DISSERTATION ZUR ERLANGUNG DES DOKTORGRADES
DER FAKULTÄT CHEMIE UND PHARMAZIE
DER LUDWIG-MAXIMILIANS UNIVERSTITÄT MÜNCHEN

ADVANCED ENERGETIC MATERIALS BASED ON 5-AMINOTETRAZOLE

– SYNTHESIS, CHARACTERIZATION, TESTING AND SCALE-UP

VORGELEGT VON

JÖRG STIERSTORFER

MÜNCHEN

2009

Erklärung

Diese Dissertation wurde im Sinne von § 13 Abs. 3 bzw. 4 der Promotionsordnung vom 29. Januar 1998 von Prof. Dr. Thomas M. Klapötke betreut.

Ehrenwörtliche Versicherung

Diese Dissertation wurde selbständig, ohne unerlaubte Hilfsmittel erarbeitet.

München, den 6. Februar 2009

……..

(Jörg Stierstorfer)

Dissertation eingereicht am:	06.02.2009
1. Gutachter	Prof. Dr. Thomas M. Klapötke
2. Gutachter	Prof. Dr. Konstantin Karaghiosoff
Mündliche Prüfung am	19.03.2009

Dedicated to my Parents

Acknowledgements

First of all, I would like to thank *Prof. Dr. Thomas M. Klapötke* for his invaluable mentoring, his support and pleasantness during the last three years and also in times before this study. In particular, I want to thank him for the scientific reliance and also his financial support enabling many official journeys.

Next, I would like to thank *Prof. Dr. Konstantin Karaghiosoff* for many helpful discussions and support and for being the second corrector. Thank you also for many NMR and X-ray measurements, quite a lot of them having been started at midnight and also during the weekends. Thank you for being the "good soul" of the research group.

I would like to thank the whole group of Prof. Klapötke for the warm atmosphere and their support. With this, a few persons are worth to mention. *Michael Göbel*, I want to thank you for being a good friend and colleague, equipped with a good scientific knowledge and a good taste of music in the lab D3.110. *Hendrik Radies*, I also want to thank you for your north-german character and help with many technical problems. *Stefan Sproll*, I want to thank you for the pleasant and scientific lab atmosphere, many inspired discussions about organic synthesis, many amusing hours in the practical courses and also for several conjoint projects. I also want to express my gratitude to *Norbert Mayr* and *Xaver Steemann* for their time-consuming help with the Koenen tests and also the high-speed movies. Thank you, *Karina*, for many fruitful collaborations and your intensive proof-reading.

I am especially thankful to *Matthias Scherr* (Dr. Maddi), *Niko Fischer* (Der Finch) and *Franz Martin* (Tiger Woods) for being great friends and colleagues.

I also want to thank my "precursor" *Dr. Jan J. Weigand* for being an excellent teacher and friend.

I want to acknowledge the great help of my entire research students Ines, Karina, Norma, Vroni, as well as Andreas, Georg, Hans, Marco, Marius and Michael.

I would like to express my thankfulness to the best secretary I know, Ms. Irene Scheckenbach, for her kindness.

I am indebted to and thank many of the members of the Department of Chemistry and Biochemistry, particularly Dr. Peter Mayer for invaluable help with many X-ray problems; the “NMR Mayer” for measuring numerous NMR spectra as well as perfect support with the conference posters; Mrs. Käser and Mr. Eicher for their efforts measuring the correct elemental analyses and also their friendliness; Mr. Andres and Mr. Fischer for their great endeavors to find the correct mass peaks; Prof. Ingo Lorenz for his help with nomenclature of complexes; Dr. Margaret-Jane Crawford for correcting several manuscripts and Dr. Brigit Weber for measuring the SQUID experiments.

I want to express my gratitude towards Dr. Betsy Rice and Dr. Ed Byrd for their support, several enjoyable E-Mail correspondences and also for giving me a very warm welcome to the United States.

Of course, I want to thank all the people, not mentioned before, who supported me writing up this thesis.

In particular, I want thank my parents Helma and Manfred for being the best parents in the world. Thank you for my education, your belief in me and finally being what I am. Last but not least, I want to thank Alexandra and all my good friends for accepting me like I am.

Preface

Green energetic materials research

Anybody may ask me: “What are the results of your dissertation?” My answer would be: “You can’t see them, you can’t smell them. It is nothing, it is only hot air.” Of course, this answer may be quite disappointing at first glance. However, from my point of view, it is one of the most desirable scopes of this work: Green Energetic Materials Research! In contrast, it is disappointing to realize how difficult it can be, to explain the manifold challenges of this project to those friends, who are not familiar with the great concepts of chemistry. It is not only difficult to explain modern chemistry, but also to rationalize the motivation. I learned during the three years: You cannot invent a new world. However, you can improve it! And you can also love it! As far as I can say, this thesis contains a lot of useful information and compounds, some of them under current investigation as applied energetic materials, and some of them bearing the potential of possibly serving as roadmap towards next generation energetic materials. Other compounds that were initially considered to be potential at the time under study proved to be less useful for practical applications, but still are of academic relevance.

As Marie Curie said: “We must not forget that when radium was discovered no one knew that it would prove useful in hospitals. The work was one of pure science. And this is a proof that scientific work must not be considered from the point of view of the direct usefulness of it. It must be done for itself, for the beauty of science, and then there is always the chance that a scientific discovery may become like the radium a benefit for humanity.”

Jörg Stierstorfer

LIFE IS TOO SHORT - PLAY HARD !

Table of Contents

List of Compounds

Color explanation:

red: secondary explosives (V_{Det} > 8200 m s^{-1})

green: primary explosive (highly sensitive)

pink: light inducible primary explosive (laser ignition)

blue: nitrogen-rich propellant (N% > 75 %)

orange: colorant for pyrotechnics (green, orange, red or blue flames)

lilac: interesting starting material

brown: extremely sensitive and dangerous

1	1,2,3,4-1*H*-Tetrazole
2	5-Amino-1*H*-tetrazole
3	Azidoformamidinium nitrate
4	Aminoguanidinium nitrate
5	Dicyandiamide
6	Cyanamide
7	5-Aminotetrazolium nitrate
8	5-Aminotetrazolium picrate
9	5-Aminotetrazolium chloride
10	1-Methyl-5-aminotetrazole
11	2-Methyl-5-aminotetrazole
12	1-Methyl-5-aminotetrazolium nitrate
13	1-Methyl-5-aminotetrazolium perchlorate
14	1-Methyl-5-aminotetrazolium picrate
15	1,4-Dimethyl-aminotetrazolium iodide
15a	1,4-Dimethyl-aminotetrazolium nitrate
15b	1,4-Dimethyl-aminotetrazolium perchlorate
15c	1,4-Dimethyl-aminotetrazolium azide
15d	1,4-Dimethyl-aminotetrazolium dinitramide
15e	1,4-Dimethyl-aminotetrazolium azotetrazolate
16	Sodium 5-5-azotetrazolate pentahydrate
16a	Hydrazinium 5-5-azotetrazolate
16b	Guanidinium 5-5-azotetrazolate

16c	1-Aminoguanidinium 5-5-azotetrazolate
16d	1,3-Diaminoguanidinium 5-5-azotetrazolate
16e	1,3,5-Triaminoguanidinium 5-5-azotetrazolate
16f	Azidoformamidinium 5-5-azotetrazolate
17	5,5'-Bis(tetrazolyl)hydrazine
18	Silver 5-nitrotetrazolate
19	1,5-Diaminotetrazole
19a	1,5-Diaminotetrazolium nitrate
19b	1,5-Diaminotetrazolium perchlorate
20	1,5-Diamino-4-methyl-tetrazolium iodide
20a	1,5-Diamino-4-methyl-tetrazolium nitrate
20b	1,5-Diamino-4-methyl-tetrazolium perchlorate
20c	1,5-Diamino-4-methyl-tetrazolium dinitramide
21	Lithium 5-aminotetrazolate
22	Sodium 5-aminotetrazolate trihydrate
23	Potassium 5-aminotetrazolate
24	Rubidium 5-aminotetrazolate
25	Cesium 5-aminotetrazolate
26	Magnesium 5-aminotetrazolate
27	Calcium 5-aminotetrazolate
28	Strontium 5-aminotetrazolate
29	Barium 5-aminotetrazolate
30	Hydrazinium 5-aminotetrazolate
31	5-Aminotetrazolium dinitramide
32	Azidoformamidinium dinitramide
33	1,5-Diaminotetrazolium dinitramide
34	1-Methyl-5-aminotetrazolium dinitramide
35	2-Methyl-5-aminotetrazolium dinitramide
36	Tetrazolium dinitramide
37	Triaminoguanidinium dinitramide
38	5-Aminotetrazolium perchlorate
38·At	5-Aminotetrazolium perchlorate · 5-aminotetrazole
39	Aminoguanidium perchlorate
40	Triaminoguanidinium perchlorate
41	Azidoformamdinium perchlorate
42	Tetrazolium perchlorate
43	5-Nitriminotetrazole
43·H_2O	5-Nitriminotetrazole monohydrate
44	1-Methyl-5-nitriminotetrazole
44·H_2O	1-Methyl-5-nitriminotetrazole monohydrate

45 2-Methyl-5-nitraminotetrazole
46 1-(2-Hydroxyethyl)-5-aminotetrazole
47 2-(2-Hydroxyethyl)-5-aminotetrazole
48 1-(2-Chloroethyl)-5-aminotetrazole
49 1-(2-Azidoethyl)-5-aminotetrazole
50 1-(2-Hydroxyethyl)-5-nitriminotetrazole
51 1-(2-Chloroethyl)-5-nitriminotetrazole
52 1-(2-Nitratoethyl)-5-nitriminotetrazole
53 1-(2-Azidoethyl)-5-nitriminotetrazole
54 Potassium 1-(2-azidoethyl)-5-nitriminotetrazolate
55 Sodium 1-(2-chloroethyl)-5-nitriminotetrazolate
56 Ammonium 1-(2-chloroethyl)-5-nitriminotetrazolate
57 1-(2-Hydroxyethyl)-5-aminotetrazolium nitrate
58 1-(2-Azidoethyl)-5-aminotetrazolium nitrate
59 1-(2-Azidoethyl)-5-aminotetrazolium perchlorate monohydrate
60 $[Cu(1\text{-}EtOH\text{-}AtNO_2)_2(H_2O)_2]$
61 $[Cu(1\text{-}EtCl\text{-}AtNO_2)_2(H_2O)_2]\cdot 2H_2O$
62 $[Cu(1\text{-}EtN_3\text{-}AtNO_2)_2(H_2O)_2]$
63 1,3,5-Trimethylhexahydro-1,3,5-triazine
64 2-Nitro-2-azapropyl acetate
65 1-Chloro-2-nitro-2-azapropane
66 1-(2-Nitro-2-azapropyl)-5-aminotetrazole
67 1-(2-Nitro-2-azapropyl)-tetrazole
68·H_2O 1-(2-Nitro-2-azapropyl)-5-nitriminotetrazole monohydrate
68·EtOH 1-(2-Nitro-2-azapropyl)-5-nitriminotetrazole·ethanol
69 2,5-Bis(2-nitro-2-azapropyl)-nitriminotetrazole
70 1-Methyl-5-(2-nitro-2-azapropyl)-5-nitraminotetrazole
71 1-Methyl-4-(2-nitro-2-azapropyl)-5-nitriminotetrazole
72 1-Methyl-5-(2-nitro-2-azapropyl)-5-aminotetrazole
73 2-Methyl-5-(2-nitro-2-azapropyl)-5-nitraminotetrazole
74 1,4-Dimethyl-5-nitriminotetrazole
75 Ammonium 1-methyl-5-nitriminotetrazolate
76 Ammonium 2-methyl-5-nitriminotetrazolate
77 Lithium 1-methyl-5-nitriminotetrazolate
78 Sodium 1-methyl-5-nitriminotetrazolate
79 Potassium 1-methyl-5-nitriminotetrazolate
80 Rubidium 1-methyl-5-nitriminotetrazolate
81 Cesium 1-methyl-5-nitriminotetrazolate
82 Strontium bis(1-methyl-5-nitriminotetrazolate)
83 Strontium bis(2-methyl-5-nitriminotetrazolate)

84	Silver 1-methyl-5-nitriminotetrazolate
85	Guanidinium 1-methyl-5-nitriminotetrazolate
86	1-Aminoguanidinium 1-methyl-5-nitriminotetrazolate
87	1,3-Diaminoguanidinium 1-methyl-5-nitriminotetrazolate
88	1,3,5-Triaminoguanidinium 1-methyl-5-nitriminotetrazolate
89	Azidoformamidinium 1-methyl-5-nitriminotetrazolate
90	Calcium bis(5-nitrimino-1*H*-tetrazolate)
90·5H_2O	Calcium bis(5-nitrimino-1*H*-tetrazolate) pentahydrate
91	Potassium 5-nitriminotetrazolate
92	Magnesium 5-nitriminotetrazolate
93	Calcium bis(5-nitrimino-1*H*-tetrazolate)
94	Strontium bis(5-nitriminotetrazolate)
95	Strontium 5-nitriminotetrazolate
96	Barium 5-nitriminotetrazolate
97	Cadmium 5-nitriminotetrazolate
98	Zinc bis(5-nitriminotetrazolate) tetrahydrate
99	Zinc bis(1-methyl-5-nitriminotetrazolate) hexahydrate
100	Hydrazinium 5-nitriminotetrazolate
101	Dihydrazinium 5-nitriminotetrazolate monohydrate
102	5-Amino-1-methyltetrazolium 5-nitriminotetrazolate monohydrate
103	5-Amino-2-methyltetrazole · 5-nitriminotetrazole
104	$[Cu(HAtNO_2)_2(H_2O)_4]$
105	$(NH_4)_2[Cu(AtNO_2)_2]$
106	$[Cu(AtNO_2)(NH_3)_3]_2$
107	$[Cu(1MeAtNO_2)_2(H_2O)_2]$·2 H_2O
108	$[Cu(1MeAtNO_2)_2(H_2O)_2]$
109	$[Cu(1MeAtNO_2)_2]$
110	$[Cu(1MeAtNO_2)_2(H_2O)_2]$·2 MeOH
111	$[Cu(1MeAtNO_2)_2(NH_3)_2]$
112	$[Cu(2MeAtNO_2)_2(2MeHAtNO_2)_2]$
113	$[Cu(2MeAtNO_2)_2]$
114	$[Cu(2MeAtNO_2)_2(NH_3)_2]$
115	$[Cu(2MeAtNO_2)_2(NH_3)_4]$·$H_2O$
116	5,5'-Bis(1*H*-tetrazolyl)triazene
117	1-(1*H*-tetrazol-5-yl)-2-benzylidene hydrazine
118	5,5'-Bis(1-methyltetrazolyl)triazene
119	5,5'-Bis(2-methyltetrazolyl)triazene
120	Ammonium 5,5'-bis(1-methyltetrazolyl)triazenate
121	Ammonium 5,5'-bis(2-methyltetrazolyl)triazenate
122	Sodium 5,5'-bis(1-methyltetrazolyl)triazenate

123 Sodium 5,5’-bis(2-methyltetrazolyl)triazenate

124 5,5’-Bis(1-methyltetrazolyl)-1-methyl-triazene

125 5,5’-Bis(2-methyltetrazolyl)-1-methyl-triazene

126 Magnesium 5,5’-bis(2-methyltetrazolyl)triazenate

127 Ammonium tetrazolate

128 Hydrazinium tetrazolate

129 Lithium tetrazolate

130 Sodium tetrazolate

131 Potassium tetrazolate

132 Rubidium tetrazolate

133 Cesium tetrazolate

134 Strontium tetrazolate pentahydrate

135 5-Azido-1*H*-tetrazole

136 Hydrazinium 5-azidotetrazolate

137 Ammonium 5-azidotetrazolate

138 Aminoguanidinium 5-azidotetrazolate

139 Guanidinium 5-azidotetrazolate semihydrate

140 Lithium 5-azidotetrazolate monohydrate

141 Sodium 5-azidotetrazolate monohydrate

142 Potassium 5-azidotetrazolate

143 Cesium 5-azidotetrazolate

144 Calcium 5-azidotetrazolate hydrate

145 1-Methyl-5-azidotetrazole

146 2-Methyl-5-azidotetrazole

147 5-Nitro-2*H*-tetrazole

148 1-Methyl-5-nitrotetrazole

149 2-Methyl-5-nitrotetrazole

150 1-Methyl-5-chlorotetrazole

151 Bis-(1-methyltetrazol-5-yl)-diazene N-oxide

152 1,5-Bistetrazole

152·H_2O 1,5-Bistetrazole monohydrate

153 2-Methyl-1,5-bistetrazole

154 Ammonium 1,5-bistetrazolate

155 Sodium 1,5-bistetrazolate

156 Potassium 1,5-bistetrazolate

157 Bis(aqua-(1,5-bistetrazolato))copper(II)

158 Bis(ammine(1,5-bistetrazolato))copper(II)

159 Bis(chloro(2-methyl-1,5-bistetrazole)copper(II)

160· H_2O 5,5’-Bis(1*H*-tetrazolyl)amine monohydrate

160 5,5’-Bis(1*H*-tetrazolyl)amine

161 5,5’-Bis(2-methyltetrazolyl)amine

162 5,5’-Bis(2-methyltetrazol)methylamine

163 5-(1*H*-Tetrazol-5-yl)-5’-(2-methyltetrazol-5-yl)amine

164 5-(1*H*-Tetrazol-5-yl) -5’-(2-ethyltetrazol-5-yl)amine

165 $[Zn(H_2bta)_2(H_2O)_2](NO_3)_2 \cdot 0.5H_2O$

166 $[Zn(H_2bta)_2(ClO_4)_2] \cdot H_2O$

167 $[Cu(H_2bta)_2](NO_3)_2 \cdot 0.5H_2O$

168 $[Cu(H_2bta)_2(ClO_4)_2]$

169 $[Cu(Me_2bta)_2(NO_3)_2]$

170 $[Cu(Me_2bta)_2(ClO_4)_2]$

171 $[Cu(Me_3bta)_3](ClO_4)_2$

172 $[Cu(Me_3bta)Cl_2]$

173 5-Aminotetrazolium tetrafluoroborate

174 Tosyl-azidoformamidine

175 OCX (Octopus Explosive)

176 3-[2-(2-Nitrato-ethyl)-2*H*-tetrazol-5-yl]-[1,2,3,4]oxatriazol-5-one

177 5-Nitratoethyl-5-nitramino-1*H*-tetrazole

178 1,4-Di(2-chloroethyl)-5-aminotetrazolium chloride

179 5-Cyano-2*H*-tetrazole

180 *1H*-Tetrazole-5-carboxylic acid amide

181 *1H*-Tetrazole-5-carboxylic acid nitramine

182 Ammonium sodium 5-cyanotetrazolate dihydrate

183 1,4-Diamino-2,3,5,6-tetrazine

184 Sodium 5-chlorotetrazole dihydrate

Chapter 1.

Introduction

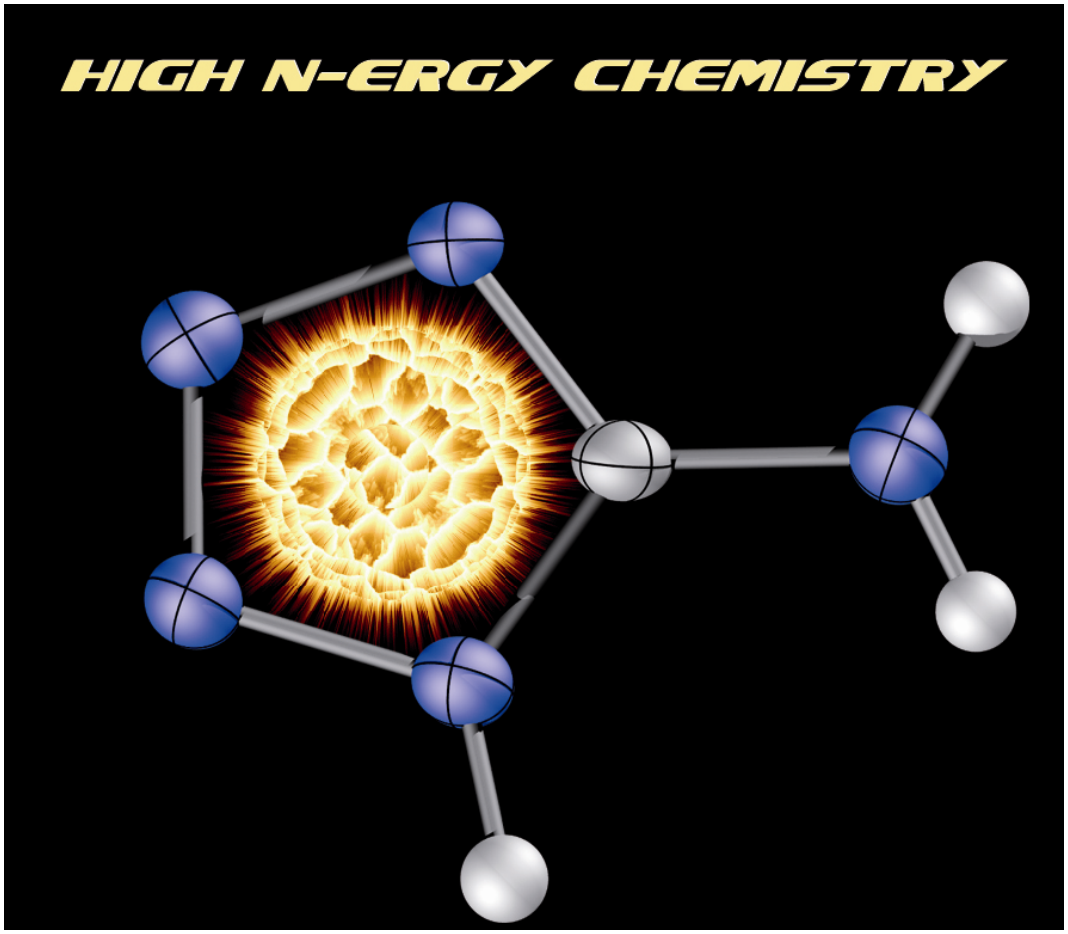

1.1 Energetic Materials

1.1.1 Classification

The research of new energetic materials is an ongoing project in many research groups world-wide.[1,2,3,4,5,6] Before the discussion of recent developments of new **e**nergetic **m**aterials (EM), a few definitions must be given.

One of the most recent definitions of an *energetic material* according to ASTM (American Society for Testing and Materials) says: "*Energetic materials are defined as chemical compounds or compositions that contain both fuel and oxidizer and rapidly react to release energy and gas. Examples of energetic materials are high explosives, gun propellants, rocket and missile propellants, igniters, primers, initiators, and pyrotechnic (e.g. illuminants, smoke, delay, decoy, flare and incendiary) compounds and compositions. Energetic materials may be thermally, mechanically, and electrostatically initiated and do not require atmospheric oxygen to sustain the reaction.*"

In order to describe the energetic materials presented in this work, this definition is very inconvenient. Most of the compounds are not characterized by an balanced oxygen content. Many of the most explosive derivatives neither contain oxygen. Therefore, it is necessary to introduce a more general definition of energetic materials: "*Energetic materials are chemical compounds or compositions, which may react rapidly under release of energy and gas. The reaction may be a detonation, explosion, deflagration, decomposition or combustion.*

In the following only *Chemical Energetics* are described. Atomic and physical explosions, which can be more than a million greater in energy than produced from a chemical explosion are not described in this work.

Many variations of classification of chemical energetic materials have been found throughout this century.[7] The main difference of classifications is with respect to their chemical nature and to their performance and uses. Classifying explosives by the presence of certain molecular groups (e.g. azides, nitro compounds, nitramines, nitric esters) contains neither information of the energetic performance nor of possible applications. A more suitable way to classify **h**igh **e**nergy **d**ense **m**aterials (HEDM) is by performances and uses. Using this classification, HEDMs are divided into three classes (**Figure 1.1**): (i) explosives, (ii) propellants, and (iii) pyrotechnics.

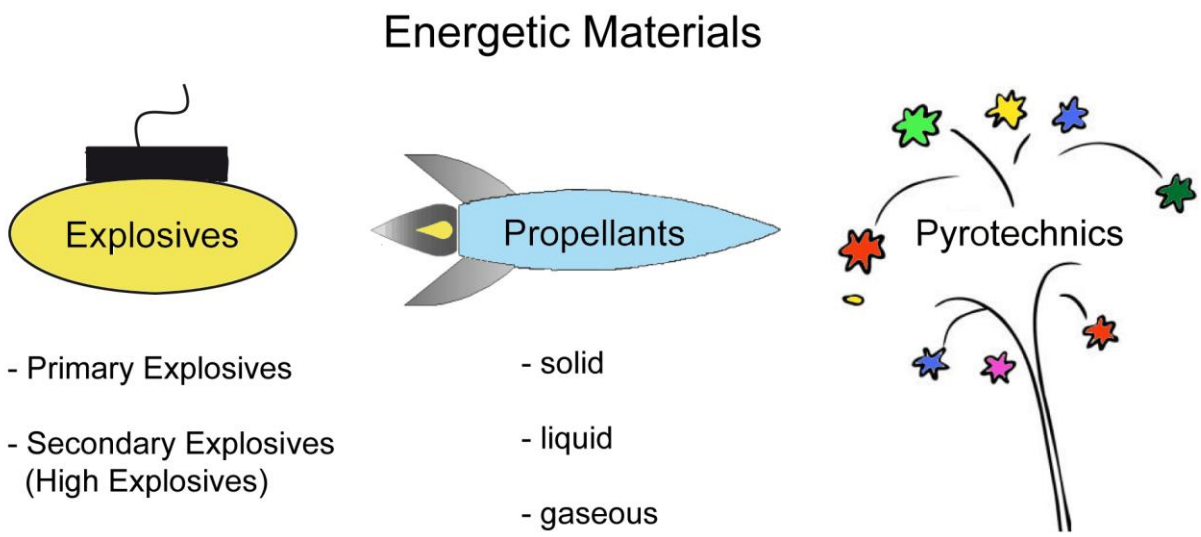

Figure 1.1 Classification of Energetic Materials.

The class of *explosives* is divided into *primary explosives* and *secondary explosives*, also called *high explosives*.

A convenient definition for an explosion is described by Meyer and Köhler:[8] *An explosion is a sudden increase in volume and release of energy in a violent manner, usually with generation of high temperatures and release of gases. An explosion causes pressure waves in the local medium in which it occurs. Explosions are categorized as deflagrations if these waves are subsonic and detonations if they are supersonic.*

Primary explosives

Compounds considered to the class of *primary explosives* are mostly highly sensitive towards friction, impact and electrical sparks. They usually detonate with velocities between 3500 and 5500 m s^{-1}. Primary explosives differ from secondary explosives by they undergo a very rapid transition from burning to detonation. The detonation is often used for ignition of less sensitive explosives. Famous examples (**Figure 1.2**) are lead azide (a), silver azide,[9] mercury fulminate[10](b) and lead styphnate (c). A problem of most primary explosives is the presence of heavy metals, due to its corresponding environmental impact when the primary explosives are brought to function. Therefore modern lead-free primary explosives, e.g. 1,3,5-triazido-2,4,6-trinitrobenzene (d), (TATNB),[11] are preferred.

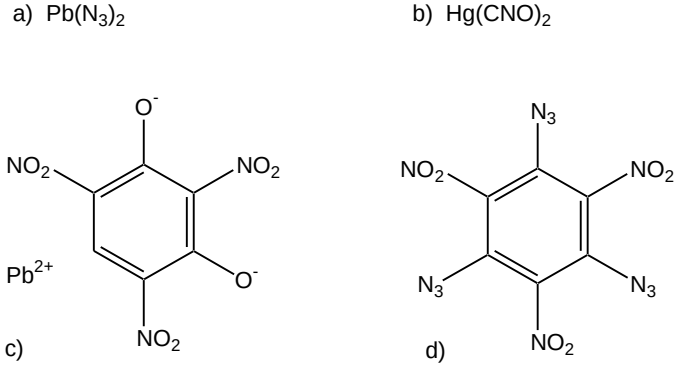

Figure 1.2 Primary explosives. a) lead azide b) mercury fulminate, c) lead styphnate, d) TATNB.

Secondary Explosives

Secondary explosives detonate or explode with higher detonation velocities (> 5500 m s^{-1}) and detonation pressures under formation of a shockwave. Mostly, they are only slightly sensitive and kinetically stable, therefore they cannot be detonated readily by heat or shock and the explosion has to be stimulated using a detonator containing a primary explosive. Examples of commonly known secondary explosives (**Figure 1.3**) are TNT (2,4,6-trinitrotoluene), RDX (royal demolition explosive, hexogen, hexahydro-1,3,5-trinitro-1,3,5-triazine),[12] HMX (high melting explosive, her majesties explosive, octogen, octahydro-1,3,5,7-tetranitro-1,3,5,7-tetrazine) [13] and PETN (pentaerythritol tetranitrate).[14]

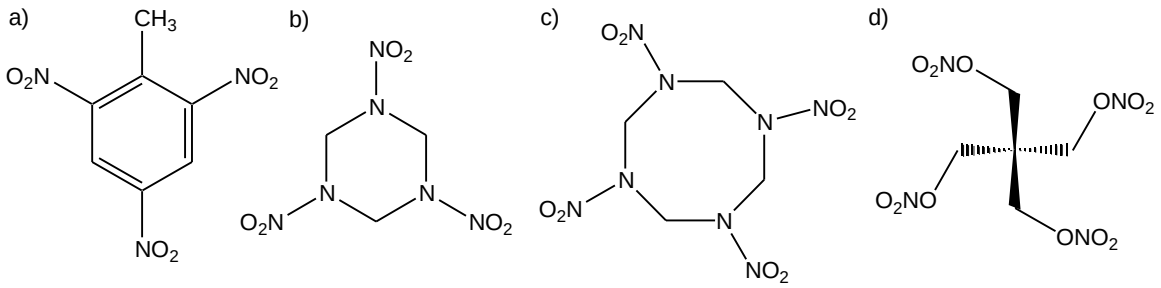

Figure 1.3 Commonly used secondary explosives: a) TNT b) RDX c) HMX d) PETN.

In the field of secondary explosives, especially in military applications, many new energetic molecules have been synthesized (**Figure 1.4**).[15] Based on computational simulations,[16] as well as experiences from the field of organic chemistry, new high density materials have been defined and can be achieved if the molecular structure contains fused ring and/or strained ring systems. Trinitroazetidine (TNAZ, **Figure 1.4.f**) for example is a new energetic material with a high thermal stability (mp.: 101 °C, $T_{Dec.}$:

240 °C) which is under current investigations for replacement of TNT based explosives. It delivers a detonation velocity of 8950 m s^{-1}, as well as a detonation pressure of 357 kbar.[17] A further novel insensitive explosive is diaminodinitroethylen (DADE), abbreviated also as FOX-7.[18] It decomposes at 220 °C and shows a suitable detonation velocity (8870 m s^{-1}, calc.) and pressure (340 kbar, calc.).[19] Examples of other modern secondary explosives are hexanitrostilben (HNS), 1,3,5-triamino-2,4,6-trinitrobenzene (TATB), hydrazinium nitroformate (HNF), nitrotriazoloxid (NTO), ammonium-dinitramide (ADN), 2,4,6,8,10,12-hexanitro-2,4,6,8,10,12-hexaaza-tetracyclo-dodecan (CL-20), 4,10-dinitro-2,6,8,12-tetraoxa-4,10-diazatetracylododecane (TEX) [20] and octanitro cubane (ONC).[21]

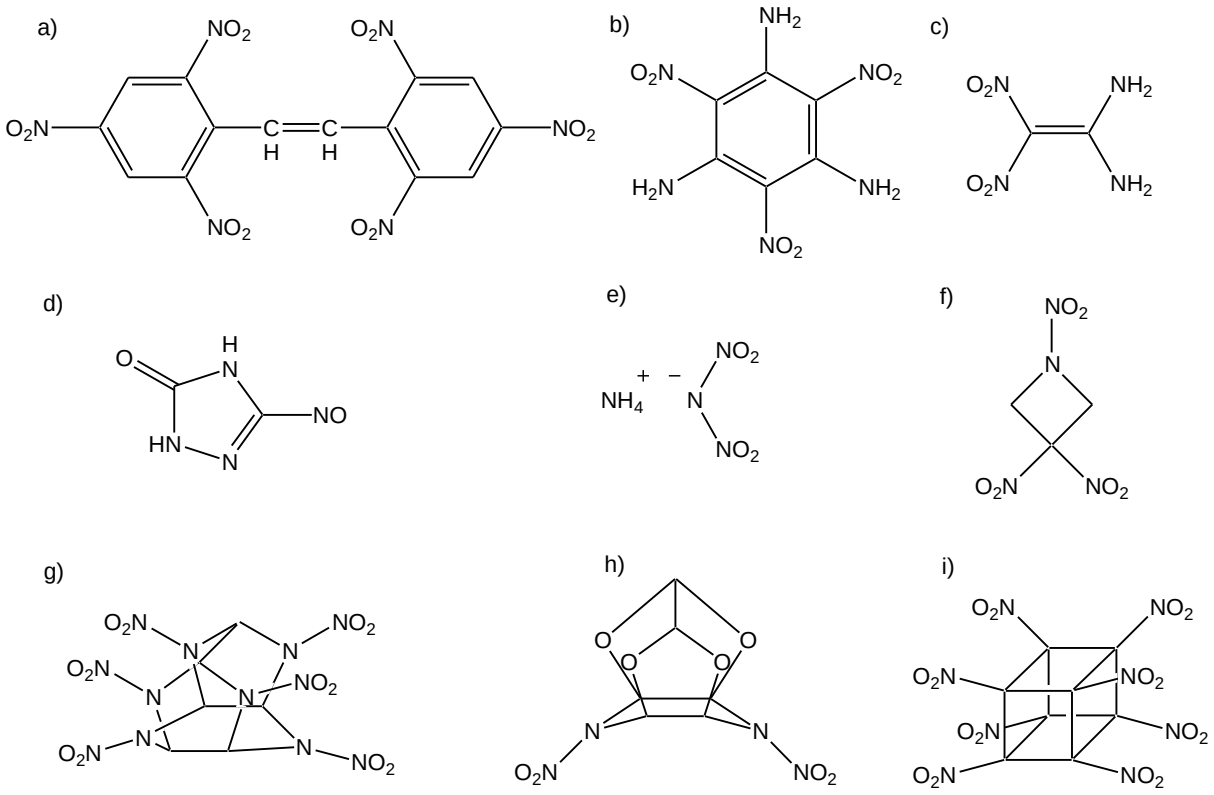

Figure 1.4 Modern Explosives: a) HNS b) TATB c) FOX-7 d) NTO e) ADN f) TNAZ g) CL-20 h) ONC.

Propellants

Propellants are combustible materials, at best containing within themselves all the oxygen needed for the combustion. They are used in rocket engines, e.g. in the space shuttle mission setup (**Figure 1.5**), in missiles or as gun powders. For this applications, mostly mixtures containing a fuel and an oxidizer are used. They differ from primary

and secondary explosives in that their prime objective is to deflagrate. For obtaining a large specific impulse I_{sp} a high burning temperature and a small averaged mole weight of the gaseous combustion products is needed. Propellants can be initiated by flames or sparks. By deflagrating, propellants build up relatively high pressures without the presence of a higher velocity shock wave. The most famous example of a propellant is black powder. For propellants, the chemistry of the compounds can be divided into three groups. Single based (SB), double based (DB) and semi-nitramine/nitramine propellants belonging to the gelatinized nitrocellulose-based propellants (NC-based), which are most widely used in gun applications.[22] A further group of propellants is based on a synthetic polymer binder system with an inorganic oxidizing system, commonly a perchlorate, and called composite propellant. This class is widely used for rocket propulsion in solid state booster.

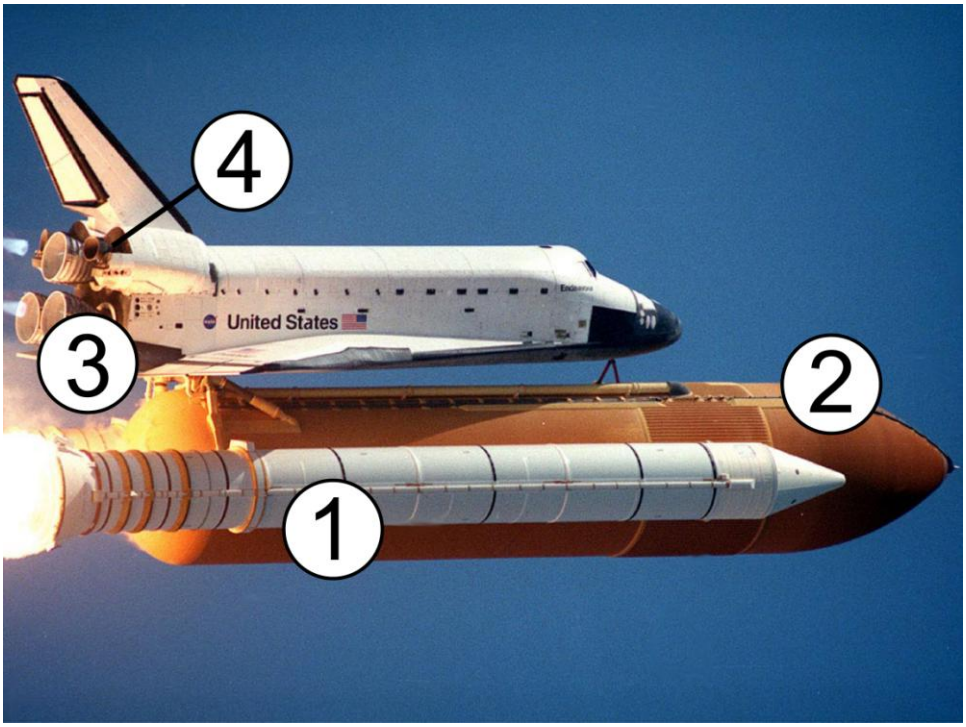

Figure 1.5 Space shuttle mission setup. **1**: Solid-propellant booster containing 454 t propellant: NH_4ClO_4 (70 %), Al (16 %), polybutadiene acrylic acid acrylonitrile (12 %), epoxy-curing agent (2 %), Fe_2O_3 (0.07 %). **2**: Cryogenic propellant carrier: liquid oxygen (LOX) and liquid hydrogen (LH_2). **3**: Combustion engine of LOX/LH_2. **4**: Orbital Maneuvering Subsystem (OMS): Hypergolic mixture of monomethyl hydrazine (MMH) and nitrogen tetroxide (N_2O_4).

Finally there are the liquid and gaseous propellants, which are mainly used in space exploration and technology. Hydrazine, monomethylhydrazine (MMH), and unsymmetrical dimethylhydrazine (UDMH) are liquid rocket fuels. They are used in a wide variety of rocket engines requiring high performance and long storage times. Hydrazines used as liquid fuel build hypergolic (self-igniting) systems when mixed with various oxidizers such as N_2O_4, HNO_3 or F_2.

Pyrotechnics

Pyrotechnics are mixtures or compounds designed to produce effects such as heat, light, sound, gas or smoke. This results of a non-detonative, self sustaining exothermic chemical reaction. The expression *pyrotechnics* is based on the Greek words pyros (fire) and techne (art). Pyrotechnic devices combine high reliability with very compact and efficient energy storage, in the form chemical energy which is converted to expanding hot gases either through deflagration or detonation. The controlled action of a pyrotechnic device, initiated by an electrical signal or mechanical impetus, makes possible a wide range of automated or remote mechanical actions, e.g. deployment of safety equipment and services or precisely timed release sequences. The majority of the technical pyrotechnic devices use propellants in their function. The other part use primary or secondary explosives to obtain very fast and powerful mechanical actions, e.g. cable cutters or exploding bolts.

Figure 1.6 Smokeless firework.

1.1.2 Characteristics

To introduce a new suitable explosive, e.g. for replacement of RDX, many requirements have to be fulfilled. In the following poster the main desired characteristics are illustrated.

Figure 1.7 Wanted poster of a new secondary explosive.

Performance: A new high explosives should at least exceed the detonation power of TNT (trinitrotoluene) at best also that of RDX (royal demolition explosive). The most important characteristics and parameter of performance are the detonation velocity ($V_{Det.}$), the detonation pressure ($p_{C\text{-}J}$) and the detonation energy (U_{Det}). Typical values of these characteristics are:[23] TNT: $V_{Det.}$ = ~6950 m s^{-1}, p = ~210 kbar, $U_{Det.}$ = ~5000 kJ kg^{-1}, RDX: $V_{Det.}$ = 8750 m s^{-1}, $p_{C\text{-}J}$ = 347 kbar, $U_{Det.}$ = 6033 kJ kg^{-1}. When testing a new high explosive, at least a detonation velocity of 8500 m s^{-1} should be exceeded. For new compounds these parameters can be calculated using computer codes such as "EXPLO5" or "Cheeta" by knowing the sum formula, density and heat of formation (ΔH_f). Perhaps the most critical parameter is the density ρ of a explosive, since the detonation pressure is directly proportional to the squared density ρ^2. The detonation velocity depends also on the molar quantity N of formed gaseous products. In addition high, negative reaction enthalpies are required for effective energetic materials. The estimation of ΔH_f of HEDMs is also a difficult project since bomb calorimetric measurements often create wrong combustion energies. This can be reasoned by an incomplete combustion due to the tendency to explode. A simple method for estimating the explosion power is the "Koenen" Steel Sleeve Test (1.3.18).

Thermal stability: A further fundamentally characteristic of new high explosives is a good thermal stability. This is necessary since safety aspects surpass all other criteria of explosives. Not only the risks in production processes have to keep low, but also high thermal impacts have to be overcome while bearing the pure or converted explosives. A typical desirable temperature of decomposition of new high explosives are above 180 °C. If melting points are detected, there should be a huge range (~80 °C) between melting and decomposition, which may also be used in melt casting production. TNT decomposes above 160° C, while it melts at 80 °C. RDX decomposes while melting above 204 °C. Melt- and decomposition temperatures of HEDMs are usually determined automatically using DSC (differential scanning calorimetry), DTA (differential thermal analysis) or TGA (thermal gravimetric analysis) devices.

High density: High densities are a basic condition of energetic materials. As mentioned already, detonation velocity and pressure are both functions of the density, but also of the heat of reaction, moles of gas produced and the average molecular weight of the products. The detonation pressure varies directly as the square of the density.

Insensitivity: The trend of designing new energetic materials goes to synthesis of "insensitive" materials. Since many accidents happened during handling or work up processes on high explosives this point becomes more important. Common explosives show sensitivities towards different stimuli. The most important criteria are the sensitivity towards impact, towards friction and electrical sparks. Energetic materials are classified to their sensitivities by the "Recommendations on the transport of dangerous goods" into extremely sensitive, very sensitive, sensitive, low sensitive or not sensitive. The sensitivities can be discovered e.g. by using BAM (Bundesamt für Materialwissenschaften) methods (drophammer and friction tester, see 1.3.12 and 1.3.13).

Chemical and hydrolytical stability: New materials should of course be kinetically and thermodynamically stable. The stability towards hydrolysis is obvious, since water vapor is present all-around.

Toxicity: The main disadvantage of RDX is its toxicity against aquatic creatures. However, it is not only desirable to design non toxic products, also its decomposition products should be environmentally benign. In addition toxic starting materials, products, byproduct or solvents have to be avoided in technical syntheses. Therefore explosives containing high nitrogen contents are desired, because of dinitrogen N_2 as the main reaction product, whereby nitrogen oxides, NH_3 or HCN are not desired. Besides the lower environmental pollution, the reduction of detectable plume signatures in propellants is another benefit. High-nitrogen materials such as tetrazen are also promising approaches finding replacements for toxic primary explosives (e. g. $Pb(N_3)_2$) used in large scales in ammunition.

Low solubility: To avoid ground water pollution, new explosive should be low soluble in water. An important indication gives the octanol/water coefficient (see 1.3.19).

Compatibility: An indispensable characteristic of a new explosive is its compatibility with, e.g. binders and plasticizers used in explosive compositions. First information can be obtained by running thermal analysis of mixtures with methyl ammonium nitrate and nitroguanidine.

Longevity: A further important criteria for technically used explosives is their long term stability. This often correlates with the decomposition and melting temperature as well as the vapor pressure. Usually, salts are better storable than neutral compounds. To increase the periods of storage often scavengers, based on hydroquinone and substituted phenols, are added to explosive compositions. Long term stability test can be performed using TSC (Thermal Safety Calorimeter) devices.

Yield: High yields are not only necessary to decrease the costs of production. A quantitative reaction is desired, since usually the purification and work-up is more complex than the synthesis itself. Also highly sensitive or toxic byproducts should be avoided in industrial scales.

Price: Secondary explosives are produced in thousands of tons worldwide, therefore the synthesis should be cost-effective and profitably.

1.1.3 History and Future Research

The research of new energetic materials shows a long term history. However, many of commonly used explosives have been not invented for use as explosive, naturally. **Figure 1.8** shows a time scale of the first description of famous EM.

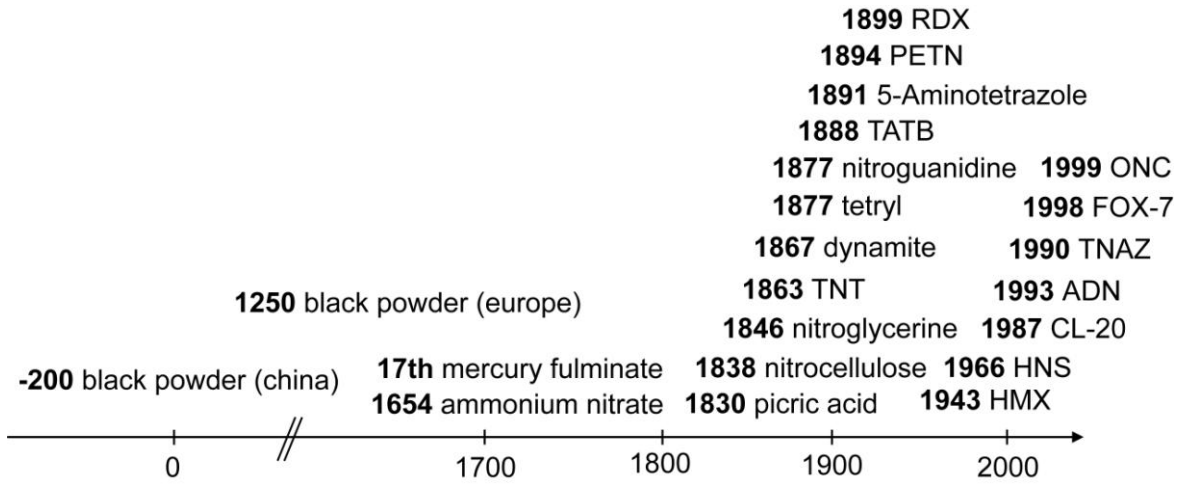

Figure 1.8 Time scale of invention of new energetic materials.

TATB (triamino-trinitro benzene), for example, has been synthesized for the first time in 1888, but was described not until 1978 as an explosive. The existence of black powder in

220 BC is reported to be likely the first explosive composition. Not until 1400 years later black powder was reinvented in Europe for military use to blow up walls and protective barriers. Till now, most of the EM have been synthesized in the last 180 years. Interestingly, the development has never stopped and perhaps will never stop.

Development of new high explosives - A never ending challenge! Ongoing worldwide research of new energetic materials for both, civilian and military applications are currently developing pyrotechnics with reduced smoke and new explosives and propellants with higher performance or enhanced insensitivity to thermal or shock insults. The introduction of a new compound into technical application is even hard (or harder) as commercial launch of new pharmaceuticals. Numerous requirements must be fulfilled, which are not conceivable when designing and synthesizing new energetic materials. One approach is the use of *high nitrogen* or *all-nitrogen* compounds. Up to date, there is no example of a homo-polyatomic nitrogen compound which could be used as HEDM, since neither thermodynamic nor kinetic stabilization with respect to decomposition into N_2 has been achieved. Therefore, experimental investigations [24] are elusive compared to the large number of theoretical studies.[25] The azide anion and the N_5^+ cation [26] are the only homopolyatomic nitrogen species which are stable at ambient conditions. However, a polymeric single-bonded cubic form of nitrogen (*cg*-N) was described by Eremets *et al.*.[27] This material was synthesized directly from molecular nitrogen at temperatures above 2000 K and pressures above 110 GPa in a laser-heated diamond-cell. At room temperature *cg*-N is metastable only at pressures above 42 GPa. Also the polymerization of nitrogen in sodium azide at pressures as high as 120 GPa was reported.[28] Quite recently, also by using high pressure polymeric nitrogen, stable at room temperature, has been observed by pressing a mixture of H_2/N_2.[29]

A further approach is the use of nitrogen-rich heterocycles, particularly, the class of tetrazole derivatives. Therefore, the development of tetrazole compounds as new energetic materials [30] for civil and military applications is of great interest in many research programs worldwide. Tetrazoles have the outstanding property of often combining a high nitrogen content with good thermal and kinetic stabilities, due to their aromatic ring system. “High-nitrogen” compounds form a unique class of energetic materials whose energy is derived from their very high heats of formation rather than from the overall heat of combustion. The enthalpy criteria of energetic materials are governed by their molecular structure, and therefore, the move to heterocycles with a higher nitrogen content (e.g. from imidazole ($\Delta_f H°_{cryst.}$ = 14.0 kcal mol^{-1}),[31] over

1,2,4-triazole ($\Delta_f H°_{cryst.}$ = 26.1 kcal mol^{-1}) to 1,2,3,4-tetrazole ($\Delta_f H°_{cryst.}$ = 56.7 kcal mol^{-1})[32]) the trend in the heats of formation is obvious. The high heat of formation is directly attributable to the large number of energetic N–N, N–C and N–O bonds.[33] Especially energetic ionic salts of tetrazoles have been utilized in energetic roles owing to their higher heats of formation, density and oxygen balance compared to those of their carbocyclic analogues. In the following an introduction into tetrazole chemistry is given.

1.2 Tetrazoles

Tetrazoles are aromatic heterocycles containing one carbon atom as well as four nitrogen atoms. The most elementary tetrazole is 1,2,3,4-1*H*-tetrazole (**1**). Due to the delocalization of its electronic system and a [1,5]*H*-shift two main tautomers can be observed: 1*H*-tetrazole and 2*H*-tetrazole. The 5*H*-tetrazole tautomere has never been detected since its loss of aromaticity (**Scheme 1.1**).

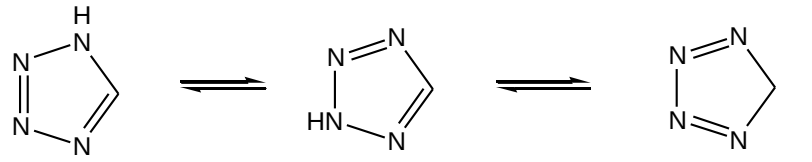

Scheme 1.1 Tautomers of 1,2,3,4-tetrazole.

1.2.1 History and Applications

Uniquely natural tetrazoles are not known yet. The first tetrazole, 5-cyano-2-phenyltetrazole, was discovered by E. Fischer in 1878 by the reaction process shown in **Scheme 1.2**.[34] However, the structure was elucidated not until 1885.[35] In 1947 ~300 tetrazole derivatives have been known, particularly, with regards for possible applications in colorants, agrochemistry and propellant systems. Since 1960 tetrazoles were booming due to the discovery of their biochemical and pharmaceutical activities.[36] Tetrazoles have been proofed to exhibit, e.g. antibacterial, fungicidal and anitiallergical properties.[37] In addition some tetrazoles inhibits blood clotting as well as increase of cancer cells.[38,39] Tetrazoles are also used as additives in silver halogenide

emulsions in photography techniques to obtain better color resolutions.[40] Up to now more than 318000 entries regarding tetrazole chemistry are found in the Scifinder database.[41]

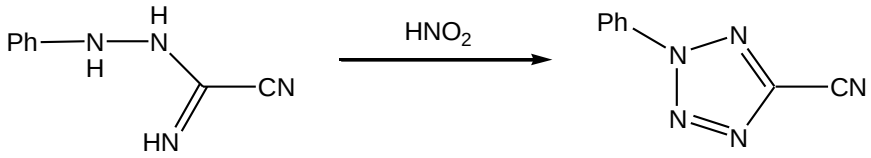

Scheme 1.2 First synthesis of a tetrazole derivative.

1.2.2 Syntheses

Several different synthetic routes for tetrazole derivatives are found in the literature. The most important are (A) (2+3)-dipolar cycloadditions, (B) ring closure of azidoformamidinium derivatives and (C) ring assembly by three components. Examples for reaction types A,[42] B and C are depicted in **Scheme 1.3**.

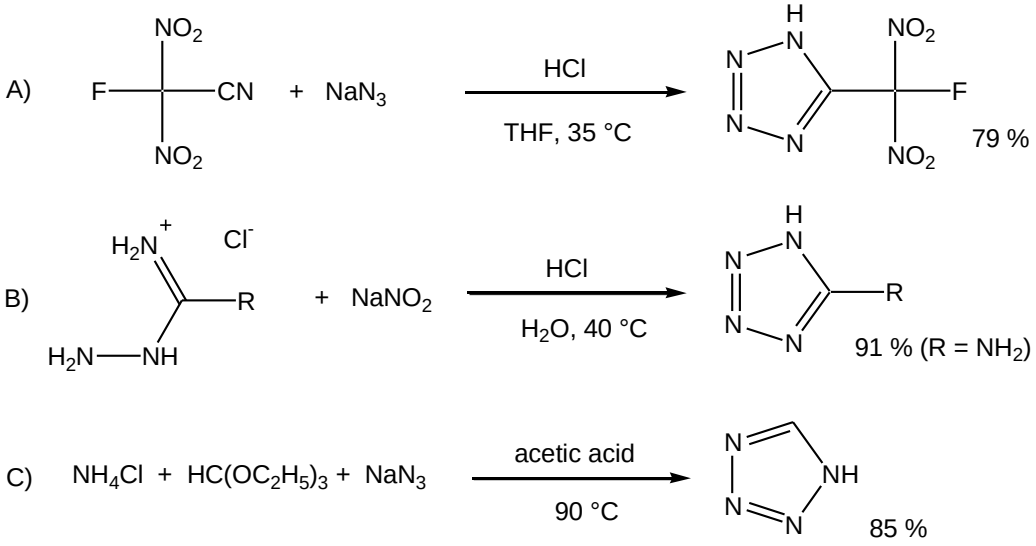

Scheme 1.3 Synthetic strategies preparing tetrazoles.

1.2.3 Properties and Characteristics

Tetrazoles are mostly polar compounds. For unsubstituted tetrazole, a dipole moment of 5.11 D was determined in 1,4-dioxane.[43] The solubility of tetrazoles depends on the substituents at the ring moiety. Oftentimes, water, alcohols as well as solvents like MeCN, THF or ethyl acetate are the solvents of choice for syntheses. All neutral tetrazoles investigated in this thesis are soluble in DMSO. All investigated salts are soluble in water and could recrystallized, mostly, from ethanol/water mixtures.

By comparison of the relative energies of 1*H*-tetrazole and 2*H*-tetrazole in the gas phase, the 2*H*-tetrazole is slightly favored.[44,45] However, due to solvatation effects, in solution also the 1*H*-tautomere can be observed.

In **Scheme 1.4** three different monosubstituted tetrazoles are shown. For 5-substituted tetrazoles, the locating of the hydrogen atom strongly depends on the substituent. There is again a tautomeric form with the hydrogen atom located in position 2, but in solution the 1*H*-tautomere is favored as measurements of the dipole moment show.[36,46,47,48]

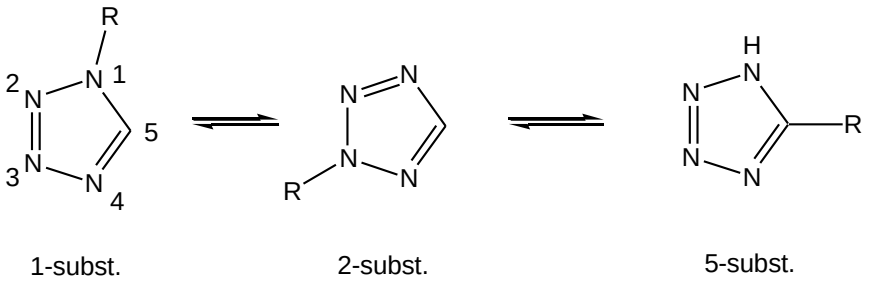

Scheme 1.4 Monosubstituted tetrazoles.

5-Substituted tetrazoles can be further substituted leading to di- and trisubstituted tetrazoles. The 1,5- and the 2,5-disubstituted tetrazoles are liable to the so called tetrazole-tetrazoline tautomerization, which especially can be observed with tetrazoles containing an exocyclic oxygen or sulphur atom (X = O, S). The tetrazole-tetrazoline tautomerization is depicted in **Scheme 1.5**.

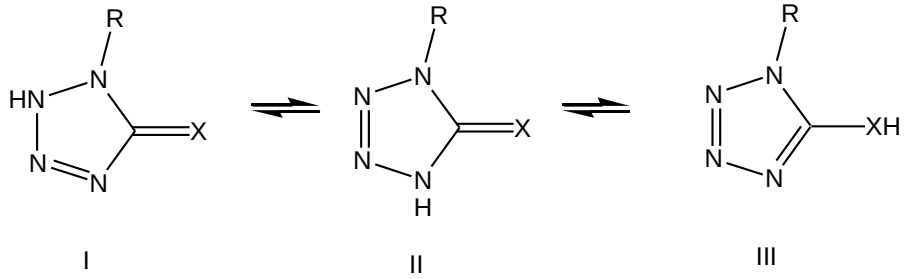

Scheme 1.5 Tetrazole-tetrazoline tautomerization.

In contrast to 5-hydroxy- and the 5-mercapto-tetrazole, aminotetrazoles (X = NH-R) are only observed in the form of tautomer III.[49]

Another tautomerization, which includes ring opening and closure is the α-azido-imine-tetrazole-tautomerization, which is a special form of the equilibrium of molecules containing an azido group next to a sp^2 carbon atom of a π-system.

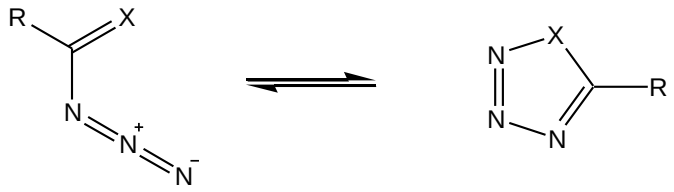

Scheme 1.6 α-Azido-imine-tetrazole-tautomerization.

In the case of X = N-R_1, an equilibrium can be observed which depends on several factors including the nature of R and R_1, the temperature and the solvent.[50,51]

On the basis of the tautomerization shown in **Scheme 1.6**, there are several examples of isomerizations,[36] which also have relevance for the synthesis of various 1-substituted tetrazoles (**Scheme 1.7**).

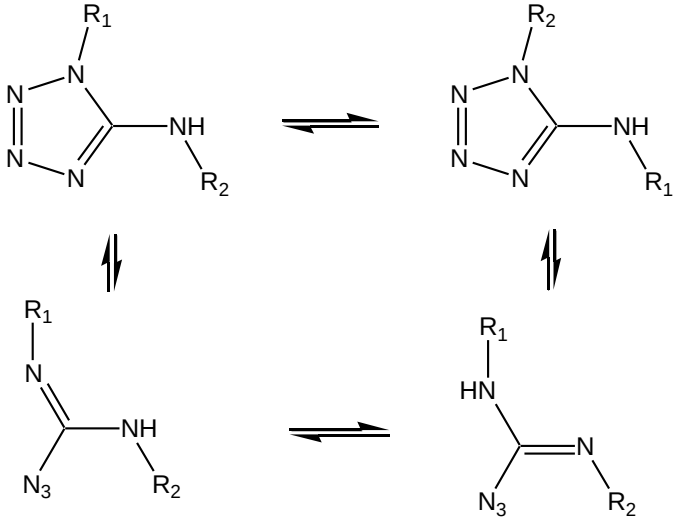

Scheme 1.7 1,5-Isomerization of 1-substituted 5-aminotetrazoles.

Most of the tetrazoles are stable at room temperature. The melting points of 5-monosubstituted tetrazoles are higher than that of the corresponding 1,5- and 2,5-disubstituted homologues due to the formation of hydrogen bonds at the cyclic NH-group. Due to higher dipole moments, the melting and boiling points of 1-alkylated tetrazoles are commonly higher than those of 2-alkylated tetrazoles.

Thermolysis of 5-substituted tetrazoles leads to the corresponding nitrile and HN_3. A second pathway results in the nitrilimine and molecular nitrogen (**Scheme 1.8**).

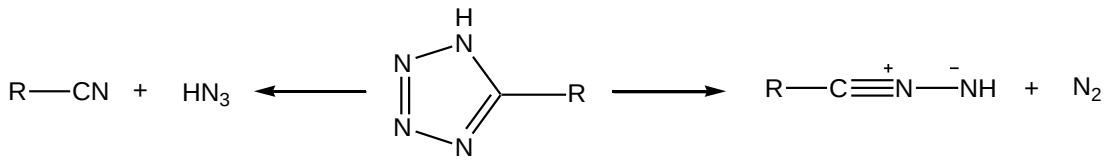

Scheme 1.8 Decomposition pathway of 5-substituted tetrazoles.

Photolysis of tetrazoles with UV light usually leads to reactive intermediates, whereas the formation of molecular nitrogen can be observed. The intermediates are further stabilized through fragmentation and isomerisation.[36,40]

With respect to acidic properties, tetrazoles and the 5-substituted tetrazoles are weak acids with pK_S-values reaching from 1.14 (5-trifluoromethyl-1*H*-tetrazole) to 6.33 (5-diethylamino-1*H*-tetrazole). Therefore, most of them can easily be deprotonated with alkaline metal and alkaline earth metal hydroxides. Nevertheless tetrazoles also have basic properties (pK_B 9.7–12.9). The tetrazole ring can be protonated by using strong acids, usually at nitrogen atom N4,[52] sometimes also at N3.[53]

The substitution reactions of tetrazoles are in first instance reactions with eletrophiles, whereas the nitrogen atoms react as the nucleophiles. Acylations mostly take place at the N2 of the tetrazole ring,[54] whereas alkylations lead to mixtures of 1,5- and 2,5-disubstituted tetrazoles.[55]

1.2.4 Classification and Nomenclature of Tetrazoles

The best way to classify tetrazole derivatives is by using the substituent connected to the carbon atom (position 5). With this, different classes of tetrazoles can be declared, e.g. 5*H*-tetrazoles, 5-alkyltetrazoles, 5-aminotetrazoles, 5-cyanotetrazoles, 5-halogenotetrazoles, 5-hydroxytetrazoles, 5-mercaptotetrazoles, 5-methyltetrazoles and 5-nitrotetrazoles. However, by all the rules this nomenclature is incorrect. According to IUPAC the tetrazole ring has a low priority and often time, by having functional substituents, the nomenclature has to be changed. 5-Amino-1*H*-tetrazole should be 1*H*-tetrazol-5-yl-amine; 5-cyanotetrazole should be 1*H*-tetrazol-5-yl-carbonitrile! However, 5-nitro-2-tetrazole stays 5-nitro-2-tetrazole.

Annotation of the author:

To establish understanding to the reader, the nomenclature used in this thesis is not consequently according to IUPAC and follows the style of "5-amino-1*H*-tetrazole". It was also dispensed from the (sometimes confusing) nomenclature of alkylated tetrazoles, e.g. 1,5-diamino-1*H*-tetrazole is simplified written as 1,5-diaminotetrazole. In addition, it is hard find the right nomenclature of condensed tetrazole heterocycles, e.g. of 1*H*-[1,5']bistetrazole described in Chapter 14. For these classes of tetrazoles often abbreviations, e.g. 1,5-BT are used, in particular, when these compounds are used as ligands in transition metal complexes.

1.3 Energetic Tetrazole Derivatives: Status Quo

Many tetrazole derivatives have been synthesized and introduced as new energetic materials also in the research group of Prof. Thomas M. Klapötke. A selection of the most important and modern comforts are described in the following.

1.3.1 Synthesis of 5-Aminotetrazole

5-Aminotetrazole (**5-At, 2**) [56] is a valuable intermediate in the preparation of tetrazole compounds [57] because of its varied reactions and its ease of preparation. It is obtained by the reaction of nitrous acid with aminoguanidine (**Scheme 1.9**, A) [58] or by the reaction of hydrazoic acid with dicyandiamide (**Scheme 1.9**, B).[59] The first reaction (**A**) forms azidoformamidinium nitrate (**3**) (starting from aminoguanidinium nitrate (**4**) which after deprotonation rearranges to **5-At**. In the second reaction (**B**) the dicyandiamide (**5**) depolymerises to cyanamide (**6**), which then reacts with hydrazoic acid to give **5-At**. In both cases, **5-At** is obtained as monohydrate.

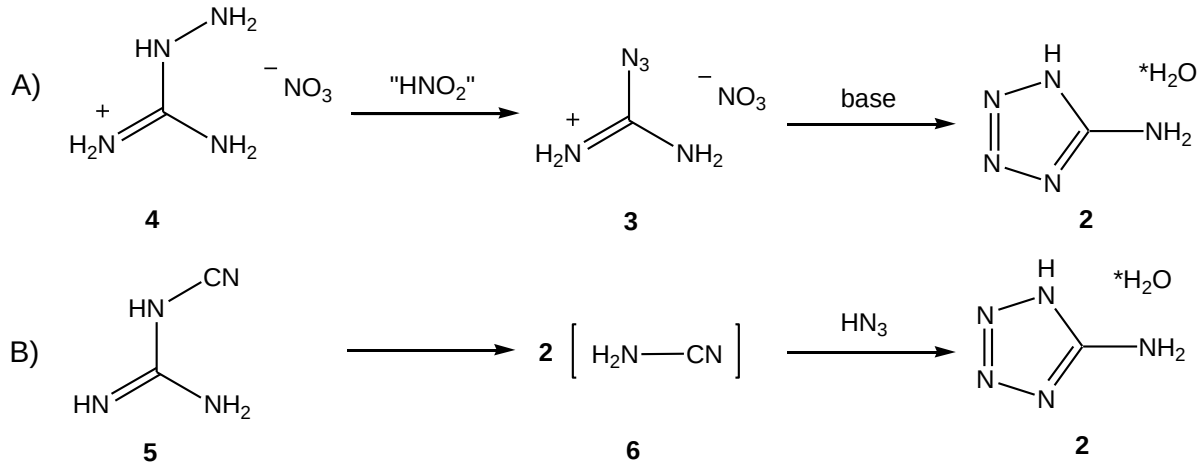

Scheme 1.9 Syntheses of 5-At (**2**).

1.3.2 Structure of 5-Aminotetrazole

The crystal structure of 5-aminotetrazole monohydrate was determined by Bray and White in 1979 [60] and was also reinvestigated in this work. **Figure 1.9** shows three different valence structures and the X-ray molecular structure of **2**·H_2O. In the

discussion of the molecular structure, Bray and White mentioned: *The localization of the proton would suggest that (I) is the valence-bond description of this tautomer. However, this is an oversimplification, since the bonds from C5 to N1, N4 and N5 are almost exactly equal, while N2–N3 is longer and the adjacent single bonds are shorter than standard values. It has been shown in other meso-ionic compounds that a conventional description does not necessarily correspond to observed bond distances.*

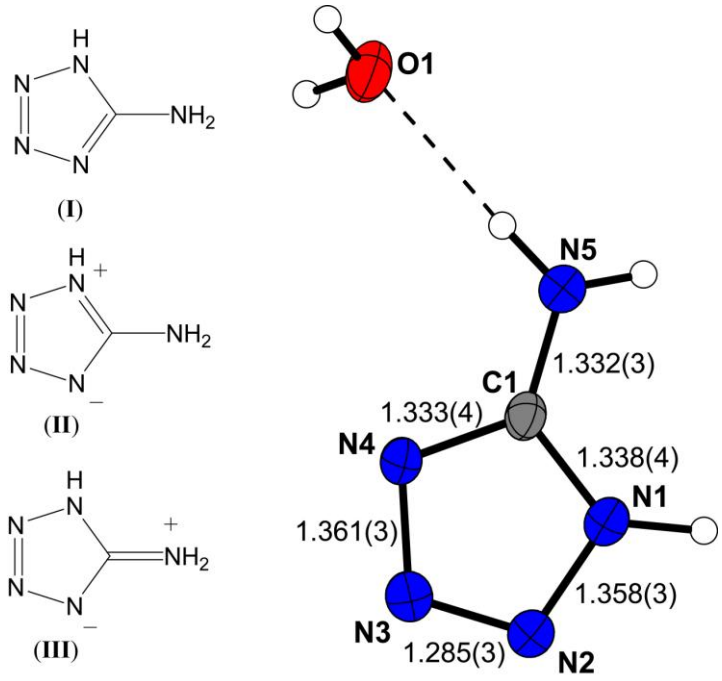

Figure 1.9 Valence bond descriptions of 5-aminotetrazole (**2**) monohydrate and its molecular structure determined by XRD. Thermal ellipsoids represent the 50 % probability level. Bond lengths are given in Å.

1.3.3 Protonation and Deprotonation of 5-Aminotetrazole

Energetic derivatives of **5-At** can easily obtained by the formation of 5-aminotetrazolium salts in combination with oxygen-rich counteranions. In spite of their large number of electron pairs, **5-At** is only weakly basic and therefore only protonated by strong acids. 5-Aminotetrazolium nitrate (**7**) [61] as well as 5-aminotetrazolium picrate (**8**) [62] have been described recently (**Scheme 1.10**). Also 5-aminotetrazolium chloride (**9**) has been described as valuable starting material in syntheses of energetic materials.[63] Chapter 3 of this thesis describes the synthesis and characterization of 5-aminotetrazolium perchlorate (**38**) as well as the

5-aminotetrazolium dinitramide (**31**).[64] The obtained salts are highly energetic materials, characterized by good oxygen balances.

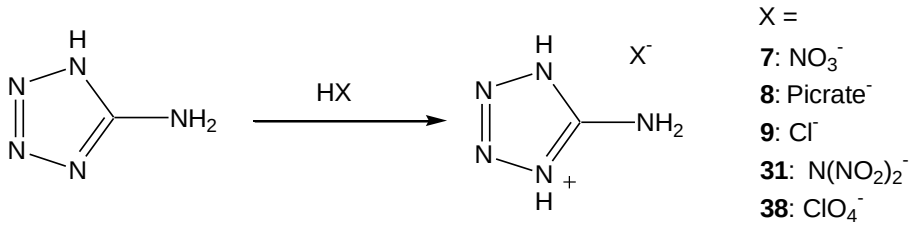

Scheme 1.10 Syntheses of energetic 5-aminotetrazolium salts.

Energetic salts have been also prepared by protonation of 1-methyl-5-aminotetrazole (**10**) and 2-methyl-5-aminotetrazole (**11**), which are obtained easily by methylation of **5-At**.[65,66]

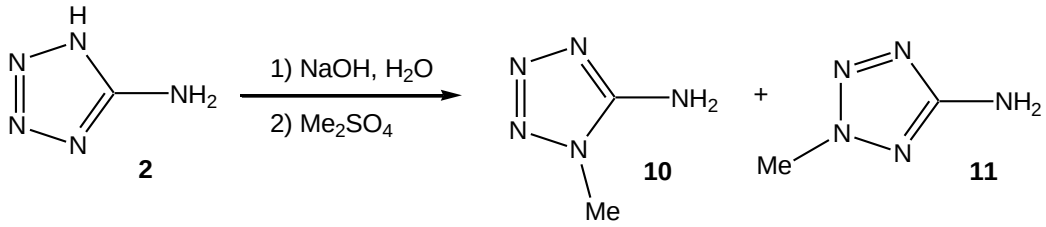

Scheme 1.11 Synthesis of 1-methyl-5-aminotetrazole (**10**) and 2-methyl-5-aminotetrazole (**11**).

Deprotonation of **2** is, without much doubt, the most facile reaction of **2**. Although 5-aminotetrazole is known for a long time, its salts are rarely described. A full characterization and testing of the series of alkali salts, valuable intermediates in syntheses of alkylated 5-aminotetrazoles as well as high nitrogen colorants in modern pyrotechnic compositions can be found in Chapter 2.[67]

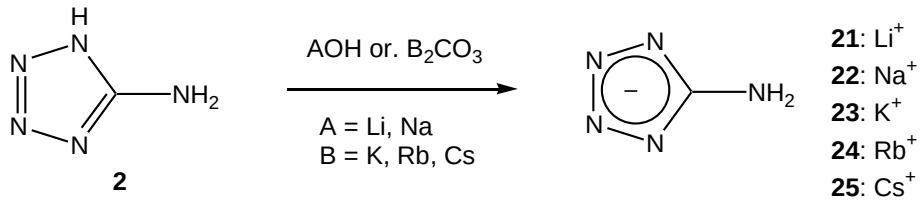

Scheme 1.12 Synthesis of alkali 5-aminotetrazolates.

Methyl-5-aminotetrazolium salts are also only obtained by the use of strong acids (**Scheme 1.14**). Combinations with classic energetic and oxidizing anions such as ClO_4^- and NO_3^- have recently published within this research group. [68] The dinitramide salt is also described in Chapter 3.

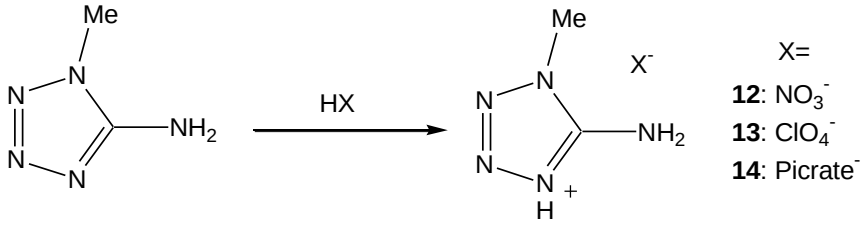

Scheme 1.13 Syntheses of energetic 1-methyl-5-aminotetrazolium salts.

The basicity of 1- and 2-methyl-5-aminotetrazole can be further reduced by introducing a second methyl group at the N4 nitrogen atom. By metathesis reaction using 1,4-dimethyl-5-aminotetrazolium iodide also the azide and dinitramide salts have been synthesized.[68,69]

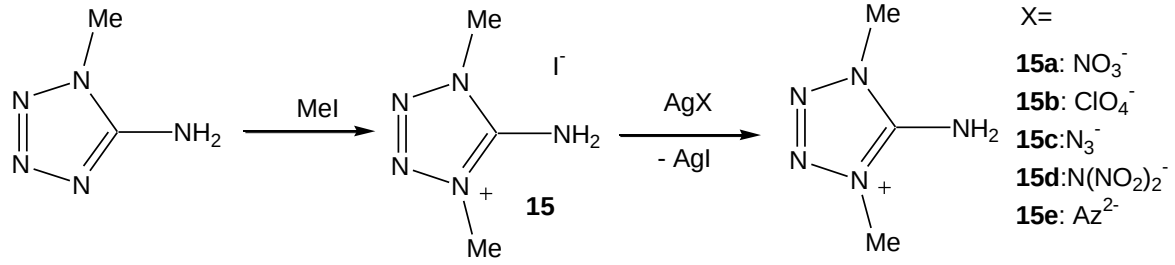

Scheme 1.14 Syntheses of energetic 1,4-dimethyl-5-aminotetrazolium salts.

1.3.4 5,5'-Azotetrazolates

The formation of sodium 5,5'-azotetrazolate (**16**) was firstly described in 1893 by J. Thiele (**Scheme 1.15**).[70] Salts of the 5,5-azotetrazolate anion are particularly suitable target molecules, since these salts have a considerable nitrogen content and are expected to have appropriate stabilities toward friction, impact, and heat. Salts of 5,5'-azotetrazolates have been extensively studied.[71] Also complete data of N-rich guanidinium derivatives (**16b–16e**) of 5,5'-azotetrazolate are described in literature.[72]

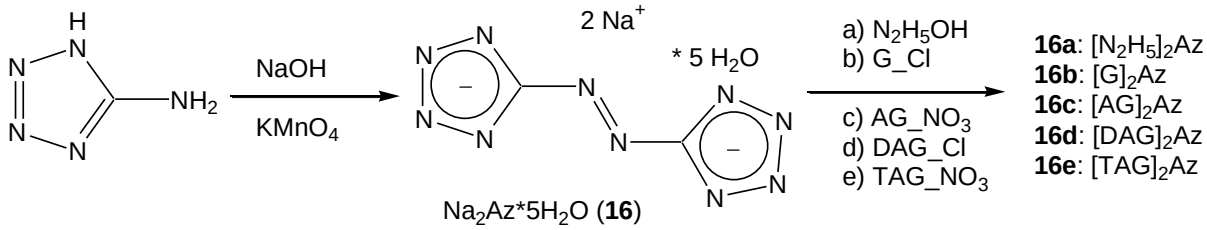

Scheme 1.15 Syntheses of nitrogen rich 5,5'-azotetrazolate salts.

1.3.5 5,5'-Bis(tetrazolyl)hydrazines

The reduction of **16** with magnesia yields to 5,5'-bis(tetrazolyl)hydrazine (BTH, **17**) according to **Scheme 1.16**. **BTH** has been also described by J. Thiele [73] and was reinvestigated in our research group quite recently.[74] **BTH** can be deprotonated forming 5,5'-bis(tetrazolato)hydrazines in combination with metals or nitrogen rich cations.

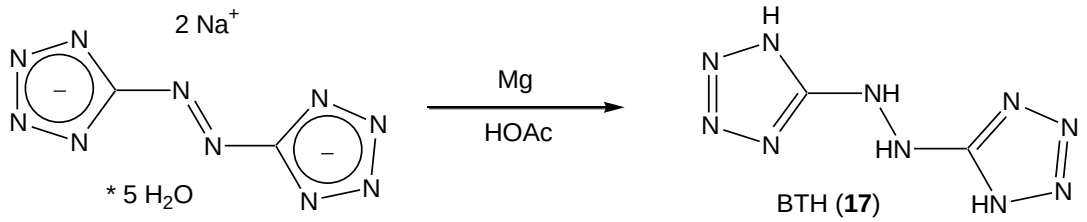

Scheme 1.16 Formation of 5,5'-bis(tetrazolyl)hydrazine (BTH).

1.3.6 5-Nitrotetrazoles

Nitrogen rich salts of 5-nitro-2*H*-tetrazole has been described as promising energetic compounds. They were synthesized by metathesis reaction using silver 5-nitrotetrazolate (**18**) and the corresponding guanidinium chlorides.[75,76,77,78] Synthesis and characterization 1-methyl and 2-methyl-5-nitrotetrazole are described in Chapter 13.

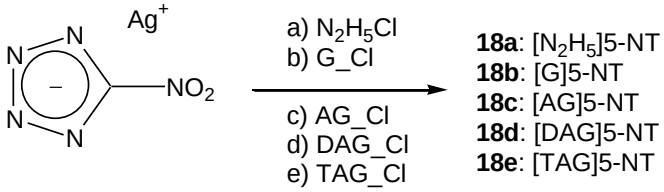

Scheme 1.17 Synthesis of nitrogen-rich 5-nitrotetrazolates.

1.3.7 1,5-Diaminotetrazoles

1,5-Diaminotetrazole (**19**) and its derivatives have previously been considered as gas-generating agents, and some work has been done using **19** as a valuable intermediate in the preparation of **h**igh-**e**nergy-**d**ense **m**aterials [79] or other useful tetrazole-containing compounds.[80] A problem is the difficult accessibility of **19**. Three different synthesis of **19** are depicted in **Scheme 1.18**. Amination of **5-At** leads to insufficient yields of a mixture of 19 and 2,5-diaminotetrazole. Perhaps the best synthesis is the 1933 reported one of Stolle *et al.*,[81] who synthesized **19** by reacting thiosemicarbazide with lead(II)

oxide and sodium azide in a CO_2 atmosphere in ethanol as the solvent. However, this synthesis is hard to scale up due to the risk of explosion during the work up procedure while filtrating from lead sulfide, which is impured by highly sensitive lead azide.

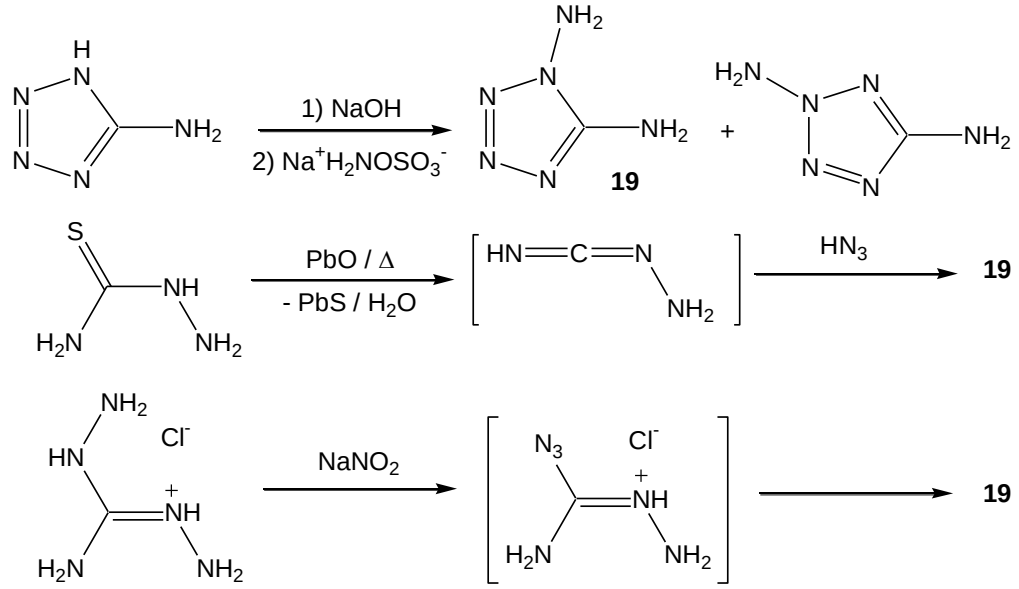

Scheme 1.18 Syntheses of 1,5-diaminotetrazole.

Protonation of **19** is only described with nitric as well as perchloric acid. The synthesis of diaminotetrazolium dinitramide is described in Chapter 3. The reaction **19** with iodomethane yields 1,5-diamino-4methyl-tetrazolium iodide (**20**). **20** can be reacted by the metathesis with silver nitrate, silver dinitramide, or silver azide yielding the energetic salts 1,5-diamino-4-methyl-tetrazolium nitrate, dinitramide and azide.

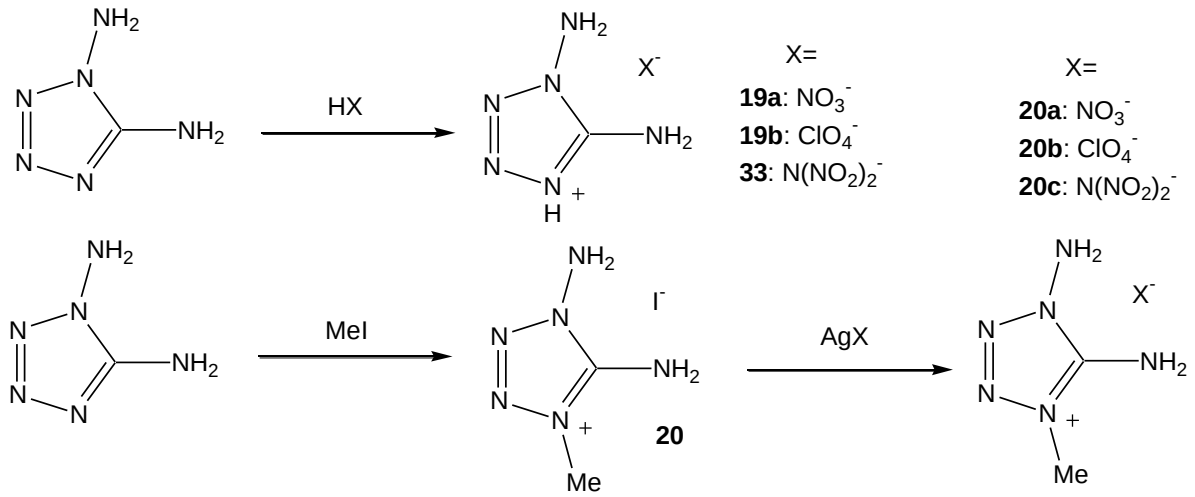

Scheme 1.19 Synthesis of 1,5-diaminotetrazolium and 1,5-diamino-4-methyl-tetrazolium salts.

1.4 Analytic, Testing and Calculation Methods

1.4.1 X-ray Diffraction (XRD)

Most of the crystal structures were determined on the Oxford Xcalibur3 diffractometer using a Spellman generator (voltage 50 kV, current 40 mA) and a KappaCCD detector. Suitable single crystals were picked from the crystallization mixture, mounted in Kel-F oil on a glass fiber on the goniometer head, which was transferred to the N_2 stream (100K, 150 K, 200 K) of the diffractometer. The data collection was undertaken using the CRYSALIS CCD software [82] and the data reduction was performed with the CRYSALIS RED software.[83] The structures were solved either with SIR-92,[84] SIR-97 [85] or SHELXS-97.[86] The datasets were refined with SHELXL-97 [87] implemented in the program package WinGX [88] and finally checked using the PLATON SOFTWARE.[89] The .cif files [90] have been finalized with CIFTOOLS and checked using the CIFCHECK.[91] Sup files have been created with the PLATON Taskbar v1.081. Illustrations of molecular as well as crystal structures have been drawn with DIAMOND 2.[92] The data for a smaller amount of crystal structures were collected on a Nonius Kappa CCD diffractometer under an N_2 stream as well. Data collection and reduction was done by the Bruker "Collect" and the "HKL Denzo and Scalepack" software.[93] In the case of chiral space groups, e.g. *Pn*, $P2_1$, $P2_12_12_1$, the *Friedel pairs* have been merged.

Figure 1.10 Oxford Xcalibur 3 diffractometer

1.4.2 Vibrational Spectroscopy (IR/Raman)

Infrared (IR) spectra were either recorded using Perkin-Elmer Spektrum One FT-IR instruments. Samples were measured in KBr disks or pure with an ATR (*attenuated total reflection)* device. In the former case solids were measured as KBr disks, liquids between NaCl plates and gases in an IR gas cell with NaCl windows.

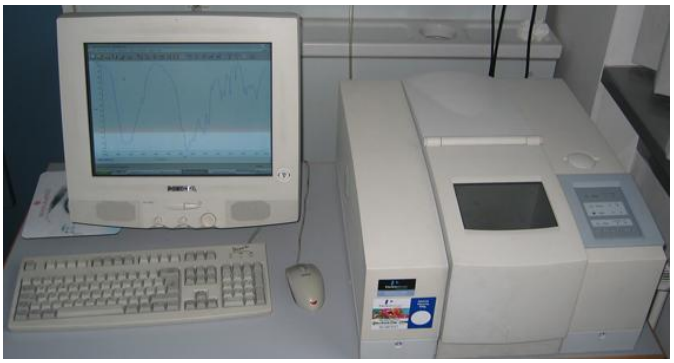

Figure 1.11 FT-IR spectrometer

Raman spectra were measured using a Perkin-Elmer Spektrum 2000R NIR FT-Raman instrument equipped with a Nd:YAG laser (1064 nm) at laser powers between 100 and 450 mW.

Figure 1.12 Raman spectrometer

1.4.3 NMR Spectroscopy

^{1}H and ^{13}C spectra were recorded with a Jeol Eclipse 270, Jeol EX 400 or a Jeol Eclipse 400 instrument. All chemical shifts are quoted in ppm relative to TMS (^{1}H, ^{13}C), $MeNO_2$ (^{14}N, ^{15}N) and LiCl (^{7}Li) as external standards. Neutral compounds were mostly measured in d_6-DMSO as the solvent, ionic compounds in D_2O.

Figure 1.13 Jeol EX 400 NMR instrument

1.4.4 Mass Spectrometry (MS)

Mass spectrometry was performed on the JEOL MS station JMS-700. Different ionization modes (EI, DEI, MALDI, CI, FAB^+, FAB^-) have been used. Mass peaks of neutral tetrazoles are mostly obtained well by electrical ionization.

Figure 1.14 JEOL MStation JMS-700

1.4.5 Elemental Analysis (EA)

Elemental Analyses were performed with a Netsch STA 429 Simultaneous Thermal Analyzer. Organic compounds are combusted under presence of O_2 to CO_2, H_2O, N_2, NO, NO_2, SO_2 and SO_3, followed by a reduction using copper at 850 °C to CO_2, H_2O and N_2. Energetic samples containing a nitrogen content of > 70 % are hard to determine, since they tend to explode. In this cases, it was proofed to use very small amounts of the samples (< 1.5 mg).

Figure 1.15 Netsch C,H,N,S Analyzer

1.4.6 UV/Vis Spectroscopy

A Varian Cary 5000 spectrometer was used to record the UV-VIS spectra. In all cases methanol or ethanol was used as the solvent.

Figure 1.16 Varian UV-Vis spectrometer

1.4.7 Melting Points

With respect to protect the DSC machines against unregulated explosions and to ensure exothermic peaks (melting points, phase transitions, loss of solvent) the thermal behavior of nearly all compounds was discovered with a BÜCHI melting-point apparatus B-540 in glass capillaries.

Figure 1.17 Büchi melting-point device

1.4.8 Differential Scanning Calorimetry (DSC)

DSC measurements were performed in covered Al-containers with a nitrogen flow of 20 mL min^{-1} on either a Linseis PT10 DSC [94] or on a Perkin Elmer Pyris 6 DSC [95] calibrated by pure indium and zinc standards at a heating rate of 2 and 5 °C min^{-1}.

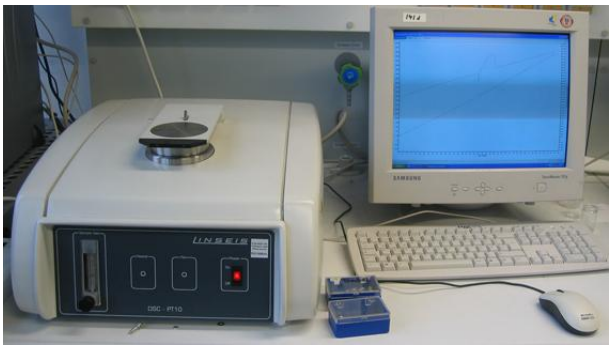

Figure 1.18 Linseis PT10 DSC

Figure 1.19 left: Perkin Elmer Pyris 6 DSC; right: DSC Aluminum sample container

1.4.9 Bomb Calorimetry

Figure 1.20 Parr 1356 bomb calorimeter equipped with a Parr 1108CL oxygen bomb.

Heats of combustion were determined experimentally using a Parr 1356 bomb calorimeter (static jacket) equipped with a Parr 1108CL oxygen bomb.[96] To achieve better combustion, the samples (~200 mg) were pressed with a defined amount of benzoic acid (~800 mg) forming a tablet, and a Parr 45C10 alloy fuse wire was used for ignition. In all measurements, a correction of 2.3 cal cm^{-1} wire burned has been applied and the bomb was examined for evidence of noncombusted carbon after each run. A Parr 1755 printer was furnished with the Parr 1356 calorimeter to produce a permanent record of all activities within the calorimeter. The reported values are the average of three separate measurements. The calorimeter was calibrated by combustion of certified benzoic acid (SRM, 39i, NIST) in an oxygen atmosphere at a pressure of 3.05 MPa. The standard molar enthalpy of combustion ($\Delta_c H°$) was derived from the equation:

$\Delta_c H° = \Delta_c U + \Delta nRT$ ($\Delta n = \Delta n_i$ (products, g) – Δn_i(reactants, g); Δn_i is the total molar amount of gases in the products or reactants).

The enthalpy of formation, $\Delta_f H°$, for each of the compounds was calculated at 298.15 K using Hess' law and the ideal combustion reaction.

$$C_nH_mN_xO_y + \left(n + \frac{m}{4} - \frac{y}{2}\right)O_2 \rightarrow nCO_2 + \frac{m}{2}H_2O + \frac{x}{2}N_2$$

Enthalpies of formation: carbon dioxide ($\Delta_f H°_{298}(CO_2(g))$ = −394 kJ mol^{-1})
water ($\Delta_f H°_{298}(H_2O(g))$ = −242 kJ mol^{-1})

1.4.10 Thermal Safety Calorimetry (TSC)

Long term stabilities tests were performed using a Systag FlexyTSC [97] (Thermal Safety Calorimetry) in combination with a RADEX V5 oven and the SysGraph Software. The test were undertaken as long-term isoperibolic evaluations in Glass test vessels at Atmospheric pressure with ~200 mg of the compounds. It was shown that tempering the substance for 48 hours at 40 degrees under the decomposition point results in a storage period of 58 years at room temperature.

Figure 1.21 Systag Flexy TSC device

1.4.11 Thermal Gravimetry (TG)

TGA (Thermal Gravimetry Analysis) measurements were performed in nitrogen atmosphere in open Al_2O_3 crucibles (sample weight ~ 4 – 10 mg) at a heating rate of 1–5 °C min^{-1} with a Setaram DTA–TGA 92 thermogravimetric analyzer [98] in the temperature range from 30 °C – 400 °C. For the removal of moisture, the samples were dried *in vacuo*.

1.4.12 Drophammer

First impression of the impact sensitivity of new compounds can be received by the older drophammer shown in **Figure 1.22**. By using this drophammer only an impact energy of 30 J can be set.

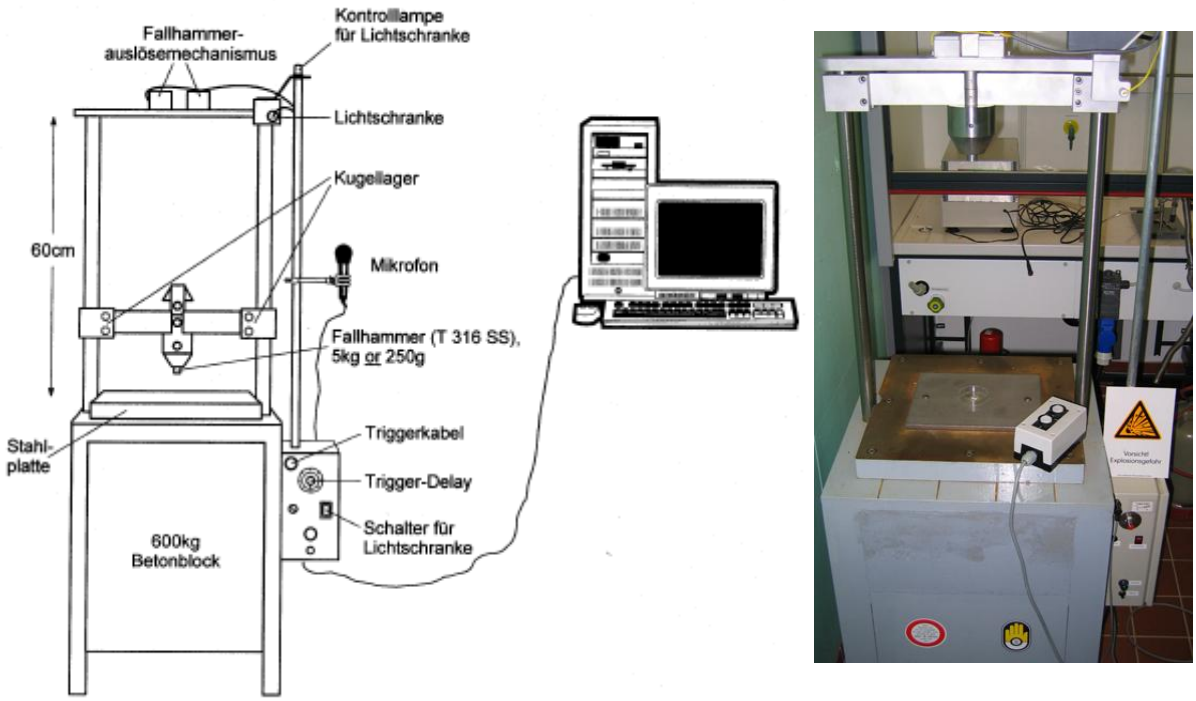

Figure 1.22 Drophammer (old version).

The recent impact sensitivity tests were carried out according to STANAG 4489 [99] modified according to instruction [100] using a BAM (Bundesanstalt für Materialforschung) [101] drophammer.[102] The sample, placed between two flat, parallel, hardened steel surfaces, is subjected to an impact by dropping a weight. The impact may result in initiation depending on the sensitivity of the material, weight mass, and its drop height (impact energy). The impact energy is calculated by:

$$E_{IS}\,(J) = m\,(kg) \cdot g\,(9.81\ m\ s^{-2}) \cdot h\,(m)$$

Initiation is observed by sound, light effects, smoke, or by inspection. The BAM impact apparatus, known to give fairly reproducible results, is shown in **Figure 1.23**. Typically drop weights having a mass of 1, 5 or 10 kg are used and the lowest energy required to

create a detonation is recorded. Thus drop-weight and drop-height at which the initiation of the sample occurs are the main parameters determined from impact testing. The drop height at which detonation is observed is thus a measure of impact sensitivity of an *explosive*. The maximum height in which no explosion was observed has to be confirmed in six independent trials.

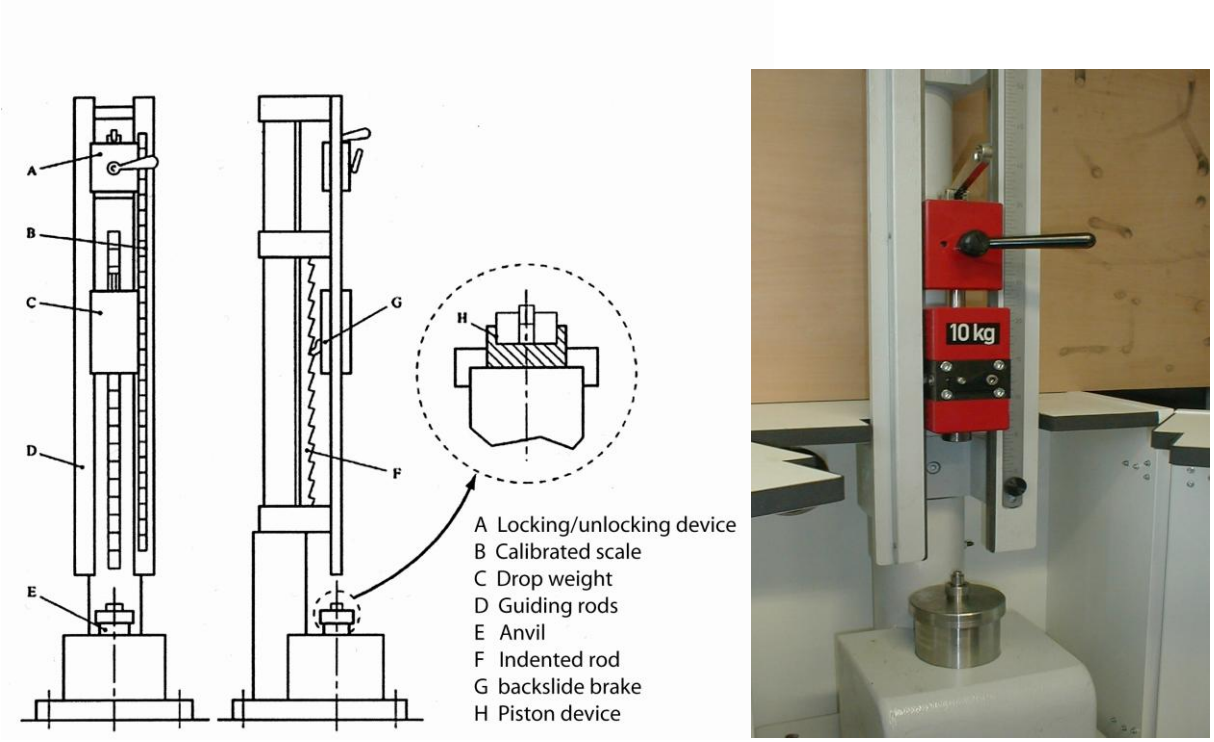

Figure 1.23 BAM drophammer.

Table 1.1 Impact sensitivity of selected energetic materials.

Substance	Impact energy [J]
Ethylnitrate	1
$N_2H_5ClO_4$	2
$Pb(N_3)_2$	2.5
Lead styphnate	5
Nitroglycerin (NG)	1
$Hg(ONC)_2$	1
PETN	3
RDX	5
Tetryl (dry)	4

1.4.13 Friction Test

The friction sensitivity tests were carried out according to STANAG 4487 [103] modified according to instruction [104] using the BAM friction tester (**Figure 1.24**).[105,106] The sample is placed on a rough ceramic plate and a force (created by different weights on the lever) is loaded on the sample trough a stationary pin in contact with the plate. The plate is motor driven trough a complete cycle pass beneath the pin. The test sample is subjected to the friction created by the rubbing of the pin against the plate. Normally the test is run with a pin load of 5 – 10 – 20 – 40 – 60 – 80 – 120 – 160 – 240 – 360 N or values in between depending of the weight and the used groove. Each experiment is evaluated with respect to "no reaction", decomposition (change of color, smell) or explosion (bang, crackle, spark formation, ignition) and continued, by changing the pin load, until no explosion occurred within six single tests. However, only explosions are evaluated as "positive". A compound is classified as not friction sensitive if each single test with a friction load of 360 N was evaluated as decomposition or "no reaction". In this thesis, the classification of impact and friction sensitivities were assigned according to the "UN recommendations on the transport of dangerous goods".[107]

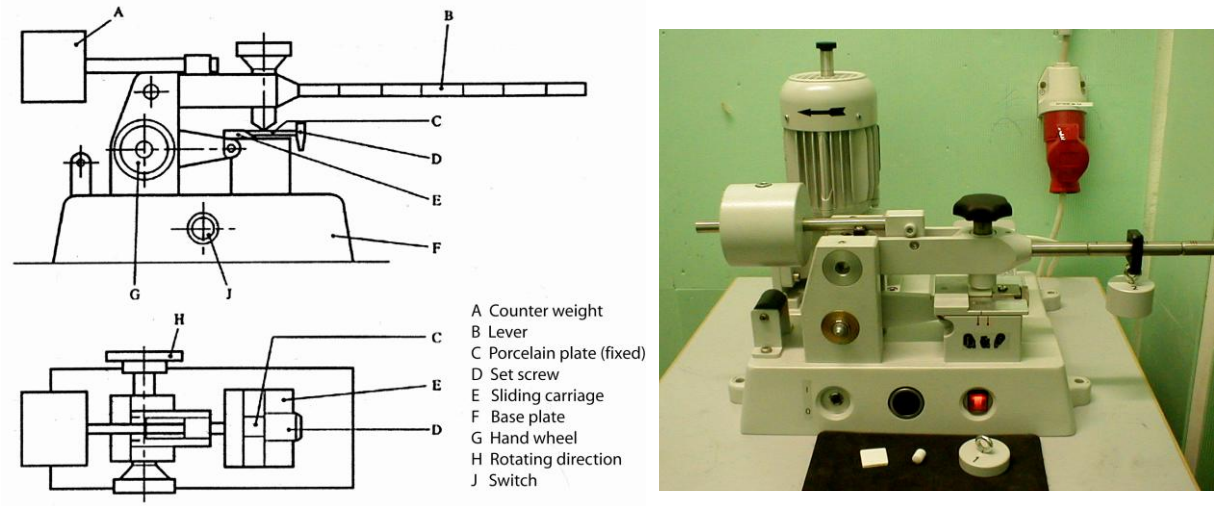

Figure 1.24 Scheme of the BAM friction tester.

1.4.14 Electrical Spark Device (ESD)

Electrostatic discharge is one of the most frequent and the least characterized causes of accidental explosions of energetic materials. Electrostatic sensitivity tests were carried out using an electric spark tester ESD 2010EN (OZM Research) operating with the "Winspark 1.15 software package".[108] This tester allows to precisely measure both total

spark energy discharged into the sample and a fraction of this energy really absorbed by the sample initiating its explosion. This feature allows to determine the true minimum energy sufficient for accidental initiation of the sample. The tester can load the sample with very wide range of spark energies from $1 \cdot 10^{-5}$ to 17 J – allowing to test all categories of energetics ranging from extremely sensitive primary explosives to insensitive high explosives. During operation of the instrument, a small amount of the sample is placed on a grounded metal plate anode. The metal plate with the sample is placed on the holder in the instrument, and the desired amount of energy of an electric spark is selected by setting appropriate capacitor and voltage. The energy is calculated by the equation $E\ (J) = ½\ C\ V^2$ with C = capacitance in farads (F) and V = charging voltage (V). An electric discharge is performed between the anode with the sample and the discharge needle-electrode above the sample. Initiation is considered to have occurred if either smoke, flame, flash or the characteristic smell of the reaction products is observed.

Table 1.2 Electrical Spark Sensitivity of selected materials.

Substance	Electric spark energy [J]
RDX	0.15–0.20
HMX	0.21–0.23
TNT	0.46–0.57
TATB	2.5–4.25
PETN	0.19
NQ	0.60
$Pb(N_3)_2$	0.005
Human body	0.005–0.02

Figure 1.25 OZM small scale electrical discharge device

Annotation: The electrical spark sensitivity strongly dependents on the particle size and shape. As a matter of principle powders are more sensitive than crystalline materials. For appropriate comparison, materials must be sieved before testing.

In earlier times tests towards electrical discharge have been performed either by using a tesla coil or a electrical piezo device removed from an lighter (**Figure 1.26**).

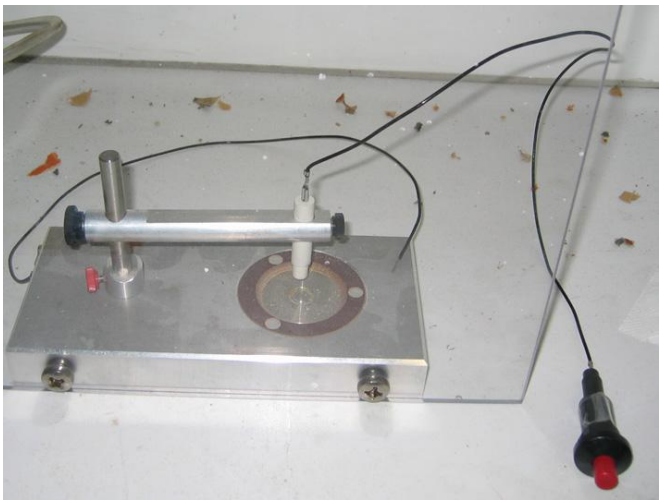

Figure 1.26 Outdated electrostatic discharge device.

The following **Figure 1.27** shows a picture series of a high speed movie clip of the electrical ignition of compound **109** using a tesla coil.

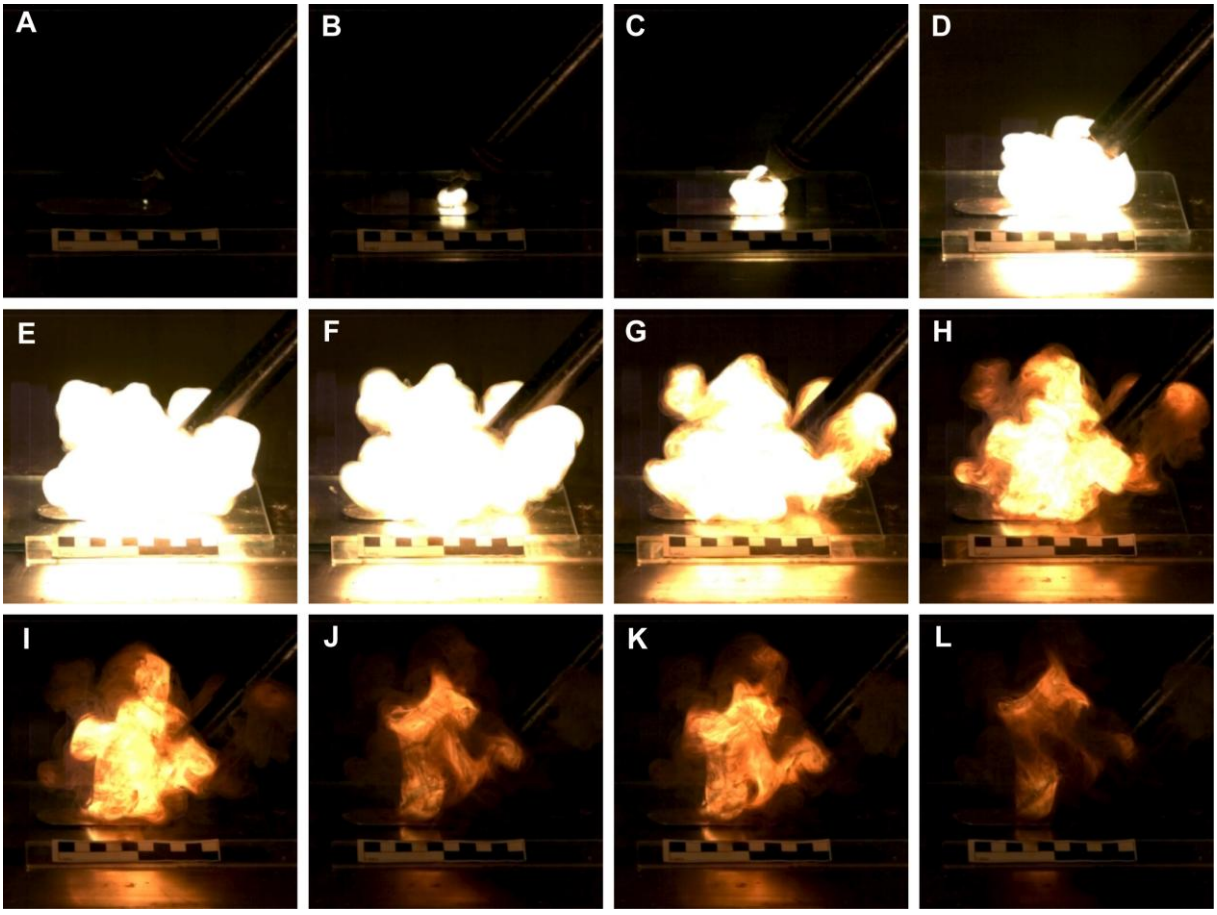

Figure 1.27 Picture series of the old ESD test of compound **109** using a tesla coil.

1.4.15 Hot Plate Test

The hot plate test (**Figure 1.28**) was introduced in the research lab D3.110 to investigate the fast cook up of new compounds in the small scale without direct contact to flames. This test is extremely useful, since it can be performed in the fume hood and can be watched and recorded from safe distance. For this, the energetic material is placed on a copper plate (15 x 15 x 0.25 cm), which is warmed from below using a bunsen burner (distance ~5 cm).

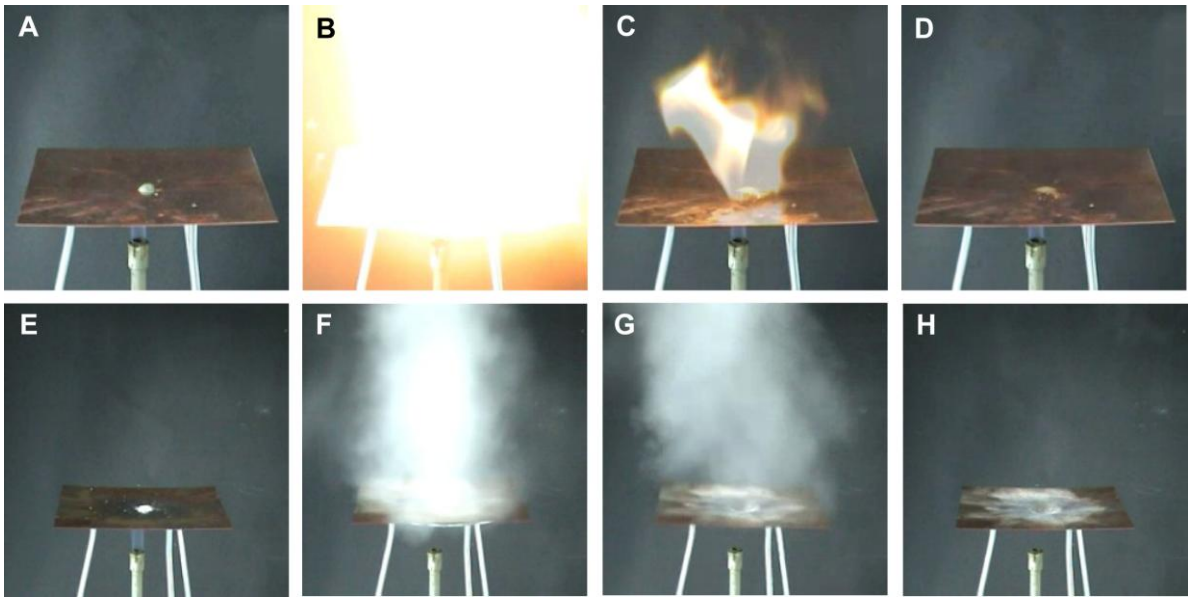

Figure 1.28 Two picture series of the hot plate test. A–D: Compound **100** under emission of light, E–H: Compound **90**, violent explosion without light emission.

1.4.16 Flame Test

In contrast to the "Hot plate test" the compound is directly placed with a spatula into the flame of Bunsen burner. The flame test (**Figure 1.29**) provides first details of the combustibility and also energetic character of a new energetic material. The evaluation of residues (coal) can also be an indication of the nitrogen content of a molecule. The results can be divided into (i) fulmination, (ii) fast combustion, (iii) low combustion, (iv) decomposition, (v) melting or (vi) no reaction (not combustible).

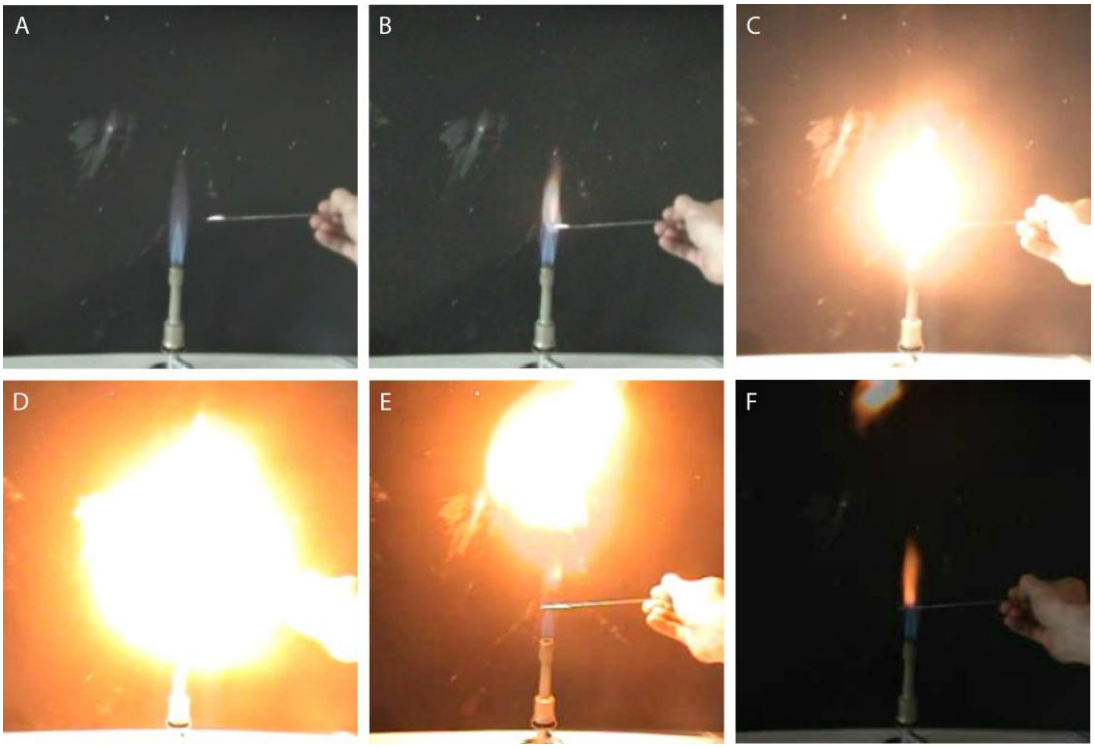

Figure 1.29 Picture series of the flame test of 1,5-bistetrazole **152**.

1.4.17 Burn Rate Test

There exist two kinds of burning rates.[109] The "burning rate" (BR) and the "linear burning rate" (LBR). The BR

$$\frac{dz}{dt} \text{ (z: ratio of volumes } \frac{(V_0 - V)}{V_0} \text{)}$$

describes the velocity with which the volume of the burning propellant changes. The BR is proportional to the LBR, which is the velocity with which a chemical reaction progresses as a result of thermal conduction or radiation. The LBR depends next to the chemical composition on several further conditions, like the pressure, temperature, humidity and particle size and shape. A more "quantitative" determination of the linear burn rate can be performed by simple burning a line of a compound in a definite length and volume. The time scale can be controlled by filming using a high speed camera. A picture series of the burn rate test of 1,5-bistetrazole (**90**) is shown in **Figure 1.30**. In this test the burn rate was estimated to be in the range of 1.9–2.1 m s^{-1}.

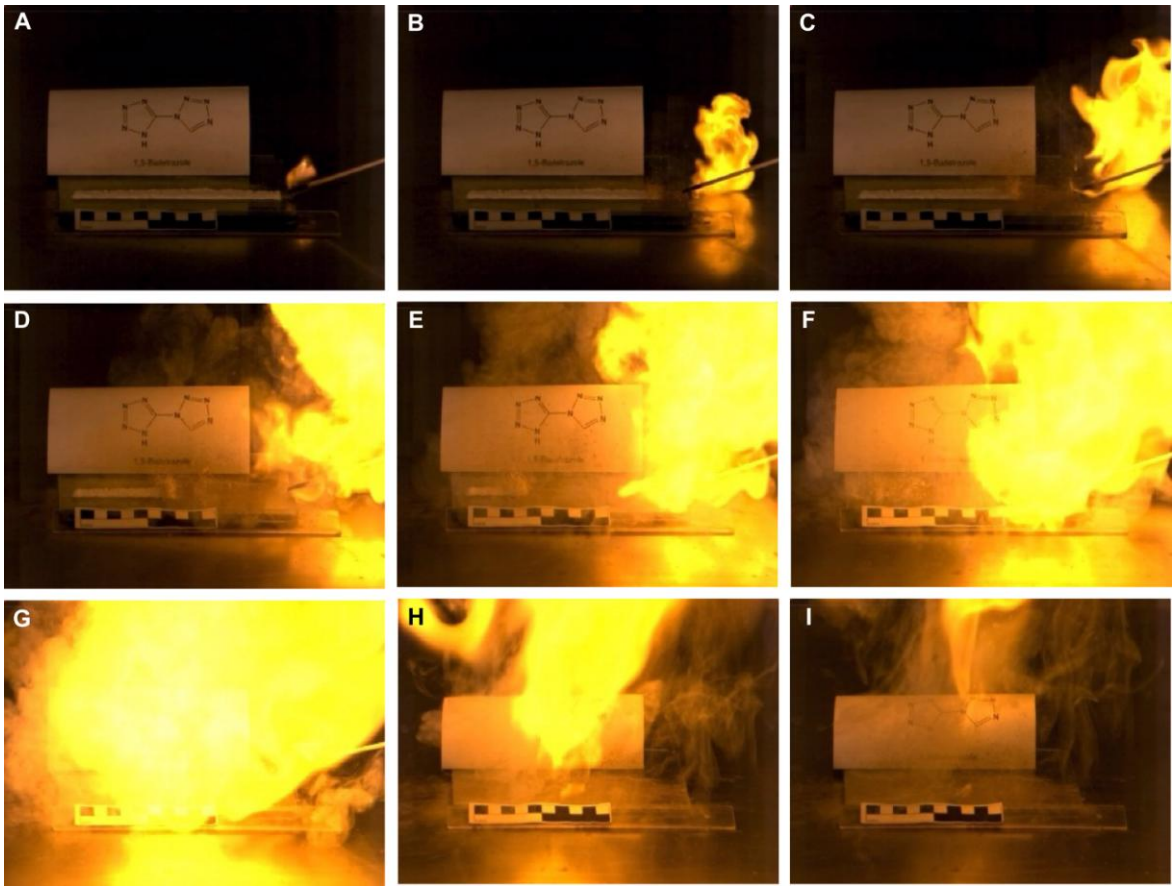

Figure 1.30 Burn rate determination of **90**.

1.4.18 Koenen Test

The shipping classification and also relative explosion performance under confinement of energetic materials can be investigated by the *Koenen test* steel sleeve test.[110,111] In case of the shipping classification in containers the degree of venting required to avoid an explosion during processing operations can be evaluated. The explosive is placed in a non-reusable open-ended flanged steel tube, which is locked up by a closing plate with variable orifice (0–10 mm), through which formed gaseous decomposition products are vented. A defined volume of 25 mL of the compound is loaded into the flanged steel tube and a threaded collar is slipped onto the tube from below. The closing plate is fitted over the flanged tube and secured with a nut. The explosion is initiated via thermal ignition using four *Bunsen* burners, which are started simultaneously. The test is completed when either rupture of the tube or no reaction is observed, after heating the tube for a minimal time period of at least 5 min. In case of the tube's rupture the fragments are collected and weighed. The appearance of the fragmentation degree (**Table 1.3**) decides if an explosion occurred or not. The reaction is evaluated as an explosion if the tube is

destroyed into three or more pieces. TNT destroys the steel sleeve up to an orifice width of 6 mm, RDX and HMX even up to 8 mm.[112]

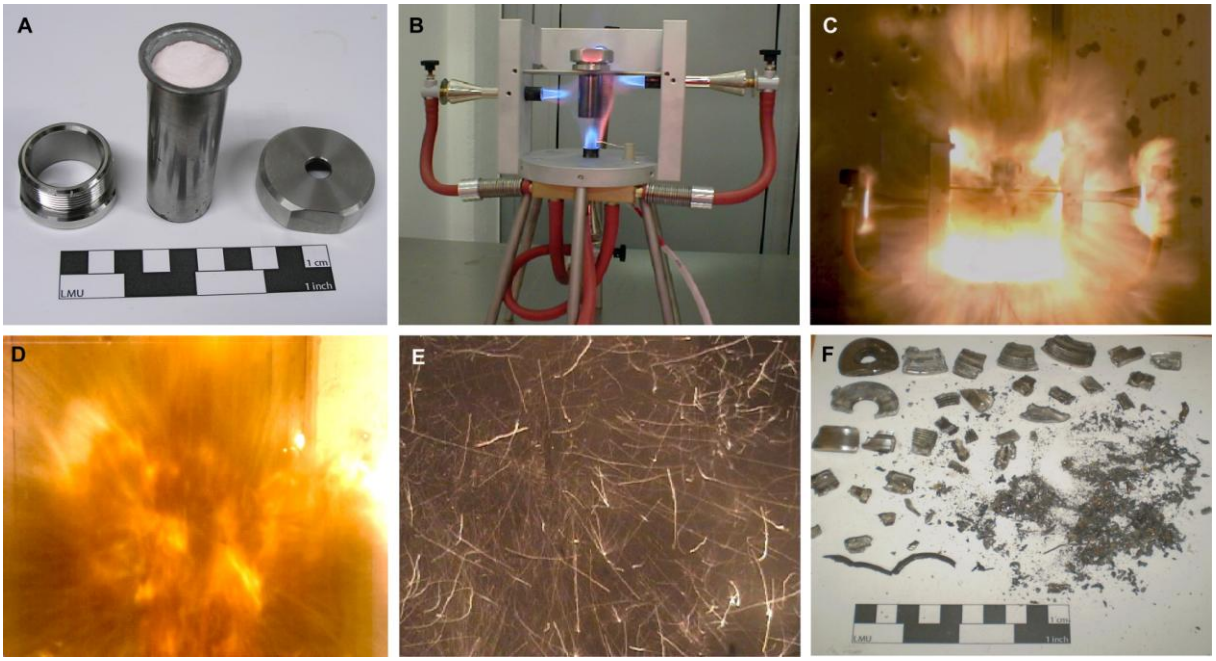

Figure 1.31 A) Steel sleeve with screwing element (hole width 10 mm), B) Koenen test setup, C) Start of detonation, D) 0.5 ms after start of detonation, E) Blistering metal shivers, F) Blistering metal shivers.

Table 1.3 Fragmentation degree.

Types of Fragments	Description	Result
0	Thimble is unchanged	–
A	T. plate is dented in	–
B	T. plate and sides are dented in	–
C	T. plat is broken	–
D	T. is teared up	–
E	T. is put in two parts	–
F	T. is destroyed in three or more big pieces, which can be connected	Explosion
G	T. is destroyed into little pieces, top is undamaged	Explosion
H	T. is damaged in a lot of little pieces, the top is damaged too	Explosion

The valuation of a substance in order to its thermal sensitivity under confinement is combined in **Table 1.4**.

Table 1.4 Validation guidelines.

Valuation	Diameter [mm]
non sensitive	Ø < 2
few sensitive	2 ≤ Ø < 10
sensitive	10 ≤ Ø < 16
very sensitive	16 ≤ Ø < 20
extreme sensitive	Ø ≥ 20

1.4.19 Octanol/Water Partition Coefficient

With regard to environmental compatibility of new energetic materials the n-octanol/water partition coefficient [113] should be determined. The partition coefficient of a substance between water and a lipophilic solvent (*n*-octanol) is one model variable which may be used to describe the transfer of a substance from the aquatic environment into an organism and the potential bioaccumulation of the substance. Studies show a highly significant relationship between the partition coefficient of different substances in the system water/*n*-octanol and their bioaccumulation in fish described in the literature.[114] It has also been shown to be a useful parameter in other forms of biological activity. The partition coefficient (P_{ow}) is defined as the ratio of the equilibrium concentrations (C_i) of a dissolved substance in a two-phase system consisting of two largely immiscible solvents. In the case *n*-octanol and water: $P_{ow} = C_{n\text{-octanol}}/C_{water.}$ The partition coefficient (P_{ow}) therefore is the quotient of two concentrations and is usually given in the form of its logarithm to base ten (log *P*). The tests in this thesis were carried out with a mixture of analytical grade *n*-octanol and distilled water at 22 °C (±1 °C).

Reference substances: The reference substances (**Table 1.5**) need not be employed in all cases when investigating a new substance. They are provided primarily so that calibration of the method may be performed from time to time and to offer the chance to compare the results when another method is applied.

Table 1.5 Data for Reference Substances

Test Substance	P_{ow}
Di(2-ethylhexyl)phthalate (OECD)	$1.3 \cdot 10^5$ ($4.6 \cdot 10^4$–$2.8 \cdot 10^5$)
Hexachlorobenzene (OECD)	$3.6 \cdot 10^5$ ($1.1 \cdot 10^5$–$8.3 \cdot 10^5$)
o-Dichlorobenzene (EEC)	$5.1 \cdot 10^3$ ($1.5 \cdot 10^3$–$2.3 \cdot 10^4$)
Dibutyl phthalate (EEC)	$1.3 \cdot 10^4$ ($1.7 \cdot 10^3$–$2.8 \cdot 10^4$)
Trichloroethylene (OECD)	$2.0 \cdot 10^3$ ($5.2 \cdot 10^2$–$3.7 \cdot 10^3$)
Urea (OECD)	$6.2 \cdot 10^{-2}$ ($2.0 \cdot 10^{-2}$–$2.4 \cdot 10^{-1}$)

1.4.20 Calculation of Heat of formation

Due to the highly energetic character of new HEDMs, bomb calorimetric measurements oftentimes can only be performed with very small amounts, consequently doubtful combustion energies are obtained. Therefore extended computational studies were accomplished, which are presented in the following. In earlier times ab initio calculations based on the ideal gas phase reaction enthalpy (method 1) were used. However, it has been shown that by using the atomization energy method (method 2) more precise results are obtained. All calculations were carried out using the Gaussian G03W (revision B.03) program package.[115]

Method 1

The method is explained in the following by computing the heat of formation of triaminoguanidinium dinitramide (TAG^+DN^-, Chapter 3). The structure, energy and frequency calculations were performed at the Hartree-Fock level followed by a Møller-Plesset correlation energy correction, truncated at second order.[116] For all atoms H, C, N and O an augmented correlation consistent polarized double-zeta basis set was used (aug-cc-pVDZ).[117] The ab initio computational results are summarized in **Table 1.6**.

The molecular volumes of TAG and DN were taken or back-calculated from literature-known X-ray structural data (**Table 1.7**). The lattice energies (U_L) and lattice enthalpies (ΔH_L) of TAG-DN were calculated according to the equations provided by Jenkins *et al.*.[118] and are summarized in **Table 1.8**.

Table 1.6 MP2/aug-cc-pVDZ computational results.

Compound	Formula	Symbol	Point group	$-E$ / a.u.	*zpe* [a] / kcal mol^{-1}
triamino-guanidinium	$CH_9N_6^+$	TAG	C_3	370.773187	100.8
dinitramide	$N_3O_4^-$	DN	C_2	463.977161	17.9
water	H_2O		C_{2v}	76.260910	13.4
dinitrogen	N_2		$D_{\infty h}$	109.280650	3.1
carbon dioxide	CO_2		$D_{\infty h}$	188.169700	7.1
dioxygen	O_2		$D_{\infty h}$	150.004290	2.0

[a] The zero point energies (*zpe*) were calculated at the B3LYP/aug-cc-pVDZ level of theory

Table 1.7 Molecular volumes.

	Symbol	V_M / Å^3	V_M / nm^3
NH_4^+ [118]	A	21.0	0.021
$C(NHNH_2)_3^+$ [119]	TAG	112	0.112
$N(NO_2)_2^-$ [120]	DN	89.1	0.089

Table 1.8 Lattice energies (U_L) and lattice enthalpies (ΔH_L) of TAG-DN.

	V_M / nm^3	U_L / kJ mol^{-1}	ΔH_L / kJ mol^{-1}
TAG-DN	0.201	504.3	509.3

$C(NHNH_2)_3^+(g) + N(NO_2)_2^-(g) + 1.25\ O_2(g) \rightarrow CO_2(g) + 4.5\ H_2O(g) + 4.5\ N_2(g)$

With the values given in **Table 1.9** the $\Delta E^{el.}$ was calculated (all species in the gas phase):

$\Delta E_{el.}$ (TAG-DN) = –2232.8 kJ mol^{-1}

The $\Delta E^{el.}$ value was converted into the gas phase reaction enthalpy ($\Delta_{rxn}H$) after correction for the work term ($p\Delta V$), the vibrational correction ($\Delta_{vib}U$), the translational ($\Delta_{trans}U$) and rotational term ($\Delta_{rot}U$):[121]

Table 1.9 Gas phase reaction enthalpy

	equations
$P\Delta V = \Sigma\, \nu_i\, RT$	6.75 RT
$\Delta_{vib}U = \Sigma\, \nu_i\, (zpe)_i$	–166.7 kJ mol^{-1}
$\Delta_{trans}U = \Sigma\, \nu_i\, (1.5)\, RT$	10.125 RT
$\Delta_{rot}U = \Sigma\, \nu_i\, (F_{rot} / 2)\, RT$	8 RT
$\Delta_{rxn}H_{298}$ / kJ mol^{-1}	–2337.9

Using the lattice enthalpies and the enthalpy of vaporization for water ($\Delta_{vap}H$ = 44.0 kJ mol^{-1}) [122] the enthalpy of combustion according to the following equation was calculated.

$$[C(NHNH_2)_3]^+[N(NO_2)_2]^-(s) + 1.25\ O_2(g) \rightarrow CO_2(g) + 4.5\ H_2O(l) + 4.5\ N_2(g)$$

$\Delta_{comb.}H_{298}$(TAG-DN) = – 1828.6 kJ mol^{-1} (for H_2O(g)) = – 2026.6 kJ mol^{-1} (for H_2O(l))

With the known enthalpies of formation of carbon dioxide ($\Delta_fH°_{298}(CO_{2(g)})$ = –393.5 kJ mol^{-1} [122]) and water ($\Delta_fH°_{298}(H_2O_{(g)})$ = –241.8 kJ mol^{-1} [122]) the enthalpy of formation of TAG-DN can now be calculated to:

$\Delta_fH°_{298}$(TAG-DN(s)) = +347.0 kJ mol^{-1}.

The energy of formation ($\Delta_fU^o_{298}$) can be obtained from the above calculated enthalpy of formation according to the following equation with Δn being the change of moles of the gaseous components (Δn(TAG-DN) = –11):

$$\Delta_fU°_{298} = \Delta_fH°_{298} - \Delta n\, RT$$

$\Delta_fU°$(TAG-DN(s)) = +374.3 kJ mol^{-1} = +1772.7 kJ kg^{-1}

Method 2

This method is explained by computing the heat of formation of 5-aminotetrazolium dinitramide (HAT^+DN^-, Chapter 3). The enthalpies (H) and free energies (G) were calculated using the complete basis set (CBS) method of Petersson and coworkers in

order to obtain very accurate energies. The CBS models use the known asymptotic convergence of pair natural orbital expressions to extrapolate from calculations using a finite basis set to the estimated complete basis set limit. CBS-4 begins with a HF/3-21G(d) structure optimization; the zero point energy is computed at the same level. It then uses a large basis set SCF calculation as a base energy, and a MP2/6-31+G calculation with a CBS extrapolation to correct the energy through second order. A MP4(SDQ)/6-31+(d,p) calculation is used to approximate higher order contributions. In this study we applied the modified CBS-4M method (M referring to the use of minimal population localization) which is a re-parametrized version of the original CBS-4 method and also includes some additional empirical corrections.[123,124] The enthalpies of the gas-phase species M were computed according to the atomization energy method (eq. 1) (**Tables 1.10–1.12**).[125,126]

$$\Delta_f H^\circ_{(g,\,M,\,298)} = H_{(Molecule,\,298)} - \sum H^\circ_{(Atoms,\,298)} + \sum \Delta_f H^\circ_{(Atoms,\,298)} \qquad (\mathbf{1})$$

Table 1.10 CBS-4M results.

	p.g.	$-H^{298}$ / a.u.	$-G^{298}$ / a.u.	*NIMAG*
HAT^+	C_s	313.534215	313.567694	0
DN^-	C_2	464.499549	464.536783	0
AF	C_s	313.533549	313.570115	0
2-MeHAT	C_1	352.783676	352.821342	0
HTZ^+	C_{2v}	258.229407	258.259436	0
H		0.500991	0.514005	0
C		37.786156	37.803062	0
N		54.522462	54.539858	0
O		74.991202	75.008515	0

Table 1.11 Literature values for atomic $\Delta_f H^\circ$ / kcal mol^{-1}.

	Ref. [125]	NIST [122]
H	52.6	52.1
C	170.2	171.3
N	113.5	113.0
O	60.0	59.6

Table 1.12 Enthalpies of the gas-phase species M.

M	M	$\Delta_f H°$(g,M) / kcal mol^{-1}
HAT^+	CH_4N_5	+235.0
DN^-	$N(NO_2)_2^-$, $N_3O_4^-$	–29.6
AF^+	$(H_2N)_2CN_3^+$, $CH_4N_5^+$	+235.4
HTZ^+		+246.3
2-MeHAT^+	$C_2H_6N_5^+$	+221.2

The lattice energies (U_L) and lattice enthalpies (ΔH_L) were calculated from the corresponding molecular volumes (**Table 1.13**) according to the equations provided by Jenkins *et al.* [118] and are summarized in **Table 1.14**.

Table 1.13 Molecular volumes.

	V_M / Å^3	V_M / pm^3
DN^-	89 [a]	0.089
$[HAT]^+$	69 [b]	0.069
$[NH_4][DN]$	110 [120]	0.110

[a] this work, back-calculated from V(ADN) using the molecular volume for NH_4^+ from the literature; [b] The molecular volume of $[HAT]^+$ was calculated from the molecular volume of $[HAT][NO_3]$ – $V_M(NO_3^-)$.

Table 1.14 Lattice energies and lattice enthalpies.

	V_M / nm^3	U_L / kJ mol^{-1}	ΔH_L / kJ mol^{-1}	ΔH_L / kcal mol^{-1}
[HAT][DN]	0.172	525.6	530.6	126.8

With the calculated lattice enthalpies the gas-phase enthalpies of formation (**Table 1.12**) were converted into the solid state (standard conditions) enthalpies of formation (**Table 1.15**). These molar standard enthalpies of formation (ΔH_m) were used to calculate the molar solid state energies of formation (ΔU_m) according to eq. (**2**).

$$\Delta U_m = \Delta H_m - \Delta n\, RT \quad (\Delta n \text{ being the change of moles of gaseous components}) \qquad (\mathbf{2})$$

The enthalpy of formation of the solid species M ($\Delta_f H°$(s,M)) was calculated to be +78.6 kcal mol^{-1}.

Table 1.15 Solid state energy of formation ($\Delta_f U°$)

	$\Delta_f H°$(s) / kcal mol^{-1}	Δn	$\Delta_f U°$(s) / kcal mol^{-1}	M / g mol^{-1}	$\Delta_f U°$(s) / kJ kg^{-1}
[HAT][DN]	+78.6	–8	83.3	192.1	+1813.3

1.4.21 Calculation of Detonation Parameters using EXPLO5

The prediction of energetic properties of new compounds can be performed by computing its detonation parameter. Very important parameters are: energy of explosion ($U_{Exp.}$), detonation pressure $p_{C\text{-}J}$, detonation velocity ($V_{Det.}$), temperature of explosion ($T_{Ex.}$), volume of decomposition gases (V). By using the energy of formation and the density either obtained by X-ray crystallography or by pycnometer measurements several detonation parameters of energetic compounds including the atoms C, H, N, O, Al and F can be calculated by using the EXPLO5 computer program.[127,128] This program is based on the steady-state model of equilibrium detonation and uses BKW E.O.S for gaseous detonation products and Cowan-Fickett E.O.S. for solid carbon.[129] The calculation of the equilibrium composition of the detonation products is done by applying modified White, Johnson and Dantzig's free energy minimization technique. The program is designed to enable the calculation of detonation parameters at the CJ point. The BKW equation in the following form was used with the BKWN set of parameters (α, β, κ, θ) as stated below the equations and X_i being the mol fraction of i-th gaseous product, k_i is the molar covolume of the i-th gaseous product:

$$pV / RT = 1 + xe^{\beta x} \qquad x = (\kappa \Sigma X_i k_i) / [V (T + \theta)]^{\alpha}$$

$\alpha = 0.5$, $\beta = 0.176$, $\kappa = 14.71$, $\theta = 6620$.

1.5 Concept and Goals

The goal of this thesis is according to the title *Energetic materials based on 5-Aminotetrazole* the synthesis of new energetic materials, which are appropriate for civil as well as military energetic applications.

There exist three main goals for the research of energetic materials in this thesis:

- Replacement of RDX, which is a powerful secondary explosive with low sensitivities, a good thermal stability and a low priced synthesis. However, RDX was found to be polluting, in particular, to aquatic creatures.

- Replacement of toxic heavy metal barium salts as green colorants as well as new perchlorate-free red colorants in pyrotechnical compositions and flares.

- New high-nitrogen materials for use in smokeless and low-erosive solid propellants. Possible applications would be rocket engines in missiles, propelling charges in gun barrel weapons and gas-generators.

- Replacement of lead(II) azide in priming charges. Lead azide is not only very toxic, but also its explosion performance is sometimes too low, e.g. for initiation of HNS (hexanitrostilbene). Therefore "green" alternatives with good thermal stabilities and great performances are in the focus of many researcher world-wide.

Due to their highly energetic character of HEDMs, the chemical as well as physico-chemical properties of all compounds have to be fully characterized. Due to safety reasons, the sensitivities towards impact, friction and heat have to be clarified, before synthesizing larger amounts (> 250 mg). A main challenge in this work is the investigation of solid, crystalline materials. X-ray determination is a valuable method to understand the molecular as well as the crystal structure of new materials, which often can related to the thermal stability, sensitivity and also performance. In addition, the density, which is a main characteristic of new high explosives, is obtained by X-ray methods. Heats of formation have to be determined either by bomb calorimeter measurements or by theoretical calculations. By using the energy of formation and the X-ray density, important detonation parameters such as the detonation velocity and

pressure can be calculated. The synthetic procedure of well performing compounds should be optimized in order to produce larger scales (10–30 g).

An auspicious starting material for new syntheses of energetic compounds is 5-amino-1*H*-tetrazole (**2**), which is commercially available (500 g ~ 100 €), but also accessible via different synthetic routes in the lab as well in the technical scale. Nearly all synthesis in this thesis are based on this 5-aminotetrazole. 5-Aminotetrazole is also commercially available as its monohydrate, but with slightly higher costs. Water-free 5-aminotetrazole is a colorless powder, which is not hygroscopic and stable up to 200 °C. Perhaps the sole disadvantage is its low solubility in organic solvents, e.g. CH_2Cl_2 and diethyl ether. In addition, it is also only slightly soluble in cold alcohols and water.

Figure 1.32 5-Aminotetrazole by Aldrich

Scheme 1.20 gives an overview of the present dissertation. All compounds described in this thesis could be synthesized starting with 5-aminotetrazole. However, in few cases it was proofed to become more facile to use other starting materials. For example, there exists much better synthetic routes to 1,5*H*-tetrazole (Chapter 11) in comparison to the described deamination reaction of 5-amino-1*H*-tetrazole.

In the following short descriptions of all chapter including the references of the published articles are given:

Chapter 2 – 5-Aminotetrazolate salts

Chapter 2 describes deprotonation reactions of 5-amino-1*H*-tetrazole with alkaline and alkaline earth metal hydroxides and carbonates, respectively, as well as hydrazine.[67,130]

Chapter 3 – Nitrogen-rich perchlorates and dinitramides

In chapter 3, the synthesis, characterization and testing of several nitrogen-rich perchlorates [131,132] is described, which act as starting material for high nitrogen

dinitramides.[133,134,135,136] These compounds deliver the highest performances in this thesis and are partly characterized by a balanced oxygen content.

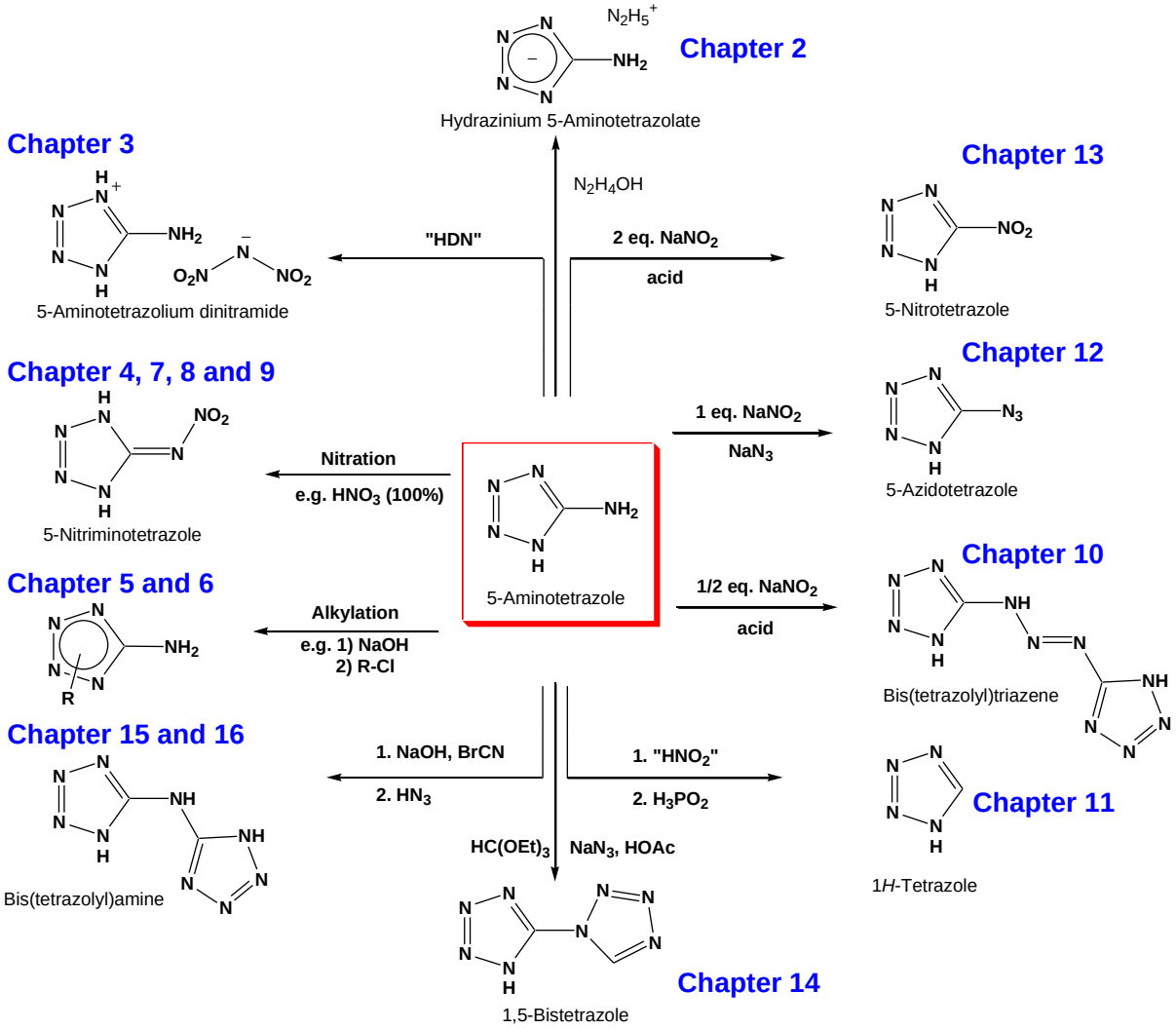

Scheme 1.20 Synthetic overview of the present thesis: Energetic Materials Based on 5-Aminotetrazole.

Chapter 4 – Nitration Products of 5-aminotetrazoles

Chapter 4 describes the products of the nitration reaction of 5-aminotetrazole and its methyl analogues with fuming nitric acid.[137,138,139] The neutral compounds are highly energetic and act as starting materials for the synthesis of salts and complexes

Chapter 5 – Functionalized 1-ethyl-5-aminotetrazoles and 1-Ethyl-5-nitrimino-tetrazoles

Alkylation of 5-aminotetrazole with 2-chloroethanol leads to a mixture of the *N*-1- and *N*-2-isomers 1-(2-hydroxyethyl)-5-aminotetrazole (**46**) and 1-(2-hydroxyethyl)-5-

aminotetrazole (**47**). Several reactions to a large amount of neutrals, salts and complexes are presented, which are all based on compound **46**.[140]

Chapter 6 – 2-Aza-2-nitro-propyl-tetrazoles

In this chapter, products obtained by the alkylation of different tetrazolates with 2-aza-2-nitro-propyl chloride are introduced. In addition 1,4-dimethyl-5-nitriminotetrazole is rejudged.[141]

Chapter 7 – Salts of 1-methyl-5-nitriminotetrazole

Promising alkaline, alkaline earth as well as nitrogen-rich salts containing the 1-methyl-5-nitriminotetrazolate anion (and also in part its 2-methyl analogue) are described. The salts have different properties and can be used as colorants in pyrotechnics as well as new well performing materials for the replacement of RDX.[142,143,144,145,146]

Chapter 8 – Salts of 5-nitriminotetrazole

5-Nitriminotetrazole can be deprotonated twice. In this chapter a selection of investigated metal salts are described. Auspicious calcium 5-nitriminotetrazolate (**90**) may be used as green replacement for lead azide in priming charges.[147,148]

Chapter 9 – Copper complexes of 5-nitriminotetrazole

Chapter 9 describes the synthesis and characterization of copper complexes of 5-nitriminotetrazole and its methyl analogues. In addition to the standard analytical methods, such as XRD the magnetic properties were determined by SQUID measurements. The energetic properties of the complexes range from primary explosive to insensitive green colorants for pyrotechnics.[149,150]

Chapter 10 – Bis(tetrazolyl)triazenes

The reaction of 5-aminotetrazoles with half an equivalent of sodium nitrite in acid solution yield bis(tetrazolyl)triazenes. In particular, the bis(methyltetrazolyl)triazenes are in spite of their high nitrogen content characterized by a good thermal stability and can also reacted with ammonia solution to ammonium bis(methyltetrazolyl)triazenates. These represent new insensitive nitrogen-rich derivatives with decomposition temperatures above 200 °C.[151]

Chapter 11 – Salts of 1*H*-tetrazole

In chapter 11, ammonium, hydrazinium, alkali as well as alkaline earth metal salts of 1*H*-tetrazole are specified. Especially the strontium salt shows promise as new smokeless red colorant in pyrotechnical compositions.[152]

Chapter 12 – 5-azidotetrazoles

The reaction of 5-aminotetrazoles with one equivalent of sodium nitrite followed by an acidic work-up yields 5-azidotetrazoles. 5-Azido-1*H*-tetrazole, which is the tetrazole with the highest nitrogen content (to date) was fully reinvestigated (X-ray, multinuclear NMR spectroscopy, sensitivities, calculations) and a new as well as safer synthesis is described. With this, several extremely explosive salts have been prepared, which contain the CN_7^- anion. Hydrazinium 5-azidotetrazolate, which represents the tetrazole salt with the highest nitrogen content ever reported was characterized comprehensively. All salts have been determined by X-ray diffraction and a detailed description is given.[153,154]

Chapter 13 – Methyl-5-nitrotetrazoles and derivatives

The reaction of methyl-5-aminotetrazoles with an excess of sodium nitrite yields 5-nitrotetrazoles. 1-Methyl- and 2-Methyl-5-nitrotetrazole have been synthesized and characterized.[155] In addition, the interesting byproduct bis(1-methyltetrazolyl)diazene-N-oxide is discussed. 1-Methyl-5-chlorotetrazole is presented as the main-product in the presence of chloride during the diazotation product.

Chapter 14 – 1,5-Bistetrazoles

Chapter 14 introduces 1,5-bistetrazoles, which are obtained by the reaction of 5-aminotetrazoles with triethyl orthoformate and sodium azide in glacial acetic acid. The chemical as well as physico-chemical properties of neutral and ionic 1,5-bistetrazoles were determined. In addition, three copper complexes were synthesized to investigate the ligand behavior of 1,5-bistetrazoles.

Chapter 15 – Bis(tetrazolyl)amines

5,5'-Bis(tetrazolyl)amine (**H_2bta**) can also be synthesized from 5-aminotetrazole. However, the best synthesis, which can also performed in larger scale is the reaction of sodium dicyanamide with 2. eq. sodium azide in acidic solution. H_2bta is an extremely promising nitrogen-rich material with astonishing stability towards heat and outer

stimuli and may be used as secondary explosive as well as nitrogen fuel in solid propellants. It can be further alkylated which is shown by methylation reactions, substituting the ring protons in the first step and also the amine proton in a second step. All compounds were fully characterized, including X-ray determinations of these very low soluble compounds.[156]

Chapter 16 – Complexes of bis(tetrazolyl)amines

In chapter 16, the introduced bis(tetrazolyl)amines (Chapter 15) have been used as chelating ligands in zinc and copper complexes in combination with oxygen-rich counter anions. Most of the copper complexes show photo-chemical behavior and explode in the Raman device. This makes them promise for use as light inducible primary explosives.[157,158]

Chapter 17 – Exciting reactions, ongoing projects and selected structures

Chapter 17 depict various reactions and selected crystal structures, which do not fit in one of the previous chapters. For example, the structure of 5-cyano-2*H*-tetrazole is presented and also connecting reactions are proposed. The products obtained open a large field of energetic materials for further research. In addition, the first structure of a deprotonated 5-chlorotetrazole is introduced. Salts of 5-chlorotetrazoles could be very interesting materials as colorants in pyrotechnics in future times.

Chapter 2.

5-Aminotetrazolate Salts

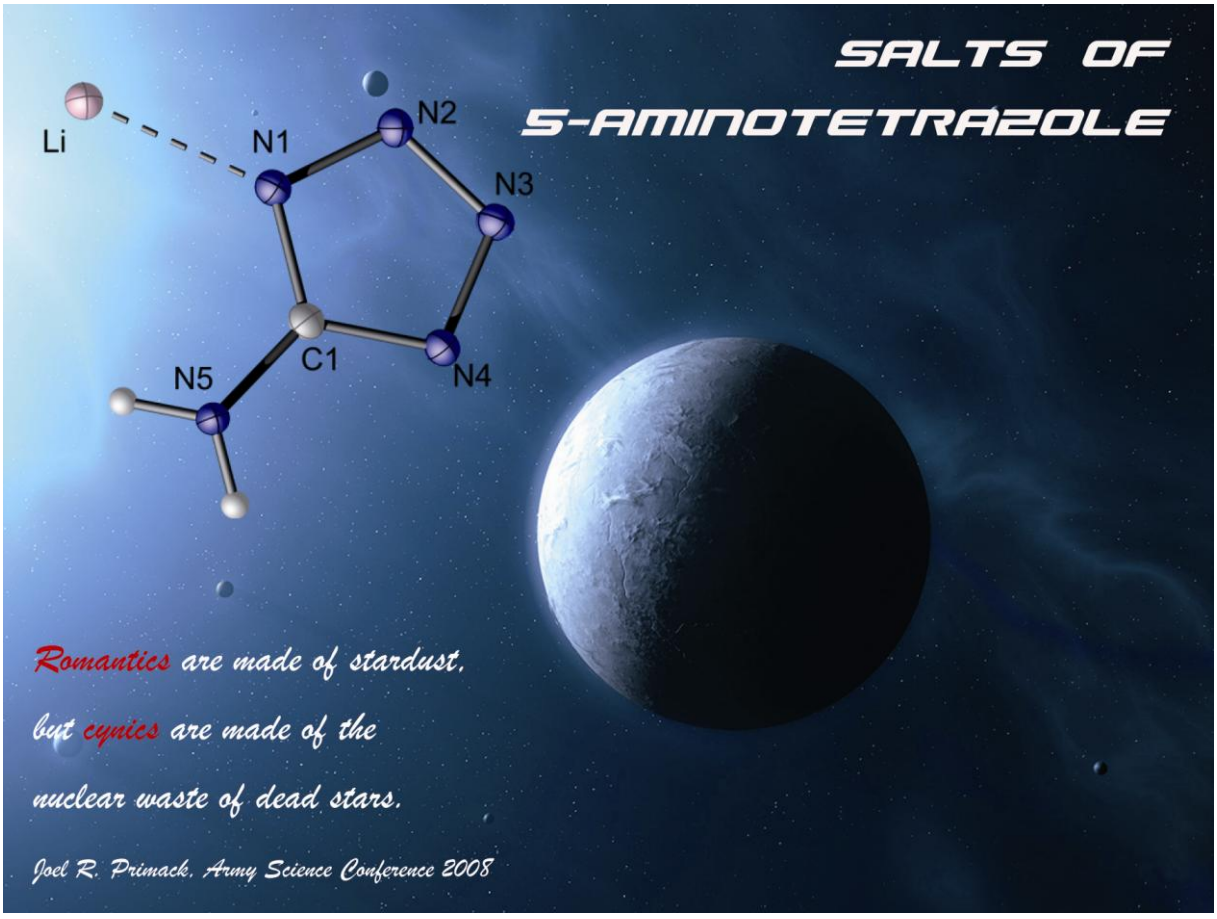

2.1 Introduction

Metal salts of tetrazoles [159,160] are still an important field of the inorganic chemistry due to the practical and theoretical significance of these unique compounds and diversity of their properties. They are used as starting materials and intermediate in alkylation processes of tetrazoles but can also be used as colorants in pyrotechnical compositions. Regarding the development of new energetic materials one approach is also the synthesis of high-nitrogen tetrazole salts which combine a positive heat of formation ($\Delta_f H > 0$) and therefore high explosive and propulsive power with relatively high thermal stability and low volatility and therefore low inhalation toxicity.[30] Usually salts with a nitrogen content above 80 % show definite sensitivities. However, these values strongly depend on the constitution of the atoms and cannot be correlated to the nitrogen content. Nitrogen-rich salts can be used as energetic materials for application, e.g. in propellant charges.

Tetrazole and the 5-substituted derivatives are weak acids with pK_a-values in the range of 1.1−6.3, which is comparable with that of carbonic acids.[40,47] The acidity increases in the case of 5-aryl-substituted tetrazoles because of a better resonance stabilization of the anion. In the case of strong π-delocalization in the anion, e.g. 5-azido-1*H*-tetrazole, [161] the acidity approaches that of a strong acid. The tetrazole ring itself shows a basicity lower than that of aniline. Typical pK_b-values are found in the range of 9.7 (1-methyl-1*H*-tetrazol) to 12.9 (5-amino-1-phenyl-1*H*-tetrazole). Protonation takes place preferentially at N4.[162] Electrophiles attack tetrazoles usually at one of the ring nitrogen atoms. [163] While acylation [164] of 5-monosubstituted tetrazoles proceeds in most cases selectively at N2, alkylation is not selective and yields mixtures of 1,5- and 2,5-disubstituted tetrazoles.[165] The position attacked by the electrophile strongly depends on the substituent at C5, the reaction conditions, and the reagent. While electron withdrawing groups (CN, NO_2) at C5 lead to substituents at the nitrogen atom N2, electron donating groups (NH_2, OH) lead to alkylation at the nitrogen atom N1.

In the following the deprotonation of 5-At using alkali as well as alkaline earth hydroxides and carbonates is described. The formed alkali and earth alkaline 5-aminotetrazolates (**21**–**29**) were analyzed comprehensively and a detailed characterization is given in this work.

Also the synthesis of hydrazinium 5-aminotetrazolate (**30**) is described. The motivation of this study is the insensitivity of **30** in combination with an extraordinarily high

calculated detonation pressure and velocity, even succeeding those of HMX. Here we report on an easy one-step synthesis of **30**, a full characterization as well as calculations of the detonation and propulsion parameters.

2.2 Synthesis

The synthesis of the alkali 5-aminotetrazolates comply with **Scheme 2.1**. All reactions were performed in water, in case of Li^+ and Na^+ the metal hydroxides, in case of K^+, Rb^+ and Cs^+ the corresponding carbonates were used. Single crystals were obtained by recrystallization from water or water-ethanol solutions.

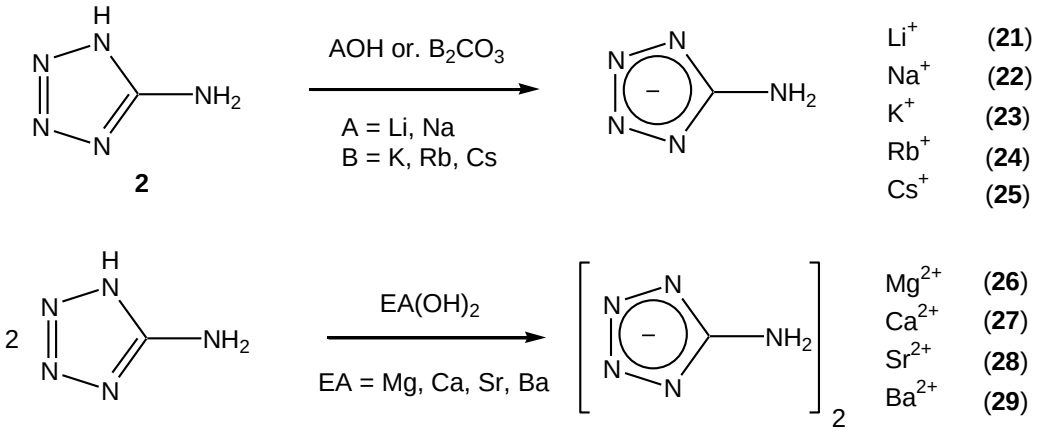

Scheme 2.1 Synthesis of alkali and alkaline earth metal salts of 5-At (**21**-**29**).

Hydrazinium 5-aminotetrazolate (**30**) can be synthesized via two facile routes (**Scheme 2.2**). (i) The synthesis under exclusion of water by the reaction of 5-amino-1*H*-tetrazole (**2**) with hydrazine in THF yields **30** in high purity and yield. **30** is recrystallized from hot ethanol yielding colorless needle shaped crystals which can be washed with diethyl ether. (ii) Also possible is the reaction of **2** or its monohydrate with hydrazine hydrate in water or in alcoholic (MeOH, EtOH) solutions.

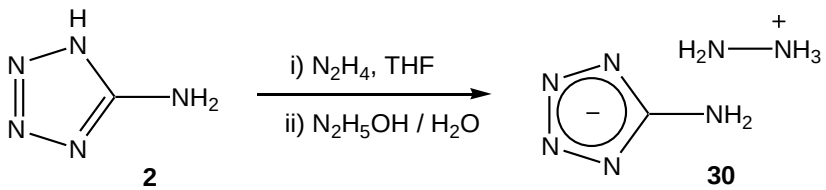

Scheme 2.2 Two synthetic protocols of the formation of hydrazinium 5-aminotetrazolate (**30**).

2.3 Structures

Suitable single crystals of compounds **21**–**26**, **29** and **30** have been determined by X-ray diffraction. A detailed description follows.

2.3.1 Lithium 5-aminotetrazolate (**21**)

21 crystallizes in the monoclinic space group $P2_1/c$ with four molecules in the unit cell. The N–N bond distances in the tetrazolate ring are between N–N single bonds (1.454 Å) and N=N double bonds (1.245 Å).[166,167] The shortest distance is between the atoms N2–N3 of 1.307(2) Å, the longest between the nitrogens N1 and N2 of 1.359(2) Å. In comparison with the crystal structure of the neutral 5-aminotetrazole as its monohydrate [60] the distances between the ring atoms are very similar in contrast to the distance to the NH_2 group. In 5-At the C1–N5 bond length is 1.330(2) Å while **6** shows a longer distance of 1.393(2) Å. Within this the bond angle N4–C1–N1 is larger (112.4(1)°) than in 5-aminotetrazole (107.9(1)°). The five membered tetrazolate ring is almost planar (torsion angle N1–N2–N3–N4 = 0.55(2)°) which is the basic requirement for a delocalized 6π-aromatic system. Due to the bonding-geometry of the amine nitrogen N5, a hybridization between an sp^2 and an sp^3 atom is suggested. The hydrogen atoms (bond angles between 111.7–113.8°) do not lie in the plane and are bent ~30° out of plane. A detailed record of the bond and torsion angles is given in **Table 2.1** and **Table 2.2**. The molecular unit is given in **Figure 2.1**.**a**. **Figure 2.1**.**b** shows the unit cell along the *a* axis.

The lithium cations are coordinated via four different nitrogen atoms building a distorted tetrahedral coordination sphere, which can be seen in **Figure 2.1**.**c**. Three of the Li–N bond distances are very similar (Li–N1 = 2.025(2) Å, Li–$N2^{i}$ = 2.041(4) Å, Li–$N4^{ii}$ = 2.028(5) Å) while the Li–$N5^{iii}$ distance to the primary amine group is elongated to 2.200(8) Å ((i) –x, –y, –z; (ii) –1+x, 0.5–y, –0.5+z; (iii) x, 0.5–y, –0.5+z).

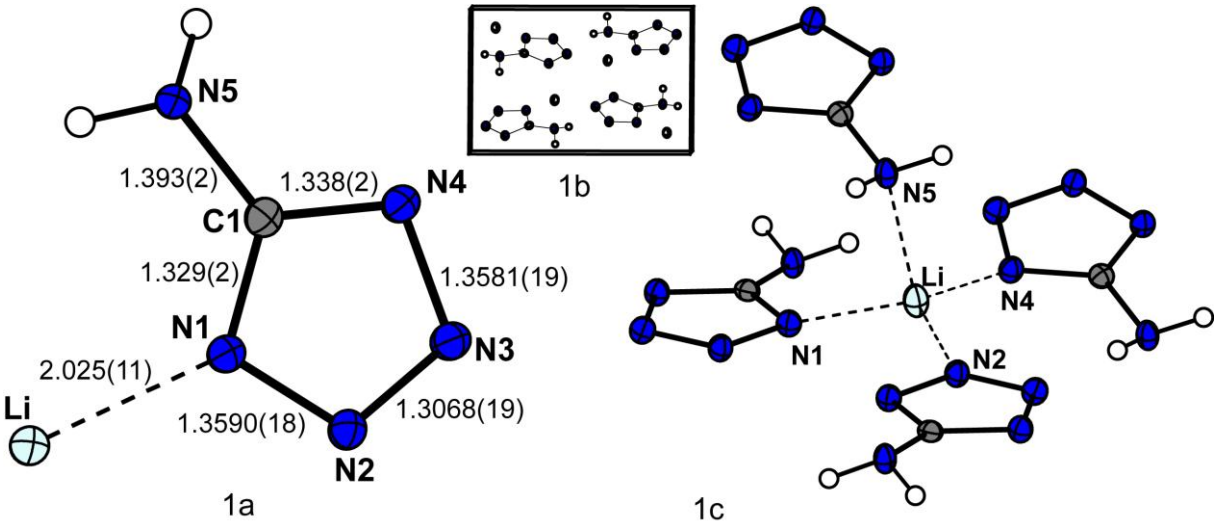

Figure 2.1 a) A view of the molecular unit of **21**, showing the atom-labeling scheme and bond-distances (Å) with standard deviations. Thermal ellipsoids represents 50 % probability and hydrogen atoms are shown as small spheres of a arbitrary radii. b) Unit cell, viewing along the *a* axis. c) coordination geometry of the lithium cations.

2.3.2 Sodium 5-aminotetrazolate trihydrate (**22**)

22 could only obtained crystalline as its trihydrate. **22** crystallizes in the centro-symmetric triclinic space group *P*–1 with four molecules in the unit cell. The bond distances and angles in the tetrazolate anion are only insignificant smaller than in the lithium salt. For an easier illustration only one molecule of the two found in the asymmetric unit is shown in **Figure 2.2**. The sodium atoms are coordinated octahedrally by one nitrogen atom (N3–Na1 = 2.44(1) Å) and three different oxygen atoms (O1–Na1 = 2.431(9) Å, O2–Na1 = 2.420(2) Å, O3–Na1 = 2.390 Å). The packing is affected by several strong hydrogen bonds, e.g. O2–H2A···N1^{i} (D–A = 2.836(2) Å, 172(2)°), O3–H3A···N4^{ii} (2.812(2) Å, 174(2)°) and O1–H1B···O2^{iii} (2.888(2) Å, 169(3)°); (i) –1–x, 1–y, 2–z; (ii) –x, –y, 2–z; (iii) 1+x, y, z.

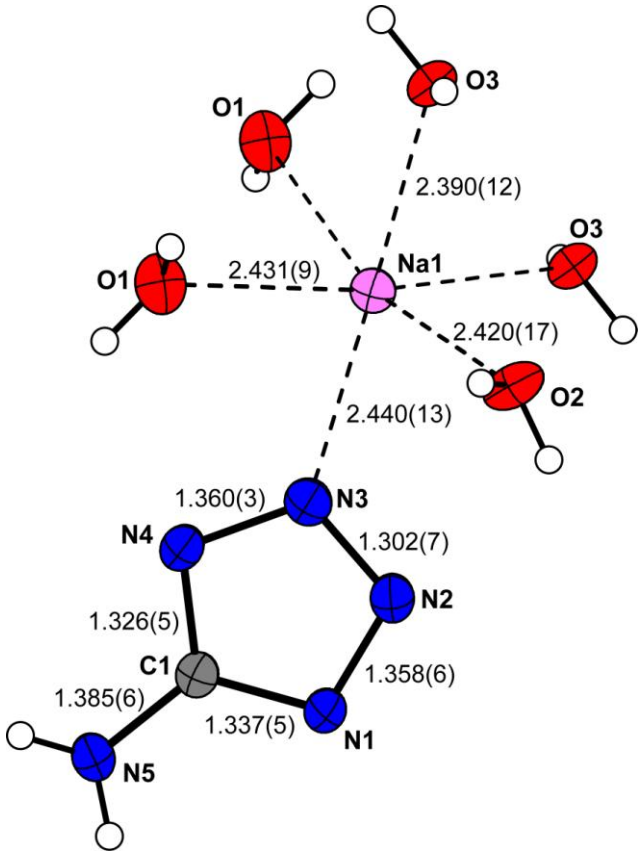

Figure 2.2 A view of the molecular unit of **22** and the coordination of the Na^+ cations, showing the atom-labeling scheme and bond-distances (Å) with standard deviations. Thermal ellipsoids represent 50 % probability and hydrogen atoms are shown as small spheres of a arbitrary radii.

2.3.3 Potassium 5-aminotetrazolate (**23**)

Potassium 5-aminotetrazolate crystallizes in the monoclinic space group $P2_1/c$ with four molecules in the unit cell. The bond distances and angles are similar to the discussed alkali salts and are given in **Figure 2.3a**. The packing is affected by an alternating tilted layer structure, which can be seen in **Figure 2.3b**. The layers are connected via a distorted trigonal coordination of the potassium cations (**Figure 2.3c**) to three different nitrogen atoms. The shortest distance K1–N2 of 2.763(2) Å lies within these layers, while the N1–K1^{i} and the N4–K1^{ii} distances have values of 2.832(2) Å and 2.824(2) Å ((i) 2–x, 0.5+y, 2.5–z; (ii) 1–x, 0.5+y, 1.5–z).

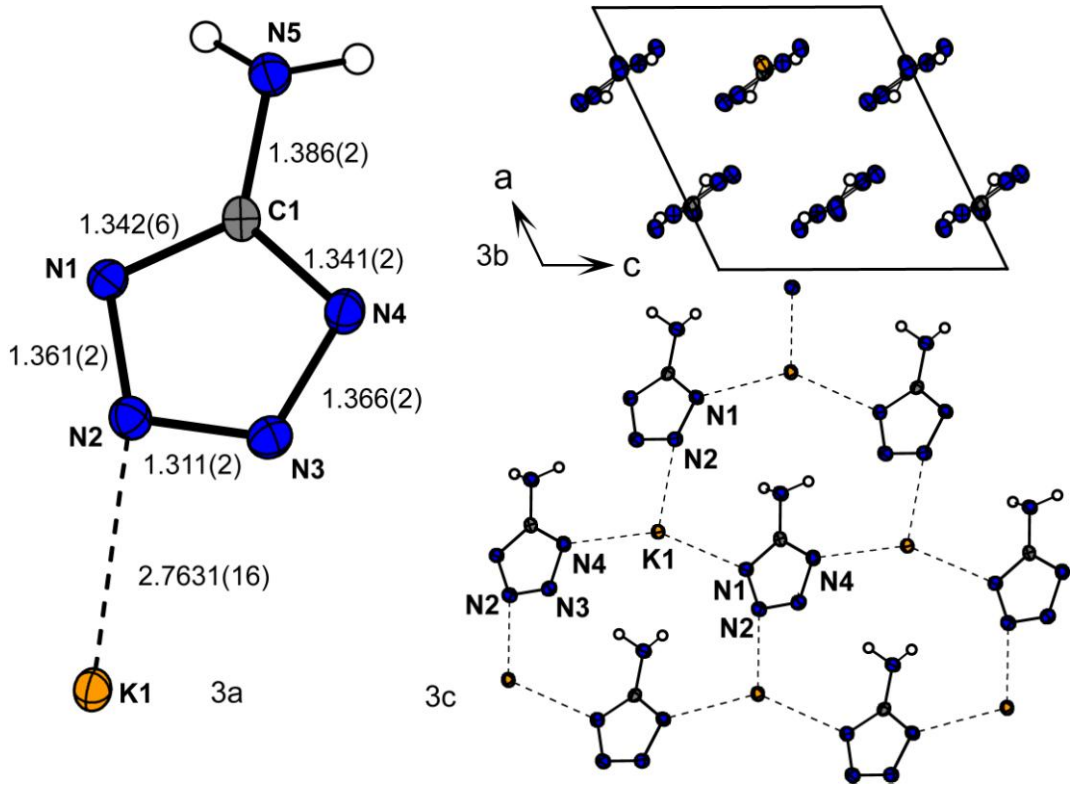

Figure 2.3 a) A view of the molecular unit of **23**, showing the atom-labeling scheme and bond-distances (Å) with standard deviations. Thermal ellipsoids represents 50 % probability and hydrogen atoms are shown as small spheres of a arbitrary radii. b) Unit cell, view along the *b* axis, showing the layers c) coordination geometry of the potassium cations.

2.3.4 Rubidium 5-aminotetrazolate (**24**)

The rubidium salt **24** crystallizes without inclusion of crystal water in the orthorhombic space group *Pnma* with four molecules in the unit cell. Three atoms lie on special positions (Rb1: 0.48244, ¼, 0.29766; C1: 0.2824, ¼, 0.7598; N5: 0.2699, ¼, 0.6064) representing a mirror plane dividing the molecular unit (**Figure 2.4a**). Again, there are no anomalies in the structure of the anion. As it can be seen in **Figure 2.4a** and **b**, **24** crystallizes in weak staggered layers where the rubidium cations are formally coordinated tenfold by nine nitrogen atoms in a distance between 3.09 and 3.18 Å and one nitrogen atom with a longer distance about 4 Å.

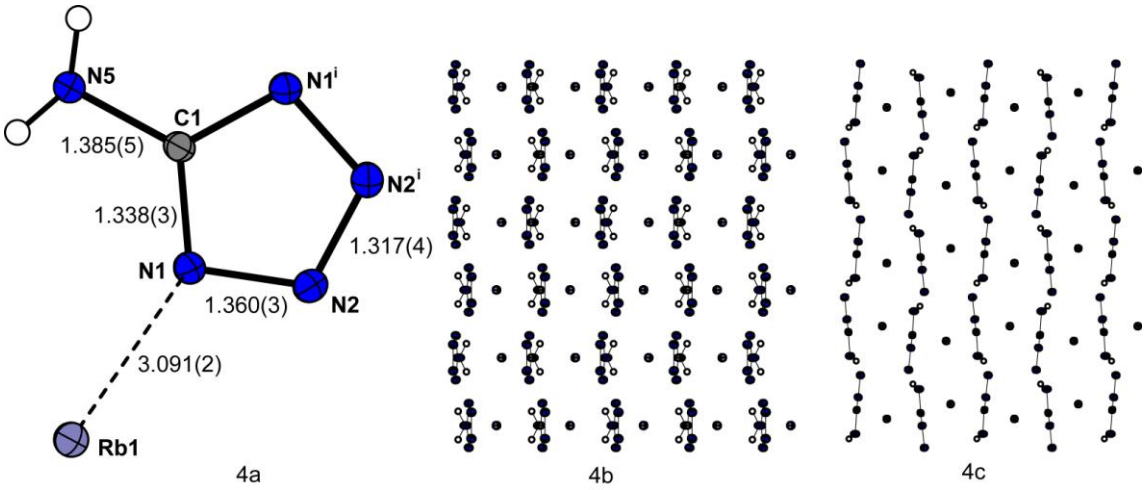

Figure 2.4 a) A view of the molecular unit of **24**, showing the atom-labeling scheme and bond-distances (Å) with standard deviations. Thermal ellipsoids represent 50 % probability and hydrogen atoms are shown as small spheres of a arbitrary radii (i = x, 0.5–y, z). b) View on a super cell along the *b* axis c) View on a super cell along the *c* axis.

2.3.5 Cesium 5-aminotetrazolate (**25**)

25 crystallizes in the orthorhombic space group *P*nma with four molecules in the unit cell. The molecular unit and a view on the unit cell along 1,1,0 can be seen in **Figure 2.5**. It crystallizes with the highest density (ρ = 2.837 g cm^{-3}) within the alkali 5-aminotetrazolate series. The packing resembles with the structure of **24**, again the Cs^+ cations and atoms C1 and N5 lie on special positions. The similarity of the structures can also be seen in the vibrational spectra (see below). The crystal metric is mainly elongated along the *a* axis by about 0.63 Å, whereas the *b* and *c* axis are only ~0.1 Å longer. The volume of the unit cell in **25** is 508.05(8) Å^3 in comparison to the smaller volume in **24** (455.26(9) Å^3). These values fit to the larger ion radii of Cs^+ (1.95 Å, CN = 10) as compared to Rb^+ (1.80 Å, CN = 10).[168]

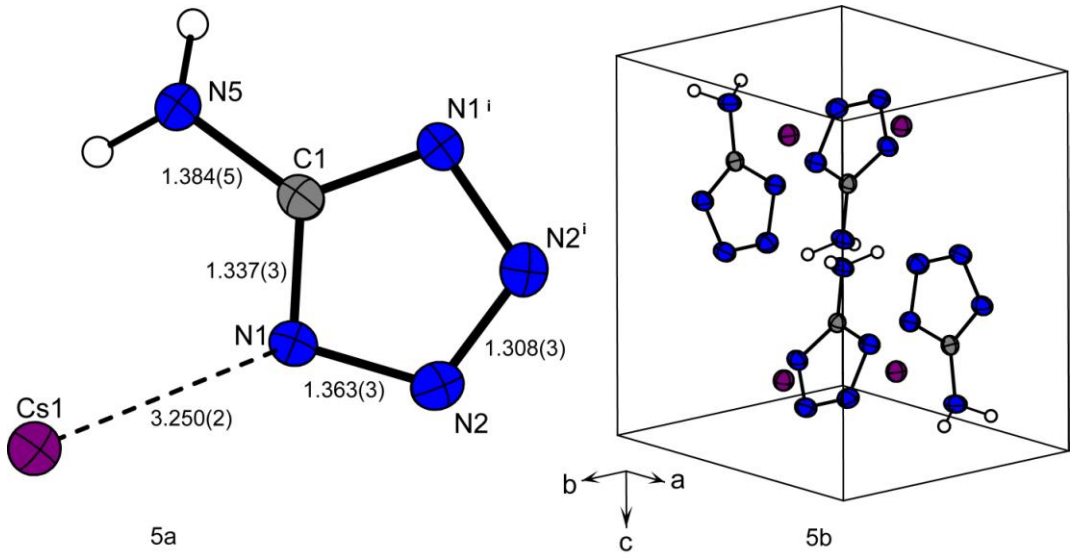

Figure 2.5 a) A view of the molecular unit of **25**, showing the atom-labeling scheme and bond-distances (Å) with standard deviations. Thermal ellipsoids represent 50 % probability and hydrogen atoms are shown as small spheres of a arbitrary radii (i = x, 0.5–y, z). b) Unit cell, view along 110.

Table 2.1 and **Table 2.2** show the relevant bond lengths, bond angles as well as selected torsion angles of the 5-aminotetrazolate anions in **21–25**.

Table 2.1 Selected angles [°]of the anions of **21–25**.

Atoms 1–2–3	1–2–3 [°]	1–2–3 [°]	1–2–3 [°]	1–2–3 [°]	1–2–3 [°]
	21	**22**	**23**	**24**	**25**
N1–N2–N3	109.7(1)	109.6(1)	109.7(1)	109.6(1)	109.6(1)
N2–N3–N4	109.3(1)	109.5(1)	109.6(1)	109.6(1)	109.6(1)
C1–N1–N2	104.3(1)	104.2(1)	104.3(1)	104.0(2)	104.1(2)
C1–N4–N3	104.3(1)	104.5(1)	104.2(1)	104.0(2)	104.1(2)
N1–C1–N4	112.4(1)	112.2(1)	112.2(1)	112.8(3)	112.6(3)
N1–C1–N5	123.3(1)	123.6(1)	124.5(1)	123.5(2)	123.7(2)
N4–C1–N5	124.2(1)	123.9(1)	123.3(1)	123.5(2)	123.7 (2)
C1–N5–H5a	114(1)	113(1)	114(1)	112(2)	115(2)
C1–N5–H5b	114(1)	112(1)	115(1)	112(2)	115(2)

Table 2.2 Selected torsion angles [°] of the anions of **21–25**.

Atoms 1–2–3–4 [°]	Tors. Angle 1–2–3–4	Tors. Angle 1–2–3–4	Tors. Angle 1–2–3–4	Tors. Angle 1–2–3–4	Tors. Angle 1–2–3–4
	21	**22**	**23**	**24**	**25**
N1–N2–N3–N4	–0.6(2)	–0.47(2)	0.4(2)	0.00(3)	0.00(3)
C1–N1–N2–N3	0.2(2)	–0.71(2)	–0.2(2)	0.5(2)	0.1(2)
N2–N3–N4–C1	0.7(2)	0.02(2)	–0.2(2)	–0.5(2)	–0.1(2)
N2–N1–C1–N5	–175.2(1)	175.0(1)	–177. 6(2)	177.3(4)	–176.5(3)
N3–N4–C1–N5	174.9(1)	–174.7(1)	177.8(2)	177.3(4)	–176.5(3)

2.3.6 Magnesium 5-aminotetrazolate tetrahydrate (**26**)

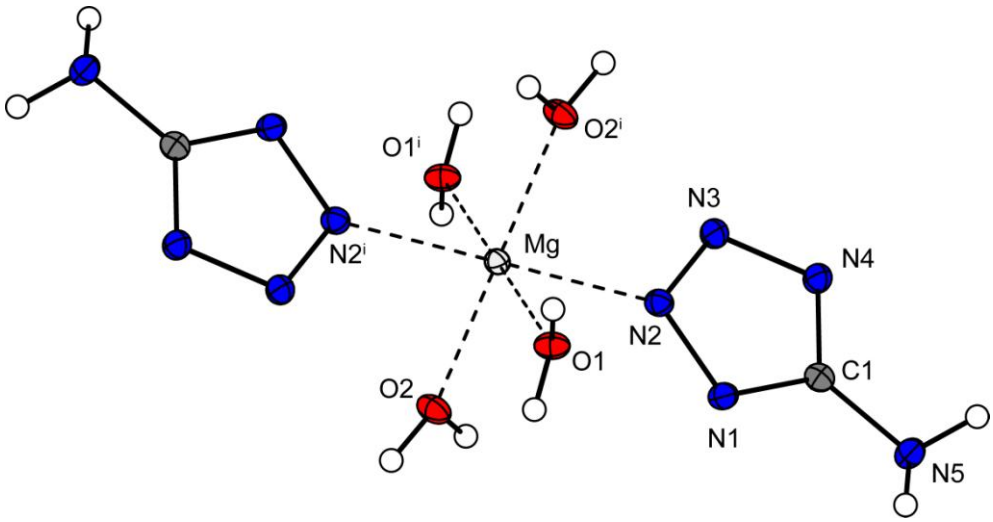

Figure 2.6 Molecular moiety of $Mg(At)_2 \cdot 4H_2O$. Hydrogen atoms shown as spheres of arbitrary radius and thermal displacements set at 50 % probability. Selected geometries: distances (Å) N1–N2 = 1.361(1), N2–N3 = 1.306(2), N3–N4 = 1.354(1), N4–C1 = 1.345(2), N1–C1 = 1.332(2), N5–C1 = 1.390(1), Mg–N2 = 2.196(1), Mg–O1 = 2.064(9), Mg–O2 = 2.059(1); angles (°) N1–C1–N4 = 112.2(1), N2–Mg–O1 = 90.90(4), N2–Mg–O2 = 92.65(5), O2–Mg–O1 = 92.30(4); i: –x, 1–y, –z.

Magnesium 5-aminotetrazolate tetrahydrate crystallizes in the triclinic space group *P*–1 with one molecular moiety in the unit cell. The molecular structure of the 5-aminotetrazolate anions is comparable to those observed for the corresponding alkali

salts. The C–N bonds within the ring show lengths of 1.345(2) (N4–C1) and 1.332(2) (N1–C1), which is between typical C–N single (1.30 Å) and C=N double (1.47 Å) bonds. The coordination of the magnesium cations located at the centre of inversion is nearly octahedral, whereby typical Mg–O and Mg–N bond lengths in the range of ~2.0–2.2 Å are observed (**Figure 2.6**). The packing of **26** is formally described as a layer structure along the *a* axis, whereby the discrete layers are connected by several hydrogen bonds, basically formed by the water molecules.

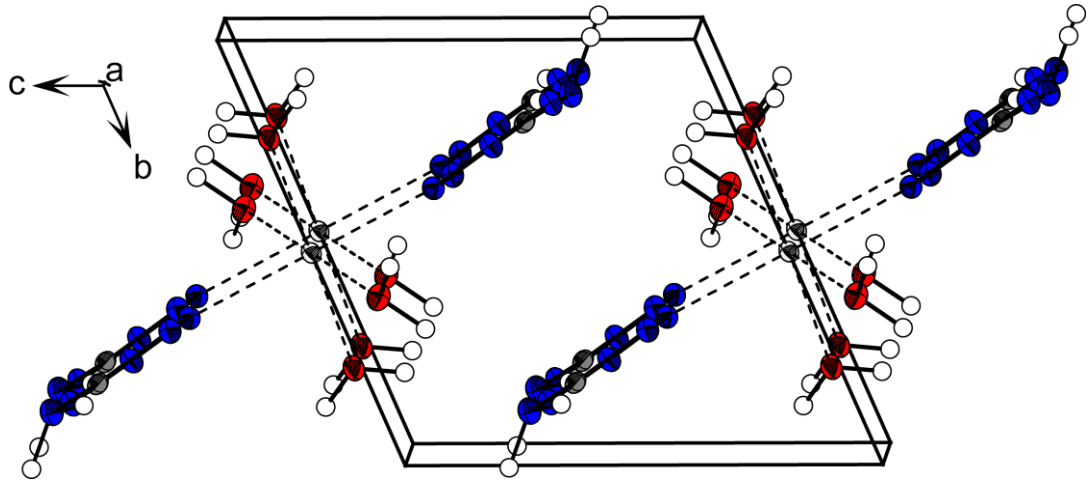

Figure 2.7 Unit cell of **26**, viewing along the *a* axis.

Although single crystals of compounds **27** and **28** have been obtained it was not possible to collect suitable datasets, since both compounds crystallize in very thin needles.

2.3.7 Barium 5-aminotetrazolate hydrate (**29**)

The structure of barium 5-aminotetrazolate (**29**) is best described by the formation of a binuclear complex, which is depicted in **Figure 2.8**. The barium atoms within one complex have a distance of 4.4462(6) Å. Both show different coordination spheres, which are build by nitrogen and oxygen atoms in the range of ~1.8–3.0 Å. The water molecules are strongly disordered.

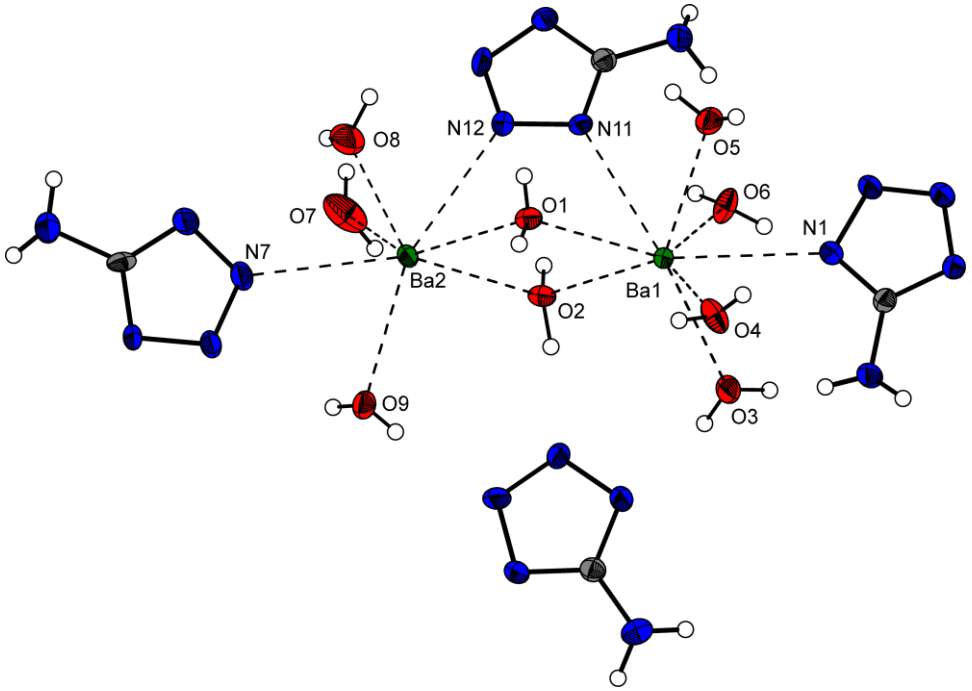

Figure 2.8 Molecular moiety of $Ba_2(At)_4 \cdot 9\ H_2O$. Hydrogen atoms shown as spheres of arbitrary radius and thermal displacements set at 50 % probability.

2.3.8 Hydrazinium 5-aminotetrazolate (**30**)

Hydrazinium 5-aminotetrazolate crystallizes as correctly published in 1958 [169] in the chiral orthorhombic space group $P2_12_12$ with four molecules in the unit cell. However, in the previously solved structure no hydrogen atoms have been located. Therefore a short reinvestigation is given in this work. The density of **30** was calculated to be 1.547 g cm^{-3}. The planar tetrazolate ring system as well as the bond lengths and angles are comparable to other 5-aminotetrazolates e.g. triaminoguanidinium 5-aminotetrazolate or alkali 5-aminotetrazolate salts in the literature.[170] The NH_2 protons of the anion do not follow the planarity of the ring system and are angulated showing torsion angles of N1–C1–N5–H5a = 31.3(2) ° and N4–C1–N5–H5b = 24.1(2)°. The hydrazine bond with an distance of 1.455(3) Å fits exactly to value observed for other tetrazole hydrazinium structures in literature, e.g. dihydrazinium bis(tetrazolato)hydrazine [171] and dihydrazinium azotetrazolate.[172] **30** forms an extensive hydrogen bond network, which could be the reason for the stability and low sensitivities. All nitrogen atoms of the anions (depicted in **Figure 2.9**) as well of the hydrazinium cations participate in hydrogen bonds.

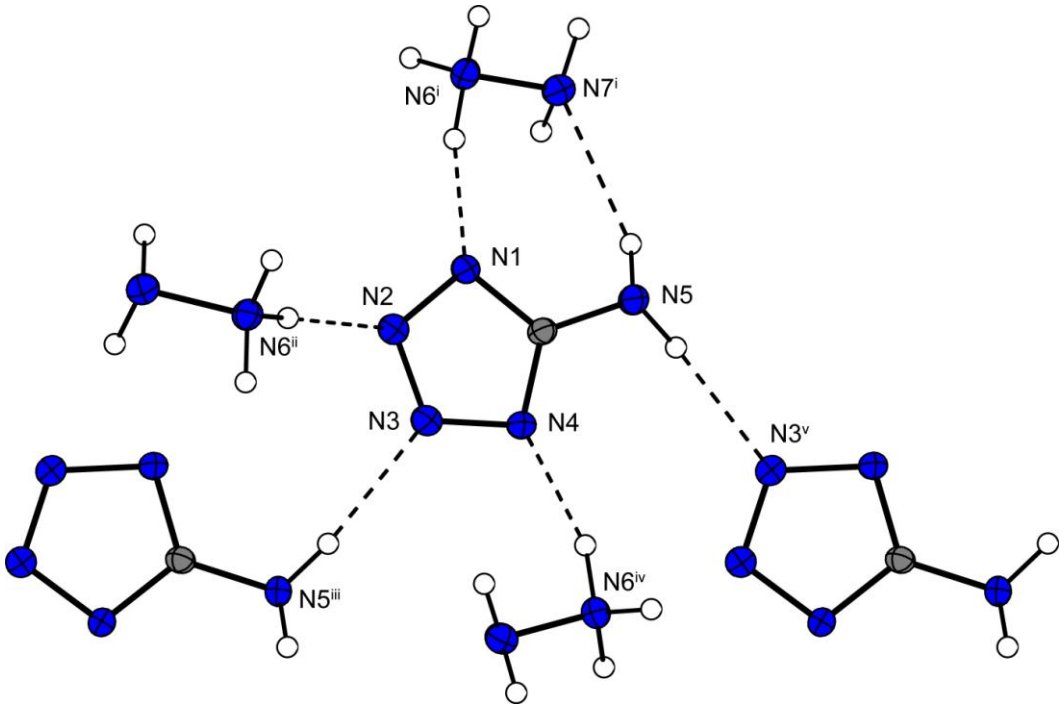

Figure 2.9 View of the hydrogen bonds of one 5-aminotetrazolate anion in hydrazinium 5-aminotetrazolate. i: x, y, 1+z; ii: 1–x, –y, z; iii: –0.5+x, 0.5–y, 1–z; iv: 1.5–x, 0.5+y, –z; v: 0.5+x, 0.5–y, 1–z. Hydrogen atoms shown as spheres of arbitrary radius and thermal displacements set at 50 % probability.

2.4 Vibrational Spectroscopy

2 and its salts **21**–**25** can be easily identified by vibrational spectroscopy. After deprotonation, the absorption band of 5–aminotetrazole at 1670–1580 cm^{-1} (C=N stretching) is found at lower wave numbers (1500–1450 cm^{-1}). In the case of **21**, there are more similarities to the protonated form due to the more covalent lithium-nitrogen bonds. The Raman spectra of the 5-At salts contain further characteristic absorption bands: 3400–3000 cm^{-1} [$\nu_{sym}(NH_2)$, $\nu_{asym}(NH_2)$], 1680–1470 cm^{-1} [ν(C=N), $\delta(NH_2)$], 1550–1350 cm^{-1} [ν(ring)], 1350–700 cm^{-1} [ν(NCN), ν(NN), γ(CN), δ tetrazolate ring], < 700 cm^{-1} [$\omega(NH_2)$]. **24** and **25**, which crystallize analogously show almost exact the same spectra.

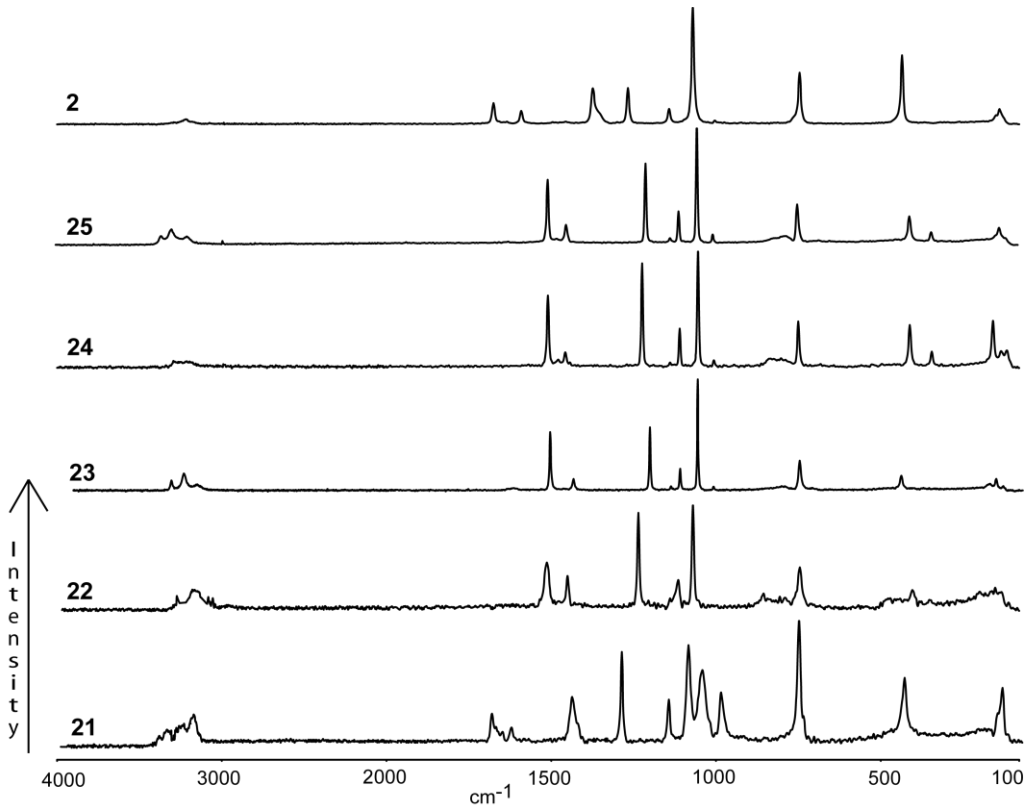

Figure 2.10 Raman spectra of 5-At (**2**) and alkali 5-aminotetrazolates (**21–25**).

2.5 Physico-Chemical Properties

2.5.1 Differential Scanning Calorimetry

DSC measurements for determining the thermal behavior of the alkali 5-aminotetrazolate salts were performed in covered Al-containers with a nitrogen flow of 20 mL min^{-1} on a Perkin-Elmer Pyris 6 DSC, at a heating rate of 5 °C min^{-1}. The melting points are given as onset temperatures. **21** shows a well-defined melting point at 196 °C, while the neutral 5-At melts under decomposition at a onset temperature of 202 °C. **22** is characterized by the loss of its crystal water below 100 °C in several imprecise steps. **22** as its trihydrate loses a undefined amount of crystal water even on standing in air and is accordingly not stable over time at ambient temperature. The further thermal behavior of **22** is characterized by a high melting point at 306 °C. Alkali salts **23**, **24** and **25** have descending melting points at 263 °C, 238 °C and 223 °C. Again, the exceptional position of the lithium salt can be seen at the lowest melting point. The heating of **24** is characterized by an irreversible first order phase transition at 197 °C.

None of the compounds show a exothermic decomposition as far as 350 °C. The DSC plots in **Figure 2.11** show the thermal behavior of ~1.5 mg of **21–25** in the temperature range from 50–350 °C.

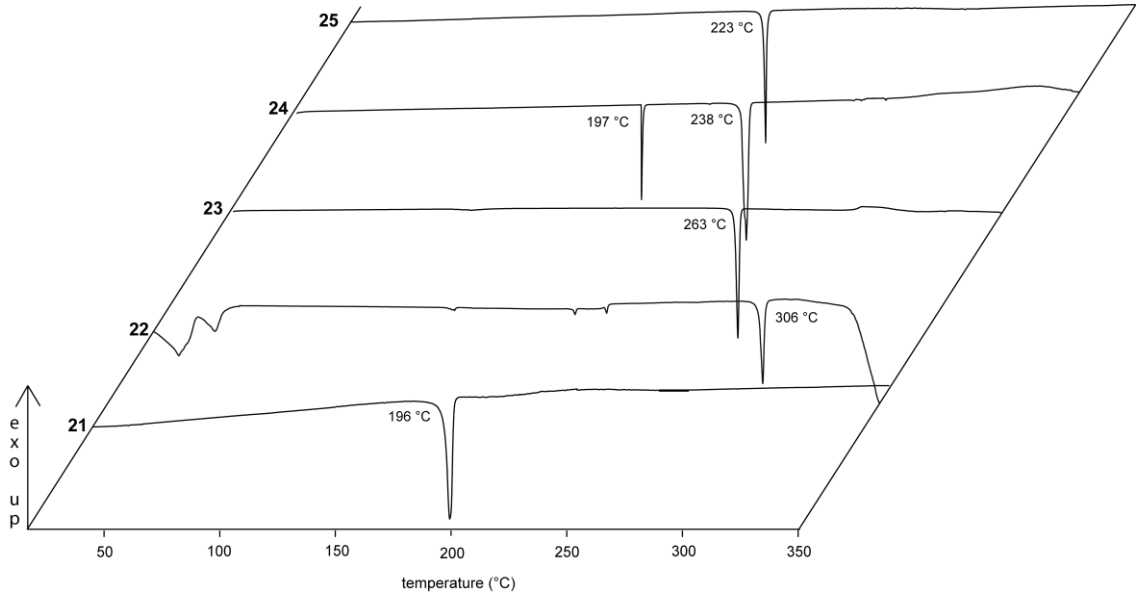

Figure 2.11 DSC plots (endo down) of compounds **21–25**. (5 °C min^{-1}); melting points, T_{onset} **21**: 196 °C, **22**: 306 °C, **23**: 263 °C, **24**: a) phase transition: 197 °C, b) melting point: 238 °C, **25**: 223 °C.

2.5.2 Bomb Calorimetry

The heats of combustion were determined as previously described in the introduction. The enthalpy of formation, $\Delta_f H°$, for each of the salts was calculated at 298.15 K using the Hess' law and the following combustion reactions. The heats of formation are summarized in **Table 2.3**.

$$LiCH_2N_5 + 7/4\ O_2 \longrightarrow 1/2\ Li_2O + CO_2\ (g) + H_2O\ (l) + 5/2\ N_2$$

$$NaCH_2N_5 * 3\ H_2O + 2\ O_2 \longrightarrow 1/2\ Na_2O_2 + CO_2\ (g) + 4\ H_2O\ (l) + 5/2\ N_2$$

$$KCH_2N_5 + 5/2\ O_2 \longrightarrow KO_2 + CO_2\ (g) + H_2O\ (l) + 5/2\ N_2$$

$$RbCH_2N_5 + 5/2\ O_2 \longrightarrow RbO_2 + CO_2\ (g) + H_2O\ (l) + 5/2\ N_2$$

$$CsCH_2N_5 + 5/2\ O_2 \longrightarrow CsO_2 + CO_2\ (g) + H_2O\ (l) + 5/2\ N_2$$

Scheme 2.3 Combustion equations of alkali salts **21–25**

2.5.3 Sensitivities and Flame Colors

For initial safety testing, the impact and friction sensitivities were tested. Except for **21**, which shows a low sensitivity towards impact (> 75 J) all compounds are insensitive neither towards impact nor friction and show no reaction under electrical discharge (tesla coil).
For testing the flame-colors the salts were combusted in the flame of a "Bunsen burner". All compounds show the cation specific flame colors summarized in **Table 2.3**.

Table 2.3 Physico-chemical properties of alkali 5-At (**21–25**).

	21	**22**	**23**	**24**	**25**
Formula	$LiCN_5H_2$	$NaCN_5H_8O_3$	KCN_5H_2	$RbCN_5H_2$	$CsCN_5H_2$
FW (g mol^{-1})	91.02	161.11	123.18	169.55	216.99
Impact sensitivity (J)[a]	> 75 J	–	–	–	–
Friction sens. (N)[b]	–	–	–	–	–
Flame color	red	orange	purple	lavender	pink
N (%)[c]	76.96 %	43.47 %	56.86 %	41.31 %	32.28%
Ω (%)[d]	–61.52 %	–39.72 %	–64.95%	–47.18 %	–36.87 %
Combustion	yes	yes	yes	yes	yes
T_{melt} (°C)[e]	196	306	263	238	223
Density (g cm–^{3})[f]	1.736	1.554	1.961	2.474	2.837
$-\Delta_c U$ (cal g^{-1})[g]	1535	980	1484	1330	1079
$-\Delta_c H°$ (kJ mol^{-1})[h]	581	657	763	942	978
$\Delta_f H°$ (kJ mol^{-1})[i]	–399	–1136	–202	–26	3

[a] BAM drophammer (grain size < 0.08–0.12 mm); [b] BAM friction tester (grain size < 0.08–0.12 mm); [c] Nitrogen content; [d] Oxygen balance; [e] Temperature of melting by DSC (β = 5 °C min^{-1}); [f] estimated from XRD; [g] Experimental (constant volume) combustion energy; [h] Experimental molar enthalpy of combustion; [i] Molar enthalpy of formation.

2.6 Energetic Properties and Detonation Experiments of Hydrazinium 5-aminotetrazolate

2.6.1 Theoretical Calculations

The enthalpies and free energies of formation were calculated according the atomization energy method, described in the introduction. For compound **30** the following energy and enthalpy of formation were calculated:

$\Delta_f H°$(**30**,s) = +373.2 kJ mol^{-1} $\Delta_f U$(**30**,s) = +3333.6 kJ kg^{-1}.

The detonation parameters calculated with the EXPLO5 program using the experimentally determined density (X-ray) are summarized in **Table 2.4**.

Table 2.4 Calculated detonation parameters for compound **30**.

	$[N_2H_5]^+[CH_2N_5]^-$ (**30**)
ρ (g cm^{-3})	1.547
Ω (%)	–75.1
Q_v (kJ kg^{-1})	–4295
T_{ex} (K)	2759
$p_{C\text{-}J}$ / kbar	296
$V_{Det.}$ (m s^{-1})	9516
V_0 (L kg^{-1})	959

ρ = density, Ω = oxygen balance, Q_v = heat of detonation, T_{ex} = detonation temperature, $p_{C\text{-}J}$ = detonation pressure, $V_{Det.}$ = detonation velocity, V_0 = Volume of detonation gases.

Particularly, the calculated velocity of detonation of 9516 m s^{-1} shows an astonishing high value. It is in the same range of these observed for HMX and CL-20. Therefore the velocity of **30** should be determined experimentally, which is described in the following.

2.6.2 Experimental Study

In order to evaluate the detonation velocity and the initiation properties of compound **30** experimentally, it was prepared on a 100 g (!) scale. The detonation velocity tests were performed in an OZM laboratory detonation chamber (model KV-250). The

measurement of the detonation velocity was performed using the OZM detonating velocity measuring system EXPLOMET-FO-2000. The use of the fiber optic technique insures excellent electrical noise immunity (**Figure 2.12**) The system used had five independent timers measuring the time intervals (in μs) between the illumination of two adjacent optical probes and calculated the velocity of detonation (m s^{-1}). The WinExplomet software package was used to transfer the results to a PC via a serial interface. For the detonation velocity measurement a 14 mm PE tube was equipped with two optical fibers in a distance of 2 cm. The amount of compound **30** used for the test was 15 g. The compound was loaded into the PE tube and manually compressed with ~50 N. As a booster charge 2 g of nitropenta (PETN) were added on top and carefully compressed manually using ~20 N force. Initiation was achieved with an electrically ignited (40 V, 5 A) PETN-SAcN detonator (1 g PETN, 0.2 g silver acetylide nitrate).

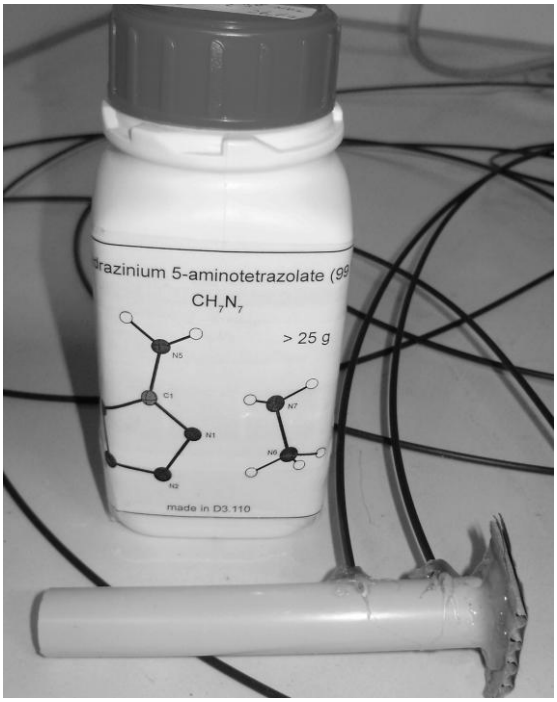

Figure 2.12 left: Setup for determination of the velocity of detonation showing a plastic tube filled with **30**. right: OZM laboratory detonation chamber (model KV-250).

Although initiation of the detonator and the booster charge were achieved without any problems, compound **30** could not be initiated using this setup. This clearly shows the insensitivity of compound **30** towards initiation even when a PETN booster charge was used. Although one could try to initiate with a RDX booster charge, for practical applications the use of a detonator that has already been fielded is always preferred.

2.6.3 Specific Impulse

Due to the failed initiation experiments, the use of **30** as fuel solid propellants was calculated and tested experimentally. The performance of propellants is best characterized by their specific impulse (I_{sp}). Moreover, for gun propellants, erosivity is an additional concern and lower reaction temperatures and a high N_2/CO ratio of the reaction gases are desirable.[173] Equally important, an increase of the I_{sp} of only 20 s would be expected to increase the payload or range by ~100 %. Moreover, smokeless combustion, which is an inherent feature of high-nitrogen compounds, is not only of environmental but particularly of strategic interest since location of the gun, missile or rocket is much more difficult.

In order to evaluate the properties of compound **30** as a potential energetic component in gun or missile propellants we calculated the specific impulses and combustion temperatures under isobaric conditions at 45 and 70 bar, representative for rocket and gun propellants, using the EXPLO5 code.

Table 2.5 summarizes the computed isobaric combustion temperatures ($T_{c,}$ the lower the better for gun-propellants), the specific impulses (I_{sp}) and the molar N_2/CO ratios for mixtures of **30** with ADN and three typical conventional gun-propellants (single-, double-, triple-base) at 70 bar.

Whereas single-base propellants are used in all guns from pistols to artillery weapons, the more powerful (see I_{sp}) double-base propellants are commonly used in pistols and mortars. The disadvantage of double-base propellants is the excessive erosion of the gun barrel (see N_2/CO ratio) by the much higher flame temperatures, and the presence of a muzzle flash (fuel-air explosion of the combustion products). In order to reduce erosion and muzzle flash, triple-base propellants with up to 50 % nitroguanidine are used in tank guns, large caliber guns and naval guns. However, the performance of triple-base propellants is lower than that of double-base propellants. A formulation of **30** with ADN (**30**:ADN = 40:60) shows a relatively low combustion temperature (comparable to single- and triple-base propellants), with excellent molar N_2/CO ratios (which are usually 0.5 for conventional propellants). The computed specific impulse for such a

mixture make a possible application of **30** as promising energetic component in erosion-reduced gun propellants very interesting.

Table 2.5 Computed propulsion parameters (70 bar chamber pressure) for formulations of **30** with ADN and for single-, double- and triple-base propellants for comparison.

O	*F*	ρ / g cm^{-3}	Ω / %	T_c / K	I_{sp} / s	N_2/CO
ADN [a]	Hy-At					
10	90	1.573	–65.0	1863	227	9.6
20	80	1.599	–55.0	1922	229	9.2
30	70	1.625	–44.9	2110	236	4.6
40	60	1.651	–34.8	2377	246	5.2
50	50	1.678	–24.7	2653	254	6.3
60	40	1.704	–14.6	2916	260	8.7
70	30	1.730	–4.5	3091	261	17.7
80	20	1.756	+5.6	2954	250	88.8
90	10	1.782	+15.7	2570	229	1440.0
NC [b]		1.66	–30.2	2750	232	0.3
NC[b]/NG (50:50)		1.63	–13.3	3287	248	0.7
NC [b]/NG [c]/NQ [d] (25:25:50)		1.70	–22.0	2663	235	1.4

[a] ADN, ammonium dinitramide; [b] NC-13.3 (N content 13.3 %); [c] NG, nitroglycerine; [d] NQ, nitroguanidine.

Table 2.6 summarized the propulsion parameters for formulations of **30** with ADN at 45 bar pressure and for a stoichiometric formulation of AP/Al which is presently used in large booster motors (e.g. ARIANE5, Space Shuttle).

A 60:40 mixture of **30** with ADN possesses a calculated specific impulse of 251 s which is ~20 s higher than that of a mixture of AP/Al commonly used in solid state boosters.
The combustion property of the 60:40 mixture (~10 g) was tested experimentally. By adding the ADN to **30**, the mixture was obtained to become a tough-flowing liquid, which may be a reason of hygroscopicity of this mixture. It was transferred to a plastic

tube and ignited using a sparkler. The resulted combustion (**Figure 2.13**) was smokeless and very homogenously over a long period of time (~2 min).

Table 2.6 Computed propulsion parameters (70 bar chamber pressure) for formulations of **30** with ADN and for an AP/Al formulation for comparison.

O	*F*	ρ / g cm^{-3}	Ω / %	T_c / K	I_{sp} / s
ADN [a]	Hy-At				
10	90	1.573	–65.0	1857	220
20	80	1.599	–55.0	1909	221
30	70	1.625	–44.9	2106	229
40	60	1.651	–34.8	2375	238
50	50	1.678	–24.7	2648	245
60	40	1.704	–14.6	2903	251
70	30	1.730	–4.5	3063	251
80	20	1.756	+5.6	2932	240
90	10	1.782	+15.7	2563	221
AP [b]	Al [c]				
70	30	2.178	–2.9	4199	232

[a] ADN, ammonium dinitramide; [b] ammonium perchlorate, [c] aluminum.

Figure 2.13 Combustion of 60:40 mixture of **30** with ADN.

2.7 Experimental Part

*Lithium 5-aminotetrazolate (**21**):* 5-Aminotetrazole (8.51 g, 100 mmol) and lithium hydroxide (2.4 g, 100 mmol) were combined and dissolved in 150 mL water. The water was evaporated and the colorless product was recrystallized from water/ethanol (1:5) yielding colorless crystals (8.30 g, 91 % yield). **DSC** (T_{onset}, 5 °C min^{-1}): 197 °C; **IR** (KBr, cm^{-1}): $\tilde{\nu}$ = 3484 (s), 3383 (s), 3275 (s), 3198 (s), 2933 (m), 2776 (m), 2631 (m), 2507 (m), 1775 (m), 1670 (s), 1641 (s), 1451 (m), 1298 (m), 1243 (w), 1159 (m), 1062 (s), 995 (m), 915 (m), 756 (m), 741 (m), 690 (w), 547 (m); **Raman** (1064 nm, 200 mW, 25 °C, cm^{-1}): $\tilde{\nu}$ = 3259 (29), 3205 (33), 2614 (18), 1694 (33), 1634 (24), 1450 (45), 1298 (77), 1155 (43), 1095 (82), 1053 (64), 996 (49), 759 (100), 437 (59), 139 (52); **^{1}H NMR** (D_2O, 25 °C, ppm): δ = 4.67 (s, NH_2); **^{13}C NMR** (D_2O, 25 °C, ppm): δ = 157.1; **EA** (CH_2N_5Li, 91.05): calcd. C 13.20, H 2.22, N 76.96 %; found: C 13.03, H, 2.30, N 76.79 %.

*Sodium 5-aminotetrazolate trihydrate (**22**):* 5-Aminotetrazole (8.51 g, 100 mmol) and sodium hydroxide (4.0 g, 100 mmol) were combined and solved in 150 mL water. The water was evaporated and the colorless product was recrystallized from a small amount of hot water (11.21 g, 68 % yield). **DSC** (T_{onset}, 5 °C min^{-1}): 306 °C; **IR** (KBr, cm^{-1}): $\tilde{\nu}$ = 3591 (s), 3415 (s), 3389 (s), 3266 (s), 3190 (s), 2267 (w), 1644 (s), 1520 (s), 1454 (m), 1298 (w), 1233 (m), 1137 (m), 1111 (m), 1067 (m), 1011 (w), 848 (m), 800 (m), 756 (m), 717 (m), 594 (m); **Raman** (1064 nm, 200 mW, 25 °C, cm^{-1}): $\tilde{\nu}$ = 3178 (39), 1512 (59), 1450 (49), 1235 (94), 1114 (45), 1069 (100), 853 (35), 745 (55), 403 (39), 152 (41); **^{1}H NMR** (D_2O, 25 °C, ppm): δ = 4.67 (s, NH_2); **^{13}C NMR** (D_2O, 25 °C, ppm): δ = 164.3; **EA** ($CH_8N_5NaO_3$, 161.05): calcd. C 7.46, H 5.01, N 43.47 %; found: C 7.61, H 4.72, N 43.28 %.

*Potassium 5-aminotetrazolate (**23**):* 5-Aminotetrazole (4.25 g, 50 mmol) and potassium carbonate (3.5 g, 25 mmol) were added to 150 mL water. The solution was heated until the release of CO_2 stopped. The water was evaporated and the colorless product was recrystallized from a hot water/ethanol (1:4) mixture (590 mg, 96 % yield). **DSC** (T_{onset}, 5 °C min^{-1}): 267 °C; **IR** (KBr, cm^{-1}): $\tilde{\nu}$ = 3390(s), 3310 (m), 3325 (m), 2730 (w), 2241 (w), 2137 (w), 1737 (w), 1704 (w), 1688 (w), 1637 (s), 1635 (s), 1564 (m), 1502 (vs), 1473 (m), 1454 (s), 1208 (s), 1139 (s), 1111 (s), 1057 (m), 1008 (m), 802 (s), 744 (m),

687 (m), 665 (m), 484 (w); **Raman** (1064 nm, 200 mW, 25 °C, cm^{-1}): $\tilde{\nu}$ = 3390 (9), 3313 (16), 3229 (6), 1631 (3), 1517 (53), 1445 (11), 1207 (57), 1142 (4), 1114 (20), 1058 (100), 1010 (4), 799 (4), 742 (27), 426 (14), 151 (6), 132 (11); **^{1}H NMR** (d_6-DMSO, 25 °C, ppm): δ = 4.09 (s, NH_2); **^{13}C NMR** (d_6-DMSO, 25°C, ppm): δ = 164.8; **EA** (CH_2KN_5, 122.99): calcd. C 9.75, H 1.64, N 56.86 %; found: C 9.73, H 1.68, N 56.48 %.

*Rubidium 5-aminotetrazolate (**24**):* 5-Aminotetrazole (4.25 g, 50 mmol) and rubidium carbonate (5.77 g, 25 mmol) were added to 150 mL water. The solution was heated for five minutes until the release of CO_2 stopped. The water was evaporated and the colorless product was recrystallized from a water/ethanol (1:5) mixture (760 mg, 90 % yield). **DSC** (T_{onset}, 5 °C min^{-1}): 238 °C; **IR** (KBr, cm^{-1}): $\tilde{\nu}$ = 3391 (s), 3310 (s), 3226 (s), 2240 (w), 1633 (s), 1515 (s), 1454 (m), 1208 (m), 1138 (m), 1111 (m), 1058 (w), 1008 (w), 805 (m), 745 (m), 707 (m), 689 (m); **Raman** (1064 nm, 200 mW, 25 °C, cm^{-1}): $\tilde{\nu}$ = 3283 (85), 1509 (62), 1453 (9), 1223 (90), 1109 (34), 1054 (100), 750 (40), 411 (37), 340 (8), 159 (40); **^{1}H NMR** (D_2O, 25 °C, ppm): δ = 4.79 (s, NH_2); ^{13}C NMR (D_2O, 25 °C, ppm): δ = 164.6; **EA** (CH_2N_5Rb, 168.94): calcd. C 7.08, H 1.19, N 41.31 %; found: C 7.14, H 1.18, N 41.50 %.

*Cesium 5-aminotetrazolate (**25**):* 5-Aminotetrazole (4.25 g, 50 mmol) and cesium carbonate (8.15 g, 25 mmol) were added to 150 mL water. The solution was heated for five minutes until the release of CO_2 stopped. The water was evaporated and the colorless product was recrystallized from a small amount of hot water (931 mg, 86 % yield). **DSC** (T_{onset}, 5 °C min^{-1}): 223 °C; **IR** (KBr, cm^{-1}): $\tilde{\nu}$ = 3372 (s), 3214 (s), 2762 (m), 2257 (m), 2133 (m), 1643 (s), 1523 (s), 1508 (s), 1453 (s), 1384 (m), 1239 (w), 1221 (m), 1137 (s), 1111 (s), 1050 (m), 1004 (m), 782 (s), 746 (m), 721 (m), 669 (m), 477 (m); **Raman** (1064 nm, 200 mW, 25 °C, cm^{-1}): $\tilde{\nu}$ = 3358 (7), 3296 (13), 3201 (7), 1506 (56), 1450 (17), 1209 (70), 1108 (29), 1050 (100), 1005 (9), 749 (35), 408 (24), 342 (11), 136 (15); **^{1}H NMR** (D_2O, 25 °C, ppm): δ = 4.78 (s, NH_2); **^{13}C NMR** (D_2O, 25°C, ppm): δ = 164.7; **EA** (CH_2CsN_5, 216.94): calcd. C 5.54, H 0.93, N 32.28 %; found: C 5.56, H 0.95, N 32.29 %.

*General procedure of synthesis of **26–29**:* To 5-aminotetrazole (9.50 g, 0.1 mol) and half an equivalent of an alkaline earth metal hydroxide (magnesium hydroxide (2.91 g, 0.05 mol), calcium hydroxide (3.7 g, 0.05 mol), strontium hydroxide octahydrate (13.29 g, 0.05 mol), barium hydroxide octahydrate (15.58, 0.05 mol)) 100 mL water was

added and the mixture was heated to reflux for 10 min. The solution was filtrated and left for crystallization.

*Magnesium 5-aminotetrazolate tetrahydrate (**26**):* **DSC** (T_{onset}, 5 °C min^{-1}): 324 °C; **IR** (KBr, cm^{-1}): $\tilde{\nu}$ = 3434 (s), 3374 (s), 3163 (s), 2395 (m), 2301 (m), 2170 (w), 1648 (m), 1528 (s), 1458 (m), 1382 (m), 1253 (m), 1160 (m), 1141 (s), 1083 (m), 1028 (w), 873 (s), 784 (m), 752 (m), 716 (m), 694 (m), 464 (w); **Raman** (1064 nm, 200 mW, 25 °C, cm^{-1}): $\tilde{\nu}$ = 3372 (11), 3154 (14), 1520 (39), 1454 (14), 1255 (62), 1142 (45), 1083 (100), 1031 (11), 888 (15), 750 (38), 418 (22), 364 (11), 219 (19), 186 (40), 130 (13); **^{1}H NMR** (D_2O, 25 °C, ppm): δ = 4.78 (s, NH_2); **^{13}C NMR** (D_2O, 25 °C, ppm): δ = 164.5; **EA** ($C_2H_{12}MgN_{10}O_4$, 264.49): calcd. C 9.08, H 4.57, N 52.96 %; found: C 9.10, H 4.50, N 52.63 %.

*Calcium 5-aminotetrazolate tetrahydrate (**27**):* **DSC** (T_{onset}, 5 °C min^{-1}): 350 °C; **IR** (KBr, cm^{-1}): $\tilde{\nu}$ = 3422 (s), 3350 (s), 2363 (w), 2171 (w), 1648 (m), 1622 (m), 1541 (m), 1519 (m), 1451 (m), 1384 (m), 1232 (m), 1176 (m), 1124 (m), 1104 (m), 1009 (w), 765 (m), 576 (m); **Raman** (1064 nm, 200 mW, 25 °C, cm^{-1}): $\tilde{\nu}$ = 3235 (13), 2986 (32), 1616 (14), 1553 (23), 1445 (12), 1234 (37), 1140 (22), 1127 (34), 1067 (100), 1007 (11), 750 (33), 430 (22), 170 (23), 186 (40), 130 (13); **^{1}H NMR** (D_2O, 25 °C, ppm): δ = 3.80 (s, NH_2); **^{13}C NMR** (D_2O, 25 °C, ppm): δ = 163.5; **EA** ($C_2H_{12}CaN_{10}O_4$, 280.26): calcd. C 8.57, H 4.32, N 49.98 %; found: C 8.66, H 4.04, N 50.24 %.

*Strontium 5-aminotetrazolate tetrahydrate (**28**):* **DSC** (T_{onset}, 5 °C min^{-1}): 354 °C; **IR** (KBr, cm^{-1}): $\tilde{\nu}$ = 3440 (s), 3350 (s), 2168 (w), 1650 (m), 1616 (m), 1547 (m), 1521 (m), 1453 (m), 1414 (m), 1226 (m), 1177 (m), 1126 (m), 1088 (m), 1004 (w), 763 (m), 594 (m), 432(m); **Raman** (1064 nm, 200mW, 25°C, cm^{-1}): $\tilde{\nu}$ = 3175 (13), 2986 (32), 1616 (14), 1553 (23), 1445 (12), 1234 (37), 1140 (22), 1127 (34), 1067 (100), 1007 (11), 750 (33), 430 (22), 170 (23), 186 (40), 130 (13); **^{1}H NMR** (D_2O, 25 °C, ppm): δ = 4.79 (s, NH_2); **^{13}C NMR** (d_6-DMSO, 25 °C, ppm): δ = 162.2; **EA** ($C_2H_{12}N_{10}O_4Sr$, 327.80): calcd. C 7.33, H 3.69, N 42.73 %; found: C 7.29, H 3.65, N 41.65 %.

*Barium 5-aminotetrazolate · 4.5 H_2O (**29**):* **DSC** (T_{onset}, 5 °C min^{-1}): 359 °C; **IR** (KBr, cm^{-1}) $\tilde{\nu}$ = 3411 (s), 3350 (s), 2263 (w), 2145 (w), 1625 (m), 1521 (m), 1439 (m), 1381 (w), 1236 (w), 1156 (w), 1127 (m), 1013 (w), 754 (m), 600 (m); **Raman** (1064 nm, 200 mW, 25 °C, cm^{-1}): $\tilde{\nu}$ = 3264 (25), 3129 (21), 1935 (19), 1611 (24), 1540 (45), 1442 (27),

1225 (38), 1128 (60), 1069 (100), 1012 (27), 744 (45), 430 (28), 334 (28), 200 (33); **^{1}H NMR** (D_2O, 25 °C, ppm): δ = 4.79 (s, NH_2); **^{13}C NMR** (D_2O, 25 °C, ppm): δ = 162.3; **EA** ($C_2H_{12}BaN_{10}O_4$, 377.51): calcd. C 6.36, H 3.20, N 37.10 %; found: C 6.40, H 3.21, N 37.15 %.

*Hydrazinium 5-aminotetrazolate (**30**): Method 1:* 5-Aminotetrazole (42.54g, 0.5 mol) was suspended in 300 mL of THF (dry, over mol. sieves) and the suspension was heated to 50 °C. Hydrazine (1M in THF, 500 mL, 0.5 mol) was added in small portions under vigorous stirring. Insoluble hydrazinium 5-aminotetrazolate formed instantaneously as a white, flocculent precipitate in quantitative yields. After being stirred for further 5 minutes, the solid was filtered off and dried. The crude product was recrystallized from hot ethanol. *Method 2:* 5-Aminotetrazole (42.54 g, 0.5 mol) was suspended in 100 mL water and heated to 50 °C. Hydrazinium hydrate 25.03 g, 0.5 mol) was added drop wise to the suspension until the 5-aminotetrazole was completely deprotonated and the solution was clear. The water was removed under reduced pressure and the crude product was recrystallized from ethanol. **DSC** (T_{onset}, 5 °C min^{-1}): 118–122 °C (mp.), 186 °C (dec.); **IR** (KBr, cm^{-1}): $\tilde{\nu}$ = 3405 (vs), 3351 (vs), 3290 (vs), 3195 (s), 2964 (s), 2721 (s), 2160 (m), 1630 (s), 1522 (s), 1442 (m), 1232 (m), 1106 (s), 1083 (s), 961 (m), 939 (m), 756 (w), 658 (w), 558 (w); **Raman** (1064 nm, 400 mW, 25 °C, cm^{-1}): $\tilde{\nu}$ = 3286 (17), 3181 (21), 1630 (14), 1523 (56), 1452 (17), 1235 (55), 1116 (32), 1085 (30), 1064 (100), 1009 (17), 962 (22), 941 (30), 758 (29), 427 (25), 229 (30); **^{1}H NMR** (d_6-DMSO, 25 °C, ppm): δ = 7.43 (s); **^{13}C NMR** (d_6-DMSO, 25 °C, ppm): δ = 161.5(CN_4); **^{15}N NMR** (d_6-DMSO, 25 °C, ppm): δ = –8.0 (N1), −116.4 (N2), −332.0 (H_2N–NH_3^+), –342.4 (N5); ***m/z*** (FAB^+): 33 (100); ***m/z*** (FAB^-): 84 (100); **EA** (CH_7N_7, 117.11): calcd.: C 10.26, H 6.02, N 83.72 %; found: C 10.65, H 5.72, N 83.85 %; **impact sensitivity**: 100 J; **friction sensitivity**: > 360 N; **ESD**: 3.0 J; **Flame test**: low flammable.

2.8 Conclusion

From this studies of 5-aminotetrazolate salts the following conclusions can be drawn:

- 5-Amino-1*H*-tetrazole (**2**) can be easily deprotonated in aqueous solution using alkali and alkali earth metal hydroxides or carbonates forming the corresponding 5-aminotetrazolate salts (**21–29**) in nearly quantitative yields. The reaction of

hydrazine hydrate or hydrazine solution (in THF) yields hydrazinium 5-aminotetrazolate.

- **21–29** can be recrystallized from water/ethanol mixtures yielding to single crystals. Except for the calcium and strontium salts, since these compounds crystallize in very thin needles, all salts were determined by low temperature X-ray diffraction.

- The crystal structures of lithium 5-aminotetrazolate (**21**), sodium 5-aminotetrazolate trihydrate (**22**), potassium 5-aminotetrazolate (**23**), rubidium 5-aminotetrazolate (**24**), cesium 5-aminotetrazolate (**25**), magnesium 5-amino-tetrazolate tetrahydrate (**26**) and barium 5-aminotetrazolate hydrate (**29**) were determined using low-temperature single crystal diffraction.

- A comprehensive analytical characterization of the chemical and thermo-chemical properties and sensitivities of **21–25** is given. The thermal behavior is characterized by defined melting points and no decompositions till 350 °C. **24** shows a first order phase transition at 197 °C. The heats of formation were calculated using bomb calorimetric measurements and step up endothermic within the alkali row. All compounds are in spite of their high nitrogen content non energetic materials with characteristic flame colors and are safe to handle. Except for **21**, which shows a very low impact sensitivity of more than 75 J, all compounds are insensitive towards friction and impact.

- Extremely high detonation parameters ($V_{Det.}$ ~ 9500 m s^{-1}) have been computed for **30**. However, it was not possible to initiate **30** even with PETN based priming charges.

- Hydrazinium 5-aminotetrazolate (**30**) is a promising nitrogen-rich salt, which may be suitable as a powerful, low-erosive, smokeless and environmentally benign ingredient for gun-propellants and solid boosters. A mixture of **30** and ADN (ammonium dinitramide) becomes liquid and shows consistently and smokeless combustion.

Chapter 3.

Nitrogen-Rich Perchlorates and Dinitramides

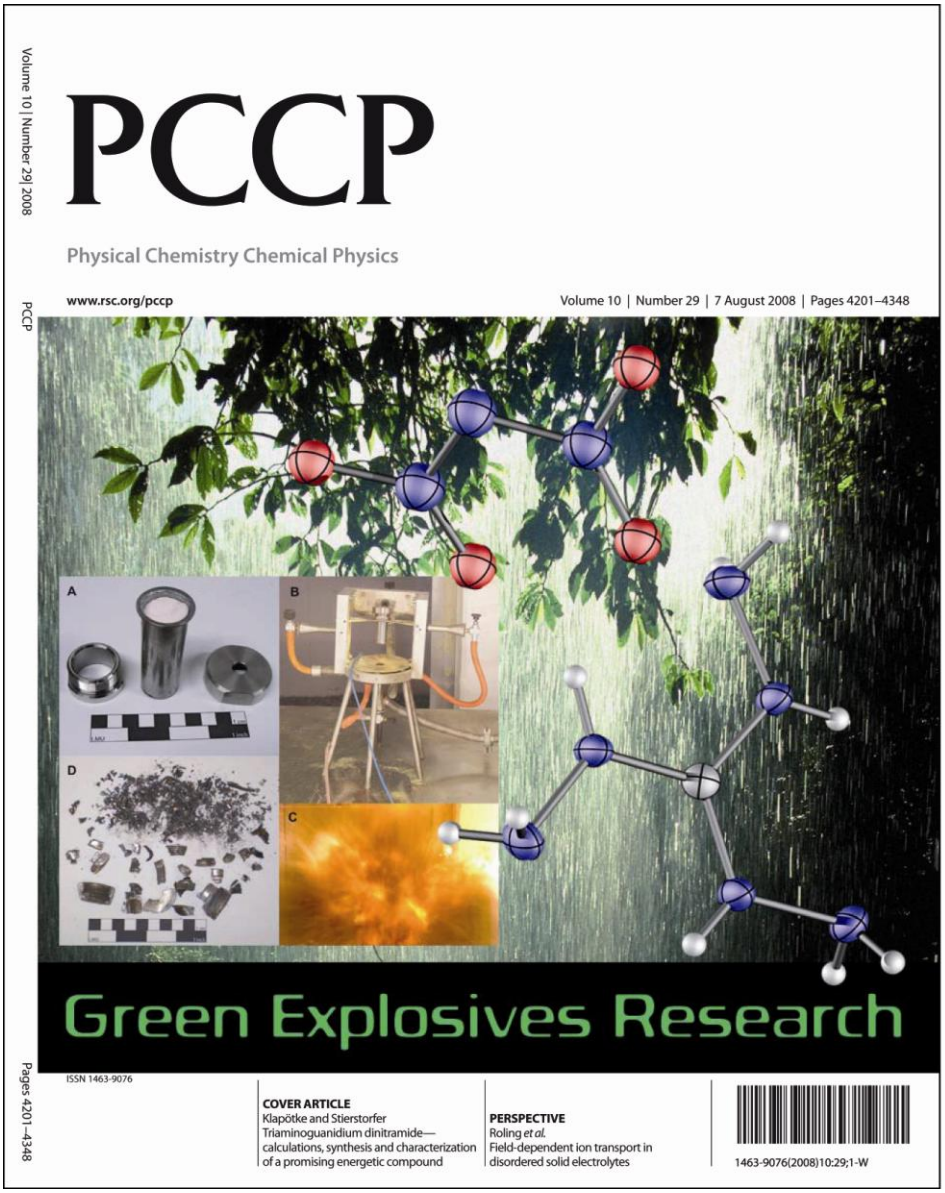

3.1 Introduction

The following chapter describes the synthesis of tetrazolium dinitramides and other nitrogen rich cations in combination with the dinitramide anion. These are 5-aminotetrazolium dinitramide (**31**), azidoformamidinium dinitramide (**32**), 1,5-diaminotetrazolium dinitramide (**33**), 1-methyl-5-aminotetrazolium dinitramide (**34**), 2-methyl-5-aminotetrazolium dinitramide (**35**), 5*H*-tetrazolium dinitramide (**36**) and triaminoguanidinium dinitramide (**37**). Many salts with oxygen rich counter-anions have been prepared as mentioned in the introduction. Interestingly, only few salts include the highly energetic dinitramide. The reason may be, that there is still a misbelieve in the strongness of dinitramine acid, which indeed is a very strong acid (p*K*s = –5.6).[174] Salts containing the dinitramide anion, $N(NO_2)_2^-$ (DN),[175] are of potential interest as high explosives, gas generators or components in propellants or propellant charges.[176,64,177,178] At present more than 90% of the energetic materials used for industrial purposes are ammonium nitrate based.[179] The development of nitrogen-rich *HEDMs* [30] is an ongoing area of interest in our research group. The first generation of high-nitrogen compounds such as hydrazinium azotetrazolate (HZT) [180] and triaminoguanidinium azotetrazolate (TAGZT),[72] did indeed meet the criteria for being nitrogen-rich and have proven to be very desirable ingredients in erosion-reduced gun propellants. However, due to the unfavorable oxygen balance (Ω) such compounds are not suitable as energetic fillers in high explosive compositions.

The oxygen balance indicates the relative amount of oxygen available for the ideal combustion reactions without adding outer oxygen: carbon to carbon dioxide, hydrogen to water and sulfur to sulfur dioxide. The oxygen balance can be easily calculated by the equation: $\Omega\ (\%) = (w\mathrm{O} - 2x\mathrm{C} - 1/2y\mathrm{H} - 2z\mathrm{S})1600/M$. ($w$: number of oxygen atoms, x: number of carbon atoms, y: number of hydrogen atoms, z: number of sulfur atoms, M: molecular weight). The compound is said to have a positive oxygen balance if it contains more oxygen than is needed for the combustion. It then belongs to the class of "oxidizer". A negative oxygen balance exists if it contains less oxygen than is needed. The combustion will then be incomplete and significant amounts of toxic gases like carbon monoxide will be emerged. Compounds with a negative oxygen balance are related to the class of "fuels".

The second generation of high-nitrogen energetic materials such as 5-aminotetrazolium dinitramide (HATDN, **31**) and azidoformamidinium dinitramide (AFDN, **32**) presented

in this chapter combine desirable high nitrogen contents and also very good oxygen balance and such compounds are therefore suitable for use in high-explosive formulations.[181] Moreover, due to the balanced oxygen situation these compounds will also be suitable as powerful ingredients in solid rocket propellants. High energetic salts have the main advantages of often possessing a high thermal stability, a low vapor pressure and higher densities, due to their lattice energies.[145,182] Many N-rich dinitramides like guanidinium dinitramide,[183] aminoguanidinium dinitramide,[184] bisguanidinium dinitramide,[185] 1,4-dimethyl-5-aminotetrazolium dinitramide,[68] 1,5-diamino-4-methyltetrazolium dinitramide [186] were synthesized and characterized as energetic materials. 5-Aminotetrazolium dinitramide (**31**) has also been described as an energetic material for potential applications as a gas generator in literature.[64,178,187] However, no spectroscopic data are available, the synthesis described uses non commercially available barium dinitramide and the thermal behavior and several energetic properties were proofed to be wrong. Azidoformamidinium dinitramide (**32**) has never been synthesized and was only mentioned in theoretical calculations.[177] The azidoformamidinium cation is a highly energetic N-rich cation, which, unfortunately, often shows high sensitivities and low decomposition temperatures. Azidoformamidinium, which is obtained by the reaction of nitrous acid with aminoguanidine, [188,189] undergoes cyclization under basic conditions and 5-aminotetrazole is formed (**Scheme 3.1**). The azidoformamidinium and 5-aminotetrazolium cations have the same sum formula and are therefore isomers.

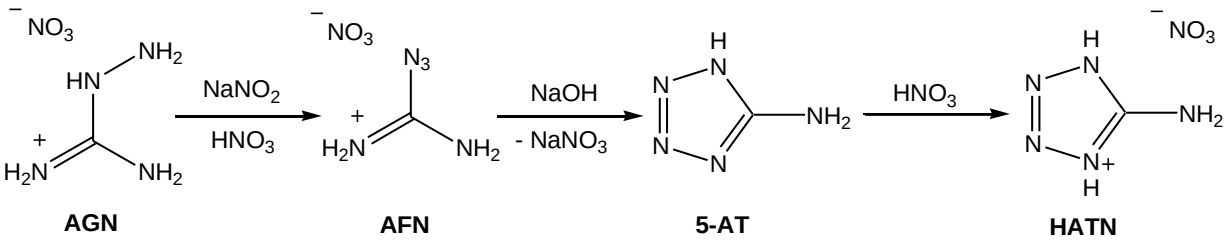

Scheme 3.1 Isomerization of azidoformamidinium nitrate (**AFN**) to 5-amino-tetrazolium nitrate (**HATN**).

The following chapter also includes the synthesis and characterization of the new compound 1,5*H*-tetrazolium dinitramide (**36**). This compound has only been mentioned in two dubious patents [187] for use as ingredients in propellant systems. However, for example, the highly hygroscopic character was not mentioned. Therefore **36** is more of academic interest or can be used at least in water based liquid propellants. Also 1,4*H*-

tetrazolium perchlorate is rarely described [190,191] and a comprehensive characterization cannot be found. **36** and **42** are the first protonated 1,4*H*-tetrazoles, which are characterized by single X-ray crystallography. This is a consequence, since the protonation of 1*H*-tetrazole requires very strong acids. Compounds **31** and **32** are characterized by an oxygen balance [192] of Ω = 0, which is as mentioned before always desirable for energetic materials but reached only in a few compounds, e.g. a) ethylene glycol dinitrate,[193] b) nitroisobutylglycerol trinitrate [194] and c) bis(2,2,2-trinitroethyl)urea [195] which are shown in **Figure 3.1**. Next to bis(2,2,2-trinitroethyl)urea, isomers **31** and **32** are the second crystallographic determined compounds with Ω = 0. In addition, next to triazidocarbenium dinitramide, **32** is the second compound, which carries both an azide as well as a dinitramide group combined in one compound.

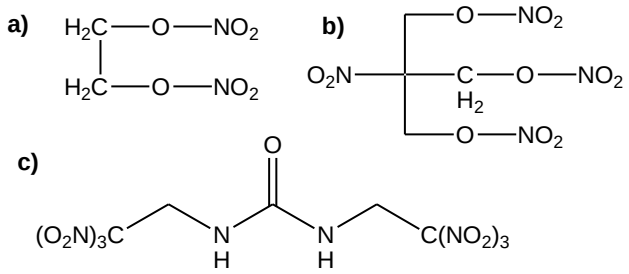

Figure 3.1 Compounds with a balanced oxygen content. a) ethylene glycol dinitrate ($C_2H_4N_2O_6$), b) nitroisobutylglycerol trinitrate ($C_4H_6N_4O_{11}$), c) bis(2,2,2-trinitroethyl)urea ($C_5H_6N_8O_{13}$).

All dinitramide salts have been prepared by the reaction of the corresponding perchlorate and potassium dinitramide under precipitation of low soluble potassium perchlorate. Since most of the desired perchlorates are unknown or insufficiently described, appropriate syntheses and a comprehensive characterization of the perchlorate salts, 5-aminotetrazolium perchlorate (**38**), aminoguanidinium perchlorate (**39**), triaminoguanidinium perchlorate (**40**), azidoformamidinium perchlorate (**41**) and tetrazolium perchlorate (**42**) are described in this chapter. Perchlorate salts are, in spite of their toxicity,[196] still used in many energetic compositions [197] since they are, despite of their high oxygen content, often more stable and less sensitive than the corresponding chlorates due to a steric (kinetic) barrier.[198] Ammonium perchlorate [199] for example is used in combinations with aluminum as the solid propellant [200] in boosters of the space shuttle. Potassium perchlorate is still used in pyrotechnic compositions for accomplishing a suitable oxygen balance.[192] This and further special energetic

properties can be fulfilled by combining nitrogen rich cations with the ClO_4^- anion. Since the pK_s of perchloric acid is very low (–10) [201] salts can be prepared even in combination with different tetrazole derivatives, *e.g.* 1,5-diaminotetrazole or 1-methyl-5-aminotetrazole.[202,203,68] Also some guanidinium perchlorate salts are known but rarely described and only a few crystal structures of guanidinium perchlorate [204] as well as 1-carbamoylguanidine [205] and biguanidine [206] have been reported in the literature. In this work we present a full characterization, including the crystal structures and properties, of three cationic derivatives of guanidine as their perchloric salts.[207] These compounds, namely aminoguanidinium perchlorate (**39**, $AGClO_4$), triaminoguanidinium perchlorate (**40**, $TAGClO_4$) and azidoformamidinium perchlorate (**41**, $AFClO_4$) are not only interesting energetic derivatives but can also be used as synthetic building blocks in the preparation of further nitrogen rich salts by the reaction of potassium salts with the formation of low soluble potassium perchlorate.

3.2 Synthesis of Nitrogen-Rich Perchlorates

5-Amino-1*H*-tetrazole (**2**) is a weak base, which is only protonated by strong acids ($pK_a \leq 0$) under normal conditions. 5-At was reacted with an excess of perchloric acid in water at room temperature, yielding 5-amino-1*H*-tetrazolium perchlorate (**38**) (**Scheme 3.2**) after storing the reaction mixture in the fridge for three weeks. When an equivalent amount of diluted perchloric acid was used, the reaction was incomplete and an adduct between **38** and 5-At (**2**) was formed.[132] An alternative synthesis of **38** is the reaction of 5-amino-1*H*-tetrazolium bromide with anhydrous silver perchlorate either in methanol or ethanol.

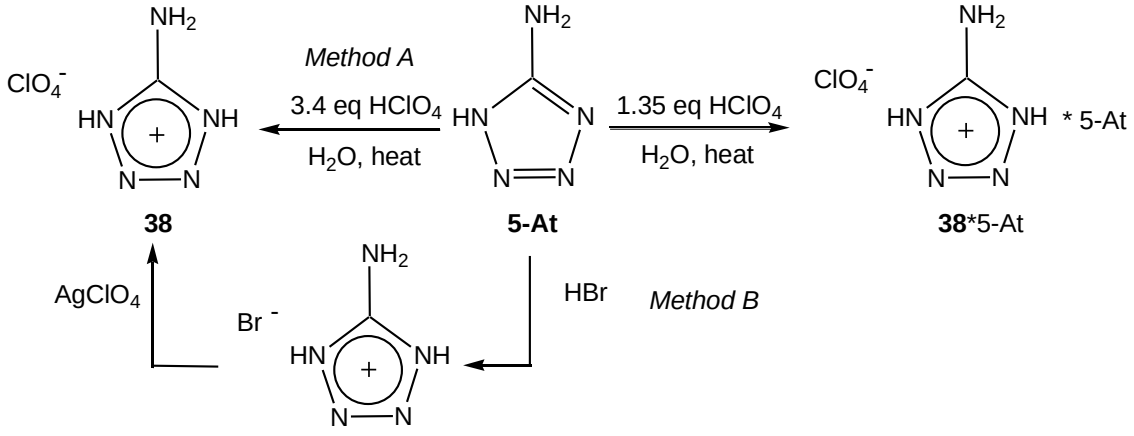

Scheme 3.2 Synthesis of the perchlorate salt **38** and its 5-aminotetrazole adduct.

The perchlorate salts (**39–45**) were synthesized according to **Scheme 3.3**. Aminoguanidinium perchlorate ($AGClO_4$, **39**) is obtained by neutralization of the cheap starting material aminoguanidinium hydrogen carbonate using one equivalent of perchloric acid solution. After completion of the CO_2 release the product was isolated by evaporation and was recrystallized from ethanol.[131]

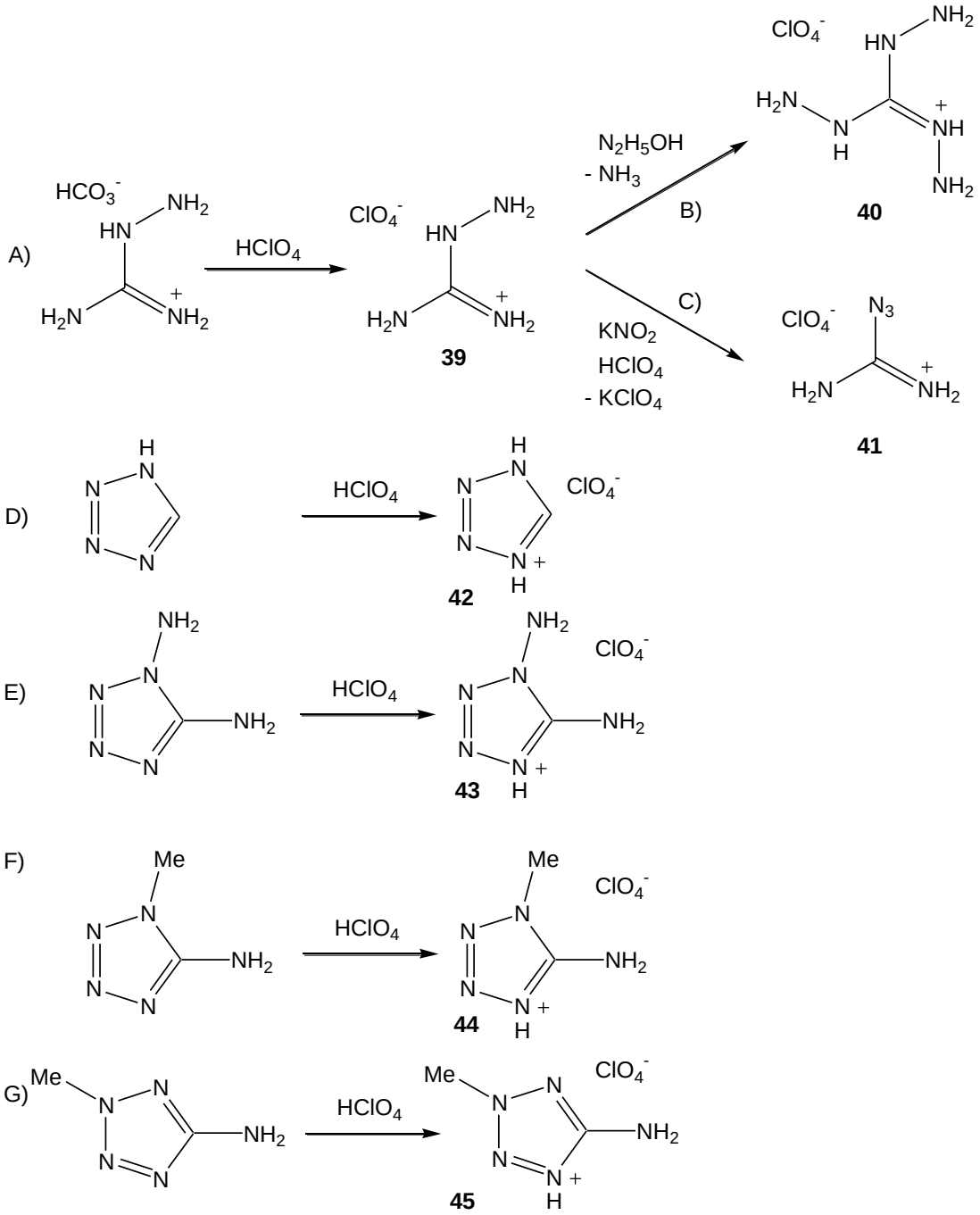

Scheme 3.3 Synthesis of the perchlorate alts **39–45**.

$TAGClO_4$ (**40**) was formed in excellent yields by the reaction of $AGClO_4$ (**39**) with an excess of hydrazinium hydrate in dioxane as the solvent. The end of the reaction can be easily detected by cessation of NH_3 release while refluxing the mixture at ~80 °C.

$AFClO_4$ (**41**) was obtained by the reaction of the hydrazine group of **$AGClO_4$** (**39**) with HNO_2, formed from potassium nitrite in dilute aqueous perchloric acid solution. After filtration of $KClO_4$ the product was isolated simply by removing the solvent.

1*H*-Tetrazolium perchlorate (**42**) is obtained by the reaction of 1*H*-tetrazole with an equivalent amount of 1 N perchloric acid. Single crystals of highly hygroscopic **42** were obtained by slow evaporation of an ethanol solution under high vacuum conditions. The product should be stored under dry nitrogen or argon. *It should be also mentioned that all nitrogen-rich perchlorates show increased sensitivities towards impact and friction and belong to the class of primary explosives.*

Diaminotetrazolium perchlorate (**43**) as well as 1-methyl-5-aminotetrazolium perchlorate (**44**) and 2-methyl-5-aminotetrazolium perchlorate (**45**) were prepared according to recently published procedures of our research group.[202,68]

3.3 Synthesis of Nitrogen-Rich Dinitramides

5-Aminotetrazolium dinitramide (**31**), azidoformamidinium dinitramide (**32**), 1,5 diaminotetrazolium dinitramide (**33**), 1*H*-tetrazolium dinitramide (**34**) 1-methyl-5-aminotetrazolium dinitramide (**35**), 2-methyl-5-aminotetrazolium dinitramide (**36**) and triaminoguanidinium dinitramide (**37**) were prepared according to the new synthetic routes presented in **Scheme 3.4**. The impetus of the reaction of azidoformamidinium, 5-aminotetrazolium, 1,5-diaminotetrazolium, 1-methyl-5-aminotetrazolium, 2-methyl-5-aminotetrazolium perchlorate, 1*H*-tetrazolium and triaminoguanidinium perchlorate with potassium dinitramide (KDN) is the precipitation of low soluble $KClO_4$ which can be separated by filtration.

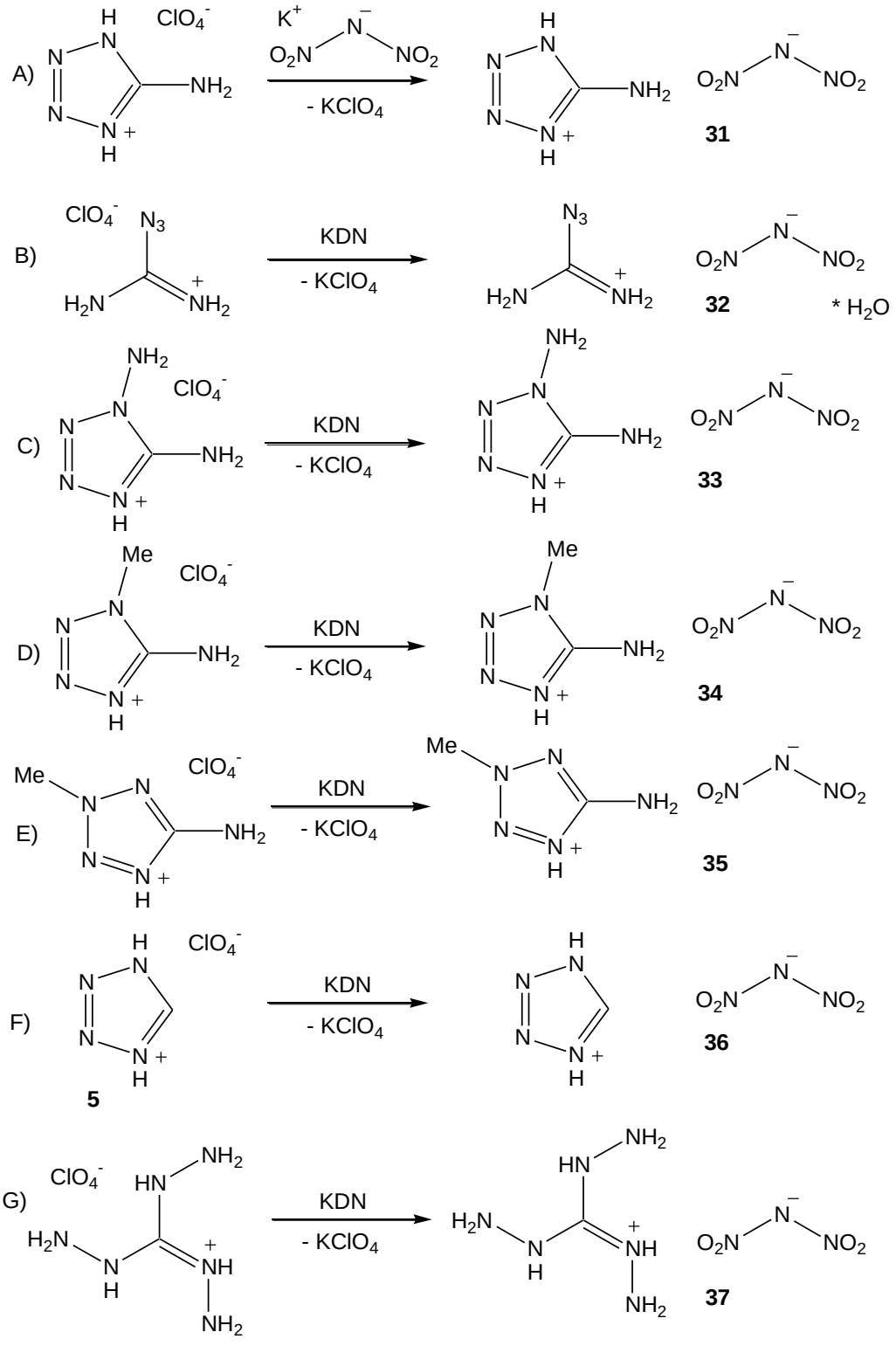

Scheme 3.4 Synthesis of A) 5-aminotetrazolium dinitramide (**31**), B) azidoformamidinium dinitramide (**32**), C) 1,5-diaminotetrazolium dinitramide (**33**), D) 1-methyl-5-aminotetrazolium dinitramide (**34**), E) 2-methyl-5-aminotetrazolium dinitramide (**35**), F) 5*H*-tetrazolium dinitramide (**36**) and G) triaminoguanidinium dinitramide (**37**).

3.4 Crystal Structures

3.4.1 5-Aminotetrazolium perchlorate (**38**) and 5-aminotetrazolium perchlorate · 5-aminotetrazole (**38**·5-At)

As mentioned in the synthesis section, depending on the amount of perchloric acid used to react with 5-At, either the perchlorate salt **38** is obtained or an adduct between the starting material and the product forms. **Figure 3.2** shows the asymmetric unit of both compounds with the labeling scheme. The angles and distances for the tetrazolium cations in both compounds are similar and agree with the previous report of the nitrate salt [61a] and are listed in **Table 3.1**. However, the C2–N6 and the N8–N9 distances in the second tetrazole ring in the structure of **2** are longer and shorter, respectively than the analogous distances in the tetrazolium cation, in agreement with the published structure of 5-amino-1*H*-tetrazolium monohydrate.[60]

Table 3.1 Selected bond lengths /Å and angles /° in the tetrazole rings of perchlorate salts **38** and **38**·5At.

atoms	**38**	**38**·5At (5-AtH$^+$)	**38**·5At (5-At)
N5–C1	1.301(5)	1.312(2)	1.342(2)
C1–N1	1.333(5)	1.342(2)	1.328(2)
N1–N2	1.353(5)	1.363(2)	1.366(2)
N2–N3	1.266(1)	1.271(2)	1.283(2)
N3–N4	1.352(5)	1.357(2)	1.359(2)
N4–C1	1.334(5)	1.341(2)	1.343(2)
N5–C1–N1	128.8(4)	127.9(1)	126.9(1)
C1–N1–N2	110.9(4)	109.7(1)	105.4(1)
N1–N2–N3	107.6(3)	108.0(1)	111.9(1)
N2–N3–N4	107.8(3)	108.0(1)	105.6(1)
N4–C1–N5	128.2(4)	128.0(1)	125.0(1)
N4–C1–N1	103.0(3)	104.0(1)	107.9(1)

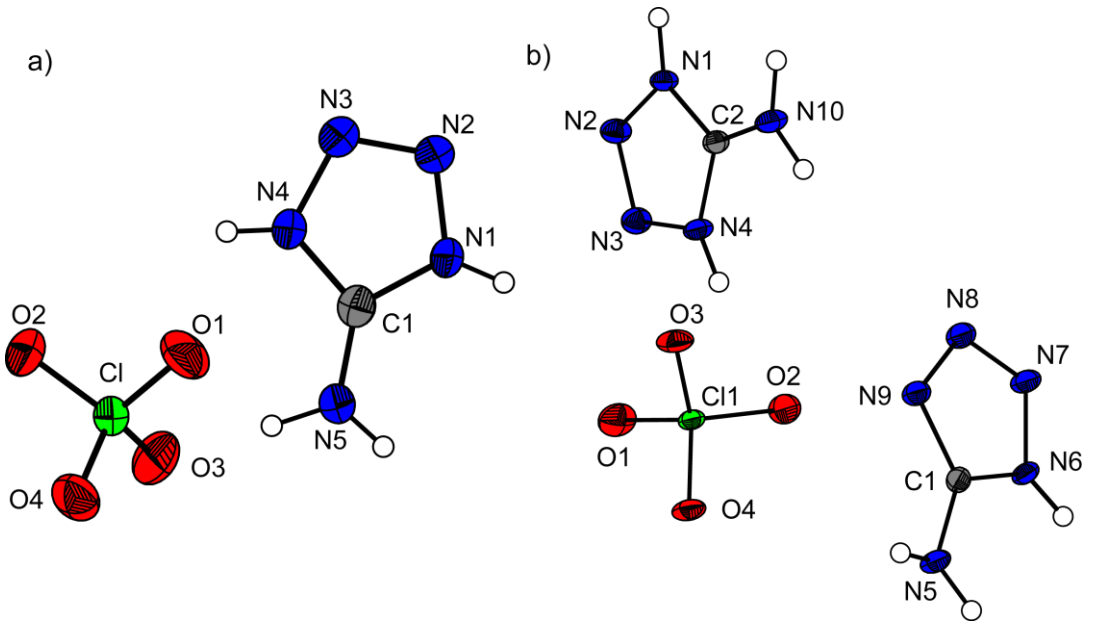

Figure 3.2 Asymmetric unit of perchlorate salts **38** (a) and **38**·5At (b) with their labeling schemes.

The cations in **38** orient very symmetrically forming layers, which in contrast to the nitrate salt [61a] are not planar due to the non-planarity of the perchlorate anion and cut the *a* and *c* axis at an angle of ~45°. **Figure 3.3** shows a view of the unit cells along the *a* axis with a sample of the extensive hydrogen-bonding found in the structure.

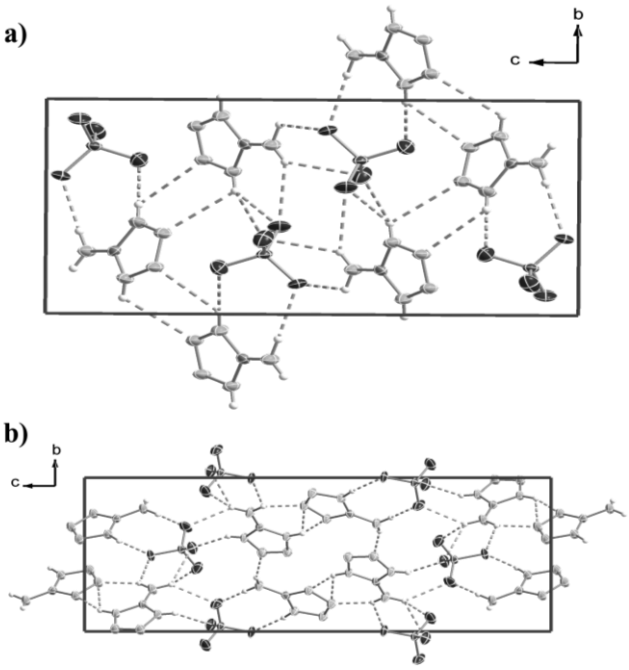

Figure 3.3 Hydrogen-bonding in the unit cell of perchlorate salts **38** (a) and **38**·5At (b). Views along the *a* axis.

The extensive hydrogen-bonding networks are better explained in the formalism of graph-set analysis as introduced by Berstein *et al.* [208] and using the computer program *RPLUTO.*[209] At the secondary level, the combination of all hydrogen bonds summarized yield only a few chain patterns with the descriptor **C2,2(X)** (X = 6, 8), whereas the rest of the graph-sets are ring motifs with the following labels: **R1,2(6)**, **R2,2(X)** (X = 4, 6, 8), **R4,2(8)** and **R4,4(X)** (X = 12, 16).

The presence of one molecule of neutral 5-At in the structure of **38**·5-At modifies the packing considerably. The perchlorate anions arrange along the *b* axis forming smooth waves with large gaps between them (~6–11 Å) occupied by tetrazolium cations and neutral tetrazole molecules. In contrast to **38** where the tetrazolium cations orients forming layers in the same direction, in **38**·5-At there exist planar layers of tetrazoles in one direction, which are interrupted by the above-mentioned waves of anions and the following layers of tetrazoles are approximately orthogonal to the first ones and are cut again by the anions so that the following layers are coplanar to the first ones. The structure contains even more hydrogen bonds (14) than the perchlorate salt described above (9), which are at least as strong, however, the non formation of infinite layers as it is the case for **38** makes the compound to be less dense (1.874 g cm^{-3}). An interesting feature about the structure is (as mentioned before) that, in contrast to **38** where cations and anions alternate, here there exist spaces between anions being occupied by the tetrazolium cations and 5-At molecules, which hydrogen-bond to each other and make the structure very stable, which is in turn reflected in the relatively low sensitivity of the compound (see Energetic Discussion).

3.4.2 Aminoguanidinium perchlorate (**39**)

$AGClO_4$ (**39**) crystallizes in the monoclinic space group $P2_1/c$ with four molecules in the unit cell with a density of 1.764 g cm^{-3}. The asymmetric unit is shown in **Figure 3.4**. The bond lengths in the aminoguanidinium cation are in the same range as observed for example in aminoguanidinium chloride [210] or nitrate [211] in the literature. The C–N bond distances are between 1.30 and 1.33 Å which is crucially shorter than C–N single bonds (1.47 Å) but significantly longer than C=N double bonds (1.22 Å) and show the delocalization of the positive charge. The hydrazine N1–N2 bond has a length of 1.402(3) Å. The Cl–O bond distances in the ClO_4^- anion lie between 1.41 and 1.44 Å, which is quite normal and can be found in other perchlorate structures.[68]

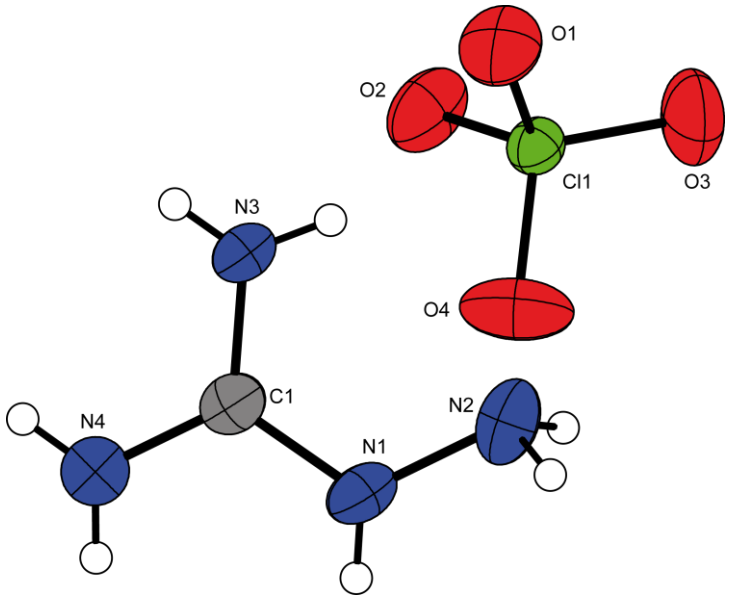

Figure 3.4 Molecular structure of **39.** Displaced ellipsoids are drawn at the 50 % probability level.

The packing of the structure is influenced by several moderate N–H···O hydrogen bonds, in which all oxygen atoms of the perchlorate anions as well as all hydrogen atoms of the cations participate. The coordination of one aminoguanidinium cation is illustrated in **Figure 3.5**.

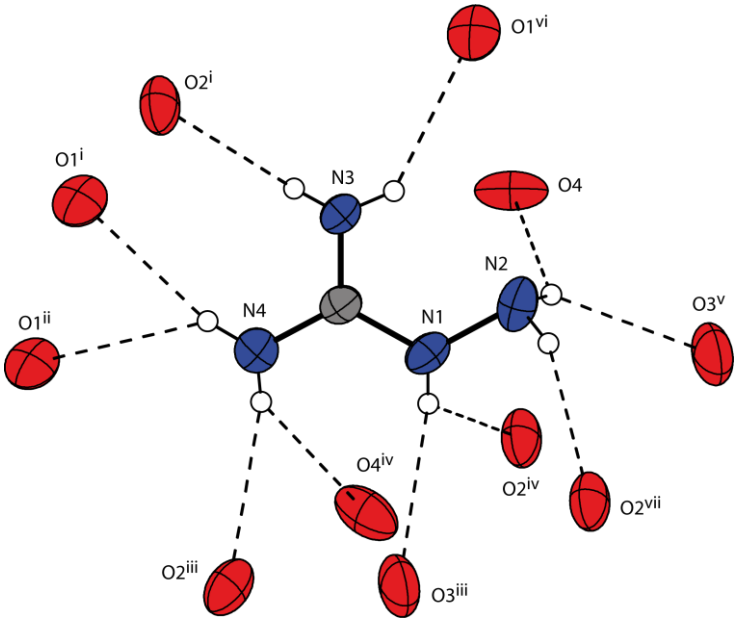

Figure 3.5 Hydrogen bonding of the aminoguanidinium cation in the structure of **39**. Symmetry codes: (i) 2–x, 0.5+y, 1.5–z; (ii) x, –0.5–y, –0.5+z; (iii) x, 1+y, z; (iv) 1–x, 0.5+y, 1.5–z; (v) 1–x, –1–y, 2–z; (vi) 2–x, –1–y, 2–z; (vii) x, –0.5–y, 0.5+z.

3.4.3 Triaminoguanidinium perchlorate (**40**)

$TAGClO_4$ (**40**) crystallizes in the monoclinic space group $P2_1/c$, whereby eight molecules can be found in the unit cell. In **Figure 3.6** one molecule of the asymmetric unit containing two independent molecular moieties is shown. The Cl–O distances in the perchlorate anions lie again between 1.42 and 1.44 Å. The structure of the cation is comparable to those observed for triaminoguanidinium chloride [212] and nitrate [213] in the literature. Again the positive charge is delocalized, which can be seen by the similar C–N bond lengths (d(C1–N1) = 1.327(3) Å, d(C1–N3) = 1.317(3) Å, d(C1–N5) = 1.332(3) Å) building a planar fragment. The hydrazine bonds have similar lengths between 1.40 and 1.42 Å. Again the packing is influenced by several N–H···O and N–H···N hydrogen bonds resulting in a high density of 1.740 g cm^{-3}.

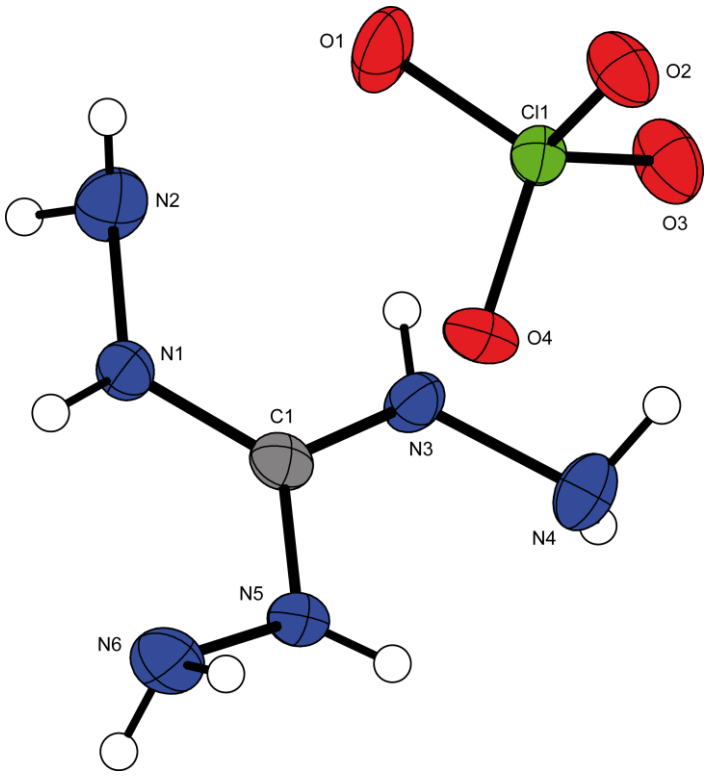

Figure 3.6 Molecular structure of **40**. Displaced ellipsoids are drawn at the 50 % probability level.

3.4.4 Azidoformamidinium perchlorate (**41**)

$AFClO_4$ (**41**) crystallizes in the orthorhombic space group *Pbca* with eight formula moieties in the unit cell and a density of 1.826 g cm^{-3}. The azidoformamidinium moiety

(**Figure 3.7**) is not planar (torsion angle (N2–N1–C1–N4) = 19.5(3)°) and the azide has a N1–N2–N3 angle of 170.1(2)°, which is quite common for covalent azide groups and can be explained by hyperconjugation effects.[214] The NH_2 groups are in plane with the carbon atom, displaying a N4–C1–N5 angle of 123.3(2)°. The C–N distances and intraatomic angles are similar to those found in 1972 by Bärnighausen who investigated azidoformamidinium chloride.[215]

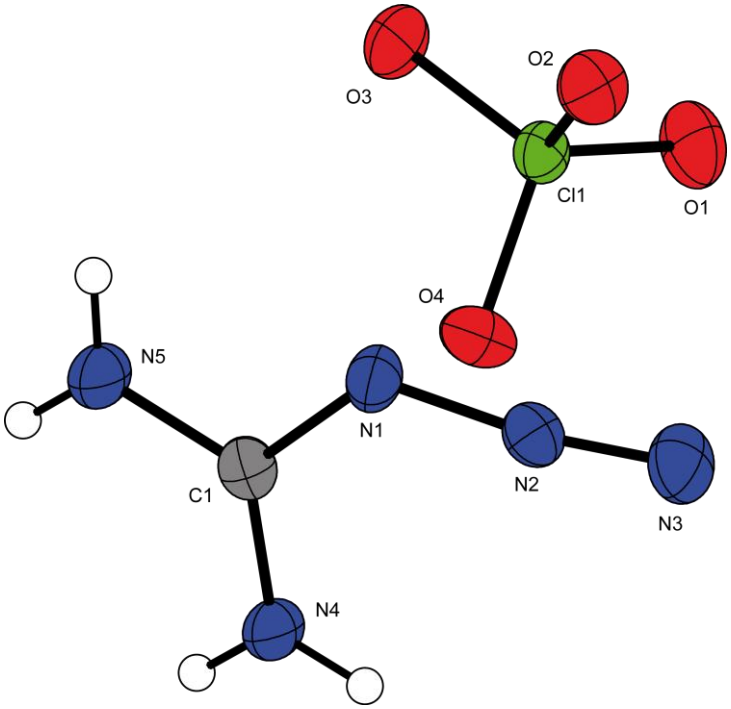

Figure 3.7 Molecular structure of **41.** Displaced ellipsoids are drawn at the 50 % probability level. Selected distances: d(C1–N1) = 1.390(3), d(C1–N4) = 1.306(3), d(C1–N5) = 1.302, d(N1–N2) = 1.256(2), d(N2–N3) = 1.116(2) Å.

3.4.5 Tetrazolium perchlorate (**42**)

1,4*H*-Tetrazolium perchlorate, shown in **Figure 3.8**, crystallizes in the monoclinic space group $P2_1/n$ with four molecules in the unit cell. The density of 2.021 g cm^{-3} is the highest density observed for the investigated perchlorates in this chapter. The packing of the structure is influenced by several moderate N–H···O hydrogen bonds, in which all oxygen atoms of the perchlorate anions as well as all nitrogen bonded hydrogen atoms of the cations participate. The Cl–O bond distances in the ClO_4^- anion lie between 1.43 and 1.45 Å, which is quite normal and can be found in other perchlorate structures, e.g. in 1-carbamoylguanidinium [216] and biguanidinium [217] perchlorate.

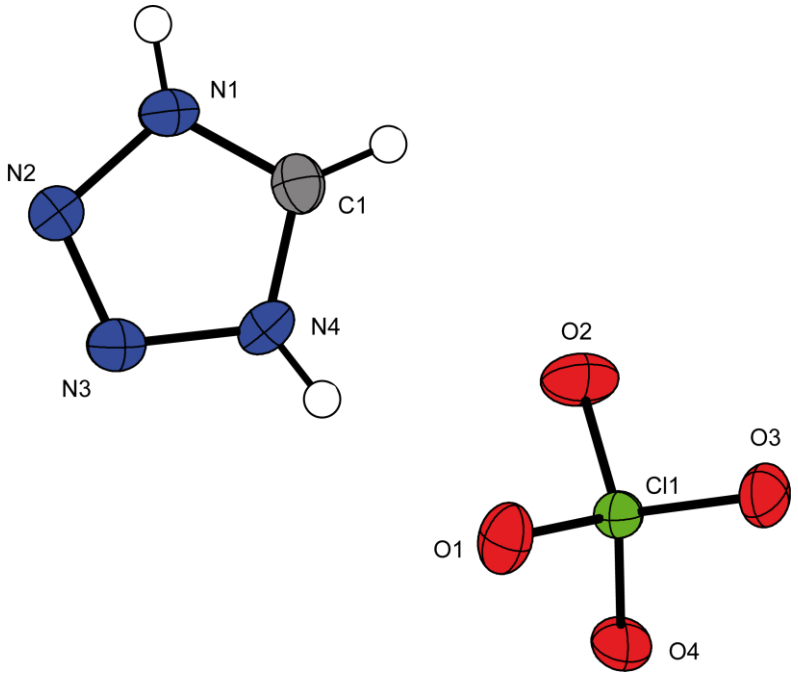

Figure 3.8 Molecular moiety of **42**. Thermal ellipsoids represent the 50 % probability level. Selected geometries: distances (Å): Cl1–O2 = 1.435(1), Cl1–O4 = 1.436(1), Cl1–O3 = 1.441(1), Cl1–O1 = 1.445(1), N2–N3 = 1.274(2), N2–N1 = 1.347(2), N1–C1 =1.305(2), N3–N4 = 1.346(2), N4–C1 = 1.303(2); angles (°): O(1,2,3,4)–O(1,2,3,4) = 108.47(7)–109.95(7), N3–N2–N1 = 107.(1), C1–N1–N2 = 110.1(1), N2–N3–N4 = 107.5(1), C1–N4–N3 = 110.0(1); torsion angles (°): N1–N2–N3–N4 = –0.1(2).

3.4.6 5-Aminotetrazolium dinitramide (**31**)

5-Aminotetrazolium dinitramide crystallizes without inclusion of crystal water in the chiral monoclinic space group *Pc* with two molecules in the unit cell. The density observed (1.856 g cm^{-3}) is very high in comparison to other tetrazoles or tetrazolium salts in literature. The molecular moiety is shown in **Figure 3.9**. The bond lengths in the aminotetrazolium cation correspond exactly to the values observed for 5-aminotetrazolium nitrate [218] and picrate.[219] The twisted geometry of the dinitramide anion is comparable to those of other N-rich dinitramides like guanidinium dinitramide,[183] aminoguanidinium dinitramide,[184] bisguanidinium dinitramide [185] or 4-methyl-1,5-diaminotetrazolium dinitramide.[202]

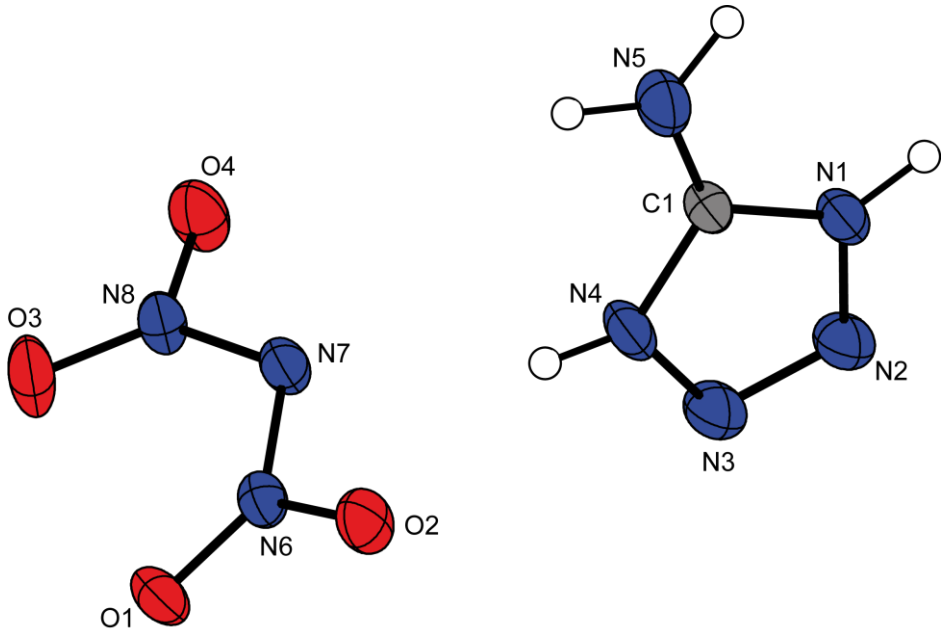

Figure 3.9 Molecular moiety of **31**. Thermal ellipsoids represent the 50 % probability level. Selected geometries: distances (Å): C1–N1 = 1.336(2), N1–N2 = 1.360(2), N2–N3 = 1.267(2), N3–N4 = 1.363(3), C1–N4 = 1.331(2), C1–N5 = 1.308(3), N6–N7 = 1.352(2), N7–N8 = 1.384(2), N6–O1 = 1.227(2), N6–O2 = 1.254(2), N8–O3 = 1.218(2), N8–O4 = 1.241(2); angles (°): N1–C1–N4 = 103.3(2), N1–C1–N5 = 128.9(2), C1–N1–N2 = 110.8(2), N1–N2–N3 = 107.5(2), N2–N3–N4 = 107.8(2), C1–N4–N3 = 110.6(2), N6–N7–N8 = 114.7(1), N6–N7–O1 = 126.2(2), N7–N6–O2 = 112.3(1), O1–N6–O2 = 121.4(2), N7–N8–O3 = 125.6(2), N7–N8–O4 = 111.5(1), O3–N8–O4 = 122.8(2); torsion angles (°): C1–N1–N2–N3 = –0.8(2), N1–N2–N3–N4 = 0.0(2); N2–N1–C1–N5 = –179.1(2), O1–N6–N7–N8 = 13.4(3), O2–N6–N7–N8 = –169.6(2), N6–N7–N8–O3 = 14.7(3), N6–N7–N8–O4 = –168.8(2).

In spite of the high density, no layer structure is formed. The packing of **31** is characterized by a 3-dimensional network, which is build by different hydrogen bonds. All hydrogen atoms of the cations, as well as the oxygen atoms and N7 of the dinitramide anions participate in these bridges. The aminotetrazolium cation and the dinitramide anion lay nearly orthogonal to each other, which can be seen in **Figure 3.10**.

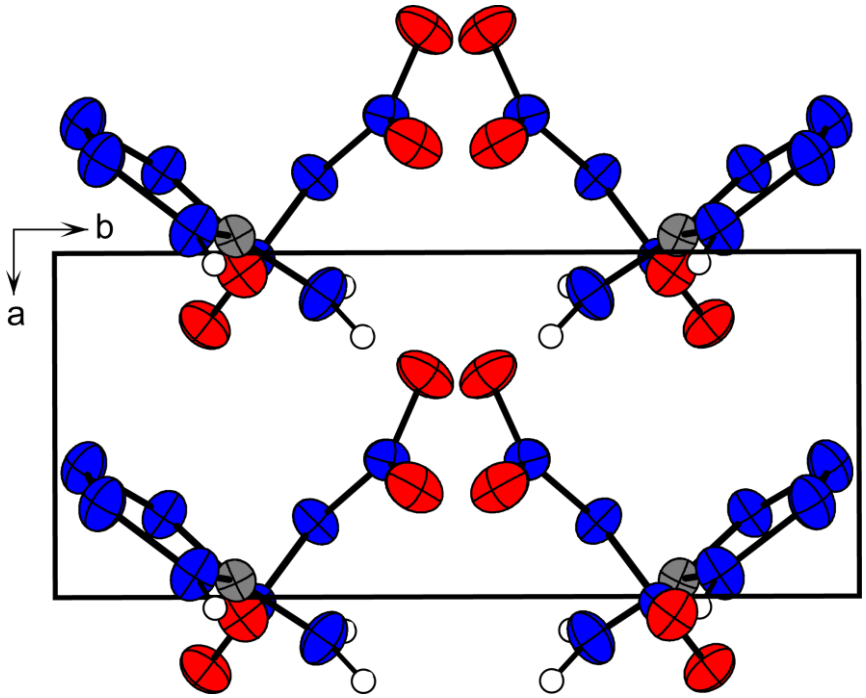

Figure 3.10 View on the packing of **31** along the *c* axis.

3.4.7 Azidoformamidinium dinitramide monohydrate (**32**)

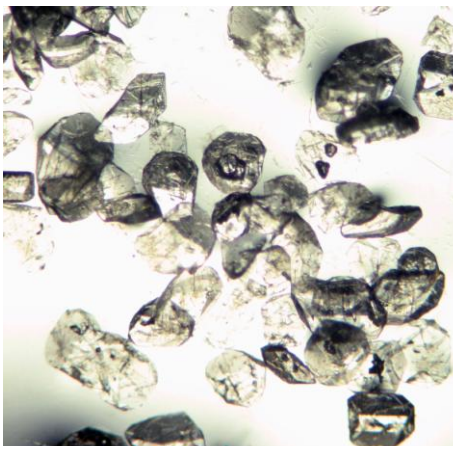

Azidoformamidinium dinitramide crystallizes as a monohydrate (**32**·H_2O) in the monoclinic space group $P2_1/m$ with two molecules in the unit cell and a density of 1.754 g cm^{-3}. To the best of our knowledge **32**·H_2O is the first structurally characterized compound, containing a planar dinitramide moiety. The structure of the azidoformamidinium cation is shown in **Figure 3.11** and does not correspond to that of other compounds containing azidoformamidinium cations e.g. azidoformamidinium chloride [215] and bis-azidoformamidinium 5,5-azotetrazolate.[72] The azidoformamidinium moiety is found to be completely planar. Similar to other azidoformamidinium cations is the angulated (angle N6–N7–N8 = 169.3(2)°) azide group, which is quite common for covalent azide groups due to hyperconjugation effects.[214] The angles N4–C1–N5 = 124.7(2)°, N5–C1–N6 = 112.3(2)° and N4–C1–N6 = 123.0(2)° are in agreement to an idealized sp^2 hybridisized carbon atom C1.

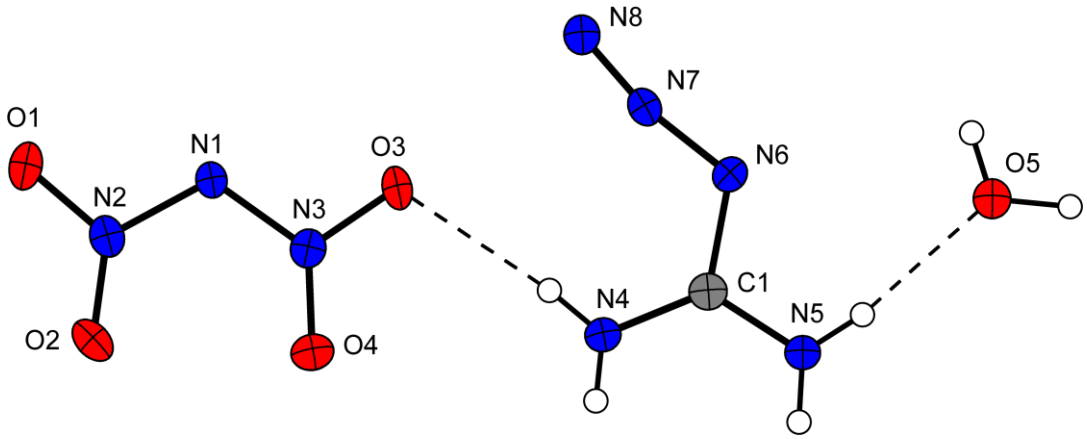

Figure 3.11 Molecular unit of **32**·H_2O. Thermal ellipsoids represent the 50 % probability level. Selected geometries: distances (Å): O1–N2 = 1.246(2), O2–N2 = 1.218(2), O3–N3 = 1.247(2), O4–N3 = 1.207(2), N1–N2 = 1.375(2), N1–N3 = 1.372(2), N6–N7 = 1.259(2), N7–N8 = 1.109(2), N4–C1 = 1.315(3), N5–C1 = 1.303(3), N6–C1 = 1.386(3); angles (°): O1–N2–O2 = 123.2(2), O2–N2–N1 = 126.4(2), O1–N2–N1 = 110.4(2), O4–N3–N1 = 127.7(2), O3–N3–O4 = 122.1(2), O3–N3–N1 = 110.2(2), N7–N6–C1 = 117.9(2), N6–N7–N8 = 169.3(2), N5–C1–N6 = 112.3(2), N4–C1–N5 = 124.7(2), N4–C1–N6 = 123.0(2), N2–N1–N3 = 116.0(1); torsion angles (°): N7–N6–C1–N4 = 0, N7–N6–C1–N5 = 180, N3–N1–N2–O2 = 0, N2–N1–N3–O4 = 0.

The high density can be explained by the formation of a layer structure (**Figure 3.12**), in which the cations, the anions as well as the crystal water are connected by strong hydrogen bonds. The layers show gaps of ~3 Å.

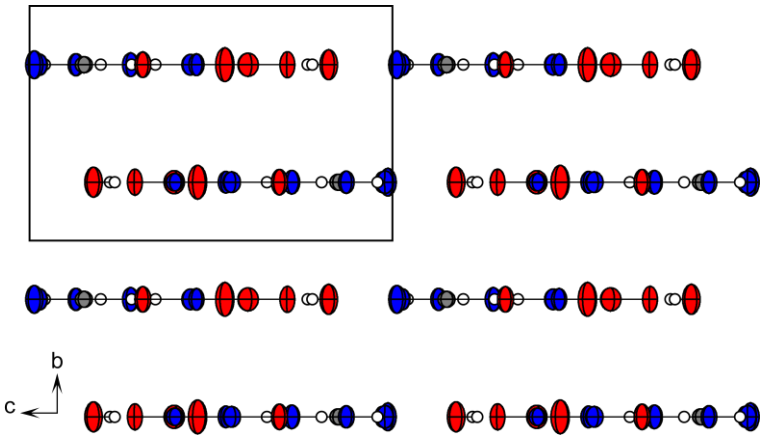

Figure 3.12 View on the layer packing of **32**·H_2O along the *a* axis.

3.4.8 1,5-Diaminotetrazolium dinitramide (**33**)

33 crystallizes in the monoclinic space group $P2_1/c$ with eight molecules in the unit cell and a calculated density of 1.771 g cm^{-3}. The structure of the 1,5-diaminotetrazolium cation (**Figure 3.13**) is consistent with the one found for diaminotetrazolium nitrate in literature.[13b] The bond lengths between the tetrazolate ring atoms N1, N2, N3 and N4 vary from 1.26 to 1.37 Å and fit in the range between N–N single bonds (1.45 Å) and N=N double bonds (1.25 Å).[167] Also the equal distances between C1–N1 (1.327(2) Å) and C1–N4 (1.327(2) Å) lie within the values for C–N single and C=N double bonds. However, also the bond N1–N6 (1.381(2) Å) to the external amino group is significantly shorter than a N–N single bond. The structure of the dinitramide anion is comparable to that of 1,5-diamino-4-methyltetrazolium dinitramide in which also two different N–N bond lengths (N7–N8 = 1.355(2) Å, N8–N9 = 1.377(2) Å) are found.

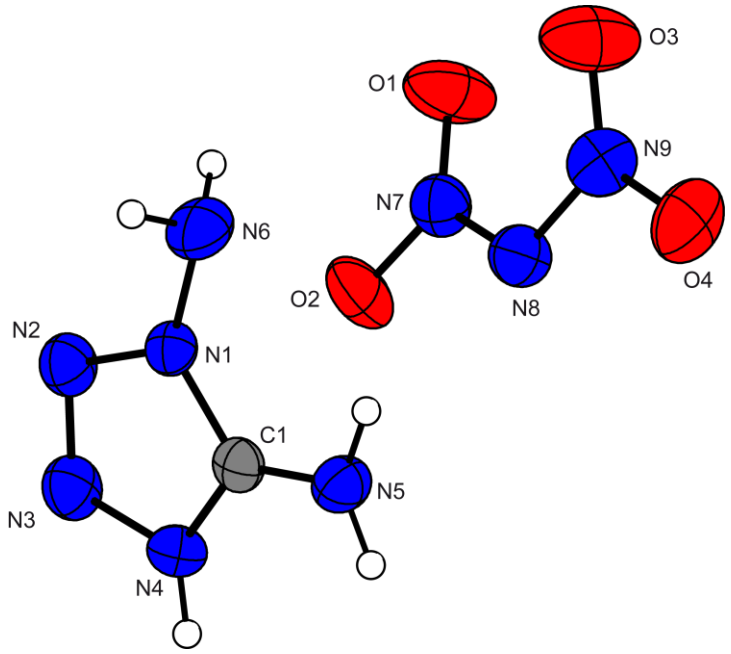

Figure 3.13 Molecular unit of **33**. Thermal ellipsoids represent the 50 % probability level. Selected geometries: distances (Å): N1–C1 = 1.327(2), N1–N2 = 1.365(2), N1–N6 = 1.381(2), N2–N3 = 1.264(2), N3–N4 = 1.358(2), N4–C1 = 1.327(2), N5–C1 = 1.311(3), N7–N8 = 1.355(2), N8–N9 = 1.377(2), O1–N7 =1.214(2), O2–N7 =1.245(2), O3–N9 = 1.213(3), O4–N9 = 1.239(2); angles (°): N2–N1–C1 = 110.6(2), N2–N1–N6 = 124.9(2), N6–N1–C1 = 124.4(2), N1–N2–N3 = 107.1(2), N2–N3–N4 = 108.1(2), N3–N4–C1 = 110.5(2), N4–C1–N5 = 130.4(2), N1–C1–N5 = 126.0(2),

N1–C1–N4 = 103.7(2), O2–N7–N8 = 112.0(2), O1–N7–O2 = 122.0(2), O1–N7–N8 = 125.9(2), N7–N8–N9 = 116.0(2), O3–N9–N8 = 125.8(2), O3–N9–O4 = 123.04(2), O4–N9–N8 = 111.1(2); torsion angles (°): C1–N1–N2–N3 = –0.7(2), N2–N1–C1–N4 = 1.3(2), N6–N1–N2–N3 = –179.2(2), N6–N1–C1–N5 = –0.6(3), O1–N7–N8–N9 = 11.2(3), O2–N7–N8–N9 = –172.9(2), N7–N8–N9–O3 = 16.0(3), N7–N8–N9–O4 = –167.6(2).

The packing of the structure is dominated by an two-dimensional network in which single plains are connected by several strong hydrogen bonds. A view on the hydrogen bonds of one plane and the unit cell along the *b* axis is shown in **Figure 3.14**.

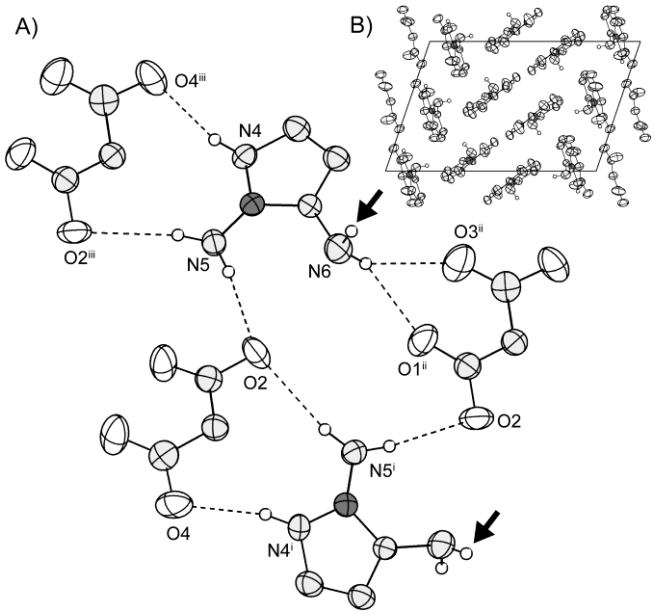

Figure 3.14 A) View on the planes in the structure of **33**, connected by hydrogen bonds. The arrows mark anchors for the formation of hydrogen bonds upright to these planes. B) View on the unit cell of **33** along the *b* axis.

3.4.9 1-Methyl-5-aminotetrazolium dinitramide (**34**)

1-Methyl-5-aminotetrazolium dinitramide crystallizes in the monoclinic space group $P2_1/m$ with two molecules in the unit cell and a density of 1.646 g cm^{-3}. The structure of the 1-methyl-5-aminotetrazolium moiety is similar to these found for other 1-methyl-5-aminotetrazolium salts, e.g. the nitrate salt in literature.[68] The molecular moiety is shown in **Figure 3.15**. Since the appearance of the mirror plane in $P2_1/m$ the dinitramide anions are completely planar. However, again there are two different N–N bond lengths found in the anions (N6–N7 = 1.353(3), N7–N8 = 1.393(3) Å) forming the

N6–N7–N8 angle of 115.4(2)°. The occurrence of a planar dinitramide is very rare. To the best of our knowledge, we found, except to the structure of **32**, no alternative crystal structure containing planar dinitramide anions.

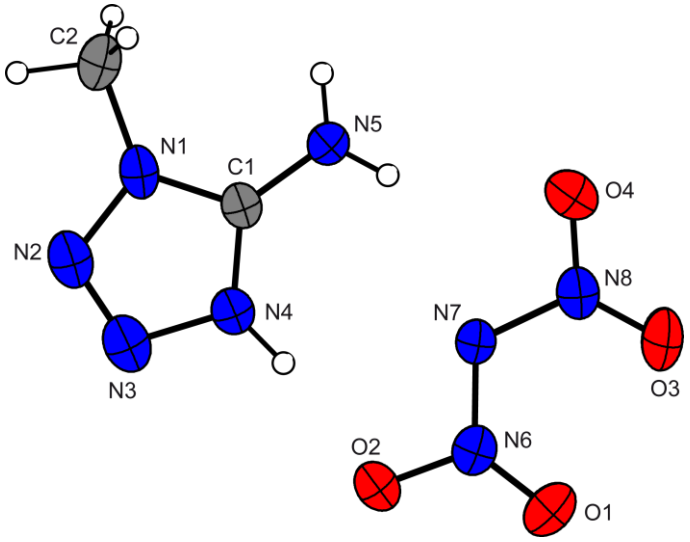

Figure 3.15 Molecular unit of **34**. Thermal ellipsoids represent the 50 % probability level. Selected geometries: distances (Å): N1–N2 = 1.372(4), N1–C1 = 1.344(4), N2–N3 = 1.273(4), N3–N4 = 1.367(4), N4–C1 = 1.323(4), N1–C2 = 1.464(5), N5–C1 = 1.315(4), N6–N7 = 1.353(3), N7–N8 = 1.393(3), O1–N6 = 1.202(3), O2–N6 = 1.277(3), O3–N8 = 1.204(3), O4–N8 = 1.233(4); angles (°): N2–N1–C1 = 109.1(3), N2–N1–C2 = 122.0(2), C1–N1–C2 = 128.9(3), N1–N2–N3 = 108.4(2), N2–N3–N4 = 107.3(3), N3–N4–C1 = 110.7(2), N1–C1–N5 = 125.9(3), N4–C1–N5 = 129.5(3), N1–C1–N4 = 104.7(2), O2–N6–N7 = 110.1(2), O1–N6 –O2 = 121.7(2), O1–N6–N7 = 128.2(2), N6–N7–N8 = 115.4(2), O3–N8–N7 = 125.7(3), O4–N8–N7 = 111.0(2) O3–N8–O4 = 123.4(2); torsion angles (°):C1–N1–N2–N3 = 0.00(1), O1–N6–N7–N8 = 0.00(1).

The packing of **34** is characterized by the formation of a layer structure containing the anions and cations. All oxygen atoms of the dinitramide (marked in **Figure 3.16**) participate in several strong hydrogen bonds. Also a strong non-classical hydrogen bond ($C2^{ii}$–H2B···O3 = 1.03(4), 2.33(4), 3.294(4) Å, 155(3)°) is found in the structure.

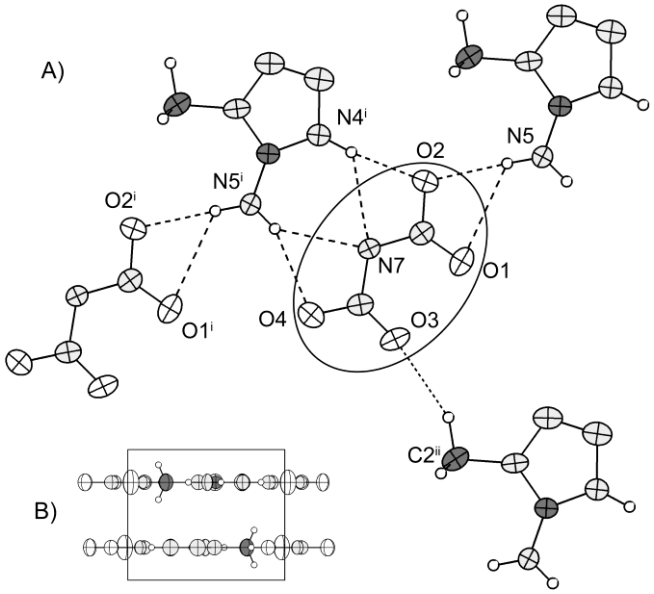

Figure 3.16 A) Coordination of one dinitramide anion. Selected hydrogen bonds: N4^{i}–H4···O2 = 0.91(3), 1.95(3), 2.855(3) Å, 173(3)°; N4^{i}–H4···N7 = 0.91(3), 2.40(4), 3.052(3), 128(3); N5–H5A···O2 = 0.88(3), 2.05(3), 2.934(4) Å, 178(3)°; N5–H5A···O1 = 0.88(3), 2.65(3), 3.24(4) Å, 125.4(2)°; C2^{ii}–H2B···O3 = 1.03(4), 2.33(4), 3.294(4) Å, 155(3)°; N5^{i}–H5B···N7 = 0.85(3), 2.37(4), 3.109(4) Å, 147(3)°; N5^{i}–H5B···O4 = 0.85(3), 2.30(3), 3.101(4) Å, 158(3)°; (i) –1+x, y, z; (ii) x, y, –1+z. B) View on the unit cell of **34** along the *c* axis.

3.4.10 2-Methyl-5-aminotetrazolium dinitramide (**35**)

35 crystallizes in the triclinic space group *P*–1 with two molecules in the unit cell and the lowest density of 1.659 gcm^{-3} observed in this work. The molecular moiety is shown in **Figure 3.17**. The structure of the cation is in the range of other 2-methyl-5-aminotetrazolium salts, e.g. the perchlorate [68] and picrate.[220] The dinitramide anion is not planar and comparable to those observed in **33**.

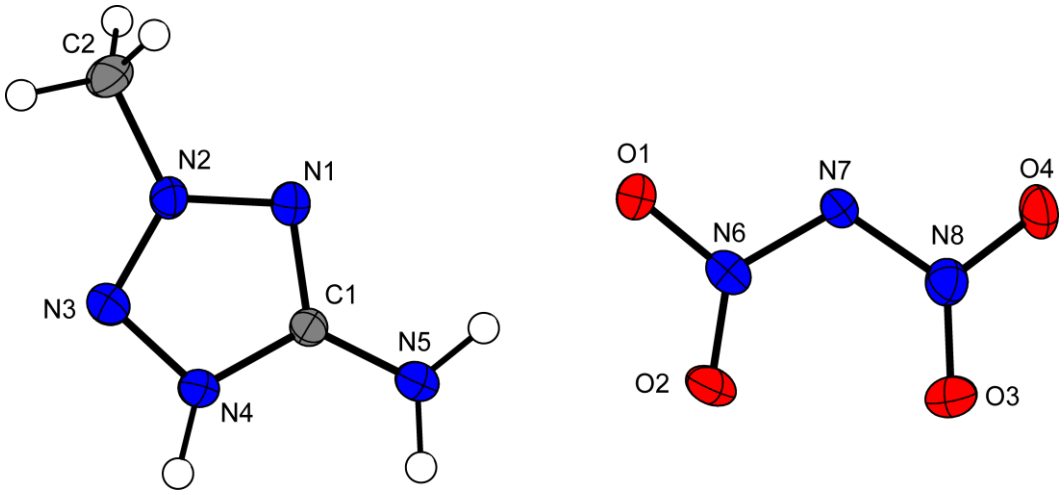

Figure 3.17 Molecular moiety of **35**. Thermal ellipsoids represent the 50 % probability level. Selected geometries: distances (Å): C1–N1 = 1.323(3), N1–N2 = 1.338(2), N2–C2 = 1.461(3), N3–N2 = 1.291(3), N5–C1 = 1.329(3), N4–N3 = 1.345(3), N4–C1 = 1.349(3), O1–N6 = 1.277(2), O2–N6 = 1.214(2), N7–N6 = 1.351(3), N7–N8 = 1.396(3), N8–O3 = 1.207(2), O4–N8 = 1.243(2); angles (°): N1–C1–N5 = 125.4(2), N1–C1–N4 = 108.6(2), C1–N1–N2 = 102.7(2), N1–N2–C2 = 121.1(2), O2–N6–O1 = 121.2(2), O2–N6–N7 = 127.8(2), O1–N6–N7 = 111.0(2), O3–N8–O4 = 124.5(2), O3–N8–N7 = 125.7(2), O4–N8–N7 = 109.8(2); torsion angles (°): N3–N4–C1–N5 = 179.8(2), N4–C1–N1–N2 = 0.8(3), N4–N3–N2–C2 = –178.3(3), N8–N7–N6–O1 = –179.4(2), N6–N7–N8–O3 = –10.4(3).

3.4.11 Tetrazolium dinitramide (**36**)

36 crystallizes in the monoclinic space group *C*2/*c* with four molecules in the unit cell and a density of 1.824 g cm^{-3}. The crystal structures of **36** and **42** represent the first examples of protonated 1*H*-tetrazolium salts determined by X-ray diffraction. The structure of the tetrazolium cations can be compared with those of the few 5-N substituted tetrazolium cations, e.g. aminotetrazolium nitrate [61] or perchlorate (**38**). However, the bond distances and angles of the planar ring system are all between typical C–N and N–N single bonds and C=N and N=N double bonds, respectively. The lengths and angles fit to neutral 1*H*-tetrazole [221] and other 5-C substituted tetrazoles, e.g. 5-methyl-tetrazole,[222] bis(1*H*-tetrazolyl)methane [223] and 5,5'-bistetrazole.[224] The dinitramide anions are strongly disordered, which is demonstrated in **Figure 3.18**.

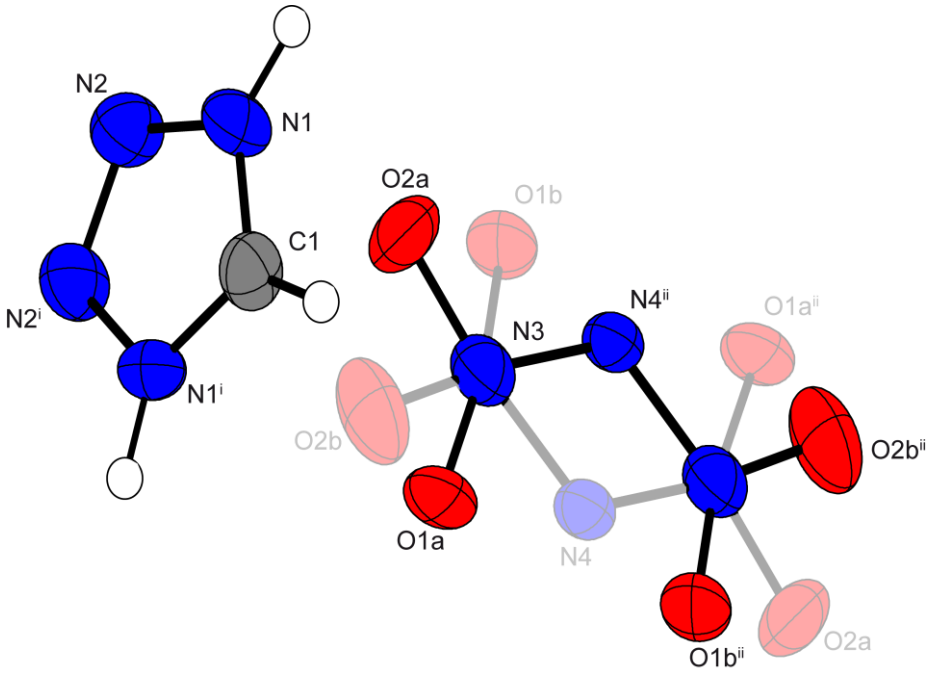

Figure 3.18 Molecular moiety of **36**. Thermal ellipsoids represent the 50 % probability level. The light ellipsoids label the disorder of the dinitramide anion. Selected geometries: distances (Å): N3^{ii}–O1b^{ii} = 1.198(3), N3^{ii}–O2b^{ii} = 1.202(3), N3–O1a = 1.218(3), N3–O2a = 1.280(3), C1–N1 = 1.295(2), N2–N1 = 1.342(2), N2–N2^{i} =1.276(2), N3–N4^{ii} = 1.336(3); angles (°): O2b^{ii}–N3^{ii}–O1b^{ii} = 127.6(3), O1a–N3–O2a = 119.3(3), N3–N4^{ii}–N3^{ii} = 115.8(2), N1–C1–N1^{i} = 106.0(2), C1–N1–N2 = 109.8(2); torsion angles (°): N1^{i}–C1–N1–N2 = –0.12(8), O1a–N3–N4^{ii}–N3^{ii} = 1.8(3); (i): 1–x, y, 0.5–z; (ii) –x, –y, 1–z.

3.4.12 Triaminoguanidinium dinitramide (**37**)

1,3,5-Triaminoguanidinium dinitramide crystallizes in the orthorhombic space group *Pbca* with eight molecular moieties in the unit cell and a density of 1.628 g cm^{-3}. The molecular moiety is shown in **Figure 3.19**. The bond lengths in the triaminoguanidinium cation correspond exactly to the values observed for triaminoguanidinium nitrate.[213] The hydrazine bond lengths (N1–N2, N3–N4, N5–N6, all ~1.41 Å) are marginally shorter than the bonds in isolated hydrazine (1.45 Å).[225] The twisted geometry of the dinitramide anion is comparable to those of other N-rich dinitramides like guanidinium dinitramide,[183] aminoguanidinium dinitramide,[184] bisguanidinium dinitramide [185] or 4-methyl-1,5-diaminotetrazolate dinitramide.[202]

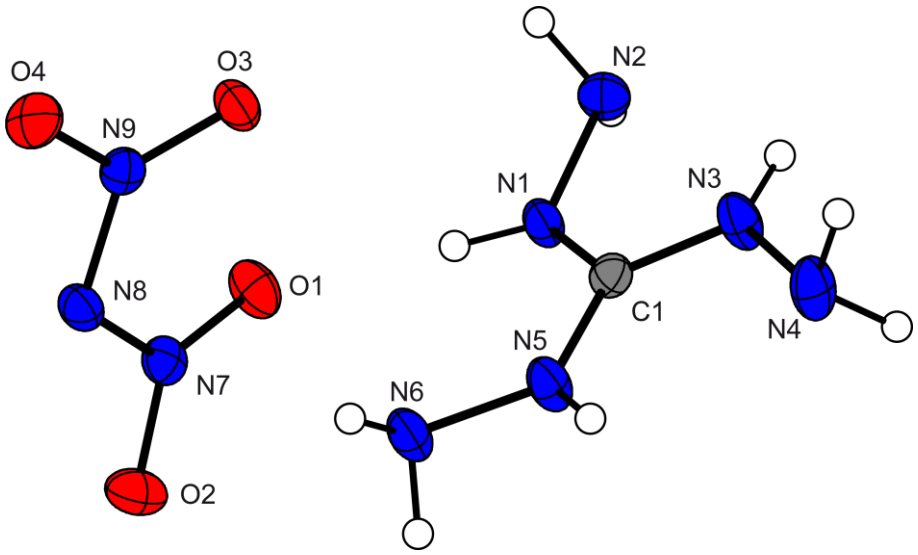

Figure 3.19 Molecular unit of **37**. Thermal ellipsoids represent the 50 % probability level. Selected geometries: distances (Å): C1–N1 = 1.323(2), N1–N2 = 1.408(2), C1–N3 = 1.322(2), N3–N4 = 1.411(2), C1–N5 = 1.327(2), N5–N6 = 1.407(2), N7–N8 = 1.365(2), N8–N9 = 1.373(2), N7–O1 = 1.234(1), N7–O2 = 1.240(2), N9–O3 = 1.232(1), N9–O4 = 1.233(1); angles (°): N1–C1–N3 = 119.9(1), N1–C1–N5 = 119.9(1), C1–N1–N2 = 117.6(1), C1–N3–N4 = 117.9(1), C1–N5–N6 = 118.4(1), N7–N8–N9 = 114.8(1), N8–N7–O1 = 126.0(1), N8–N7–O2 = 112.4(1), O1–N7–O2 = 121.5(1), N8–N9–O3 = 125.7(1), N8–N9–O4 = 112.3(1), O3–N9–O4 = 121.9(1); torsion angles (°): N3–C1–N1–N2 = –8.5(2), N3–C1–N5–N6 = 177.6(1), O1–N7–N8–N9 = –12.1(2), O2–N7–N8–N9 = 170.7(1), N7–N8–N9–O3 = –10.7(2), N7–N8–N9–O4 = 172.1(1).

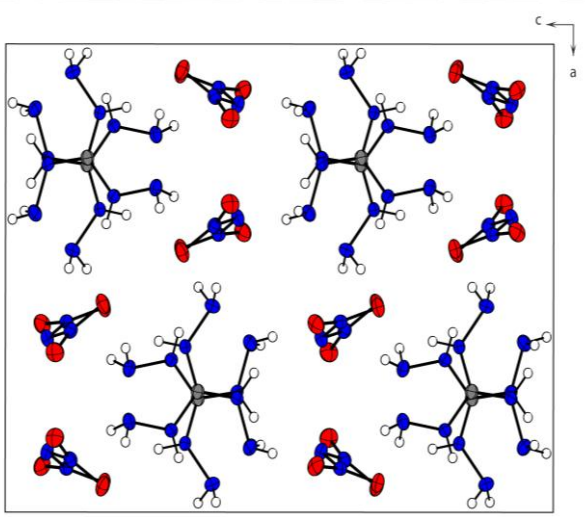

Figure 3.20 View on the packing of **37** along the *b* axis.

The packing of **37** is characterized by a 3-dimensional network, which is built by ten different hydrogen bonds. All hydrogen atoms of the cations, as well as the oxygen atoms and N8 of the dinitramide anions participate in these bridges. The dinitramide anions build 1-dimensional stacks along the *b* axis, which can be seen in **Figure 3.20**, whereby the cations lie nearly orthogonal to these stacks.

3.5 NMR spectroscopy

Compounds **31–37** were investigated using ^{1}H, $^{13}C\{^{1}H\}$, ^{14}N and ^{15}N NMR as well as $^{15}N\{^{1}H\}$ spectroscopy and the chemical shifts are given with respect to TMS (^{1}H, ^{13}C) as well as $MeNO_2$ (^{14}N, ^{15}N) as external standard. In the spectra of **31**–**34** $D_3C–OD$ was used, in the spectra of **35**–**37** d_6-DMSO was used as the solvent. Due to the fast proton exchange in $D_3C–OD$, the ^{1}H spectra of **31** and **32** show only one signal assigned to the cations (**31**: 6.84, **32**: 8.75). The crystal water protons of **32** are located at 4.62 ppm. The C–H proton of **35** can be found at 9.23 ppm, while the acidic N–H protons are shifted to lower fields (11.83 ppm). In the ^{1}H spectrum of **36** only two signals are observed at 6.17 ppm (NH_2) and 4.29 (CH_3). In the ^{1}H spectrum of **37** two broad signals were obtained at 8.57 (–N*H*–) and 4.45 ppm (NH_2) with intensities of 1:2. In the spectra of all compounds a low field signal at 159.3 (**32**), 150.3 (**31**), 143.0 (**35**), 160.5 (**36**) and 159.6 ppm (**37**) can be assigned in the **^{13}C** spectra for the tetrazole carbon atom. The methyl groups in **34** and **35** is found at 32.7 and 40.6 ppm, respectively. ^{13}C resonances are probably the best method for differentiating tetrazole derivatives and also isomers **31** and **32**. ^{15}N spectra of **31**–**37** were recorded and are shown in **Figure 3.21** (**31**–**36**) and **Figure 3.22**. (**37**). The assignments of the signals are based on the analysis of the observed $^{15}N–^{1}H$ coupling constants and by comparison with the literature.[57] In the ^{15}N NMR spectrum of **32**, no signal (~310 ppm) could be obtained for the α azide nitrogen atom bonded to the carbon atom. Except for **32** and **37** no resonances of the central dinitramide nitrogen atom could have been detected. This is a consequence of the long relaxation time (> 5 s) of the central dinitramide nitrogen atom.

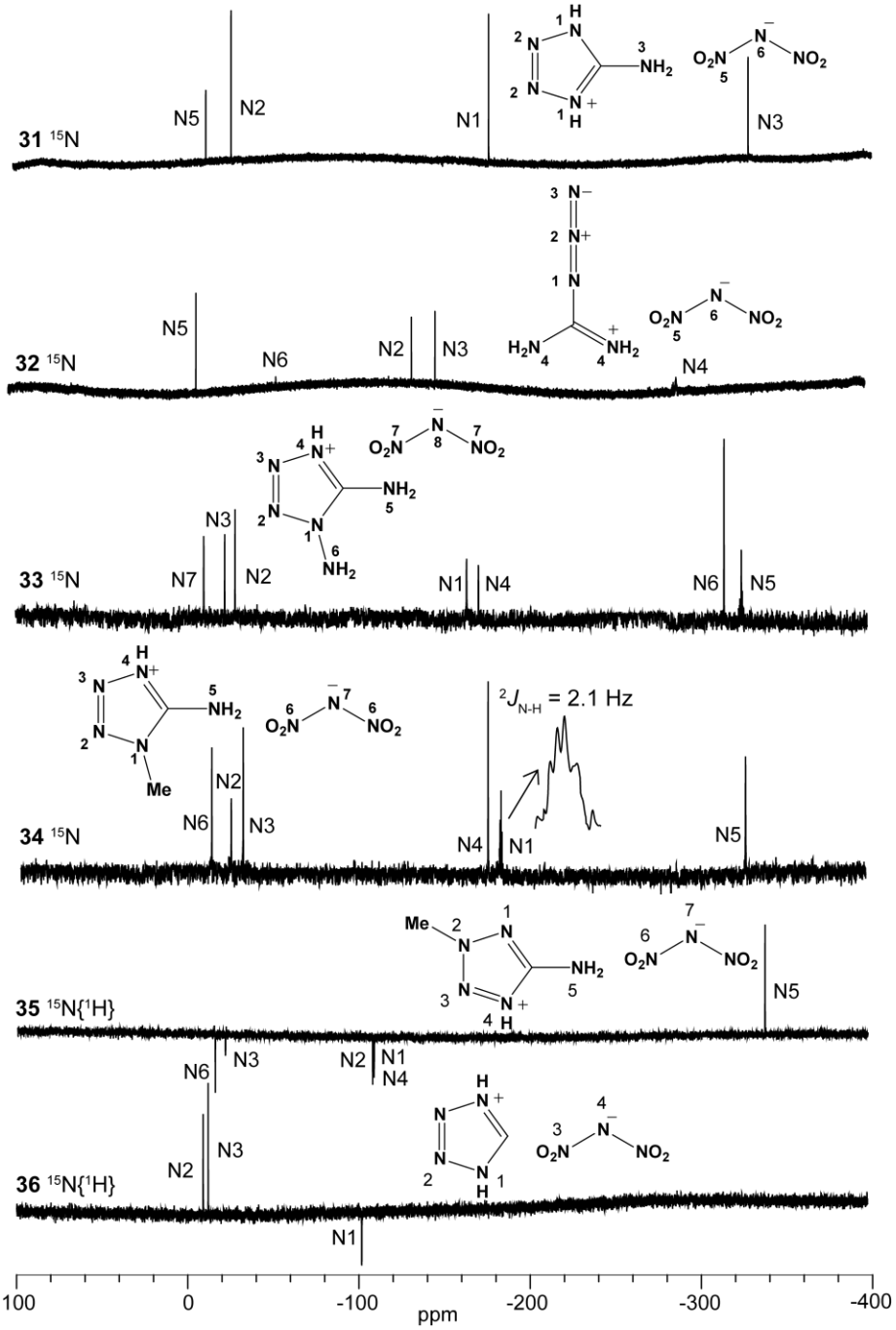

Figure 3.21 ^{15}N (**31**–**34**) and $^{15}N\{^1H\}$ (**35** and **36**) NMR spectra. **31**: δ (ppm) = –12.5 (N5, NO_2), –27.1 (N2), –177.6 (N1), –329.2 (NH_2, N3); **32**: δ (ppm) = –11.9 (N5, NO_2), –58.4 ($N(NO_2)_2$, N6), –137.5 (N2), –151.3 (N3), –290.8 (NH_2, N4); **33**: δ (ppm) = –12.8 ($N(NO_2)_2$), –21.5 (N3), –34.7 (N2), –165.8 (N1), –172.5 (N4), –318.6 (N6) –330.7 (N5); **34**: δ (ppm) = –12.8 ($N(NO_2)_2$), –24.3 (N2, q, $^3J_{NH}$ = 1.9 Hz), –31.3 (N3,), –176.3 (N4), –183.4 (N1, q, $^2J_{NH}$ = 2.1 Hz), –328.7 (N5). **35**: –8.1 (N2), –11.1 (NO_2), –101.4 (N1); **36**: –14.5 ($N(NO_2)_2$), –20.5 (N3, $^3J_{NH}$ = 1.7 Hz), 107.4 (N2, q, $^2J_{NH}$ = 2.1 Hz), –108.0 (N4, $^3J_{NH}$ = 1.7 Hz)), –108.2 (N1), –339.2 (N5).

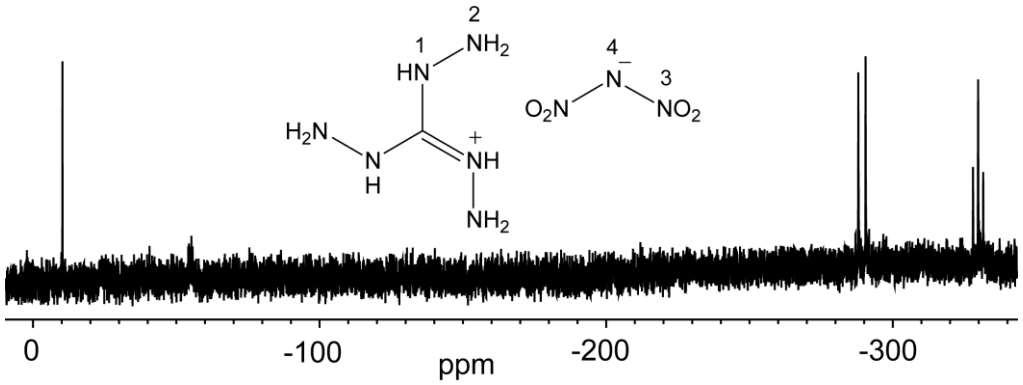

Figure 3.22 ^{15}N NMR spectrum of **37** in d_6-DMSO. δ (ppm) = –10.3 (NO_2), –55.3 ($N(NO_2)_2$), –289.2 (NH, d, $^1J_{N–H}$ = 103 Hz), –329.8 (NH_2, t, $^1J_{N–H}$ = 73 Hz).

The high symmetry of the 5-aminotetrazolium cation contributes to the simplicity of the NMR spectra of **38**. In d_6-DMSO the exchange of the ring protons with those of the amino group is faster than the time scale necessary to record the spectrum, so that an averaged broad resonance is observed at low field (9.70 ppm) for compound **38**, whereas the presence of the 5-At moiety in **38**·5-At causes this signal to shift to 8.04 ppm (higher field), which is lower field than the analogous signal in 5-At itself (6.50 ppm). The carbon signal for the tetrazolium cations in the ^{13}C NMR is found at δ ~154.5 ppm for both materials, whereas the 5-At carbon atom resonance in **38**·5-At is shifted to lower field at 157.2 ppm, in agreement with other nitrogen-rich heterocyclic compounds. [226,227]

The ^{15}N{^{1}H} NMR spectrum of the 5-amino-1*H*-tetrazolium cation is shown in

Figure 3.23 and shows the three expected signals, all of them in the negative region. The signal at the highest field (–325.1 ppm) can easily be assigned to the amino-group nitrogen atom resonance, whereas the other two signals can be differentiated by the PIS (proton induced effect),[228] which causes a shift to higher field of the resonances of the protonated nitrogen atoms. The protonated nitrogen atoms N2 and N5 can be identified as the signal at –167.8 ppm, whereas N3 and N4 are found at lower field (–27.0 ppm), keeping in with 5-amino-1*H*-tetrazolium nitrate.[61a]

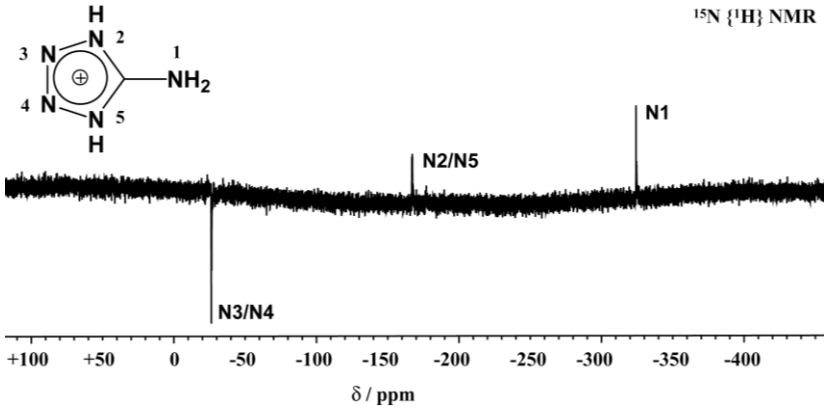

Figure 3.23 ^{15}N {^{1}H} NMR spectrum of the 5-AtH^{+} cation in compound **38**.

The ^{13}C and ^{15}N NMR chemical shifts of **39**–**41** are presented in **Table 3.2**. For compounds **39**–**41** the proton coupled as well as the proton decoupled ^{15}N NMR spectra (**Figure 3.24**) with full NOE (nuclear overhauser effect) were recorded. The assignments are given based on the values of the ^{15}N–^{1}H coupling constants. The chemical shifts are given with respect to CH_3NO_2 (^{15}N) and TMS (^{1}H, ^{13}C) as external standards. In the case of ^{15}N NMR, negative shifts are up-field from CH_3NO_2. In all cases D_2O was used as the solvent.

In the ^{15}N NMR spectra of $AGClO_4$ three signals are observed which can be assigned to the nitrogen N1 (–285.6 ppm), N2 (–327.6 ppm) as well as N3/N4 (–312.4 ppm). $TAGClO_4$ shows only two signals at –289.1 ppm (N1, N3, N5) and –329.4 ppm (N2, N4, N6), while in $AFClO_4$ four different nitrogen shifts are observed. The azide group is shifted in contrast to carbon bonded covalent azides [229] in a different order, which can be explained by the presence of the positive charge building a formal carbenium ion. The azide nitrogen atoms can be found at –138.2 ppm (N3), –152.7 (N2) and –305.9 (N1) ppm. The NH_2 nitrogen resonance is found at –292.2 ppm.

Table 3.2 ^{15}N NMR and ^{13}C NMR chemical Shifts of **39**–**41**.

compound	δ(N1)/ppm	δ(N2)	δ(N3)	δ(N4)	δ(N5)	δ(N6)	δ(C1)/ppm
39	–285.6	–327.6	–312.4	–312.4	---	---	159.3
40	–289.1	–329.4	–289.1	–329.4	–289.1	–329.4	159.5
41	–305.9	–152.7	–138.2	–292.2	–292.2	---	159.2

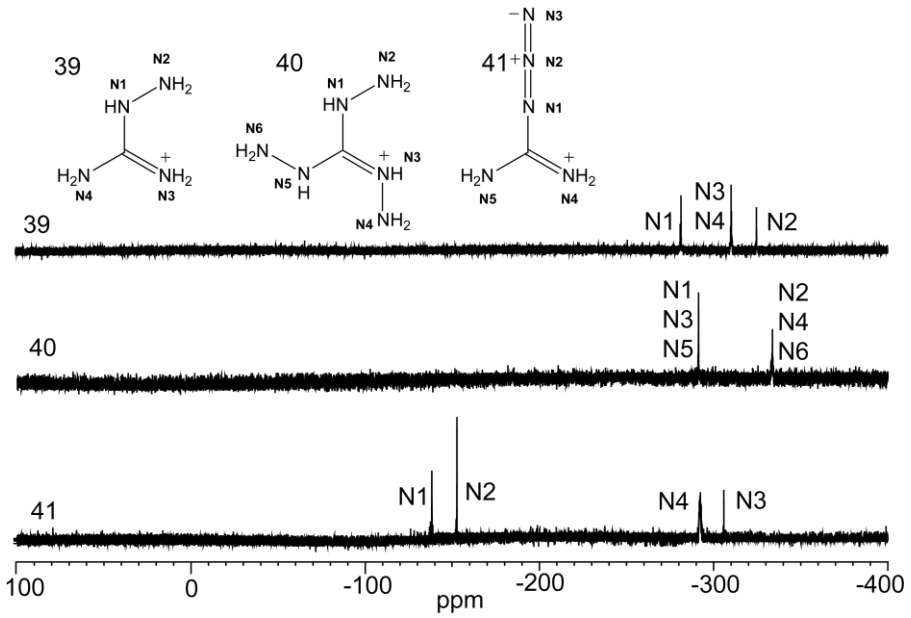

Figure 3.24 ^{15}N NMR spectra of **39**–**41**.

3.6 Vibrational Spectroscopy

Vibrational spectroscopy (IR and Raman) is also a suitable method for identifying dinitramide anions. **37** shows characteristic vibrations in the Raman spectrum, which is shown in **Figure 3.25**. Several vibrations could be assigned on the basis of a frequency analysis on the optimized structures and by comparison with the literature:[175] 3310–3370 cm^{-1} ν_s(N–H, NH_2), 1513 cm^{-1} ν_s(NO_2), 1326 cm^{-1} ν_s(NO_2), 1100–1200 cm^{-1} δ_s and δ_{as}(N–H, NH_2), 953 cm^{-1}ν_s(N_3), 821 cm^{-1} δ_{sciss}(NO_2), 488 cm^{-1} δ_{wag}(NO_2).

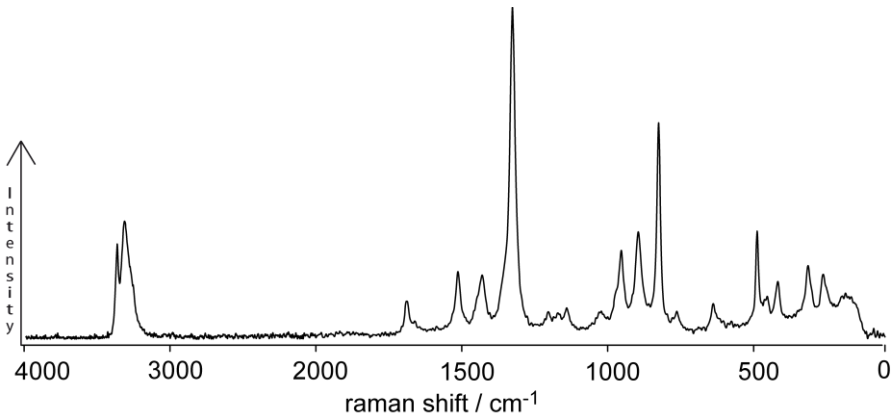

Figure 3.25 Raman spectrum of **37**

Both compounds (**38** and **38**·5-At) were characterized by elemental analysis (EA), mass spectrometry (MS), vibrational (IR/Raman) and multinuclear NMR (^{1}H, ^{13}C and ^{15}N) spectroscopy. Both materials were found to be analytically pure on the basis of a CHN analysis (±0.5%). In some instances the nitrogen content was found to deviate considerably from the calculated value, due to the relatively high nitrogen amount of the compounds. The vibrational spectra measured show the characteristic bands of the perchlorate anion. These are observed as a strong stretch with its maximum at 1088 (**38**) and 1087 (**38**·5-At) cm^{-1} in the infrared spectra (**Figure 3.26**) and as strong, sharp bands at 940 and 457 cm^{-1} (**38**) and at 937 and 457 cm^{-1} (**38**·5-At) in the Raman spectra (**Figure 3.27**).[230] These results are in agreement with previously published tetrazolium perchlorate salts in our an other groups.[68,231]

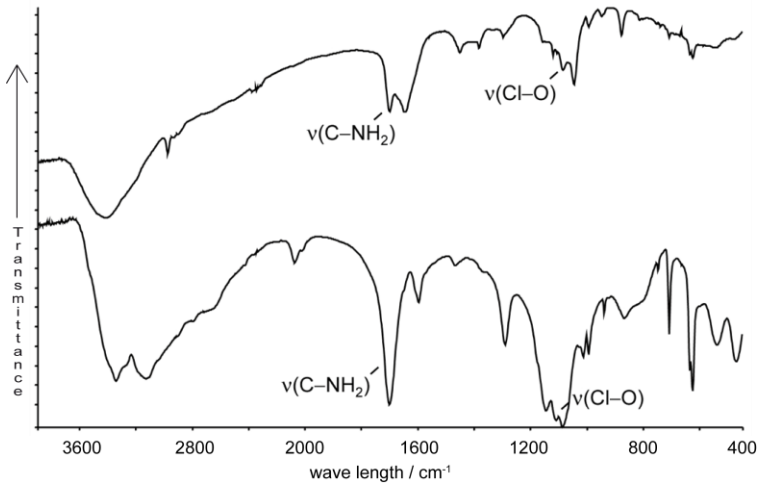

Figure 3.26 IR spectra of 5-amino-1*H*-tetrazolium perchlorate (**38**) (below) and its 5-At adduct (above).

Apart from the intense bands corresponding to the anion just mentioned above, the IR and Raman spectra of the compounds also contain a set of bands that are characteristic for the cation. Broad strong bands in the N–H stretching region are observed in the IR spectra of **38** and **38**·5-At. These bands are of very low intensity in the respective Raman spectra. In addition to the anion stretch bands, the strongest absorption in the IR spectra is the combined C=NH_2 stretching and the NH_2 deformation modes found at 1701 cm^{-1} for both compounds, which supposes a red shift in comparison to other tetrazolium salts, which generally shown bands at ~1685 cm^{-1}.[68] Lastly, the rest of the bands are of lower intensity and can be assigned as follows: 1550–1350 cm^{-1} [ν(tetrazole ring)], 1350–700 cm^{-1} [ν(N–C–N), ν(N–N), γ(CN), δ(tetrazole ring)], < 700 cm^{-1} [δ out-of-plane bend (N–H), ω(NH_2)].[232]

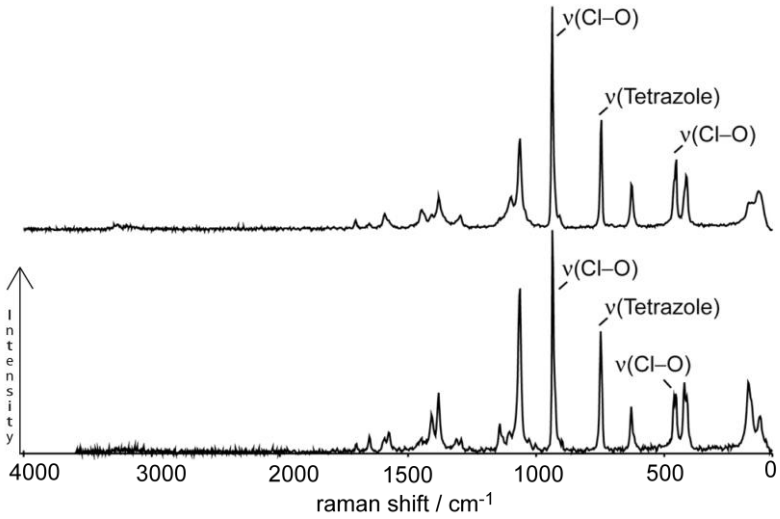

Figure 3.27 Raman spectra of 5-amino-1*H*-tetrazolium perchlorate (**38**) (above) and its 5-At adduct (below).

Also compounds **39**–**41** can be easily identified using vibrational spectroscopy such as IR and Raman spectroscopy. In the Raman spectra (**Figure 3.28**) the most intense band at about 930 cm^{-1} is caused by the $\nu_s(ClO_4^-)$ vibration, which is not active in the IR spectra. The perchlorate anion shows further characteristic vibrations at about 459 cm^{-1} (δ_s), 625 cm^{-1} (δ_{as}) and 1119 cm^{-1} (ν_{as}). The N–H stretch vibrations can only be obtained as weak peaks in the Raman spectra in the range of 3200–3400 cm^{-1}. The azidoformamidinium cation in **41** causes the characteristic vibrations at 2189 and 2128 cm^{-1} in the Raman spectra, which can be assigned to the ν_{sym} and ν_{asym} of the covalent azide. The very weak vibrations in the range of 1400–1700 cm^{-1} can be assigned to C–N and N–N stretching vibrations of the cations.

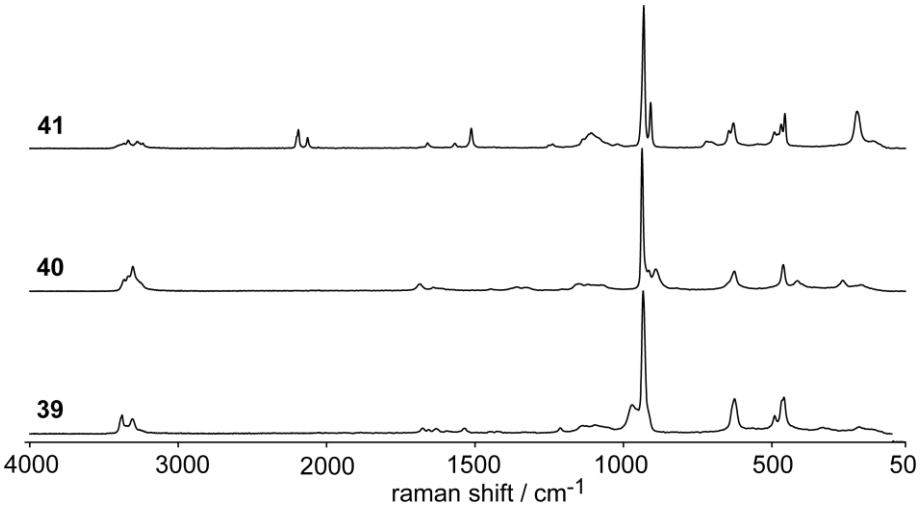

Figure 3.28 Raman spectra of **39**–**41**.

3.7 Thermodynamic and Energetic Properties

The thermal stability and sensitivity to impact, friction, electrostatic discharge and thermal shock of the dinitramide and perchlorate salts **31–42** were experimentally determined by DSC measurements and standard sensitivity tests, respectively. In addition heats of formation were determined and detonation parameters have been calculated. The results of the tests are summarized in **Table 3.9**.

3.7.1 Differential Scanning Calorimetry (DSC)

In order to determine the decomposition temperatures, a Linseis DSC PT 10 with a heating rate (β) of 5 K min^{-1} and a nitrogen flow of 5 L h^{-1} was used. The measurements with ~1.5 mg of **31–37** were performed in pressed Al-containers, containing a hole (0.1 mm) for the gas release. The DSC plots in **Figure 3.29** show the thermal behavior of **31–37** in the 50–360 °C temperature range. Temperatures are given as "onset temperatures". **31** melts at 85 °C and decomposes at 117 °C, while its isomer **32** decomposes violently at nearly the same temperature of 116 °C. **32** cannot be dehydrated until its decomposition temperature. However, water free **32** should be hard to handle due to its high sensitivities even as monohydrate. We cannot confirm the decomposition temperature of **31** of 180 °C reported in literature![176] In contrast to **34**, which melts at 75 °C and decomposes above 145 °C, **33** decomposes without prior melting at 135 °C. **35** and **36** are also characterized by low melting (**35**: 70, **36**: 90 °C) and decomposition temperatures (**35**: 154, **36**: 110 °C). Unfortunately all decomposition temperatures investigated in this work are quite low for use in technical applications, whereas the salts are not volatile and seem to be long term stable in TSC (thermal safety calorimetry) experiments up to a temperature of 80 °C.

DSC revealed high thermal stabilities for compounds **38** and **38**·5-At with highly exothermic decompositions. **38** shows distinctive melting followed by vigorous decomposition beyond the melting point, whereas **38**·5-At melts with concomitant decomposition. The DSC plots in **Figure 3.30** show the thermal behavior of ~2.0 mg of **39**, **40** and **41** in the 50–400 °C temperature range. The temperature of decomposition can be related to the sensitivity of the compounds. $AFClO_4$ has the lowest decomposition point (125 °C), $TAGClO_4$ is second (180 °C) and $AGClO_4$ is the most stable compound and

decomposes not until 250 °C. The investigated salts have discrete melting points, whereby melting temperatures do not follow the trend of the decomposition temperatures. $TAGClO_4$ has the highest melting point within this row (**39**: 72 °C, **40:** 125 °C, **41**: 75 °C), which can be explained by the many hydrogen bonds observed in this structure.

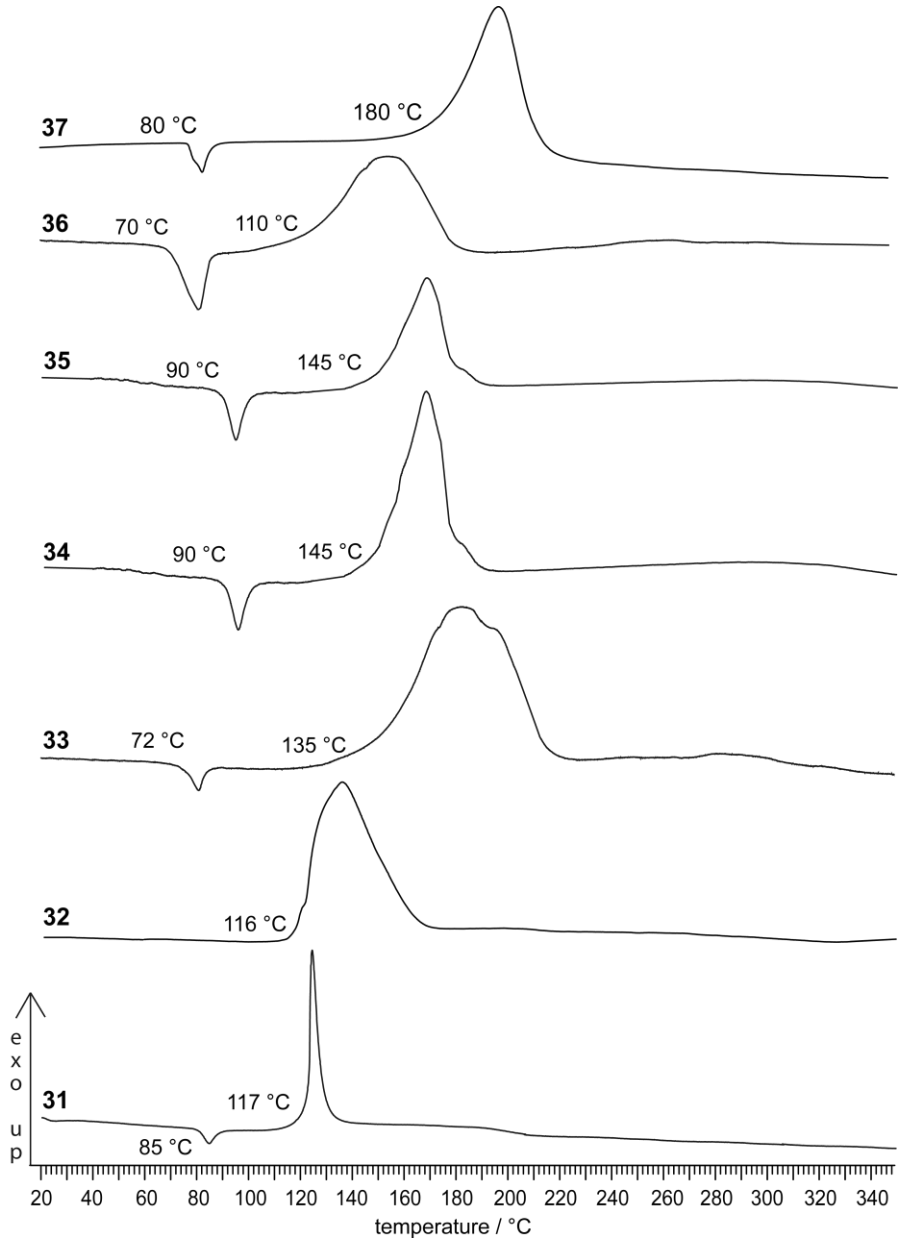

Figure 3.29 DSC plots (exo up) of **31**–**37** (β = 5 °C min^{-1}).

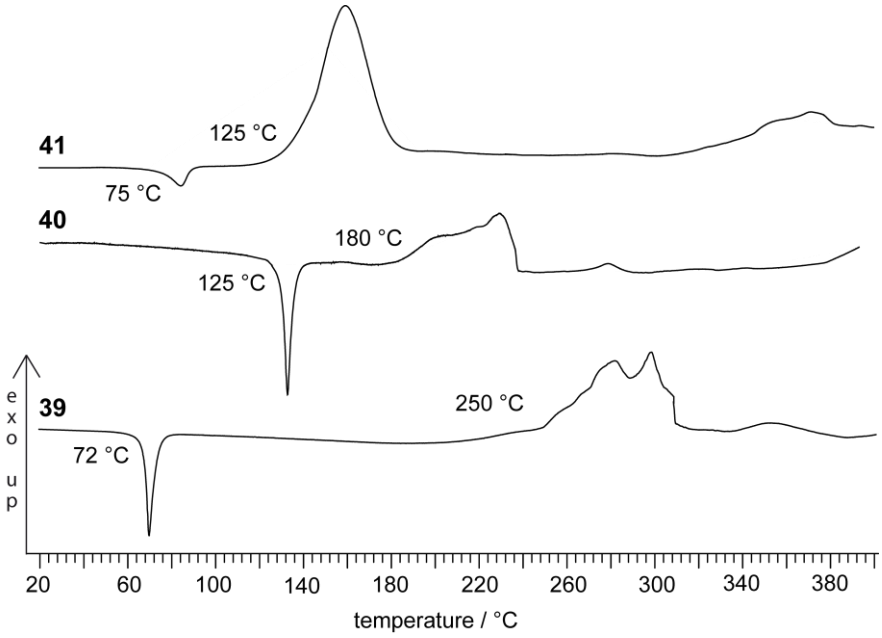

Figure 3.30 DSC plots (exo up) of **39**–**41** (β = 5 °C min^{-1}).

3.7.2 Heats of Formation

The heats of formation of **31**–**36** have been calculated by the atomization energy method, which was explained in Chapter 1. **Tables 3.4–3.9** summarizes the calculation pathway.

Table 3.3 CBS-4M results.

	p.g.	$-H^{298}$ / a.u.	$-G^{298}$ / a.u.	*NIMAG*
HAT^+	C_s	313.534215	313.567694	0
DN^-	C_2	464.499549	464.536783	0
AF	C_s	313.533549	313.570115	0
$HDAT^+$	C_1	368.793548	368.829752	0
1-MeHAT^+	C_1	352.779155	352.816869	0
2-MeHAT	C_1	352.783676	352.821342	0
HTZ^+	C_{2v}	258.229407	258.259436	0
H		0.500991	0.514005	0
C		37.786156	37.803062	0
N		54.522462	54.539858	0
O		74.991202	75.008515	0

Table 3.4 Literature values for atomic $\Delta H°_f^{298}$ / kcal mol^{-1}.

	Ref. [125]	NIST [122]
H	52.6	52.1
C	170.2	171.3
N	113.5	113.0
O	60.0	59.6

Table 3.5 Enthalpies of the gas-phase species M.

M	M	$\Delta_f H°$(g,M) / kcal mol^{-1}
HAT^+	CH_4N_5	+235.0
DN^-	$N(NO_2)_2^-$, $N_3O_4^-$	–29.6
AF^+	$(H_2N)_2CN_3^+$, $CH_4N_5^+$	+235.4
$HDAT^+$	$CH_5N_6^+$	+252.2
1-$MeHAT^+$	$C_2H_6N_5^+$	+224.0
HTZ^+		+246.3
2-$MeHAT^+$	$C_2H_6N_5^+$	+221.2

The lattice energies (U_L) and lattice enthalpies (ΔH_L) (**Table 3.7**) were calculated from the gas-phase enthalpies (**Table 3.5**) and the corresponding molecular volumes (**Table 3.6**) according to the equations, provided by Jenkins *et al.*. [118]

Table 3.6 Molecular volumes.

	V_M / Å^3	V_M / pm^3
DN^-	89 [a]	0.089 [c]
$[HAT]^+$	69 [b]	0.069 [b]
$[NH_4][DN]$	110 [61]	0.110
[AF][DN]	174 [d]	0.174
$[HDAT]^+$	93 [e]	0.093
[1-$MeHAT]^+$	99 [f]	0.099
[HDAT][DN]	182 [g]	0.182
[1-MeHAT][DN]	208 [h]	0.208
[2-MeHAT][DN]	206.4 [i]	0.206
[2-$MeHAT]^+$	117.4 [j]	0.117

$[HTZ]^+[DN]^-$	161.3	0.161

[a] this work, back-calculated from V(ADN) using the molecular volume for NH_4^+ from the literature; [b] The molecular volume of $[HAT]^+$ was calculated from the molecular volume of $[HAT][NO_3]$ – $V_M(NO_3^-)$. [c] from single crystal X-ray data; [d] The molecular volume of anhydrous [AF][DN] was calculated from the experimental volume of $[AF][DN]\cdot H_2O$ – $V_M(H_2O$, hydrate); [e] The molecular volume of $[HDAT]^+$ was calculated from the molecular volumes of $[HDAT][NO_3]$ and $[HDAT][ClO_4]$; [f] from single crystal X-ray data; [g] The molecular volume of [HDAT][DN] was taken to be equal to $V([HDAT]^+) + V([DN]^-)$; [h] from X-ray data, V = 416 Å^3, Z = 2; [j] from X-ray data, V = 412.8 Å^3, Z = 2; [j] the molecular volume of $[2\text{-MeHAt}]^+$ was calculated as $V([2\text{-MeHAt}]^+) = V([2\text{-MeHAt}]^+[DN]^-) - V([DN])$.

Table 3.7 Lattice energies and lattice enthalpies.

	V_M / nm^3	U_L / kJ mol^{-1}	ΔH_L / kJ mol^{-1}	ΔH_L / kcal mol^{-1}
[AF][DN]	0.174	524.0	529.0	126.4
[HAT][DN]	0.172	525.6	530.6	126.8
[HDAT][DN]	0.182	517.8	522.8	124.9
[1-MeHAT][DN]	0.208	499.7	504.7	120.6
$[HTZ]^+[DN]^-$	0.161	535.0	540.0	129.1
[2-MeHAT][DN]	0.206	501.1	506.1	121.0

With the calculated lattice enthalpies (**Table 3.7**) the gas-phase enthalpies of formation (**Table 3.5**) were converted into the solid state (standard conditions) enthalpies of formation (**Table 3.8**). These molar standard enthalpies of formation (ΔH_m) were used to calculate the molar solid state energies of formation (ΔU_m) (**Table 3.8**) according to the following equation:

$\Delta U_m = \Delta H_m - \Delta n\, RT$ (Δn being the change of moles of gaseous components).

Table 3.8 Solid state energies of formation ($\Delta_f U°$).

	$\Delta_f H°$(s) / kcal mol^{-1}	Δn	$\Delta_f U°$(s) / kcal mol^{-1}	M / g mol^{-1}	$\Delta_f U°$(s) / kJ kg^{-1}
[HAT][DN] (**31**)	+78.6	–8	+83.3	192.1	+1813.3
[AF][DN] (**32**)	+79.4	–8	+84.0	192.1	+1829.6
[HDAT][DN] (**33**)	+97.7	–9	+103.0	207.1	+2080.8

[1-MeHAT][DN] (**34**)	+73.8	–9	+79.1	206.1	+1605.8
[2-MeHAT][DN] (**35**)	+70.6	–9	+75.9	206.1	+1540.8
[HTZ][DN] (**36**)	+87.6	–7	+91.7	177.1	+2166.4
[TAG][DN] (**37**)[a]	+59.6	–11	+66.1	211.1	+1310.1

[a] The heat of formation of **37** has been computed using the *ab initio* method as described in the introduction.

3.7.3 Sensitivities

The sensitivities of **31**–**41** were tested using the BAM drop hammer, BAM friction tester and the OZM small scale electrical spark device. The compounds were fine grinded (0.08 – 0.12 mm) before testing. The sensitivities are summarized in **Table 3.9**.

Compounds **31**–**37** are very sensitive towards impact: **31** (2 J), **32**·H_2O (2 J), **33** (2 J), **34** (4 J), **35** (5 J), **36** (2 J) and **37** (2 J). In addition **31**–**37** show also increased sensitivities towards friction: **31** (20 N), **32**·H_2O (7 N), **33** (5 N), **34** (112 N), **35** (64 N), **36** (28 N) and **37** (24 N). According to the "UN Recommendations on the transport of dangerous goods", **31**–**37** are classified as "very sensitive" or at least "sensitive" (**35**) in both categories. Therefore compounds **31**–**33** as well as **36** and **37** are assigned to the class of primary explosives. To reduce these highly sensitive values several attempts were performed by adding wax, cyclodextrine or polyvinyl alcohol to **37**. The best results were obtained by adding wax in the 3 % and 5 % scale. (97 % TAGDN, 3 % wax: impact = 4.5 J, friction = 42 N; 95 % TAGDN, 5 % wax: impact = 5.0 J, friction = 50 N).

The electrical spark sensitivities of **31**–**37** (crystal size 75–125 µm) were determined to be 750 mJ (**31**), 930 mJ (**32**·H_2O), 670 mJ (**33**), 980 mJ (**34**), 800 mJ (**35**), 500 mJ (**36**) and 200 mJ (**37**) which are less sensitive compared to RDX (~200 mJ) and lead azide (5 mJ). However, these values should be treated with reserve, since the electrical spark sensitivity is strongly dependent on the particle size and shape.

The perchlorate salt **38** is a hazardous material with a high impact sensitivity (*IS*) of 1.5 J, accompanied by a high friction sensitivity (*FS*) of 8 N. These values classify **38** as a very sensitive (impact) and extremely sensitive (friction) material according to the "UN Recommendations on the Transport of Dangerous Goods".[107] Comparison with

commonly used materials is useful for assessing the energetic properties of this compound. **38** is more sensitive to impact than lead azide (*IS* = 3.0–6.5 J, for technical grade product) and has a comparable friction sensitivity to other initiator explosives.[34] However, the presence of neutral 5-At in perchlorate salt **38**·5-At results in a complex hydrogen-bonded network (see X-ray discussion above), which translates in decreased sensitivity values and the material is less impact sensitive than common secondary explosives such as TNT (22 vs. 15 J) although more friction sensitive (260 vs. 355 N). This is the principal reason why compounds that can form multiple hydrogen bonds are of interest as prospective insensitive materials with high densities and performances.[35,36] Comparison with similar nitrate and perchlorate salts reported in our group shows an expected increased sensitivity to both impact and friction for the perchlorate salts in comparison to the analogous nitrate salts. The formal replacement of the methyl group in 1-methyl-5-amino-1*H*-tetrazolium perchlorate by a proton in compound **38** increases both, impact and friction sensitivity only slightly.

Compound **39**, as well as compound **40** are sensitive towards impact (**39**: > 4 J, **40**: > 3 J) and therefore are classified as "sensitive". Since the impact sensitivity (> 2 J) of **41** is lower than that of lead azide,[308] it is classified as "extremely sensitive" and should be considered to be a primary explosive. Therefore, **41** should only be handled with appropriate precautions! Also the extreme friction sensitivity of 5 N is the highest observed in this chapter. Compounds **39** and **40** are significantly less sensitive towards friction (**39**: > 110 N, **40**: > 45 N). Tetrazolium perchlorate (**42**) has not been tested towards its sensitivities, due to its high hygroscopicity.

3.7.4 Detonation Parameters

The calculation of the detonation parameters of compounds **31**–**37** was performed with the program package EXPLO5 (version 5.02). The results are summarized in **Table 3.9**.

Especially the detonation parameters of compound **31** and **36** show very promising values exceeding these of TNT and RDX and in part even these of HMX. The most important criteria of high explosives are the detonation velocity ($V_{det.}$= **31**: 9429, **36**:

9215, TNT: 7000, RDX: 8936, HMX: 9100 m s^{-1}), the detonation pressure ($p_{det.}$ = **31**: 384, **36**: 365 RDX: 346 kbar) and the energy of explosion ($\Delta_E U°$ = **31**: –6186, **36**: –6227, RDX: –60432 kJ kg^{-1}).

Table 3.9 Sensitivities and Detonation parameters of **31**–**37**.

	31	**32**	**32**·H_2O	**33**	**34**	**35**	**36**	**37**	**RDX**
Molec. Mass (g mol^{-1})	192.1	192.1	210.1	207.1	206.1	206.1	177.1	211.2	222.1
Impact sensitivity [a] (J)	2		2	2	4	5	2	2	7
Friction sens. [b] (N)	20		7	5	112	64	28	24	120
ESD [c] (J)	0.75		0.93	0.67	0.98	0.80	0.50	0.20	0.2
Koenen test [d] (mm)	≥10							≥10	8
N [e] (%)	58.33	58.33	53.33	60.87	54.36	54.36	36.14	59.7	37.8
Ω [f] (%)	0	0	0	–3.9	–23.3	–23.3	4.5	–18.9	–21.6
$T_{dec.}$ [g] (°C)	117		116	135	145	148	130	180	213
Density [h] (g cm^{-3})	1.856		1.754	1.771	1.646	1.659	1.824	1.628	1.82
$-\Delta_c H$ [i] (kJ mol^{-1})			1560					2027	2105
$\Delta_f H_m°$ [j] (kJ mol^{-1})	329	332	109	431	331	296	367	251	67
$\Delta_f U°$ [k] (kJ kg^{-1})	1813	1830	631	2081	1606	1541	2166	1310	400
calculated values by EXPLO5:									
$-\Delta_E U°$ [l] (kJ kg^{-1})	6186	6168	5806	6192	5842	5785	6227	5902	6043
T_E [m] (K)	4657	4710	4302	4632	4280	4266	4880	3986	4321
p_{C-J} [n] (kbar)	384	338	330	360	287	290	365	299	346
$V_{Det.}$ [o] (m s^{-1})	9429	9013	8971	9306	8481	8548	9215	8796	8936
Gas vol. [p] [L kg^{-1}]	822	823	857	865	844	842	794	932	794

[a] BAM drophammer (grain size: 75–125 µm); [b] BAM friction tester (grain size: 75–125 µm); [c] OZM small scale electrostatic discharge device; [d] hole width of steel sleeve (see Chapter 1); [e] Nitrogen content; [f] Oxygen balance; [g] Temperature of decomposition by DSC (β = 5 °C); [h] Calc. by X-ray determination; [i] Experimental (constant volume) combustion energy; [j] Molar enthalpy of formation; [k] Energy of formation; [l] Energy of explosion; [m] Explosion temperature [n] Detonation pressure; [o] Detonation velocity; [p] Assuming only gaseous products.

3.7.5 Koenen Tests

5-Aminotetrazolium dinitramide (**31**) and triaminoguanidinium dinitramide (**37**), were investigated according to their explosion performance under confinement using a *"Koenen test"* steel sleeve apparatus (see introduction). The *Koenen* test was performed with 26.0 g **31** as well as 23.6 g of triaminoguanidinium dinitramide (**37**) using closing plates with an orifice of 10 mm. The first trials were successful indicated by the rupture of the steel tube into partly powder like pieces, which are shown in **Figure 3.31** and **Figure 3.32**. TNT destroys the steel sleeve up to an orifice width of 6 mm, RDX and HMX even up to 8 mm. Compared to these applied explosives the performance of **31** and **37** are obviously better, which in the first one was suggested by the detonation parameters, which exceeds the values of RDX and HMX. The explosion occurred within 1 ms, which was observed using a high speed camera (4000 frames s^{-1}). The experimental detonation velocities were also estimated to be close to 9000 ± 500 m s^{-1}.

Figure 3.31 A) Steel Sleeve loaded with 25 mL explosive; B) Koenen test setup showing the four Bunsen burners; C) Moment of explosion (0.25 ms) of HATDN; D) Collected fragments.

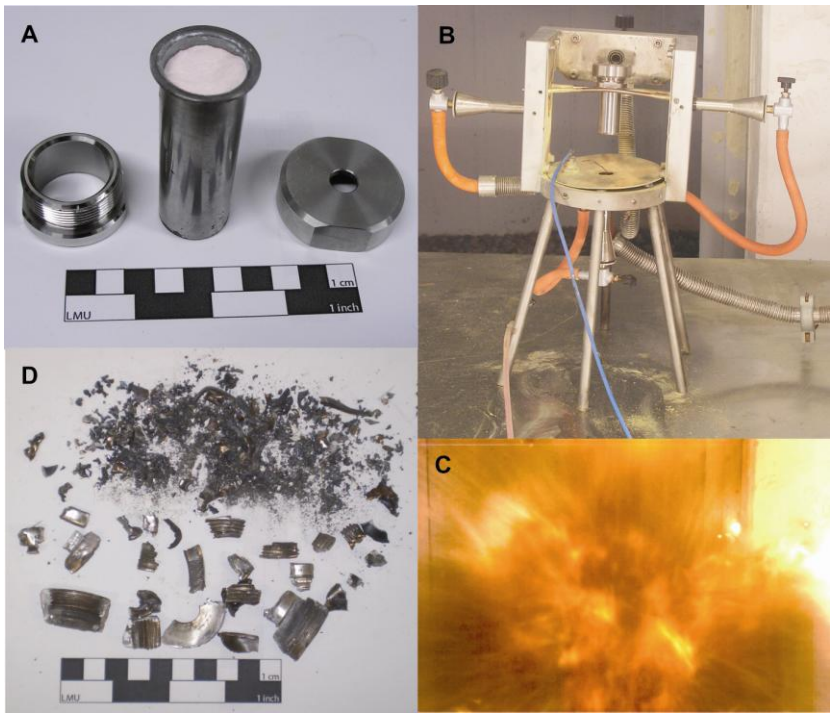

Figure 3.32 A) Steel sleeve loaded with 23.6 g of **37**; B) *Koenen* test setup showing four *Bunsen* burners; C) Moment of explosion filmed using a high speed camera (4000 frames s^{-1}); D) Result of the Koenen test showing the collected fragments.

3.8 Experimental Part

WARNING! All compounds in this chapter are highly energetic and also partly very sensitive materials. Proper protective measures should be used during all synthetic steps! Kevlar gloves and ear plugs are absolutely mandatory!

*5-Aminotetrazolium dinitramide (**31**).* A solution of 5-aminotetrazolium perchlorate (5.56 g, 30 mmol) in 15 mL water was combined with a solution of potassium dinitramide (4.35 g, 30 mmol) in 25 mL water. 10 mL of ethanol were added and the mixture was stirred for 20 min. The potassium perchlorate precipitated was filtered off and the solution was evaporated to dryness using high vacuum (5.36 g, 92 %). Single crystals suitable for X-ray diffraction were obtained by recrystallization from ethanol. **DSC** (T_{onset}, 5 °C min^{-1}): 85 °C, 117 °C (dec.); **IR** (KBr, cm^{-1}): $\tilde{\nu}$ = 3332 (s), 3154 (s), 2077 (w), 1698 (s), 1535 (s), 1430 (m), 1343 (m), 1291 (m), 1199 (s), 1177 (vs), 1023 (s), 953 (m), 826 (w), 761 (w), 731 (m), 719 (w), 624 (m), 543 (m), 470 (m); **Raman** (1064 nm,

200 mW, 25 °C, cm^{-1}): $\tilde{\nu}$ = 3315 (6), 1692 (5), 1594 (6), 1577 (8), 1536 (8), 1449 (14), 1391 (10), 1325 (100), 1163 (9), 1066 (43), 1032 (10), 1017 (11), 958 (15), 824 (48), 749 (59), 490 (29), 416 (25), 319 (17); **^{1}H NMR** (d_6-DMSO, 25 °C, ppm): δ = 6.84 (br, s, 4*H*); **^{13}C NMR** (d_6-DMSO, 25 °C, ppm): δ = 150.3 (C1); **^{14}N NMR** (d_6-DMSO, 25 °C, ppm): δ = –12 (NO$_2$); **^{15}N NMR** (D$_3$C–OD, 25 °C, ppm): δ = –12.5 (NO$_2$), –27.2 (N2,N3), –177.6 (N1,N4), –329.2 (NH$_2$); ***m/z*** (FAB$^+$): 86; (FAB$^-$): 106; **EA** ($CH_4N_8O_4$, 192.09) calcd.: C 5.69, H 4.30, N 59.70 %; found: C 5.67, H 4.01, N 58.66 %; **impact sensitivity**: 2 J; **friction sensitivity**: 20 N; **ESD**: 750 mJ.

*Azidoformamidinium dinitramide monohydrate (**32**·H_2O)*. To a solution of azidoformamidinium perchlorate (1.86 g, 10 mmol) in 15 mL water a solution of potassium dinitramide (1.45, 10 mmol) in 20 mL water was added drop wise. After stirring for one hour at room temperature the precipitate formed was filtered off and the solution was evaporated to dryness. The colorless crude product was recrystallized from a small amount of ethanol. **32** was obtained as its monohydrate (1.89 g, 90 %). **DSC** (T_{onset}, 5 °C min^{-1}): 120 °C (dec.); **IR** (ATR, cm^{-1}): $\tilde{\nu}$ = 3615 (s), 3541 (m), 3330 (vs), 3248 (s), 3136 (s), 2184 (s), 2127 (m), 1676 (s), 1652 (s), 1623 (m), 1523 (s), 1490 (s), 1447 (s), 310 (w), 1250 (m), 1187 (s), 1075 (w), 1018 (m), 898 (w), 743 (m), 647 (m); **Raman** (1064 nm, 200 mW, 25 °C, cm^{-1}): $\tilde{\nu}$ = 3326 (6), 2184 (40), 2115 (10), 1647 (6), 1503 (12), 1454 (17), 1321 (100), 1232 (7), 1172 (11), 1107 (13), 1014 (9), 962 (16), 904 (41), 824 (47), 763 (7), 660 (16), 500 (19), 485 (19), 471 (24), 298 (24), 218 (43); **^{1}H NMR** (D$_2$O, 25 °C, ppm): δ = 8.50 (br, NH$_2$); **^{13}C NMR** (D$_2$O, 25 °C, ppm): δ = 159.9 (C1); **^{15}C NMR** (D$_2$O, 25 °C, ppm): δ = 11.9 (NO$_2$), –58.4 (N(NO$_2$)$_2$), –137.5 (–N=N_β=N), –151.3 (–N=N=N_γ), –290.8 (NH$_2$); ***m/z*** (FAB$^+$): 86; (FAB$^-$): 106; **EA** ($CH_6N_8O_5$, 210.11) calcd.: C 5.72, H 2.88, N 53.33 %; found: not determinable; **impact sensitivity:** 2 J; **friction sensitivity:** 7 N; **ESD**: 930 mJ.

*1,5-Diaminotetrazolium dinitramide (**33**)*: A solution of 1,5-diaminotetrazolium perchlorate (4.00 g, 20 mmol) in 10 mL water was combined with a solution of potassium dinitramide (2.90 g, 20 mmol) in 10 mL water. 10 mL of ethanol were added and the mixture was stirred for 30 min. The potassium perchlorate precipitated was filtered off and the solution was evaporated to dryness using high vacuum. The residue was dissolved in 15 mL EtOH and remained $KClO_4$ was again removed by filtration. After evaporation of EtOH the product was obtained as colorless crystalline residue. (3.94 g, 85 %). Single crystals suitable for X-ray diffraction were obtained by recrystallization

from ethanol. **DSC** (T_{onset}, 5 °C min^{-1}): 72 °C, 135 °C (dec.); **IR** (KBr, cm^{-1}): $\tilde{\nu}$ = 3318 (s), 3251 (s), 3153 (s), 3093 (s), 1781 (vs), 1616 (w), 1535 (s), 1429 (m), 1343 (m), 1290 (m), 1202 (s), 1177 (s), 1143 (m), 1119 (m), 1022 (s), 951 (w), 827 (w), 813 (w), 761 (m), 749 (w), 731 (m), 703 (w), 689 (w), 653 (w), 626 (m), 567 (m); **Raman** (1064 nm, 200 mW, 25 °C, cm^{-1}): $\tilde{\nu}$ = 3367 (12), 3305 (22), 3251 (11), 1717 (10), 1624 (9), 1581 (13), 1512 (19), 1447 (26), 1350 (26), 1313 (100), 1186 (11), 1130 (11), 1002 (26), 962 (25), 932 (15), 821 (63), 783 (80), 691 (26), 487 (45), 315 (46), 302 (47), 239 (24); **^{1}H NMR** (d_4-MeOH, 25 °C, ppm): δ = 5.14 (s, NH, NH_2); **^{13}C NMR** (d_4-MeOH, 25 °C, ppm): δ = 150.5 (CN_4; **^{14}N NMR** (d_4-MeOH): δ (ppm): = –11 (N(NO_2); **^{15}N NMR** (d_4–MeOH): δ = –12.8 (N(NO_2)$_2$), –21.5 (N3), –34.7 (N2), –165.8 (N1), –172.5 (N4), –318.6 (N6), –330.7 (N5); ***m/z*** (FAB^+): 101; (FAB^-): 106; **EA** ($CH_5N_9O_4$, 207.11) calcd.: C 5.80, H 2.43, N 60.87 %; found: not determinable; **impact sensitivity**: 2 J; **friction sensitivity**: < 5 N; **ESD**: 670 mJ.

*1-Methyl-5-aminotetrazolium dinitramide (**34**)*: A solution of 1-methyl-5-aminotetrazolium perchlorate (1.99 g, 10 mmol) in 10 mL water was combined with a solution of potassium dinitramide (1.45 g, 10 mmol) in 10 mL water. 10 mL of ethanol were added and the mixture was stirred for 20 min. The potassium perchlorate precipitated was filtered off and the solution was evaporated to dryness using high vacuum (1.96 g, 95 %). Single crystals suitable for X-ray diffraction were obtained by recrystallization from ethanol. **DSC** (T_{onset}, 5 °C min^{-1}): 90 °C, 145 °C (dec.); **IR** (KBr, cm^{-1}): $\tilde{\nu}$ = 3352 (s), 3258 (s), 3179 (s), 3105 (s), 2860 (m), 2739 (m), 2677 (m), 1692 (vs), 1542 (s), 1462 (m), 1417 (m), 1352 (m), 1200 (s), 1066 (w), 1030 (s), 972 (w), 953 (w), 804 (m), 777 (m), 745 (m), 714 (m), 665 (w), 627 (w), 485 (m), 448 (w); **Raman** (1064 nm, 200 mW, 25 °C, cm^{-1}): $\tilde{\nu}$ = 3262 (5), 3052 (10), 3013 (8), 2962 (22), 1715 (8), 1610 (6), 1535 (18), 1511 (8), 1464 (27), 1452 (29), 1419 (13), 1356 (17), 1302 (62), 1272 (27), 1235 (8), 1150 (8), 1064 (8), 1043 (14), 1013 (20), 975 (14), 810 (36), 777 (100), 672 (19), 487 (31), 464 (21), 450 (15), 301 (57), 229 (21); **^{1}H NMR** (d_6-DMSO, 25 °C, ppm): δ = 8.48 (2*H*, s), 3.68 (3*H*, CH_3); **^{13}C NMR** (d_6-DMSO, 25 °C, ppm): δ = 153.7 (CN_4), 32.7 (CH_3); **^{14}N NMR** (d_6-DMSO, 25 °C, ppm): δ = –11 (N(NO_2); **^{15}N NMR** (d_4-MeOH, 25 °C, ppm): δ (ppm): = –12.8 (N(NO_2)$_2$), –24.3 (N2, q, $^{3}J_{NH}$ = 1.9 Hz), –31.3 (N3), –176.3 (N4), –183.4 (N1, q, $^{2}J_{NH}$ = 2.1 Hz), –328.7 (N5); ***m/z*** (FAB^+): 100; (FAB^-): 106; **EA** ($C_2H_6N_8O_4$, 206.12): calc. C 11.65, H 2.93, N 54.36 %; found: C 12.00, H 3.04, N 54.06 %; **impact sensitivity**: 4 J; **friction sensitivity**: 112 N; **ESD**: 980 mJ.

*2-Methyl-5-aminotetrazolium dinitramide (**35**):* A solution of 2-methyl-5-aminotetrazolium perchlorate (1.99 g, 10 mmol) in 10 mL water was combined with a solution of potassium dinitramide (1.45 g, 10 mmol) in 10 mL water. 10 mL of ethanol were added and the mixture was stirred for 20 min at 0 °C. The potassium perchlorate precipitated was filtered off and the solution was evaporated to dryness using high vacuum (1.96 g, 95 %). Single crystals suitable for X-ray diffraction were obtained by recrystallization from ethanol. **DSC** (T_{onset}, 5 °C min^{-1}): 90 °C, 148 °C (dec.); **IR** (KBr, cm^{-1}): $\tilde{\nu}$ = 3283 (s), 3181 (s), 3098 (s), 2754 (m), 1662 (vs), 1586 (m), 1532 (s), 1431 (s), 1343 (m), 1182 (vs), 1078 (w), 1021 (s), 952 (w), 827 (w), 803 (w), 761 (m), 731 (m), 969 (s), 647 (m), 552 (w), 481 (w); **Raman** (1064 nm, 200 mW, 25 °C, cm^{-1}): $\tilde{\nu}$ = 3297 (11), 3060 (20), 3038 (17), 2970 (40), 1674 (12), 1591 (12), 1541 (18), 1500 (16), 1437 (43), 1384 (39), 1305 (100), 1179 (19), 1088 (28), 1028 (37), 963 (28), 934 (21), 816 (56), 647 (54), 488 (39), 474 (40), 323 (26), 300 (34), 228 (23), 181 (26); **^{1}H NMR** (d_6-DMSO, 25 °C, ppm): δ = 6.17 (2H, s), 4.29 (3H, CH_3); **^{13}C NMR** (d_6-DMSO, 25 °C, ppm): δ = 160.5 (CN_4), 40.6 (CH3); **^{14}N NMR** (d_6-DMSO, 25 °C, ppm): δ = –14 ($N(NO_2)_2$); **^{15}N NMR** (d_6-DMSO, 25 °C, ppm): δ = –14.5 ($N(NO_2)_2$), –20.5 (N3, q, $^{3}J_{NH}$ = 1.7 Hz), 107.4 (N2, q, $^{2}J_{NH}$ = 2.1 Hz), –108.0 (N4, q, $^{3}J_{NH}$ = 1.7 Hz), –108.2 (N1), –339.2 (N5); ***m/z*** (FAB^+): 100; (FAB^-): 106; **EA** ($C_2H_6N_8O_4$, 206.12): calc. C 11.65, H 2.93, N 54.36 %; found: C 11.64, H 3.14, N 53.96 %; **impact sensitivity**: 4 J; **friction sensitivity**: 112 N; **ESD**: 980 mJ.

*Tetrazolium dinitramide (**36**):* To 10 mL of an aqueous tetrazolium perchlorate (850 mg, 5.0 mmol) solution, 10 mL of an aqueous potassium dinitramide (725 mg, 5.0 mmol) solution was added. After stirring for 1 h at 0 °C the precipitated potassium perchlorate was filtered off and the solvent was removed by evaporation. 20 mL of ethanol were added and remaining $KClO_4$ was filtered off. After removing the solvent at room temperature using high vacuum, hygroscopic colorless crystals were obtained (8.35 g, 98 %). **DSC** (T_{onset}, 5 °C min^{-1}): 70 °C (mp.), 110 °C (dec.); **IR** (KBr, cm^{-1}): $\tilde{\nu}$ = 3140 (s), 3060 (s), 2902 (m), 2587 (w), 2361 (w), 1525 (vs), 1456 (s), 1329 (w), 1309 (m), 1176 (vs), 1136 (s), 1017 (s), 953 (m), 824 (m), 741 (s); **Raman** (1064 nm, 300 mW, 25 °C, cm^{-1}): $\tilde{\nu}$ = 3138 (6), 1538 (11), 1489 (9), 1460 (15), 1416 (5), 1332 (100), 1312 (54), 1220 (9), 1143 (9), 1063 (17), 976 (16), 828(28), 478 (13), 443 (6), 313 (19), 202 (6); **^{1}H NMR** (d_6-DMSO, 25 °C, ppm): δ = 11.83 (s, 2*H*, N*H*), 9.23 (s, 1*H*, C*H*); **^{13}C NMR** (d_6-DMSO, 25 °C, ppm): δ = 143.7; **^{14}N NMR** (d_6-DMSO, 25 °C, ppm): δ = –11; **^{15}N NMR** (d_6-DMSO, 25 °C, ppm): δ = –8.1 (N2), –11.1 (NO_2), –101.4 (N1); ***m/z*** (FAB^+): 71; (FAB^-):

106; **EA** ($CH_3N_7O_4$, 177.08): calc. C 6.78, H 1.71, N 36.14 %; found: not determinable; **impact sensitivity**: 2 J; **friction sensitivity**: 28 N.

*Triaminoguanidinium dinitramide (**37**):* Triaminoguanidinium perchlorate (20.47 g, 0.10 mol) was dissolved in 70 mL of water. To this a solution of potassium dinitramide (14.51 g, 0.10 mol) in 50 mL of water was added drop wise while $KClO_4$ started to precipitate. The mixture was stirred for 30 min and was then filtered off. The filtrate was evaporated at 40 °C and the residue was recrystallized from hot ethanol yielding TAG-DN as colorless needles (17.3 g, 82 %). **DSC** (T_{onset}, 5 °C min^{-1}): 80 °C, 180 °C (dec.); **IR** (KBr, cm^{-1}): $\tilde{\nu}$ = 3360 (s), 3299 (vs), 3273 (vs), 1676 (s), 1491 (s), 1414 (m), 1362 (w), 1325 (m), 1155 (m), 1131 (s), 989 (m), 947 (s), 916 (s), 821 (m), 759 (m), 740 (m), 639 (w); **Raman** (1064 nm, 250 mW, 25 °C, cm^{-1}): $\tilde{\nu}$ = 3361 (28), 3311 (35), 1687 (11), 1513 (20), 1430 (19), 1326 (100), 1200 (7), 1169 (7), 1140 (9), 953 (26), 895 (32), 825 (65), 638 (10), 488 (32), 452 (12), 417 (17), 313 (22), 261 (19); **^{1}H NMR** (d_6-DMSO, 25 °C, ppm): δ = 8.57 (3*H*, s, -N*H*-), 4.45 (6*H*, s, -NH_2); **^{13}C NMR** (d_6-DMSO, 25 °C, ppm): δ = 159.6 (C1); **^{15}N NMR** (d_6-DMSO, 25 °C, ppm): δ = –10.3 (NO_2), –55.3 ($N(NO_2)_2$), –289.2 (*N*H, d, $^1J_{N\text{-}H}$ = 103 Hz), –329.8 (NH_2, t, $^1J_{N\text{-}H}$ = 73 Hz); ***m/z*** (FAB^+): 105; (FAB^-): 106; **EA** ($CH_9N_9O_4$, 211.14): calc. C 5.69, H 4.30, N 59.70 %; found: C 5.67, H 4.01, N 58.66 %; **BAM drophammer**: 2 J; **BAM friction test**: 24 N; **ESD**: 0.20 J.

*5-Amino-1H-tetrazolium perchlorate (**38**). Method A*: 5-Amino-1*H*-tetrazole monohydrate (0.153 g, 1.48 mmol) was suspended in 2 mL water and reacted carefully with a large excess of 70–72% concentrated perchloric acid (0.724 g, 5.05 mmol) to give a colorless solution. The reaction mixture was brought to boiling and refluxed for 5 min. The hot solution was then carefully transferred into a shell and left to stand. Large platelets of the compound suitable for X-ray analysis start to precipitate in the course of three weeks in excellent yield and purity (0.229 g, 83%). *Method B*: Alternatively 5-amino-1*H*-tetrazolium bromide monohydrate (0.184 g, 1.00 mmol) was reacted with anhydrous silver perchlorate (weighed out in a glove box) (0.207 g, 1.00 mmol) in 15 mL methanol for 2 h. Yellow silver bromide precipitated immediately and the solution (slightly yellow) was filtered and the solvent left to evaporate yielding either directly pure material or material which was pure after recrystallization by diffusing ether into a methanolic solution of the compound (0.155 g, 84%). **DSC** (T_{onset}, 2 °C min^{-1}): 176 (mp.), ~180 (dec.); **IR** (KBr, cm^{-1}): $\tilde{\nu}$ = 3348 (s), 3186 (s), 2076 (w), 1701(vs), 1599 (w), 1466 (w), 1383 (w), 1291 (m), 1145 (s), 1110 (vs), 1088 (vs), 1014 (m), 995 (m), 940 (w),

869 (w), 749 (w), 710 (m), 670(w), 636 (m), 626 (m), 540 (w), 472 (m), 412 (w), 400 (w), 313 (w); **Raman** (1064 nm, 200 mW, 25 °C, cm^{-1}): $\tilde{\nu}$ = 3279 (2), 1706 (5), 1592 (5), 1449 (6), 1381 (10), 1299 (4), 1100 (12), 1066 (23), 940 (100), 749 (48), 629 (25), 457 (31), 416 (27), 138 (9); **^{1}H NMR** (d_6-DMSO, 25 °C, ppm): δ = 9.70 (4H, s, NH/NH_2); **^{13}C NMR** (d_6-DMSO, 25 °C, ppm): δ = 154.7 (1C, C–NH_2); **^{35}Cl NMR** (d_6-DMSO, 25 °C, ppm): δ = 1.0 (ClO_4); ***m/z*** (FAB^+): 86.1 $(CH_4N_5)^+$, 171.1 $(CH_3N_5)_2H)^+$; **EA** ($CH_4N_5O_4Cl$, 185.53) calc.: C 6.47, H 2.17, N 37.75 %; found: C 6.43, H 2.27, N 37.55 %; **impact sensitivity**: 1.5 J; **friction sensitivity**: 8 N.

*5-Aminotetrazolium perchlorate · 5-Amino-1H-tetrazole (**38**·5-At):* 5-Amino-1*H*-tetrazole monohydrate (0.165 g, 1.60 mmol) was suspended in 1 mL water and reacted carefully with a small excess of 70–72% concentrated perchloric acid (0.310 g, 2.16 mmol). The insoluble compound dissolved on careful short heating to reflux using a heat gun giving a clear colorless solution, which was left to cool slowly overnight. Colorless single crystals of the adduct precipitated within 2–3 days (0.118 g, 55%). **DSC** (T_{onset}, 2 °C min^{-1}): 170 (dec.); **IR** (KBr, cm^{-1}): $\tilde{\nu}$ = 3420 (s), 2976 (m), 2378 (m), 2346 (m), 1701 (m), 1650 (m), 1452 (w), 1384 (w), 1298 (w), 1121 (m), 1087 (m), 1047 (m), 995 (w), 878 (w), 710 (w), 636 (w); **Raman** (1064 nm, 200 mW, 25 °C, cm^{-1}): $\tilde{\nu}$ = 3117 (3), 3066 (3), 1704 (4), 1652 (7), 1575 (9), 1409 (17), 1382 (27), 1313 (6), 1144 (13), 1066 (74), 937 (100), 750 (54), 631 (21), 457 (26), 424 (31), 174 (31), 128 (16); **^{1}H NMR** (d_6-DMSO, 25 °C, ppm): δ = 8.04 (7H, s, NH/NH_2); **^{13}C NMR** (d_6-DMSO, 25 °C, ppm): δ = 157.2 (CN_4), 154.5 (1C, CN_4^+); **^{35}Cl NMR** (d_6-DMSO, 25 °C, ppm): δ = 1.0 (ClO_4); ***m/z*** (FAB^+): 86.1 $(CH_4N_5)^+$, 171.1 $(CH_3N_5)_2H)^+$; **EA** ($C_2H_7N_{10}O_4Cl$, 270.60) calcd.: C 8.88, H 2.61, N 51.76 %; found: C 8.64, H 2.65, N 50.69 %; **impact sensitivity**: 22 J; **friction sensitivity**: 260 N.

*Aminoguanidinium perchlorate (**39**):* To aminoguanidinium bicarbonate (13.61 g, 0.10 mol) 1 M perchloric acid solution (100 mL) was added under continuous stirring. After the release of CO_2 stopped, the solvent was evaporated and the crude product was recrystallized from ethanol yielding colorless **39** (16.80 g, 96 % yield). **DSC** (T_{onset}, 5 °C min^{-1}): 72 °C, 250 °C (dec.); **IR** (ATR, cm^{-1}): $\tilde{\nu}$ = 3459 (s), 3371 (vs), 1652 (s), 1599 (m), 1537 (w), 1420 (w), 1204 (w), 1039 (s), 930 (m), 622 (m); **Raman** (1064 nm, 200 mW, 25 °C, cm^{-1}): $\tilde{\nu}$ = 3377 (13), 3307 (10), 1676 (4), 1533 (4), 1213 (4), 1137 (5), 1096 (6), 970 (20), 933 (100), 625 (24), 490 (12), 459 (25); **^{1}H NMR** (D_2O, 25 °C, ppm): δ = 8.49 (s, 1H, N*H*–NH_2), 7.15 (s, 2H, NH_2), 6.65 (s, 2H, NH_2), 4.60 (s, 2H, NH–NH_2); **^{13}C NMR**

(D_2O, 25 °C, ppm): δ = 159.3 (C1); **^{15}N NMR** (D_2O, 25 °C, ppm): δ = –285.6 (N1), –312.4 (N3, N4), –327.6 (N2); ***m/z*** (FAB^+): 75 (cation); ***m/z*** (FAB^-): 99 (ClO_4^-); **EA** ($CH_7N_4ClO_4$, 174.56) calc.: C 6.88, H 4.04, N 32.10 %; found: C 6.71, H 4.34, N 31.57 %; **impact sensitivity**: > 4 J; **friction sensitivity**: > 110 N; $\Delta U_{comb.}$: 1632 cal g^{-1}.

*Triaminoguanidinium perchlorate (**40**):* Aminoguanidinium perchlorate (8.73 g, 0.05 mol) was suspended in 40 mL of dioxane and 3 eq. of hydrazine hydrate (7.50 g, 0.15 mole, 7.3 mL) were added. The mixture was refluxed for 4 h at 90 °C until the release of NH_3 stopped. Afterwards the solvent was evaporated and the crude product was recrystallized from hot ethanol yielding **40** (9.72 g, 95 % yield). **DSC** (T_{onset}, 5 °C min^{-1}): 125 °C, 180 °C (dec.); **IR** (ATR, cm^{-1}): $\tilde{\nu}$ = 3293 (vs), 1680 (s), 1359 (w), 1218 (w), 1056 (s), 955 (m), 936 (m), 707 (w), 618 (m); **Raman** (1064 nm, 200 mW, 25 °C, cm^{-1}): $\tilde{\nu}$ = 3363 (8), 3305 (17), 1686 (4), 1638 (2), 1361 (2), 1146 (4), 937 (100), 890 (15), 626 (13), 461 (18), 414 (7), 260 (7); **^{1}H NMR** (D_2O, 25 °C, ppm): δ = 8.55 (N*H*–NH_2), 4.43 (NH–N*H*$_2$); **^{13}C NMR** (D_2O, 25 °C, ppm): δ = 159.5 (C1); **^{15}N NMR** (D_2O, 25 °C, ppm): δ = –291.2 (N1, N3, N5), –333.6 (N2, N4 N6); ***m/z*** (FAB^+): 105; ***m/z*** (FAB^-): 99 (ClO_4^-); **EA** ($CH_9N_6ClO_4$, 204.57) calc.: C 5.87, H 4.43, N 41.08 %; found: C 6.02, H 4.42, N 40.58 %; **impact sensitivity**: > 3 J; **friction sensitivity**: > 45 N; $\Delta U_{comb.}$: 2058 cal g^{-1}.

*Azidoformamidinium perchlorate (**41**):* Aminoguanidinium perchlorate (6.98 g, 0.04 mol) was dissolved in 40 mL 1 M perchloric acid solution (0.04 mol). To this, a solution of potassium nitrite (3.40 g, 0.04 mol) in 20 mL of water was added dropwise while cooling the solution at O °C. The ice bath was removed and the mixture was stirred for 30 min at RT. Afterwards urea (150 mg) was added, the precipitated potassium perchlorate was filtered off and the solvent was removed using a rotating evaporator, equipped with a water bath not hotter than 60 °C. The crude product was dissolved in a small amount of ethanol, again filtered and the ethanol was removed using high vacuum yielding colorless **41** (6.53 g, 88 % yield). Single crystals suitable for X-ray diffraction were obtained by recrystallization from 2-propanol. **DSC** (T_{onset}, 5 °C min^{-1}): 75 °C, 125 °C (dec.); **IR** (ATR, cm^{-1}): $\tilde{\nu}$ = 3394 (vs), 3336 (s), 3260 (s), 3198 (s), 2474 (w), 2410 (w), 2189 (s), 2128 (m), 1685 (vs), 1651 (m), 1503 (s), 1240 (m), 1048 (s), 928 (w), 904 (w), 714 (w), 629 (m); **Raman** (1064 nm, 200 mW, 25 °C, cm^{-1}): $\tilde{\nu}$ = 3337 (5), 3275 (5), 3237 (3), 2189 (13), 2128 (7), 1659 (3), 1567 (3), 1512 (14), 1238 (3), 1108 (11), 1019 (3), 931 (100), 908 (32), 719 (5), 644 (12), 629 (18), 491 (11), 468 (17), 456 (24), 212 (26); **^{1}H NMR** (D_2O, 25 °C, ppm): δ = 8.99 (s, 2H, N*H*$_2$), 8.56 (s, 2H, N*H*$_2$); **^{13}C NMR** (D_2O, 25 °C,

ppm): δ = 159.2 (C1); **^{15}N NMR** (D_2O, 25 °C, ppm): δ = –138.2 (N3), –152.7 (N2), –292.2 (N4, N5), –305.9 (N1); ***m/z*** (FAB^+): 86; ***m/z*** (FAB^-): 99 (ClO_4^-); **EA** ($CH_4N_5ClO_4$, M = 185.53) calc.: C 6.47, H 2.17, N 37.75 %; found: not determinable; **impact sensitivity**: > 2 J; **friction sensitivity**: > 5 N; $\Delta U_{comb.}$: 1285 cal g^{-1}.

3.9 Conclusions

From this extended study of nitrogen-rich perchlorates as well as dinitramides the following conclusions can be drawn:

- 5-Aminotetrazolium dinitramide (HAT-DN, **31**), azidoformamidinium dinitramide (AF-DN·H_2O, **32**), 1,4-diaminotetrazolium dinitramide (HDAT-DN, **33**), 1-methyl-5-aminotetrazolium dinitramide (1MeHAT-DN, **34**) 2-methyl-5-aminotetrazolium dinitramide (2MeHAT-DN, **35**), tetrazolium dinitramide (HTZ-DN, **36**) and triaminoguanidinium dinitramide (TAG-DN, **37**) were prepared in high yields from the reaction of potassium dinitramide and 5-aminotetrazolium perchlorate (**38**), azidoformamidinium perchlorate (**41**), 1,4-diaminotetrazolium perchlorate, 1-methyl-5-aminotetrazolium perchlorate, 2-methyl-5-amino-tetrazolium perchlorate, tetrazolium perchlorate (**42**) and triaminoguanidinium perchlorate (**40**), respectively.

- Protonation of 5-amino-1*H*-tetrazole (5-At) with an excess of perchloric acid afforded the corresponding perchlorate salt (**38**). Using one equivalent of perchloric acid results in the formation of an adduct between **38** and 5-At .

- Aminoguanidinium perchlorate (**39**), triaminoguanidinium perchlorate (**40**) and azidoformamidinium perchlorate (**41**) can be synthesized in high yields and purity by facile and cheap routes starting from aminoguanidinium bicarbonate.

- Strongly hygroscopic tetrazolium perchlorate (**42**) is formed by the reaction of 1*H*-tetrazole with 1 eq. of diluted perchloric acid.

- All compounds were recrystallized from ethanol or water/ethanol mixtures yielding single crystals. The solid state structures of **31**–**42** were determined by single crystal X-ray diffraction.

- The explosive and detonation parameters of **31**–**37** were obtained from a combined experimental and computational study. The obtained detonation velocity and pressure, particularly for **31** and **36**, exceeds these of RDX and also these of HMX.

- Regarding the decomposition temperature triaminoguanidinium dinitramide (180 °C) is most promising. By comparison with the detonation values reported for RDX it can be concluded that triaminoguanidinium dinitramide (TAG-DN, **37**) may also be a valuable ingredient as an energetic filler in high explosive compositions or due to its high sensitivity as an energetic component in liquid monopropellants.

- The investigated compounds **31**–**42** are highly energetic compounds with increased sensitivities towards impact and friction and should only be handled with appropriate safety precautions.

- **31** and **37** were tested in a Koenen steel sleeve apparatus using hole widths of 10 mm. Both compounds exploded violently destroying the steel tube into powder like pieces.

Chapter 4.

Nitration Products of 5-Amino-tetrazole and Methyl-5-aminotetrazoles

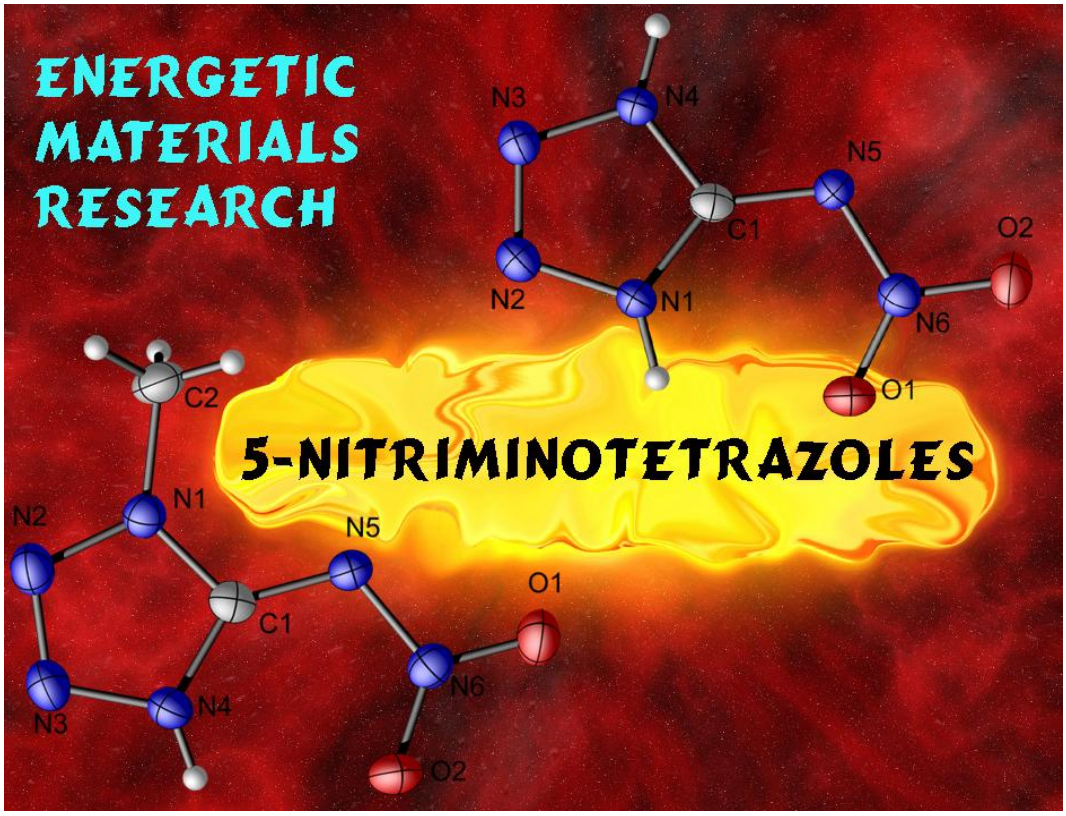

4.1 Introduction

The combination of a tetrazole ring with energetic groups containing oxygen such as nitro groups (R–NO_2),[11] nitrate esters (R–O–NO_2) [233] or nitramines (R_2N–NO_2) [234] is of particular interest. Energetic materials based on tetrazoles show the desirable properties of high nitrogen contents on the one hand, and astonishing kinetic and thermal stabilities due to aromaticity on the other. Compounds with a high nitrogen content are potential candidates for replacing common secondary explosives like RDX [235] (hexahydro-1,3,5-trinitro-*S*-triazine) and HMX [236] (octahydro-1,3,5,7-tetranitro-1,3,5,7-tetrazine), or in high-tech propellants when combined with a suitable oxidizer.[237] Nitroaminotetrazoles are of special interest because they combine both the oxidizer and energetic nitrogen-rich backbone in one molecule.

The nomenclature of nitroaminotetrazoles also referred to as nitramino-, nitriminotetrazoles or nitroiminotetrazoles is usually inconsistent in literature, [238] as a result of incomplete characterization of the previously reported compounds. Therefore, a complete characterization of three well-known nitroaminotetrazoles is given in this work. The crystal structures show the first examples of neutral 5-aminotetrazoles which has been nitrated at the primary NH_2 group. For 5-nitroaminotetrazole only the cell parameters have been published previously,[239] while several examples of 5-methyl-5-nitro-aminotetrazoles have been structurally characterized and reported in the literature.[240] On the basis of the crystal structures obtained, the nitration product of 5-aminotetrazole (**2**) is now referred to as 5-nitriminotetrazole (**43**).

Nitriminotetrazoles and corresponding metal nitraminotetrazolates [241,242,243] have been known for a long time since they are cheap and easy to manufacture via various routes. However there are two main methods. The first synthesis uses protonation of 5-aminotetrazole (**2**) [244] using warm concentrated HNO_3, to form 5-aminotetrazole nitrate, followed by dehydration with concentrated sulfuric acid [245] to form **43**. Another synthetic route is based on the cyclization of nitroguanylazide [246,247] (also known as nitroazidoformamidine).

4.2 Synthesis

The syntheses of 5-nitriminotetrazole (**43**), 1-methyl-5-nitriminotetrazole (**44**) and 2-methyl-5-nitroaminotetrazole (**45**) are presented in **Scheme 4.1**. All of the syntheses are easy, one-pot reactions using 100 % nitric acid, whereby the products are available in high quantities and good yields. Recrystallization from solvents such as ethanol, diethyl ether, acetone, THF, and also nitric acid yields water-free crystals of **43** and **44**. Recrystallization from pure water yielded the monohydrates **43**·H_2O and **44**·H_2O. The compounds are neither hygroscopic nor sensitive towards light and air. However, the crystal water is being completely lost by simple standing at room temperature in an open vessel for a few weeks.

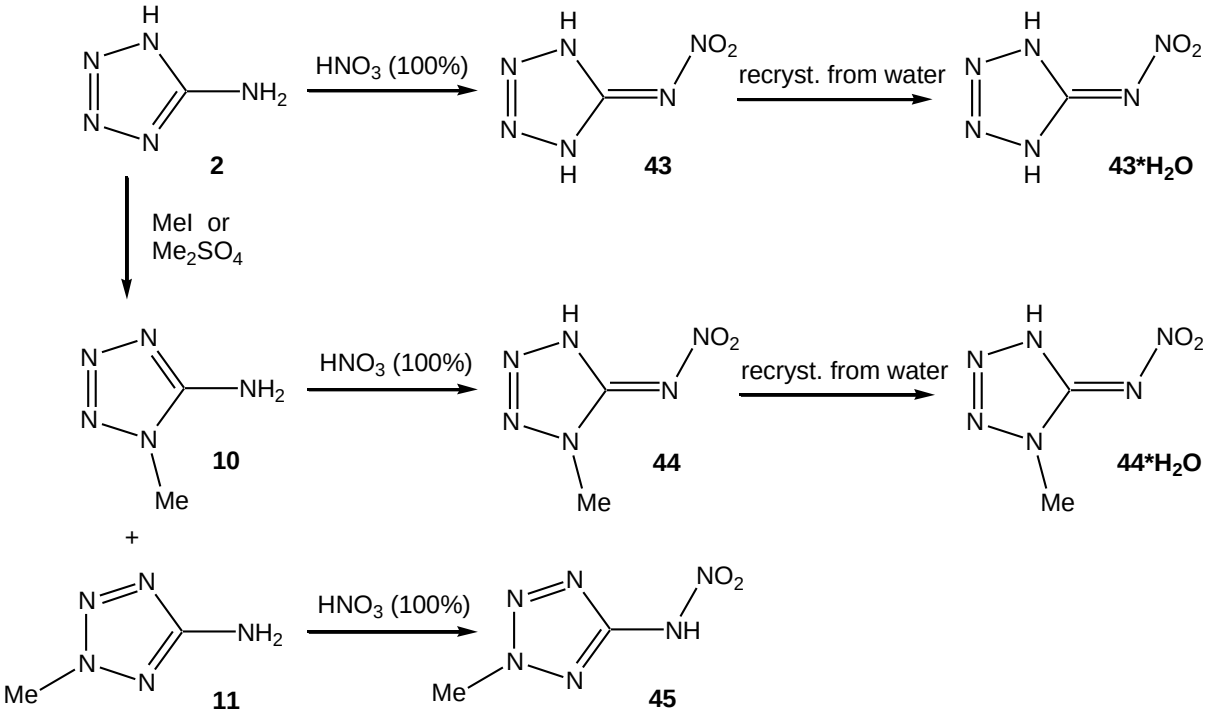

Scheme 4.1 The reaction of 5-aminotetrazole (**2**), 1-methyl-5-aminotetrazole (**10**) and 2-methyl-5-aminotetrazole (**11**) with 100 % HNO_3.

4.3 Crystal Structures

4.3.1 5-Nitriminotetrazole (**43**)

5-Nitrimino-1,4*H*-tetrazole **43** was characterized as a dibasic acid with pK_a values of 2.5 and 6.1,[245] previously it was not possible to locate the hydrogen atoms and it was assumed that the more acid hydrogen is located at the nitramino group.[248] However using single crystal diffraction both hydrogen atoms were located on the tetrazole ring at the nitrogen atoms N1 and N4. The ^{15}N NMR spectrum (see below) shows only four signals, which suggests the same connectivity present in solution. Even in the gas phase, DFT calculations (see below) show this isomer to be the lowest in energy. The molecular unit can be seen in **Figure 4.1**.

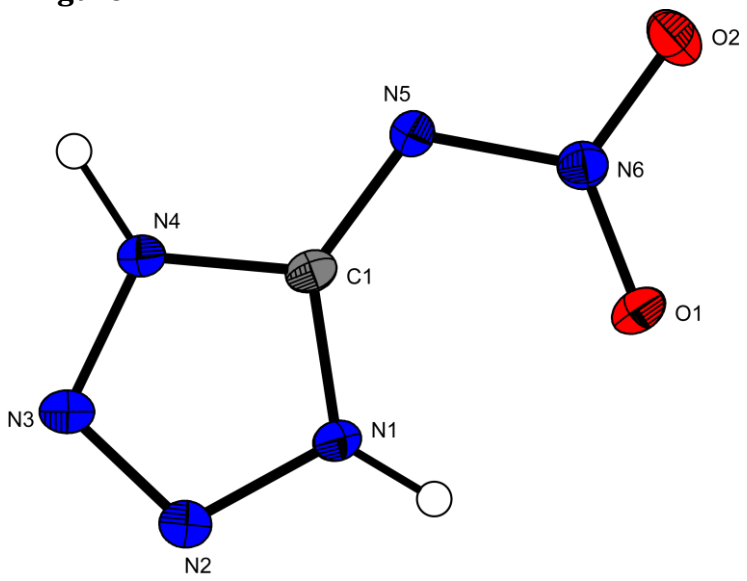

Figure 4.1 Molecular moiety of **43**. Ellipsoids of non-hydrogen atoms are drawn at the 50 % probability level.

The structure of the tetrazole ring in **43** can be compared with that of 5-aminotetrazole monohydrate (5-At).[60] The bond lengths in **43** are slightly shorter than in 5-At, with the shortest distance in **43** between the atoms N2 and N3 with 1.278(1) Å and the longest between N1 and N2 with 1.358(1) Å. The C1–N5 bond length is 1.341(1) Å, which is closer to a C=N double bond (1.28 Å) rather than a C–N single bond (1.46 Å) where as the nitramine bond N5–N6 is considerably longer (1.363(1) Å). The angles in **43** differ in comparison with those in 5-At. The N4–C1–N1 angle in **43** (103.9(1)°) is smaller than in 5-At (107.9(1)°), which can be explained using the VSEPR model,[249] in which a double bond requires more space. One condition of the 6π-Hückel-aromaticity is a planar ring

system, which can be seen at the torsion angle between N1–N2–N3–N4 of 0.5(1)°. The nitramine group also shows only slight deviations from the planarity (torsion angle C1–N5–N5–O1 1.8(1)°), and is stabilized via a intramolecular hydrogen bond between N1–H1···O1 (D···A 2.562(2) Å, D–H···A 107(1)°). In addition there are several intermolecular hydrogen bonds illustrated in **Figure 4.2**, which are one reason for the high density of 1.867 g cm^{-3}. The strongest intermolecular hydrogen bonds are between the nitrogen atoms N1 and N2^{i} (D···A 2.948(1) Å, D–H···A 156(1)°, (i): 1–x, –0.5+y, 0.5–z) and the atoms N4 and N5^{ii} (D···A 2.850(2) Å, D–H···A 175(2)°, (ii): –x, 0.5+y, 0.5–z). Bond lengths and angles for the non-hydrogen atoms in **43** are given in **Table 4.1** and **Table 4.2**.

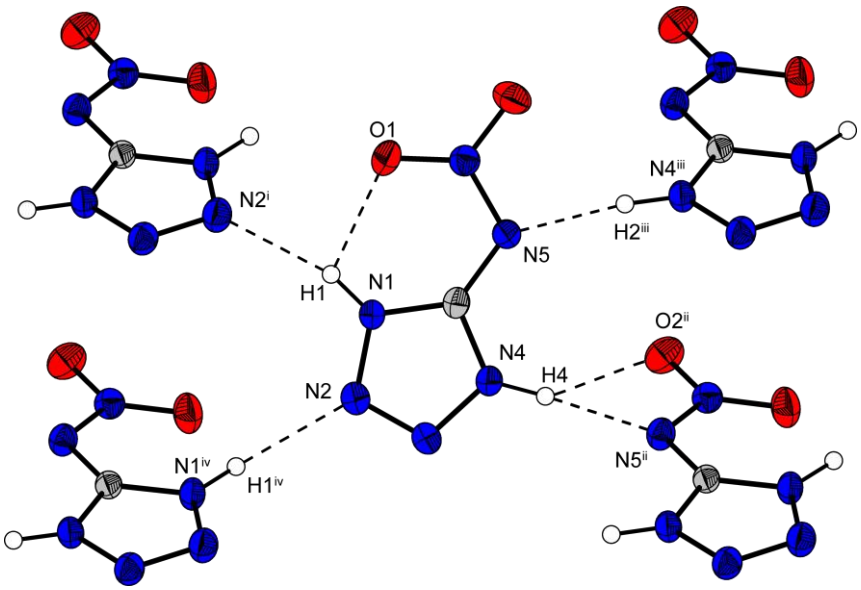

Figure 4.2 H-bonding in **43**: (N1–H1···N2^{i}: D–H 0.89(2) Å, H···A 2.11(2) Å, D···A 2.948(1) Å, D–H···A 156(1)°; N4–H4···N5^{ii}: 0.98(2) Å, 1.83(2) Å, 2.850(2) Å, 175(2)°; N4–H4–O2^{ii}: 0.98(2) Å, 2.48(2) Å, 3.146(1) Å, 125(1)°; (i): 1–x, –0.5+y, 0.5–z (ii): –x, 0.5+y, 0.5–z).

4.3.2 5-Nitriminotetrazole monohydrate (**43**·H_2O)

43·H_2O crystallizes in agreement to its water-free analogue in the monoclinic space group $P2_1/c$ with four molecules in the unit cell. The density of 1.808 g cm^{-3} is lower than that of water-free **43**. However, the molecular structure (**Figure 4.3**) is very similar to that of **43**. Again both hydrogen atoms are located at the tetrazole ring. The nitrimine group follows the planarity (C1–N5–N6–O1 = –1.1(2)°) and is fixed by an intramolecular H-bond (**S1,1(6)**, N1–H1···O1: 0.90(2), 2.23(2), 2.588(2) Å, 103(1)°). The C1–N5 bond

length is 1.340(2) Å, which again is closer to a C=N double bond (1.28 Å) than a C–N single bond (1.46 Å),[250] where as the nitramine bond N5–N6 is considerably longer (1.363(1) Å). The exact bond lengths and angles of both compounds are given in **Table 4.1** and **Table 4.2**.

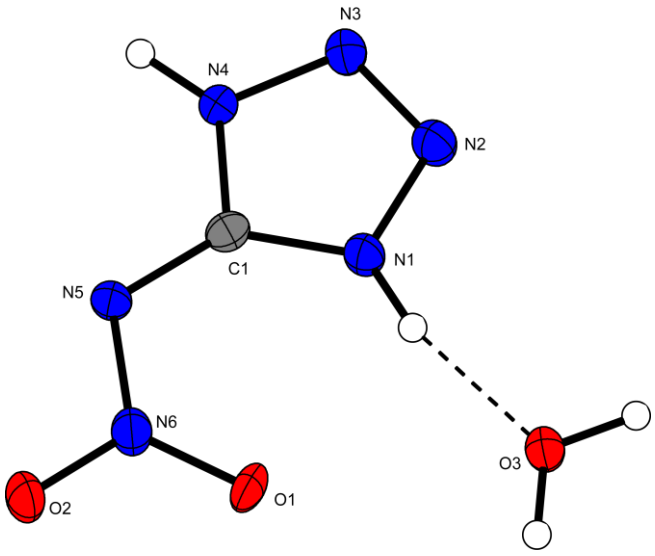

Figure 4.3 Molecular moiety of **43**·H_2O. Ellipsoids of non-hydrogen atoms are drawn at the 50 % probability level.

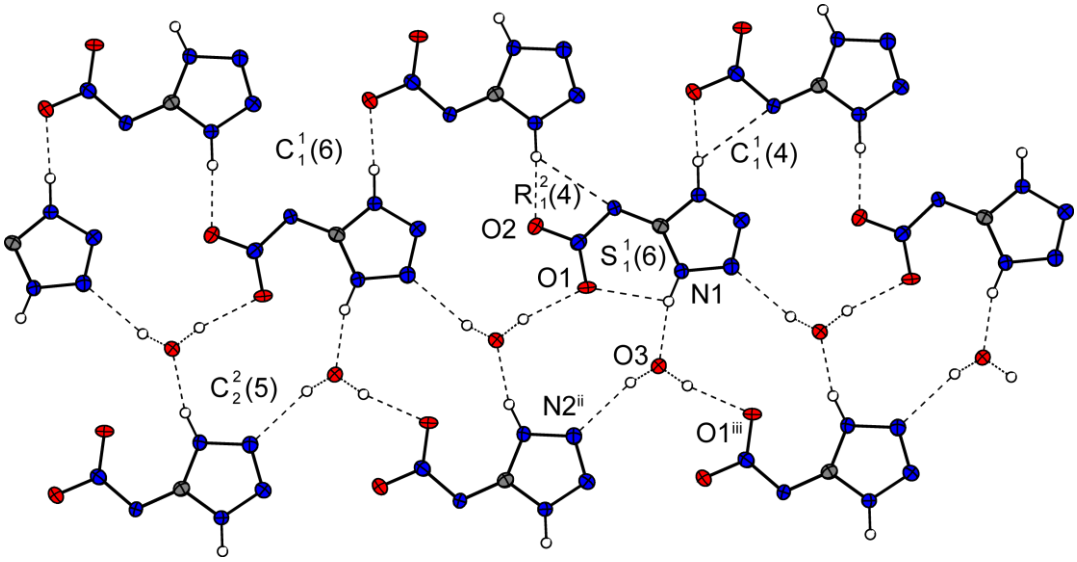

Figure 4.4 View on the hydrogen bond network in the layers of **43**·H_2O. Selected hydrogen bonds (Å, Å, Å, °): N1–H1···O3 = 0.89(2), 1.77(2), 2.637(2), 164(2); N4–H4···O2^{i} = 0.91(2), 1.87(2), 2.781(2), 178(2); N4–H4···N5^{i} = 0.91(2), 2.53(2), 3.142(2), 125(2); O3–H3B···N2^{ii} = 0.89(2), 2.10(2), 2.970(2), 165(2); O3–H3A···O1^{iii} = 0.93(2), 1.93(2), 2.841(2), 167(2); (i) –x, 0.5+y, 0.5–z; (ii) 1–x, –0.5+y, 1.5–z; (iii) 1–x, 0.5+y, 1.5–z.

The packing of **43**·H_2O is characterized by the formation of layers, in which a strong hydrogen bond network appear. The layers have distances of ~3.1 Å. A view on a layer is shown in **Figure 4.4**. By analyzing the graph sets [208] several chains (**C1,1(6)**, **C1,1(4)** and **C2,2(5)**) can be found within the layers. Between two 5-nitriminotetrazole molecules a bifurcated hydrogen bond with the graph set **R2,1(4)** can be detected including the nitrimine atoms N5 and O2 as double acceptor system.

4.3.3 1-Methyl-5-nitriminotetrazole

Accordingly, the densities of **44** and **45** decrease because of the presence of the methyl-group. The molecular unit of **44** (**Figure 4.5**) shows a similar connectivity to that of **43**, whereby one hydrogen atom in **43** has been substituted by a methyl group at the atom N1. Again, in **44** the nitro group is tilted towards the side where the hydrogen atom is located, forming an intramolecular hydrogen bond. In **44**, the nitrimine unit is also found to lie in the plane of the tetrazole ring (torsion angle O1–N6–N5–C1 of 4.3(2)°), whereby the tetrazole ring in **44** shows comparable bond lengths with those observed in **43**. The most significant difference is the nitramine bond between N5 and N6, which is shorter in compound **44** (d (N5–N6) = 1.338(2) Å). Finally, there are no significant differences for the angles observed in compound **43** and **44**.

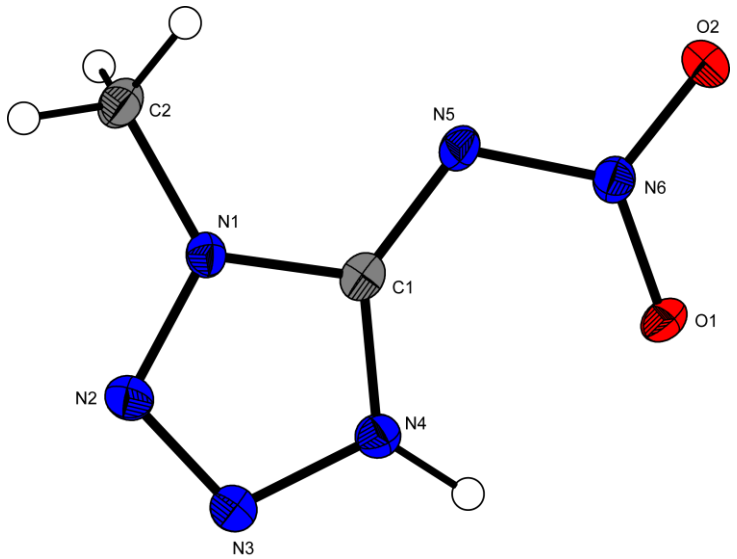

Figure 4.5 A view of the molecular structure of **44**, representing the half of the asymmetric unit. Thermal ellipsoids are drawn at the 50 % probability level and hydrogen atoms are shown as small spheres of arbitrary radii.

The structure observed for **44** in the crystalline state is again influenced by several strong intermolecular hydrogen bonds, which are illustrated in **Figure 4.6**.

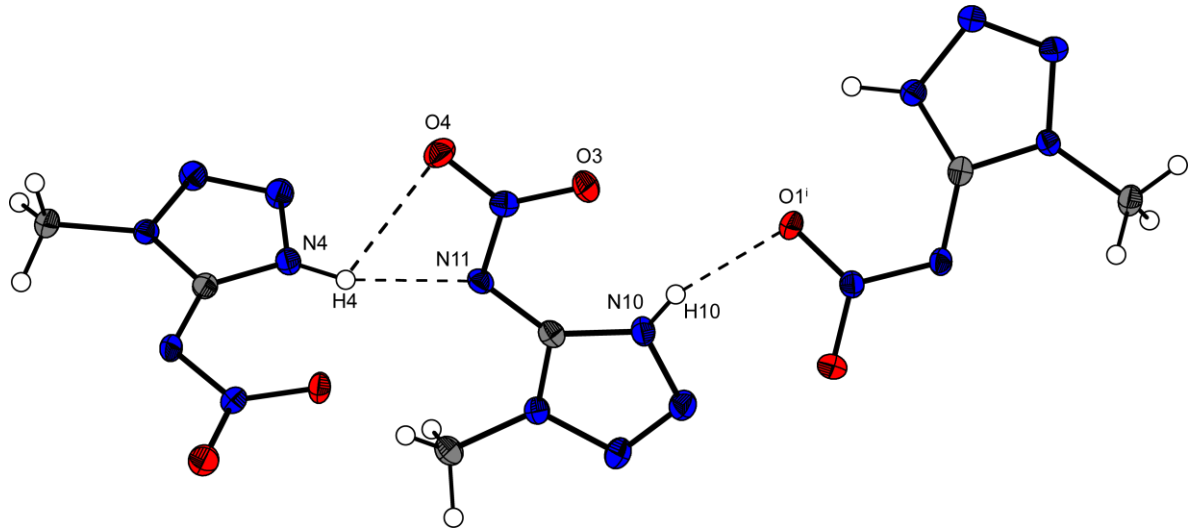

Figure 4.6 H-bonding in **44** (N4–H4···N11^{i}: D–H 0.93(2) Å, H···A 1.96(2) Å, D···A 2.848(2) Å, D–H···A 158(2)°; N4–H4···O4: 0.93(19) Å, 2.59(2) Å, 3.098(2) Å, 115 (2)°; N10–H10···O1^{i}: 0.80(2) Å, 2.10(2) Å, 2.874(2) Å, 163(2)°; (i): –x, 0.5+y, 0.5–z).

4.3.4 1-Methyl-5-nitriminotetrazole monohydrate (**44**·H_2O)

The molecular structure of 1-methyl-5-nitriminotetrazole monohydrate is shown in **Figure 4.7**. It crystallizes in the monoclinic space group $P2_1/n$ with four molecules in the unit cell. The density of 1.643 g cm^{-3} is also lower than this observed for water-free **44** (1.755 g cm^{-3}). The molecular structure again is very similar to this observed for water-free **44**. Again the nitro group is only slightly shifted out from the tetrazole ring plane (N4–C1–N5–O1 = 10.9(3)°), but also directed by the intramolecular H-bond N1–H1···O1 (0.96(2), 2.26(2), 2.621(2) Å, 101(2)°). The water molecule is coordinated via the H-bond N4–H4···O3 (0.96(3), 1.67(3), 2.607(2), 165(3)°) to the proton located at ring nitrogen atom N4.

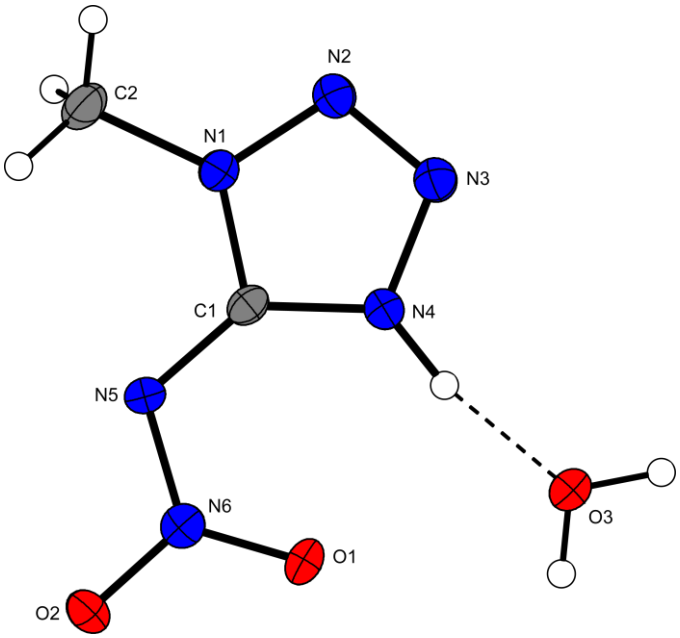

Figure 4.7 Molecular moiety of **44**·H_2O. Ellipsoids of non-hydrogen atoms are drawn at the 50 % probability level.

In accordance to the water-free structure of **44**, also in the packing of **44**·H_2O the formation of an three-dimensional network can be observed. In **Figure 4.8** the hydrogen bonds are depicted. Only the ring nitrogen atoms N1 participate in the hydrogen bonds. In addition nitrogen atom N5 is takes part in a weak hydrogen bond. This may be a reason for the lower density observed in this structure.

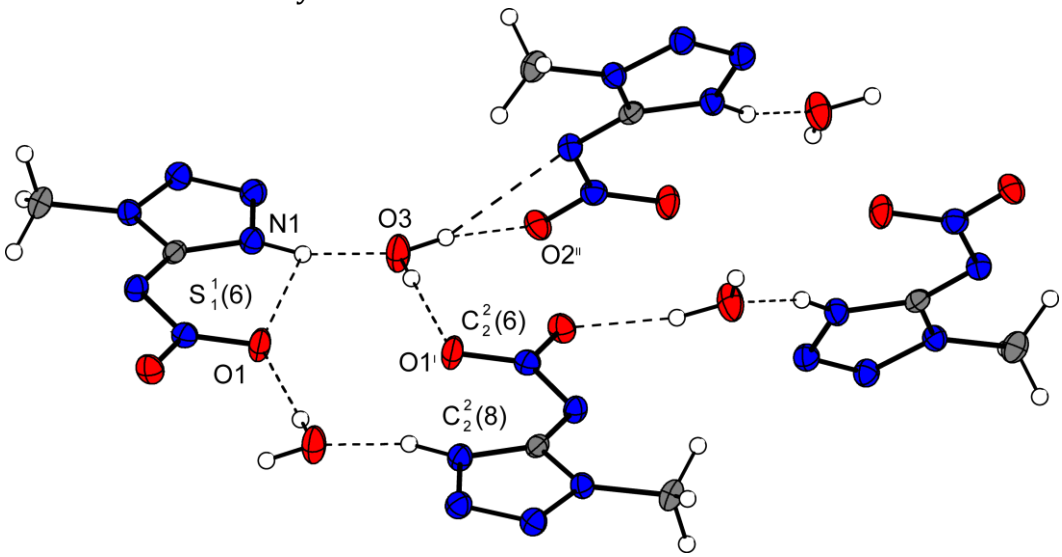

Figure 4.8 View on the hydrogen bond network in the layers of **44**·H_2O. Selected hydrogen bonds (Å, Å, Å, °): O3–H3A···O1^{i} = 0.83(3), 2.07(3), 2.895(2), 172(2); O3–H3B···O2^{ii} = 0.91(3), 1.95(3), 2.836(2), 165(2); O3–H3B···N5^{ii} = 0.91(3), 2.56(3), 3.296(2), 139(2); (i) 2–x, –y, 1–z; (ii) 0.5+x, 0.5–y, 0.5+z.

4.3.5 2-Methyl-5-nitraminotetrazole (**45**)

The structure of **45** is considerably different to the structures of **43** and **44** discussed previously. The methyl group at the nitrogen atom N2 directs the remaining proton to the nitrogen atom N5, building a nitraminotetrazole (**Figure 4.9**).

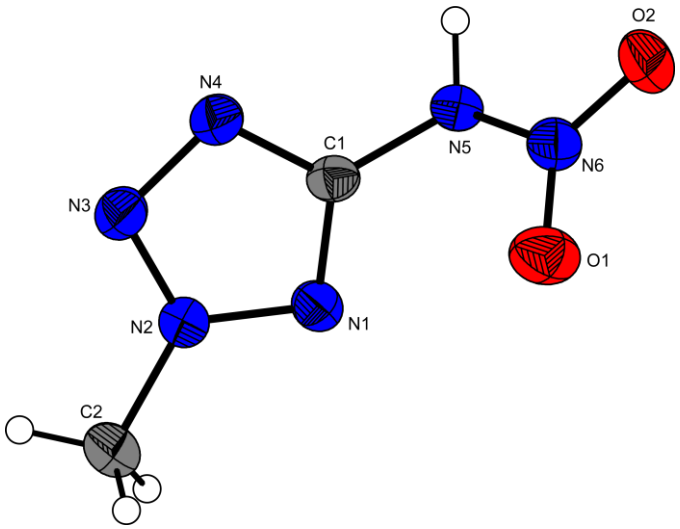

Figure 4.9 A view of the molecular structure of **45**. Thermal ellipsoids are drawn at the 50 % probability.

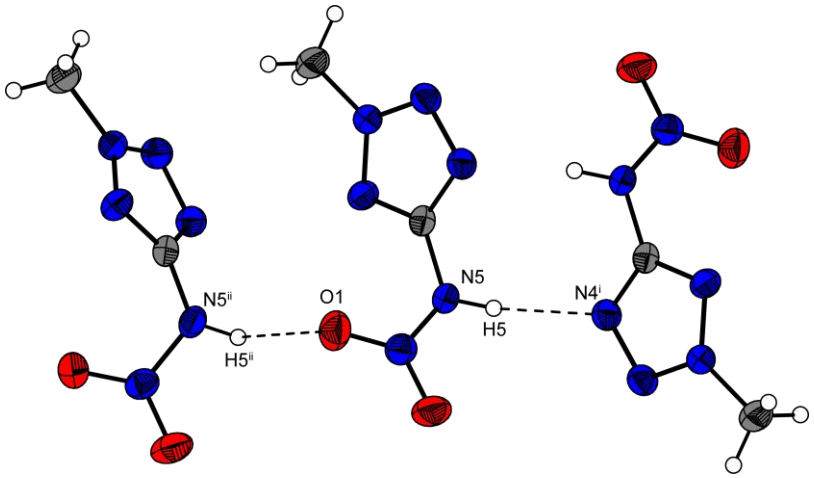

Figure 4.10 H-bonding in **45**. (N5–H1···N4^{i}: D–H 0.86(2) Å, H···A 2.13(2) Å, D···A 2.965(2) Å, D–H···A 163(2)°; N5 ^{ii}–H1^{ii}···O1: 0.86(2) Å, 2.66(2) Å, 3.070(2) Å, 111(2)°; (i) 1–x, –y, 1–z (ii): x, –0.5–y, –0.5+z).

In **45**, the C1–N5 bond length is crucially longer with a distance of 1.397(2) Å and the nitramine unit does not lie in the plane of the tetrazole ring, as is clearly shown by the C1–N5–N6–O1 torsion angle of –19.2(2)°. The N6–N5–C1 angle (117.9(1)°) is larger than observed in **43** and **44** and the N5–N6 nitramine bond of 1.379(2) Å is the longest in this

series of compounds which can be seen as contributing to the low density of 1.667 g cm^{-3}, which is the lowest among the three water-free structures discussed in this chapter. Further reasons for the lower density of **45** are the absence of strong intramolecular hydrogen bonds, and the presence of only two moderately strong hydrogen bonds as are illustrated in **Figure 4.10**. Relevant structural parameters are listed below.

Table 4.1 Bond lengths [Å] of **43**, **43**·H_2O, **44**, **44**·H_2O and **45**.

Atoms	**43**	**43**·H_2O	**44**	**44**·H_2O	**45**
O2–N6	1.234(1)	1.251(2)	1.234(2)	1.224(2)	1.224(2)
O1–N6	1.237(1)	1.249(2)	1.266(2)	1.217(2)	1.217(2)
N1–N2	1.358(1)	1.362(2)	1.355(2)	1.327(2)	1.327(2)
N1–C1	1.341(1)	1.340(2)	1.345(2)	1.325(2)	1.325(2)
N4–C1	1.336(1)	1.337(2)	1.338(2)	1.339(2)	1.339(2)
N4–N3	1.352(1)	1.351(2)	1.3639(2)	1.321(2)	1.321(2)
N2–N3	1.278(1)	1.280(2)	1.2836(2)	1.318(2)	1.318(2)
N5–N6	1.363(1)	1.335(2)	1.3375(2)	1.379(2)	1.379(2)
N5–C1	1.341(1)	1.350(2)	1.3458(2)	1.397(2)	1.397(2)
N1–C2			1.455(2)	1.459(2)	1.459(2)

Table 4.2 Bond angles [°] of **43**, **43**·H_2O, **44**, **44**·H_2O and **45**.

Atoms	**43**	**43**·H_2O	**44**	**44**·H_2O	**45**
N2–N1–C1	109.87(9)	109.1(1)	110.4(1)	110.4(2)	101.0(1)
C1–N4–N3	110.5(1)	110.7(1)	110.2(1)	110.2(2)	105.8(1)
N1–N2–N3	107.97(9)	108.7(1)	107.8(1)	107.8(2)	114.1(1)
N6–N5–C1	115.43(9)	115.0(1)	115.7(1)	114.9(2)	117.9(1)
N2–N3–N4	107.73(9)	107.2(1)	107.7(1)	107.7(2)	106.0(1)
O1–N6–O2	123.5(1)	121.3(2)	121.6(1)	121.4(2)	126.1(2)
O1–N6–N5	122.07(9)	122.8(1)	121.9(1)	123.0(2)	118.2(1)
O2–N6–N5	114.44(9)	116.0(1)	116.5(1)	115.6(2)	115.6(2)
N4–C1–N1	103.9(1)	104.4(2)	103.9(1)	103.8(2)	113.2(2)
N4–C1–N5	121.4(1)	120.1(2)	136.9(1)	137.1(2)	122.3(1)
N1–C1–N5	134.6(1)	135.4(2)	119.2(1)	119.1(2)	124.5(2)

4.4 Spectroscopy

4.4.1 Vibrational Spectroscopy

Vibrational spectroscopy is a suitable method for identifying nitraminotetrazoles. The IR and Raman (**Figure 4.11**) spectra of compounds **43**, **44** and **45** show the vibrations expected from comparison with similar compounds in the literature.[251] The *N*–NO_2 groups result in the strong absorptions in the 1280–1300 ($\nu_{sym}(NO_2)$) and 1560–1620 ($\nu_{asym}(NO_2)$) cm^{-1} regions as well as a weak band at 945–970 (ν(N–N)) cm^{-1}.[252] The IR and Raman spectra of compounds **43**, **44** and **45** show further characteristic absorption bands in the regions listed below: 3250–3100 cm^{-1} [ν(N–H)], 3000–2850 [ν(C–H) **44**, **45**], 1680–1550 [ν(N–H)], 1550–1350 [ν, tetrazole ring, $\nu_{as}(CH_3)$], ~1380 [$\nu(CH_3)$], 1350–700 [ν(N1–C1–N4), ν(N–N), ν(N–H), ν, tetrazole ring], < 700 [ν δ_{oop} N–H)].

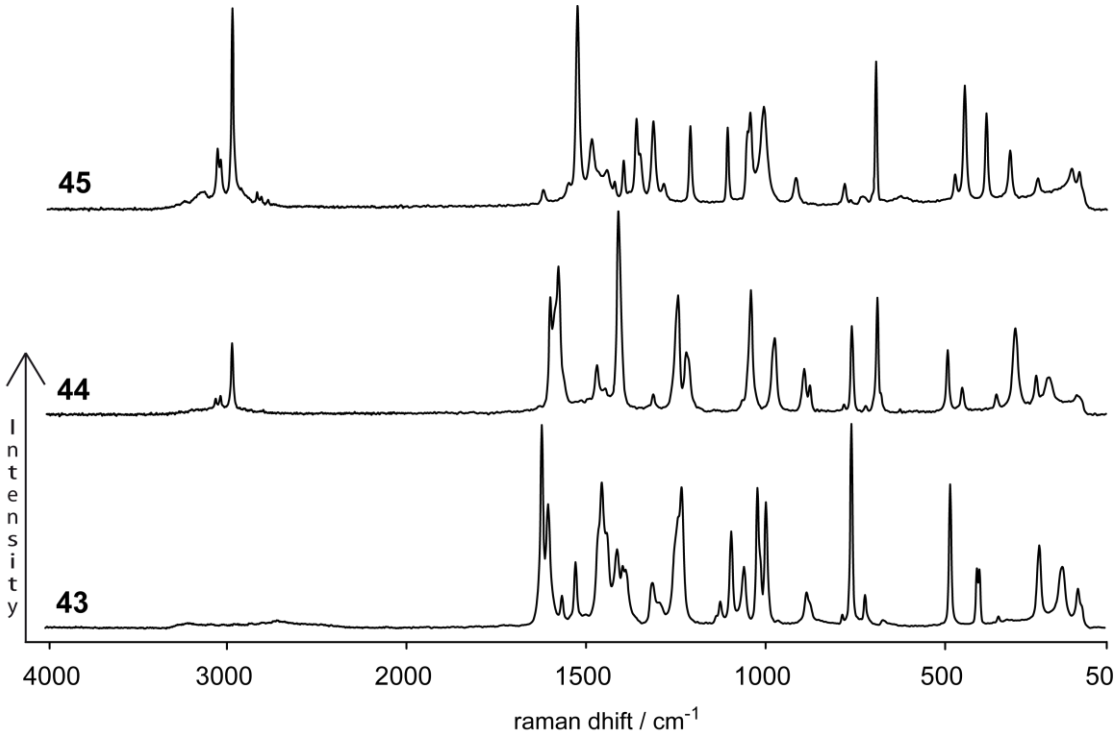

Figure 4.11 Solid state Raman spectra of compounds **43**, **44** and **45**.

4.4.2 NMR Spectroscopy

The ^{13}C and ^{15}N NMR chemical shifts and the $^{15}N–^{1}H$ coupling constants are presented in **Table 4.3** and can be seen in **Figure 4.12**. For all compounds the proton coupled as well as the proton decoupled ^{15}N NMR spectra (with full NOE) were recorded. The assignments are given based on the values of the $^{15}N–^{1}H$ coupling constants and by comparison with the literature.[240] The chemical shifts are given with respect to CH_3NO_2 (^{15}N) and TMS (^{13}C) as external standards. In the case of ^{15}N NMR, negative shifts are upfield from CH_3NO_2. For all compounds d_6-DMSO was used as the solvent, and additionally d_6-aceton was used for observing the solvent shift in compound **43**. In the d_6-DMSO spectra only three signals could be observed for **43**, while in d_6-aceton the five expected signals could be located and assigned.

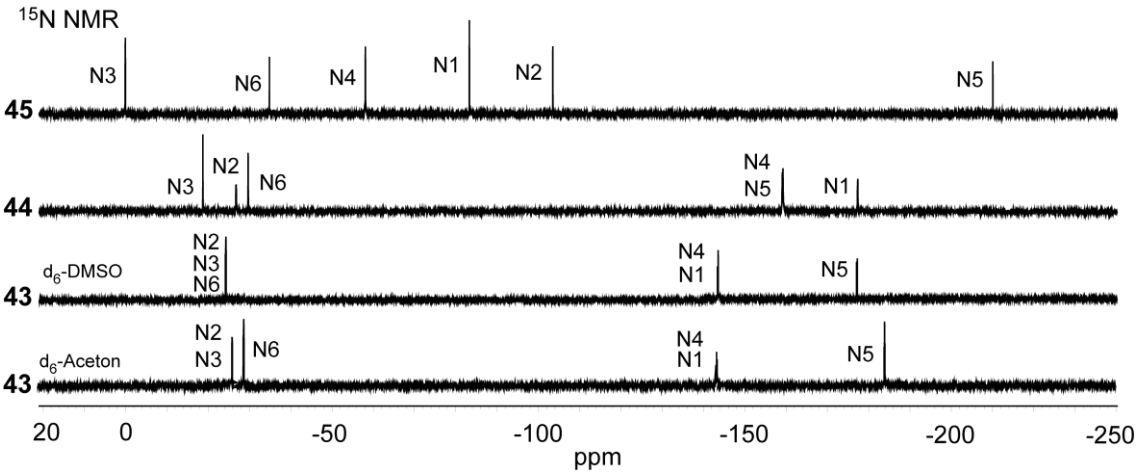

Figure 4.12 ^{15}N NMR spectra of compounds **43**, **44** and **45**.

Table 4.3 ^{15}N NMR and ^{13}C NMR chemical shifts and $^{15}N–^{1}H$ coupling constants.

	δ(N1)/ppm	δ(N2)	δ(N3)	δ(N4)	δ(N5)	δ(N6)	δ(C1)
43 (acetone)	–143.4	–26.4	–26.4	-143.4	-143.3	–29.0	151.8
43 (DMSO)	–144.6	–24.6	–24.6	-144.6	-174.9	–24.6	152.6
44	–177.4	–26.8	–29.8	-159.2	-159.3	–18.8	150.3
	$^{2}J_{N-H}$= 2.1 Hz	$^{3}J_{N-H}$= 1.9 Hz					
45	–83.4	–103.6	–0.3	–58.3	-209.3	–35.0	157.6
	$^{3}J_{N-H}$= 1.9 Hz	$^{2}J_{N-H}$=2.2 Hz	$^{3}J_{N-H}$= 1.9 Hz				

4.5 Thermodynamic and Energetic Properties

4.5.1 Differential Scanning Calorimetry (DSC)

DSC measurements to determine the decomposition temperatures of **43**, **44** and **45** were performed in covered Al-containers with a nitrogen flow of 20 mL min^{-1} on a Perkin-Elmer Pyris 6 DSC at a heating rate of 5 °C min^{-1}. The DSC plots in **Figure 4.13** show the thermal behavior of 1.0 mg of **43**, **44** and **45** in the 50–300 °C temperature range. Compound **43** shows the lowest decomposition point at 122 °C, whereby compounds **44** and **45** decompose during melting at 125 °C and 123 °C, as is shown by the curve of **Figure 4.13**.

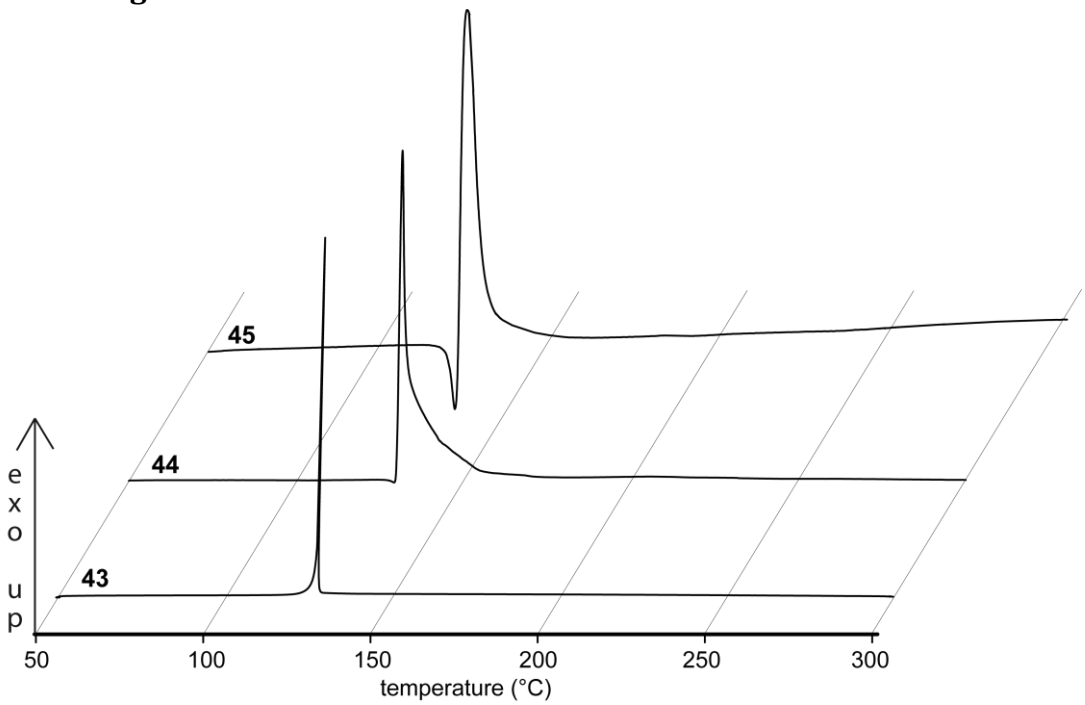

Figure 4.13 DSC plot (exo up) of compounds **43**, **44** and **45**. (5 °C min^{-1}) T_{onset}: **43** = 122 °C, **44** = 125 °C, **45** = 123 °C.

To determine the heats of decomposition, a Linseis DSC PT10 was used. Three samples (~1 mg) were heated with a heating rate of 2 °C min^{-1} and a fixed nitrogen flow of 5 L h^{-1} over the decomposition peaks. The surface was integrated using the Linseis software and the average of three measurements was calculated to yield heats of decomposition $\Delta_{dec.}H°$ of 2638 (**43**), 1685 (**44**) and 2158 J g^{-1} (**45**).

4.5.2 Heats of Formation

The enthalpies of energetic materials are governed by the molecular structure of the compounds, and therefore, heterocycles with a higher nitrogen show higher heats of formation. The heats of combustion for the compounds **43**, **44** and **45** were determined experimentally, using a Parr 1356 bomb calorimeter as described in the introduction. The enthalpy of formation, $\Delta_f H°$, for each of the compounds was calculated at 298.15 K using Hess' law and the following combustion reactions, which shows that **43**, **44** and **45** are strongly endothermic compounds ($\Delta_f H°$: **43**: +264, **44**: +260, **45**: +380 kJ mol^{-1}).

43: $CH_2N_6O_2 + 1/2\ O_2 \longrightarrow CO_2 + H_2O + 3\ N_2$

44, 45: $C_2H_4N_6O_2 + 2\ O_2 \longrightarrow 2\ CO_2 + 2\ H_2O + 3\ N_2$

In addition, the heats of formation of **43** and **44** as well as of **43**·H_2O and **44**·H_2O have been computed by the atomization energy method.

From the gas-phase enthalpies of formation $\Delta_f H°$(g) (**43**: 398 kJ mol^{-1}, **43**·H_2O: 128 kJ mol^{-1}, **44**: 362 kJ mol^{-1} and **44**·H_2O: 97 kJ mol^{-1}), the enthalpies of the solid state can be calculated using the enthalpies of sublimation by the equation:

$$\Delta_f H°(s) = \Delta_f H°(g) - (\Delta_{sub} H)$$

For a solid compound the enthalpy of sublimation ($\Delta_{sub} H$) can be approximated on the basis of TROUTON's rule [253] if the melting temperature, in our case the decomposition temperature (T_m in K) is known: $\Delta_{sub} H.$ [J mol^{-1}] = 188 T_m [K]

With the known enthalpies of formation of carbon dioxide ($\Delta_f H°_{298}(CO_{2(g)})$ = −394 kJ mol^{-1}) and water ($\Delta_f H°_{298}(H_2O_{(g)})$ = −242 kJ mol^{-1}) the enthalpies of formation of **43** (322 kJ mol^{-1}), **43**·H_2O (54 kJ mol^{-1}), **44** (287 kJ mol^{-1}) and **44**·H_2O (22 kJ mol^{-1}) have been calculated. Only the value of **44** is in good agreement with those (**43**: 264 kJ mol^{-1}, **44**: 260 kJ mol^{-1}) measured by bomb calorimetry. Differences of $\Delta(\Delta_f H°(\mathbf{43}) - \Delta_f H°(\mathbf{43}\cdot H_2O)$ = 268 kJ mol and $\Delta(\Delta_f H°(\mathbf{44}) - \Delta_f H°(\mathbf{44}\cdot H_2O)$ = 265 kJ mol can be calculated. This differences are in agreement to measured heats of formations of H_2O (g: –242 kJ mol^{-1}, l: 286 kJ mol^{-1}).

4.5.3 Sensitivities

For initial safety testing, the impact and friction sensitivities were tested according to BAM methods with the "BAM drophammer" and "BAM friction tester". Compound **43** is very sensitive towards impact (< 1.5 J) and friction (< 8 N) and since the value is comparable with lead azide, it should be considered to be a primary explosive, and should therefore only be handled with appropriate precautions. Compound **44** is moderately sensitive towards impact (< 12.5 J) and friction (< 160 N), however **45** shows increased sensitivities. (impact: < 3.0 J, friction: < 145 N)**.** Accordingly, **44** and **45** fall into the group of compounds described as "sensitive". The impact sensitivities of **43**·H_2O (9 J) and **44**·H_2O (19 J) are significantly lower compared to their water free analogues. The same trends are observed regarding the friction sensitivities. While **43** is extremely sensitive towards friction, **43**·H_2O is significantly lower. Interestingly, again a lower ratio is observed in the testing of **44** (160 N) and **44**·H_2O (320 N).

4.5.4 Decomposition Products

In order to determine the thermal decomposition [254] products, the compounds were heated in an evacuated steel tube for ~30 s at about 100 °C above the decomposition temperature and the gaseous products were transferred into an evacuated IR gas cell. In **Figure 4.14**, the gas phase IR spectra of the decomposition products of **43**, **44** and **45** are shown.

The thermal decomposition of **43** results in the formation of only two main products which could be identified using IR spectroscopy namely CO_2 [40] and CO.[41] In addition trace amounts of HCN and CH_4 were visible in the gas-phase IR spectrum, however no evidence for the formation of water vapor was found. In the methylated compounds, many more decomposition products were observed using gas-phase IR spectroscopy. Besides CO_2 and CO larger amounts of CH_4 [122] and HCN were found in the decomposition of **44** and **45**, in comparison with **43**. In contrast to **44**,

where bigger amounts of expected NH_3 were detected, the thermal decomposition of **45** shows only traces of NH_3 but moderate amounts of N_2O.[43]

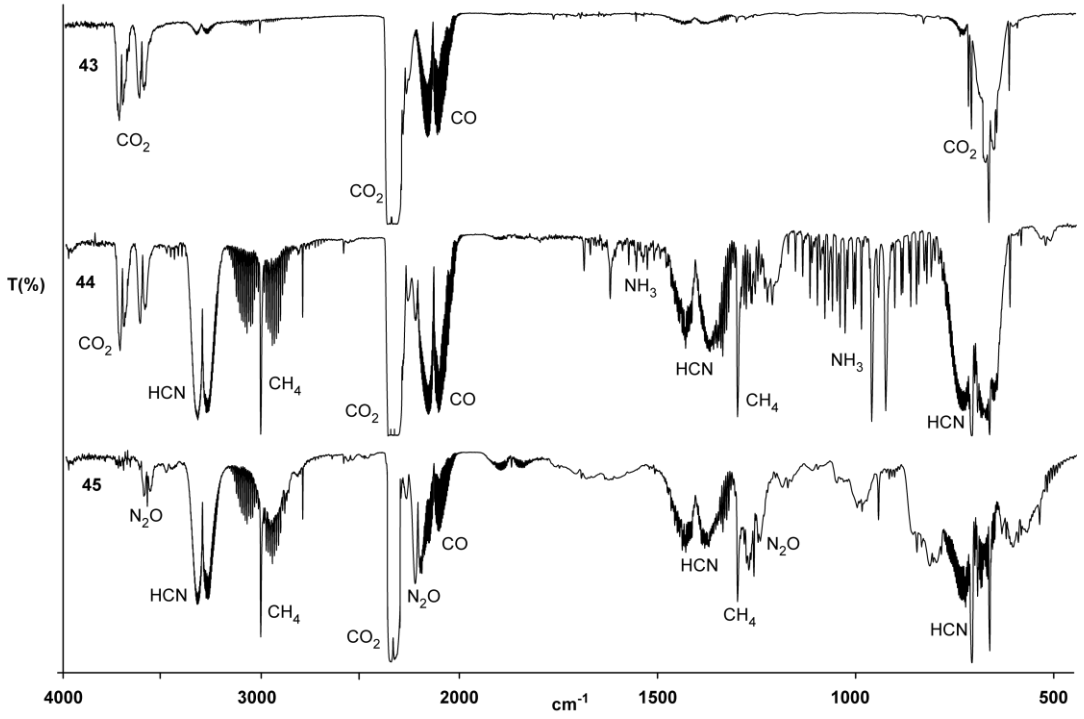

Figure 4.14 IR spectra showing the gas-phase decomposition products of **43** (top), **44** (middle) and **45** (bottom).

4.5.5 Detonation Parameters

The detonation parameters were calculated using the program EXPLO5 V5.02. **43** shows a very high calculated detonation pressure of 394 kbar and a detonation velocity of 9450 m s^{-1} (higher than those of TNT ($p_{C\text{-}J}$ = 202 kbar, $V_{Det.}$ = 7150 m s^{-1}). Also compound **44** shows promising values for the detonation pressures (295 kbar) and detonation velocity (8433 m s^{-1}). The influence of the density on the properties of energetic materials is clearly shown by **45**, which shows the lowest detonation pressure of 289 kbar in spite of the highest positive heat of

Flame test of **43**

formation due to its low density. The influence of the inclusion of water and also the lower density can be seen on the decreased values of **43**·H_2O and **44**·H_2O (see **Table 4.4**), which are significantly lower than those of **43** and **44**.

Table 4.4 Sensitivities, energetic properties and detonation parameter.

	43	**43**·H_2O	**44**	**44**·H_2O	**45**
Formula	$CH_2N_6O_2$	$CH_4N_6O_3$	$C_2H_4N_6O_2$	$C_2H_6N_6O_3$	$C_2H_4N_6O_2$
Molecular Mass [g mol^{-1}]	130.09	148.10	144.11	162.13	144.11
Impact sensitivity [J][a]	1.5	9	12.5	19	3.0
Friction sensitivity [N][b]	8	140	160	320	145
ESD-test [J]	0.19	0.38	0.28	0.35	0.20
N [%][c]	64.61	51.84	58.32	57.15	58.32
Ω [%][d]	–12.3	–10.8	–44.4	–39.5	–44.4
$T_{dec.}$ [°C][e]	122	122	125	125	122
Density [g cm^{-3}][f]	1.867	1.808	1.755	1.643	1.67
$\Delta_{dec.}H_m°$ [J g^{-1}][g]	2638		1685		2158
$-\Delta U_{comb}$ [cal g^{-1}][h]					2902
$\Delta_f H_m°$ [kJ mol^{-1}][i]	322	54	287	22	380
$\Delta_f U°$ [kJ kg^{-1}][j]	2574	472	2096	250	2742
calculated values by EXPLO5:					
$-\Delta_E U°$ [kJ kg^{-1}][k]	5746	5003	5382	4669	5998
T_E [K][l]	4563	3861	3900	3425	4283
$p_{C\text{-}J}$ [kbar][m]	394	323	299	239	289
$V_{Det.}$ [m s^{-1}][n]	9450	8849	8464	7894	8434
Gas vol. [L kg^{-1}][o]	800	838	783	832	413

[a] BAM drophammer (grain size: 75–125 µm); [b] BAM friction tester (grain size: 75–125 µm); [c] Nitrogen content; [d] Oxygen balance; [e] Temperature of decomposition by DSC (β = 5 °C); [f] X-ray density; [g] experimental enthalpy of decomposition using DSC; [h] Experimental (constant volume) combustion energy; [i] Molar enthalpy of formation; [j] Energy of formation; [k] Energy of Explosion; [l] Explosion temperature; [m] Detonation pressure; [n] Detonation velocity; [o] Assuming only gaseous products.

4.5.6 Koenen Test

The explosion performance under confinement of compound **44** was investigated using a "Koenen test" steel sleeve apparatus using a hole width of 8 mm as well as 10 mm. The explosions as well as the result of the Koenen tests can be seen in **Figure 4.15**. Compound **44** destroyed the steel tube into more than 20 fragments using a hole width of 8 mm and 10 mm, respectively. It can therefore be assumed that compound **44** offers a greater explosion performance than RDX.

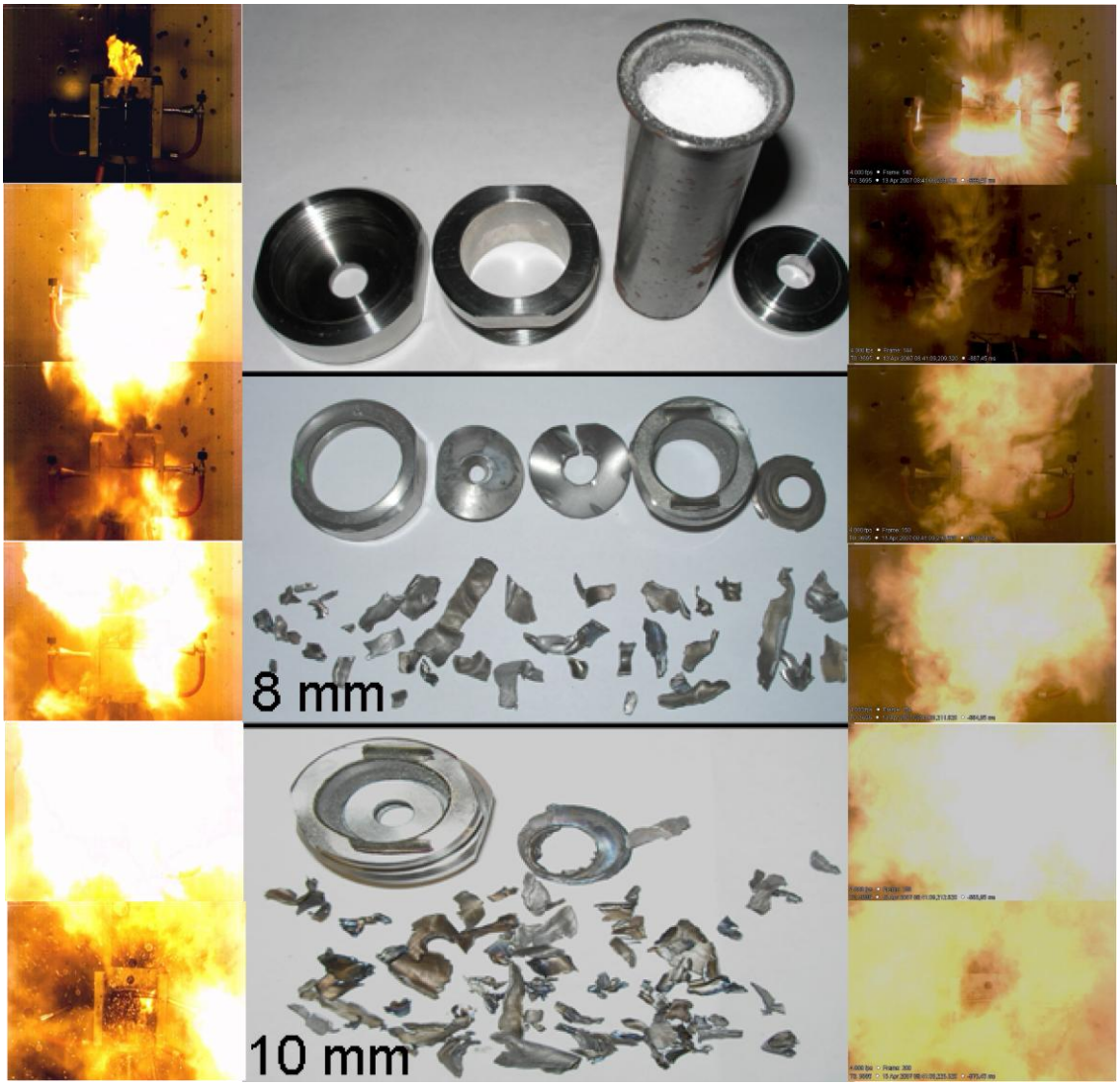

Figure 4.15 top: steel sleeve loaded with 25 ml (30 g) of compound **44**. middle: collected fragments using a hole width of 8mm. below: collected fragments using a hole width of 10 mm.

4.5.7 Long Term Stability Tests

Long term stabilities tests were performed using a Systag FlexyTSC (Thermal Safety Calorimetry) in combination with a RADEX V5 oven and the SysGraph Software. The tests were undertaken as long-term isoperibolic evaluations in glass test vessels at atmospheric pressure with ~300 mg of the compounds. It was shown that tempering the substance for 48 hours at 40 degrees under the decomposition point results in a storage period of > 50 years at ambient temperature. In our cases we chose a temperature of 80 °C and investigated the possible occurrence of exo- or endothermic behavior over a period of 48 hours (**Figure 4.16**). **43** and **44** were completely stable for 48 hours, while **45** showed negligible minimal exothermic steps in the first 6 hours. It can therefore be stated, that all three compounds show long-term stabilities, which is a basic requirement for possible applications.

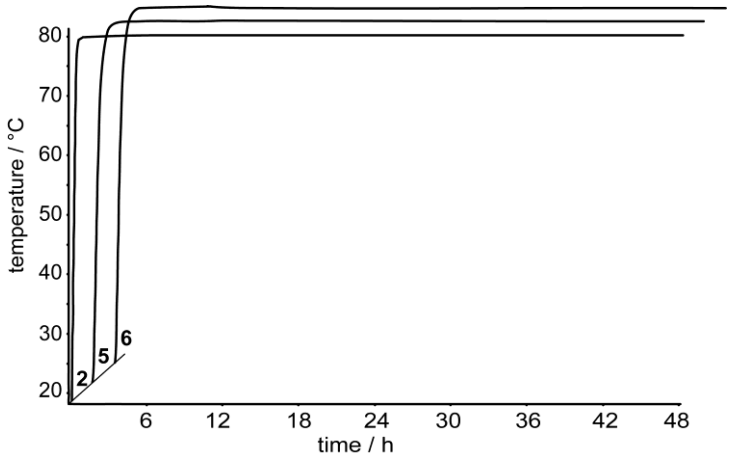

Figure 4.16 Long term stability screen of **43**, **44** and **45** using a FlexyTSC (80 °C, 48 hours).

4.5.8 Electrostatic Potential

The electrostatic potentials were illustrated after computing an optimal structure at the B3LYP/6-31G(d,p) level of theory using the program package HyperChem 7.52.[255] **Figure 4.17** shows the 0.001 electron bohr^{-1} isosurface of electron density for **43**, **44** and **45**. In these diagrams a Jorgensen-Salem representation was chosen with an electrostatic potential contour value of 0.1 hartree. The dark regions represent extremely electron-rich regions (V(r) < 0.1 hartree) and the light regions extremely electron-deficient regions (V(r) > 0.1 hartree). In general, the patterns of the calculated

electrostatic potentials of the surface of molecules can be related to the impact sensitivities.[256,257] In contrary to non sensitive organic molecules where the area the positive potential is larger but weaker in strength, in nitro and azo compounds usually more extensive regions with larger and stronger positive potentials are observed which can be related to the increased impact sensitivities.

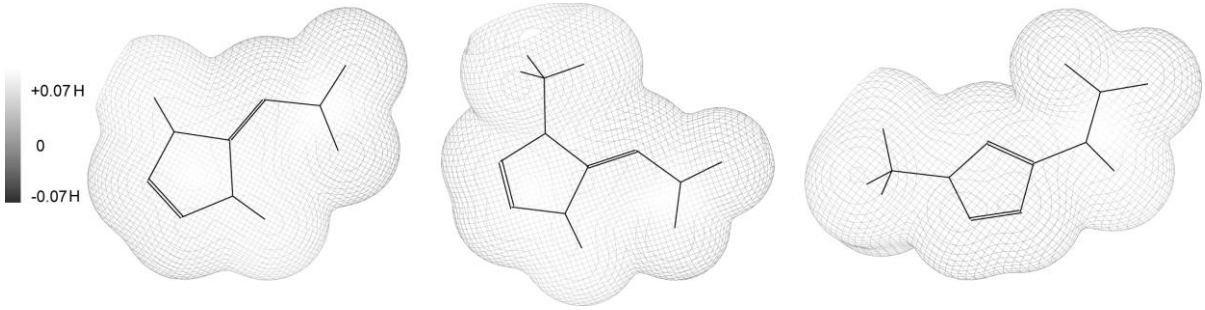

Figure 4.17 Calculated (B3LYP/DFT/6-31G*(p,d)) electrostatic potential of **43** (left), **44** (middle) and **45** (right). The dark regions represent electron-rich regions, the light regions extremely electron-deficient regions.

4.6 Experimental Part

All reagents and solvents were used as received (Sigma-Aldrich, Fluka, Acros Organics) if not stated otherwise. 5-Aminotetrazole (97 %) was purchased from Aldrich, HNO_3 (100 %) from Fluka and methyl iodide from Acros Organics.

CAUTION !

*The nitri- and nitraminotetrazoles prepared are energetic materials which show increased sensitivities towards various stimuli. Proper protective measures (safety glasses, face shield, leather coat, earthened equipment and shoes, Kevlar® gloves and ear plugs) should be used when handling compound **43**, **44** and **45**. **Extra** safety precautions should be taken, especially when compound **43** is prepared on larger scale (> 1 g).*

*5-Nitriminotetrazole (**43**):* 5-Aminotetrazole (4.25 g, 0.05 mol) was added in small portions to 12 mL of ice-cooled HNO_3 (100 %). After 2 hours the ice bath was removed and the solution was stirred for further 20 hours in an open vessel. (A closed reaction vessel favors the formation of the highly explosive N,N-5-dinitraminotetrazole!) The reaction was then quenched with 15 mL of cold water and the HNO_3 was reduced in volume under vacuum until the colorless product started to precipitate. Single crystals

suitable for X-ray diffraction were obtained by recrystallization of the crude product from half-conc. HNO_3 (5.98 g, 92 % yield). **DSC** (T_{onset}, 5 °C min^{-1}): 122 °C (dec.); **IR** (KBr, cm^{-1}): $\tilde{\nu}$ = 3214 (m), 3081 (m), 2936 (m), 2857 (m), 1798 (m), 2720–2685 (m, br), 2093 (w),1708 (w), 1613 (s), 1507 (s), 1450 (m), 1405 (m), 1383 (m), 1515 (vs), 1236 (s), 1226 (s), 1130 (w), 1054 (m), 1021 (m), 995 (m), 878 (m), 780 (m), 752 (m), 714 (m), 653 (m), 478 (w), 399 (m); **Raman** (1064 nm, 200 mW, 25 °C, cm^{-1}): $\tilde{\nu}$ = 3210 (2), 2707 (3), 1617 (98), 1599 (60), 1561 (15), 1523 (32), 1450 (70), 1407 (38), 1391 (30), 1309 (22), 1228 (68), 1120 (12), 1089 (47), 1054 (29), 1016 (68), 993 (61), 879 (17), 755 (100), 717 (16), 480 (70), 405 (29), 398 (28), 231 (40), 167 (29), 124 (19); **^{1}H NMR** (d_6-DMSO, 25 °C, ppm): δ = 14.21 (s, br, 2H); **^{13}C NMR** (d_6-DMSO, 25 °C, ppm): δ = 152.6 (C1); **^{14}N NMR** (d_6-DMSO, 25°C): δ: –24.6 (NO_2); **^{15}N NMR** (d_6-DMSO, 25°C, ppm): δ = –24.6 (N2, N3, NO_2), –144.6 (N1, N4), –174.9 (N5); *m/z* (DCI): 131 $[M+H]^+$, 85 $[M+H–NO_2]^+$, 71 $[CH_2N_4+H]^+$, 69 $[M+H–H_2N_2O_2]^+$; ***m/z*** (DEI): 130 $[M]^+$, 84 $[M–NO_2]^+$, 46 $[NO_2]^+$, 42 $[N_3]^+$, 28 $[N_2]^+$; **EA** ($CH_2N_6O_2$, 130.09) calcd.: N 64.6, C 9.2, H 1.6; found: N 64.4, C 9.3, H 1.7 %; **impact sensitivity**: < 1.5 J; **friction sensitivity**: 8 N; **$\Delta_c U$**: 1700 cal g^{-1}.

5-Nitriminotetrazole monohydrate (**43**·H_2O): A small amount of **43** was dissolved in water and left for crystallization. After one day colorless rods were obtained. **DSC** (T_{onset}, 5 °C min^{-1}): 122–124 °C (dec.); **IR** (KBr, cm^{-1}): $\tilde{\nu}$ = 3538 (m), 3463 (m), 3070 (w), 2930 (w), 2670 (w), 1614 (s), 1591 (s), 1508 (m), 1451 (m), 1355 (s), 1320 (vs), 1259 (s), 1242 (s), 1120 (w), 1062 (m), 1016 (w), 993 (m), 910 (w), 879 (w), 846 (m), 777 (m), 755 (w), 727 (w), 655 (w); **Raman** (1064 nm, 350 mW, 25 °C, cm^{-1}): $\tilde{\nu}$ = 1635 (10), 1585 (62), 1556 (12), 1423 (87), 1372 (7), 1305 (6), 1251 (11), 1083 (15), 1065 (17), 1017 (100), 989 (37), 855 (11), 758 (34), 732 (23), 492 (22), 418 (30), 358 (9), 237 (25), 172 (30); **EA** ($CH_4N_6O_3$, 148.10) calcd.: C 8.22, H 2.72, N 56.75 %; found: C 8.26, H 2.49, N 57.15 %; **impact sensitivity**: 9 J; **friction sensitivity**: 140 N; **ESD**: 0.38 J.

1-Methyl-5-aminotetrazole and 2-Methyl-5-aminotetrazole: The methylated 5-aminotetrazoles were synthesized by methylation of 5-aminotetrazole using Me_2SO_4 or MeI according to the literature procedures.[65] An alternative synthesis occurs via cyclization reactions according to the literature.[66]

*1-Methyl-5-nitriminotetrazole (**44**):* 1-Methyl-5-aminotetrazole (1.98 g, 0.02 mol) was added in small portions to 6 mL of ice-cooled HNO_3 (100 %). After 2 hours the ice bath was removed and the solution was stirred for further 20 hours. Afterwards the reaction

was quenched with 10 mL of cold water and the HNO_3 was removed using high vacuum until the colorless product started to precipitate. Single crystals suitable for X-ray structure determination were obtained by recrystallization from half-conc. HNO_3 (2.74 g, 95 % yield). **DSC** (T_{onset}, 5 °C min^{-1}): 125 °C (dec.); **IR** (KBr, cm^{-1}): $\tilde{\nu}$ = 3091–3056 (m, br), 2885 (m), 2636 (m), 2282 (w), 2217 (w), 2082 (w), 1925 (w), 1591 (vs), 1515 (s), 1496 (s), 1455 (s), 1441 (m), 1411 (m), 1400 (m), 1384 (m), 1330 (vs), 1308 (s), 1261 (s), 1213 (vs), 1135 (m), 1065 (w), 1037 (s), 970 (s), 813 (m), 778 (m), 716 (s), 685 (m), 669 (m), 450 (m); **Raman** (1064 nm, 200 mW, 25 °C, cm^{-1}): $\tilde{\nu}$ = 3057 (8), 3031 (9), 2966 (35), 1597 (58), 1574 (73), 1467 (24), 1441 (13), 1407 (100), 1310 (10), 1241 (59), 1218 (31), 1038 (61), 972 (38), 890 (23), 874 (15), 757 (44), 686 (57), 490 (32), 450 (14), 354 (10), 302 (42), 244 (19), 208 (19), 129 (10); **^{1}H NMR** (d_6-DMSO, 25 °C, ppm): δ = 14.09 (1H, s, NH), 3.73 (3H, s, CH_3); **^{13}C NMR** (d_6-DMSO, 25 °C, ppm): δ = 150.3 (C1), 34.0 (C2); **^{14}N NMR** (d_6-DMSO, 25 °C, ppm): δ = –18.8 (NO_2); **^{15}N NMR** (d_6-DMSO, 25 °C, ppm): δ = –26.8 (N2, $^{3}J_{N-H}$= 1.9 Hz), –29.8 (N3), –159.2 (N4), –159.3 (N5), –177.4 (N1, $^{2}J_{N-H}$= 2.1 Hz); ***m/z*** (DEI): 144 $[M]^+$, 46 $[NO_2]^+$, 43 $[HN_3]^+$, 15 $[CH_3]^+$; **EA** ($C_2H_4N_6O_2$, 144.11) calcd.: C 16.7, H 2.8, N 58.3 %; found: C 16.6, H 2.8, N 58.5 %; **impact sensitivity**: 12.5 J; **friction sensitivity**: 160 N; **$\Delta_c U$**: 2700 cal g^{-1}.

*1-Methyl-5-nitriminotetrazole monohydrate (**44**·H_2O)*: A small amount of **44** was dissolved in warm water and left for crystallization. After one day colorless crystals were obtained. **DSC** (T_{onset}, 5 °C min^{-1}): 124-126 °C (dec.); **IR** (KBr, cm^{-1}): $\tilde{\nu}$ = 3568 (w), 3443 (w), 3084 (m), 3049 (m), 2879 (m), 2634 (w), 1727 (w), 1700 (w), 1591 (vs), 1515 (s), 1498 (s), 1455 (s), 1411 (m), 1400 (m), 1330 (s), 1307 (s), 1213 (vs), 1135 (m), 1065 (m), 1038 (s), 970 (s), 812 (m), 778 (m), 753 (m), 716 (s), 686 (w), 669 (m); **Raman** (1064 nm, 350 mW, 25 °C, cm^{-1}): $\tilde{\nu}$ = 3034 (10), 3014 (15), 2958 (36), 1582 (95), 1469 (24), 1418 (79), 1340 (12), 1275 (40), 1231 (27), 1088 (19), 1056 (38), 1044 (100), 984 (22), 880 (25), 761 (53), 693 (50), 682 (23), 495 (35), 454 (16), 300 (36), 270 (21), 247 (27), 166 (23); **EA** ($C_2H_6N_6O_3$, 162.11): calcd.: C 14.82, H 3.73, N 51.84 %; found: C 14.60, H 3.51, N 52.11 %; **impact sensitivity**: 19 J; **friction sensitivity**: 320 N; **ESD**: 0.35 J.

*2-Methyl-5-nitraminotetrazole (**45**):* 2-Methyl-5-aminotetrazole (1.98 g, 0.02 mol) was added in small portions to 8 ml of ice-cooled HNO_3 (100 %). After 2 hours the ice bath was removed and the solution was stirred at room temperature over night. The reaction was then quenched with 10 ml of ice, while the product precipitated. The colorless

powder obtained was then recrystallized from hot water (2.62 g, 91 % yield). **DSC** (T_{onset}, 5 °C min^{-1}): 123 °C (dec.); **IR** (KBr, cm^{-1}): $\tilde{\nu}$ = 3237 (m), 3144 (m), 3051 (s), 2927 (m), 2819 (m), 2691 (w), 2402 (w), 1613 (vs), 1526 (m), 1479 (s), 1462 (m), 1384 (m), 1351 (s), 1313 (vs), 1207 (m), 1102 (w), 1051 (w), 1041 (w), 1001 (w), 920 (m), 779 (m), 759 (m), 734 (m), 691 (m), 618 (w), 482 (w); **Raman** (1064 nm, 200 mW, 25 °C, cm^{-1}): $\tilde{\nu}$ = 3133 (9), 3052 (30), 2970 (98), 2828 (6), 1618 (10), 1524 (100), 1483 (35), 1438 (18), 1395 (24), 1359 (44), 1312 (43), 1209 (41), 1105 (40), 1042 (47), 1004 (50), 915 (16), 779 (13), 725 (6), 692 (72), 472 (17), 445 (61), 384 (47), 318 (29), 241 (15), 147 (20), 126 (18); **^{1}H NMR** (d_6-DMSO, 25 °C, ppm): δ = 11.74 (1H, br, s, NH), 4.37 (3H, s, CH_3); **^{13}C NMR** (d_6-DMSO, 25 °C, ppm): δ = 157.6 (CN_4), 40.9 (CH_3); **^{14}N NMR** (d_6-DMSO, 25 °C, ppm): δ = –35.0 (NO_2); **^{15}N NMR** (d_6-DMSO, 25 °C, ppm): δ = –0.3 (N3, $^{3}J_{N-H}$= 1.9 Hz), –35.0 (NO_2), –58.3 (N4), –83.4 (N1), –103.6 (N2, $^{2}J_{N-H}$= 2.2 Hz), –209.3 (N5), –159.2 (N4), –159.3 (N5), –177.4 (N1, $^{3}J_{N-H}$= 1.9 Hz); ***m/z*** (DEI): 144 (51) $[M]^+$, 98 (77) $[M-NO_2]^+$, 71 $[CH_3N_4]^+$, 70 $[CH_2N_4]^+$, 69 $[CHN_4]^+$, 56 (27) $[N_4]^+$, 55 (30) $[CHN_3]^+$, 46 (21) $[NO_2]^+$, 43 (100) $[HN_3]^+$, 28 (43) $[N_2]^+$, 15 (33) $[CH_3]^+$; ***m/z*** (DCI): 289 $[2M+H]^+$, 145 $[M+H]^+$, 99 $[M-NO_2]^+$, 85 $[CH_3N_5]^+$, 71 $[CH_3N_4]^+$; **EA** ($C_2H_4N_6O_2$, 144.11): calcd.: C 16.7, H 2.8, N 58.3 %; found: C 16.8, H 2.9, N 58.4 %; **impact sensitivity:** 3.0 J; **friction sensitivity**: 145 N; $\Delta_c U$: 2902 cal g^{-1}.

4.7 Conclusion

From this experimental study the following conclusions can be drawn:

- 5-Nitriminotetrazole (**43**), 1-methyl-5-nitrimino-tetrazole (**44**) and 2-methyl-5-nitraminotetrazole (**45**) can be synthesized in high yields and purity from 5-aminotetrazole and 1- and 2-methyl-5-aminotetrazole respectively in simple one step syntheses by reaction with fuming HNO_3. Recrystallization of **43** and **44** from water yields the monohydrates **43**·H_2O and **44**·H_2O.

- The described synthesis of **43** yielded to several *violent explosions*! It is necessary to use an open vessel while stirring over night. It has been proved, that after pouring the nitration mixture on ice, the solution should be stirred for further 24 hours at room temperature. *Highest safety precautions should be used anyway!* It is also possible to neutralize the nitration mixture carefully by adding an excess

of KOH. The potassium salt precipitated can be recrystallized from ethanol/water. Afterwards, the addition of one equivalent diluted hydrochloric acid yields 5-nitriminotetrazole, which can be extracted using diethyl ether.

- The crystal structures of 5-nitriminotetrazole (**43**), 1-methyl-5-nitrimino-tetrazole (**44**) and 2-methyl-5-nitraminotetrazole (**45**) were determined using low-temperature single crystal X-ray diffraction. In the structure of **43** both hydrogen atoms could be located at the tetrazole ring forming a nitriminotetrazole. A similar structure can be observed for **44**, whereas **45** corresponds to a nitraminotetrazole, where the hydrogen atom is located at the nitrogen atom of the nitramine group. In addition, the crystal structures of **43**·H_2O and **44**·H_2O are presented. Both crystal packings have, although possessing more hydrogen bonds, lower densities as their water-free analogues. All of the compounds are stabilized in the crystalline state of the presence of strong hydrogen bonds.

- Thorough characterization of the chemical, thermo-chemical and energetic properties of **43**, **44** and **45** is reported. All compounds presented in this chapter are highly performing energetic materials. However, they show increased sensitivities towards friction and impact and also low decomposition temperatures in the range of 122–124 °C. In the case of **43**, increased precautions should be undertaken when the compound is prepared on a larger scale.

- **43**·H_2O and **44**·H_2O show decreased sensitivities (impact, friction, electrical discharge) but also detonation parameter in comparison to the water-free analogues.

- The heats of formation of the monohydrates **43**·H_2O (54 kJ mol^{-1}) and **44**·H_2O (22 kJ mol^{-1}) are ~265 kJ mol^{-1} lower than those of the water-free analogues.

- The detonation parameters of the **43**–**45** were computed with the EXPLO5.V2 software. Since the water free compounds have higher densities, they show also higher calc. performances. 5-Nitriminotetrazole (**43**) is characterized by an extremely high V_{Det} = 9450 m s^{-1} and $p_{C\text{-}J}$ = 394 kbar.

Chapter 5.

Functionalized 1-Ethyl-5-aminotetrazoles and 1-Ethyl-5-nitriminotetrazoles

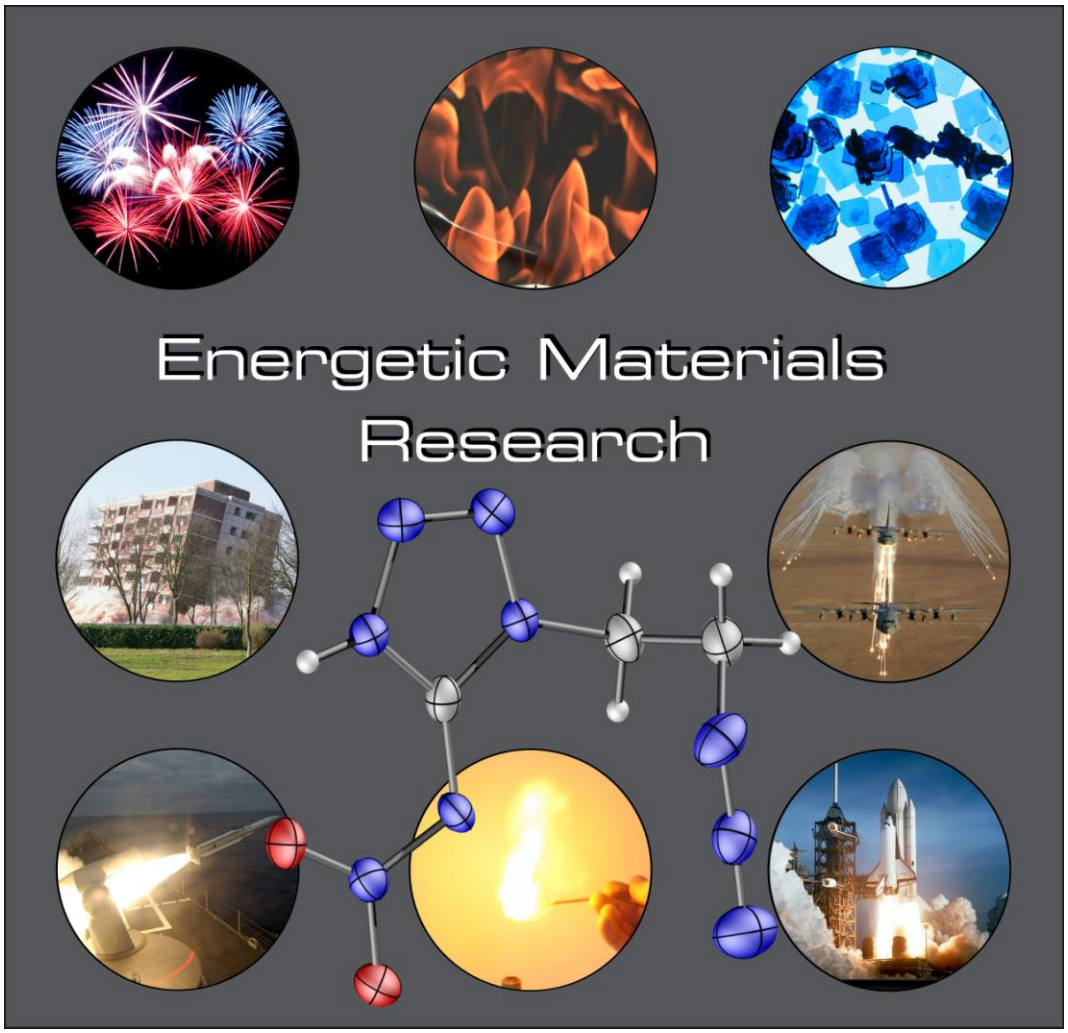

5.1 Introduction

Tetrazoles have the outstanding property of often combining high nitrogen contents and high positive heats of formation with good thermal stabilities, due to their aromatic ring system. Of particular interest are tetrazoles, which exhibit energetic nitrogen-oxygen containing functional groups such as nitro groups (R–NO_2),[155,258,259] nitrate esters (R–O–NO_2) [233] or nitramine functionalities (R_2N–NO_2).[138,260] Also the formation of tetrazolium salts with oxygen rich counter anions such as NO_3^- [61,68] or $N(NO_2)_2^-$ [175a,134,135] are in the focus of the research, since these compounds have balanced oxygen contents. 5-Nitriminotetrazoles have been known for a long time, since they are obtainable via facile synthetic routes.[261] 1-Substituted 5-nitriminotetrazoles, e.g. 1-methyl-5-nitriminotetrazole and 1-ethyl-5-nitriminotetrazole were first described in 1957.[262] 1-Methyl-5-nitriminotetrazole (1MeHAtNO_2) is synthesized by methylation of 5-aminotetrazole (5-At) forming 1-methyl-5-aminotetrazole (1MeAt) followed by nitration of the primary amine.

In this work we present the syntheses of several new 1-functionalized 5-nitriminotetrazoles and derivatives, which are also accessible by nitration of the corresponding 5-aminotetrazoles.[65,263] The compounds belong to all classes of energetic materials. Thus, 1-(2-azidoethyl)-5-aminotetrazole represents a nitrogen rich fuel for propellant charges, 1-(2-azidoethyl)-5-nitriminotetrazole represents a powerful secondary explosive and the copper complexes can be used as colorants (green and blue) in modern smokeless pyrotechnical compositions.

5.2 Synthesis

The syntheses of functionalized 1-ethyl-5-aminotetrazoles and 1-ethyl-5-nitriminotetrazoles were performed according to **Scheme 5.1**. The *N*-alkylation of 5-aminotetrazole using 1-chloroethanol was prepared as described by Henry and Finnegan.[65] The alkylation yields the isomers 1-(2-hydroxyethyl)-5-aminotetrazole (**46**) and 2-(2-hydroxyethyl)-5-aminotetrazole (**47**) in 32 % and 58 % yield, respectively. The 1-isomer was separated by recrystallization from ethanol. The 2-isomer, which shows a great crystallization-delay, is not described in this work. Single crystals of **46** were obtained from water. Treatment of **46** with $SOCl_2$ yielded 1-(2-chloroethyl)-5-aminotetrazole (**48**) in 75 % yield.[263] Single crystals were also

obtained by recrystallization from hot water. The substitution of chlorine with azide was tried in different solvents (MeCN, acetone, H_2O, DMF) using different azide sources (NaN_3, Me_3SiN_3, AgN_3). Only the reaction of **48** with NaN_3 in DMF as the solvent yielded 1-(2-azidoethyl)-5-aminotetrazole (**49**) in good yields (76 %). Two different kinds of single crystals (polymorphs **49a** and **49b**) both suitable for XRD could be obtained by recrystallization from hot water and hot ethanol. The nitration of **46**, **48** and **49** using 100 % nitric acid yielded the products 1-(2-hydroxyethyl)-5-nitriminotetrazole (**50**), 1-(2-chloroethyl)-5-nitriminotetrazole (**51**) and 1-(2-nitratoethyl)-5-nitriminotetrazole monohydrate (**52**). The reactions were performed simply by adding **46**, **48** and **49** to an ice cooled excess of 100 % nitric acid and stirring for 12 hours. Afterwards the reactions were poured on ice and the solvent was removed using high vacuum. Single crystals of **50**–**52** were obtained by simple evaporation of aqueous solutions on air at ambient temperature. In the case of **46** or **50** the hydroxyl group could not have been nitrated by using fuming nitric acid. Interestingly, nitration of **49** did not yield 1-(2-azidoethyl)-5-nitriminotetrazole (**53**) since the azide group was substituted by an ONO_2 group. **52** was only obtained solid as its monohydrate. Compound **53** could be synthesized by NO_2BF_4 as a mild nitration agent. Unfortunately the yields are low (38 %) and the purification is tricky, since HBF_4 has to be removed. Therefore, potassium hydroxide was added to an ethanolic solution of the nitration mixture, first precipitating KBF_4 and second potassium 1-(2-azidoethyl)-5-nitriminotetrazolate (**54**), which both were isolated by filtration. The starting material can be easily removed, since it cannot be deprotonated and it is soluble in ethanol. Other attempts to synthesize **53** by chlorine-azide substitution of **51** failed due to the formation of sodium 1-(2-chloroethyl)-5-nitriminotetrazolate (**55**), which cannot be substituted by the azide anion. The deprotonation of **51** was also proven by the formation of the ammonium salt **56** by using aqueous ammonia solution. In addition, protonation of 1-substituted 5-aminotetrazoles was performed using diluted nitric acid on **46** and **49** as well as perchloric acid on **49**. With this, 1-(2-hydroxyethyl)-5-aminotetrazolium nitrate (**57**), 1-(2-azidoethyl)-5-aminotetrazolium nitrate (**58**) and 1-(2-azidoethyl)-5-amino-tetrazolium perchlorate (**59**) were obtained in nearly quantitative yields, which were recrystallized from water/ethanol mixtures.

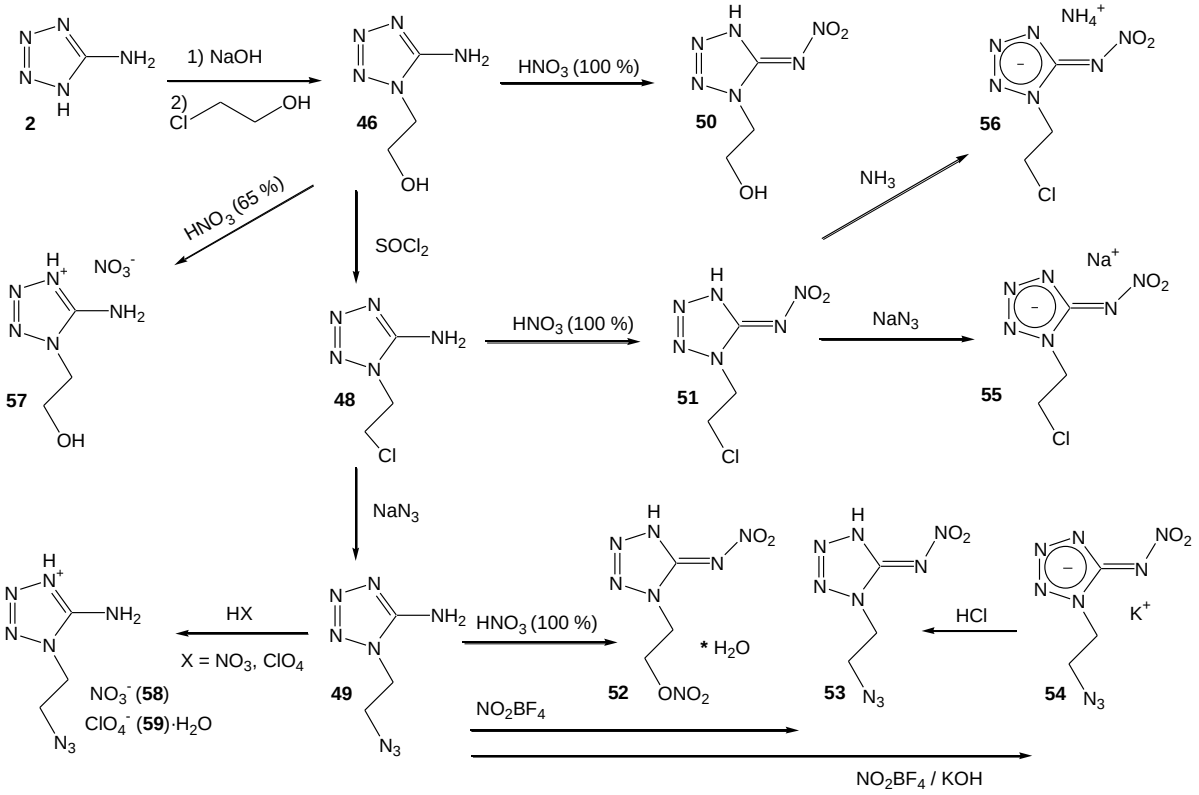

Scheme 5.1 Synthesis of 1-functionalized 5-amino- and 5-nitriminotetrazoles.

In addition to the complexes presented in Chapter 9, three copper complexes have been synthesized, in which the nitrimino-tetrazole moieties act as bidentate ligands.[149] One of the complexes was shown to be a promising alternative to toxic lead azide as a new primary explosive. Therefore, **50**, **51** and **53** were reacted with copper(II) nitrate in hot aqueous solutions to yield the complexes *trans*[diaqua-bis(1-(2-hydroxyethyl)-5-nitriminotetrazolato*N4,O1*)copper (II)] (**60**), *trans*[diaqua-bis(1-(2-chloroethyl)-5-nitriminotetrazolato-*N4,O1*)copper(II)] dihydrate (**61**) and [diaqua-bis(1-(2-azidoethyl)-5-nitriminotetrazolato-*N4,O1*)copper-(II)] (**62**) (**Scheme 5.2**). Green single crystals of complexes **60** - **62** precipitated from concentrated aqueous solutions over night.

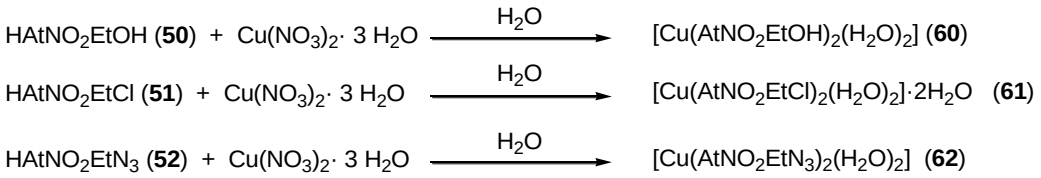

Scheme 5.2 Synthesis of the copper complexes **60** –**62**.

5.3 Crystal Structures

The molecular structures and crystal structures of **46–62** are described in the following paragraph. Structural parameter (bond length and angles) are given at the end of this section. In general, all tetrazole rings follow the geometries observed for other tetrazole derivatives in the CCDC database. The five membered ring is planar building an aromatic system. The ring moiety of **46**, **47**, **48**, **49a**, **49b** and **57–59** are in agreement with the structure observed for 5-amino-1*H*-tetrazole monohydrate [60] and 1-phenyl-5-aminotetrazole.[264] The nitrated 5-aminotetrazoles **50**, **51**, **52** and **53** are in agreement with both the structure of 1-methyl-5-nitriminotetrazole (Chapter 4) and of 1-(2-nitro-2-azapropyl)-5-nitriminotetrazole monohydrate (Chapter 6).

5.3.1 1-(2-Hydroxyethyl)-5-aminotetrazole (**46**)

46 crystallizes in the monoclinic space group $P2_1/c$ with four molecules in the unit cell and a density of 1.497 g cm^{-3}. Its molecular structure (**Figure 5.1**) can be compared with the one of 1-(2-hydroxyethyl)-tetrazole described 2007 by Lyakhov *et al.*.[265]

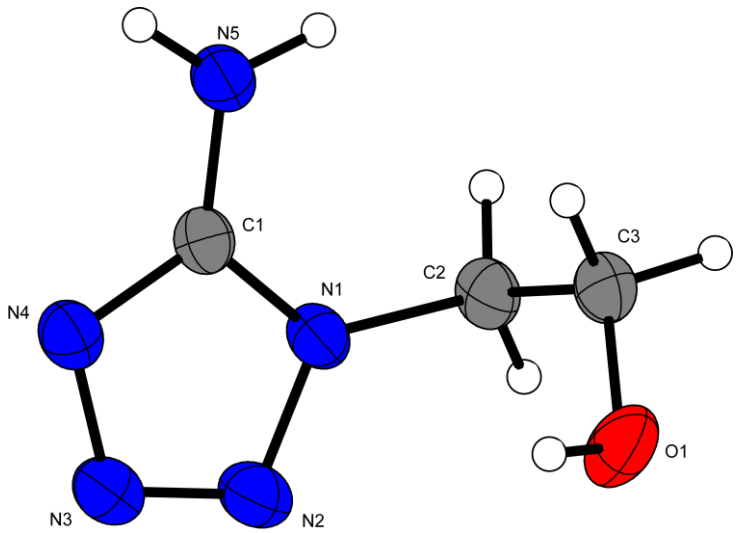

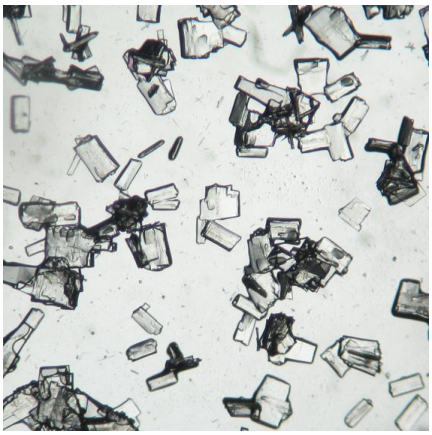

Figure 5.1 Molecular structure of **46**. Thermal ellipsoids represent the 50 % probability level.

In the packing of **46** the tetrazole moieties crystallize in layers, whereas the ethyl substituent is nearly orthogonal to the planes (**Figure 5.2**). Interactions (**Figure 5.3**) can be observed between the alkyl chains on the one hand side, as well as an intensive

H-bond network can be found on the other side. The layers are built by **R4,4(13)** graph sets including a OH group of a neighbored layer.

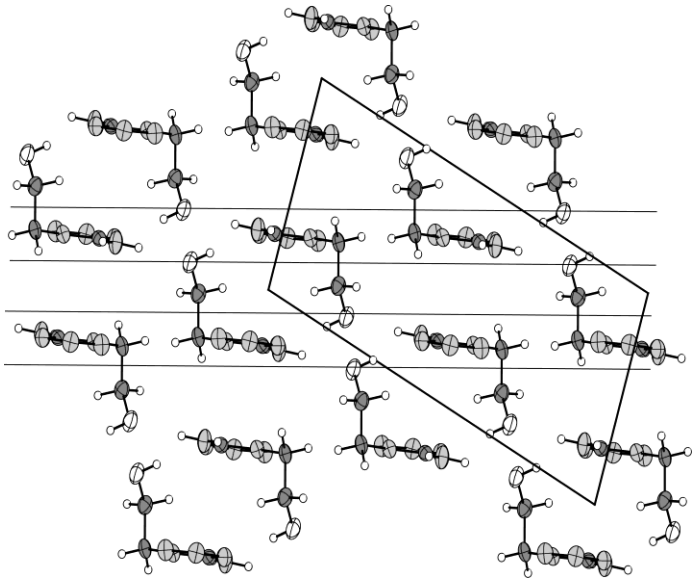

Figure 5.2 View on the packing of **46** illustrating the planes build by the 5-aminotetrazole moieties.

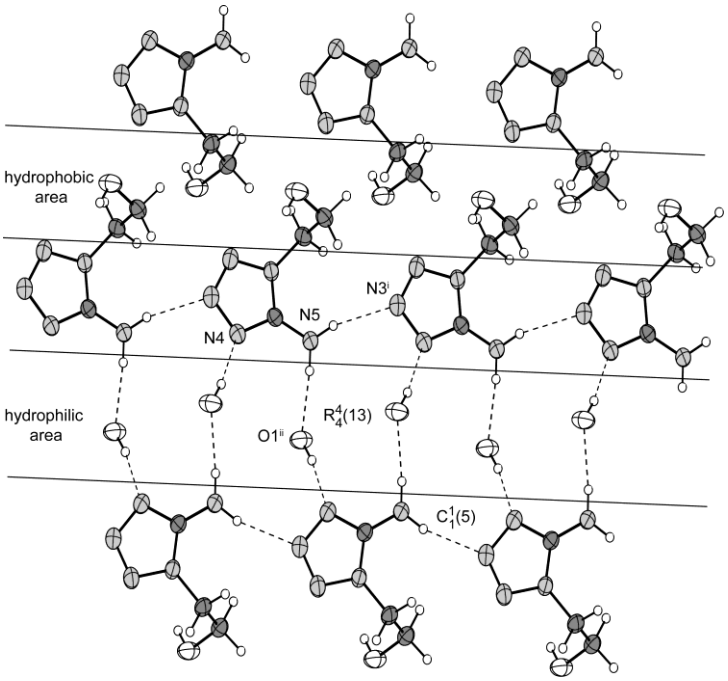

Figure 5.3 H-bonding in the structure of **46**. Two graph sets are marked. Selected hydrogen bonds (Å, Å, Å,°): N5–H5A···N3^{i} = 0.88(3), 2.16(3), 3.012(3), 162(2); N5–H5B···O1^{ii} = 0.86(3), 1.98(3), 2.828(3), 173(3); O1–H1···N4^{iii} = 0.86(4), 1.99(4), 2.842(3), 171(3); (i) x, 1+y, z; (ii) x, 0.5–y, 0.5+z; (iii) 2–x, –y, 1–z.

5.3.2 2-(2-Hydroxyethyl)-5-aminotetrazole (**47**)

The molecular structure of 2-substiuted **47** is depicted in **Figure 5.4**. **47** crystallizes in the monoclinic space group $P2_1/c$ with four molecules in the unit cell. The structure of the tetrazole ring is in agreement to this of 2-methyl-5-aminotetrazole.[283] All hydrogen atoms participate in the following hydrogen bonds: O1–H1···N4^{i} (0.89(2), 1.93(2), 2.810(2) Å, 170(2)°), N5–H5B···N1^{ii} (0.84(2), 2.31(2), 3.136(2) Å, 171(2)°) and N5–H5A···O1^{iii} (0.87(2), 2.04(2), 2.913(2) Å, 175(1)°) ((i) x, 0.5–y, 0.5+z; (ii) 1–x, –y, 1–z; (iii) 1–x, –0.5+y, 0.5–z).

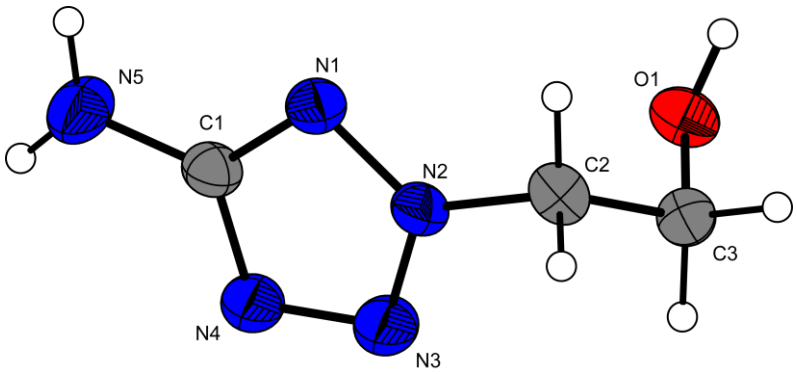

Figure 5.4 Molecular structure of **47**. Thermal ellipsoids represent the 50% probability level. Bond distances (Å): O1–C3 = 1.418(2), N2–N3 = 1.299(2), N2–N1 = 1.338(2), N2–C2 = 1.466(2), N1–C1 = 1.336(2), N3–N4 = 1.332(2), N4–C1 = 1.348(2), N5–C1 = 1.345(2), C3–C2 = 1.506(2).

5.3.3 1-(2-Chloroethyl)-5-aminotetrazole (**48**)

48 crystallizes with a density of 1.547 g cm^{-3} and two molecules in a triclinic unit cell with the space group *P*–1.The molecular structure (**Figure 5.5**) of **48** can be compared with those of 1-(2-chloroethyl)-tetrazole [266] and 1-ethyl-tetrazole, which also have been described as ligands in copper complexes.[267] The packing is very similar to that observed for **46**.

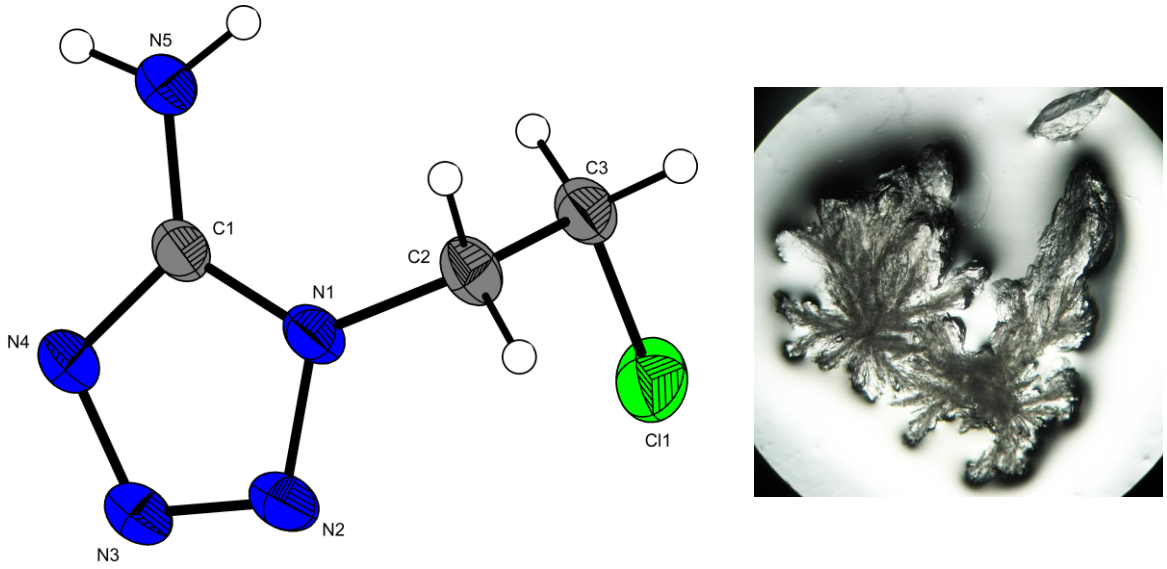

Figure 5.5 Molecular structure of **48**. Thermal ellipsoids represent the 50 % probability level.

In the packing of **48** no continuous layers are formed. However, again regions dominated by H-bonds as well as alkyl interactions can be found (**Figure 5.6**). The hydrogen bonding modes are depicted in **Figure 5.7**. **C1,1(5)** chains as well as two symmetric ring graph sets (**R4,4(8)**, **R5,5(10)**) can be found in the structure of **46**.

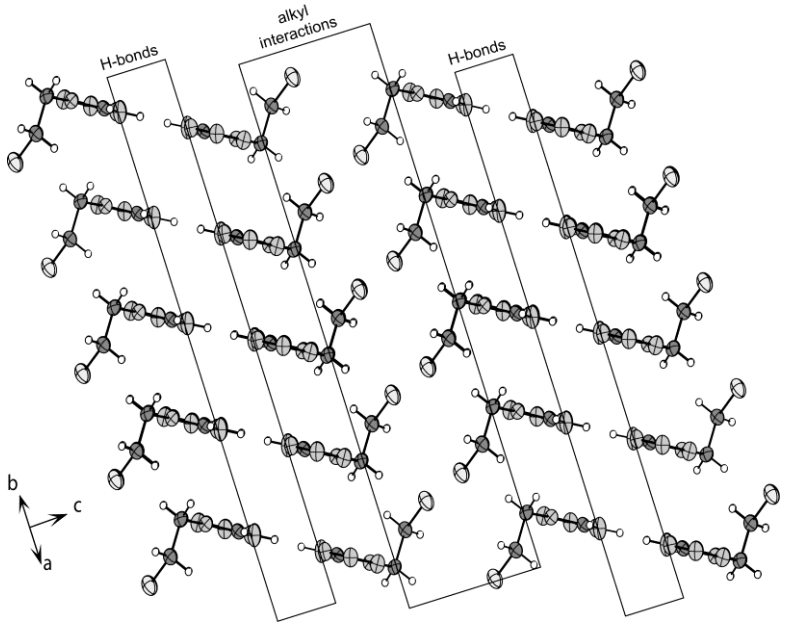

Figure 5.6 View on the packing of **48** illustrating the planes built by the 5-aminotetrazole moieties.

The observed hydrogen bonds form endless **C1,1(5)** chains and also ring systems with the graph sets **R4,4(10)** and **R2,2(8)**.

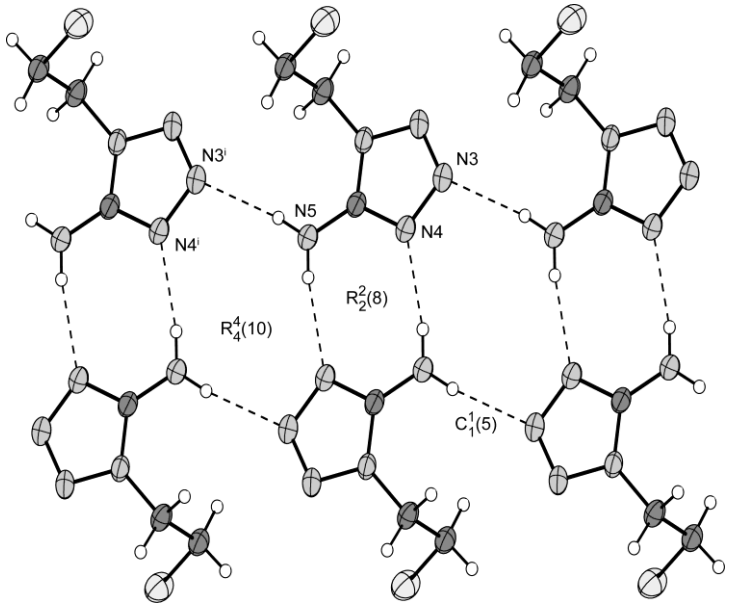

Figure 5.7 H-bonding in the structure of **48**. Two graph sets are marked. Selected hydrogen bonds (Å, Å, Å,°): N5–H5B···N3^{i} = 0.86(2), 2.17(2), 3.020(2), 171(2); N5–H5A···N4^{ii} = 0.84(2), 2.17(2), 3.001(2), 169(2); (i) –1+x, –1+y, z; (ii) 1–x, –y, 1–z.

5.3.4 1-(2-Azidoethyl)-5-aminotetrazole (**49**)

Interestingly, two polymorphs of **49** have been obtained. Recrystallization from water yielded the structure **49a** shown in **Figure 5.8**, whereas recrystallization from ethanol yielded the molecular structure (**49b**) shown in **Figure 5.9**. Single point calculations at the experimentally observed structures (X-ray) of **49a** and **49b** showed that latter molecule is ~32 kJ mol^{-1} lower in electronic energy (B3LYP/cc-pVDZ). **49a** crystallizes in the monoclinic space group $P2_1/c$ with four molecules in the unit cell and a density of 1.50 g cm^{-3}. In contrast **49b** crystallizes in the triclinic within the space group $P\bar{1}$ with two molecules in the unit cell and a calculated density of 1.49 g cm^{-3}. The molecular structures are akin and a comparison of the bond lengths is given in **Table 5.1**. Within the standard deviations there are no differences within the bond lengths. The greatest difference is observed in the bond angles C1–N1–C2 and N2–N1–C2 which are responsibly for displacement of the 2-azidoethyl substituent. The structures can be compared with the complex bis(1-(2-azidoethyl)-tetrazole-*N4*) copper(II) chloride described in 2001 by Ivashkevich *et al.*.[268] A neutral 1-(2-azidoethyl)tetrazole moiety cannot be found in the literature.

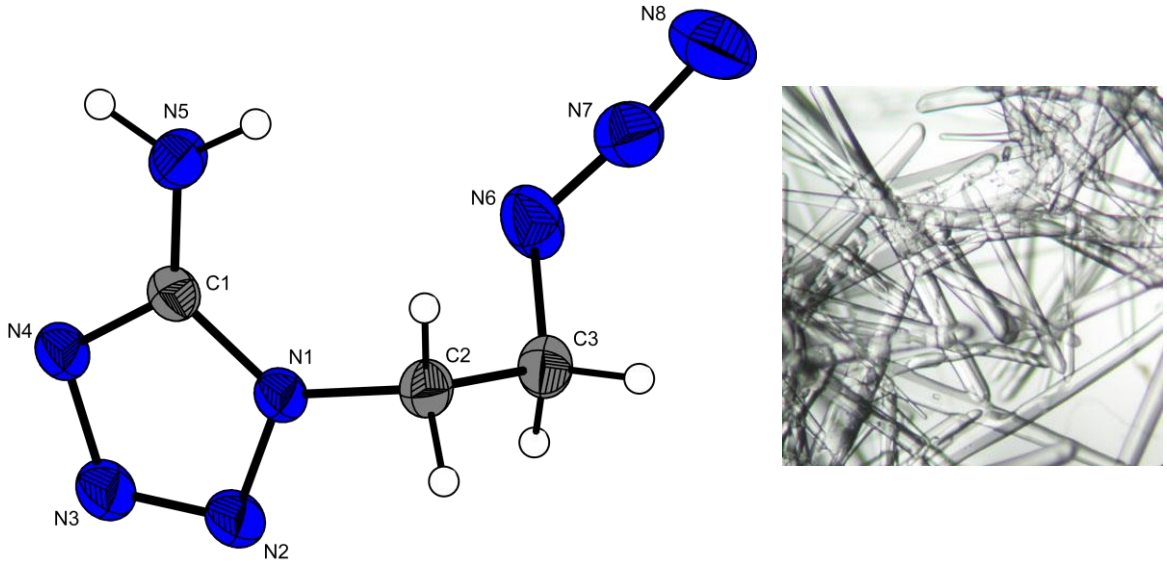

Figure 5.8 Molecular structure of **49a** (crystals from water). Thermal ellipsoids represent the 50 % probability level.

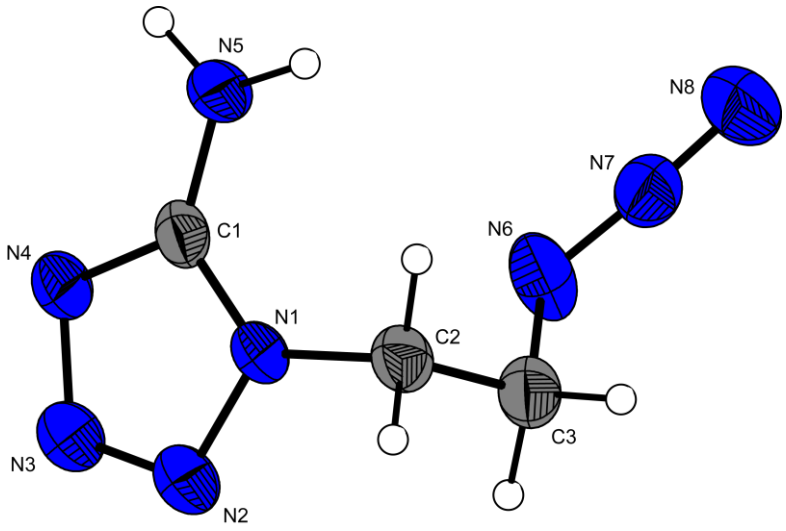

Figure 5.9 Molecular structure of **49b** (crystals from ethanol). Thermal ellipsoids represent the 50 % probability level.

In **Figure 5.10** and **Figure 5.11** the hydrogen bond motif of **49a** and **49b** are depicted. However, the same motifs are observed in the structure of polymorph **49b**. The analysis of the hydrogen bond graph sets [208] shows that due to **C1,1(5)** and **R2,2(8)** isolated chains are formed. Between the chains only weak interactions can be observed. This is a consequence of the low density of 1.50 g cm^{-3}. A view on larger sections of **49a** and **49b** (**Figure 5.12** and **Figure 5.13**) point up the different space group (**49a**: $P2_1/c$, **49b**: $P\bar{1}$) symmetries.

Table 5.1 Bond lengths (Å) and angles (°) of polymorphs **49a** and **49b**.

atoms 1–2	**49a**	**49b**	atoms 1–2–3	**49a**	**49b**
N1–C1	1.347(2)	1.349(2)	C1–N1–N2	108.4(1)	108.6(1)
N1–N2	1.366(2)	1.363(2)	N3–N2–N1	106.0(1)	105.8(1)
N2–N3	1.287(2)	1.280(2)	N2–N3–N4	112.0(1)	112.4(1)
N3–N4	1.363(2)	1.357(2)	C1–N4–N3	105.4(1)	105.4(1)
N4–C1	1.335(2)	1.335(2)	N4–C1–N1	108.3(1)	107.9(1)
N5–C1	1.331(2)	1.330(2)	N5–C1–N1	126.0(1)	126.2(2)
N1–C2	1.463(2)	1.460(2)	N5–C1–N4	125.8(1)	126.0(2)
C2–C3	1.512(2)	1.509(3)	C1–N1–C2	131.1(1)	130.2(1)
N6–C3	1.483(2)	1.479(3)	N2–N1–C2	120.5(1)	121.2(1)
N6–N7	1.222(2)	1.222(2)	N1–C2–C3	112.1(1)	111.7(2)
N7–N8	1.131(2)	1.130(2)	N6–C3–C2	111.5(1)	111.4(2)
			N7–N6–C3	115.2(1)	115.8(2)
			N8–N7–N6	173.5(2)	173.3(2)

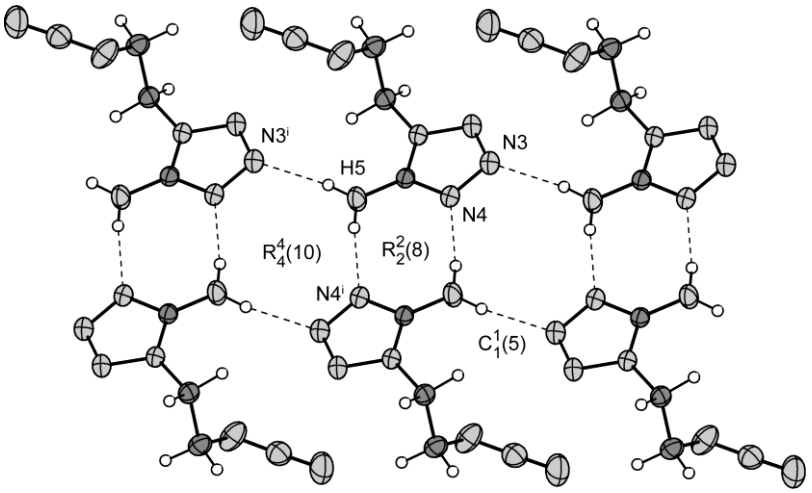

Figure 5.10 Hydrogen bonding in **49a**. Three graph sets are marked. Selected hydrogen bonds (Å, Å, Å,°): N5–H5B···N3^{i} = 0.89(2), 2.12(2), 3.006(2), 172(2); N5–H5A···N4^{ii} = 0.88(2), 2.15(2), 3.015(2), 172(2); (i) –1+x, y, z; (ii) 1–x, 1–y, 1–z.

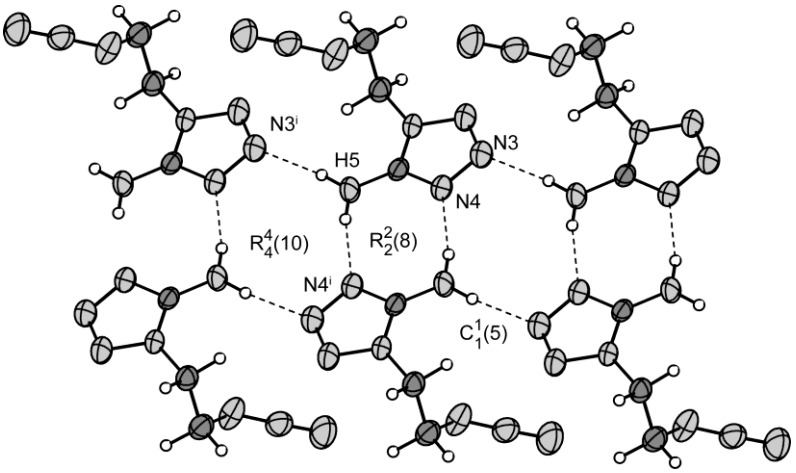

Figure 5.11 H-bonding in the structure of **49b**. Three graph sets are marked. Selected hydrogen bonds (Å, Å, Å,°): N5–H5B···N3^{i} = 0.92(2), 2.11(2), 3.025(2), 175(2); N5–H5A···N4^{ii} = 0.89(2), 2.09(2), 2.966(2), 168(2); (i) x, –1+y, z; (ii) –1–x, 1–y, 1–z.

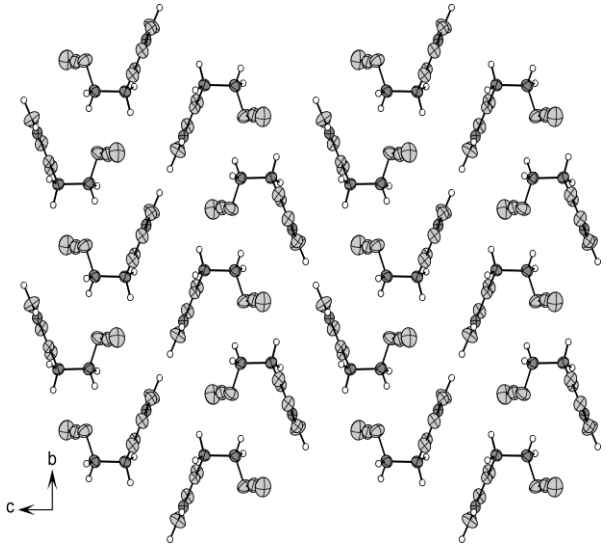

Figure 5.12 View on the packing of **49a** along the *a* axis.

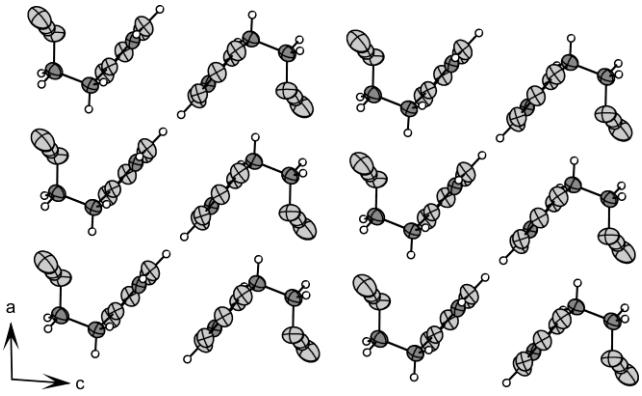

Figure 5.13 View on the packing of **49b** along the *b* axis.

5.3.5 1-(2-Hydroxyethyl)-5-nitriminotetrazole (**50**)

50 crystallizes in the triclinic space group *P*–1 with two molecules in the unit cell and a density of 1.733 g cm^{-3}. The molecular structure, depicted in **Figure 5.14**, is in agreement to that observed for 1-methyl-5-nitriminotetrazole but also neutral 5-nitriminotetrazole. The C1–N5 bond length is 1.343(2) Å, which is closer to a C=N double bond (1.28 Å) than a C–N single bond (1.46 Å). The nitramine bond N5–N6 shows a distance of 1.362(2) Å.

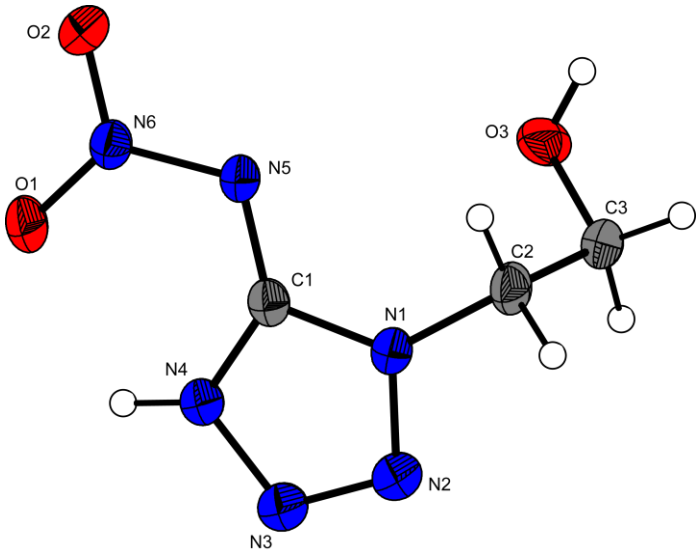

Figure 5.14 Molecular structure of **50**. Thermal ellipsoids represent the 50 % probability level.

A view on the crystal packing of **50** as well as a view on the hydrogen bonds can be seen in **Figure 5.15** and **Figure 5.16**.

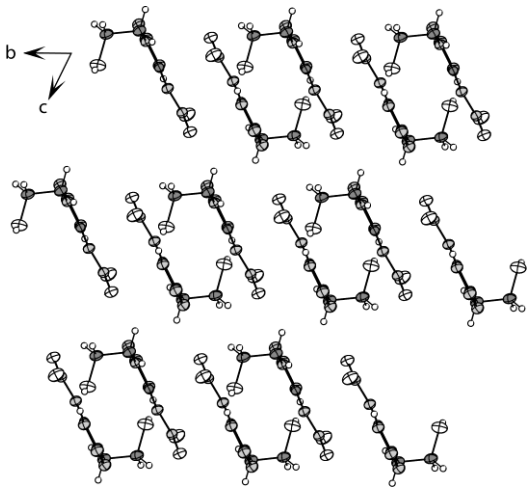

Figure 5.15 View on the packing of **50** along the *b* axis.

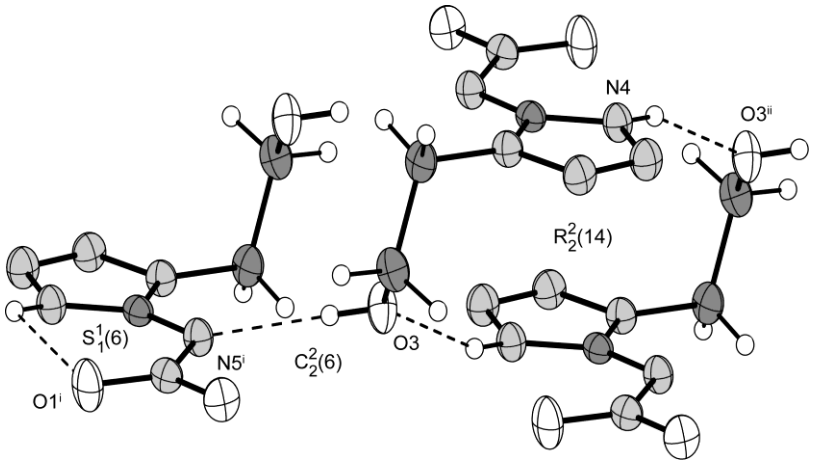

Figure 5.16 H-bonding in the structure of **50**. Three graph sets are marked. Selected hydrogen bonds (Å, Å, Å,°): O3–H3···N5^{i} = 0.83(2), 2.06(2), 2.893(2), 177(2); N4–H4···O3^{ii} = 0.87(2), 1.90(2), 2.719(2), 155(2); (i) –x, 3–y, –z; (ii) –1–x, 3–y, –z.

5.3.6 1-(2-Chloroethyl)-5-nitriminotetrazole (**51**)

1-(2-Chloroethyl)-5-nitriminotetrazole crystallizes in the orthorhombic space group $P2_12_12_1$ with four molecules in the unit cell and a density of 1.724 g cm^{-3}. The molecular moiety is shown in **Figure 5.17**.

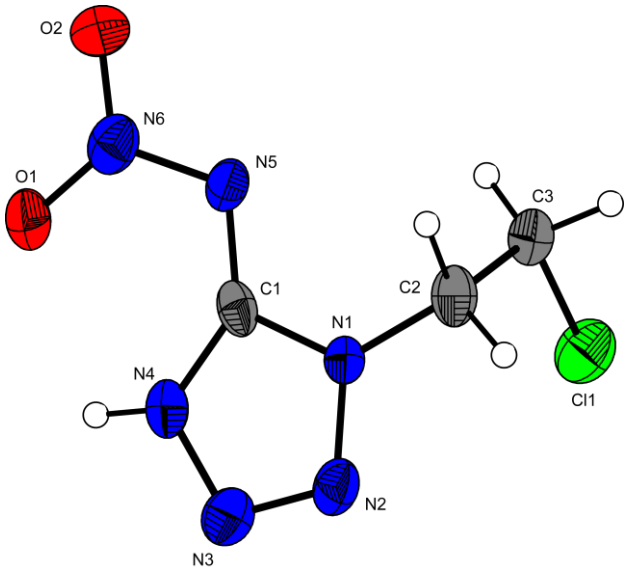

Figure 5.17 Molecular structure of **51**. Thermal ellipsoids represent the 50 % probability level.

The structure of **51** shows similar interactions, also observed in structures **46**–**49**. The packing can be divided into areas containing alkyl chain interactions as well as polar

areas containing the hydrogen bond network. A view on the packing of **51** is depicted in **Figure 5.18**.

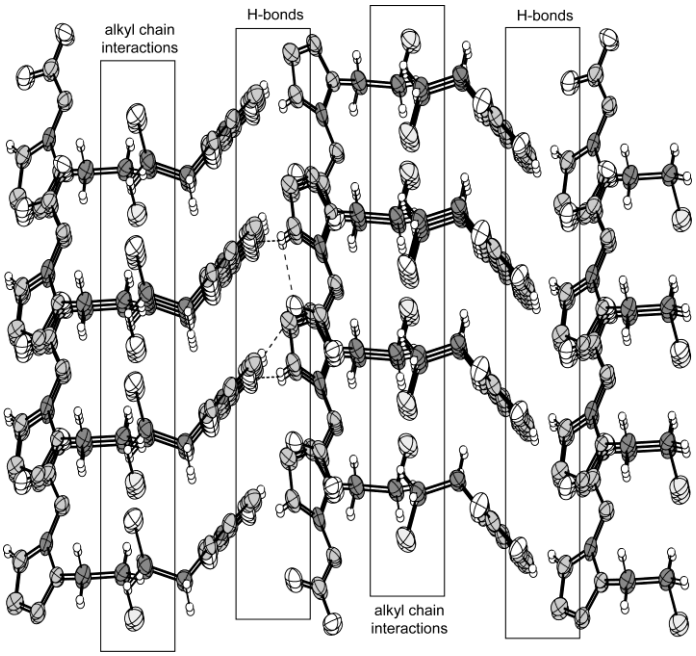

Figure 5.18 View on the packing of **51** illustrating the planes build by the 5-nitriminotetrazole moieties.

The following **Figure 5.19** gives an overview about the hydrogen bonds observed in the structure of **51**. Only one hydrogen bond is responsible for the formation of **C1,1(6)** chains.

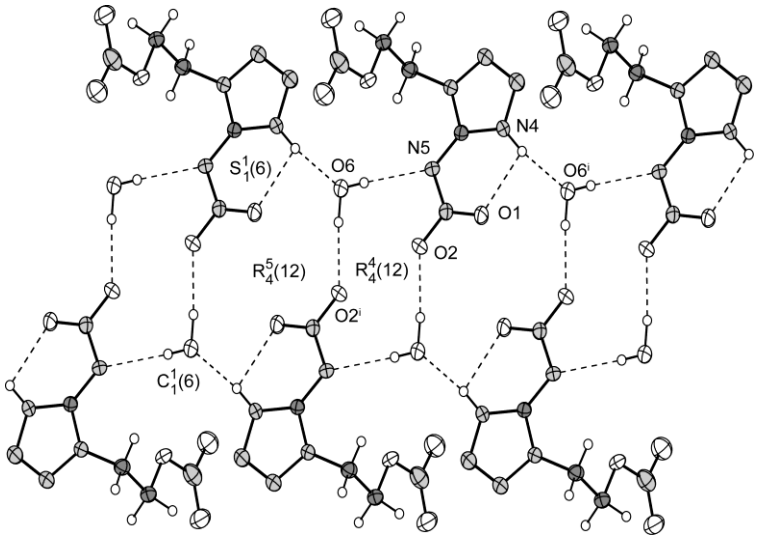

Figure 5.19 H-bonding in the structure of **51**. Two graph sets are marked. N4–H1···O1^i = 0.82(4), 2.03(4), 2.805(5), 159(4); (i) –0.5+x, 0.5–y, 1–z.

5.3.7 1-(2-Nitratoethyl)-5-nitriminotetrazole monohydrate (**52**)

Figure 5.20 shows the molecular structure of 1-(2-nitratoethyl)-5-nitriminotetrazole monohydrate, which crystallizes in the triclinic space group *P*-1. The density of 1.781 g cm^{-3} is higher than the ones observed for **50** and **51**, although **52** includes one crystal water molecule. This may be a reason of the intensive hydrogen bond network, depicted in **Figure 5.22**.

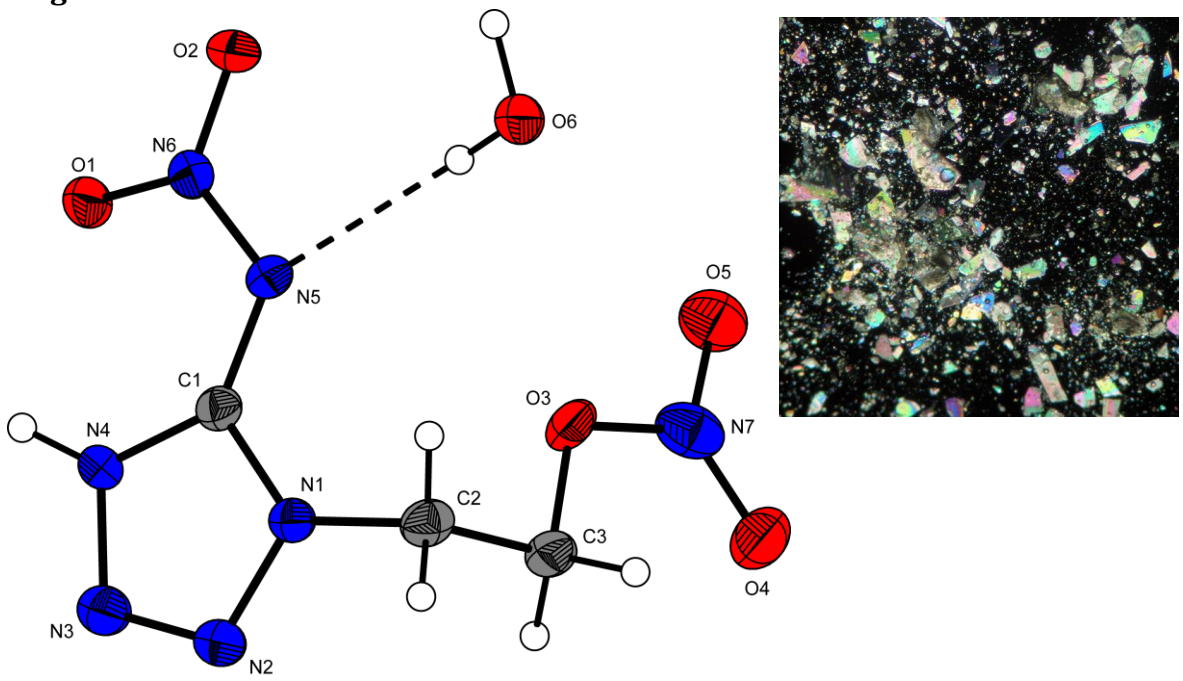

Figure 5.20 Molecular structure of **52**. Thermal ellipsoids represent the 50 % probability level.

Figure 5.21 shows a view on the packing of **52** along the *b* axis. Again alternation layers formed by H-bonds and alkyl chain interactions can be observed.

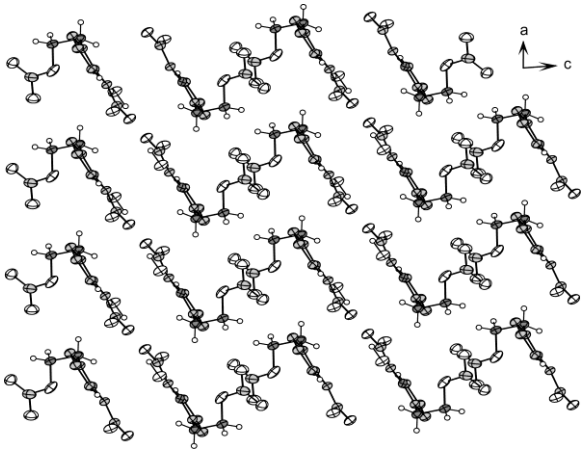

Figure 5.21 View on the packing of **52** along the *b* axis.

All atoms of the crystal water molecules participate in strong H-bond interactions connected to three different 5-nitriminotetrazole moieties, which is shown in **Figure 5.22**. Again the formation of **C1,1(6)** chains can be observed.

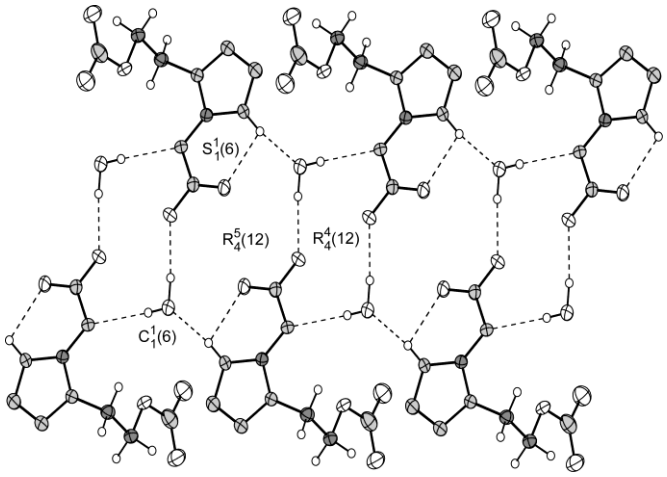

Figure 5.22 H-bonding in the structure of **52**. Four graph sets are marked. Selected hydrogen bonds (Å, Å, Å,°): N4–H4···O6^{i} = 0.87(4), 1.81(5), 2.678(4), 170(4); O6–H6A···N5 = 0.78(6), 2.19(6), 2.946(4), 166(5); O6–H6A···O2 = 0.78(6), 2.56(5), 3.080(4), 126(4); O6–H6B···O2^{ii} = 0.94(5), 2.01(5), 2.951(4), 174(4); (i) x, –1+y, z; (ii) 1–x, 1–y, 1–z.

5.3.8 2-Azidoethyl-5-nitriminotetrazole (**53**)

The lowest density (1.665 g cm^{-3}) of nitriminotetrazoles **50**–**53** is calculated for 1-(2-azidoethyl)-5-nitriminotetrazole (**53**), which crystallizes in the monoclinic space group $P2_1/c$. The molecular structure is depicted in **Figure 5.23**. Interestingly, next to the classical H-bonds, dimer pairs are formed by an uncommon linear azide-nitro interaction (shorter than the sum of *vdW* radii), which is shown in **Figure 5.24**. A possible explanation of this can be done using the concept of "σ-hole bonding". The noncovalent interaction based on positive holes in the electrostatic surface is best explained by Murray and Politzer *et al.*.[269] In our case the σ-hole is likely to be located on the oxygen atom along the extension of the N–O bond of the nitro group which can interact linearly with a negative region of the outer azide nitrogen atom. Due to this electrostatic interaction the N–O bond is elongated. The best lewis structure is also shown in **Figure 5.24**.

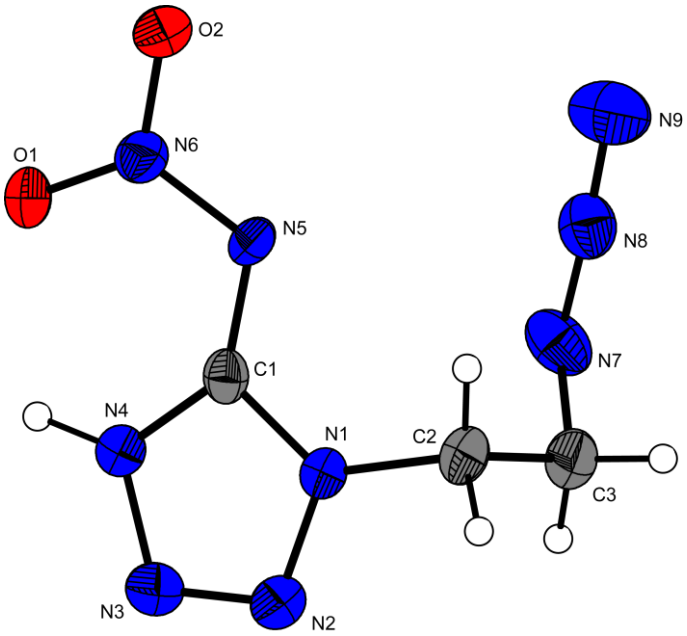

Figure 5.23 Molecular structure of **53**. Thermal ellipsoids represent the 50 % probability level.

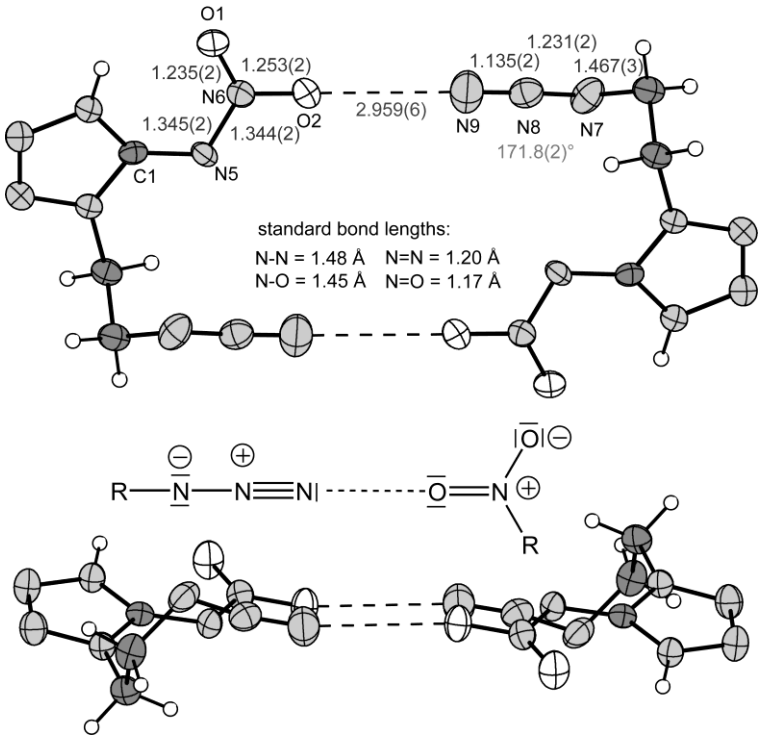

Figure 5.24 Azide-nitro σ-hole bonding interaction in **53** with the corresponding Lewis structure.

In contrast to the previously discussed packings, wave like pattern can be found in the structure of **53** (**Figure 5.25**).

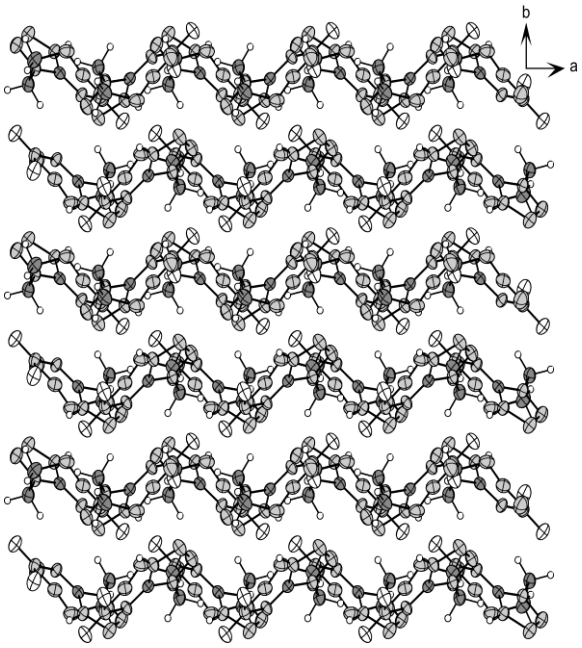

Figure 5.25 View on the wave like pattern in the structure of **53** along the *c* axis.

Next to one strong intermolecular H-bond and the typical intramolecular H-bond (**S1,1(6)**) one strong non-classical H-bond is found in the structure of **53**, which can be seen in **Figure 5.26**.

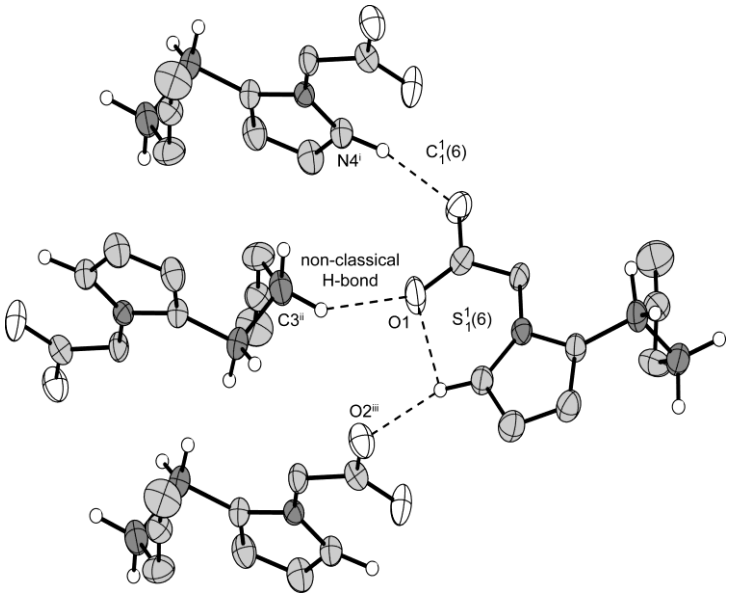

Figure 5.26 H-bonding in the structure of **53**. Two graph sets are marked. Selected hydrogen bonds (Å, Å, Å,°): N4^{i}–H4^{i}···O2 = 0.96(2), 1.95(2), 2.873(2), 159(2); N4–H4···O1 = 0.96(2), 2.19(2), 2.590(5), 104(2); C3^{ii}–H3b···O1 = 0.97(2), 2.41(2), 3.220(3), 142(1); (i) –0.5–x, 0.5+y, 1.5–z; (ii) –0.5+x, 0.5–y, 0.5+z; (iii) –0.5–x, –0.5+y, 1.5–z.

5.3.9 Potassium 1-(2-azidoethyl)-5-nitriminotetrazolate (**54**)

54 crystallizes triclinic with 2 x 3 (!) independent molecular moieties in the unit cell. For better clearness only one is shown in **Figure 5.27**.

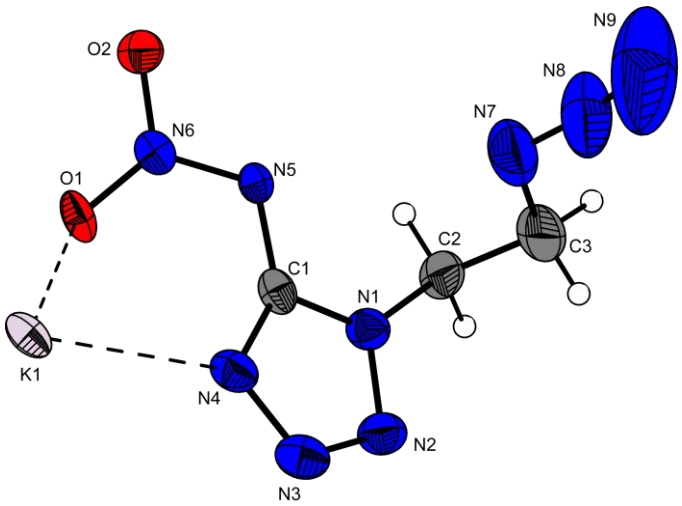

Figure 5.27 One molecular moiety of the crystal structure of **54**. Thermal ellipsoids represent the 50 % probability level. The disorder of the outer azide nitrogen atoms can be seen at the large ellipsoids.

The following **Figure 5.28** shows a view on the isolated chains formed in the structure of potassium 1-(2-azidoethyl)-5-nitriminotetrazolate.

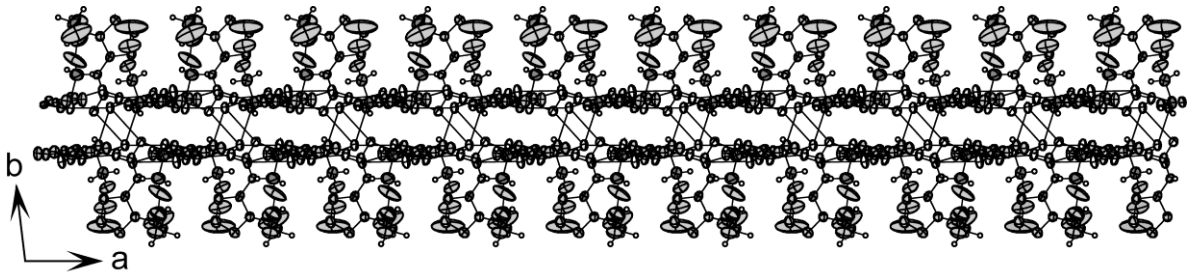

Figure 5.28 View on the chains in the structure of **54** along the *c* axis.

5.3.10 Sodium (**55**) and ammonium (**56**) 1-(2-chloroethyl)-5-nitriminotetrazolate

55 and **56** crystallize in the monoclinic space group $P2_1/c$ with four molecules in the unit cell and densities of 1.862 and 1.637 g cm^{-3}, respectively. The densities and also the bond lengths and angles of the molecular structures (shown in **Figure 5.29** and **Figure 5.30**) are in agreement with those of ammonium 5-nitriminotetrazolate [270] and other

1-substituted 5-nitriminotetrazolates, e.g. ammonium 1-methyl-5-nitriminotetrazolate and sodium 1-methyl-5-nitriminotetrazolate (Chapter 7). The sodium atoms in **55** are coordinated by six atoms (O1, O2, N4 and N3) building no regular coordination polyeder. Since the oxygen atom O1 coordinates to two different sodium atoms dimers are formed (**Figure 5.31**). In the packing of **56** an extensive hydrogen bond network is formed. The hydrogen atoms of one ammonia cations participate in several strong H-bonds to different atoms (O1, O2, N3, N4 and N5) of five different nitriminotetrazolate anions.

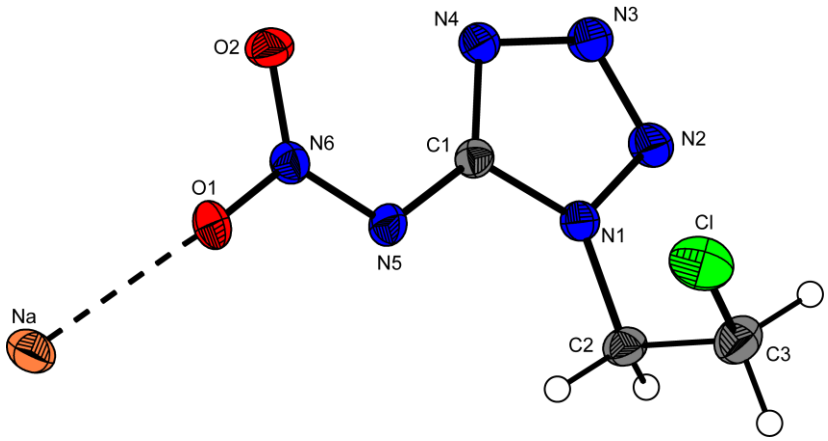

Figure 5.29 Molecular structure of **55**. Thermal ellipsoids represent the 50 % probability level.

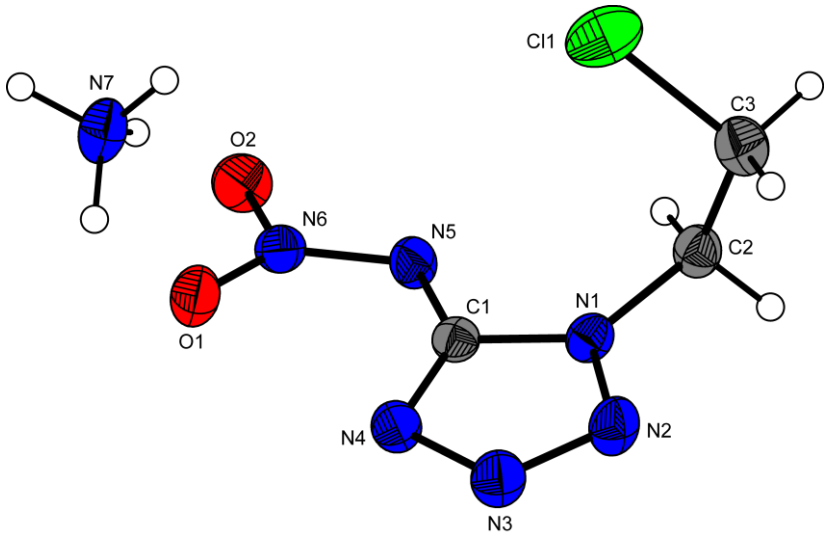

Figure 5.30 Molecular structure of **56**. Thermal ellipsoids represent the 50 % probability level.

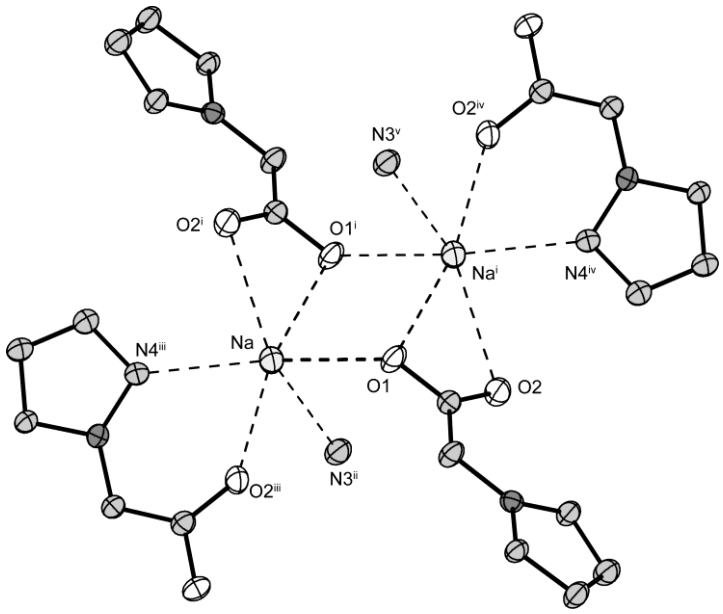

Figure 5.31 View on the dimers in the structure of **55**. Thermal ellipsoids represent the 50 % probability level. Symmetry codes: (i) –x, –y, –z; (ii) –x, 0.5+y, 0.5–z; (iii) –x, –y, 1–z; (iv) x, –0.5–y, –0.5+z; (v) x, y, –1+z.

A view on the packing of ammonium 1-(2-chloroethyl)-5-nitriminotetrazolate (**56**) is given in **Figure 5.32**.

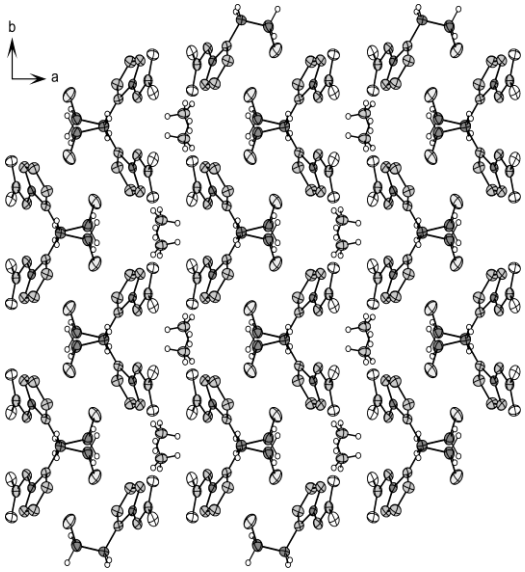

Figure 5.32 View on the packing of **56** along the *c* axis.

All hydrogen atoms of the ammonia cations participate in strong hydrogen bonds, which are shown in **Figure 5.33**.

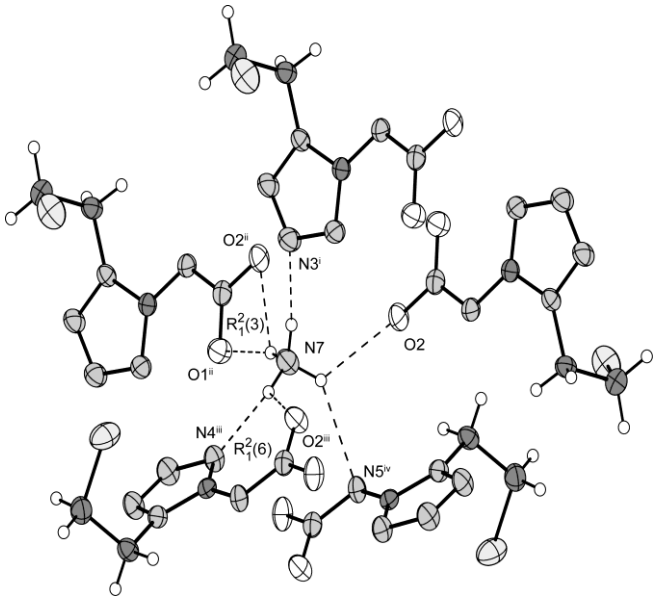

Figure 5.33 H-bonding of one ammonium cation in the structure of **55**. Two graph sets are marked. Selected hydrogen bonds (Å, Å, Å,°): N7–H7A···O2 = 0.92(3), 2.42(3), 2.928(3), 115(2); N7–H7C···N3^{i} = 0.95(4), 2.18(4), 3.125(3), 173(3); N7–H7B···O1^{ii} = 0.92(3), 2.00(3), 2.894(3), 165(2); N7–H7B···O2^{ii} = 0.92(3), 2.46(3), 3.187(3), 136(2); N7–H7D···N4^{iii} = 0.89(3), 2.01(3), 2.889(3), 167(2); N7–H7D···O1^{iii} = 0.89(3), 2.33(3), 2.850(3), 117(2); N7–H7A···N5 = 0.92(3), 2.46(3), 3.184(3), 136(2); (i) –1–x, 1–y, –z; (ii) –1–x, 1–y, –1–z; (iii) –1–x, –0.5+y, –0.5–z; (iv) x, 0.5–y, –0.5+z.

5.3.11 1-(2-Hydroxyethyl)-5-aminotetrazolium nitrate (**57**)

Protonation of **46** takes place at the expected nitrogen atom N4, due to the similarity to protonation of 1-methyl-5-aminotetrazole, which has been investigated in detail.[68] 1-(2-Hydroxyethyl)-5-aminotetrazolium nitrate (**57**) crystallizes in the monoclinic space group $P2_1/c$ with four molecules in the unit cell. The molecular unit is shown in **Figure 5.34**. The density of 1.602 g cm^{-3} is lower than that of 1-methyl-5-aminotetrazolium nitrate (1.653 g cm^{-3}).[68]

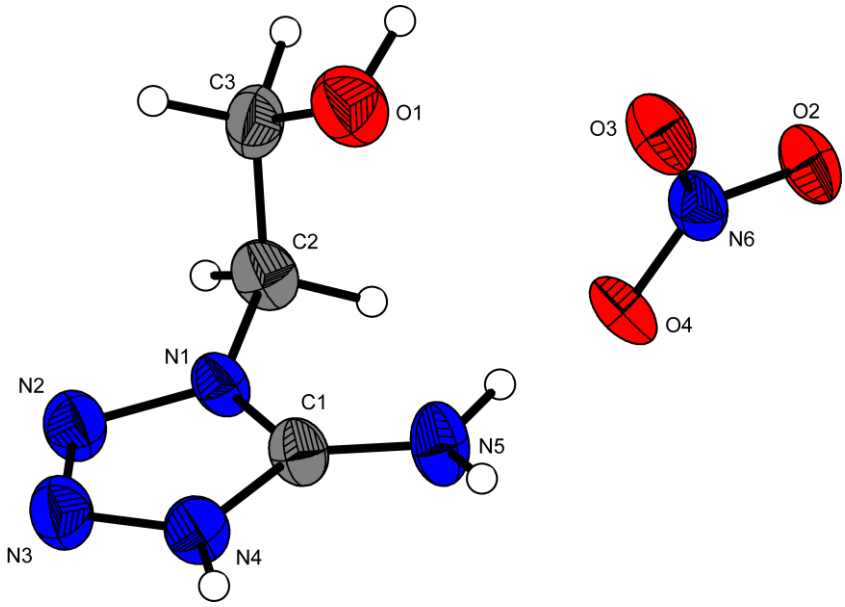

Figure 5.34 Molecular structure of **57**. Thermal ellipsoids represent the 50 % probability level.

The hydrogen bonds appearing in the structure of **57** are shown in **Figure 5.35**. Several H-bond graph sets can be detected.

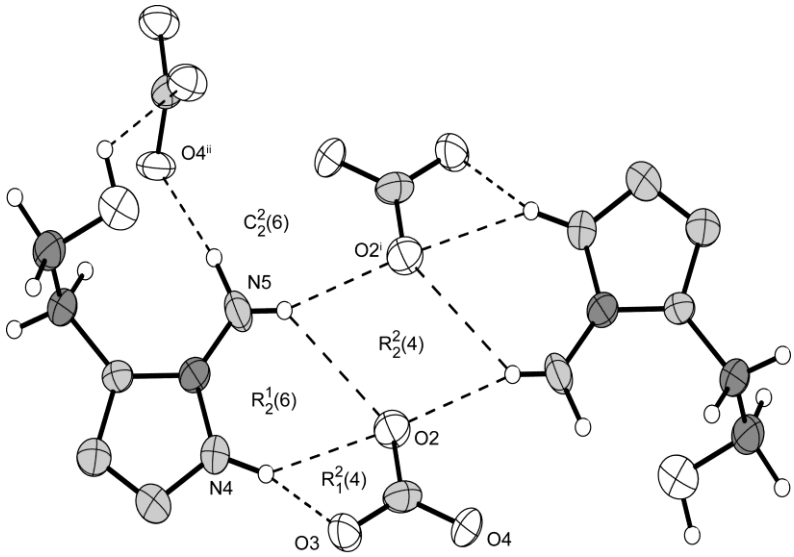

Figure 5.35 H-bonding in the structure of **57**. Four graph sets are marked. Selected hydrogen bonds (Å, Å, Å,°): N4–H4···O3 = 0.95(5), 1.74(5), 2.660(5), 162(4), N4–H4···O2 = 0.95(5), 2.42(5), 3.176(6), 137(3), N5–H5B···O4^{ii} = 0.97(6), 2.14(6), 3.076(6), 163(5); N5–H5A··· O2^{i} = 0.81(4), 2.32(5), 3.071(6), 154(4); (i) x, –1+y, z; (ii) 1–x, –0.5+y, 0.5–z.

The packing of **57** is illustrated in **Figure 5.36**. Again layers containing the amine and nitrate moieties connected by hydrogen bonds can be distinguished.

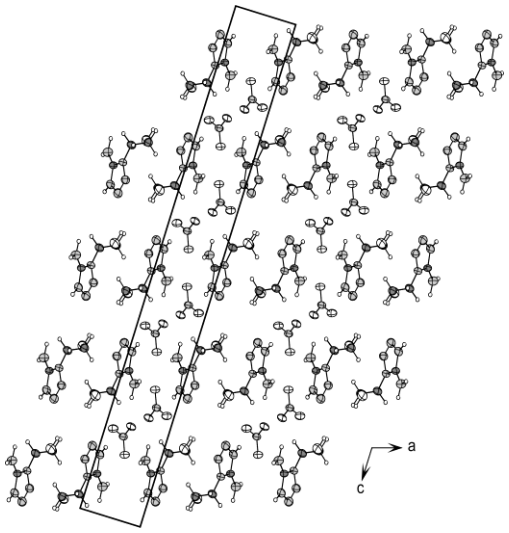

Figure 5.36 View on the packing of **57** along the *b* axis.

5.3.12 1-(2-Azidoethyl)-5-aminotetrazolium nitrate (**58**) and 1-(2-Azidoethyl)-5-aminotetrazolium perchlorate monohydrate (**59**)

The 1-(2-azidoethyl)-5-aminotetrazolium salts **58** and **59** also crystallize in the monoclinic space group $P2_1/c$ with four molecules in the unit cell. In both molecular structures, which are shown in **Figure 5.37**and **Figure 5.40**, protonation takes place at the nitrogen atom N4.

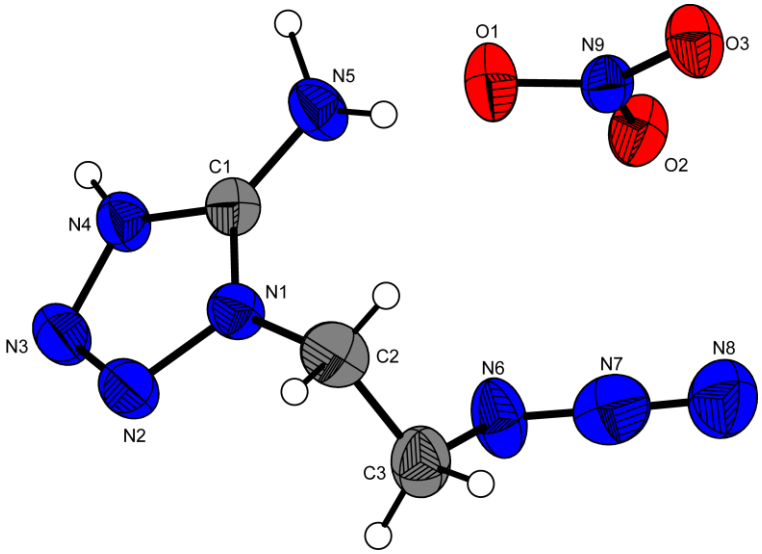

Figure 5.37 Molecular structure of **58**. Thermal ellipsoids represent the 50 % probability level.

The densities of 1.663 (**58**) and 1.655 g cm^{-3} (**59**), respectively, are in the range of 1-methyl-5-aminotetrazolium nitrate and perchlorate,[68] but significantly lower than that of 1,5-diaminotetrazolium nitrate (1.72 g cm^{-3}) and perchlorate (1.90 g cm^{-3}).[202] The packing of **58** is analogous to that observed for **57**. A view along the *b* axis is shown in **Figure 5.38**.

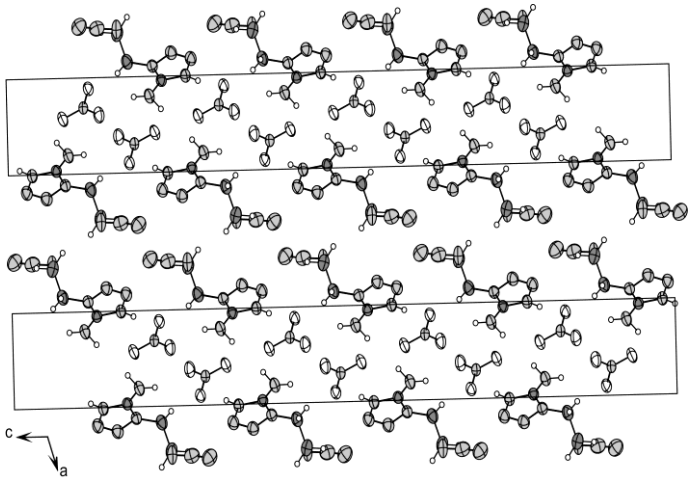

Figure 5.38 View on the packing of **58** along the *b* axis.

Also hydrogen bonding (**Figure 5.39**) of **58** is in agreement with the structure of **57**.

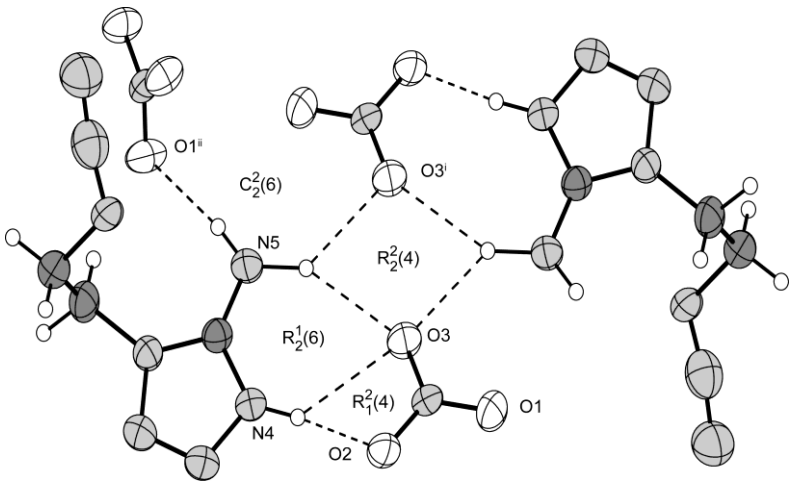

Figure 5.39 H-bonding in the structure of **58**. Four graph sets are marked. Selected hydrogen bonds (Å, Å, Å,°): N4–H4···O2 = 0.91(4), 1.75(4), 2.65(1), 172(3), N4–H4···O3 0.91(4), 2.47(4), 3.13(3), 129(3), N5–H5B···O3^{i} = 1.13(3), 2.15(4), 3.061(6), 136(3); N5–H5A··· O1^{ii} = 0.86(4), 2.62(5), 3.06(3), 155(4); (i) 1–x, –0.5+y, 0.5–z; (ii) x, –0.5–y, –0.5+z.

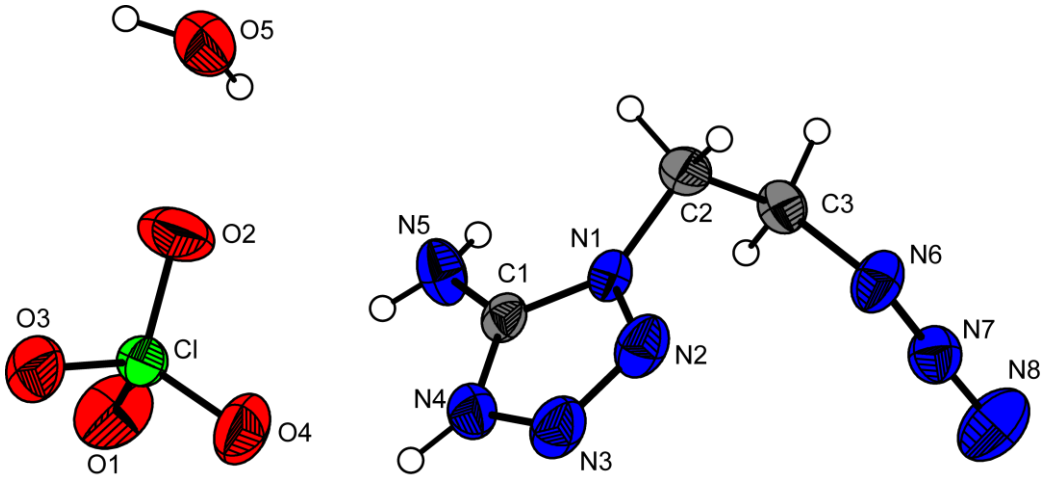

Figure 5.40 Molecular structure of **59**. Thermal ellipsoids represent the 50 % probability level.

Also compound **59** crystallizes in a similar way compared to **57** and **58**. A view along the *c* axis can be found in **Figure 5.41**.

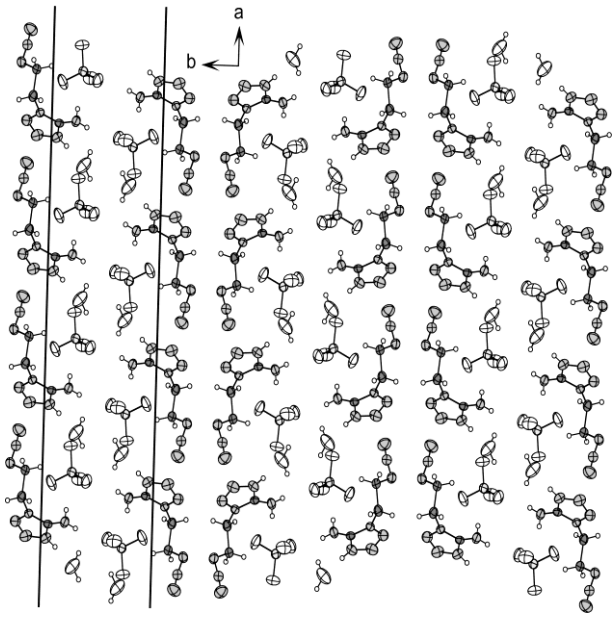

Figure 5.41 View on the packing of **59** along the *c* axis.

A view on selected hydrogen bonds created in the structure of **59** are shown in **Figure 5.42**. Further H-bonds are present between the water hydrogen atoms and neighboring perchlorate anions.

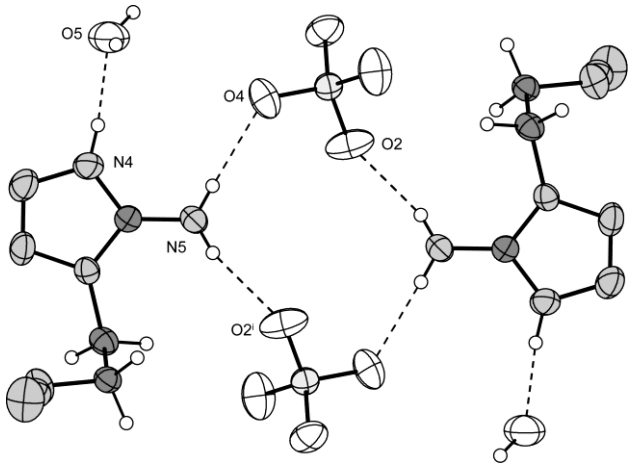

Figure 5.42 H-bonding in the structure of **59**. Selected hydrogen bonds (Å, Å, Å,°): N5–H5B···O4 = 0.79(3), 2.22(3), 3.001(3), 169(3); N4–H4···O5 = 0.85(3), 1.79(3), 2.635(3), 174(3); N5–H5A···O2^{i} = 0.80(2), 2.15(3), 2.925(4), 164(2); (i) x, y, –1+z.

5.3.13 $[Cu(AtNO_2EtOH)_2(H_2O)_2]$ (**60**)

trans[Diaquabis(1-(2-hydroxyethyl)-5-nitriminotetrazolato-*N4,O1*)copper(II)] (**60**) crystallizes in the triclinic space group *P*–1 with one molecule in the unit cell. The copper atoms are located on the centre of inversion, whereby the 5-nitriminotetrazolate acts as bidentate ligand with a bite angle of 74.84(6)°. The coordination distance of N4–Cu is 1.997(4) Å, which is a typical Cu–N coordination length, also found in copper nitriminotetrazolates (Chapter 9), but also found in copper nitrogen complexes like $[Cu(NH_3)_4(NO_3)_2]$.[333] The distances observed between the copper and oxygen atoms are Cu–O1 = 2.405(2) Å and Cu–O3 = 1.983(2) Å resulting in a Jahn Teller distorted octahedral coordination sphere (**Figure 5.43**). This coordination geometry of the elongated octahedron is typical for this kind of chromophores distorted by the Jahn Teller effect and is similar to those found for other complexes of both 2-substituted and 1-substituted tetrazoles.[335]

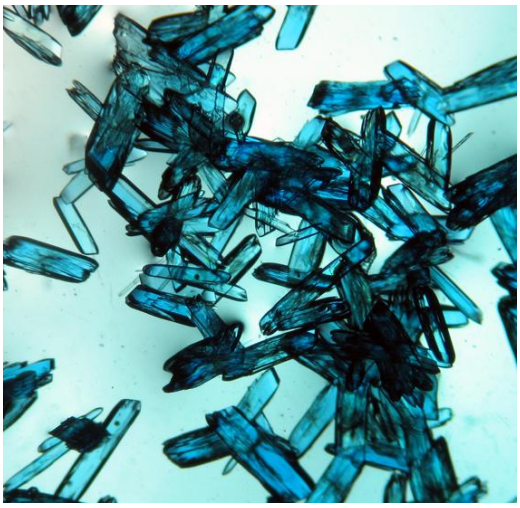

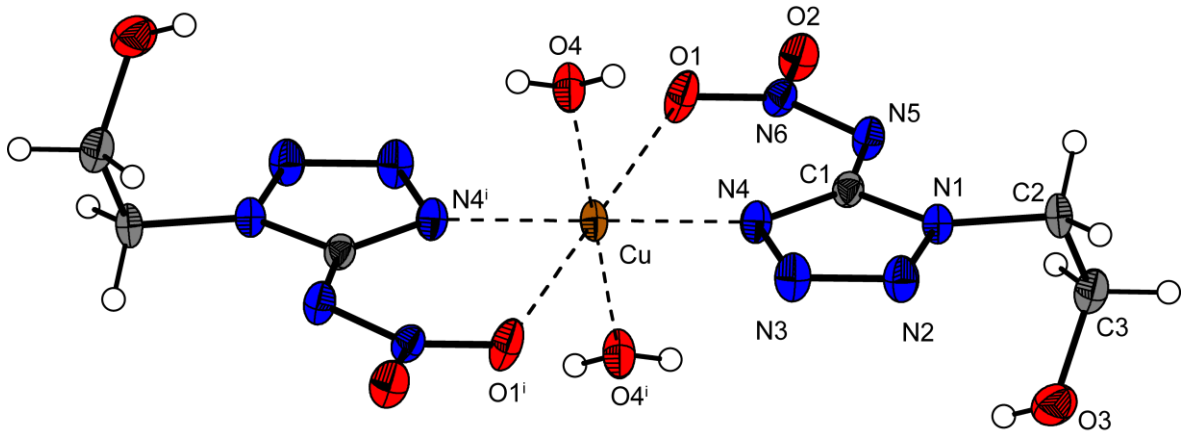

Figure 5.43 Molecular structure of **60**. Thermal ellipsoids represent the 50 % probability level. Selected coordination geometries distances (Å): Cu–N4 = 1.977(2), Cu–O1 = 2.405(2), Cu–O4 = 1.983(2); angles (°): N4–Cu–O1 = 74.84(6), N4–Cu–O4 = 89.00(7), O4–Cu–O1 = 91.99(6).

5.3.14 $[Cu(AtNO_2EtCl)_2(H_2O)_2](H_2O)_2$ (**61**)

The molecular structure of **61** is shown in **Figure 5.44**. Although no comparable neutral complex can be found in literature, **61** is a further example of 1-(2-chloroethyl) substituted tetrazole complexes. In 2001, 2002 and 2003 Stassen *et al.* reported on the synthesis and X-ray structure of bis(1-(2-chloroethyl)-tetrazole)bis(nitrato)-copper(II) nitrate [271] chloride [272] and perchlorate,[273] while also several 1-(2-chloroethyl)-tetrazole iron complexes are described in literature.[274] The copper cations are coordinated by the atoms N4 and O1 with a bite angle of 77.29(5)°. Again a Jahn Teller distorted octahedral coordination sphere is observed. The axial positions are occupied by the oxygen atoms O1 with a distance of 2.367(1) Å.

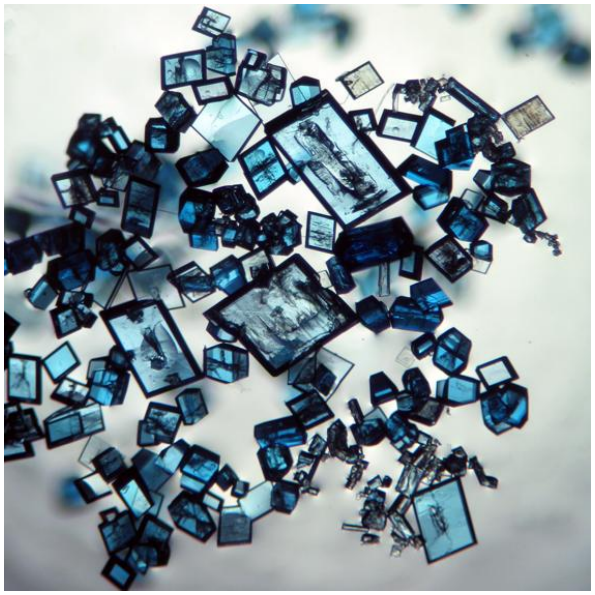

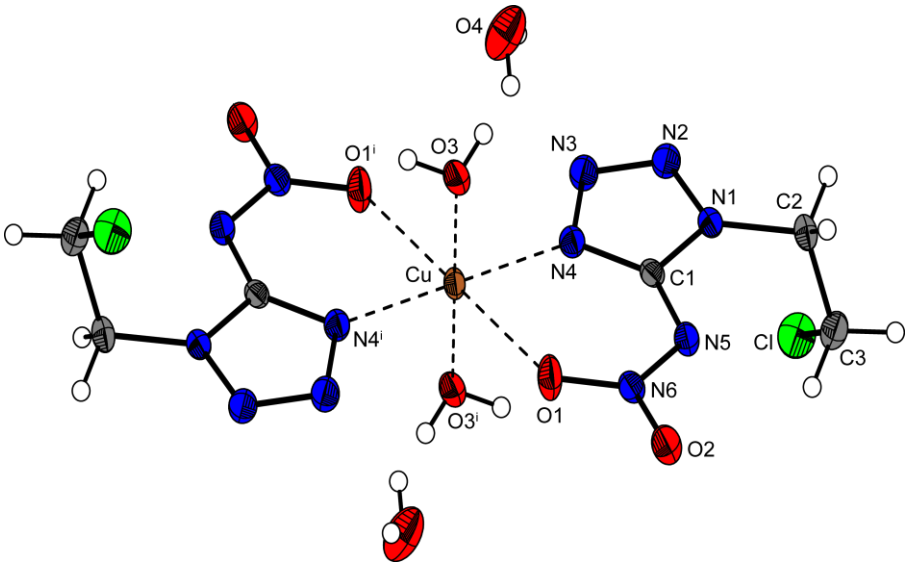

Figure 5.44 Molecular structure of **61**. Thermal ellipsoids represent the 50 % probability level. Selected coordination geometries distances (Å): Cu–N4 = 1.982(1), Cu–O1 = 2.367(1), Cu–O3 = 1.9849(14); angles (°): N4–Cu–O1 = 77.30(5), N4–Cu–O3 = 91.24(6), O4–Cu–O1 = 86.26(6).

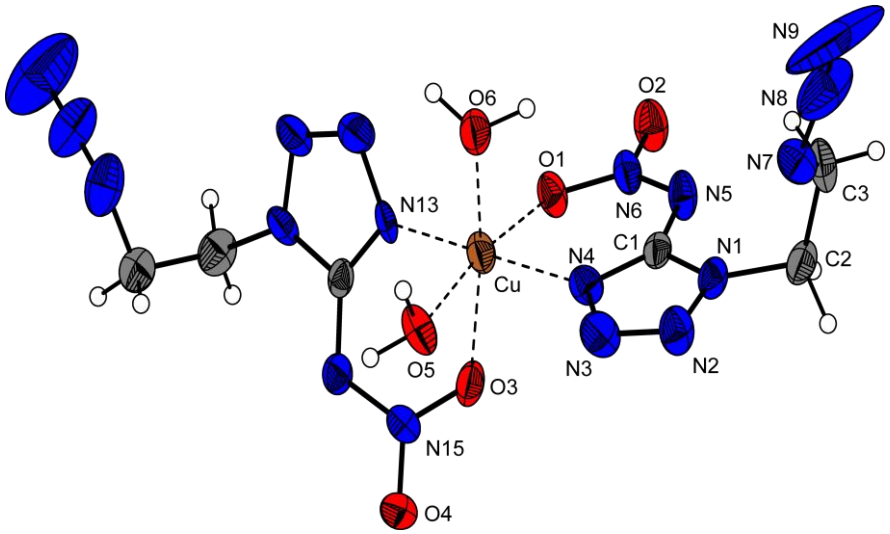

Figure 5.45 Molecular structure of **62**. Thermal ellipsoids represent the 50 % probability level. The outer azide nitrogen atoms are strongly disordered. Selected coordination geometries distances (Å): Cu–N4 = 1.950(5), Cu–N13 = 1.961(5), Cu–O5 = 2.013(5), Cu–O1 = 2.066(4), Cu–O6 = 2.181(5), Cu–O3 = 2.343(5); angles (°): N4–Cu–N13 = 169.2(2), N4–Cu–O5 = 92.6(2), N13–Cu–O5 = 95.9(2), N4–Cu–O1 = 83.4(2), N13–Cu–O1 = 87.2(2), O5–Cu–O1 = 170.5(2), N4–Cu–O6 = 88.5(2), N13–Cu–O6 = 98.3(2), O5–Cu–O6 = 89.2(2), O1–Cu–O6 = 99.2(2), N4–Cu–O3 = 97.2(2), N13–Cu–O3 = 76.7(2), O5–Cu–O3 = 86.5(2), O1–Cu–O3 = 85.5(2), O6–Cu–O3 = 173.1(2).

5.3.15 $[Cu(AtNO_2EtN_3)_2(H_2O)_2]$ (**62**)

Interestingly, there is one copper complex of 1-azidoethyl-5*H*-tetrazole known in the literature.[268] Ivashkevic *et al.* describe poly-bis[1-(2-azidoethyl)-tetrazole-*N4*]copper(II)-di-chlorido as an example of a layered polymeric crystal structure with the formula $CuCl_2L_2$. [Diaquabis(1-(2-azidoethyl)-5-nitriminotetrazolato-*N4,O1*)copper(II)] (**62**), shown in **Figure 5.45**, crystallizes in the monoclinic space group $P2_1/c$ with four molecules in the unit cell forming the lowest density (1.764 g cm^{-3}) of the investigated copper complexes. In contrast to the structures of **60** and **61**, the copper atoms are not located at the centre of inversion.

5.4 Spectroscopy

NMR spectroscopy, particularly ^{13}C and ^{15}N NMR, are valuable methods to identify 5-aminotetrazoles as well as 5-nitriminotetrazoles. By comparing the tetrazole carbon atom shifts, it can be seen that the 5-aminotetrazole derivatives are all found in the same range (156.5 ppm (**46**), 155.9 ppm (**48**), and 156.3 ppm (**49**)). The same trend is observed for the 5-nitriminotetrazole derivatives (150.9 ppm (**50**, **51**), 151.1 ppm (**53**)) or salts (157.2 ppm (**55**) and 158.8 ppm (**56**)). The signals of the 5-aminotetrazole derivatives correspond to the one of unsubstituted 5-aminotetrazole (156.6 ppm).[275] The shift of the tetrazolates (**54–56**) signals to lower fields can be explained with orbital effects.[276] The signals of the CH_2 groups are all in the same range, whereas the ones of **46** and **50** are shifted to higher ppm values due to the hydroxy moiety. ^{15}N spectra measured in d_6-DMSO of **46, 48–51** as well as **53** can be seen in **Figure 5.46**. The assignments were done by evaluation of the ^2J and ^3J $^1H–^{15}N$ coupling constants and by comparison with the values given in literature.[202]

Also ***vibrational spectroscopy*** (IR and Raman) can be used for specific characterization of substituted tetrazole derivatives. The characteristic vibrations of the tetrazole ring framework at 1000–1030, 1045–1085 and 1095–1120 cm^{-1} [277] and the stretching motion of the –N–N=N fragment at 1265–1320 cm^{-1} [36] appear in every IR-spectra of all investigated compounds. The signal caused by the stretching motion of the cyclic (C=N)-bond at 1580–1600 cm^{-1} is in the same range like the exocyclic one of the nitriminotetrazoles (**51**–**56**).[278] The N–H and C–H valence vibrations generate broad signals in the same range at 2800–3200 cm^{-1}. In the case of the 5-nitriminotetrazoles the

symmetric valence vibration of the NNO_2 fragment appears at 1330 cm^{-1}. The OH valence motion is found at 3330–3380 cm^{-1} in the spectra of **46**, **50** and **57**. The ν_{as} of the azide group in **49**, **53**, **54**, **58**, **59** and **62** appears between 2110 and 2150 cm^{-1}.

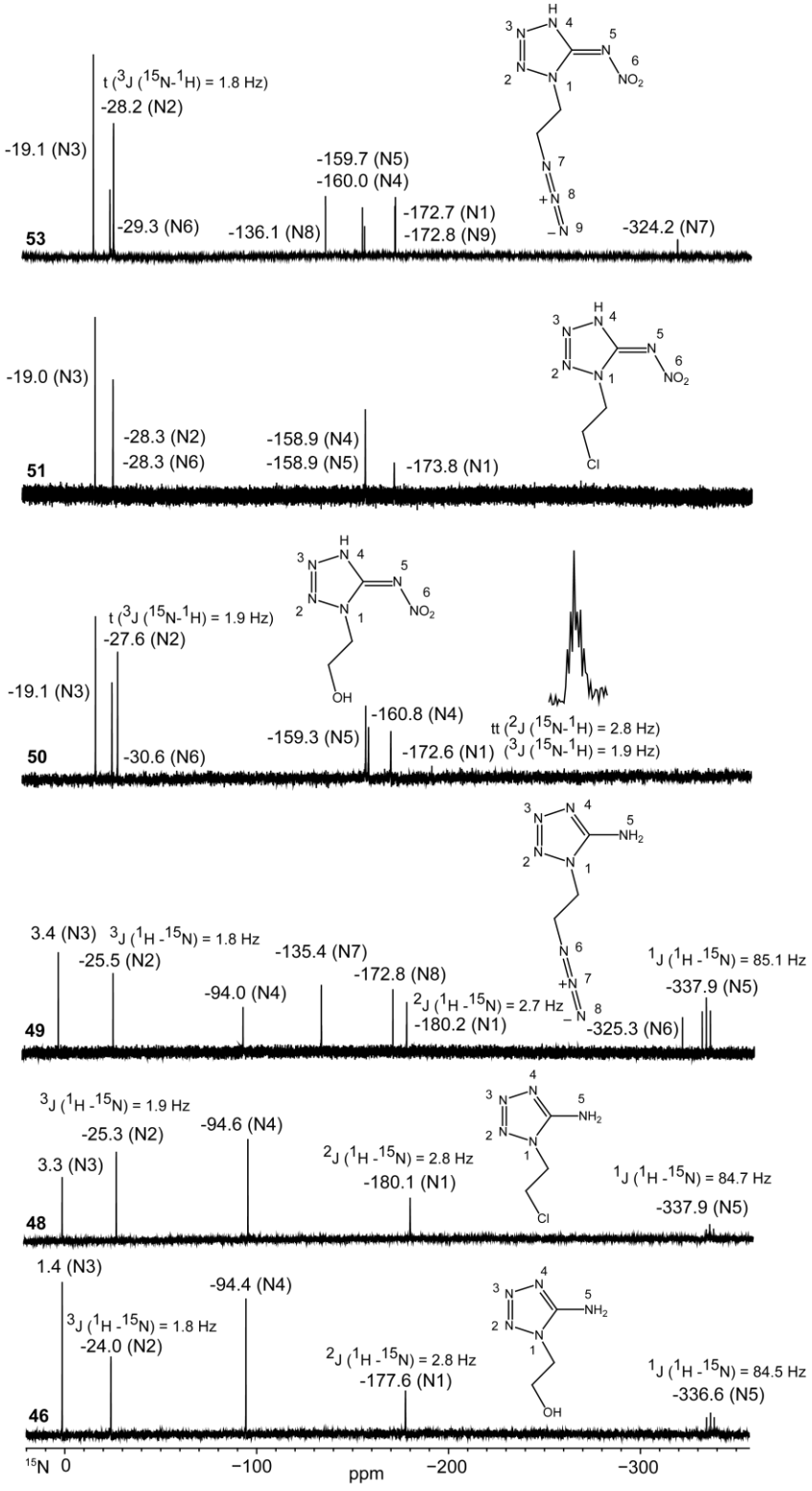

Figure 5.46 ^{15}N NMR spectra of **46, 48–51** and **53** measured in d_6-DMSO. Chemical shifts are given in ppm with respect to $MeNO_2$ as external standard.

5.5 Physico-Chemical Properties

Since **46**–**62** are partly high energetic compounds with exceedingly nitrogen contents, the energetic behavior was investigated and a detailed description is given in the following.

5.5.1 Thermal Behavior

The thermal behavior of **46** and **48**–**62** (~1.5 mg) was investigated on a Linseis PT10 DSC as well as a Perkin Elmer Pyris 6 DSC at heating rates of 5 ° min^{-1}. The thermograms of the 50 –300 °C temperature range are shown in **Figure 5.48**. The 5-aminotetrazoles **46**, **48** and **49** show melting points between 130 and 158 °C, followed by a broad decomposition range of the melt. Compounds **50**–**53** have decomposition temperatures between 112 and 142 °C. Except for **51** no prior melting could be observed. Salts **54**, **55** and **56** show significantly higher decomposition temperatures than neutral **51** and **53**, which is usually observed comparing tetrazoles with their corresponding tetrazolates. In contrast to that, protonation of tetrazoles mostly decreases the decomposition temperature, which is in agreement with the thermo-plots of **57**–**59**. In addition **57**–**59** show melting points at 85 (**59**), 95 (**58**) and 135 °C (**57**).

The copper complexes **60**–**62** show the highest as well as the sharpest decomposition temperatures of 217 (**62**), 233 (**61**) and 245 °C (**60**). In none of the thermo-plots in **Figure 5.47** melting points or loss of crystal water could be observed.

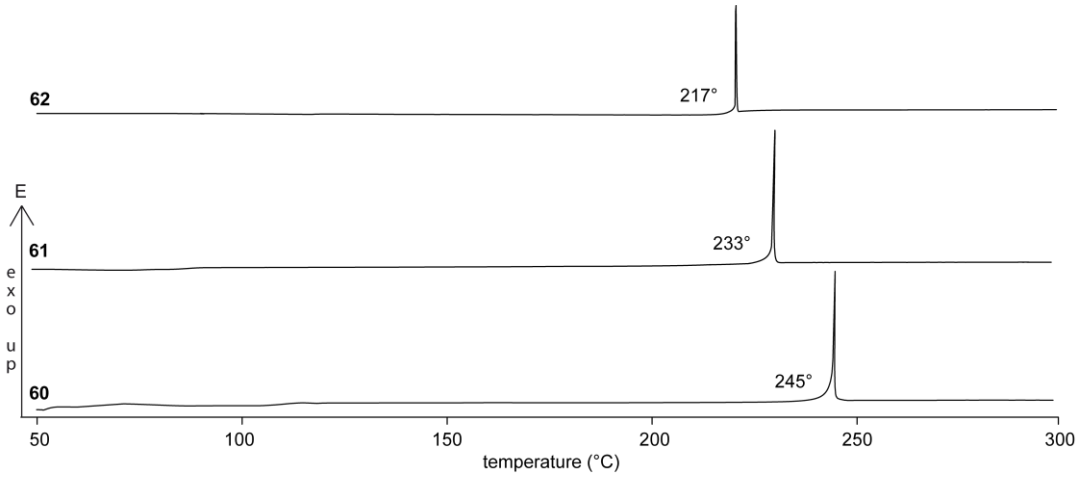

Figure 5.47 Thermograms (exo-up) of **60**–**62** in the 50–300 °C temperature range.

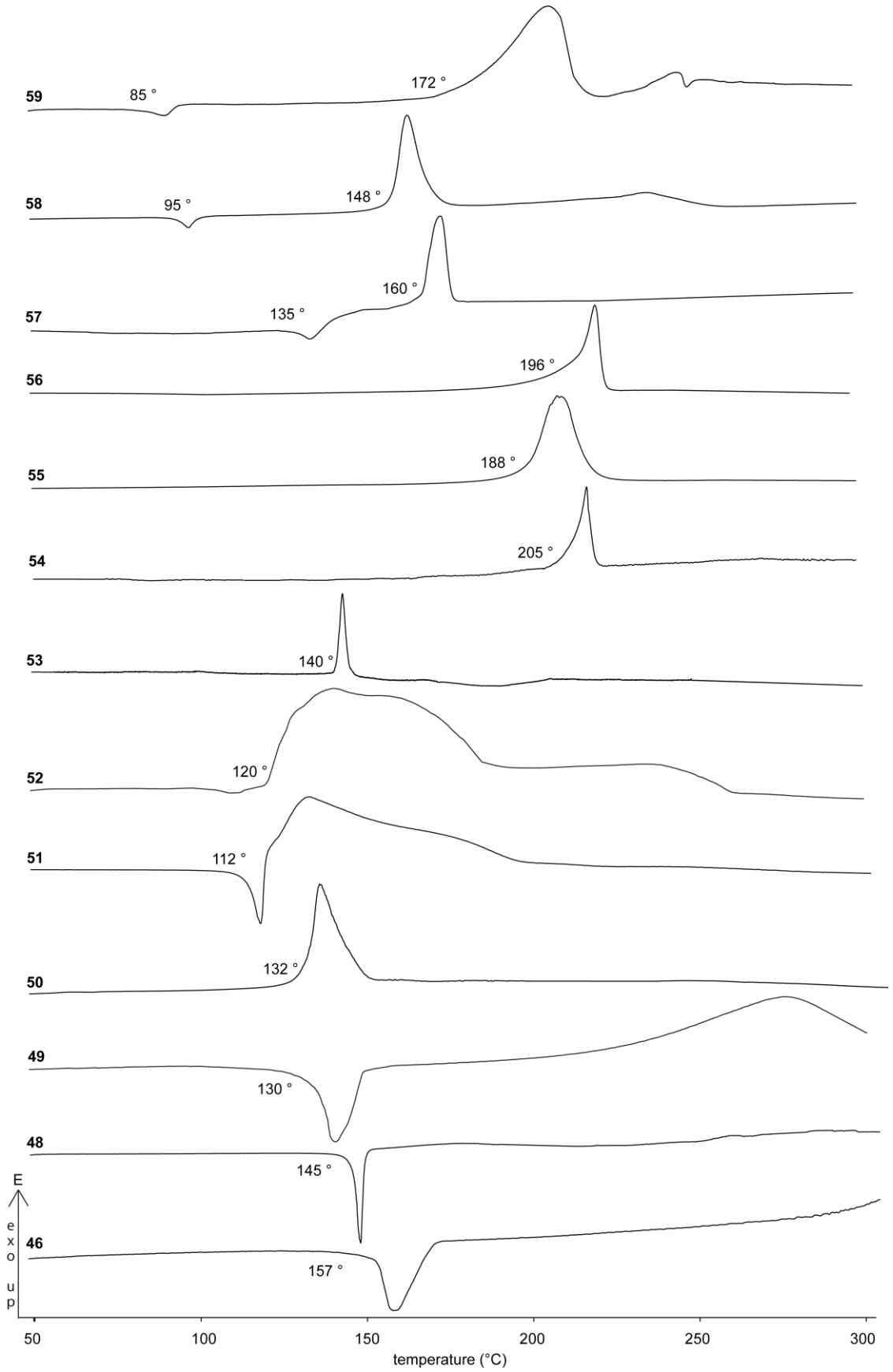

Figure 5.48 Thermo-plots (exo-up) of **46**, **48**–**59** in the 50–300 °C temperature range. Temperatures are given as T_{onset}.

5.5.2 Heats of Formation

The heats of formation of **46, 48–52** as well as **57** and **58** have been calculated using experimentally obtained heats of combustion. In bomb calorimetric measurements nitrogen-rich highly energetic compounds, such as **49** and **53** carrying the covalent azide group, tend to burn incompletely due to the tendency to explode. Often, wrong heats of combustion ($\Delta_c H$) and finally wrong heats of formation ($\Delta_f H°$) are obtained. Therefore, the heats of formation of **49** and **53** were computed on the CBS level and using the atomization method. The enthalpy of formation, $\Delta_f H°$, for each of the compounds **46, 48–52** as well as **57** and **58** was calculated at 298.15 K using the Hess thermochemical cycle and the following combustion reactions.

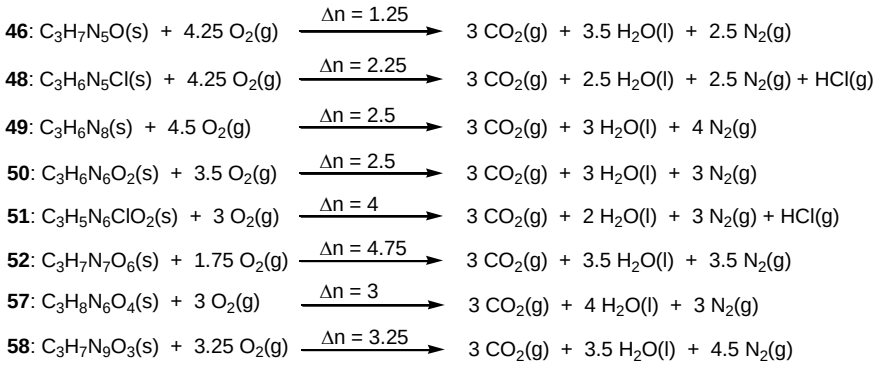

Scheme 5.3 Combustion equations of **46, 48–52** as well as **57** and **58**.

The heats of formation of the combustion products H_2O (l) (–286 kJ mol^{-1}), CO_2 (g) (–394 kJ mol^{-1}) and HCl (g) (–92 kJ mol^{-1}) were adopted from the literature.[122] Except for **46**, all compounds were calculated to have positive enthalpies of formation. The detailed values are summarized in **Table 5.2** and **Table 5.3**. Within the covalent derivatives, compound **53** was calculated to have the largest positive heat of formation (+629 kJ mol^{-1}). In the course of all salts, **58** shows the highest value (+457 kJ mol^{-1}).

5.5.3 Detonation Parameters

The calculation of the detonation parameters was performed with the program package EXPLO5 (version 5.02). Unfortunately, only compounds containing C, H, N, O, Al, or F can be calculated. Therefore, it was not possible to calculate compounds **48**, **51**, **54**, **55**, **56** and **59**, which contain chlorine. The detonation parameters, calculated with the EXPLO5

program using the experimentally determined densities (X-ray), are summarized in **Table 5.2** and **Table 5.3**.

Among the investigated compounds **52** shows the best detonation parameters. The calculated detonation velocity of 8943 m s^{-1} even exceeds the values of RDX. Regarding the detonation pressure (**52**: 341 kbar, RDX: 346 kbar) similar values are calculated. The detonation velocities of compounds **53**, **58** and **58** reveal values significantly higher than 8000 m s^{-1}. Although showing detonation pressures of $p_{C\text{-}J}$ = 280 (**50**), 275 (**53**) and 271 kbar (**58**) and explosion temperatures of more than 3500 K, the performance data are lower than those of RDX. The influence of the density can clearly be seen on the values of **49**, which, although it is formed very endothermically, shows low calculated detonation parameters. The other compounds stay below $V_{Det.}$ = 8050 m s^{-1}. However, they also exceed the detonation parameter of TNT ($V_{Det.}$ = ~7000 m s^{-1}).

Table 5.2 Physico-chemical properties of **46**, **48–53**.

	46	**48**	**49**	**50**	**51**	**52**	**53**
Formula	$C_3H_7N_5O$	$C_3H_6ClN_5$	$C_3H_6N_8$	$C_3H_6N_6O_3$	$C_3H_5ClN_6O_2$	$C_3H_7N_7O_6$	$C_3H_5N_9O_2$
FW / g mol^{-1}	129.14	147.58	154.16	174.14	192.58	237.16	199.16
Impact sens. [a] / J	> 100	> 100	10	6	28	25	2
Friction sens. [b] / N	> 360	> 360	360	55	> 360	360	80
N [c] / %	54.24	47.46	72.70	48.27	43.64	44.75	63.31
Ω [d] / %	–105.32	–64.88	–93.42	–55.13	–49.85	–23.61	–52.2
$T_{dec.}$ [e] / °C	160(mp)	150(mp)	130(mp)	138	130	128	140
Density [f] / g cm^{-3}	1.50	1.55	1.50	1.73	1.72	1.781	1.67
$\Delta_c H$ [g] / kJ mol^{-1}	3852	3460	3652	3080	2655	2570	---
$\Delta_f H_m°$ [h] / kJ mol^{-1}	–105	143	413/550*	201	278	165	629*
$\Delta_f U°$ [i] / kJ kg^{-1}	–689	1976	2824/3679*	1261	1534	800	3256*
calculated values by EXPLO5:							
$-\Delta_E U_m°$ [j] / kJ kg^{-1}	1842	---	3455/4321*	5353	---	6160	–5719*
T_E [k] / K	1643	---	2581/3010*	3710	---	4352	4184*
$p_{C\text{-}J}$ [l] / kbar	133	---	191/218*	280	---	341	275*
$V_{Det.}$ [m] / m s^{-1}	6645	---	7619/8043*	8254	---	8943	8320*

[a] BAM drophammer; [b] BAM methods; [c] Nitrogen content; [d] Oxygen balance; [e] Decomposition temperature from DSC (β = 5 °C); [f] determined by X-ray crystallography; [g] Enthalpy of combustion [h] Molar enthalpy of formation; [i] Energy of formation; [j] Total energy of detonation, EXPLO5 V5.02; [k] Explosion temperature; [l] Detonation pressure; [m] Detonation velocity; * calculated $\Delta_f H_m°$.

Table 5.3 Physico-chemical properties of **54–59** in comparison with RDX.

	54	**55**	**56**	**57**	**58**	**59**	**RDX**
Formula	$C_3H_4KN_9O_2$	$C_3H_4ClN_6NaO_2$	$C_3H_8ClN_7O_2$	$C_3H_8N_6O_4$	$C_3H_7N_9O_3$	$C_3H_9ClN_8O_5$	$C_3H_6N_6O_6$
FW / g mol^{-1}	237.25	214.56	209.61	192.15	217.15	272.61	222.11
Impact sens. [a]/J	25	> 50	> 50	> 50	7	5	7
Friction sens.[b]/N	300	> 360	> 360	> 360	160	120	120
N [c] / %	53.14	39.17	46.78	43.74	58.05	41.10	37.8
Ω [d] / %	–53.95	–48.47	–57.24	–49.96	–47.89	–29.35	–21.6
$T_{dec.}$ [e] / °C	205	184	196	160	148	172	~213
Density [f] / g cm^{-3}	1.78	1.86	1.64	1.60	1.66	1.66	1.82
$\Delta_c H$ [g] / kJ mol^{-1}	---	---	---	2912	2910	---	---
$\Delta_f H_m°$ [h] / kJ mol^{-1}	---	---	---	11	457	---	2105
$\Delta_f U°$ [i] / kJ kg^{-1}	---	---	---	173	2674	---	66.5
calculated values by EXPLO5:							
$-\Delta_E U_m°$ [j]/ kJ kg^{-1}	---	---	---	5107	6010	---	6043
T_E [k] / K	---	---	---	3512	4176	---	4321
$p_{C\text{-}J}$ [l] / kbar	---	---	---	233	271	---	346
$V_{Det.}$ [m] / m s^{-1}	---	---	---	7784	8329	---	8750

[a] BAM drophammer; [b] BAM methods; [c] Nitrogen content; [d] Oxygen balance; [e] Decomposition temperature from DSC (β = 5 °C); [f] determined by X-ray crystallography; [g] Enthalpy of combustion [h] Molar enthalpy of formation; [i] Energy of formation; [j] Total energy of detonation, EXPLO5 V5.02; [k] Explosion temperature; [l] Detonation pressure; [m] Detonation velocity.

5.5.4 Sensitivities

For initial safety testing, the impact and friction sensitivity as well as the electrostatic sensitivity were determined and are summarized in **Table 5.2** and **Table 5.3**. The

sensitivity data strongly depend from the particle size, shape and texture. *Although we tried to use fine crystalline materials (1–100 µm) we cannot guarantee on exact values for these new energetic materials. Appropriate tests should be repeated before the compounds are synthesized in larger scales.* Compound **50** (IS: 6 J, FS: 55 N) and **53** (IS: 2 J, FS: 80 N) are the most sensitive compounds investigated in this work, while **46**, **47**, **55**, **56** and **67** are completely insensitive towards impact and friction. Using the "UN recommendations on the transport of dangerous goods" [82] **53** is classified as *very sensitive* regarding the impact sensitivity, while **50** is classified as *very sensitive* towards friction. Also **58** and **59** are classified as *sensitive* in both categories. As a matter of principle the nitrated 5-aminotetrazoles (**50**–**54**) or compounds carrying a covalent azide group (**49**, **53**, **54**, **58** and **59**) are higher in sensitivities. The inclusion of crystal water decreases the sensitivity, which can be seen on the values of **52** (IS: 25, FS: 360 N). We could not observe any differences in the sensitivities of polymorphs **49a** and **49b**. Complexes **50**–**62** were also tested regarding to their impact sensitivity. Only **62** (10 J) was found to be moderately sensitive towards impact.

5.6 Experimental Part

WARNING! Although most of the compounds described in this Chapter 5 are characterized by lower sensitivities and good thermal stabilities, they are nevertheless powerful energetic materials. Therefore, special precautions and safety equipment are needed, particularly, when handling 5-nitriminotetrazole as starting material.

*1-(2-Hydroxyethyl)-5-aminotetrazole (**46**):* A solution of 5-aminotetrazole (85.1 g, 1.0 mol) and NaOH (40.0 g, 1.0 mol) in 200 mL H_2O was refluxed at 120 °C for one hour. 2-Chloroethanol (74 mL, 1.1 mol) was added in drops and further procedure followed as described in the literature [27] (41.3 g, 32 % yield). **DSC** (T_{onset}, 5 °C min^{-1}): 160–161 °C; **IR** (KBr, cm^{-1}): $\tilde{\nu}$ = 3331 (s, br), 3153 (s, br), 2965 (m), 2946 (s), 2881 (m), 2749 (m), 2684 (m), 2577 (w), 2478 (w), 2437 (w), 2265 (w), 2217 (w), 2132 (w), 2067 (vw), 2019 (vw), 1925 (vw), 1869 (vw), 1662 (s), 1598 (s), 1484 (m), 1450 (s), 1422 (w), 1396 (w), 1355 (w), 1335 (w), 1289 (m), 1279 (m), 1245 (w), 1200 (vw), 1142 (w), 1123 (m), 1100 (s), 1071 (s), 1040 (s), 983 (m), 952 (w), 860 (m), 779 (m), 744 (m), 698 (w), 664 (m), 502 (m), 464 (w); **Raman** (1064 nm, 200 mW, 25 °C, cm^{-1}): $\tilde{\nu}$ = 3335 (6), 3151 (11), 3007 (15), 2967 (19), 2948 (41), 2881 (5), 2756 (3), 1662 (13), 1595 (18),

1481 (15), 1454 (20), 1427 (7), 1357 (16), 1333 (20), 1293 (40), 1248 (10), 1125 (19), 1098 (14), 1073 (17), 986 (22), 951 (12), 861 (37), 778 (100), 667 (18), 498 (7), 467 (17), 363 (10), 324 (14), 269 (18), 215 (9), 181 (22); **^{1}H NMR** (d_6-DMSO, 25 °C, ppm): δ = 6.63 (br s, 2H, NH_2), 4.73 (br s, 1H, OH), 4.18 (t, ^3J=6 Hz, 2H, CH_2), 3.71 (t, ^3J=6 Hz, 2H, CH_2); **^{13}C NMR** (d_6-DMSO, 25 °C, ppm): δ = 156.5 (C), 59.6 (CH_2), 47.8 (CH_2); ***m/z*** (DEI): 129 [$(M)^+$, (100)], 98 (78), 86 (43), 70 (14), 57 (14), 45 (48), 43 (78), 31 (15), 28 (31), 27 (13). **EA** ($C_3H_7N_5O$, 129.12) calcd.: C 27.91, H 5.46, N 54.24 %; found: C 27.85, H 5.45, N 54.07 %; **impact sensitivity**: > 100 J; **friction sensitivity**: > 100 N.

*1-(2-Chloroethyl)-5-aminotetrazole (**48**).* The preparation of **48** was performed according to the literature using 25.8 g (0.2 mol) 1-(2-hydroxyethyl)-5-aminotetrazole (**46**).[27] Recrystallization from water yielded colorless **48** (22.1 g, 75 % yield). **DSC** (T_{onset}, 5 °C min^{-1}): 150–151 °C; **IR** (KBr, cm^{-1}): $\tilde{\nu}$ = 3312 (s, br), 3241 (s, br), 3102 (s, br), 2829 (m), 2741 (m), 2658 (m, br), 1773 (w), 1694 (s), 1651 (m), 1645 (m), 1557 (w), 1552 (w), 1505 (w), 1488 (w), 1439 (m), 1384 (w), 1364 (w), 1311 (m), 1283 (w), 1249 (m), 1209 (w), 1112 (w), 1056 (w), 1029 (m), 994 (w), 944 (w), 904 (w), 814 (w), 771 (w), 711 (w), 670 (m), 601 (m), 504 (w); **Raman** (1064 nm, 200 mW, 25 °C, cm^{-1}): $\tilde{\nu}$ = 3235 (3), 3082 (9), 3021 (23), 2989 (32), 2970 (61), 2954 (58), 2863 (7), 1692 (11), 1496 (13), 1441 (40), 1366 (33), 1282 (11), 1250 (34), 1207 (14), 1109 (5), 1070 (12), 1033 (34), 996 (15), 946 (8), 908 (9), 770 (100), 712 (8), 671 (67), 647 (36), 506 (12), 427 (14), 339 (24), 307 (21), 231 (41), 188 (28); **^{1}H NMR** (d_6-DMSO, 25 °C, ppm): δ = 7.08 (br s, 2H, NH_2), 4.50 (t, ^3J=6 Hz, 2H, CH_2), 3.95 (t, ^3J=6 Hz, 2H, CH_2). **^{13}C NMR** (d_6-DMSO, 25 °C, ppm): δ = 155.9 (C), 46.8 (CH_2), 42.5 (CH_2); **EA** ($C_3H_6N_5Cl$, 147.57) calcd.: C 24.42, H 4.10, N 47.46 %; found: C 24.44, H 3.77, N 47.44 %; **impact sensitivity**: > 100 J; **friction sensitivity**: > 100 N.

*1-(2-Azidoethyl)-5-aminotetrazole (**49**):* A solution of **48** (2.0 g, 13.6 mmol) in 30 mL DMF was combined with NaN_3 (1.0 g, 15 mmol) in 30 mL DMF and refluxed at 100 °C for 4 hours. The warm solvent was evaporated and the crude product was recrystallized from H_2O yielding colorless needles (1.57 g, 76 % yield). **DSC** (T_{onset}, 5 °C min^{-1}): 129–130 °C; **IR** (KBr, cm^{-1}): $\tilde{\nu}$ = 3342 (s), 3262 (m), 3160 (s), 2955 (w), 2741 (w), 2438 (vw), 2231 (vw), 2133 (s), 2096 (s), 2039 (m), 1652 (s), 1593 (s), 1479 (m), 1445 (m), 1434 (m), 1375 (vw), 1349 (w), 1333 (w), 1303 (m), 1287 (m), 1221 (w), 1134 (w), 1105 (m), 1055 (w), 1009 (w), 970 (vw), 954 (vw), 910 (vw), 821 (w), 781 (vw), 744 (w), 694 (vw), 664 (m), 647 (w), 631 (w), 521 (m); **Raman** (1064 nm, 200 mW, 25 °C, cm^{-1}): $\tilde{\nu}$ =

3150 (19), 3000 (24), 2988 (26), 2962 (71), 2868 (10), 2127 (11), 2097 (13), 1668 (14), 1594 (22), 1474 (16), 1445 (37), 1374 (25), 1351 (30), 1334 (26), 1291 (41), 1258 (15), 1221 (15), 1138 (28), 1100 (15), 1058 (17), 1011 (20), 972 (14), 956 (17), 822 (22), 780 (100), 667 (16), 630 (21), 450 (17), 356 (28), 317 (31), 270 (36), 232 (54), 162 (33); **^{1}H NMR** (d_6-DMSO, 25 °C, ppm): δ = 6.80 (s, 2H, NH_2), 4.31 (t, ^{3}J=6 Hz, 2H, CH_2), 3.71 (t, ^{3}J=6 Hz, 2H, CH_2); **^{13}C NMR** (d_6-DMSO, 25 °C, ppm): δ = 156.3 (C), 49.4 (CH_2), 44.6 (CH_2); ***m/z*** (ESI): 309 [$(2M+H)^+$, (100)], 155 [$(M+H)^+$, (34)]; **EA** ($C_3H_6N_8$, 154.13) calcd.: C 23.38, H 3.92, N 72.70 %; found: C 23.38; H 3.91; N 72.36 %; **impact sensitivity**: 10 J; **friction sensitivity**: 360 N.

General procedure for preparation of **50**, **51** and **52**. To 20 mL of a cooled solution of nitric acid (100 %) the respective 1-ethyl-5-aminotetrazoles (**46**, **48**, and **49**) (25 mmol) was added portion wise. After stirring the solution for 12 hours at room temperature, it was poured on ice. The solvent was removed using high vacuum to obtain the crude product, which was washed until it became free of acid. Recrystallization resulted from an appropriate solvent (see below).

*1-(2-Hydroxyethyl)-5-nitriminotetrazole (**50**):* Recrystallization from diluted HNO_3 yielded colorless rods (4.13 g, 95 % yield). **DSC** (T_{onset}, 5 °C min^{-1}): 137–139 °C (dec.); **IR** (KBr, cm^{-1}): $\tilde{\nu}$ = 3359 (m, br), 3153 (w), 2966 (m), 2881 (w), 2637 (w), 1786 (vw), 1586 (s), 1506 (s), 1448 (m), 1427 (w), 1379 (m), 1352 (w), 1337 (m), 1293 (m), 1257 (s), 1234 (s), 1215 (s), 1140 (w), 1076 (m), 1058 (m), 1041 (m), 979 (m), 956 (w), 875 (vw), 861 (w), 779 (w), 755 (vw), 720 (m), 680 (vw), 649 (w), 522 (vw); **Raman** (1064 nm, 200 mW, 25 °C, cm^{-1}): $\tilde{\nu}$ = 3023 (13), 3001 (19), 2973 (44), 1571 (100), 1505 (14), 1454 (19), 1445 (27), 1414 (64), 1348 (24), 1290 (34), 1258 (26), 1224 (64), 1138 (14), 1073 (23), 1030 (41), 985 (23), 883 (23), 859 (12), 758 (39), 652 (27), 484 (38), 440 (20), 369 (19), 308 (50), 277 (28), 205 (21); **^{1}H NMR** (d_6-DMSO, 25 °C, ppm): δ = 4.85 (br s, 1H, OH), 4.22 (t, ^{3}J=5 Hz, 2H, CH_2), 3.77 (t, ^{3}J=5 Hz, 2H, CH_2); **^{13}C NMR** (d_6-DMSO, 25 °C, ppm): δ = 150.9 (C), 58.1 (CH_2), 50.4 CH_2); ***m/z*** (DEI): 174 [$(M)^+$ (1)], 147 (1), 131 (66), 129 (8), 98 (9), 85 (66), 55 (38), 45 (100), 28 (73), 27 (38); **EA** ($C_3H_6N_6O_3$, 174.12) calcd.: C 20.66, H 3.36, N 48.28 %; found: C 20.69, H 3.47, N 48.27 %; **impact sensitivity**: 6 J; **friction sensitivity**: 55 N.

*1-(2-Chloroethyl)-5-nitriminotetrazole (**51**):* Recrystallization from H_2O yielded colorless **51** (4.48 g, 93 % yield). **DSC** (T_{onset}, 5 °C min^{-1}): 111–112 °C; **IR** (KBr, cm^{-1}): $\tilde{\nu}$ =3170 (m),

3113 (m, br), 3025 (m), 2977 (m), 2885 (w), 2448 (vw), 2084 (vw), 1899 (vw), 1583 (s), 1574 (s), 1492 (s), 1450 (m), 1437 (s), 1418 (m), 1384 (w), 1328 (m), 1319 (m), 1285 (w), 1246 (m), 1209 (s), 1200 (s), 1125 (vw), 1058 (w), 1033 (m), 987 (m), 952 (vw), 905 (w), 866 (vw), 801 (vw), 777 (w), 723 (m), 682 (w), 648 (vw), 439 (w); **Raman** (1064 nm, 200 mW, 25 °C, cm^{-1}): $\tilde{\nu}$ = 3028 (14), 3003 (18), 2977 (52), 2946 (32), 1582 (100), 1571 (71), 1490 (10), 1442 (23), 1406 (77), 1369 (15), 1328 (17), 1278 (19), 1241 (32), 1224 (24), 1205 (25), 1128 (6), 1055 (21), 1032 (23), 990 (60), 957 (22), 891 (8), 868 (22), 752 (40), 683 (21), 679 (16), 650 (79), 501 (41), 473 (15), 439 (14), 351 (9), 310 (32), 260 (29), 214 (15), 168 (22); **^{1}H NMR** (d_6-DMSO, 25 °C, ppm): δ = 12.64 (br s, 1*H*, NH), 4.55 (t, ^3J=6 Hz, 2H, CH_2), 4.04 (t, ^3J=6 Hz, 2H, CH_2); **^{13}C NMR** (d_6-DMSO, 25 °C, ppm): δ = 150.9 (C), 48.9 (CH_2), 41.4 (CH_2); ***m/z*** (DEI): 192 [$(M)^+$ (22)], 157 (24), 111 (24), 103 (77), 63 (96), 55 (73), 46 (23), 30 (46), 28 (64), 27 (100); **EA** ($C_3H_5N_6ClO_2$, 192.56) calcd.: C 18.71, H 2.62, N 43.64 %; found: C 18.71, H 2.74, N 43.34 %; **impact sensitivity**: 28 J; **friction sensitivity**: > 360 N.

*1-(2-Nitratoethyl)-5-nitriminotetrazole monohydrate (**52**):* Recrystallization from very diluted HNO_3 gave colorless **52** after two days (2.46 g, 45 % yield). **DSC** (T_{onset}, 5 °C min^{-1}): 120 °C (dec.); **IR** (KBr, cm^{-1}) $\tilde{\nu}$ = 3571 (m), 3374 (s, br), 3127 (s, br), 3016 (s), 2961 (s), 2648 (m), 2067 (w), 1690 (m), 1643 (s), 1583 (s), 1496 (s), 1448 (s), 1384 (s), 1312 (s), 1283 (s), 1250 (s), 1141 (m), 1031 (s), 978 (m), 892 (m), 846 (m), 779 (m), 755 (m), 720 (m), 678 (w), 649 (w), 579 (vw), 565 (vw), 543 (vw), 522 (vw), 504 (vw); **Raman** (1064 nm, 200 mW, 25 °C, cm^{-1}) $\tilde{\nu}$ = 3020 (31), 2979 (69), 1621 (26), 1584 (100), 1508 (39), 1452 (43), 1422 (86), 1316 (38), 1279 (75), 1263 (78), 1247 (70), 1159 (21), 1084 (25), 1038 (56), 996 (40), 881 (37), 849 (31), 758 (92), 706 (25), 662 (38), 567 (33), 493 (48), 446 (26), 353 (32), 312 (55), 237 (41), 209 (37), 175 (42); **^{1}H NMR** (d_6-DMSO, 25 °C, ppm) δ = 8.18 (s, 1H, NH), 4.88 (t, ^3J=5 Hz, 2H, CH_2), 3.76 (t, ^3J=5 Hz, 2H, CH_2); **^{13}C NMR** (d_6-DMSO, 25 °C, ppm) δ = 151.1 (C), 48.7 (CH_2), 41.6 (CH_2); **EA** ($C_3H_5N_7O_4$, 219.12) calcd.: C 16.44, H 2.30, N 44.75 %; found: C 16.31, H 2.62, N 44.55 %; **impact sensitivity**: 25 J; **friction sensitivity**: 360 N.

*1-(2-Azidoethyl)-5-nitriminotetrazole (**53**):* An equimolar amount of diluted (1N) hydrochloric acid was added to potassium 1-(2-azidoethyl)-5-nitriminotetrazolate (**54**). The solvent was evaporated and acetone was added to the residue. The KCl was removed by filtration and the acetone was evaporated. The crude product was recrystallized from a small amount of methanol yielding colorless **53** (90 %). **DSC** (T_{onset},

5 deg min^{-1}): 140 °C (dec.); **IR** (KBr, cm^{-1}): $\tilde{\nu}$ = 3444 (w), 3019 (m), 2962 (m), 2115 (s), 1625 (m), 1581 (vs), 1495 (s), 1448 (m), 1308 (s), 1254 (s), 1152 (w), 1033 (m), 976 (w), 873 (w), 780 (w), 722 (w), 661 (w), 633 (w), 555 (w), 440 (w); **Raman** (1064 nm, 200 mW, 25 °C, cm^{-1}): $\tilde{\nu}$ = 3024 (8), 3000 (7), 2977 (12), 2119 (16), 1583 (100), 1505 (55), 1416 (72), 1330 (15), 1308 (17), 1278 (39), 992 (40), 957 (22), 868 (22), 755 (51), 656 (79), 480 (15), 311 (30), 170 (22); **^{1}H NMR** (d_6-DMSO, 25 °C, ppm): δ = 9.58 (s, 1H, NH), 4.40 (t, ^3J = 6 Hz, 2H, CH_2), 3.81 (t, ^3J = 6 Hz, 2H, CH_2); **^{13}C NMR** (d_6-DMSO, 25 °C, ppm): δ = 151.3 (C), 49.9 (CH_2), 46.6 (CH_2); EA ($C_3H_5N_9O_2$, 199.13) calcd.: C 18.10, H 2.53, 63.30 %; found: C 17.78, H 2.91, N 62.72 %; **impact sensitivity**: 2 J; **friction sensitivity**: 80 N.

*Potassium 1-(2-azidoethyl)-5-nitriminotetrazolate (**54**):* 1-(2-Azidoethyl)-5-amino-tetrazole (**49**) (0.39 g, 3 mmol) was dissolved in MeCN (10 mL) and cooled using an ice bath. To this, nitronium tetrafluoroborate (0.33 g, 3 mmol) was added. The solution was stirred for 30 min at 0 °C and for one hour at 25 °C. The solvent was evaporated and a solution of KOH (168 mg, 3 mmol) in 20 mL ethanol was added. Precipitated KBF_4 was removed by filtration and a further equivalent of KOH (168 mg, 3 mmol) in 20 mL ethanol was added. The solvent was evaporated and 20 mL cold water was added. The insoluble starting material was removed by filtration and the water was evaporated. The crude product was recrystallized from hot ethanol yielding **54** (0.24 g, 33 % yield). **DSC** (T_{onset}, 5 °C min^{-1}): 205 °C (dec.); **IR** (KBr, cm^{-1}): $\tilde{\nu}$ = 2944 (w), 2142 (m), 2108 (m), 1506 (s), 1456 (s), 1432 (m), 1384 (s), 1355 (vs), 1343 (vs), 1235 (m), 1143 (m), 1103 (m), 1032 (m), 950 (w), 881 (w), 786 (w), 776 (w), 727 (w), 659 (w), 628 (w), 514 (w), 441 (w); **Raman** (1064 nm, 200 mW, 25 °C, cm^{-1}): $\tilde{\nu}$ = 3012 (7), 2982 (15), 2968 (14), 2123 (3), 1513 (100), 1457 (12), 1430 (11), 1388 (13), 1349 (12), 1321 (32), 1225 (7), 1106 (15), 1050 (15), 1035 (50), 884 (9), 836 (6), 756 (13), 662 (8), 633 (7), 488 (9), 375 (10), 213 (13); **^{1}H NMR** (d_6-DMSO, 25 °C, ppm): δ = 4.22 (t, ^3J = 6 Hz, 2H, CH_2), 3.69 (t, ^3J = 6 Hz, 2H, CH_2); **^{13}C NMR** (d_6-DMSO, 25 °C, ppm): δ = 157.6 (C), 49.2 (CH_2), 45.6 (CH_2); **EA** ($C_3H_4KN_9O_2$, 237.25) calcd.: C 15.13, H 2.12, N 52.92 %; found: C 15.00, H 2.31, N 52.90 %; **impact sensitivity**: 25 J; **friction sensitivity**: 300 N.

*Sodium 1-(2-chloroethyl)-5-nitriminotetrazolate (**55**):* A solution of 1-(2-chloroethyl)-5-nitriminotetrazole (**51**) (339 mg, 1.8 mmol) and NaOH (80 mg, 2.0 mmol) in 10 mL H_2O was heated at 100 °C for two minutes. The solvent was removed under high vacuum to obtain colorless crystals. Recrystallization from EtOH yielded colorless crystals (378 mg,

98 % yield). **DSC** (T_{onset}, 5 °C min^{-1}): 183–184 °C (dec.); **IR** (KBr, cm^{-1}): $\tilde{\nu}$ = 3425 (m, br), 3018 (m), 2972 (m), 2736 (w), 2373 (w), 1978 (w), 1580 (m), 1502 (s), 1462 (s), 1454 (s), 1440 (s), 1391 (s), 1363 (s, br), 1289 (s), 1256 (m), 1237 (s), 1131 (m), 1104 (m), 1042 (m), 993 (w), 951 (w), 910 (m), 872 (w), 775 (m), 757 (w), 739 (w), 676 (m), 655 (m), 518 (vw), 477 (vw); **Raman** (1064 nm, 200 mW, 25 °C, cm^{-1}): $\tilde{\nu}$ = 3015 (5), 2977 (7), 2984 (5), 1550 (3), 1498 (100), 1462 (5), 1433 (7), 1377 (8), 1347 (15), 1323 (8), 1298 (8), 1264 (3), 1134 (2), 1108 (10), 1037 (38), 992 (2), 875 (4), 759 (9), 678 (4), 653 (9), 510 (3), 443 (2), 370 (4), 307 (6), 246 (8), 208 (6); **^{1}H NMR** (d_6-DMSO, 25 °C, ppm): δ = 4.41 (t, ^3J=6 Hz, 2H, CH_2), 3.98 (t, ^3J=6 Hz, 2H, CH_2); **^{13}C NMR** (d_6-DMSO, 25 °C, ppm): δ = 157.2 (C), 47.8 (CH_2), 42.1 (CH_2); **EA** ($C_3H_4ClN_6NaO_2$, 214.55) calcd.: C 16.79, H 1.88, N 39.17 %; found: C 16.81, H 1.77, N 38.99 %; **impact sensitivity**: > 50 J; **friction sensitivity**: > 360 N.

*Ammonium 1-(2-chloroethyl)-5-nitriminotetrazolate (**56**):* 1-(2-Chloroethyl)-5-nitrimino-tetrazole (385 mg, 2.0 mmol) in 10 mL NH_3 (25 %) was heated for 10 minutes. The solvent was removed under high vacuum. Recrystallization from H_2O resulted in colorless crystals (402 mg, 96 % yield). **DSC** (T_{onset}, 5 °C min^{-1}): 233 °C (dec.); **IR** (KBr, cm^{-1}): $\tilde{\nu}$ = 3571 (w), 3176 (s, br), 3065 (s), 2840 (m), 2237 (w), 2340 (w), 2159 (w), 1879 (w), 1675 (w), 1648 (w), 1547 (m), 1426 (s), 1393 (s), 1360 (s), 1292 (m), 1267 (m), 1225 (m), 1146 (m), 1124 (m), 1084 (m), 1059 (m), 1037 (m), 1014 (m), 866 (w), 777 (vw), 756 (w), 730 (vw), 622 (w), 480 (vw); **Raman** (1064 nm, 200 mW, 25 °C, cm^{-1}): $\tilde{\nu}$ = 3077 (5), 1552 (10), 1473 (72), 1441 (100), 1371 (18), 1273 (8), 1210 (27), 1151 (23), 1126 (28), 1084 (18), 1016 (71), 976 (9), 867 (9), 761 (15), 732 (14), 478 (11), 383 (22), 205 (25); **^{1}H NMR** (d_6-DMSO, 25 °C, ppm): δ = 7.32 (s, 4H, NH_4^+), 4.35 (t, ^3J=6 Hz, 2H, CH_2), 3.94 (t, ^3J=6 Hz, 2H, CH_2); **^{13}C NMR** (d_6-DMSO, 25 °C, ppm): δ = 158.8 (C), 48.0 (CH_2), 42.3 (CH_2); **EA** ($C_3H_8ClN_7O_2$, 209.59) calcd.: C 17.19, H 3.85, N 46.78 %; found: C 17.16, H 3.98, N 46.35 %; **impact sensitivity**: > 50 J; **friction sensitivity**: > 360 N.

*1-(2-Hydroxyethyl)-5-aminotetrazolium nitrate (**57**):* 1-(2-Hydroxyethyl)-5-amino-tetrazole (**46**) (645 mg, 5 mmol) was heated with HNO_3 2N (10 mL) to 60 °C for 15 min. The solvent was evaporated to obtain the crude product. After recrystallization from EtOH colorless needles were obtained (845 mg, 88 % yield). **DSC** (T_{onset}, 5 °C min^{-1}): 135–136 °C, 160 °C (dec.); **IR** (KBr, cm^{-1}): $\tilde{\nu}$ = 3346 (s, br), 3154 (s, br), 2965 (m), 2945 (m), 2881 (m), 2792 (m), 2750 (m), 2661 (m), 2489 (m), 2396 (m), 2132 (w), 2069 (w),

1923 (w), 1762 (w), 1688 (s), 1666 (s), 1598 (s), 1484 (m), 1433(m), 1386 (s), 1339 (w), 1309 (m), 1280 (m), 1264 (m), 1234 (m), 1123 (m), 1100 (m), 1071 (s), 1039 (s), 983 (m), 945 (m), 860 (m), 825 (w), 779 (w), 769 (w), 744 (w), 721 (w), 697 (w), 663 (m), 502 (m), 465 (w); **Raman** (1064 nm, 300 mW, 25 °C, cm^{-1}): $\tilde{\nu}$ = 3423 (8), 3305 (5), 3153 (5), 3001 (10), 2950 (24), 1689 (8), 1663 (8), 1581 (12), 1482 (16), 1460 (28), 1430 (23), 1386 (16), 1357 (19), 1335 (18), 1294 (25), 1247 (18), 1124 (12), 1074 (22), 1038 (98), 987 (16), 950 (14), 862 (24), 813 (12), 778 (58), 766 (83), 727 (17), 718 (22), 669 (14), 649 (19), 468 (14), 451 (14), 356 (16), 257 (25), 182 (28), 91 (23); **^{1}H NMR** (d_6-DMSO, 25 °C, ppm): δ = 4.10 (t, 2H, CH_2), 3.67 (t, 2H, CH_2); **^{13}C NMR** (d_6-DMSO, 25 °C, ppm): δ = 156.1 (C), 59.4 (CH_2), 47.9 (CH_2); EA ($C_3H_8N_6O_4$, 192.13) calcd.: C 18.75, H 4.20, N 43.74 %; found C 18.77, H 4.19, N 43.60 %; **impact sensitivity**: > 50 J; **friction sensitivity**: 360 N.

*1-(2-Azidoethyl)-5-aminotetrazolium nitrate (**48**):* 1-(2-Azidoethyl)-5-aminotetrazole (**59**) (462 mg, 3.0 mmol) was combined with HNO_3 2N (5 mL) and heated to 60 °C for 15 min. The solvent was evaporated and the crude product was recrystallized from wet EtOH yielding colorless rods (521 mg, 80 % yield). **DSC** (T_{onset}, 5 °C min^{-1}): 95 °C, 148 °C (dec.); **IR** (KBr, cm^{-1}): $\tilde{\nu}$ = 3354 (m), 3244 (m), 3166 (m), 3012 (w), 2948 (w), 2450 (w, br), 2132 (s), 2100 (s), 2035 (w), 1764 (w), 1690 (s), 1497 (m), 1401 (s), 1382 (s), 1328 (s), 1301 (s), 1237 (m), 1126 (w), 1084 (w), 1042 (m), 996 (w), 966 (w), 913 (w), 818 (w), 768 (w), 724 (w), 603 (w), 550 (w), 508 (w); **Raman** (1064 nm, 300 mW, 25 °C, cm^{-1}): $\tilde{\nu}$ = 3347 (4), 3297 (5), 3263 (6), 3011 (8), 2971 (18), 2949 (17), 2872 (5), 2665 (4), 2527 (5), 2424 (4), 2212 (4), 2136 (10), 1934 (5), 1889 (6), 1821 (5), 1746 (5), 1598 (9), 1501 (12), 1441 (22), 1375 (12), 1303 (17), 1226 (13), 1082 (12), 1051 (80), 996 (12), 818 (16), 770 (44); 719 (13), 695 (5), 662 (14), 626 (17), 564 (6), 545 (6), 443 (12), 345 (15), 304 (16), 259 (26), 230 (29), 166 (17); **^{1}H NMR** (d_6-DMSO, 25 °C, ppm): δ = 7.32 (s, 2H, NH_2), 4.30 (t, 2H, CH_2), 3.70 (t, 2H, CH_2); **^{13}C NMR** (d_6-DMSO, 25 °C, ppm): δ = 155.7 (C), 49.3 (CH_2), 44.7 (CH_2); **^{14}N NMR** (d_6-DMSO, 25 °C, ppm): δ = –12.90 (NO_3^-), –135 (N_β), –177 (N_γ), 327 (N_α); **EA** ($C_3H_7N_9O_3$, 217.15) calcd.: C 16.59, H 3.25, N 58.05 %; found: 16.55, H 3.27, N 57.55 %; **impact sensitivity**: 7 J; **friction sensitivity**: 160 N.

*1-(2-Azidoethyl)-5-aminotetrazolium perchlorate monohydrate (**59**):* 1M Perchloric acid (9 mL) was added in drops to a solution of **49** (1.39 g, 9 mmol) in 7 mL H_2O. The solution was heated to 80 °C for 15 min. After evaporating the solvent, the crude product was recrystallized from EtOH to give colorless rods (2.33 g, 95 % yield). **DSC** (T_{onset}, 5 °C

min^{-1}): 85 °C, 172 °C (dec.); **IR** (KBr, cm^{-1}): $\tilde{\nu}$ = 3363 (s, br), 3298 (s), 2934 (w), 2871 (w), 2651 (w, br), 2531 (w, br), 2264 (w), 2147 (s), 2134 (s); 2102 (w), 1682 (s), 1505 (w), 1436 (m), 1368 (m), 1345 (m), 1288 (s), 1262 (m), 1246 (m), 1141 (s, br), 1088 (s, br), 1043 (s, br), 1043 (s), 1011 (s), 932 (m), 834 (w), 718 (w), 626 (s), 554 (m); **Raman** (1064 nm, 300 mW, 25 °C, cm^{-1}): $\tilde{\nu}$ = 3191 (4), 3015 (10), 2070 (17), 2047 (15), 2134 (8), 2095 (8), 1706 (12), 1607 (12), 1505 (18), 1445 (26), 1431 (28), 1370 (25), 1345 (18), 1307 (19), 1283 (23), 1223 (15), 1131 (19), 1039 (14), 977 (14), 932 (100), 834 (26), 767 (65), 652 (14), 624 (32), 456 (35), 366 (16), 255 (31), 205 (26); **^{1}H NMR** (d_6-DMSO, 25 °C, ppm): δ = 6.75 (s br, 2H, NH_2), 4.30 (t, 2H, CH_2), 3.70 (t, 2H, CH_2); **^{13}C NMR** (d_6-DMSO, 25 °C, ppm): δ = 155.7 (C), 49.3 (CH_2), 44.8 (CH_2); **EA** ($C_3H_9ClN_8O_5$, 272.61) calcd.: C 13.22, H 3.33, N 41.10 %; found: C 13.00, H 3.71, N 41.09 %; **impact sensitivity**: 5 J; **friction sensitivity**: 120 N.

General procedure for preparation of **60**, **61** and **62**: To a hot solution of $Cu(NO_3)_2{\cdot}3H_2O$ (242 mg, 1.0 mmol) in 5 mL water, a warm aqueous solution (10 mL) containing two eq. of the corresponding nitriminotetrazole (**50**, **51**, **53**) was added and stirred for 10 min at 80 °C. The solution was filtrated and left for crystallization. After 1 or 2 days single crystals of **60–62** were obtained which have been isolated by filtration.

*Trans[diaqua-bis(1-(2-hydroxyethyl)-5-nitriminotetrazolato-N4,O1)copper(II)] (**60**):* **DSC** (T_{onset}, 5 °C min^{-1}): 245 °C; **IR** (KBr, cm^{-1}): $\tilde{\nu}$ = 3376 (s), 2987 (m), 2959 (m), 2364 (w), 1649 (w), 1536 (vs), 1491 (s), 1483 (s), 1459 (m), 1434 (vs), 1396 (m), 1348 (m), 1325 (m), 1291 (s), 1274 (s), 1239 (s), 1221 (s), 1119 (w), 1075 (w), 1057 (m), 1019 (m), 882 (w), 732 (m), 659 (w), 579 (w), 485 (w); **EA** ($C_6H_{14}CuN_{12}O_8$, 445.80) calcd.: C 16.17, H 3.17, N 37.70 %; found: C 16.12, H 3.12, N 37.55 %; **impact sensitivity**: > 50 J.

*Trans-[diaqua-bis(1-(2-chloroethyl)-5-nitri-minotetrazolato-N4,O1)copper(II)] dihydrate (**61**):* **DSC** (T_{onset}, 5 °C min^{-1}): 233°C (dec.); **IR** (KBr, cm^{-1}): $\tilde{\nu}$ = 3596 (m), 3501 (m), 3177 (s, br), 2960 (m), 2341 (w), 2307 (w), 1654 (w), 1593 (m), 1517 (s), 1465 (s), 1425 (s), 1390 (vs), 1351 (vs), 1314 (vs), 1297 (vs), 1267 (s), 1211 (s), 1138 (m), 1110 (s), 1036 (m), 1010 (m), 960 (m), 905 (m), 872 (m), 814 (m), 773 (m), 764 (m), 741 (m), 685 (s), 662 (m), 509 (w); **EA** ($C_6H_{16}Cl_2CuN_{12}O_8$, 518.72) calcd.: C 13.89, H 3.11, N 32.40 %; found: C 13.89, H 3.13, N 32.34; **impact sensitivity**: > 50 J.

*[Diaqua-bis(1-(2-azidoethyl)-5-nitriminotetrazolato-N4,O1)copper (II)] (**62**)*: **DSC** (T_{onset}, 5 °C min^{-1}): 217 °C (dec.); **IR** (KBr, cm^{-1}): $\tilde{\nu}$ = 3456 (m, br), 2963 (w), 2118 (s), 1637 (m), 1582 (s), 1528 (m), 1481 (s), 1417 (s), 1343 (s), 1303 (vs), 1261 (s), 1112 (w), 1033 (w), 874 (w), 802 (w), 757 (w), 675 (w), 628 (w), 555 (w); **EA** ($C_6H_{12}CuN_{18}O_6$, 495.92) calcd.: C 14.53, H 2.44, N 50.85 %; found: C 14.07, H 2.97, N 49.99 %; **impact sensitivity**: 10 J.

5.7 Conclusion

Functionalized 1-ethyl-5-amino- and 1-ethyl-5-nitriminotetrazoles were synthesized and characterized with regard to develop new energetic materials (explosives, propellants and pyrotechnics). From this combined experimental and theoretical work, the following conclusions can be drawn:

- Functionalized 1-ethyl-5-aminotetrazoles can be synthesized starting by the reaction of sodium 5-aminotetrazolate with 2-chloroethanol. The substituent is stable towards hydrolysis and can be modified by typical S_N2 reaction conditions. Several 5-nitriminotetrazoles were obtained by nitration of the 5-aminotetrazole derivatives.

- The crystal structures of 1-(2-hydroxyethyl)-5-aminotetrazole (**46**), 1-(2-hydroxyethyl)-5-aminotetrazole (**47**), 1-(2-chloroethyl)-5-aminotetrazole (**48**), 1-(2-azidoethyl)-5-aminotetrazole (**49**), 1-(2-hydroxyethyl)-5-nitriminotetrazole (**50**), 1-(2-chloroethyl)-5-nitriminotetrazole (**51**), 1-(2-nitratoethyl)-5-nitriminotetrazole monohydrate (**52**), 1-(2-azidoethyl)-5-nitriminotetrazole (**53**), potassium 1-(2-azidoethyl)-5-nitriminotetrazolate (**54**), sodium 1-(2-chloroethyl)-5-nitriminotetrazolate (**55**), ammonium 1-(2-chloroethyl)-5-nitriminotetrazolate (**56**), 1-(2-hydroxyethyl)-5-aminotetrazolium nitrate (**57**), 1-(2-azidoethyl)-5-aminotetrazolium nitrate (**58**), 1-(2-azidoethyl)-5-aminotetrazolium perchlorate monohydrate (**59**) were determined by low temperature single crystal X-ray diffraction.

- 5-Nitriminotetrazoles can be used as bidentate ligands. Therefore, the coordination ability of **50**, **51** and **53** was tested by the reaction with copper

nitrate trihydrate yielding the copper complexes diaqua-bis(1-(2-hydroxyoethyl)-5-nitriminotetrazolato copper(II) (**60**), diaqua-bis(1-(2-chloroethyl)-5-nitriminotetrazolato copper(II) (**61**) and diaqua-bis(1-(2-azidoethyl)-5-nitrimino-tetrazolato copper(II) (**62**).

- The energetic properties and sensitivities of all compounds were determined. They range from insensitive (**46**, **48**, **55**, **56**) to "very sensitive" (**53**). The calculated energetic performances, based on the X-ray densities and heats of formation, range from values assigned to the group of *propellants* (**49**) to values of *high explosives* (**50**, **52**, **53**). Unfortunately, most of the compounds show low decomposition temperatures in the range of 120–150 °C.

- The color performance of the copper complexes **60**–**62** was tested with regard to find application as coloring agents in "green" pyrotechnics. **60** and **62** show a brilliant green flame and in the case of **61** a bright blue flame color was observed. The complexes combust almost smokeless, which makes them to promising coloring agents in modern pyrotechnical compositions.

Chapter 6.

2-Nitro-2-aza-propyl-tetrazoles

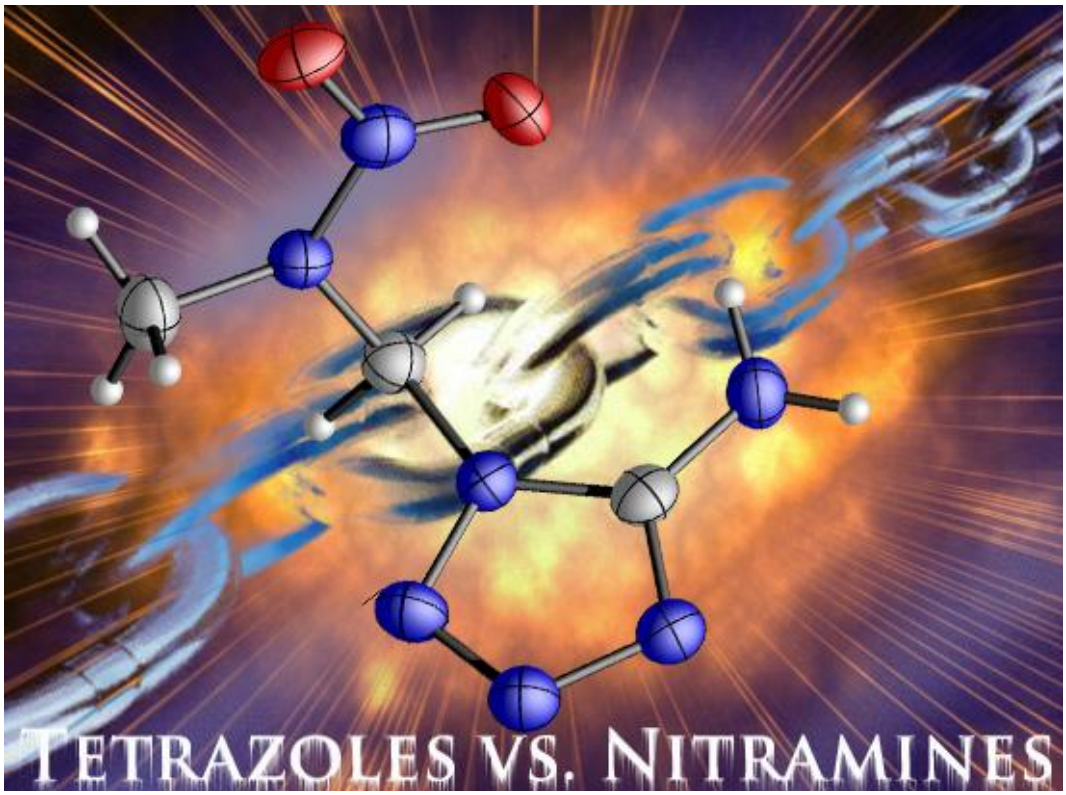

6.1 Introduction

The synthesis of energetic, non-nuclear materials (explosives, propellants and pyrotechnics) for possible military or civil application has been a long term goal in our research group.[279] We recently reported on the synthesis and characterization of 2-(2-nitro-2-azapropyl)-5-nitrotetrazole,[280] which has an appropriate oxygen balance similar to that of RDX. The oxygen balance indicates the relative amount of oxygen available for the following ideal combustion reactions without adding outer oxygen: carbon to carbon dioxide, hydrogen to water, nitrogen to dinitrogen and sulfur to sulfur dioxide. The oxygen balance can easily be calculated by the equation: Ω (%) = (wO – 2xC – 1/2yH – 2zS)1600/M. (w: number of oxygen atoms, x: number of carbon atoms, y: number of hydrogen atoms, z: number of sulfur atoms, M: molecular weight). In this chapter, the synthesis of several new neutral energetic materials containing a tetrazole moiety and a nitramine (2-nitro-2-azapropyl) substituent are presented. In all cases, alkylation reactions of 2-nitro-2-azapropyl chloride with tetrazolate anions were used to introduce the nitramine function.

6.2 Synthesis

The preparative route to chloro 2-nitro-2-azapropyl (**65**) [281] is divided into two steps (**Scheme 6.1**). The first step is a nitration reaction of the cyclic amine 1,3,5-trimethylhexahydro-1,3,5-triazine (**63**), which is carried out with the help of acetic anhydride, furnishing 2-nitro-2-azapropyl acetate (**64**).[282] The fuming nitric acid is added to the acetic anhydride, which is used in large excess, in a slightly exothermic process. To this mixture, **63** dissolved in glacial acetic acid is added drop wise. To finish the nitration, the whole mixture is heated to 70–75 °C, whereas it is important to heat it very slowly, because of the strong exothermicity of the reaction. If the temperature exceeds 80°C, the reaction may get out of control resulting in further rise of the temperature and possible formation of highly explosive undesired nitration products.

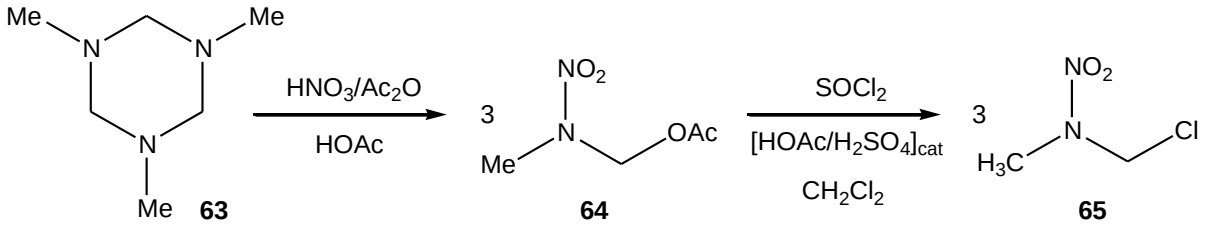

Scheme 6.1 Synthesis of 1-chloro-2-nitro-2-azapropane (**65**)

64 has to be converted into the chloro 2-nitro-2-azapropyl (**65**) because of the better properties of the chloride as leaving group compared to the acetic acid ester. This is achieved by treating the 2-nitro-2-azapropyl acetate with thionyl chloride in dichloromethane as solvent and with some acetic acid and sulfuric acid as catalysts. To finish the reaction, the mixture is refluxed for 1 hour after the entire thionyl chloride was added.

The tetrazole derivatives **66–73** were synthesized according to **Scheme 6.2**. The starting tetrazoles were either purchased commercially (5-amino-1*H*-tetrazole (**2**)) or synthesized according to procedures described in literature (1*H*-tetrazole (**1**) (Chapter 11), 5-nitriminotetrazole, 1-methyl-5-nitriminotetrazole, 2-methyl-5-nitramino-tetrazole (Chapter 4)). For the S_N2-like mechanism, one nitrogen atom of the tetrazole moiety serves as nucleophile, either the nitrogen atoms N1 and N2 or the nitrogen N5 of a 5-aminotetrazole or a 5-nitriminotetrazole. The nucleophilic attack takes place at the methylene group of 2-nitro-2-azapropyl chloride; the chloride serves as leaving group. For increasing the nucleophility of the tetrazole moiety, it has to be activated by deprotonation of the corresponding tetrazole or nitriminotetrazole. This is achieved in two different ways: The first way is to synthesize an alkali metal salt of the tetrazole or the nitriminotetrazole, which then is reacted with the chloro 2-nitro-2-azpropyl. The disadvantage is, the involvation of two separate reaction steps. The alkali metal salt has to be isolated first before being used in the coupling reaction. The second way is to deprotonate the nucleophilic center *in situ* by using triethyl amine to absorb the HCl formed. In this case, the entire coupling reaction involves only one step. As solvents, the moderately polar and aprotic solvents acetone and tetrahydrofurane are used. In case of using an alkali metal salt as starting material, the reaction has to be performed in suspension. However, the solubility of the product is very high, which makes it easy to isolate by filtration and removal of the solvent. The advantage of carrying out the reaction with the help of triethyl amine is the low solubility of the formed triethyl ammonium chloride in acetone and THF. The chloride can be removed from the reaction

mixture and the progress of the reaction is observed by the formation of a white precipitate.

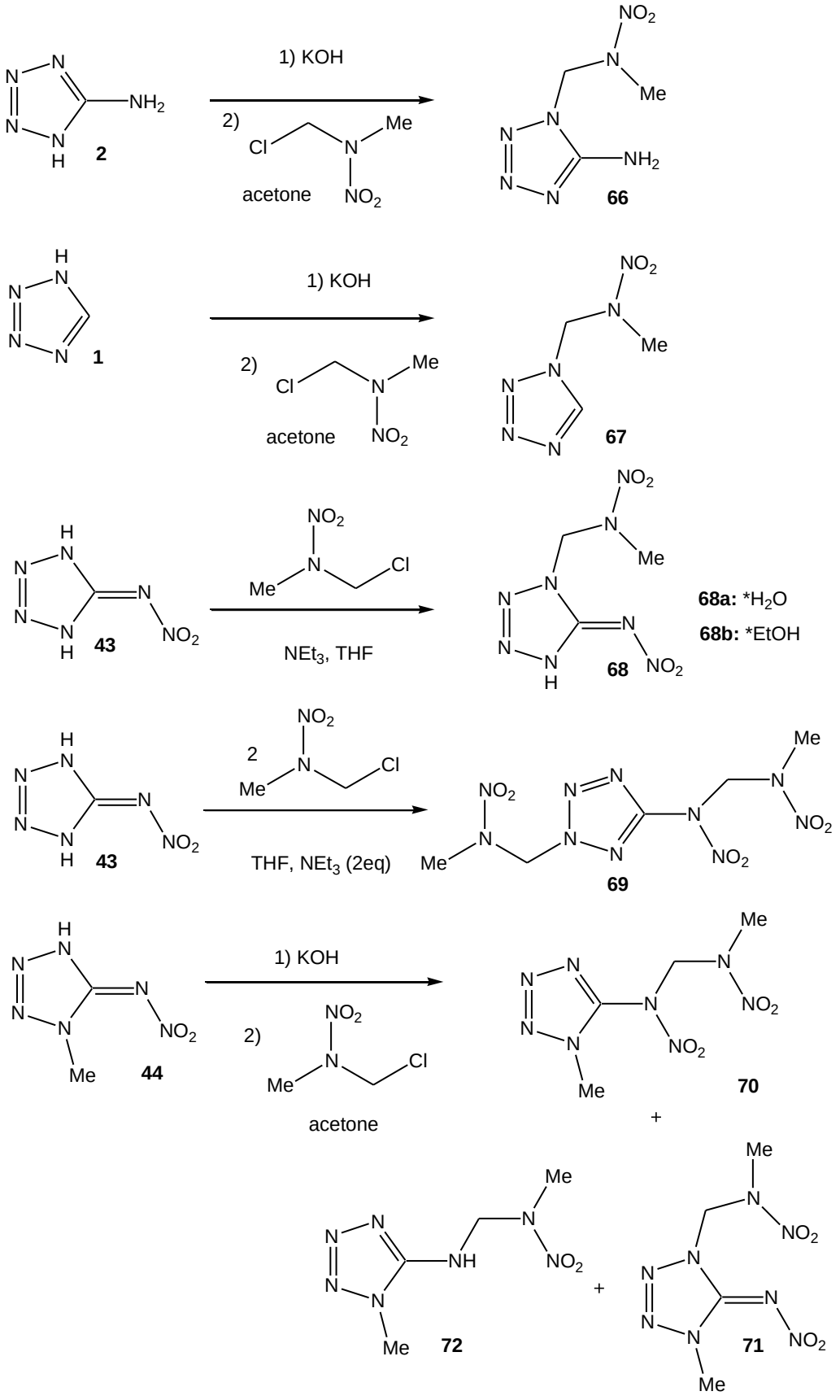

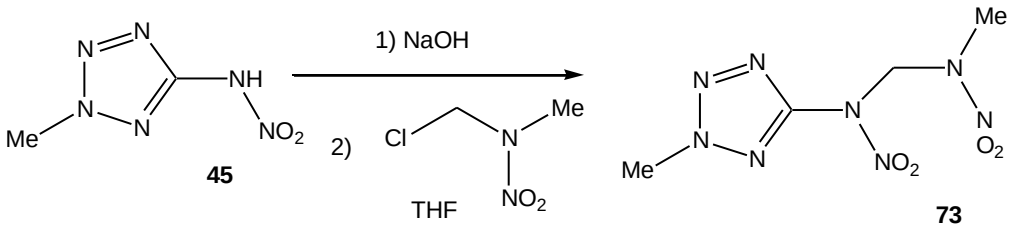

Scheme 6.2 Synthesis of 2-nitro-2-azapropyl-tetrazoles **66**–**73**.

1-(2-Nitro-2-azapropyl)-5-aminotetrazole (**66**) was synthesized by stirring a mixture of potassium 5-aminotetrazolate and 2-nitro-2-azapropyl chloride in acetone overnight. The potassium salt of 5-aminotetrazole was synthesized according to Chapter 2 using aqueous NaOH solution and recrystallized from ethanol. 1-(2-Nitro-2-azapropyl)-5*H*-tetrazole (**67**) was prepared analogue to **66** by using potassium tetrazolate. 1-(2-Nitro-2-azapropyl)-5-nitriminotetrazole (**68**) could successfully synthesized by using the monodeprotonated potassium salt of 5-nitriminotetrazole as suspension in THF. After the addition of **65**, the mixture was stirred at ambient temperature overnight.. It is important, that the potassium salt is used in more than double excess. In any case the potassium salt and the 2-nitro-2-azapropyl chloride were used in equimolar amounts, it was not possible to isolate one single product, but always a mixture of **68** and 2,5-bis(2-nitro-2-azapropyl)-nitriminotetrazole (**69**). Compound **68** could not be obtained in crystalline form without inclusion of any solvent. Recrystallization from water or wet methanol furnished the monohydrate **68a**, recrystallization from ethanol furnished the ethanol adduct **68b**. Compound **69** is synthesized best by stirring two equivalents of **65** with **43**, which is deprotonated *in situ* by two equivalents of triethyl amine. The reaction of potassium 1-methyl-5-nitriminotetrazolate [143] with **65** ended in three products. The main product, 1-methyl-5-(2-nitro-2-azapropyl)-5-nitraminotetrazole (**70**), was obtained in 60 % yield. The isomer 1-methyl-4-(2-nitro-2-azapropyl)-nitriminotetrazole (**71**) was obtained only in very low yield and was detected by its different crystal shape, while crystal picking of **70**. A third product (~12 % yield), 1-methyl-5-(2-nitro-2-azapropyl)-5-aminotetrazole (**72**) was obtained as colorless crystalline solid by allowing the mother liquor to stand for a few days. The mechanism of the formation of **72** could not be clarified, yet. The coupling reaction of **65** and 2-methyl-5-nitraminotetrazole (**45**) was carried out as suspension reaction with THF as solvent using one equivalent of triethyl amine as base. The mixture was not heated and after filtration and evaporation, 2-methyl-5-(2-nitro-2-azapropyl)-nitraminotetrazole (**73**) was obtained in 94 % yield. The synthesis using the potassium salt of 2-methyl-5-nitraminotetrazole was unsuccessful. With this, yellow oil was obtained, which could not be recrystallized.

The alkylation process of deprotonated **44** was investigated further by methylation of potassium 1-methyl-5-nitraminotetrazolate using dimethyl sulfate (**Scheme 6.3**). In contrast to the previously described alkylations of **44**, only one product, 1,4-dimethyl-5-nitriminotetrazole (**74**), could be isolated in high yields (85 %).

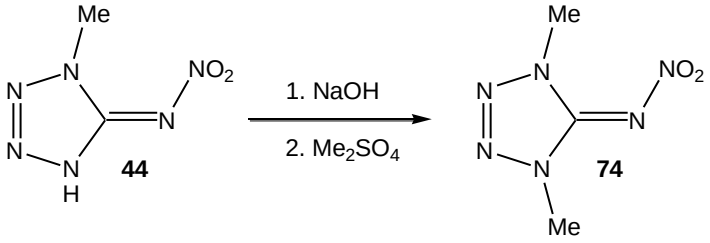

Scheme 6.3 Synthesis of 1,4-dimethyl-5-nitriminotetrazole (**74**)

6.3 Crystal Structures

Suitable single crystals of **66 - 74** were picked from the crystallization mixtures and were measured on an Oxford Xcalibur3 diffractometer. A detailed description of the molecular as well as the crystal structures is given in the following section.

6.3.1 1-(2-Nitro-2-azapropyl)-5-aminotetrazole (**66**)

1-(2-Nitro-2-azapropyl)-5-aminotetrazole (**66**) crystallizes in the monoclinic space group $P2_1/c$ with four molecules in the unit cell. The molecular moiety is depicted in **Figure 6.1**. The density of 1.628 g cm^{-3} is higher than that of 5-aminotetrazole monohydrate (**2**·H_2O).[60] Bond lengths can be found in **Table 6.1** and are comparable to those of **2**·H_2O. As a matter of course, the tetrazole ring is planar, (as observed in all structures in this work) building an aromatic 6π ring system. The distance C1–N5 (1.341(2) Å) is significantly shorter than that of a typical C–N single bond. The protons at the primary amine N5 are twisted only slightly (15–20°) out of the ring plane. The N1–C2 bond length of 1.459(2) Å follows exactly the distance of C–N single bonds. Nitrogen atom N6 is surrounded nearly trigonal planar, whereby also the nitro oxygen atoms lay in this plane. A weak intramolecular hydrogen bond is found between the atoms N5 and O1 (N5–H5B···O1: 0.89(2), 2.49(2), 3.165(2) Å, 134(3)°).

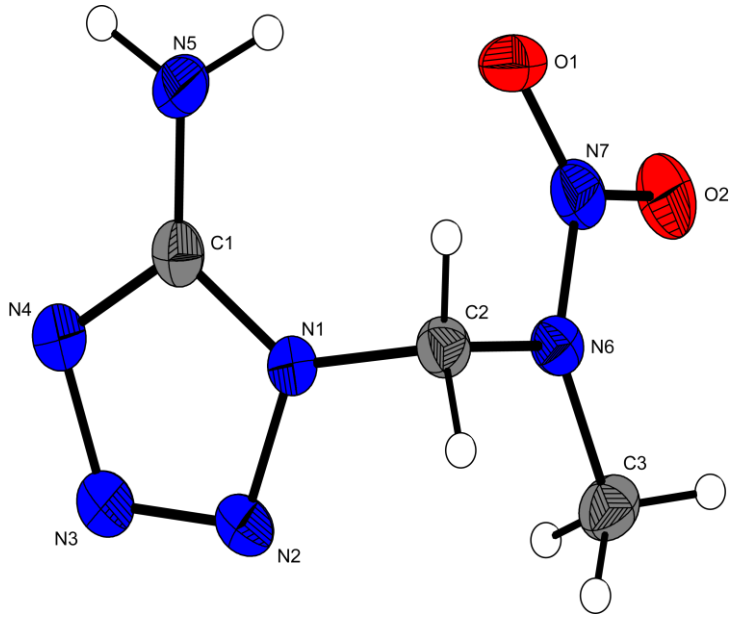

Figure 6.1 Molecular moiety of **66**. Ellipsoids of non-hydrogen atoms are drawn at the 50 % probability level.

The packing of **66** is characterized by a wave like pattern, which can be seen in **Figure 6.2**. This motive is fixed by the strong hydrogen bond N5–H5a···N4^{i} (0.90(2), 2.10(2), 2.987(2) Å, 169(2)°).

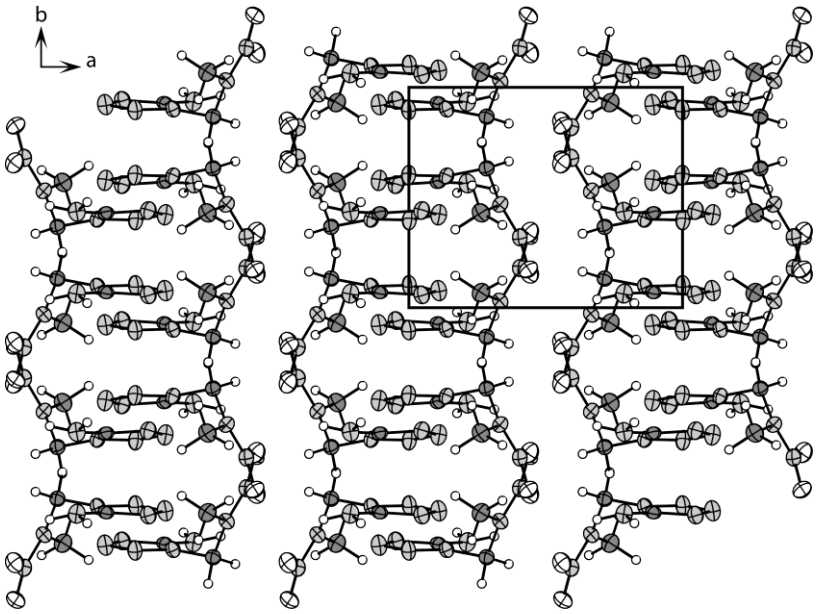

Figure 6.2 View on the packing of **66** along the *b* axis. One unit cell is marked.

6.3.2 1-(2-Nitro-2-azapropyl)- tetrazole (**67**)

1-(2-Nitro-2-azapropyl)-tetrazole (**67**) crystallizes in the chiral monoclinic space group $P2_1$ with two molecules in the unit cell. The density of 1.612 g cm^{-3} is only slightly lower than that of **8**, although no classical hydrogen bonds can be formed. However, the proton located at the carbon atom C1 is forming a weak non-classical H-bond (C1–H1···N1: 0.92(2), 2.66(2), 3.534(2) Å, 160(2)°). The molecular structure (**Figure 6.3**) is similar to that of **66**. Again, nitrogen atom N5 is enclosed trigonal planar (torsion angle C2–N5–N6–O2 = 178.6(1)°).

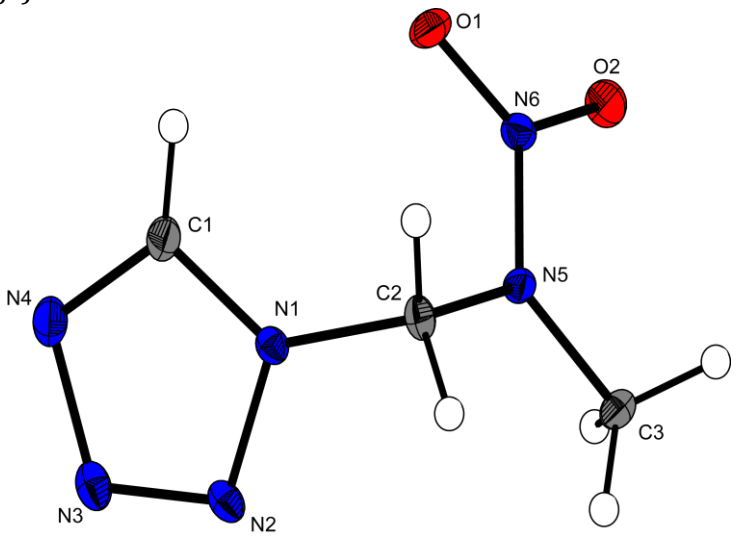

Figure 6.3 Molecular moiety of **67**. Ellipsoids of non-hydrogen atoms are drawn at the 50 % probability level.

6.3.3 1-(2-Nitro-2-azapropyl)-5-nitrimino-1*H*-tetrazole (**68**)

Compound **68** was only obtained crystalline with one molecule of water or ethanol, as shown in **Figure 6.4** and **Figure 6.5**. Both crystallize with densities of 1.746 g cm^{-3} (**68**·H_2O) and 1.562 g cm^{-3} (**68**·EtOH) in the space group $P2_1/c$ with four molecules in the unit cell. The molecular geometries are very similar and comparable to that of other 1-subtituted 5-nitriminotetrazoles, e.g. 1-methyl-5-nitriminotetrazole. The 2-nitro-2-azapropyl substituent follows the structure found in **66** and **67**. The remaining ring proton forms a very strong hydrogen bond to the crystal water (**Figure 6.4**) as well as to the ethanol oxygen atom (N4–H4···O5: 0.89(4), 1.79(4), 2.648(3) Å, 161(4)°) (**Figure 6.5**). This may explain that the solvent free compound was only obtained as colorless oil. The OH group of the ethanol forms on his part a strong hydrogen bond to one of the nitro oxygen atoms of a neighbored molecule (O5–H5···O1^{i}: 0.93(5), 2.01(5), 2.930(3) Å,

168(4)°; (i) 1–x, 1–y, 1–z). Also the water hydrogen atoms form strong hydrogen bonds to the atoms O2 and N5 of different neighbored molecules, which is a reason for the relatively high density observed for this compound.

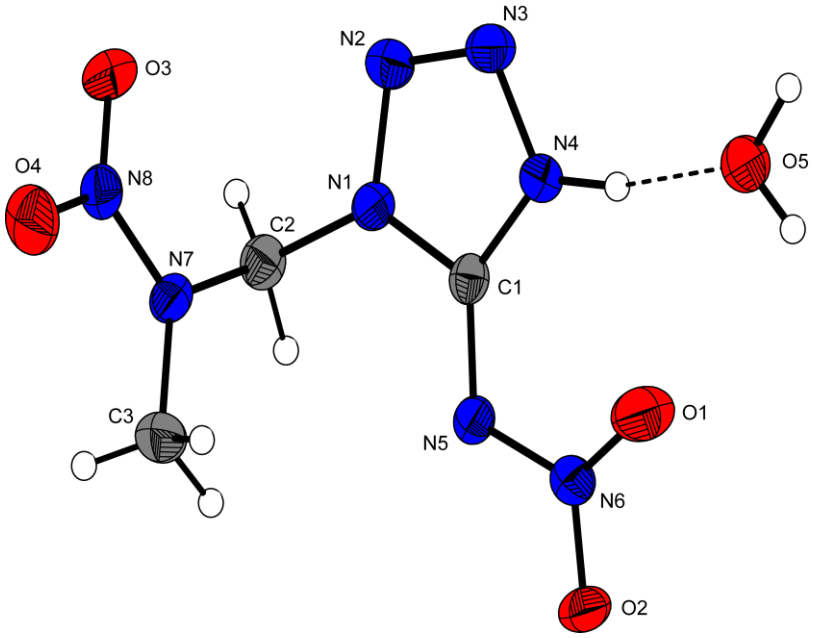

Figure 6.4 Molecular moiety of **68**·H_2O. Ellipsoids of non-hydrogen atoms are drawn at the 50 % probability level. Marked hydrogen bond: N4–H4···O5: 0.94(3), 1.77(3), 2.691(2) Å, 166(2)°.

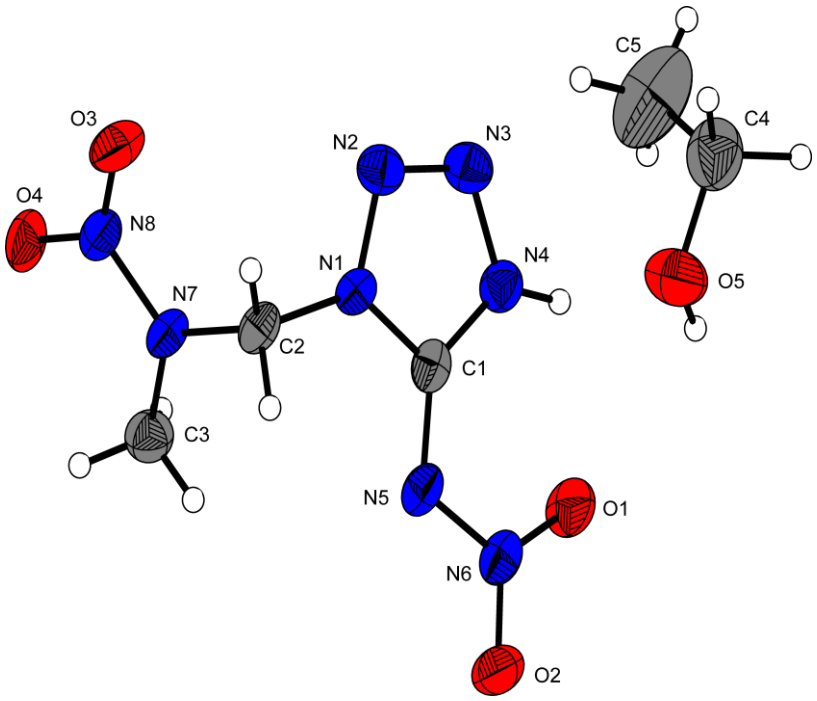

Figure 6.5 Molecular moiety of **68**·EtOH. Ellipsoids of non-hydrogen atoms are drawn at the 50 % probability level.

6.3.4 2,5-Bis(2-nitro-2-azapropyl)-5-nitraminotetrazole (**69**)

The doubly alkylated compound **69**, crystallizes in the monoclinic space group $P2_1$ with two molecules in the unit cell. No classical or non-classical hydrogen bonds can be found in the packing of **69**. However, the resulting density of 1.606 g cm^{-3} is in the range of the other structures discussed in this work. The molecular moiety is shown in **Figure 6.6**. Interestingly alkylation takes place at the nitrogen atoms N2 and N5. The structure of both 2-nitro-2-aza-propyl chains is nearly the same.

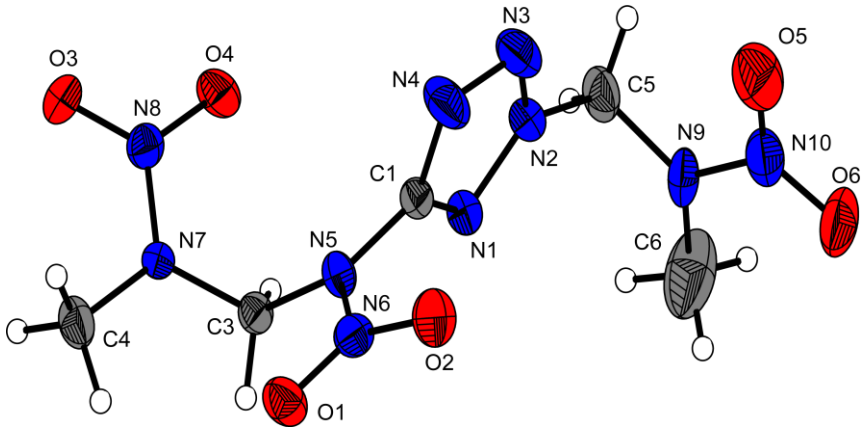

Figure 6.6 Molecular moiety of **69**. Ellipsoids of non-hydrogen atoms are drawn at the 50 % probability level. Selected distances not given in Table 6.1: N9–N10 = 1.353(3), N9–C4 = 1.424(4), N9–C5 = 1.435(4), N10–O5 = 1.213(3), N10–O6 = 1.220(3), C4–N2 = 1.455(4).

6.3.5 1-Methyl-5-(2-nitro-2-azapropyl)-5-nitraminotetrazole (**70**) and 1-Methyl-4-(2-nitro-2-azapropyl)-5-nitraminotetrazole (**71**)

The alkylation products of 1-methyl-5-nitriminotetrazole **70** and **71** crystallize in common space groups (**70**: $P2_1/c$, **71**: *Pbca*). The molecular structures (**Figure 6.7** and **Figure 6.8**) show significant differences. While in **70** the nitro group is strongly twisted out of the ring plane (torsion angle N1–C1–N5–N6 = –75.6(2)°) it is less twisted (N1–C1–N5–N6 = 39.3(6)°) in **71**. Also the C1–N5 bond lengths differ obviously. In the structure of **70** this bond of 1.399(2) Å is closer to a C–N single bond, while in **71** a distance (1.327(4) Å) closer to a C=N double bond is observed. The density of **71** (1.663 g cm^{-3}) is significantly higher than that of **70** (1.594 g cm^{-3}). It might be a general trend that 1,4-substituted nitriminotetrazoles have higher densities than 1,5-substituted ones,

which also can be observed by comparing 1,4-dimethyl-5-nitriminotetrazole (**74**, 1.536 g cm^{-3}) with 1,5-dimethyl-5-nitriminotetrazole (1.522 g cm^{-3}).[240,57]

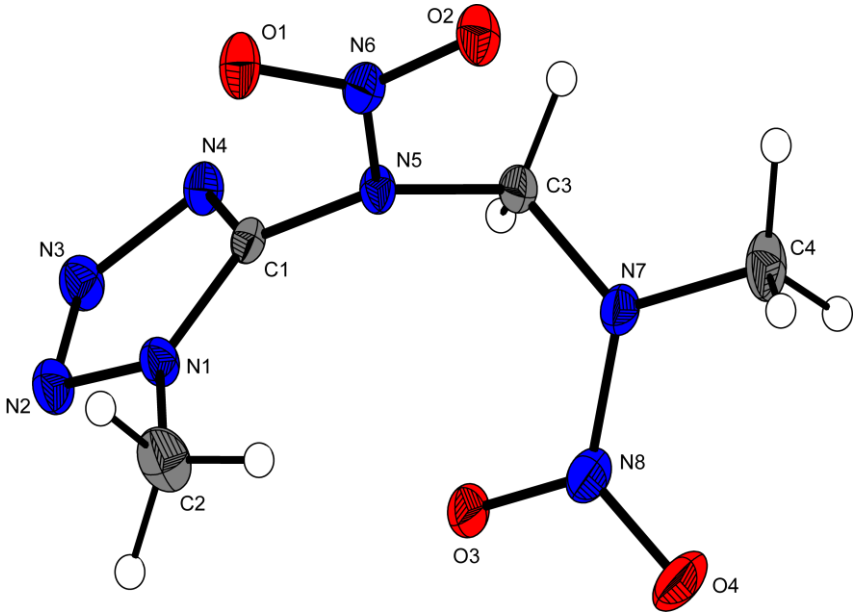

Figure 6.7 Molecular moiety of **70**. Ellipsoids of non-hydrogen atoms are drawn at the 50 % probability level.

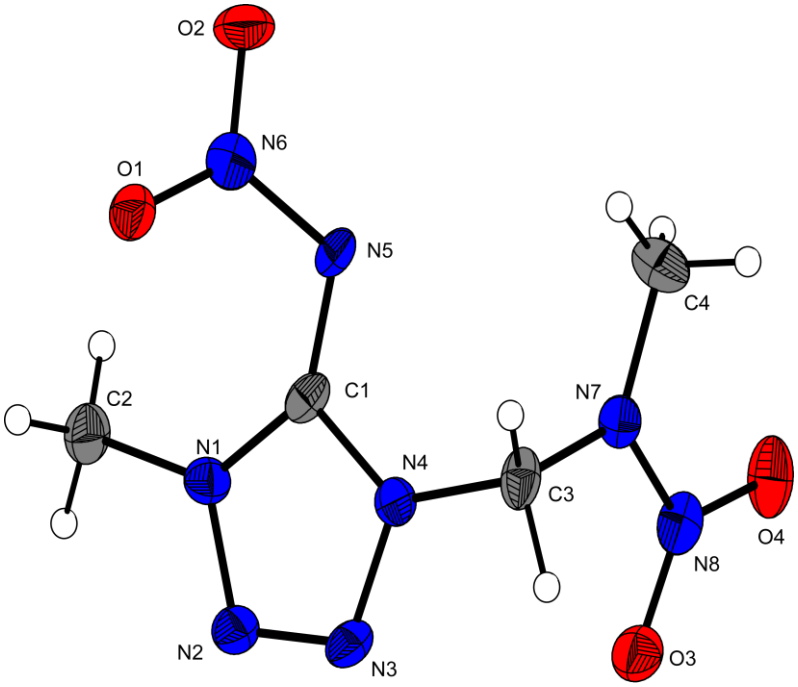

Figure 6.8 Molecular moiety of **71**. Ellipsoids of non-hydrogen atoms are drawn at the 50 % probability level.

6.3.6 1-Methyl-5-(2-nitro-2-azapropyl)-5-aminotetrazole (**72**)

The lowest density observed in this chapter was calculated for compound **72** (1.525 g cm^{-3}), which crystallizes in the monoclinic space group $P2_1/c$ with four molecules in the unit cell. The 2-nitro-2-azapropyl unit bonded (N5–C3 = 1.454(3) Å) at nitrogen atom N5 follows the constitution observed for the other structures discussed in this work. The left part in **Figure 6.9** is comparable to the structure of 1-methyl-5-aminotetrazole and its salts. The C1–N5 bond length of 1.347(3) Å is similar to this observed for **66**.

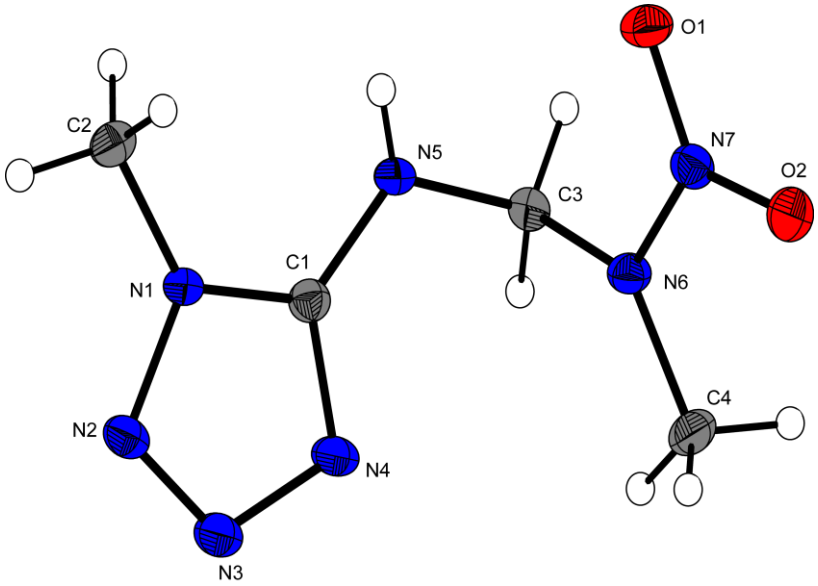

Figure 6.9 Molecular moiety of **72**. Ellipsoids of non-hydrogen atoms are drawn at the 50 % probability level.

6.3.7 2-Methyl-5-(2-nitro-2-azapropyl)-5-nitraminotetrazole (**73**)

Compound **73** crystallizes in the monoclinic space group $P2_1/c$ with four molecules in the unit cell. The density of 1.592 g cm^{-3} is similar to that observed for the corresponding 1-methyl compound **70** (1.596 g cm^{-3}). The molecular moiety is shown in **Figure 6.10**. The left part is in agreement to the structure observed for 2-methyl-5-aminotetrazole described by Bryden.[283] The N5–C1 bond length of 1.399(2) Å is also comparable to that of **70**. Therefore, **73** should be described as a "5-nitr*a*minotetrazole".

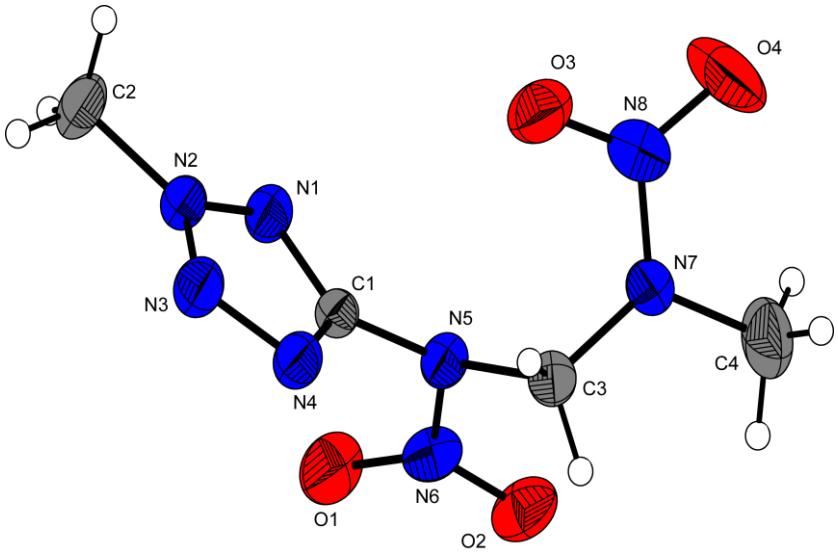

Figure 6.10 Molecular moiety of **73**. Ellipsoids of non-hydrogen atoms are drawn at the 50 % probability level.

6.3.8 1,4-Dimethyl-5-nitriminotetrazole (**74**)

1,4-Dimethyl-5-nitriminotetrazole crystallizes in the orthorhombic space group *Pbca* with 16 molecules in the unit cell. In **Figure 6.11** only one molecular moiety is shown.

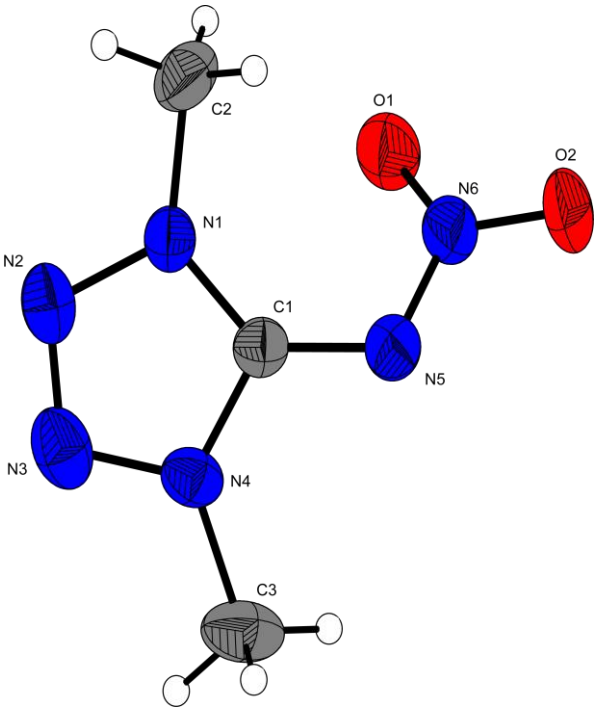

Figure 6.11 Molecular moiety of **74**. Ellipsoids of non-hydrogen atoms are drawn at the 50 % probability level.

Both methyl groups are bonded with the same distance of 1.458(3) Å (N1–C2) and 1.454(3) Å (N4–C3) to the tetrazole nitrogen atoms. The C1–N5 bond length of 1.341(2) Å is closer to a C=N double bond, which legitimates the nomenclature "nitrimine". The nitrimine group is strongly twisted out of the ring plane forming a torsion angle N4–C1–N5–N6 of 142.9(2)°. Since no hydrogen bonds can be formed the observed density of 1.536 g cm^{-3} is low in comparison with other 5-nitriminotetrazoles. For comparison, 5-nitriminotetrazole and 1-methyl-5-nitrimino-tetrazole show densities of 1.894 g cm^{-3} and 1.716 g cm^{-3}, respectively.

Table 6.1 Bond distances [Å] of compounds **66–74**.

Atoms	**66**	**67**	**68**·H_2O	**68**·EtOH	**69**	**70**	**71**	**72**	**73**	**74**
N1–N2	1.371(2)	1.351(2)	1.370(2)	1.364(3)	1.331(3)	1.345(2)	1.363(3)	1.365(2)	1.326(2)	1.358(2)
N2–N3	1.294(2)	1.295(2)	1.268(2)	1.279(3)	1.318(3)	1.311(2)	1.285(3)	1.292(2)	1.311(2)	1.282(2)
N3–N4	1.360(2)	1.373(2)	1.360(2)	1.355(3)	1.319(3)	1.362(2)	1.365(3)	1.366(2)	1.320(2)	1.354(2)
N5–N6			1.350(2)	1.358(3)	1.381(3)	1.395(2)	1.371(3)		1.403(2)	1.350(2)
N6–O1			1.243(2)	1.247(3)	1.219(3)	1.220(2)	1.252(3)		1.216(2)	1.241(2)
N6–O2			1.220(2)	1.225(3)	1.219(3)	1.223(2)	1.236(3)		1.214(2)	1.236(2)
N1–C1	1.339(2)	1.335(2)	1.356(2)	1.348(3)	1.320(3)	1.334(2)	1.354(4)	1.336(2)	1.318(2)	1.337(3)
N4–C1	1.330(2)	1.317(2)	1.335(2)	1.344(4)	1.334(3)	1.315(2)	1.348(4)	1.333(2)	1.336(2)	1.340(2)
N5–C1	1.341(2)		1.341(2)	1.341(3)	1.392(3)	1.399(2)	1.327(4)	1.353(2)	1.399(2)	1.347(3)
N1(4,5)–C2(3)	1.459(2)	1.464(2)	1.461(2)	1.463(3)	1.457(3)	1.458(2)	1.479(4)	1.436(3)	1.459(2)	1.454(3)
N1–Me						1.460(2)	1.464(5)	1.455(3)	1.456(2)	1.458(3)
C2(3)–N(NO_2)Me	1.445(2)	1.442(2)	1.438(2)	1.435(3)	1.439(3)	1.448(2)	1.434(4)	1.462(3)	1.440(2)	
N–NO_2	1.358(2)	1.340(1)	1.355(2)	1.355(3)	1.337(3)	1.347(2)	1.365(4)	1.344(2)	1.348(2)	
N(NO_2)–Me	1.468(2)	1.458(2)	1.457(2)	1.457(4)	1.457(3)	1.458(2)	1.460(5)	1.454(2)	1.446(3)	
N(Me)–O1(3)	1.233(2)	1.241(1)	1.229(2)	1.227(3)	1.230(2)	1.240(2)	1.239(3)	1.243(2)	1.234(2)	
N(Me)–O2(4)	1.231(2)	1.233(1)	1.228(2)	1.229(3)	1.236(2)	1.233(2)	1.230(3)	1.236(2)	1.218(2)	

6.4 Spectroscopy

6.4.1 Multinuclear NMR Spectroscopy

Compounds **66–73** were investigated using ^{1}H, $^{13}C\{^{1}H\}$, and ^{15}N or $^{15}N\{^{1}H\}$ NMR spectroscopy. The chemical shifts are given with respect to TMS (^{1}H, ^{13}C) as well as $MeNO_2$ (^{14}N, ^{15}N) as external standards. All spectra were measured in d_6-DMSO.

^{1}H NMR: Compared to the starting material **65**, all proton signals of the methylene group of **66–73** are strongly shifted downfield due to the coordination of the 2-nitro-2-azapropyl moiety to the electron withdrawing tetrazole ring system. They exhibit values of 6.06 ppm (**70**) to 6.81 ppm (**69**). Compound **69** contains two of the 2-nitro-2-azapropyl groups attached to the tetrazole ring. One exception from that rule is **72**, in which the 2-nitro-2-azapropyl moiety is attached to the 5-amino group of 1-methyl-5-aminotetrazole with a chemical shift of 5.21 ppm for CH_2 protons and a C–H coupling constant of 6.3 Hz. The same applies for the methyl group of the 2-nitro-2-azapropyl moiety with chemical shifts of 3.47 ppm to 3.55 ppm for **67–73**. The methyl group of **66** is shifted upfield to 3.13 ppm. The aromatic proton of **67** (9.58 ppm) is slightly shifted downfield compared to 1*H*-tetrazole (Chapter 11). The methyl protons directly attached to the tetrazole ring in **70**, **72** and **73** exhibit chemical shifts of 4.03 ppm, 3.71 ppm and 4.49 ppm, which is downfield of the chemical shifts for 1-methyl-5-aminotetrazole (3.69 ppm) and 2-methyl-5-aminotetrazole (4.07 ppm) respectively. In addition, for **68**·H_2O and **68**·EtOH the signals of water and ethanol can be seen with chemical shifts according to those for H_2O and EtOH as residual solvents in DMSO.

^{13}C NMR: The aromatic tetrazole carbon atoms exhibits chemical shifts between 145.2 ppm (**67**) and 159.5 ppm (**69**), with the trend to downfield shifted signals for the 2-substituted tetrazoles **69** and **73** of 159.5 ppm and 159.1 ppm, respectively, and upfield shifted signals for the 1-sustituted compounds **70** and **72** of 150.6 ppm and 155.7 ppm as well as for the unsubstituted **67** (145.2 ppm). Comparison of **66** and **68** allows the conclusion, that nitration of the 5-amino group at the tetrazole results in a significant upfield shift of the cyclic carbon atom (**66**: 156.2 ppm, **68**: 151.4 ppm). The chemical shifts for the methylene and the methyl group of the 2-nitro-2-azapropyl moiety are in the expected range of 59.6 ppm to 67.4 ppm for the methylene group and

39.0 ppm to 39.9 ppm for the methyl group, which are almost identical to the chemical shifts observed for the starting material, however slightly shifted downfield.

^{15}N NMR spectra of compounds **66–70**, as well as **72** and **73** can be seen in **Figure 6.12**. Although the ^{15}N NMR spectrum of **66** was measured proton decoupled all seven nitrogen atoms of **66** could clearly be assigned according to the ^{15}N NMR of 1-methyl-5-aminotetrazole.[284] Nitrogen atoms N3 (6.9 ppm) and N2 (–26.6 ppm) are shifted most to lower field due to two neighboring nitrogen atoms in the tetrazole ring. Atom N4 with one neighboring nitrogen atom and one carbon atom is shifted to –94.7 ppm, whereas the two nitrogen atoms neighbored by two carbon atoms, N1 and N6, are shifted to –176.2 ppm and –205.3 ppm with the higher shift for the nitramine nitrogen. The electron rich 5-amino-group is found at –335.9 ppm and the nitro group of the nitramine at –30.0 ppm.

A similar explanation also applies to the ^{15}N NMR spectra of **67–73**. Proton coupled ^{15}N NMR spectroscopy is more suitable for alkyl substituted tetrazoles, since the assignments can be done by evaluating the ^{2}J and ^{3}J coupling constants.. Thus, the assignments can be done by evaluating the ^{15}N–^{1}H coupling constants. Interestingly, in the case of the 2-nitro-2-azapropyl substituent only the ^{3}J coupling (triplet, ~1.5 Hz) can be observed significantly, while the ^{2}J coupling is hard to detect. All spectra are in agreement with similar ones found for 1- and 2-methyl-5-nitraminotetrazole (Chapter 4). There are strong similarities between the NMR spectra of **70**, **72,** and **73**, which only differ in the position of the methyl group (**70** and **73**) or concerning the nitro group at N5 (**70** and **72**). In all spectra, N3 is shifted downfield (9.9 ppm (**70**), 1.3 ppm (**72**)), and 1.4 ppm (**73**). The resonance of the nitrogen core N2 strongly varies depending on the substitution of the tetrazole ring. It exhibits chemical shifts of –5.5 ppm (**70**) and –20.3 ppm (**72**) for the 1-sustituted tetrazoles and is shifted to –101.6 ppm in the case of **73**, where the tetrazole ring is substituted in position 2. The chemical shifts of nitrogen atom N4 range from –53.4 ppm in **73** to –93.8 ppm in **72**, where it splits up into a doublet with a coupling constant of $^{3}J_{NH}$ = 2.2 Hz due to the coupling with the remaining proton of the 5-amino group. N4 in **70** can be assigned to the resonance at –57.8 ppm. The resonance of the 5-amino group of **72** exhibits a doublet with $^{1}J_{N-H}$ = 94 Hz at –324.4 ppm.

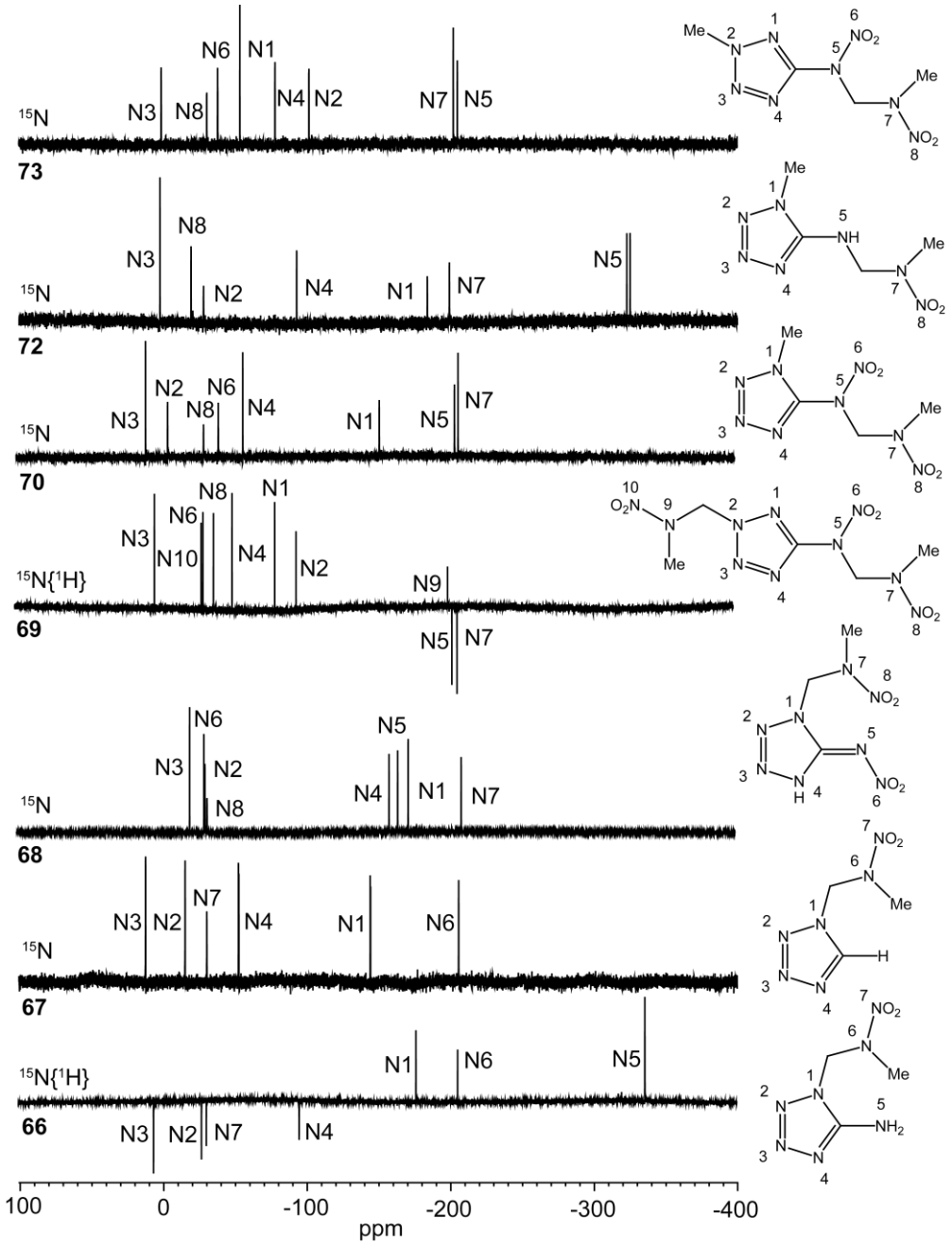

Figure 6.12 ^{15}N NMR spectra of **66**, **67**, **68**·H_2O, **69**, **70**, **72** and **73** measured in d_6-DMSO. δ (ppm): **66** = 6.9 (N3), –26.6 (N2), –30.0 (N7), –94.7 (N4), –176.2 (N1), –205.3 (N6), –333.9 (N5); **67** = 12.2 (N3), –15.3 (N2), –30.4 (N7), –52.6 (N4), –144.3 (N1), –205.9 (N6); **68**·H_2O = –20.2 (N3), –30.1 (N6), –30.8 (N2), –32.2 (N8), –159.1 (N4), –165.1 (N5), –172.4 (N1), –209.4 (N7); **69** = 2.9 (N3), –29.7 (N10), –30.9 (N6), –38.2 (N8), –51.2 (N4), –80.9 (N1), –95.7 (N2), –201.3 (N9), –204.2 (N5), –207.8 (N7); **70** = 9.9 (N3), –5.5 (N2), –30.4 (N8), –40.8 (N6), –57.8 (N4), –152.7 (N1), –205.0 (N7), –207.5 (N5); **72** = 1.3 (N3), –20.3 (N2), –29.0 (N8), –93.8 (N4), –184.5 (N4), –199.9 (N1), –324.4 (N5); **73** = 1.4 (N3), –30.4 (N8), –37.9 (N6), –53.4 (N4), –77.9 (N1), –101.6 (N2), –202.1 (N5), –204.9 (N7).

6.4.2 Vibrational Spectroscopy

Vibrational spectroscopy is adequate to identify 1-substituted 5-amino- as well as 5-nitriminotetrazoles. All absorptions measured were assigned according to commonly observed absorptions described in literature.[285,286,287]

The infrared and Raman spectra of **66–73** are mainly determined by the stretching and deformation vibrations of aliphatic methylene and methyl groups, nitro groups and vibrations of the tetrazole ring. The bands of the C–H stretching vibrations are located in the range of 3055–2837 cm^{-1}, whereas, three or four bands can be distinguished in all cases. Stretching and deformation vibrations of the tetrazole ring can be assigned to one distinct band, which is located within the range of 1020–1025 cm^{-1} and two or three further absorptions in the range from 1038 cm^{-1} to 1147 cm^{-1}. Apart from that, a different absorption of the tetrazole moiety is observed between 1265 cm^{-1} and 1320 cm^{-1}. The most characteristic absorptions, however, derive from the nitro-groups. Compounds **66**, **67** and **73** exhibit one set of absorptions each, which are located at 1297 cm^{-1} and 1521 cm^{-1} (**66**), 1281 cm^{-1} and 1533 cm^{-1} (**67**) and 1300 cm^{-1} and 1600 cm^{-1} (**73**). Compounds **68**·H_2O, **70** and **72**, having two nitro groups each, exhibit two sets of absorptions: 1265 cm^{-1}, 1525 cm^{-1}, 1295 cm^{-1} and 1577 cm^{-1} (**68**·H_2O), 1266 cm^{-1}, 1530 cm^{-1}, 1288 cm^{-1}, 1584 cm^{-1} (**70**) and 1261 cm^{-1}, 1531 cm^{-1}, 1282 cm^{-1} and 1585 cm^{-1} (**72**). For **69**, even three sets of nitro group absorptions can be seen according to the three nitramine units contained in the molecule. The absorptions are located in the same range given for the nitro groups discussed above. For **66**, the stretching and deformation vibration of the 5-amino group can be assigned additionally at 3424 cm^{-1} and 1646 cm^{-1}, respectively. The vibrations of the molecular units of **68**·H_2O and **68**·EtOH are almost equal and therefore not discussed separately. The most obvious difference is the O–H stretching vibration of the water molecule in the monohydrate **68**·H_2O at 3484 cm^{-1} and the O–H stretching vibration of the ethanol hydroxy group in **68**·H_2O at 3540 cm^{-1}. Compound **67** additionally exhibits absorption bands for the C_{ring}–H stretching and the deformation vibration at 3128 and 1479 cm^{-1}, respectively.

6.4.3 Mass Spectrometry

Mass spectra of the neutral compounds **66**–**73** were measured either in EI, DEI, FAB or ESI technique. All compounds measured could be clearly identified by the molecule peak $[M+H]^+$. Further fragments visible in all mass spectra are the 2-nitro-2-azapropyl fragment at *m/z* 89 and the azide moiety resulting from the cleavage of the tetrazole ring at *m/z* 43. In the cases of **70** and **67**, the remaining fragment $[M–NNO_2]^+$ can be seen at *m/z* 99.1, 157.2 and 112.1 respectively. The tetrazole ring $[CHN_4]^+$ at *m/z* 69.1 can be observed in the spectra of **66**, **67** and **70.** Often, the loss of one or even two nitro groups is observed, which exemplarily is discussed for compound **69**:

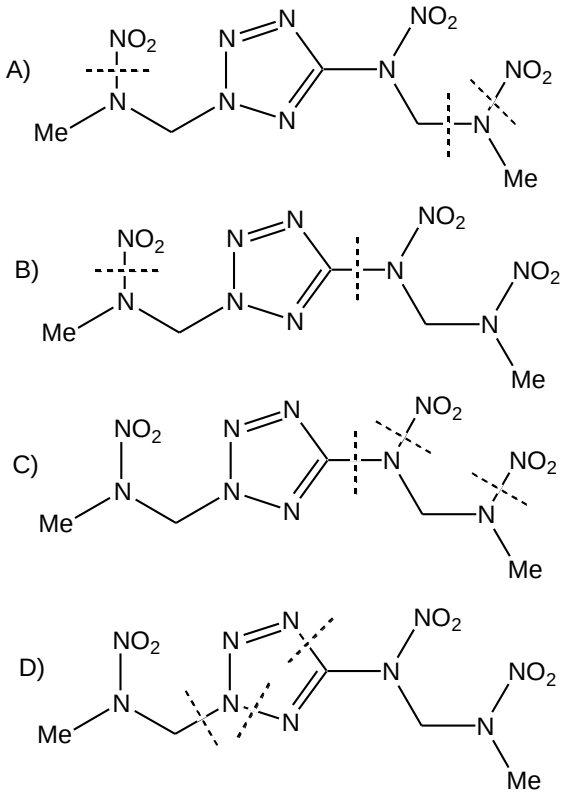

Figure 6.13 Possible fragmentation pattern of cleaving in the mass spectrum of **69**.

The molecule peak $[M+H]^+$ is observed at *m/z* 307.2. The successive cleavage of the three bonds, depicted in **Figure 6.13**, leads to three fragments at *m/z* 260.2 $[M–NO_2]^+$, 215.2 $[M+H–2NO_2]^+$ and *m/z* 186.2 $[M+H–CH_3NNO_2–NO_2]^+$. Different pathways are shown in the second and third fragmentation (B), (C) way. The loss of a nitro group and the cleavage of the C–N bond in position 5 of the tetrazole ring leads to the fragments at *m/z* 111.1 $[CN_4CH_2NCH_3]^+$ and *m/z* 57.1 $[CH_3NCH_2]^+$. Finally, the 2-nitro-2-azapropyl moiety is separated and the tetrazole ring is further fragmented (D) to yield the peaks at *m/z* 89.1 $[CH_3NNO_2CH_2]^+$ and at *m/z* 43.1 $[N_3]^+$.

6.5 Energetic Properties

6.5.1 Differential Scanning Calorimetry

Differential scanning calorimetry (DSC) measurements to determine the melting and decomposition temperatures of **66–73** (~1.5 mg of each energetic material) were performed in covered Al-containers containing a hole in the lid with a nitrogen flow of 20 mL/min on a Linseis PT10 DSC at a heating rate of 5 °C min^{-1}. The DSC plots in **Figure 6.14** show the thermal behavior in the 50–400 °C temperature range. Temperatures are given as onset temperatures.

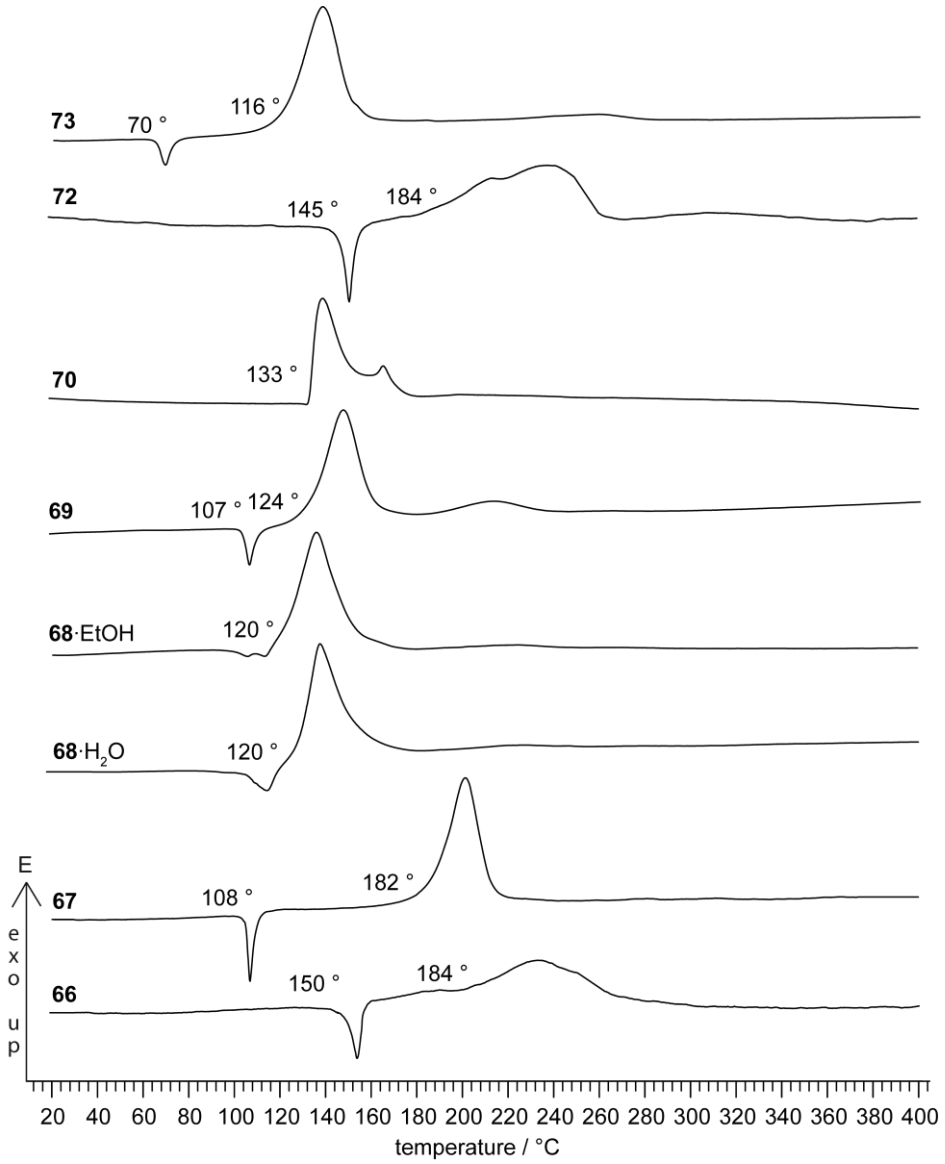

Figure 6.14 DSC thermograms (exo-up) of compounds **66–73** (heating rates: 5 °C min^{-1}).

The examined samples **66–73** exhibit decomposition temperatures between 116 °C and 184 °C. Apart from **70**, all compounds melt before decomposition and therefore have a definite liquidity range, which ranges e.g. for **67** more than 70 °C from melting to decomposition. The highest decomposition temperatures of 184 °C belong to **66** and **72**, which are the two 5-aminotetrazole derivatives. The amino group attached to the tetrazole ring stabilizes the compounds compared to those connected to the nitramine unit. All nitriminotetrazole compounds **68**·H_2O, **68**·EtOH **69**, **70**, and **73** have decomposition temperatures, which are far below those of **66, 67** and **72**. Comparing the two isomers **70** and **73**, the decomposition of **70** at 133 °C starts very precisely, whereas the decomposition peak of molten **73** is observed very broad. Also its melting point is observed much lower at 70 °C, which is the lowest melting point observed in this chapter.

6.5.2 Bomb Calorimetry

The heats of combustion of compounds **66–73** were determined experimentally using a Parr 1356 bomb calorimeter. The enthalpy of formation, $\Delta_f H°$, for each of the compounds was calculated at 298.15 K using Hess' law and the following combustion reaction.

$$C_nH_mN_xO_y + \left(n + \frac{m}{4} - \frac{y}{2}\right)O_2 \rightarrow nCO_2 + \frac{m}{2}H_2O + \frac{x}{2}N_2$$

The heats of formation of the combustion products H_2O (l) (–286 kJ mol^{-1}) and CO_2 (g) (–394 kJ mol^{-1}) were obtained from the literature.[288,289] The values for $\Delta_f H°$ as well as those for $\Delta_c H°$ are summarized in **Table 6.2**. The heats of formation for the synthesized compounds are in a broad range from even exothermic (–639 kJ mol^{-1}, **68**·EtOH) to strongly endothermic (+383 kJ mol^{-1}, **66**). The other tetrazole derivatives are all formed endothermically ($\Delta_f H°$ **67** = 286, **68**·H_2O = 18, **69** = 296, **70** = 254, **72** = 121, **73** = 333 kJ mol^{-1}).

The difference of isomers **73** and **70** is 81 kJ mol^{-1}. Usually, 2-substituted isomers are formed more endothermical (see Chapter4). However, this can also be due to measuring inaccuracies of the bomb calorimeter or while preparing the. The values for **68**·H_2O and **68**·EtOH are very low due to water or ethanol solvate molecules contained. Considering the molar heat of formation of gaseous water of 242 kJ mol^{-1}, the value for **68**·H_2O is in the range of the other compounds. From the experimentally determined heats of formation and X-ray densities, various thermochemical properties have been calculated using the EXPLO5 software (see below) and are summarized in **Table 6.2**.

6.5.3 Sensitivities

For initial safety testing, the impact and friction sensitivities as well as the electrostatic sensitivity were determined. The detailed values are summarized in **Table 6.2**. The only compound containing three nitramine groups (**69**) stands out with its low impact sensitivity of 2 J. The compounds containing two nitramine groups, one directly connected to the tetrazole ring and a second within the 2-nitro-2-azapropyl moiety fill the range between 5 J and 12 J, which are the methylated isomers **70** (5 J) and **73** (8 J) and on the other hand the unsubstituted homologues **68**·H_2O (12 J) and **68**·EtOH (10 J), which prospectively should be more sensitive, but as they crystallize with one molecule of water and ethanol respectively, the sensitivities are lower. Tetrazole **67** has an intermediate sensitivity of 15 J, whereas **66** and **72** are completely insensitive. The friction sensitivities vary from moderately sensitive to insensitive. Again, the molecules containing a nitriminotetrazole moiety are more sensitive. The electrostatic sensitivity tests were carried out using an electric spark tester ESD 2010EN (OZM Research) operating with the "Winspark 1.15 software package". The electrical spark sensitivities on crystalline material were determined to be 0.22 J (**66**), 1.45 J (**67**), 1.04 (**68**·H_2O), 0.75 (**68**·EtOH), 0.50 (**69**), 0.20 (**70**), 0.60 (**72**) and 0.07 (**73**). Except for the methyl substituted compounds **70** and **73**, all have values lower than commonly primary explosives ($Pb(N_3)_2$: 0.005 J) and secondary explosives (RDX: 0.2 J). It should be mentioned that the test towards electrical discharge strongly depends on the particle size and shape. Although we tried to use fine crystalline materials (75–125 µm) a guarantee for the determined values (especially value of **73**) cannot be given.

6.5.4 Detonation parameters

The calculation of the detonation parameters was performed with the program package EXPLO5 (version 5.02). Among the investigated compounds **66**, **67** and **68**·H_2O reveal detonation velocities significantly higher than 8000 ms^{-1}. Although showing detonation pressures of $p_{C\text{-}J}$ = 273 (**66**), 247 (**67**), and 281 kbar (**68**·H_2O) and an explosion temperature of more than 3500 K, the performance data are lower than those of RDX. The detonation velocities of **68**·EtOH, **69**, **70**, **72**, and **73** are below $V_{Det.}$ = 8000 ms^{-1}, but, however, succeeding easily the detonation parameter of TNT. A reason for the lower $p_{C\text{-}J}$ and $V_{Det.}$, in comparison to those of RDX, are the low densities observed for **66–73**.

The explosion temperatures seem to be associated with the amount of nitramine moieties contained in the molecule. The explosion temperature of **69**, containing three nitramine units almost reaches 4000 K (3905 K). The value of the highest explosion temperature is also associated with a very high explosion energy of 5470 kJ kg^{-1}. The explosion temperature of **72**, which is the methylated 5-aminotetrazole derivative is low (2644 K). The remaining values are spread over the range between 2700 K and 3700 K (except from **68**·EtOH) with the trend to higher temperatures for nitriminotetrazole derivatives (**70**: 3695 K; **73**: 3664 K).

Table 6.2 Physico-chemical properties of **66–70** as well as **72** and **73**.

	66	**67**	**68**·H_2O	**68**·EtOH	**69**	**70**	**72**	**73**
Formula	$C_3H_7N_7O_2$	$C_3H_6N_6O_2$	$C_3H_8N_8O_5$	$C_5H_{12}N_8O_5$	$C_5H_{10}N_{10}O_6$	$C_4H_8N_8O_4$	$C_4H_9N_7O_2$	$C_4H_8N_8O_4$
Molecular Mass [g mol^{-1}]	173.13	158.14	236.15	264.20	306.20	232.16	187.16	232.16
Impact sensitivity [J][a]	> 100	15	12	10	2	5	40	8
Friction sensitivity [N][b]	120	128	144	84	108	240	120	96
ESD–test [J]	0.22	1.45	1.04	0.75	0.50	0.20	0.60	0.065
N [%][c]	56.63	53.15	47.45	42.41	45.74	48.27	52.39	48.27
Ω [%][d]	–69.3	–70.8	–33.8	–66.6	–47.0	–55.1	–89.8	–55.1
$T_{dec.}$ [°C][e]	184	194	120	120	124	133	192	116
Density [g cm^{-3}][f]	1.628	1.612	1.746	1.562	1.606	1.663	1.525	1.592
$-\Delta U_{comb}$ [cal g^{-1}][g]	3547	3520	2380	2760	2892	3068	3812	3149
$-\Delta H_{comb}°$ [kJ mol^{-1}][h]	2564	2324	2342	3044	3694	2972	2982	3051
$\Delta_f H_m°$ [kJ mol^{-1}][i]	383	286	18	–639	296	254	121	333
$-\Delta_E U°$ [kJ kg^{-1}][j]	5368	5341	4971	2374	5470	5285	3775	5569
T_E [K][k]	3554	3494	3594	2025	3905	3695	2644	3882
$p_{C\text{-}J}$ [kbar][l]	273	247	281	138	245	254	194	243
$V_{Det.}$ [m s^{-1}][m]	8467	8085	8311	6408	7936	7977	7542	7902
Gas vol. [L kg^{-1}][n]	802	776	822	804	791	780	798	783

[a] BAM drophammer, grain size (75–150 µm); [b] BAM friction tester, grain size (75–150 µm); [c] Nitrogen content; [d] Oxygen balance; [e] Temperature of decomposition by DSC (β = 5 °C); [f] estimated from a structure determination; [g] Experimental (constant volume) combustion energy; [h] Experimental molar enthalpy of combustion; [i] Molar enthalpy of formation; [j] Energy of Explosion; [k] Explosion temperature; [l] Detonation pressure; [m] Detonation velocity; [n] Assuming only gaseous products.

6.6 Experimental

*CAUTION! The prepared tetrazoles **66–74** and their starting materials are energetic compounds with increased sensitivities against heat, impact and friction. Although we had no problems in synthesis, proper protective measures (safety glasses, face shield, leather coat, earthened equipment and shoes, Kevlar® gloves and ear plugs) should be used during work on **66–74**.*

*2-Nitro-2-azapropyl acetate (**64**):* The reaction was carried out according to modified procedure described in the literature.[281] A 500 mL three-necked reaction flask equipped with a thermometer and a dropping funnel was charged with acetic anhydride (88 mL, 936 mmol) and cooled to 0°C with an ice bath. Fuming nitric acid (28 mL, 666 mmol) was slowly added taking care, that the temperature does not exceed 5 °C for the reaction is somewhat exothermic. To the reaction mixture a solution of 1,3,5-trimethylhexahydro-1,3,5-triazine (25.2 mL, 184 mmol) in glacial acetic acid (25 mL, 436 mmol) was added drop wise within 1 hour before it was heated to 70–75 °C under refluxing conditions for 1 hour. The mixture was allowed to cool down to room temperature, 100 mL of water were added and it was extracted with dichloromethane (8 x 25 mL). Either the organic and the aqueous phase was nearly neutralized (pH 6) with ammonium carbonate, the organic phase was washed with 100 mL of water and the combined aqueous phases were again extracted with dichloromethane (4 x 25 mL). The organic phases were dried over magnesium sulfate, the solvent was removed in a rotary evaporator and the crude product was distilled under reduced pressure (3 mbar, 89 °C) to give 50.20 g (61% yield) of 2-nitro-2-azapropyl acetate as a colorless liquid. **IR** (KBr, cm^{-1}): $\tilde{\nu}$ = 3482 (w), 2996 (m), 2955 (m), 1751 (vs), 1547 (vs), 1470 (s), 1431 (s), 1630 (s), 1393 (s), 1369 (s), 1301 (s), 1214 (s), 1126 (m), 1017 (s), 958 (s), 857 (m), 829 (m), 770 (m), 681 (m), 647 (w), 603 (m), 495 (m); **^{1}H NMR** ($CDCl_3$, 25 °C, ppm): δ = 5.68 (s, CH_2), 3.41 (s, $H_3C–N(NO_2)$), 2.09 (s, $H_3C–C(O)O$); **^{13}C NMR** ($CDCl_3$, 25 °C, ppm): δ = 170.6($C(O)CH_3$), 72.8 (CH_2), 38.6 ($H_3C–N(NO_2)$), 20.6 ($C(O)CH_3$).

*2-Nitro-2-azapropyl chloride (**65**):* The reaction was carried out according to modified procedure described in the literature.[282] A 250 mL reaction flask was charged with 2-nitro-2-azapropyl acetate (24.7 g, 167 mmol), glacial acetic acid (0.7 mL, 12.3 mmol), conc. H_2SO_4 (2 drops) and 35 mL of dichloromethane and thionyl chloride (23.4 g,

334 mmol) was added dropwise over a period of 90 minutes. The mixture was then heated to 40–45 °C under refluxing conditions for 1 hour, before the solvent was removed under reduced pressure. For purification the pale yellow oil was distilled in vacuum (2 mbar, 48 °C) to give 2-nitro-2-azapropyl chloride (18.14 g, 87% yield) as a colorless liquid. **^{1}H NMR** ($CDCl_3$, 25 °C, ppm): δ = 5.60 (s, CH_2), 3.38 (s, $H_3C–N(NO_2)$; **^{13}C NMR** ($CDCl_3$, 25 °C, ppm): δ = 60.4(CH_2Cl), 37.6 (CH_3).

*1-(2-Nitro2-azapropyl)-5-aminotetrazole (**66**):* 5-Aminotetrazole (17.0 g, 200 mmol) is suspended in a solution of 100 mL water and 13.2 g, 200 mmol) KOH (85%). The suspension is heated to 50°C and the 5-aminotetrazole is dissolved. Evaporation of the solvent gives the potassium-5-aminotetrazolate in quantitative yields. The pale yellow solid can be recrystallized from water/ethanol with 92% yield (22.7 g). The potassium 5-aminotetrazolate (7.39 g, 60 mmol) is suspended in 50 mL of acetone and the 2-nitro-2-azapropyl chloride (8.22 g, 66 mmol) is slowly added through a dropping funnel. The suspension is stirred overnight, filtered off and the solid is washed with warm acetone. The solvent is removed in a rotary evaporator and a yellowish solid remains, which is recrystallized from hot ethanol to give 6.02 g of **66** (58 % yield). **DSC** (T_{onset}, 5 °C min^{-1}): 147–153 °C (mp.), 184 °C (dec.); **IR** (KBr, cm^{-1}): $\tilde{\nu}$ = 3424 (s), 3300 (m), 3134 (m), 3097 (m), 2721 (s), 1646 (s), 1579 (s), 1521 (vs), 1472 (m), 1446 (m), 1424 (m), 1387 (w), 1354 (m), 1297 (s), 1261 (s), 1206 (s), 1116 (m), 1074 (m), 1021 (m), 992 (m), 927 (w), 846 (w), 795 (m), 764 (m), 740 (w), 719 (w), 680 (m), 654 (m), 604 (w), 485 (w); **Raman** (1064 nm, 400 mW, 25 °C, cm^{-1}): $\tilde{\nu}$ = 3038 (36), 2995 (42), 2964 (36), 1648 (10), 1582 (14), 1529 (10), 1443 (27), 1424 (21), 1356 (23), 1318 (29), 1262 (50), 1128 (18), 1094 (14), 1070 (14), 1021 (15), 928 (17), 849 (100), 793 (57), 655 (14), 603 (22), 445 (27), 398 (23), 304 (19), 235 (27); **^{1}H NMR** (d_6-DMSO, 25 °C, ppm): δ = 6.98 (s, NH_2), 6.14 (s, CH_2), 3.13 (s, CH_3); **^{13}C NMR** (d_6-DMSO, 25 °C, ppm): δ = 156.2 (CN_4), 59.6 (CH_2), 39.4 (s, CH_3); **^{15}N NMR** (d_6-DMSO, 25 °C, ppm): δ = 6.9 (N3), –26.6 (N2), –30.0 (N7), –94.7 (N4), –176.2 (N1), –205.3 (N6), –333.9 (N5); ***m/z*** (DEI): 173.1 $[M]^+$; **EA** ($C_3H_7N_7O_2$, 173.13) calcd.: C 20.81, H 4.08, N 56.63; found: C 22.14, H 4.25, N 55.09; **impact sensitivity**: > 100 J (neg.); **friction sensitivity**: > 120 N; **ESD**: > 0.22 J; **RADEX** (130 °C, 50 h): no decomposition.

*1-(2-Nitro-2-azapropyl)-tetrazole (**67**):* 1*H*-Tetrazole (700.5 mg, 10 mmol) was suspended in a solution of KOH (85 %) (660.1 mg, 10 mmol) in 15 mL of water. The tetrazole is dissolved and after evaporation of the water under reduced pressure, the

potassium tetrazolate formed as a colorless solid. The potassium tetrazolate was directly suspended in 20 mL of acetone without being recrystallized. To this suspension, 2-nitro-2-azapropyl chloride (1.245 g, 10 mmol) which previously was dissolved in a few milliliters of acetone, was added drop wise. After being stirred overnight, the suspension was heated to reflux for 1 hour and filtered off afterwards. The acetone was removed under reduced pressure and the remaining solid was recrystallized from ethanol to give 1.17 g (74% yield) **67** as colorless crystals. **DSC** (T_{onset}, 5 °C min^{-1}): 108 °C (mp.), 182 °C (dec.); **IR** (KBr, cm^{-1}): $\tilde{\nu}$ = 3450 (vs), 3128 (m), 3051 (w), 1634 (m), 1533 (m), 1479 (m), 1383 (w), 1341 (w), 1303 (m), 1281 (m), 1168 (m), 1096 (m), 1038 (w), 959 (w), 885 (w), 854 (w), 766 (m), 750 (m), 718 (w), 672 (m), 614 (m); **Raman** (1064 nm, 350 mW, 25 °C, cm^{-1}): $\tilde{\nu}$ = 3127 (33), 3050 (37), 3003 (65), 2959 (36), 1529 (22), 1478 (26), 1448 (33), 1428 (35), 1410 (37), 1374 (27), 1335 (31), 1294 (53), 1264 (34), 1169 (36), 1095 (36), 1038 (29), 1012 (61), 852 (100), 750 (33), 641 (27), 613 (38), 444 (31), 407 (24), 352 (24), 265 (24), 209 (19); **^{1}H NMR** (d_6-DMSO, 25 °C, ppm): δ = 9.58 (s, N_4CH), 6.46 (s, CH_2), 3.52 (s, CH_3); **^{13}C NMR** (d_6-DMSO, 25 °C, ppm): δ = 145.2 (CN_4), 61.9 (CH_2), 39.5 (CH_3); **^{15}N NMR** (d_6-DMSO, 25 °C, ppm): δ = 12.2 (N3), –15.3 (N2), –30.4 (N6), –52.6 (N4), –144.3 (N1), –205.9 (N5); ***m/z*** (FAB$^+$): 159.2 $[M+H]^+$; **EA** ($C_3H_6N_6O_2$, 158.12) calcd.: C 22.79, H 3.82, N 53.15 %; found: C 22.71, H 3.57, N 52.47 %; **impact sensitivity**: > 15 J; **friction sensitivity:** > 128 N; **ESD**: > 1.45 J.

*1-(2-Nitro-2-azapropyl)-5-nitriminotetrazole monohydrate (**68**·H_2O)*: 5-Nitrimino-tetrazole (4.43 g, 34 mmol) was suspended in an ethanolic solution of KOH (85%, 2.25 g, 34 mmol) and stirred for 15 minutes. The suspension was filtered off, the solid dried to give 5.27 g (31.5 mmol, 92%) of potassium 5-nitriminotetrazolate. The salt was suspended in 50 mL of THF and 2-nitro-2-azapropyl chloride (1.87 g, 15 mmol), previously dissolved in 25 mL of THF, was added drop wise. The suspension was stirred at room temperature overnight and the remaining solid, consisting of potassium 5-nitriminotetrazolate and potassium chloride, was filtered off. The THF was removed from the filtrate under reduced pressure, the remaining colorless oil was dissolved in a small amount of water/ethanol for recrystallization to give **68**·H_2O as colorless crystals in 22% yield (783 mg, 3.3 mmol). **DSC** (T_{onset}, 5 °C min^{-1}): 112–118 °C (mp.), 120 °C (dec.); **IR** (KBr, cm^{-1}): $\tilde{\nu}$ = 3484 (m), 3049 (w), 1577 (vs), 1554 (s), 1525 (m), 1450 (m), 1408 (m), 1337 (m), 1295 (s), 1265 (s), 1201 (m), 1135 (m), 1113 (w), 1083 (m), 1022 (m), 1007 (m), 916 (m), 799 (m), 765 (m), 746 (m), 686 (w), 673 (w), 643 (m), 607 (m); **Raman** (1064 nm, 300 mW, 25 °C, cm^{-1}): $\tilde{\nu}$ = 3051 (37), 2995 (66), 2962 (43), 1585

(58), 1560 (22), 1526 (55), 1441 (31), 1424 (45), 1400 (42), 1293 (49), 1264 (100), 1133 (11), 1059 (28), 1009 (40), 987 (46), 883 (24), 869 (41), 850 (68), 758 (50), 748 (36), 707 (28), 604 (34), 496 (33), 421 (22), 394 (24), 318 (25), 257 (46), 239 (28); **^{1}H NMR** (d_6-DMSO, 25 °C, ppm): δ = 9.78 (s, NH), 6.12 (s, CH_2), 3.50 (s, CH_3), 3.43 (s, H_2O); **^{13}C NMR** (d_6-DMSO, 25 °C, ppm): δ = 151.4 (CN_4), 61.2 (CH_2), 39.8 (CH_3); **^{15}N NMR** (d_6-DMSO, 25 °C, ppm): δ = –20.2 (N3), –30.1 (NO_2, N6), –30.8 (N2, t, $^{3}J_{N-H}$ = 1.5 Hz), –32.2 (NO_2, N8, m), –159.1 (N4), –165.1 (N5), –172.4 (N1), –209.4 (N7); ***m/z*** (FAB$^+$): 219.2 $[M+H]^+$; **EA** ($C_3H_8N_8O_5$, 236.15) calcd.: C 15.26, H 3.41, N 47.45 %; found: C 15.74, H 3.67, N 47.59 %; **impact sensitivity**: > 12 J; **friction sensitivity**: > 144 N; **ESD**: > 1.04 J.

*1-(2-Nitro-2-azapropyl)-5-nitriminotetrazole · EtOH (**68**·EtOH):* Nitriminotetrazole (3.96 g, 30.5 mmol) is dissolved in 50 mL of THF and triethyl amine (3.08 g, 30.5 mmol) are slowly added to the solution. A white precipitate, which immediately forms, disappears after a few seconds. 2-Nitro-2-azapropyl chloride (1.87 g, 15 mmol) is dissolved in 25 mL of THF and slowly added through a dropping funnel over a period of 1 hour. A white, crystalline precipitate of triethylammonium chloride is formed. The reaction is stirred overnight, the precipitate is filtered off and the solvent is removed from the filtrate. A pale yellow oil is remaining, which was dried under vacuum and taken up in ethanol for recrystallization to give 1.76 g of **68**·EtOH as colorless crystals (22 % yield). The product achieved from the reaction crystallizes with one equivalent of ethanol as solvate as X-ray single crystal structure studies showed. **DSC** (T_{onset}, 5 °C min^{-1}): 112–118 °C (mp.), 120°C (dec.); **IR** (KBr, cm^{-1}): $\tilde{\nu}$ = 3540 (s), 3488 (s), 3051 (m), 2826 (m), 2737 (m), 2663 (m), 1634 (m), 1586 (vs), 1525 (vs), 1442 (m), 1497 (vs), 1439 (s), 1397 (m), 1356 (s), 1311 (s), 1283 (s), 1260 (s), 1207 (s), 1108 (w), 1057 (m), 1007 (s), 927 (m), 884 (w), 777 (m), 761 (m), 748 (m), 705 (m), 602 (m), 576 (m), 475 (w); **Raman** (1064 nm, 300 mW, 25 °C, cm^{-1}): $\tilde{\nu}$ = 3072 (14), 3005 (37), 2970 (36), 2927 (30), 1571 (100), 1453 (37), 1416 (48), 1260 (80), 1056 (30), 1035 (32), 1064 (100), 984 (44), 876 (32), 850 (61), 757 (71), 709 (24), 604 (14), 487 (25), 252 (32); **^{1}H NMR** (d_6-DMSO, 25 °C, ppm): δ = 9.78 (s, NH), 6.12 (s, CH_2), 3.50 (s, CH_3), 3.44 (q, J = 6.8 Hz, CH_2OH), 1.05 (t, J = 6.8 Hz, CH_3); **^{13}C NMR** (d_6-DMSO, 25 °C, ppm): δ = 151.4 (CN_4), 61.2 (CH_2), 56.6 (CH_2OH), 39.8 (CH_3), 19.0 (CH_3CH_2OH); ***m/z*** (FAB$^+$): 219.2 $[M+H]^+$; **EA** ($C_5H_{12}N_8O_5$, 264.20) calcd.: C 22.73, H 4.58, N 42.41 %; found: C 20.32, H 4.13, N 43.79 %; **impact sensitivity**: > 10 J; **friction sensitivity**: > 84 N; **ESD**: > 0.75 J.

*2,5-(Bis(2-nitro-2-azapropyl)-nitriminotetrazole (**69**):* 5-Nitriminotetrazole (1.30 g, 10 mmol) was dissolved in 40 mL of THF and triethyl amine (2.02 g, 20 mmol) was added dropwise. A white precipitate, which formed at first, dissolves again after a few seconds. 2-Nitro-2-azapropyl chloride is dissolved in 10 mL of THF and slowly added to the reaction mixture through a dropping funnel. A white precipitate of triethylammonium chloride starts to form. The mixture is further stirred overnight, the precipitate is filtered off and the solvent is evaporated from the filtrate to give a yellow, viscous oil. After a few hours, in the oil the product started to crystallize. The oil/crystal-mixture was vigorously stirred with a small amount of ethanol for 2 hours and a white crystalline product could be filtered off. It was recrystallized from ethanol to give 1.27 g (42% yield) of **69**. **DSC** (T_{onset}, 5 °C min^{-1}): 107 °C (mp.), 124 °C (dec.); **IR** (KBr, cm^{-1}): $\tilde{\nu}$ = 3448 (m), 3048 (m), 2999 (w), 2960 (w), 1577 (vs), 1553 (vs), 1449 (s), 1408 (s), 1295 (vs), 1267 (vs), 1201 (s), 1135 (s), 1114 (m), 1083 (s), 1023 (s), 943 (m), 917 (s), 852 (w), 799 (s), 766 (s), 746 (s), 686 (m), 674 (m), 643 (s), 608 (s), 460 (w), 419 (m); **Raman** (1064 nm, 350 mW, 25 °C, cm^{-1}): $\tilde{\nu}$ = 3050 (52), 3000 (57), 2962 (44), 2900 (13), 1588 (14), 1559 (20), 1526 (78), 1449 (29), 1401 (34), 1345 (24), 1294 (64), 1269 (33), 1010 (50), 943 (17), 919 (18), 869 (85), 855 (100), 606 (29), 460 (19), 422 (18), 385 (14), 316 (19), 239 (30); **^{1}H NMR** (*d*$_6$-DMSO, 25 °C, ppm): δ = 6.81 (s, 2–CH_2), 6.10 (s, 5–CH_2), 3.55 (s, 5–$H_3CN(NO_2)$), 3.47 (s, 2–$H_3CN(NO_2)$); **^{13}C NMR** (*d*$_6$-DMSO, 25 °C, ppm): δ = 159.5 (CN_4), 67.4 (5–CH_2), 67.0 (2–CH_2), 39.8 (5–$H_3CN(NO_2)$), 39.4 (2–$H_3CN(NO_2)$); **^{15}N NMR** (*d*$_6$-DMSO, 25 °C, ppm): δ = 2.9 (N3), –29.7 (NO_2, N10), –30.9 (NO_2, N6), –38.2 (NO_2, N8), –51.2 (N4), –80.9 (N1), –95.7 (N2), –201.3 (NNO_2(9)), –204.2 (NNO_2, N5), –207.8 (NNO_2, N7); ***m/z*** (FAB$^+$): 307.2 $[M+H]^+$; **EA** ($C_5H_{10}N_{10}O_6$, 306.20) calcd.: C 19.61, H 3.29, N 45.74 %; found: C 19.81, H 3.26, N 46.85 %; **impact sensitivity**: > 2 J; **friction sensitivity**: > 108 N; **ESD**: > 0.50 J.

*1-Methyl-5-(2-nitro-2-azapropyl)-nitriminotetrazole (**70**):* 1-Methyl-5-nitriminotetrazole (4.32 g, 30 mmol) was dissolved in a KOH solution (prepared from 1.98 g KOH (85 %) and 50 mL of water), the water was evaporated and the potassium 1-methyl-5-nitriminotetrazolate (5.47 g, 30 mmol) was used for the coupling reaction with 2-nitro-2-azapropyl chloride without recrystallization. The potassium salt was suspended in 25 mL of acetone and 2-nitro-2-azapropyl chloride (4.11 g, 33 mmol), dissolved in 10 mL of acetone, was added drop wise to the suspension. The mixture was stirred overnight, refluxed for 90 minutes and filtered off. The solvent was removed from the filtrate in vacuum which afforded more than 7 g of a yellow oil. The oil was taken up in

hot ethanol and recrystallized, which yielded 4.18 g (60 % yield) of **70** as colorless crystals. In the crystallization mixture also a few crystals of **71** were detected. **DSC** (T_{onset}, 5 °C min^{-1}): 133 °C (dec.); **IR** (KBr, cm^{-1}): $\tilde{\nu}$ = 3432 (m), 3051 (w), 3034 (w), 1584 (vs), 1530 (s), 1480 (m), 1449 (m), 1408 (m), 1390 (m), 1288 (vs), 1266 (s), 1123 (m), 1092 (m), 1015 (m), 913 (m), 855 (w), 766 (m), 748 (m), 700 (m), 659 (w), 643 (m), 604 (m); **Raman** (1064 nm, 350 mW, 25 °C, cm^{-1}): $\tilde{\nu}$ = 3035 (21), 2970 (45), 1545 (39), 1449 (14), 1414 (23), 1309 (23), 1264 (23), 988 (12), 916 (12), 857 (93), 799 (20), 700 (37), 660 (16), 644 (10), 606 (26), 491 (20), 474 (24), 388 (12), 303 (13), 176 (12); **^{1}H NMR** (*d*$_6$-DMSO, 25 °C, ppm): δ = 6.06 (s, CH_2), 4.03 (s, $H_3CN(NO_2)$), 3.51 (s, CH_3); **^{13}C NMR** (*d*$_6$-DMSO, 25 °C, ppm): δ = 150.6 (CN_4), 67.6 (CH_2), 39.9 ($H_3CN(NO_2)$), 34.7 (CH_3); **^{15}N NMR** (*d*$_6$-DMSO, 25 °C, ppm): δ = 9.9 (N3), –5.5 (N2, q, $^3J_{N-H}$ = 1.9 Hz), –30.4 (N8, NO_2), –40.8 (N6, NO_2), –57.8 (N4), –152.7 (N1, q, $^2J_{N-H}$ = 2.3 Hz), –295.0 (N7), –207.5 (N5); ***m/z*** (DEI$^+$): 233.3 $[M+H]^+$; **EA** ($C_4H_8N_8O_4$, 232.16) calcd.: C 20.69, H 3.47, N 48.27 %; found: C 20.23, H 2.86, N 47.62 %; **impact sensitivity**: > 5 J; **friction sensitivity**: > 240 N; **ESD**: > 0.20 J.

*1-Methyl-4-(2-nitro-2-azapropyl)-aminotetrazole (**72**):* The coupling reaction between potassium 1-methyl-5-nitriminotetrazolate and **65** in acetone described above did not only deliver the 1-methyl-5-NAP-nitriminotetrazole, but also the 1-methyl-5-NAP-aminotetrazole. It could be separated from **70** due to its different solubility in ethanol. **72** was obtained from the mother liquor in 12 % yield (0.68 g). **DSC** (T_{onset}, 5 °C min^{-1}): 142–147 °C (mp.), 184 °C (dec.); **IR** (KBr, cm^{-1}): $\tilde{\nu}$ = 3262 (m), 3122 (m), 3040 (m), 1617 (vs), 1500 (vs), 1450 (s), 1343 (m), 1300 (vs), 1288 (s), 1248 (vs), 1226 (m), 1082 (m), 1041 (m), 1021 (m), 1002 (m), 843 (w), 768 (m), 742 (w), 668 (m), 653 (m), 619 (w), 562 (m); **Raman** (1064 nm, 350 mW, 25 °C, cm^{-1}): $\tilde{\nu}$ = 3055 (30), 3027 (30), 2952 (65), 1605 (39), 1467 (31), 1450 (39), 1342 (21), 1306 (54), 1244 (35), 1116 (33), 1081 (18), 1000 (61), 843 (90), 780 (100), 664 (23), 620 (16), 563 (13), 423 (21), 253 (36), 181 (21); **^{1}H NMR** (*d*$_6$-DMSO, 25 °C, ppm): δ = 8.09 (t, J = 6.3 Hz, NH), 5.21 (d, J = 6.3 Hz, CH_2), 3.71 (s, CH_3), 3.53 (s, $H_3CN(NO_2)$); **^{13}C NMR** (*d*$_6$-DMSO, 25 °C, ppm): δ = 155.7 (CN_4), 60.8 (CH_2), 39.0 ($H_3CN(NO_2)$), 32.4 (CH_3); **^{15}N NMR** (*d*$_6$-DMSO, 25 °C, ppm): δ = 1.3 (s, N3), –20.3 (s, N2), –29.0 (m, $^3J_{NH}$ = 2.5 Hz, NO_2), –93.8 (d, $^3J_{NH}$ = 2.2 Hz, N4), –184.5 (t, $^2J_{NH}$ = 2.2 Hz, N1), –199.9 (s, NNO_2), –324.4 (d, $^1J_{NH}$ = 94 Hz, NH); ***m/z*** (FAB$^+$): 188.2 $[M+H]^+$; **EA** ($C_4H_9N_7O_2$, 187.16) calcd.: C 25.67, H 4.85, N 52.39 %; found: C 25.71, H 4.84, N 52.51 %; **impact sensitivity**: > 40 J; **friction sensitivity**: > 120 N; **ESD**: 0.60 J.

*2-Methyl-5-(2-nitro-2-azapropyl)-nitriminotetrazole (**73**):* 2-Methyl-5-nitraminotetrazolate (4.32 g, 30 mmol) was suspended in 25 mL of THF and triethyl amine (3.04 g, 30 mmol) was added. A white precipitate, which first was formed, disappears within half a minute. 2-nitro-2-azapropyl chloride (3.74 g, 30 mmol), dissolved in 10 mL of THF, was added drop wise. The mixture was stirred at room temperature overnight, filtered off and the solvent was removed from the filtrate. The remaining yellow oil was suspended in 30 mL of pentane and stirred vigorously. After a few minutes all the oil was converted into fine, crystalline material, which was filtered off (6.55 g, 94% yield). and recrystallized from ethanol/methanol. **DSC** (T_{onset}, 5 °C min^{-1}): 68 – 78 °C (mp.), 116 °C (dec.); **IR** (KBr, cm^{-1}): $\tilde{\nu}$ = 3435 (m), 3043 (m), 1585 (vs), 1531 (vs), 1467 (s), 1458 (s), 1441 (m), 1412 (m), 1397 (s), 1365 (w), 1304 (s), 1282 (s), 1261 (s), 1214 (m), 1195 (m), 1147 (m), 1066 (m), 1048 (m), 1025 (m), 911 (m), 855 (w), 800 (m), 769 (m), 749 (m), 704 (w), 663 (m), 649 (m), 602 (m), 494 (w), 453 (w); **Raman** (1064 nm, 350 mW, 25 °C, cm^{-1}): $\tilde{\nu}$ = 3043 (30), 2994 (43), 2969 (91), 2875 (15), 2837 (9), 1592 (15), 1517 (59), 1457 (20), 1402 (25), 1366 (23), 1337 (18), 1291 (68), 1214 (10), 1197 (15), 1146 (6), 1067 (8), 1046 (26), 1018 (73), 915 (16), 857 (100), 799 (13), 751 (5), 704 (28), 763 (12), 751 (12), 603 (23), 495 (11), 464 (32), 394 (30), 374 (11), 327 (13), 308 (22), 243 (13), 221 (14); **^{1}H NMR** (*d*$_6$-DMSO, 25 °C, ppm): δ = 6.09 (s, CH_2), 4.49 (s, CH_3), 3.47 (s, CH_3NNO_2); **^{13}C NMR** (*d*$_6$-DMSO, 25 °C, ppm): δ = 159.1 (CN_4), 67.1 (CH_2), 41.2 (CH_3), 39.7 (CH_3NNO_2); **^{15}N NMR** (*d*$_6$-DMSO, 25 °C, ppm): δ = 1.4 (N3, q, $^{3}J_{N-H}$ = 1.5 Hz), –30.4 (N8), –37.9 (N6), –53.4 (N4), –77.9 (N1, q, $^{3}J_{N-H}$ = 1.8 Hz), –101.6 (N2, q, $^{2}J_{N-H}$ = 2.4 Hz), –202.1 (N5, t, $^{2}J_{N-H}$ = 1.9 Hz), –204.9 (N7); ***m/z*** (DEI^{+}): 233.3 [M+H]$^{+}$; **EA** ($C_2H_3KN_6O_2$, 182.18) calcd.: C 20.69, H 3.47, N 48.27 %; found: C 21.71, H 3.81, N 47.08 %; **impact sensitivity**: > 8 J; **friction sensitivity**: > 96 N; **ESD**: > 0.07 J.

*1,4-Dimethyl-5-nitriminotetrazole (**74**):* 1-Methyl-5-nitriminotetrazole (1.44 g, 10 mmol) was deprotonated using 40 mL of aqueous KOH solution (570 mg, 10 mmol). To this, dimethyl sulfate was added drop wise at 60 °C and the mixture was refluxed for three hours. Afterwards the solvent was reduced by half and the product was extracted using CH_2Cl_2 (2 x 30 mL). After evaporating the solvent, the crude product was recrystallized from hot water yielding 1.34 g colorless crystals (85 % yield). **DSC** (T_{onset}, 5 °C min^{-1}): 85 °C (mp.), 200 °C (dec.); **IR** (KBr, cm^{-1}): $\tilde{\nu}$ = 3029 (w), 2442 (w), 2265 (w), 2115 (w), 1685 (w), 1664 (s), 1495 (m), 1436 (s), 1412 (m), 1376 (s), 1352 (m), 1258 (vs, br), 1229 (vs), 1115 (m), 1049 (m), 1007 (s), 918 (w), 874 (w), 791 (s), 774 (s), 750 (m), 676 (s); **Raman**: (1064 nm, 200 mW, 25 °C, cm^{-1}): $\tilde{\nu}$ = 3032 (31), 2964 (93), 1568 (81), 1467

(26), 1439 (27), 1415 (46), 1378 (38), 1353 (41), 1278 (17), 1232 (15), 1050 (18), 1010 (62), 876 (11), 796 (31), 775 (11), 752 (38), 621 (100), 522 (7), 482 (29), 349 (10), 283 (33), 209 (13), 161 (15); **^{1}H NMR** (d_6-DMSO, 25 °C, ppm): δ = 3.78 (s, 3H, CH_3); **^{13}C NMR** (d_6-DMSO, 25 °C, ppm): δ = 39.7 (CH_3), 168.0 (CN_4); **^{14}N NMR** (d_6-DMSO, 25°C, ppm): δ = –19.6 (NO_2); **^{15}N NMR** (d_6-DMSO, 25 °C, ppm): δ = –359.4 (N7, NH_4^+), –149.3 (N5), –111.8 (C2, ^2J(N–H) = 2.1 Hz), –93.8 (N1, ^{3}J(N–H) = 1.8 Hz), –63.9 (N4), –15.4 (N6, NO_2), –6.4 (N3, ^3J(N–H) = 1.8 Hz); ***m/z*** (DEI): 158(34) $[M]^+$, 112(58) $[M–NO_2]^+$, 89(10), 83 (6) $[M–NO_2–2CH_3]^+$, 70(5), 69(10), 57(8), 56(20), 55(12), 53(7), 46 (6) $[NO_2]^+$, 45(24), 43 (100) $[HN_3]^+$, 42 (12) $[N_3]^+$, 41(11), 28(35) $[N_2]^+$, 18(23), 15(34) $[CH_3]^+$; **EA** ($C_3H_6N_6O_2$, 158.12) calcd.: C 22.79, H 3.82, N 53.15 %; found: C 23.10, H 3.84, N 52.99 %; **impact sensitivity**: > 30 J; **friction sensitivity**: > 360 N.

6.7 Conclusions

From this experimental study the following conclusions can be drawn:

- 1-(2-Nitro-2-azapropyl)-5-aminotetrazole (**66**), 1-(2-nitro-2-azapropyl)-5*H*-tetrazole (**67**), 1-(2-nitro-2-azapropyl)-5-nitriminotetrazole (**68**·H_2O, **68**·EtOH), 1,5-bis(2-nitro-2-azapropyl)-5-nitraminotetrazole (**69**), 1-methyl-5-(2-nitro-2-azapropyl)-5-nitraminotetrazole (**70**), 1-methyl-4-(2-nitro-2-azapropyl)-5-nitriminotetrazole (**71**), 1-methyl-5-(2-nitro-2-azapropyl)-5-aminotetrazole (**72**) and 2-methyl-5-(2-nitro-2-azapropyl)-nitraminotetrazole (**73**) can be synthesized, mostly in good yields from deprotonated 5-amino-1*H*-tetrazole (**2**), 1*H*-tetrazole (**1**), 5-nitriminotetrazole (**43**), 1-methyl-5-nitriminotetrazole (**44**) and 2-methyl-5-nitraminotetrazole (**45**), respectively.

- 1,4-dimethyl-5-nitriminotetrazole (**74**) was synthesized by methylation of potassium 1-methyl-5-nitriminotetrazolate with dimethyl sulfate.

- The crystal structures of **66**–**74** were determined by low-temperature single crystal X-ray diffraction. The compounds crystallize in common space groups ($P2_1/c$: **66**, **68**·H_2O, **68**·EtOH, **70**, **72** and **73**; $P2_1$: **67** and **69**; *Pbca*: **71** and **74**) with densities between 1.52 and 1.75 g cm^{-3}. In addition **66**–**74** were characterized comprehensively by vibrational spectroscopy (IR and Raman),

multinuclear (^{1}H, ^{13}C, ^{14}N and ^{15}N) NMR spectroscopy, mass spectrometry, elemental analysis and differential scanning calorimetry.

- The thermal behavior of **66**–**74** was investigated by DSC measurements. The decomposition temperatures reach from 116 °C (**73**) to 184 °C (**66**, **72**).

- The sensitivities towards impact, friction and electrical discharge of compounds **66**–**74** were determined by using the BAM drophammer and friction tester as well as a small scale electrical discharge tester. The values are mostly lower than commonly used secondary explosives e.g. RDX or HMX. The most sensitive compound is The impact sensitivity range from 2 →100 J. Most of the compounds are only moderately sensitive towards friction. The sensitivity towards electrical discharge, of course, strongly depends on the particle sizes and range from 0.07–1.45 J.

- The heats of formation $\Delta_f H^\circ$ were calculated using heats of combustion obtained from bomb calorimetric measurements. All compounds, except for **68**·EtOH (–639 kJ mol^{-1}) are formed endothermically with values between 18 kJ mol^{-1} (**68**·H_2O) and 383 kJ mol^{-1} (**66**).

- By using $\Delta_f H^\circ$ and the maximum densities obtained from XRD several detonation parameter (heat of explosion, explosion temperature, detonation pressure and velocity) were computed with the EXPLO5 software. The highest detonation pressures (273 and 281 kbar) as well as velocities (8467 and 8311 m s^{-1}) were calculated for compounds **66** as well as **68**·H_2O.

Chapter 7.

Salts of 1-Methyl-5-nitriminotetrazole

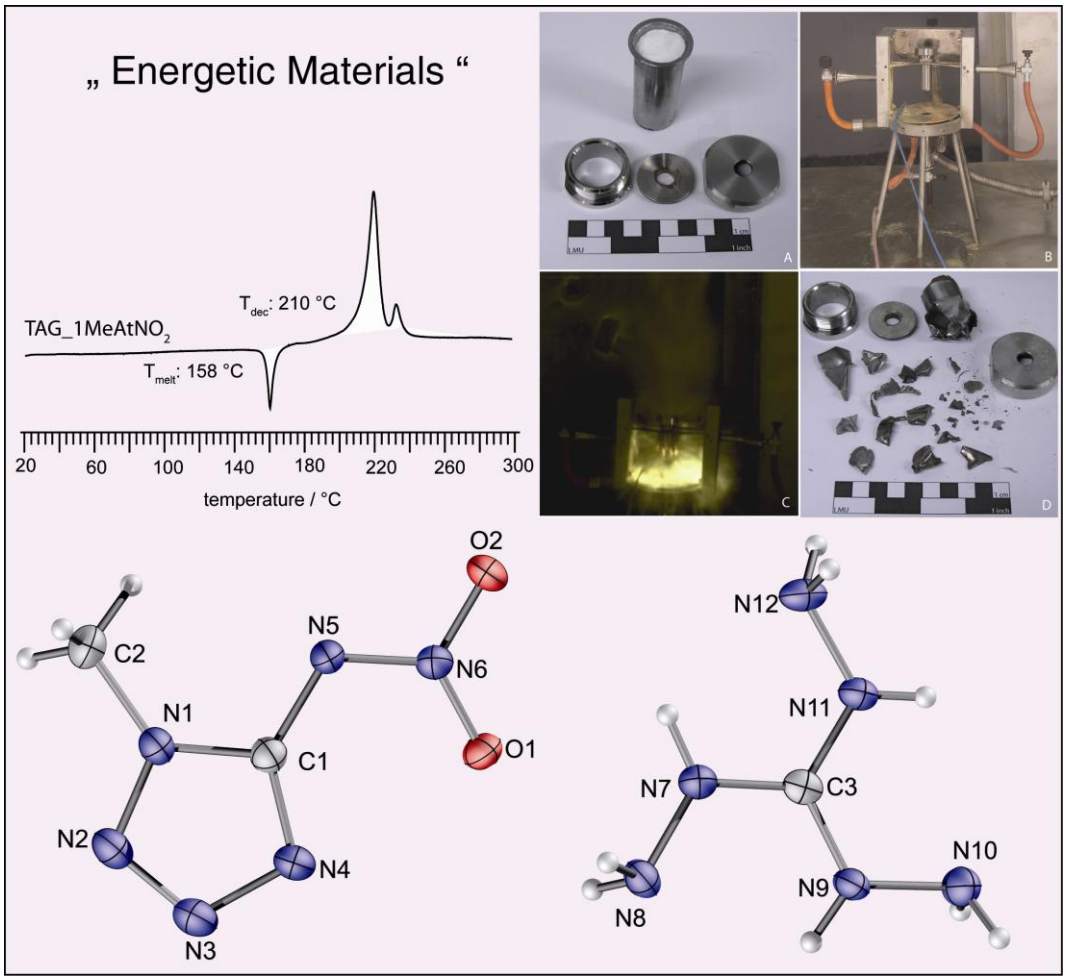

7.1 Introduction

Increasing environmental concerns over the last few years also raised the requirements of *HEDM*s, and new replacements for the commonly used toxic hexogen are wanted.[290] Therefore explosives containing high nitrogen contents are in the focus, because of the environmentally benign dinitrogen (N_2) molecule as reaction product, whereby nitrogen oxides (N_xO_y), NH_3 or HCN are not desired.[71d,72,291,186] The high, negative enthalpy of formation for the decomposition products and the diminution of carbon residues are further advantages of nitrogen rich compounds. The following chapter is about synthesis and characterization of new energetic materials based on 1-methyl-5-nitriminotetrazole, which is also synthesized from commercially available 5-amino-1*H*-tetrazole (**2**, **5-At**) and its derivatives.[292,67] Due to its considerable nitrogen content and its stability towards impact, friction and heat and also its cheap availability, it is an appropriate precursor for the formation of new explosives. In contrast, substituted groups with an electron acceptor effect destabilize the synthesized compound. To prepare new energetic materials often tetrazoles,[30b,293] tetrazolates [294] and tetrazolium [202,295] salts are used, since they are mostly endothermic compounds with a high nitrogen content. In addition, these compounds are considered mostly less toxic, easy to handle due to their high kinetic and thermal stability and easy to prepare. Disadvantage of tetrazolates and tetrazolium compounds are the possible contamination of ground water since these ionic structures feature a high solubility. On the other side, they show mostly high densities and stabilities based on their lattice energy. The formation of ionic structures is a popular approach for the synthesis of new energetic materials. However, it is hard to fulfill all requirements for new energetic materials.

The compounds described in this chapter are N-rich as well as alkaline and alkaline earth metal salts of the anion 1-methyl-5-nitriminotetrazolate. This is a valuable compound, due to the combination of the nitrogen-rich backbone as a fuel and the nitro-group as an oxidizer. The first investigations on neutral 1-methyl-5-nitriminotetrazole (1MeHAtNO_2, **44**) were published in 1957.[296] The nitration of the amino group in **5-At** leads to an increased energetic character as well as higher sensitivities compared to **5-At** and improves the oxygen balance. The methyl group lowers the sensitivity in comparison to non-methylated 5-nitriminotetrazole (H_2AtNO_2, **44**). Deprotonation of 1-methyl-5-nitriminotetrazole yields more suitable compounds with higher

decomposition temperatures. For this reason 5-nitriminotetrazolate anions are convenient components for new ionic energetic materials.

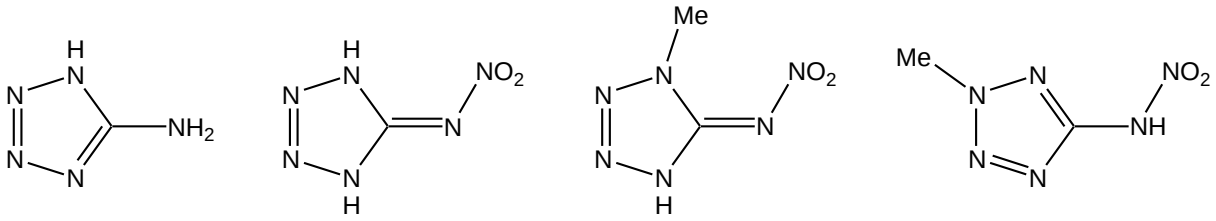

Figure 7.1 5-Aminotetrazole (**2**, 5-At), 5-nitriminotetrazole (**43**, H_2AtNO_2), 1-methyl-5-nitriminotetrazole (**44**, 1-MeHAtNO$_2$) and 2-methyl-5-nitriminotetrazole (**45**, 2-MeHAtNO$_2$).

According to the performance in energetic salts the same requirements have to be applied for the cations of the energetic material. Therefore, 1-methyl-5-nitriminotetrazole salts containing nitrogen rich cations are in the focus of this chapter. Firstly, the ammonium 1-methyl-5-nitriminotetrazolate and ammonium 2-methyl-5-nitriminotetratolate salts are described, whereby the second is characterized by a too low decomposition temperature.[142] Therefore, most of the further salts described are synthesized only by using the 1-methyl analogue. The ammonium ion is very popular due to its environmental compatibility and its structure containing only nitrogen and hydrogen atoms. However, 1-methyl-5-nitriminotetrazole as its ammonia salt does not show a resounding thermal, but a good kinetic stability, a high density and acceptable performance. A promising strategy for improving the performance is the replacement of the ammonium ion by cations with higher nitrogen contents. Following this approach different guanidinium salts of **44** were synthesized and are presented in this work. Guanidine chemistry has extended over a period of more than 100 years, and many useful compounds have been identified. The spectrum of uses of these compounds is highly diverse, ranging from biologically active molecules to highly energetic materials, thus indicating the manifold usability of the guanidine moiety as building block.[297] But also, metal salts of tetrazoles [67] are still an important field of organic and inorganic chemistry due to the theoretical and practical significance of these unique compounds and the diversity of their properties. Alkali and alkaline earth metal salts of tetrazoles [148] can be used as coloring agents in modern pyrotechnic compositions [298] due to their brilliant flame colors and simple accessibility.[299]

7.2 Synthesis

The ammonium salts were synthesized according to **Scheme 7.1** by deprotonation of 1-methyl-5-nitriminotetrazole and 2-methyl-5-nitraminotetrazole using aqueous ammonia solutions. **44** and **45** were obtained by the reaction of 1-methyl-5-aminotetrazole and 2-methyl-5-aminotetrazole with HNO_3 (100 %) as described in Chapter 4.

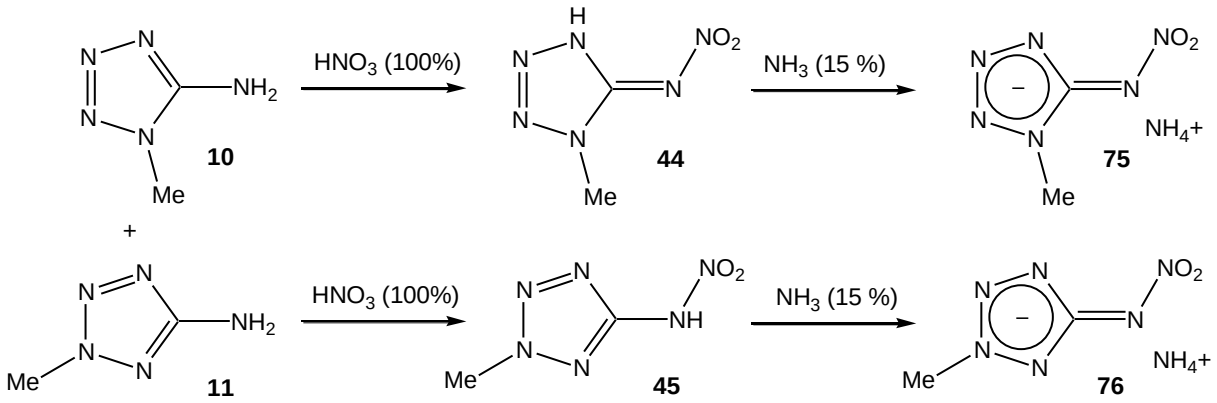

Scheme 7.1 Synthesis of ammonium 1-methyl-5-nitriminotetrazolate (**75**) and ammonium 2-methyl-5-nitriminotetrazolate (**76**).

The synthesis of the alkali and strontium salts of 1-methyl-5-nitriminotetrazolate is shown in **Scheme 7.2**. All reactions were performed in water, in case of Li^+ and Na^+ the metal hydroxides, in case of K^+, Rb^+ and Cs^+ the corresponding carbonates were used. Single crystals were obtained by recrystallization from water or water/ethanol solutions. The syntheses of **82** and **83** were also performed in water using strontium hydroxide octahydrate and 1-methyl-5-nitriminotetrazole (**44**) and 2-methyl-5-nitraminotetrazole (**45**), respectively, according to **Scheme 7.2**. **82** and **83** are slightly soluble in cold water and can be recrystallized from hot water (**83**) or ethanol/water mixtures (**82**), whereby single crystals were obtained. The reaction of **45** with strontium octahydrate yielded a light yellow solution, from which **83** precipitated as colorless solid, which shows a very low solubility in cold water. After two recrystallizations from water, **83** was obtained as colorless crystals.

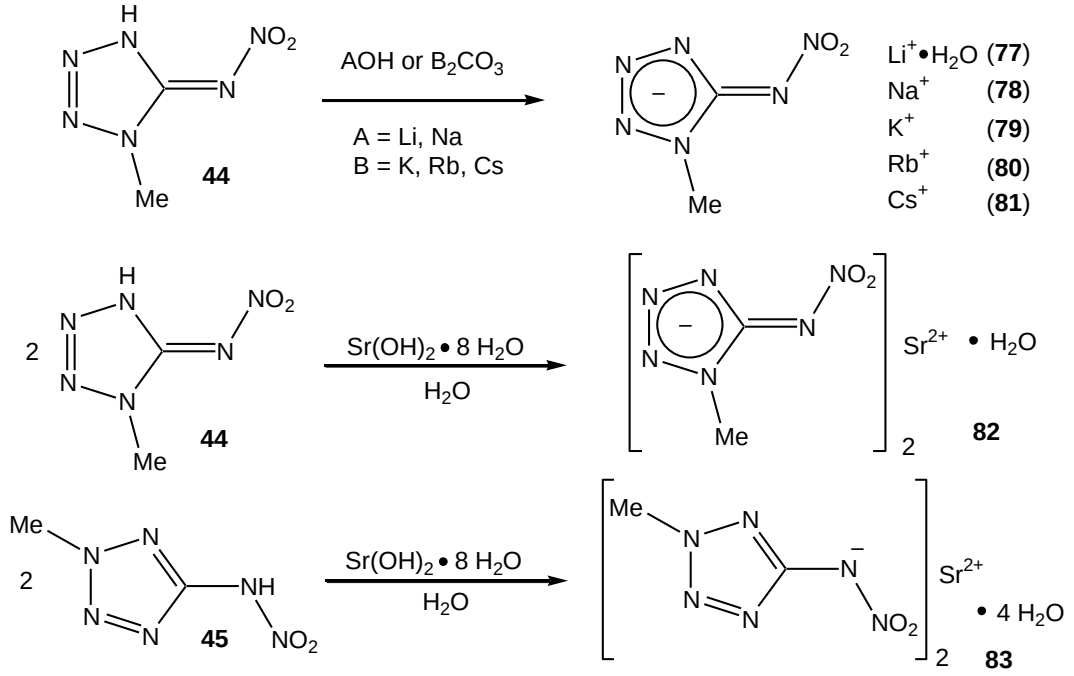

Scheme 7.2 Synthesis of the compounds **77**–**83**.

Scheme 7.3 shows a general survey of syntheses of the guanidinium 1-methyl-5-nitriminotetrazolate salts. All these compounds were synthesized using silver 1-methyl-5-nitriminotetrazolate (Ag_1-MeAtNO$_2$, **84**), which was used in the wet state. **84** was obtained by metathesis reaction of potassium 1-methyl-5-nitriminotetrazolate (K_1MeAtNO$_2$, **79**) and silver nitrate. The reaction products guanidinium 1-methyl-5-nitriminotetrazolate (G_1MeAtNO$_2$, **85**), 1-aminoguanidinium 1-methyl-5-nitriminotetrazolate (AG_1MeAtNO$_2$, **86**), 1,3-diaminoguanidinium 1-methyl-5-nitriminotetrazolate (DAG_1MeAtNO$_2$, **87**), 1,3,5-triaminoguanidinium 1-methyl-5-nitriminotetrazolate (TAG_1MeAtNO$_2$, **88**), and azidoformamidinium 1-methyl-5-nitriminotetrazolate (AF_1MeAtNO$_2$, **89**) were formed by the reaction of **84** with the corresponding chloride salts. Thereby, the impetus of these reactions is the formation of silver chloride, which features a very low solubility in water and can be easily removed by filtration.

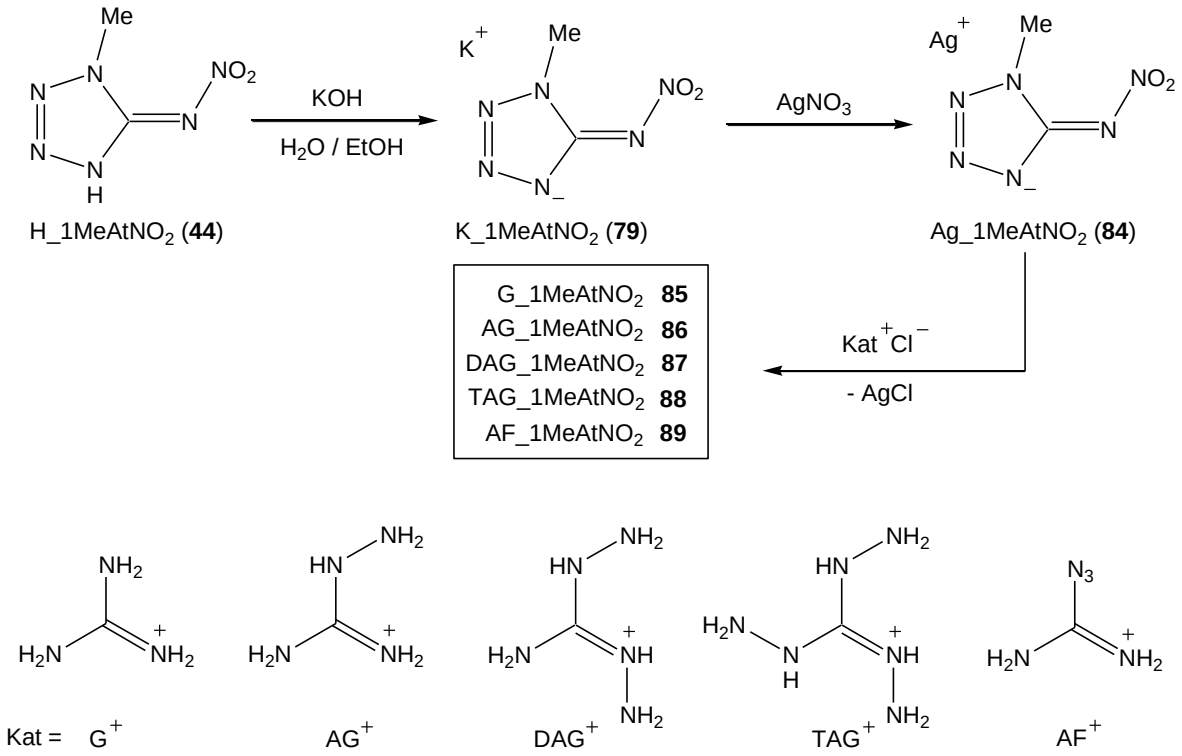

Scheme 7.3 Syntheses of compounds **84**–**89** via the formation of AgCl.

An alternative procedure forming **85**–**89** is the reaction of the potassium salt **79** and the corresponding guanidinium perchlorates (**39**–**41**) under the formation of low soluble potassium perchlorate (**Scheme 7.4**). This method does not include an intermediate and therefore the reaction yields are slightly better and nearly quantitative. As the perchlorates are more sensitive than the chlorides, appropriate security measures have to be applied.

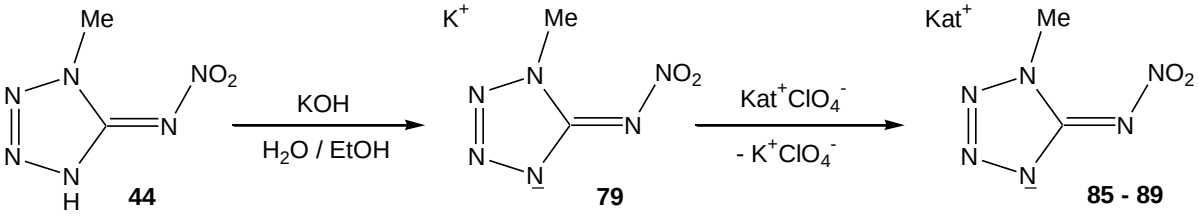

Scheme 7.4 Syntheses of compounds **84**–**89** via the formation of KClO4.

Since triaminoguanidinium 1-methyl-5-nitriminotetrazolate (**88**, TAG_1MeAtNO$_2$) was investigated to be a promising new energetic compound for applications as secondary explosive, a cheap and facile synthetic route is desired. The previously published syntheses (**Schemes 7.3** and **7.4**) either use silver 1-methyl-5-nitriminotetrazolate, which is expensive and sensitive towards light or triaminoguanidinium perchlorate, which is highly sensitive towards impact and friction.

The new synthesis of **88** follows the protocol presented in **Scheme 7.5**. The deprotonation reaction was performed in water obtaining a yield of 97 %. The second reaction was performed in a dioxane/water mixture using a small excess of hydrazine hydrate.

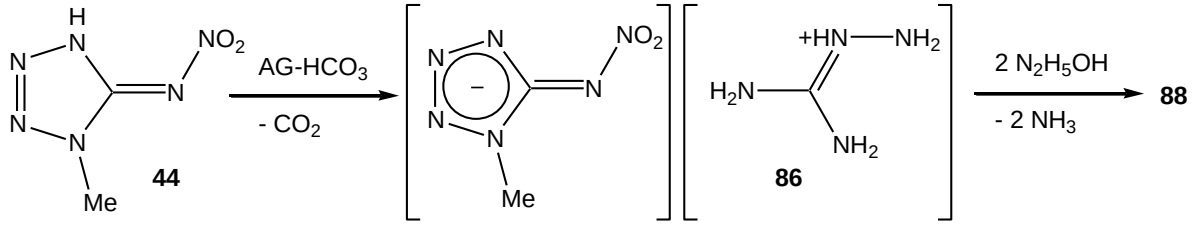

Scheme 7.5 Improved Synthesis of **88**.

The new synthesis is able to reduce the five step protocol of the previously described synthesis of **88** to "only" two steps.

7.3 Crystal Structures

7.3.1 Ammonium 1-methyl-5-nitriminotetrazolate (**75**)

75 crystallizes in the monoclinic space group $P2_1/c$ with four molecules in the unit cell. The density of 1.64 g/cm^3 is lower than in the neutral **44** (1.76 g cm^{-3}). The bond distances in the nitraminotetrazolate anion are quite normal and are comparable to them of the protonated form. The tetrazolate ring is planar due to its aromaticity and the nitramine unit follows this planarity exactly (torsion angle C1–N5–N6–O1 = 0.0(3)°) The shortest bond distance in the tetrazolate ring is between the nitrogen atoms N2 and N3 (1.298(2) Å), the longest between N3 and N4 (1.365(2) Å) all between the length of N–N single bonds (1.46 Å) and N=N double bonds (1.25 Å). Remarkable is the bond distance between the atoms C1 and N5 with 1.373(2) Å between a C–N single bond (1.47 Å) and C=N double bonds (1.28 Å) and the short bonding between N5 and N6 of 1.314(2) Å. The molecular unit is shown in **Figure 7.2**. The structure is affected by several hydrogen bonds in which all protons of the ammonia cation are involved. The stronger ones are directed to oxygen atoms of the nitro groups. N7–H7B···O1^{i}: 0.97(3) Å, 1.94(3) Å, 2.900(2) Å, 168(2)°; N7–H7D···O2^{ii}: 0.92(2) Å, 1.95(2) Å, 2.850(2) Å, 164(2)°; N7–H7C···N3^{iii}: 0.98(3) Å, 2.01(3) Å, 2.991(3) Å, 176(2)°; N7–H7A···N4: 0.94(3) Å, 2.02(3) Å, 2.946(3) Å, 171.(2)°; (i) –1+x, y, z; (ii) –1+x, 0.5–y, 0.5+z; (iii) x, 0.5–y, –0.5+z.

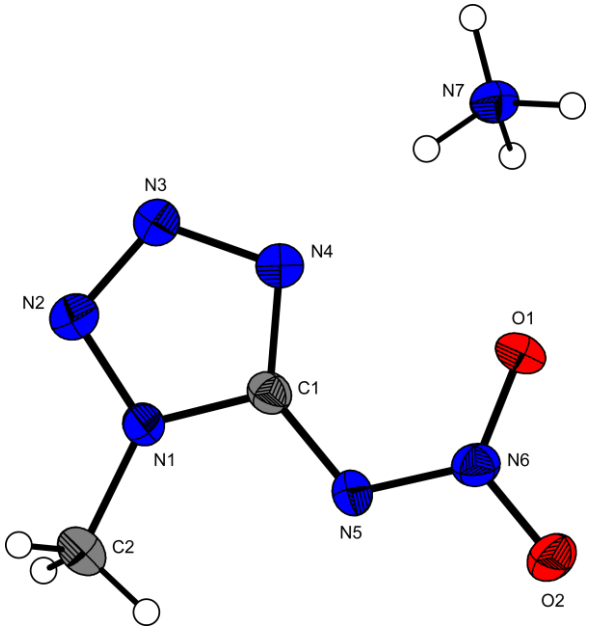

Figure 7.2 A view of the molecular unit of **75**, showing the atom-labeling scheme. Thermal ellipsoids represent 50 % probability.

7.3.2 Ammonium 2-methyl-5-nitriminotetrazolate (**76**)

The ammonium salt of 2-methyl-5-nitraminotetrazole (**76**) crystallizes in the chiral monoclinic space group $P2_1$ with two molecules in the unit cell. The density of 1.65 g cm^{-3} is comparable to **75** and interestingly even similar to compound **45**, which crystallizes with a density of 1.67 g cm^{-3}. The molecular unit can be seen in **Figure 7.3**.

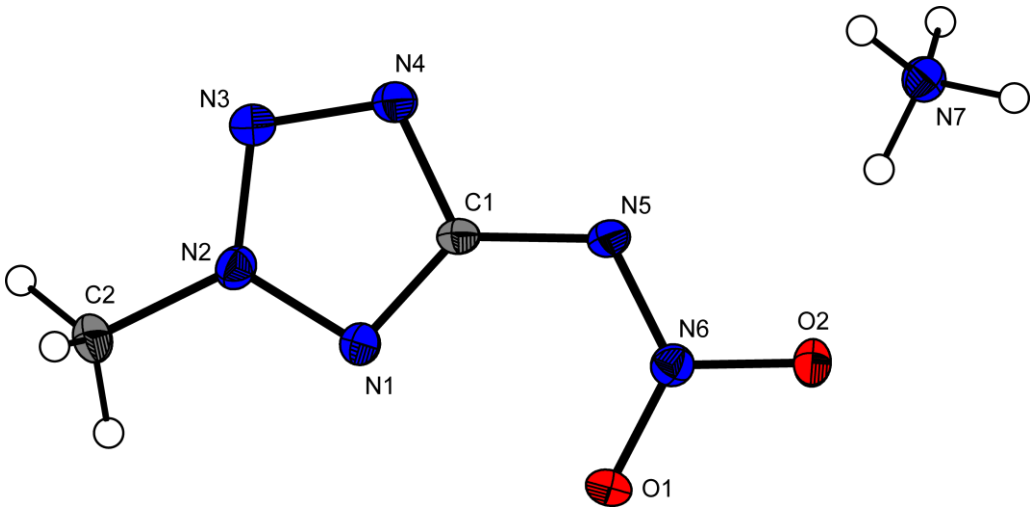

Figure 7.3 A view of the molecular unit of **76**, showing the atom-labeling scheme. Thermal ellipsoids represents 50 % probability and hydrogen atoms are shown as small spheres of a arbitrary radii.

The bond distances in **76** are very similar to those of **75** and are given in **Table 7.1**. The significant bond length between the atoms C1 and N5 of 1.386(2) Å for differentiating a nitraminotetrazole from a nitriminotetrazole is again between a C–N single and a double bond and can be interpreted optionally. Again there are several strong hydrogen bonds created by the ammonia cation: N7–H7B···N4^{i}: 0.92(2) Å, 2.05(2) Å, 2.973(2) Å, 174(2)°; N7–H7C···O2^{ii}: 0.94(2) Å, 2.05(2) Å, 2.856(2) Å, 143(2)°; N7–H7A–O2: 0.94(3) Å, 1.93(3) Å, 2.863(2) Å, 171(2)°; N7–H7A–N5: 0.94(3) Å, 2.60(3) Å, 3.301(2) Å, 132.(2)°; N7–H7D···O1^{iii}: 0.93(3) Å, 2.00(3) Å, 2.906(2) Å, 163(2)°; (i) 1–x, 0.5+y, –z; (ii) 1–x, –0.5+y, –z; (iii) 2–x, –0.5+y, –z.

Table 7.1 Selected bond lengths[Å], angles[°] and torsion angles[°] of **75** and **76**.

Atoms 1–2	d(1–2) [Å]	d(1–2) [Å]
	75	**76**
N1–N2	1.347(2)	1.338(2)
N2–N3	1.298(2)	1.315(2)
N3–N4	1.365(2)	1.324(2)
N1–C1	1.347(2)	1.337(2)
N4–C1	1.333(2)	1.362(2)
N5–C1	1.373(2)	1.386(2)
N1(2)–C2	1.467(3)	1.468(2)
N5–N6	1.314(2)	1.298(2)
N6–O1	1.263(2)	1.263(2)
N6–O2	1.259(2)	1.285(2)
Atoms 1–2–3	∢(1–2–3) [°]	∢(1–2–3) [°]
	75	**76**
N1–N2–N3	106.1(2)	114.8(1)
N2–N3–N4	111.4(2)	105.7(1)
C1–N1–N2	109.2(2)	101.2(2)
C1–N4–N3	105.5(1)	106.4(2)
N1–C1–N4	108.0(2)	111.9(2)
N1–C1–N5	116.0(2)	131.8(2)
N4–C1–N5	136.0(2)	116.3(2)
C1–N1–C2	129.4(2)	
N2–N1–C2	121.4(2)	

N1–N2–C2		122.4(2)
N3–N2–C2		122.8(2)
N6–N5–C1	116.6(2)	117.4(2)
O1–N6–O2	119.7(2)	118.6(2)
O2–N6–N5	116.3(2)	115.7(2)
O1–N6–N5	123.9(2)	125.7(2)
Atoms 1–2–3–4	∢(1–2–3–4) [°]	∢(1–2–3–4) [°]
	75	**76**
N1–N2–N3–N4	0.0(2)	–0.1(2)
C1–N1–N2–N3	0.0(2)	–0.27(2)
N2–N1–C1–N5	178.6(2)	–179.9(2)
N6–N5–C1–N1	176.3(2)	4.2(3)
C1–N5–N6–O1	0.0(3)	–2.5(2)
C1–N5–N6–O2	–179.3(2)	177.1(1)

7.3.3 Lithium 1-methyl-5-nitriminotetrazolate monohydrate (**77**)

77 crystallizes as the monohydrate in the monoclinic space group $P2_1$ with two molecules in the unit cell. The molecular moiety can be found in **Figure 7.4**. The bond lengths in the planar (torsion angle N1–N2–N3–N4 –0.2(4)°) tetrazolate ring are between 1.297(5) (N2–N3) and 1.361(5) Å (N3–N4). The distance between the atoms C1 and N5 is 1.374(5) Å, which corresponds more with a C=N double bond (1.30 Å) than a C–N single bond (1.48 Å) and is relevant to the nomenclature nitrimino- vs. nitraminotetrazole. The nitramine bond distance N5–N6 is 1.325(4) Å.

The lithium cations are pentacoordinated by two water molecules at a distance of 2.060(8) Å, by the *N*,*O*-chelating nitriminotetrazolate *d*(Li–O1) = 2.092(8) Å and *d*(Li–N4) = 2.027(8) Å and the oxygen atom O2 of a neighboring tetrazolate *d*(Li–O2^{i}) = 2.087(8) Å; (i) –1–*x*, –0.5+*y*, –3–*z*. This coordination results in endless chains with the units bridged by the oxygen atoms of the nitro groups as illustrated in **Figure 7.5**.

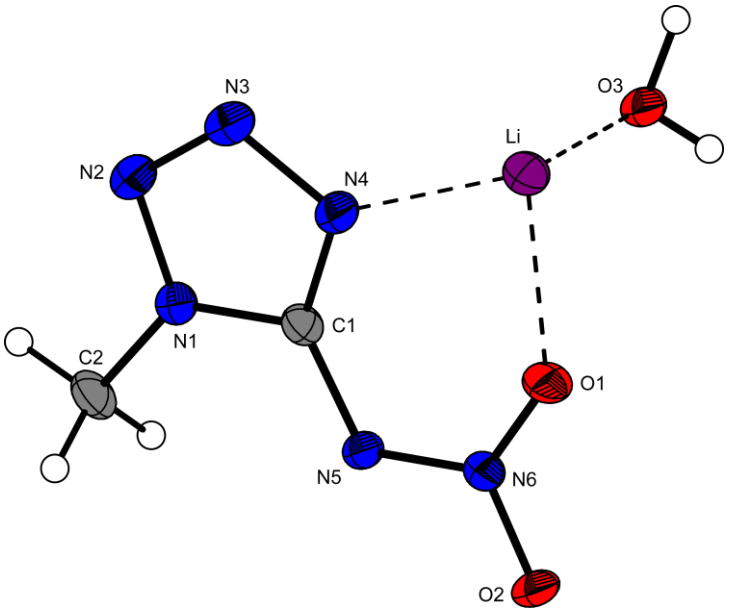

Figure 7.4 A view of the molecular unit of **77**. Ellipsoids represent 50 % probability.

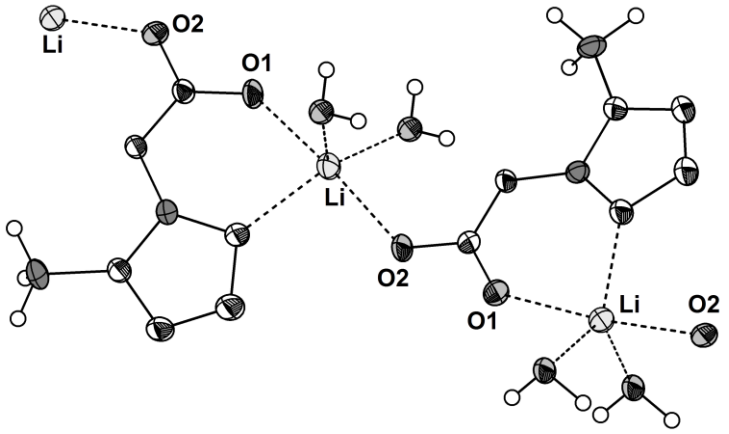

Figure 7.5 A view of the coordination of the lithium cations in **77** leading to endless chains.

7.3.4 Sodium 1-methyl-5-nitriminotetrazolate (**78**)

The sodium salt **78** of 1-methyl-5-nitriminotetrazole crystallizes in the monoclinic space group $P2_1/c$ with four molecules in the unit cell. The bond distances and angles in the molecular unit (**Figure 7.6**) are similar to those observed in **77** and can be found in **Table 7.2**. Again the tetrazolate ring is planar and the nitramine group lies in this plane (torsion angle C1–N5–N6–O1 = 2.3(4)°).

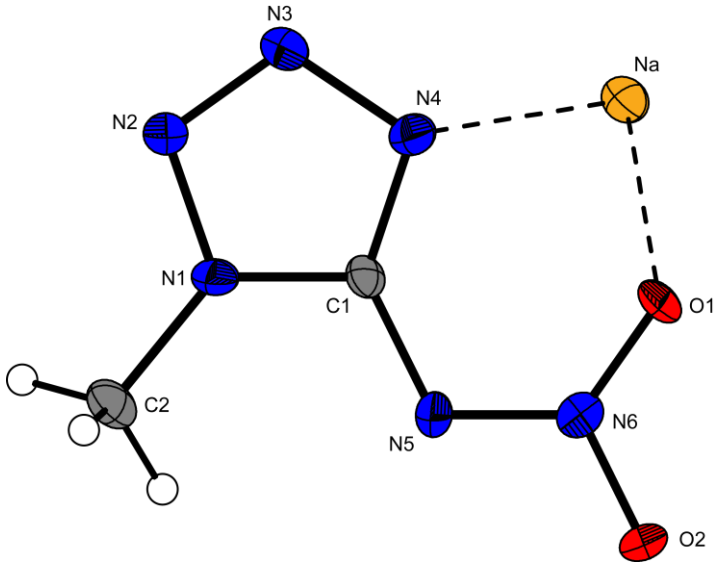

Figure 7.6 A view of the molecular unit of **78**. Ellipsoids represent 50 % probability.

The sodium cations are hexa-coordinated by the atoms O1 (2.561(2) Å), O2 (2.441(2) Å), N3^{i} (2.513(3) Å), O2^{ii} (2.430(2) Å), O1^{iii} (2.349(2) Å) and N4^{iii} (2.392(2) Å) building no regular geometry ((i) x, 1+y, z; (ii) –1+x, y, z); (iii) 2–x, –0.5+y, 0.5–z). The packing (**Figure 7.6**) can be described as a two-dimensional structure with hooked stacking.

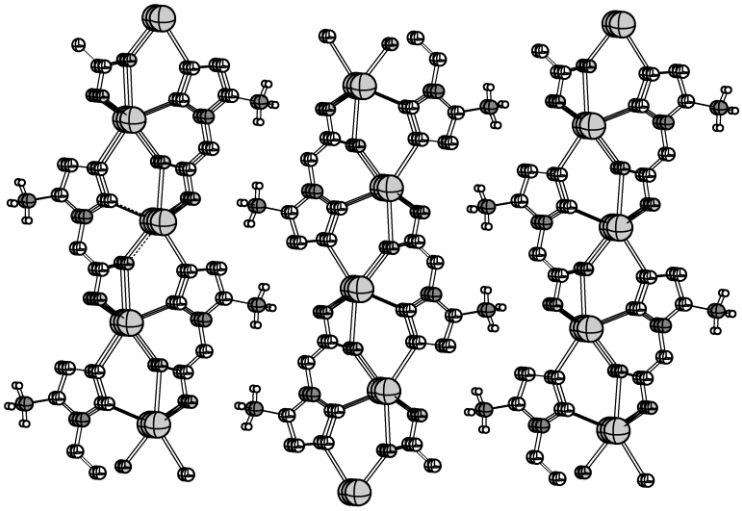

Figure 7.7 A view of the packing and coordination in **78**. The sodium cations are represented as light grey balls.

7.3.5 Potassium 1-methyl-nitriminotetrazolate (**79**)

Potassium 1-methyl-nitriminotetrazolate crystallizes analogously to compound **77** in the monoclinic space group $P2_1/c$ with four molecules in the unit cell and a density of 1.947 g cm^{-3}. There are nearly no differences in the molecular moiety (**Figure 7.8**) as

well as in the packing. The relationship to the sodium salt can also be seen in the similar Raman spectra (see below).

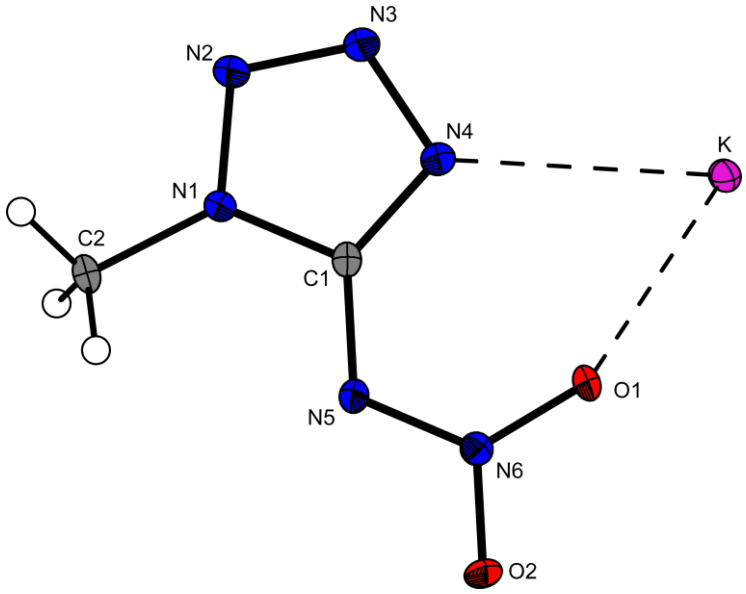

Figure 7.8 A view of the molecular unit of **79**. Ellipsoids represent 50 % probability.

7.3.6 Rubidium 1-methyl-nitriminotetrazolate (**80**)

The rubidium salt **80** crystallizes in the monoclinic space group $P2_1/n$ with eight molecules in the unit cell and a density of 2.258 g cm^{-3}. One molecular unit is illustrated in **Figure 7.9**. The bond lengths and angles are similar to those described above.

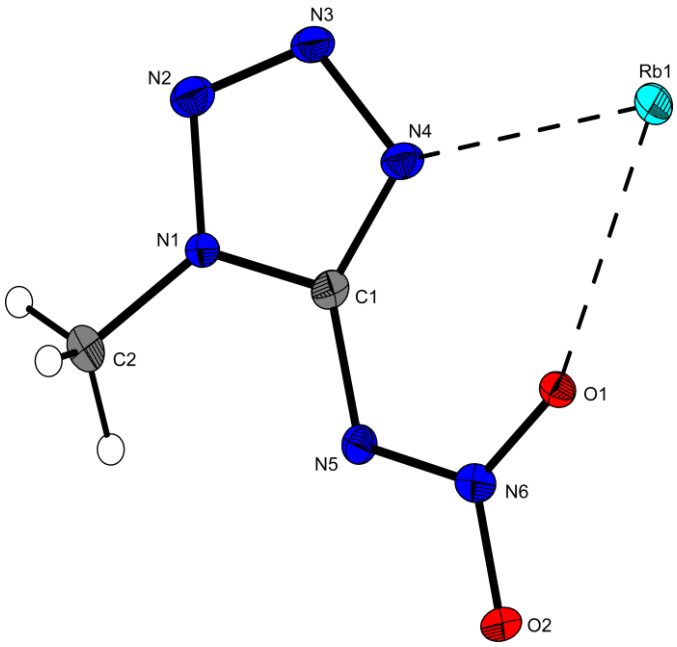

Figure 7.9 A view of the molecular unit of **80**. Ellipsoids represent 50 % probability.

7.3.7 Cesium 1-methyl-5-nitriminotetrazolate (**81**)

81 crystallizes also in the monoclinic crystal system in the space group $P2_1/n$ with four molecules in the unit cell and a density of 2.617 g cm^{-3}. The molecular moiety and the nearest coordination distances to the cesium cations (d(Cs–O2) = 3.038 Å, d(Cs–N4) = 3.132 Å) can be seen in **Figure 7.10**. The packing of the structure, in which the cations and anions form one-dimensional stags along the *a* axis is illustrated in **Figure 7.11**.

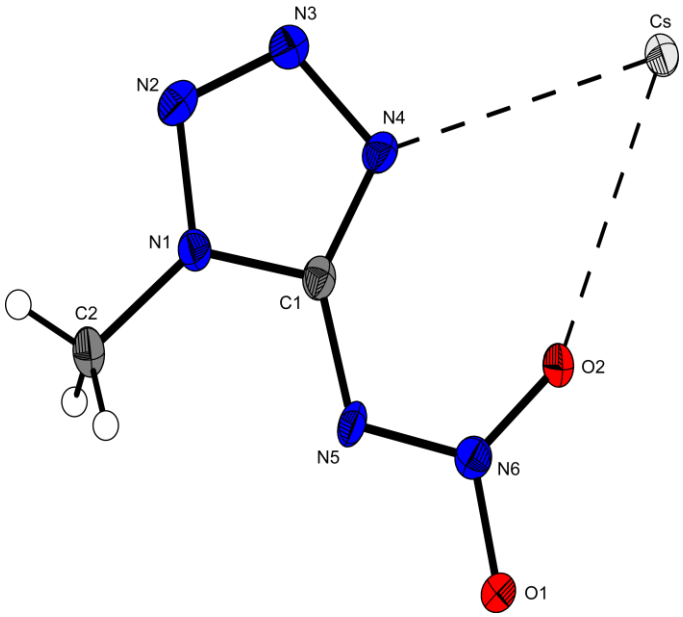

Figure 7.10 A view of the molecular unit of **81**. Ellipsoids represent 50 % probability.

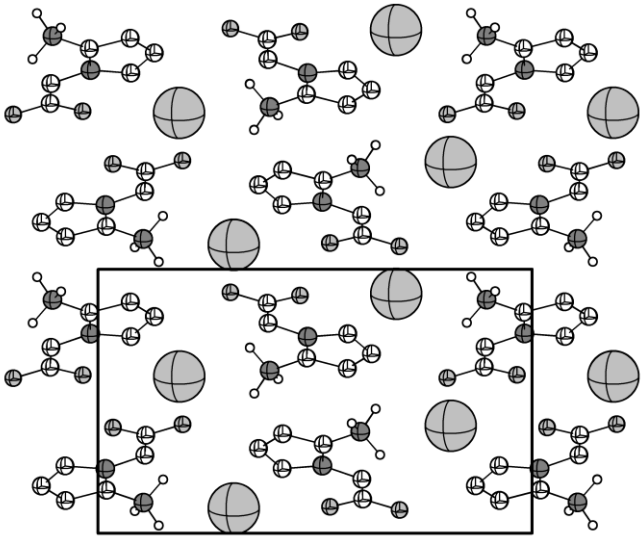

Figure 7.11 A view of the packing of compound **81** including one unit cell. View along the *a* axis; atoms are represented as balls.

Table 7.2 Selected bond lengths (Å), angles (°), and dihedral angles (°) for **77**–**81** with estimated standard deviations in parentheses.

	77	**78**	**79**	**80**	**81**
Distances (Å)					
O1–N6	1.246(4)	1.258(2)	1.267(2)	1.243(3)	1.259(4)
O2–N6	1.253(4)	1.271(2)	1.263(2)	1.256(3)	1.246(4)
N1–N2	1.348(5)	1.347(2)	1.345(2)	1.340(4)	1.351(4)
N2–N3	1.297(5)	1.304(2)	1.298(2)	1.301(4)	1.293(5)
N3–N4	1.361(5)	1.375(2)	1.366(2)	1.367(4)	1.362(5)
N4–C1	1.339(5)	1.331(3)	1.336(2)	1.335(4)	1.320(5)
N1–C1	1.355(5)	1.347(3)	1.352(2)	1.343(4)	1.350(5)
C1–N5	1.374(5)	1.374(3)	1.375(2)	1.381(4)	1.378(5)
N5–N6	1.325(4)	1.311(2)	1.305(2)	1.320(4)	1.328(4)
N1–C2	1.456(5)	1.460(3)	1.463(2)	1.461(4)	1.463(5)
N4–A	2.027(8)			3.027(3)	3.132(3)
O1–A	2.087(8)			2.745(2)	3.234(3)
Angles (°)					
N1–N2–N3	106.9(3)	106.1(2)	106.2(1)	105.9(3)	106.0(3)
N2–N3–N4	111.2(3)	111.2(2)	111.6(1)	111.5(3)	111.8(3)
N3–N4–C1	105.5(3)	105.1 (2)	105.2(1)	105.0(3)	105.1(3)
N4–C1–N1	117.2(3)	108.5(2)	108.1(1)	108.1(3)	108.9(3)
N4–C1–N5	134.7(4)	135.0(2)	135.2(1)	134.6(3)	135.9(3)
C1–N5–N6	116.4(3)	116.1(2)	116.7(1)	116.2(3)	117.4(3)
N5–N6–O1	124.2(3)	125.3(2)	124.3(1)	124.2(3)	115.1(3)
O1–N6–O2	119.7(3)	118.7(2)	119.1(1)	120.1(3)	120.8(3)
N4–M–O1	80.0(3)	67.6(1)	56.5(1)	55.6(1)	52.0(1)
Dihedral angles (°)					
N1–N2–N3–N4	–0.2(4)	–1.1(3)	0.5(2)	–0.3(3)	0.0(4)
C1–N5–N6–O1	–3.7(5)	2.3(4)	–1.5(2)	–0.8(4)	–178.6(3)

7.3.8 Strontium bis(1-methyl-5-nitriminotetrazolate) monohydrate (**82**)

Strontium bis(1-methyl-5-nitriminotetrazolate) crystallizes as a monohydrate in the monoclinic space group *C*2/*c* with four molecules in the unit cell and a calculated density of 2.189 g cm^{-3}. The strontium cations are coordinated ninefold by the atoms O1, O2 and N4 (1.73–1.82 Å) of four different 1-methyl-5-nitriminotetrazolate anions and O3 of the crystal water (Sr–O3 = 2.582(3) Å).

The molecular structure (**Figure 7.12**) of the anions is comparable to those of alkali and several guanidinium 1-methyl-5-nitriminotetrazolates in this Chapter. Again the C1–N5 bond length of 1.380(3) Å is significantly shorter than a C–N single bond. The NNO_2 group is twisted ~ 10 ° out of the tetrazole ring plane.

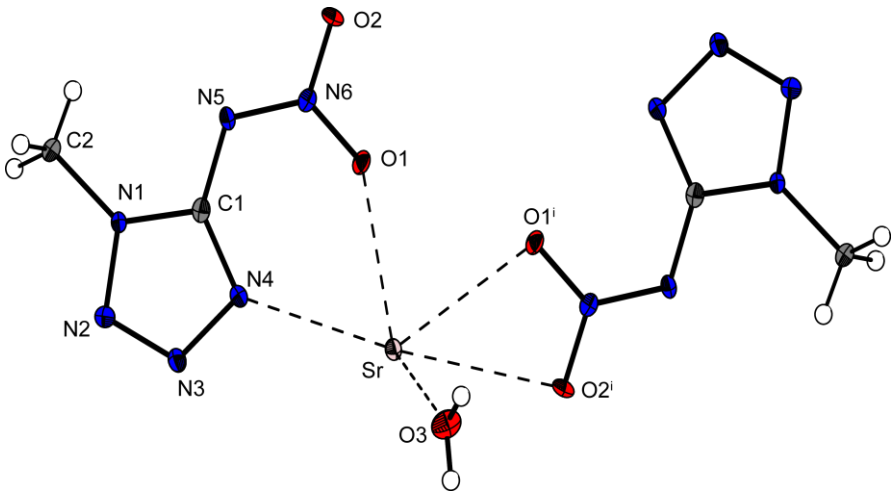

Figure 7.12 Molecular moiety of **82**. Hydrogen atoms shown as spheres of arbitrary radius and thermal displacements set at 50 % probability. Selected geometries: distances (Å) N1–N2 = 1.347(2), N1–C2 = 1.463(3), N1–C1 = 1.349(3), N2–N3 = 1.298(3), N3–N4 = 1.364(2), N4–C1 = 1.329(3), C1–N5 = 1.380(3), N5–N6 = 1.301(3), O1–N6 = 1.291(2), O2–N6 = 1.252(2), Sr–O1 = 1.811(1), Sr–O3 = 2.582(3), Sr–N4 = 2.733(2), Sr–O2^{i} = 2.768(1); angles(°) N1–C1–N4 = 108.2(2), N1–C1–N5 = 117.7(2), O1–N6–N5 = 124.1(2), O1–N6–O2 = 118.2(2), O1–Sr–N4 = 57.78(5); torsion angles (°) N6–N5–C1–N1 = −159.6(2), C1–N5–N6–O1 = −1.1(3); (i) x, –y, 0.5+z.

The packing of **82** is again strongly influenced by the formation of stacks along the *c* axis (**Figure 7.13**). The connection within the stacks are generated by the tridentate coordination modes of the atoms N4, O1 and O2 within one anion. The crystal water affects no bridging and is coordinated alternating up and down.

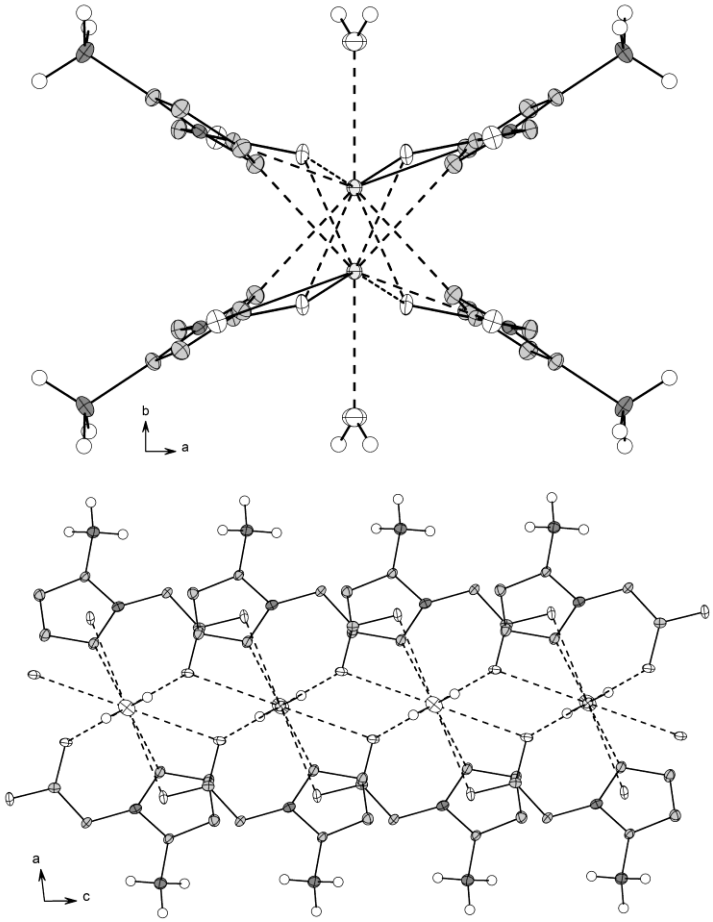

Figure 7.13 View through (along *c* axis, top) and on (along *a* axis, below) the stacks in **82**.

7.3.9 Strontium bis(2-methyl-5-nitriminotetrazolate) tetrahydrate (**83**)

83 crystallizes also in the monoclinic space group $C2/c$ with four molecules in the unit cell and the lowest density of 1.834 g cm^{-3}. The molecular moiety presented in **Figure 7.14** shows an octuple coordinated strontium cation, which is met by four crystal water molecules in a distance of 2.527(3) Å (Sr–O3) and 2.574(2) Å (Sr–O4) and by the atoms O1 (2.669(2) Å) and N5 (2.697(2) Å) of the 2-methyl-5-nitriminotetrazolate anion. The isolated coordination sphere within the molecular moiety is unique in comparison to the other structures observed in this work. The low density of **83** may be a reason of this isolated complexes, which are connected by weak hydrogen bonds raised by the water molecules. In contrast to the molecular structure of neutral 2-methyl-5-nitraminotetrazole (**45**), in which a C1–N5 bond distance of 1.40 Å is found, in **83** this bond length is shorter (1.386(4) Å) and also in the range of **82**. However, it is the longest C1–N5 distance observed in this work.

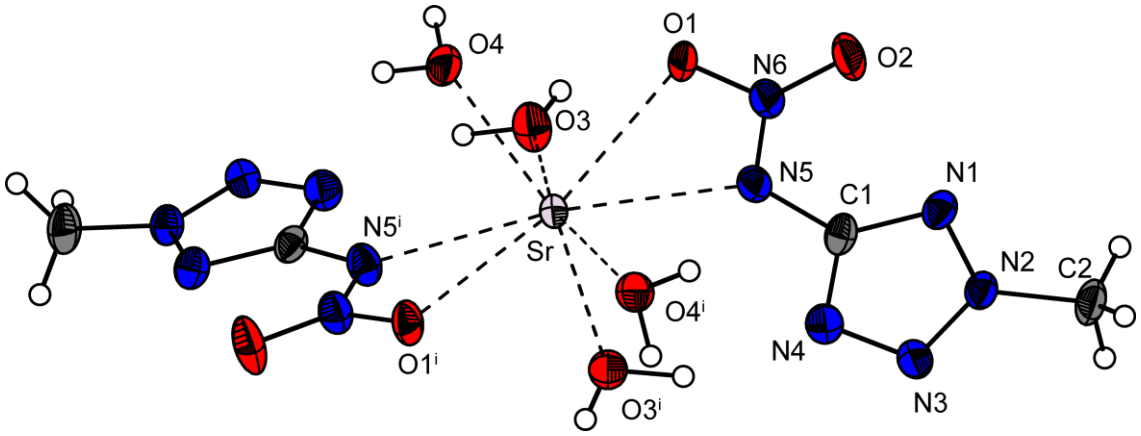

Figure 7.14 Molecular moiety of **83**. Hydrogen atoms shown as spheres of arbitrary radius and thermal displacements set at 50 % probability. Selected geometries: distances (Å) N1–N2 = 1.332(4), N2–C2 = 1.456(4), N1–C1 = 1.338(4), N2–N3 = 1.320(4), N3–N4 = 1.313(4), N4–C1 = 1.345(4), C1–N5 = 1.386(4), N5–N6 = 1.305(4), O1–N6 = 1.284(3), O2–N6 = 1.229(3), Sr–N5 = 2.697(2), Sr–O1 = 2.669(2), Sr–O3 = 2.527(3), Sr–O4 = 2.574(2); angles(°) N1–C1–N4 = 113.1(2), N1–C1–N5 = 131.3(3), O1–N6–N5 = 112.9(2), O1–N6–O2 = 121.3(3), O1–Sr–N5 = 47.41(7); torsion angles (°) N6–N5–C1–N1 = –2.5(5), C1–N5–N6–O1 = –176.3(3); (i) 2–x, y, 2.5–z.

1-Methyl-5-nitriminotetrazole and its crystal structure is described in Chapter 4. Its structure is very similar compared to the molecular structures of the anions participating in the investigated 1-methyl-5-nitriminotetrazolate salts. Only the position of the nitramine group to the tetrazole ring plane differs significantly since there are various hydrogen bonds influencing this building block. **Table 7.6** contains selected geometric details of these anions.

7.3.10 Silver 1-methyl-5-nitriminotetrazolate (**84**)

The silver salt **84** crystallizes in the monoclinic space group $P2_1/c$, with four formula units in the unit cell resulting in a calculated density of 2.947 g cm^{-3}. **Figure 7.15** represents the asymmetric unit and its labeling scheme. The distances between the tetrazole ring atoms are conform to the results for **85**, **87**, **88** and **89** and are described in detail in the structure of **85**. The tetrazole ring is planar (torsion angle N1–C1–N4–N3 = –0.9(3) °) indicating a delocalized, aromatic π system. The nitramine-group is considerably twisted out of this plane (torsion angle N4–C1–N5–N6 = 31.8(5) °) and the

bond length C1–N5 (1.37(4) Å) corresponds more to a C=N double bond. This result is very similar to latest investigations on alkali salts of 1-methyl-5-nitriminotetrazole.

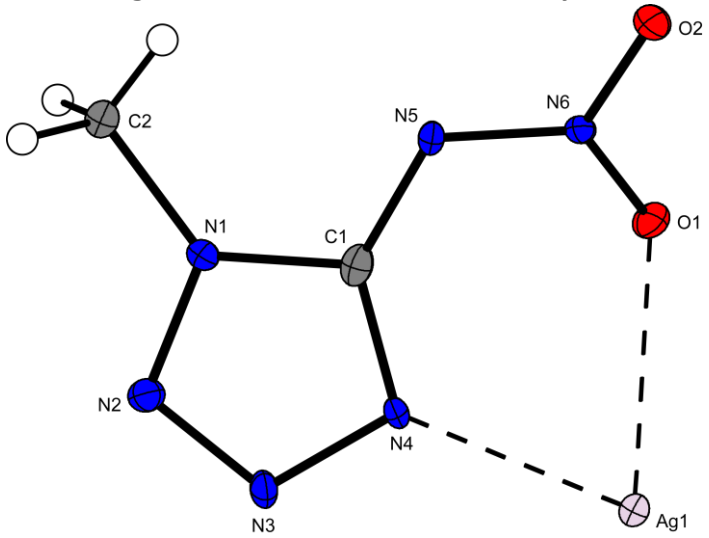

Figure 7.15 Formula unit of **84**. Thermal ellipsoids represent the 50 % probability level.

The ions of compound **84** are packed in a complex three-dimensional structure, which contains endless, two-dimensional layers as structural units, which are illustrated in **Figure 7.16**. As no classic hydrogen bonds can be detected in the crystal, the packing is only influenced by electrostatic forces.

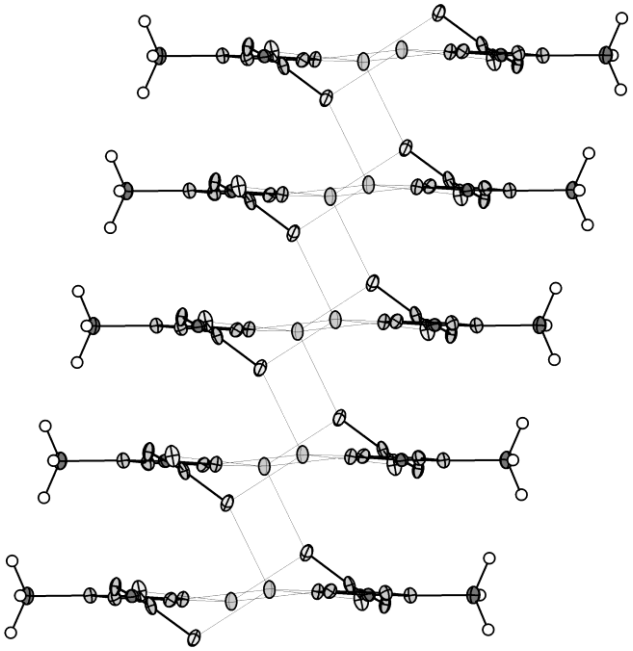

Figure 7.16 View on the 2-dim layers in the crystal structure of Ag_1-MeAtNO$_2$ along the *b* axis.

Within this structure the silver cations are pentacoordinated by the *N,O*-chelating nitriminotetrazolate with *d*(Ag1–N4) = 2.27(2) Å, and *d*(Ag1–O1) = 2.61(3) Å, by the oxygen atom of a neighboring tetrazolate *d*(Ag1–O1^{i}) = 2.77(4) Å [(i) x, –0.5–y, 0.5+z], by one nitrogen atom with *d*(Ag1–N3^{ii}) = 2.33 Å [(ii) 1–x, –0.5+y, 1.5–z] and the nitro group of another neighboring 5-nitriminotetrazolate anion with *d*(Ag1–O2^{iii}) = 2.46(2) Å; (iii) 1–x, 0.5+y, 1.5–z. The geometry of this coordination can be described as a distorted trigonal bipyramide. The distances for the metal coordinating bonds are very similar compared to those, found in alkali 5-nitriminotetrazolates.

7.3.11 Guanidinium 1-methyl-5-nitriminotetrazolate (**85**)

Figure 7.17 shows the molecular moiety of **85**, which crystallizes in the monoclinic space group *C*2/*c*. There are eight formula moieties in the unit cell and the crystal structure features a density of 1.550 g cm^{-3}. The C–N distances in the cations vary from 1.30 to 1.32 Å, which is between the typical values for C–N single bonds (1.47 Å) and C=N double bonds (1.22 Å) and show the delocalization of the positive charge. The observed bond lengths in the guanidinium cation match the typical values found in the literature for guanidinium nitrate [300] and guanidinium chloride.[301] The tetrazolate ring is again planar (torsion angle C1–N1–N2–N3 = –0.1(3)°). In contrast to this, the nitramine unit is significantly twisted from the ring plane (torsion angle N4–C1–N5–N6 = 8.2(4) °). The bond lengths between the tetrazolate ring atoms N1, N2, N3, and N4 vary from 1.29 to 1.36 Å and fit exactly in the range between N–N single bonds (1.45 Å) an N=N double bonds (1.25 Å). Also the distances between C1–N1 (1.35(4) Å) and C1–N4 (1.33(3) Å) lie within the values for C–N single and C=N double bonds. In contrast to this, the bond N1–C2 (1.46(3) Å), which links the methyl group to the tetrazolate ring, can definitely be identified as a C–N single bond. As the bond N5–N6 (1.31(2) Å) can be identified neither as single nor as double bond, also the electrons within the nitramine group participate in the delocalization.

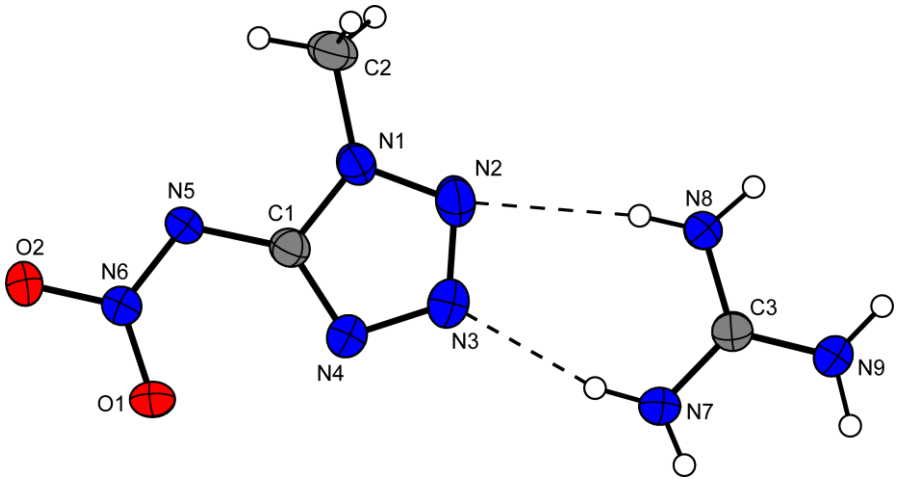

Figure 7.17 Formula unit of **85**. Thermal ellipsoids represent the 50 % probability level.

The packing of the crystal structure of **85** is dominated by several classical hydrogen bonds, which are summarized in **Table 7.3**. Because of these hydrogen bonds cations and anions are linked as one-dimensional, infinite chains, which are shown in **Figure 7.18** with the view along the *b* axis. Within these chains one guanidinium cation links two anions. There are two hydrogen bonds with O1 and O2 as acceptor and N8–H8b and N9–H9a as donor. In the other two hydrogen bonds (N2–H7b···N7, N3–H8a···N8) nitrogen atoms act as acceptor and as well as donor. In contrast, **Figure 7.19** shows the linkage of two of these infinite chains via hydrogen bonds along the *c* axis. This motif is responsible for the package of the crystal. One hydrogen atom, bonded to N7 at the guanidinium cation of one chain, interacts with the atoms N4 and O1 of the 1-methyl-5-nitriminotetrazolate of the second chain, which link the chains to each other.

Table 7.3 Hydrogen bonds in the crystal structure of **85**.

Atoms	d(D–H) [Å]	d(H···A) [Å]	d(D···A) [Å]	∢(D–H···A) [°]
N8–H8b···O2	0.86(3)	2.03(3)	2.890(3)	178(3)
N8–H8a···N2	0.82(3)	2.35(3)	3.167(3)	172(3)
N8–H8a···N3	0.82(3)	2.67(3)	3.368(3)	143(2)
N7–H7a···N4	0.82(3)	2.39(3)	3.016(3)	134(2)
N7–H7a···O1	0.82(3)	2.52(3)	3.265(3)	151(3)
N7–H7b···N3	0.85(4)	2.14(4)	2.970(3)	166(3)
N9–H9a···O1	0.90(4)	2.04(4)	2.930(3)	174(3)
N9–H9b···O2	0.90(4)	2.07(4)	2.942(3)	164(3)

N9–H9b···N5	0.90(4)	2.45(4)	3.139(3)	133(3)
N9–H9b···N6	0.90(4)	2.66(4)	3.524(3)	161(3)

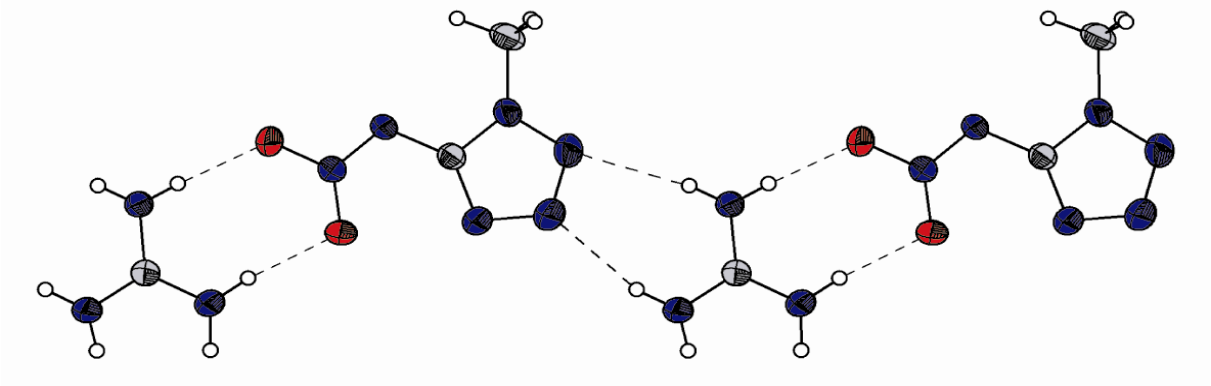

Figure 7.18 Cation coordination via hydrogen bonds within the one-dimensional chains. View along axis *b*; thermal ellipsoids represent the 50 % probability level.

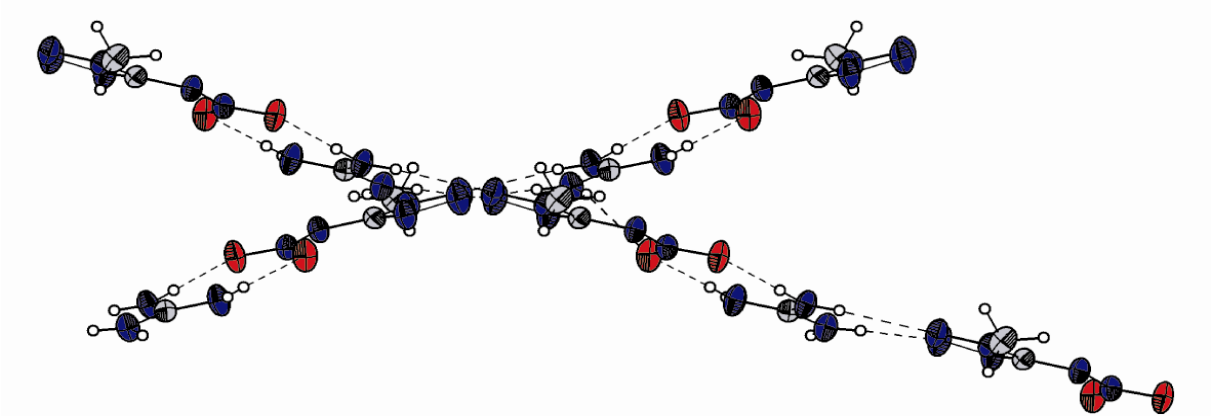

Figure 7.19 Connection between the 1-dim chains. View along axis *c*.

Info: Although aminoguanidinium 1-methyl-5-nitriminotetrazolate (**86**) could be recrystallized from wet ethanol forming colorless crystals, a suitable solution of the X-ray determination was not practicable due to an unsolvable twin problem. The elemental analysis confirmed no inclusion of crystal water.

7.3.12 Diaminoguanidinium 1-methyl-5-nitriminotetrazolate monohydrate (**87**)

Figure 7.20 shows the molecular moiety of compound **87** and its labeling scheme. It crystallizes in the triclinic space group *P*-1, with two formula units in the unit cell and a

calculated density of 1.605 g cm^{-3}. The bond lengths within the 1-methyl-5-nitriminotetrazolate fit the values, observed for **85** almost exactly. In contrast, to that the steric constitution of the nitramine-group to the ring plane is different. The aromatic cycle and the nitramine group lie together in one plane (torsion angle N4–C1–N5–N6 = 0.4(2)°). Only the oxygen atoms O1 and O2 are slightly twisted out of the plane (torsion angles C1–N5–N6–O1 = 1.5(2)°, C1–N5–N6–O2 = -178.5(1)°). The distances N7–C3 (1.33(6) Å), N9–C3 (1.32(2) Å) and N11–C3 (1.33(2) Å) within the diaminoguanidinium cation are comparable to the structure found in diaminoguanidinium 3-nitro-1,2,4-triazol-5-one [302] and are slightly longer than the values found in the guanidinium cation (**85**), which can be explained by the influence of the two additional amino groups. The hydrazine bonds (d(N7–N8) = 1.41(2) Å, d(N9–N10) = 1.41(7) Å) are marginally shorter than the bonds in isolated hydrazine (1.45 Å).[225]

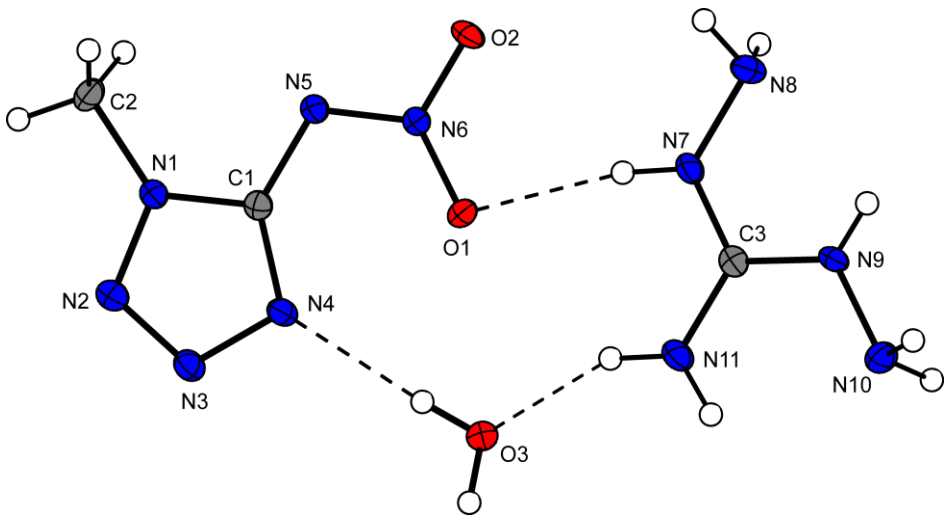

Figure 7.20 Molecular moiety of **87**. Thermal ellipsoids represent the 50 % probability level.

The packing of the structure is again influenced by several classical hydrogen bonds. The ions are packed as two-dimensional, infinite layers within the crystal structure. In these layers one anion is coordinated by three cations and two molecules crystal water via the five hydrogen bonds: N2–H9···$N9^{i}$: 0.78(2), 2.20(3), 2.90(2) Å, 146.6(1)°, (i): 1-x, -y,1-z; N4–H3A···$O3^{ii}$: 0.84(2), 2.04(2), 2.87(2) Å, 170.5(2)°, (ii): x, y, z; N5–H3B···$O3^{iii}$: 0.90(2), 2.06(2), 2.94(2) Å, 164.9(2)°, (iii): -1+x,y,z; O2–H11B···$N11^{iv}$: 0.85(2), 2.28(2), 2.86(2) Å, 126.7(1)°, (iv): -x,1-y,-z; O1–H7···$N7^{v}$: 0.85(2), 2.04(2), 2.88(2) Å, 167.1(1)°, (v): 1-x,1-y,-z. These two-dimensional structural units are arranged in a parallel way and connected only via hydrogen bonds. The distance between two infinite layers is ~5 Å. Due to the

moderate interactions the layer-structure is tight and the calculated density for **87** is fairly high (1.605 g cm^{-3}). **Figure 7.21** gives a clear impression of the three-dimensional structure and the dense assembly of layers.

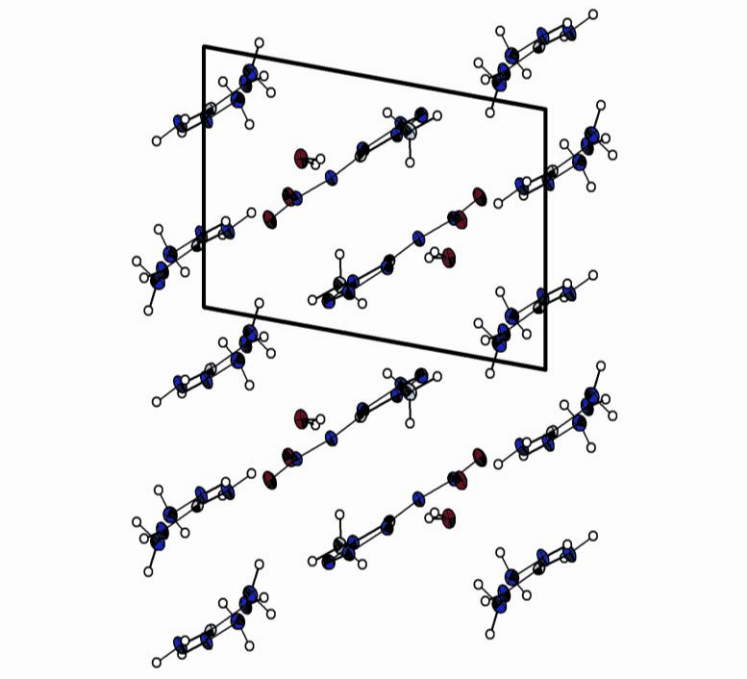

Figure 7.21 View on the layers in the crystal structure of **87** along the *a* axis. The unit cell is drawn.

7.3.13 Triaminoguanidinium 1-methyl-5-nitriminotetrazolate (**88**)

The unit cell of **88**, which crystallizes with a calculated density of 1.569 g cm^{-3} in the triclinic space group *P*-1, contains two formula moieties. The bond lengths in the 1-methyl-5-nitriminotetrazolate anion, which is depicted in **Figure 7.22**, are also very similar to the values found and discussed for **85** and **87**. Although again there are differences in the steric constitution compared to **87**, which can be seen on the nitramine-group strongly twisted out of the aromatic ring plane (torsion angle N4–C1–N5–N6 = 16.9(3)°). Even the oxygen atoms O1 and O2 of the nitro group stick significantly up the ring plane (torsion angles N4–C1–N5–O1 = 17.8(2)°, N4–C1–N5–O2 = 15.3(2)°). Within the triaminoguanidinium cation the bond lengths correspond exactly to the N–N values of **87** and those observed for triaminoguanidinium nitrate.[213]

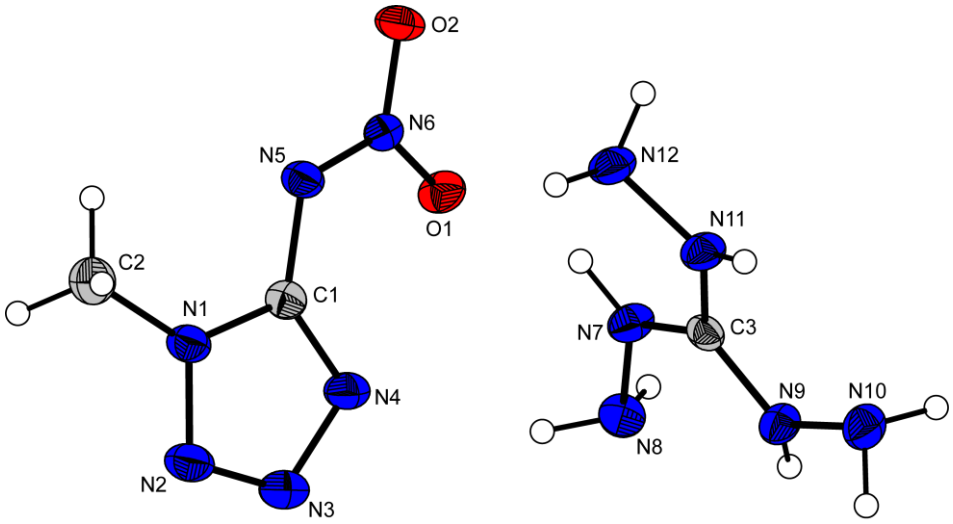

Figure 7.22 Molecular moiety of **88**. Thermal ellipsoids represent the 50 % probability level.

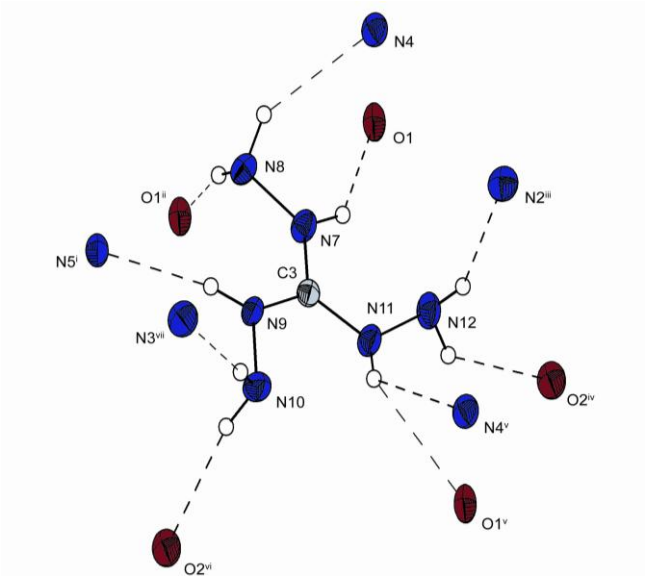

Figure 7.23 Hydrogen bonding of the triaminoguanidinium cation. Symmetry codes: (i) x, –1+y, z; (ii) –x, –1–y, 1–z ; (iii) 1–x, –y, 2–z; (iv) 1–x, –y, 1–z; (v) 1+x, y, z; (vi) 1–x, 1–y, 1–z; (vii) 1–x, 1–y, 2–z.

There are several moderate hydrogen bonds listed in **Table 7.4**, which strongly influence the packing of the crystal structure of **88**. Each N–H or N–H_2 group of the triaminoguanidinium ion acts as hydrogen bond donor, thus the coordination of this cation dominates the resulting structure. An overview of the hydrogen bonds based on the donor groups of the cation is displayed in **Figure 7.23**. Since the interactions via hydrogen bonds are mostly weak and there are no layers or chains, the packing of the molecules is not as dense (1.569 g cm^{-3}) as those observed in **85** and **87**.

Table 7.4 Hydrogen bonds in the crystal structure of **88**.

Atoms	d(D–H) [Å]	d(H···A) [Å]	d(D···A) [Å]	∢(D–H···A) [°]
N9–H9···N5	0.86(2)	2.17(2)	2.98(2)	159.9(2)
N7–H7···O1	0.90(2)	2.13(2)	2.87(2)	138.4(2)
N7–H7···N6	0.90(2)	2.68(2)	3.55(2)	160.5(2)
N12–H12B···O2	0.90(2)	2.24(2)	2.95(2)	136.0(2)
N12–H12A···N2	0.92(2)	2.38(2)	3.23(2)	153.8(2)
N11–H11···O1	0.83(2)	2.56(2)	3.08(2)	121.8(2)
N11–H11···N4	0.83(2)	2.64(2)	3.29(2)	136.0(2)
N8–H8B···N4	0.92(2)	2.40(2)	3.21(2)	146.7(2)
N10–H10B···N3	0.94(2)	2.35(2)	3.28(2)	169.0(2)
N8–H8A···O1	0.88(2)	2.15(2)	3.01(2)	163.9(2)
N10–H10A···O2	0.91(2)	2.30(2)	3.20(2)	168.0(2)

7.3.14 Azidoformamidinium 1-methyl-5-nitriminotetrazolate (**89**)

Azidoformamidinium 1-methyl-5-nitrimintetratolate (**89**) crystallizes in the monoclinic space group $P2_1/c$, with four molecules in the unit cell and a calculated density of 1.612 g cm^{-3}. The asymmetric unit and its labeling scheme are displayed in **Figure 7.24**. The steric constitution of the anion in **89** is comparable to this observed for compound **85**. Again the nitramine group is twisted out of the aromatic ring plane (torsion angle N4–C1–N5–N6 = 6.9(2)°). The structure of the azidoformamidinium cation corresponds to that of azidoformamidinium chloride.[215] The azidoformamidinium unit is not planar (torsion angle N11–C3–N7–N8 = 13.6(2)°) and the azide group is angulated (angle N7–N8–N9 = 171.1(1)°), which is quite common, for covalent azide groups due to hyperconjugation effects.[303] The amino-groups of N10 and N11 building a planar fragment with the carbon atom C3 (angle N11–C3–N10 = 122.1(1)°).

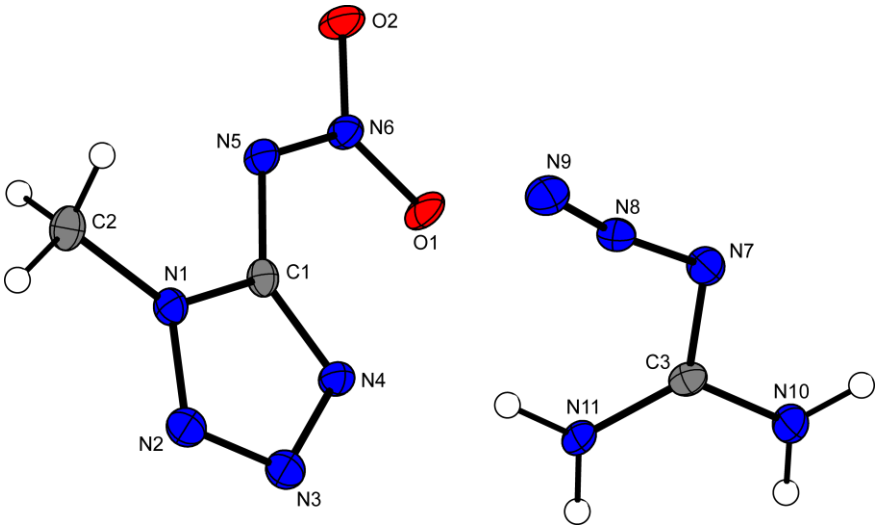

Figure 7.24 Molecular moiety of **89**. Thermal ellipsoids represent the 50 % probability level.

The three-dimensional structure of compound **89** is again significantly influenced by several hydrogen bonds. The molecular network contains one-dimensional, infinite chains as structural units. Six different hydrogen bonds can be found in the investigated structure, listed in **Table 7.5**. The coordination of one azidoformamidinium cation is shown in **Figure 7.25**, representing the smallest moiety of the molecular packing.

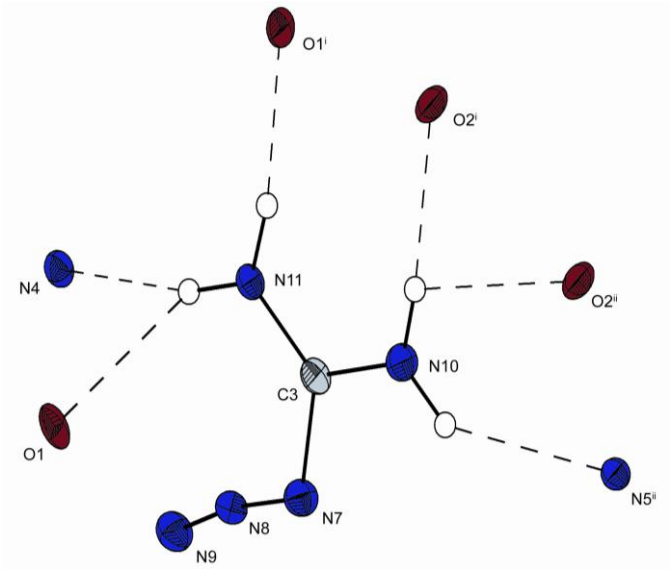

Figure 7.25 Hydrogen bonding of the azidoformamidinium cation. Symmetry codes: (i) 1–x, 0.5+y, 1.5–z; (ii) x, –0.5–y, 0.5+z.

The nitrogen atoms of the azide group do not participate in any of the hydrogen bonds. The density of **89** (1.612 g cm^{-3}) is comparable to the density of bis(azidoformamidinium) 5,5'-azotetrazolate (1.624 g cm^{-3}), which had been recently investigated in this research group.[72]

Table 7.5 Hydrogen bonds in the crystal structure of **89**.

Atoms	d(D–H) [Å]	d(H···A) [Å]	d(D···A) [Å]	∢(D–H···A) [°]
N10–H10A···O2^{i}	0.88(2)	2.03(2)	2.90(2)	168.3(2)
N10–H10A···O2^{ii}	0.88(2)	2.36(2)	2.83(2)	113.6(1)
N11–H11B···N4	0.89(2)	2.02(2)	2.89(2)	164.7(2)
N11–H11B···O1	0.89(2)	2.42(2)	2.97(2)	120.7(1)
N11–H11A···O1^{i}	0.91(2)	2.05(2)	2.96(2)	171.1(2)
N10–H10B···N5^{ii}	0.87(2)	2.37(2)	3.09(2)	141.3(2)

Table 7.6 Selected bond lengths (Å), angles (°), and dihedral angles (°) for compounds **84**, **85**, **87**, **88** and **89**.

	84	**85**	**87**	**88**	**89**
Distances:					
C1–N1	1.355(4)	1.354(3)	1.346(2)	1.351(2)	1.355(2)
C2–N1	1.465(4)	1.455(3)	1.460(2)	1.457(2)	1.461(2)
N1–N2	1.343(3)	1.344(3)	1.348(2)	1.344(2)	1.349(2)
N2–N3	1.301(4)	1.292(3)	1.297(2)	1.295(2)	1.298(2)
N3–N4	1.362(3)	1.357(3)	1.364(2)	1.363(2)	1.369(2)
N4–C1	1.336(4)	1.330(3)	1.333(2)	1.335(2)	1.336(2)
N5–C1	1.365(4)	1.368(3)	1.382(2)	1.374(2)	1.379(2)
N5–N6	1.317(3)	1.309(3)	1.318(2)	1.319(2)	1.319(2)
N6–O1	1.265(3)	1.249(3)	1.252(1)	1.257(2)	1.261(1)
N6–O2	1.261(3)	1.264(3)	1.256(1)	1.249(2)	1.260(2)
Angles:					
C1–N1–C2	129.8(3)	129.4(2)	130.2(1)	129.3(1)	129.3(1)
C2–N1–N2	120.7(2)	121.9(2)	121.7(1)	121.8(1)	122.0(1)
N1–N2–N3	106.1(2)	106.1(2)	106.9(1)	106.4(1)	106.6(1)
N2–N3–N4	111.2(2)	111.9(2)	110.9(1)	111.4(1)	111.2(1)
N3–N4–C1	106.0(2)	105.4(2)	105.4(1)	105.4(1)	105.6(1)
N4–C1–N5	134.7(3)	134.9(2)	134.8(1)	135.5(1)	135.4(1)
N5–C1–N1	117.6(3)	117.1(2)	116.6(1)	116.5(1)	116.6(1)
C1–N5–N6	116.3(2)	116.4(2)	115.9(1)	117.1(1)	116.4(1)
N5–N6–O1	123.7(2)	124.5(2)	123.4(1)	122.9(1)	124.1(1)

N5–N6–O2	116.1(3)	115.4(2)	116.6(1)	116.3(1)	115.9(1)
O1–N6–O2	120.2(2)	120.1(2)	120.0(1)	120.8(1)	120.0(1)
Dihedral angles:					
N2–N1–C1–N5	–172.2(3)	–177.9(2)	–179.8(1)	–176.2(1)	–174.7(1)
N4–C1–N5–N6	31.8(5)	8.3(4)	0.4(2)	16.9(2)	6.9(2)

7.4 NMR Spectroscopy

The proton coupled ^{15}N NMR spectra of compound **75** and **76** are shown in **Figure 7.26**. The ^{15}N NMR shifts, the values of the ^{15}N, ^{1}H coupling constants and the ^{13}C NMR shifts of the tetrazole carbon atoms are presented in **Table 7.7**. For all compounds the proton coupled as well as the proton decoupled NMR spectra (with full NOE) were recorded. The assignments are based on the analysis of the ^{15}N, ^{1}H coupling constants. All Shifts are given with respect to CH_3NO_2 (^{15}N) and TMS (^{13}C) as external standard. In both cases D_2O was used as solvent.

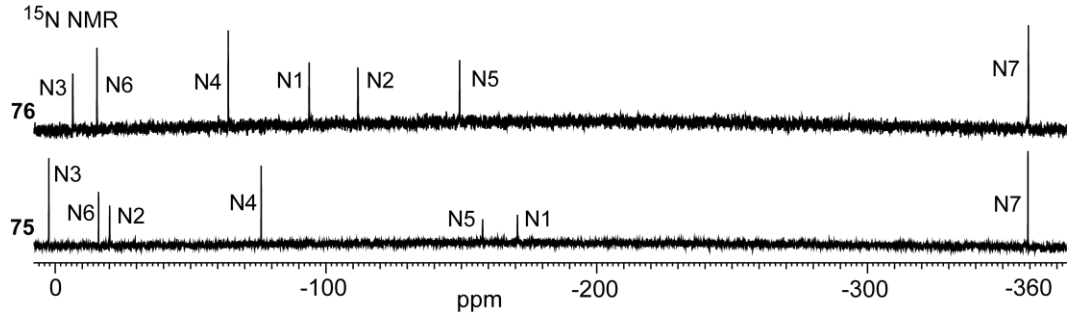

Figure 7.26 ^{15}N NMR spectra of compounds **75** (below) and **76** (top).

Table 7.7 ^{15}N NMR and ^{13}C NMR Chemical Shifts and ^{15}N, ^{1}H coupling constants.

	N1	N2	N3	N4	N5	N6	N7	C1
75	–170.7	–20.1	2.4	–76.1	–157.9	–16.0	–359.3	157.5
	^{2}J(N–H) = 2.1Hz	^{3}J(N–H) = 1.8Hz						
76	–93.8	–111.8	–6.4	–63.9	–149.3	–15.4	–359.4	168.0
	^{3}J(N–H) = 1.8 Hz	^{2}J(N–H) = 2.1Hz	^{3}J(N–H) = 1.8 Hz					

The alkali salts **77–81** were characterized using multinuclear (^{1}H, ^{7}Li, ^{13}C, ^{14}N, ^{15}N) NMR spectroscopy. All shifts are given with respect to LiCl (^{7}Li), CH_3NO_2 (^{14}N, ^{15}N) and TMS (^{1}H, ^{13}C) as external standard. In all cases D_2O was used as solvent. In the ^{1}H spectra only the methyl protons and in the case of the monohydrate the crystal water can be seen. The ^{7}Li spectrum of **77** shows one signal at –1.00 ppm. The ^{13}C NMR spectra show two signals, caused by the methyl groups and the high-field shifted tetrazole carbon atom. For compound **78** the proton coupled as well as the proton decoupled NMR spectra (with full NOE) were recorded. The assignments are based on the analysis of the ^{15}N–^{1}H coupling constants and on comparison with known compounds. The proton coupled ^{15}N NMR spectrum of compound **78,** representative for all five alkali salts, is shown in **Figure 7.27**.

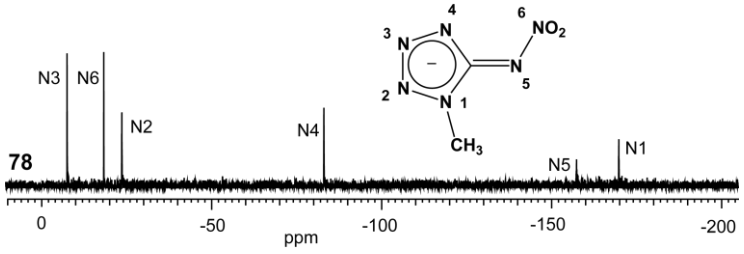

Figure 7.27 ^{15}N NMR spectrum of **78**.

Also compounds **85–89** were investigated using ^{1}H, ^{13}C and ^{15}N NMR (proton coupled) spectroscopy and the chemical shifts are given with respect to TMS (^{1}H, ^{13}C) as well as $MeNO_2$ (^{15}N) as external standard. In all cases *d*$_6$-DMSO or D_2O were used as the solvent. All recorded ^{1}H spectra show one signal caused by the protons of the methyl group (C2) at ~3.66 ppm. The proton signals of the cations are shifted to lower field in the range of 4.5–11 ppm. Two signals can be assigned in the ^{13}C spectra, caused by the methyl groups (33.1 ppm) and the low-field shifted tetrazole carbon atom (157.7 ppm). Since **88** and **89** have the highest nitrogen content within the investigated derivatives, the proton-coupled ^{15}N spectra in *d*$_6$-DMSO (**88**) and D_2O (**89**), respectively, were recorded and are shown in **Figure 7.28**. The solvent shift of the ^{15}N signals to higher fields in D_2O can be seen clearly.

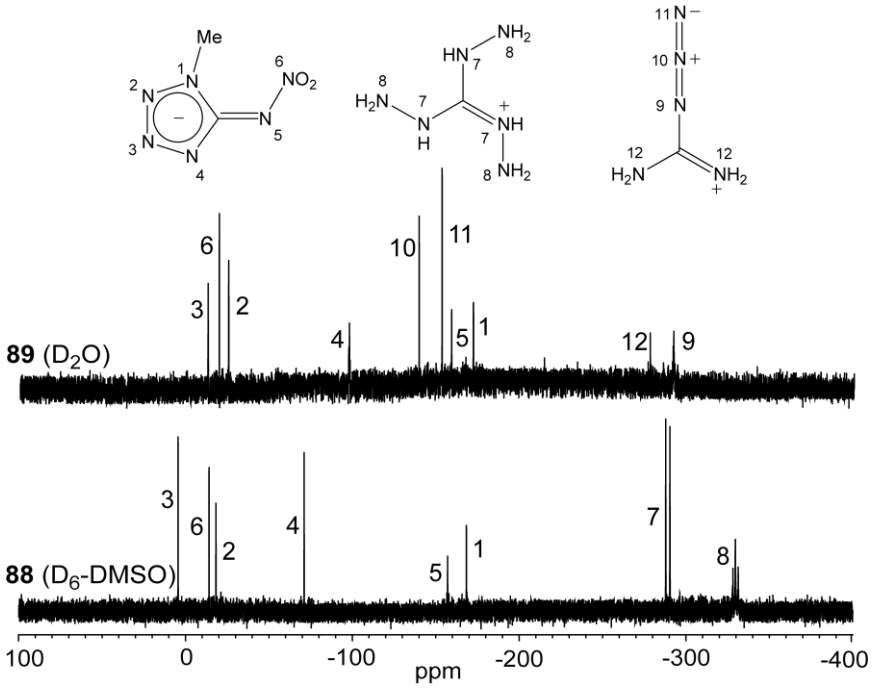

Figure 7.28 ^{15}N NMR spectra of **88** and **89**. **88**: δ = 4.5 (N3), –14.1 (N6), –18.3 (N2, q, $^{3}J_{NH}$ = 1.9 Hz), –71.2 (N4), –157.2 (N5), –168.4 (N1, q, $^{2}J_{NH}$ = 2.2 Hz), –289.1 (N7, d, $^{1}J_{NH}$ = 102.7 Hz), –329.7 (N8, t, $^{1}J_{NH}$ = 69.4 Hz) ppm; **89**: δ = –12.4 (N3), –19.0 (N6), –24.7 (N2, q, $^{3}J_{NH}$ = 1.9 Hz), –97.1 (N4), –139.0 (N10), –152.7 (N11), –158.5 (N5), –171.5 (N1, q, $^{2}J_{NH}$ = 2.2 Hz), –277.6 (N12), –291.8 (N9).

7.5 Vibrational Spectroscopy

Deprotonated methyl-5-nitriminotetrazoles as well as their neutral analogues can be easily identified using vibrational spectroscopy (IR and Raman). The Raman spectra of **75** and **76** are shown in **Figure 7.29**. After deprotonation, the absorption band of the 1-methyl-5-nitriminotetrazoles at about 1600 cm^{-1} (C=N stretching) is found at lower wavenumbers (1508 cm^{-1}). In the case of **76** these difference is much smaller due to longer C1–N5 nitramine bond length in **45**. The Raman spectra of the ammonia salts contain further characteristic absorption bands, which were assigned by calculating (DFT B3LYP/CC-PVDZ) the vibrational spectra after optimizing the structure of the anions: 3080–3000 cm^{-1} [$\nu_{sym}(CH_3)$], 2865–2960 cm^{-1} [$\nu_{sym}(NH_4^+)$], 1480–1560 cm^{-1} [$\nu_{asym}(NO_2)$, ν(C=N),], 1460–1400 cm^{-1} [ν_{asym} CH_3], 1550–1350 cm^{-1} [ν tetrazolate ring,

ν (C–N)], 1050–980 [$\nu_{sym}(NNO_2)$], 1350–700 cm^{-1} [ν(NCN), ν(NN), γ(CN), δ(tetrazolate ring)].

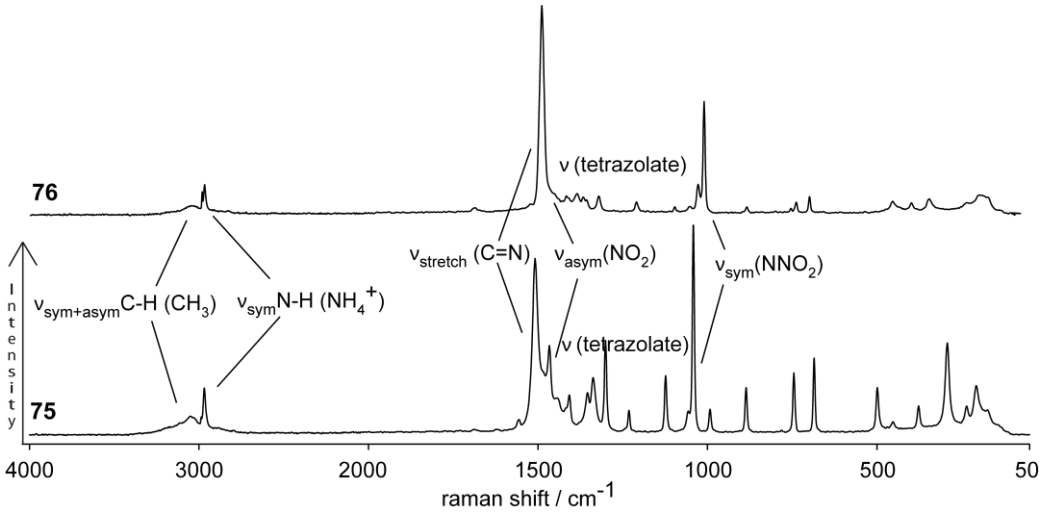

Figure 7.29 Raman spectra of compounds **75** and **76** (25 °C, 1064 nm) showing characteristic vibrations.

Also the alkaline metal salts **77–81** were identified using vibrational spectroscopy (IR and Raman). Again, after deprotonation, the absorption band of the C=N stretching of 1-methyl-5-nitriminotetrazole (**44**) at 1670–1580 cm^{-1} is found at lower wavenumbers (1500–1550 cm^{-1}). The Raman spectra of **77–81** are shown in **Figure 7.30**.

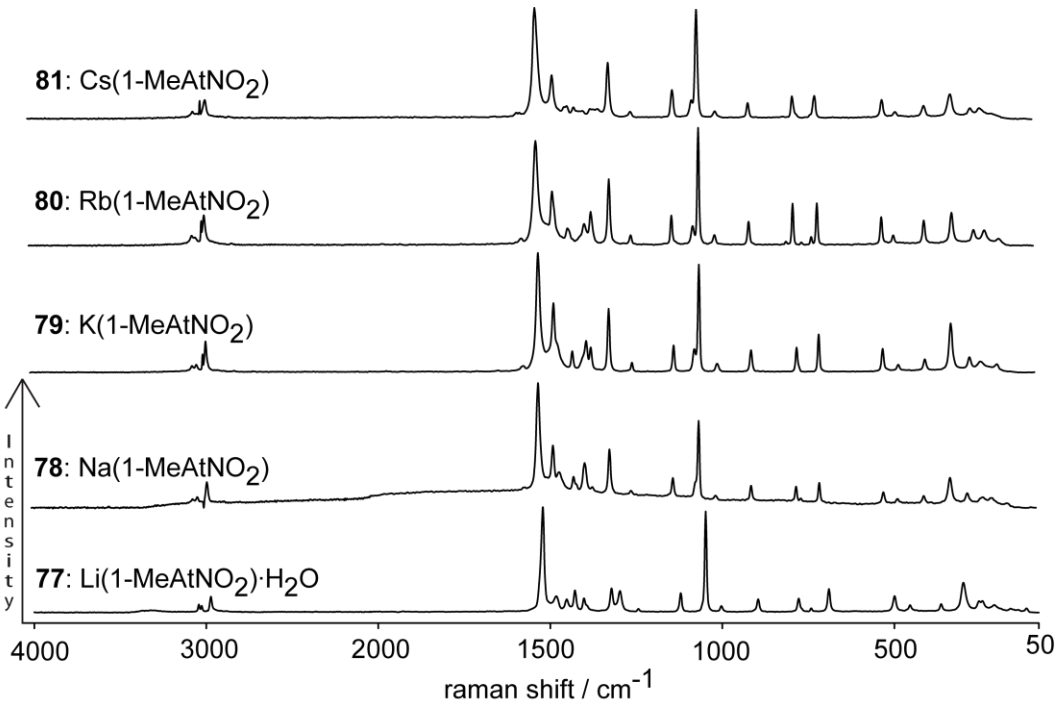

Figure 7.30 Raman spectra of the alkali salts **77–81**.

The Raman spectra of **44** and its salts **85–89** are shown in **Figure 7.31**. The absorption band of the C=N stretching vibration is the most significant peak in the Raman spectrum of 1-methyl-5-nitriminotetrazole (**44**) and lies in the range from 1670–1580 cm^{-1}. This absorption band is shifted to lower wavenumbers (1550–1500 cm^{-1}) for its salts **85–89**. It can be seen that the anions are much higher in intensity in comparison to the cations. The N–H stretch vibrations of the cations can only be obtained as weak absorption bands in the range from 3400–3200 cm^{-1}. Also the C–N and N–N stretching vibrations can be assigned to weak peaks ranging from 1700–1400 cm^{-1}. In the spectrum of **89** there are two absorption bands (2189 and 2112 cm^{-1}), which can be identified as ν_{sym} and ν_{asym}, respectively, of the covalent-bonded azide group.

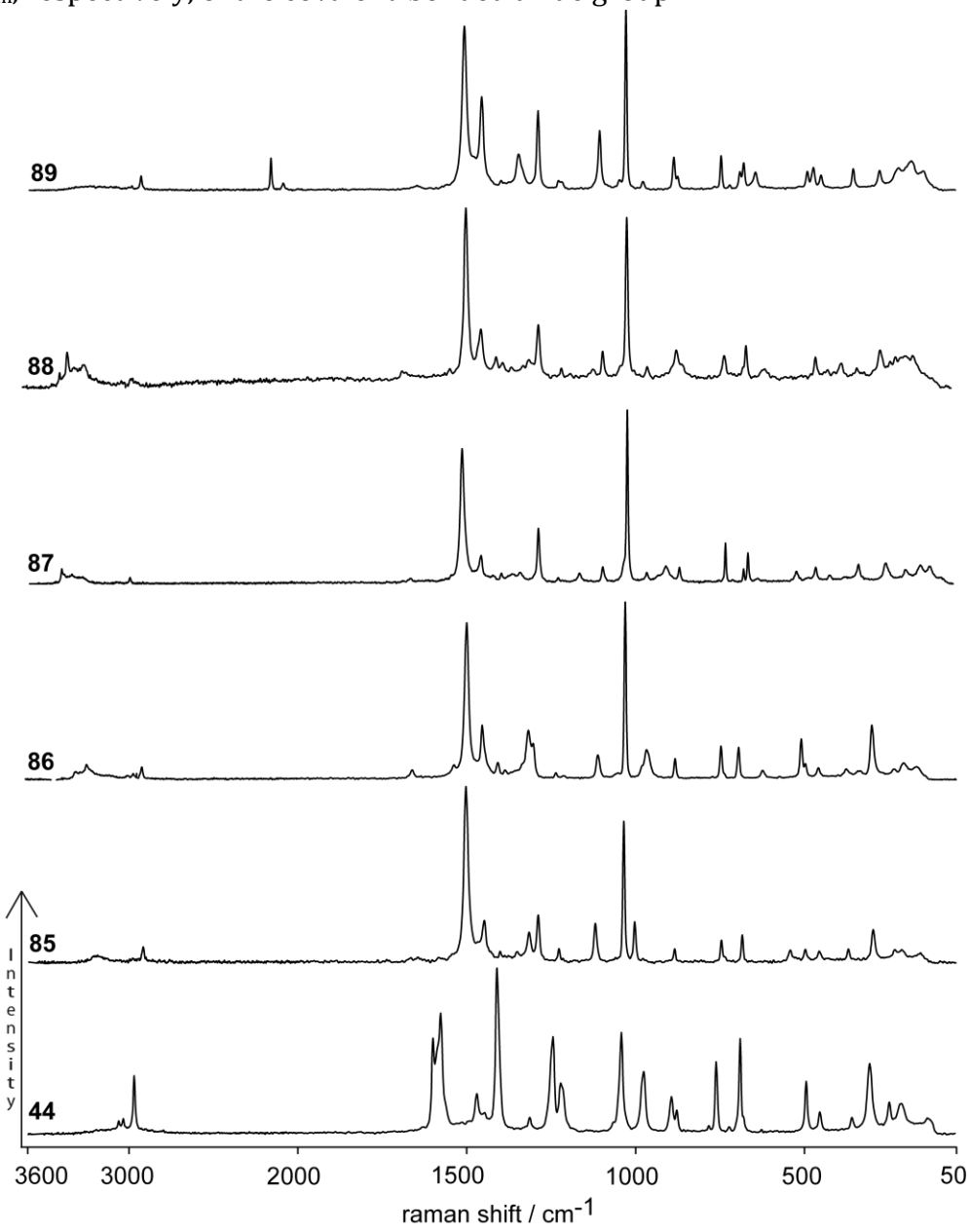

Figure 7.31 Raman spectra of 1-methyl-5-nitriminotetrazole (**44**) and its salts **85**–**89**.

7.6 Physico-Chemical Properties

Due to the promising energetic characteristics of **75–89** their physico-chemical properties were investigated.

7.6.1 Differential Scanning Calorimetry (DSC)

The thermal behavior of the 1-methyl-5-nitriminotetrazolate salts (**75–89**) was determined, using DSC measurements. The measurements of the ammonium methyl-5-nitriminotetrazolate salts **75** and **76** were performed in covered Al-containers on the Perkin-Elmer Pyris 6 DSC, at different heating rates (2, 5, 10, 15 and 20 K min^{-1}). The decomposition points are given as onset temperatures. **75** shows a well-defined decomposition point at 188 °C while **76** starts to decompose at about 150 °C in three steps. The DSC plots in **Figure 7.32** illustrates the thermal behavior of ~1 mg of **75** and **76** in the temperature range from 50–350 °C showing the dependency of the decomposition temperature from the heating rate.

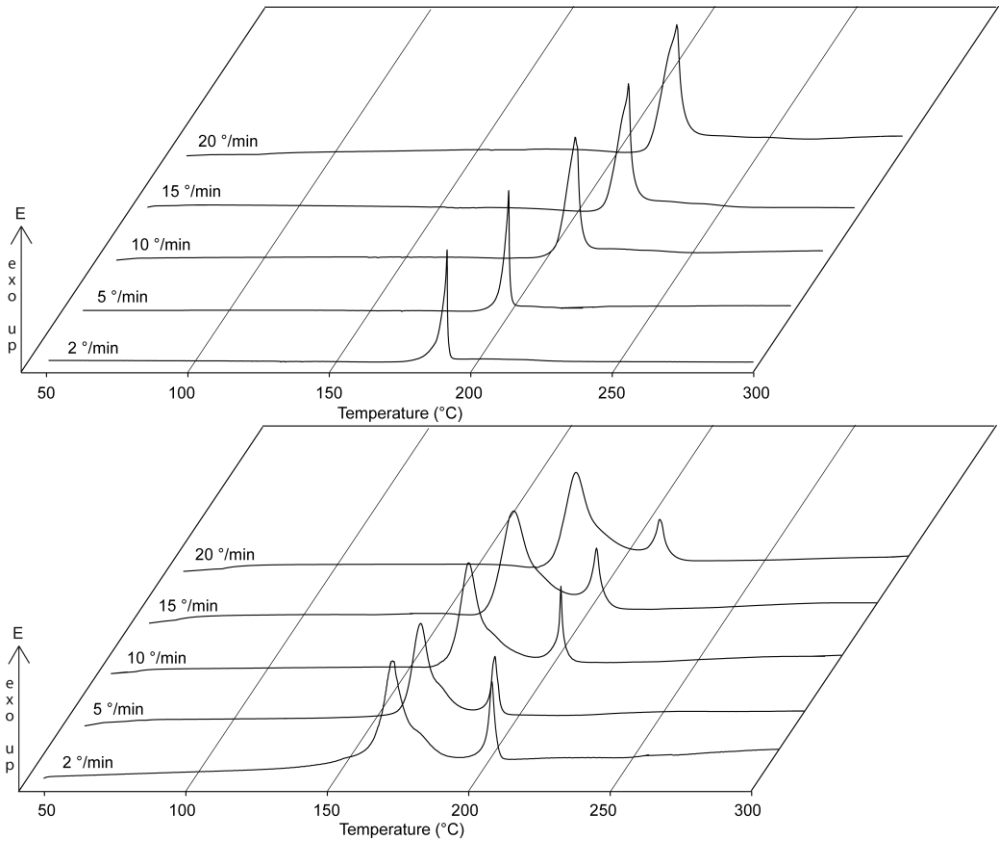

Figure 7.32 DSC plots (exo-up) of the thermal behavior of **75** (top) and **76** (below) at different heating rates (2, 5, 10, 15, 20 °C min^{-1}).

For determining the heats of decomposition the Linseis DSC PT 10 was used. Three samples (~2 mg) were heated with a heating rate of 2 °C min^{-1} and a nitrogen flow of 5 L h^{-1} over the decomposition peaks and the surface was integrated using the Linseis software yielding the following values. $\Delta_{Dec.}H_m°$ (J g^{-1}) **75:** –2189, **76:** –2420.

DSC measurements determining the thermal behavior of the metal salts of 1-methyl-5-nitriminotetrazole **77–82** and strontium 2-methyl-5-nitraminotetrazolate (**83**) were performed in covered Al-containers with a nitrogen flow of 20 mL min^{-1} on the Perkin-Elmer Pyris 6 DSC (**77**–**81**) as well as on the Linseis PT10 DSC (**82**, **83**) at heating rates of 5 °C min^{-1}. The DSC plots in **Figure 7.33** show the thermal behavior of ~1.5 mg of **77–83** in the temperature range from 50–400 °C. The salts **77–81** show melting points between 230 and 280 °C followed by decompositions above 300 °C. The lithium salt **77** shows the loss of its crystal water starting at a temperature of 140 °C. **82** is characterized by the highest decomposition temperature of 350 °C. The loss of its crystal water can be detected in the range of 120–170 °C. **83** melts under release of water above 165 °C followed by a brought decomposition starting at 230 °C.

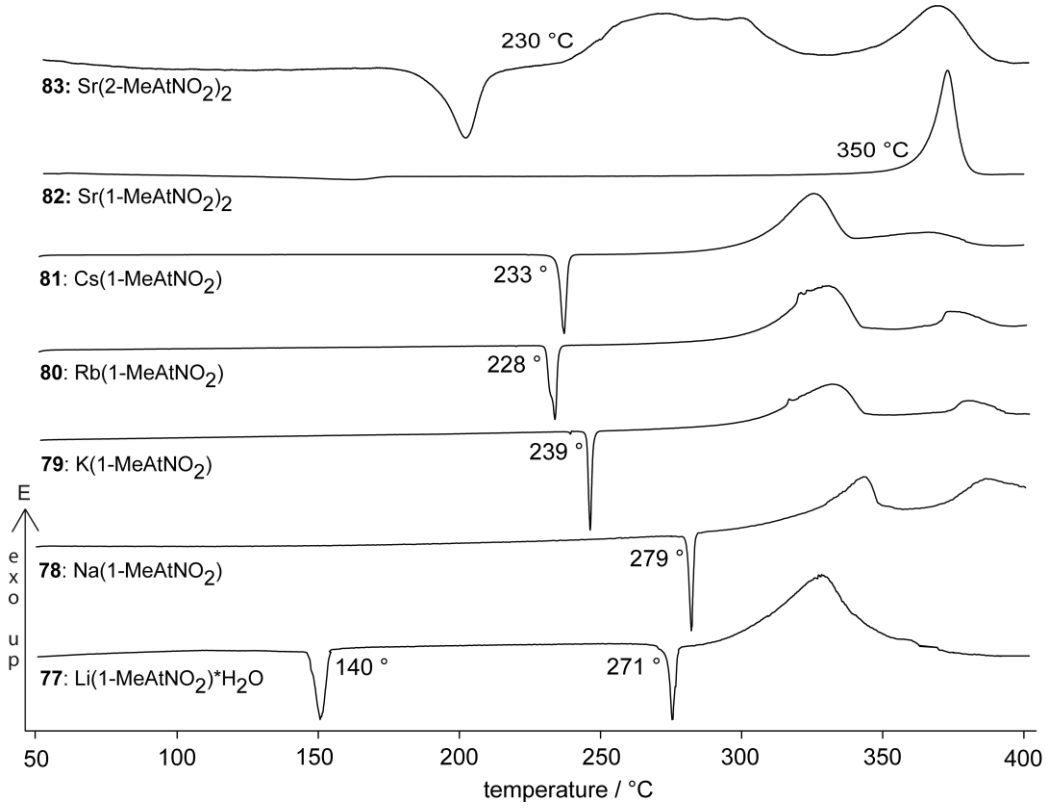

Figure 7.33 DSC plots (endo up) of compounds **77–83**. (5 °C min^{-1}); melting points, T_{onset} **77**: 271 °C, **78**: 279 °C, **79**: 239 °C, **80**: 228 °C, **81**: 233 °C, **83**: 165 °C.

Also DSC measurements of the nitrogen-rich salts **85–89** were performed under constant nitrogen flow (20 mL min^{-1}) in covered Al-containers with a hole (0.1 mm) for gas release on a Linseis PT 10 DSC, at a heating rate of 5 °C min^{-1}. The thermal behavior of ~2 mg of the compounds **85–89** in the temperature range from 50 to 300 °C is illustrated as thermograms in **Figure 7.34**. The melting points and the temperatures of decomposition are given as onset temperatures. The well-defined melting points depend on the number of hydrogen bonds, which can be found in the corresponding crystal structures. Compounds **87** and **89** melt at significantly lower temperatures (120 and 118 °C) than **85**, **86** and **88** since the packing of the molecules within the crystal structure is only influenced by five and six hydrogen bonds, respectively. In contrast at least ten hydrogen bonds can be found in the structures of **85** and **88** resulting in higher melting points (192 and 158 °C). Except for **89**, all salts decompose at temperatures slightly higher than 200 °C in a range from 208 to 216 °C. This is about 90 °C higher than the decomposition temperature of the neutral 1MeHAtNO_2, which decomposes at 125 °C. It is also higher than the decomposition temperature of the ammonium salt (188 °C) and the influence of the deprotonation and the selection of the cation can be seen. The second decomposition of **86–88** could not be clarified yet. The intensive endothermic point of **87** at 120 °C results both from the dehydration and also melting of compound **87**. **89** decomposes at a temperature of 165 °C since it contains an azido group, which is more sensitive towards temperature.

7.6.2 Long Term Stability Tests

Long term stability tests were performed using a Systag FlexyTSC. The tests were undertaken as long-term isoperibolic runs in glass test vessels at atmospheric pressure with ~300 mg of the compounds. Temperatures 40 °C below the decomposition points were chosen and possible occurrences of exo- or endothermic behaviors over a period of 48 hours were monitored. (**Figure 7.35**) However, **75** and **76** were completely stable for 48 hours at a oven temperature of 150 °C used for compound **75** as well as 80 °C used for compound **76**. It can therefore be reasoned, that both compounds show long-term stabilities, which is a basic requirement for possible applications.

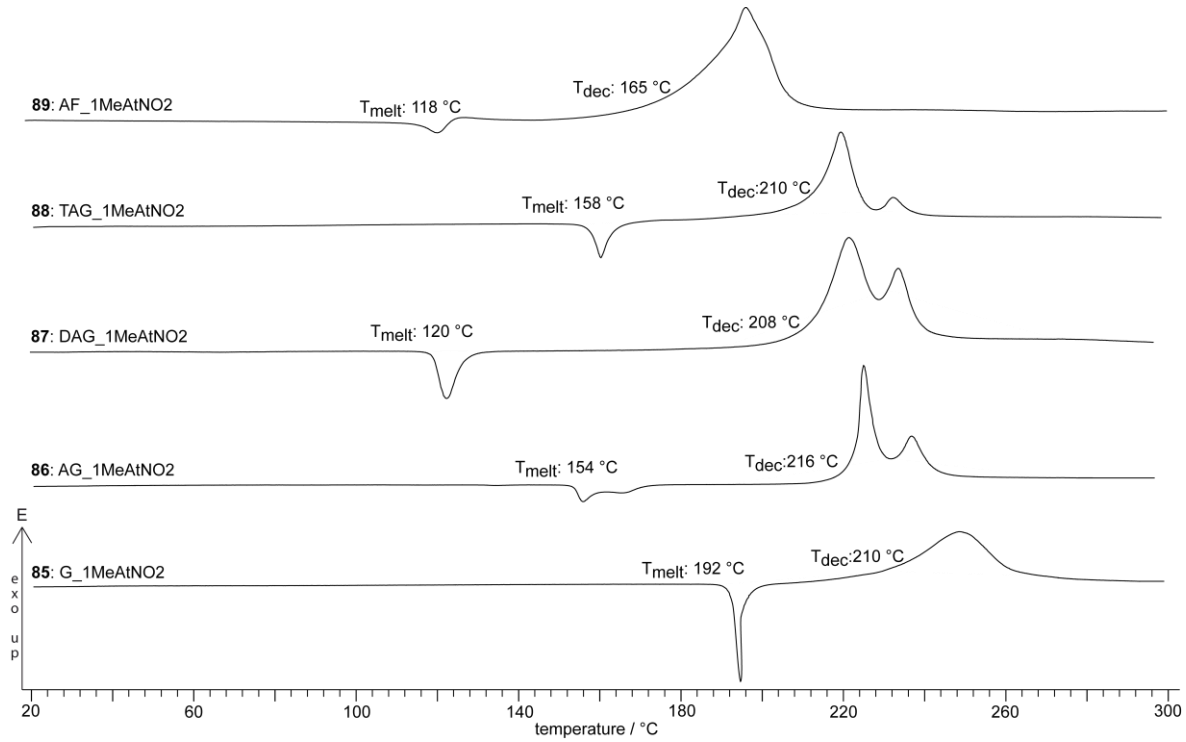

Figure 7.34 DSC plots (endo down) of compounds **85**–**89** (5 °C min^{-1}); melting points, T_{onset} **85**: 192 °C, **86**: 154 °C, **87**: 120 °C, **88**: 158 °C, **89**: 118 °C; temperature of decomposition, T_{onset} **85**: 210 °C, **86**: 216 °C, **87**: 208 °C, **88**: 210 °C, **89**: 165 °C.

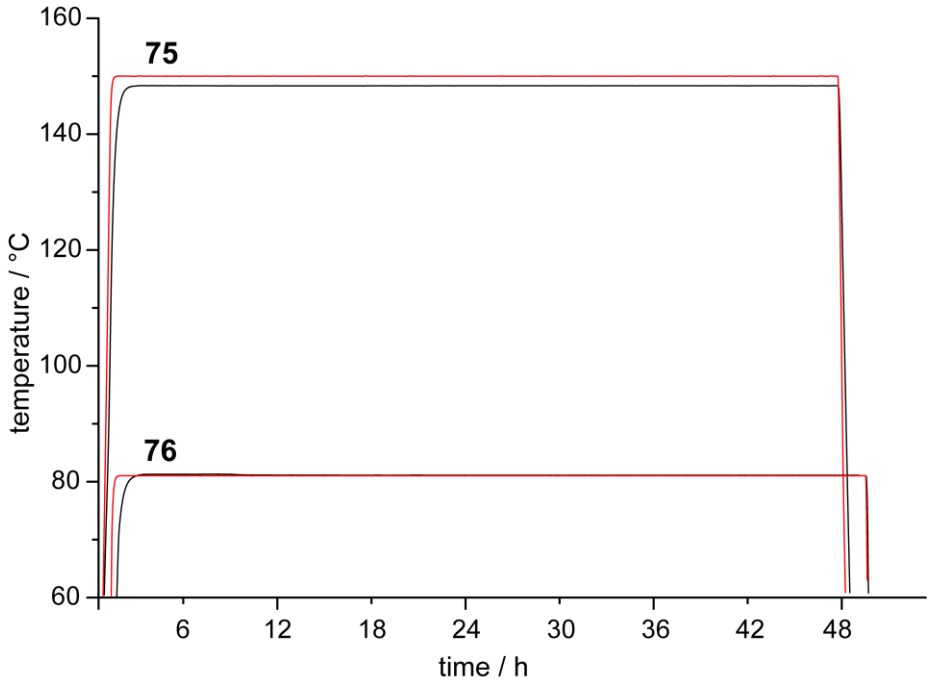

Figure 7.35 Screen of the isoperibolic TSC long term stability tests of **75** (top) at 150 °C and **76** (below) at 80 °C. (Red line: oven temperature, black line: sample temperature).

Also compounds **85**–**89** seem to be long term stable at room temperature. This was proofed by heating **85**–**89** 50 °C below their decomposition temperatures for 48 hours. After this time, the Raman spectra of all compounds were unaltered.

7.6.3 Bomb Calorimetry

The heat of formation of compounds **75**–**81** as well as **85**–**89** were determined using bomb calorimetric measurements. For all calorimetric measurements the procedure described in the Introduction was used. The enthalpy of formation, $\Delta_f H°$, for each of the salts was calculated at 298.15 K using the Hess thermochemical cycle and the following combustion reactions.

75, 76: $C_2H_7N_7O_2 + 11/4\ O_2 \longrightarrow 2\ CO_2(g) + 3.5\ H_2O(l) + 3.5\ N_2(g)$

77: $LiC_2H_3N_6O_2{*}H_2O + 2\ O_2 \longrightarrow 1/2\ Li_2O + 2\ CO_2(g) + 2.5\ H_2O(l) + 3\ N_2$

78: $NaC_2H_3N_6O_2 + 2.25\ O_2 \longrightarrow 1/2\ Na_2O_2 + 2\ CO_2(g) + 1.5\ H_2O(l) + 3\ N_2$

79: $KC_2H_3N_6O_2 + 2.75\ O_2 \longrightarrow KO_2 + 2\ CO_2(g) + 1.5\ H_2O(l) + 3\ N_2$

80: $RbC_2H_3N_6O_2 + 2.75\ O_2 \longrightarrow RbO_2 + 2\ CO_2(g) + 1.5\ H_2O(l) + 3\ N_2$

81: $CsC_2H_3N_6O_2 + 2.75\ O_2 \longrightarrow CsO_2 + 2\ CO_2(g) + 1.5\ H_2O(l) + 3\ N_2$

85: $C_3H_9N_9O_2 + 4.25\ O_2 \longrightarrow 3\ CO_2(g) + 4.5\ H_2O(l) + 4.5\ N_2(g)$

86: $C_3H_{10}N_{10}O_2 + 4.5\ O_2 \longrightarrow 3\ CO_2(g) + 5\ H_2O(l) + 5\ N_2(g)$

87: $C_3H_{11}N_{11}O_2 + 4.75\ O_2 \longrightarrow 3\ CO_2(g) + 5.5\ H_2O(l) + 5.5\ N_2(g)$

88: $C_3H_{12}N_{12}O_2 + 5\ O_2 \longrightarrow 3\ CO_2(g) + 6\ H_2O(l) + 6\ N_2(g)$

89: $C_3H_7N_{11}O_2 + 3.75\ O_2 \longrightarrow 3\ CO_2(g) + 3.5\ H_2O(l) + 5.5\ N_2(g)$

Scheme 7.6 Combustion equations of the salts **75–81** as well as **85–89**.

The heats of formation $\Delta_f H°_{298}$ of **75** and **76** have been computed to be –17 and +111 kJ mol^{-1}. Within the nitrogen-rich salts in this chapter, **75** is the only salt, which is formed exothermically. The results of the determination of the heats of formation of **77**–**81** show the trend of decreasing in the endothermic character for compounds **77**–**81**. The inclusion of crystal water leads to exothermic heats of formation as it can be seen on compound **77**. While the sodium salt is slightly endothermic, the cesium salt is

characterized by a strong exothermic character. ΔH_f (kJ mol^{-1}) **77**: –401, **78**: +9, **79**: +4, **80**: –148, **81**: –217.
The results of the determination of the heats of formation for compounds **85–89** show their endothermic characters since the calculated values are all significantly positive.

The heats of formation show the significant trend of increasing endothermicity for compounds **85–88**. The increase of the endothermic character is based on the compounds rising nitrogen content and N–N single bonds in the row from the guanidinium to the triaminoguanidinium cation. This trend of **85**–**88** corresponds to the sensitivities of the investigated compounds. Solitary is the value of the azidoformamidinium derivative. $\Delta_f H°_{298}$ (kJ mol^{-1}) **85**: +155, **86**: +257, **87**: +352, **88**: +569, **89**: +405.

7.6.4 Sensitivities and Flame Colors

For initial safety testing, the impact and friction sensitivities were tested according to BAM methods using the BAM drophammer as well as the BAM friction tester and are summarized in **Table 7.8**. Neutral 1-methyl-5-nitriminotetrazole (**44**) shows increased sensitivities towards impact (> 12.5 J) and friction (> 160 N) and should only be handled with appropriate precautions. Compound **75** is also sensitive towards impact (< 24 J) but not friction sensitive below 360 N. Interestingly, **76** shows an increased sensitivity towards impact (< 10 J), but also no sensitivity towards friction below 360 N. According to the UN recommendations on the transport of dangerous goods both compounds are classified as “sensitive”. **75** and **76** burn very well and show no sensitivity against electrical discharge by using a 20 kV tesla-coil spark device.

The alkali salts are neither sensitive towards impact (> 100 J) nor friction (> 360 N). All salts are characterized by a nearly smokeless combustion and the generation of brilliant flame colors, which are based on the alkali cations. (Li^+: red, Na^+: yellow, K^+: light red, Rb^+: purple, Cs^+: lavender). Strontium salts **82** and **83** are also only slightly sensitive towards impact (**82**: 40 J, **83**: > 50 J) and not sensitive towards friction (**82**: > 360 N, **83**: > 360) and thereby classified according to the “UN Recommendations on the transport of dangerous goods” as “less sensitive” in both categories.

The electrical spark sensitivities of pulverized samples (0.075–0.125 mm) were determined to be 0.9 J (**82**), 1.2 J (**83**, crystals), 0.01 J (**83**, powder), which in the case of **82** consider with values observed for insensitive energetic materials. Due to the hard recrystallization of **83** also the electrical spark sensitivity (ES) as powder was tested resulting in a high value of 0.01 J. However, this correlation can also be found for other energetic materials in the literature.[108]

Strontium bis(1-methyl-5-nitriminotetrazolate) monohydrate (**82**) shows the best color performance of all strontium salts investigated in this thesis. Its flame color in a Bunsen burner is intensively red. The flame color of strontium bis(2-methyl-5-nitraminotetrazolate) (**83**) is orange-red. It is the most improper salt for application as colorant in pyrotechnics. However, the combustion is also smokeless and no solid residues could be observed.

Figure 7.36 Combustion of lithium (**77**, left), sodium (**78**, middle) and strontium 1-methyl-5-nitriminotetrazolate (**82**, right).

7.6.5 Detonation Parameters

The detonation parameters of explosion of the pure compounds were calculated using the program EXPLO5 V5.02 and are summarized in **Table 7.8**. **75** shows a high calculated detonation pressure of 221 kbar and a detonation velocity of 7884 m s^{-1} comparable to TNT (p = 202 kbar, v = 7150 m/s). Compound **76** is characterized by slightly higher values of 237 kbar for the detonation pressure and 7984 m s^{-1} for the detonation velocity. The calculated values for the ammonium salts **75** and **76** (**Table 7.8**) are smaller compared to the protonated starting materials **44** and **45** owing to the fact that the latter ones are not only considerably more endothermic compounds, but

also have higher densities. The difference in the volume of the gaseous decomposition products (**75**: 860 L kg^{-1}, **76**: 835 L kg^{-1}) is founded on the different detonation temperatures (**75**: 2549 K, **76**: 2965 K) and their influence on the Boudouard-equilibrium.

Table 7.8 Physico-chemical properties of **75**, **76** and **85–89**.

	75	**76**	**85**	**86**	**87**	**88**	**89**
Formula	$C_2H_7N_7O_2$	$C_2H_7N_7O_2$	$C_3H_9N_9O_2$	$C_3H_{10}N_{10}O_2$	$C_3H_{11}N_{11}O_2$	$C_3H_{12}N_{12}O_2$	$C_3H_7N_{11}O_2$
FW (g mol^{-1})	161.15	161.15	206.16	218.18	233.19	248.21	229.16
IS (J)[a]	< 24	< 10	40	10	7.5	6	4
FS (N)[b]	> 360	> 360	> 360	> 360	> 360	240	160
N (%)[c]	60.85	60.85	62.05	64.20	66.07	67.72	67.23
Ω (%)[d]	–54.61	–54.61	–66.94	66.00	–65.18	–64.46	–52.36
Combustion	yes	yes	yes	yes	yes	yes	yes
$T_{dec.}$ (°C)[e]	188	150	210	216	208	210	165
ρ (g cm^{-3})[f]	1.639	1.651	1.550	1.57 (exp.)	1.61	1.57	1.61
$-\Delta H_{comb.}°$ (kJ mol^{-1})[g]	1771	1899	2622	2867	3105	3465	2586
$\Delta_f H_m°$ (kJ mol^{-1})[h]	–17	111	155	257	352	569	405
EXPLO5 values:							
$-\Delta_E U_m°$ (J g^{-1})[i]	3277	3998	3656	3959	4224	4888	4174
T_E (K)[j]	2549	2965	2692	2805	2916	3210	3210
$p_{C\text{-}J}$ (kbar)[k]	221	237	206	227	261	273	230
$V_{Det.}$ (m s^{-1})[l]	7884	7984	7747	8062	8559	8770	7910
V_0 (L kg^{-1})[m]	860	835	844	859	872	886	802

[a] BAM drophammer; [b] BAM friction tester; [c] Nitrogen content; [d] Oxygen balance; [e] Temperature of decomposition by DSC (β = 5°C); [f] estimated from a structure determination; [g] Experimental molar enthalpy of combustion; [h] Molar enthalpy of formation; [i] Energy of explosion; [j] Explosion temperature; [k] Detonation pressure; [l] Detonation velocity; [m] Assuming only gaseous products.

7.6.6 Decomposition Products

In order to determine the thermal decomposition products the compounds were heated in a evacuated steel tube for ~30 s over the decomposition temperature and the gaseous products were passed in a background corrected evacuated gas IR cell. In **Figure 7.37** the gas phase IR spectra of the IR detectable decomposition products are illustrated. The thermal decomposition of **75** results in the formation of five main products, which were identified using IR spectroscopy, namely CO_2,[304] CO,[305] HCN,[122] CH_4 and NH_3.[306] However, no evidence for the formation of water vapor was found. Compound **76** showed more decomposition products observed in the gas phase. Besides CO, large amounts of CH_4 and HCN were found in the decomposition of **76**. Astonishing is the absence of CO_2 and the formation of N_2O, showing a complex decomposition mechanism, which could not investigated ordinarily yet.

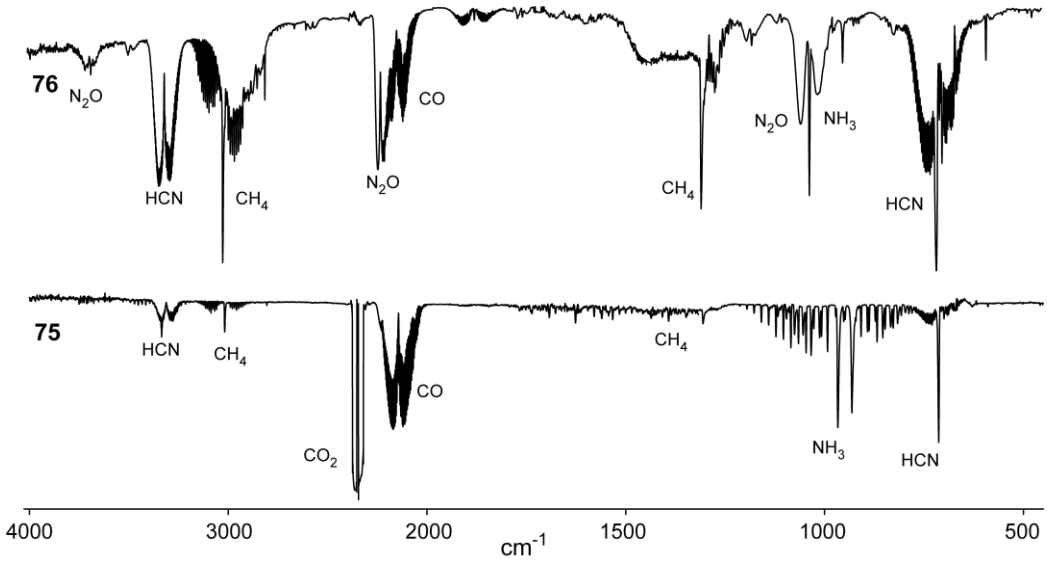

Figure 7.37 Gas phase IR spectrum of the decomposition products of **75** and **76**.

7.6.7 Koenen Test of Triaminoguanidinium 1-Methyl-5-nitriminotetrazolate

Compound **88** was investigated according to its explosion performance under confinement using a *"Koenen test"* steel sleeve apparatus. The *Koenen test* was performed with 27 g of triaminoguanidinium 1-methyl-5-nitriminotetrazolate using a closing plate with an orifice of 10 mm. The first trial was successful indicated by the rupture of the steel tube into more than 15 fragments, which are shown in **Figure 7.38**.

TNT destroys the steel sleeve up to an orifice width of 6 mm, RDX even up to 8 mm. Compared to these applied explosives the explosion performance under confinement by thermal ignition of compound **88** is obviously better, although the calculated detonation parameters of RDX are slightly higher.

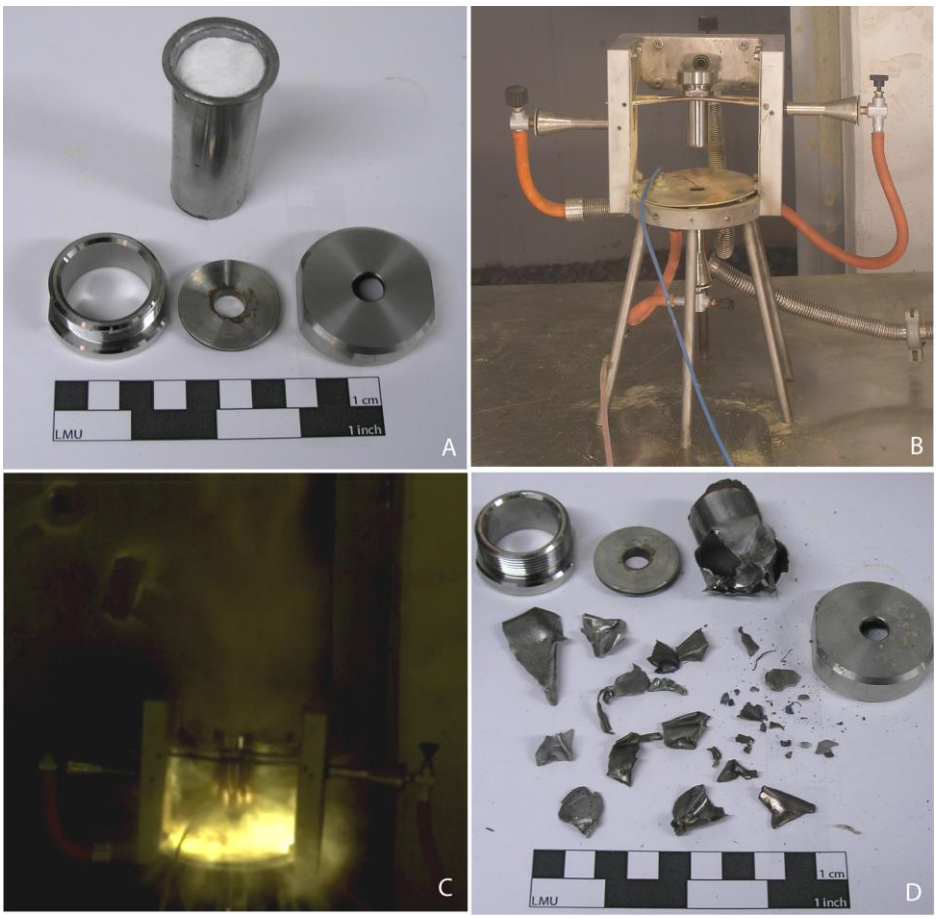

Figure 7.38 A) Steel sleeve loaded with 27.0 g of **88**. B) *Koenen* test setup showing four *Bunsen* burners. C) Moment of explosion filmed using a high speed camera (2500 frames s^{-1}). D) Result of the Koenen test showing the collected fragments.

7.7 Experimental Part

Caution! 1-Methyl-5-nitriminotetrazole and its salts are energetic materials with increased sensitivities towards shock and friction. Therefore, proper security precautions (safety glass, face shield, earthened equipment and shoes, Kevlar® gloves and ear plugs) have to be applied synthesizing and handling the described compounds. Especially compounds

described containing the azido or perchlorate group are extremely sensitive and have to be handled very carefully.

*Ammonium 1-methyl-5-nitriminotetrazolate (**75**):* A solution of 1-methyl-5-nitriminotetrazole (2.88 g, 20 mmol) in half-conc. ammonia solution (15 %, 20 mL) was stirred for 10 min at 60 °C and was concentrated under vacuum. The obtained solid was recrystallized from water to furnish the product as white crystals (3.16 g, 98%). **DSC** (T_{onset}, 2 °C min^{-1}): 188 °C (dec.); **IR** (KBr, cm^{-1}): $\tilde{\nu}$ = 3166 (m), 3103 (m), 3040 (m), 2865 (m), 2380 (w), 2354 (w), 2327 (w), 1913 (w), 1779 (w), 1731 (w), 1681 (w), 1507 (m), 1438 (s), 1404 (m), 1328 (vs), 1296 (vs), 1238 (s), 1225 (s), 1117 (s), 1054 (m), 1033 (s), 985 (m), 877 (s), 827 (m), 774 (s), 740 (s), 687 (s); **Raman** (1064 nm, 200 mW, 25 °C, cm^{-1}): $\tilde{\nu}$ = 3050(9), 2968 (22), 1556 (7), 1508 (84), 1466 (42), 1407 (19), 1353 (20), 1337 (27), 1300 (45), 1231 (11), 1119 (28), 1048 (10), 1037 (100), 988 (12), 881 (22), 745 (29), 685 (36), 499 (22), 452 (6), 377 (14), 292 (43), 235 (13), 207 (23); **^{1}H NMR** (d_6-DMSO, 25 °C, ppm): δ = 3.64 (s, 3H, CH_3), 7.17 (s, 4H, NH_4^+); **^{13}C NMR** (d_6-DMSO, 25 °C): δ = 33.0 (CH_3), 157.5 (CN_4); **^{14}N NMR** (d_6-DMSO, 25 °C, ppm): δ = –14.8 (NO_2), –359.3 (NH_4^+); **^{15}N NMR** (d_6-DMSO, 25 °C, ppm): δ = –359.3 (N7, NH_4^+), –170.7 (N1, ^{2}J(N–H) = 2.1Hz), –157.9 (N5), –76.1 (N4), –20.1 (N2, ^{3}J(N–H) = 1.8Hz), –16 (N6, NO_2), 2.4 (N3); ***m/z*** (FAB^-): 142 (anion); **EA** ($C_2H_7N_7O_2$, 161.15) calcd.: C 14.91, H 4.38, N 60.85 %; found: C 14.88, H 4.12, N 60.98 %; **impact sensitivity**: < 24 J; **friction sensitivity**: > 360 N; $\Delta_c U$ = 2635 cal g^{-1}.

*Ammonium 2-Methyl-5-nitriminotetrazolate (**76**):* A solution of 2-methyl-5-nitraminotetrazole (2.88 g, 20 mmol) in diluted ammonia solution (10 %, 20 mL) was stirred for 2 h at room temperature and was concentrated in vacuo. The obtained solid was recrystallized from water to furnish the product as white crystals (3.16 g, 98%). **DSC** (T_{onset}, 2 °C min^{-1}): 149 °C (dec.); **IR** (KBr, cm^{-1}): $\tilde{\nu}$ = 3178 (m), 3083 (m), 1688 (w), 1487 (s), 1434 (s), 1385 (vs), 1353 (s), 1323 (s), 1272 (m), 1206 (m), 1096 (m), 1041 (m), 1029 (m), 1010 (m), 883 (m), 764 (m), 755 (w), 742 (w), 704 (m), 678 (w), 475 (w); **Raman** (1064 nm, 200 mW, 25 °C, cm^{-1}): $\tilde{\nu}$ = 2986 (11), 2971 (14), 1688 (3), 1490 (100), 1418 (9), 1387 (10), 1369 (8), 1323 (9), 1211 (6), 1098 (4), 1030 (14), 1012 (54), 886 (4), 740 (6), 701 (9), 456 (6), 400 (6), 348 (7), 199 (9); **^{1}H NMR** (d_6-DMSO, 25 °C, ppm): δ = 4.16 (s, 3H, CH_3), 7.32 (s, 4H, NH_4^+); **^{13}C NMR** (d_6-DMSO, 25°C, ppm): δ = 39.7 (CH_3), 168.0 (CN_4); **^{14}N NMR** (d_6-DMSO, 25 °C): δ = –359.4 (NH_4^+), –359.4 (NO_2);

^{15}N NMR (d_6-DMSO, 25 °C, ppm): δ = –359.4 (N7, NH_4^+), –149.3 (N5), –111.8 (C2, ^{2}J(N–H) = 2.1 Hz), –93.8 (N1, ^{3}J(N–H) = 1.8Hz), –63.9 (N4), –15.4 (N6, NO_2), –6.4 (N3, ^{3}J(N–H) = 1.8Hz); ***m/z*** (FAB$^-$): 142 (anion); **EA** ($C_2H_7N_7O_2$, 161.15) calcd.: C 14.91, H 4.38, N 60.85 %; found: C 15.10, H 4.44, N 60.53 %; **impact sensitivity**: < 10 J; **friction sensitivity**: > 360 N; $\Delta_c U$ = 2825 cal g^{-1}.

*Lithium 1-methyl-5-nitriminotetrazolate monohydrate (**77**):* 1-Methyl-5-nitrimino-tetrazole (0.64 g, 4.4 mmol) and lithium hydroxide (0.11 g, 4.4 mmol) were dissolved in 20 mL of warm water. Afterwards, the two solutions were combined and the water was evaporated to leave colorless rods (0.41 g, yield 61 %). **DSC** (T_{onset}, 5 °C min^{-1}): 271 °C, 301 °C (dec.); **IR** (KBr, cm^{-1}): $\tilde{\nu}$ = 3375 (m), 3319 (m), 3041 (w), 2973 (w), 2231 (w), 1668 (w), 1520 (m), 1481 (m), 1422 (m), 1319 (s), 1295 (s), 1242 (m), 1118 (m), 1055 (m), 999 (m), 893 (m), 769 (m), 739 (m), 683 (s), 584 (s); **Raman** (1064 nm, 200 mW, 25 °C, cm^{-1}): $\tilde{\nu}$ = 3314 (2), 3037 (4), 2973 (15), 1522 (100), 1481 (15), 1450 (11), 1427 (21), 1401 (13), 1321 (23), 1297 (20), 1120 (18), 1047 (96), 1000 (5), 896 (12), 777 (13), 689 (22), 498 (15), 362 (8), 298 (28); **^{1}H NMR** (D_2O, 25 °C, ppm): δ = 3.45 (s, crystal water), 3.62 (s, CH_3); **^{7}Li NMR** (D_2O, 25 °C, ppm): δ = –1.00; **^{13}C NMR** (D_2O, 25 °C, ppm): δ = 33.0 (CH_3) 164.4 (CN_4); **^{14}N NMR** (D_2O, 25 °C, ppm): δ = –17.8 (NO_2); **EA** ($C_2H_5LiN_6O_3$, 168.04) calcd.: C 14.29, H 3.00, N 50.01 %; found: C 14.27, H 3.10, N 49.95 %; $\Delta_c U$ = –2000 cal g^{-1}.

*Sodium 1-methyl-5-nitriminotetrazolate (**78**):* 1-Methyl-5-nitriminotetrazole (1.44 g, 10 mmol) and sodium hydroxide (0.40 g, 10 mmol) were added to 50 mL of warm water. After stirring at 90 °C for 5 min the water was evaporated. The crude product was recrystallized from a hot ethanol/water mixture (5:1) yielding colorless rods suitable for X-ray diffraction (1.54 g, yield 93 %). **DSC** (T_{onset}, 5 °C min^{-1}): 278 °C (dec.); **IR** (KBr, cm^{-1}): $\tilde{\nu}$ = 3049 (w), 2967 (m), 2697 (m), 2378 (w), 1917 (w), 1786 (w), 1513 (s), 1462 (s), 1379 (vs), 1300 (s), 1238 (s), 1113 (m), 1039 (s), 986 (w), 882 (m), 774 (m), 751 (w), 738 (m), 690 (m), 497 (w); **Raman** (1064 nm, 200 mW, 25 °C, cm^{-1}): $\tilde{\nu}$ = 3053 (7), 3025 (9), 2969 (21), 1512 (100), 1468 (50), 1450 (2), 1407 (25), 1375 (36), 1302 (47), 1239 (14), 1116 (24), 1040 (69), 990 (10), 886 (18), 754 (17), 696 (20), 497 (13), 379 (10), 302 (24), 251 (12); **^{1}H NMR** (D_2O, 25 °C, ppm): δ = 3.82 (s, CH_3); **^{13}C NMR** (D_2O, 25 °C, ppm): δ = 33.0 (CH_3) 157.6 (CN_4); **^{14}N NMR** (D_2O, 25 °C, ppm): δ = –17.9 (NO_2); **^{15}N NMR** (D_2O, 25 °C, ppm): δ = –7.4 (N3), –18.2 (NO_2), –23.5

(N2), –82.9 (N4), –157.3 (N5), –169.7 (N1); **EA** ($C_2H_3NaN_6O_2$, 166.07) calcd.: C 14.46, H 1.82, N 50.60 %; found: C 14.62, H 1.73, N 50.58 %; $\Delta_c U$ = –2140 cal g^{-1}.

*Potassium 1-methyl-5-nitriminotetrazolate (**79**):* A solution of 1-methyl-5-nitriminotetrazole (1.44 g, 10 mmol) in 30 mL water was reacted with potassium carbonate (0.69 g, 50 mmole) by heating till the release of CO_2 stopped. After stirring at 90 °C for 5 min the water was evaporated. The crude product was recrystallized from a hot ethanol/water mixture (3:1) yielding colorless crystals suitable for X-ray diffraction (1.71 g, 94 % yield). **DSC** (T_{onset}, 5 °C min^{-1}): 239 °C (dec.); **IR** (KBr, cm^{-1}): $\tilde{\nu}$ = 3454 (w), 3046 (w), 2970 (w), 2380 (w), 1508 (s), 1457 (s), 1408 (s), 1382 (s), 1364 (vs), 1355 (vs), 1298 (m), 1229 (m), 1107 (m), 1035 (m), 979 (w), 879 (m), 774 (m), 740 (m), 687 (m), 494 (w); **Raman** (1064 nm, 200 mW, 25 °C, cm^{-1}): $\tilde{\nu}$ = 3033 (4), 3023 (6), 2986 (15), 2968 (26), 1550 (5), 1508 (100), 1462 (58), 1407 (17), 1366 (23), 1353 (21), 1300 (53), 1231 (8), 1109 (22), 1048 (19), 1035 (90), 981 (7), 882 (18), 748 (21), 683 (31), 495 (20), 449 (6), 371 (11), 295 (41), 241 (12), 208 (9), 160 (7); **^{1}H NMR** (D_2O, 25 °C, ppm): δ = 3.87 (s, CH_3); **^{13}C NMR** (D_2O, 25 °C, ppm): δ = 32.0 (s, CH_3), 156.2 (s, CN_4). **^{14}N NMR** (D_2O, 25 °C, ppm): δ = –17.9 (NO_2); **EA** ($C_2H_3KN_6O_2$, 182.19) calcd.: C 13.19, H 1.66, N 46.13 %; found: C 13.22, H 1.70, N 46.47 %; $\Delta_c U$ = –1980 cal g^{-1}.

*Rubidium 1-methyl-5-nitriminotetrazolate (**80**):* To a warm solution of 1-methyl-5-nitriminotetrazole (1.44 g, 10 mmol) in 30 mL water rubidium carbonate (1.30 g, 5 mmol) was added. The solution was stirred at 90 °C till the release of CO_2 stopped. After evaporation of the solvent, the crude product was recrystallized from a hot ethanol/water mixture (2:1), yielding colorless crystals (2.12 g, 93 % yield). **DSC** (T_{onset}, 5 °C min^{-1}): 228 °C (dec.); **IR** (KBr, cm^{-1}): $\tilde{\nu}$ = 3433 (m), 3039 (m), 2968 (w), 2716 (w), 2342 (m), 1509 (s), 1456 (s), 1411 (s), 1380 (s), 1363 (vs), 1349 (vs), 1294 (s), 1230 (s), 1109 (m), 1049 (m), 1033 (m), 982 (m), 881 (m), 774 (m), 754 (m), 739 (w), 728 (m), 700 (m), 687 (s), 494 (w), 460 (w); **Raman** (1064 nm, 200 mW, 25 °C, cm^{-1}): $\tilde{\nu}$ = 3041 (8), 2985 (21), 2970 (26), 1553 (6), 1511 (90), 1462 (46), 1417 (15), 1368 (18), 1348 (29), 1295 (57), 1231 (9), 1112 (26), 1049 (17), 1033 (100), 985 (9), 885 (20), 755 (36), 701 (7), 684 (36), 495 (24), 460 (9), 370 (21), 289 (28), 224 (13), 193 (13), 151 (6); **^{1}H NMR** (D_2O, 25 °C, ppm): δ = 3.87 (CH_3); **^{13}C NMR** (D_2O, 25 °C, ppm): δ = 33.0 (CH_3), 156.2 (CN_4); **^{14}N NMR** (D_2O, 25 °C, ppm): δ = –17.9 (NO_2); **EA** ($C_2H_3N_6O_2Rb$, 228.58) calcd.: C 10.51, H 1.32, N 36.77 %; found: C 10.52, H 1.32, N 37.04 %; ΔU_c = –1422 cal g^{-1}.

*Cesium 1-methyl-5-nitriminotetrazolate (**81**):* Cesium carbonate (1.63 g, 5 mmole) was added to a solution of 1-methyl-5-nitriminotetrazole (1.44 g, 10 mmol) in 30 mL water and stirred for 5 min at 90 °C. After the water was evaporated, the crude product was recrystallized from a ethanol / water (1:1) mixture (2.59 g, 94 % yield). **DSC** (T_{onset}, 5 °C min^{-1}): 233 °C (dec.); **IR** (KBr, cm^{-1}): $\tilde{\nu}$ = 3446 (m), 3027 (w), 2954 (w), 2342 (w), 1798 (w), 1506 (s), 1458 (s), 1414 (m), 1388 (s), 1336 (vs), 1322 (vs), 1290 (s), 1233 (m), 1102 (m), 1049 (w), 1033 (m), 978 (w), 881 (m), 776 (m), 751 (w), 739 (m), 685 (m), 487 (w); **Raman** (1064 nm, 200 mW, 25 °C, cm^{-1}): $\tilde{\nu}$ = 3028 (6), 2986 (16), 2956 (17), 1559 (5), 1509 (100), 1459 (39), 1415 (11), 1395 (10), 1325 (9), 1294 (50), 1229 (6), 1105 (26), 1049 (17), 1035 (98), 980 (7), 883 (14), 753 (20), 688 (21), 490 (17), 451 (6), 367 (12), 289 (22), 231 (9), 204 (9); **^{1}H NMR** (D_2O, 25 °C, ppm): δ = 3.84 (s, CH_3); **^{13}C NMR** (D_2O, 25 °C, ppm): δ = 33.1 (CH_3), 156.2 (CN_4); **^{14}N NMR** (D_2O, 25 °C, ppm): δ = –17.9 (NO_2); **EA** ($C_2H_3CsN_6O_2$, 276.01) calcd.: C 8.70, H 1.10, N 30.45 %; found: C 8.77, H 1.10, N 30.75 %; $\Delta_c\boldsymbol{U}$ = –1125 cal g^{-1}.

*Strontium 1-methyl-5-nitriminotetrazolate monohydrate (**82**):* 1-Methyl-5-nitrimino-tetrazole (14.4 g, 0.10 mol) and strontium hydroxide octahydrate (13.4 g, 0.05 mol) were added to 50 mL of warm water. After stirring for 5 min at 90 °C the water was evaporated. The crude product was recrystallized from a hot ethanol/water mixture (1:1) yielding colorless rods suitable for X-ray diffraction (18.2 g, yield 93 %). **DSC** (T_{onset}, 5 °C min^{-1}): 350 °C (dec.); **IR** (Diamond-ATR, cm^{-1}): $\tilde{\nu}$ = 3609 (vw), 3544 (w), 3319 (vw), 3140 (vw), 2401 (vw), 2354 (vw), 2311 (vw), 1668 (vw), 1616 (w), 1515 (m), 1468 (s), 1421 (m), 1374 (s), 1324 (vs), 1293 (s), 1240 (s), 1114 (m), 1056 (w), 1024 (s), 990 (m), 878 (m), 771 (m), 760 (m), 738 (m), 705 (w), 694 (m); **Raman** (1064 nm, 200 mW, 25 °C, cm^{-1}): $\tilde{\nu}$ = 2965 (11), 1514 (100), 1470 (34), 1419 (9), 1376 (16), 1346 (30), 1299 (23), 1239 (5), 1117 (14), 1055 (5), 1027 (59), 992 (6), 882 (10), 788 (4), 762 (13), 739 (2), 691 (12), 505 (11), 464 (4), 388 (6), 303 (12), 249 (6), 217 (7), 187 (10); **^{1}H NMR** (d_6-DMSO, 25 °C, ppm): δ = 3.68 (s, 6H, CH_3), 3.37 (s, 2H, H_2O); **^{13}C NMR** (d_6-DMSO, 25 °C, ppm): δ = 33.1 (CH_3), 157.6 (CN_4); **^{15}N NMR:** (d_6-DMSO, 25 °C) δ = 4.45 (N3), –14.12 (N6), –18.29 (N2, t, $^{3}J_{NH}$ = 1.9 Hz), –71.15 (N4), –157.16 (N5), –168.38 (N1, d, $^{2}J_{NH}$ = 2.2 Hz; **EA** ($C_4H_8N_{12}O_5Sr$, 391.80) calcd.: C 12.26, H 2.06, N 42.90 %; found: C 12.41, H 2.25, N 43.18 %; **impact sensitivity**: 40 J; **friction sensitivity**: > 360 N; **ESD**: 0.9 J.

*Strontium 2-methyl-5-nitriminotetrazolate tetrahydrate (**83**):* 2-Methyl-5-nitraminotetrazole (3.63 g, 50 mmol) was dissolved in 100 mL of warm (90 °C) water and combined with 50 mL of an aqueous suspension containing strontium hydroxide octahydrate (6.64 g, 25 mmol). After stirring for 5 min at 90 °C the water was evaporated. The crude product was recrystallized two times from hot water yielding colorless crystal. (5.7 g, yield 51 %). **DSC** (T_{onset}, 5 °C min^{-1}): 165 °C, 230 °C (dec.); **IR** (KBr, cm^{-1}): $\tilde{\nu}$ =3485 (s), 3405 (s), 3298 (s), 3044 (w), 2959 (w), 2440 (w), 2336 (w), 2212 (w), 1782 (m), 1763 (m), 1670 (s), 1650 (m), 1543 (m), 1506 (s), 1431 (vs), 1325 (vs), 1285 (s), 1225 (s), 1102 (s), 1062 (m), 1041 (s), 1019 (m), 906 (m), 771 (m), 755 (m), 744 (m), 712 (s), 675 (m), 621 (m), 562 (m), 493 (w); **Raman** (1064 nm, 200 mW, 25 °C, cm^{-1}): $\tilde{\nu}$ = 2963 (4), 1494 (100), 1506 (100), 1429 (6), 1384 (5), 1326 (2), 1226 (3), 1063 (3), 1021 (32), 906 (2), 746 (5), 722 (6), 447 (2), 401 (2), 341 (7), 200 (4); **^{1}H NMR** (d_6-DMSO, 25 °C, ppm): δ = 4.16 (s, 3H, CH_3), 3.40 (s, H_2O); **^{13}C NMR** (d_6-DMSO, 25°C, ppm): δ = 39.7 (CH_3), 168.0 (CN_4); ***m/z*** (FAB^-): 143 (anion); **EA** ($C_4H_{14}N_{12}O_8Sr$, 445.89) calcd.: C 10.78, H 3.17, N 37.70 %; found C 10.50, H 3.31, N 37.28 %; **impact sensitivity**: > 50 J; **friction sensitivity**: > 360 N; **ESD**: 0.01 J (powder), 1.2 J (crystals).

*Silver 1-methyl-5-nitriminotetrazolate (**84**):* Silver nitrate (1.70 g, 0.01 mol) was dissolved in 20 mL water and added to a solution of potassium 1-methyl-5-nitriminotetrazolate (1.82 g, 0.01 mol) in 20 mL water. The silver salt precipitated immediately as a colorless powder. The reaction mixture was stirred for 30 minutes under exclusion of light. The product was filtered off and dried using high vacuum also under the exclusion of light. To obtain suitable crystals for X-ray diffraction analysis small amounts of product **84** were recrystallized from hot water. For the synthesis of **84** a reaction yield of 97 % (2.42 g) could be achieved. **IR** (KBr, cm^{-1}): $\tilde{\nu}$ = 2966 (w), 1505 (s), 1456 (s), 1400 (m), 1381 (m), 1329 (vs), 1301 (vs), 1260 (m), 1232 (s), 1123 (m), 1052 (w), 1034 (w), 985 (w), 878 (w), 764 (w), 756 (w), 728 (w), 696 (w); **Raman** (1064 nm, 400 mW, 25 °C, cm^{-1}): $\tilde{\nu}$ = 2986 (35), 2971 (14), 1503 (100), 1463 (19), 1403 (14), 1387 (13), 1331 (20), 1306 (25), 1233 (11), 1124 (14), 1034 (66), 987 (5), 880 (8), 758 (23), 730 (5), 688 (14), 504 (20), 466 (5), 372 (8), 303 (19), 245 (7), 211 (8), 86 (4); **EA** ($C_2H_3N_6AgO_2$, 250.95) calcd.: C 9.57, H 1.20, N 33.49 %, found: C 10.10, H 1.51, N 33.08 %; **impact sensitivity**: > 50 J; **friction sensitivity**: > 360 N.

*Guanidinium 1-methyl-5-nitriminotetrazolate (**85**):* Potassium 1-methyl-5-nitriminotetrazolate (3.34 g, 0.02 mol) was dissolved in 20 mL water. Under constant

stirring a solution of silver nitrate (3.38 g, 0.02 mol) in water was added. **84**, which started instantly to precipitate, was filtered and washed with small amounts of water. The wet powder was completely transferred into a reaction vessel, which contained a solution of guanidinium chloride (1.62 g, 0.02 mol) in water. Silver chloride started to precipitate immediately, indicating the successful course of the reaction. The silver chloride was filtered off and the filtrate was collected in a volumetric reaction flask. The solvent was removed by a rotary evaporator. To purify product **85** the solid residue was recrystallized from an ethanol/water (4:1) mixture. Analytically pure **85** was achieved as colorless needles after filtration and washing with ethanol and diethyl ether. According to this procedure a reaction yield of 78 % (3.17 g) could be obtained. All steps should be performed under exclusion of light. **DSC** (T_{onset}, 5 °C min^{-1}): 197 °C, 236 °C (dec.); **IR** (ATR, cm^{-1}): $\tilde{\nu}$ = 3433 (s), 3350 (s), 3282 (s), 3173 (vs), 2955 (m), 2796 (w), 1666 (s), 1654 (s), 1595 (w), 1556 (w), 1505 (m), 1455 (m), 1412 (w), 1323 (vs), 1234 (s), 1123 (s), 1039 (m), 1006 (m), 888 (m), 767 (w), 748 (w), 737 (m), 686 (m); **Raman** (1064 nm, 400 mW, 25 °C, cm^{-1}): $\tilde{\nu}$ = 2987 (9), 2959 (9), 1514 (100), 1459 (24), 1325 (17), 1298 (27), 1236 (8), 1127 (22), 1042 (81), 1009 (23), 890 (8), 750 (13), 688 (16), 544 (7), 499 (8), 370 (8), 296 (19); **^{1}H NMR** (d_6-DMSO, 25 °C, ppm): δ = 6.94 (s, 6H, NH_2), 3.68 (s, 3H, CH_3); **^{13}C NMR** (d_6-DMSO, 25 °C, ppm): δ = 158.4 (G^+), 157.6 (CN_4), 33.1 (CH_3); ***m/z*** (FAB$^+$): 60 (cation); ***m/z*** (FAB$^-$): 143 (anion); **EA** ($C_3H_9N_9O_2$, 203.16) calcd.: C 17.74, H 4.47, N 62.05 %; found: C 17.69, H 4.35, N 61.76 %; **impact sensitivity**: > 40 J; **friction sensitivity**: > 360 N, $\Delta_c U$: 3093 cal g^{-1}.

*Aminoguanidinium 1-methyl-5-nitriminotetrazolate (**86**):* **Method 1**: The synthesis of **86** was carried out similar to the synthesis of **85**. Potassium 1-methyl-5-nitriminotetrazolate (3.34 g, 0.02 mol) and aminoguanidinium chloride (2.21 g, 0.02 mol) were used as starting materials. After recrystallization from water/ethanol colorless crystals were obtained (3.75 g, yield 86 %). **Method 2**: 1-Methyl-5-nitriminotetrazole (7.20 g, 50 mmol) dissolved in 50 mL of water was combined under release of carbon dioxide with a suspension of aminoguanidine bicarbonate (6.80 g, 50 mmol). The solution was stirred for 5 min at 50 °C. Subsequently the solvent was removed by evaporation. The analytically pure obtained aminoguanidinium 1-methyl-5-nitriminotetrazolate was washed with 50 mL of an ethanol/diethyl ether mixture and separated by filtration. (10.6 g, 97 % yield). **DSC** (T_{onset}, 5 °C min^{-1}): 155 °C, 226 °C (dec.); **IR** (KBr, cm^{-1}): $\tilde{\nu}$ = 3430 (m), 3354 (s), 3252 (s), 3142 (s), 1657 (vs), 1505 (m), 1459 (s), 1342 (vs), 1322 (vs), 1294 (vs), 1234 (s), 1217 (s), 1102 (m), 1031 (m), 949

(m), 880 (m), 772 (w), 738 (w), 690 (m); **Raman** (400 mW, 25 °C, cm^{-1}): $\tilde{\nu}$ = 3285 (4), 2986 (27), 2959 (9), 1670 (6), 1508 (100), 1461 (34), 1415 (11), 1390 (5), 1323 (31), 1307 (21), 1239 (4), 1116 (15), 1034 (99), 969 (14), 885 (11), 747 (19), 694 (16), 621 (4), 507 (21), 457 (6), 372 (6), 296 (34), 201 (10); **^{1}H NMR** (d_6-DMSO, 25 °C, ppm): δ = 8.57 (s, 1H, NH–NH_2), 7.24 (s, 2H, NH_2), 6.75 (s, 2H, NH_2), 4.68 (s, 2H, NH–NH_2), 3.66 (s, 3H, CH_3); **^{13}C NMR** (d_6-DMSO, 25 °C, ppm): δ = 159.3 (AG^+), 157.7 (CN_4), 33.1 (CH_3); ***m/z*** (FAB^+): 75 (cation); ***m/z*** (FAB^-): 143 (anion); **EA** ($C_3H_{10}N_{10}O_2$, 218.18) calcd.: C 16.52, H 4.62, N 64.20 %; found: C 16.51, H 4.75, N 63.79 %; **impact sensitivity**: > 10 J; **friction sensitivity**: > 360 N; $\Delta_c U$: 3148 cal g^{-1}.

*Diaminoguanidinium 1-methyl-5-nitriminotetrazolate (**87**):* The synthesis of **87** was carried out similar to the synthesis of **85**. Potassium 1-methyl-5-nitriminotetrazolate (3.34 g, 0.02 mol) and diaminoguanidinium chloride (2.51 g, 0.02 mol) were used as starting materials. After recrystallization from water/ethanol colorless crystals were obtained (3.82 g, yield 82 %). **DSC** (T_{onset}, 5 °C min^{-1}): 122 °C, 216 °C (dec.); **IR** (KBr, cm^{-1}): $\tilde{\nu}$ = 3468 (m), 3364 (w), 3311 (s), 3246 (s), 3203 (s), 1672 (m), 1617 (w), 1506 (s), 1456 (s), 1407 (m), 1341 (vs), 1294 (vs), 1228 (s), 1162 (m), 1108 (s), 1036 (s), 947 (m), 880 (m), 772 (w), 740 (m), 686 (m); **Raman** (1064 nm, 400 mW, 25 °C, cm^{-1}): $\tilde{\nu}$ = 3354 (17), 2986 (15), 2959 (8), 1518 (100), 1464 (25), 1297 (41), 1178 (8), 1111 (13), 1039 (99), 927 (13), 889 (11), 755 (21), 691 (18), 551 (9), 494 (11), 369 (13), 292 (17), 192 (12); **^{1}H NMR** (d_6-DMSO, 25 °C, ppm): δ = 8.54 (s, 2H, N*H*–NH_2), 7.16 (s, 2H, C–NH_2), 4.59 (s, 4H, NH–NH_2), 3.67 (s, 3H, CH_3); **^{13}C NMR** (d_6-DMSO, 25 °C, ppm): δ = 160.3 (DAG^+), 157.7 (CN_4), 33.1 (CH_3); ***m/z*** (FAB^+): 90 (cation); ***m/z*** (FAB^-): 143 (anion); **EA** ($C_3H_{11}N_{11}O_2$, 233.19) calcd.: C 15.45, H 4.75, N 66.07 %; found: C 15.32, H 4.88, N 65.71 %; **impact sensitivity**: > 7.5 J; **friction sensitivity**: > 360 N; $\Delta_c U$: 3190 cal g^{-1}.

*Triaminoguanidinium 1-methyl-5-nitriminotetrazolate (**88**):* **Method 1**: The synthesis of **88** was carried out similar to the synthesis of **85**. Potassium 1-methyl-5-nitriminotetrazolate (3.34 g, 0.02 mol) and triaminoguanidinium chloride (2.80 g, 0.02 mol) were used as starting materials. After recrystallization from water/ethanol colorless needles were obtained (4.52 g, yield 91 %). **Method 2**: To aminoguanidinium 1-methyl-5-nitriminotetrazolate (8.73 g, 40 mmol) 50 mL dioxane, 10 mL water and hydrazine hydrate (5.0 g, 100 mmol) were added. The mixture was heated to 90 °C for 3 h. Afterwards the solvent was evaporated and the precipitation was initiated by the addition of small amounts of ethanol and diethyl ether. The crude product was

recrystallized from a hot ethanol/water mixture(10:1) (8.2 g, 83 % yield). **DSC** (T_{onset}, 5 °C min^{-1}): 158 °C, 225 °C (dec.); **IR** (KBr, cm^{-1}): $\tilde{\nu}$ = 3469 (w), 3371 (m), 3322 (vs), 3207 (s), 1676 (s), 1618 (w), 1507 (s), 1455 (vs), 1340 (vs), 1228 (s), 1194 (m), 1132 (m), 1107 (s), 1036 (m), 979 (m), 880 (m), 773 (m), 739 (m), 687 (m); **Raman** (1064 nm, 400 mW, 25 °C, cm^{-1}): $\tilde{\nu}$ = 3331 (20), 3229 (12), 2986 (16), 1506 (100), 1462 (32), 1418 (17), 1295 (35), 1228 (11), 1108 (20), 1038 (94), 978 (12), 894 (21), 754 (18), 691 (23), 637 (10), 489 (17), 414 (13), 301 (21), 207 (18); **^{1}H NMR** (d_6-DMSO, 25 °C, ppm): δ = 8.60 (s, 3H, NH–NH_2), 4.50 (s, 6H, NH–NH_2), 3.67 (s, 3H, CH_3); **^{13}C NMR** (d_6-DMSO, 25 °C, ppm): δ = 159.6 (TAG$^+$), 157.7 (CN_4), 33.1 (CH_3); **^{15}N NMR** (d_6-DMSO, 25 °C, ppm): δ = 4.45 (N3), –14.12 (N6), –18.29 (N2, t, $^3J_{NH}$ = 1.9 Hz), –71.15 (N4), –157.16 (N5), –168.38 (N1, d, $^2J_{NH}$ = 2.2 Hz), –289.13 (N7, $^1J_{NH}$ = 102.7 Hz), –329.66 (N8, $^1J_{NH}$ = 69.4 Hz); ***m/z*** (FAB$^+$): 105 (cation); ***m/z*** (FAB$^-$): 143 (anion); **EA** ($C_3H_{12}N_{12}O_2$, 248.21) calcd.: C 14.52, H 4.87, N 67.72 %; found: C 14.52, H 4.77, N 67.45 %; **impact sensitivity**: > 6 J; **friction sensitivity**: > 240 N; **$\Delta_c U$**: 3345 cal g^{-1}.

*Azidoformamidinium 1-methyl-5-nitriminotetrazolate (**89**):* The synthesis of **89** proceeded analogical to the synthesis of **85**. Potassium 1-methyl-5-nitriminotetrazolate (3.34 g, 0.02 mol) and azidoformamidinium chloride (2.80 g, 0.02 mol) were used as starting materials. After recrystallization from water/ethanol colorless needles were obtained. (4.25 g, yield 93 %). **DSC** (T_{onset}, 5 °C min^{-1}): 119 °C, 180 °C (dec.); **IR** (ATR, cm^{-1}): $\tilde{\nu}$ = 3396 (m), 3325 (m), 3235 (s), 3186 (s), 2963 (m), 2796 (m), 2440 (w), 2354 (w), 2187 (s), 2112 (w), 1699 (s), 1660 (s), 1571 (w), 1507 (s), 1462 (s), 1407 (m), 1380 (m), 1312 (vs), 1295 (vs), 1240 (s), 1227 (vs), 1124 (m), 1106 (s), 1051 (m), 1032 (s), 981 (m), 902 (m), 884 (m), 772 (m), 732 (m), 690 (s), 659 (m), 580 (m); **Raman** (1064 nm, 400 mW, 25 °C, cm^{-1}): $\tilde{\nu}$ = 2986 (21), 2958 (8), 2189 (18), 2112 (3), 1659 (2), 1521 (91), 1469 (52), 1411 (5), 1360 (20), 1302 (44), 1239 (5), 1120 (33), 1059 (5), 1042 (100), 990 (4), 900 (18), 760 (19), 703 (10), 693 (15), 658 (10), 504 (10), 486 (12), 464 (8), 368 (12), 290 (11), 233 (12), 196 (16), 159 (10); **^{1}H NMR** (d_6-DMSO, 25 °C, ppm): δ = 9.10 (s, 2H, NH_2), 8.72 (s, 2H, NH_2), 3.75 (s, 3H, CH_3); **^{13}C NMR** (d_6-DMSO, 25 °C, ppm): δ = 159.2 (AF$^+$), 157.1 (CN_4), 33.8 (CH_3); **^{15}N NMR** (D_2O, 25 °C, ppm): δ = –12.35 (N3), –19.03 (N6), –24.68 (N2, q, $^3J_{NH}$ = 1.9 Hz), –97.11 (N4), –138.97 (N8), –152.72 (N9), –158.46 (N5), –171.48 (N1, q, $^2J_{NH}$ = 2.2 Hz), –277.64 (N7), –291.81 (N10); ***m/z*** (FAB$^+$): 86 (cation); ***m/z*** (FAB$^-$): 143 (anion); **EA** ($C_3H_7N_{11}O_2$, 229.16) calcd.: C 15.72, H 3.08, N 67.23 %; found: C 15.31, H 3.09, N, 65.68 %; **impact sensitivity**: > 4 J; **friction sensitivity**: > 160 N; **$\Delta_c U$**: 2708 cal g^{-1}.

7.8 Conclusion

From this experimental study the following conclusions can be drawn:

- 1-Methyl-5-nitriminotetrazole and 2-methyl-5-nitraminotetrazole can be easily deprotonated by using aqueous ammonia solution as well as metal hydroxides or carbonates forming ammonium 1-methyl-5-nitriminotetrazolate (**75**) and ammonium 1-methyl-5-nitriminotetrazolate (**76**) as well as the corresponding alkali and alkali earth metal salts **77**–**83**. These form silver 1-methyl-5-nitriminotetrazolate (**84**) by the reaction with $AgNO_3$ in aqueous solutions.

- The nitrogen-rich salts guanidinium 1-methyl-5-nitriminotetrazolate (**85**), 1-aminoguanidinium 1-methyl-5-nitriminotetrazolate (**86**), 1,3-diaminoguanidinium 1-methyl-5-nitriminotetrazolate (**87**), 1,3,5-triaminoguanidinium 1-methyl-5-nitriminotetrazolate (**88**), and azidoformamidinium 1-methyl-5-nitriminotetrazolate (**89**) can easily be obtained via metathesis reactions using silver 1-methyl-5-nitriminotetrazolate and the guanidinium chlorides in aqueous solution with high yields and good purity. An alternative synthesis route is the reaction of guanidinium perchlorates with potassium 1-methyl-5-nitriminotetrazolate. This route eliminates the light sensitive silver salt. **85**–**89** can be recrystallized from water/ethanol mixtures resulting in colorless crystals.

- The compounds are energetic materials due to their high nitrogen content and the partly increased sensitivities as well as the promising detonation parameters compared to common explosives like TNT and RDX.

- The crystal structures of **75**–**89** were determined using low temperature X-ray diffraction showing a similar structure of the 1-methyl-5-nitriminotetrazolate anion. Only the constitution of the nitramine group is variable since the coordination of the anions via classical hydrogen bonds is different. The compounds crystallize in monoclinic (**75**–**85** and **89**) or triclinic (**87** and **88**) space groups.

- A comprehensive analytical characterization of the chemical and thermochemical properties and sensitivities of compounds **75**–**89** is given. The salts show higher decomposition points than the neutral compounds **44** and **45**.

- In contrast to the neutral 1-methyl-5-nitriminotetrazole, its alkali and alkali earth metal salts are neither sensitive towards friction nor impact and show melting points between 230 and 280 °C followed by decompositions ranges above 300 °C. The combustion is nearly smokeless and brilliant flame colors are produced.

- Compounds **75**, **76** and **85**–**89** are stable at air even at higher temperatures. The long term stabilities 40 °C below the decomposition temperatures were tested successfully using a FlexyTSC (Thermal Safety Calorimeter).

- Promising detonation parameters were calculated especially for **85**–**89** compared to common explosives like TNT and RDX. The performance (calculated values: $p_{C\text{-}J}$ = 273 kbar; $V_{Det.}$ = 8770 m s^{-1}) of triaminoguanidinium 1-methyl-5-nitriminotetrazolate (**88**), even successful in the *Koenen test* using a critical diameter of 10 mm, qualifies it for further investigations concerning military applications.

Chapter 8.

Energetic Salts of 5-Nitriminotetrazole

8.1 Calcium 5-Nitriminotetrazolate – A green replacement for lead azide in priming charges.

All classes of energetic materials (explosives, propellants, pyrotechnics) contain polluting ingredients and decomposition products. Nitrogen rich derivatives are promising alternatives in energetic materials, since the generation of molecular nitrogen as an end-product of propulsion or explosion is highly desired in order to avoid environmental pollution and health risks, as well as to reduce detectible plume signatures.[307] However, also the application of heavy metal salts, e.g. lead azide and lead styphnate, should be strongly reduced. Lead azide is employed as an initiating explosive in blasting caps, since it is cheap and easy to manufacture and shows a appropriate thermal stability ($T_{dec.}$: 320–340 °C). When used as a primary charge, it is effective in smaller quantities than mercury fulminate.[308] Primary charges are the secondary component in ignition trains, which are designed to initiate secondary explosives, e.g. TNT or RDX. Next to the high toxicity, lead azide is also decomposed by atmospheric CO_2 and shows very high sensitivity towards impact (1–4 J) and friction (0.1–1 N). Several substitutes for lead azide have been presented in the last decades.[309] Less toxic silver azide (T_{dec}: 270–275 °C) gives a very satisfactory initiation effect which is superior to that of $Pb(N_3)_2$. Nevertheless, its practical use is limited, because it is light sensitive and also very high sensitive towards friction. The hardest criteria for new primary explosives [310] are a good thermal stability in combination with great performances. Zhillin *et al.* presented the two high-energy-capacity complexes tetraammine-*cis*-bis(5-nitro-2*H*-tetrazolato-*N*2)-cobalt(III) perchlorate [311] and tetra-ammine-bis(1-methyl-5-aminotetrazole-*N*3,*N*4)cobalt(III) perchlorate,[312] whereby the first mentioned is presently used in missile manufacture and mining industry. Also several replacements based on copper bis(tetrazole-5-yl)amines are presented in Chapter 16. In this section, one of the most powerful and qualified replacement for lead azide, calcium 5-nitriminotetrazolate (**90**) is described. A facile synthetic route, which can be also performed in larger scales, a comprehensive characterization including safety tests as well as an initiation experiment are described in the following.

The one step synthesis of **90**, shown in **Scheme 8.1**, can be divided into two steps. In the first reaction 5-amino-1*H*-tetrazole (**2**) is nitrated by using 100 % nitric acid. After

pouring the reaction on ice, it is not necessary to isolate 5-nitriminotetrazole (**43**) and, therefore, the solution is neutralized (while cooling) by the addition of calcium hydroxide. The precipitate formed is recrystallized from hot water yielding calcium 5-nitriminotetrazolate pentahydrate (**90**·5H_2O). The second reaction step is the dehydration at higher temperatures (150 °C) and lower pressures (1·10^{-1} mbar) yielding water-free **90**.

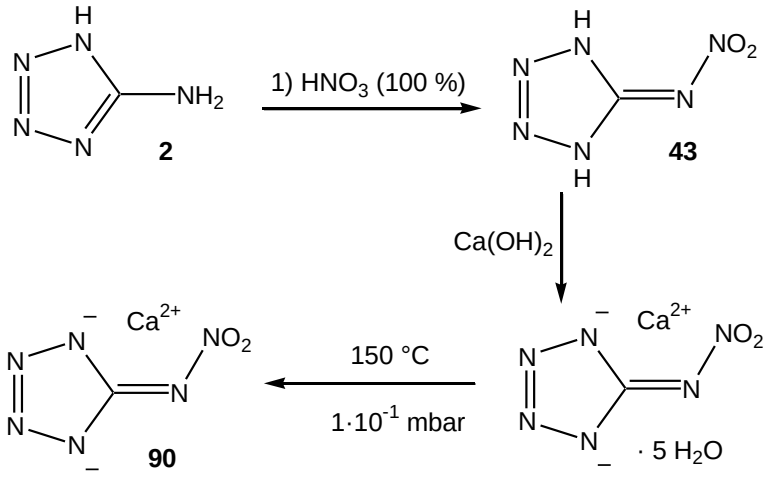

Scheme 8.1 Preparative route to calcium 5- nitriminotetrazolate (**90**).

A thermogravimetry (TG) curve as well as a differential scanning calorimetry (DSC) thermogram are depicted in **Figure 8.1**. The TG curve shows that the loss of water occurs over two discrete steps, which can be explained by having a look on the crystal structure (**Figure 8.2**). Four water molecules are lost between 72 and 85 °C. The fifth water is removed at temperatures above 92 °C. Above 145 °C the compound is completely dry. Dehydration was performed by simple putting **90**·5H_2O in an 200 °C oven for 48 hours. The DSC plot demonstrates the auspicious thermal stability up to temperatures above 360 °C. This decomposition temperature even surpasses that of lead and silver azide.

The structure of **90**·5H_2O in the crystalline state was determined by X-ray diffraction. Relevant data and parameters of the X-ray measurements and refinements are given in the appendix. Calcium 5-nitriminotetrazolate pentahydrate crystallizes in the triclinic space group *P*-1 with two molecular moieties in the unit cell. A density of 1.89 g cm^{-3} has been calculated. **90**·5H_2O is described best by the formation of a binuclear complex, which is depicted in **Figure 8.2**. The 5-nitriminotetrazolate dianions coordinate by the atoms N1 and O1 to the calcium cations forming a bite angle of 67.06(6)°. In accordance

to the TG experiment four molecules water are μ_1-coordinated, whereby one is bridging the calcium cations by a μ_2-coordination.

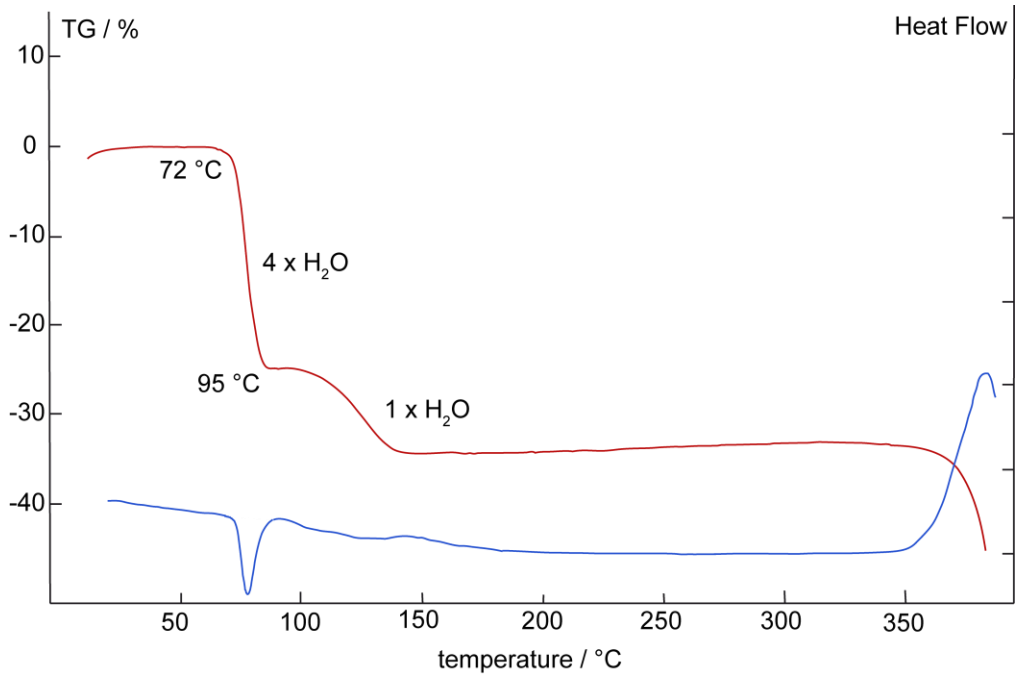

Figure 8.1 Thermogravimetry plot of compound **90**·5 H_2O, showing the loss of mass (left axis, red curve) and the DTA curve (right axis, blue curve).

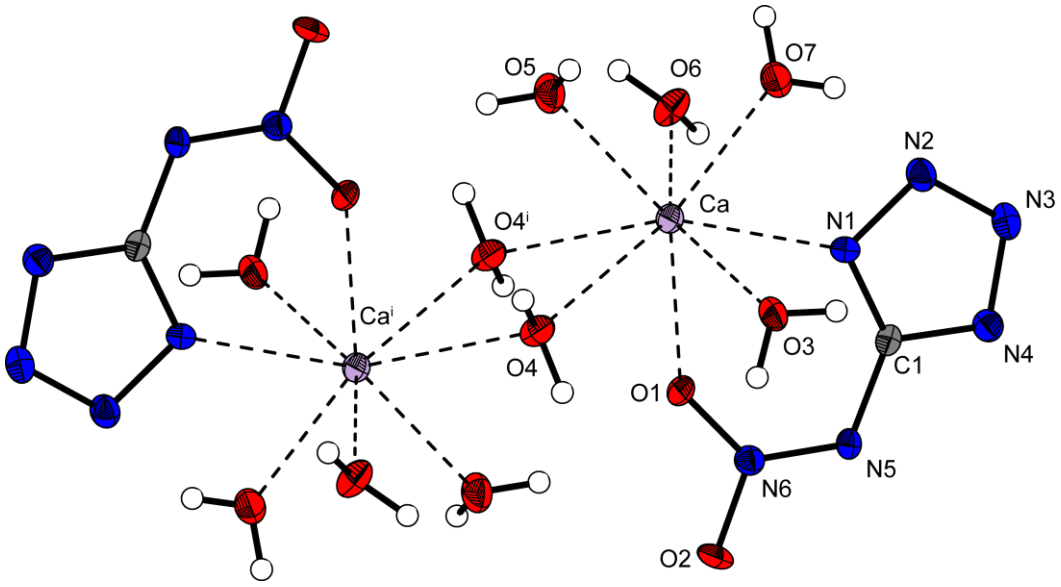

Figure 8.2 Molecular moiety of **90**·5H_2O. Ellipsoids of non-hydrogen atoms are drawn at the 50 % probability level. Selected coordination distances (Å): Ca–N1 = 2.492(2), Ca–O1 = 2.413(2), Ca–O3 = 2.516(2), Ca–O4 = 2.577(2), Ca–O5 = 2.3975(2), Ca–O6 = 2.365(2), Ca–O7 = 2.397(2).

90 as well as its pentahydrate were investigated by several specific tests determining the energetic behavior. The sensitivities towards impact, friction and electrical discharge of fine powdered (75–125 µm) **90** and **90**·5H_2O have been explored by the BAM drophammer and friction tester as well as the electric spark tester ESD 2010EN. Interestingly, **90**·5H_2O is more sensitive towards impact (15 J) than its water-free analogue (50 J). However, its sensitivity towards friction is lower (**90**: 112, **90**·5H_2O: 240 N). Also the electrical discharge sensitivity is significantly lower (**90**: 0.15 J, **90**·5H_2O: 1.05 J). This value is comparable to that of the secondary explosive RDX (~0.2 J) and significantly lower than that of lead azide (0.005 J). The friction and impact sensitivity values are also lower than these of used lead azide, which sensitivities must be reduced by the addition of dextrine. A comparison is given in **Table 8.1**. In order to investigated the durability of **90**, long term stability tests were performed using a Systag FlexyTSC (Thermal Safety Calorimeter) in combination with a RADEX V5 oven. The tests were undertaken as long-term isoperibolic runs in glass test vessels at atmospheric pressure with 300 mg of the compound at a temperature of 265 °C. 48 hours at this temperature do not yield to any decomposition reaction or loss of mass.

The heat of formation $\Delta_f H°$(s,M) of **90** has been calculated by the atomization energy method: $\Delta_f H°_{(g, M, 298)} = H_{(Molecule, 298)} - \sum H°_{(Atoms, 298)} + \sum \Delta_f H°_{(Atoms, 298)}$

The enthalpies (H) and free energies (G) were calculated using the complete basis set (CBS) method described by Petersson and coworkers using the Gaussian G03W (revision B.03) program package. With the calculated gas phase enthalpies (Ca^{2+}: 1927.3 kJ mol^{-1}, $AtNO_2^{2-}$: 399.0 kJ mol^{-1}) and the lattice enthalpy ($CaAtNO_2$: 2283.3 kJ mol^{-1}) computed by the *Jenkins equation*, $\boldsymbol{\Delta_f H°}$(s, M) has been calculated to be **32.8 kJ mol^{-1}**. With this value also the enthalpy of explosion $\boldsymbol{\Delta_{Ex} H}$ has been calculated according to the following equation and $\Delta_f H°$: CaO(s) = –635.6; $\Delta_f H°$, CO(g) = –110.5 kJ mol^{-1}) from the literature [122] to have a great value of **–778.9 kJ mol^{-1}**.

90 (s) → CaO (s) + CO (g) + 5/2 N_2 (g)

Table 8.1 Comparison of **90** with lead azide

	90	**90**·5H_2O	$Pb(N_3)_2$
Formula	$CCaN_6O_2$	$CH_{10}CaN_6O_7$	N_6Pb
FW / g mol^{-1}	168.13	258.23	291.23
$\rho_{calc.}$ / g cm^{-3}	~2.0	1.9	4.8

$\Delta_f H°$ / kJ kg^{-1}	195.1	---	1637.7
$\Delta_{Ex} H°$ / kJ kg^{-1}	–4632	---	–1638
Impact sensitivity* / J	50	15	2–4
Friction Sensitivity* / N	112	240	0.1–1
ESD* / J	0.15	1.05	0.005
Hot plate test	fulmination	fulmination	fulmination
$T_{dec.}$ / °C	360	360	320

* grain size: 75–125 µm

Hexanitrostilbene (HNS) is a secondary explosive with low sensitivities and a high thermally stability ($T_{dec.}$ = 318 °C). It can be used individually, but is also manufactured as an additive to cast TNT (trinitrotoluene), to improve the fine crystalline structure. However, HNS is hard to initiate and primary explosives with performances equal or greater than silver azide are needed. **90** was proofed to initiate HNS using the setup shown in **Figure 8.3** (A and B). A standard explosive train was used. A copper tube (∅ = 1.0 cm) was loaded with 2 g HNS and 0.5 g **90** on the top. As igniter, a "Austin Powder Firing Parameter Type I" was fixed on top without direct contact to **90**. Immediately after firing the upper igniter, **90** exploded violently and a successfully initiation of the HNS charge could be observed. The entire amount of HNS had been detonated by destroying the setup even in powder like pieces. Larger collected fragments of the copper tube and clamp are shown in **Figure 8.3** (C).

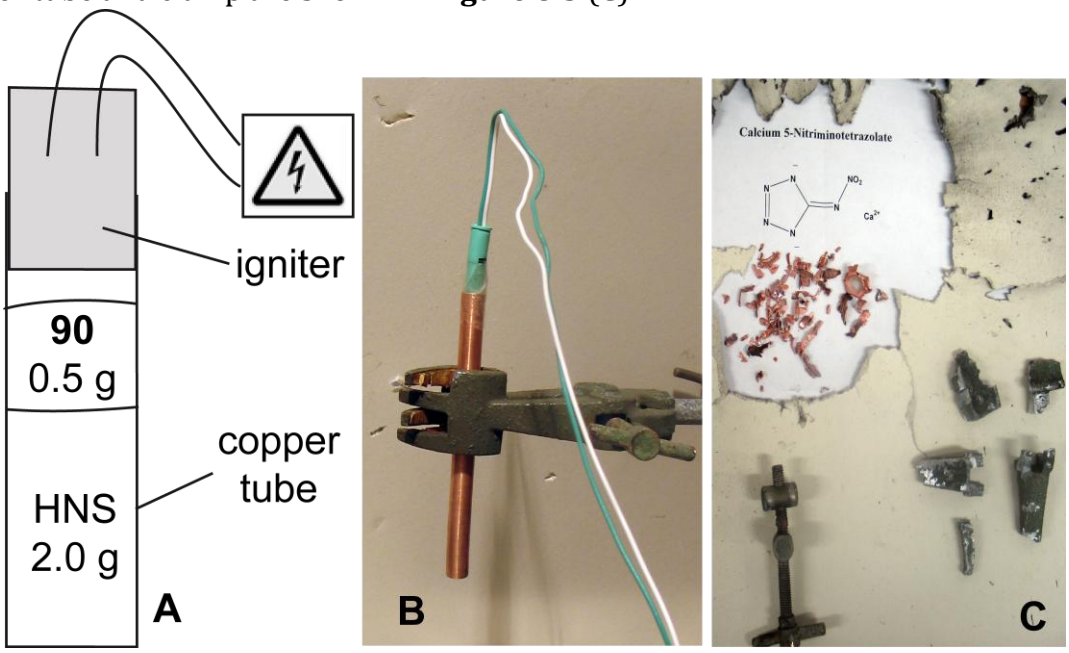

Figure 8.3 Initiation test of HNS using **90** as the primary explosive. A) theoretical setup; B) experimental setup; C) collected fragments of initiation test.

8.2 Alkali Metal Salts

Several mono-deprotonated as well as deprotonated alkali metal salts of 5-nitriminotetrazole are described in literature.[313] Also its ammonium salts have been published.[314] Except for the dipotassium 5-nitriminotetrazolate (**91**) no further alkali salts are characterized in this thesis. The alkali salts can be easily synthesized by deprotonation of **43** using one as well as two equivalents of alkali hydroxides or carbonates, respectively. The DSC curve (**Figure 8.13**) of **91** shows an almost straight line until 364 °C implying, that no crystal water is contained, which was also proofed by elemental analysis. In general the mono-deprotonated species are low soluble, also in cold water, but can be recrystallized from hot water. In contrast to the alkaline earth metals salts, the doubly deprotonated alkali salts of **43** are well soluble in water and can be recrystallized from water/ethanol mixtures. They represent appropriate starting materials for alkylations as shown in Chapter 6.

8.3 Alkaline Earth Metal Salts

Next to the doubly deprotonated calcium salt **90**, further alkaline earth metal salts have been prepared to investigate their energetic behavior.

8.3.1 Magnesium 5-nitriminotetrazolate tetrahydrate (**92**)

The magnesium salt of **43** was prepared by the reaction of 5-nitriminotetrazole with one equivalent of $Mg(OH)_2$. The resulted magnesium salt could only obtained as very thin needles and could not be determined by XRD. However, due to the elemental analysis the formula $Mg(AtNO_2)\cdot 4H_2O$ can be calculated. The compound is insoluble in organic solvents, moderate soluble in cold water and can be recrystallized from an ethanol/water mixture.

8.3.2 Calcium bis(5-nitrimino-1*H*-tetrazolate) pentahydrate (**93**)

The mono-deprotonated calcium salt has been prepared to compare its stabilities as well as sensitivities with the corresponding doubly deprotonated salt **90**. **93** crystallizes in

agreement to **90** also as its pentahydrate in the monoclinic space group $P2_1/c$ with four molecules in the unit cell. The density of 1.852 g cm^{-3} is lower than that of **90**. The molecular moiety is shown in **Figure 8.4**. The structure of the monodeprotonated 5-nitriminotetrazole is in agreement with that of e.g. ammonium 5-nitriminotetrazolate.[315] The calcium cations are surrounded by seven oxygen atoms with distances between 2.35 and 2.50 Å forming a distorted pentagonal bipyramide.

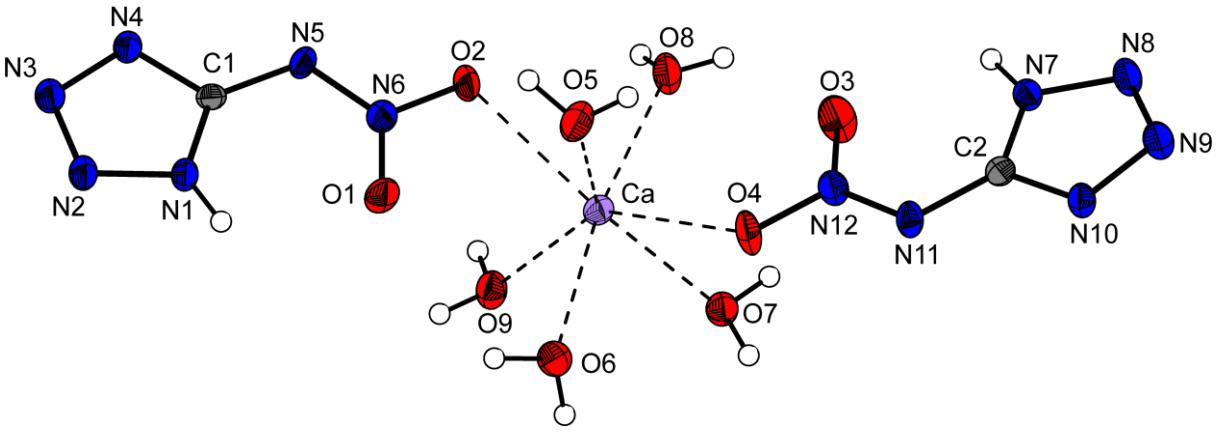

Figure 8.4 Molecular moiety of $Ca(HAtNO_2)\cdot 5H_2O$. Ellipsoids of drawn at the 50 % probability level. Selected coordination distances (Å): Ca–O6 = 2.359(2), Ca–O8 = 2.385(2), Ca–O5 = 2.402(2), Ca–O7 = 2.446(2), Ca–O2 = 2.459(2), Ca–O9 = 2.484(2), Ca–O4 = 2.498(2), Ca–O1 = 2.950(2).

8.3.3 Strontium bis(5-nitriminotetrazolate) tetrahydrate (**94**)

Strontium bis(1-hydro-5-nitriminotetrazolate) tetrahydrate (**94**) crystallizes orthorhombic in the *Pbcn* space group with four molecules in the unit cell. The molecular moiety is depicted in **Figure 8.5**. The density of 2.202 g cm^{-3} is lower in comparison to that observed for strontium bis(1-methyl-5-nitriminotetrazolate) monohydrate (**95**). The bond distances and angles of the anions follow those observed in other mono-deprotonated 5-nitriminotetrazoles in the literature and are also in the range of these in **95**. The C1–N5 distance of N5–C1 = 1.375(4) Å is nearer to a C–N double bond than a single bond. The nitrimino-group is only slightly twisted (~6°) out of the ring plane. This may be a consequence of the formation of an intramolecular hydrogen bond between the atoms N1–H1···O2.

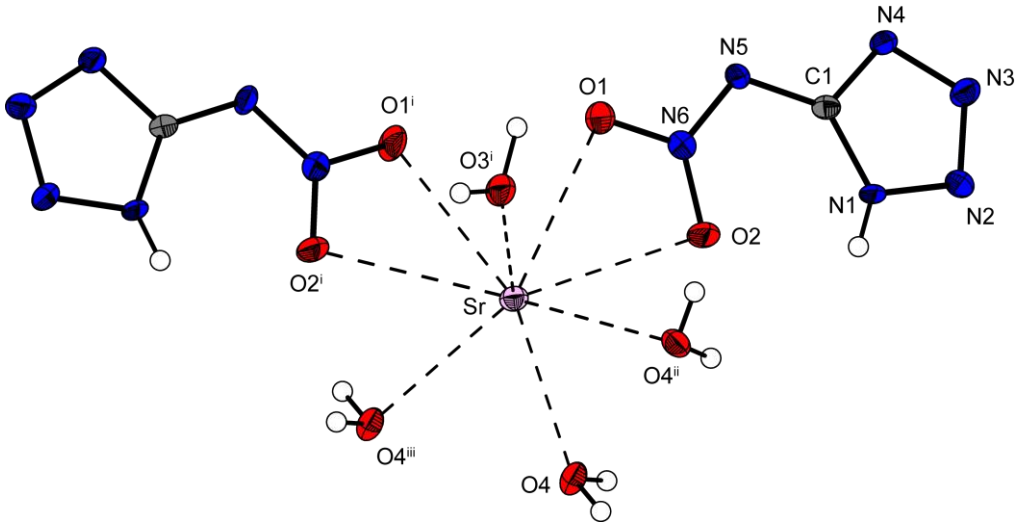

Figure 8.5 Molecular moiety of $Sr(HAtNO_2)\cdot 5H_2O$. Ellipsoids of drawn at the 50 % probability level. Selected geometries: distances: (Å) N1–C1 = 1.336(4), N1–N2 = 1.344(4), N2–N3 = 1.297(4), N3–N4 = 1.349(4), N4–C1 = 1.331(4), N5–C1 = 1.375(4), N5–N6 = 1.311(4), O1–N6 = 1.262(4), O2–N6 = 1.256(4), Sr–O1 = 2.764(2), Sr–O2 = 2.868(2), Sr–O3 = 2.610(3), Sr–O4 = 2.694(3); angles (°): N6–N5–C1 = 115.9(3), O1–Sr–O2 = 45.13(7), O2–N6–O1 = 118.5(3); torsion angles (°): N6–N5–C1–N1 = −6.1(7), C1–N5–N6–O2 = −0.9(5).

The packing of **94** is characterized by the formation of stacks along the *c* axis. The stacks are build by bridging water molecules in the centers as can be seen in **Figure 8.6**. Both 5-nitriminotetrazolate anions coordinated to one strontium atom are located at the same side.

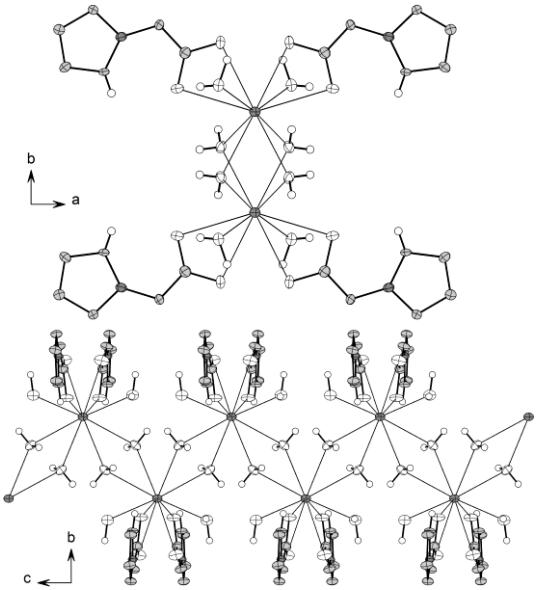

Figure 8.6 View on the stacks in **94** along the *c* axis (top) and *a* axis (below).

8.3.4 Strontium 5-nitriminotetrazolate dihydrate (**95**)

Strontium 5-nitriminotetrazolate dihydrate (**95**) crystallizes in the chiral orthorhombic space group *Fdd*2 with 16 molecules in the unit cell and a density of 2.423 g cm^{-3}. The "Flack" parameter was estimated to be −0.007(7). **Figure 8.7** shows the molecular unit of **95**, in which the 5-nitriminotetrazolate dianion is coordinated by the atoms N4 and O2 to the strontium cation. The molecular structure of the dianions again corresponds to the nomenclature "5-nitrimino-", since the C1–N1 distance of 1.375(4) Å is nearer at a C=N double bond (1.30 Å) than a C–N single bond (1.47 Å). The bond lengths and angles follow the values observed for e.g. **90** and **96**. The nitrimino-group is slightly twisted (~6°) out of the planar aromatic tetrazole ring system.

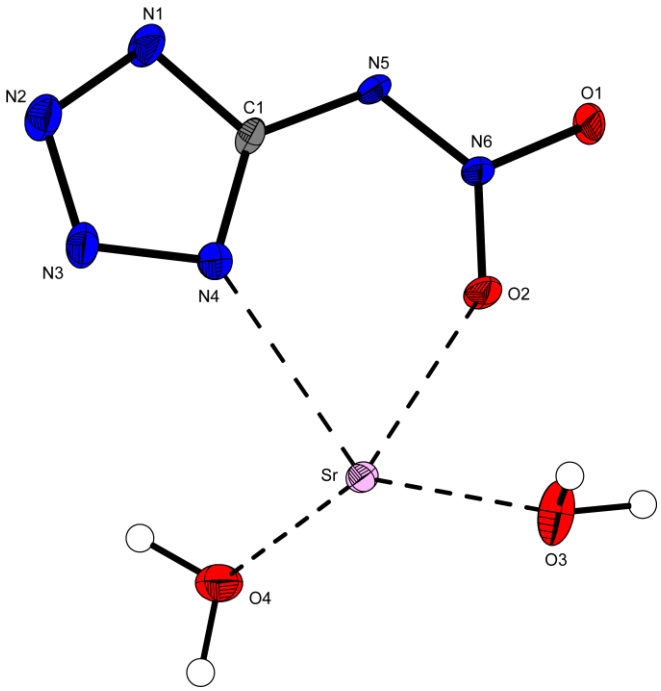

Figure 8.7 Molecular moiety of **95**. Hydrogen atoms shown as spheres of arbitrary radius and thermal displacements set at 50 % probability. Selected geometries: distances (Å) N1–N2 = 1.344(4), N2–N3 = 1.297(4), N3–N4 = 1.349(4), N4–C1 = 1.331(4), N1–C1 = 1.336(4), N5–N6 = 1.311(4), N5–C1 = 1.375(4), O1–N6 = 1.262(4), O2–N6 = 1.256(4), Sr–N1 = 2.864(2), Sr–O3 = 2.610(3), Sr–O4 = 2.694(3), Sr–O1 = 2.764(2), Sr–O2 = 2.868(5); angles (°) N6–N5–C1 = 118.3(2), O2–N6–N5 = 127.1(2), O2–N6–O1 = 116.8(2), N4–Sr–O2 = 61.16(2); torsion angles (°) N6–N5–C1–N4 = 6.0(5), C1–N5–N6–O2 = 0.5(5).

The packing of **95** is characterized by the formation of a three dimensional network. The strontium cations are coordinated ninefold by two crystal water molecules and by the nitrogen atoms N1 and N4 and oxygen atoms O1 and O2 of four different 5-nitriminotetrazolate dianions. The coordination of one dianion can be seen in **Figure 8.8**. Except for the atoms C1 and N6 all atoms participate in different coordination modes. The two strongest hydrogen bonds in the packing are formed between the ring nitrogen atoms N2 and N3 and the two crystal water molecules (O4–H4A···N3: 0.90(2), 1.89(2), 2.788(3) Å, 179(4)°; O3–H3B···N2: 0.90(3), 1.92(3), 2.799(3) Å, 166(4)°).

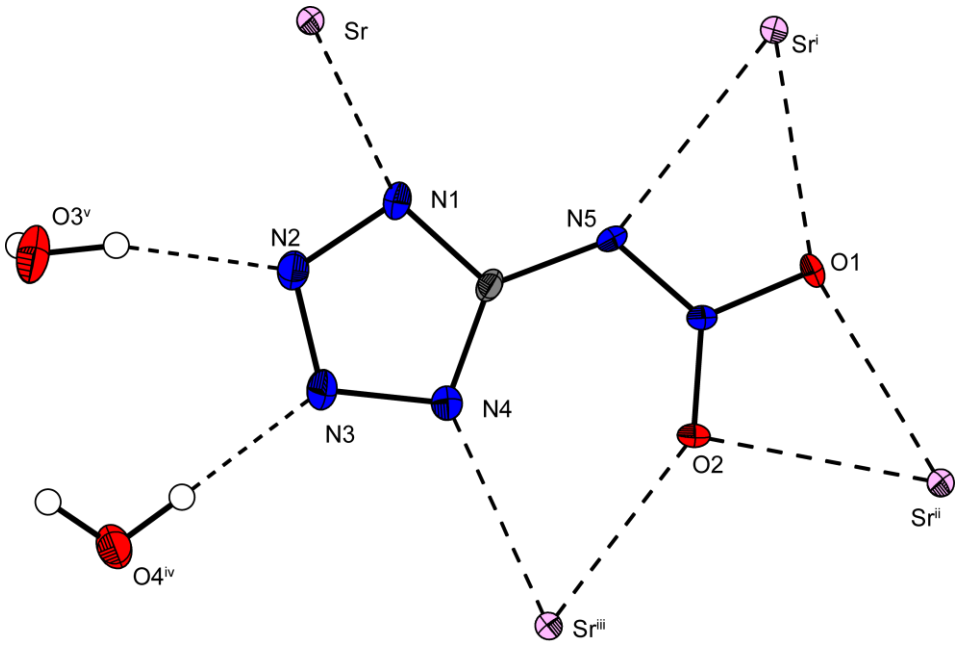

Figure 8.8 Coordination modes of the 5-nitriminotetrazolate anions. (i) 0.25+x, 2.25−y, 0.25+z; (ii): 0.5+x, y, 0.5+z; (iii): 2−x, 2.5−y, 0.5+z; (iv): 1−75−x, 0.25+y, 0.75+z; (v): 1.5−x, 2.5−y, z.

8.3.5 Barium 5-nitriminotetrazolate dihydrate (**96**)

$Ba(AtNO_2)\cdot 2H_2O$ (**96**) crystallizes with a density of 2.911 g cm^{-3} in the triclinic space group *P*–1 containing two molecular units in the elemental cell. Again two barium centers are connected via two bridged water molecules forming a binuclear complex (**Figure 8.9**).

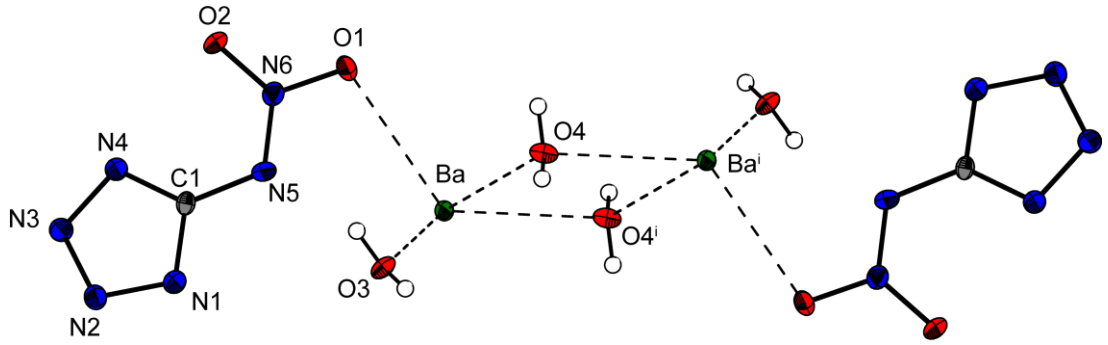

Figure 8.9 A view of the dimers in $BaAtNO_2 \cdot 2H_2O$, showing the atom-labeling scheme. Thermal ellipsoids represent 50 % probability and hydrogen atoms are shown as small spheres of a arbitrary radii.

8.4 Transition Metal Salts

8.4.1 Cadmium 5-nitriminotetrazolate dihydrate (**97**)

The cadmium salt **97** of the doubly deprotonated nitriminotetrazole was synthesized in aqueous solution using **43** and $CdCO_3$ as starting materials. The motivation of this toxic compound was to investigate the energetic characteristics, since cadmium azide is more powerful than lead and silver azide. **97** is absolutely insoluble in H_2O, DMSO and DMF and all other organic solvents. Therefore, no single crystals for X-ray analysis could be obtained. It precipitates from water as its dihydrate, which was examined by elemental analysis. **97** can be dehydrated at 150 °C under lower pressure ($2 \cdot 10^{-2}$ mbar). **97** performs very well in the *Hot Plate test*. However, its thermal stability ($T_{Dec.}$ = 333°) is lower than that observed for the earth alkaline salts.

8.4.2 $[Zn(HAtNO_2)_2(H_2O)_4] \cdot 2H_2O$ (**98**)

The zinc complexes **98** and **99** (see below) have been synthesized because (i) the coordination ability of 5-nitriminotetrazoles to zinc should be investigated (ii) zinc is a non-toxic cation in novel green energetic complexes. It was not possible to form crystalline material of a doubly deprotonated zinc 5-nitriminotetrazole. However, both compounds are not appropriate as new energetic materials, since they show lower decomposition temperatures on the one hand and are hard to dehydrate on the other hand. The structure of **98** was solved in the monoclinic space group $P2_1/c$ with four

molecular units in the unit cell and a high density of 1.967 g cm^{-3}. The zinc cation is coordinated octahedral by four water molecules and two nitriminotetrazoles as shown in **Figure 8.10**. The coordination bonds are formed between the N1/N7 atoms and the zinc cation. The nitriminotetrazolates are oppositely coordinated in the equatorial position. The torsion angels of N1–N2–N3–N4 0.2(3) ° and N7–N8–N9–N10 0.3(3)° point towards the suspected planarity of the tetrazole rings. The torsion angel N10–C2–N11–N12 is 7.1(4)° which shows that the nitrimino group is nearly coplanar to the tetrazole ring. There are four different zinc oxygen distances which are between 2.065(4) and 2.115(3) Å which match with other zinc water coordinations.[316]

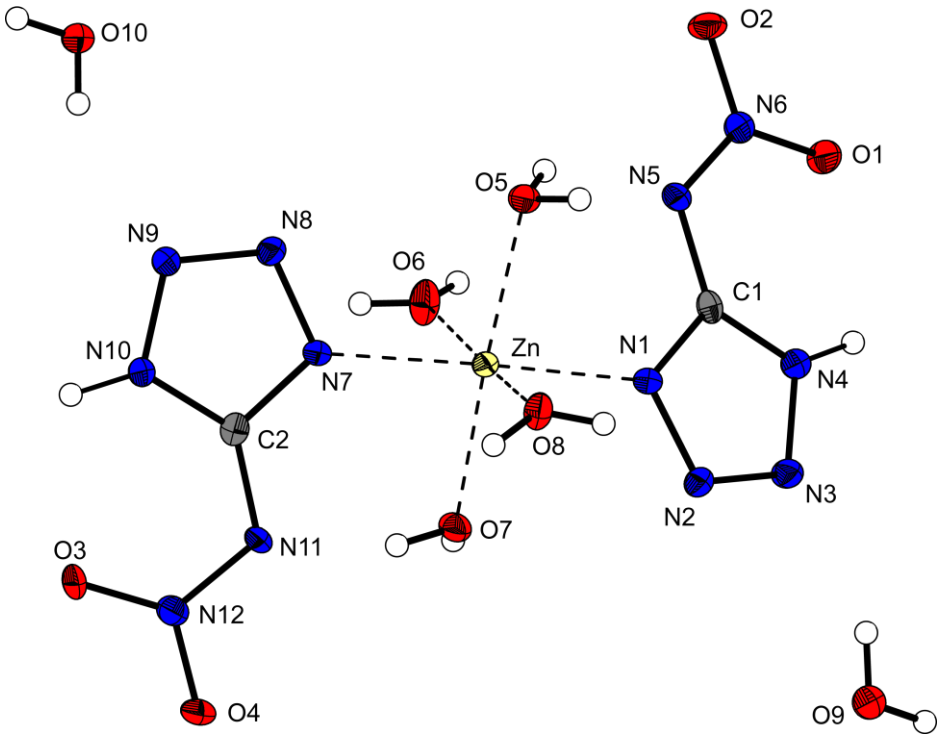

Figure 8.10 Molecular structure of $[Zn(HAtNO_2)_2(H_2O)_4]\cdot 2H_2O$ (**98**). Hydrogen atoms shown as spheres of arbitrary radius and thermal displacements set at 50 % probability. Selected coordination geometries: distances (Å): Zn–O7 = 2.065(2), Zn–O8 = 2.083(2), Zn–O5 = 2.097(2), Zn–O6 = 2.115(2), Zn–N1 = 2.152(2), Zn–N7 = 2.158(2); angles (°): O7–Zn–O8 = 93.74(8), O7–Zn–O5 = 176.62(7), O8–Zn–O5 = 87.28(8), O7–Zn–O6 = 90.98(8), O8–Zn–O6 = 174.25(7), O5–Zn–O6 = 88.19(8), O7–Zn–N1 = 87.14(7), O8–Zn–N1 = 94.90(8), O5–Zn–N1 = 89.56(7), O6–Zn–N1 = 88.61(8), O7–Zn–N7 = 89.96(7), O8–Zn–N7 = 88.44(7), O5–Zn–N7 = 93.29(7), O6–Zn–N7 = 88.28(8), N1–Zn–N7 = 175.71(7).

8.4.3 $[Zn(H_2O)_6](1MeAtNO_2)_2$ (**99**)

The structure of **99** has been solved in the orthorhombic space group *Pbca* with four molecules in the unit cell and a lower density of 1.900 g cm^{-3}. The crystal water molecules coordinate the zinc octahedrally and there is no direct bonding from the zinc cation to the nitriminotetrazolates (**Figure 8.11**). The torsion angels of N1–N2–N3–N4 with –0.3(4)° and of N4–C1–N6–N7 with –9.0(6)° show that the tetrazole rings are planar and that the nitrimino-group is in the plane of the tetrazole ring, whereas also the methyl group is coplanar to the ring. The zinc oxygen distances are 2.095(3), 2.063(3) and 2.094(3) Å similar to other zinc molecules, which are hexahedrally coordinated by water.[317]

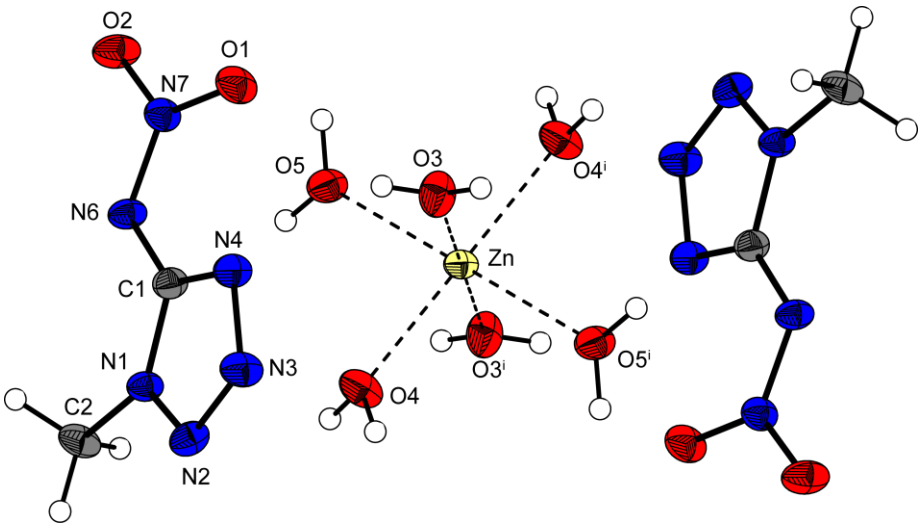

Figure 8.11 Molecular structure of $[Zn(H_2O)_6]\cdot(1MeAtNO_2)_2$ (**99**). Hydrogen atoms shown as spheres of arbitrary radius and thermal displacements set at 50 % probability. Selected coordination geometries: distances (Å): Zn–O5 = 2.064(3), Zn–O4 = 2.094(3), Zn–O3 = 2.095(3); (i) –x, –y, –z.

8.5 Hydrazinium Salts

8.5.1 Hydrazinium 5-nitrimino-1*H*-tetrazolate (**100**)

The hydrazinium salts hydrazinium 5-nitrimino-1*H*-tetrazolate (**100**) and bis(hydrazinium) 5-nitriminotetrazolate monohydrate (**101**) were synthesized according to **Scheme 8.2**. Since **100** seems to be soluble in THF to a certain amount, the yield drops to 56 %. **100** can be recrystallized from methanol. However, no crystals suitable for X-ray analysis could be obtained.

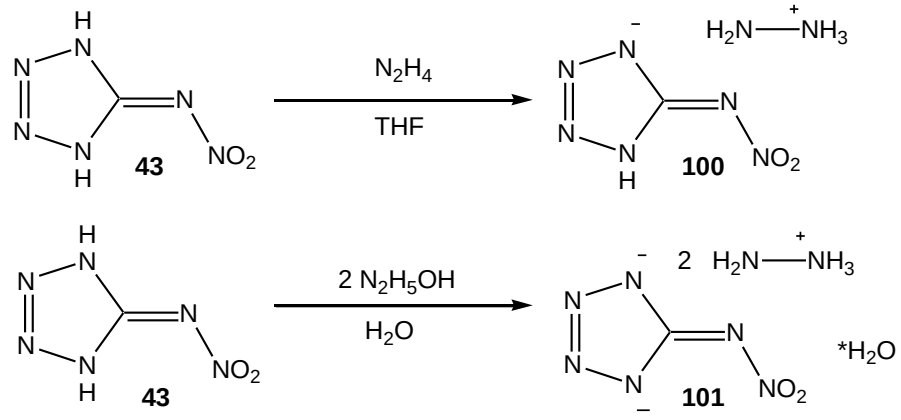

Scheme 8.2 Syntheses of hydrazinium 5-nitriminotetrazolates **100** and **101**.

Compound **100** is the only compound in this chapter, which shows appropriate characteristics for use as a new secondary explosive. In order to calculate its detonation parameters, the density has been determined in a small scale solvent pycnometer and should be in the range of 1.66 to 1.70 g cm^{-3}. The heat of formation was computed using experimentally obtained heats of combustion. The energetic properties of **100** are summarized in **Table 8.2**.

Table 8.2 Physico-Chemical Properties of **100**.

	100
Formula	$CH_6N_8O_2$
FW /g mol^{-1}	162.11
Impact sensitivity [a] / J	3
Friction sensitivity [b] / N	56
ESD-test [c] / J	0.40
N [d] / %	69.12
Ω [e] / %	–29.6
$T_{dec.}$ [f] / °C	188
Density [g] / g cm^{-3}	1.680
$-\Delta U_{comb}$ [h] / cal g^{-1}	2263
$-\Delta H_{comb}$ [i] / kJ mol^{-1}	1530
$\Delta_f H°_m$ [j] / kJ mol^{-1}	279
EXPLO5 values:	
$-\Delta_E U_m°$ [k] / kJ kg^{-1}	4996
T_E [l] / K	3584
p [m] / kbar	301
$V_{Det.}$ [n] / m s^{-1}	8856
Gas vol. [o] / L kg^{-1}	892

[a] BAM drophammer; [b] BAM friction tester; [c] OZM small scall electrostatic discharge device; [d] Nitrogen content; [e] Oxygen balance; [f] Temperature of decomposition by DSC (β = 5 °C min^{-1}); [g] estimated from solvent pycnometry; [h] Experimental (constant volume) combustion energy; [i] Experimental molar enthalpy of combustion; [j] Molar enthalpy of formation; [k] Energy of Explosion; [l] Explosion temperature; [m] Detonation pressure; [n] Detonation velocity; [o] Assuming only gaseous products.

8.5.2 Bis(hydrazinium) 5-nitriminotetrazolate monohydrate (**101**)

Compound **101** has been synthesized by the reaction of 5-nitriminotetrazole (**43**) with two equivalents of hydrazine hydrate. Recrystallization from ethanol/water afforded unfortunately only the monohydrate (**101**), which is depicted in **Figure 8.12**. It crystallizes in the orthorhombic space group $P2_12_12_1$ with four molecules in the unit cell. The Friedel pairs have been merged. The density of 1.635 g cm^{-3} is slightly lower than that determined for **100**. The structure of the anions as well as cations is in agreement to previously discussed structures. The packing is strongly dominated by several H-bonds (listed in **Table 8.3**).

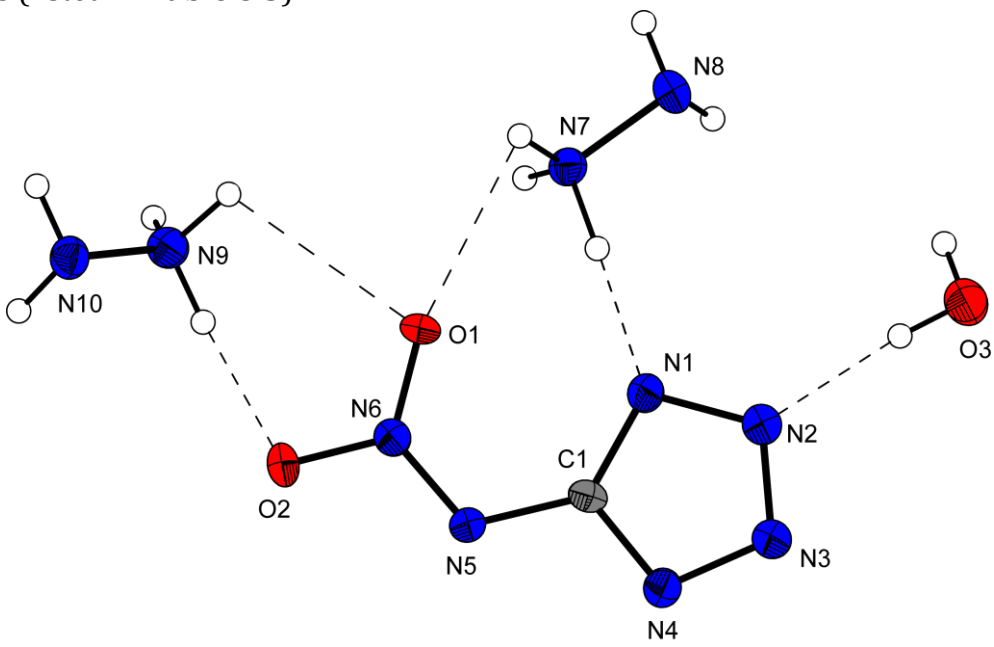

Figure 8.12 Molecular structure of bis(hydrazinium) 5-nitriminotetrazolate monohydrate (**101**). Hydrogen atoms shown as spheres of arbitrary radius and thermal displacements set at 50 % probability.

Table 8.3 Hydrogen bonding in the structure of **101**. Hydrogen atoms without standard deviations.

D–H···A	d(D–H)	d(H···A)	d(D–A)	∢(D–H···A)
N7–H1–N1	1.05	1.81	2.858(4)	176.8
N7–H2–N4^{i}	0.92	1.97	2.880(4)	176.6
N7–H3–O1^{ii}	1.02	2.0200	3.019(4)	166.4
N7–H3–N1^{ii}	1.02	2.57	3.085(4)	111.0

N8–H4–N5^{iii}	0.88	2.45	3.322(4)	167.8
N8–H5–O3^{iv}	0.81	2.56	3.120(3)	127.0
N9–H6–N3^{i}	1.01	1.94	2.906(3)	160.5
N9–H7–N10^{ii}	0.96	1.98	2.915(5)	163.1
N9–H8–O2	0.93	1.99	2.841(3)	151.6
N9–H8–O1	0.93	2.55	3.047(3)	113.9
N9–H8–N6	0.93	2.61	3.373(3)	139.9
N10–H9–N8^{v}	0.89	2.67	3.084(3)	110.1
N10–H10–O2^{vi}	0.89	2.39	3.021(3)	128.1
N10–H10–N5^{vi}	0.89	2.48	3.328(3)	158.4
O3–H11–N2	0.86	2.04	2.875(3)	166.0
O3–H12–O3^{iv}	0.81	2.07	2.855(3)	162.5

(i) 2–x, –0.5+y, 0.5–z; (ii) –1+x, y, z; (iii) 1–x, –0.5+y, 0.5–z; (iv) –0.5+x, 0.5–y, 1–z; (v) 1.5–x, –y, –0.5+z; (vi) –0.5+x, 0.5–y, –z.

8.6 Energetic Properties

The thermal behavior as well as the sensitivities of compounds **91**–**97** as well as **100** are described in the following. The characteristics of **90** are described in section 8.1.

8.6.1 Thermal Stability

All of the decomposition temperatures, determined by DSC measurements, are higher than the decomposition temperature of the corresponding non-ionic acid **43**. A general trend seems to be, that hydrazinium and ammonium salts decompose at lower temperatures in comparison to alkali metal and alkaline earth metal salts. However, also the hydrazinium salt **100** shows an appropriate decomposition temperature of 188 °C. The thermo plots of **90**–**97** as well as **100** are depicted in **Figure 8.13**. The investigated metal salts potassium (**91**), magnesium (**92**), calcium (**93**), strontium (**94**, **95**), barium (**96**) and cadmium (**97**) nitriminotetrazolate show very good thermal stabilities. The mono-deprotonated salts **93** and **94** show the lowest decomposition temperatures of 200 °C and 224 °C, respectively. With regard to $T_{Dec.}$, most promising are next to **90** the doubly deprotonated potassium salt **91** as well as the strontium salt **95** and the corresponding barium salt **96**.

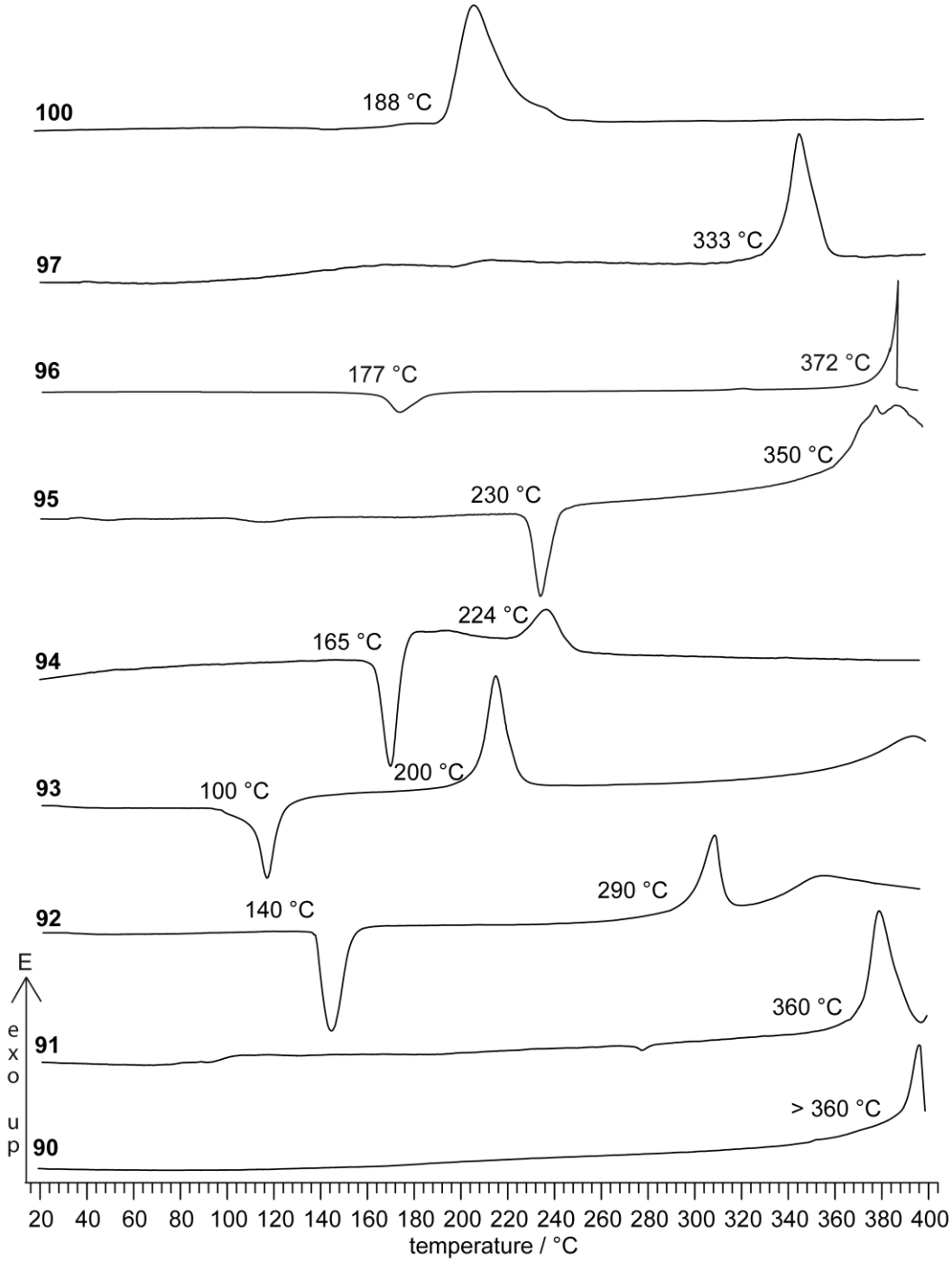

Figure 8.13 DSC plots (exo-up) of compounds **90**–**97** as well as **100**.

8.6.2 Sensitivities

The impact sensitivities of the ionic compounds are spread over a very large range reaching from very sensitive to insensitive. Hydrazinium 5-nitrimino-1*H*-tetrazolate (**100**) is sensitive towards impact (3 J) and friction (56 N). As already mentioned, **90**·5H_2O is moderately sensitive, whereas the dried calcium salt **90** is completely

insensitive. The further alkali and alkali earth metal salts of nitriminotetrazole show low (360N) to moderate (112 N) friction sensitivities depending on the water content. Only the heavy metal salt **97** is very sensitive towards friction (12 N). Further sensitivity data are summarized in **Table 8.4**.

Table 8.4 Physico-chemical properties of **91–98**.

	91	**92**	**93**	**94**	**95**	**97**	**98**
Formula	$CK_2N_6O_2$	$CH_8MgN_6O_6$	$C_2H_{12}CaN_{12}O_9$	$C_2H_{10}N_{12}O_8Sr$	$CH_4N_6O_4Sr$	$CH_4BaN_6O_4$	$CCdN_6O_2$
FW / g mol^{-1}	206.25	224.42	388.27	417.84	251.72	301.41	240.46
Impact sens. / J	10	> 40	10	20	30	45	17
Friction sens. / N	240	> 360	240	> 360	> 360	> 360	12
ESD-test / J	0.4	0.9	1.0	0.4	1.9	1.2	0.01
N / %	40.75	37.45	43.29	40.23	33.39	27.88	67.23
$T_{dec.}$ / °C	364	290	200	224	350	372	333

8.7 The Reaction of 5-Nitriminotetrazole with Methyl-5-aminotetrazoles

The formation of nitrogen-rich tetrazolate or tetrazolium salts leads to interesting energetic materials. Also the combination of two tetrazole derivatives (forming tetrazolium tetrazolates) is possible, which has been successfully described on the formation of 5-aminotetrazolium 5-nitriminotetrazolate by Shreeve et. al..[3] In this section the reactions of 5-nitriminotetrazole (**43**) with 1-methyl-5-aminotetrazole (**10**) as well as 2-methyl-5-aminotetrazole (**11**) are described. In the first reaction **10** was protonated yielding 1-methyl-5-aminotetrazolium 5-nitrimino-1*H*-tetrazolate monohydrate (**102**). In the latter case no protonation could be observed and the co-crystallization product **103** of 5-nitraminotetrazole and 2-methyl-5-aminotetrazole was obtained.

8.7.1 Synthesis

The synthesis of 1-methylaminotetrazolium nitriminotetrazolate (**102**) and 2-methyl-5-aminotetrazole · 5-nitriminotetrazole (**103**) was performed according to **Scheme 8.3**. 5-

Nitriminotetrazole was dissolved in water and the 1-methyl-5-aminotetrazole and 2-methylaminotetrazole, respectively, was added. After heating the mixture and removing the solvent, both have been recrystallized from ethanol in good yields (77 % (**102**), 81% (**103**)). As shown in many studies, tetrazoles behave as weak bases.[36] They are protonated only in the media whose acidity can be described by the empiric scales of acidity function. In the case of weak bases the pK_{BH+} value is a suitable criterion for the basicity. To the best of our knowledge, we could not find exact values for 1-methyl- and 2-methyl-5-aminotetrazole. However values are given for 1-methyl-5*H*-tetrazole (pK_{BH+} = –3.00) and 2-methyl-5*H*-tetrazole (–3.25) as well as 1-methyl-5-aryl-tetrazole (–2.50) and 2-methyl-5-aryl-tetrazole (–3.27), which show that latter molecule is the weaker base and can therefore harder be protonated.[318] However, the differences are no of the size that the failed protonation of **11** clearly explained. Also in DMSO solution no protonation is obtained, which can be seen clearly in the ^{13}C NMR spectrum.

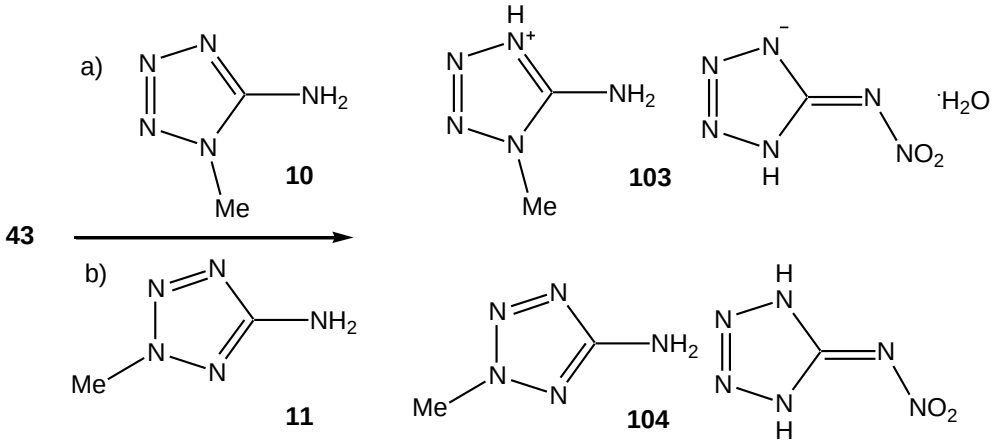

Scheme 8.3 Products of the reaction of 5-nitriminotetrazole with 1-methyl-5-aminotetrazole and 2-methyl-5-aminotetrazole, respectively.

8.7.2 Structure of 1-Methyl-5-aminotetrazolium nitriminotetrazolate (**102**) and 2-Methyl-5-aminotetrazole · 5-nitraminotetrazole (**103**)

103, also abbreviated with 1MeHAt_HAtNO$_2$·H$_2$O crystallizes in the monoclinic space group $P2_1/c$ with a calculated density of 1.590 g cm^{-3}. The complete molecular moiety is build planar (**Figure 8.14**). The structure of the 1-methyl-5-aminotetrazolium cation is in agreement with those observed for e.g. 1-methyl-5-aminotetrazolium nitrate or dinitramide.[68,134] Within the 5-nitriminotetrazolate anions an intramolecular hydrogen bond (N4–H4···O2 = 0.89(2), 2.32(2), 2.661(2) Å, 102(2)°, graph set **S1,1(6)**) stabilizes

the planar structure. This is also found e.g. in 5-aminotetrazolium 5-nitrimino-tetrazolate.[3b]

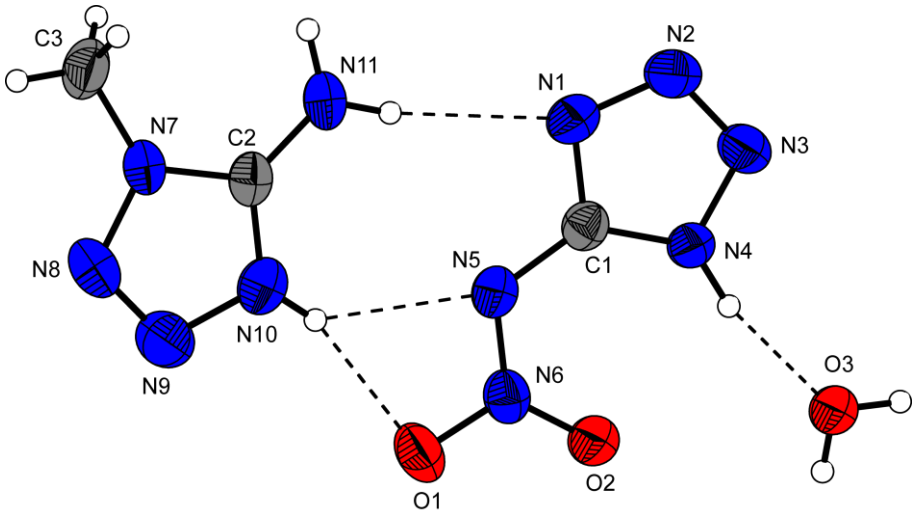

Figure 8.14 Molecular moiety of **102**. Ellipsoids of non-hydrogen atoms are drawn at the 50 % probability level. Bond distances (Å): O1–N6 = 1.274(2), O2–N6 = 1.238(2), N6–N5 = 1.302(2), N4–N3 = 1.344(2), N4–C1 = 1.346(2), C1–N1 = 1.328(2), C1–N5 = 1.372(2), N1–N2 = 1.348(2), N3–N2 = 1.301(2), N7–C2 = 1.342(2), N7–N8 = 1.369(2), N7–C3 = 1.446(2), N11–C2 = 1.315(2), C2–N10 = 1.330(2), N10–N9 = 1.365(2), N8–N9 = 1.266(2).

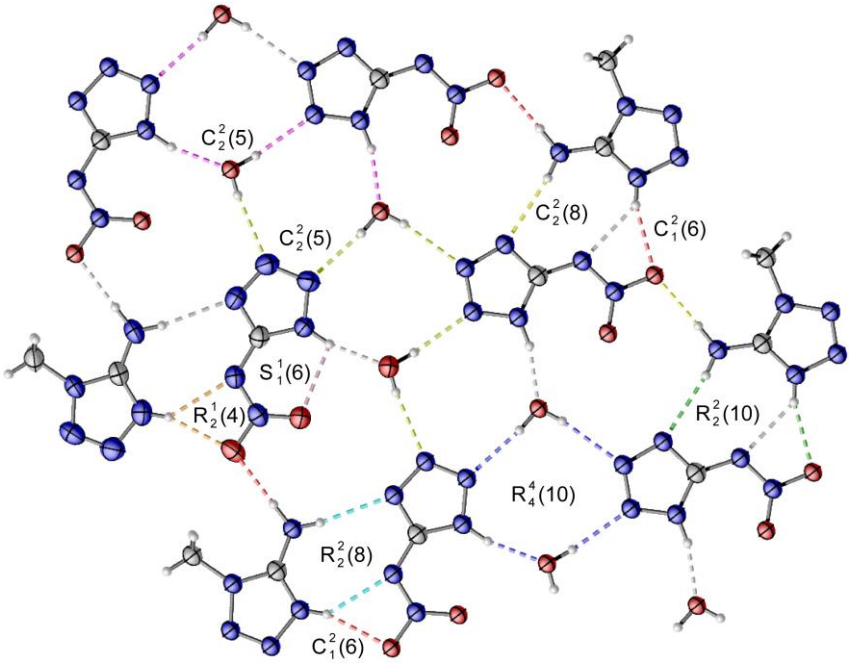

Figure 8.15 Hydrogen bonding in the layers of **102**. Selected hydrogen bonds (Å, Å, Å,°): N4–H1···O3 = 0.89(2), 1.86(2), 2.733(2), 167(2); N11–H3···N1 = 0.83(2), 2.32(2), 3.137(2), 172(2); N11–H3···N5 =

0.83(2), 2.62(2), 3.242(2), 133(2), N11–H4···O1^{i} = 0.90(3), 1.97(3), 2.865(2), 174(2); N11–H4···N6^{i} = 0.90(3), 2.66(3), 3.479(2), 152(2); N10–H2···O1= 0.80(2), 2.13(2), 2.903(2), 162(2); N10–H2···N5 = 0.80(2), 2.27(3), 2.925(2), 140(2); N10–H2···N6 = 0.80(2), 2.62(3), 3.408(2), 169(2); O3–H8···N3^{ii} = 0.85(3), 2.10(3), 2.941(2), 170(2); O3–H9···N2^{iii} = 0.79(3), 2.21(3), 2.977(2), 164(2); (i) x, 1+y, z; (ii) 1–x, –0.5+y, –0.5–z; (iii) x, –1+y, z.

The packing of **103** is characterized by the formation of layers along the *b* axis. The layers have distances of ~2.25 Å. Within the layers a distinctive hydrogen bond network is formed. (**Figure 8.15**). Several graph sets are drawn and illustrated with different colors (**S1,1(6)** purple, **R1,2(4)** orange, **R2,2(8)** turquoise, **R2,2(10)** dark green, **R4,4(10)** blue, **C2,1(6)** red, **C2,2(5)** pink, **C2,2(5)** light green, **C2,2(8)** yellow).

As previously described the reaction of 5-nitriminotetrazole with 2-methyl-5-aminotetrazole does not yield to the formation of a salt but to the formation the co-crystallization product **103**. The compound abbreviated with 2MeAt_H_2AtNO_2 also crystallizes in the monoclinic space group $P2_1/c$ with a higher calculated density of 1.657 g cm^{-3} in comparison to **102**. Again the complete molecular moiety is build planar. (**Figure 8.16**) The structure of the 2-methyl-5-aminotetrazole molecule is in agreement with those observed for 2-methyl-5-aminotetrazole described by Bryden.[283] However, the structure of H_2AtNO_2 is observed in special way. While in the structure of 5-nitriminotetrazole or 5-nitriminotetrazole monohydrate (Chapter 4) both hydrogen atoms are located at the tetrazole ring (at N1 and N4), in this structure the second hydrogen atom is connected at the atom N5. This yields to an elongation of the C1–N5 bond length (1.385 Å vs. 1.332(2) Å in 5-nitriminotetrazole), which is now closer to a C–N single bond than a C=N double bond. With this, the first constitution isomer of **43**, which should be named "5-nitramino-1*H*-tetrazole", was observed.
Again an intramolecular hydrogen bond (N4–H4···O2 = 0.96(2), 2.24(2), 2.629(2) Å, 103(1)°, graph set **S1,1(6)**) appear in the structure of this 5-nitraminotetrazole. A reason of the formation of this isomer is the strong hydrogen bond network, which is observed in the packing of **103**. Again a layer structure (distances ~3.12 Å) is formed.

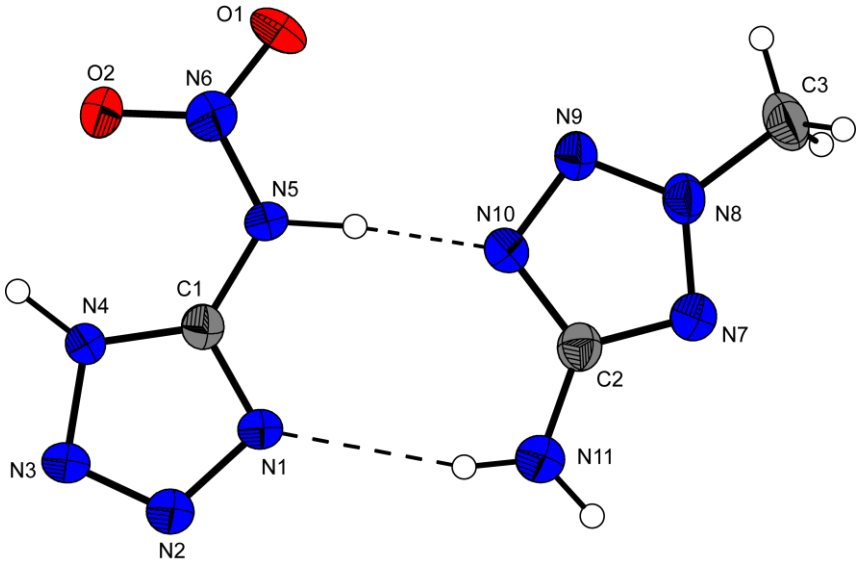

Figure 8.16 Molecular moiety of 2MeAt·H_2AtNO_2. Bond distances (Å): Ellipsoids of non-hydrogen atoms are drawn at the 50 % probability level. N1–C1 = 1.318(2), N1–N2 = 1.370(2), N8–N9 = 1.301(2), N8–N7 = 1.337(2), N8–C3 = 1.461(2), N4–C1 = 1.325(2), N4–N3 = 1.355(2), N9–N10 = 1.335(2), N10–C2 = 1.355(2), O2–N6 = 1.228(2), O1–N6 = 1.226(2), N5–N6 = 1.343(2), N5–C1 = 1.386(2), N3–N2 = 1.286(2), N11–C2 = 1.348(2), N7–C2 = 1.334(2).

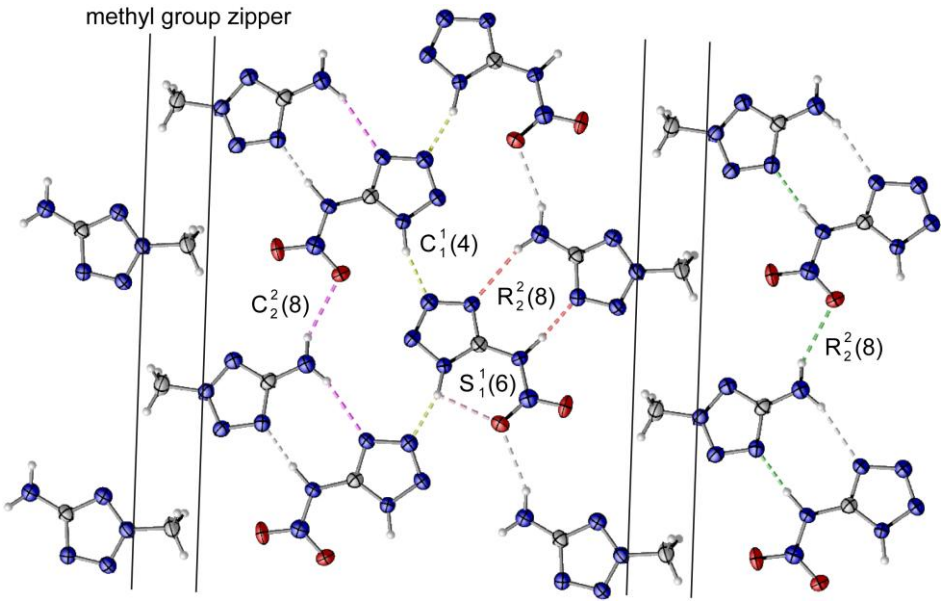

Figure 8.17 Hydrogen bonding in the layers of **103**. Selected hydrogen bonds (Å, Å, Å,°): N5–H5···N10 = 1.00(2), 1.73(2), 2.719(2), 174(2); N11–H11A···O2^{i} = 0.88(2), 2.32(2), 3.124(2), 152(2); N4–H4···N2^{ii} = 0.96(2), 1.81(2), 2.738(2), 160(2); (i) x, 1.5–y, 0.5+z; (ii) 1–x, 0.5+y, 1.5–z.

A view on one layer is shown in **Figure 8.17**, whereby important graph sets are drawn ((**S1,1(6)** purple, **R2,2(8)** red, **C2,2(8)** dark green, **C2,2(8)** pink, **C1,1(4)** light green). Due to the three chain graph sets, alternating tapes are formed. The tapes are connected and a "hydrophobic zipper" is build by the methyl groups of 2-methyl-5-aminotetrazole.

8.7.3 Physico-Chemical Properties of **102** and **103**

Differential scanning calorimetry (DSC) measurements to determine the melt- and decomposition temperatures of **102** and **103** (~1.5 mg of each energetic material) were performed in covered Al-containers containing a hole in the lid with a nitrogen flow of 20 mL min^{-1} on a Linseis PT10 at a heating rate of 5 °C min^{-1}. The DSC plots in **Figure 8.18** show the thermal behavior of **102** and **103** in the 50–400°C temperature range. Temperatures are given as onset temperatures. **102** decomposes at temperatures above 138 °C. Even more interesting is the curve of **103**. The formation of the tautomeric form of **43** yields to an increase of the decomposition temperature of 36 °C to 158 °C.

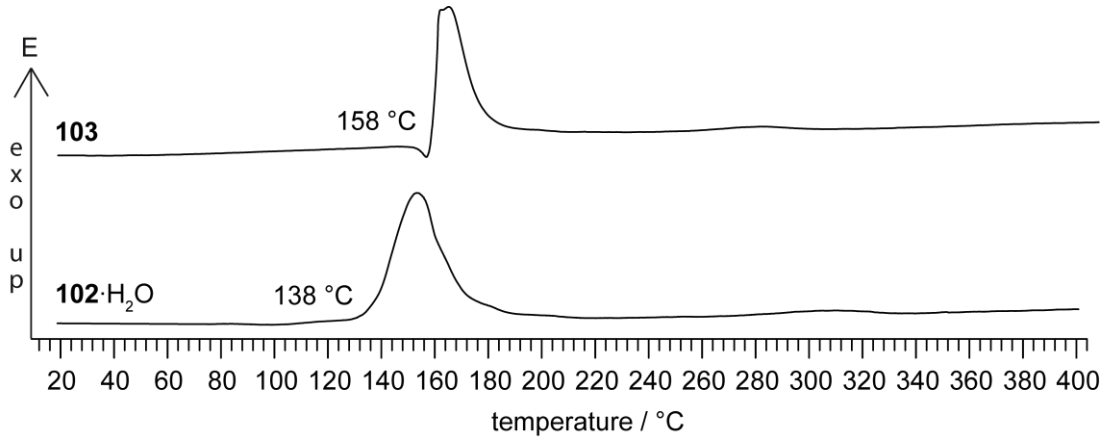

Figure 8.18 DSC thermograms (exo up) of compounds **102** and **103** (heating rate of 5 °C min^{-1}).

The heats of combustion of compounds **102** and **103** were determined experimentally using a Parr 1356 bomb calorimeter. The standard molar enthalpy of combustion ($\Delta_c H°$) was derived from

$\Delta_c H° = \Delta_c U + \Delta nRT$ ($\Delta n = \Delta n_i$ (products, g) – Δn_i(reactants, g); Δn_i is the total molar amount of gases in the products or reactants).

The enthalpy of formation, $\Delta_f H°$, for each of the compounds was calculated at 298.15 K using Hess' law and the following combustion reactions:

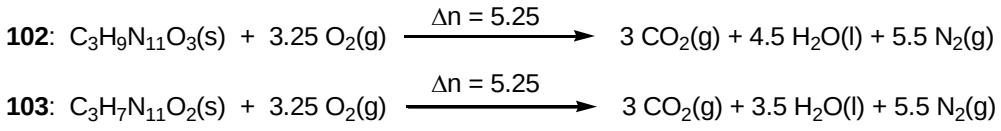

$\Delta_f H°$ H_2O (l) = –286 kJ mol^{-1} and $\Delta_f H°$ CO_2 (g) = –394 kJ mol^{-1}

The final heats of formation of **102** and **103** have been calculated to be 122 kJ mol^{-1} (**102**) and 444 kJ mol^{-1} (**103**). By comparing these values, again the influence of inclusion of crystal water can be seen.

From the determined energies of formation and X-ray densities, various thermochemical properties have been calculated using the EXPLO5 software (see below) and are summarized in **Table 8.5**. The energy of formation ($\Delta_f U°_{298}$) can easily be obtained from the following equation:

$\Delta_f U° = \Delta_f H° - \Delta n$ RT (Δn being the change of moles of gaseous components)

Unfortunately, compounds **102** and **103** have only a moderate detonation performance, which may be a reason of the low densities. However, both have better calculated detonation criteria than still used TNT.

Last but not least the sensitivities of **102** and **103** were discovered. The compounds were pulverized and sieved resulting in a particle size of 0.075–0.125 mm. **102** (3 J) as well as **103** (2 J) are highly sensitive towards impact. Regarding the friction sensitivity, again neutral **103** is more sensitive (72 N) and is classified as *very sensitive* in contrast to **102** (144 N), which is classified "only" as *sensitive*. The electrical spark sensitivities of **102** (1.50 J) and **103** (0.46 J) are lower than those of RDX (0.2 J).

Table 8.5 Sensitivities, energetic properties and detonation parameter.

	102	**103**
Formula	$C_3H_9N_{11}O_3$	$C_3H_7N_{11}O_2$
FW /g mol^{-1}	247.18	229.16
Impact sensitivity [a] / J	3	2
Friction sensitivity [b] / N	144	72
ESD-test [c] / J	1.50	0.46
N [d] / %	62.33	67.23
Ω [e] / %	–48.5	–52.4
$T_{dec.}$ [f] / °C	139	159
Density [g] / g cm^{-3}	1.590	1.657
$-\Delta U_{comb}$ [h] / cal g^{-1}	2514	2749
$-\Delta H_{comb}$ [i] / kJ mol^{-1}	122	444
$\Delta_f H°_m$ [j] / kJ mol^{-1}	611	2047
EXPLO5 values:		
$-\Delta_E U_m°$ [k] / kJ kg^{-1}	3716	4347
T_E [l] / K	2889	3266
p [m] / kbar	208	247
$V_{Det.}$ [n] / m s^{-1}	7619	8093
Gas vol. [o] / L kg^{-1}	834	801

[a] BAM drophammer; [b] BAM friction tester; [c] OZM small scale electrostatic discharge device; [d] Nitrogen content; [e] Oxygen balance; [f] Temperature of decomposition by DSC (β = 5 °C min^{-1}); [g] estimated from solvent pycnometry; [h] Experimental (constant volume) combustion energy; [i] Experimental molar enthalpy of combustion; [j] Molar enthalpy of formation; [k] Energy of Explosion; [l] Explosion temperature; [m] Detonation pressure; [n] Detonation velocity; [o] Assuming only gaseous products.

8.8 Experimental Part

*WARNING! Although salts **90**–**101** are characterized by low sensitivities and good thermal stabilities, they are nevertheless powerful energetic materials. Therefore special precautions and safety equipment are needed, particularly, when handling 5-nitriminotetrazole as starting material.*

*Calcium nitriminotetrazolate pentahydrate (**90**·5H₂O):* 5-Nitriminotetrazole (2.60 g, 20 mmol) was dissolved in 20 mL of water, calcium hydroxide (1.48 g, 20 mmol) was added and the suspension was heated to 60 °C and filtered off. The product was directly recrystallized from water, the crystals filtered off and washed with ethanol/ether to yield 2.86 g (11 mmol, 55%) of calcium nitriminotetrazolate pentahydrate. **DSC** (T_{onset}, 5 °C min^{-1}): 74–125 °C (– 5 H_2O), > 360 °C (dec.); **IR** (KBr, cm^{-1}): $\tilde{\nu}$ = 3532 (m), 3360 (s), 3309 (s), 2167 (w), 1647 (m), 1622 (m), 1559 (w), 1540 (w), 1474 (s), 1412 (s), 1338 (m), 1299 (s), 1158 (m), 1135 (m), 1087 (m), 1042 (w), 1026 (s), 883 (m), 835 (w), 754 (w), 722 (w), 610 (w), 566 (w); **Raman** (1064 nm, 350 mW, 25 °C, cm^{-1}): $\tilde{\nu}$ = 1487 (100), 1431 (9), 1406 (6), 1220 (7), 1160 (8), 1138 (7), 1091 (9), 1047 (7), 1029 (18), 727 (5), 611 (5), 406 (9); **^{1}H NMR** (*d*$_6$-DMSO, 25 °C, ppm): δ = 3.45 (s, H_2O); **^{13}C NMR** (*d*$_6$-DMSO, 25 °C, ppm): δ = 164.4 (CN_4); ***m/z*** (FAB$^-$): 129.1 $[HAtNO_2]^-$; **EA** ($CaCH_{10}N_6O_7$, 258.2) calcd.: C 4.65, H 3.90, N 32.55 %; found: C 4.66, H 3.65, N 32.54 %; sensitivities of the anhydrous compound: **impact sensitivity**: > 70 J; **friction sensitivity**: > 112 N; **ESD**: > 156 mJ.

*Potassium 5-nitriminotetrazolate (**91**):* A dilute solution of potassium hydroxide (2.59 g, 39.4 mmol) in water was poured on dry nitriminotetrazole (2.56 g, 19.7 mmol). A white precipitate of monodeprotonated 5-nitriminotetrazolate, which formed firstly, was dissolved again very quickly. The water was removed in vacuo and the white residue was recrystallized from ethanol to give potassium 5-nitriminotetrazolate in quantitative yields. Recrystallization from water afforded larger crystals. **DSC** (T_{onset}, 5 °C min^{-1}): 364 °C (dec.); **IR** (KBr, cm^{-1}): $\tilde{\nu}$ = 3432 (m), 2395 (w), 1645 (m), 1453 (s), 1398 (vs), 1295 (s), 1198 (w), 1145 (w), 1110 (w), 1069 (m), 1028(m), 1010 (m), 861 (m), 831 (w), 763 (m), 737 (w); **Raman** (1064 nm, 350 mW, 25 °C, cm^{-1}): $\tilde{\nu}$ = 1445 (100), 1391 (5), 1201 (6), 1146 (7), 1111 (7), 1072 (6), 1050 (10), 1028 (9), 1011 (26), 883 (4), 739 (5), 474 (3), 411 (13), 391 (8), 235 (4); **^{13}C NMR** (D_2O, 25 °C, ppm): δ = 164.5 (CN_4); ***m/z*** (FAB$^+$): 39.0 $[K]^+$; ***m/z*** (FAB$^-$): 129.1 $[HAtNO_2]^-$; EA ($CK_2N_6O_2$, 206.25): calcd.: C 5.82, N 40.75 %; found: C 6.15, N 40.62 %; **impact sensitivity**: > 10 J; **friction sensitivity**: > 240 N; **ESD**: > 0.40 J.

*Magnesium nitriminotetrazolate tetrahydrate (**92**):* 5-Nitriminotetrazole (390 mg, 3 mmol) was dissolved in 15 mL of water and magnesium hydroxide (174 mg, 3 mmol) was added. The suspension was stirred for 10 min at 60 °C (the magnesium hydroxide was not dissolved completely). The white suspension was filtered off, the filtrate was

evaporated to dryness and the remaining white solid was recrystallized from water/ethanol to yield magnesium nitriminotetrazolate tetrahydrate in nearly quantitative yields. **DSC** (T_{onset}, 5 °C min^{-1}): 140 °C (–H_2O), 290 °C (dec.); **IR** (KBr, cm^{-1}): $\tilde{\nu}$ = 3576 (m), 3458 (vs), 3387 (vs), 3180 (s), 2343 (w), 1653 (m), 1489 (vs), 1421 (vs), 1408 (vs), 1335 (s), 1190 (m), 1157 (w), 1113 (m), 1043 (m), 890 (m), 732 (m), 720 (m), 685 (m), 636 (m), 536 (m); **Raman** (1064 nm, 350 mW, 25 °C, cm^{-1}): $\tilde{\nu}$ = 1646 (2), 1486 (100), 1412 (7), 1239 (10), 1187 (14), 1160 (5), 1115 (5), 1043 (36), 891 (2), 754 (3), 498 (3), 426 (14), 405 (9), 221 (6); **^{1}H NMR** (*d_6*-DMSO, 25 °C, ppm): δ = 3.43 (s, H_2O); **^{13}C NMR** (*d_6*-DMSO, 25 °C, ppm): δ = 164.9 (CN_4); ***m/z*** (FAB^-): 129.1 $[HAtNO_2]^-$; **EA** ($CH_8MgN_6O_6$, 224.42) calcd.: C 5.35, H 3.59, N 37.45 %; found: C 5.54, H 3.68, N 37.99 %; **impact sensitivity**: > 50 J; **friction sensitivity**: > 360 N; **ESD**: > 0.90 J.

*Calcium bis(5-nitrimino-1H-tetrazolate) pentahydrate (**93**):* 5-Nitriminotetrazole (520 mg, 4 mmol) was dissolved in 20 mL of water and calcium hydroxide (148 mg, 2 mmol) was added. After stirring for 15 min at 90 °C the solution was filtrated off and left for crystallization. Single crystals of colorless **93** were obtained after one day (535 mg, 69 % yield). **DSC** (T_{onset}, 5 deg min^{-1}): 100–130 °C (–H_2O), 200 °C (dec.); **IR** (KBr, cm^{-1}): $\tilde{\nu}$ = 3405 (s), 1645 (m), 1545 (s), 1424 (vs), 1363 (s), 1328 (s), 1242 (m), 1152 (w), 1063 (m), 1003 (m), 872 (m), 744 (w), 696 (w), 524 (w); **Raman** (1064 nm, 350 mW, 25 °C, cm^{-1}): $\tilde{\nu}$ = 2974 (1), 1543 (100), 1429 (6), 1400 (4), 1361 (14), 1336 (28), 1242 (2), 1154 (8), 1102 (4), 1093 (5), 1062 (7), 1037 (41), 1006 (30), 873 (4), 750 (5), 500 (4), 429 (8), 417 (10), 374 (9), 231 (6); **^{1}H NMR** (*d_6*-DMSO, 25 °C, ppm): δ = 3.34 (s, H_2O); **^{13}C NMR** (*d_6*-DMSO, 25 °C, ppm): δ = 158.3 (CN_4); ***m/z*** (FAB^-) 129.0 $[HAtNO_2]^-$; **EA** ($CaC_2H_{12}N_{12}O_9$, 388.27) calcd.: C 6.19, H 3.12, N 43.29 %; found: C 6.53, H 3.13, N 43.33 %; **impact sensitivity**: > 10 J; **friction sensitivity**: > 240 N; **ESD**: > 1.0 J.

*Strontium bis(5-nitrimino-1H-tetrazolate) tetrahydrate (**94**):* 5-Nitriminotetrazole (0.50 g, 3.83 mmol) and strontium hydroxide octahydrate (0.51 g, 1.92 mmol) were solved in 25 mL water and refluxed for 15 minutes. After cooling to room temperature colorless crystals could be obtained. Recrystallization from water yielded colorless rods suitable for XRD (0.72 g, 92 %). **DSC** (T_{onset}, 5 °C min^{-1}): 163 °C, 224 °C (dec.); **IR** (Diamond-ATR, cm^{-1}): $\tilde{\nu}$ = 3377 (s), 3251 (s), 2913 (m), 2797 (m), 2675 (m), 2544 (m), 2359 (m), 1910 (vw), 1823 (vw), 1659 (w), 1526 (m), 1416 (m), 1357 (m), 1323 (s), 1254 (m), 1175 (w), 1159 (w), 1117 (w), 1068 (m), 1036 (m), 983 (m), 934 (m), 866 (w), 771 (w), 740 (m), 717 (m), 699 (m), 595 (w); **Raman** (1064 nm, 400 mW, 25 °C,

cm^{-1}): $\tilde{\nu}$ =3354 (2), 1660 (2), 1544 (100), 1448 (2), 1386 (9), 1333 (34), 1175 (3), 1165 (9), 1130 (6), 1069 (7), 1040 (49), 987 (14), 915 (2), 870 (9), 760 (14), 741 (3), 705 (2), 506 (7), 445 (7), 418 (10), 372 (9), 227 (13), 184 (22), 157 (7); **^{1}H NMR** (d_6-DMSO, 25 °C, ppm): δ = 3.27 (s, crystal water); **^{13}C NMR** (d_6-DMSO, 25°C, ppm): δ = 158.4; **EA** ($C_2H_{10}N_{12}O_8Sr$, 417.80) calcd.: C 5.75, H 2.41, N 40.23 %; found: C 5.62, H 2.38, N 39.69 %; **impact sensitivity**: 20 J; **friction sensitivity**: 288 N; **ESD**: 0.4 J.

*Strontium 5-nitriminotetrazolate dihydrate (**95**):* 5-Nitriminotetrazole (3.9 g, 0.03 mol) and strontium hydroxide octahydrate (7.97 g, 0.03 mol) were added to 40 mL water and refluxed for 3 minutes. After filtration, the crude product was recrystallized from a hot water/ethanol mixture (1:4) obtaining colorless blocks suitable for XRD. (6.7 g, yield 89 %) **DSC** (T_{onset}, 5 °C min^{-1}): 230 °C, 350 °C (dec.); **IR** (KBr, cm^{-1}): $\tilde{\nu}$ = 3454 (s), 3335 (s), 2484 (w), 2435 (w), 2342 (w), 1957 (w), 1648 (m), 1465 (s), 1418 (s), 1396 (s), 1313 (m), 1257 (m), 1160 (m), 1138 (w), 1082 (m), 1016 (m), 869 (m), 829 (w), 753 (m), 726 (w), 593 (m); **Raman** (1064 nm, 200 mW, 25 °C, cm^{-1}): $\tilde{\nu}$ =1956 (0), 1462 (100), 1314 (1), 1214 (3), 1164 (4), 1142 (4), 1085 (3), 1035 (4), 1025 (22), 881 (1), 752 (1), 494 (1), 422 (8), 406 (2), 262 (2), 164 (2), 136 (1); **^{1}H NMR** (d_6-DMSO, 25 °C, ppm): δ = 3.39 (s, crystal water); **^{13}C NMR** (d_6-DMSO, 25 °C, ppm): δ = 164.8; **EA** ($CH_4N_6O_4Sr$, 251.70) calcd.: C 4.77, H 1.60, N 33.39 %; found: C 4.73, H 1.96, N 32.35 %; **impact sensitivity**: 30 J; **friction sensitivity**: > 360 N; **ESD**: 1.0 J.

*Barium 5-nitriminotetrazolate dihydrate (**96**):* 5-Nitriminotetrazole (3.5 g, 0.027 mol) was solved in 20 mL water and added to 25 mL of a barium hydroxide octahydrate (8.5 g, 0.027 mol) solution. Additionally 50 mL water was added and the solution was refluxed for 10 minutes. After filtration, the crude product was recrystallized from hot water obtaining light orange needles suitable for XRD. (2.38 g, yield 29 %) **DS**C (T_{onset}, 5 °C min^{-1}): 370°C (dec.); **IR** (KBr, cm^{-1}): $\tilde{\nu}$ = 3443 (m), 3210 (m), 2341 (w), 2173 (w), 1651 (m), 1462 (s), 1405 (s), 1385 (s), 1304 (s), 1138 (m), 1079 (m), 1038 (m), 1018 (m), 880 (m), 835 (w), 772 (m), 751 (m), 695 (m), 564 (m); **Raman** (1064 nm, 200 mW, 25 °C, cm^{-1}): $\tilde{\nu}$ = 3215 (4), 2537 (2), 1450 (100), 1383 (7), 1215 (10), 1142 (7), 1082 (3), 1039 (4), 1015 (24), 881 (1), 767 (1), 705 (1), 492 (2), 428 (5), 400 (6), 259 (1), 152 (3); **^{1}H NMR** (d_6-DMSO, 25 °C, ppm): δ = 3.35 (s, crystal water); **EA** ($CH_4BaN_6O_4$, 301.41) calcd.: C 3.98, H 1.34, N 27.88 %; found: C 4.15, H 1.39, N 27.96 %.

*Cadmium nitriminotetrazolate dihydrate (**97**):* 5-Nitriminotetrazole (1.30 g, 10 mmol) was dissolved in 20 mL of water and a suspension of cadmium carbonate (1.72 g, 10 mmol) in 30 mL of water was added. A slightly gas evolution could be observed, but the suspension did not cleared up completely. The slightly pink cadmium nitriminotetrazolate, which is insoluble in water was filtered off, washed with ethanol and dried. **DS**C (T_{onset}, 5 °C min^{-1}): 333°C (dec.); **IR** (KBr, cm^{-1}): $\tilde{\nu}$ = 3379 (s), 3227 (s), 1635 (m), 1489 (s), 1467 (vs), 1424 (s), 1401 (vs), 1271 (s), 1181 (m), 1164 (w), 1137 (w), 1099 (w), 1036 (w), 1016 (s), 867 (m), 770 (w), 751 (w), 735 (w), 603 (w), 503 (w); **Raman** (1064 nm, 350 mW, 25 °C, cm^{-1}): $\tilde{\nu}$ = 1471 (100), 1436 (16), 1400 (8), 1366 (2), 1297 (2), 1235 (4), 1181 (9), 1163 (8), 1139 (5), 1099 (2), 1037 (3), 1015 (20), 869 (2), 775 (4), 756 (2), 717 (1), 504 (1), 428 (3), 406 (4), 283 (3), 209 (4); **^{13}C NMR** (DCl, 20 % in D_2O, 25 °C, ppm): δ = 148.4; ***m/z*** (FAB$^-$): 129.1 $[HAtNO_2]^-$; **EA** ($CH_4CdN_6O_4$, 240.46) calcd.: C 4.34, H 1.46, N 30.40 %; found: C 4.67, H 1.58, N 28.68 %; sensitivities of the water-free salt: **impact sensitivity**: > 17 J; **friction sensitivity**: > 12 N; **ESD**: > 10.3 mJ(!).

*Zinc bis(5-nitrimino-1H-tetrazolate) hexahydrate (**98**):* 5-Nitriminotetrazole (1.30 g, 10 mmol) was dissolved in 20 mL of water and 10 mL of an aqueous solution containing zinc perchlorate hexahydrate (1.86 g, 5 mmol) was added. The mixture was stirred for 110 min at 70 °C and the solution was left for crystallization. Colorless crystals of **98** were obtained after 4 days, which were isolated and washed with a small amount of diethyl ether. **EA** ($C_2H_{14}N_{12}O_{10}Zn$, 431.59) calcd.: C 5.57, H 3.27, 37.07 %; found: C 5.61, H 3.09, N 38.97 %.

*Zinc 1-methyl-5-nitriminotetrazolate hexahydrate (**99**):* Potassium 1-methyl-5-nitriminotetrazolate (3.64 g, 20 mmol) was dissolved in water (10 mL) and zinc perchlorate hexahydrate (3.72 g, 10 mmol) was added. The solvent was removed under high pressure and the crude product was recrystallized from water to obtain colorless rods (455 mg, 10 % yield). **DS**C (T_{onset}, 5 °C min^{-1}): 154–155 °C, 258 °C (dec.); **IR** (KBr, cm^{-1}): $\tilde{\nu}$ = 3547 (m), 3376 (m, br), 3034 (m), 2956 (m), 2650 (w), 2301 (w), 2029 (w), 1621 (m), 1534 (s), 1484 (s), 1429 (s), 1413 (s), 1301 (s), 1338 (s), 1246 (s), 1119 (s), 1087 (br, s), 1029 (m), 1002 (m), 940 (w), 886 (m), 756 (m), 735 (m), 688 (m), 626 (s); **Raman** (1064 nm, 300 mW, 25 °C, cm^{-1}): 2958 (8), 1537 (100), 1490 (18), 1427 (11), 1340 (32), 1121 (17), 1038 (29), 943 (42), 890 (11), 761 (13), 692 (15), 629 (19), 504

(17), 464 (24), 311 (19), 247 (10); **EA** ($C_4H_{18}N_{12}O_{10}Zn$, 459.64): calcd.: C 10.45, H 3.95, 34.81 %; found: C 11.15, H 4.64, N 33.99 %.

*Hydrazinium 5-nitrimino-1H-tetrazolate (**100**):* 5-Nitriminotetrazole (650 mg, 5 mmol) is dissolved in 20 mL of THF (dry, over mol. sieves) and a solution of hydrazine in THF (1 M, 5 mL, 5 mmol $H_2N–NH_2$) is added under vigorous stirring. A thick, white precipitate starts to form instantaneously, which is filtered off, washed with diethyl ether and dried. Yield: 480 mg (2.80 mmol, 56%, calculated as hemihydrate). The product can be recrystallized best from methanol. **DSC** (T_{onset}, 5 °C min^{-1}): 176–180°C (mp.), 188 °C (dec.); **IR** (KBr, cm−1): $\tilde{\nu}$ = 3433 (s), 3323 (m), 3019 (m), 1621 (w), 1547 (s), 1444 (s), 1351 (s), 1319 (vs), 1225 (m), 1148 (w), 1097 (m), 1059 (m), 1036 (w), 1027 (w), 1000 (w), 983 (w), 865 (w), 775 (w), 743 (w), 697 (w), 512 (w), 419 (w); **Raman** (1064 nm, 350 mW, 25 °C, cm^{-1}): $\tilde{\nu}$ = 3178 (3), 1625 (8), 1578 (6), 1530 (100), 1442 (11), 1391 (8), 1375 (13), 1316 (58), 1140 (11), 1104 (9), 1058 (13), 1019 (80), 1008 (48), 981 (17), 869 (10), 753 (17), 690 (3), 478 (18), 417 (19), 377 (13), 256 (16); **^{1}H NMR** (d_6-DMSO, 25 °C, ppm): δ = 8.20 (s, $H_2N–NH_3^+$); **^{13}C NMR** (d_6-DMSO, 25 °C, ppm): δ = 158.4; ***m/z*** (FAB^+): 100.1 $[2\text{-MeAT}]^+$; ***m/z*** (FAB^-): 129.1 $[HAtNO_2]^-$; *m/z* (FAB^+): 33.0 $[N_2H_5]^+$; ***m/z*** (FAB^-): 130.1 $[AtNO_2]^-$; **EA** ($CH_6N_8O_2$, 162.11) calcd.: C 7.41, H 3.73, N 69.11 %; found: C 7.19, H 4.08, N 68.64 %; **impact sensitivity**: > 3 J; **friction sensitivity**: > 56 N; **ESD**: > 0.40 J.

*Bis(hydrazinium) 5-nitriminotetrazolate monohydrate (**101**):* 5-Nitriminotetrazole (650 mg, 5 mmol) was dissolved in 10 mL of water. To this hydrazine hydrate (510 mg, 12 mmol) was added and the obtained solution was evaporated. The residue was recrystallized from MeOH yielding colorless **101** (692 mg, 65 % yield). **IR** (KBr, cm^{-1}): $\tilde{\nu}$ = 3442 (m), 3350 (m), 3316 (m), 3126 (m), 3058 (m), 2616 (w), 1619 (m), 1545 (m), 1450 (s), 1384 (s), 1363 (s), 1319 (vs), 1117 (s), 1090 (s), 1021 (m), 973 (m), 938 (s), 869 (w), 761 (m), 696 (w); **EA** ($CH_{12}N_{10}O_3$, 212.17) calcd.: C 5.66, H 5.70, N 66.02 %; found C 5.43, H 6.01, N 65.51 %.

*1-Methylaminotetrazolium nitriminotetrazolate (**102**):* 5-Nitriminotetrazole (650.4 mg, 5 mmol) was dissolved in 10 mL of water and 1-methyl-5-aminotetrazole (495.5 mg, 5 mmol) was added to the solution. It was heated to 60°C, until the 1-methyl-5-aminotetrazole was completely dissolved. After evaporation of the water in vacuo, a poorly water-soluble white powder was obtained, which could be recrystallized from

ethanol to give 705 mg (2.85 mmol, 57 % yield) 1-methylaminotetrazolium nitriminotetrazolate monohydrate. The structure determination by X-ray crystallography resulted in the monohydrated compound. **DSC** (T_{onset}, 5 °C min^{-1}): 138 °C (dec.); **IR** (KBr, cm^{-1}): $\tilde{\nu}$ = 3464 (s), 3367 (s), 3112 (s), 2870 (m), 1698 (vs), 1641 (m), 1548 (s), 1447 (s), 1357 (s), 1328 (s), 1227 (m), 1156 (m), 1076 (m), 1061 (m), 1028 (m), 1001 (w), 968 (w), 876 (w), 833 (w), 777 (w), 748 (w), 696 (w), 559 (m), 493 (w); **Raman** (1064 nm, 350 mW, 25 °C, cm^{-1}): $\tilde{\nu}$ = 3150 (11), 2952 (31), 2572 (5), 1661 (13), 1594 (19), 1412 (13), 1320 (29), 1279 (22), 1119 (18), 1046 (9), 973 (8), 788 (100), 680 (18), 478 (10), 313 (27), 219 (17); **^{1}H NMR** (*d_6*-DMSO, 25 °C, ppm): δ = 6.83 (s, NH_2), 3.66 (s, CH_3); **^{13}C NMR** (*d_6*-DMSO, 25 °C, ppm): δ = 156.1 (CN_4(1-MeAt$^+$)), 153.5 (CN_4($AtNO_2^-$)), 32.1 (CH_3); ***m/z*** (FAB^+): 100.1 [1-MeAt]$^+$; ***m/z*** (FAB^-): 129.1 [$AtNO_2$]$^-$; **EA** ($C_3H_9N_{11}O_3$, 247.18): calcd.: C 14.58, H 3.67, N 62.33 %; found: C 13.78, H 2.95, N 61.41 %; **impact sensitivity**: > 3 J; **friction sensitivity**: > 144 N; **ESD**: > 1.53 J.

*2-Methylaminotetrazole · 5-nitriminotetrazole (**103**):* 5-Nitriminotetrazole (1.30 g, 10 mmol) was dissolved in 20 mL of water and 2-methylaminotetrazole (991 mg, 10 mmol) was added. The suspension was heated to 60°C, which did not result in a clear solution, but the solution showed a certain opalescence. The water was removed in a rotary evaporator and the remaining solid was recrystallized from methanol. The crystals were washed with water and pentane to give 1.62 g (7.1 mmol, 71 %) of the 2-methylaminotetrazole nitriminotetrazole adduct. **DSC** (T_{onset}, 5 °C min^{-1}): 158 °C (dec.); **IR** (KBr, cm^{-1}): $\tilde{\nu}$ = 3450 (s), 3341 (s), 3112 (m), 2883 (m), 2705 (m), 2608 (m), 1628 (s), 1554 (m), 1516 (m), 1438 (w), 1405 (w), 1365 (m), 1330 (s), 1310 (vs), 1258 (m), 1194 (m), 1103 (m), 1097 (m), 1058 (m), 1002 (w), 917 (w), 830 (w), 755 (w), 728 (m), 652 (w), 472 (w); **Raman** (1064 nm, 350 mW, 25 °C, cm^{-1}): $\tilde{\nu}$ = 3040 (19), 3027 (17), 2965 (58), 1623 (37), 1570 (72), 1437 (25), 1380 (100), 1262 (44), 1197 (28), 1142 (16), 1097 (49), 1018 (92), 648 (60), 460 (34), 390 (28), 347 (24), 316 (30), 211 (21), 171 (21); **^{1}H NMR** (*d_6*-DMSO, 25 °C, ppm): δ = 9.56 (s, NH($AtNO_2$)), 4.06 (s, CH_3); **^{13}C NMR** (*d_6*-DMSO, 25 °C, ppm): δ = 167.7 (CN_4(2-MeAt$^+$)), 153.3 (CN_4($AtNO_2^-$)), 39.3 (CH_3); ***m/z*** (FAB^+): 100.1 [2-MeAt]$^+$; ***m/z*** (FAB^-): 129.1 [$AtNO_2$]$^-$; ***m/z*** (DCI^+): 229.2 [M]$^+$, 131.2 [$AtNO_2$+H]$^+$, 100.1 [2-MeAt+H]$^+$; **EA** ($C_3H_9N_{11}O_3$, 229.16): calcd.: C 15.72, H 3.08, N 67.23 %; found: C 16.04, H 3.09, N 67.01 %; **impact sensitivity**: > 2 J; **friction sensitivity**: > 72 N; **ESD**: > 0.46 J.

8.9 Conclusions

From this extensive study about salts of 5-nitriminotetrazole the following conclusions can be drawn:

- Several metal salts (potassium, magnesium, calcium and cadmium) of 5-nitriminotetrazole (**43**) were synthesized and characterized. The reaction of 5-nitriminotetrazole with one equivalent magnesium, calcium, strontium and barium hydroxide as well as cadmium carbonate yields the corresponding metal salts $Mg(AtNO_2)\cdot 4H_2O$ (**92**), $Ca(AtNO_2)\cdot 5H_2O$ (**90**$\cdot 5H_2O$), $Sr(AtNO_2)\cdot 2H_2O$ (**95**), $Ba(AtNO_2)\cdot 2H_2O$ (**96**) and $Cd(AtNO_2)\cdot 2H_2O$ (**97**), respectively. By using half an equivalent of calcium as well as strontium hydroxide $Ca(HAtNO_2)_2\cdot 5H_2O$ (**93**) and $Sr(HAtNO_2)_2\cdot 4H_2O$ (**94**) are obtained. The reaction of two equivalents of potassium hydroxide yields the twice deprotonated potassium salt $K_2(AtNO_2)$ (**91**). The structures in the solid states of **90**, **93–96** were determined by X-ray crystallography.

- The dehydration (T > 150 °C) of **90**$\cdot 5H_2O$, **95**, **96** and **97** yielded highly powerful compounds which can be used as low sensitive primary explosives. Several hot plate tests were performed resulting in violent explosions.

- **90**$\cdot 5H_2O$ was tested by a Koenen Steel Sleeve experiment using a critical diameter of 20 mm. Three fragments could be collected.

- **90** can be initiated by standard “igniter caps”. The shock wave produced lead to an initiation of HNS. In addition, several long term tests have been carried out. **90** is stable at temperatures above 265 °C in TSC (Thermal Safety Calorimetry) tests. Although this positive behavior, $Ca(AtNO_2)$ decomposes not until 370 °C! The

barium and cadmium salts would also fulfill these criteria. However, barium and cadmium salts are highly toxic and should be avoided.

- In order to investigate the ability of 5-nitriminotetrazoles to coordinate to zinc cations, the two new zinc complexes $[Zn(HAtNO_2)(H_2O)_4]\cdot 2H_2O$ (**98**) and $[Zn(H_2O)_6](1MeAtNO_2)_2$ (**99**) have been synthesized and characterized. It was not possible to form a zinc salt of doubly deprotonated **43**. In contrast to the copper complexes (Chapter 9), 5-nitriminotetrazoles do not act as bidentate ligands to zinc(II). The complexes obtained are not suitable as energetic materials, due to their large amount of crystal water, which cannot removed before decomposition.

- Two promising hydrazinium salts have been synthesized and characterized. Hydrazinium 5-nitrimino-1*H*-tetrazolate (**100**) and bis(hydrazinium) 5-nitriminotetrazolate (**101**) were synthesized by the reaction of hydrazine in THF as well as hydrazine hydrate, respectively, with 5-nitriminotetrazole. Unfortunately, no crystal structure of **100** could be obtained.

- The detonation parameters of **100** were computed with the EXPLO5 program by using a solvent pycnometer density of 1.68 g cm^{-3} and a heat of formation of 279 kJ mol^{-1}, determined by bomb calorimeter measurements. A detonation velocity of 8856 m s^{-1} was obtained which makes **100** together with its thermal stability of 188 °C to a promising new high explosive.

- The reaction of 5-nitriminotetrazole (**43**) with 1-methyl-5-aminotetrazole (**10**) as well as 2-methyl-5-aminotetrazole (**11**) resulted in two different products. In the first case the salt 1-methyl-5-aminotetrazolium 5-nitriminotetrazolate monohydrate (**102**) is obtained. In the second reaction a co-crystallization product (**103**) was obtained. In this compound, the first constitution isomer of 5-nitriminotetrazole could have been stabilized by strong hydrogen bonds. In this molecule, which should be named 5-nitraminotetrazole only one hydrogen atom is located at the tetrazole ring. Both compounds were fully characterized, e.g. X-ray structures, multinuclear NMR, vibrational spectroscopy, bomb calorimetry, DSC, sensitivities, calculation of detonation parameter.

Chapter 9.

Copper 5-Nitriminotetrazolates

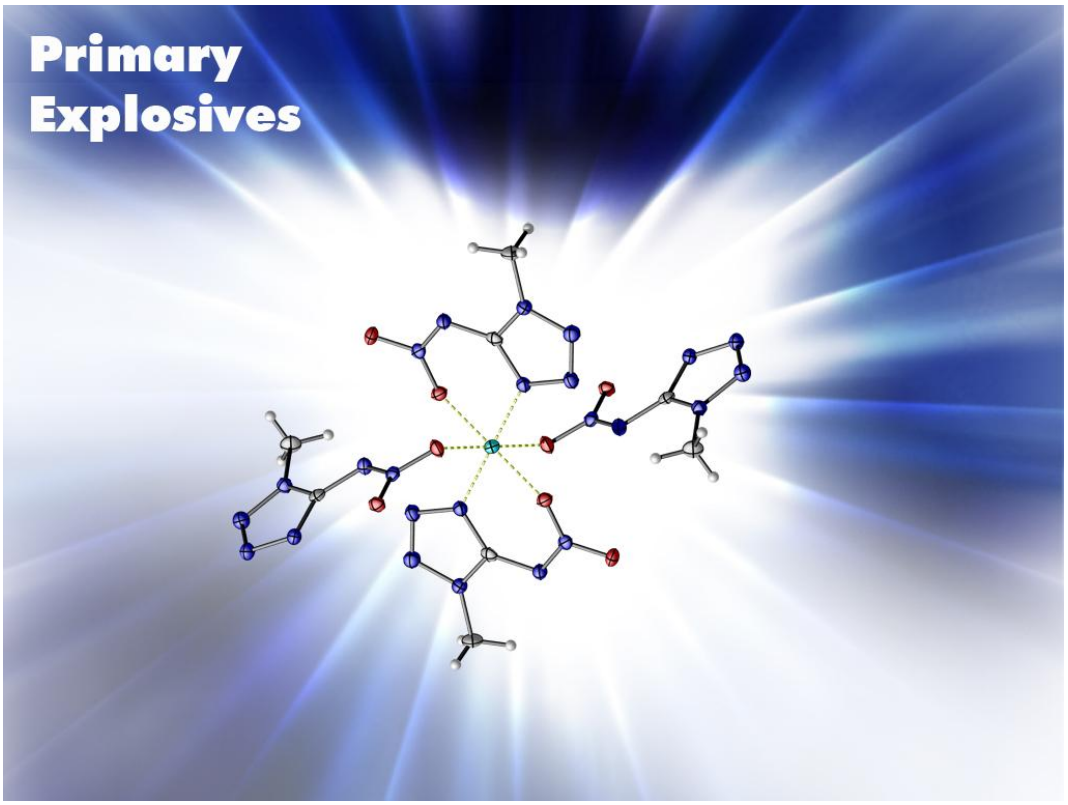

9.1 Introduction

The fascination of many chemists to copper-nitrogen compounds usually starts at the beginning of their education. The bright blue color, which occurs when ammonia is added to aqueous copper(II) salts, not only is the best proof for Cu^{2+} in the qualitative practical but also is one of the most impressive colors accessible in aqueous media. This famous $[Cu(NH_3)_4(H_2O)_2]$ d^9 complex is also the paradigm for distorted octahedral coordination spheres due to the Jahn Teller effect.[319]

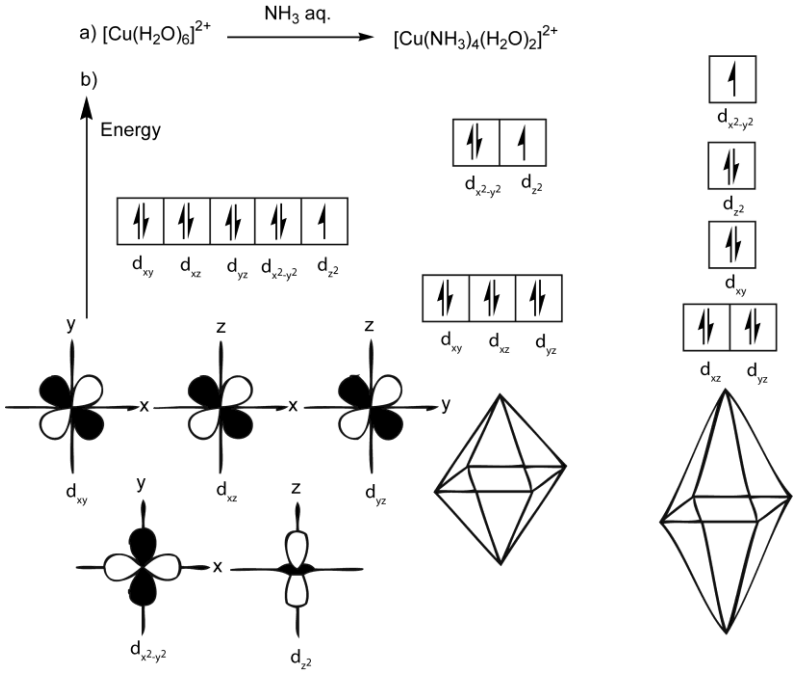

Figure 9.1 Jahn Teller Effect.

Until now uncountable further copper-nitrogen complexes were synthesized and characterized in literature. Of particular interest are copper complexes with nitrogen rich ligands, since they can be used as energetic materials. Nitrogen rich copper complexes can be used as (i) lead free primary explosives (ii) green or blue colorants in pyrotechnical compositions or (iii) as burn rate accelerator in modern solid propellants. Commonly used and highly sensitive primary explosives [320,321] still include poisonous and polluting compounds like lead azide ($Pb(N_3)_2$),[322,323,324] lead styphnate (2,4,6-Trinitroresorcinate) [325] or mercury fulminate ($Hg(CNO)_2$).[326] Finding suitable new substitutes for lead or mercury containing primary explosives is an important aspect of current energetic materials research. Primary explosives only consisting of

C,N,H such as tetrazene [327] which is used as a sensitizer exist, but are often difficult to synthesize. A recently employed idea is the formation of non-toxic metal complexes containing zinc or copper instead of toxic heavy metals.[149,328]

Copper tetrazole complexes are also suitable materials for modern pyrotechnical compositions.[329] Common pyrotechnic compositions are non-explosive combustible mixtures consisting fuels and oxidizers, which generate bright colored light, heat or acoustic effects.[330] High-nitrogen materials have been investigated for use in pyrotechnic compositions in order to reduce smoke production.[331] A low-smoke pyrotechnic composition should include a nitrogen-rich energetic material (e.g. tetrazoles) with a low carbon content, an oxidizer and a colorant. Another development in research of pyrotechnics is the substitution of toxic ingredients like barium and perchlorate salts in pyrotechnical compositions. Brilliant green flames previously were generated by barium salts, e.g. $Ba(NO_3)_2$. However, also bright green flames can be obtained by combusting copper(II) complexes with nitrogen rich ligands, e.g. triazoles or tetrazoles,[30b] as mentioned in the literature.[202,332] Particularly, tetrazoles show appropriate properties such as a high positive heat of formation and a high nitrogen content, but also a good thermal and kinetic stability due to the aromatic ring system. Last but not least, it was shown that copper salts or complexes can increase the burn rate in solid propellants.

In this chapter several copper(II) complexes of different 5-nitriminotetrazoles are presented. Generally, 5-nitriminotetrazoles are a unique class of energetic tetrazole derivatives, since (i) they combine both the oxidizer (NO_2) and the fuel (tetrazole backbone) in one molecule, (ii) they can be deprotonated yielding in thermally stable anions, which can be used in nitrogen-rich salts or as ligands in several metal complexes. In this chapter the focus is on complexes of 5-nitriminotetrazole, 1-methyl-5-nitriminotetrazole and 2-methyl-5-nitraminotetrazole either obtained from water or ammonia solution. Particularly, coordinated ammonia is of special interest since the nitrogen content can be improved.

9.2 Synthesis

The copper complexes **104**–**115** were synthesized according to **Scheme 9.1** by combination of either aqueous copper nitrate trihydrate or aqueous copper chloride solutions with **43**, **44** and **45**. Complex **104** is obtained in high yields by simple combining two solutions containing two eq. of 5-nitriminotetrazole (H_2AtNO_2, **43**) and one eq. of copper nitrate, respectively. **105** is obtained in good yields by adding an excess of aqueous ammonia solution to the reaction solution of the synthesis of **104**. Small amounts of complex **106** are obtained from the mother liquor after isolating **105**. The 1-methyl-5-nitriminotetrazole copper complexes $[Cu(C_2H_3N_6O_2)_2(H_2O)_2] \cdot 2H_2O$ (**107**) and $[Cu(C_2H_3N_6O_2)_2(H_2O)_2]$) (**108**) were by the addition of an aqueous solution of copper nitrate trihydrate to an aqueous solution containing two equivalents 1-methyl-5-nitriminotetrazole ($1MeHAtNO_2$, **44**) at 80 °C. **107** was observed as the main product (yield 85%), while **108** was obtained on allowing the mother liquor to stand for a few days. The highly explosive $[Cu(C_2H_3N_6O_2)_2]$ (**109**), which does not contain crystal water was obtained by dehydration of **107** using high vacuum ($1 \cdot 10^{-2}$ bar) at 120 °C for two hours. In order to remove the four water molecules, heating to 120 °C is sufficient but it requires twice the time. Single crystals of **109** were obtained by recrystallization of **109** from dry methanol, whereas recrystallization from wet methanol leads to the formation of crystals of compound **110**, which contains two coordinated water molecules and two free methanol molecules. The addition of two eq. of 1-methyl-5-nitriminotetrazole to an aqueous copper nitrate solution followed by the addition of conc. ammonia solution leads to complex **111**. The reaction of 2-methyl-5-nitraminotetrazole ($2MeHAtNO_2$, **45**) with Cu^{2+} in aqueous solutions only succeeds if four equivalents of ligand are used. By using only two equivalents of **45**, the ligand crystallized back from the aqueous solution as colorless needles. Compound **112** crystallized within one day as beautiful green plates in a yield of 80 %. After isolating **112** by filtration the mother liquor was concentrated and left for crystallization for several days, whereby **113** crystallized in small amounts in form of green rods. Complex **114** is formed, if two eq. of **45** are added to one equivalent of a Cu^{2+} salt and two equivalents of aqueous ammonia are added. If the previous reaction is performed in concentrated ammonia, **115** is obtained in high yields in form of lavender colored needles.

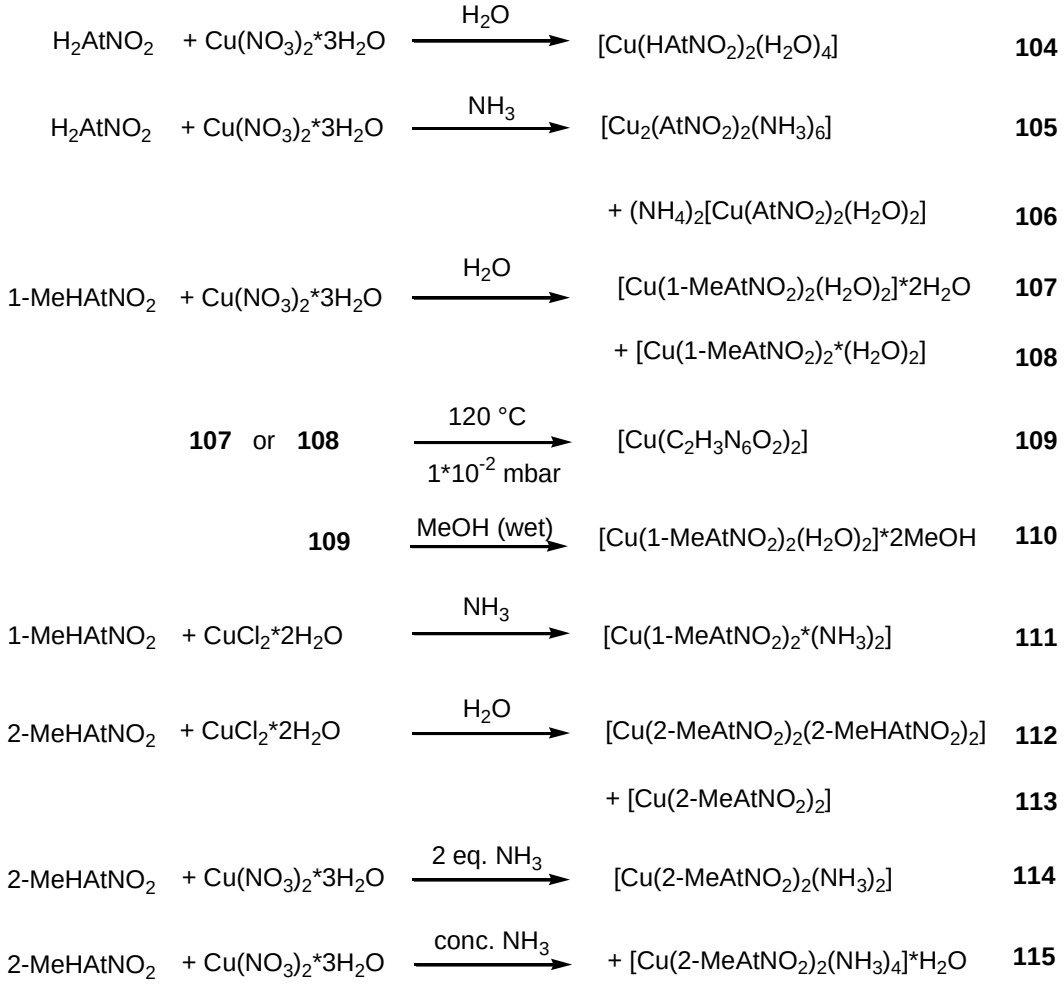

Scheme 9.1 Synthesis of copper complexes **104**–**115**.

9.3 Crystal Structures

Compounds **104**–**115** were determined by low temperature singly crystal X-ray diffraction. A description of the molecular structures as well as of selected packings follows.

9.3.1 $[Cu(CHN_6O_2)(H_2O)_4]$ (**104**)

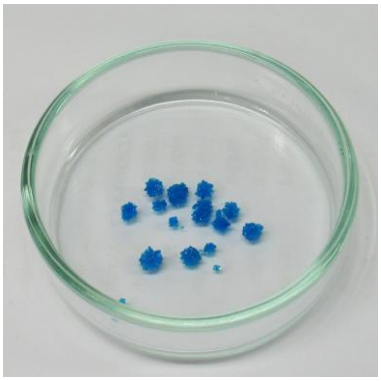

trans[Tetra-aqua-bis-5-nitriminotetrazolato-*N*(4)] copper(II) crystallizes in the triclinic space group with one molecule in the unit cell. The copper atoms lie on the centre of inversion (0,0.5,0). The coordination distance of N4–Cu is 1.997(1) Å, which is a typical Cu–N coordination length and also found in copper nitrogen

complexes like $[Cu(NH_3)_4(NO_3)_2]$.[333] The distances observed between the copper and oxygen atoms, Cu–O3 = 2.532(2) Å and Cu–O4 = 1.959(2) Å, result in a Jahn Teller distorted octahedral coordination sphere (**Figure 9.2**). This coordination geometry of the elongated octahedron is typical for this kind of chromophores distorted by the Jahn Teller [334] effect and is similar to those found for other complexes of both 2-substituted and 1-substituted tetrazoles.[335] The Cu–O3 distance is the longest Cu–O coordination bond observed in this work and leads to the most elongated octahedron. The structures observed for **104** and **115** represent examples, in which the nitriminotetrazoles are not coordinated as a bidentate ligand via one nitrogen atom and one oxygen atom of the nitramine group building a six membered ring.

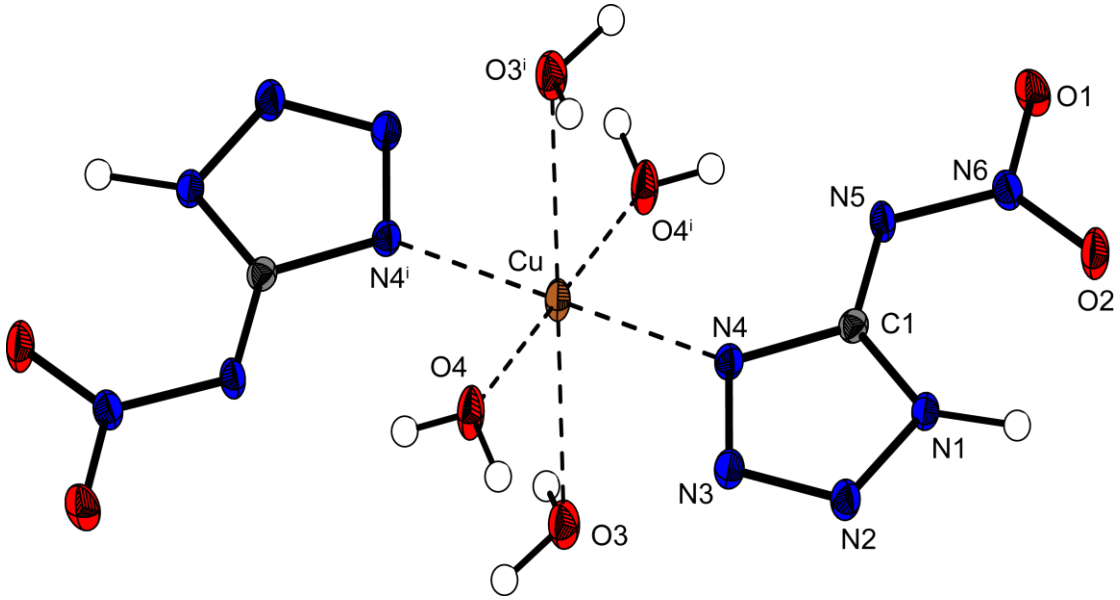

Figure 9.2 Molecular moiety of **104**. Hydrogen atoms shown as spheres of arbitrary radius and thermal displacements set at 50 % probability. Selected geometries: distances (Å): Cu1–O4 = 1.959(2), Cu1–N4 = 2.006(2), Cu1–O3 = 2.532(2), O1–N6 = 1.242(2), O2–N6 = 1.249(2), N1–C1 = 1.342(3), N1–N2 = 1.356(2), N2–N3 = 1.281(2), N3–N4 = 1.357(2), N4–C1 = 1.347(3), N5–N6 = 1.335(2), N5–C1 = 1.363(3); angles (°): O4–Cu1–N4 = 89.42(7), O4–Cu1–N4ⁱ = 90.58(7), O3–Cu1–O4 = 92.9(1), O3–Cu1–O4ⁱ = 87.1(1); (i) –x, 1–y, –z.

The packing of **104** is characterized by columns along the *b* axis (**Figure 9.3**). The shortest copper distances are observed along the unit cell axes.

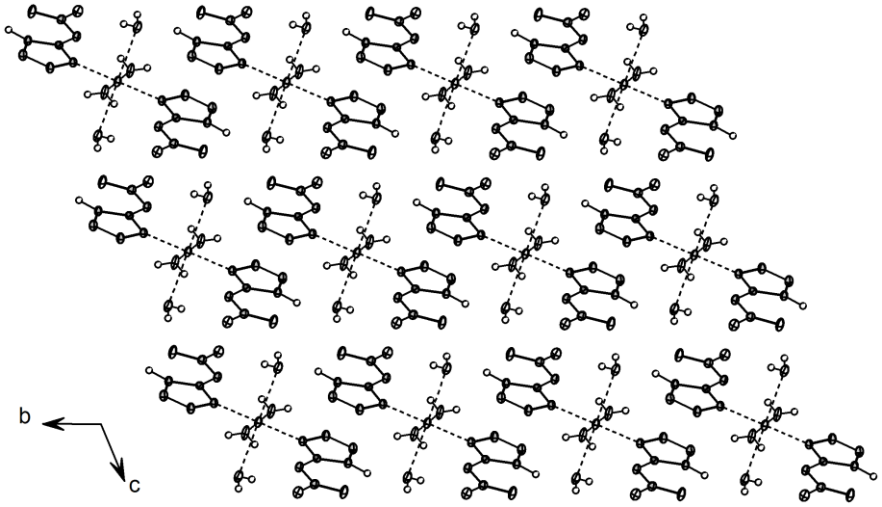

Figure 9.3 View of the packing of **104** along the *a* axis.

9.3.2 $[Cu(CN_6O_2)(NH_3)_3]_2$ (**105**)

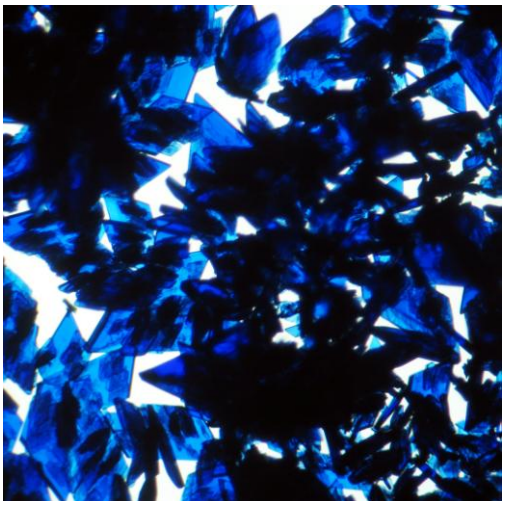

The dark blue complex **105** crystallizes in the monoclinic space group $P2_1/c$ with two molecules in the unit cell. The density was calculated to be 2.011 g cm^{-3}, which is similar to that of **106** (2.010 g cm^{-3}). A view on the binuclear complex is depicted in **Figure 9.4**. The coordination of the copper cations is again an elongated octahedron, whereby the longer coordination distances are Cu–O1 = 2.418(2) and Cu–N2^{i} = 2.399(2). The shorter Cu–N distances are found to be between 2.00 and 2.05 Å. Interestingly, the same formation of dimers can be found in the corresponding nickel complex $[Ni(AtNO_2)_2(NH_3)]_2$ in the literature.[336] The structure of the nitriminotetrazolate dianion is comparable to other crystal structures containing this dianion, e.g. diammonim nitriminotetrazolate [337] or strontium nitriminotetrazolate monohydrate (Chapter 8). The nitrimine unit is coplanar with the planar tetrazole ring plane. Literally **105** must be assigned to be a nitraminotetrazolate. The bond distance N5–C1 of 1.397(4) corresponds more with a C–N single bond (1.48 Å) than a C=N double bond (1.30 Å), which is relevant to the nomenclature nitrimino- vs. nitraminotetrazole. The nitramine bond distance N5–N6 is 1.325(4) Å. In the neutral ligand **43** the N5–C1 bond length is nearer a double bond and

therefore the nomenclature of **105** is also maintained. The dimers form closed motives in the packing of **105**, whereby columns are formed by several hydrogen bonds between the coordinated ammonia and nitriminotetrazolate molecules.

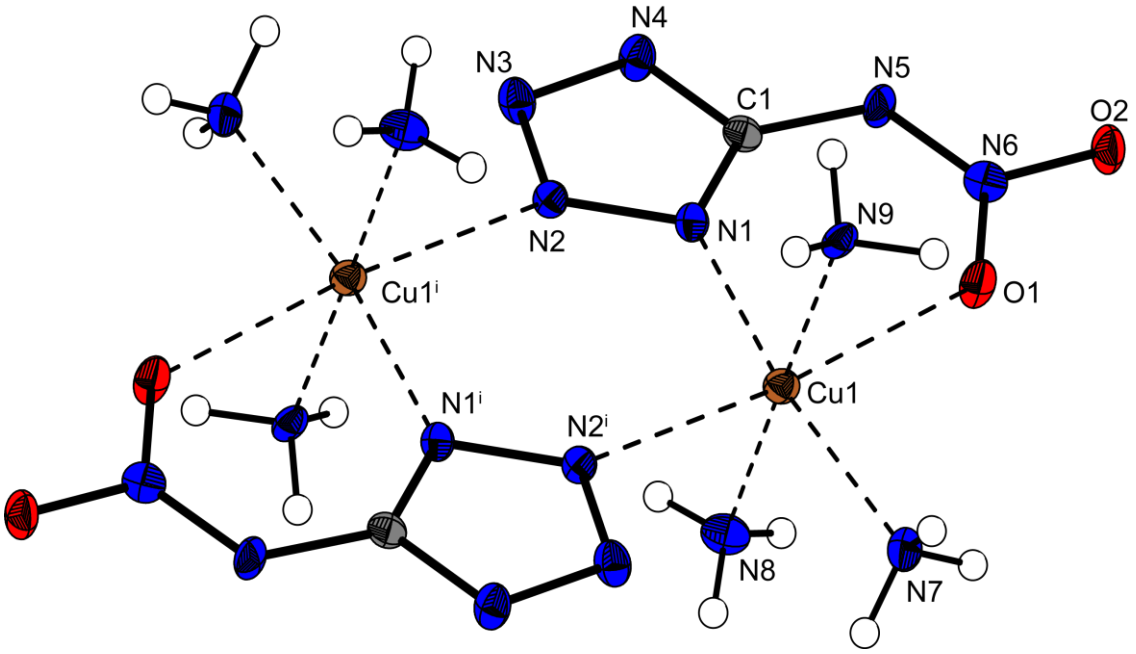

Figure 9.4 View on the dimers in the structure of **105**. Hydrogen atoms shown as spheres of arbitrary radius and thermal displacements set at 50 % probability. Selected geometries: distances (Å): Cu–Cuⁱ = 4.180(3), Cu–N1 = 2.033(2), Cu–O1 = 2.418(2), Cu–N7 = 2.043(3), Cu–N8 = 2.004(3), Cu–N9 = 2.005(3), Cu–N2ⁱ = 2.399(2), O2–N6 = 1.276(3), O1–N6 = 1.269(3), N5–N6 = 1.286(3), N5–C1 = 1.397(4), N1–C1 = 1.347(4); angles (°): N1–Cu–N2 = 100.67(9), N1–Cu–O1 = 75.33(8), O1–Cu–N2 = 174.79(8), N1–Cu–N7 = 168.1(1), N8–Cu–N9 = 179.2(1), N8–Cu–N1 = 87.7(1); (i) 1–x, –y, 1–z.

9.3.3 $(NH_4)_2[Cu(CN_6O_2)_2(H_2O)_2]$ (**106**)

Compound **106** crystallizes monoclinic in the space group $P2_1/n$. The doubly deprotonated 5-nitriminotetrazolate acts as a bidentate ligand coordinating via its atoms N1 and O1 with distances of Cu–N1 = 1.922(1) and Cu–O1 = 2.026(1) Å (**Figure 9.5**). The water molecules are coordinated in a longer distance of 2.382(1) Å. However, the resulting octahedral is less elongated than observed in **104**. The molecular structure of the dianions is similar to that observed for **105**.

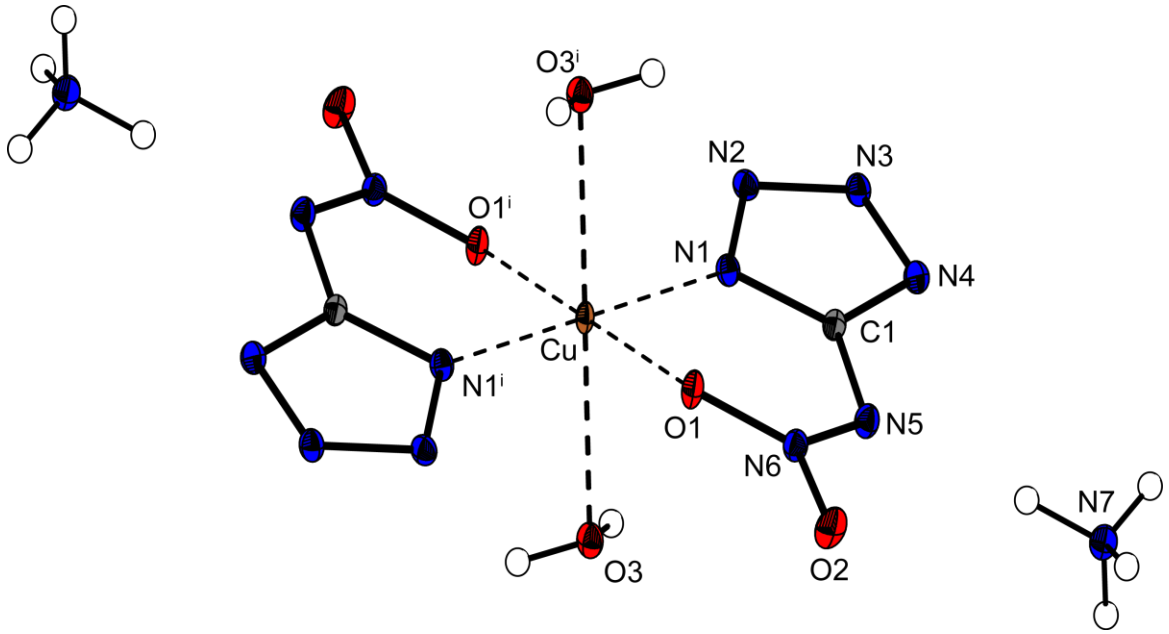

Figure 9.5 Molecular moiety of **106**. Hydrogen atoms shown as spheres of arbitrary radius and thermal displacements set at 50 % probability. Selected geometries: distances (Å): Cu–N1 = 1.922(1), Cu–O1 = 2.026(1), Cu–O3 = 2.382(1), O2–N6 = 1.252(2), O1–N6 = 1.293(2), N5–N6 = 1.301(2), N5–C1 = 1.382(2), N1–C1 = 1.343(2); angles (°): N1–Cu–O1 = 85.92(5), N1–Cu–O1^{i} = 94.08(5), N1–Cu–O3 = 89.71(5), O1–Cu–O3 = 88.53(5); (i) –x, –y, –z.

In the packing of **106** layers are formed by several hydrogen bonds involving the ammonium cations and the coordinated water molecules of the next layer (**Figure 9.6**). The nearest copper distances within the layers are 10.449(5) Å. Significantly nearer Cu–Cu distances of 6.687(1) Å are observed along the *c* axis.

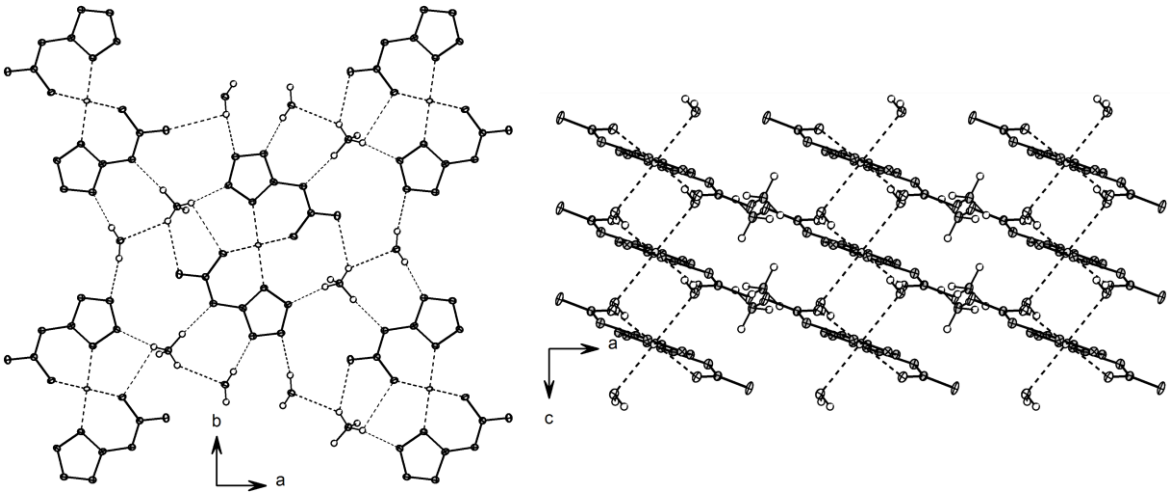

Figure 9.6 Illustration of the layers formed in the structure of **106** and the extensive hydrogen bonding.

9.3.4 $[Cu(C_2H_3N_6O_2)_2(H_2O)_2]\cdot 2H_2O$ (**107**) and $[Cu(C_2H_3N_6O_2)_2(H_2O)_2]$ (**108**)

The reaction of ligand **44** with copper(II) nitrate yields two different compounds (**107**, $[Cu(C_2H_3N_6O_2)_2(H_2O)_2]\cdot 2H_2O$ and **108**, $[Cu(C_2H_3N_6O_2)_2(H_2O)_2]$) which can be easily distinguished by their color. The blue colored main product **107** is characterized by the inclusion of two water molecules, which do not participate in the coordination sphere. In these two structures the effects of the inclusion of water can clearly be seen e.g. in the variation of the density (**107**: 1.870 g cm^{-3}, **108**: 2.035 g cm^{-3}). Both compounds crystallize with two molecules in the unit cell in the monoclinic crystal system, **107** in the space group $P2_1/c$, and **108** in the alternative setting $P2_1/n$. The coordination geometry of the copper cations is characterized by an elongated octahedral arrangement due to the Jan Teller effect. This coordination geometry is typical for transition metals with d^9 valence electron configurations distorted by the Jahn Teller effect and is similar to those found for other complexes of both 2-substituted and 1-substituted tetrazoles.[335] The Cu–N bond lengths show considerable variation. Whereas a typical Cu–N4 distance of 1.997(1) Å is found in **107** and is considerable with complexes with e.g. 1,10-phenantroline as ligand system [338] in compound **108** the distance Cu–N4 of 1.919(2) Å is importantly shorter. The differences in the Cu–O bond lengths are however, less significant (**107**: d(Cu–O3) 1.971(1) Å, d(Cu–O1) 2.393(1) **108**: d(Cu1–O1) 2.048(2) Å, d(Cu1–O3) 2.337(2) Å). The geometries of the 1-methyl-5-nitriminotetrazolates in **107** and **108** are essentially unaffected by the inclusion of water in **107**. In the following **Figure 9.7** and **Figure 9.8** the molecular moieties of the complexes **107** and **108** are shown.

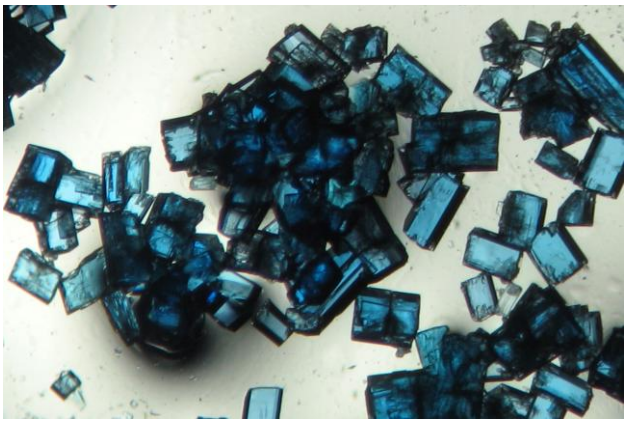

Crystals of complex **107**

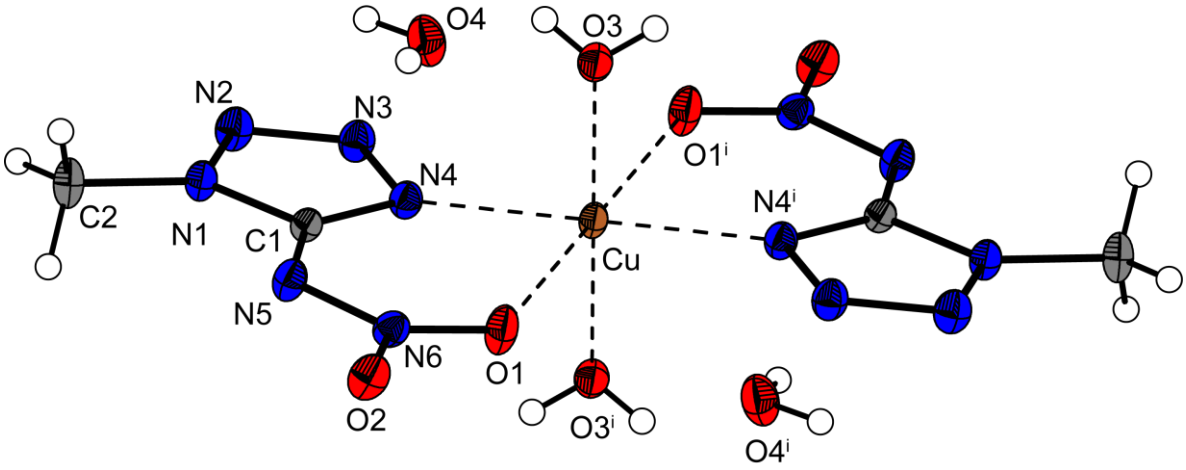

Figure 9.7 Crystal structure of **107** showing the molecular unit and atom labeling scheme. Ellipsoids represent 50 % probability; (i) 2–x, 1–y, 1–z.

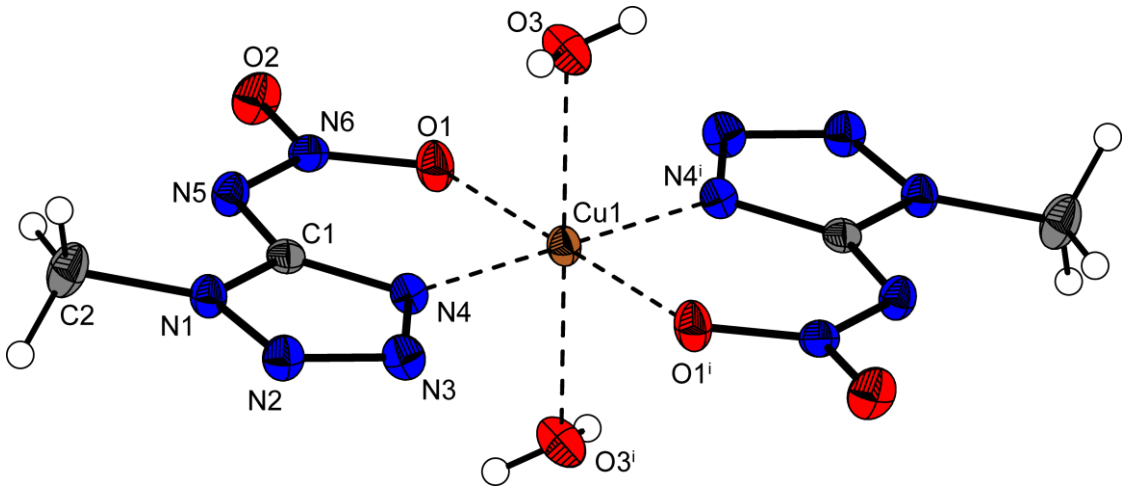

Figure 9.8 Crystal structure of **108** showing the molecular unit and atom labeling scheme. Ellipsoids represent 50 % probability; (i) –x, 1–y, 1–z.

9.3.5 $[Cu(C_2H_3N_6O_2)_2]$ (**109**)

The primary explosive **109** crystallizes in the monoclinic space group $P2_1/c$ with two molecules in the unit cell and a density of 2.067 g cm^{-3}. The copper cations lay on the center of inversion and are coordinated in a distorted octahedral arrangement by two nitrogen atoms (d(Cu–N4) = 1.923(2) Å), which is also found in copper nitrogen complexes, such as $[Cu(NH_3)_4(NO_3)_2]$ [333] and four oxygen atoms (d(Cu–O1) = 1.974(2) Å), d(Cu–O4^i) = 2.589(2) Å; i: 2–x, –0.5+y, 1.5–z). The shorter coordination distances Cu–N4 and Cu–O1 are between one chelating 1-methyl-5-nitriminotetrazolato ligand, whereby a longer coordination to the other oxygen atom of the nitro group is also

observed, which is longer than in typical Jahn Teller distorted d^9 copper complexes (see structures of **107**, **108** and **110**). Accordingly, every nitro-group participates in coordination to two copper centers, which results in an endless three-dimensional network. The extended molecular structure of **109**, which illustrates the coordination of the nitro-groups in the crystalline state, is shown in **Figure 9.9**.

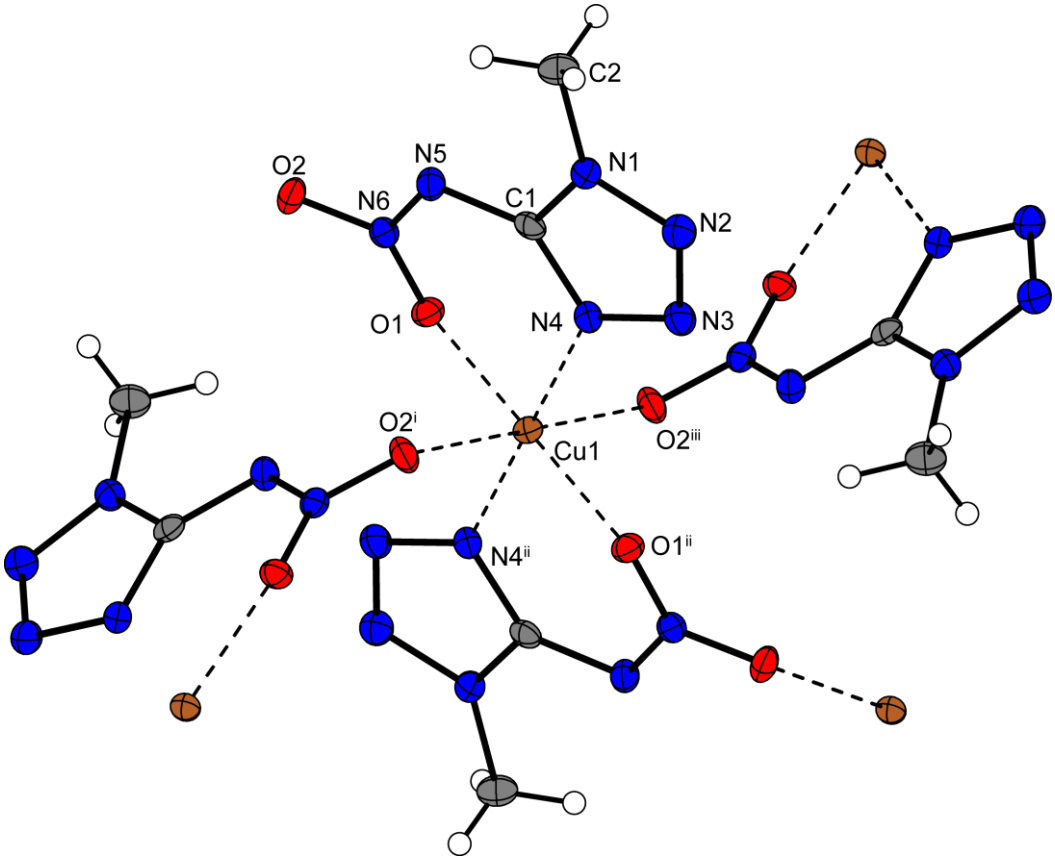

Figure 9.9 Crystal structure of **109** showing an extended molecular unit and atom labeling scheme. Ellipsoids represent 50 % probability. (i) 2–x, –0.5+y, 1.5–z; (ii) 2–x, –y, 2–z; (iii) x, 0.5–y, 0.5+z.

9.3.6 $[Cu(C_2H_3N_6O_2)_2(H_2O)_2]\cdot MeOH$ (**110**)

Compound **110** crystallizes in the monoclinic space group $P2_1/c$ with two molecules in the unit cell and the lowest density of 1.74 g cm^{-3} observed in this work. The structure is analogues to that of **107**, however instead of two water molecules in **107**, two methanol molecules complete the packing of compound **110.** The methanol is not coordinated to

any copper centers, therefore it is not further discussed. The molecular structure of **110** in the crystalline state is shown in **Figure 9.10**.

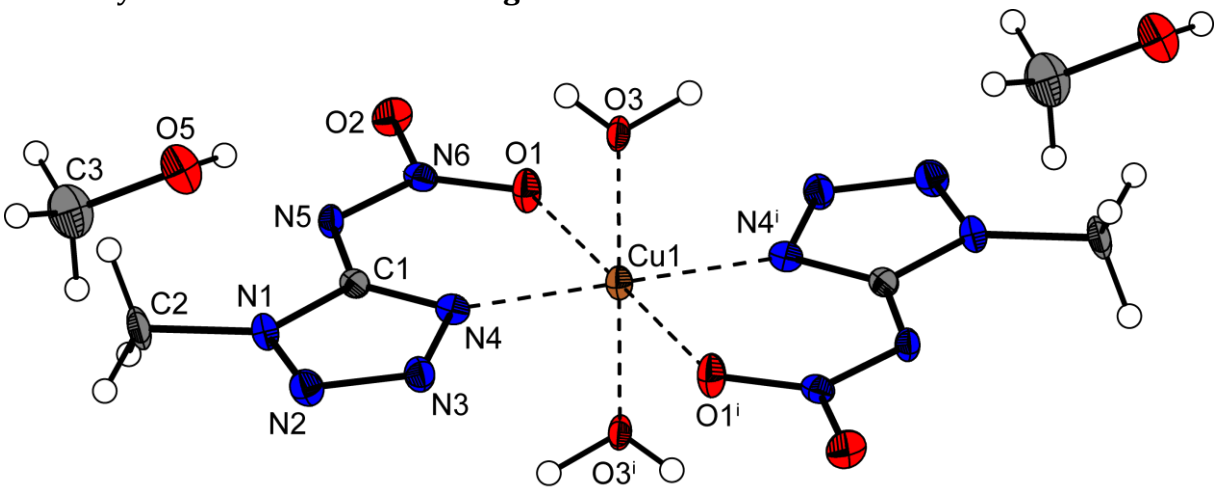

Figure 9.10 Molecular structure of **110** showing the molecular unit and atom labeling scheme. Ellipsoids represent 50 % probability; (i) –x, –y, –z.

The bond lengths and bond distances of the discussed crystal structures **107–110** are given in **Table 9.1**.

Table 9.1 Bond lengths [Å] and angles [°].

atoms A–B	**107**	**108**	**109**	**110**
	d(A–B) [Å]	d(A–B) [Å]	d(A–B) [Å]	d(A–B) [Å]
Cu–O3	1.971(1)	2.337(2)	---	1.998(2)
Cu–N4	1.997(1)	1.919(2)	1.923(2)	1.960(2)
Cu–O1	2.393(1)	2.048(2)	1.974(2)	2.326(2)
O2–N6	1.261(2)	1.241(3)	1.248(3)	1.252(2)
O1–N6	1.246(2)	1.284(3)	1.291(3)	1.255(2)
N1–C1	1.347(2)	1.344(3)	1.340(3)	1.339(3)
N1–N2	1.349(2)	1.352(3)	1.352(3)	1.353(3)
N1–C2	1.462(2)	1.467(3)	1.467(4)	1.466(3)
N5–N6	1.324(2)	1.311(3)	1.306(3)	1.328(3)
N5–C1	1.365(2)	1.366(3)	1.362(3)	1.361(3)
N2–N3	1.294(2)	1.293(3)	1.287(3)	1.288(3)
N3–N4	1.365(2)	1.365(3)	1.365(3)	1.365(3)
N4–C1	1.343(2)	1.337(3)	1.334(3)	1.343(3)

atoms A–B–C	angle [°]	angle [°]	angle [°]	angle [°]
O3–Cu–N4	89.84(6)	87.08(9)	---	89.27(8)
O3–Cu–O1	88.97(5)	91.39(8)	---	88.35(7)
N4–Cu–O1	76.57(5)	85.57(8)	86.23(8)	78.18(7)
C1–N1–N2	109.5(1)	109.4(2)	108.8(2)	109.8(2)
C1–N1–C2	128.8(1)	129.2(2)	129.5(2)	128.4(2)
N2–N1–C2	121.7(1)	121.1(2)	121.7(2)	121.8(2)
N6–N5–C1	117.8(2)	118.3(2)	117.5(2)	118.5(2)
N3–N2–N1	106.6(1)	107.0(2)	107.4(2)	107.1(2)
O1–N6–O2	120.8(1)	117.6(2)	117.8(2)	121.0(2)
O1–N6–N5	124.9(1)	125.1(2)	125.2(2)	124.0(2)
O2–N6–N5	114.3(1)	117.4(2)	116.9(2)	115.0(2)
N2–N3–N4	110.6(1)	109.7(2)	109.6(2)	109.5(2)
C1–N4– N3	106.5(1)	107.4(2)	107.1(2)	107.7(2)

9.3.7 $[Cu(C_2H_3N_6O_2)_2(NH_3)_2]$(**111**)

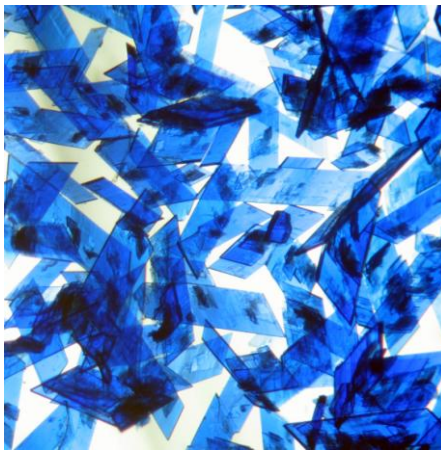

Complex **111** crystallizes in the monoclinic space group $P2_1/c$ with two molecules in the unit cell. The structure is comparable to those of complexes **107** and **108**, in which water is included in the coordination sphere of the copper(II) centers. Again the coordination of the copper(II) cations is affected by a Jahn Teller distorted octahedral sphere, where the shorter distances are between the copper and the nitrogen atoms and the elongated coordination bond is between the copper cations and the oxygen atom O1 of the nitro-group, (d(Cu–N7) = 1.996(2) Å, d(Cu–N4) = 2.016(2) Å, d(Cu–O1) = 2.361(2) Å). The N4–Cu–O1 chelate angle is 75.88(6) Å. The density of 1.850 g cm^{-3} is also comparable to those observed for **107** and **108**. However, it is significantly lower than those of the other structures presented in this work. An illustration of the molecular unit is presented in **Figure 9.11**. The structure of the 1-methyl-5-nitriminotetrazolate anions is comparable to those of alkali and several guanidinium 1-methyl-5-nitriminotetrazolates in the literature.[144] The C1–N5 bond length of 1.364(3) Å is closer to a double bond and is

significantly shorter than a C–N single bond. Furthermore, the nitrimine unit does not follow the ring planarity and is twisted ~27° out of this plane.

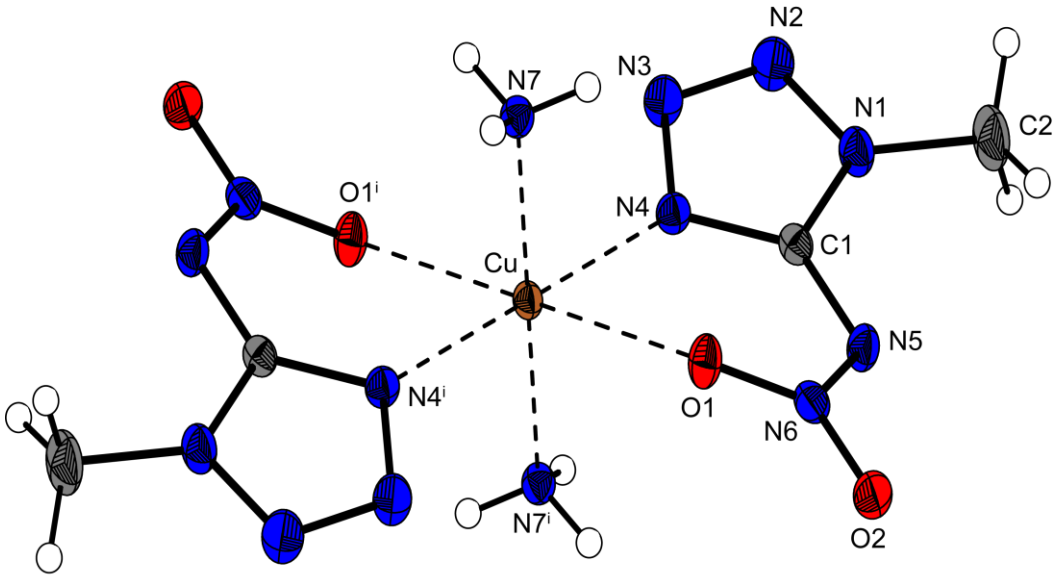

Figure 9.11 Molecular moiety of **111**. Hydrogen atoms shown as spheres of arbitrary radius and thermal displacements set at 50 % probability. Selected geometries: distances (Å): Cu–N4 = 2.016(2), Cu–N7 = 1.996(2), Cu–O1 = 2.361(2), O1–N6 = 1.277(2), O2–N6 = 1.240(2), N5–N6 = 1.319(3), N5–C1 = 1.364(3), N1–C1 = 1.342(3), N1–N2 = 1.348(3), N1–C2 = 1.463(3), C1–N4 = 1.338(3), N3–N2 = 1.290(3), N3–N4 = 1.360(3); angles (°): N7–Cu–N4 = 91.13(9), N7–Cu–O1 = 92.85(8), N4–Cu–O1 = 75.88(6), O2–N6–O1 = 119.2(2), N4–C1–N5 = 134.5(2); torsion angles (°): N4–Cu–O1–N6 = –39.9(2), N6–N5–C1–N4 = –26.7(4), C1–N5–N6–O1 = –0.5(3); (i) –x, –y, –z.

With regard to the highest antiferromagnetic coupling observed for **111** (see magnetic measurements, section 9.4), a view of the packing is depicted in **Figure 9.12**. Interestingly, no dimers, chains or layer pattern could be detected. Therefore. the molecular moiety is packed isolated, connected by medium strong hydrogen bonds formed by all hydrogen atoms of the ammonium cations (N7–H7C–N3^{ii}: D–A = 3.171(3) Å, 178(3)°; N7–H7A–O2^{iii}: 3.213(3) Å, 171(2)°; N7–H7B–O1^{iv}: 3.036(3) Å, 168.(3)°; (ii) x, 0.5–y, –0.5+z; (iii) –x, 0.5+y, –0.5–z; (iv) x, –0.5–y, –0.5+z). The shortest copper distance of 5.611(1) Å is found along *b*-*c*, while the second one (7.266(2) Å) is observed along the *c* axis.

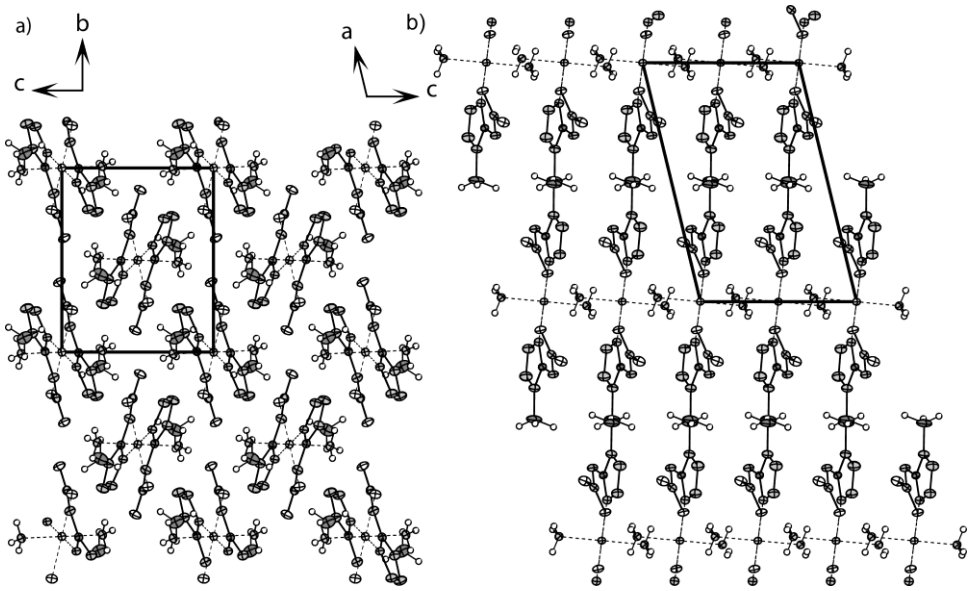

Figure 9.12 View on the packing of **111** a) along the *a* axis and b) along the *b* axis. The unit cell is marked.

9.3.8 [Cu(2-MeAtNO$_2$)$_2$(2-MeHAtNO$_2$)$_2$] (**112**)

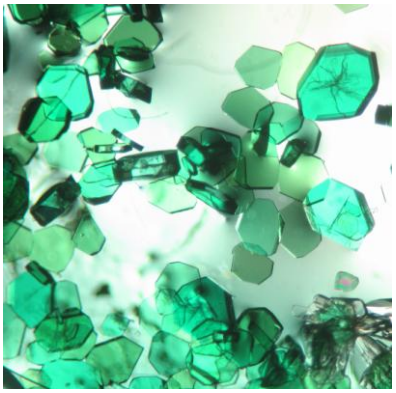

Trans-bis[(2-methyl-5-nitraminotetrazole-*N*)(2-methyl-5-nitraminotetrazolato-*N,O*)-copper(II)] (**112**) crystallizes in green prisms in the triclinic space group *P*-1 with two molecules in the unit cell and represents together with **109** and **113** the class of copper complexes in this chapter, which crystallizes without any inclusion of water or ammonia. With the best of our knowledge it is the first Cu(II) complex in literature which has a closed coordination sphere by four tetrazole derivatives (**Figure 9.13**). The charge balance is given by two deprotonated 2-methyl-5-nitraminotetrazole molecules, which are again coordinated as a bidentate ligand with a N4–Cu–O1 angle of 78.68(5)°, whereby the oxygen atoms with the longest bond lengths (d(Cu–O1) = 2.348(2) Å) represent the top of the elongated octahedral. The plane is build from coordination of the nitrogen atoms of the tetrazoles, whereby the Cu–N10 distance to the neutral 2-methyl-5-nitraminotetrazol is about 0.05 Å longer than the observed Cu–N4 distance to the deprotonated tetrazole (d(Cu–N4) = 1.997(2) Å, d(Cu–N10) = 2.049(2) Å). It is the first compound, in which both forms occur in one molecule. The structure of **45** is considerably different to the structure of ligands **43** and **44**. The methyl group at the nitrogen atom N2 directs the remaining proton to the nitrogen atom N5, building a

nitraminotetrazole. In neutral **45**, the C3–N11 bond length of 1.397(2) Å is crucially longer than in neutral **43** and **44** (Chapter 4) and the nitramine unit does not lie in the plane of the tetrazole ring, as is clearly shown by the N7–C3–N11–N12 torsion angle of 63.7(2)°. The deprotonated form shows a N5–C1 bond length of 1.376(2) Å and also the N6–N5–C1–N1 torsion angle of 161.6(2)° is more flat. The tetrazole bond distances and angles show only insignificantly alterations.

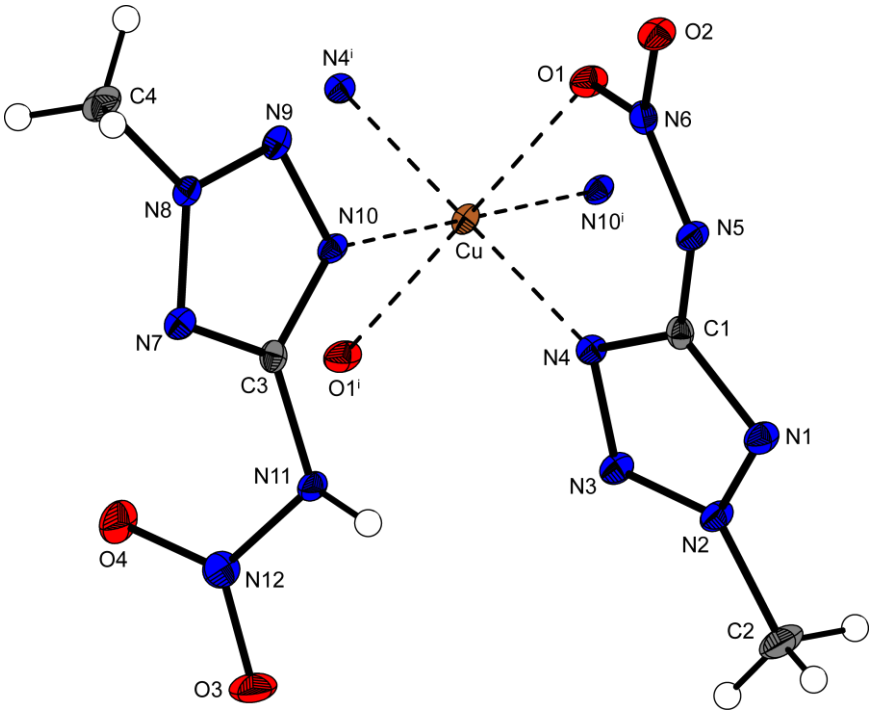

Figure 9.13 Molecular moiety of **112**. Hydrogen atoms shown as spheres of arbitrary radius and thermal displacements set at 50 % probability. Selected geometries: distances (Å): Cu–N4 = 1.997(2), Cu–N10 = 2.049(2), Cu–O1 = 2.358(1), O2–N6 = 1.270(2), O1–N6 = 1.266(2), N5–N6 = 1.312(2), N5–C1 = 1.376(2), N1–N2 = 1.340(2), N1–C1 = 1.344(2), N2–N3 = 1.308(2), N3–N4 = 1.343(2), N4–C1 = 1.356(2), N2–C2 = 1.465(2), O3–N12 = 1.232(2), O4–N12 = 1.223(2), N7–N8 = 1.332(2), N7–C3 = 1.330(2), N8–N9 = 1.312(2), N12–N11 = 1.369(2), C3–N10 = 1.359(2), C3–N11 = 1.397(2), N9–N10 = 1.327(2), N8–C4 = 1.460(2); angles (°): N4–Cu–O1 = 78.68(5), N4–Cu–N10 = 91.32(6), N10–Cu–O1 = 88.52(5), N6–N5–C1 = 118.6(2), N1–C1–N4 = 111.2(2), O1–N6–O2 = 119.4(2), N12–N11–C3 = 118.3(2), N7–C3–N10 = 112.3(2), O4–N12–O3 = 125.9(2); torsion angles (°): N6–N5–C1–N1 = 161.6(2), N4–Cu–O1–N6 = –29.1(1), N7–C3–N11–N12 = 63.7(2); (i) –x, –y, 1–z.

In the packing of **112** (**Figure 9.14**) no characteristic motives can be found. The four tetrazole ligands shield the copper complexes from each other. The two remaining protons on the neutral nitraminotetrazole ligand, which are suitable for H-bonds result in a loose interaction between the complexes. This leads to a lower density of 1.859 g cm^{-3}. The shortest Cu–Cu distance of 7.558(1) Å is found along the *a* axis.

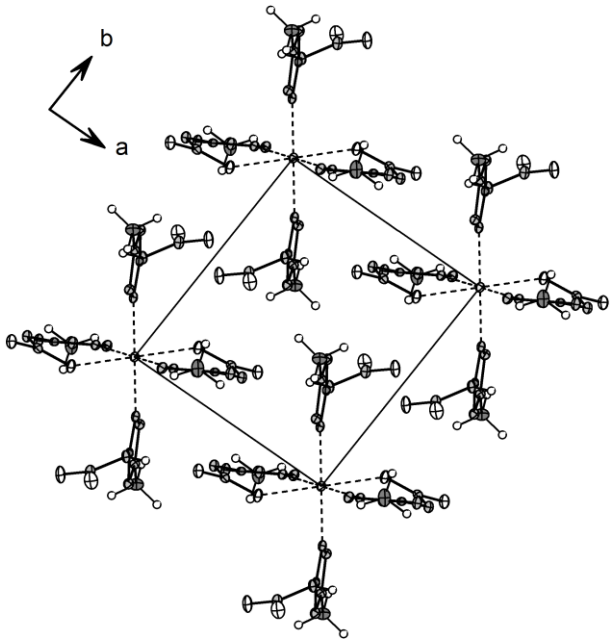

Figure 9.14 View on the unit cell of **112** along the *c* axis

9.3.9 $[Cu(2MeAtNO_2)_2]_\infty$ (**113**)

Bis(2-methyl-5-nitraminotetrazolato-*N,O*) copper(II) (**113**) crystallizes in the monoclinic space group $P2_1/c$ with two molecules in the unit cell and a calculated density of 2.073 g cm^{-3}. A projection of the molecular structure is depicted in **Figure 9.15**. The molecular structure of the anions is comparable to that of **112** and also with other salts, e.g. ammonium 2-methyl-5-nitramniotetrazolate.[142] The nitramine-unit is twisted ~10° out of the ring plane, whereby a N1–Cu–O1 chelate angle of 85.27(7)° is formed. The top and bottom of the elongated octahedral coordination sphere is occupied by the oxygen atoms O2 of neighboring anions in a distance of 2.403(2) Å. From this a three-dimensional network results. It can be explained by having a view on the copper cations, which are arranged in planes, marked in **Figure 9.16**. Within this planes they are connected by the nitro-groups. Between the planes the tetrazoles are arranged as it can be seen in **Figure 9.16**. The nearest Cu–Cu distances of 5.921(1) Å are found in the copper planes, whereby to the next layer distances of 8.689(1) Å are observed.

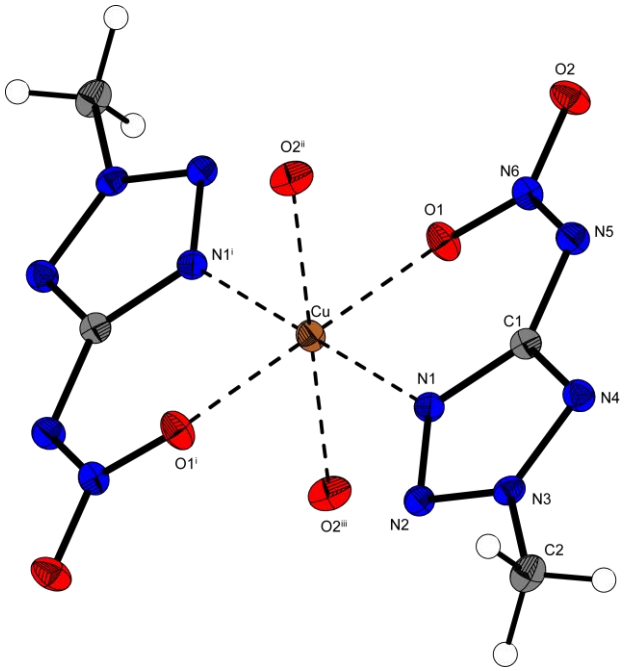

Figure 9.15 Molecular moiety of **113**. Hydrogen atoms shown as spheres of arbitrary radius and thermal displacements set at 50 % probability. Selected geometries: distances (Å): Cu–N1 = 1.938(2), Cu–O1 = 1.966(2), Cu–O2^{ii} = 2.403(2), O2–N6 = 1.246(2), O1–N6 = 1.294(2), N3–N2 = 1.308(3), N3–N4 = 1.334(2), N3–C2 = 1.462(3), N2–N1 = 1.332(3), N4–C1 = 1.335(3), N6–N5 = 1.303(2), N5–C1 = 1.375(3), N1–C1 = 1.355(3); angles (°): N1–Cu–O1 = 85.27(7), N1–Cu–O2 = 92.30(6), O1–Cu–O2 = 85.41(7), O2–N6– O1 = 116.6(2), N1–C1–N5 = 131.0(2), N4–C1–N1 = 110.8(2); torsion angles (°): O1–Cu–N1–C1 = 30.0(2), N6–N5–C1–N1 = –7.8(3), O1–N6–N5–C1 = –2.0(3); (i) 2–x, –y, 2–z; (ii) x, 0.5–y, –0.5+z; (iii) 2–x, –0.5+y, 2.5–z.

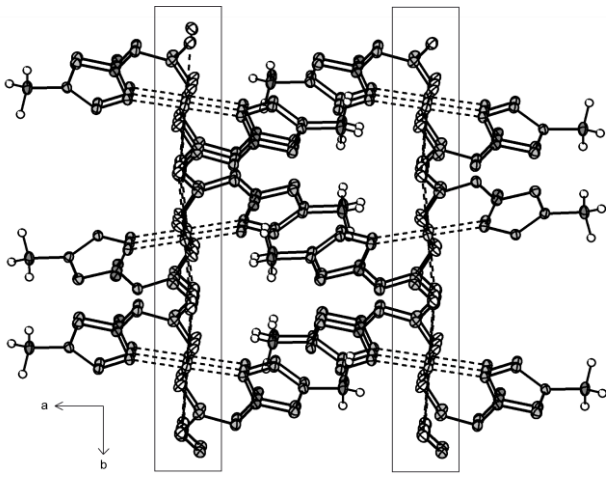

Figure 9.16 View on the three-dimensional network formed in the packing of **113**. The layers of copper atoms, which are connected by the nitro-groups are marked with squares.

9.3.10 [Cu(2-MeAtNO$_2$)$_2$(NH$_3$)$_2$] (**114**)

Trans-bis(ammine-(2-methyl-5-nitraminotetrazolato-*N,O*) copper(II) (**114**) crystallizes in the monoclinic space group *C*2/*c* with four molecules in the unit cell. The density of 1.864 g cm^{-3} is in the same range as observed for the corresponding 1-methyl-nitriminotetrazolate complex **111**. The copper(II) atoms are coordinated by an elongated octahedral coordination sphere (**Figure 9.17**).

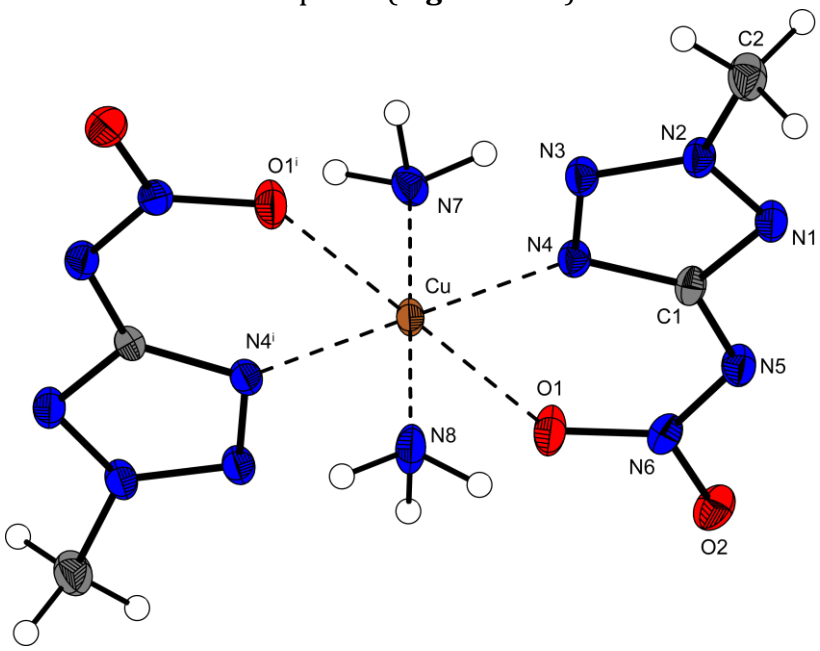

Figure 9.17 Molecular moiety of **114**. Hydrogen atoms shown as spheres of arbitrary radius and thermal displacements set at 50 % probability. Selected geometries: distances (Å): Cu–N4 = 2.020(2), Cu–N7 = 1.999(3), Cu–N8 = 2.006(3), Cu–O1 = 2.340(2) O1–N6 = 1.262(2), O2–N6 = 1.250(2), N1–N2 = 1.322(3), N1–C1 = 1.337(3), N5–N6 = 1.306(2), N5–C1 = 1.378(3), N3–N2 = 1.310(2), N2–C2 = 1.463(3), N3–N4 = 1.330(2), N4–C1 = 1.361(3); angles (°): N7–Cu–N8 = 180.0, N7–Cu– N4 = 90.29(6), N8–Cu–N4 = 89.71(6), N4–Cu–O1 = 76.42(6), O2–N6–O1 = 119.3(2), N1–C1–N5 = 133.1(2), N4–C1–N1 = 110.6(2); torsion angles (°): N6–N5–C1–N4 = 177.8(2), C1–N5–N6–O1 = 2.3(3), O1–Cu–N4–C1 = 3.1(2); (i) 1–x, y, 0.5–z.

The closest coordination distances (~2 Å) are build by the nitrogen atoms N1 of the tetrazolates and the coordinated ammonia molecules. Again the elongated bond is formed by the oxygen atoms (d(Cu–O1) = 2.340(2) Å), whereby the nitrogen atoms show distances of d(Cu–N1) = 2.020(2) Å, d(Cu–N7) = 1.999(3) Å and d(Cu–N8) = 2.006(3) Å. Therefore, these distances of the copper amine bonds of **114** and these of

115 are comparable to those of **111** and copper amino complexes like $Cu(NH_3)_4SO_4 \cdot H_2O$.[339] The copper cation as well as atom N7 and N8 lie on a C_2 axis. However, hydrogen atoms connected to N7 and N8 break this symmetry and are also half-occupied. The packing of **114** is characterized by an alternating layer structure which can be seen best along the *a* axis (**Figure 9.18**). The layers have distances of 4.38 Å along *b*. Although the copper cations have closed coordination spheres, the shortest Cu–Cu distances are found to be 5.614(1) Å.

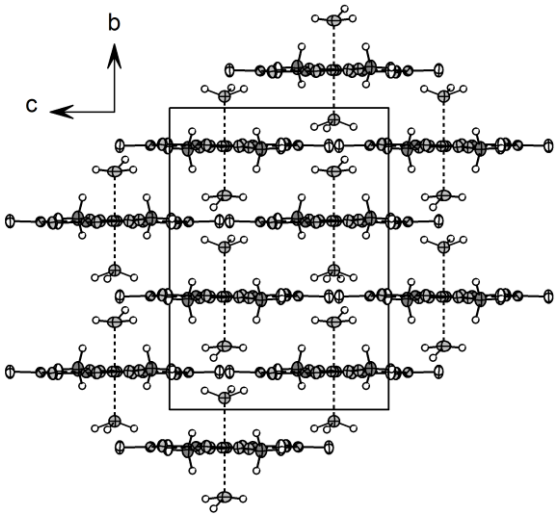

Figure 9.18 View on the unit cell of **114** along the *a* axis.

9.3.11 $[Cu(2MeAtNO_2)_2(NH_3)_4] \cdot H_2O$ (**115**)

Tetrammine-bis(2-methyl-5-nitraminotetrazolato-*N,O*) copper(II) (**115**) crystallizes in lavender needles in the triclinic space group *P*–1, with two molecules in the unit cell and a calculated density of 1.718 g cm^{-3}, which is the lowest observed in this work. The molecular unit is illustrated in **Figure 9.19**, in which the Cu(II) coordination sphere is formed by the four ammonia nitrogen atoms N13–N16 and the ring nitrogen atoms N4 and N9. However the coordination distance between Cu–N9 of 2.688(6) Å is the longest observed in this chapter, but significantly shorter than the copper-nitrogen van der Waals radius $r_{Cu} + r_N$ = 3.0 Å.[340] The long distance might be caused by the sterical influence of the methyl group. Interestingly, it could never be observed a coordination via the N(3) tetrazole nitrogen atom yet. The presence of the non-coordinated water molecule might not only be the reason for the low density, but also, due to the formation of a hydrogen bond to the nitrogen atom N11, a reason for the uncommonly coordination mode of this tetrazole ring. The trend of lowering the density by the inclusion of crystal water has also been observed in **107** and **108**.

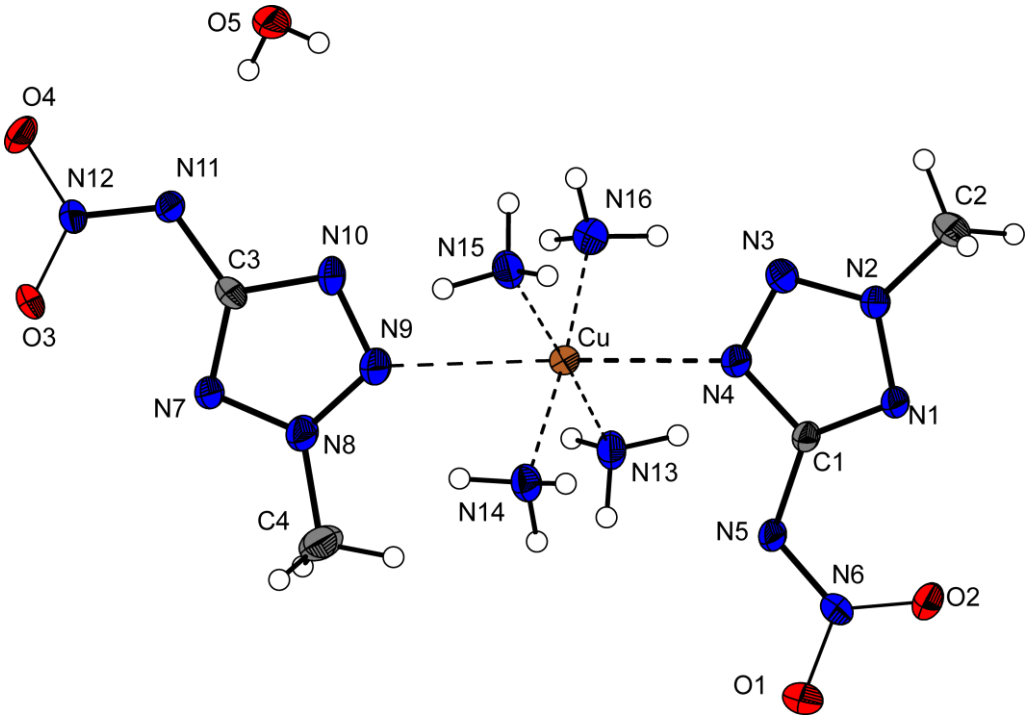

Figure 9.19 Molecular moiety of **115**. Hydrogen atoms shown as spheres of arbitrary radius and thermal displacements set at 50 % probability. Selected geometries: distances (Å): Cu–N4 = 2.425(5), Cu–N13 = 2.031(5), Cu–N14 = 2.035(5), Cu–N15 = 2.037(5), Cu–N16 = 2.044(5), Cu–N9 = 2.688(6); angles (°): N13–Cu–N4 = 90.1(2), N14–Cu–N4 = 90.8(2), N15–Cu–N4 = 93.8(2), N16–Cu–N4 = 93.9(2), N4–Cu–N9 = 177.9(2), N9–Cu–N13 = 88.2(2), N9–Cu–N14 = 88.1(2) N13–Cu–N14 = 92.6(2), N13–Cu–N15 = 176.1(2), N14–Cu–N15 = 87.6(2), N13–Cu–N16 = 87.9(2), N14–Cu–N16 = 175.3(2), N15–Cu–N16 = 91.6(2).

The packing of **115** can be described by the formation of layers in the *b*-*c* plane (**Figure 9.20**). Within the layers the water molecules are fixed by hydrogen bonds. The nearest Cu–Cu distance is found between the layers and is about 7.3 Å.

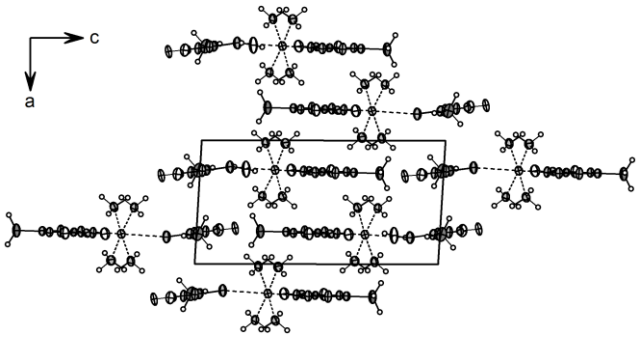

Figure 9.20 View on the unit cell of **116** along the *b* axis demonstrating the layers in the *b*-*c* plane.

9.4 Magnetic Measurements

The magnetic susceptibility of the complexes **104**, **105**, **111**, **112**, **114** and **115** was determined in the temperature range from 5 to 300 K. Magnetic measurements of the fine crystalline samples were performed on a Quantum-Design-MPMSR-XL-SQUID-Magnetometer. All measurements were carried out at two field strengths (0.2 and 0.5 T) in the settle mode. The data were corrected for the magnetization of the sample holder. Diamagnetic corrections were estimated using Pascal's constants. The $\chi_M T$ product at room temperature is with 0.47 $cm^3K\ mol^{-1}$ (**104**), 0.44 $cm^3K\ mol^{-1}$ (**111**), 0.48 $cm^3K\ mol^{-1}$ (**112**), 0.41 $cm^3K\ mol^{-1}$ (**114**), and 0.44 $cm^3K\ mol^{-1}$ (**115**) larger than the spin-only value of 0.37 expected for a single copper (II) ion (S = 1/2) assuming g = 2.00. For the dinuclear complex **105** a room temperature moment of $\chi_M T$ = 0.88 $cm^3K\ mol^{-1}$ is obtained, again larger than the theoretically expected value (0.74 cm^3K/mol). For the dinuclear complex **105** the $\chi_M T$ product starts to decrease below 50 K, an indication for magnetic exchange interactions over the bridging tetrazole ring. Assuming the formula given in [341a] for the magnetic interactions in a S_1 = 1/2 and S_2 = 1/2 spin system with $H = -J\ S_2 \cdot S_2$, a weak antiferromagnetic interaction can be estimated to be J = −6.0±0.2 cm^{-1} (g = 2.07±0.01) by fitting the observed data given in **Figure 9.21**. As the N1 nitrogen atoms of the bridging tetrazole belong to the basal plane of Cu, but N2 occupies an axial position of the elongated octahedral coordination sphere on the neighboring Cu^{2+}, the interactions between the magnetic orbitals of the two copper centers are very weak leading to small coupling parameters.

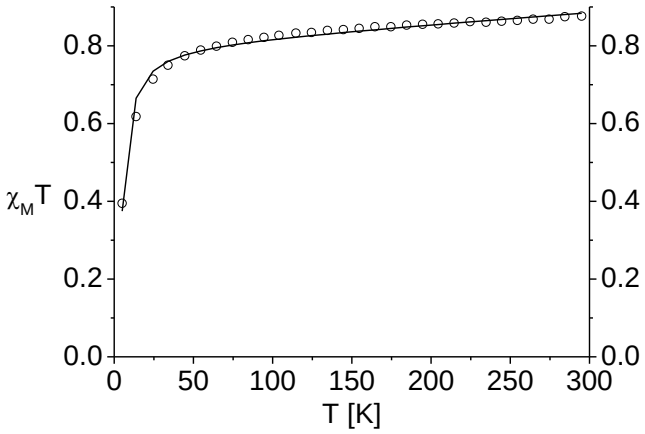

Figure 9.21 Plot of $\chi_M T$ vs. T for **105** under an applied magnetic field of 0.02 T. Solid line represent the best fit of the data with the model described in the text.

The temperature dependence of the $\chi_M T$ product of the mononuclear complexes strongly depends on the packing of the molecules in the crystal, especially on the formed hydrogen bonds. The susceptibility data can be fitted very well with the Curie-Weiss law ($\chi_M = C/(T - \Theta)$) with the parameters Θ = –11.5 K, C = 0.48 cm^{3}K mol^{-1} for **112**; Θ = –23.2 K, C = 0.49 cm^{3}K mol^{-1} for **104**; Θ = –39.0 K, C = 0.45 cm^{3}K mol^{-1} for 11; Θ = –77.8 K, C = 0.42 cm^{3}K mol^{-1} for **114**; and Θ = –90.8 K, C = 0.47 cm^{3}K mol^{-1} for compound **111**. In compound **112** with nearly ideal Curie-behavior no pathway for magnetic exchange interactions is available as all hydrogen bonds are formed between substituents of the coordinated ligands. In contrast to this for compound **111** a 2D layer of hydrogen bonds between the NH_3 hydrogen and the coordinated oxygen of the nitro-group of the tetrazole ligand is formed. Here a significant decrease of the magnetic moment below 100 K is observed and the fit according to the Curie-Weiss law gives a negative Weiss constant in agreement with the antiferromagnetic interactions. In **Figure 9.22** the results from the magnetic measurements are displayed for the three selected examples **112**, **115** and **111**. In all cases the exchange pathway (the hydrogen bonds) connects one position in the equatorial plane of the first copper centre with one position of the linked copper centre in the axial position of the elongated octahedral coordination sphere. The interactions between the magnetic orbitals are always weak, leading to comparable small interaction parameters.

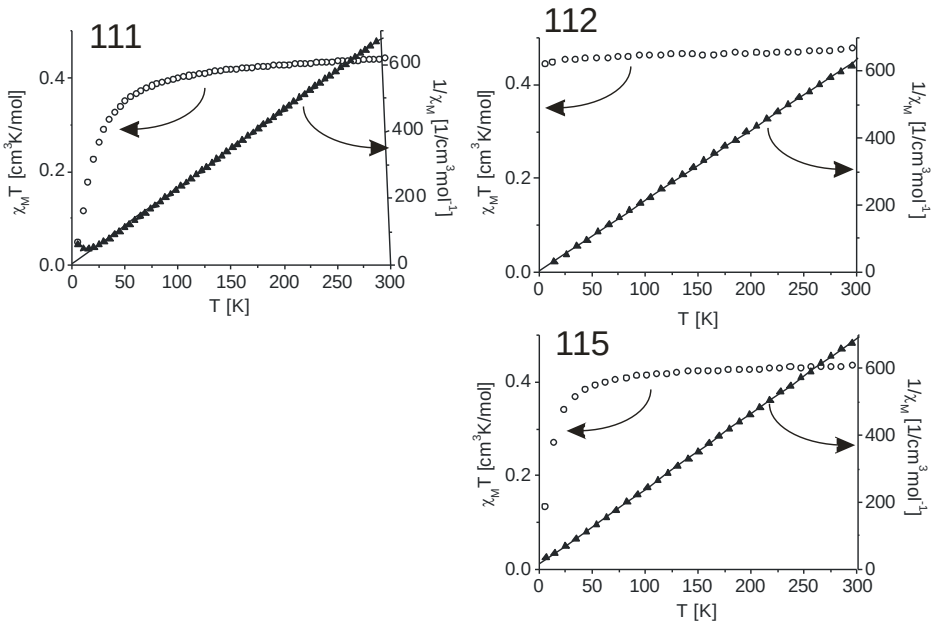

Figure 9.22 Plot of $\chi_M T$ vs. T and $1/\chi_M$ vs. T for the complexes **112** (top), **115** (middle) and **111** (bottom) under an applied magnetic field of 0.05 T. Solid lines represent the best fit of the data with the model described in the text.

9.5 Energetic Properties

9.5.1 Differential Scanning Calorimetry

DSC measurements determining the thermal behavior of the copper(II) 5-nitriminotetrazolate complexes were performed in covered Al-containers with a nitrogen flow of 20 mL min^{-1} on a Linseis PT 10 DSC at heating rates of 5 °C min^{-1}. The DSC plots in **Figure 9.23** show the thermal behavior of ~2 mg of **104–109** and **111–115** in the temperature range from 50–400 °C. Interestingly, the deprotonation in combination with the coordination to the copper(II) centers results in a substantial increase in the decomposition points in comparison to the neutral ligands **43–45**, which decomposes at temperatures of 120–125 °C. The lowest decomposition temperature is observed for complex **112** (124 °C), in which two neutral ligands are coordinated. This temperature of decomposition corresponds to that of **45**. The second lowest temperature (128 °C) is observed for **104**, in which 5-nitriminotetrazole is only deprotonated once. The decomposition follows immediately the loss of water. Complexes **105**, **106**, **111**, **112** and **113** show decomposition points in the range of 200–243 °C. Compound **109** shows a decomposition temperature of 252 °C, which is in the same range of the hydrates **107** and **108** ($T_{dec.}$ = 256 °C). Interestingly, solely **115** decomposes above 300 °C at a temperature of 317 °C. **115** lose its non coordinated crystal water above temperatures of 110 °C. This high decomposition temperature can only be explained by the uncommon coordination mode of the tetrazole ligand (see crystal structures).

To determine the heats of decomposition of **107** and **109** three samples (~2 mg) were heated with a heating rate of 2 °C min^{-1} and a fixed nitrogen flow of 5 L h^{-1} over the decomposition peaks. The surface was integrated using the Linseis software and the average of three measurements was used to calculate the heats of decomposition $\Delta_{dec.}H°$. **109**: 2739 J g^{-1} (958 kJ mol^{-1}); **107**: 2218 J g^{-1} (936 kJ mol^{-1}).

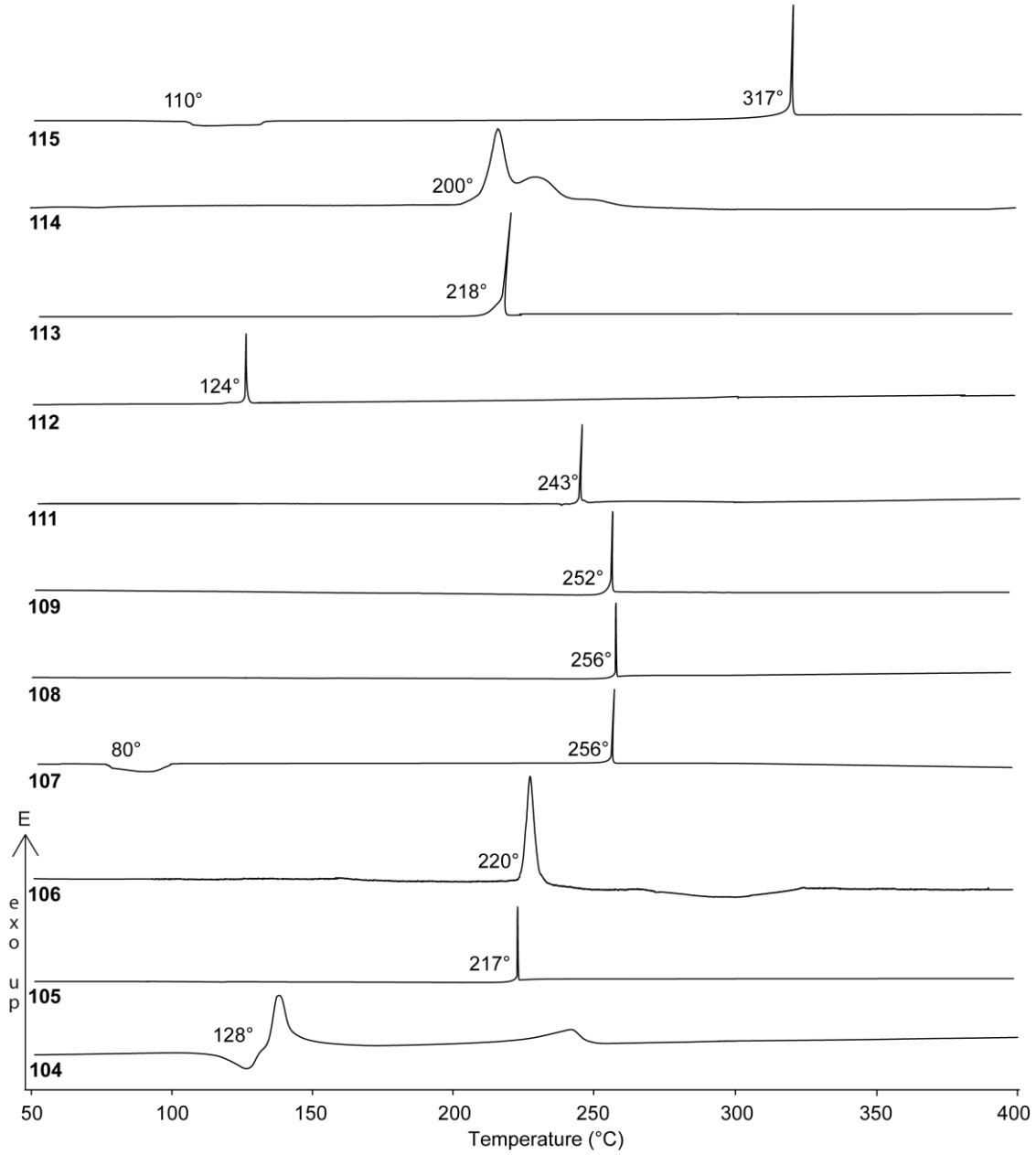

Figure 9.23 DSC thermograms (exo-up) of compounds **104–109** as well as **111–115** (heating rate of 5 °C min^{-1}).

9.5.2 Thermogravimetry

Thermogravimetry (TG) was used to investigate the dehydration of **107** and was performed using a Setaram TG-DTA 92-16 in a helium atmosphere with a heating rate of 1 °C min^{-1} to a maximum temperature of 350 °C. For the measurement, 5.351 mg of a pulvered sample in an aluminum oxide pan was used. The TG curve as well the DTA curve are shown in **Figure 9.24**. The loss of water occurs over a wide range, starting at before 50 °C and ending at about 85 °C. It depends on the heating rate and occurs at

higher temperatures when higher heating rates are used (see DSC measurements). The loss of 0.878 mg weight corresponds to the loss of all four water molecules in compound **107**, resulting in a fine green powder. It is not possible to stop the dehydration process at compound **108**. In the second step at about 245 °C a loss of mass of 3.932 mg was observed, which is more than the expected mass for remaining copper(II) oxide as solid residues. Through the explosion, which releases a huge amount of nitrogen, some of the Cu(II)O must be removed from the open set up.

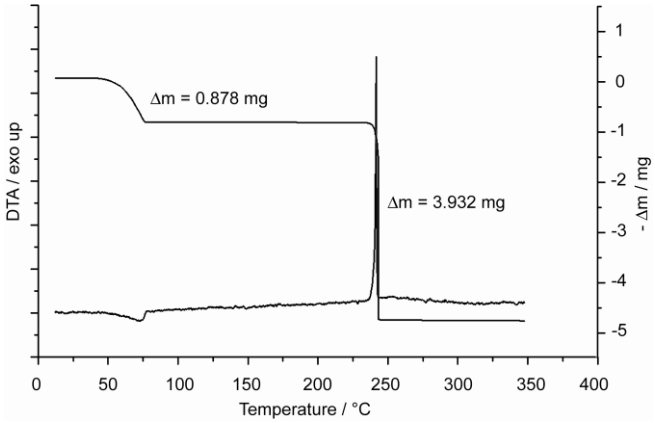

Figure 9.24 Thermogravimetry plot of compound **107**, showing the loss of mass (right axis) and the DTA curve (left axis).

9.5.3 Sensitivities and Flame Colors

Since the investigated copper-tetrazole complexes **104**–**115** are energetic compounds with increased nitrogen contents, the sensitivities towards friction and impact were tested. The results are summarized in **Table 9.2**. Also the sensitivities of the starting materials **43**–**55** are listed for better comparison. While the methyl derivatives are moderately sensitive, 5-nitriminotetrazole is a highly energetic compound and very sensitive towards outer stimuli and should therefore only be handled with great care. Its copper complexes **104**–**106** show lower sensitivities. Generally the sensitivity corresponds to the amount of included water or ammonia molecules. At this, crystal water lowers the sensitivities in higher spades than ammonia. Compounds **107** and **110** are not sensitive towards impact (< 100 J) and friction (< 360 N). Compound **108** shows only a very low impact sensitivity (> 55 J) and is not sensitive towards friction. Compound **109** is very sensitive towards impact (1 J) and friction (40 N) and since the

value is comparable with lead azide, it should be considered to be a primary explosive. Next to **109**, compounds **112** and **113** show the highest sensitivities towards impact as well as friction. According to the "UN Recommendations on the Transport of Dangerous Goods" compounds **109**, **112** and **113** are classified as "very sensitive".

Except for **109**, **112** and **113**, which deflagrate violently when brought to a flame, all complexes burn with a brilliant green flame color. The burning is also nearly smokeless and free of carbon residues. This makes, especially **104**–**108** as well as **110**, **114** and **115** to promising candidates for green colorants in modern smokeless pyrotechnical compositions.

Flame test of **110**

Table 9.2 Sensitivity data of **104–109** as well as **111–115**. (impact, friction and flame test)

	43	**44**	**45**	**104**	**105**	**106**	**107**	**108**	**109**	**111**	**112**	**113**	**114**	**115**
IS [J]	1	12	3	30	> 50	> 40	> 100	55	1	15	2	1	20	40
FS[N]	8	160	145	360	> 360	360	> 360	> 360	40	> 360	30	18	300	30
flame test	defl.	defl.	defl.	green comb.	green comb.	green comb.	green comb.	green comb.	defl.	green comb.	defl.	defl.	green comb.	green comb.

Since lead azide is still used in modern priming charges and the U.S. army alone consumes more than 1000 pounds,[342] a comparison with the most promising compound **109** is shown in **Table 9.3**.

Table 9.3 Energetic Properties of **109** and lead azide.

	109	lead azide
impact sensitivity	1 J	2.5–4.0 J (pure) 3.0–6.5 J (techn.)
friction sensitivity	> 40 N	0.1–1 N
decomp. temperature	252 °C	> 315 °C

9.6 Experimental Part

*CAUUTION: The prepared nitri- and nitraminotetrazoles and -tetrazolates are energetic materials with increased sensitivities against various stimuli. Although we had no problems preparing the compounds **104–115** proper protective measures (safety glasses, face shield, leather coat, earthened equipment and shoes, Kevlar® gloves and ear plugs) should be used. Extra precautions should be taken, when the ligands are prepared on larger scales.*

*[Cu(HAtNO$_2$)$_2$(H$_2$O)$_4$] (**104**):* Copper(II) nitrate trihydrate (242 mg, 1.0 mmol) was dissolved in 2 mL hot water and combined with a hot solution of 5-nitriminotetrazole (**43**) (260 mg, 2 mmol) in 4 mL water. Light blue crystals suitable for X-ray analysis were obtained after several hours of crystallization at room temperature (340 mg, yield 43 %). **DSC** (T_{onset}, 5 °C min^{-1}): 138 °C (dec.); **IR** (KBr, cm^{-1}): $\tilde{\nu}$ = 3431 (vs), 3096 (s), 2906 (s), 2609 (m), 1816 (w), 1652 (m), 1539 (s), 1492 (m), 1457 (s), 1369 (s), 1324 (vs), 1260 (s), 1159 (s), 1099 (m), 1064 (s), 1009 (s), 881 (m), 805 (m), 774 (m), 744 (s), 694 (m), 572 (w), 486 (w); **EA** ($C_2H_{10}CuN_{12}O_8$, 393.72) calcd.: C 6.10, H 2.56, N 42.69 %; found: C 6.16, H 2.62, N 42.55 %; **impact sensitivity**: 30 J; **friction sensitivity**: 360 N.

*[Cu(AtNO$_2$)(NH$_3$)$_3$]$_2$ (**105**):* Copper(II) nitrate trihydrate (242 mg, 1.0 mmol) was dissolved in 2 mL hot water and combined with a hot solution of 5-nitriminotetrazole (**43**) (260 mg, 2 mmol) in 10 mL ammonium hydroxide solution (25 %). The solution was refluxed for 5 min. After cooling to room temperature and waiting for one day the product started to precipitate forming blue crystals (203 mg, yield 64 %). **DSC** (T_{onset}, 5 °C min^{-1}): 220 °C (dec.); **IR** (KBr, cm^{-1}): $\tilde{\nu}$ = 3332 (s), 3242 (s), 3168 (s), 2605 (w), 2477 (w), 2362 (w), 2346 (w), 2294 (w), 2175 (w), 2019 (w), 1934 (w), 1891 (w), 1762 (w), 1733 (w), 1627 (m), 1462 (s), 1462 (s), 1399 (s), 1371 (s), 1303 (s), 1251 (s), 1237 (s), 1214 (m), 1153 (m), 1135 (w), 1094 (m), 1026 (s), 866 (m), 753 (m), 738 (m), 721 (w), 699 (w), 636 (w), 482 (w); **EA** ($C_2H_{18}Cu_2N_{18}O_4$, 485.38) calcd.: C 4.95, H 3.74, Cu 26.18, N 51.94, O 13.19 %; found: C 4.98, H 3.42, N 51.93 %; **impact sensitivity**: > 50 J; **friction sensitivity**: > 360 N.

*$(NH_4)_2[Cu(AtNO_2)_2(H2O)_2]$ (**106**):* Small amounts of complex **106** are obtained from the mother liquor after isolating **105** (170 mg, yield 21 %). **DSC** (Tonset, 5 °C min^{-1}): 217 °C (dec.); **EA** ($C_2H_{12}CuN_{14}O_6$, 391.75) calcd.: C 6.13, H 3.09, N 50.06 %; found: C 6.41, H 3.43, N 49.73 %; **impact sensitivity**: 40 J; **friction sensitivity**: 360 N.

*$[Cu(C_2H_3N_6O_2)_2(H_2O)_2]\cdot(H_2O)_2$ (**107**):* Copper(II) nitrate trihydrate (240 mg, 1.0 mmol) was dissolved in 2 mL hot water and combined with a hot solution of 1-methyl-5-nitriminotetrazole (288 mg, 2 mmol) in 15 mL water and refluxed for 5 min. After cooling to room temperature and standing for 24 hours, blue crystals of **107** started to precipitate (299 mg, yield 71 %). After filtration the mother liquid was left, whereby green crystals of **108** were obtained (39 mg, yield 10 %). **DSC** (T_{onset}, 5 °C min^{-1}): 256 °C (dec.); **IR** (KBr, cm^{-1}): $\tilde{\nu}$ = 3504 (m), 3461 (m), 3220 (m), 2963 (m), 2148 (w), 1801 (w), 1662 (w), 1526 (m), 1476 (s), 1398 (m), 1384 (m), 1339 (s), 1305 (s), 1256 (m), 1120 (m), 1037 (m), 1010 (w), 929 (w), 887 (w), 859 (w), 776 (w), 737 (w), 654 (w), 585 (w); **EA** ($C_4H_{14}CuN_{12}O_8$, 421.78) calcd.: C 11.39, H 3.35, N 39.85 %; found: C 11.32, H 3.38, N 39.69 %; **impact sensitivity**: > 100 J; **friction sensitivity**: > 360 N.

*$[Cu(C_2H_3N_6O_2)_2(H_2O)_2]$ (**108**):* **DSC** (T_{onset}, 5 °C min^{-1}): 251 °C (dec.); **IR** (KBr, cm^{-1}): $\tilde{\nu}$ = 3481 (m), 2963 (w), 1798 (w), 1628 (m), 1539 (m), 1487 (m), 1417 (s), 1404 (s), 1385 (s), 1339 (m), 1298 (s), 1247 (m), 1125 (m), 1030 (m), 877 (w), 772 (w), 757 (w), 734 (m), 701 (m), 537 (w); **EA** ($C_4H_{10}CuN_{12}O_6$, 385.75) calcd.: C 12.45, H 2.61, N 43.57 %; found: C 12.28, H 2.71, N 43.11 %; **impact sensitivity**: 55 J; **friction sensitivity**: > 360 N.

*$[Cu(C_2H_3N_6O_2)_2]$ (**109**):* The highly explosive copper complex **109** was obtained by dehydration of powdered **107** at 120 °C and reduced pressure ($1\cdot10^{-2}$ mbar) for two hours. Single crystals suitable for X-ray diffraction were grown from dry methanol. **DSC** (T_{onset}, 5 deg min^{-1}): 252° C (dec.); **IR** (KBr, cm^{-1}): $\tilde{\nu}$ = 3498 (m), 3456 (m), 3223 (m), 2861 (m), 2926 (m), 2346 (w), 1618 (m), 1528 (m), 1494 (m), 1477 (m), 1438 (m), 1384 (m), 1339 (s), 1303 (s), 1245 (m), 1229 (m), 1120 (m), 1037 (w), 1001 (m), 873 (m), 776 (w), 733 (w), 698 (w), 588 (w), 512 (w); **EA** ($C_4H_6CuN_{12}O_4$, 349.71) calcd.: C 13.74, H 1.73, N 48.06 %; found: C 13.77, H 1.83, N 48.29 %; **impact sensitivity**: 1 J; **friction sensitivity**: 40 N.

*[Cu(C$_2$H$_3$N$_6$O$_2$)$_2$(H$_2$O)$_2$]·(MeOH)$_2$ (**110**):* The light blue colored methanol containing complex **110** was obtained by recrystallization of **109** from wet methanol. **EA** ($C_6H_{18}CuN_{12}O_8$, 449.83) calcd.: C 16.02, H 4.03, N 37.37 %; found: C 15.81, H 3.92, N 37.65 %; **impact sensitivity**: > 100 J; **friction sensitivity**: > 360 N.

*[Cu(1MeAtNO$_2$)$_2$(NH$_3$)$_2$] (**111**):* A solution of **44** (288 mg, 2.0 mmol) in 8 mL ammonium hydroxide solution (25 %) was heated and combined with a hot solution of copper(II) chloride dihydrate (171 mg, 1.0 mmol) in 1 mL water. The dark blue solution was heated for 5 min at 90 °C. After one day of crystallization at room temperature, dark-blue crystals suitable for X-ray analysis were obtained (184 mg, yield 48 %). **DSC** (T_{onset}, 5 °C min^{-1}): 240 °C (dec.); **IR** (KBr, cm^{-1}): $\tilde{\nu}$ = 3450 (w), 3330 (s), 3242 (m), 3188 (m), 3042 (w), 2509 (w), 1748 (w), 1632 (w), 1522 (s),1473 (s), 1412 (s), 1379 (s), 1324 (s), 1287 (vs), 1242 (s), 1123 (m), 1054 (w), 1030 (w), 1001 (w), 877 (w), 772 (w), 757 (m), 735 (m), 703 (m), 689 (w), 496 (w), 467 (w); **EA** ($C_4H_{12}CuN_{14}O_4$, 383.78) calcd.: C 12.52, H 3.15, N 51.10 %; found: C 12.37, H 3.19, N 50.79 %; **impact sensitivity**: 15 J; **friction sensitivity**: > 360 N.

*[Cu(2MeAtNO$_2$)$_2$(2MeHAtNO$_2$)] (**112**):* A solution of **45** (576 mg, 4.0 mmol) in 7 mL water was heated to 80 °C. To this solution copper(II) chloride dihydrate (170 mg, 1.0 mmol) in 4 mL water was added and the mixture was heated for 15 min at 80 °C. After five days time of crystallization at room temperature, dark-green crystals suitable for X-ray analysis were obtained (491 mg, yield 77 %). **DSC** (T_{onset}, 5 °C min^{-1}): 124 °C (dec.); 1458 (m), 1426 (s), 1403 (s), 1369 (s), 1339 (vs), 1314 (vs), 1220 (w), 1193 (w), 1152 (m), 1134 (w), 1073 (w), 1036 (w), 1024 (w), 1008 (w), 918 (w), 871 (w), 776 (w), 759 (m), 741 (w), 708 (m), 679 (w), 628 (w), 512 (w), 469 (w); **EA** ($C_8H_{14}CuN_{24}O_8$, 637.90) calcd.: C 15.06, H 2.37, N 52.70 %; found: C 15.02, H 2.27, N 52.66 %; **impact sensitivity**: > 2 J; **friction sensitivity**: 30 N.

*[Cu(2MeAtNO$_2$)$_2$] (**113**):* A small amount of blue crystals is obtained by long standing of the mother liquor after isolating complex **112**. **DSC** (T_{onset}, 5 °C min^{-1}): 218 °C (dec.); **EA** ($C_4H_6CuN_{12}O_4$, 349.72) calcd.: C 15.06, H 2.37, N 52.70 %; found: not determinable due to explosion; **impact sensitivity**: 1 J; **friction sensitivity**: 30 N.

*[Cu(2MeAtNO$_2$)$_2$(NH$_3$)$_2$] (**114**):* Copper(II) nitrate trihydrate (242 mg, 1.0 mmol) was dissolved in 2 mL hot water and combined with a hot solution of **45** (288 mg, 2.0 mmol)

in 4 mL water. To this 0.25 mL of conc. ammonia solution was added drop wise. After heating to 80 °C for 10 min the solution was left for crystallization. After separation of small amounts of **115**, complex **114** crystallized within two days as blue crystals (195 mg, yield 51 %). **DSC** (T_{onset}, 5 °C min^{-1}): 200 °C (dec.); **IR** (KBr, cm^{-1}): $\tilde{\nu}$ = 3467 (m), 3340 (s), 3238 (s), 3183 (s), 2956 (w), 2367 (w), 2161 (w), 1925 (w), 1782 (w), 1655 (m), 1637 (m), 1489 (vs), 1391 (s), 1351 (vs), 1324 (s), 1269 (s), 1249 (s), 1210 (s), 1103 (m), 1095 (m), 1046 (s), 1028 (m), 1010 (w), 885 (m), 768 (m), 753 (m), 741 (s), 728 (s), 704 (s), 676 (w), 635 (w), 614 (w), 538 (w), 469 (w); **EA** ($C_4H_{12}CuN_{14}O_4$, 383.78) calcd.: C 12.52, H 3.15, N 51.10 %; found: C 12.54, H 3.11, N 49.15 %; **impact sensitivity**: 20 J; **friction sensitivity**: 300 N.

*[Cu(2MeAtNO$_2$)$_2$(NH$_3$)$_4$]·H$_2$O (**115**):* Copper(II) chloride dihydrate (171 mg, 1.0 mmol) was dissolved in 1 mL water and added to a hot solution of **45** (288 mg, 2.0 mmol) in 3 mL water. To this light-green solution 1 mL aqueous ammonia solution (25 %) was added. The dark-blue mixture was heated for 5 min at 90 °C and left for crystallization at room temperature. After two hours fine dark-blue crystals suitable for X-ray analysis were obtained (326 mg, yield 75 %). **DSC** (T_{onset}, 5 °C min^{-1}): 110 °C, 317 °C (dec.); **IR** (KBr, cm^{-1}): $\tilde{\nu}$ = 3462 (s), 3350 (s), 3182 (m), 2957 (w), 2918 (w), 2857 (w), 1639 (m), 1489 (s), 1404 (s), 1391 (s), 1353 (vs), 1325 (s), 1250 (s), 1211 (m), 1144 (w), 1095 (m), 1046 (m), 1029 (w), 885 (w), 797 (w), 769 (w), 741 (w), 728 (w), 702 (w); **EA** ($C_4H_{20}CuN_{16}O_5$, 435.85) calcd.: C 11.02, H 4.63, N 51.42 %; found: C 11.28, H 4.39, N 51.25 %; $\Delta_c U$: –2271 cal g^{-1}; **impact sensitivity**: 40 J; **friction sensitivity**: 30 N.

9.7 Conclusions

From this experimental study the following conclusions can be drawn:

- 5-Nitriminotetrazole (**43**), 1-methyl-5-nitriminotetrazole (**44**), 2-methyl-5-nitraminotetrazole (**45**) can be used as mono- and bidentate as well as in the case of **105** as bridging ligands. Novel copper complexes are formed including different amounts of crystal water or ammonia depending on the reaction conditions.

- In this chapter the following compounds are presented: $[Cu(HAtNO_2)_2(H_2O)_4]$ (**104**), $[Cu(AtNO_2)(NH_3)_3]_2$ (**105**), $(NH_4)_2[Cu(AtNO_2)_2(H_2O)_2]$ (**106**), $[Cu(1MeAtNO_2)_2(H_2O)_2]\cdot(H_2O)_2$ (**107**), $[Cu(1MeAtNO_2)_2(H_2O)_2]$ (**108**), $[Cu(1MeAtNO_2)_2]$ (**109**), $[Cu(1MeAtNO_2)_2(H_2O)_2]\cdot(MeOH)_2$ (**110**), $[Cu(1MeAtNO_2)_2(NH_3)_2]$ (**111**), $[Cu(2MeAtNO_2)_2(2MeHAtNO_2)_2]$ (**112**), $[Cu(2MeAtNO_2)_2]$ (**113**), $[Cu(2MeAtNO_2)_2(NH_3)_2]$ (**114**), $[Cu(2MeAtNO_2)_2(NH_3)_4]\cdot H_2O$ (**115**). All compounds are obtained via facile routes and except for **106**, **108** and **113** also in good yields. All complexes are crystalline materials, which are neither hygroscopic nor sensitive towards air.

- The crystal structures of **104**–**115** were determined and discussed with respect to the coordination spheres of the copper centers. All complexes crystallizes in distorted octahedral coordination modes characterized by the Jahn-Teller effect.

- The magnetic susceptibility of the complexes **104**, **105**, **111**, **112**, **114** and **115** was determined in the temperature range from 5 to 300 K.

- In the case of **107** and **108** the crystal water can be completely removed at higher temperatures forming promising primary explosive bis(1-methyl-5-nitriminotetrazolate) copper(II) **109**. The dehydration proceeds in discrete steps, determined by differential thermogravimetry. **109** is a primary explosive due to its high sensitivity towards impact (1 J), but shows a lower sensitivity towards friction (40 N) compared with common primary explosives. It is stable up to 250 °C and shows even long term stability when tested at a temperature of 190 °C. In comparison with the commonly used lead azide, it shows suitable

properties, particular the friction and impact sensitivities and a lower toxicity. The thermal decomposition provides a heat of decomposition of 2730 J g^{-1}, measured using differential scanning calorimetry.

- Most of the complexes show energetic behaviors. The sensitivities towards impact and friction as well as the decomposition temperatures were discovered. The decrease of sensitivity corresponds with the amount of coordinated solvent. The temperatures of decomposition vary from 124 (**112**) to 317 °C (**115**). Most of the complexes show smokeless combustion with bright green flame colors. By combining different complexes, the energetic properties as well as the green flame tone can be adjusted. This could be utilized in modern barium-free pyrotechnical compositions.

- Especially complexes **105**, **106**, **107, 108**, **109**, **114** and **115** are certainly of interest as additives in pyrotechnics, AP-based propellants, or other applications, as they show promising properties with respect to stability, sensitivity, and energetic aspects.

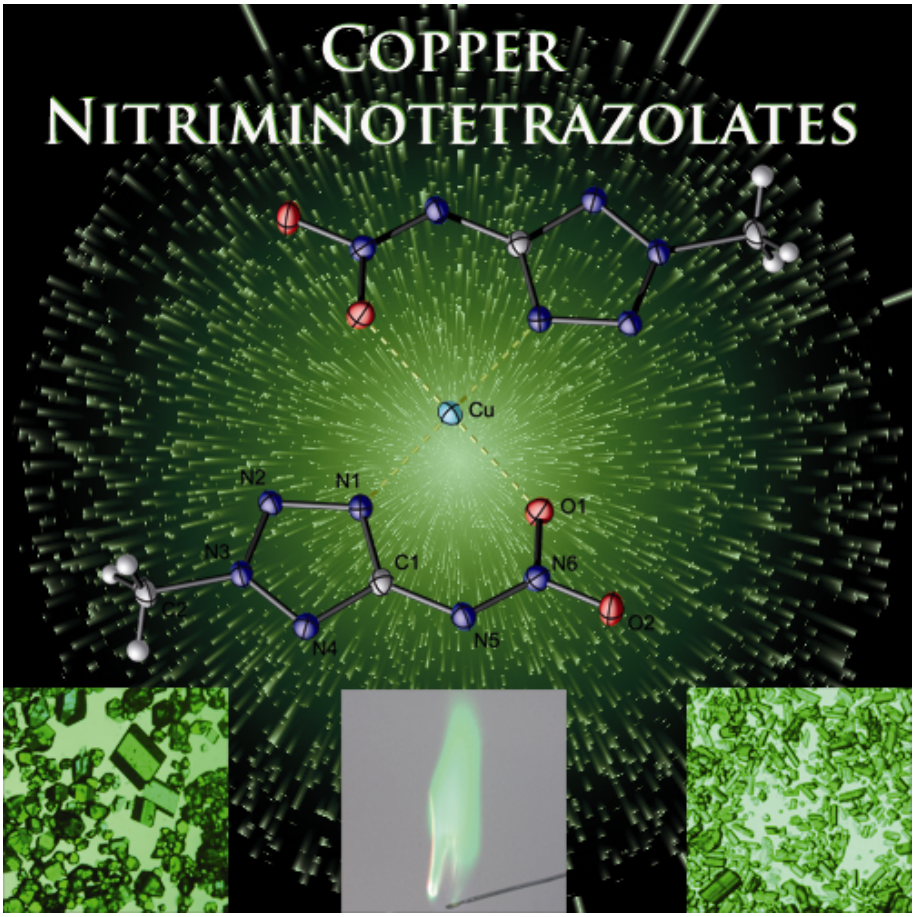

Chapter 10.

Bis(tetrazolyl)triazenes

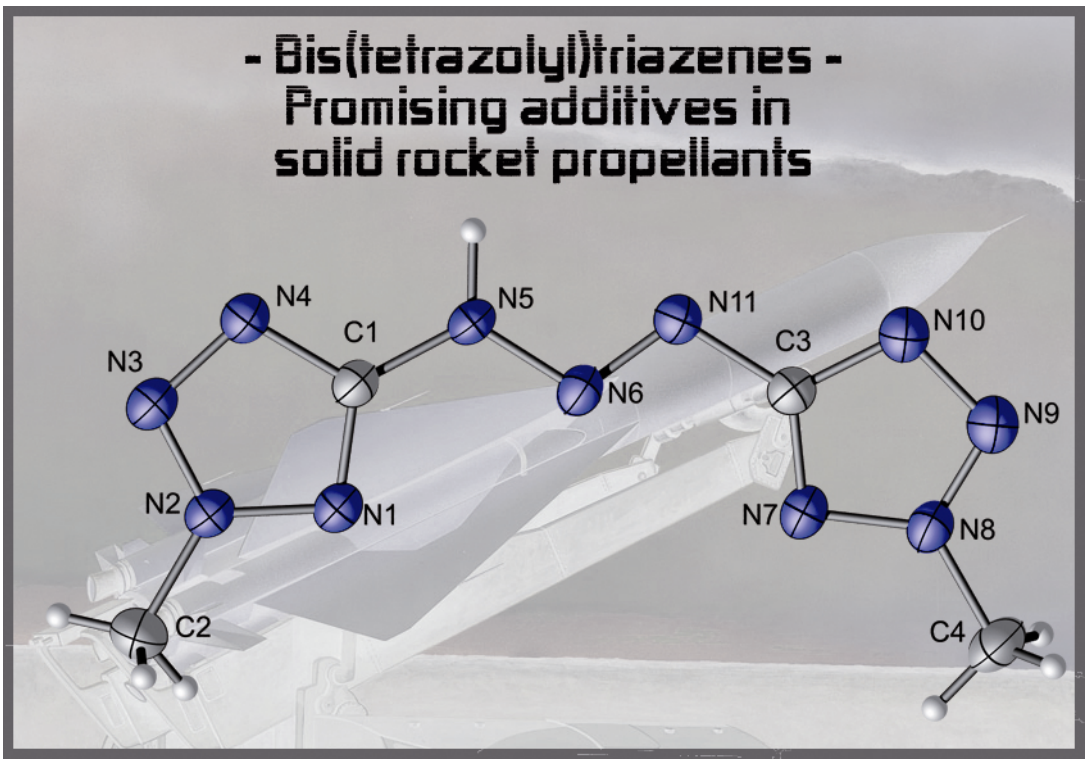

10.1 Introduction

The compounds described in this chapter are due to their high nitrogen content but lower densities highly suitable as novel additives in solid propellants. In contrast to high explosives, propellants need to release their energy in form of deflagration. In this way they produce high pressure without fracturing the containment chamber. Black powder [343] was one of the first propellants used in guns and motors. Today it is still used in pyrotechnic formulations, especially in small firework rockets. However, the use of black powder as propellant for larger objects like missiles and space rockets shows disadvantages, like the unpredictability of the behavior and also the development of polluting gases.[344] Rocket propellants need to fulfill a couple of requirements: (i) The energetic material must have a high energy content and slow burning rate to sustain a high specific impulse over a period of time. (ii) Additionally, the substance needs to be stable over a long time period and in a wide as possible temperature range. To compare different propellants in their performance the specific impulse I_{sp} is used. It is defined as the thrust divided by the mass flow rate of the explosive (equation 1).

$$I_{sp} = \frac{thrust\ of\ motor}{mass\ flow\ rate\ through\ nozzle} \qquad (\mathbf{1})$$

The specific impulse is also a function of the temperature in the combustion chamber and the average molar mass of the gases:

$$I_{sp} \propto \sqrt{\frac{temperature\ of\ combustion\ chamber}{average\ molar\ mass\ of\ gaseous\ products}} \qquad (\mathbf{2})$$

Therefore I_{sp} depends on the properties of the propellant, on the design of the combustion chamber and the rocket motor respectively. The two main types of solid rocket propellant are double-base propellants and composite propellants. Double-base propellants are homogenous and composed of nitrocellulose with nitroglycerine or other nitroglycols as energetic plasticizers. Because the dimension of propellant grains based on this type of mixture is limited, composite propellants were developed during the second world war. The most important composite propellant today is a mixture of aluminum as fuel and ammonium perchlorate as oxidizer. Polymers, like hydroxy- or carboxy-terminated polybutadiene serve as binding agents. These type of mixtures are used as solid rocket boosters at the US Space Shuttle and also in the European Ariane

rockets (see introduction). Depending on the kind of binder and other additives used the specific impulse reaches about 2400–2600 Ns kg^{-1} (engl. (I_{sp} g^{-1}): 245–265 s) and the flame temperature is about 2850–3500 K.

Although the performance of ammonium perchlorate is highly suitable as rocket propellant, it has one big disadvantage. As it can be seen from the decomposition equation (**3**) a high amount of HCl is produced.

$$2\ NH_4ClO_4 \rightarrow N_2 + 3\ H_2O + 2\ HCl + 2.5\ O_2 \qquad (\mathbf{3})$$

With the fact of 500.000 kg propellant per booster for the Space Shuttle there is a total output of 217 tons of HCl per launch. With the humidity in the air a huge quantity of acid mist is released, which leads to acid rain. In addition the resulting Al_2O_3 is harmful for living creatures and plants. Some endeavors were made to reduce the environmental pollution, especially, concerning the HCl impact. One possibility is to add $NaNO_3$ to build up NaCl:[345]

$$NH_4ClO_4 + NaNO_3 \rightarrow NH_4NO_3 + NaClO_4 \rightarrow \text{production of NaCl} \qquad (\mathbf{4})$$

The simplest way to reduce the environmental pollution would be using propellants which contain no chloride and do not produce any other harmful residues. Many scientists are searching for new energetic materials with good performance and at the same time having environmental friendly properties. Examples for this new class of energetic materials are 5,5'-bis(1*H*-tetrazolyl)amine (H_2bta) (Chapter 15) and salts of 5,5'-bis*(*1*H*-tetrazolyl)hydrazine (BTH) [74] as well as *5,5'*-azotetrazolates (Atz), which syntheses are illustrated in **Scheme 10.1**.

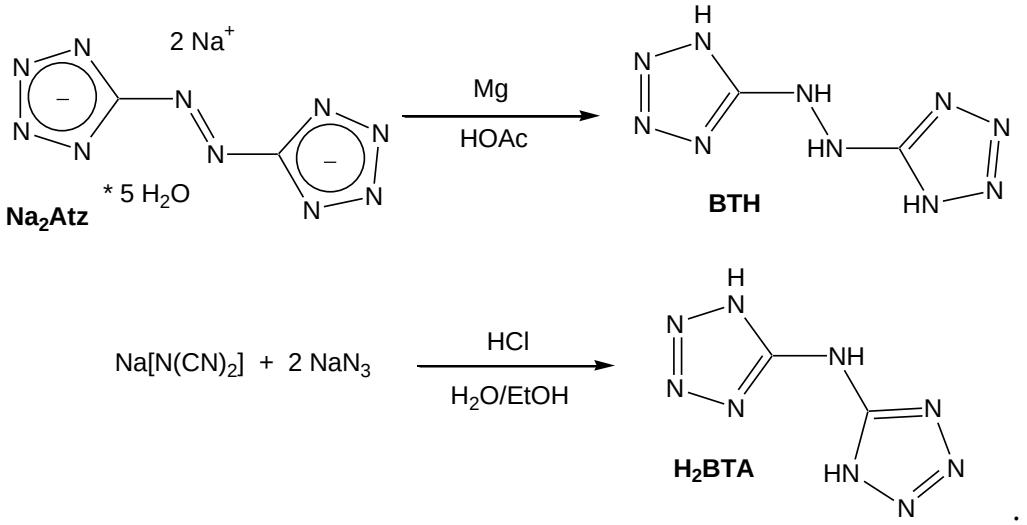

Scheme 10.1 Syntheses of the nitrogen-rich materials 5,5'-bis*(*1*H*-tetrazolyl)hydrazine (BTH) and 5,5'-bis(1*H*-tetrazolyl)amine (H_2bta).

Compounds containing the 5,5'-azotetrazolate anion are particularly suitable target molecules, since these salts have a considerable nitrogen content and are expected to have appropriate stabilities toward friction, impact and heat. Metal salts of 5,5'-azotetrazolates have been extensively studied [71] and also N-rich guanidinium derivatives of 5,5'-azotetrazolate are described in literature as possible additives in solid propellants.[72] The main disadvantage is the incompatibility towards acids. Suitable alternatives for 5,5'-azotetrazolates are derivatives of bis-tetrazolyl-triazenes, which are stable towards acid conditions. Derivates of bis-tetrazolyl-triazenes have also high nitrogen contents and a very high positive heat of formation. Due to their high nitrogen content the main decomposition product is also dinitrogen. In 1910, Hofmann and Hock synthesized bis*(1H*-tetrazol-5-yl)-triazene (**116**) for the first time,[346] which decomposes slowly by simple exposure to air but can be used as precursor producing 1-(1*H*-tetrazol-5-yl)-2-benzylidene hydrazine (**117**) (see end of this Chapter). A great deal better are methylated derivatives of bis*(1H*-tetrazol-5-yl)triazene since they are thermally stable and show lower sensitivities towards outer stimuli. These properties can still be improved by deprotonation of the triazene group forming triazenates. Bis(1-methyltetrazol-5-yl)-triazene is unknown in literature. Bis(2-methyl-tetrazolyl)-*5,5'*-triazene was synthesized accidentally by Hattori *et al.* during the attempt producing methylated 5-hydroxytetrazole, but was not further described.[347] It has been also mentioned in literature as intermediate in synthesis of arylidene-2-methyl-2*H*-tetrazol-5-yl-hydrazones [348] and 1,3,4,6-tetrakis(2-methyltetrazol-5-yl)hexaaza-1,5-diene.[349] In the work of A. Lyakhov deprotonated bis(2-methyl-tetrazol-5-yl)triazene was used as a chelate ligand for Ni(II).[350] In this chapter, facile synthetic routes to several bis(methyltetrazol-5-yl)triazenes, bis(methyltetrazol-5-yl)-triazenates and bis(methyl-tetrazol-5-yl)methyltriazenes are presented, which were fully characterized and also tested with regard to their energetic properties.

10.2 Synthesis

1-Methyl-5-aminotetrazole (**10**) and 2-methyl-5-aminotetrazole (**11**) were synthesized by methylation of 5-aminotetrazole (**2**) using dimethyl sulfate according to literature.[65] The diazotation of **10** was carried out in water, according to **Scheme 10.2**. A matter of particular interest is the sequence of addition. In this case a solution of 1-methyl-5-aminotetrazole in diluted hydrochloric acid is slowly dropped to an ice cold solution of

half an eq. of sodium nitrite. Bis(1-methyltetrazol-5-yl)triazene (**118**) starts to precipitate after a few minutes (from this solution) and was isolated by filtration. Recrystallization from hot water yielded single crystals of the monohydrate suitable for XRD. Bis(2-methyltetrazol-5-yl)triazene (**119**) can also be synthesized via this route, but also, due to its solubility in organic solvents, by the reaction in THF as solvent and *i*-pentylnitrite as the diazotation agent. Recrystallization from hot water yielded also light yellow single crystals. A small amount of single crystals of magnesium bis(2-methyl-tetrazol-5-yl)triazenate dodecahydrate (**126**) was accidentally obtained on working up one of the reactions originally carried out to establish the reaction conditions towards **119** using $MgSO_4$ as drying agent.

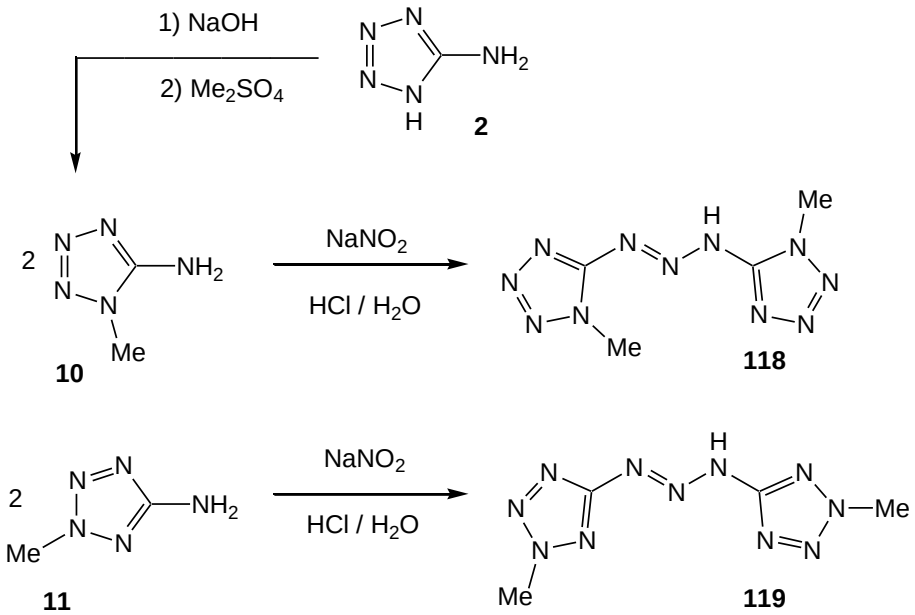

Scheme 10.2 Synthesis of bis(1-methyltetrazol-5-yl)triazene (**118**) and bis(2-methyl-tetrazol-5-yl)triazene (**119**).

Deprotonation (**Scheme 10.3**) of **118** and **119** can be performed in water by adding common bases e.g metal hydroxides or carbonates. The reactions with conc. ammonia solution yielded the water free salts ammonium bis(1-methyltetrazol-5-yl)triazenate (**120**) and ammonium bis(2-methyltetrazol-5-yl)triazenate (**121**). Both compounds are low soluble in water below ~50 °C and crystallize as microcrystalline materials. Many attempts to obtain single crystals for X-ray determination failed. To obtain other crystals containing the bis(methyltetrazol-5-yl)triazenate anions the salts sodium bis(1-methyl-tetrazol-5-yl)triazenate (**122**) and sodium bis(2-methyltetrazol-5-yl)triazenate (**123**) were synthesized by the reaction of **118** and **119** with aqueous sodium hydroxide

solutions. Suitable single crystals could be obtained of **122** by recrystallization from water or a H_2O/MeOH mixture, whereby only the methanol adduct could be determined by X-ray diffraction.

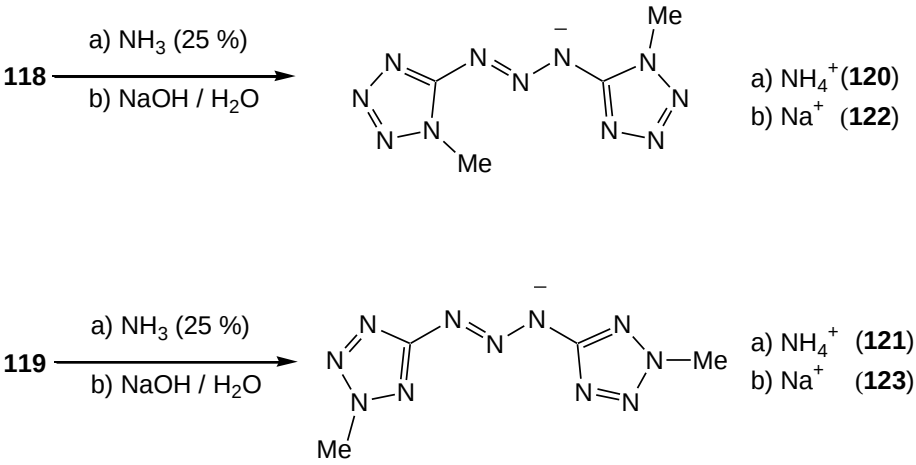

Scheme 10.3 Deprotonation of **118** and **119** using aqueous NH_3 and NaOH solution.

The triazenate unit can be alkylated by common alkylation reagents at one of the marginal nitrogen atoms. This was proofed by the reactions of **122** and **123** with methyl iodide and dimethyl sulfate, respectively, yielding bis(1-methyltetrazol-5-yl)-3-methyl-1-triazene (**124**) and bis(2-methyltetrazol-5-yl)-3-methyl-1-triazene (**125**) depicted in **Scheme 10.4**. The products are insoluble in water, slightly soluble in solvents like MeCN, THF, acetone and good soluble in DMF or DMSO. **124** and **125** could be recrystallized from hot EtOH.

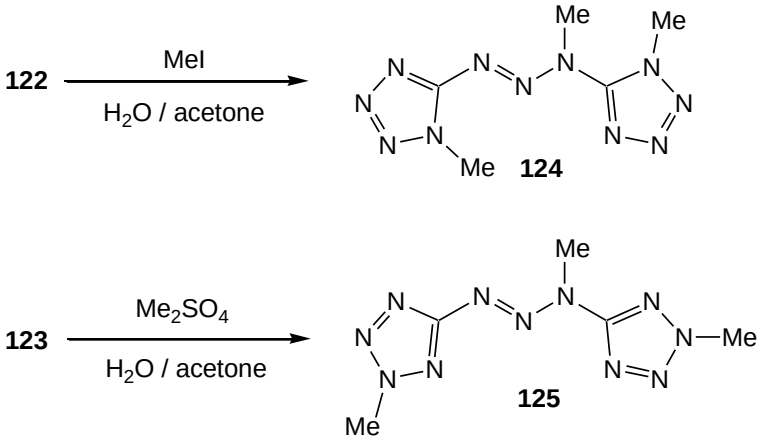

Scheme 10.4 Methylation of **122** and **123** yielding bis(1-methyltetrazolyl)-3-methyl-1-triazene (**124**) and bis(2-methyltetrazolyl)-3-methyl-1-triazene (**125**).

10.3 Crystal Structures

Suitable single crystal of **118**·H_2O, **119**, **122**·MeOH, **124** and **126** were investigated by low temperature X-ray diffraction. A detailed description follows.

10.3.1 Bis(1-methyltetrazol-5-yl)triazene (**118**)

The monohydrate of **118** crystallizes in the orthorhombic space group *Pnma* with four molecules in the unit cell. The density was calculated to be 1.529 g cm^{-3}, which is low in comparison to other 5-N substituted tetrazoles in the literature, such as 5-amino-1*H*-tetrazole,[60] 5-nitro-2*H*-tetrazole,[155] 5-azido-1*H*-tetrazole (Chapter 12) and 5-nitriminotetrazole (Chapter 4). The molecular moiety, which is shown in **Figure 10.1** is affected by a planar setup. All nonhydrogen atoms lie on the mirror plane in the *a*-*c* layer. The water molecule is coordinated via a strong hydrogen bond to the nitrogen atom N5. The structure of the triazene unit follows that expected by the "Lewis structure". The distance between the atoms N6–N7 of 1.264(2) Å corresponds with the bond length of a N=N double bond (1.20 Å), while the N6–N5 distance of 1.331(2) is significantly longer, but also shorter than a N–N single bond (1.48 Å). The geometries of the two tetrazole rings differ considerably. In 5-N substituted tetrazoles, usually the shortest N–N distances are observed between the atoms N2 and N3 (1.297(2) Å) as well as N9 and N10 (1.294(3) Å) which is also the case in the right tetrazole ring of **118**. The other ring shows an opposed trend. In this ring, the N9–N10 distance is found to be the longest (1.354(3) Å). The bond lengths to the external methyl groups have typical values (1.46 Å) found for C–N single bonds.

The packing of **118**·H_2O is characterized by a layer structure along the *c*-*a* plane (**Figure 10.2a**). The layers have distances of ~3.15 Å. Within the layers, strong hydrogen bonds involving the NH group and water molecules, are observed (**Figure 10.2b**). On this account columns along the *c* axis are formed.

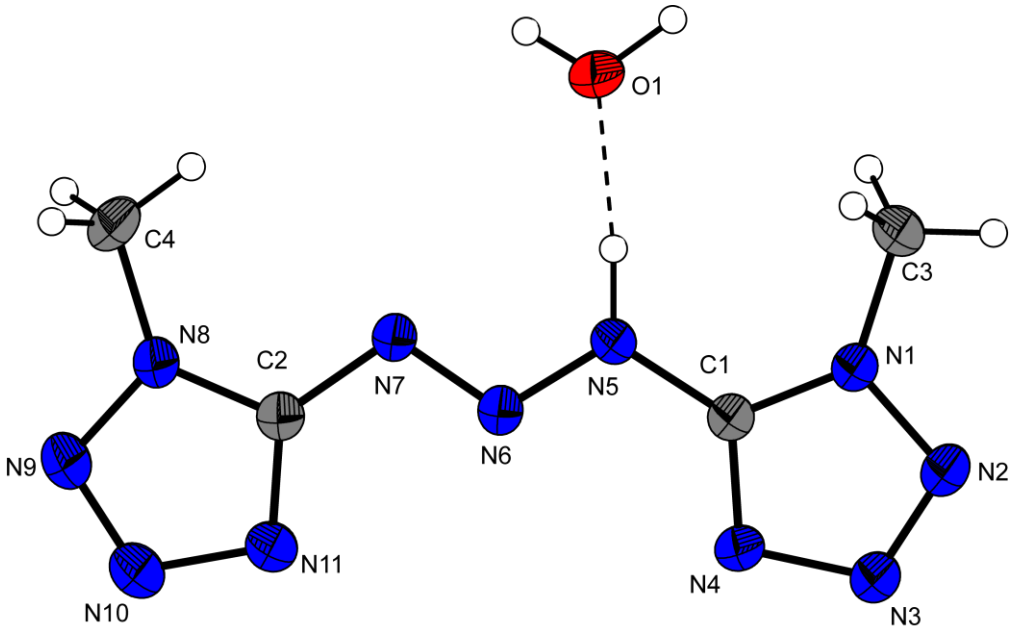

Figure 10.1 Molecular moiety of **118**·H_2O. Ellipsoids of non-hydrogen atoms are drawn at the 50 % probability level.

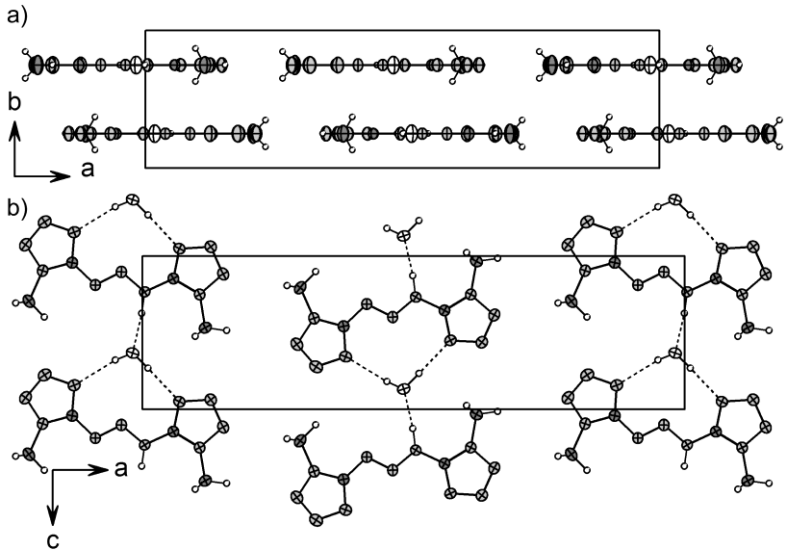

Figure 10.2 View on the unit cell of **118**·H_2O along a) the *c* axis showing the layers, b) the *b* axis showing the connections within the layers. Hydrogen bonds: O1–H1a···N11 = 0.81(3), 2.10(3), 2.902(3) Å, 172(3)°; N5–H5···O1 = 0.94(3), 1.76(3), 2.703(2) Å, 175(3)°; O1–H1b···N1 = 0.94(4), 1.99(4), 2.934(3) Å, 178(4)°.

10.3.2 Bis(2-methyltetrazol-5-yl)triazene (**119**)

119 crystallizes in the monoclinic space group $I2/a$ with eight molecules in the unit cell and a slightly higher density of 1.532 g cm^{-3} in comparison to **118**. The molecular structure, depicted in **Figure 10.3** in terms of the bond lengths is similar to that observed for **118**. Exact bond distances can be found in **Table 10.1**. However, **119** is not completely planar. While the triazene unit is found to be planar (torsion angle C1–N5–N6–N11 = 179.7(2)°), the tetrazole rings are slightly out of phase, which can be seen on the N10–C3–C1–N4 torsion angle of 12.3(4)°.

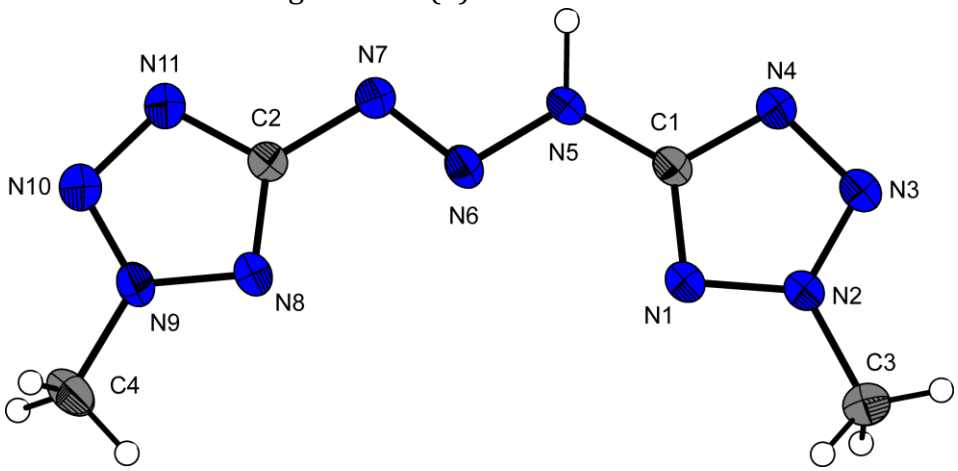

Figure 10.3 Molecular moiety of **119**. Ellipsoids of non-hydrogen atoms are drawn at the 50 % probability level.

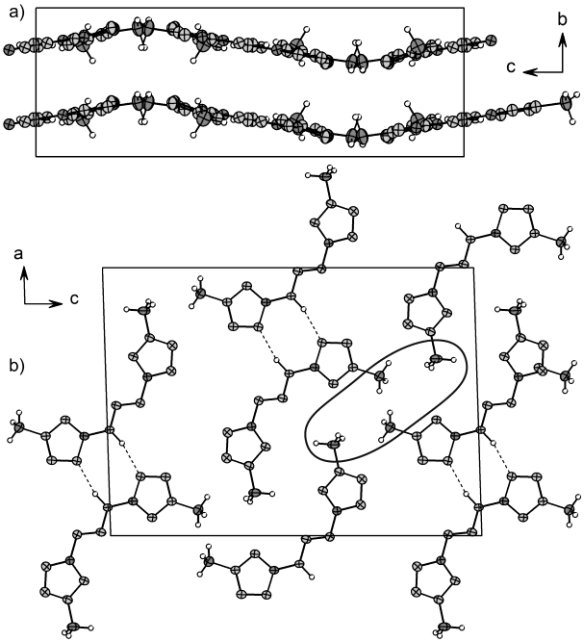

Figure 10.4 View on the unit cell of **119** along a) the *a* axis; b) the *b* axis illustrating the formation of dimers.

On inspection along the a axis wave like pattern can be detected (**Figure 10.4a**). The discrete layers are connected by two kinds of interactions. On the one hand dimers are formed by the O1–H1···N7^{i} hydrogen bond (0.79(3) Å, 2.05(3) Å, 2.838(2) Å, 178(3)°; (i) –1–x, y, 0.5–z), on the other hand hydrophobic areas are build by the interaction of the methyl groups (marked in **Figure 10.4b**).

10.3.3 Sodium bis(1-methyltetrazol-5-yl)triazenate · MeOH

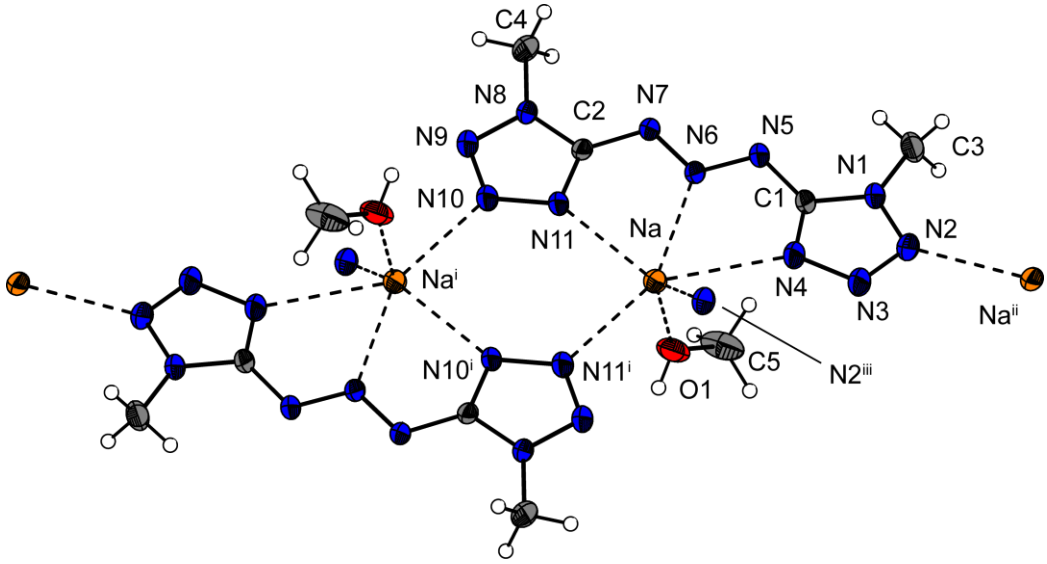

Figure 10.5 View on the dimers in **122**·MeOH. Selected distances (Å): Na–O1 = 2.475(2), Na– N11 = 2.498(2), Na–N6 = 2.640(2), Na–N4 = 2.766(2), Na–N2^{iii} = 2.668(2), O1–C5 = 1.561(3); (i) 2–x, –y, 1–z; (ii) 2–x, 0.5+y, 1.5–z; (iii) 2–x, –0.5+y, 1.5–z.

122·MeOH crystallizes in the monoclinic space group $P2_1/c$ with four molecules in the unit cell and a calculated density of 1.327g cm^{-3}. The sodium cations are coordinated sixfold by an distorted pentagonal-pyramidal coordination sphere. The bis(1-methyl-tetrazol-5-yl)triazenate anions act as tridentate ligands by the coordination of its atoms N4, N6, and N11. The fourth coordination position is filled by the methanol oxygen atom O1, while the fifth and sixth positions are filled by the nitrogen atoms N2 and N11 of two neighbored bis(1-methyl-tetrazol-5-yl)triazenate. Here dimers (**Figure 10.5**) can be detected as a structural motive.

Single crystals of **122** were obtained from hot water and measured at the Oxford Xcalibur3 diffractometer. However, the data set could not be refined completely. This

may be a consequence that the methyl groups are partly disordered and also huge amounts of partly strong disordered crystal water are included in the packing. Therefore a discussion of this structure with a sum formula $C_{12}H_{48}N_{33}Na_3O_{15}$ is abdicated. However the wR_2 value could be lowered to ~14 % and the coordination of two of the sodium atoms representing a distorted octahedron is depicted in **Figure 10.6**.

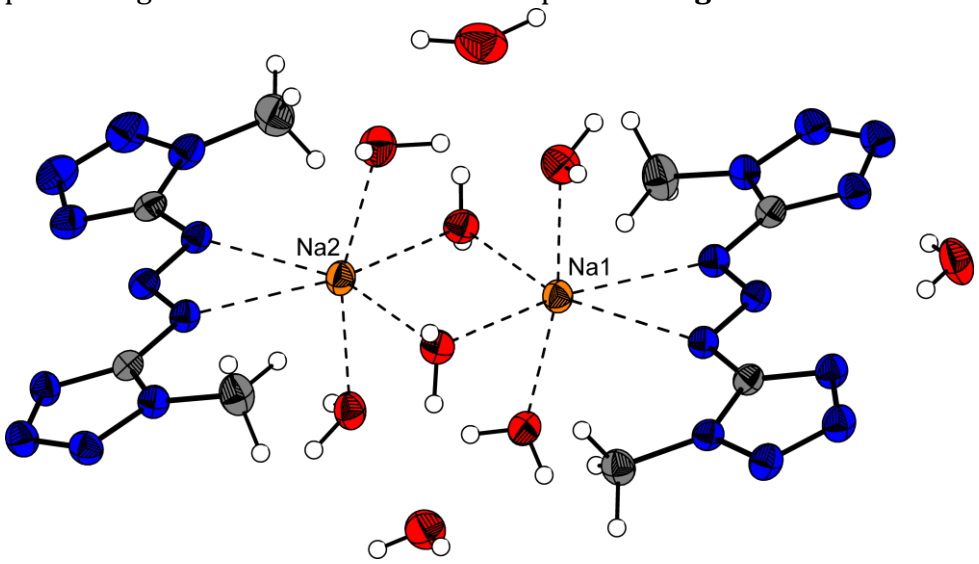

Figure 10.6 A selected view on the coordination sphere of the sodium atoms of **122**·5H_2O. Several water molecules and one anion and cation were removed for better clearness. Selected crystallographic data: a = 6.865(1) Å, b = 11.929(2) Å, c = 27.155(5) Å, α = 80.87(3)°, β = 88.48(3)°, γ = 76.45(3)°, V = 2134.5(7), Z = 2, Å^3, ρ = 1.50 g cm^{-3}.

10.3.4 Bis(1-methyltetrazol-5-yl)-1-methyl-triazene (**124**)

124 crystallizes in the orthorhombic space group $Pca2_1$ with eight molecules in the unit cell. For better clearness only one molecule of the asymmetric unit is shown in **Figure 10.7**. Although no hydrogen bonds can be formed, the highest density of 1.559 g cm^{-3} is be observed. The methyl group bonded at the nitrogen atom N5 does not influence the geometry of the triazene unit. The distances N5–N6 (1.324(5) Å) and N6–N7 (1.269(5) Å) are similar to the other structures discussed in this work. Also the C–N bonds of the triazene group to the tetrazole rings are not affected. While the atoms C1, N5, N6, N7 and C2 lie in one plane, the tetrazole rings are twisted 16.1° (torsion angle N5–C2–C1–N4 molecule) as well as 33.9° to each other.

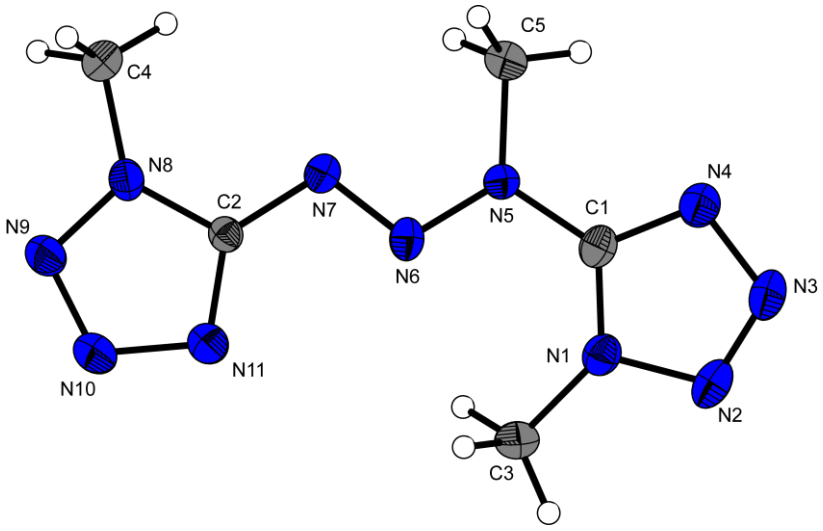

Figure 10.7 Molecular moiety of **124**. Ellipsoids of non-hydrogen atoms are drawn at the 50 % probability level.

A view on the unit cell along the *b* axis is shown in **Figure 10.8**. Thereby alternating columns can be found, which are mainly connected by "Van der Waals" forces.

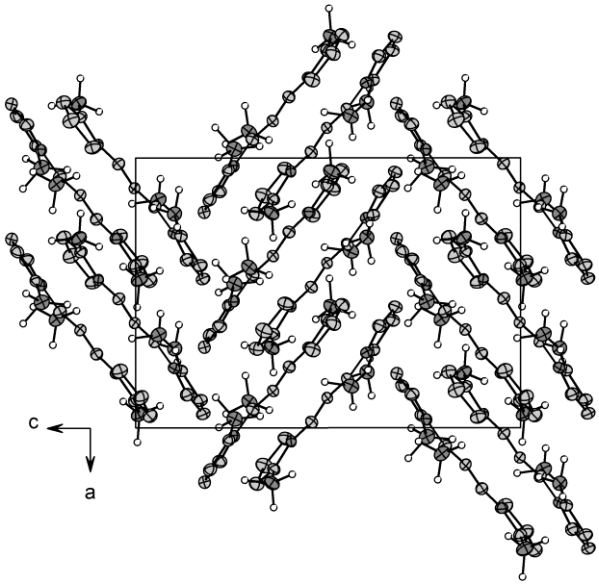

Figure 10.8 View on the unit cell of in **124** along the *b* axis.

10.3.5 Magnesium bis(2-methyltetrazol-5-yl)triazenate (**126**)

Single crystals of **123** could not have been measured since the crystal size was too small for reaching a adequate dataset. However, suitable crystals of magnesium bis(2-methyl-tetrazol-5-yl)triazenate dodecahydrate (**126**) were accidentally obtained on a different work up procedure of **119** using $MgSO_4$ as drying agent. **126** crystallizes with one

molecular moiety in the unit cell in the triclinic space group *P*–1. The bis(2-methyl-tetrazol-5-yl)triazenate anions do not participate in the coordination of the magnesium cations (**Figure 10.9**). These are surrounded by six water molecules building a regular octahedral coordination sphere with distances between 2.05 and 2.10 Å.

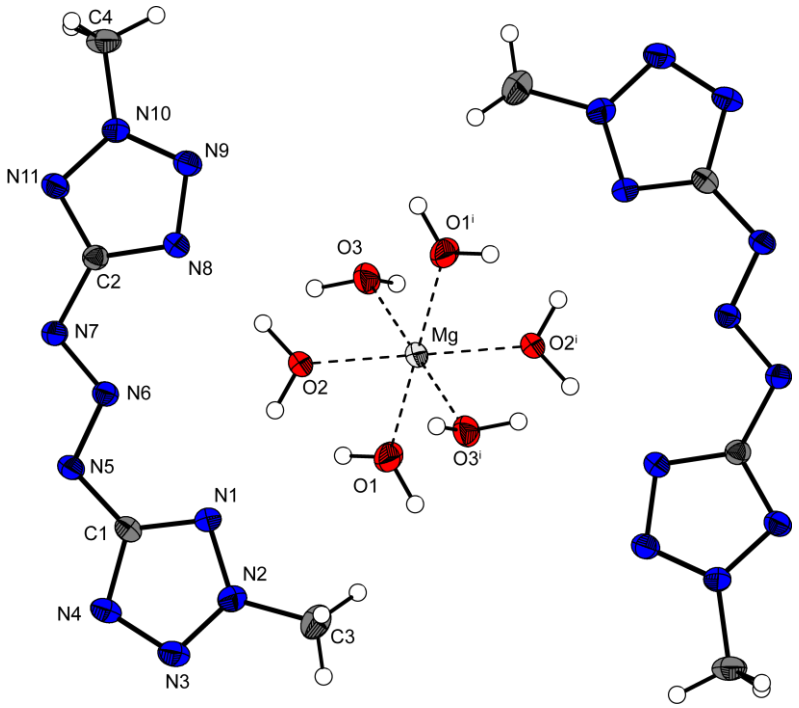

Figure 10.9 View on the molecular moiety of **126**. Non-coordinated crystal water was removed for better clearness. Selected distances (Å): Mg–O1 = 2.050(1), Mg–O2 = 2.097(1), Mg–O3 = 2.071(1); selected angles (°): O1–Mg–O2 = 90.04(5), O1–Mg–O3 = 89.66(6); (i) 1–x, –y, –z.

Table 10.1 Bond distances [Å] of **118**·H_2O, **119**, **122**·MeOH, **124** and **126**.

Atoms	**118**·H_2O	**119**	**122**·MeOH	**124** (a)	**124** (b)	**126**
N1–N2	1.354(2)	1.340(2)	1.362(2)	1.360(5)	1.357(5)	1.333(2)
N2–N3	1.297(2)	1.308(2)	1.372(2)	1.277(6)	1.292(5)	1.311(2)
N3–N4	1.364(2)	1.329(2)	1.378(2)	1.359(5)	1.364(5)	1.333(2)
N5–N6	1.331(2)	1.336(2)	1.352(2)	1.343(5)	1.328(5)	1.309(2)
N6–N7	1.264(2)	1.263(2)	1.313(2)	1.282(5)	1.270(5)	1.305(2)
N8–N9	1.351(2)	1.318(2)	1.412(2)	1.341(4)	1.355(5)	1.337(2)
N9–N10	1.294(3)	1.330(2)	1.311(2)	1.307(5)	1.293(5)	1.312(2)
N10–N11	1.354(3)	1.330(2)	1.394(2)	1.364(5)	1.356(5)	1.322(2)

N1–C1	1.334(3)	1.325(2)	1.396(2)	1.330(5)	1.348(5)	1.338(2)
N4–C1	1.325(3)	1.345(2)	1.380(2)	1.313(5)	1.300(5)	1.356(2)
N5–C1	1.372(3)	1.375(2)	1.385(2)	1.400(5)	1.389(5)	1.382(2)
N7–C2	1.395(3)	1.404(2)	1.430(2)	1.383(5)	1.399(5)	1.386(2)
N8–C2	1.329(3)	1.329(3)	1.345(2)	1.347(6)	1.346(5)	1.334(2)
N11–C2	1.323(3)	1.347(2)	1.383(2)	1.333(5)	1.314(5)	1.358(2)
N1(2)–C3	1.458(3)	1.462(3)	1.539(3)	1.468(5)	1.460(5)	1.455(3)
N8(9)–C4	1.452(3)	1.458(3)	1.487(2)	1.447(5)	1.448(5)	1.446(2)
N5–C5				1.455(5)	1.465(4)	

10.4 Spectroscopy

Multinuclear NMR spectroscopy: NMR spectroscopy is a valuable method to identify bis(methyltetrazol-5-yl)triazenes. All Shifts are given with respect to TMS (^{1}H, ^{13}C) and CH_3NO_2 (^{14}N, ^{15}N) as external standards. d_6-DMSO (**118**, **119**, **120**, **121** and **123**), D_2O (**122**) and $CDCl_3$ (**124**, **125**) were used as solvents. The ^{1}H NMR spectra of **118** and **119** measured in d_6-DMSO show singlets at 4.04 ppm and 4.32 ppm, respectively. The hydrogen atom at the triazene unit in **118** provides no visible signal, because of fast proton exchange in polar solvents like DMSO. In **119** it is found weakly at 14.10 ppm. Deprotonation of the triazene unit decrease the hydrogen resonances to higher fields (**120**: 3.86, **121**: 4.20 ppm). Methylation affords a down field shift and also a split into two resonances (**124**: 4.12, 4.11 ppm, **125**: 4.38, 4.39 ppm). The ^{13}C NMR resonances of the methyl carbon atoms and the tetrazole carbon in **118** and **119** are found at 34.9 ppm and 155.2 ppm (**118**) as well as 40.5 and 162.9 ppm (**119**). In the ammonia salts the methyl resonances are found at higher fields (**120**: 33.1, **121**: 39.7) while the tetrazole carbon shifts significantly increase to 161.9 (**120**) and 173.7 (**121**). In the case of the methylated compounds **124** and **125**, two signals are observed for the tetrazole carbon atoms (**124**: 157.9, 154.2; **125**: 169.5 and 165.0) whereby the higher ones can be assigned to the carbon atoms closer to the introduced methyl group. ^{14}N NMR spectroscopy of bis(methyltetrazol-5-yl)triazenes yields featureless spectra due to the quadrupole moment of the ^{14}N core. Solely in the ^{14}N spectra of **120** and **121** the ammonia nitrogen atoms could be detected at –358 ppm (**120**) and –359 ppm (**121**). ^{15}N NMR spectroscopy yields sharp signals, however, it is hard to measure due to the low frequency of the ^{15}N core. (0.3 %) Therefore, high concentrations are required,

which is hard to fulfill for the investigated compounds due to their low solubility. To exemplify, the proton coupled ^{15}N NMR spectra of compound **119** and **125** are shown in **Figure 10.10**. The assignments are based on the analysis of the ^{15}N–^{1}H coupling constants and on comparison with known tetrazole derivatives.

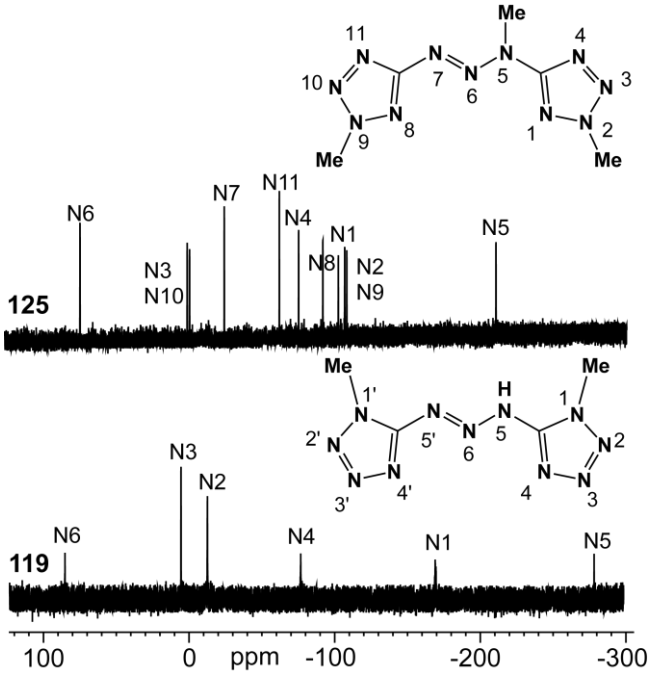

Figure 10.10 ^{15}N NMR spectra of **119** and **125**. δ(ppm): (**119**): 85.2 (N6), 5.54 (N3/N3'), –76.6 (N4), –12.7 (N2/N2', q, $^{3}J_{NH}$ = 1.8 Hz), –168.7 (N1, q, $^{2}J_{NH}$ = 2.1 Hz), –265.0 (N5/N5'); (**125**): 72.6 (N6), –0.6 (N3, q, $^{3}J_{NH}$ = 1.8 Hz), –2.2 (N10, q, $^{3}J_{NH}$ = 1.8 Hz), –25.8 (N7), –63.5 (N11), –76.6 (N4), –93.2 (N8, q, $^{3}J_{NH}$ = 1.8 Hz), –103.7 (N1, q, $^{3}J_{NH}$ = 1.8 Hz), –108.1 (N9, q, $^{2}J_{NH}$ = 2.2 Hz), –109.5 (N2, q, $^{2}J_{NH}$ = 2.3 Hz), –211.3 (N5, q, $^{2}J_{NH}$ = 2.4 Hz).

Vibrational Spectroscopy: The investigated compounds **118–125** can be easily identified using IR and Raman spectroscopy. The Raman spectra of **118** and **119** are dominated by the asymmetric stretching mode $\nu_{asym}(N{=}N_{triazene})$ providing signals in the range of 1430–1460 cm^{-1}. This vibration is lower in energy in the spectra of the deprotonated triazenes **120**–**123**. The IR spectra contain more vibrations with high intensities. Of course, the O–H vibration caused by the crystal water in **118**, **122** and **123** and the symmetric bending mode of the ammonia cations in **120** and **121** can be observed as broad signals above 3150 cm^{-1}. The vibrational spectra contain further vibrations: 3080–2980 cm^{-1} [$\nu_{sym}(CH_3)$], 3430–3140 cm^{-1} [$\nu_{sym/asym}(NH_4^+)$], 1680 –1550 [ν(N–H)], 1550–1350 [ν, tetrazole ring, $\nu_{as}(CH_3)$], ~1380 [$\nu(CH_3)$], 1350–700 [ν(N1–C1–N4), ν(N–N), ν(N–H), ν, tetrazole ring], < 700 [ν, δ_{oop} (N–H)].

UV/VIS spectroscopy: The UV-VIS spectra of compounds (**118–125**) were measured in diluted methanol solutions. In general the observed resonances are n→π* transitions. All substances show absorptions below the visible wavelength region. These results are consistent with the visible impressions since all substances are colorless or slightly yellow colored. The UV-VIS spectrum of **118** contains one absorption at 315 nm. The two corresponding salts **120** and **122** show both a maximum peak red shifted about 15 nm. In addition, the spectra of **120** and **122** include a shoulder at 240 nm. The absorption of the methylated compound **124** is blue shifted towards 299 nm. **119** shows a maximum value for the absorption at 291 nm, whereby a shoulder can be found at 244 nm. The spectrum of salts **121** and **123** is nearly equal to this observed for **119**. The resonance of **125** is blue shifted to 281 nm.

Mass spectrometry: In all DEI⁺ mass spectra of the neutral compounds (**118**, **119**, **124** and **125**) the mass peaks at *m/z* 209 and 223, respectively, could have been detected. In the spectra of the 1-methyl-tetrazolylderivatives the 1-methyl-5-azotetrazolyl radical was observed with a peak at *m/z* 111 as a main fragmentation product. In **Scheme 10.5**, one possible fragmentation pathway is shown, which is comparable to that of azotetrazoles.[57]

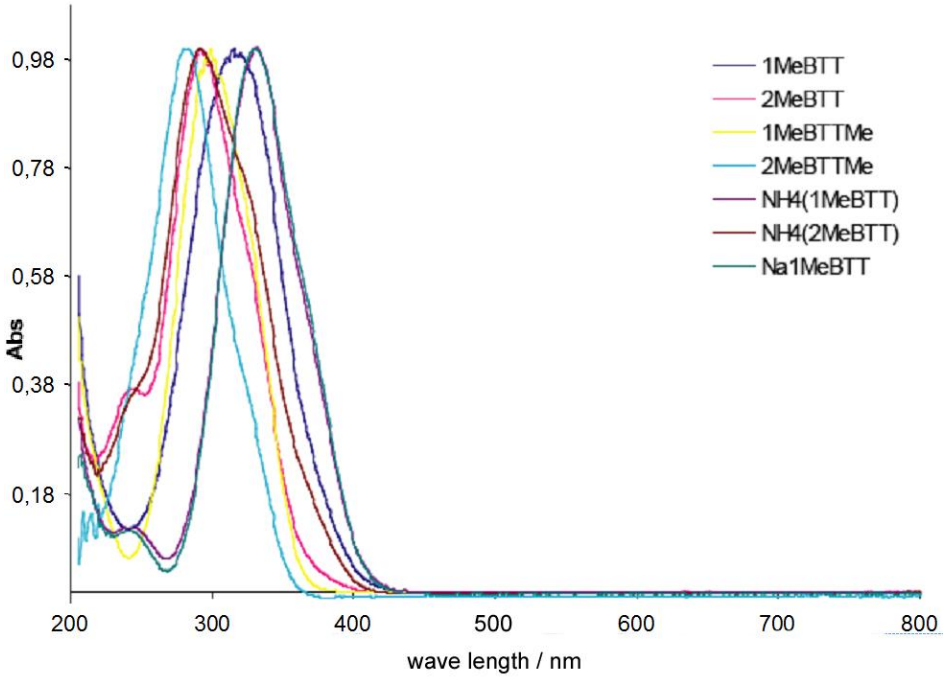

Figure 10.11 UV-VIS spectra of compounds **118**–**122** as well as **124** and **125**; values are normalized to 1.

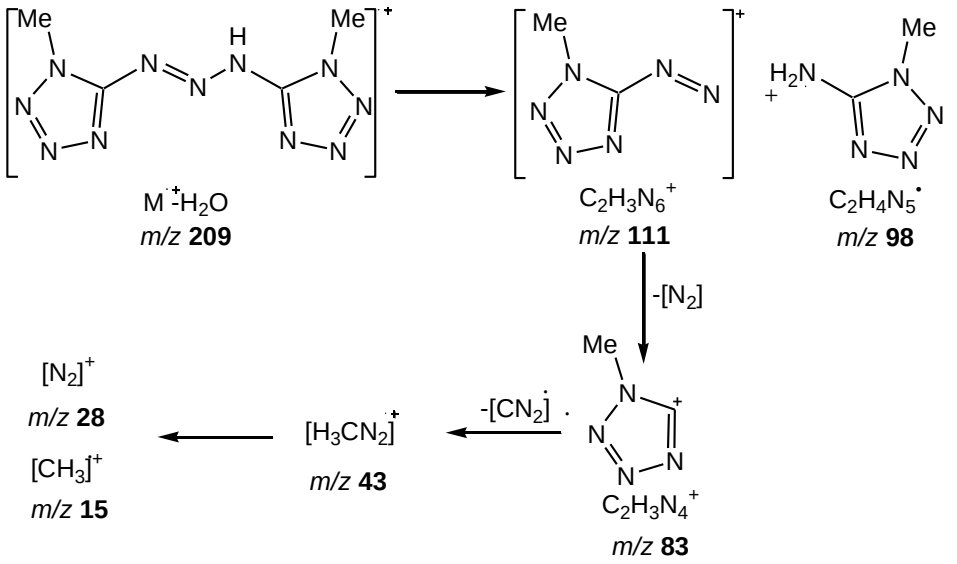

Scheme 10.5 Possible fragmentation pathway of **118**.

119 shows analogue fragmentation than that of **118** (**Scheme 10.5**). An additional peak at 181 *m/z* was detected, which is generated by the loss of dinitrogen ($M^+–N_2$). Again N_2^+ (28 *m/z*) and CH_3^+ (15 *m/z*) arise as further intensive fragmentation products. The ammonium salts were measured in the FAB^- mode, in which the mass peak *m/z* 208 of the anion could have been detected.

10.5 Energetic Properties

10.5.1 Differential Scanning Calorimetry

DSC measurements to determine the melt- and decomposition temperatures of **118–125** were performed in covered Al-containers containing a hole in the lid with a nitrogen flow of 20 mL min^{-1} on a Linseis PT10 DSC at a heating rate of 5 °C min^{-1}. The DSC plots in **Figure 10.12** show the thermal behavior of ~1.5 mg energetic material in the 50–400°C temperature range. Temperatures are given as onset temperatures. In general it can be seen that the position of the methyl group does not influence the thermal behavior a lot. The neutral compounds **118** and **119** melt under exothermic decomposition at temperatures of 182 °C and 183 °C, respectively. Deprotonation increase the decomposition temperatures, which can be seen on the curves of **120**–**123**. **120** decomposes without melting above a temperature of 236 °C. On the other hand

ammonium salt **121** decomposes at lower temperatures of 205 °C. However, both nitrogen-rich salts decomposes above 200 °C, which is one of the most important criteria of new energetic materials for use in technical applications. The sodium salt **122** even decomposes not until 340 °C, which is more than 100 °C higher comparing with the corresponding ammonium salt. However, sodium salt **123** loses its five crystal water molecules in two steps at 74 and 100 °C followed by the decomposition above 256 °C. The methylation products **124** and **125** show discrete melting points at 133 °C and 135 °C, respectively, followed by a broad decomposition area starting at 160 °C (**124**) as well as 200 °C (**125**). These thermal behaviors are caused by that no classical hydrogen bonds could be formed in the structures of **124** and **125**.

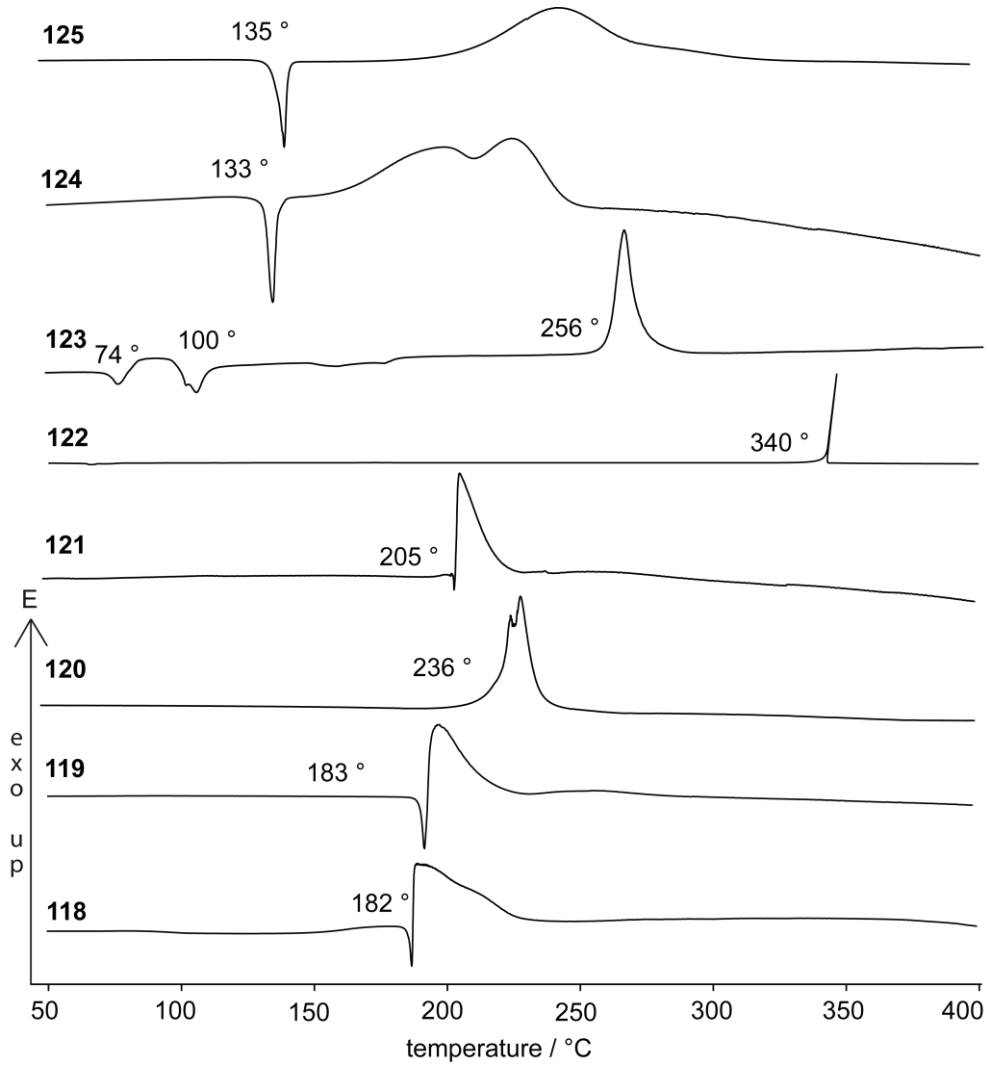

Figure 10.12 DSC thermograms (exo-up) of compounds **118–125** (heating rate of 5 °C min^{-1}).

10.5.2 Bomb Calorimetry

The heats of combustion of compounds **118–121**, **124** and **125** were determined experimentally using a Parr 1356 bomb calorimeter (see introduction). To achieve better combustion, the samples (~200 mg) were pressed with a defined amount of benzoic acid (~800 mg) forming a tablet. The experimental results of the constant volume combustion energy ($\Delta_c U$) of the salts are summarized in **Table 10.2**. The standard molar enthalpy of combustion ($\Delta_c H°$) was derived from $\Delta_c H° = \Delta_c U + \Delta nRT$ ($\Delta n = \Delta n_i$ (products, g) – Δn_i(reactants, g); Δn_i is the total molar amount of gases in the products or reactants). The enthalpy of formation, $\Delta_f H°$, for each of the compounds was calculated at 298.15 K using Hess' law and the following combustion reactions.

118: $C_4H_9N_{11}O\ (s) + 5.75\ O_2\ (g) \longrightarrow 4\ CO_2\ (g) + 4.5\ H_2O\ (l) + 5.5\ N_2\ (g)$

119: $C_4H_7N_{11}\ (s) + 5.75\ O_2\ (g) \longrightarrow 4\ CO_2\ (g) + 3.5\ H_2O\ (l) + 5.5\ N_2\ (g)$

120, **121**: $C_4H_{10}N_{12}\ (s) + 6.5\ O_2\ (g) \longrightarrow 4\ CO_2\ (g) + 5\ H_2O\ (l) + 6\ N_2\ (g)$

124, 125: $C_5H_9N_{11}\ (s) + 7.25\ O_2\ (g) \longrightarrow 5\ CO_2\ (g) + 4.5\ H_2O\ (l) + 5.5\ N_2\ (g)$

All investigated tetrazoles are strongly endothermic, which was expected by comparison with the literature ($\Delta_f H°$ **118**·H_2O: +514, **119**: + 792, **120**: + 650, **121**: + 647, **124**: + 686, **125**: + 586 kJ mol^{-1}). The influence of crystal water can be seen at the lower $\Delta_f H°$ of **118**·H_2O, in comparison with **119**.

From the experimentally determined heats of formation and densities obtained from single crystal structure X-ray diffraction, various thermochemical properties have been calculated using the EXPLO5 software (see below) and are summarized in **Table 10.2**.

10.5.3 Sensitivities

Since the investigated bis(methyltetrazol-5-yl)triazenes **118–121**, **124** and **125** are energetic compounds with high nitrogen contents, the sensitivities toward friction and impact were tested. Powdered (grain size 75–125 µm) **118** and **119** are sensitive towards impact (**118**: 3 J, **119**: 2.5 J). However, monohydrate **118** is only very weak sensitive towards friction (360 N), while **119** is very friction sensitive (70 N). The ammonium salts **120** (IS: 7.5 J, FS: 360 N) and **121** (IS: 4 J, FS: > 360 N) are lower sensitive than their corresponding neutral derivatives. Interestingly, also the methyl

derivatives **124** and **125** containing a higher carbon and hydrogen content are very sensitive towards impact (**124**: 3 J, **125**: 3 J). Again only the 2-methyltetrazol-5-yl derivative **125** is very sensitive towards friction (20 N) while **124** is nearly insensitive (360 N). According to the UN Recommendations on the Transport of Dangerous Goods, compounds **118**·H_2O, **119**, **124** and **125** are classified as "very sensitive" regarding the impact sensitivity, while **120** and **121** are classified "only" as sensitive. Regarding the friction sensitivities **121** is classified as insensitive, **118**, **120** and **124** are less sensitive and **119** and **125** are classified as "very sensitive". Therefore, all derivatives should only be handled with care and appropriate precaution. Thus compound **120** is not only most promising in terms of the thermal stability but also in terms of the sensitivities.
Electrostatic sensitivity tests of **120** were carried out using an electric spark tester ESD 2010EN. The electrical spark sensitivity of microcrystalline (75–125 μm particle size) **120** was determined to be 1.2 (±0.1) J.

10.5.4 Detonation Parameters

Some detonation parameters such as pressure, temperature, velocity, the heat of explosion, and the amount of gaseous decomposition products were calculated with the EXPLO5 V5.02 software. The results are given in **Table 10.2**. The most useful values for classifying new explosives are the detonation pressure and detonation velocity. In comparison with common explosives such as TNT (Trinitrotoluene, $p_{C\text{-}J}$ = 202 kbar, $V_{Det.}$ = 7150 m s^{-1}), compounds **118–121**, **124** and **125** show higher detonation pressures (**118**·H_2O: 209, **119**: 221, **120**: 248, **121**: 248, **124**: 220, **125**: 215 kbar). Due to the correlation of the detonation pressure and velocity, the same trend can be found in the detonation velocities. (**118**·H_2O: 7825, **119**: 7982, **120**: 8484, **121**: 8484, **124**: 8014, **125**: 7961 m s^{-1}). Unfortunately all compounds show lower values than those of commonly used RDX (hexogen, $p_{C\text{-}J}$ = 347 kbar, $V_{Det.}$ = 8750 m s^{-1}). This may be a reason of the lower densities and that the compounds contain no oxygen resulting in a strongly negative oxygen balance. Therefore, their use as solid propellants was investigated by calculating the specific impulse.

Table 10.2 Physico-chemical properties of **118–121**, **124** and **125**.

	118·H_2O	**119**	**120**	**121**	**124**	**125**
Formula	$C_4H_9N_{11}O$	$C_4H_7N_{11}$	$C_4H_{10}N_{12}$	$C_4H_{10}N_{12}$	$C_5H_9N_{11}$	$C_5H_9N_{11}$
Molecular Mass [g mol^{-1}]	227.19	209.17	226.20	226.20	223.20	223.20
Impact sensitivity [J][a]	3	2.5	7.5	4	3	3
Friction sensitivity [N][b]	360	70	360	> 360	360	20
N [%][c]	67.82	73.66	74.31	74.31	69.03	69.03
Ω [%][d]	–80.99	–87.97	–91.95	–91.95	–103.94	–103.94
Combustion	good	good	good	good	moderate	moderate
$T_{dec.}$ [°C][e]	182	183	236	205	175	200
Density [g cm^{-3}][f]	1.528	1.532	1.6 (exp.)	1.6 (exp.)	1.559	1.55(est.)
$-\Delta U_{comb}$ [cal g^{-1}][g]	3556	3861	3867	3864	4225	4206
$-\Delta H_{comb}$° [kJ mol^{-1}][h]	3375	3367	3654	3651	3940	3922
$\Delta_f H_m$° [kJ mol^{-1}][i]	514	792	650	647	686	668
calculated values using EXPLO5:						
$-\Delta_E U$° [kJ kg^{-1}][j]	3934	4450	3714	3701	3840	3759
T_E [K][k]	2843	3136	2626	2620	2704	2673
$p_{C\text{-}J}$ [kbar][l]	209	221	248	248	220	215
$V_{Det.}$ [m s^{-1}][m]	7825	7982	8484	8484	8014	7961
Gas vol. [L kg^{-1}][n]	799	760	816	816	757	757

[a] BAM drophammer; [b] BAM friction tester; [c] Nitrogen content; [d] Oxygen balance; [e] Temperature of decomposition by DSC (β = 5 °C); [f] estimated from a structure determination; [g] Experimental (constant volume) combustion energy; [h] Experimental molar enthalpy of combustion; [i] Molar enthalpy of formation; [j] Energy of Explosion; [k] Explosion temperature; [l] Detonation pressure; [m] Detonation velocity; [n] Assuming only gaseous products.

10.5.5 Specific Impulse

Whereas the performance of HEs can be related to heat of explosion (U_{Ex}), detonation pressure (p) and detonation velocity ($V_{Det.}$), the performance of rocket/missile propellants is best characterized by their specific impulse (I_{sp}), as mentioned in the introduction. Moreover, for gun propellants, erosivity is an additional concern. Also lower reaction temperatures and a high N_2/CO ratio of the reaction gases are desirable. Equally important, an increase of the I_{sp} of only 20 s would be expected to increase the

payload or range by ~100 %. Moreover, smokeless combustion, which is an inherent feature of high-nitrogen compounds, is not only of environmental but particularly of strategic interest since localization of the gun, missile or rocket is much more difficult.

In order to evaluate the properties of the most suitable compound **120** as potential energetic component in gun or missile propellants we calculated the specific impulses and combustion temperatures under isobaric conditions at 45 and 70 bar, representative for rocket and gun propellants, using the EXPLO5 code. **Table 10.3** summarizes the computed isobaric combustion temperatures (T_c, the lower the better for gun-propellants), the specific impulses (I_{sp}) and the molar N_2/CO ratios for mixtures of **120** with ADN and three typical conventional gun-propellants (single-, double-, triple-base) at 70 bar.

Table 10.3 Computed propulsion parameters for formulations of **120** with ADN and for single-, double- and triple-base propellants (70 bar chamber pressure).

O [a]	F [b]	ρ / g cm^{-3}	Ω / %	T_c / K	I_{sp} / s	N_2/CO
ADN [c]	**120**					
10	90	1.621	–80.17	1843	207	7.96
20	80	1.642	–68.40	1853	208	3.81
30	70	1.662	–56.62	1865	209	2.43
40	60	1.683	–44.85	2016	214	2.16
50	50	1.704	–33.08	2384	231	2.61
60	40	1.725	–21.30	2741	243	3.43
70	30	1.746	–9.53	3037	251	5.82
80	20	1.766	2.25	3035	244	21.19
90	10	1.787	14.02	2649	227	316.60
NC [d]		1.66	–30.2	2750	232	0.3
NC [d]/NG (50:50)		1.63	–13.3	3287	248	0.7
NC [d]/NG [e]/NQ [f] (25:25:50)		1.70	–22.0	2663	235	1.4

[a] oxidizer; [b] fuel; [c] ADN, ammonium dinitramide; [d] NC-13.3 (N content 13.3%); [e] NG, nitroglycerine; [f] NQ, nitroguanidine.

Whereas single-base propellants are used in all guns from pistols to artillery weapons, the more powerful (see I_{sp}) double-base propellants are commonly used in pistols and mortars. The disadvantage of double-base propellants is the excessive erosion of the gun barrel (see N_2/CO ratio) by the much higher flame temperatures, and the presence of a muzzle flash (fuel-air explosion of the combustion products). In order to reduce erosion and muzzle flash, triple-base propellants with up to 50% nitroguanidine are used in tank guns, large caliber guns and naval guns. However, the performance of triple-base propellants is lower than that of double-base propellants. A formulation of **120** with ADN (**120**: ADN = 30:70) shows a suitable combustion temperature (3037 K, between single and double based propellants), with an excellent molar N_2/CO ratio of 5.82 (which are usually 0.5 for conventional propellants). The computed specific impulse of 251 s for such a mixture make a possible application of **120** as promising energetic component in erosion-reduced gun propellants very interesting. **Table 10.4** summarized the propulsion parameters for formulations of **120** with ADN at 45 bar pressure and for a stoichiometric formulation of AP/Al which is presently used in large booster motors (e.g. ARIANE5, Space Shuttle).

Table 10.4 Computed propulsion parameters for formulations of **120** with ADN and for an AP/Al formulation for comparison (45 bar chamber pressure).

O	F	ρ / g cm^{-3}	Ω / %	T_c / K	I_{sp} / s
ADN [a]	**120**				
10	90	1.621	–80.17	1835	200
20	80	1.642	–68.40	1845	201
30	70	1.662	–56.62	1857	203
40	60	1.683	–44.85	2016	214
50	50	1.704	–33.08	2383	224
60	40	1.725	–21.30	2735	235
70	30	1.746	–9.53	3016	241
80	20	1.766	2.25	2706	236
90	10	1.787	14.02	2640	218
AP [b]	Al [c]				
70	30	2.178	–2.9	4199	232

[a] ADN, ammonium dinitramide; [b] ammonium perchlorate; [c] aluminum.

10.5.6 Decomposition Experiments

A specially equipped IR cell was loaded each with 200 mg of **118**, **119** and their corresponding ammonia salts **120** and **121**. After heating the cell to 300 °C, the resulting combustion products were analyzed via IR spectroscopy.

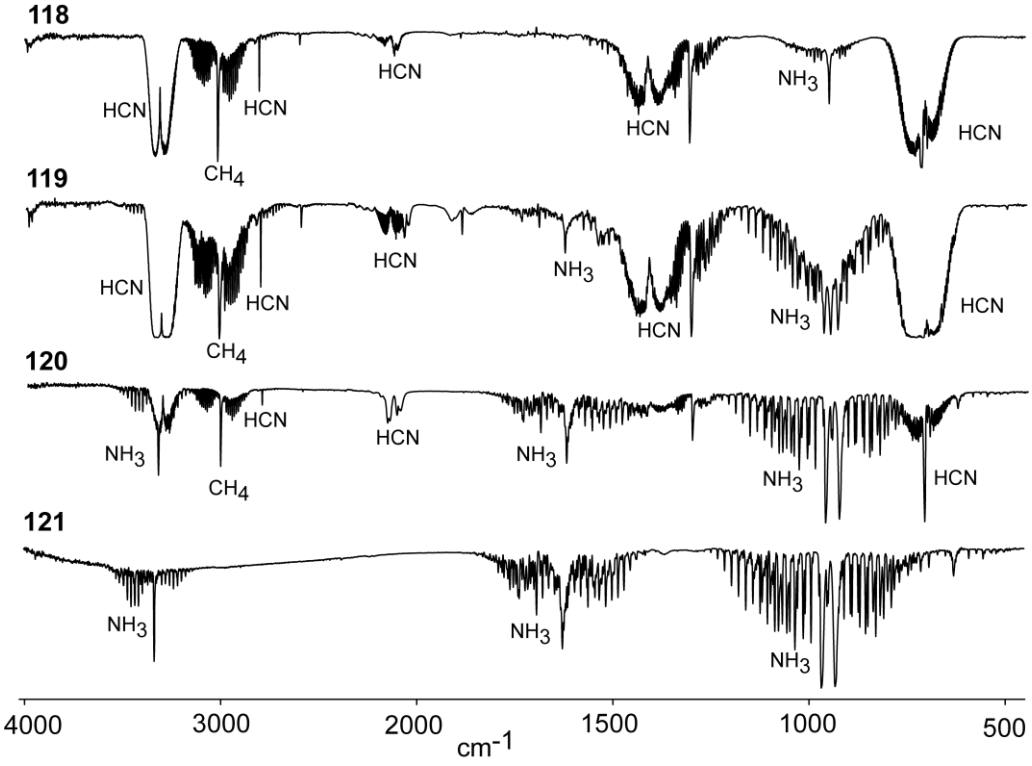

Figure 10.13 Gas IR spectra of thermal decomposition products of **118**–**121**.

As it can be seen in **Figure 10.13** the IR active gaseous decomposition products are hydrogen cyanide (HCN), methane (CH_4) and ammonia (NH_3). The IR spectrum of **118** shows intensive resonances of HCN at 3300–3400 cm^{-1} and 1300–1500 cm^{-1}. In the region of 750 cm^{-1}, the signals are broadened due to a superposition with vibrational bands of methane.

This effect is even more obvious in the spectrum of **119**. Furthermore, signals at 1300 cm^{-1} and in the range of 3100–2900 cm^{-1} confirm the existence of methane in the explosion products. In the spectrum of **120**, the vibrational resonances of methane in the low frequency area (750 cm^{-1}) appear almost without interference. In this spectrum only traces of HCN could be detected. The main products seem to be NH_3 and methane. Interestingly, in the spectrum of the ammonia salt **121** only vibrational signals originating from NH_3 are visible. This contradicts with the expectation of seeing additional methane and HCN as explosion products. One possible reason could be an

incomplete combustion because of insufficient heating. From the mass spectroscopic analysis of **118** and **119** of course N_2 arises as the main decomposition product.

10.5.7 Long Term Stabilities

The long term stability test of **120** was performed using a Systag FlexyTSC (Thermal Safety Calorimeter) in combination with a RADEX V5 oven. The test was undertaken as long-term isoperibolic evaluation in a glass test vessel at atmospheric pressure with 400 mg of **120**. It was previously shown that tempering a substance for 48 hours at 40 degrees under the decomposition point results in storage periods about over 50 years at room temperature. Initially for **120** a temperature of 190 °C was chosen and possible occurrences of exo- or endothermic behavior were investigated over period of 48 hours. **120** was completely stable during this period. It can therefore be reasoned, that **120** is long-term stable even at higher temperatures, which is a basic requirement for possible applications.

10.5.8 *n*-Octanol/Water Partition Coefficient

With regard to environmental compatibility of new energetic materials the n-octanol/water partition coefficients (see introduction) of **118–121** were tested. The partition coefficient of a substance between water and a lipophilic solvent (*n*-octanol) is one model variable which may be used to describe the transfer of a substance from the aquatic environment into an organism and the potential bioaccumulation of the substance. The tests were carried out with a mixture of analytical grade *n*-octanol and distilled water at 22 °C (±1 °C). The partition coefficients of **118** and **119** could not be determined, since the compounds are neither soluble in *n*-octanol nor in water. This represents the ideal case of new compounds. The partition coefficients (*P*) of **120** and **121** were determined to be 0.081 (log*P* = –1.09, **120**) and 0.078 (log*P* = –1.11, **121**). This is a appropriate value (comparable to that of urea (0.062, log*P* = –1.21)) for a new compound, which could be upscaled for application in future times.

10.6 Outlook

Bis(tetrazolyl)triazenes are an exciting class of nitrogen-rich energetic derivatives. Neutral bis(1*H*-tetrazol-5-yl)triazene (**116**) is a sensitive nitrogen-rich (N > 83 %) compound, which is not long term stable at air. However, its salt and methyl derivatives are promising high thermally stable derivatives and could be used as additives in solid propellant charges. Due to a poor crystallization behavior of **116** and its salts, no compounds containing bis(1*H*-tetrazol-5-yl)triazene are described in this thesis. However, the synthesis of hydrazinium bis(tetrazolate)triazene or ammonium bis(tetrazolate)triazene proceeds in facile syntheses. The synthesis of bis(1*H*-tetrazol-yl)triazene (**116**) takes course by diazotation 5-aminotetrazole (**2**). **116** can be reduced with $SnCl_2$ in concentrated hydrochloric acid to give the tetrazolyl hydrazine. 1-Tetrazolyl-2-benzylidene-hydrazine (**117**) is a stable intermediate on the way to the synthesis of 5-hydrazinotetrazoles. Due to poor solubility of the tetrazolyl hydrazine in organic solvents, it cannot be separated from the tin(II) chloride, which is soluble in water and almost any organic solvent, by recrystallization. Therefore benzaldehyde is added to the mixture and the formed phenylhydrazone precipitates instantaneously, which can be recrystallized from ethanol very easily to give the product as nice white needles. The subsequent hydrolysis of the phenyl hydrazone by passing hot steam through an aqueous solution delivers the 5-hydrazino-1*H*-tetrazole (**Scheme 10.6**).

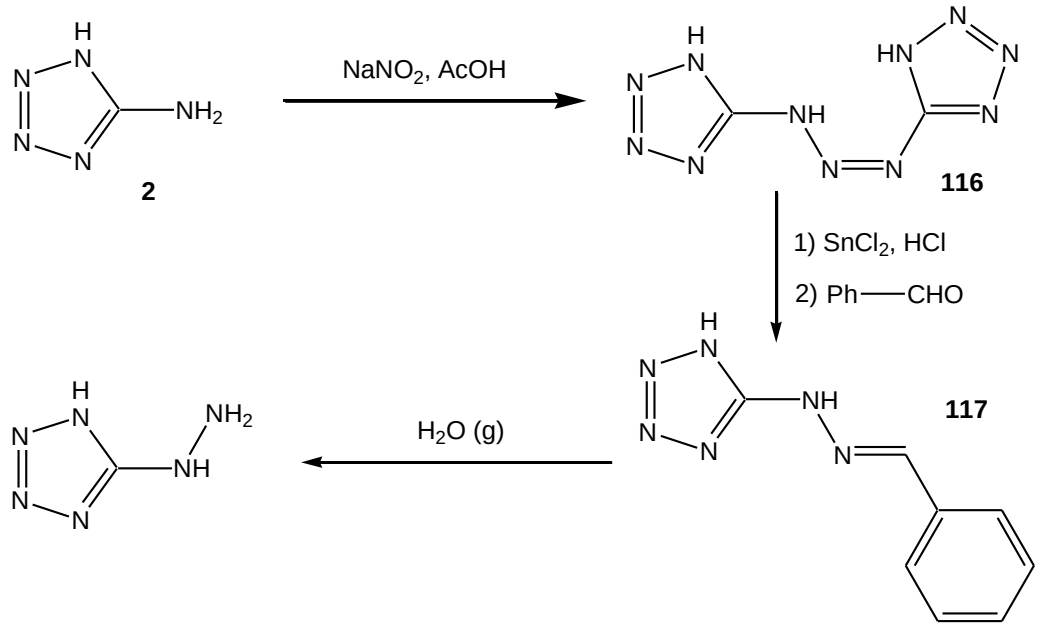

Scheme 10.6 Synthesis of 5-hydrazino-1*H*-tetrazole.

1-Tetrazolyl-2-benzylidenehydrazine (**117**) crystallizes with four molecules in the unit cell in the triclinic space group *P*-1. For better clearness only one molecule is depicted in **Figure 10.14**. The proton at the tetrazole ring is located at the N1 position. This is result, due to the electron donating substituent at the carbon atom. The N5–N6 bond length of 1.375(2) Å is between a N–N single (1.48 Å) and a N=N double (1.20 Å) bond.

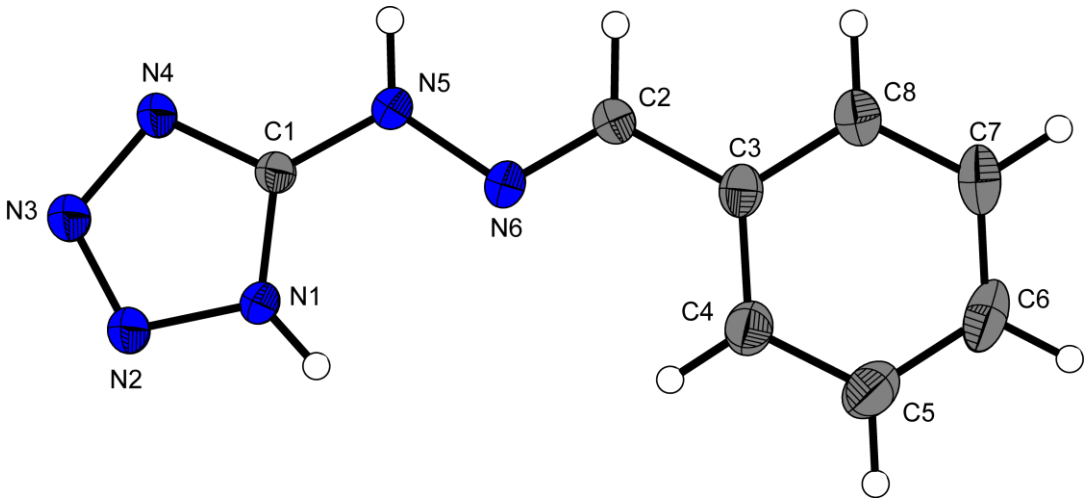

Figure 10.14 Molecular structure of 1-tetrazolyl-2-benzylidenehydrazine (**117**). Ellipsoids represent 50 % probability. Selected bond distances (Å): N5–C1 = 1.343(2), N5–N6 = 1.375(2), N6–C2 = 1.278(2), C3–C2 = 1.460(2).

10.7 Experimental Part

*CAUTION! The prepared compounds **118–125** are energetic compounds with increased sensitivities against heat, impact and friction. Although we had no problems in synthesis, proper protective measures (safety glasses, face shield, leather coat, earthened equipment and shoes, Kevlar® gloves and ear plugs) should be used during work on **118–125**.*

*Bis(1-methyltetrazol-5-yl)triazene monohydrate (**118**):* 1-Methyl-5-aminotetrazole (19.82 g, 200 mmol) was elutriated in 100 mL water and cooled to 0 °C. After adding concentrated HCl (21.24 g, 200 mmol), 1-methyl-5-aminotetrazole was solved completely. A solution of $NaNO_2$ (6.90 g, 10 mmol) in 40 mL water was added drop wise within 20 min. Thereafter the solution was stirred for 24 h, the resulting colorless solid was isolated by filtration and washed with water. Single crystals were obtained from a wet methanol solution (11.0 g, yield 52.6 %). **DSC** (T_{onset}, 5 °C min^{-1}): 160 °C, 182 °C

(dec.); **IR** (KBr, cm^{-1}): $\tilde{\nu}$ = 3375 (m), 3270 (m), 3081 (w), 3031 (w), 2662 (m), 2554 (m), 1664 (m), 1631 (s), 1530 (m), 1502 (m), 1458 (m), 1437 (s), 1396 (m), 1308 (m), 1268 (s), 1247 (m), 1226 (m), 1194 (s), 1102 (w), 1036 (m), 1003 (w), 983 (w), 936 (m), 806 (m), 747 (m), 729 (m), 699 (s), 666 (m), 641 (m), 605 (m), 482 (w); **Raman** (1064 nm, 200 mW, 25 °C, cm^{-1}): $\tilde{\nu}$ = 2987 (59), 1619 (17), 1531 (54), 1453 (43), 1429 (100), 1306 (8), 1284 (28), 1246 (12), 1250 (8), 1221 (11), 1113 (24), 938 (9), 697 (15), 485 (10), 421 (11), 393 (9), 220 (28), 184 (10); **^{1}H NMR** (d_6-DMSO, 25 °C, ppm): δ = 4.04 (s, 6*H*, CH_3); **^{13}C NMR** (d_6-DMSO, 25 °C, ppm): δ = 34.9 (s, CH_3), 155.2 (tetrazole); **^{15}N NMR** (d_6-DMSO, 25 °C, ppm): δ = –265.0 (s, N5, N7), –168.7 (d, $^{2}J_{NH}$ = 2.1 Hz, N1), –76.59 (s, N4), –12.72 (d, $^{3}J_{NH}$= 1.8 Hz, N2), 5.54 (s, N3), 85.20 (s, N6); **EA** ($C_4H_9N_{11}O$, 227.19) calcd.: C 21.15, H 3.99, N 67.82 %; found: C 21.18, H 3.89, N 67.48 %; ***m/z*** (DEI^+): 209 [$M^+ - H_2O$] (11), 111 [$C_2H_3N_6^+$] (100), 83 [$C_2H_3N_4^+$] (12), 53 (19), 43 [$CH_3N_2^+$] (45), 28 [N_2^+] (64); **UV/VIS** (MeOH): λ_{max} = 315 nm; $\Delta_c U$: –3556 cal g^{-1}; **BAM drophammer**: 3 J; **friction tester**: 360 N.

*Bis(2-methyl-tetrazol-5-yl)triazene (**119**):* 2-Methyl-5-aminotetrazole (8.72 g, 88 mmol) was solved in 80 mL THF and cooled to 0° C. After adding concentrated HCl (4.58 g, 44 mmol), the formation of a colorless solid could be observed. Within 30 min 5.9 mL *i*-pentylnitrite (5.15 g, 44 mmol) were added drop wise, the suspension turned into light yellow and was stirred for 24 h at room temperature afterwards. The resulting solid was recrystallized from methanol to obtain the colorless product (15.1 g, 82 %). **DSC** (T_{onset}, 5 °C min^{-1}): 183 °C (dec.); **IR** (KBr, cm^{-1}): $\tilde{\nu}$ = 3445 (m), 3190 (m), 3136 (m), 3060 (m), 2995 (m), 2920 (m), 2857 (m), 2686 (w), 2384 (w), 1598 (s), 1521 (m), 1468 (s), 1409 (m), 1389 (m), 1349 (m), 1285 (m), 1205 (s), 1100 (w), 1063 (w), 1040 (m), 1018 (m), 949 (m), 808 (m), 758 (m), 744 (m), 705 (m), 686 (m), 672 (m), 661 (m), 590 (w), 491 (w); **Raman** (1064 nm, 200 mW, 25 °C, cm^{-1}): $\tilde{\nu}$ = 2980 (4), 2963 (8), 1601 (12), 1528 (24), 1455 (100), 1413 (8), 1361 (5), 1291 (7), 1193 (4), 1100 (7), 1079 (6), 1049 (9), 942 (6), 703 (4), 489 (3), 434 (2), 376 (3), 174 (5); **^{1}H NMR** (d_6-DMSO, 25 °C, ppm): δ = 4.32 (s, 6*H*, CH_3), 14.10 (s, 1*H*, NH); **^{13}C NMR** (d_6-DMSO, 25 °C, ppm): δ = 40.5 (CH_3), 162.9 (tetrazole); **EA** ($C_4H_7N_{11}$, 209.17) calcd.: C 22.97, H 3.37, N 73.66 %; found: C 22.78, H 3.31, N 73.17 %; ***m/z*** (DEI^+): 209 [M^+] (5), 181 [$M^+ - N_2$] (18), 111 [$C_2H_3N_6^+$] (39), 83 [$C_2H_3N_4^+$] (3), 55 (8), 42 (11), 43 [$CH_3N_2^+$] (100), 28 [N_2^+] (37), 15 [CH_3^+] (16); **UV/VIS** (MeOH): λ_{max} = 291 nm; $\Delta_c U$: –3861 cal g^{-1}; **BAM drophammer**: 2.5 J; **friction tester**: 70 N.

*Ammonium bis(1-methyltetrazol-5-yl)-triazenate (**120**):* Bis(1-Methyltetrazol-5-yl)-triazene monohydrate (2.27 g, 10.0 mmol) was elutriated in 20 mL water. The suspension was heated to 80 °C and an excess of concentrated ammonia (25 %, 25 mL) was added until the reactant was completely dissolved. The ammonium salt crystallized after cooling down to room temperature, was washed with ethanol and diethyl ether and finally dried using high vacuum (1.58 g, 70 % yield). **DSC** (T_{onset}, 5 °C min^{-1}): 236 °C (dec.); **IR** (KBr, cm^{-1}): $\tilde{\nu}$ = 3425 (m), 3158 (m), 3062 (m), 2956 (m), 2857 (m), 2760 (m), 2197 (w), 2125 (w), 1971 (w), 1720 (w), 1612 (w), 1519 (s), 1478 (s), 1451 (s), 1313 (s), 1229 (m), 1209 (m), 1119 (w), 1105 (w), 1047 (w), 1009 (w), 807 (w), 749 (m), 705 (m), 666 (m), 613 (m), 498 (w); **Raman** (1064 nm, 200 mW, 25 °C, cm^{-1}): $\tilde{\nu}$ = 2987 (5), 2962 (6), 1529 (100), 1478 (14), 1467 (16), 1415 (7), 1327 (35), 1290 (14), 1204 (18), 1127 (14), 1007 (3), 948 (6), 707 (12), 498 (15), 422 (5), 405 (4), 221 (22); **^{1}H NMR** (d_6-DMSO, 25 °C, ppm): δ = 3.86 (s, 6H, 2xCH_3), 7.42 (s, 4H, NH_4^+); **^{13}C NMR** (d_6-DMSO, 25 °C, ppm): δ = 33.1 (CH_3), 161.9 (tetrazole); **^{14}N NMR** (d_6-DMSO, 25 °C, ppm): δ = –358 (NH$_4^+$); **EA** ($C_4H_{10}N_{12}$, 226.2) calcd.: C 21.24, H 4.46, N 74.31 %; found: C 21.16, H 4.39, N 73.86 %; ***m/z*** (FAB$^-$): 208 [anion]; **UV/VIS** (MeOH): λ_{max} = 329 nm; **$\Delta_c U$**: –3867 cal g^{-1}; **BAM drophammer**: 7.5 J; **friction tester**: 360 N.

*Ammonium bis(2-methyltetrazol-5-yl)triazenate (**121**):* Bis(2-methyltetrazol-5-yl)-triazene (2.09 g, 10 mmol) was elutriated in 20 mL water. The suspension was heated to 80 °C and concentrated ammonia (25 %, 27.3 g, 0.4 mol) was added until the reactant was completely dissolved. The ammonium salt crystallized after cooling down to room temperature, was washed with ethanol and diethyl ether and afterwards dried in vacuum (1.63 g, 72 % yield). **DSC** (T_{onset}, 5 °C min^{-1}): 205 °C (dec.); **IR** (KBr, cm^{-1}): $\tilde{\nu}$ = 3434 (w), 3137 (m), 3063 (m), 2910 (m), 2756 (m), 2554 (m), 2115 (w), 1183 (w), 1701 (w), 1599 (w), 1563 (w), 1511 (m), 1461 (s), 1423 (m), 1408 (m), 1382 (m), 1322 (s), 1272 (s), 1205 (m), 1052 (m), 1030 (m), 812 (m), 767 (m), 710 (m), 671 (w), 519 (w), 432 (w); **Raman** (1064 nm, 200 mW, 25 °C, cm^{-1}): $\tilde{\nu}$ = 2961 (4), 1509 (100), 1469 (5), 1410 (5), 1259 (12), 1259 (6), 1106 (7), 1050 (3), 1037 (3), 964 (11), 520 (5), 185 (4); **^{1}H NMR** (d_6-DMSO, 25 °C, ppm): δ = 4.20 (s, 6H, CH_3), 6.10 (s br, 4H, NH_4^+); **^{13}C NMR** (d_6-DMSO, 25 °C, ppm): δ = 39.7 (CH_3), 173.7 (tetrazole); **^{14}N NMR** (d_6-DMSO, 25 °C, ppm): δ = –359 (NH$_4^+$); **EA** ($C_4H_{10}N_{12}$, 226.2) calcd.: C 21.24, H 4.46, N 74.31 %; found: C 21.27, H 4.48, N 74.31 %; ***m/z*** (FAB$^-$): 208 [anion]; **UV/VIS** (MeOH): λ_{max} = 292 nm; **ΔU_c**: –3864 cal g^{-1}; **BAM drophammer**: 4 J; **friction tester**: > 360 N.

*Sodium bis(1-methyltetrazol-5-yl)triazenate (**122**):* Bis(1-methyltetrazol-5-yl)triazene monohydrate (2.27 g, 10 mmol) was deprotonated using 100 mL of an aqueous NaOH (0.40 g, 10 mmol) solution. After stirring for five min at 80 °C, the solution was cooled while the product started to precipitate. The light yellow micro crystals were filtered off and washed with ethanol and diethyl ether. The elemental analysis fits to the monohydrate (2.39 g, 96 % yield). The raw product could be recrystallized either from a small amount of water including five water molecules or from a water/methanol mixture co crystallizing with one molecule methanol. **DSC** (T_{onset}, 5 °C min^{-1}): 135 °C, 195 °C (dec.); **IR** (KBr, cm^{-1}): $\tilde{\nu}$ = 3445 (m), 3203 (w), 1622 (w), 1519 (s), 1474 (m), 1456 (w) 1323 (vs), 1284 (m), 1218 (m), 1205 (w), 707 (w); **Raman** (1064 nm, 200 mW, 25 °C, cm^{-1}): $\tilde{\nu}$ = 2987 (7), 2965 (7), 1546 (100), 1473 (11), 1402 (6), 1338 (22), 1288 (15), 1206 (24), 1129 (15), 1012 (5), 711 (10), 500 (22), 412 (9), 222 (22); **^{1}H NMR** (D_2O, 25 °C, ppm): δ = 3.94 (s, 6*H*, CH_3); **^{13}C NMR** (D_2O, 25 °C, ppm): δ = 161.0 (CN_4), 33.0 (*C*H_3); **EA** ($C_4H_8N_{11}NaO$, 249.2) calcd.: C 19.28, H 3.24, N 61.84 %; found: C 19.27, H 3.27, N 61.32 %; **UV/VIS** (MeOH): λ_{max} = 330 nm.

*Sodium bis(2-methyltetrazol-5-yl)triazenate pentahydrate (**123**):* To bis(2-methyltetrazol-5-yl)triazene (2.09 g, 10 mmol) 20 mL of an 0.5 M NaOH (10 mmol) solution was added. After stirring for 10 min at 80 °C, the solution was evaporated. The raw product was recrystallized from hot ethanol, isolated by filtration and washed with small amounts of diethyl ether. (3.08 g, 96 % yield). **DSC** (T_{onset}, 5 °C min^{-1}): 74 °C(–H_2O), 100 °C (–H_2O), 256 °C (dec.); **IR** (KBr, cm^{-1}): $\tilde{\nu}$ = 3588 (m), 3479 (s), 3422 (s), 3180 (s), 2163 (w), 1735 (w), 1682 (m), 1630 (m), 1517 (m), 1469 (vs), 1441 (m), 1419 (m), 1388 (m), 1340 (vs), 1274 (s), 1252 (s), 1212 (m), 1056 (m), 1031 (w), 820 (w), 767 (m), 710 (m), 669 (m), 594 (w), 505 (w); **Raman** (1064 nm, 200 mW, 25 °C, cm^{-1}): $\tilde{\nu}$ = 3025 (1), 2961 (3), 1512 (100), 1463 (10), 1415 (7), 1372 (2), 1334 (2), 1250 (8), 1200 (1), 1107 (7), 962 (10), 712 (1), 503 (3), 420 (2), 316 (2), 211 (2); **^{1}H NMR** (*d_6*-DMSO, 25 °C, ppm): δ = 4.18 (s, 6*H*, CH_3), 3.46 (s, 10*H*, H_2O); **^{13}C NMR** (*d_6*-DMSO, 25 °C, ppm): δ = 174.8 (tetrazole), 39.7 (*C*H_3); **EA** ($C_4H16_6N_{11}NaO_5$, 321.23) calcd.: C 14.96, H 5.02, N 47.96 %; found: C 14.91, H 5.36, N 46.53 %; **UV/VIS** (MeOH): λ_{max} = 295 nm.

*Bis(1-methyltetrazol-5-yl)-3-methyltriaz-1-ene (**124**):* Bis(1-methyltetrazol-5-yl)triazene monohydrate (4.54 g, 20 mmol) was stirred in 200 mL of an aqueous NaOH (800 mg, 20 mmol) solution for 5 min at 60 °C. Then 1.1 equivalent of methyl iodide (1.4 mL) was added drop wise and the solution was stirred for 2 h at 80 °C. The light yellow

precipitate was filtered off and washed with water and a small amount of ethanol (3.04 g, 68 % yield). Single crystals were obtained by recrystallization from hot ethanol. **DSC** (T_{onset}, 5 °C min^{-1}): 140 °C, 175 °C (dec.); **IR** (KBr, cm^{-1}): $\tilde{\nu}$ = 3431 (w, br), 1574 (s), 1519 (m), 1491 (m), 1473 (m), 1454 (s), 1423 (vs), 1393 (m), 1322 (w), 1281 (s), 1263 (w), 1231 (m), 1194 (m), 1155 (s), 1098 (w), 991 (m), 914 (w), 742 (w), 731 (m), 723 (m), 701 (w), 688 (w), 649 (m), 570 (m), 499 (w); **Raman** (1064 nm, 200 mW, 25 °C, cm^{-1}): $\tilde{\nu}$ = 2950 (11), 1573 (100), 1518 (44), 1490 (20), 1449 (54), 1422 (38), 1396 (42), 1322 (5), 1265 (25), 1230 (6), 1100 (18), 1033 (4), 991 (7), 916 (6), 724 (11), 708 (12), 568 (7), 501 (7), 421 (10); **^{1}H NMR** ($CDCl_3$, 25 °C, ppm): δ = 4.12 (s, 3*H*, CH_3), 4.11 (s, 3*H*, CH_3), 3.83 (s, 3*H*, CH_3); **^{13}C NMR** ($CDCl_3$, 25 °C, ppm): δ = 157.9 (tetrazole), 154.2 (tetrazole), 37.6 (CH_3), 35.9 (CH_3), 34.0 (CH_3); **EA** ($C_5H_9N_{11}$, 223.2) calcd.: C 26.91, H 4.06, N 69.03 %; found: C 26.90, H 3.97, N 68.54 %; ***m/z*** (DEI^+): 43 [$CH_3N_2^+$] (100), 83 [$C_2H_3N_4^+$] (20), 111 [$C_2H_3N_6^+$] (17), 223 $[M]^+$ (38); **UV/VIS** (MeOH): λ_{max} = 299 nm; **$\Delta_c U$**: –4225 cal g^{-1}; **BAM drophammer**: 3 J; **friction tester**: 360 N.

*Bis(2-methyltetrazol-5-yl)-3-methyltriaz-1-ene (**125**):* Bis(2-methyltetrazol-5-yl)triazene (2.09 g, 10 mmol) was stirred in 100 mL of an aqueous NaOH (400 mg, 10 mmol) solution for 5 min at 60 °C. Then 0.65 eq. of Me_2SO_4 (0.62 mL) were added drop wise and the solution was stirred for 2 h at 80 °C. The light yellow precipitate was filtered off and washed with water and a small amount of ethanol (1.29 g, 58 % yield). **DSC** (T_{onset}, 5 °C min^{-1}): 135 °C, 200 °C (dec.); **IR** (KBr, cm^{-1}): $\tilde{\nu}$ = 3446 (w), 3038 (w), 1613 (w), 1569 (vs), 1476 (vs), 1422 (m), 1398 (vs), 1292 (w), 1234 (s), 1218 (s), 1175 (m), 1071 (m), 1032 (m), 980 (m), 916 (w), 801 (w), 761 (w), 745 (m), 713 (m), 631 (w), 590 (w), 99 (w); **Raman** (1064 nm, 200 mW, 25 °C, cm^{-1}): $\tilde{\nu}$ = 3041 (3), 1964 (10), 1563 (85), 1478 (100), 1399 (20), 1360 (6), 1293 (10), 1207 (4), 1179 (3) 1083 (3), 1034 (15), 982 (10), 915 (4), 762 (2), 746 (2), 717 (7), 638 (2), 501 (7), 444 (6), 345 (3), 183 (5);); **^{1}H NMR** ($CDCl_3$, 25 °C, ppm): δ = 3.74 (s, 3*H*, triazene-CH_3), 4.38 (s, 3*H*, CH_3), 4.39 (s, 3*H*, tetrazole-CH_3); **^{13}C NMR** ($CDCl_3$, 25 °C, ppm): δ = 169.5 (tetrazole), 165.0 (tetrazole), 40.2 (CH_3), 40.1 (CH_3), 33.7 (triazene-CH_3); **^{15}N NMR** ($CDCl_3$, 25 °C, ppm): δ = 72.6 (s, N7), –0.57 (s, N3), –2.20 (s, N3'), –25.8 (s, N6), –63.5 (s, N4), –76.6 (s, N4'), –93.2 (s, N1), –103.7 (s, N1'), –108.1 (s, N2), –109.5 (d, $^{2}J_{NH}$= 2.3 Hz, N2'), –211.3 (s, N8); **EA** ($C_5H_9N_{11}$, 223.1) calcd.: C 26.91, H 4.06, N 69.03 %; found: C 26.90, H 3.97, N 68.54 %; ***m/z*** (DEI^+): 43 [$CH_3N_2^+$] (100), 55 (17), 83 [$C_2H_3N_4^+$] (8), 111 [$C_2H_3N_6^+$] (86), 223 $[M]^+$ (7); **UV/VIS** (MeOH): λ_{max} = 281 nm; **$\Delta_c U$**: –4491 cal g^{-1}; **BAM drophammer**: 3 J; **friction tester**: 20 N.

*1-Tetrazol-5-yl-2-benzylidene hydrazine (**117**):* 5-Amino-1*H*-tetrazole (3.402 g, 40 mmol) was suspended in 12 mL of water and 8 mL of glacial acetic acid and cooled to 0°C in an ice bath. A solution of $NaNO_2$ (1.38 g, 20 mmol) in 12 mL of water is dropwise added over a period of 2.5 hours. A yellow precipitate of 1,3-bis-(5-tetrazolyl)triazene forms. The mixture is further stirred at room temperature for 2 hours and filtered off. The 1,3-bis-(1*H*-tetrazol-5-yl)triazene is added to a solution of $SnCl_2{\cdot}2H_2O$ (9.04 g, 40 mmol) in 50 mL of concentrated hydrochloric acid in small portions and the mixture is finally stirred for 2 hours at 35°C before being filtered. Benzaldehyde was added to the filtrate dropwise, until the solution noticeably smelled like it.[351,352] A white precipitate of tetrazolyl phenyl hydrazone began to form. It was filtered off and recrystallized from ethanol. (604 mg, 16% yield). **DSC** (T_{onset}, 5 °C min^{-1}): 238 °C (dec.); **IR** (KBr, cm^{-1}): $\tilde{\nu}$ = 3450 (m), 3182 (m), 3013 (m), 2952 (m), 2851 (m), 1639 (vs), 1608 (s), 1597 (s), 1532 (m), 1495 (m), 1446 (w), 1379 (m), 1337 (w), 1272 (w), 1224 (w), 1138 (w), 1110 (m), 1048 (s), 1040 (s), 998 (w), 940 (m), 822 (m), 794 (w), 757 (m), 728 (w), 687 (m), 612 (w), 537 (w), 510 (w); **Raman** (1064 nm, 300 mW, 25 °C, cm^{-1}): $\tilde{\nu}$ = 3064 (6), 1633 (9), 1612 (81), 1600 (100), 1575 (40), 1499 (2), 1449 (8), 1373 (3), 1342 (3), 1311 (2), 1293 (4), 1277 (4), 1225 (30), 1178 (10), 1162 (7), 1143 (5), 1134 (6), 1109 (13), 1074 (4), 1056 (4), 1029 (3), 1001 (24), 897 (2), 619 (3), 340 (2), 238 (6); **^{1}H NMR** (*d_6*-DMSO, 25 °C, ppm): δ = 15.38 (s, NH-tetrazole), 11.80 (s, NH-hydrazine), 8.04 (s, CH), 7.78 (m, 2 o-H), 7.40 (m, 2 m-H, 1 p-H); **^{13}C NMR** (*d_6*-DMSO, 25 °C, ppm): δ = 157.0 (CN_4), 143.7 (CN), 134.9 (ipso-C_{ar}), 130.0 (p-C_{ar}), 129.2 (o-C_{ar}), 127.3 (m-C_{ar}); **EA** ($C_8H_8N_6$, 188.19) calcd.: C 51.06, H 4.28, N 44.66 %; found: C 50.86, H 4.04, N 45.17 %.

10.8 Conclusion

From this experimental study the following conclusions can be drawn:

- Bis(1-methyltetrazol-5-yl)triazene (**118**) and bis(2-methyltetrazol-5-yl)triazene (**119**) were synthesized by diazotation of 1-methyl-5-aminotetrazole (**10**) and 2-methyl-5-aminotetrazole (**11**), respectively, by using half an equivalent of sodium nitrite. The sodium and ammonium salts of **118** and **119** were synthesized by aqueous ammonia as well as sodium hydroxide solution. These triazenate salts can be methylated yielding bis(1-methyltetrazol-5-yl)-3-

methyltriaz-1-ene (**124**) and bis(2-methyltetrazol-5-yl)-3-methyltriaz-1-ene (**125**). All syntheses could be performed via facile routes in good yields using cheap available precursors.

- The molecular structures of **118**·H_2O, **119**, sodium bis(1-methyltetrazol-5-yl)triazenate (**120**), magnesium bis(2-methyltetrazol-5-yl)triazenate (**126**) and **124** were determined using low temperature single crystal X-ray diffraction and a detailed description is given in this work.

- All compounds were characterized by Raman, IR, multinuclear NMR and UV/VIS spectroscopy, mass spectrometry, elemental analysis and differential scanning calorimetry. The decomposition temperature of the investigated compounds range from 182 to 340 °C.

- All substances show desirable high positive heat of formation (514–792 kJ mol^{-1}) determined in bomb calorimetric measurements. With these values and densities either obtained by X ray or pycnometry several detonation parameter were computed by the EXPLO5 program, resulting in values much higher than those of TNT but lower than those of RDX. In addition, promising specific impulses of mixtures of ammonium dinitramide (ADN) and ammonium bis(1-methyltetrazol-5-yl)triazenate (**120**) with good N_2/CO ratios were calculated.

- The sensitivities towards impact and friction were determined by the BAM drophammer and friction tester varying from very sensitive comparable to those of primary explosives to completely insensitive.

- The most promising new energetic material is ammonium bis(1-methyltetrazol-5-yl)triazenate (**120**), which combine a high decomposition temperature and high heat of formation with a low sensitivity and good long term stability.

- The molecular structure of 1-tetrazol-5-yl-2-benzylidene-hydrazine (**117**) is described, which was obtained by reduction of bis(1*H*-tetrazol-5-yl)triazene (**116**). **116** is a valuable starting material for the synthesis of nitrogen-rich compounds.

Chapter 11.

Salts of 1*H*-Tetrazole

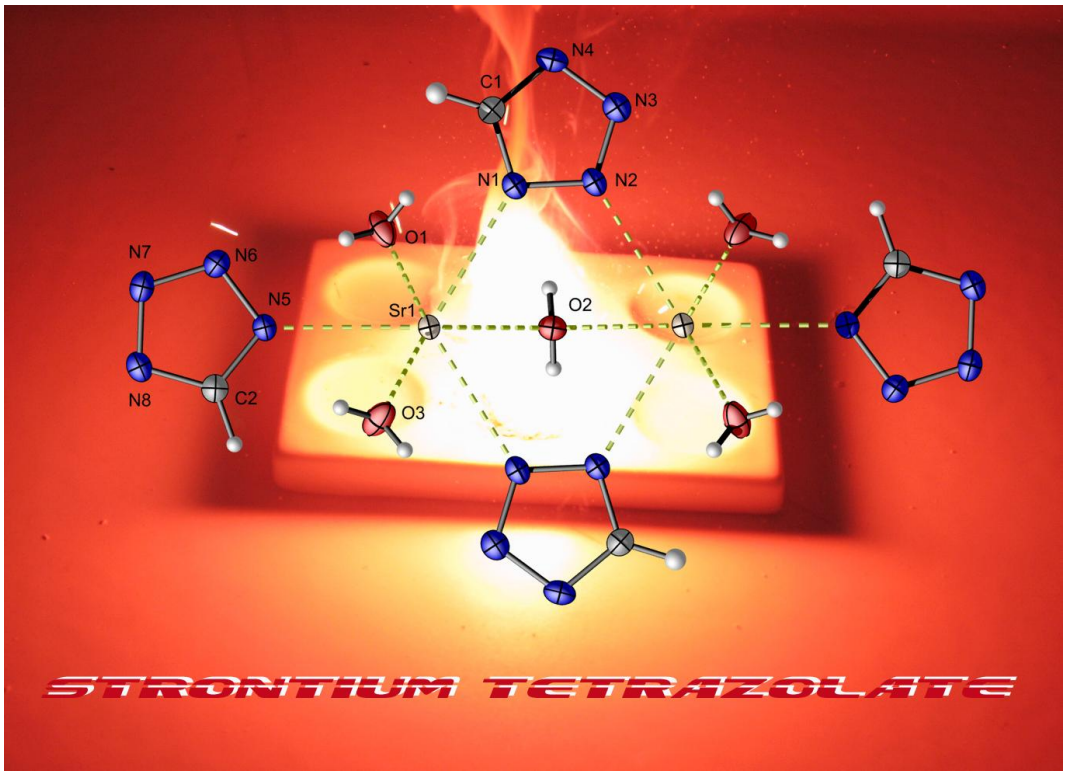

11.1 Introduction

The most basic tetrazole is 1*H*-1,2,3,4-tetrazole (**1**), as already mentioned in the introduction. Tetrazoles are a unique class of heterocyclic compounds with various interesting properties. They can be used for example in pharmaceuticals,[353] as synthetic building blocks in coordination chemistry [354] and as energetic materials with high nitrogen contents [71d,72] in modern explosive compositions.[30] In the latter, particularly tetrazoles play an important role in the development of environmentally benign explosives. Due to the possibility of deprotonation, protonation and alkylation amongst other reactions, the properties of tetrazoles can be considerably varied and result in numerous possible derivatives. Although the chapter about salts of 1*H*-tetrazole (**1**) is integrated into this thesis by the deamination reaction of 5-aminotetrazole using sodium nitrite and phosphorous acid (**Scheme 11.1**D), there are two main synthetic routes to **1**. In the lab scale, the reaction C) of ammonium chloride, triethyl orthoformate and sodium azide in concentrated acetic acid is the most facile one.[355]

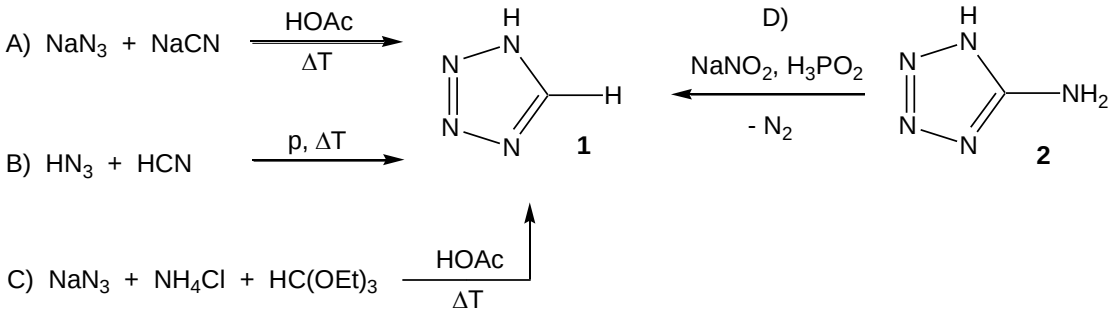

Scheme 11.1 Synthesis of 1*H*-tetrazole.

The (2+3) dipolar cycloaddition (**Scheme 11.1.A** and **B**) between HN_3 and HCN [356] or NaN_3 and NaCN [357] can only be performed by the use of pressure, catalysts or long reaction times due to the HOMO and LUMO energies of these compounds.

1*H*-Tetrazole is an endothermic compound (ΔH_f = 237 kJ mol^{-1}),[358] and therefore its use as an energetic material in propellant systems is discussed. For practical applications, **1** possesses too low density (ρ = 1.53 g cm^{-3}) and a low decomposition temperature at 188 °C. However, the second problem can be improved by deprotonation, which results in salts with higher thermal stability. The strontium salt (**134**) for example, is stable up to temperatures of 335 °C. In this work, several salts of 1*H*-tetrazole are presented including the ammonium and hydrazinium salts as compounds with high nitrogen

contents. The properties of the latter two which determine suitability for use in energetic compositions were investigated, and since modern, smokeless pyrotechnic mixtures could contain alkali and alkaline earth metal salts, several corresponding metal tetrazole salts are also presented in this chapter.

11.2 Synthesis

1 was synthesized by the reaction of ammonium chloride, triethyl orthoformate and sodium azide in concentrated acetic acid at 80 °C for six hours (**Scheme 11.2**), followed by recrystallization from ethyl acetate. Salts **127–134** were obtained by deprotonation of **1** using the bases indicated in **Scheme 11.3**. All salts were recrystallized from water, ethanol, or water / ethanol mixtures.

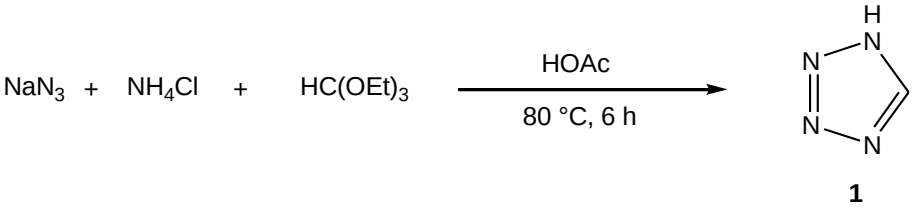

Scheme 11.2 Synthesis of 1*H*-tetrazole (**1**).

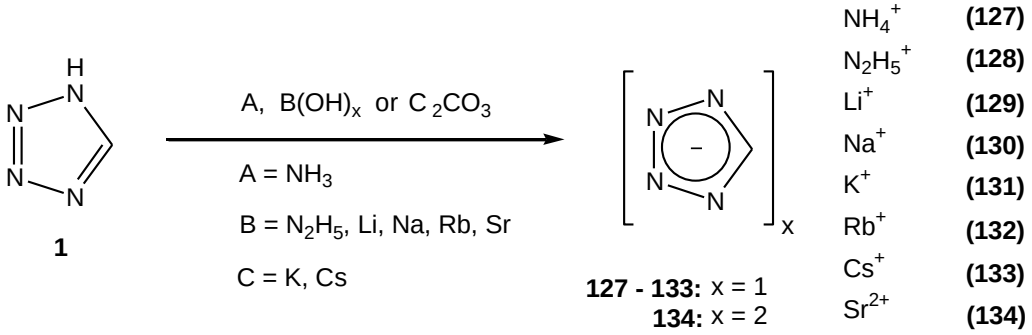

Scheme 11.3 Synthesis of salts of 1*H*-tetrazole **127–134**.

11.3 Crystal Structures

The tetrazolate salts **127–134** were investigated using low temperature X-ray diffraction and a detailed description of the crystal structures is given in the following section.

11.3.1 Ammonium tetrazolate monohydrate (**127**·H_2O)

Ammonium tetrazolate (**127**) crystallizes as a monohydrate in the monoclinic space group $P2_1/n$ with four molecules per unit cell. The ammonium cation is coordinated in a tetrahedral arranged by three different nitrogen atoms of three different tetrazolate rings and one oxygen atom from one molecule of crystal water by hydrogen bonds as shown in **Figure 11.1**.

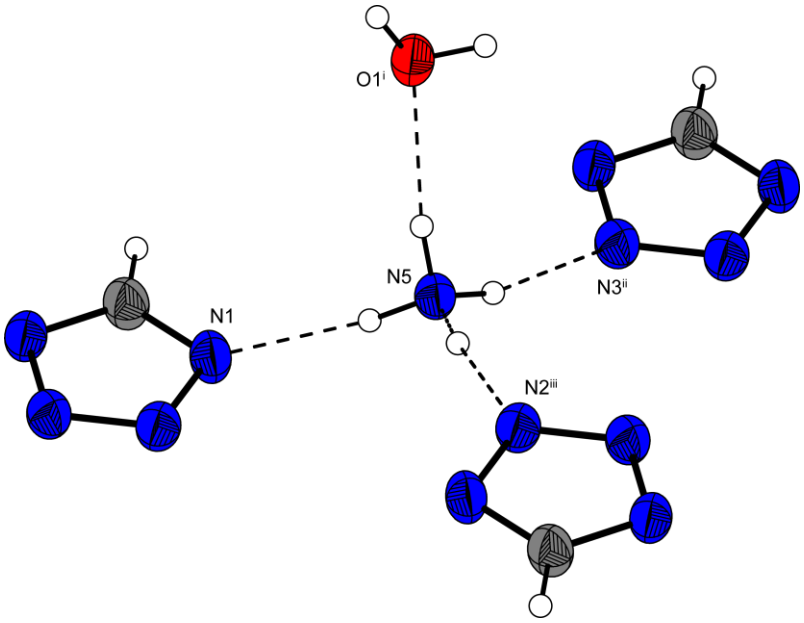

Figure 11.1 Coordination sphere of the NH_4^+ cations in ammonium tetrazolate monohydrate (**127**). Thermal ellipsoids are drawn at the 50 % probability level and hydrogen atoms are shown as small spheres of arbitrary radii. Hydrogen bonds: N5–H5a···N1: D–H 0.90(2) Å, H···A 2.03(2) Å, D···A 2.918(2) Å, D–H···A 171(2)°; N5–H5c···N2: 0.94(2) Å, 2.00(2) Å, 2.927(2) Å, 173(2)°; N5–H5d···N3: 0.92(2) Å, 2.06(2) Å, 2.962(2) Å, 166(2)°; N5–H5b···O1ⁱ: 0.91(2) Å, 1.97(2) Å, 2.851(2) Å, 164(2)°; (i): –1+x, –1+y, z; (ii) –1+x, y, z; (iii): –x, –2+y, 2–z.

A three-dimensional structure of alternating tetrazolate and ammonium ions forming a zig-zag pattern in the *a,c*-plane is observed, stabilized by an extended network of hydrogen bonds involving all four hydrogen atoms of the ammonium cation, similar to those observed for other related ammonium tetrazolate salts found in the literature.[359,142] The zig-zag chains are connected by hydrogen bonds formed between the ammonium cation to the nitrogen atoms N1, N2 and N3 of the tetrazolate ring. Furthermore, the zig-zag chains are stabilized by additional hydrogen bonds between the nitrogen atom N4 of the tetrazolate anion and a molecule of crystal water

(O1–H1···N4: D–H 0.88(2) Å, H–A 1.87(2) Å, D···A 2.725(2) Å, D–H···A 165(2)°) which itself forms a hydrogen bond to the ammonium cation. The N4–C1 bond length of 1.320(2) Å is a slightly shorter than the N1–C1 bond (1.326(2) Å) what may be a result of the influence of the stronger hydrogen bond to the oxygen atom of crystal water in comparison with the nitrogen atom of the ammonium cation. The bond lengths of the tetrazolate anion are in the range of those found in ammonium 5-nitriminotetrazolate.[270] Surprisingly, **127** has the lowest density of all compounds **127–134** (ρ = 1.343 g cm^{-3}), which is a extremely low value for tetrazolate salts.

11.3.2 Hydrazinium tetrazolate (**128**)

128 crystallizes in an orthorhombic crystal system with 16 molecules per unit cell. The space group was fixed as *Ccca.* Since only very thin plates could be obtained by different crystallization methods and a poor structure solution with a final wR_2 of approximately 20 % only a short description of the structure is given in this work. The molecular unit can be seen in **Figure 11.2**.

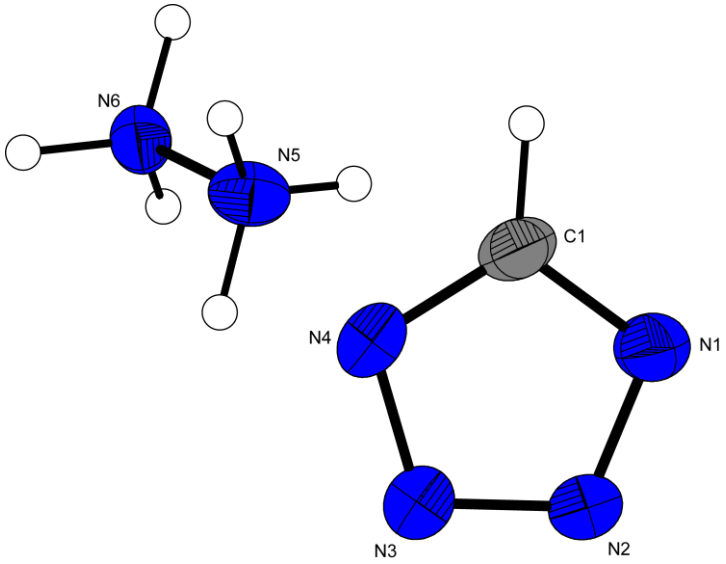

Figure 11.2 Structure of hydrazinium tetrazolate (**128**). Thermal ellipsoids are drawn at the 50 % probability level and hydrogen atoms are shown as small spheres of arbitrary radii.

Again, the low density of 1.385 g cm^{-3} of **128** is unexpected in comparison with the densities of other hydrazinium salts of tetrazoles derivates.[169,360] The bond lengths and angles in the tetrazolate anion are within the range observed for other structures described in this work. The N–N bond length of 1.445(5) Å in the hydrazinium cation has

the standard value reported for N–N single bonds found in literature.[166] In the crystal packing, two different hydrazinium cations can be found, alternating in each second layer and resulting in a channel structure which may be the cause of the low density observed in this structure.

11.3.3 Lithium tetrazolate (**129**)

129 crystallizes in the orthorhombic space group $C222_1$, containing eight molecules per unit cell. The cations are coordinated in a distorted tetrahedral arrangement by four different nitrogen atoms of four different tetrazolate rings with N–Li–N angles between 102° and 115°. All of the nitrogen atoms of each of the tetrazolate rings are coordinated to four different lithium cations, illustrated in **Figure 11.3** (d(N1–Li2) = 2.054(4) Å, d(N2–Li1) = 2.050(4) Å, d(N3–Li4) = 2.054(5) Å, d(N4–Li3) = 2.049(5) Å). The geometric distortion corresponds with the small variation of both the N1–N2 and N3–N4 (1.345(3) Å compared to 1.344(3) Å) and N1–C1 and N4–C1 bond lengths, respectively (1.333(3) Å compared to 1.328(3) Å). The observed bond lengths correspond to the calculated values of different lithium azoles found in the literature.[361]

11.3.4 Sodium tetrazolate monohydrate (**130**)

Sodium tetrazolate monohydrate crystallizes in the orthorhombic space group *Pmma* containing two molecules per unit cell. The former structure described by Palenik [362] which reported the *Pmcm* space group should be corrected. The sodium cations are coordinated in an octahedral arrangement by the N1 nitrogen atoms of four tetrazolate rings in the plane (d(N1–Na) = 2.541(1) Å and two molecules of crystal water perpendicular to this plane (**Figure 11.4**). **Figure 11.5** shows the resulting layer structure of sodium tetrazolate in the *b,c*-plane with the crystal water arranged along the *c*-axis, stabilized by O–H···N2 hydrogen bonds (D–H 0.80(2) Å, H···A 2.08(2) Å, D···A 2.883(2) Å, D–H···A 178(2)°). The N1–N2 bond (d(N1–N2) = 1.351 Å) is the longest observed among all of the salts characterized in this work, which confirms the strong influence of both coordination partners.

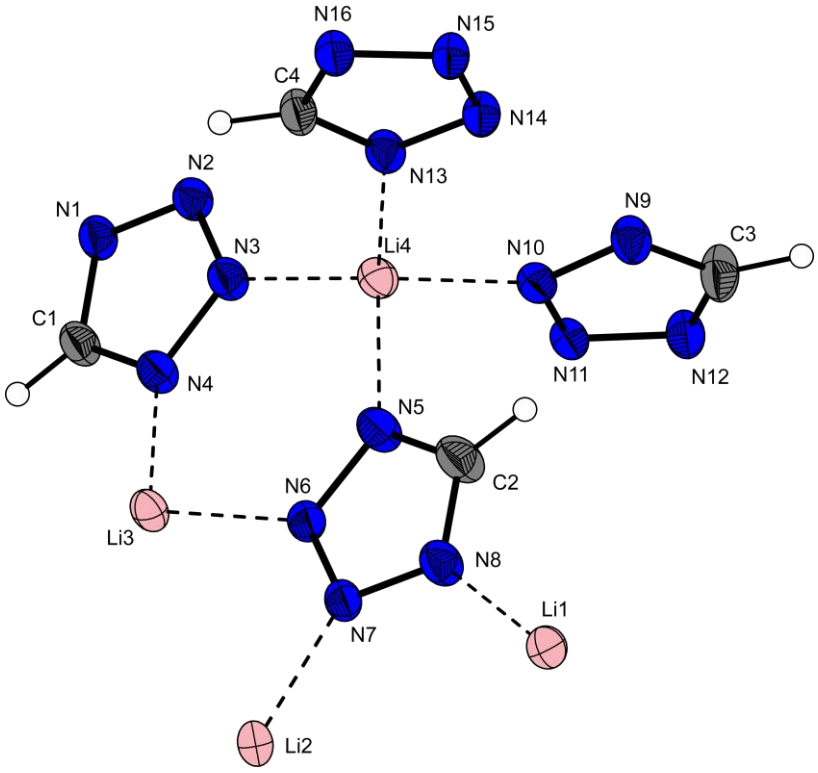

Figure 11.3 Extended structure of lithium tetrazolate (**129**). Thermal ellipsoids are drawn at the 50 % probability level and hydrogen atoms are shown as small spheres of arbitrary radii.

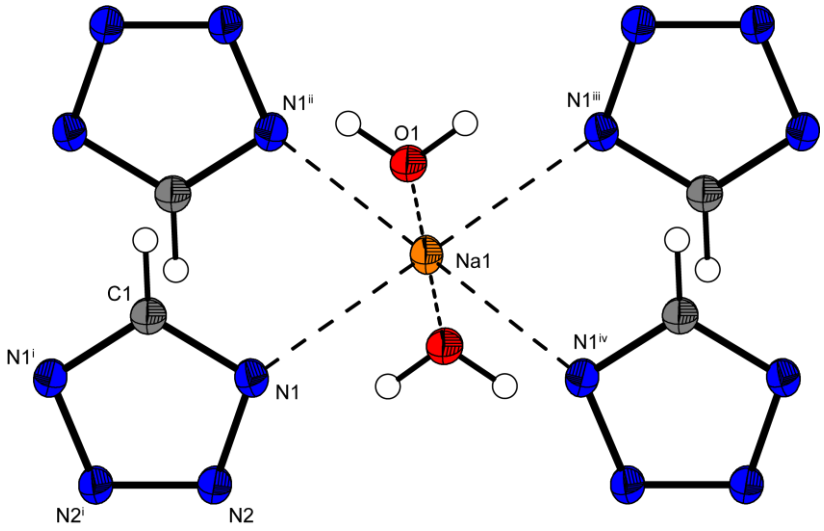

Figure 11.4 Coordination sphere of sodium tetrazolate monohydrate (**130**). Thermal ellipsoids are drawn at the 50 % probability level and hydrogen atoms are shown as small spheres of arbitrary radii. (i): –0.5–x, 1+y, z; (ii): 1–x, y, –z; (iii): –0.5+x, –y, –z; (iv): 1.5–x, –y, z.

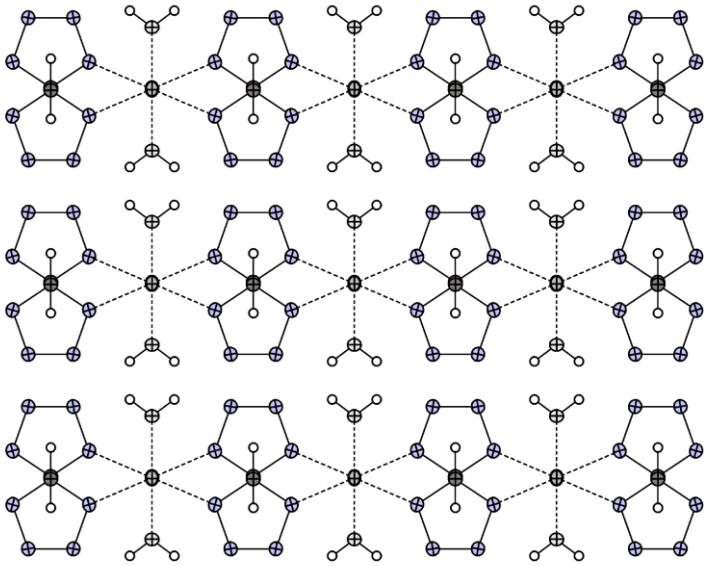

Figure 11.5 View on the packing of sodium tetrazolate monohydrate (**130**) along the *a* axis.

11.3.5 Potassium tetrazolate (**131**)

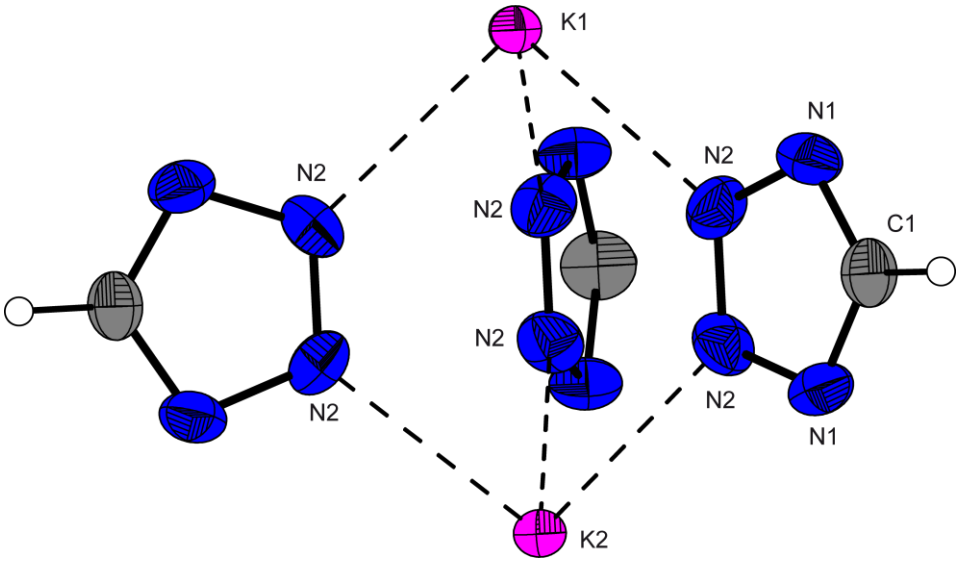

Figure 11.6 Coordination sphere of potassium tetrazolate (**131**). Thermal ellipsoids are drawn at the 50 % probability level and hydrogen atoms are shown as small spheres of arbitrary radii.

131 crystallizes in the hexagonal space group *P*–6 with six molecules in the unit cell. The crystal structure is composed of K_2TZ_3-units in which two potassium atoms are coordinated trigonal by the same three tetrazolate rings involving both equivalent nitrogen atoms N2 (**Figure 11.6**). The N–K–N angles are between 85° and 88°.

According to the regular K_2TZ_3-structure, the tetrazolate anions are symmetric, with bond lengths of 1.319(4) Å for the two C–N-bonds C1–N1 and C1–N4, 1.345(5) Å for the N–N bonds N1–N2 and N3–N4 and 1.300(5) Å for N2–N3. N1–N2 and N3–N4 bond lengths are the average of the values found in literature for N–N single (1.48 Å) and N=N double bonds (1.20 Å) which suggests the presence of a delocalized ring. The units are all together arranged along the *c* axis at different levels resulting in a three-dimensional structure.

11.3.6 Rubidium tetrazolate (**132**)

132 crystallizes in the hexagonal space group *P*63*/m* with six molecules in the unit cell. The tetrazolate ions are arranged alternating in the *a,c*- and *b,c*-plane, respectively, each building an edge of a hexagon with rubidium in the center and in the middle between three hexagons coordinated in an octahedral arrangement as illustrated in **Figure 11.7**. Each rubidium is coordinated in a facial arrangement by three N1 and three N2 atoms with bond lengths of 3.082(4) Å (Rb–N1) and 2.970(5) Å (Rb–N2) (**Figure 11.8**). The distances between rubidium and the nitrogen atoms of the tetrazolate anion are shorter than have been observed for other rubidium tetrazolate derivates found in literature.[71d] The C–N and N–N bond lengths observed in the tetrazolate anion are by far the shortest determined for compounds **127–134** (d(N2–N3) = 1.272(9) Å, d(N1–N2) = 1.308(6) Å, d(N1–C1) = 1.298(5) Å), which corresponds nicely with the increased density of 2.367 g cm^{-3} observed for **132**. The bond angles however match well those obtained for the other tetrazolate salts. (∢(N2–N1–C1) = 103.4(4)°, ∢(N1–N2–N3) = 110.0(3)°, ∢(N4–C1–N1) = 113.2(7)°, ∢(N1–C1–H1) = 123.2(6)°). Although rubidium tetrazolate crystallizes in the same crystal system as potassium tetrazolate, considerable differences in the crystal structure are observed, for example, the difference in the calculated densities, as well as the coordination spheres around the metal cations. Whereas **131** only shows a trigonal coordination of three tetrazolate nitrogen atoms to the potassium cations, **132** shows a octahedral coordination around the Rb cations, which may be due to the larger ionic radius of Rb^+ in comparison with K^+.

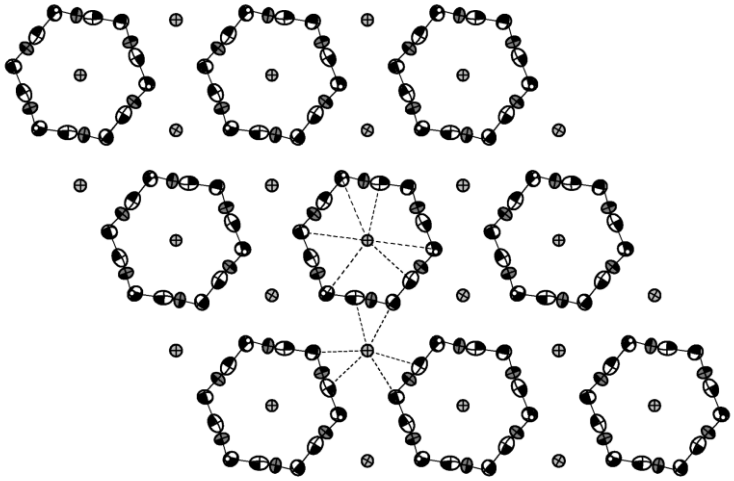

Figure 11.7 Rubidium tetrazolate (**132**): view along the *c* axis.

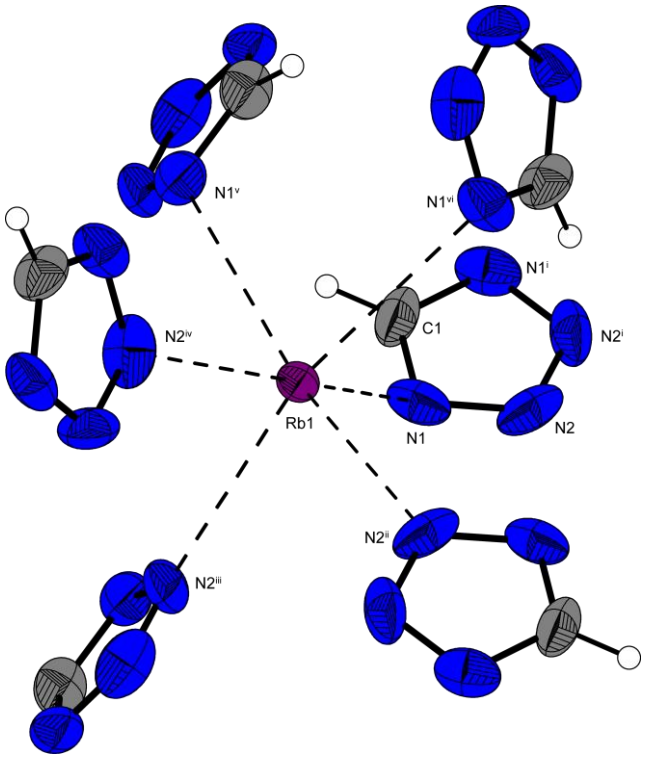

Figure 11.8 Coordination sphere of rubidium tetrazolate (**132**). Thermal ellipsoids are drawn at the 50 % probability level and hydrogen atoms are shown as small spheres of arbitrary radii; (i) x, y, –0.5–z; (ii) 1–x, –y, –z; (iii) 1–x, –y, –z; (iv) 1+y, 1–x+y, –z; (v) 1–x+y, 1–x, z; (vi) 1–y, x–y, z.

11.3.7 Cesium tetrazolate (**133**)

133 crystallizes in the orthorhombic crystal system *Pbca* with eight molecules per unit cell. Each cesium atom is coordinated in a distorted octahedral arrangement by six tetrazolate anions involving nine nitrogen atoms since three tetrazolate rings are coordinated by two nitrogen atoms each. The distances between the cesium and the nitrogen atoms of the tetrazolate rings are between 3.154(5) Å (Cs–N3) and 3.370(5) Å (Cs–N5) and can be compared to those found in cesium 5-cyanotetrazolate.[363] The coordination sphere of **133** is shown in **Figure 11.9**.

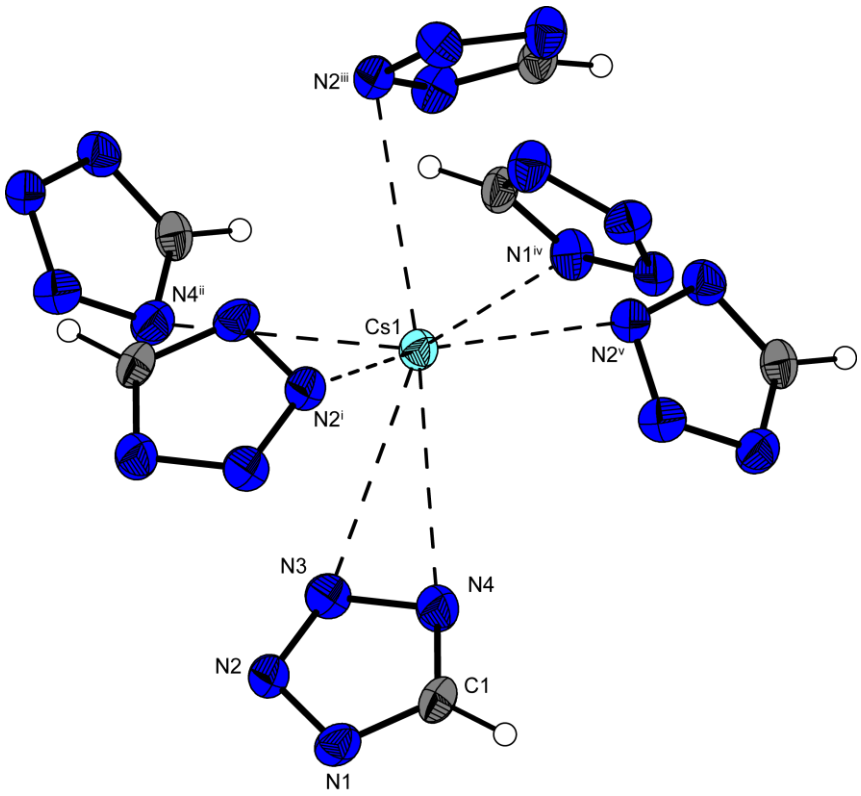

Figure 11.9 Coordination sphere of cesium tetrazolate (**133**). Thermal ellipsoids are drawn at the 50 % probability level; (i) –x, 2–y, 2–z; (ii) –0.5+x, 1.5–y, 2–z; (iii) x, 1.5–y, 0.5+z; (iv) 0.5–x, 2–y, 0.5+z; (v) 0.5+x, 1.5–y, 2–z.

As a result of the two different coordination modes of the tetrazolate to the Cs cations, the tetrazolate rings show the largest variation in bond lengths of compounds **127–134**. The C1–N4 bond (d = 1.316(8) Å) is approximately 0.01 Å longer than the C1–N1 bond (d = 1.306(8) Å). The ring N–N bonds also show considerable variations. The N1–N2 bond length is 1.346(7) Å, whereas N3–N4 is 1.339(8) Å. Cesium tetrazolate shows the highest density (3.118 g cm^{-3}) of compounds **127–134** and shows the shortest bond

lengths except for rubidium tetrazolate. In addition, in comparison to other cesium tetrazolate derivates reported in literature,[364] the density of **133** is surprisingly high. In the crystalline state **133** forms a layer structure of alternating cesium and tetrazolate layers in the *a,c*-plane. (**Figure 11.10**)

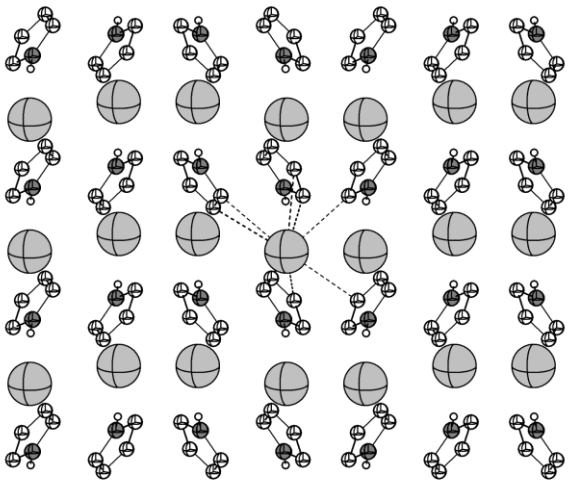

Figure 11.10 Cesium tetrazolate (**133**): view along the *a* axis

11.3.8 Strontium tetrazolate pentahydrate (**134**)

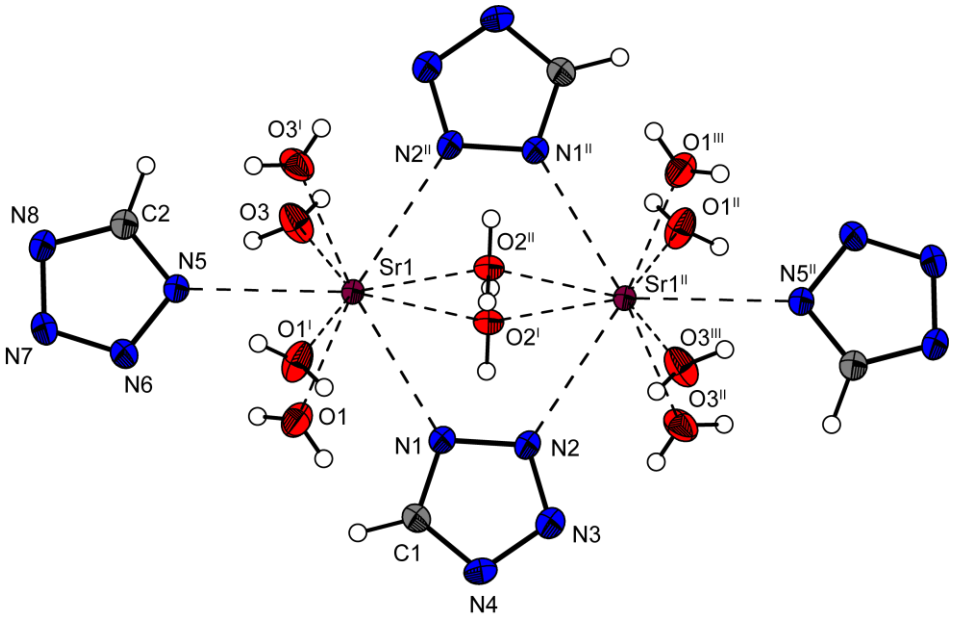

Figure 11.11 Coordination sphere of strontium tetrazolate pentahydrate (**134**) forming $Sr_2TZ_4 \cdot 10\ H_2O$ dimers. Thermal ellipsoids are drawn at the 50 % probability level and hydrogen atoms are shown as small spheres of arbitrary radii; (i) x, y, –z; (ii) 2–x, –y, z; (iii) 2–x, –y, –z.

Strontium tetrazolate crystallizes as a pentahydrate in the orthorhombic space group *Pnnm* with four moieties in the unit cell. A three-dimensional network of **134** (**Figure 11.12**) is formed by dimeric strontium tetrazolate pentahydrate units, $Sr_2TZ_4 \cdot 10\ H_2O$ whose structure is shown in **Figure 11.11**. Each strontium atom is ninefold coordinated by six molecules of crystal water and three tetrazolate rings. The two strontium atoms of each unit are connected *via* two water molecules and two tetrazolate anions, acting as μ_2-bridges in diametrically opposed arrangements. Both the two bridging and the two end-on coordinated tetrazolate rings are each arranged in-plane diametrically opposite each other (torsion angles: ∢(N5–Sr1–N1–N2) = 180.0(1)°, ∢(N5–Sr1–N1–C1) = 0.0(1)°, ∢(N1–Sr1–N5–N6) = 0.0(1)°, ∢(N1–Sr1–N5–C2) = 180.0(1)°).

Despite the different coordination sphere of the tetrazolate ring, both show similar bond lengths and angles. The ring is asymmetrical with bond lengths of 1.341(3) Å and 1.344(3) Å for N1–N2 respectively N3–N4, 1.328(4) Å and 1.322(4) Å for N1–C1 respectively N4–C1 and 1.310(3) Å for N2–N3. The bond angles (∢(N2–N1–C1) = 104.2(2)°, ∢(N4–N3–C1) = 104.1(2)°, ∢(N1–N2–N3) = 109.4(2)°, ∢(N2–N3–N4) = 109.6(2)°, ∢(N1–C1–N4) = 112.7(3)°, ∢(N1–C1–H1) = 123(2)°, ∢(N4–C1–H1) = 124(2)°) are very similar to the corresponding angles observed for compounds **127–134**. Although the different coordination of the tetrazolate rings apparently has no effect on their properties, in the case of crystal water it does. This effect of unequal coordination modes can be verified impressively with DSC (difference scanning calorimetry) on the basis of crystal water release as discussed below.

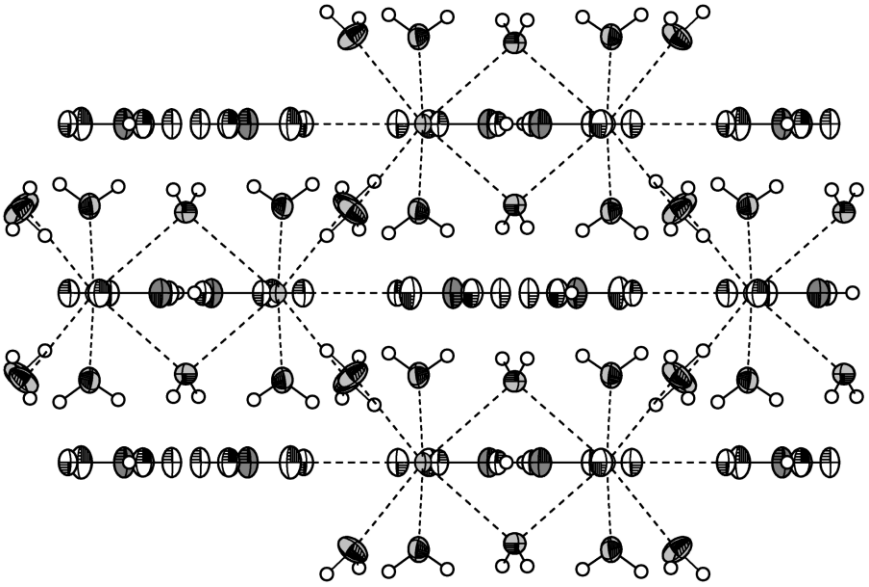

Figure 11.12 View on the packing of strontium tetrazolate pentahydrate (**134**) along the *a* axis.

Table 11.1 Bond lengths [Å] of **127–130**.

Atoms	d(1–2) [Å]	d(1–2) [Å]	d(1–2) [Å]	d(1–2) [Å]
	127	**128**	**129**	**130**
N1–N2	1.344(2)	1.341(5)	1.345(3)	1.351(1)
N1–C1	1.326(2)	1.335(5)	1.333(3)	1.328(1)
N4–C1	1.320(2)	1.327(6)	1.328(3)	1.328(1)
N4–N3	1.342(2)	1.342(5)	1.344(3)	1.351(1)
N2–N3	1.305(2)	1.310(5)	1.312(3)	1.303(2)
C1–H1	0.96(2)	0.99(5)	0.96(3)	0.91(3)

Table 11.2 Bond lengths [Å] of **131–134**.

Atoms	d(1–2) [Å]	d(1–2) [Å]	d(1–2) [Å]	d(1–2) [Å]
	131	**132**	**133**	**134**
N1–N2	1.345(5)	1.308(6)	1.346(7)	1.341(3)
N1–C1	1.319(4)	1.298(5)	1.306(8)	1.328(4)
N4–C1	1.319(4)	1.298(5)	1.316(8)	1.322(4)
N4–N3	1.345(5)	1.308(6)	1.339(8)	1.344(3)
N2–N3	1.300(5)	1.272(9)	1.294(7)	1.310(3)
C1–H1	0.950(5)	0.91(8)	0.95(7)	0.94(4)

Table 11.3 Bond angles [°] of **127–130**.

Atoms	∢(1–2–3) [°]	∢(1–2–3) [°]	∢(1–2–3) [°]	∢(1–2–3) [°]
	127	**128**	**129**	**130**
N2–N1–C1	104.1(1)	104.4(4)	104.1(2)	104.2(1)
C1–N4–N3	104.5(1)	104.5(3)	104.3(2)	104.2(1)
N1–N2–N3	109.6(1)	109.4(3)	109.6(2)	109.6(6)
N2–N3–N4	109.4(1)	109.6(3)	109.6(2)	109.6(6)
N4–C1–N1	112.5(1)	112.0(4)	112.5(2)	112.5(2)
N4–C1–H1	123(1)	124(3)	123.4(2)	123.8(7)

Table 11.4 Bond angles [°] of **131–134**.

Atoms	∢(1–2–3) [°]	∢(1–2–3) [°]	∢(1–2–3) [°]	∢(1–2–3) [°]
	131	**132**	**133**	**134**
N2–N1–C1	103.8(3)	103.4(4)	103.5(5)	104.2(2)
C1–N4–N3	103.8(3)	103.4(4)	103.4(5)	104.1(2)
N1–N2–N3	109.6(2)	110.0(3)	109.5(5)	109.4(2)
N2–N3–N4	109.6(2)	110.0(3)	109.8(5)	109.6(2)
N4–C1–N1	113.3(5)	113.2(7)	113.9(6)	112.7(3)
N4–C1–H1	123.4(5)	123.2(6)	124(4)	124(2)

11.4 Spectroscopy

11.4.1 Vibrational Spectroscopy

1*H*-Tetrazole (**1**) and its salts **127–134** can be easily identified using vibrational IR and Raman spectroscopy.[365] The vibrational spectra of salts containing the tetrazolate anion were assigned by calculating (DFT B3LYP/cc-pVDZ) the vibrational spectra of the tetrazolate anion after optimizing the structure using the GAUSSIAN 03 software.[115] **Table 11.5** shows a comparison of calculated (B3LYP/cc-pVDZ) and experimentally obtained vibrational spectra of the tetrazolate anion and the potassium salt **131**, respectively. A correction factor of 0.99 was used. The Raman spectra of compounds **1** as well as **127–134** are illustrated in **Figure 11.13**, whereby the red shift of the most intense $\nu_s(N_2–N_3)$ vibration in neutral **1** relative to salts **127–134** can clearly be observed.

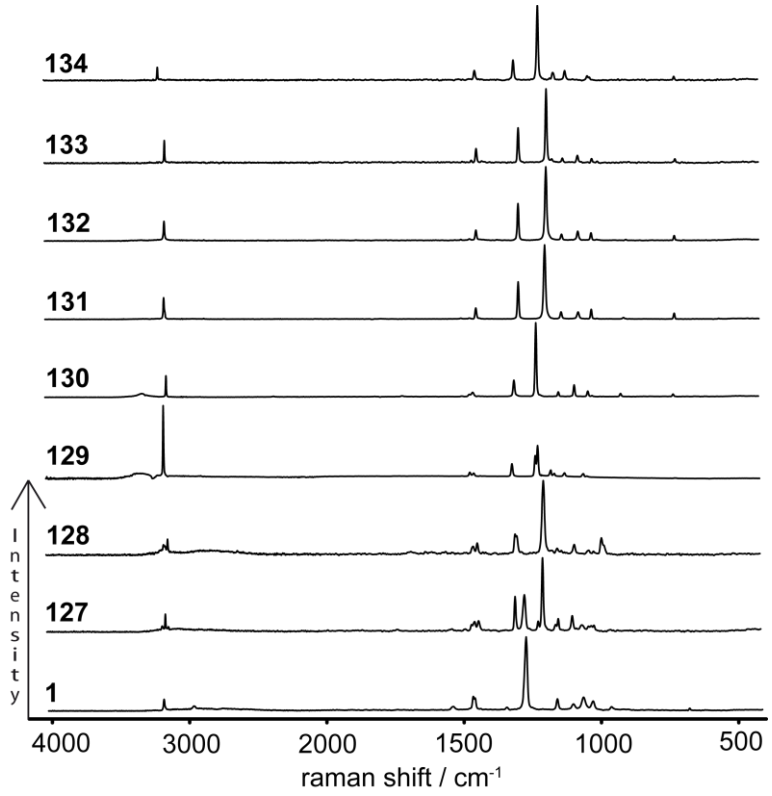

Figure 11.13 Raman spectra of compounds **1** and **127–134**.

Table 11.5 Raman and IR-data of potassium tetrazolate (**131**).

Raman			**IR**			
theory	· 0.99	Experiment	theory	· 0.99	exp.	vibr.
3200 (100)	3168	3135 (29)	3200 (100)	3168	3136 (m)	ν(C–H)
1475 (5)	1460	1430 (15)	1475 (28)	1460	1428 (s)	δ(C–H)
1297 (6)	1284	1276 (50)	1297 (2)	1284	1276 (m)	δ_s(N–C–N)
1190 (21)	1178	1180 (100)	1172 (6)	1178	1145 (s)	$\nu_s(N_2–N_3)$
1143 (7)	1131	1120 (9)	1143 (15)	1131	1120 (s)	δ(N–N)
1075 (1)	1064	1058 (9)	1075 (5)	1064	1053 (m)	$\nu_s(N_1–N_2)$
1023 (8)	1012	1010 (13)	1023 (13)	1012	1008 (s)	δ(N–C–N)
			1010 (15)	1000	995 (s)	δ(ring)
721 (1)	714	708 (8)	722 (7)	714	706 (s)	γ(N–C–N)

11.4.2 NMR Spectroscopy

1*H*-Tetrazole (**1**) and salts **127–134** were characterized in D_2O or d_6-DMSO solutions using multinuclear (^{1}H, ^{7}Li, ^{13}C, ^{14}N, ^{15}N) NMR spectroscopy. All shifts are given with

respect to TMS (^{1}H, ^{13}C), CH_3NO_2 (^{14}N, ^{15}N) and LiCl (^{7}Li) as external standards. In the case of 1*H*-tetrazole (**1**) both, the C–H and N–H hydrogens are observed as singulets (C–H = 9.29 ppm, N–H = 11.1 ppm) in the ^{1}H NMR spectrum whereby the tetrazolate anion in the ^{1}H NMR spectra of **127–134** shows only one singulet (C–H = 8.10–8.36 ppm) corresponding to the C–H group, shifted upfield relative to **1**. Additionally, compounds **127**, **130** and **134** show a signal between 4.6 and 4.7 ppm in D_2O corresponding to crystal water, **127** shows an ammonium signal at 6.7 ppm in d_6-DMSO (not observed in D_2O) and **128** shows a signal at 6.8 ppm corresponding to the hydrazinium cation. In the ^{13}C spectra, a downfield shift of the tetrazolate carbon atom in compounds **127–134** (signals between 149.7 and 150.4 ppm in D_2O) relative to 1*H*-tetrazole (142.9 ppm in D_2O) can be observed. For compound **129**, one signal at 2.3 ppm in *d6*-DMSO in the ^{7}Li spectrum can be observed. Similarly, the ^{14}N NMR spectra show also a downfield shift of the two signals for N2, N3 and N1, N4. Whereas in 1*H*-tetrazole the N1, N4 and N2, N3 signals are observed at –107 and –15 ppm respectively, the tetrazolate anions in **127–134** possess signals at between –76 and –74 ppm (N1, N4) and –9 and –7 ppm (N2, N3). In the ^{15}N NMR spectrum of 1*H*-tetrazole (**Figure 11.14**), two signals can be observed at –98 ppm (N1, N4) and –7 ppm (N2, N3) whereas the ammonium salt shows a considerable downfield shift of N1, N4 (–75.2 ppm) and an upfield shift of N2, N3 (–0.6 ppm). In addition, **127** and **128** show signals at –362 and–333 ppm, respectively, in the ^{14}N NMR spectra corresponding to the ammonium and hydrazinium nitrogen atoms respectively (**Figure 11.14**).

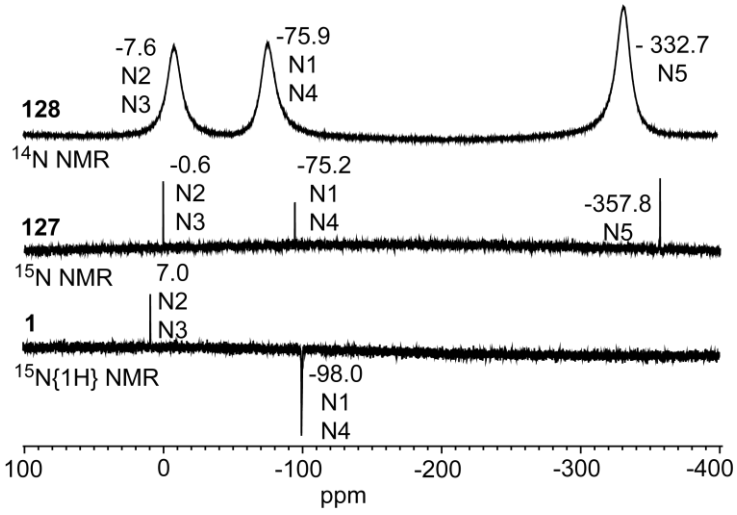

Figure 11.14 NMR spectra of compounds **1**, **127** and **128**. top: ^{14}N NMR spectrum of compound **128**. middle: ^{15}N NMR spectrum of **127**. below: ^{15}N{^{1}H} NMR spectrum of 1*H*-tetrazole (**1**).

11.5 Energetic Properties

The physico-chemical properties of **1** and **127**–**134** are summarized in **Table 11.6** and **Table 11.7**.

11.5.1 Differential Scanning Calorimetry

DSC measurements were undertaken in order to determine the thermal behavior of 1*H*-tetrazole (**1**) and its salts **127**–**134**. The measurements were performed in covered Al-containers with a nitrogen flow of 20 mL min^{-1} on a Perkin-Elmer Pyris 6 DSC, at a heating rate of 5 °C min^{-1}. The DSC plots in **Figure 11.15** show the thermal behavior of ~1.5 mg of **1** and **127**–**134** in the temperature range from 50–400 °C. 1*H*-tetrazole shows a sharp melting point at 154 °C before decomposing at 188 °C. The alkali salts **129**–**133** show melting points between 130 and 280 °C and decompose at 240 °C (**7**) and approximately 305 °C (**130**, **131**, **133**). In the case of **130**, the peak between 100 °C and 150 °C can be attributed to the release of crystal water. The lithium salt (**129**) shows the highest decomposition temperature at 380 °C without melting. **134** shows three sharp peaks corresponding to the release of crystal water between 110 °C and 130 °C. The first two similar peaks may be due to the release of monodentate coordinated crystal water molecules, whereas the third peak corresponding to the release of the μ_2-coordinating crystal water of strontium tetrazolate pentahydrate. Decomposition of **134** takes place at 335 °C.

Salts **127** and **128** both show very low melting points in the range of 40–60 °C (**127**) and 60–80 °C (**128**) and decompose at 216 °C (**127**) and 232 °C (**128**). In the case of **127** the additional endothermic peak at about 160 °C may correspond to the release of crystal water. Several endothermic steps in the DSC of hydrazinium tetrazolate between 170 and 220 °C remain unclear, but may be the result of a phase transition in the melt.

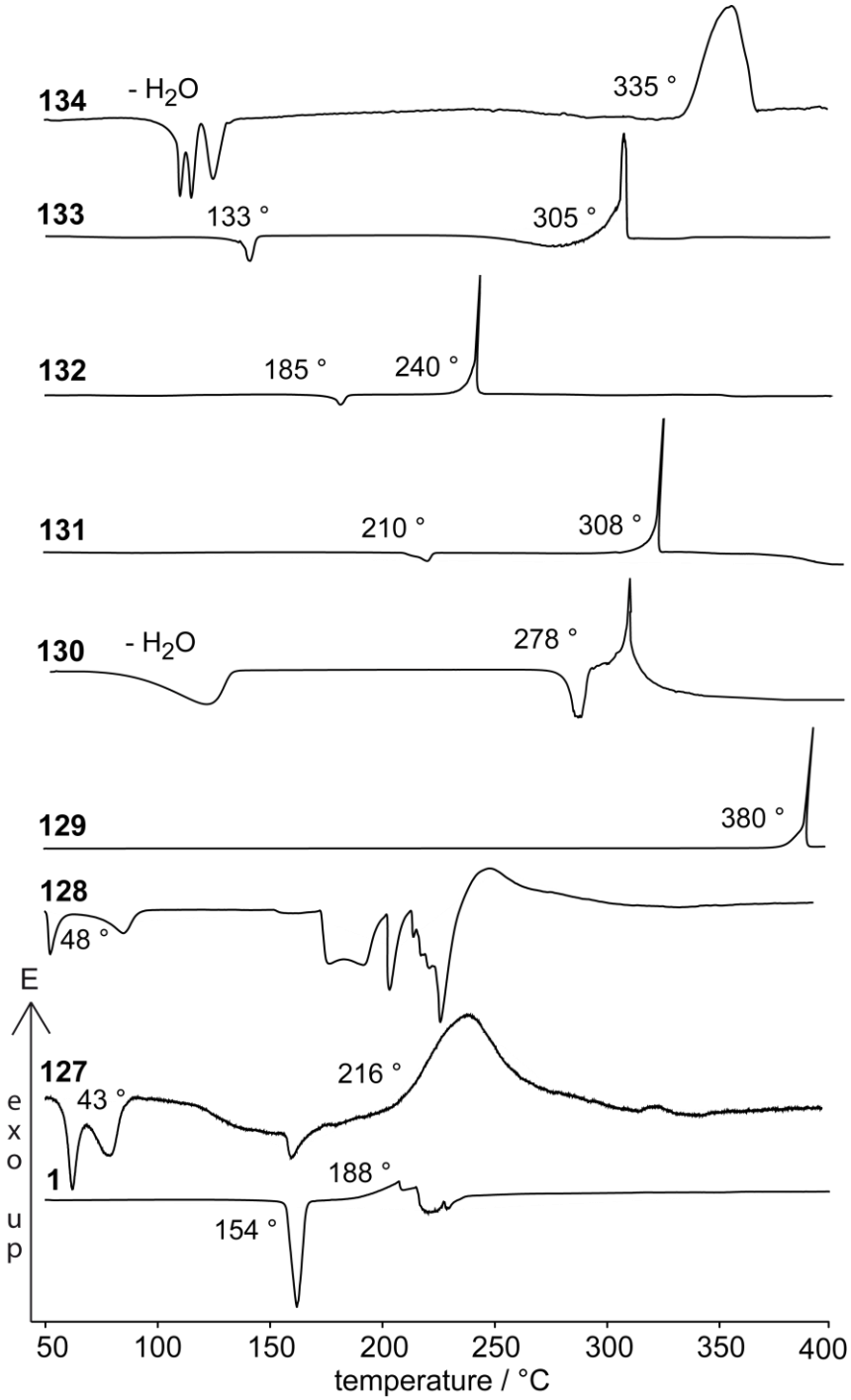

Figure 11.15 DSC plot (exo up) of compounds **1** and **127–134** (5 °C min^{-1}). $T_{Dec.}$: **1**: 188 °C, **127**: 216 °C, **128**: 232 °C, **129**: 380 °C, **130**: 303 °C, **131**: 308 °C, **132**: 240 °C, **133**: 305 °C, **134**: 335 °C.

11.5.2 Bomb Calorimetry

Since tetrazoles are usually endothermic compounds, the heats of formation (ΔH_f) of all salts presented were calculated using the energies of combustion (ΔU_c) which were

determined using bomb calorimetric measurements. The enthalpy of formation, $\Delta H_f°$, for each of the salts was calculated at 298 K using the Hess thermochemical cycle and the following combustion reactions.

127: $CH_7N_5O + 2.25\ O_2 \longrightarrow CO_2\ (g) + 3.5\ H_2O\ (l) + 2\ N_2\ (g)$

128: $CH_6N_6 + 2.5\ O_2 \longrightarrow CO_2\ (g) + 3\ H_2O\ (l) + 3\ N_2\ (g)$

129: $LiCHN_4 + 1.5\ O_2 \longrightarrow 1/2\ Li_2O\ (s) + CO_2\ (g) + 0.5\ H_2O\ (l) + 2\ N_2\ (g)$

130: $NaCH_3N_4O + 1.75\ O_2 \longrightarrow 1/2\ Na_2O_2\ (s) + CO_2\ (g) + 1.5\ H_2O\ (l) + 2\ N_2\ (g)$

131: $KCHN_4 + 2.25\ O_2 \longrightarrow KO_2\ (s) + CO_2\ (g) + 0.5\ H_2O\ (l) + 2\ N_2\ (g)$

132: $RbCHN_4 + 2.25\ O_2 \longrightarrow RbO_2\ (s) + CO_2\ (g) + 0.5\ H_2O\ (l) + 2\ N_2\ (g)$

133: $CsCHN_4 + 2.25\ O_2 \longrightarrow CsO_2\ (s) + CO_2\ (g) + 0.5\ H_2O\ (l) + 2\ N_2\ (g)$

134: $SrC_2H_{12}N_8O_5 + 3\ O_2 \longrightarrow SrO\ (s) + 2\ CO_2\ (g) + 6\ H_2O\ (l) + 4\ N_2\ (g)$

Scheme 11.4 Combustion reactions of compounds **127**–**134**.

The heats of formation of compounds **127**–**134** were calculated to $\Delta H_f°$ (kJ mol^{-1}) : **127** = 154, **128** = 145, **129** = 76, **130** = –291, **131** = 174, **132** = 150, **133** = 144, **134** = –1293. All compounds are less endothermic comparing to neutral 1*H*-tetrazole (237 kJ mol^{-1}).[358] The lowering of $\Delta H_f°$ by the inclusion of crystal water can be significantly seen on the values of **130** and **134**.

11.5.3 Sensitivities and Flame Colors

The sensitivities of all compounds **1** and **127**–**134** were tested using the BAM drophammer and friction tester. Except for, 1*H*-tetrazole (**1**) which is very sensitive towards impact (< 4 J), compounds **127**–**134** are insensitive towards impact (> 100 J). Since there is no friction sensitivity for **1** and **127**–**134** under the conditions used, all compounds can be classified (UN recommendations on the transport of dangerous goods) as insensitive towards friction (> 360 N). **1** and **127**–**134** combust nearly without smoke whereas **129–134** show brilliant flame colors as a result of the presence of the metal cations (Li^+: red, Na^+: yellow, K^+: red, Rb^+: purple red, Cs^+: pale blue, Sr^{2+}: red (**Figure 11.16**).

Figure 11.16 Combustion of a mixture containing magnesia and strontium tetrazolate pentahydrate (1:1).

Table 11.6 Physico-chemical properties of **1**, **127–130**

	1	**127**	**128**	**129**	**130**
Formula	CH_2N_4	CH_7N_5O	CH_6N_6	CHN_4Li	CH_3N_4NaO
Molecular Mass	70.05	105.12	102.10	75.99	110.05
Impact sensitivity (J)[a]	< 4	> 100	> 100	> 100	> 100
Friction sensitivity (N)[b]	> 360	> 360	> 360	> 360	> 360
N (%)[c]	79.98	66.64	82.31	73.73	20.89
Ω (%)[d]	–68.52	–68.51	–78.35	–63.17	–50.89
Combustion	yes	yes	yes	yes	yes
Flame color	colorless	colorless	colorless	red	yellow
T_{dec} (°C)[e]	188	216	232	380	303
Density (g cm^{-3})[f]	1.529 [366]	1.343	1.385	1.472	1.745
$-\Delta U_{comb.}$ (cal g^{-1})[g]	3281	2823	3287	2880	1717
$-\Delta H_{comb}$ (kJ mol^{-1})[h]	916 [358]	1240	574	913	788
$\Delta_f H_m$ (kJ mol^{-1})[i]	237	154	145	76	–291
EXPLO5 values:					
$-\Delta_E U_m°$ (J g^{-1})[k]	3941	4679	2529	-	-
T_E (K)[l]	3047	2928	2015	-	-
$p_{C\text{-}J}$ (kbar)[m]	210	211	164	-	-
$V_{Det.}$ (m s^{-1})[n]	7813	8276	7546	-	-
Gas vol. (L kg^{-1})[o]	785	994	954	-	-

[a] BAM drophammer; [b] BAM friction tester,; [c] Nitrogen content; [d] Oxygen balance; [e] Temperature of decomposition by DSC (β = 2°C); f estimated from a structure determination; g Experimental (constant volume) combustion energy; [h] Experimental molar enthalpy of combustion; [i] Molar enthalpy of formation; [j] experimental enthalpy of decomposition using DSC; [k] Energy of Explosion, EXPLO5 V5.02; [l] explosion temperature, EXPLO5 V5.02 [m] detonation pressure; [n] detonation velocity; [o] Assuming only gaseous products.

Table 11.7 Physico-chemical properties of **131–134**

	131	**132**	**133**	**134**
Formula	CHN_4K	CHN_4Rb	CHN_4Cs	$C_2H_{12}N_8O_5Sr$
Molecular Mass	108.14	154.51	201.95	315.79
Impact sensitivity (J)[a]	> 100	> 100	> 100	> 100
Friction sensitivity (N)[b]	> 360	> 360	> 360	> 360
N (%)[c]	51.81	36.26	27.74	35.48
Ω (%)[d]	–66.58	–46.60	–35.65	–30.40
Combustion	yes	yes	yes	yes
Flame color	purple red	red	pale blue	red
T_{dec} (°C)[e]	308	240	305	335
Density (g cm^{-3})[f]	1.774	2.367	3.118	1.877
$-\Delta U_{comb.}$ (cal g^{-1})[g]	2203	1510	1156	1308
$-\Delta H_{comb}$ (kJ mol^{-1})[h]	996	975	976	1722
$\Delta_f H_m$ (kJ mol^{-1})[i]	174	150	144	–1293

11.6 Experimental Part

CAUTION! 1H-Tetrazole is an energetic compound with sensitivity towards heat, impact and friction. Although we had no problems in synthesis, proper protective measures (safety glasses, face shield, leather coat, earthened equipment and shoes, Kevlar® gloves and ear plugs) should be used when undertaking work involving ***1*** *as well as* ***127–129*** *on larger scales.*

*1H-Tetrazole (**1**):* Glacial acetic acid (24.0 g, 0.40 mol) was added dropwise to a suspension of sodium azide (6.50 g, 0.10 mol) and ammonium chloride (5.30 g,

0.10 mol) in triethyl orthoformate (44.4 g, 0.30 mol) and refluxed for ten hours at 80 °C. Afterwards the suspension was evaporated to dryness and 100 mL of acetone were added. The suspension was heated and filtrated while hot. The filtrate was then evaporated to dryness and recrystallized from ethyl acetate yielding 1*H*-tetrazole as colorless single crystals (4.20 g, yield 60 %). **DSC** (T_{onset}, 2 °C min^{-1}): 154 °C, 188 °C (dec.); **IR** (ATR, cm^{-1}): $\tilde{\nu}$ = 3156 (vs), 3057 (m), 2968 (w), 2818 (s), 2689 (s), 2573 (s), 2487 (m), 2350 (w), 2307 (w), 1813 (w), 1726 (w), 1520 (s), 1444 (w), 1388 (m), 1252 (s), 1144 (m), 1083 (m), 1048 (m), 1011 (m), 935 (m), 899 (s), 660 (m); **Raman** (1064 nm, 400 mW, 25 °C, cm^{-1}): $\tilde{\nu}$ = 3159 (15), 2942 (8), 2732 (3), 1526 (6), 1453 (19), 1447 (17), 1330 (5), 1261 (100), 1147 (16), 1088 (9), 1051 (18), 1016 (13), 949 (5), 665 (3); **^{1}H NMR** (D_2O, 25°C, ppm): δ = 8.87 (s, -CH); **^{1}H NMR** (*d*$_6$-DMSO, 25 °C, ppm): δ = 9.29 (s, -CH), 11.1 (s, -NH); **^{13}C NMR** (D_2O, 25 °C, ppm): δ = 142.9 (CN_4); **^{13}C NMR** (*d*$_6$-DMSO, 25 °C, ppm): δ = 143.9 (CN_4); **^{14}N NMR** (*d*$_6$-DMSO, 25 °C, ppm): δ = –97 (N1, N4), –5 (N2, N3); **^{14}N NMR** (D_2O, 25°C, ppm): δ = –107 (N1, N4), –15 (N2, N3); **^{15}N NMR** (*d*$_6$-DMSO, 25°C, ppm): δ = –98.0 (N1, N4), –7.0 (N2, N3);); ***m/z*** (FAB$^-$): 69.1 [HCN_4]; **EA** (CH_2N_4, 70.05) calcd.: C 17.15, H 2.88, N 79.98 %; found: C 17.02, H 3.02, N 78.88 %; **impact sensitivity**: < 4 J; **friction sensitivity**: > 360 N; $\Delta_c U$: –3281 cal g^{-1}.

*Ammonium tetrazolate monohydrate (**127**):* To a solution of 1*H*-tetrazole (2.80 g, 40.0 mmol) in 20 mL water an excess of diluted ammonia solution was added. After stirring at 80 °C for five minutes, the solution was evaporated to dryness and the solid product recrystallized from ethanol yielding ammonium tetrazolate monohydrate as colorless single crystals (3.66 g, yield 87 %). **DSC** (T_{onset}, 2 °C min^{-1}): 43 °C, 216 °C (dec.); **IR** (ATR, cm^{-1}): $\tilde{\nu}$ = 3187 (s), 2999 (vs), 2861 (vs), 2349 (w), 2271 (w), 2210 (w), 2132 (w), 1975 (w), 1868 (w), 1748 (w), 1707 (m), 1464 (s), 1436 (s), 1428 (s), 1292 (w), 1276 (w), 1232 (w), 1192 (m), 1148 (w), 1087 (w), 1059 (w), 1026 (w), 1006 (w), 873 (w), 835 (w), 740 (w), 724 (w), 695 (m), 665 (w); **Raman** (1064 nm, 400 mW, 25 °C, cm^{-1}): $\tilde{\nu}$ = 3136 (27), 3039 (7), 1723 (3), 1474 (3), 1441 (11), 1427 (14), 1395 (3), 1294 (46), 1194 (100), 1137 (17), 1086 (19), 1028 (6), 1007 (8), 696 (2); **^{1}H NMR** (D_2O, 25 °C, ppm): δ = 4.66 (H_2O), 8.08 (s, -CH); **^{1}H NMR** (*d*$_6$-DMSO, 25 °C, ppm): δ = 3.44 (H_2O), 6.69 (NH_4^+), 8.36 (s, -CH); **^{13}C NMR** (D_2O, 25 °C, ppm): δ = 149.8 (CN_4); **^{13}C NMR** (*d*$_6$-DMSO, 25 °C, ppm): δ = 148.7 (CN_4); **^{14}N NMR** (D_2O, 25 °C, ppm): δ = –362 (NH_4^+), –74 (N1, N4), –7 (N2, N3); **^{15}N NMR** (*d*$_6$-DMSO, 25 °C, ppm): δ = –357.8 (NH_4^+), –75.2 (N1, N4), –0.6 (N2, N3); ***m/z*** (FAB$^-$): 69.1 [HCN_4]; **impact sensitivity**: > 100 J; **friction sensitivity**: > 360 N; $\Delta_c U$: –2823 cal g^{-1}.

*Hydrazinium tetrazolate (**128**):* 1*H*-Tetrazole (2.80 g, 40.0 mmol) and an excess of hydrazinium hydroxide (2.50 g, 50 mmol) were dissolved in 40 mL of water. The solution was refluxed for five minutes before the water was removed under vacuum. Recrystallization from ethanol yielded hydrazinium tetrazolate as colorless single crystals (3.72 g, yield 91 %). **DSC** (T_{onset}, 2 °C min^{-1}): 48 °C, 232 °C (dec.); **IR** (ATR, cm^{-1}): $\tilde{\nu}$ = 3211 (s), 3105 (s), 3057 (m), 2884 (s), 2755 (s), 2643 (vs), 2202 (m), 2125 (m), 1934 (w), 1728 (w), 1645 (m), 1545 (m), 1440 (w), 1424 (m), 1306 (w), 1281 (w), 1155 (s), 1132 (s), 1076 (m), 1020 (m), 1000 (m), 972 (m), 864 (m), 696 (m), 593 (w); **Raman** (1064 nm, 400 mW, 25 °C, cm^{-1}): $\tilde{\nu}$ = 3203 (4), 3115 (17), 1670 (3), 1447 (10), 1431 (8), 1291 (23), 1187 (100), 1138 (7), 1122 (7), 1075 (9), 1022 (6), 1008 (5), 967 (11), 946 (14), 706 (2), 271 (5), 243 (7), 205 (10), 180 (7), 141 (7); **^{1}H NMR** (*d*$_6$-DMSO, 25 °C, ppm): δ = 6.80 ($N_2H_5^+$), 8.21 (s, -CH); **^{13}C NMR** (D_2O, 25 °C, ppm): δ = 150.0 (CN_4); **^{13}C NMR** (*d*$_6$-DMSO, 25 °C, ppm): δ = 149.0 (CN_4); **^{14}N NMR** (D_2O, 25 °C, ppm): δ = –333 ($N_2H_5^+$), –76 (N1, N4), –8 (N2, N3); ***m/z*** (FAB^-): 69.1 [HCN_4]; **EA** (CH_6N_6, 102.10) calcd.: C 11.76, H 5.92, N 82.31 %; found: C 11.75, H 5.78, N 81.77 %; **impact sensitivity**: > 100 J; **friction sensitivity**: > 360 N; ΔU_c: –3287 cal g^{-1}.

*Lithium tetrazolate (**129**):* 1*H*-Tetrazole (2.80 g, 40.0 mmol) was added to a solution of lithium hydroxide (0.96 g, 40 mmol) in 20 mL of water and heated to boiling. The cooled solution was evaporated to dryness and the solid product was recrystallized from ethanol yielding **129** as colorless single crystals (2.67 g, yield 88 %). **DSC** (T_{onset}, 2 °C min^{-1}): 380 °C (dec.); **IR** (ATR, cm^{-1}): $\tilde{\nu}$ = 3372 (w), 3156 (s), 2851 (w), 2692 (w), 2568 (w), 2259 (w), 1813 (w), 1748 (w), 1652 (w), 1522 (w), 1452 (m), 1440 (m), 1300 (w), 1253 (m), 1216 (m), 1208 (m), 1152 (vs), 1110 (m), 1084 (w), 1035 (s), 1024 (s), 936 (w), 903 (w), 880 (w), 865 (s), 699 (s), 663 (w); **Raman** (1064 nm, 400 mW, 25 °C, cm^{-1}): $\tilde{\nu}$ = 3144 (53), 2986 (36), 1455 (21), 1440 (18), 1302 (46), 1217 (70), 1208 (100), 1162 (26), 1148 (17), 1111 (19), 1042 (18); **^{1}H NMR** (D_2O, 25 °C, ppm): δ = 8.45 (s, -CH); **^{1}H NMR** (*d*$_6$-DMSO, 25 °C, ppm): δ = 8.33 (s, -CH); **^{13}C NMR** (D_2O, 25 °C, ppm): δ = 149.7 (CN_4); **^{13}C NMR** (*d*$_6$-DMSO, 25 °C, ppm): δ = 148.5 (CN_4); **^{7}Li NMR** (D_2O, 25 °C, ppm): δ = 0.1 (s, Li^+); **^{7}Li NMR** (*d*$_6$-DMSO, 25 °C, ppm): δ = 2.3 (s, Li^+); ***m/z*** (FAB^-): 69.1 [HCN_4]; **EA** ($CHLiN_4$, 75.99) calcd.: C 15.81, H 1.33, N 73.73 %; found: C 15.69, H 1.54, N 73.56 %; **impact sensitivity**: > 100 J; **friction sensitivity**: > 360 N; $\Delta_c U$: –2880 cal g^{-1}.

*Sodium tetrazolate monohydrate (**130**):* 2.80 g (40.0 mmol) of 1*H*-tetrazole were added to a solution of sodium hydroxide (1.60 g, 40.0 mmol) in 40 mL of water and refluxed for five minutes. After cooling to room temperature the water was removed under reduced pressure. Recrystallization from ethanol yielded sodium tetrazolate monohydrate as colorless single crystals (4.14 g, yield 94 %). **DSC** (T_{onset}, 2 °C min^{-1}): 278 °C, 303 °C (dec.); **IR** (ATR, cm^{-1}): $\tilde{\nu}$ = 3277 (vs), 3115 (s), 2328 (w), 2268 (w), 2168 (w), 2052 (w), 1796 (w), 1689 (s), 1578 (w), 1440 (m), 1286 (m), 1208 (s), 1160 (m), 1132 (m), 1064 (m), 1020 (m), 1008 (m), 903 (m), 700 (m), 652 (s); **Raman** (1064 nm, 400 mW, 25 °C, cm^{-1}): $\tilde{\nu}$ = 3288 (4), 3115 (29), 1440 (6), 1290 (23), 1210 (100), 1128 (7), 1070 (16), 1021 (8), 900 (4), 710 (4); **^{1}H NMR** (D_2O, 25 °C, ppm): δ = 4.63 (H_2O), 8.41 (s, -CH); **^{1}H NMR** (*d*$_6$-DMSO, 25°C, ppm): δ = 3.79 (H_2O), 8.10 (s, -CH); **^{13}C NMR** (D_2O, 25 °C, ppm): δ = 150.2 (CN_4); **^{13}C NMR** (*d*$_6$-DMSO, 25 °C, ppm): δ = 149.4 (CN_4); **^{14}N NMR** (*d*$_6$-DMSO, 25 °C, ppm): δ = –59 (N1, N4), 7 (N2, N3); ***m/z*** (FAB$^-$): 69.1 [HCN_4]; **EA** (CH_3N_4NaO, 110.05) calcd.: C 10.91, H 2.75, N 50.91 %; found: C 10.66, H 2.66, N 48.87 %; **impact sensitivity**: > 100 J; **friction sensitivity**: > 360 N; $\Delta_c U$: –1717 cal g^{-1}.

*Potassium tetrazolate (**131**):* 1*H*-Tetrazole (2.80 g, 40.0 mmol) and potassium carbonate (2.76 g, 20.0 mmol) were dissolved in 20 mL of water. After the evolution of carbon dioxide gas has been ceased, the solution was refluxed for five minutes and, afterwards, evaporated to dryness. Recrystallization of the crude solid product from ethanol yielded potassium tetrazolate as colorless single crystals (3.98 g, yield 92 %). **DSC** (T_{onset}, 2 °C min^{-1}): 210 °C, 308 °C (dec.); **IR** (ATR, cm^{-1}): $\tilde{\nu}$ = 3248 (w), 3136 (m), 2575 (w), 2208 (w), 2161 (w), 2111 (w), 2029 (w), 1776 (w), 1635 (w), 1454 (w), 1428 (s), 1276 (m), 1180 (s), 1145 (s), 1120 (s), 1053 (m), 1008 (s), 995 (s), 891 (vs), 706 (s); **Raman** (1064 nm, 400 mW, 25 °C, cm^{-1}): $\tilde{\nu}$ = 3135 (29), 1430 (15), 1276 (50), 1180 (100), 1120 (9), 1058 (9), 1010 (13), 892 (2), 708 (8); **^{1}H NMR** (D_2O, 25 °C, ppm): δ = 8.43 (s, -CH); **^{13}C NMR** (D_2O, 25 °C, ppm): δ = 150.2 (CN_4); ***m/z*** (FAB$^-$): 69.1 [HCN_4]; **EA** ($CHKN_4$, 108.14) calcd.: C 11.11, H 0.93, N 51.81 %; found: C 11.11, H 1.17, N 51.33 %; **impact sensitivity**: > 100 J; **friction sensitivity**: > 360 N; $\Delta_c U$: –2203 cal g^{-1}.

*Rubidium tetrazolate (**132**):* Rubidium hydroxide (4.08 g, 40.0 mmol) and 1*H*-tetrazole (2.80 g, 40.0 mmol) were dissolved in 20 mL of water and refluxed for ten minutes. The cooled solution was evaporated to dryness and the crude solid product recrystallized from ethanol. Rubidium tetrazolate was obtained as colorless single crystals (5.50 g, 89 %). **DSC** (T_{onset}, 2 °C min^{-1}): 185 °C, 240 °C (dec.); **IR** (ATR, cm^{-1}): $\tilde{\nu}$ = 3502 (w), 3130

(m), 2658 (w), 2572 (w), 2412 (w), 2204 (w), 2156 (w), 2108 (w), 2028 (w), 1757 (w), 1621 (m), 1448 (m), 1427 (vs), 1352 (m), 1275 (m), 1173 (s), 1145 (s), 1116 (s), 1052 (m), 1008 (s), 991 (s), 880 (vs), 704 (vs); **Raman** (1064 nm, 400 mW, 25 °C, cm^{-1}): $\tilde{\nu}$ = 3129 (26), 1482 (2), 1452 (2), 1428 (14), 1275 (50), 1174 (100), 1117 (9), 1057 (13), 1009 (11), 882 (2), 706 (7); **^{1}H NMR** (D_2O, 25 °C, ppm): δ = 8.42 (s, -CH); **^{13}C NMR** (D_2O, 25 °C, ppm): δ = 150.3 (CN_4); ***m/z*** (FAB^-): 69.1 [HCN_4]; **impact sensitivity**: > 100 J; **friction sensitivity**: > 360 N; $\Delta_c U$: –1106 cal g^{-1}.

*Cesium tetrazolate (**133**):* 1*H*-Tetrazole (2.80 g, 40.0 mmol) and cesium carbonate (6.52 g, 40.0 mmol) were dissolved in 20 mL of water. After all carbon dioxide was released the solution was refluxed for five minutes and then evaporated *in vacuo*. Recrystallization of the solid product from ethanol yielded cesium tetrazolate in form of colorless single crystals (7.27 g, yield 90 %). **DSC** (T_{onset}, 2 °C min^{-1}): 133 °C, 305 °C (dec.); **IR** (ATR, cm^{-1}): $\tilde{\nu}$ = 3291 (m), 3119 (w), 2596 (w), 2412 (w), 2412 (w), 2208 (w), 2163 (w), 2109 (w), 2030 (w), 1739 (w), 1691 (w), 1444 (m), 1428 (s), 1272 (s), 1208 (w), 1171 (s), 1147 (vs), 1111 (s), 1057 (m), 1004 (s), 985 (s), 904 (w), 871 (s), 700 (s); **Raman** (1064 nm, 400 mW, 25 °C, cm^{-1}): $\tilde{\nu}$ = 3125 (30), 1442 (2), 1427 (20), 1406 (3), 1274 (48), 1172 (100), 1152 (6), 1113 (7), 1058 (10), 1006 (6), 984 (2), 703 (6); **^{1}H NMR** (D_2O, 25 °C, ppm): δ = 8.53 (s, -CH); **^{13}C NMR** (D_2O, 25 °C, ppm): δ = 150.4 (CN_4); ***m/z*** (FAB^-): 69.1 [HCN_4]; **EA** ($CHCsN_4$, 201.95) calcd.: C 5.95, H 0.50, N 27.74 %; found: C 5.93, H 0.95, N 27.17 %; **impact sensitivity**: > 100 J; **friction sensitivity**: > 360 N; $\Delta_c U$: –1156 cal g^{-1}.

*Strontium tetrazolate pentahydrate (**134**): S*trontium hydroxide octahydrate (5.32 g, 20.0 mmol) and 1*H*-tetrazole (2.80 g, 40.0 mmol) of were solved in 20 mL of water and refluxed for five minutes. The cooled solution was evaporated to dryness and the crude solid product recrystallized from wet ethanol yielding strontium tetrazolate pentahydrate in form of colorless single crystals (8.49 g, yield 94 %). **DSC** (T_{onset}, 2 °C min^{-1}): 335 °C (dec.); **IR** (ATR, cm^{-1}): $\tilde{\nu}$ = 3403 (vs), 3139 (s), 2232 (w), 1751 (w), 1637 (m), 1448 (w), 1430 (m), 1292 (m), 1184 (m), 1144 (m), 1108 (w), 1022 (m), 1006 (m), 909 (w), 879 (w), 699 (m); **Raman** (1064 nm, 400 mW, 25 °C, cm^{-1}): $\tilde{\nu}$ = 3320 (10), 3131 (76), 1682 (3), 1434 (25), 1294 (52), 1196 (100), 1187 (79), 1155 (11), 1134 (26), 1085 (15), 1024 (15), 1006 (8), 194 (8); **^{1}H NMR** (D_2O, 25 °C, ppm): δ = 4.67 (H_2O), 8.39 (s, -CH); **^{13}C NMR** (D_2O, 25 °C, ppm): δ = 150.2 (CN_4); **^{14}N NMR** (D_2O, 25 °C, ppm): δ = –76 (N1, N4), –9 (N2, N3); **EA** ($C_2H_2N_8Sr$, 225.71) calcd.: C 7.61, H 3.83, N 35.48 %;

found: C 7.55, H 3.66, N 35.04 %; **impact sensitivity**: > 100 J; **friction sensitivity**: > 360 N; $\Delta_c\mathbf{U}$: –1308 cal g^{-1}.

11.7 Conclusion

From this experimental study the following conclusions can be drawn:

- 1*H*-Tetrazole (**1**) can be synthesized using various routes, whereby the reaction of ammonium chloride, triethyl orthoformate and sodium azide in acetic acid is the most facile. Crystalline 1*H*-tetrazole is very sensitive towards impact (< 4 J) but not towards friction.

- 1*H*-Tetrazole can be easily deprotonated using common bases such as ammonia, hydrazine or the alkali and alkaline earth metal hydroxides or carbonates forming the corresponding metal tetrazolate salts. Single crystals can be obtained by recrystallization from ethanol-water mixtures.

- The structures of ammonium- (**127**), hydrazinium (**128**), lithium- (**129**), sodium- (**130**), potassium- (**131**), rubidium- (**132**), cesium- (**133**) and strontium tetrazolate (**134**) were determined using low temperature X-ray diffraction.

- Next to vibrational and NMR spectroscopy the thermal behaviors were determined using DSC measurements. Nearly all salts have melting points (in a huge range) before they decompose at higher temperatures. The heats of formation were calculated using combustion energies from bomb calorimetric measurements. **1** as well as **127**, **128**, **129**, **131**, **132** and **133** are endothermic compounds, while **130** and **134** are formed exothermic, which can be explained by the inclusion of crystal water.

- The impact and friction sensitivity, the combustion and the potential use of compounds **1** as well as **127–134** as energetic materials was tested in an extensive energetic study. Since **127** and **128** show low densities in comparison with other tetrazoles, they are “unspectacular” with regards to their performance. Compound **129** and especially **134** can be used as smokeless red colorants in novel pyrotechnical compositions.

Chapter 12.

5-Azidotetrazoles

12.1 Introduction

Many scientists are attracted to nitrogen-rich compounds, since their tendencies toward instability pose considerable technical challenges in their synthesis and isolation. N-rich molecules are considered as prime candidates for "green" energetic materials since the materials exhibit desirable performance characteristics in high explosives (HEs) or in propellant formulations, but the main combustion products are molecular nitrogen. Except for molecular nitrogen (N_2), the cubic nitrogen modification at high temperatures and pressures described by Eremets *et al.*[27,367] and the $N_3^{\cdot}$ radical in the gas phase, there is no neutral polynitrogen modification known.[368] The next member in the series of compounds containing the highest nitrogen contents (**Table 12.1**) is hydrazoic acid (HN_3, N: 97.7 %) [369] followed by $[N_5][P(N_3)_6]$ (N: 91.2 %) described by Christe et. al..[370] Unfortunately, salts containing the N_5^+ cation are often only stable at very low temperatures and require difficult preparations and are therefore unsuitable for technical use. Tetraazidomethane ($C(N_3)_4$),[371] hydrazinium azide ($N_2H_5N_3$) with the empirical formula N_5H_5,[372] ammonium azide (NH_4N_3 or N_4H_4), tetrazene (N_4H_4) [373] as well as diazene (N_2H_2) [374] all have nitrogen contents of 93.3 %. Hydrazinium azide hydrazinate ($N_2H_5N_3{\cdot}N_2H_4$) [375] and $[N_5][P(N_3)_6]$ come in eighth and ninth with 91.5 % and 91.2 % respectively. In earlier times of this thesis, 5-azido-1*H*-tetrazole (**135**, CHN_7) and its ammonia salt (**137**, NH_4CN_7) are tenth and eleventh in this series. It is worth mentioning the next highest members, of this series which are hydrazine (N_2H_4),[376] bishydrazinium azotetrazolate dihydrazinate ($[N_2H_5]_2[C_2N_{10}]{\cdot}2N_2H_4$) and bishydrazinium azotetrazolate ($[N_2H_5]_2[C_2N_{10}]$).[71c]

Table 12.1 Isolated compounds with the highest nitrogen contents.

compound	N %	compound	N %
N_2 and N_x	100 %	$[N_2H_5][N_3]{*}N_2H_4$	91.5 %
HN_3	97.7 %	$[N_5][P(N_3)_6]$	91.2 %
$[N_5][B(N_3)_4]$	95.7 %	CHN_7	88.3 %
$C(N_3)_4$	93.3 %	$[NH_4][CN_7]$	87.5 %
$[N_2H_5][N_3]$	93.3 %	N_2H_4	87.4 %
$[NH_4][N_3]$	93.3 %	$[N_2H_5]_2[C_2N_{10}]{*}2\ N_2H_4$	85.7 %
N_2H_2	93.3 %	$[N_2H_5]_2[C_2N_{10}]$	85.2 %

Tetrazoles often have the outstanding benefit of combining a high nitrogen content (yielding highly endothermic compounds) with good thermal stabilities, due to their aromatic ring system. The tetrazole with the highest N-content is 5-azido-1*H*-tetrazole (**135**), which was first described in patents in 1939 [377] and was also investigated in our research group a few years ago.[227b,378] Due to its extremely high and unpredictable explosive character, a complete characterization had not been reported. In addition, the solution of the crystal structure reported previously (wR_2 = 39 %) was poor and the position of the hydrogen atom was uncertain. Salts of the highly explosive **135** are rarely described in the literature.[379,380] The reason for this may be the extreme sensitivities. Only the IR data of the ammonium and silver 5-azidotetrazolate can be found in the literature. Although 5-azidotetrazolates are probably too sensitive for any applications, they are still interesting compounds since they contain a binary CN_x^- (x = 7) anion.

The most prominent binary carbon-nitrogen anion is the cyanide anion (CN^-). Salts of hydrogen cyanide belong to the most important chemicals used in industrial and pharmaceutical as well as agricultural processes.[381] Interestingly there are only few examples of further binary CN anions known. There are different ways to systematically divide CN anions such as the charge (singly charged ions, e.g. dicyanamide ($NC–N–CN^-$),[382] doubly charged ions, e.g. cyanamide (NCN^{2-}) [383] and triply charged ions, e.g. tricyanomelaminate ($(NC–NCN)_3^{3-}$ [384]) or the carbon-nitrogen ratio. Using the carbon-nitrogen ratio as criterion, CN anions may be grouped into three classes: (i) nitrogen-rich (C_xN_y, x < y) e.g. cyanamide and dicyanamide; (ii) carbon-rich CN anions (C_xN_y, x > y) e.g. tricyanomethanide ($C(CN)_3^-$);[385] (iii) CN anions with an equal number of carbon and nitrogen atoms (C_xN_y, x = y) e.g. cyanide. Most of the nitrogen-rich CN anions are based on the tetrazole ring such as cyanotetrazolate ($C_2N_5^-$),[386] 5-cyaniminotetrazolinediide $C_2N_6^{2-}$,[387] 5,5'-bis(tetrazolate) ($C_2N_8^{2-}$),[388] 5,5'-azotetrazolate ($C_2N_{10}^{2-}$),[71] 3,6-bis(2*H*-tetrazol-5-yl)-1,2,4,5-tetrazinediide, ($C_4N_{12}^{2-}$) [389] and 5-azidotetrazolate CN_7^-. The nitrogen-rich anions are of special interest, as they represent salts with high nitrogen contents, having high positive heats of formation and showing in the most cases remarkable thermodynamic and kinetic stabilities. A compendium of selected $C_xN_y^{z-}$ (x = max. 2, y = 1–10, z = 1–2) anions is depicted in **Figure 12.1**.

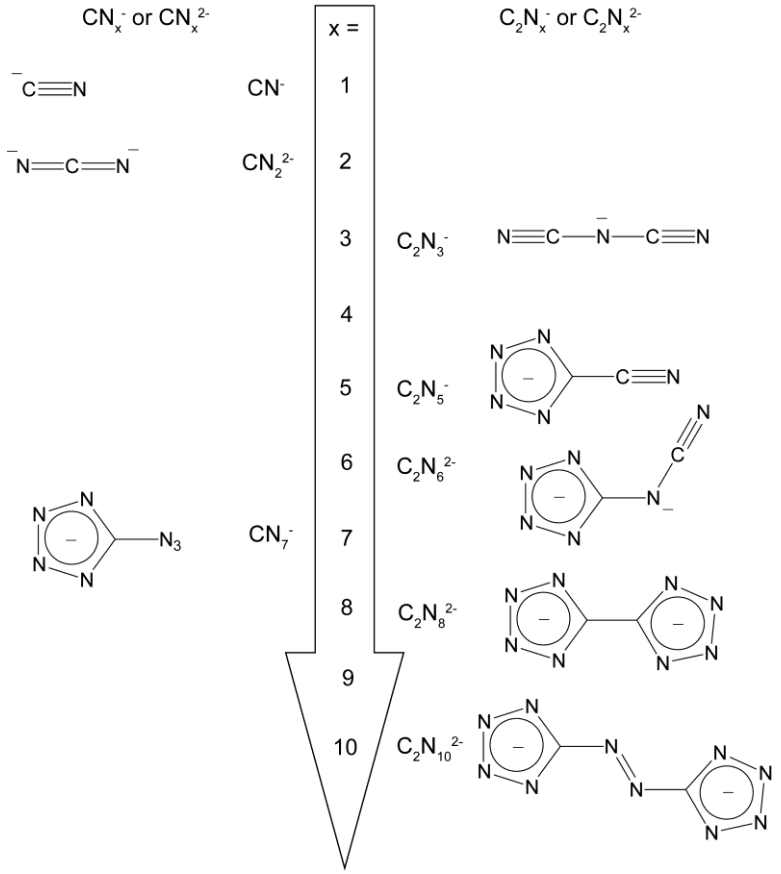

Figure 12.1 Selected N-rich C-N anions.

The CN_7^- anion represents a milestone in the development of nitrogen-rich "green" energetic materials. Energetic materials are most commonly used either in high explosives (HEs) or in propellant formulations. Whereas the performance of HEs can be related to heat of detonation ($U_{Det.}$), detonation pressure ($p_{C\text{-}J}$), and detonation velocity ($V_{Det.}$), the performance of rocket/missile propellants is best characterized by their density and specific impulse (I_{sp}). Equally important, an increase of the I_{sp} of only 20 s would be expected to increase the payload by ~100%. Moreover, for gun propellants, erosivity is an additional concern and lower reaction temperatures and a high N_2/CO ratio of the reaction gases are desirable. Recent modeling and testing have shown that the presence of high concentrations of nitrogen species in the combustion products of propellants can reduce gun barrel erosion by promoting the formation of iron nitride rather than iron carbide on the interior surface

of the barrel. Thus compounds such as hydrazinium azotetrazolate (N % = 85.19 %) or triaminoguanidinium azotetrazolate (N % = 82.32 %) show promise for use in low erosivity gun propellants. Both the U.S. Army and the U.S. Navy are pursuing new, high-nitrogen gun propellants.

In this chapter, next to a comprehensive reinvestigation of 5-azido-1*H*-tetrazole (**135**) a description of a series of highly energetic salts containing the CN_7^- anion is given, which were all characterized using X-ray diffraction. The further chemical characterization (e.g. IR, Raman, NMR, elemental analysis, DSC) is as extensive as possible, since several metal 5-azidotetrazolates, when completely dried, explode spontaneously without any handling even in the dark. While these metal salts are extremely explosive and probably only of academic interest, the nitrogen-rich salts (hydrazinium, ammonium, aminoguanidinium, and guanidinium) are stabilized via hydrogen bonds and represent promising energetic materials. In addition these salts show the highest N-content ever reported for tetrazolate salts.
Last but not least, two constitutional isomers of methyl-5-azidotetrazole are described. The hypothetical 1,3-dipolar cycloaddition of highly-explosive methylazide and cyanazide is expected to lead to the formation of isomers 1-methyl-5-azidotetrazole (**145**) and 2-methyl-5-azidotetrazole (**146**). Both highly energetic compounds have been synthesized via various routes and fully characterized.

12.2 Synthesis

The most facile and selective synthesis of 5-azido-1*H*-tetrazole (**135**) is the reaction of cyanogen bromide with 2 equivalents of sodium azide in aqueous solution at low temperatures followed by an acidic work up using diluted hydrochloric acid (**Scheme 12.1**).[379] Since 5-azidotetrazolate anions are extremely sensitive, the intermediate product should not be isolated. **135** can be extracted with diethyl ether, which is removed under reduced pressure. The product should only be handled with appropriate precautions such as safety glasses, helmet, earthened shoes, leather jacket and Kevlar gloves. In addition only plastic spatulas should be used, direct light should be avoided and the product must be stored in explosive containers due to possible spontaneous detonation. It is important to mention that explosive decomposition of **135** its salts has occurred during this work without the detonation source having been identified.

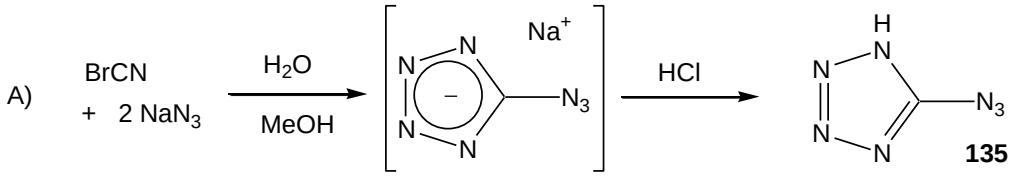

Scheme 12.1 Improved synthesis of 5-azido-1*H*-tetrazole (**135**).

The synthesis of **135** can also be achieved by the diazotation of 5-amino-1*H*-tetrazole (**Scheme 12.2.B**) with "HNO_2" followed by the addition of sodium azide or by the reaction (C) of 5-hydrazino-1*H*-tetrazole with one equivalent $NaNO_2$ and HCl in aqueous solutions.[380] However, we advise against attempting this synthesis (B) because of the formation of highly explosive tetrazole diazonium intermediates.

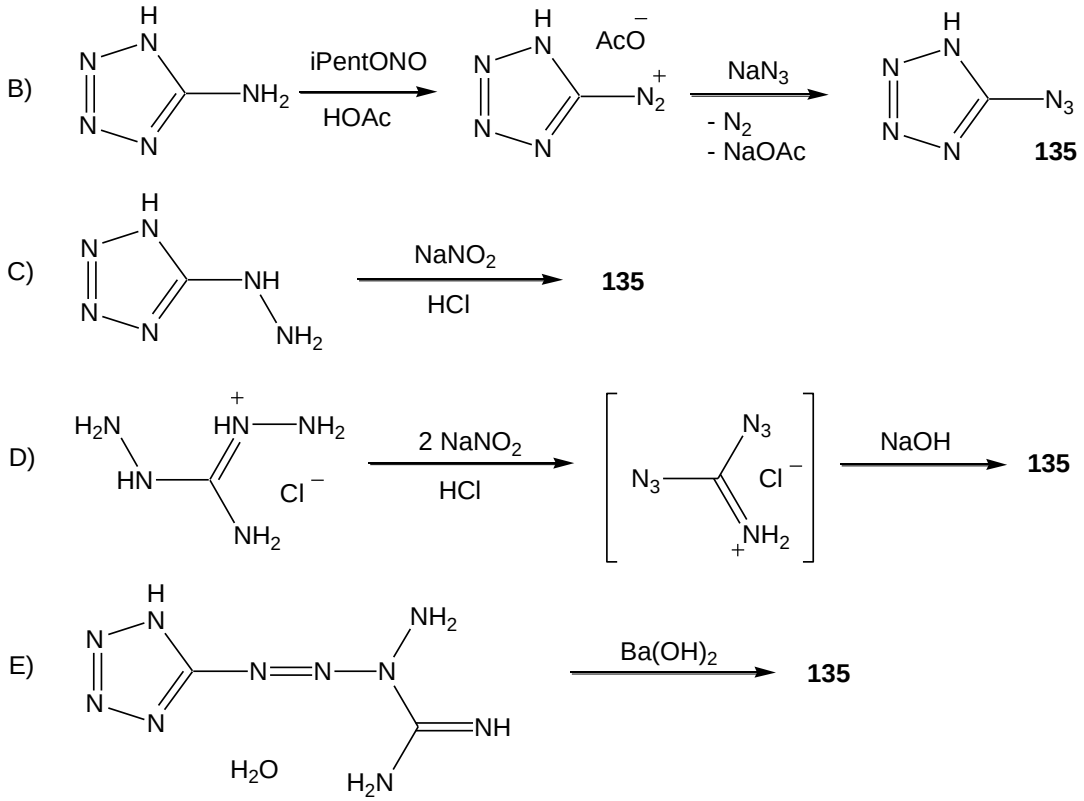

Scheme 12.2 Alternative synthetic routes to 5-azido-1*H*-tetrazole.

The reaction (D) of diaminoguanidinium salts with two equivalents of HNO_2 [390] also ends in the formation of **135**, which is also obtained as a byproduct in a advanced synthesis of 1,5-diaminotetrazole [202] by using only one equivalent of HNO_2.[391]

A quite uncommon reaction (E) is the alkaline degradation of the primary explosive tetrazene using $Ba(OH)_2$.[392]

Salts **136–144** were synthesized according to the following **Scheme 12.3**. Except for the synthesis of hydrazinium 5-azidotetrazolate (**136**) in THF, all reactions were carried out in water. Potassium and cesium 5-azidotetrazolate explode spontaneously when dry, while rubidium 5-azidotetrazolate even explodes spontaneously during the crystallization process in concentrated solution.

CAUTION: 5-Azido-1H-tetrazole as well as its salts **136–144** *are extremely energetic compounds with increased sensitivities towards various stimuli. Therefore proper protective measures (safety glasses, face shield, leather coat, earthened equipment and shoes, Kevlar® gloves and ear plugs) should be essentially used all time during work on* **136–144**. *All compounds should be stored in explosive cases since they can explode spontaneously.*

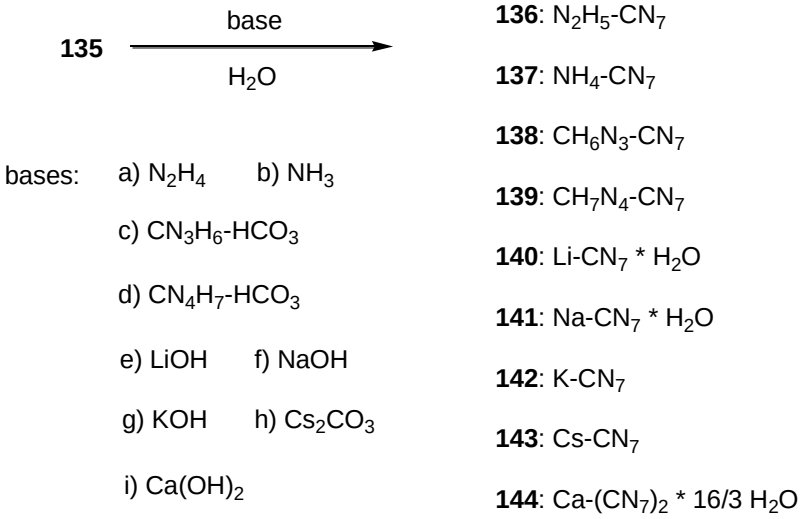

Scheme 12.3 Syntheses of the azidotetrazolate salts **136–144**.

136 was isolated by filtration after adding hydrazine in THF solution at room temperature to **135** also dissolved in THF. Single crystals could be obtained from recrystallization from a MeOH/THF mixture. The ammonium salt **137** was obtained by treating **135** with a slight excess of aqueous ammonia solution. After the solution was run dried, the colorless crude product was recrystallized from ethanol. Aminoguanidinium (**138**) and guanidinium 5-azidotetrazolate (**139**) were synthesized by the reactions of **135** with aminoguanidinium bicarbonate and guanidinium bicarbonate, respectively. Both compounds were recrystallized from wet methanol. Lithium (**140**), sodium (**141**) and potassium 5-azidotetrazolate (**142**) were obtained by simple evaporation of aqueous solutions containing **135** and one eq. of the corresponding metal hydroxide. **140** and **141** are "relatively" stable towards external

stimuli, while potassium 5-azidotetrazolate explodes violently when trying to handle a small amount. The cesium salt (**143**) was synthesized by treating **135** with half an equivalent of cesium carbonate. The aqueous solution was left for crystallization on a watch-glass and "fortunately" three single crystals could be isolated from the border of the solution. A few hours later the whole preparation exploded spontaneously. In the same way rubidium 5-azidotetrazolate was tried to synthesize a few times. However, we never obtained any solid material and the aqueous solution detonated spontaneously each time by simple standing in a dark and quiet explosive case. The calcium salt **144** could be prepared without any problems by the reaction of a aqueous suspension of $Ca(OH)_2$ with **135**. After filtration, single crystals were obtained from this solution by simple standing on air at room temperature.

2-Methyl-5-azidotetrazole (**146**) was synthesized using a similar procedure. The in situ preparation of **141**, followed by subsequent methylation with Me_2SO_4 in aqueous MeOH solution, afforded mainly the 2-substituted isomer **146** in good yield (77 %). ^{1}H NMR investigations of the reaction mixture indicate also the formation of the 1-substituted isomer **145** in a ratio of 1:5 with respect to **146** (**Scheme 12.4**). However, **146** can be precipitated from the reaction mixture upon cooling, whereas the isolation of **145** from the reaction mixture was unsuccessful. Suitable crystals for single-crystal analysis were obtained by sublimation of **146** *in vacuo* (40 °C, $1 \cdot 10^{-2}$ mbar) or by recrystallization from water.

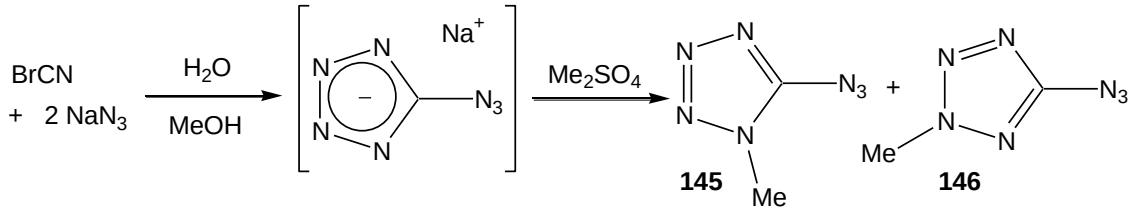

Scheme 12.4 Methylation of sodium 5-azidotetrazolate

The direct route to synthesize the 1-substituted isomer **145** involves the in situ reduction of 1-methyl-5-nitriminotetrazole (**44**) with zinc dust in aqueous HCl solution, followed by reaction with HNO_2. Azide **145** was obtained as a colorless oil after extraction from the reaction mixture with DCM (**Scheme 12.5**). Compound **145** crystallizes upon cooling (mp. 19–21 °C) and is highly soluble in common organic solvents (e.g. DMSO, Et_2O, benzene) and water. We assume that the intermediate formed after the zinc reduction of **145** is the 5-hydrazino-1-methyltetrazole, however, we abstained from isolation and full characterization of this compound.

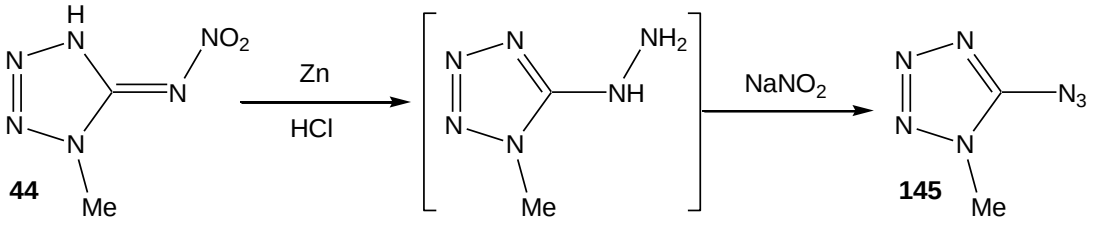

Scheme 12.5 One pot reaction converting 1-methyl-5-nitriminotetrazole (**44**) into 1-methyl-5-azidotetrazole (**145**).

12.3 Crystal Structures

Suitable single crystals of compounds **135**–**146** were determined by low temperature X-ray diffraction. A detailed description of the solutions follows.

12.3.1 5-Azido-1*H*-tetrazole (**135**)

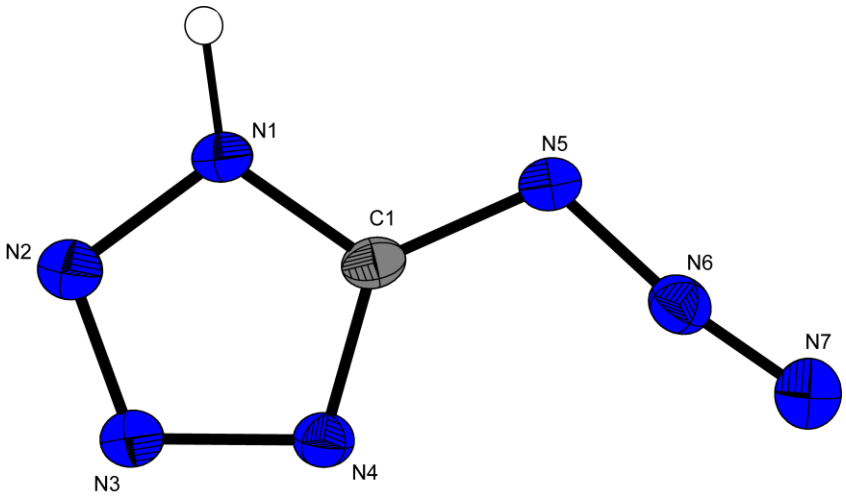

Figure 12.2 Molecular unit of **135**. Thermal ellipsoids represent the 50 % probability level. Selected geometries: distances (Å): C1–N1 = 1.327(2), N1–N2 = 1.355(2), N2–N3 = 1.295(2), N3–N4 = 1.372(2), N4–C1 = 1.321(2), C1–N5 = 1.383(2), N5–N6 = 1.267(2), N6–N7 = 1.117(2); angles (°): C1–N1–N2 = 108.3(1), N3–N2–N1 = 106.5(1), N2–N3–N4 = 110.6(1), N1–C1–N5 = 121.0 (1), C1–N4–N3 = 105.1(1), N4–C1–N5 = 129.5(2), N6–N5–C1 113.1(1), N5–N6–N7 = 171.9(2); torsion angles (°): C1–N1–N2–N3 = 0.1(2), N2–N1–C1–N5 = 178.0(1), N1–C2–N5–N6 = 174.7(1)

5-Azido-1*H*-tetrazole crystallizes in the monoclinic space group $P2_1/c$ with eight molecules in the unit cell resulting in a density of 1.720 g cm^{-3}. One molecular moiety of the asymmetric unit, containing two molecules, is shown in **Figure 12.2**. The structure

of the tetrazole ring is comparable to values observed for other tetrazole derivatives e. g. 5-aminotetrazole.[60] The N–N and C–N bond lengths are all between typical single and double bonds. The constitution of the azide group is similar to those of other covalent carbon bonded azide groups, e. g. azidoformamidinium chloride.[215] The azide group is angulated (N5–N6–N7 = 171.9(2)°), which is quite common for covalent azides and can be explained by hyperconjugation effects.[214]

The position of the hydrogen atom at the nitrogen atom N1 can be shown best by viewing on the 1-dim chains (**Figure 12.3**), which are arranged by a strong hydrogen bridge. This is the only structural motive, which is found in the packing. These chains along the *b* axis are parallel as well as nearly orthogonal to each other and are only connected by "Van der Waals" forces, which are illustrated in **Figure 12.4**.

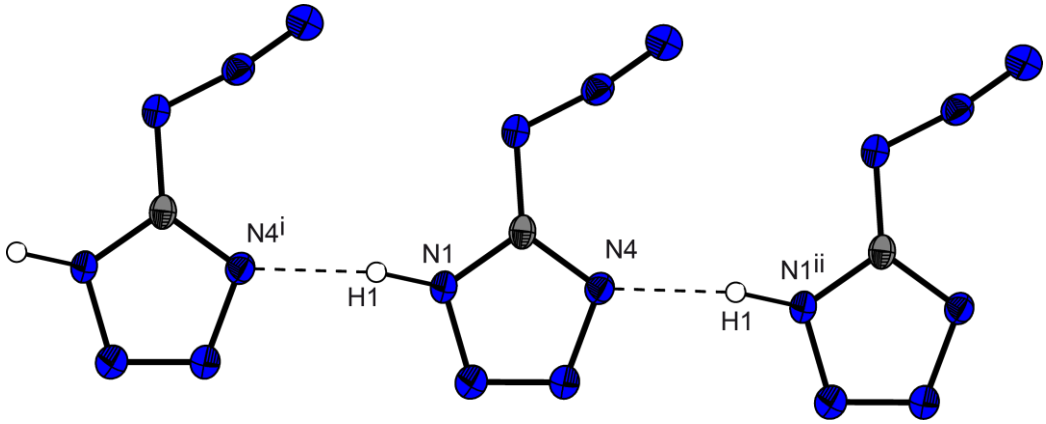

Figure 12.3 View on the 1-dim chains illustrating the hydrogen bond. (N1–H1···N4^{i}: D–H = 0.95(2), H···A = 1.87(2), D···A = 2.815(2) Å, D–H···A = 168.8(2)°; (i): x, 1+y, z, (ii): x, –1+y, z).

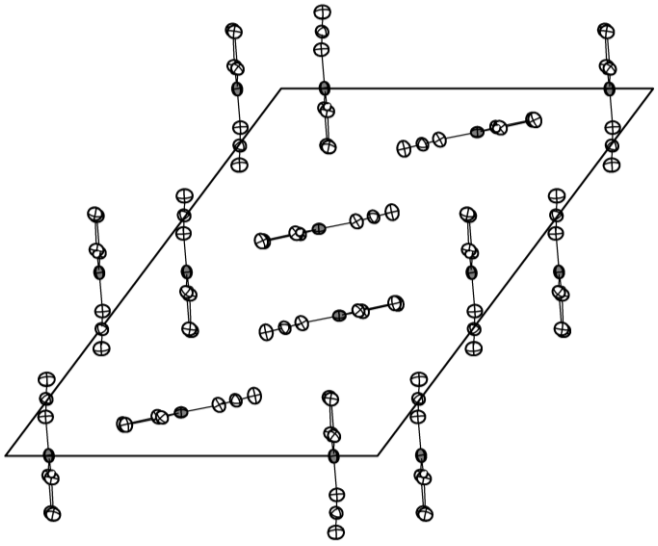

Figure 12.4 View along the *b* axis and the 1-dim chains. The unit cell is marked.

12.3.2 Hydrazinium 5-azidotetrazolate (**136**)

Hydrazinium 5-azidotetrazolate crystallizes in the monoclinic space group $P2_1/c$ with four molecules in the unit cell and a density of 1.568 g cm^{-3}. The molecular moiety is shown in **Figure 12.5**. In general, in all structures presented in this work the CN_7 anions have nearly identical geometries. The N–N and C–N bond lengths within the tetrazole ring are all between typical single and double bond lengths and are listed in **Tables 12.2–12.5**. The structure of the azidotetrazolate anion is similar to that observed for neutral 5-azido-1*H*-tetrazole (**135**). In the structures of **136**–**144**, the N1–N2 and the N5–N6 bond lengths are shorter than the neutral counterparts, while the N2–N3 as well as the C1–N5 distances are found to be longer. For the N3–N4, N1–C1, N4–C1, and N6–N7 bond distances, no similar trend is observed. The constitution of the azide group is similar to this observed in **135** and those of other covalent carbon bonded azide groups, e.g., azidoformamidinium salts. The azide group is bent (**136**: N5–N6–N7 = 171.5(3)°), which is quite common for covalent azides. Also the outer N_β–N_γ distance is significantly shorter (in the range of a N–N triple bond) than the inner one. In the structure of **136**, the hydrazine bond length of N8–N9 (1.452(2) Å) is also found in hydrazinium chloride (1.45 Å) [393] or hydrazinium 5,5'-azotetrazolate.[71]

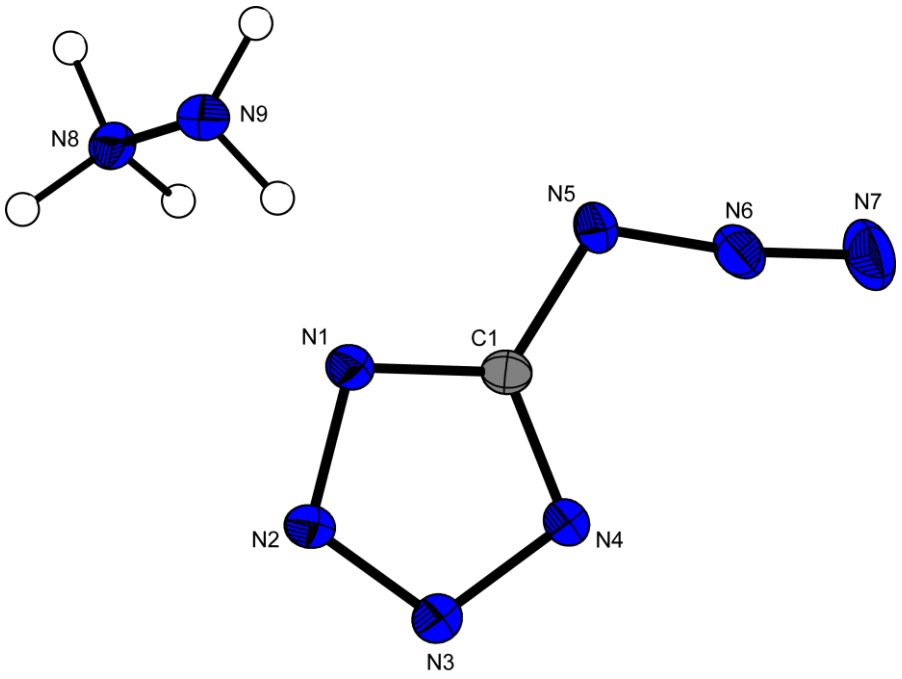

Figure 12.5 Molecular moiety of hydrazinium 5-azidotetrazolate. The ellipsoids represent the 50 % probability level.

Although **136** has the highest nitrogen content observed in this work, its sensitivities are lower in comparison to those of the water free alkaline metal salts. This may be a reason of the intense hydrogen bond network, which can be found in the packing of **136**. (**Figure 12.6**) With this layers are formed along the *b*-*c* plane. The single layers are connected by a weak hydrogen bond incorporating the outer azide nitrogen atom N7 (N9–H9A···N7 = 0.89(2), 2.60(2), 3.335(2) Å, 140(1)°).

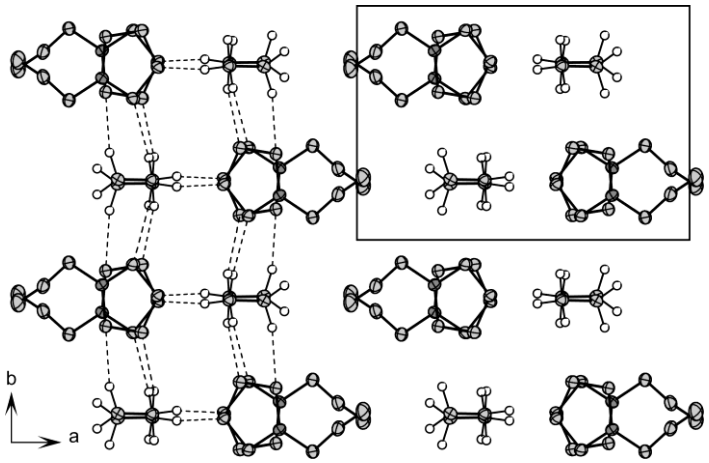

Figure 12.6 View on the packing of **136** along the *c* axis showing the hydrogen bonds. Selected hydrogen bonds within the layers: N8–H8C···N^{i} = 0.92(2), 2.01(2) 2.911(2) Å, 164(1)°; N9–H9B···N4^{ii} = 0.90(2), 2.24(2), 3.05(2) Å, 150(1)°; N8–H8A···N1^{iii} = 0.930(2), 2.035(2), 2.888(2) Å, 153 (2)°; N9–H9A···N5^{iv} = 0.89(2), 2.51(2), 3.128(2) Å, 127(1)°; (i) –x, –y, 1–z; (ii) –x, 0.5+y, 1.5–z; (iii) –x, 1–y, 1–z; (iv) –x, –0.5+y, 1.5–z.

12.3.3 Ammonium 5-azidotetrazolate (**137**)

137 crystallizes in the monoclinic chiral space group $P2_1$ with two molecules in the unit cell and a density 1.608 g cm^{-3}. A view on the coordination of the ammonia cations is illustrated in **Figure 12.7**. The packing is strongly influenced by the four different hydrogen bonds. Also the nitrogen atom N7 of the azide group participates as weak hydrogen bond acceptor. The extensive hydrogen-bonding network is better explained in the formalism of graph-set analysis as introduced by Bernstein *et al.*.[208] At this only the three strong hydrogen bonds (d(D–A) < 3 Å and D–H–A angle > 120 °) are included. The binary graph set can be described as N_2 = **C2,2(6)R2,2(5)**. This combination of chains and rings yields to endless tapes in the packing of **137** (**Figure 12.8**). The connection between the rings is formed by the forth hydrogen bridge.

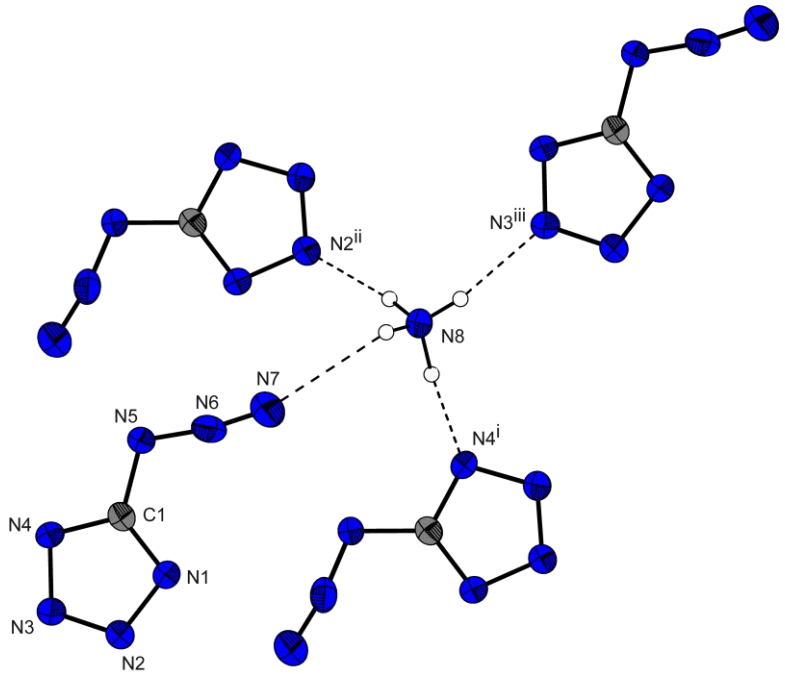

Figure 12.7 Hydrogen bonds in the packing of **137**. Selected hydrogen bonds (D–H···A, d(D–H) [Å], d(H–A) [Å], d(D–A) [Å], angle(D–H···A) [°]): N8–H8B···N4^{i}, 1.05(5), 1.89(5), 2.933(4), 175(4); N8–H8C···N2^{ii}, 0.87(3), 2.05(3), 2.917(5), 171(3); N8–H8D···N3^{iii}, 0.88(4), 2.05(4), 2.923(4), 169(6); N8–H8A···N7, 0.92(4), 2.57(3), 3.116(4), 119(2); (i) 1–x, –0.5+y, 1–z; (ii) 1–x, 0.5+y, 1–z; (iii) 1+x, y, –1+z.

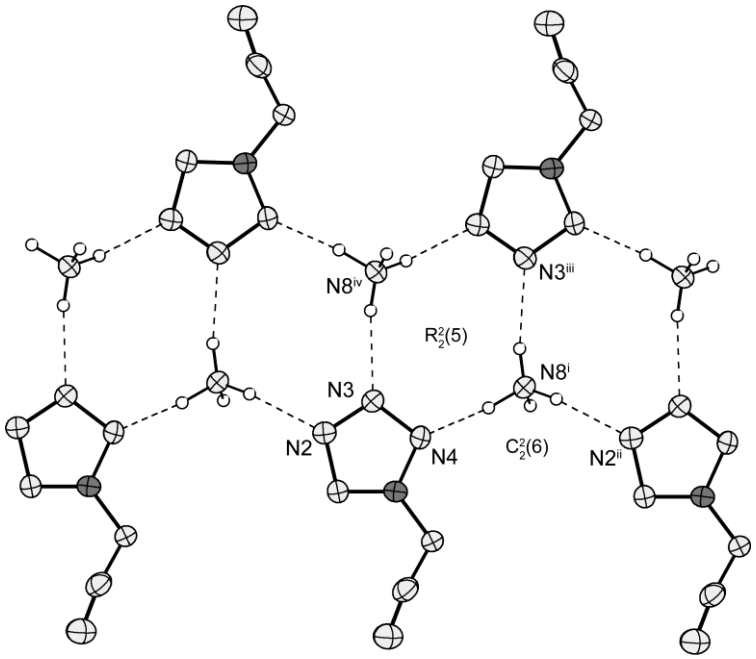

Figure 12.8 Graph-sets of interest in the packing of **137**. Symmetry codes: (i) 1–x, 0.5+y, 1–z; (ii) x, 1+y, z; (iii) –x, 0.5+y, 2–z; (iv) –1+x, y, z.

12.3.4 1-Aminoguanidinium 5-azidotetrazolate (**138**)

1-Aminoguanidinium 5-azidotetrazolate crystallizes in the triclinic space group *P*–1. The density of 1.524 g cm^{-3} is lower in comparison to those of **135–137**. The unit cell contains two different molecular moieties. In general the aminoguanidinium cations have geometries also found in aminoguanidinium chloride,[301] nitrate [394] or perchlorate.[131] They are build nearly planar (N10–C2–N8–N9 = 2.2(2)°, N20–N19–C4–N21 = –3.1(4)°), whereby different C–N bond lengths between 1.31 and 1.33 Å are observed. These distances are crucially shorter than C–N single bonds (1.47 Å) but significantly longer than C=N double bonds (1.22 Å) and show explicitly the delocalization of the positive charge.

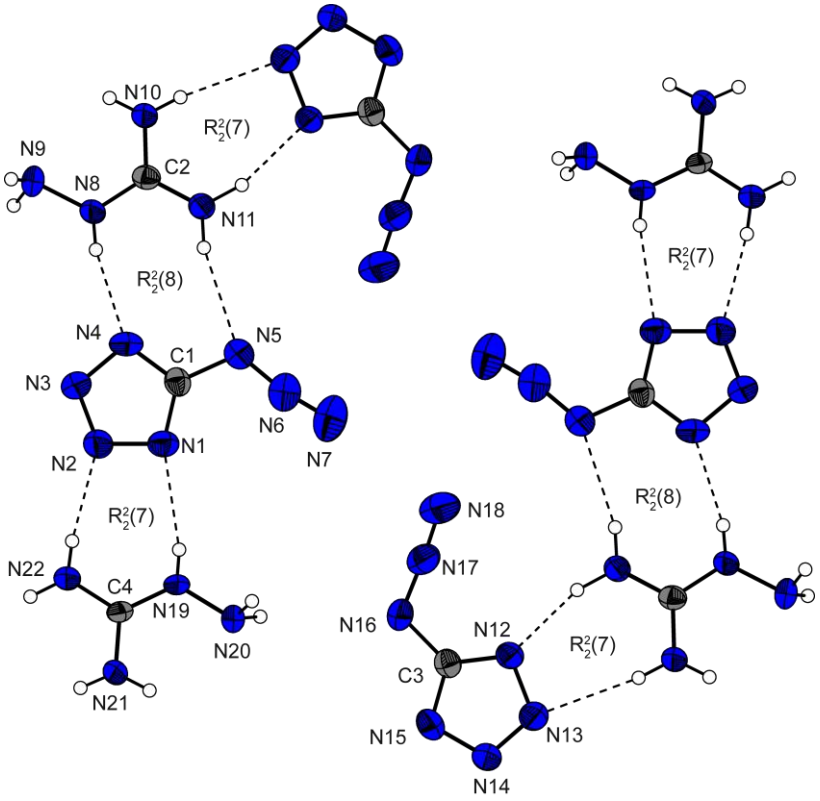

Figure 12.9 View on the layers in **138**. Thermal ellipsoids represent the 50 % probability level. Selected geometries of the cations: distances (Å): N8–N9 = 1.408(3), N8–C2 = 1.325(3), C2–N10 = 1.323(3) , C2–N11 = 1.324(3), N19–N20 = 1.397(3), N19–C4 = 1.315(3), C4–N21 = 1.315(3) , C3–N22 = 1.313(3); angles (°): C2–N8–N9 = 119.2(2), N10–C2–N11 = 120.8(3), N10–C2–N8 = 118.1(2), N11–C2–N8 = 121.1(3).

The packing of **138** is characterized by the formation of layers, which are illustrated in **Figure 12.9**. The layers have distances of ~3.25 Å. Within the layers more than ten

different hydrogen bonds, which are well within the sum of the van der Waals radii of two nitrogen atom ($r_{A(N)} + r_{D(N)}$ = 3.10 Å) [395] are formed. In contrast to the structures of **136** and **137** also nitrogen atom N5 of the azide group is participated in a weak hydrogen bond (N10–H10A···N5 = 0.87(3), 2.42(3), 3.262(3) Å, 164(2)°). In addition to the graph sets charted in **Figure 12.9**, two chains (**C2,2(9)**) are formed within the layers.

12.3.5 Guanidinium 5-azidotetrazolate semihydrate (**139**)

Guanidinium 5-azidotetrazolate semihydrate, which crystallizes in the common monoclinic space group $P2_1/c$, contains two different molecular moieties in the unit cell. The presence of crystal water increases the density to 1.546 g cm^{-3} in comparison to **138**. The structure of the guanidinium cations are in agreement to those of e.g. guanidinium chloride,[396] perchlorate [397] or bicarbonate.[398] The C–N distances between 1.30 and 1.33 Å of the cations are similar to these of **138**. Again the packing is dominated by a strong hydrogen bond network, resulting in a layer structure along the *b*-*c* plane. A view on the layers can seen in **Figure 12.10**.

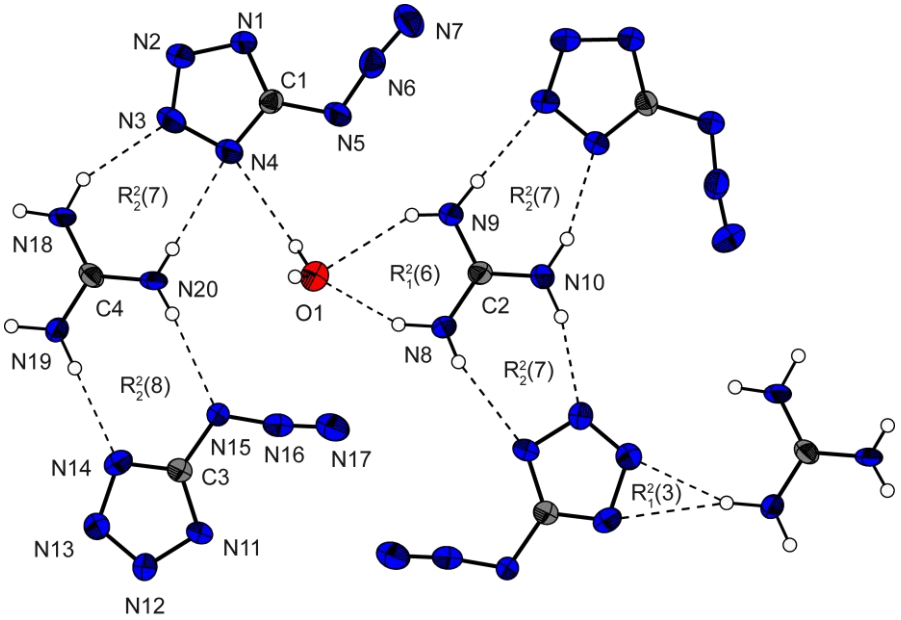

Figure 12.10 View on the layers of **139** along the *a* axis. Thermal ellipsoids represent the 50 % probability level. Selected geometries: distances (Å): C2–N8 = 1.330(5), C2–N9 = 1.330(5), C2–N10 = 1.306(5), C4–N18 = 1.318(5), C4–N19 = 1.327(5), C4–N20 = 1.317(5); angles (°): N8–C2–N9 = 118.5(4), N9–C2–N10 = 120.2(4), N10–C2–N8 = 121.2(4).

Due to the presence of the water, up to 24 different hydrogen bonds can be found. Interestingly only one hydrogen atom of the crystal water participates in the formation of the layers, while the other is directed to another layer in a distance of ~3.3 Å.

12.3.6 Lithium 5-azidotetrazolate monohydrate (**140**)

Lithium 5-azidotetrazolate monohydrate crystallizes in the monoclinic space group $P2_1/c$ with four molecules in the unit cell. The density of 1.683 g cm^{-3} is in the range of other lithium tetrazolate salts, e.g. lithium tetrazolate.[152] The lithium cations are coordinated tetrahedrally by the nitrogen atoms N2 and N3 of two different CN_7 anions and two water molecules. As expected, the Li–O coordination distance (~2.00 Å) is found to be shorter than the Li–N distances (~2.05 Å).

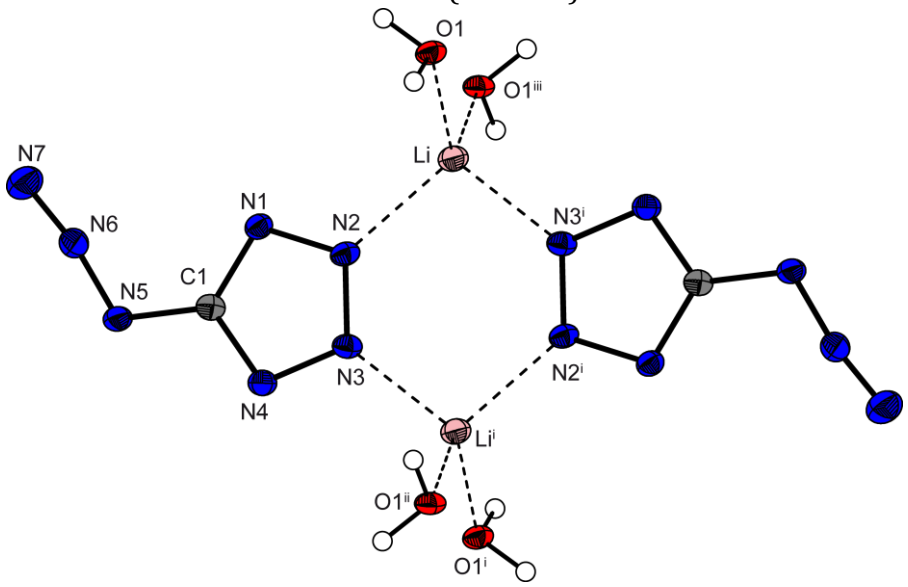

Figure 12.11 Extended molecular structure of **140**. Selected geometries: distances (Å): Li–N1 = 2.055(3), Li^{i}–N3 = 2.051(3), Li–O1 = 1.996(3); angles (°): O1–Li–N2 = 117.2(2), O1–Li–O1^{i} = 100.9(1); N2–Li–N3^{i} = 102.32(1); (i) –x, 1–y, 2–z (ii) x, 1.5–y, 0.5+z (iii) –x, –0.5+y, 1.5–z.

The water molecules bridge the extended molecular moiety (**Figure 12.11**) to layers along the *b*-*c* plane (illustrated in **Figure 12.12**) by the hydrogen bonds O1–H1A···N4 = 0.86(2), 1.94(2), 2.748(2) Å, 156(2)° and O1–H1B···N1 = 0.87(3), 1.96(3), 2.78(2) Å, 157(2)° building a **C2,2(6)** graph set.

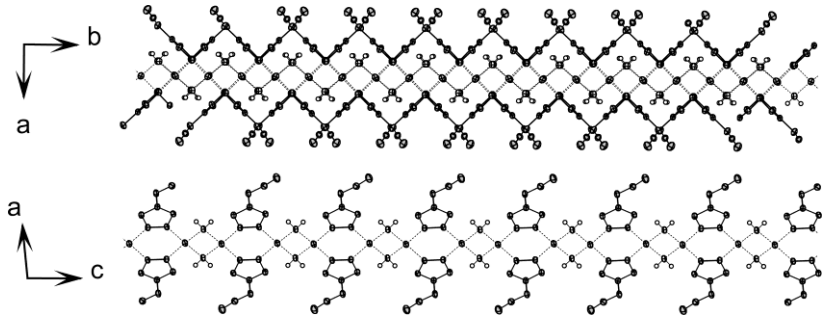

Figure 12.12 View on the layers along the *b* and *c* axes.

12.3.7 Sodium 5-azidotetrazole monohydrate (**141**)

Sodium 5-azidotetrazole crystallizes also as monohydrate in the monoclinic space group $P2_1/c$ with eight molecules in the unit cell and a calculated density of 1.743 g cm^{-3}. The constitution of the CN_7 anion is comparable to this observed for **136–140**. In this structure the azide group is twisted most out of the ring plane (N1–C1–N5–N6 = –172.6(3)° and N8–C1–N12–N13 = 9.3(4)°).

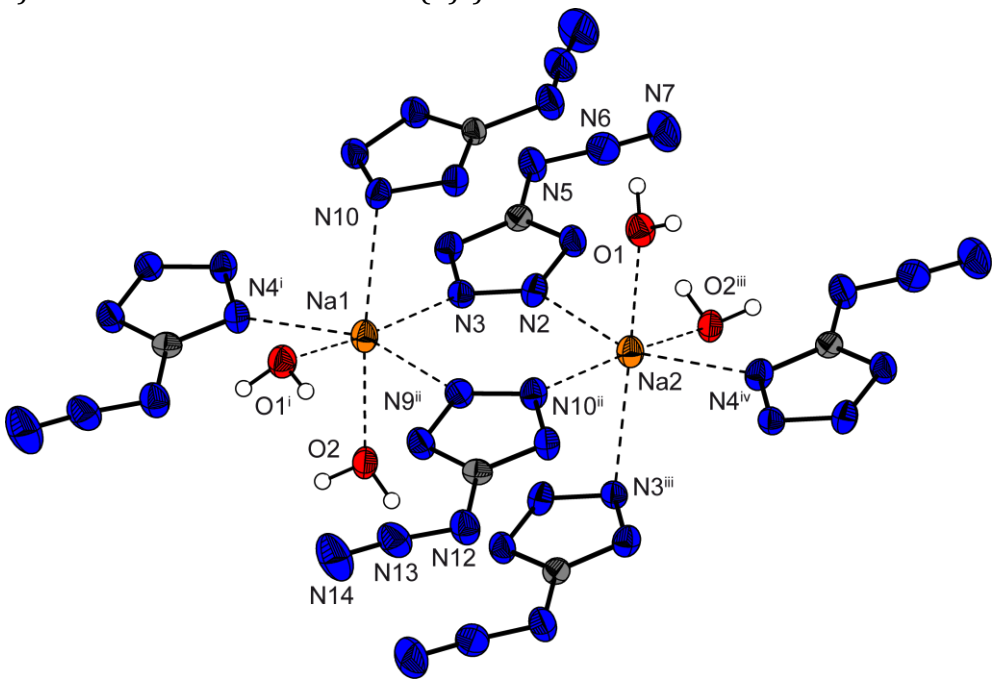

Figure 12.13 Coordination of the sodium cations in the packing of **141**. Selected coordination geometries: distances (Å): N3–Na1 = 2.499(3), O1–Na1 = 2.429(3), O2–Na1 = 2.348(4), N9–Na1 = 2.568(3), N10–Na1 = 2.711(4), N11–Na1 = 2.511(3); angles (°): O2–Na1–O1 = 97.7(1), O2–Na1–N3 = 90.56(1), O2–Na1–N11 = 87.3(1), O2–Na1–N9 = 83.88(9), O2–Na1–N10 = 173.97(8); (i) 1–x, –0.5+y, 0.5–z, (ii) 1–x, 0.5+y, 0.5–z, (iii) 1–x, 1–y, –z, (iv) x, 1+y, z.

The packing is characterized by the formation of dimeric units (**Figure 12.13**), in which the sodium atoms are coordinated nearly octahedrally by two water molecules and four ring nitrogen atoms of different tetrazolates. The azide group does not participate in any coordination to the sodium centers. However, nitrogen atoms N5 and N12 participate in hydrogen bonds (O2–H2A···N5 = 0.83(3), 2.24(3), 2.966(4) Å, 147(3)°; O1–H1A···N12 = 0.84(4), 2.22(4), 2.925(4) Å, 142(4)°). Together with the H-bonds O1–H1B···N8 = 0.72(3), 2.19(3), 2.833(4) Å, 149(4)° and O2–H2B···N1 = 0.84(3), 2.08(3), 2.825(4) Å, 148(3)°, **C2,2(6)** chains are formed.

12.3.8 Potassium 5-azidotetrazolate (**142**)

KCN_7 (**142**) crystallizes with a calculated density of 1.917 g cm^{-3} in the monoclinic space group $P2_1/c$. The coordination of one potassium cation (**Figure 12.14**), which is surrounded by six nitrogen atoms, can be described as distorted octahedral.

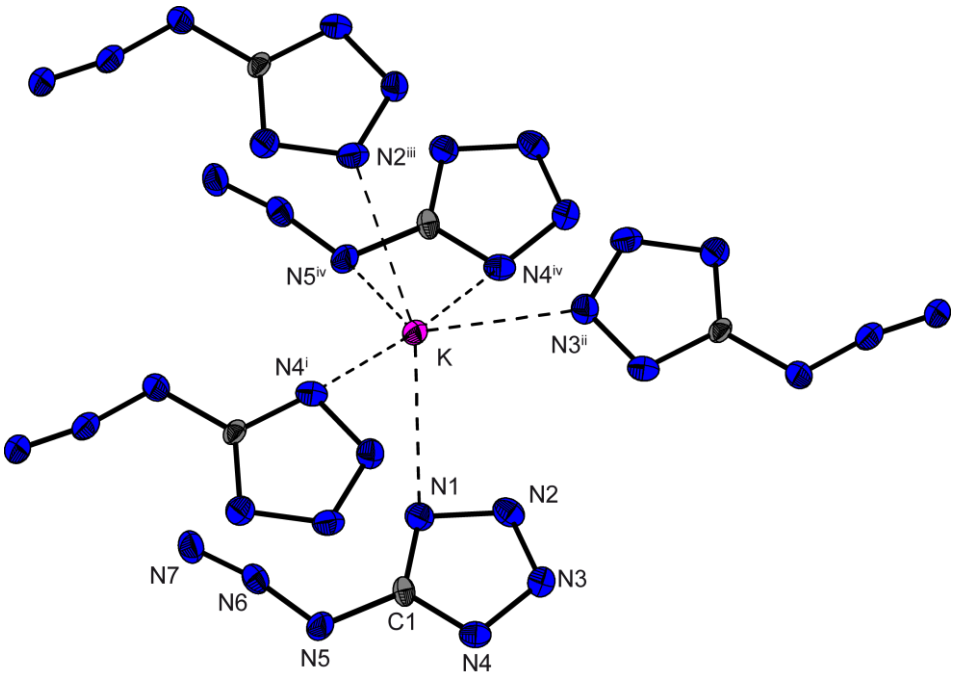

Figure 12.14 Coordination of the potassium atoms in the structure of **142**. Selected coordination geometries: distances (Å): N1–K = 2.857(2), N2–K = 3.136(2), N2^{iii}–K = 2.849(2), N3^{ii}–K = 2.818(2), N4^{i}–K = 2.878(2), N5^{iv}–K = 3.065(5), N4^{iv}–K = 3.021(2); angles (°): N1–K1–N4^{i} = 82.78(6), N1–K1–N2^{iii} = 160.24(6), N1–K1–N3^{ii} =100.87(6), N5 ^{iv}–K1–N4^{iv} = 45.69(6); (i) x, 0.5-y, 0.5+z; (ii) 2–x, 0.5+y, 0.5–z; (iii) x, 1.5–y, 0.5+z ; (iv) x, 1+y, z.

The coordination distances range from 2.85 to 3.02 Å. This coordination is comparable to that found e.g. in potassium 5-aminotetrazolate (Chapter 2) or potassium 1-methyl-5-nitriminotetrazolate.(Chapter 7) Remarkable is, that in the structure of **142** also the azide nitrogen atom N5 participates in the metal coordination sphere.

12.3.9 Cesium 5-azidotetrazolate (**143**)

Cesium 5-azidotetrazolate (**143**) crystallizes in the orthorhombic space group $P2_12_12_1$ with four molecules in the unit cell. The density of 2.810 g cm^{-3} is the highest observed in this work and also in the range of other high-nitrogen cesium salts, e.g. cesium tetrazolate (Chapter 11). As usual it is hard to determine a exact coordination number for the cesium cations. Considering only Cs–N contacts shorter than 3.5 Å, the coordination is ninefold (**Figure 12.15**).

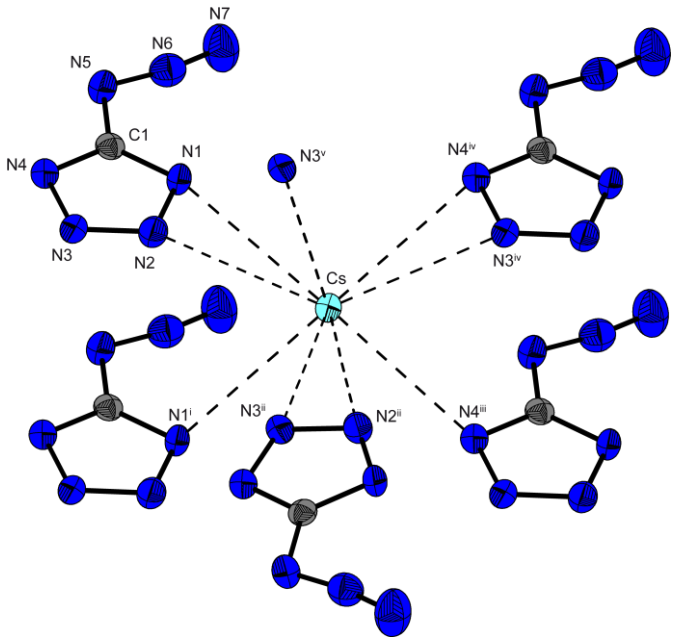

Figure 12.15 Coordination (< 3.5 Å) of the cesium cations in the structure of **143**. Ellipsoids represent the 50 % probability level. Selected geometries: distances (Å): Cs–N2 = 3.153(4), Cs–N1 = 3.357(4), Cs–N1^{i} = 3.455(4), N4^{i}–Cs = 3.250(4), Cs–N3^{ii} = 3.181(4), Cs–N2^{ii} = 3.313(4), Cs–N4^{iii} = 3.250(4), Cs–N3^{iv} = 3.242(4), Cs–N4^{iv} = 3.257(4), Cs–N3^{v} = 3.460(4); (i) 1+x, y, z; (ii) 2–x, 0.5+y, 0.5–z; (iii) 1+x, 1+y, z; (iv) x, 1+y, z; (v) 1–x, 0.5+y, 0.5–z.

The shortest distance between cesium and nitrogen is observed between the atoms Cs and N3 .The coordination mode is in agreement to these found e.g. in cesium 5-cyanotetrazolate [399] or tetrazolate. In packing of **143** the CN_7 anions are arranged in pillars along the *a* axis, which can be seen in **Figure 12.16**. Within the *b*-*c* planes the shortest Cs–Cs distance is 4.644(1) Å.

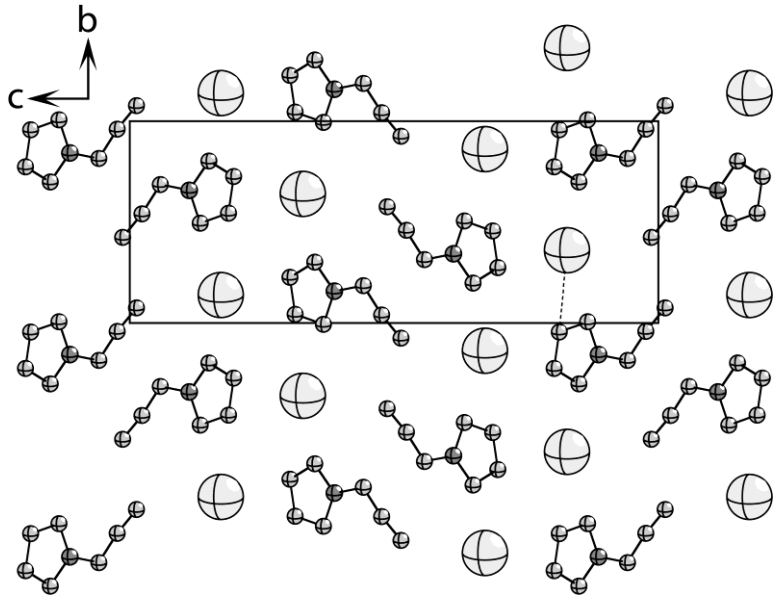

Figure 12.16 View on the packing of **133** along the *a* axis. Atoms are represented as "ball and sticks". One unit cell is marked.

12.3.10 Calcium 5-azidotetrazolate (**144**)

The molecular moiety of **144** (**Figure 12.17**) is more complex when comparing with **136**–**143**. The moiety formula is $[Ca(CN_7)_2(H_2O)_{10}][Ca(H_2O)_6](CN_7)_2$. In this structure the two most important coordination modes of Ca^{2+} are included. One calcium atom is surrounded octahedrally by six water atoms in distances of 2.30–2.34 Å, which is also found e.g. in hexaqua-calcium bis(4-hydroxyazobenzene-3-sulfonate).[400] The other calcium atoms are coordinated eightfold, by six water molecules and the nitrogen atoms N3 and N4 of two different 5-azidotetrazolate anions, while building dimers. A similar coordination mode can be found in the structure of calcium 5,5'-azotetrazolate·16 H_2O.[71] The charge balance in the structure of **144** is formed by four further non-coordinated CN_7 anions.

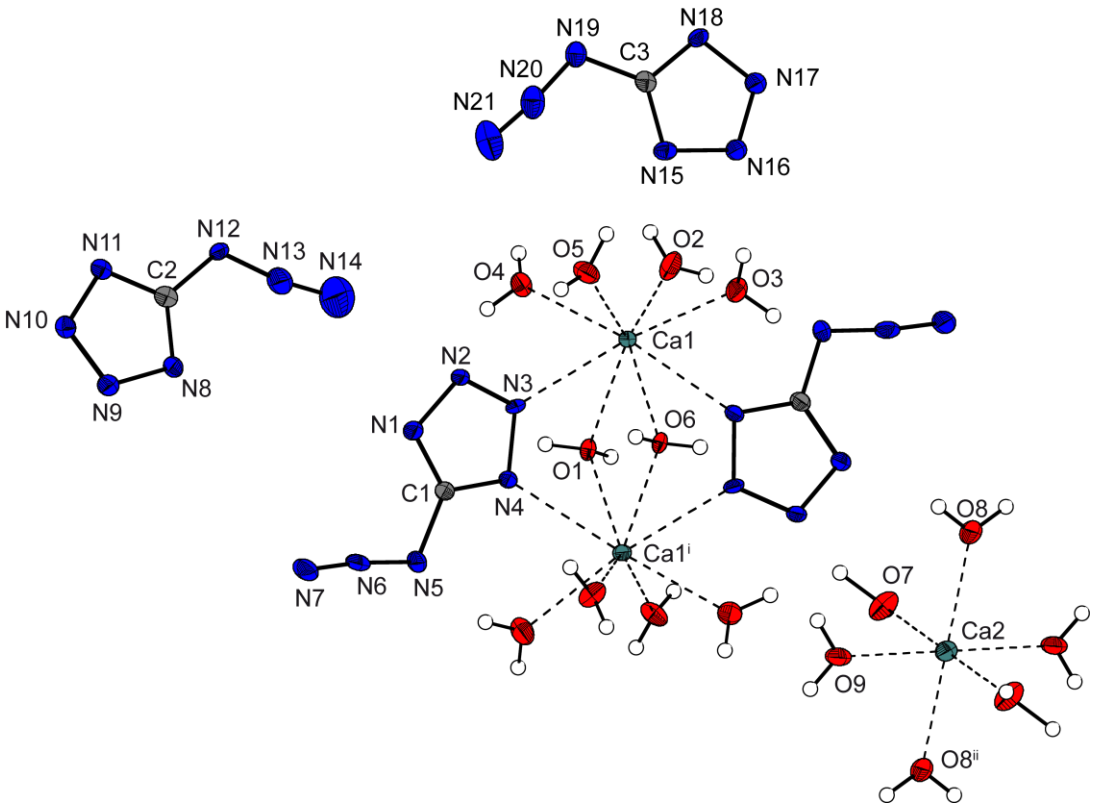

Figure 12.17 View on the molecular moiety of **144**, whereby two CN_7 anions were removed for better clearness. (i) 1–x, y, 0.5–z, (ii) 1.5–x, 0.5–y, 1–z.

Table 12.2 Bond distances (Å) of the CN_7^- anions in compounds **135–140**.

atoms	**135**	**136**	**137**	**138a**	**138b**	**139a**	**139b**	**140**
N1–N2	1.372(2)	1.348(2)	1.358(4)	1.354(3)	1.356(3)	1.351(4)	1.353(4)	1.349(2)
N2–N3	1.295(2)	1.317(2)	1.306(4)	1.300(3)	1.308(3)	1.309(4)	1.306(4)	1.315(2)
N3–N4	1.355(2)	1.352(2)	1.360(4)	1.347(3)	1.348(3)	1.359(4)	1.364(4)	1.347(2)
C1–N1	1.321(2)	1.330(2)	1.316(4)	1.319(3)	1.330(3)	1.319(4)	1.335(4)	1.335(2)
C1–N4	1.327(2)	1.327(2)	1.337(5)	1.329(3)	1.310(3)	1.333(4)	1.314(4)	1.338(2)
C1–N5	1.383(2)	1.409(2)	1.401(5)	1.403(3)	1.412(3)	1.406(5)	1.393(4)	1.390(2)
N5–N6	1.267(2)	1.252(2)	1.250(4)	1.246(3)	1.251(3)	1.255(4)	1.259(4)	1.259(2)
N6–N7	1.117(2)	1.123(2)	1.125(4)	1.103(3)	1.120(3)	1.128(4)	1.125(4)	1.121(2)

Table 12.3 Bond distances (Å) of the CN_7^- anions in compounds **141–144**.

atoms	**141a**	**141b**	**142**	**143**	**144a**	**144b**	**144c**
N1–N2	1.354(3)	1.354(3)	1.354(3)	1.354(6)	1.360(4)	1.348(4)	1.359(4)
N2–N3	1.317(3)	1.313(3)	1.316(3)	1.316(5)	1.309(4)	1.327(4)	1.306(4)
N3–N4	1.349(3)	1.350(3)	1.352(3)	1.355(6)	1.354(4)	1.351(4)	1.356(4)
C1–N1	1.317(4)	1.330(4)	1.324(3)	1.336(6)	1.330(4)	1.330(4)	1.326(4)
C1–N4	1.327(4)	1.323(4)	1.328(3)	1.315(5)	1.331(4)	1.330(4)	1.329(4)
C1–N5	1.407(4)	1.410(4)	1.411(3)	1.411(6)	1.411(4)	1.400(4)	1.405(4)
N5–N6	1.255(3)	1.255(3)	1.264(3)	1.244(6)	1.265(4)	1.257(4)	1.257(5)
N6–N7	1.117(4)	1.120(4)	1.112(3)	1.138(5)	1.119(4)	1.111(5)	1.127(5)

Table 12.4 Selected bond angles (°) and torsion angle (°) of the CN_7^- anions in compounds **135–140**.

atoms	**135**	**136**	**137**	**138a**	**138b**	**139a**	**139b**	**140**
N1–C1–N4	109.5(2)	114.0(1)	114.3(4)	113.7(2)	113.9(2)	113.7(3)	114.8(3)	112.6(2)
N1–C1–N5	121.0(1)	121.1(1)	126.8(4)	127.3(2)	126.6(2)	125.9(4)	125.6(3)	127.5(1)
N4–C1–N5	129.5 (2)	125.0(1)	118.9(3)	119.0(2)	119.4(2)	120.4(3)	119.6(3)	119.9(1)
C1–N5–N6	113.1(1)	113.7(1)	114.2(3)	115.2(2)	112.6(2)	112.9(3)	116.1(3)	114.6(1)
N5–N6–N7	171.9(2)	172.3(2)	171.5(3)	169.8(3)	175.0(3)	172.5(4)	172.3(4)	170.7(2)
N1–C1–N5–N6	174.7(1)	176.5(1)	–0.7(7)	–5.7(4)	–176.5(2)	8.0(6)	6.2(6)	–4.9(2)

Table 12.5 Selected bond angles (°) and torsion angle (°) of the CN_7^- anions in compounds **141–144** .

atoms	**141a**	**141b**	**142**	**143**	**144a**	**144b**	**144c**
N1–C1–N4	114.5(3)	114.0(2)	114.8(2)	114.0(4)	113.4(3)	114.0(3)	113.4(3)
N1–C1–N5	123.6(3)	123.8(3)	125.9(2)	126.3(4)	125.8(3)	126.6(3)	125.5(3)
N4–C1–N5	121.8(3)	122.3(3)	119.3(2)	119.7(4)	120.8(3)	119.4(3)	121.1(3)
C1–N5–N6	113.4(2)	114.0(2)	115.5(2)	113.7(4)	111.8(3)	114.8(3)	113.2(3)
N5–N6–N7	173.6(4)	171.9(3)	169.3(3)	170.7(5)	173.7(3)	169.7(4)	173.6(4)
N1–C1–N5–N6	–172.6(3)	9.3(4)	172.6(3)	5.4(7)	177.1(3)	175.4(3)	2.9(5)

12.3.11 1–Methyl-5-azidotetrazole (**145**)

1-Methyl-5-azidotetrazole crystallizes in the monoclinic space group $P2_1/m$ with four molecules in the unit cell. The, in comparison with other tetrazole derivatives, low density of 1.48 g cm^{-3} may be a reason for the low melting temperature of **145**. The tetrazole ring follows the structure also observed for 5-azido-1*H*-tetrazole (**135**) (**Figure 12.18**). The N–N and C–N bond lengths are all between typical single and double bonds. The exact bond lengths and angles can be found in **Table 12.6** and **Table 12.7**. The constitution of the azide group is similar to those of **135** and its salts **136**–**144** as well as of other covalent carbon bonded azide groups, e. g. 5-azido-triazol-3-ylamine.[401] The azide group shows an angle of N5–N6–N7 = 171.9(2)°.

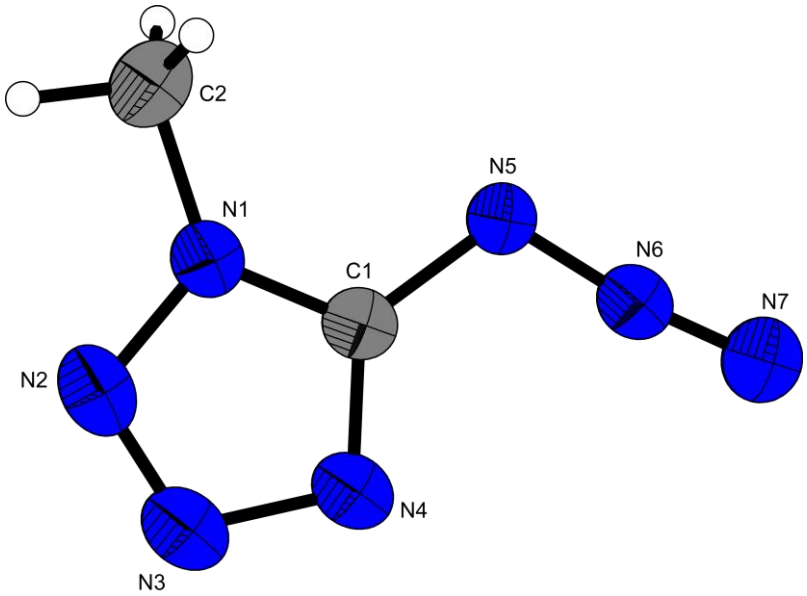

Figure 12.18 Molecular structure of **145**. Thermal ellipsoids are drawn at the 50 % probability level and hydrogen atoms are shown as small spheres of arbitrary radii.

The molecules in the structure of **145** are packed in loose layers along the *a*-*c*-plane, which can be seen in **Figure 12.19**. The layers have distances of ~3.13 Å along the *b*-axis.

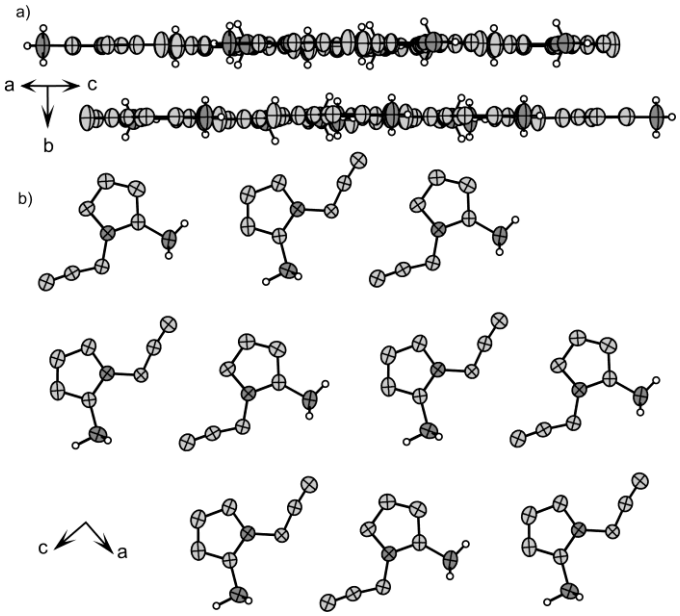

Figure 12.19 Crystal packing of **145**. a) View along the layers; b) view along the *b* axis.

12.3.12 2-Methyl-5-azidotetrazole (**146**)

2-Methyl-5-azidotetrazole crystallizes in the monoclinic space group $P2_1/c$ with four molecules in the unit cell. The molecular unit is shown in **Figure 12.20**. The density (1.571 g cm^{-3}) is significantly higher than that observed in **145**. However, the molecular unit is similar but also shows differences in the ring geometry to these in **145**. Again the molecules build a planar system (C1–N5–N6–N7 = 179.5(1)°) which are packed in layers (**Figure 12.21**). The layers have distances of ~3.10 Å.

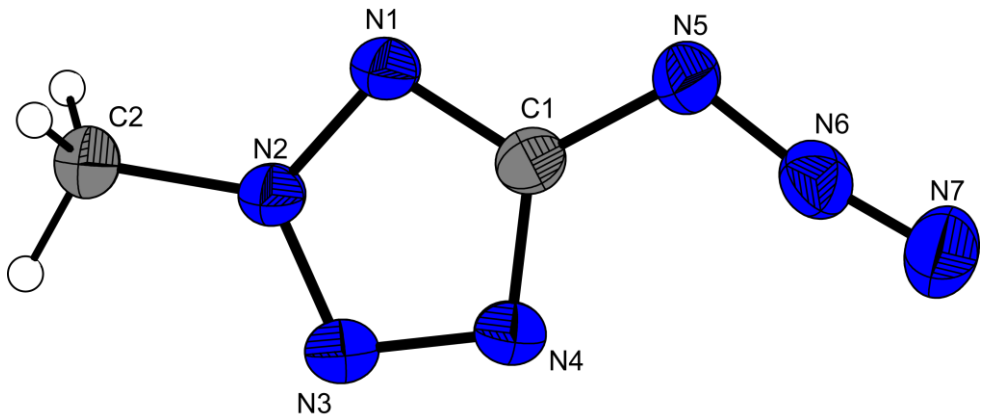

Figure 12.20 Molecular structure of **146**. Thermal ellipsoids are drawn at the 50 % probability level and hydrogen atoms are shown as small spheres of arbitrary radii.

Due to the absence of N–H and O–H protons only weak interactions can be observed. The largest discrepancy of the bond lengths of **145** and **146** is found in the distances between the atoms N3 and N4, which is significantly shorter in **146** (1.327(2) Å) in comparison to **145** (1.362(2) and 1.375(2) Å). Conspicuous in **Figure 12.20** is the small C1–N1–N2 angle of 100.6(1)° (**146**: 107.5(2) and 107.7(2)°), while angle N1–N2–N3 of 113.8(1)° is expanded.

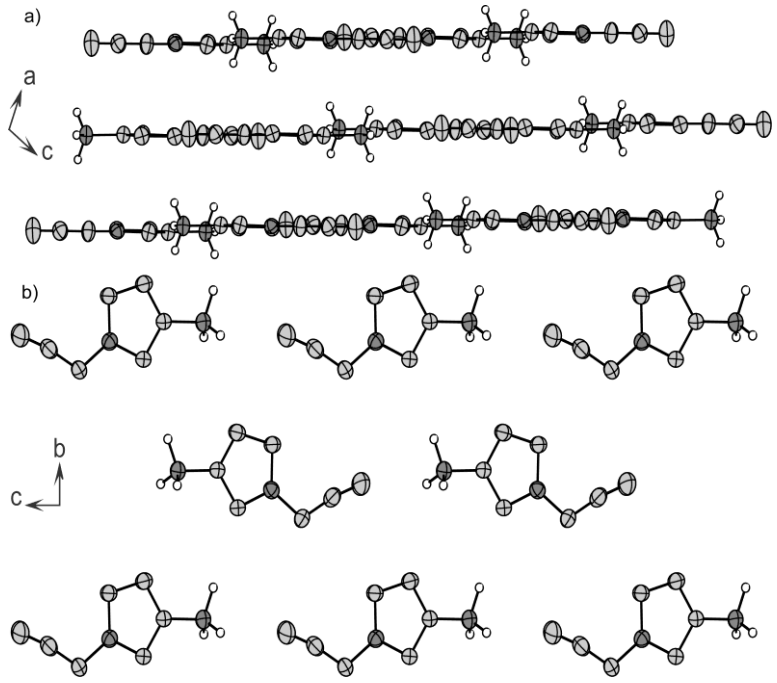

Figure 12.21 Crystal packing of **146**. a) View along the *b* axis and layers; b) View along the *a* axis on one layer.

Table 12.6 Bond lengths [Å] of **145** and **146**

Atoms	**145**(1)	**145**(2)	**146**
N1–C1	1.323(2)	1.328(3)	1.321(2)
N1–N2	1.349(2)	1.360(2)	1.339(2)
N2–N3	1.297(2)	1.295(2)	1.312(2)
N3–N4	1.362(2)	1.375(2)	1.327(2)
N4–C1	1.314(2)	1.317(3)	1.343(2)
C1–N5	1.389(2)	1.382(2)	1.394(2)
N5–N6	1.254(2)	1.254(3)	1.259(2)
N6–N7	1.111(2)	1.112(2)	1.113(2)
N1(2)–C2	1.459(3)	1.457(3)	1.448(2)

Table 12.7 Bond angles [°] and selected torsion angles [°] of **145** and **146**.

Atoms	**145**(1)	**145**(2)	**146**
C1–N1–N2	107.5(2)	107.7(2)	100.6(1)
C1–N4–N3	104.6(2)	104.4(2)	104.6(1)
N1–N2–N3	106.6(2)	106.3(2)	113.8(1)
N2–N3–N4	110.8(2)	111.1(2)	106.8(1)
N1–C1–N4	110.5(2)	110.4(2)	114.2(1)
N1–C1–N5	121.1(2)	120.1(2)	119.9(1)
N4–C1–N5	128.4(2)	129.5(2)	126.0(1)
C1–N5–N6	112.2(2)	112.5(2)	113.7(1)
N5–N6–N7	172.5(2)	173.2(2)	171.5(2)
C1–N1–C2	131.4(2)	130.2(2)	
N2–N1–C2	121.1(2)	122.1(2)	
N1–N2–C2			123.0(1)
N3–N2–C2			123.1(1)
N1– C1–N5–N6	180.0	180.0	178.9(1)
C1–N5–N6–N7	0.0	0.0	179.5(1)

12.4 Spectroscopy

12.4.1 NMR Spectroscopy

Multinuclear NMR spectroscopy, such as carbon and nitrogen NMR is a valuable method for characterization of tetrazoles and tetrazolates. The NMR spectra were measured in different solvents (*d*$_6$-DMSO (**135**, **145**, **146**), D_2O (**141**) and CD_3OD (**137**) with respect to TMS (^1H, ^{13}C) and $MeNO_2$ (^{14}N, ^{15}N) as external standards. In the ^1H and ^{13}C NMR spectra of **135** only one signal can be observed at 9.20 ppm and 157.5 ppm, respectively. In the ^1H NMR spectra of **145** and **146**, the C–H proton resonances are observed as sharp signals at 3.77 (**145**) as well as 4.28 ppm (**146**). The same trend is observed in the ^{13}C NMR spectra. Again the carbon resonances of **146** at 161.9 (C_{ring}) and 40.7 ppm (CH_3) are shifted to lower fields in comparison to that found for **145** (152.9 (C_{ring}) and 33.1 ppm (CH_3)). These trends are also observed in the corresponding NMR spectra of 1-and 2-methyl-5-aminotetrazole.[75] In the ^{13}C NMR spectra of the azidotetrazolates one

signal can be observed for the CN_7 anion in the range of 158 ppm (d_6-DMSO) and 160 ppm (D_2O), respectively.

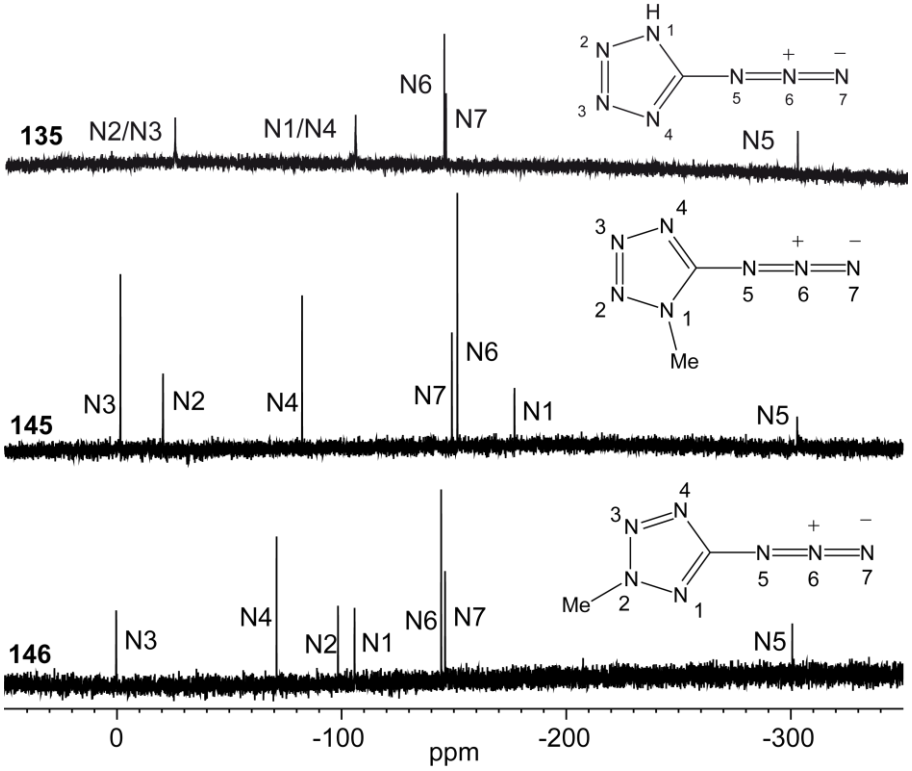

Figure 12.22 ^{15}N NMR spectrum of **135**, **145** and **146.** (δ(ppm): **135**: N2/N3 = –25.3, N1/N4 = –105.3, N6 = –144.7.2, N7 = –145.4, N5 = –301.4; **145**: 7.2 (N3), –12.2 (N2, q, $^3J_{NH}$ = 1.6 Hz), –75.6 (N4), –144.0 (N7), –146.5 (N6), –172.6 (N1, q, $^2J_{NH}$ = 2.0 Hz), –301.6 (N5); **146**: 0.4 (N1, q, $^3J_{NH}$ = 2.0 Hz), –71.0 (N4), –98.3 (N1, q, $^3J_{NH}$ = 1.9 Hz), –105.7 (N2, q, $^2J_{NH}$ = 2.3 Hz), –144.2 (N6), –146.0 (N7), –300.5 (N5).

In the ^{15}N spectrum (**Figure 12.22**) of **135**, measured in d_6-DMSO five signals are observed. The identical chemical shift of the atoms N2 and N3 as well as N1 and N4 is caused by the fast proton exchange in the polar solvent. The ^{15}N (proton coupled) spectra of **145** and **146** are also depicted in **Figure 12.22**. The assignments have been done by analyzing the ^{15}N–^1H coupling constants. In addition, the assignments in the spectra of **145** and **146** of the resonances between the three 2-coordinated nitrogen atoms can be achieved mainly by the fact that N4 (**145**: –75.6, **146**: –71.0 ppm) has one nitrogen and one carbon as nearest neighbors, whereas N2 and N3 are surrounded by two nitrogen atoms. Therefore, the signals of N2 and N3 appear at lowest field owing to electronegativity effects. This is consistent with the trends observed for other comparable ^{15}N chemical shifts.[402] Next to the observed quartet of N2 due to the $^3J_{NH}$ coupling, the assignment of peaks N2 and N3 can be achieved due to the electron

donating effect of the methyl group at N1. The electronegativity effect at N3 is lower than at N2, resulting in a low field NMR-signal for N2. Accordingly, in the spectrum of **146** nitrogen atom N2 is shifted to higher fields due to the directly connected methyl group. The ^{15}N NMR signals of the covalent azide groups are assigned according to the typical chemical shifts reported for covalent azides $-N_\alpha=N_\beta=N_\gamma$.[403] The resonance highest in intensity can be assigned to nitrogen atom N_β, while nitrogen N_α is always shifted to highest fields. Uncommonly, in the ^{15}N spectrum of **145** nitrogen atom N_γ shows a higher chemical shift than nitrogen atom N_β.

In **Figure 12.23** the ^{1}H, ^{13}C, ^{14}N, ^{15}N and ^{15}N{^{1}H} NMR spectra of hydrazinium 5-azidotetrazolate (**136**) in *d*$_6$-DMSO are depicted. In the ^{1}H spectrum a broad signal caused by the hydrazinium protons was observed at 7.07 ppm. The resonance of the ^{13}C carbon atom at 158.1 ppm is shifted to lower field when comparing with **135** (157.5 ppm). In the ^{15}N NMR spectrum six signals could be observed and assigned. (δ(ppm): 10.7 (N2/N3), –81.7 (N1/N4), –137.6 (N6), –151.0 (N7), –304.8 (N5) and 332.7 (N6)). In the ^{15}N{^{1}H} only the hydrazinium signal N6 is strong in intensity. The ^{14}N spectrum creates broad signals with low resolutions. In addition, **Figure 12.23** illustrates the ^{15}N spectra of **137** (in MeOD) and **141** (in D_2O), whereby the solvent shift can clearly be seen. (**137**: δ(ppm): N2/N3 = –2.7, N1/N4 = –92.4, N6 = –141.0, N7 = –149.0, N5 = –305.4); **141**: δ(ppm): N2/N3 = –4.5, N1/N4 = –94.0, N6 = –42.4, N7 = –146.9, N5 = –303.6)**.**

12.4.2 Vibrational Spectroscopy

Also vibrational spectroscopy, such as IR and Raman spectroscopy is adequate to identify **135**.[251] **Figure 12.24** and **Figure 12.25** illustrate the IR as well as the Raman spectrum of **135**, **145** and **146**. The assignments were done using a frequency analysis after optimizing the structure (see computational study). The most intensive vibration in the IR spectrum is the ν_{sym} vibration of the azide group, which can also be seen in the Raman spectrum. The $\nu_s(CH_3)$ and $\nu_{as}(CH_3)$ in the range of 2950–3050 cm^{-1} are strong in intensity in the Raman but low in intensity in the IR spectra of **145** and **146**. The broad signal at 1591 cm^{-1} can be assigned to the stretch vibration between the atoms C1 and N5. In the range of 980–1100 many deformation vibrations and combinations of the tetrazole ring can be found. Further characteristic absorption bands can be assigned at:

3080–2950 cm^{-1} (**145**, **146**) [$\nu_s/\nu_{as}(CH_3)$], 1560–1480 cm^{-1} [ν_s(C–N)], 1460–1400 cm^{-1} (**145**, **146**) [$\nu_{as}(CH_3)$], 1550–1350 cm^{-1} [$\nu(CN_4)$, ν(C–N)], 1350–700 cm^{-1} [ν(NCN), ν(NN), δ (NCN), $\delta(CN_4)$], < 500 [$\omega(CN_4, CH_3, N_3)$].

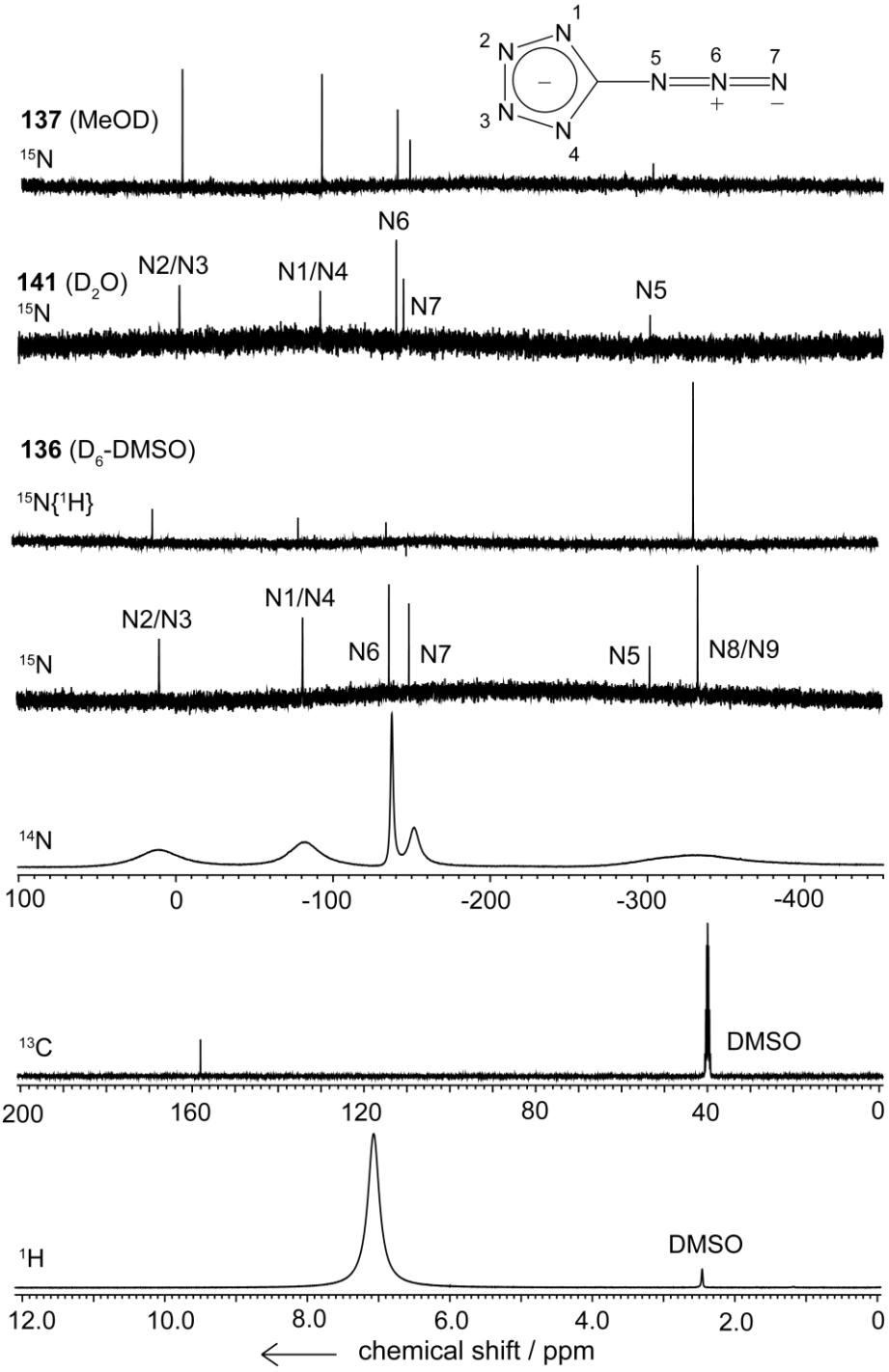

Figure 12.23 Multinuclear (^{1}H, ^{13}C, ^{14}N, ^{15}N and ^{15}N{1H}) NMR spectroscopy of **136** and ^{15}N NMR of **137** and **141** in different solvents.

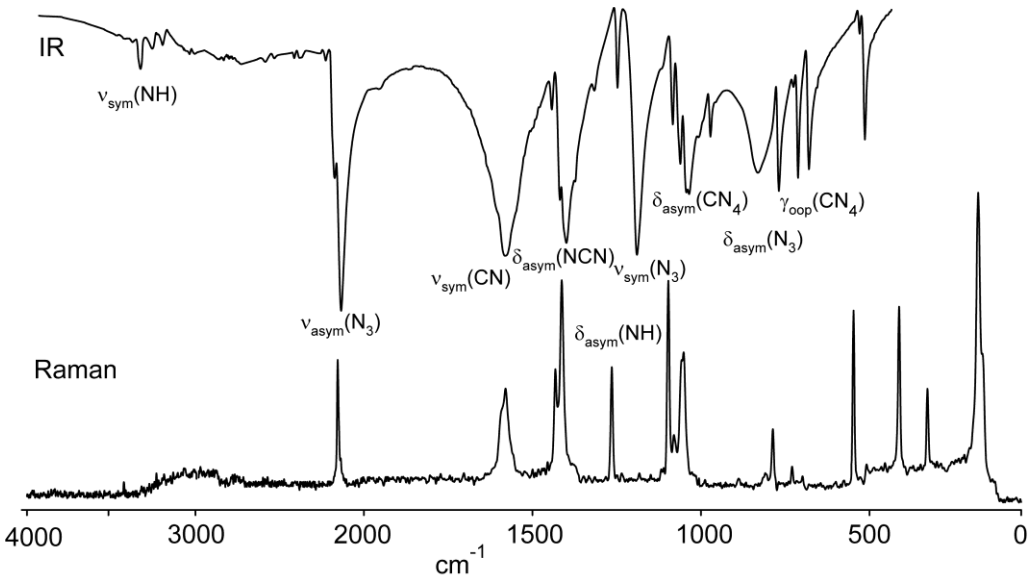

Figure 12.24 Vibrational spectroscopy of **135**. top: IR spectrum, below: Raman spectrum.

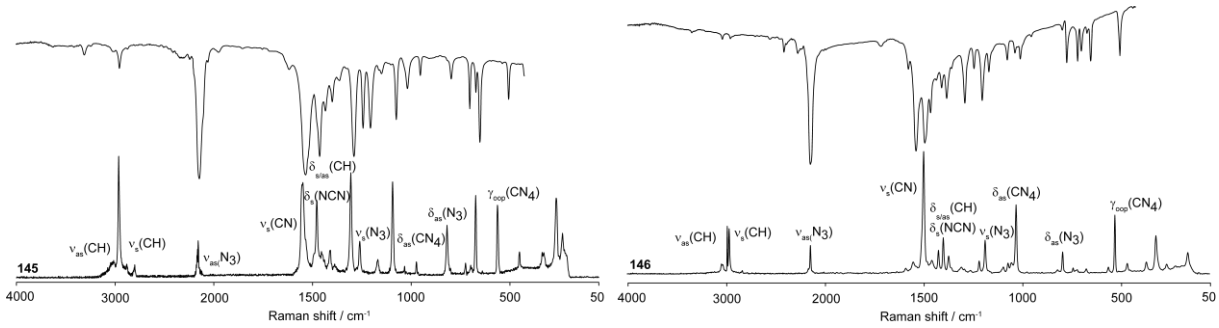

Figure 12.25 Vibrational spectroscopy of **145** (left) and (right).

12.4.3 CN_7^- anion vs. pseudohalide?

Although there is a similarity to the CN^- anion, the CN_7^- anion should not be described as a pseudohalide. Famous examples for this class of compounds are e.g. CN^-, N_3^-, OCN^-, CNO^-, SCN^- and also complexes like $Co(CO)_4^-$. There exist several criteria for pseudohalides, which are partly not fulfilled for the CN_7^- anion. While there exists the hydrogen acid and a low soluble silver salt can be formed, the synthesis of dimers as well as a halogen derivatives cannot be reached.

12.5 Computational Studies

12.5.1 5-Azidotetrazole

All calculations were carried out using the program package Gaussian03W. The structure, energy and frequency calculations of **135** were performed at the Hartree-Fock level followed by a Møller-Plesset correlation energy correction, truncated at second order.[116] For all atoms H, C and N an augmented correlation consistent polarized double-zeta basis set was used (aug-cc-pVDZ).[117] The results of the calculations are presented in **Table 12.8**. The gas phase structure of 5-azido-2*H*-tetrazole is lower in electronic energy than this of 5-azido-1*H*-tetrazole.

Table 12.8 Comparison of 1*H* and 2*H* tautomers of **135**.

	5-azido-1*H*-tetrazole	5-azido-2*H*-tetrazole
	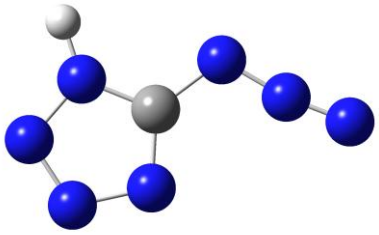	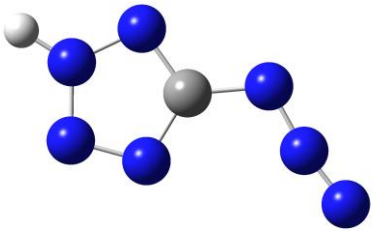
–E / a.u.	420.828841	420.834983
$E_{rel.}$ / kcal mol^{-1}	+3.85	0.00
point group	C_s	C_s
NIMAG	0	0
zpe / kcal mol^{-1}	31.0	31.5
μ / D	4.5	2.5

The two structural isomers 5-azido-1*H*-tetrazole and 5-azido-2*H*-tetrazole (both C_s symmetry) were both found to be true minima on the potential energy surface with the 5-azido-2*H*-tetrazole being more stable in the gas phase by 3.85 kcal mol^{-1} (**Table 12.8**). The fact that 5-azido-1*H*-tetrazole was unambiguously identified in the solid state can be explained by favorable hydrogen bonding of this species. Moreover, the higher dipole moment of 5-azido-1*H*-tetrazole may also favor this species in solution in polar solvents. This situation is also found for other 5-substituted tetrazoles e.g. 1*H*-tetrazole in literature.[404]

With the ab initio (MP2/aug-cc-pVDZ) computed electronic energies and the estimated heat of sublimation for 5-azido-1*H*-tetrazole of +65.5 kJ mol^{-1} (estimated as: ΔH_{sub}. [J mol^{-1}] = 188 T_m [K] [405]) and after correction for the work term ($p\Delta V$), the vibrational correction ($\Delta_{vib}U$), the translational ($\Delta_{trans}U$) and rotational term ($\Delta_{rot}U$),[121] the enthalpy of combustion of 5-azido-1*H*-tetrazole was calculated to be: $\Delta_c H$ = –1125.8 kJ mol^{-1}.

$$CHN_7(s) + 1.25\ O_2(g) \longrightarrow CO_2\ (g) + 0.5\ H_2O\ (g) + 3.5\ N_2(g)$$

With the known enthalpies of formation of carbon dioxide ($\Delta_f H°_{298}(CO_{2(g)})$ = –393.5 kJ mol^{-1}) and water ($\Delta_f H°_{298}(H_2O_{(g)})$ = –241.8 kJ mol^{-1}) the enthalpy of formation of **135** can now be calculated to: $\Delta_f H°_{298}$(**135**(s)) = +611 kJ mol^{-1}.

12.5.2 Methyl-5-azidotetrazoles

The heats of formation of **145** and **146** have been calculated using the atomization energy method, which has been proofed to be suitable especially for energetic materials. The enthalpies of the gas-phase species M were computed according to the atomization energy method equation: $\Delta_f H°_{(g,\ M,\ 298)} = H_{(Molecule,\ 298)} - \sum H°_{(Atoms,\ 298)} + \sum \Delta_f H°_{(Atoms,\ 298)}$
From the gas-phase enthalpies of formation $\Delta_f H°$(g) (**145**: 657 kJ mol^{-1}, **146**·H_2O: 634 kJ mol^{-1}), the enthalpies of the solid state can be calculated using the enthalpies of sublimation by the equation: $\Delta_f H°(s) = \Delta_f H°(g) - (\Delta_{sub} H)$
For a solid compound the enthalpy of sublimation ($\Delta_{sub}H$) can be approximated on the basis of TROUTON's rule if the melting temperatures T_m (**145**: 291 K, **146**: 335 K are known: $\Delta_{sub}H$ [J mol^{-1}] = 188 T_m [K]
With the known enthalpies of formation of carbon dioxide ($\Delta_f H°_{298}(CO_{2(g)})$ = –394 kJ mol^{-1}) and water ($\Delta_f H°_{298}(H_2O_{(g)})$ = –242 kJ mol^{-1}) the enthalpies of formation of **145** (602 kJ mol^{-1}), and **146** (571 kJ mol^{-1}) have been calculated. The values are highly endothermical and slightly lower than that calculated for 5-azido-1*H*-tetrazole (611 kJ mol^{-1}).

12.5.3 5-Azidotetrazolates

The heats of formation of **136–138** have also been calculated using the atomization energy method. The results are summarized in **Tables 12.9–12.14**.

Table 12.9 CBS-4M results

	p.g.	$-H^{298}$ / a.u.	$-G^{298}$ / a.u.	*NIMAG*
CN_7^-	C_s	420.795948	420.833397	0
$N_2H_5^+$	C_s	112.030523	112.058024	0
NH_4^+	T_d	56.796608	56.817694	0
$(H_2N)_2C(NHNH_2)^+$	C_s	260.701802	260.736515	0
H		0.500991	0.514005	0
C		37.786156	37.803062	0
N		54.522462	54.539858	0
O		74.991202	75.008515	0

Table 12.10 Literature values for atomic $\Delta_f H°^{298}$ / kcal mol^{-1}

	Ref. [125]	NIST [122]
H	52.6	52.1
C	170.2	171.3
N	113.5	113.0
O	60.0	59.6

Table 12.11 Enthalpies of the gas–phase species M.

M	M	$\Delta_f H°$(g,M) / kcal mol^{-1}
CN_7^-	CN_7^-	+114.1
$N_2H_5^+$	$N_2H_5^+$	+185.1
NH_4^+	NH_4^+	+151.9
$(H_2N)_2C(NHNH_2)^+$	AG^+	+161.0

The lattice energies (U_L) and lattice enthalpies (ΔH_L) were calculated from the corresponding molecular volumes (**Table 12.12**) according to the equations provided by Jenkins *et al.* [118] and are summarized in **Table 12.13**.

Table 12.12 Molecular volumes.

	V_M / Å^3	V_M / pm^3
$[N_2H_5][CN_7]$	151.6 [a]	0.152
$[NH_4][CN_7]$	132.3 [b]	0.132
[AG][CN_7]	201.8 [c]	0.202

[a] from X-ray data, V = 264.6 Å^3, Z = 2; [b] V = 606.5 Å^3, Z = 4; [c] V = 807.2 Å^3, Z = 4.

Table 12.13 Lattice energies and lattice enthalpies.

	V_M / nm^3	U_L / kJ mol^{-1}	ΔH_L / kJ mol^{-1}	ΔH_L / kcal mol^{-1}
$[N_2H_5][CN_7]$	0.152	543.4	548.4	131.1
$[NH_4][CN_7]$	0.132	654.6	569.6	136.1
[AG][CN_7]	0.202	503.6	508.6	121.6

With the calculated lattice enthalpies (**Table 12.13**) the gas-phase enthalpies of formation (**Table 12.11**) were converted into the solid state (standard conditions) enthalpies of formation (**Table 12.14**). These molar standard enthalpies of formation (ΔH_m) were used to calculate the molar solid state energies of formation (ΔU_m) according to eq. (1–4).

$\Delta U_m = \Delta H_m - \Delta n RT$ (Δn being the change of moles of gaseous components) (**1**)

$C(s) + 2.5\ H_2(g) + 4.5\ N_2 \rightarrow [N_2H_5]^+[CN_7]^-(s)$ (Δn = –7) (**2**)

$C(s) + 2\ H_2(g) + 4\ N_2 \rightarrow [NH_4]^+[CN_7]^-(s)$ (Δn = –6) (**3**)

$2\ C(s) + 3.5\ H_2(g) + 5.5\ N_2 \rightarrow [CN_4H_7]^+[CN_7]^-(s)$ (Δn = –7) (**4**)

Table 12.14 Solid state enthalpies ($\Delta_f H°$) and energies of formation ($\Delta_f U°$)

	$\Delta_f H°$(s) / kcal mol^{-1}	$\Delta_f H°$(s) / kJ mol^{-1}	Δn	$\Delta_f U°$(s) / kcal mol^{-1}	M / g mol^{-1}	$\Delta_f U°$(s) / kJ kg^{-1}
$[N_2H_5][CN_7]$	+168.1	+703.8	–7	+172.2	143.1	+5034.8
$[NH_4][CN_7]$	+129.9	+543.9	–6	+133.5	128.1	+4360.4
[AG][CN_7]	+153.5	+642.7	–9	+158.8	185.2	+3587.6

From **Table 12.14** it can be seen, that **136**–**138** are strongly endothermic compounds. The enthalpies of energetic materials are governed by the molecular structure of the

compounds, and therefore, heterocycles with a higher nitrogen content show higher heats of formation. The lower $\Delta_f H°$(s) of **137** in comparison to **138** can be explained by the presence of a further N–N single bond in the structure of **138**, which increase the heat of formation decisively.

12.6 Physico-chemical properties

A summary of the physico-chemical properties is given in **Table 12.15**.

12.6.1 Thermal Stability

For determining the decomposition temperature of **135**, **145** and **146** a Linseis DSC PT 10 with a heating rate of 5 K min^{-1} and a nitrogen flow of 5 L h^{-1} was used. The measurement with ~1.5 mg of **135**, **145** and **146** was performed in a pressed Al-container, containing a hole (0.1 mm) for the gas release. The DSC plot in **Figure 12.26** shows the thermal behavior of **135**, **145** and **146** in the 50–360 °C temperature range. Temperatures are given as "onset temperatures". **135** melts at 75 °C and decomposes above 165 °C. **145** and **146** show low melting temperatures, since both compounds cannot be stabilized by hydrogen bonds.

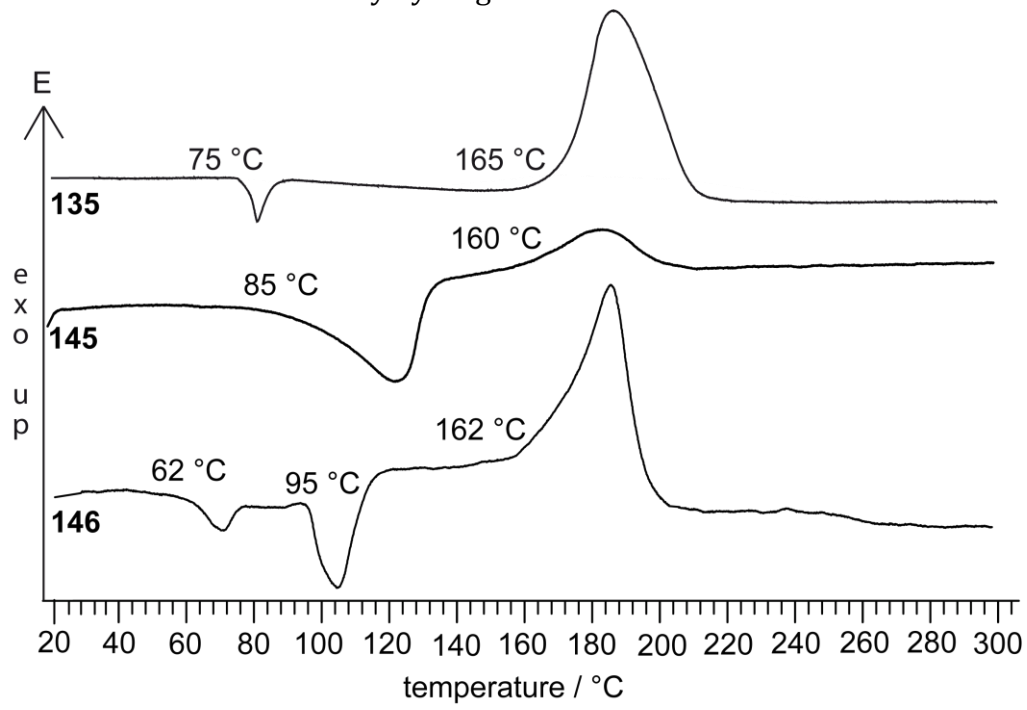

Figure 12.26 DSC plots (exo-up) of **135**, **145** and **146** (β = 5 °C min^{-1})

1-Methyl-5-azidotetrazole (**145**) is characterized by a melting point at 20 °C as well as broad boiling region starting at 85 °C. Gaseous **145** starts to decompose above temperatures of 160 °C. The 2-methylated analogue **146** is solid at room temperature. However, **146** melts at 62 °C and starts to boil at 95 °C. The decomposition temperature of 162 °C is in the range of that observed for **145**. Both compounds can be sublimated ($1 \cdot 10^{-2}$, 40 °C).

The thermal behavior of the CN_7^- salts **136–139** as well as of **141** (~1.5 mg) was also investigated on the Linseis PT10 DSC at heating rates of 5 ° min^{-1}.

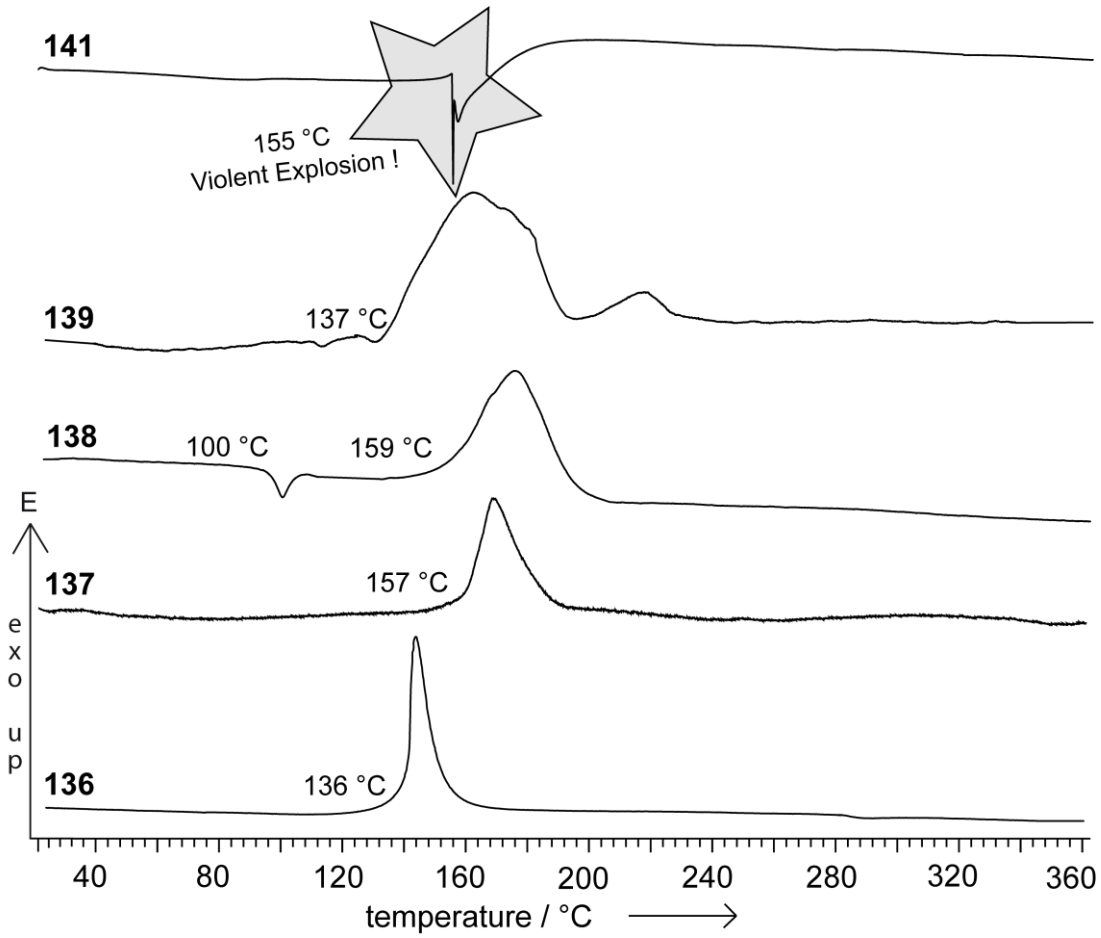

Figure 12.27 DSC plot (exo-up) of **136–139** as well as of **141**. $T_{dec.}$: **136** = 136 °C, **137** = 157 °C, **138** = 159 °C, **139** = 137 °C and **141** = 155 °C.

The compounds decompose/explode violently mostly without prior melting points. Considering only the nitrogen-rich derivatives **136–139** it can be seen from **Figure 12.27**, that **136** shows the lowest decomposition temperature of 136 °C. **137** and **138** decompose in the same range (157–159 °C), while a melting point at ~100 °C is observed

in the thermo plot of **139**. Interestingly **139**, shows broad decomposition starting at 137 °C. This may be a reason, due to the included crystal water. Sodium salt **141** decomposes at 155 °C. It is not possible to dehydrate **141** by simple heating as well as under reduced pressure. In the measurement of **141** a violent explosion appeared destroying the setup, which can be seen on its thermo plot.

12.6.2 Detonation Parameters

The detonation parameters were calculated using the program EXPLO5 V5.02. The calculation was performed using the maximum densities according to the crystal structure and the calculated heats of formation. The calculated values of compounds **135**, **145** and **146** show high calculated values exceeding these of commonly used trinitrotoluene (TNT) [406] as well as nitroglycerin (NG). Those of **135** are in the range of RDX, those of **145** and **146** are in the range of pentaerythritol tetranitrate (PETN). The most important criteria of high explosives are the detonation velocity ($V_{\mathrm{Det.}}$= **135**: 8986, **145**: 7970, **146**: 8284, TNT: ~7000, nitroglycerin: 7600, PETN: 8400, RDX: 8750 m s^{-1}, detonation pressure ($p_{\mathrm{Det.}}$ = **135**: 327, **145**: 223, **146**: 250, RDX: 346 kbar) and energy of explosion ($\Delta_{\mathrm{E}}U_{\mathrm{m}}°$ = **145**: –5284, **146**: –5043, NG: –6238, PETN: –5862, RDX: –6043 kJ kg^{-1}). Since the detonation velocity of an energetic material is directly proportional ($V_{Det.}$ α ρ) to its density, the detonation pressure even square proportional ($p_{Det.}$ α ρ^2), compound **146** is characterized by higher values regarding the pressure and velocity. However, due to the higher heat of formation compound **145** shows a higher calculated explosion energy as well as temperature in comparison with **146**.

The detonation performances of **136**–**138**, are also summarized in **Table 12.15**. The values of **136** exceed those observed for RDX [112] and also those of HMX, which is one of the most powerful secondary explosives up to date.

More importantly, the specific impulses (I_{sp}) and the molar N_2/CO ratios for the combustion gases are the relevant numbers for the characterization of propellants. Smokeless combustion, which is an inherent feature of high-nitrogen compounds, is not only of environmental interest, but particularly of strategic interest since detection of the gun, missile or rocket becomes more difficult. **Table 12.16** summarizes the computed isobaric combustion temperatures (T_{c}, the lower the better for gun-

propellants), the specific impulses (I_{sp}) and the molar N_2/CO ratios for **136**, **137**, **138**, a 60:40 mixture of **136** with ADN (ammonium dinitramide) and three typical conventional gun-propellants (single-, double-, triple-base) and a typical 70:30 solid booster mixture of AP/Al (ammonium perchlorate/aluminum).

Table 12.15 Physico-chemical properties of **135–138** as well as **145** and **146**

	135	**136**	**137**	**138**	**145**	**146**	**RDX**
Formula	CHN_7	$[N_2H_5][CN_7]$	$[NH_4][CN_7]$	$[CH_7N_4][CN_7]$	$C_2H_3N_7$	$C_2H_3N_7$	$C_3H_6N_6O_6$
FW (g mol^{-1})	111.07	143.11	128.12	185.15	125.11	125.11	222.1
IS (J)[a]	< 1	< 1	< 1	1	< 1	< 1	7
FS (N)[b]	< 5	5	5	7	< 5	< 5	120
ESD (mJ)[c]	< 20	5	10	40	50	80	> 150
N (%)[d]	88.28	88.09	87.48	79.60	81.14	81.14	37.8
Ω (%)[e]	–36.0	–50.3	–50.0	–64.8	–51.14	–51.14	–21.6
Combustion	fulm.	fulm.	fulm.	fulm.	fulm.	fulm.	comb.
$T_{dec.}$ (°C)[f]	165	136	157	159	160	162	213
ρ (g cm^{-3})[g]	1.72	1.57	1.61	1.52	1.480	1.571	1.82
$\Delta_f H_m°$ (kJ mol^{-1})[h]	611	704	540	643	602	571	2105
$\Delta_f U°$ (kJ/kg)[i]	5590	5041	4336	3588	4910	4662	66.5
EXPLO5 values:							
$-\Delta_E U_m°$ (J g^{-1})[j]	5721	5592	4829	4193	5284	5043	6043
T_E (K)[k]	4701	3813	3498	3052	3879	3718	4321
p (kbar)[l]	327	306	287	241	223	250	346
$V_{Det.}$ (m s^{-1})[m]	8986	9231	8917	8424	7970	8284	8750
Gas vol. (L kg^{-1})[n]	752	879	855	856	755	752	794

[a] impact sensitivity, BAM drophammer; [b] friction sensitivity, BAM friction tester; [c] electrical spark sensitivity, OZM small scale tester; [d] Nitrogen content; [e] Oxygen balance; [f] Decomposition temperature from DSC (β = 5 °C min^{-1}); [g] Estimated from X-ray diffraction; [h] Molar enthalpy of formation; [i] Energy of formation; [j] Energy of Explosion, EXPLO5 V5.02; [k] explosion temperature; [l] detonation pressure; [m] detonation velocity; [n] Assuming only gaseous products.

Table 12.16 Computed propulsion relevant parameters of **136–138** (isobaric combustion at p = 20 bar)

	ρ / g cm^{-3}	isobaric comb. temp., T_c / K	I_{sp} / s	N_2/CO ratio
NC [a]	1.66	2750	232	0.32
NC[a]/NG (50:50)	1.63	3308	249	0.68
NC[a]/NG[b]/NQ[c] (25:25:50)	1.70	2683	236	1.35
136	1.57	2947	265	96.6
137	1.61	2693	248	96.6
138	1.52	2249	228	93.5
136/ADN[d] (60:40)	1.66	3142	267	6.9
AP/AL (70:30)[e]	2.178	4273	252	---

[a] NC-13.3 (N content 13.3%); [b] NG, nitroglycerine; [c] NQ, nitroguanidine; [d] ADN, ammonium dinitramide; [e] AP/Al, ammonium perchlorate / aluminum.

Whereas single-base propellants are used in all guns ranging from pistols to artillery weapons, the more powerful (see I_{sp}) double-base propellants are commonly used in pistols and mortars. The disadvantage of double-base propellants is the excessive erosion of the gun barrel (see N_2/CO ratio) by the much higher flame temperatures, and the presence of a muzzle flash (fuel-air explosion of the combustion products). In order to reduce erosion and muzzle flash, triple-base propellants with up to 50 % nitroguanidine are used in tank guns, large caliber guns and naval guns. However, the performance of triple-base propellants is lower than that of double-base propellants. Compounds **136**–**138** show relatively low combustion temperatures (comparable to single- and triple-base propellants), with excellent molar N_2/CO ratios (which are usually ~0.5 for conventional propellants). The computed specific impulses of **136**, **137** and even **138** have possible applications as promising energetic components in reduced-erosion gun propellants. Moreover, a 60:40 mixture of **136** with ADN possesses a calculated specific impulse of ~15 s higher than that of a mixture of AP/Al commonly used in solid state boosters (space shuttle, Ariane 5).

12.6.3 Sensitivities

For initial safety testing, the impact and friction sensitivity as well as the electrostatic sensitivity of the neutral compounds **135**, **145** and **146** were determined. Compound **135** is very sensitive towards impact (< 1 J) and friction (< 5 J). Compounds **145** and **146** are also very sensitive towards impact (< 1 J) and towards friction (**145**: < 5 N, **146**: < 5 N) and should therefore only be handled with utmost care. **135** as well as **145** and **146** are classified according to the "UN Recommendations on the transport of dangerous goods" [107] as "extremely sensitive" in both categories. Since this values are higher than this observed for lead azide, they should be considered to be primary explosives. The electrical spark sensitivities were determined to be 20 mJ (**135**), 50 mJ (**145**) and 80 mJ (**146**), which also consider with values observed for primary explosives. These values are lower than those observed for commonly used secondary explosives like RDX (0.2 J) but higher than that of the primary explosives $Pb(N_3)_2$ (0.005 J). It should be mentioned that the test towards electrical discharge strongly depends on the particle size and shape. Although we tried to use fine crystalline materials (125–250 μm) a guarantee for the determined values, especially for low-melting **145** cannot be given.

The sensitivities of the CN_7^- salts were also discovered. However, appropriate tests could only performed with compounds **136**–**141** and **144**. **142** and **143** cannot be handled without violent explosions. Compounds **136**–**141** show all impact sensitivities of smaller than 1 J. Solely **144** explodes not until 2 J (!). However, according to the UN Recommendations on the Transport of Dangerous Goods,[107] all 5-azidotetrazolate salts are classified as "very sensitive" regarding the impact sensitivity. Also the friction sensitivity tests showed the same trends. Except for **138** (7 N), **139** (11 N) and **144** (25 N) all compounds can be initiated by forces smaller than 5 N. However, except for compound **144**, **136**–**143** are classified as extremely sensitive regarding the friction sensitivity. The electrical spark sensitivities of microcrystalline (1–50 μm particle size) material were determined to be 5 mJ (**136**), 10 mJ (**137**), 40 mJ (**138**), 70 mJ (**139**), 40 mJ (**140**), 20 mJ (**141**) and 160 mJ (**144**).

12.7 Experimental Part

*CAUTION: 5-Azido-1H-tetrazole (**135**), its salts **136–144** as well as the methyl derivatives **145** and **146** are extremely high energetic compounds with increased sensitivities towards various stimuli, therefore proper protective measures (safety glasses, face shield, leather coat, earthened equipment and shoes, Kevlar® gloves and ear plugs) should be used. All compounds should be stored in explosive cases since they can explode spontaneously.*

*5-Azido-1H-tetrazole (**135**)* Cyanogen bromide (530 mg, 5 mmol) was dissolved in a mixture of 15 mL cold water and 5 mL MeOH. To this a solution of NaN_3 (650 mg, 10 mmol) was added drop wise while cooling in an ice bath. After 2 h, 1 N HCl (5 mL, 0.5 mmol) was added slowly and the solution was allowed to come to room temperature. The mixture was extracted 3 times with 10 mL of cold diethyl ether. The organic phases were combined, dried with $MgSO_4$ and the solvent was removed at room temperature under reduced pressure, whereby 410 mg (yield 74 %) of colorless **135** was obtained. **DSC** (T_{onset}, 5 °C min^{-1}): 75 °C, 165 °C (dec.); **IR** (KBr, cm^{-1}): $\tilde{\nu}$ = 3343 (w), 3022 (m), 2897 (m), 2747 (m), 2604 (m), 2298 (m), 2194 (m), 2156 (vs), 1591 (s, br), 1454 (m), 1430 (s), 1411 (s), 1260 w), 1202 (s), 1097 (m), 1074 (m), 1048 (m), 985 (m), 845 (m, br), 783 (m), 726 (m), 694 (m), 528 (m); **Raman** (1064 nm, 200 mW, 25 °C, cm^{-1}): $\tilde{\nu}$ = 2155 (40), 1579 (32), 1431 (38), 1412 (62), 1264 (38), 1096 (32), 1051 (42), 786 (20), 729 (10), 547 (54), 412 (56), 356 (32), 177 (100); **^{1}H NMR** (d_6-DMSO, 25 °C, ppm): δ = 9.20 (1H, br); **^{13}C NMR** (d_6-DMSO, 25 °C, ppm): δ = 157.5 (1C); **^{15}C NMR** (d_6-DMSO, 25 °C, ppm): δ = –25.3 (N2/N3), –105.3 (N1/N4), –144.7 (N6), –145.4 (N7), –301.4 (N5); ***m/z*** (DEI): 111 (2), 71 (1), 69 (1), 57 (1), 55 (6), 54 (2), 53 (12), 45 (3), 44 (12), 41 (4), 42 (2), 31 (4), 29 (11), 28 (100), 27 (21), 26 (6), 18 (10); **EA** (CHN_7, 111.09) calcd.: C 10.81, H 0.91, N 88.28 %; found: not determinable; **impact sensitivity**: < 1 J; **friction sensitivity**: < 5 N; **ESD**: 20 mJ.

*Hydrazinium 5-azidotetrazolate (**136**):* 5-Azido-1*H*-tetrazole (**135**) (555 mg, 5 mmol) was dissolved in 20 mL THF and 5.5 mL of 1 M hydrazine solution in THF was added slowly. The mixture was warmed to 45 °C and methanol was added drop wise till a clear solution was obtained. From this, the product crystallized within 3 hours and was washed with diethyl ether. (458 mg, yield 64 %) **DSC** (T_{onset}, 5 °C min^{-1}): 136 °C (dec.); **IR** (KBr, cm^{-1}): $\tilde{\nu}$ =3363 (s), 3288 (w), 3211 (m), 3072 (m), 2968 (m), 2762 (m), 2641

(m), 2147 (vs), 1625 (w), 1528 (w), 1471 (s), 1403 (m), 1234 (m), 1189 (w), 1134 (m), 1122 (m), 1083 (m), 1053 (m), 1022 (w), 930 (s), 791 (m), 738 (m), 549 (w), 534 (w); **Raman** (1064 nm, 200 mW, 25 °C, cm^{-1}): $\tilde{\nu}$ = 3363 (4), 3266 (3), 3212 (5), 2139 (19), 1663 (4), 1628 (7), 1604 (5), 1521 (4), 1474 (100), 1403 (13), 1240 (3), 1233 (21), 1189 (10), 1142 (12), 1124 (21), 1082 (11), 1069 (11), 1055 (26), 1023 (3), 931 (9), 790 (10), 739 (6), 552 (18), 413 (9), 345 (23), 237 (10), 196 (9), 157 (12); **^{1}H NMR** (d_6-DMSO, 25 °C, ppm): δ = 7.07 (N_2H_5); **^{13}C NMR** (d_6-DMSO, 25 °C, ppm): δ = 158.1 (CN_7); **^{15}N NMR** (d_6-DMSO, 25 °C, ppm): δ = 10.7 (N2/N3), –81.7 (N1/N4), –137.6 (–NN_{β}N), –151.0 (–NNN_{γ}), –304.9 (–N_{α}NN), –332.7 (N_2H_5); ***m/z*** (FAB$^-$): 110. **EA** (CH_5N_9, 128.10) calcd.: 8.39, H 3.52, N 88.09 %; found: not determinable; **impact sensitivity**: < 1 J; **friction sensitivity**: < 5 N; **ESD**: 5 mJ.

*Ammonium 5-azidotetrazolate (**137**):* To 5-azidotetrazole (555 mg, 5 mmol) in 10 mL of water, concentrated ammonia solution (2 mL) was added. After stirring for 5 min the solvent was removed at room temperature under reduced pressure, and the raw product was recrystallized from a small amount of ethanol (518 mg, yield 81 %). **DSC** (T_{onset}, 5 °C min^{-1}): 157 °C (dec.); **IR** (KBr, cm^{-1}): $\tilde{\nu}$ = 3333 (m), 3156 (m), 3016 (m), 2965 (m), 2814 (m), 2161 (s), 2140 (s), 1681 (m), 1629 (w), 1474 (vs), 1445 (s), 1422 (s), 1399 (vs), 1233 (m), 1190 (m), 1137 (m), 1122 (m), 1050 (m), 789 (w), 740 (m), 548 (w), 532 (m); **Raman** (1064 nm, 200 mW, 25 °C, cm^{-1}): $\tilde{\nu}$ = 3490 (7), 3146 (1), 3019 (4), 2802 (3), 2141 (16), 1575 (3), 1482 (100), 1452 (20), 1422 (5), 1402 (10), 1334 (2) 1233 (25), 1191 (15), 1139 (20), 1123 (29), 1052 (35), 1020 (6), 787 (13), 741 (5), 550 (19), 419 (15), 348 (18), 174 (27), 155 (18); **^{1}H NMR** (D_2O, 25 °C, ppm): δ = 7.08 (NH_4, br); **^{13}C NMR** (D_2O, 25 °C, ppm): δ = 159.8 (1C); **^{15}C NMR** (D_2O, 25 °C, ppm): δ = –4.5 (N2/N3), –94.0 (N1/N4), –42.4 (N6), –146.9 (N7), –303.6 (N5); ***m/z*** (FAB$^-$): 110; **EA** (CH_4N_8, 128.10) calcd.: 9.38, H 3.15, N 87.48 %; found: not determinable; **impact sensitivity**: < 1 J; **friction sensitivity**: < 5 N; **ESD**: 50 mJ.

*Aminoguanidinium 5-azidotetrazolate (**138**):* To aminoguanidinium bicarbonate (340 mg, 2.5 mmol) suspended in 5 mL water, a solution of 5-azidotetrazole (258 mg, 2.5 mmol) in 5 mL of water was added drop wise. The colorless solution obtained was stirred for 15 min at 45 °C until the release of CO_2 has stopped and was left for crystallization. After one day **138** was obtained as colorless crystals, which were washed with a small amount of cold ethanol and diethyl ether. (440 mg, 95 % yield) **DSC** (T_{onset}, 5 °C min^{-1}): 100 °C, 159 °C (dec.); **IR** (KBr, cm^{-1}): $\tilde{\nu}$ = 3436 (s), 3316 (s), 3164 (s), 3077

(m), 2247 (w), 2143 (vs), 1671 (vs), 1521 (w), 1467 (s), 1416 (m), 1406 (m), 1231 (m), 1188 (w), 1116 (w), 1054 (w), 1011 (w), 960 (w), 787 (w), 617 (w), 511 (w); **Raman** (1064 nm, 200 mW, 25 °C, cm^{-1}): $\tilde{\nu}$ = 3272 (6), 2146 (22), 1680 (8), 1641 (6), 1559 (9), 1465 (100), 1414 (8), 1235 (29), 1190 (16), 1109 (28), 1056 (29), 963 (37), 789 (14), 741 (6), 622 (8), 551 (21), 543 (19), 517 (20), 418 (29), 335 (26), 161 (31); **^{1}H NMR** (MeOD, 25 °C, ppm): δ = 8.79 (s, 1H, NH), 7.39 (s, 2H, NH_2), 7.10 (s, 2H, NH_2), 5.07 (s, 2H, NH–NH_2); **^{13}C NMR** (MeOD, 25 °C, ppm): δ (ppm) = 159.7 (CN_7), 159.2 (AG^+); **^{15}N NMR** (MeOD, 25 °C, ppm): δ = –2.7 (N2/N3),–92.4 (N1/N4), –141.0 (N6),–149.0 (N7), 287.1 (NH), –305.4 (N5), 312.3 (NH_2), 318.4 (NH_2), 330.8 (NH_2); **EA** ($C_2H_7N_{11}$, 185.15) calcd.: 12.97, H 3.81, N 83.22 %; found: 12.21, H 4.32, N 82.69 %; **impact sensitivity**: < 1 J; **friction sensitivity**: 7 N; **ESD**: 40 mJ.

*Guanidinium 5-azidotetrazolate semihydrate (**139**):* The procedure of **139** follows that of **138** using guanidinium bicarbonate (303 mg, 2.5 mmol). **139** was obtained as colorless crystalline material. (421 mg, 94 %). **DSC** (T_{onset}, 5 °C min^{-1}): 110 °C, 137 °C (dec.); **IR** (KBr, cm^{-1}): $\tilde{\nu}$ = 3482 (s), 3369 (s), 3123 (s), 2469 (w), 2254 (w), 2144 (vs), 2037 (w), 1650 (vs), 1523 (m), 1469 (s), 1406 (s), 1237 (m), 1191 (m), 1130 (m), 1071 (w), 1049 (m), 791 (w), 741 (m), 669 (m), 632 (m), 553 (w), 534 (w); **Raman** (1064 nm, 250 mW, 25 °C, cm^{-1}): $\tilde{\nu}$ =3363 (4), 3165 (5), 2139 (15), 1644 (15), 1578 (15), 1470 (100), 1405 (22), 1337 (16) 1241 (28), 1194 (24), 1131 (24), 1119 (24), 1051 (39), 1011 (67), 792 (17), 741 (15), 545 (32), 519 (17), 421 (24), 343 (20, 167 (24); **^{1}H NMR** (MeOD, 25 °C, ppm): δ = 5.18 (s, 6H, NH_2); **^{13}C NMR** (MeOD, 25 °C, ppm): δ = 159.1 (CN_7), 158.8 (G^+); **EA** ($C_2H_7N_{10}O_{1/2}$, 179.15) calcd.: 13.41, H 3.94, N 78.19 %; found: 13.13, H 4.12, N 77.42 %; **impact sensitivity**: < 1 J; **friction sensitivity**: 11 N; **ESD**: 70 mJ.

*Lithium 5-azidotetrazolate monohydrate (**140**):* 5 mL of an aqueous lithium hydroxide (96 mg, 4 mmol) solution was added to 5-azidotetrazole (444 mg, 4 mmol) dissolved in 10 mL MeOH. After stirring for 10 min at 40 °C the solution was filtrated and left for crystallization. After 48 hours colorless single crystals were obtained, which were washed with diethyl ether. (459 mg, 85 % yield) **DSC** (T_{onset}, 5 °C min^{-1}): 152 °C (dec.); **Raman** (1064 nm, 300 mW, 25 °C, cm^{-1}): $\tilde{\nu}$ = 2157 (25), 1479 (100), 1407 (15),1243 (39), 1205 (12), 1156 (21), 1143 (21), 1068 (46), 792 (11), 746 (7), 553 (26), 429 (16), 353 (22), 167 (27); **impact sensitivity**: < 1 J; **friction sensitivity**: < 5 N; **ESD**: 40 mJ.

*Sodium 5-azidotetrazolate monohydrate (**141**):* Cyanogen bromide (530 mg, 5 mmol) was dissolved in a mixture of 15 mL cold water and 5 mL MeOH. To this a solution of NaN_3 (650 mg, 10 mmol) in 5 mL water was added drop wise while cooling in an ice bath. The solution was allowed to come to room temperature and was stirred for further 12 hours. Afterwards the solution was extracted two times with 40 mL EtOAc. The organic phases were combined and abandoned. After two days **141** was obtained as colorless needles (453 mg, yield 60 %). **DSC** (T_{onset}, 5 deg min^{-1}): 155 °C (dec.); **IR** (KBr, cm^{-1}): $\tilde{\nu}$ = 3602 (m), 3387 (m, br), 3019 (w), 2962 (w), 2855 (w), 2154 (s), 1621 (m), 1466 (s), 1415 (s), 1258 (s), 1231 (vs), 1188 (m), 1153 (m), 1132 (m), 1117 (m), 1071 (s), 1002 (s), 796 (s), 738 (w), 615 (m), 596 (m), 566 (m), 535 (w); **Raman** (1064 nm, 200 mW, 25 °C, cm^{-1}): $\tilde{\nu}$ = 3433 (7), 3044 (23), 3017 (23), 2963 (49), 2855 (25), 2145 (18), 1614 (13), 1470 (64), 1413 (18), 1261 (18), 1230 (26), 1201 (15), 1189 (15), 1133 (20), 1119 (21), 1083 (98), 1055 (23), 1001 (16), 811 (100), 739 (12), 620 (27), 596 (21), 573 (39), 550 (26), 439 (40), 422 (33), 346 (26), 273 (18), 165 (27); **^{1}H NMR** (d_6-DMSO, 25 °C, ppm): δ = 4.13 (H_2O br); **^{13}C NMR** (d_6-DMSO, 25 °C, ppm): δ = 158.2 (1C); **^{15}C NMR** (d_6-DMSO, 25 °C, ppm): δ = 8.7 (N2/N3), –83.0 (N1/N4), –138.2 (N6), –151.0 (N7), –304.9 (N5); ***m/z*** (FAB^-): 110; **EA** (NaH_2N_7O, 151.06) calcd.: C 7.85, H 1.33, N 64.90 %; found: not determinable; **impact sensitivity**: < 1 J; **friction sensitivity**: < 5 N; **ESD**: 20 mJ.

*Potassium 5-azidotetrazolate (**142**):* 5 mL of an aqueous potassium hydroxide (224 mg, 4 mmol) solution was added to 5-azido-1*H*-tetrazole (444 mg, 4 mmol) dissolved in 10 mL MeOH. After stirring for 10 min at 40 °C the solution was filtrated and left for crystallization. After 48 hours colorless single crystals were obtained, which were washed with diethyl ether (459 mg, 85 % yield). **DSC** (T_{onset}, 5 °C min^{-1}): 148 °C (dec.).

*Cesium 5-azido-1H-tetrazolate monohydrate (**143**):* To 10 mL of an aqueous 5-azidotetrazole (222 mg, 2 mmol) solution, cesium carbonate (326 mg, 1 mmol) was added. After stirring for 10 min at 40 °C the solution was filtrated and left for crystallization in an explosive case. After 48 hours three colorless single crystals could be obtained swimming on top of the solution, which were brought to KelF oil for X-ray determination. The remaining solution was placed into the explosive case again, where it detonated violently after a few hours.

*Calcium 5-azidotetrazolate hydrate (**144**):* 5 mL of aqueous CaOH (228 mg, 4 mmol) solution was added to 5-azidotetrazole (888 mg, 8 mmol) dissolved in 20 mL H_2O. After stirring for 10 min at 40 °C the solution was filtrated and left for crystallization. After 48 hours colorless single crystals were obtained, which were washed with diethyl ether (854 mg, 60 % yield). **DSC** (T_{onset}, 5 °C min^{-1}): 173 °C (dec.); **IR** (KBr, cm^{-1}): $\tilde{\nu}$ = 3607 (m), 3412 (s), 2256 (w), 2159 (vs), 2152 (s), 1654 (m), 1626 (m), 1543 (m), 1477 (s), 1423 (w), 1403 (m), 1367 (w), 1232 (s), 1210 (m), 1200 (s), 1147 (m), 1077 (w), 1053 (w), 1026 (w), 971 (w), 902 (w), 793 (w), 763 (w), 742 (w), 671 (w), 628 (w), 532 (w); **Raman** (1064 nm, 200 mW, 25 °C, cm^{-1}): $\tilde{\nu}$ = 3342 (8), 2143 (37), 1543 (8), 1489 (100), 1463 (67), 1425 (14), 1405 (15), 1247 (23), 1233 (39), 1141 (21), 1075 (23), 1055 (23), 1026 (7), 792 (10), 559 (21), 423 (26), 336 (24), 182 (35); **^{1}H NMR** (d_6-DMSO, 25 °C, ppm): δ = 3.38 (br, H_2O); **^{13}C NMR** (d_6-DMSO, 25 °C, ppm): δ = 158.4 (CN_7); **EA** ($C_6H_{32}Ca_3N_{42}O_{16}$, 1068.83) calcd.: C 6.74, H 3.02, N 55.04 %; found: C 6.71, H 3.81, N 52.94 %; **impact sensitivity**: 2 J; **friction sensitivity**: 25 N; **ESD**: 160 mJ.

*1-Methyl-5-azidotetrazole (**145**):* 1-Methyl-5-nitriminotetrazole (1.44 g, 10 mmol) was dissolved in 10 mL water. To this, an excess of zinc powder (2 g) was added and the mixture was cooled using an ice bath. 2 N hydrochloric acid (30 mL) was added in drops and the mixture was stirred for 30 min at room temperature. After the remained zinc powder was removed by filtration a solution of sodium nitrite in 10 mL water was added drop wise at temperatures below 0 °C until a clear formation of NO_2 was observed. After stirring the solution for further 5 min, the product was extracted three times with CH_2Cl_2. The organic phases were combined, washed once with 2 N hydrochloric acid and two times with a concentrated solution of Na_2CO_3. The organic phase was dried using sodium sulfate and evaporated. Liquid **145** (0.78 g, 63 % yield) was remained which could be solified by cooling in a freezer. **DSC** (T_{onset}, 5 °C min^{-1}): 20 °C (mp.), 85 °C (bp.), 160 ° (dec.); **IR** (KBr, cm^{-1}): $\tilde{\nu}$ = 2962 (w), 2160 (vs), 1630 (w), 1547 (s), 1476 (s), 1447 (m), 1413 (m), 1377 (w), 1304 (s), 1259 (s), 1221 (s), 1166 (w), 1092 (m), 1036 (w), 971 (w), 816 (w), 723 (m), 693 (w), 673 (s), 528 (w); **Raman** (1064 nm, 200 mW, 25 °C, cm^{-1}): $\tilde{\nu}$ = 3012 (13), 2963 (100), 2158 (31), 1548 (78), 1478 (63), 1454 (22), 1409 (23), 1388 (12), 1306 (86), 1260 (30), 1169 (15), 1094 (79), 973 (13), 818 (43), 673 (68), 563 (60), 451 (22), 336 (21), 265 (65), 233 (37); **^{1}H NMR** (d_6-DMSO, 25 °C, ppm): δ = 3.77 (CH_3); **^{13}C NMR** (d_6-DMSO, 25 °C, ppm): δ = 152.9 (C1), 33.1 (CH_3); **^{15}N NMR** (d_6-DMSO, 25 °C, ppm): δ = 7.2 (N3), –12.2 (N2, q, $^3J_{NH}$ = 1.6 Hz), –75.6 (N4), –144.0 (N7), –146.5 (N6), –172.6 (N1, q, $^2J_{NH}$ = 2.0 Hz), –301.6 (N5); ***m/z*** (DEI): 83 (1), 58 (13), 53 (8),

43 (42), 42 (3), 40 (4), 32 (2), 28 (13), 15 (10); EA ($C_2H_3N_7$, 125.11) calcd.: C 19.20, H 2.42, N 78.38 %; found: C 19.30, H 2.81, N 78.00; **impact sensitivity**: < 1 J; **friction tester**: < 5 N; **ESD**: 50 mJ.

*2-Methyl-5-azidotetrazole (**146**):* Cyanogen bromide (530 mg, 5 mmol) was dissolved in a mixture of 16 mL cold water and 4 mL MeOH. To this a solution of sodium azide (650 mg, 10 mmol) was added drop wise while cooling in an ice bath. After 2 h, dimethyl sulfate (0.283 mL, 378 mg, 3 mmol) was added slowly and the solution was allowed to come to room temperature. After one hour the precipitate formed was filtered off and washed with a small amount of cold water. The analytically pure **146** (287 mg, 77 % yield) can be recrystallized from hot water. **DSC** (T_{onset}, 5 °C min^{-1}): 62 °C (mp.), 162 °C (dec.); **IR** (KBr, cm^{-1}): $\tilde{\nu}$ = 3038 (w), 2956 (w), 2417 (w), 2285 (w), 2160 (vs), 1725 (w), 1588 (m), 1550 (s), 1506 (s), 1476 (s), 1421 (m), 1396 (m), 1305 (m), 1259 (w), 1218 (m), 1182 (m), 1091 (w), 1050 (w), 1026 (w), 794 (m), 739 (m), 721 (w), 674 (m), 527 (m); **Raman** (1064 nm, 200 mW, 25 °C, cm^{-1}): $\tilde{\nu}$ = 3044 (8), 2967 (37), 2143 (23), 1588 (4), 1551 (9), 1498 (100), 1456 (11), 1423 (19), 1398 (2), 1371 (14), 1306 (5), 1216 (10), 1186 (27), 1094 (5), 1070 (8), 1029 (56), 794 (18), 562 (5), 529 (48), 466 (8), 370 (9), 321 (31), 267 (8), 160 (17); **^{1}H NMR** (d_6-DMSO, 25 °C, ppm): δ = 4.28 (CH_3); **^{13}C NMR** (d_6-DMSO, 25 °C, ppm): δ = 161.9 (C1), 40.7 (CH_3); **^{15}N NMR** (d_6-DMSO, 25 °C, ppm): δ = 0.4 (N1, q, $^3J_{NH}$ = 2.0 Hz), –71.0 (N4), –98.3 (N1, q, $^3J_{NH}$ = 1.9 Hz), –105.7 (N2, q, $^2J_{NH}$ = 2.3 Hz), –144.2 (N6), –146.0 (N7), –300.5 (N5); ***m/z*** (DEI): 125 (43), 83 (1), 69 (12), 57 (1), 55 (3), 54 (23), 53 (12), 43 (100), 40 (11), 29 (11), 28 (29), 27 (12), 26 (14), 31 (8), 28(29), 18 (14), 15 (48); $C_2H_3N_7$ (125.11) calcd.: C 19.20, H 2.42, N 78.38 %; found: C 19.19, H 2.21, N 77.41; **impact sensitivity**: < 1 J **friction sensitivity**: < 5 N; **ESD**: 80 mJ.

12.8 Conclusions

From this combined experimental and theoretical work, the following conclusions can be drawn:

- The most facile synthesis of preparing 5-azido-1*H*-tetrazole (**135**) is the reaction of cyanogen bromide with two equivalents of sodium azide, followed by an acidic work up.

- The crystal structures of 5-azido-1*H*-tetrazole was determined by low temperature X-ray diffraction. The compound crystallizes monoclinic in the space group $P2_1/c$ with a density of 1.72 g cm^{-3}. The position of the hydrogen atom at the nitrogen atom N1 was confirmed by a strong hydrogen bond.

- The gas phase structures of 5-azido-1*H*-tetrazole and 5-azido-2*H*-tetrazole were compared by DFT calculations showing a lower electronic energy for the 2*H*-isomer.

- The heat of formation of **135** was calculated to be strongly endothermic ($\Delta_f H°_{298}$ = 611 kJ mol^{-1}. With this value and the density observed from the X-ray determination several detonation parameter were calculated using the EXPLO5 software. Though **135** is a primary explosive, its detonation performance can be compared with these of RDX.

- A comprehensive analytical characterization of the chemical and thermochemical properties of **135** is given. The thermal behavior is characterized by a melting point at 75 °C and a decomposition temperature of 165 °C.

- The sensitivities of **135** were determined to be extreme sensitive. **135** shows an impact sensitivity of < 1 J, a friction sensitivity of < 5 N and a electrical spark sensitivity of < 20 mJ.

- The CN_7 anion (5-azidotetrazolate) can be synthesized by deprotonation of 5-azido-1*H*-tetrazole (**135**) using common bases like ammonia, hydrazine or alkali as well as alkaline earth metal salts.

- 5-Azidotetrazolate salts are extremely sensitive and highly energetic compounds, which should be assigned to the class of primary explosive and only be handled with appropriate precautions. The sensitivities are higher than those of neutral **135**, and depend on the hydrogen bond network. Thus the metal salts (K^+, Rb^+, Cs^+) containing no crystal water molecules are highest in sensitivity and explode even in concentrated aqueous solutions.

- The molecular and crystal structures of different salts containing the CN_7 anion were determined for the first time. The structure of the anion is in agreement to that of **135**.

- Vibrational and NMR spectroscopy are valuable methods to identify CN_7 salts. An extensive ^{15}N NMR study was performed with the neutral as well as the ionic compounds.

- An extensive computational study to determine the heat of formation as well as several detonation parameter of the nitrogen-rich compounds hydrazinium (**136**), ammonium (**137**) and aminoguanidinium (**138**) 5-azidotetrazolate was performed. **136**–**138** are formed strongly endothermic and show promising detonation values as well as specific impulses when combusted with suitable oxidizers.

- The decomposition temperatures of **136**–**138** lie in the range of 135 to 160 °C.

- The CN_7 anion should not be described as a pseudohalide.

- The methylation of an aqueous solution of sodium 5-azidotetrazolate yields a mixture of 1-methyl-5-aziodotetrazole (**145**) and 2-methyl-5-azidotetrazole (**146**) in the ration 5:1.

- A selective synthetic route converting organic nitramines or nitrimines, respectively, was successfully accomplished on the reaction of 1-methyl-5-nitriminotetrazole with zinc and sodium nitrite yielding 1-methyl-5-azidotetrazole (**145**).

- The crystal structures of **145** and **146** were determined by single crystal X-ray techniques. Both compounds crystallizes monoclinic (**145**: $P2_1/m$, **146**: $P2_1/c$) forming layer structures.

- A comprehensive characterization of the chemical properties was performed and a detailed description of the vibrational and NMR spectra is given.

- The heats of formation of **145** and **146** were calculated (CMS-4M) using the atomization energy method to be 602 (**145**) and 571 kJ mol^{-1} (**146**).

- Although **145** and **146** show lower densities, promising detonation parameter have been computed using the EXPLO5 software suite. Particularly, the high calculated detonation pressure of 250 kbar makes **146** to an alternative green filler in novel priming charges.

- The sensitivities towards impact, friction and electrical discharge were tested by the BAM drophammer, friction tester as well as a small scale electrical discharge tester. The values obtained (**145**: IS < 1 J, FS < 5 N, ESD 0.05 J; **146**: IS < 1 J, FS < 5 N, ESD 0.08 J) must be assigned to the class of primary explosives and are comparable to these observed for toxic lead azide.

Chapter 13.

Methyl-5-nitrotetrazoles and Derivatives

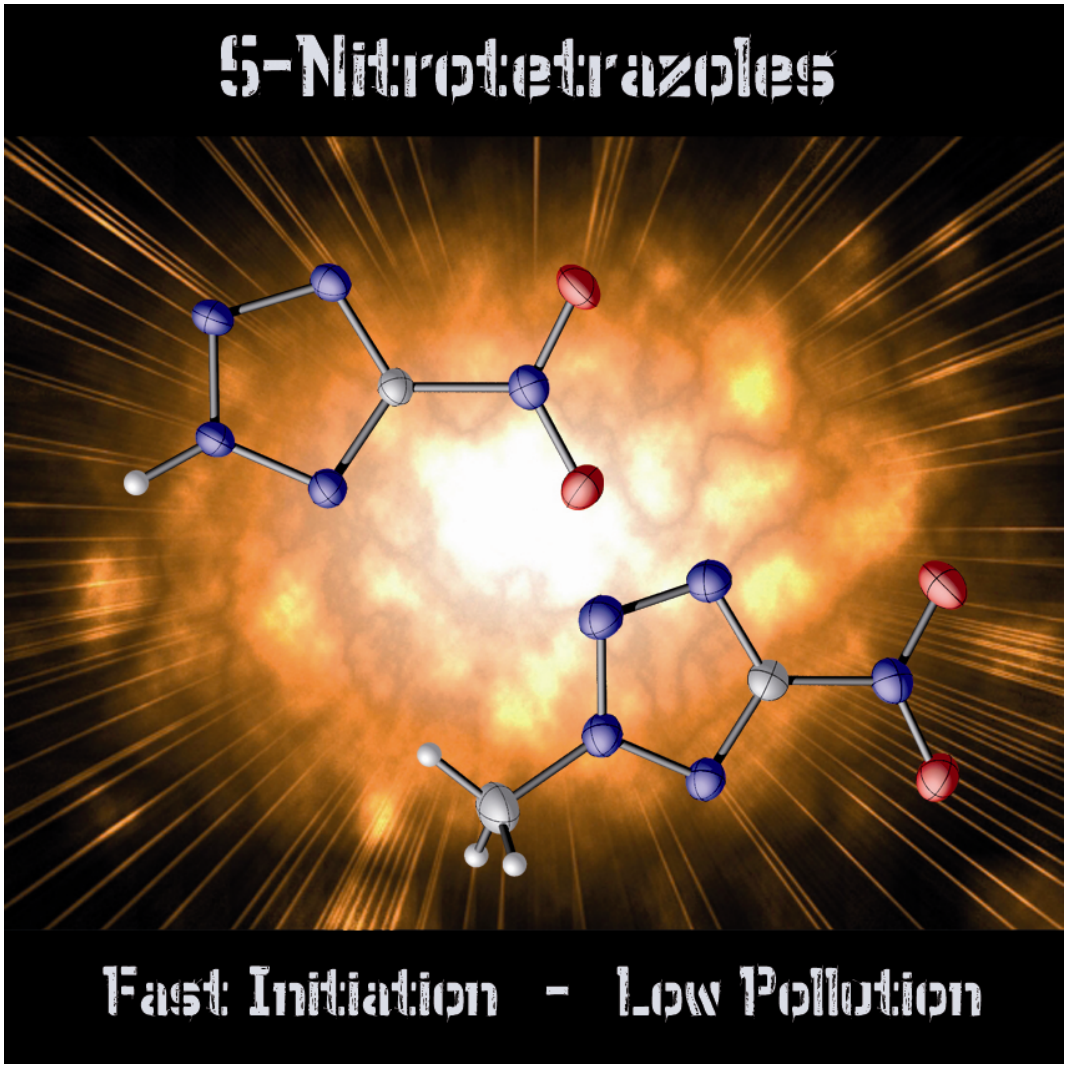

13.1 Introduction

The following chapter describes the diazotation reaction of methyl-substituted 5-aminotetrazoles using more than one equivalent of sodium nitrite. With this methyl derivatives of 5-nitro-2*H*-tetrazole can be easily synthesized. The reactions strongly depend on the order of adding the starting materials and choice of the solvents. 5-substituted tetrazoles are a promising class of energetic materials (**Figure 13.1**) due to the fact that their properties can be controlled by selection of the substituent at the carbon atom. While electron donating groups (EDGs) such as amino or hydroxy functionalities yield rather stable compounds, electron withdrawing groups (EWGs) such as nitro [407] and cyano [408] groups destabilize the ring system and increase the sensitivity of the materials. Also protonation and alkylation of the tetrazole ring is directed by the +I/–I and +M/–M effects of the substituent at the carbon atom. While EWGs direct the protonation/alkylation to the nitrogen atom labeled as N2 of the tetrazole ring,[409] EDGs favor substitution at N1.[65,410] However, there are other factors that contribute to the explosiveness of tetrazoles. For example, the high sensitivity of 5-azidotetrazole (C) (Chapter 12) and 5-nitriminotetrazole (D) (Chapters 4–9) is better explained due to the energetic nature of the azide and nitramine groups rather than based on the electronic influence of these groups on the ring system.

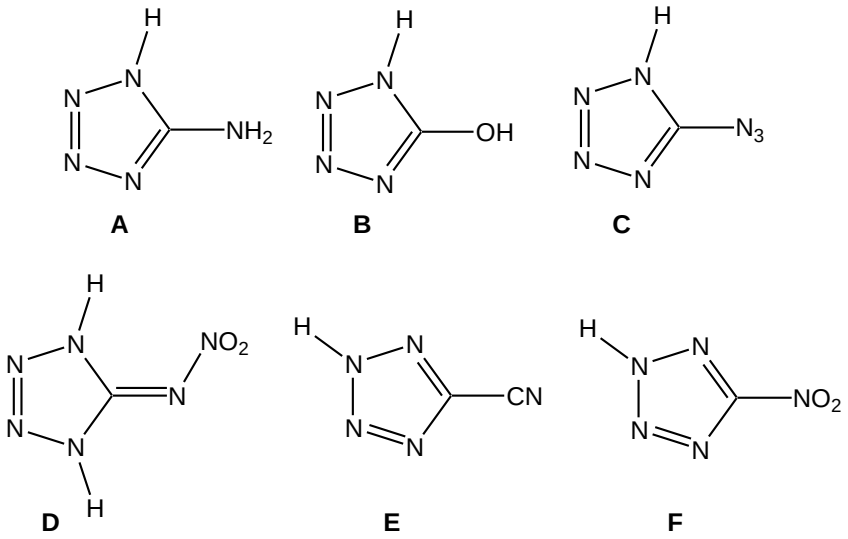

Figure 13.1 Structural formulas of neutral 5-substituted tetrazoles.

In this work, the syntheses, full analytical, spectroscopic and structural characterization of 1-methyl-5-nitrotetrazole (**148**), 2-methyl-5-nitrotetrazole (**149**) and 1-methyl-5-

chlorotetrazole (**150**) are presented. Also an interesting by-product in the reaction process of **149** is introduced, bis-1-methyltetrazol-5-yl-diazene N-oxide (**151**). In addition, the energetic properties of the compounds were assessed revealing easy initiation by impact and detonation velocities, which are almost twice as high as those of commonly used primary explosives.

13.2 Synthesis

Methylation of sodium 5-aminotetrazolate using dimethyl sulfate yields a separable mixture of the two (1-methyl and 2-methyl) isomers.[65] Both compounds can be treated similarly and diazotization with two equivalents of sodium nitrite in the presence of a non-nucleophilic acid (e.g., sulfuric acid) yields 1-methyl-5-nitrotetrazole (**148**) and 2-methyl-5-nitrotetrazole (**149**) as crystalline compounds (**Scheme 13.1**). Similar reactions are also found in the literature by using N_2O_5.[411] **148** and **149** are extracted from the reaction mixture using CH_2Cl_2. **148** and **149** are good soluble in MeOH, EtOH, acetone, MeCN, ethyl acetate, THF, CH_2Cl_2 and also in DMSO and DMF.

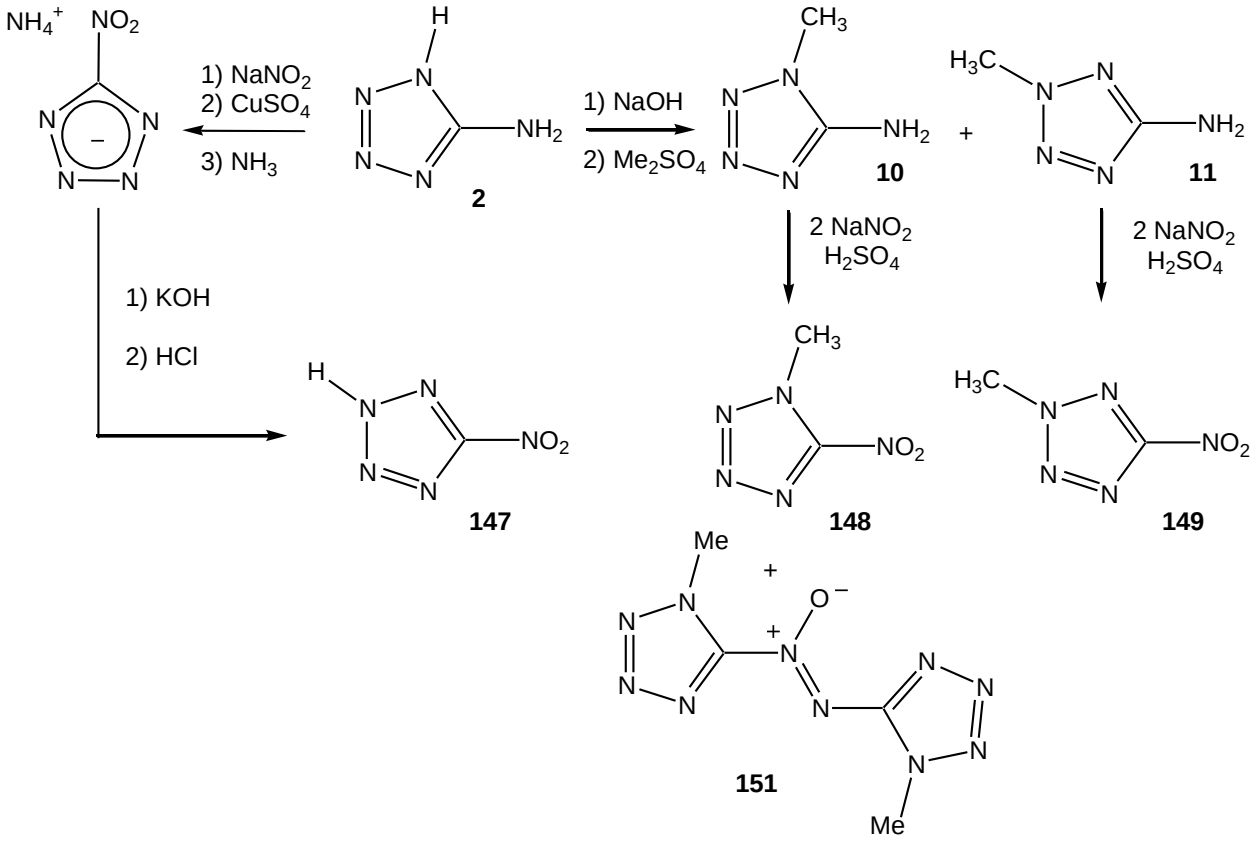

Scheme 13.1 Syntheses of neutral 5-nitrotetrazoles.

The selection of the acid for the diazotation process is of utmost importance since it affects the yield of the nitro-compound. For example using hydrochloric acid 1- or 2-methyl-5-chlorotetrazoles are obtained as the main product, which was proofed by the synthesis (**Scheme 13.2**) of 1-methyl-5-chlorotetrazole (**150**).

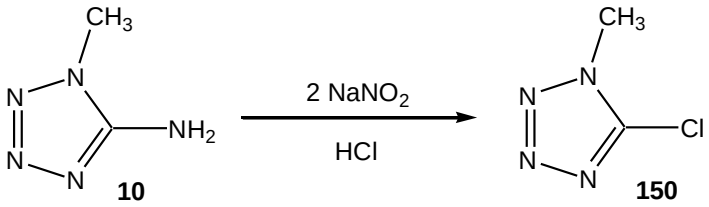

Scheme 13.2 Syntheses of 1-methyl-5-chlorotetrazole.

13.3 Crystal Structures

13.3.1 1-Methyl-5-nitrotetrazole (**148**) and 2-methyl-5-nitrotetrazole (**149**)

The unit cell of **148**, which crystallizes in the monoclinic space group $P2_1/c$ contains twelve molecules. For better clearness only one molecule of the asymmetric unit is shown in **Figure 13.2**. Since hydrogen bonds are not present in the structures of **148** and **149**, the densities (**148**: 1.628, **149**: 1.668 g cm^{-3}) are significantly lower than that observed for **147** (1.899 g cm^{-3}).

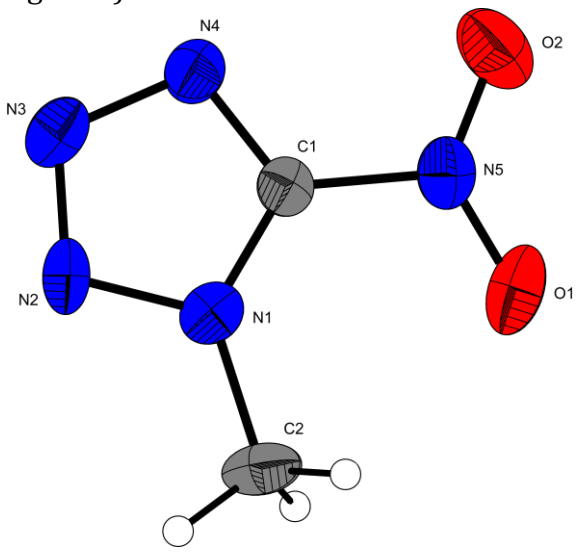

Figure 13.2 Formula unit of **148** with the labeling scheme. Hydrogen atoms shown as spheres of arbitrary radius and thermal displacements set at 30 % probability.

149 (**Figure 13.3**) crystallizes monoclinic in the space group $P2_1/c$ with four molecules in the unit cell. The molecular structure of **148** as well as of **149** is particularly comparable to that of **147** and other 5-substituted tetrazoles. All C–N and N–N bond lengths lie between single and double bonds, whereby the shortest distance (1.30–1.33 Å) is observed between the nitrogen atoms N2 and N3. In both cases (**148** and **149**) the NO_2 group is co-planar with the tetrazole ring, which confirms previously published assumptions.[412] The distances between the atoms C1 and N5 are between 1.43 and 1.48 Å, which are in the range of typical C–N single bonds. The same trend can be found for the N1–C2 and N2–C2 bond lengths (1.46–1.49 Å).

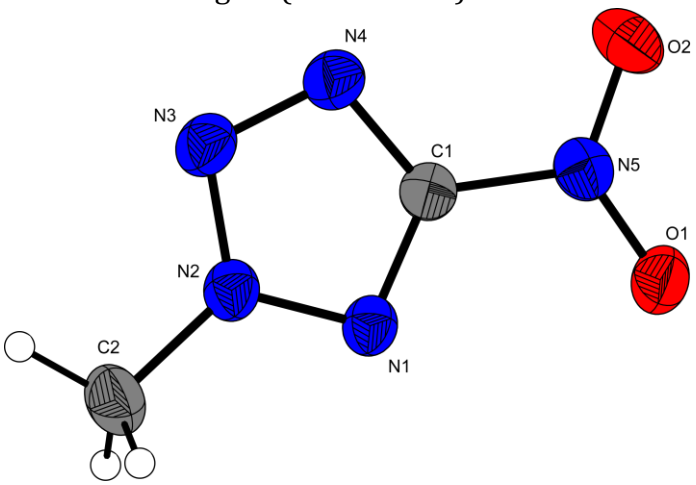

Figure 13.3 Formula unit of **149** with the labeling scheme. Hydrogen atoms shown as spheres of arbitrary radius and thermal displacements set at 50 % probability.

Table 13.1 Selected bond lengths [Å] and angles [°] for compounds **148** and **149**.

distances	**148 a**	**148 b**	**148 c**	**149**
O1–N5	1.208(6)	1.194(6)	1.196(5)	1.223(2)
O2–N5	1.191(6)	1.202(5)	1.185(5)	1.222(2)
N5–C1	1.450(7)	1.481(7)	1.438(6)	1.445(2)
N1–C1	1.326(6)	1.316(6)	1.342(6)	1.321(2)
N1–N2	1.336(6)	1.345(5)	1.354(6)	1.319(2)
N2–N3	1.297(6)	1.317(6)	1.325(6)	1.329(2)
N3–N4	1.356(7)	1.363(6)	1.317(7)	1.317(2)
N4–C1	1.303(6)	1.291(6)	1.295(6)	1.331(2)
N1(2)–C2	1.461(6)	1.478(7)	1.487(6)	1.461(2)

angles	**148 a**	**148 b**	**148 c**	**149**
O2–N5–O1	127.6(6)	127.2(5)	125.6(5)	125.1(1)
O1–N5–C1	115.8(5)	117.2(5)	117.4(5)	117.4(1)
O2–N5–C1	116.6(5)	115.7(5)	117.0(5)	117.5(1)
N1–C1–N5	125.9(5)	123.2(5)	124.8(4)	121.9(1)
C1–N1–N2	106.8(4)	106.5(4)	107.3(4)	99.9(1)
N3–N2–N1	106.6(5)	106.2(4)	104.9(4)	114.3(1)
N2–N3–N4	111.4(5)	110.8(4)	111.5(5)	106.1(1)
N3–N4–C1	103.6(5)	103.5(4)	106.6(5)	104.6(1)
N4–C1–N5	122.5(5)	123.5(5)	125.4(5)	123.0(1)
N1–C1–N4	111.6(5)	113.1(5)	109.7(5)	115.1(1)
C1–N1–C2	106.8(4)	131.9(5)	131.4(5)	
N1–N2–C2				123.6(1)
N2–N1–C2	121.1(5)	121.5(5)	121.3(5)	
N3–N2–C2				122.1(1)

13.3.2 1-Methyl-5-chlorotetrazole (**150**)

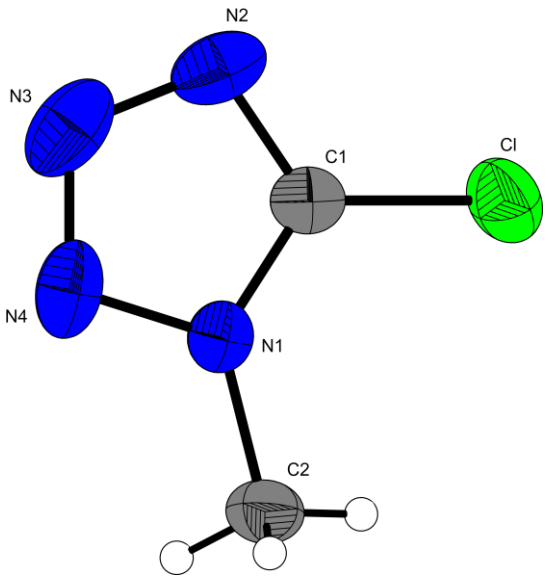

Figure 13.4 Molecular moiety of **150**. Thermal ellipsoids represent the 50 % probability level. Selected geometries: distances (Å): Cl–C1 = 1.686(2), N1–C1 = 1.330(2), N1–N4 = 1.344(2), N1–C2 = 1.464(2), N4–N3 = 1.303(3), C1–N2 = 1.311(2), N2–N3 = 1.361(3); angles (°): C1–N1–N4 = 107.4(2), N2–C1–Cl = 125.3(2), N1–C1–Cl = 124.1(1).

150 crystallizes in the orthorhombic space group *Pbca* with 8 molecules in the unit cell. The density was calculated to be 1.631 g cm^{-3}. The tetrazole ring of 1-methyl-5-chlorotetrazole, which is depicted in **Figure 13.4**, shows a structure usually found for 1-substituted neutral tetrazoles. The C–Cl bond (Cl–C1 = 1.686(2) Å) is shorter than common C–Cl single bonds (1.76 Å) found in organic molecules. In the packing of **150** only weak interactions can be found. One of these is a Cl···N3^{i} ((i): 0.5–x, –y, –0.5+z) with a distance of 3.138(2) Å, which is shorter than the sum of the vdWaals radii (r_{Cl}(1.81 Å) + r_{N}(1.54 Å) = 3.35 Å).

13.3.3 Bis(1-methyltetrazol-5-yl)diazene N-oxide (**151**)

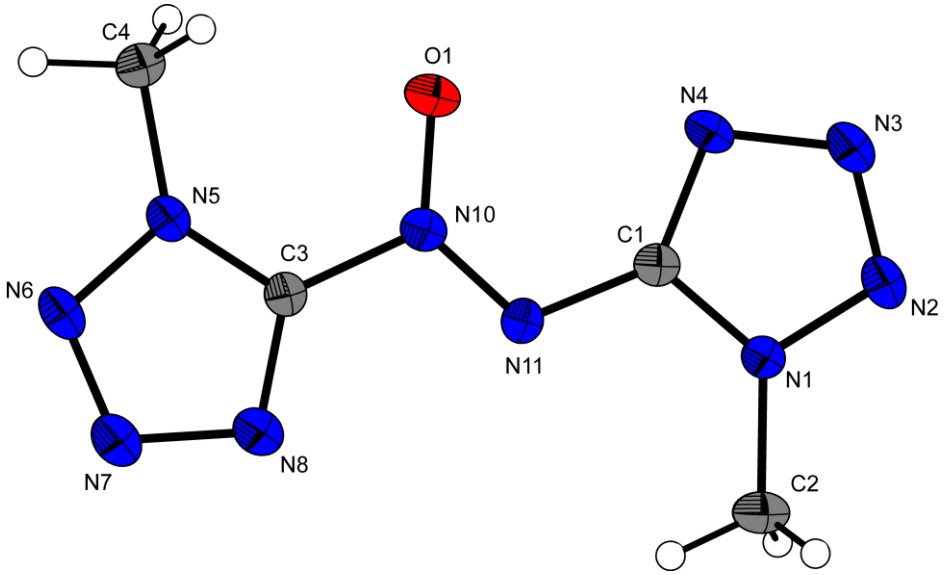

Figure 13.5 Molecular moiety of **151**. Thermal ellipsoids represent the 50 % probability level. Selected geometries: distances (Å): N1–N2 = 1.342(2), N1–C1 = 1.346(2), N1–C2 = 1.457(3), N2–N3 = 1.306(2), N3–N4 = 1.362(3), N4–C1 = 1.341(2), N5–C3 = 1.335(2), N5–N6 = 1.345(2), N5–C4 = 1.464(3), N6–N7 = 1.308(3), N7–N8 = 1.359(2), N8–C3 = 1.312(2), N11–N10 = 1.285(2), N11–C1 = 1.385(2), N10–C3 = 1.447(3), O1–N10 = 1.260(2); angles (°): N10–N11–C1 = 115.9(2), O1–N10–N11 = 128.6(2), O1–N10–C3 = 118.0(2), N11–N10–C3 = 113.4(2); torsion angles (°): C1–N11–N10–O1 = 0.0, C1–N11–N10–C3 = 180.0.

151 crystallizes in the monoclinic space group $P2_1/m$ with 2 molecules in the unit cell. Its density of 1.644 g cm^{-3} is slightly higher than this observed for **148**. The molecular moiety as well as selected geometries are given in **Figure 13.5**. The molecular backbone

(without hydrogens) is completely planar. The azo bond (N11–N10 = 1.285(2) Å) is within the expected range observed for N=N double bonds. However, also the distance O1–N10 = 1.260(2) Å is closer to a N–O double bond. **151** is packed in layers.

13.4 NMR Spectroscopy

The ^{1}H NMR spectra of **148** and **149** measured in d_6-DMSO show one single signal corresponding to the methyl group protons (**148**, δ = 3.68 ppm and **149**, δ = 4.50 ppm). The electron withdrawing character of the $-NO_2$ group shifts the proton resonances to lower field in comparison to 5-amino-1*H*-tetrazole or 1-methyl- and 2-methyl-5-amino-1*H*-tetrazole (i.e., $-NH_2$ group). The ^{13}C and ^{15}N NMR chemical shifts and the ^{15}N–^{1}H coupling constants are presented in **Table 13.2**. For both compounds the proton coupled as well as the proton decoupled ^{15}N NMR spectra (**Figure 13.6**) were recorded. The assignments are given based on the values of the ^{15}N–^{1}H coupling constants and on comparison with known compounds. The chemical shifts are given with respect to CH_3NO_2 (^{15}N) and TMS (^{1}H, ^{13}C) as external standards. In the case of ^{15}N NMR, negative shifts are upfield from CH_3NO_2. In all cases d_6-DMSO was used as the solvent.

Table 13.2 ^{15}N and ^{13}C NMR shifts of **148** and **149**.

	N1	N2	N3	N4	N5	C1	C2
148	–155.7	–0.7	6.7	–54.8	–37.6	157.4	33.1
	^{2}J(N–H) = 2.1 Hz	^{3}J(N–H)= 1.8 Hz					
149	–97.9	–76.6	5.3	–55.1	–33.5	166.4	41.9
	^{3}J(N–H) = 1.7 Hz	^{2}J(N–H)= 2.1 Hz	^{3}J(N–H) = 1.7 Hz				

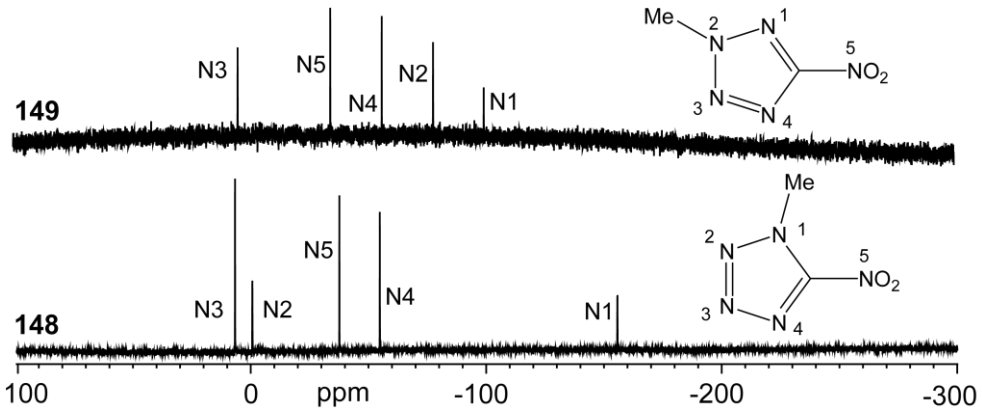

Figure 13.6 ^{15}N NMR spectroscopy of **148** and **149**.

13.5 Energetic Properties

The energetic properties of the methyl-5-nitrotetrazoles are summarized in **Table 13.5**.

13.5.1 Thermal Behavior

Figure 13.7 shows typical DSC thermographs of compounds **148** and **149**. Slow heating in a DSC apparatus (β = 5 °C min^{-1}) of samples of (~1.5 mg of each energetic material) gives rapid decomposition at temperatures above 130 °C for both compounds. Both materials show highly exothermic decompositions prior to endothermic peaks at 45 °C (**148**) and 75 °C (**149**) corresponding to the melting of the compounds.

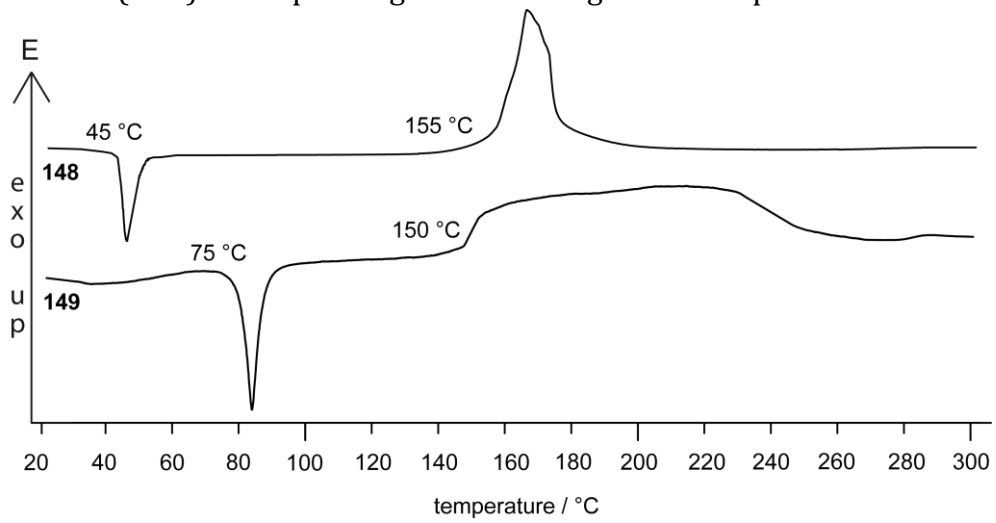

Figure 13.7 DSC thermographs (exo-up) of 5-nitrotetrazoles **148** and **149** at a heating rate of 5 °C min^{-1}.

13.5.2 Heats of Formation

The heats of formations of **148** and **149** were calculated by the atomization energy method (see introduction). With the CBS-4M results (**Table 13.3**) the enthalpies of the gas-phase species M were computed to be +80.7 (**148**) and +74.5 kcal mol^{-1} (**149**).

Table 13.3 CBS-4M results

	p.g.	$-H^{298}$ / a.u.	$-G^{298}$ / a.u.	*NIMAG*
1-Me-NT	C_s	501.427898	501.468919	0
2-Me-NT	C_s	501.437871	501.479892	0

By using the enthalpies of sublimation (14.3 (**148**), 15.6 kcal mol^{-1}(**149**)), obtained by the TROUTMAN rule the enthalpies of formation of the solid species (**Table 13.4**) have been calculated to be +66.4 (**148**), +58.9 kcal mol^{-1} (**149**). These values are in accordance to that (+67.2 kcal mol^{-1}) calculated for neutral 5-nitro-2*H*-tetrazole.

Table 13.4 Solid state energies of formation ($\Delta_f U°$)

	$\Delta_f H°$(s) / kcal mol^{-1}	$\Delta_f H°$(s) / kJ mol^{-1}	Δn	$\Delta_f U°$(s) / kcal mol^{-1}	M / g mol^{-1}	$\Delta_f U°$(s) / kJ kg^{-1}
1-Me-NT	+66.5	+279	–5	+69.5	129.08	+2252.8
2-Me-NT	+58.9	+247	–5	+61.9	129.08	+2006.4

13.5.3 Detonation Parameters

The calculation of the detonation parameters was performed with the program package EXPLO5 using the calculated energies of formation and X-ray densities. The exact values are listed in **Table 13.5**. In contrast to the extremely high calculated detonation velocity of 5-nitro-2*H*-tetrazole (**147**) of 9457 m s^{-1}, the methylated derivatives **148** and **149** have detonation velocities of ~8100 m s^{-1} and detonation pressures of ~260 kbar, higher than TNT, but lower than RDX (8800 m s^{-1}) and similar to 5,5´-azotetrazolate salts,[5,71] regardless of the high sensitivity of the compounds.

13.5.4 Sensitivities

The impact and friction sensitivities as well as the electrostatic sensitivity of powdered **148** and **149** were determined. Compounds **148** and **149** are very sensitive towards impact (**148**: 2 J and **149**: 1 J) and also sensitive towards friction (**148**: 82 N and **149**: 40 N). Grinding of the compounds in a mortar results in rattling and (in some instances) a loud explosion. According to the "UN Recommendations on the transport of dangerous goods", compounds **148** and **149** are classified as "very sensitive" regarding the impact sensitivity values. The compounds in this study are significantly more sensitive to friction and impact than nitrogen-rich salts of 5-nitro-2*H*-tetrazole [413] and the impact sensitivity approaches that of alkali metal salts of 5-nitro-2*H*-tetrazole.[414] Comparison of the energetic compounds of the materials in this study with those of

commonly used high explosives are useful to assess the potential of the materials described here. All three materials have impact sensitivity values, which are comparable to lead azide (2.5–4.0 J, pure product).

Table 13.5 Physico-chemical properties, initial safety data and predicted performance of compounds **148** and **149**.

	148	**149**	**RDX**
Formula	$C_2H_3N_5O_2$	$C_2H_3N_5O_2$	$C_3H_6N_6O_6$
Molecular Mass (g mol^{-1})	129.08	129.08	222.1
Impact sensitivity (J) [a]	2	1	7
Friction sensitivity (N) [b]	82	40	120
Electrical Discharge (J) [c]	0.50	0.20	> 0.15
N (%) [d]	54.3	54.3	37.8
$N + O$ (%) [e]	79.0	79.0	71.1
Ω (%) [f]	– 43.4	– 43.4	–21.6
Thermal Shock [g]	combustion	combustion	combustion
Combustion	good	good	good
Smokeless	+	+	–
DSC (°C) [h]	45(mp), 155 (dec)	75 (mp), 150 (dec)	213
Density (g cm^{-3}) [i]	1.628	1.668	1.82
$\Delta_f H_m°$ (kJ mol^{-1}) [j]	278	247	66.5
$\Delta_f U°$ (kJ kg^{-1}) [k]	2253	2006	400
EXPLO5 values:			
$-\Delta_E U_m°$ (J g^{-1}) [l]	5588	5368	6043
T_E (K) [m]	4226	4071	4321
p (kbar) [n]	257	262	346
D (m s^{-1}) [o]	8085	8109	8750
Gas vol. (L kg^{-1}) [p]	766	763	794

[a] BAM drophammer; [b] BAM friction tester; [c] OZM electric spark tester; [d] nitrogen content;[e] nitrogen + oxygen content, [f] oxygen balance [61]; [g] fast heating behavior; [h] decomposition temperature from DSC (β = 5°C); [i] estimated from X-ray diffraction; [j] calculated molar enthalpy of formation; [k] energy of formation; [l] energy of Explosion, EXPLO5 V5.02; [m] explosion temperature; [n] detonation pressure; [o] detonation velocity; [p] assuming only gaseous products.

The electrical spark sensitivities of microcrystalline materials (75–125 µm) were determined to be 0.50 ± 0.05 (**148**) and 0.20 (**149**) ± 0.04 J. These values can be compared to those of commonly used secondary explosives, e.g RDX (0.15 J), PETN (0.19) and TNT (0.57). However, the ESD sensitivities determined are higher than those of modern insensitive explosives such as 1,3,5-triamino-2,4,6-trinitrobenzene.[108]

13.6 Experimental Part

*CAUTION! The 5-nitrotetrazoles described here are energetic compounds, which are sensitive towards heat, impact, friction and electrostatic discharge. Although we experienced no difficulties in the synthesis of these materials, proper protective measures (safety glasses, face shield, leather coat, earthened equipment and shoes, Kevlar® gloves and ear plugs) should be used when undertaking work involving **148** and **149** on small and in particular on larger scales.*

*1-Methyl-5-nitrotetrazole (**148**):* A suspension of 1-methyl-5-aminotetrazole (2.00 g, 20 mmol) in 1M sulfuric acid (10 mL) and 30 mL of water was added at 0 °C to 30 mL water containing sodium nitrite (2.76 g, 40 mmol). After stirring at room temperature for 12 h and filtration of the precipitated bis(1-methyltetrazolyl)triazene (**118**, see Chapter 10), the solvent was evaporated. To this 80 mL dry acetone were added and the precipitated Na_2SO_4 was removed by filtration. After removing the acetone the crude product was recrystallized from a small amount of ethanol (1.52 g, yield 59 %). **DSC** (T_{onset}, 5 °C min^{-1}): 45 °C (mp.), 155 °C (dec.); **IR** (KBr, cm^{-1}): $\tilde{\nu}$ = 3038 (w), 2860 (w), 1550 (vs), 1481 (s), 1467 (m), 1408 (s), 1364 (s), 1328 (vs), 1280 (w), 1209 (m), 1073 (m), 1025 (w), 846 (s), 720 (s), 535 (w), 430 (m); **Raman** (1064 nm, 200 mW, 25 °C, cm^{-1}): $\tilde{\nu}$ = 3054)2), 2978 (6), 2964 (6), 1530 (20), 1508 (9), 1469 (100), 1463 (44), 1447 (44), 1425 (15), 1412 (11), 1329 (24), 1261 (10), 1208 (13), 1103 (11), 1085 (23), 1028 (21), 923 (7), 779 (2), 740 (2), 709 (3), 679 (4); **^{1}H NMR** (d_6-DMSO, 25 °C, ppm): δ = 3.68 (s, 6H, CH_3); **^{13}C NMR** (d_6-DMSO, 25 °C, ppm): δ = 157.6 (CN_4), 33.1 (CH_3); **^{14}N NMR** (d_6-DMSO, 25 °C, ppm): δ = –37 ($\nu_{½}$ ~60 Hz, NO_2); **^{15}N NMR** (d_6-DMSO, 25 °C, ppm): δ = 4.5 (N3), –14.1 (N6), –18.29 (N2, t, $^3J_{NH}$ = 1.9 Hz), –71.15 (N4), –157.16 (N5), –168.38 (N1, d, $^2J_{NH}$ = 2.2 Hz), –289.13 (N7, $^1J_{NH}$ = 102.7 Hz), –329.66 (N8, $^1J_{NH}$ = 69.4 Hz); ***m/z*** (DEI$^+$): 130 (19) $[M+H]^+$, 129 (65) $[M]^+$, 100 (1), 83 (8), 55 (15), 54 (17), 53 (100), 46 (38), 43 (28), 40 (7), 39 (5), 28 (45), 18 (8), 15 (4); **EA** ($C_2H_3N_5O_2$, 129.08):

calcd.: C 18.61, H 2.34, N 54.26 %; found: C 18.39, H 2.28, N 52.80 %; **impact sensitivity**: 2 J; **friction sensitivity**: 82 N; **ESD**: 0.50 ± 0.05 J; **Flame test**: combustion.

*2-Methyl-5-nitrotetrazole (**149**):* To 20 mL of an aqueous sodium nitrite (2.76 g, 0.04 mol) solution, a solution of 2-methyl-5-aminotetrazole (2.00 g, 0.02 mol) in 20 mL 1N sulfuric acid was added at 0 °C. The reaction mixture was stirred for 8 h and bis(2-methyltetrazolyl)triazene (**119**) precipitated was removed by filtration. Afterwards the product was extracted three times with 20 mL of CH_2Cl_2. The organic phases were combined, dried over $MgSO_4$ and evaporated. The crude product was recrystallized from acetone yielding single crystal suitable for XRD analysis. (1.68 g, yield 65 %) **DSC** (T_{onset}, 5 °C min^{-1}): 75 °C (mp.), 150 °C (dec.); **IR** (KBr, cm^{-1}): $\tilde{\nu}$ = 3022 (m), 1610 (m), 1565 (s), 1510 (m), 1468 (m), 1412 (s), 1285 (s), 1160 (m), 1001 (w), 880 (m), 788 (m), 750 (m), 670 (w), 610 (w), 530 (w); **Raman** (1064 nm, 200 mW, 25 °C, cm^{-1}): $\tilde{\nu}$ = 3052 (12), 2967 (60), 1555 (28), 1486 (40), 1468 (26), 1418 (100), 1369 (11), 1335 (8), 1322 (14), 1287 (12), 1209 (30), 1075 (12), 1043 (40), 1026 (44), 841 (16), 776 (17), 715 (46), 547 (10), 436 (30), 378 (18), 307 (16), 218 (16); **^{1}H NMR** (*d*$_6$-DMSO, 25 °C, ppm): δ = 4.50 (s, 3H, CH_3); **^{13}C NMR** (*d*$_6$-DMSO, 25 °C, ppm): δ = 166.4 (CN_4), 41.9 (CH_3); **^{14}N NMR** (*d*$_6$-DMSO, 25 °C, ppm): δ = –34 ($\nu_{½}$ ~50 Hz, NO_2); **^{15}N NMR** (*d*$_6$-DMSO, 25 °C, ppm): δ = 5.3 (N3), –33.5 (N5), –55.1 (N4), –76.6 (N2, ^2J(N–H) = 2.1Hz), –97.9 (N1, ^3J(N–H) = 1.7 Hz); ***m/z*** (DEI$^+$): 130 (2) $[M+H]^+$, 129 (2) $[M]^+$, 115 (1) $[M+H–CH_3]^+$, 101 (15), 58 (89), 43 (100) $[HN_3]^+$, 42 (6), 28 (3) $[N_2]^+$, 18 (29); **EA** ($C_2H_3N_5O_2$, 129.08): calcd.: C 18.61, H 2.34, N 54.26 %; found: C 18.88, H 2.35, N 52.99 %; **impact sensitivity**: 1 J; **friction sensitivity**: 40 N; **ESD**: 0.20 ± 0.04 J; **Flame test**: combustion.

*1-Methyl-5-chlorotetrazole (**150**):* The synthetic procedure of 150 has not been optimized yet. A suspension of 1-methyl-5-aminotetrazole (2.00 g, 20 mmol) in 1M hydrochloric acid (40 mL) was added at 0 °C to 20 mL of an aqueous sodium nitrite (2.76 g, 40 mmol). After stirring for 8 h at room temperature, the product was extracted using dichloromethane. Recrystallization from ethyl acetate yielded **150** in ~50 % yield. **^{1}H NMR** (*d*$_6$-DMSO, 25 °C, ppm): δ = 4.03 (s, 3*H*, CH_3); **^{13}C NMR** (*d*$_6$-DMSO, 25 °C, ppm): δ = 146.7 (CN_4), 34.6 (CH_3).

*Bis(1-methyltetrazol-5-yl)-diazene N-oxide (**151**):* **151** was obtained as byproduct in the reaction of **148**. After extraction of **148**, the water phase was evaporated and the yellow

crude product was recrystallized from acetone, yielding a small amount of yellow single crystals of **151**.

13.7 Conclusion

From this combined experimental and theoretical study the following conclusions can be drawn:

- The diazotation reaction of substituted 5-aminotetrazoles strongly depends on the amount of sodium nitrite, order of addition and choice of acid. In the case of half an equivalent nitrite is used, bis(tetrazolyl)triazenes are formed (Chapter 10). By using one equivalent of nitrite diazonium salts are obtained, which can be transferred in 5-azidotetrazoles (Chapter 12) or deaminated to 5*H*-tetrazoles (Chapter 11). In the case of an excess of nitrite and a non-nucleophilic acid is used, 5-nitrotetrazoles are generated. By using hydrochloric acid, 5-chlorotetrazoles can be synthesized.(Chapter 13)

- Convenient procedures for the synthesis of the two highly energetic neutral 1-methyl-5-nitrotetrazole (**148**) and 2-methyl-5-nitrotetrazole (**149**) are presented, which allow obtaining the materials with low cost using facile routes, good yields and excellent purities. In addition a potential synthetic procedure to 5-chlorotetrazoles (promising additives in pyrotechnics) is demonstrated on 1-methyl-5-chlorotetrazole.

- Bis(1-methyltetrazol-5-yl)-diazene N-oxide (**151**) is introduced as an interesting energetic material, which is obtained as by-product in the reaction of **148**, but has not been fully characterized yet.

- The full characterization of **148** and **149** by analytical and spectroscopic methods is described in detail. The heats of formation (+66.4 (**148**), +58.9 kcal mol^{-1} (**149**)) have been calculated by the atomization energy method. In addition the energetic properties such as thermal stability, sensitivities and calculated detonation parameters were discovered.

- The crystal structures of **148**–**151** are presented and described.

Chapter 14.

1,5-Bistetrazoles

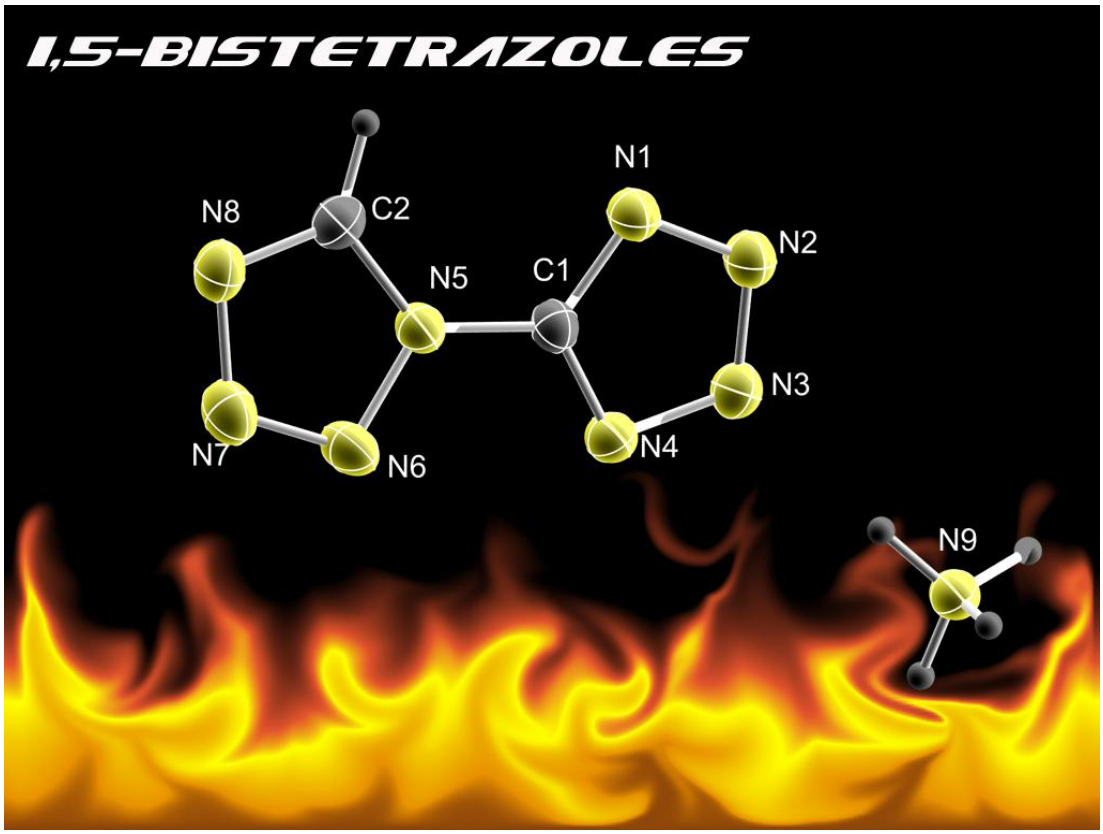

14.1 Introduction

In the research of new energetic materials, next to high performances a good thermal stability and low sensitivities are needed. Several bistetrazoles and C- or N-bridged bistetrazoles are conceivable (**Figure 14.1**). However, 1,1'-bistetrazole, containing eight nitrogen atoms in series, has never been described and is challenging. Particularly, 5,5'-bis(1*H*-tetrazolyl)amine (H_2bta) (Chapter 15) and its nitrogen-rich salts [3c] have been described combining these main requirements. 5,5'-Bis(1*H*-tetrazolyl)methane has also been described in literature.[415]

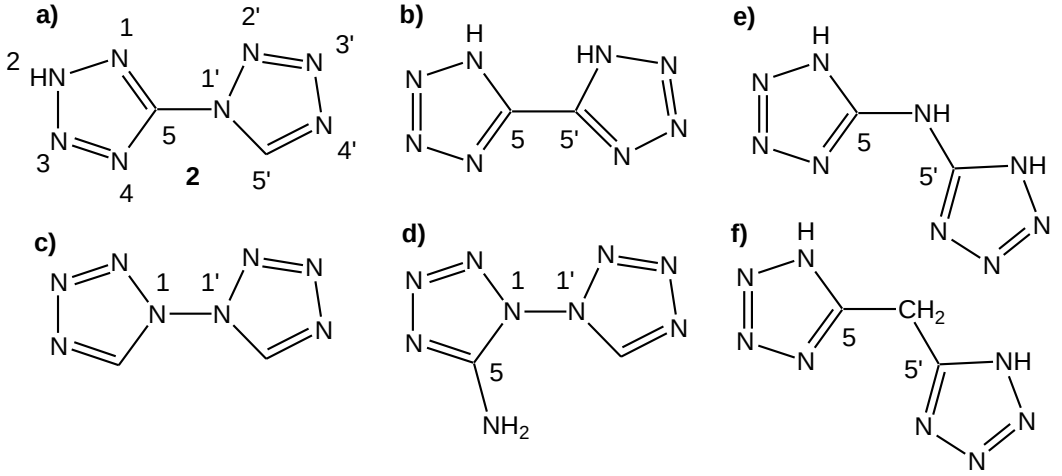

Figure 14.1 Several bistetrazoles: a) 1,5-Bistetrazole, b) 5,5'-Bistetrazole, c) 1,1'-bis-tetrazole, d) 1-(tetrazolyl-N1')-5-aminotetrazole, e) bis(tetrazolyl)-amine, f) bis(tetrazolyl)methane.

5,5'-Bistetrazole (5,5'-HBT) [416] and 1,5-bistetrazole [417,418] (**152**, 1,5-HBT) and their anions BT^- are further interesting candidates for novel nitrogen-rich materials, but also in coordination chemistry. They contain eight nitrogen atoms and may act as mono-, bi-, tri- or tetradentate ligands. **Figure 14.2** depicts various binding modes for **152** and its anion. It is, therefore, surprising that there are only a few reports on transition-metal complexes of 1,5-bistetrazole (HBT) and its anion (BT^-). However, there are numerous reports on the use of metal-containing salts of 5,5'-bistetrazole as highly energetic materials [419] or N_2 sources, including a number of patents.

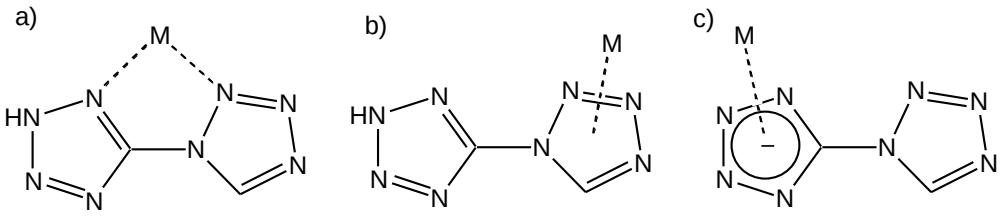

Figure 14.2 Selected coordination modes of 1,5-BT. a) chelate η^2 ; b) neutral coordination; c) deprotonated coordination.

In this chapter, a comprehensive description of the chemistry of 1,5-bistetrazole (**152**) is given. Based on these results many further derivatives can be synthesized in future times. A further motivation of this chapter is the relationship of 1,5'-bistetrazoles to 5-azidotetrazoles, described in Chapter 12. The reaction of those with HCN should lead to the 1,5-bistetrazoles. The questions are: *Is it possible to stabilize 5-azidotetrazolates by the addition of HCN? Is a delocalized electron-system formed, which increase the thermal stability and decrease the sensitivities? Or is it opposite?*

14.2 Synthesis

It has recently been shown in certain examples [420] that the interaction of a primary amine, orthoformic ester, and sodium azide leads rapidly to a 1-substituted tetrazole.[421] The ongoing work on 1,5-bistetrazoles is very profitable, thus several new derivatives have been created and characterized. **Scheme 14.1** shows a general protocol of syntheses of 1,5-bistetrazole (**152**) and 2-methyl-5-(tetrazolyl-*N1*)tetrazole (**253**, abbreviated with 2MeBT) starting from 5-aminotetrazoles. 1-Methyl-1,5-bistetrazole cannot be reacted using these conditions. This may be the consequence of a larger sterical hindrance. The synthetic route to **252** can be followed in large scales (up to 1 mol). **252** is obtained as its monohydrate (**252**·H_2O), which is good to handle. Recrystallization from half-conc. hydrochloric acid yields the water-free compound, which is extremely sensitive.

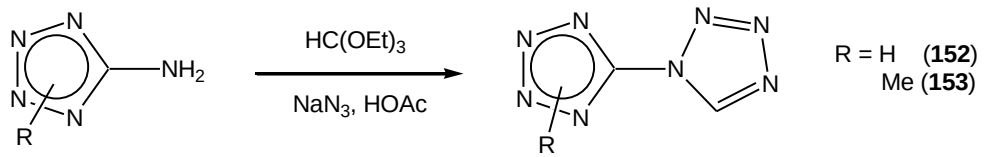

Scheme 14.1 Syntheses of 1,5-bistetrazoles.

Based on the good availability of **152** its ammonium (**154**), sodium (**155**) and potassium (**156**) salts were prepared according to **Scheme 14.2**.

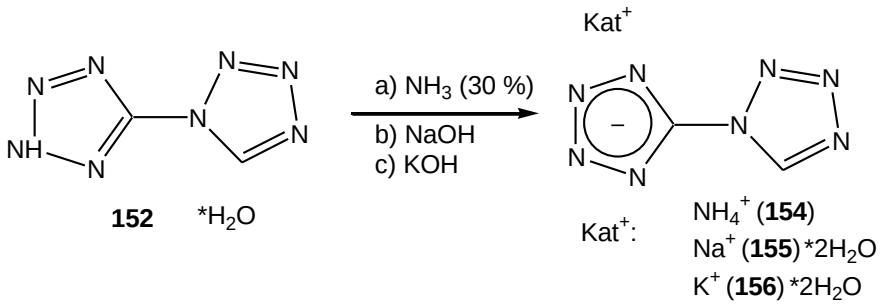

Scheme 14.2 Synthesis of ammonium 1,5-bistetrazolate (**154**).

Since there exist different possibilities of coordination modes to metal centers, three different copper complexes (**157**–**159**) were synthesized according to **Scheme 14.3**. The first and second reaction were performed in aqueous solution. It was not possible to coordinate neutral **152** to copper(II) centers, even by using conc. acids. From this three reactions it can be concluded that in anionic copper(II) complexes coordination takes place at N2 of the deprotonated ring while in neutral complexes (incl. counteranions) coordination takes place mostly at N8.

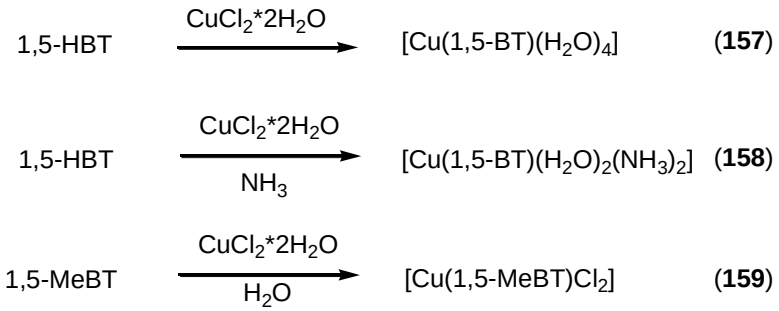

Scheme 14.3 Synthesis of copper(II) 1,5-bistetrazole complexes.

14.3 Crystal Structures

Compounds **152**, **152**·H_2O as well as **153**–**159** were determined by single crystal X-ray diffraction. A description of the solutions follows.

14.3.1 1,5-Bistetrazole monohydrate (**152**·H_2O)

1,5-Bistetrazole monohydrate (**152**·H_2O) crystallizes in the monoclinic space group $P2_1/c$ with four molecules per unit cell and a density of 1.670 g cm^{-3}, which is significantly lower than that of water-free **152**. The molecular moiety of **152**·H_2O is depicted in **Figure 14.3**. As expected, the two tetrazole rings show different bond lengths and angles. In both cases the nitrogen bond opposite to the carbon atom, N2–N3 and N6–N7, respectively, are by far the shortest bonds with 1.312(2) Å and 1.292(2) Å, respectively. It is noteworthy that the nitrogen bonds N5–N6 and N7–N8 show significantly increased bond lengths compared to the equivalent ones in the other tetrazole ring (d(N5–N6) = 1.359(2) Å, d(N7–N8) = 1.366(3) Å) what may be the result of the electron withdrawing effect of the N5-bonded ring. The C1–N5 bond connecting both tetrazole rings is with 1.404(2) Å close to a normal C–N single bond. Moreover, **152**·H_2O shows significant deviations from planarity (∢(C2–N5–C1–N4) = –2.3(3)°, ∢(C2–N5–C1–N1) = 176.6(2)°, ∢(N6–N5–C1–N4) = –178.8(2)°, ∢(N6–N5–C1–N1) = 0.1(3)°), corroborating limited aromaticity and therefore less stability. Also remarkable is the increased bond angle between N1–N2–N3 with 114.0(2)° compared to the equivalent one in the C1-bonded tetrazole ring (∢(N6–N7–N8) = 110.90°). This again may be explained referring to an increased electron density in the C1-bonded tetrazole ring as well as a decreased electron density in the N5-bonded ring, additionally generated by the hydrogen bond coordination on N2.

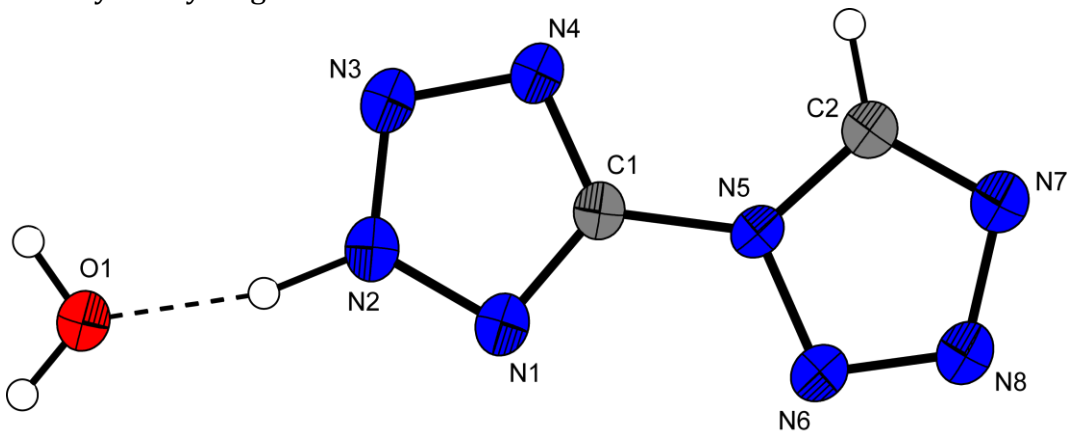

Figure 14.3 Molecular structure of **152**·H_2O. Thermal ellipsoids are drawn at the 50% probability level and hydrogen atoms are shown as small spheres of arbitrary radii.

Compared to related structures found in the literature (e.g. 4-methyl-1-(1-methyl-1*H*-tetrazol-5-yl)-1,2,4-triazolium cation),[422] the C1–N5 bond of **152**·H_2O is longer

(1.404(2) Å vs. 1.397(3) Å). However, the C1–N1 bond show similar bond lengths (d(C1–N1) = 1.314(2) Å vs. d(C1–N1) = 1.311(2) Å).

In the crystal structure, the 1,5-bistetrazole molecules build head to tail-chains forming a layer structure (**Figure 14.4**). Two molecules of **152** are connected *via* hydrogen bonds of each two water molecules involving nitrogen atoms N2, N3 and N7, N8, whereas N3 and N7 are part of a bifurcated hydrogen bond with O1–H3. The result of the graph-set analysis is depicted in **Figure 14.4.B**.

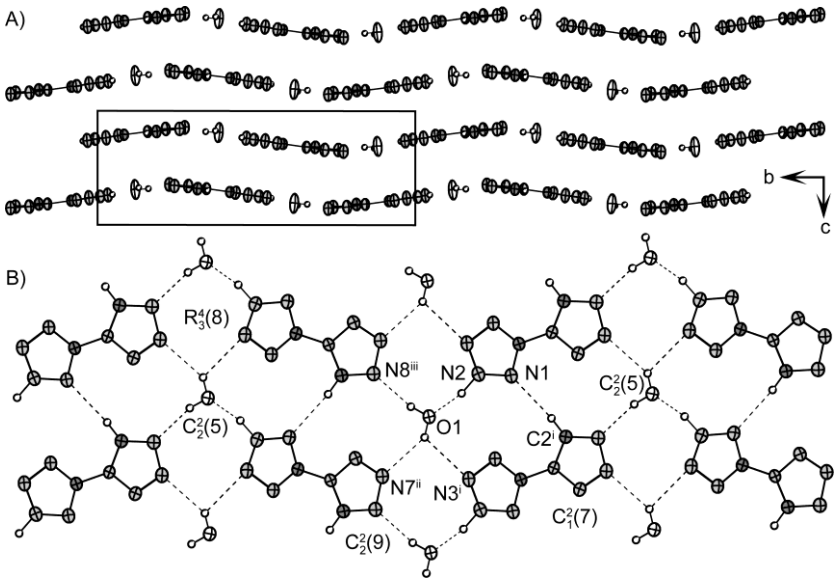

Figure 14.4 Packing of 1,5-bistetrazole monohydrate (**152**·H_2O): A) view along *a*-axis; B) hydrogen bonding; selected hydrogen bonds (Å, Å, Å,°): N2–H1···O1 = 1.03(2), 1.61(2), 2.619(2), 166(2)°; O1–H3···N3^{i} = 0.84(3), 2.48(3), 2.985(2), 120(2)°; C2^{i}–H2^{i}···N1 = 0.94(2), 2.35(2), 3.293(3), 173(2); O1–H3···N7^{ii} = 0.84(3), 2.31(3), 3.036(2), 145(2)°; O1–H4···N8^{iii} = 0.85(3), 2.01(3), 2.835(2), 167(2)°; (i) 1+x, y, z (ii) 2–x, –0.5+y, 1.5–z (iii) 1–x, –0.5+y, 1.5–z.

14.3.2 1,5-Bistetrazole (**152**)

152 crystallizes in the monoclinic space group *Pn* with four molecules in the unit cell and a density of 1.728 g cm^{-3}. Again the proton is located at the nitrogen atom N2, which is in accordance with the structure of 5-nitro-2*H*-tetrazole (**147**), but in contrast to the structure observed for 5,5-bistetrazole,[423] which exists as the 1*H*, 1'*H*-tautomer and is packed in chains held together by pairs of intermolecular hydrogen bonds. The solution

of **152** caused difficulty, since the molecules are partly disordered. This a consequence of the planar geometry. Although both rings lie within one plane, again no delocalization can be observed between the rings, due to a long C1–N5 bond length of ~1.40 Å, which is in agreement to **152**·H_2O. One of the both independent molecules of the asymmetric unit is depicted in **Figure 14.5**. Two strong hydrogen bonds are found in the packing of **152**: N10–H3···N8 = 0.90(3), 1.93(3), 2.782(7) Å, 157(2)° and N2–H1···N16 = 0.96(3), 1.89(3), 2.781(7) Å, 152(2)°). The unit cell along the *a* axis is shown in **Figure 14.6**.

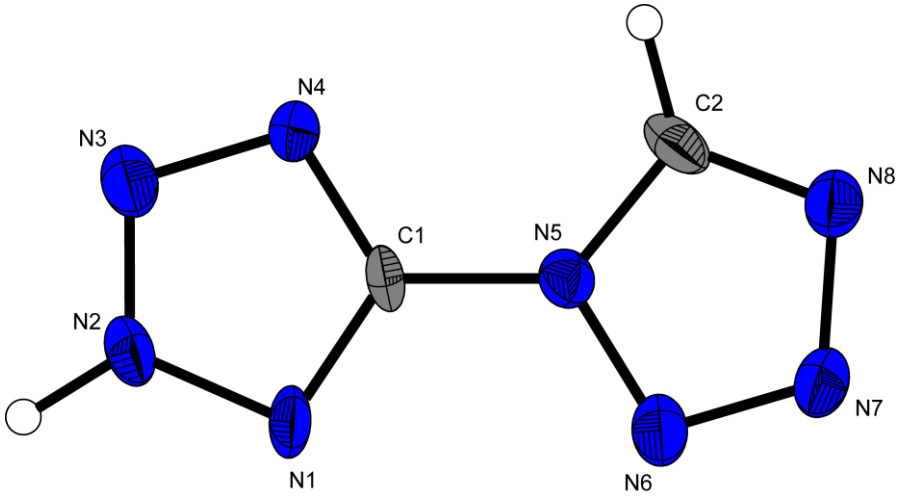

Figure 14.5 Molecular structure of **152**. Thermal ellipsoids are drawn at the 50% probability level and hydrogen atoms are shown as small spheres of arbitrary radii.

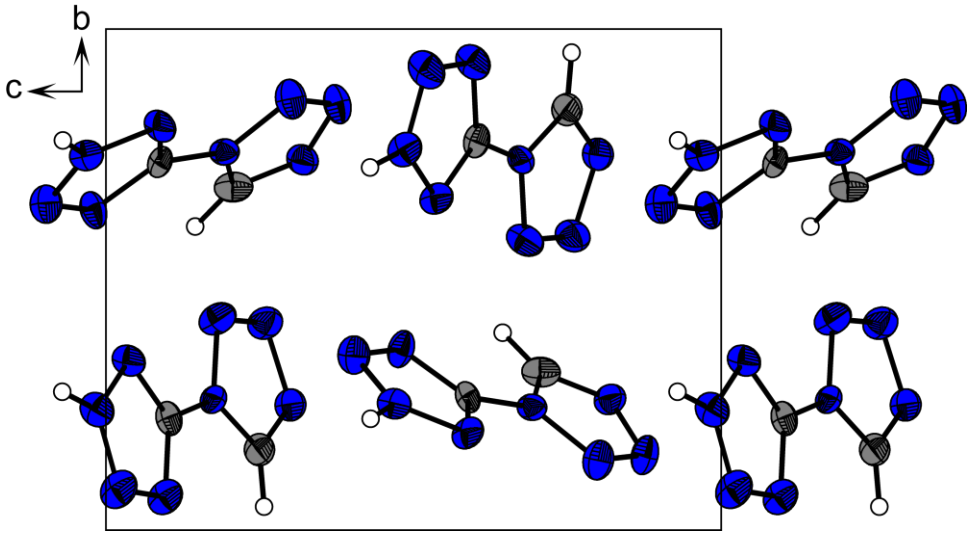

Figure 14.6 View on the unit cell of **152** along the *a* axis.

14.3.3 2-Methyl-1,5-bistetrazole (**153**)

2-Methyl-1,5-bistetrazole crystallizes in the monoclinic space group $P2_1/c$ with eight formula moieties in the unit cell, resulting in a calculated density of 1.568 g cm^{-3}. The molecular structure can be described by two tetrazole rings forming two separate delocalized π electron systems (**Figure 14.7**). The atoms C1, N1, N2, N3 and N4 are forming a planar fragment (torsion angle N3–N4–C1–N1 = 0.1(2)°), which is connected via the single bond C1–N5 (1.40(2) Å) with another 5-membered ring. This second ring system, which is formed by the atoms N5, N6, N7, N8 and C2, is also planar (torsion angle N6–N5–C2–N8 = 0.3(2) °) and significantly twisted from the plane of the first tetrazole ring (torsion angle N4–C1–N5–C2 = 29.7(3)°). The values for the bond lengths within the 5-membered rings range from 1.29 to 1.37 Å and are similar to those observed in other tetrazole derivatives. The distance between the atoms C3 and N2 (1.45(1) Å) can definitely be identified as a C–N single bond.

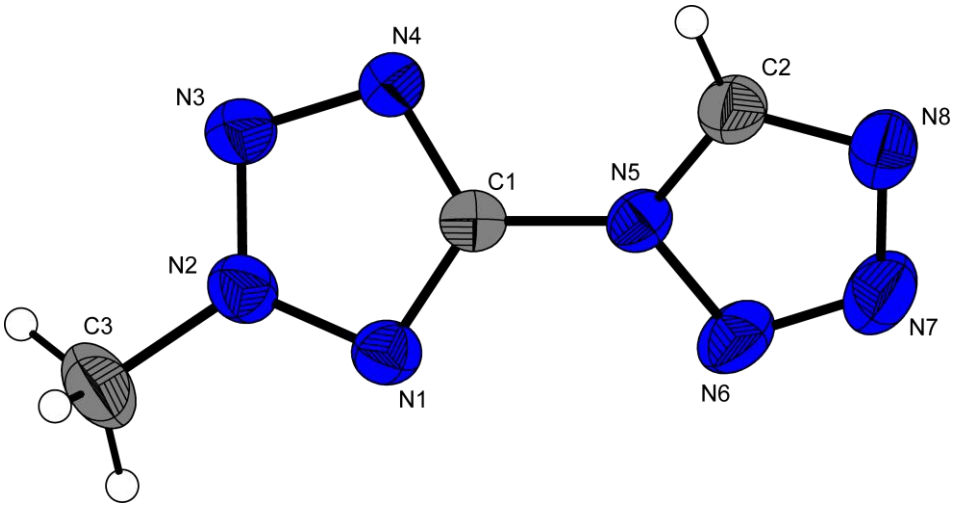

Figure 14.7 Molecular moiety of **153**. Thermal ellipsoids represent the 50 % probability level.

The neutral molecules of compound **153** crystallize in a complex, three-dimensional network, which is only influenced by van-der-waals-forces. Classic hydrogen bonds do not exist within the crystal structure, which contains neither any noticeable structural units nor clusters or aggregates. These facts explain the relative low density of 2-methyl-1,5-bistetrazole compared to other neutral tetrazoles, which are influenced by hydrogen bonds.

14.3.4 Ammonium 1,5-bistetrazolate (**154**)

154, depicted in **Figure 14.8**, crystallizes in a monoclinic crystal system (space group $P2_1/c$) with four molecules in the unit cell. The density was calculated to 1.567 g cm^{-3}. **Figure 14.9** shows the coordination of the ammonium cation: Each cation coordinates five 1,5-bistetrazolate anions *via* hydrogen bonds whereas, similar to the neutral compound **152**·H_2O, also one bifurcated hydrogen bond is involved. With exception of N1–N2 and N3–N4, all bond lengths are in the same range as observed in **152**. The deviating bonds are both considerably longer in the anion compared to the neutral compound (d(N1–N2) = 1.352(2) Å vs. d(N1–N2) = 1.326(2) Å, d(N3–N4) = 1.346(2) Å vs. d(N3–N4) = 1.332(2) Å). Almost exactly the same bond lengths as well as bond angles in the C1-bonded tetrazole ring in both compounds **152** and **153** despite an increased electron density in the anion **154** again prove the low electron delocalization between both rings. This is also validated by a significant deviation from planarity (∢(C2–N5–C1–N4) = –165.4(2)°, ∢(C2–N5–C1–N1) = 14.2(3)°, ∢(N6–N5–C1–N4) = 12.1(2)°, ∢(N6–N5–C1–N1) = –168.3(2)°). However, there is electron delocalization within the N5-bonded tetrazole ring as can be seen in terms of similar bond angles building a symmetrical ring (∢(N2–N1–C1) = 102.7(1)°, ∢(C1–N4–N3) = 102.8(1)° and ∢(N1–N2–N3) = 110.0(1)°, ∢(N2–N3–N4) = 109.7(1)°).

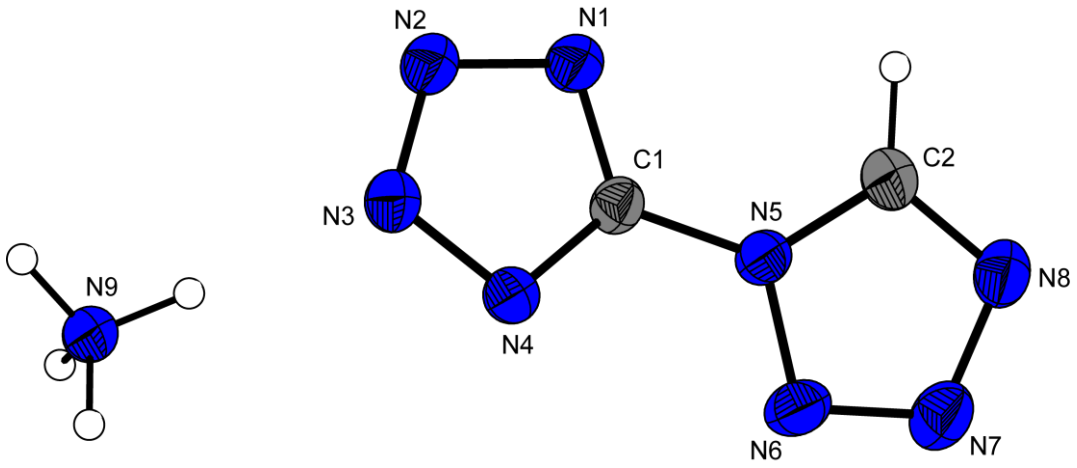

Figure 14.8 Molecular moiety of **154**. Thermal ellipsoids represent the 50 % probability level.

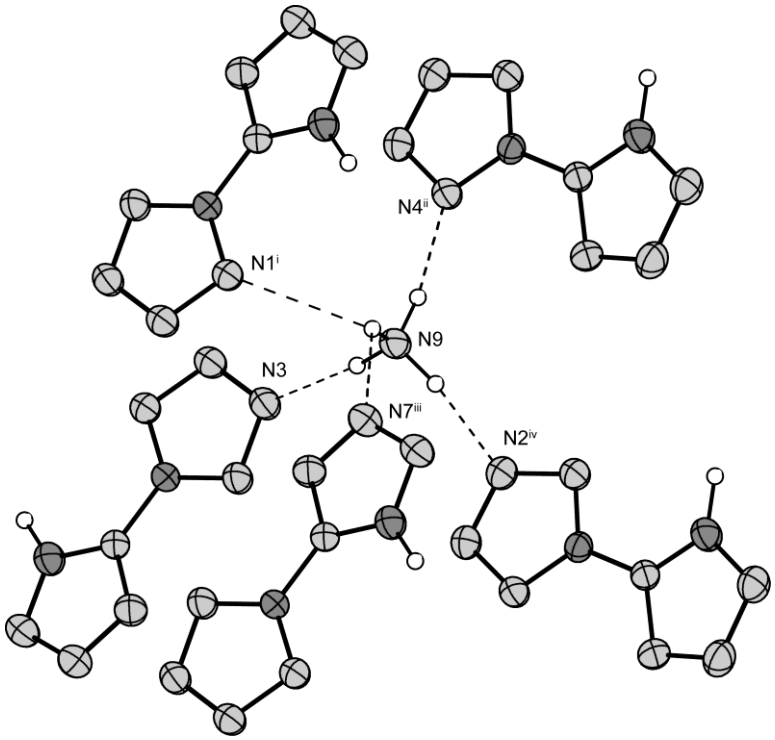

Figure 14.9 Coordination sphere of ammonium 1,5-bistetrazolate (**154**). Thermal ellipsoids are drawn at the 50% probability level and hydrogen atoms are shown as small spheres of arbitrary radii. Selected hydrogen bonds (Å, Å, Å,°): N9–H9b···N3: 0.95(2), 1.99(2), 2.926(2), 172(2)°; N9–H9a···N1^{i}: 0.98(3), 2.58(3), 3.170(2), 119(2); N9–H9d···N4^{ii}: 0.95(2), 1.99(2), 2.937(2), 171(2); N9–H9a···N7^{iii}: 0.98(3), 2.52(3), 3.183(2), 125(2); N9–H9c···N2iv: 0.97(3), 1.97(3), 2.923(2), 167(2)°; (i) –x, 1–y, 1–z (ii) –x, 0.5+y, 1.5–z (iii) –x, –y, 1–z (iv) –x, –0.5+y, 1.5–z.

14.3.5 Sodium 1,5-bistetrazolate dihydrate (**155**·2H$_2$O)

Sodium 1,5-bistetrazolate dihydrate crystallizes in the triclinic space group *P*–1 with two molecules in the unit cell. Its density of 1.654 g cm^{-3} is lower in comparison to other sodium salts in this thesis. The left tetrazole ring in **Figure 14.10**, containing the molecular unit, is strongly disordered, which can be seen on the big thermal ellipsoid of the carbon and the small ellipsoid of the N8 nitrogen atom. In the solution the positions have been splitted. The sodium atoms are coordinated octahedrally by two nitrogen atoms (Na–N8 = 2.68(1) Å) and four oxygen atoms (Na–O2 =2.360(4) Å and Na–O1 = 2.362(9) Å) building endless chains along the *a* axis, which is shown in **Figure 14.11**.

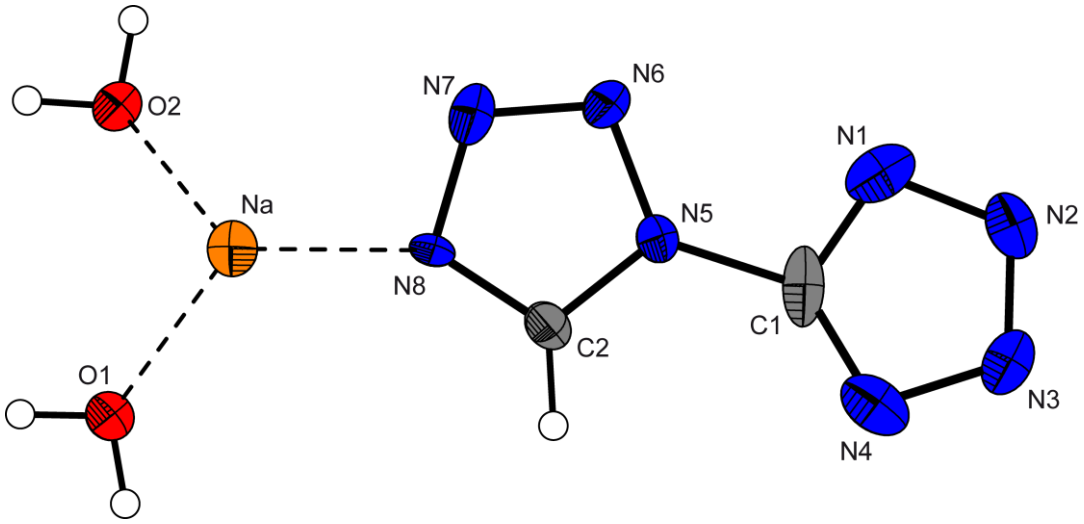

Figure 14.10 Molecular unit of sodium 1,5-bistetrazolate dihydrate (**155**·2H_2O). Thermal ellipsoids represent the 50 % probability level.

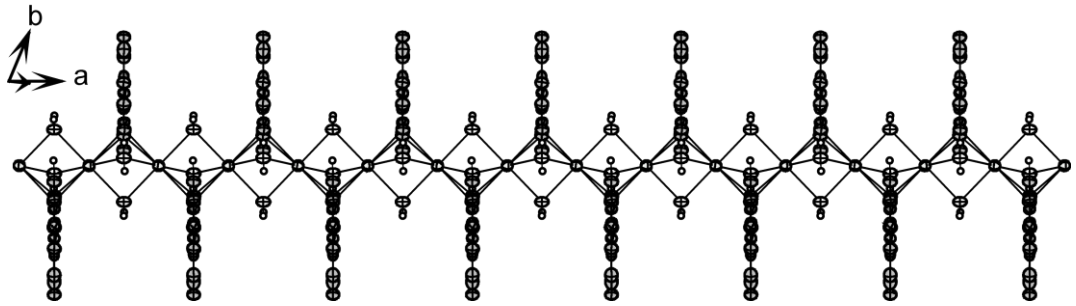

Figure 14.11 View on the chains in the structure of **155**·2H_2O.

14.3.6 Potassium 1,5-bistetrazolate dihydrate (**156**·2H_2O)

Potassium 1,5-bistetrazolate crystallizes as a dihydrate in the triclinic space group *P*–1 with two molecules in the unit cell. Surprisingly, its very low density of 1.627 g cm^{-3} is even lower than that of the sodium salt **155**. The structural motive is best described by the formation of a binuclear complex, which is shown in **Figure 14.12**. The potassium atoms are surrounded by a distorted octahedral coordination sphere by the atoms O1, O2, N1, N6 and N8. The packing can be described as an alternating layer structure, which is depicted in **Figure 14.13**.

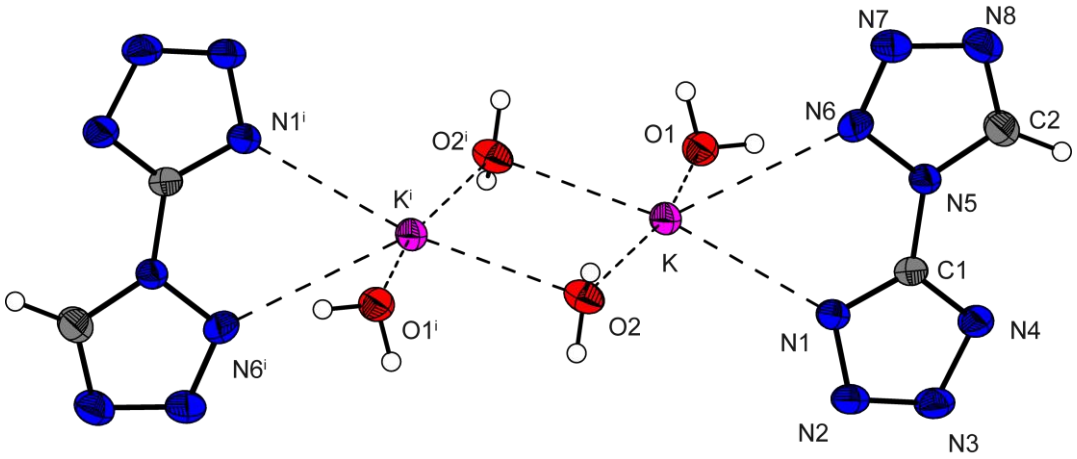

Figure 14.12 View on the binuclear complex potassium 1,5-bistetrazolate dihydrate (**156**·2H_2O). Selected distances (Å): K–O1 = 2.756(4), K–O2 = 2.705(7), K–N1 = 2.872(9), K–N6 = 3.090, K–N8^i = 2.941(8).

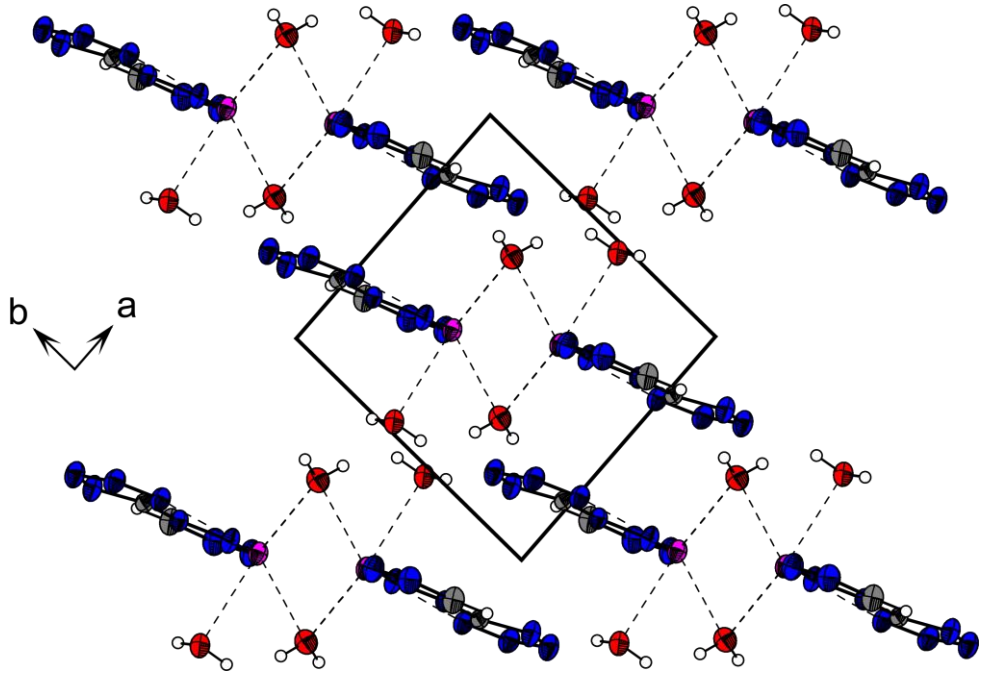

Figure 14.13 View on the packing of potassium 1,5-bistetrazolate dihydrate along the *c* axis.

14.3.7 *Trans*(tetraqua-di(1,5-bistetrazolato-*N2*)) copper(II) (**157**)

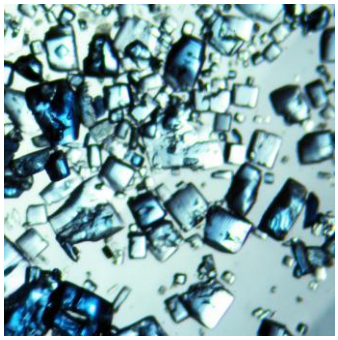

Copper complex **157** crystallizes with a density of 1.992 g cm^{-3} in the monoclinic space group $P2_1/c$ with two molecules in the unit cell. The molecular moiety is depicted in **Figure 14.14**. The 1,5-bistetrazolates coordinate with the nitrogen atom N2 to the copper atoms, which show a elongated octahedral coordination sphere, caused by the Jan Teller effect. The structure of the tetrazolates follow the geometry observed for the ammonium salt **154**.

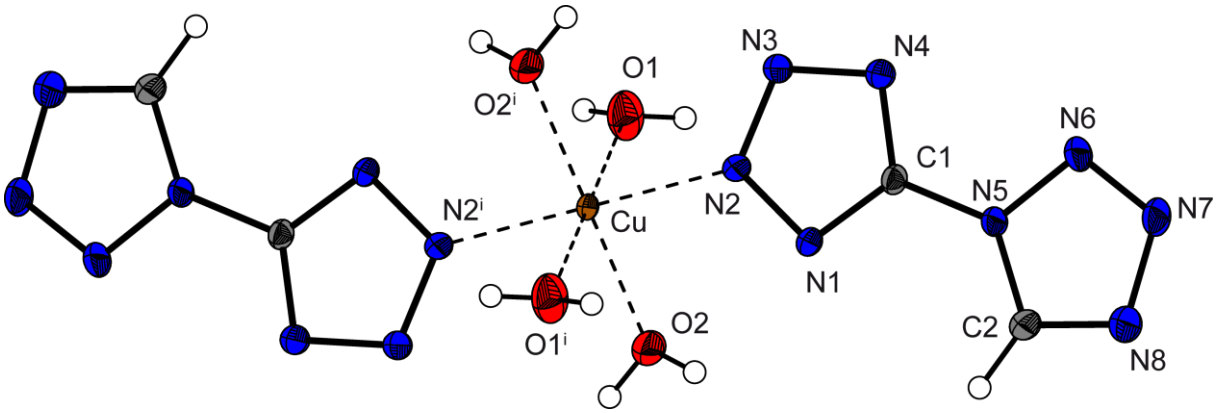

Figure 14.14 Molecular moiety of copper 1,5-bistetrazolate tetrahydrate (**157**). Thermal ellipsoids represent the 50 % probability level. Selected coordination geometries: distances (Å): Cu–N2 = 1.976(2), Cu–O2 = 1.992(2), Cu–O1 = 2.408(2); angles (°): N2–Cu–O2 = 87.75(8), N2–Cu–O1 = 88.13(8), O2–Cu–O1 = 92.50(7). (i) 2–x, –y, 2–z.

14.3.8 *Trans*(diammine-diaqua-di(1,5-bistetrazolato-*N2*)) copper(II) (**158**)

158 crystallizes according to complex **157**. Again the coordination is formed via the atoms N2 as well as an elongated octahedral coordination is observed for the copper(II) centers. The longer distance is found between the copper cations and water molecules. A view on the molecular structure of **158**, which crystallizes with a lower density of 1.829 g cm^{-3} in the triclinic space group $P\bar{1}$ with one molecule in the unit cell, is given in **Figure 14.15**.

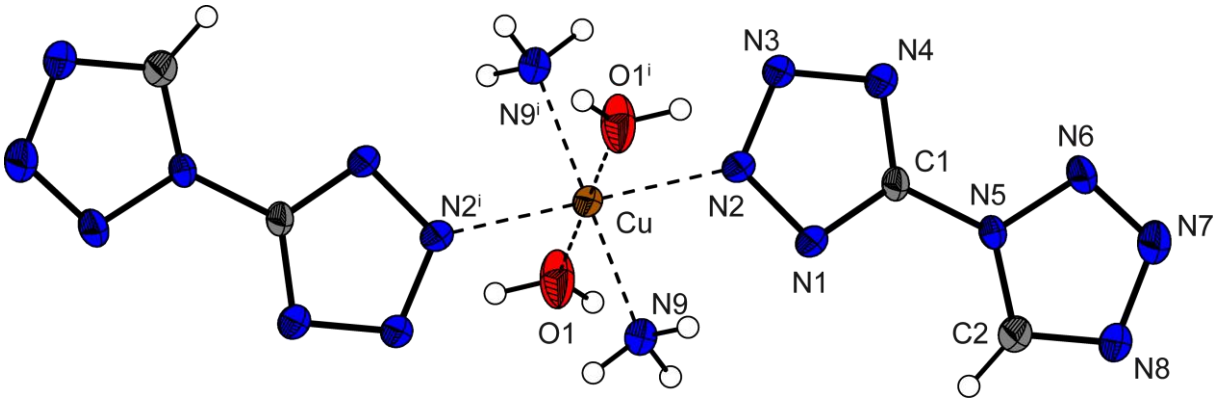

Figure 14.15 Molecular moiety of **158**. Thermal ellipsoids represent the 50 % probability level. Selected coordination geometries: distances (Å): Cu–N9 = 1.987(2), Cu–N2 = 2.034(2), Cu–O1 = 2.395(2); angles (°): N9–Cu–N2 = 88.10(9), N9–Cu–O1 = 92.2(1), N2–Cu–O1 = 90.09(8). (i) 2–x, 2–y, 1–z.

14.3.9 Bis(chlorido-(2-methyl-1,5-bistetrazole-*N8*)) copper(II) (**159**)

Copper complex **159** crystallizes as green rods in the chiral orthorhombic space group $Pna2_1$. The unit cell contains four formula moieties, one of them presented in **Figure 14.16**, resulting in a calculated density of 1.901 g cm^{-3}.

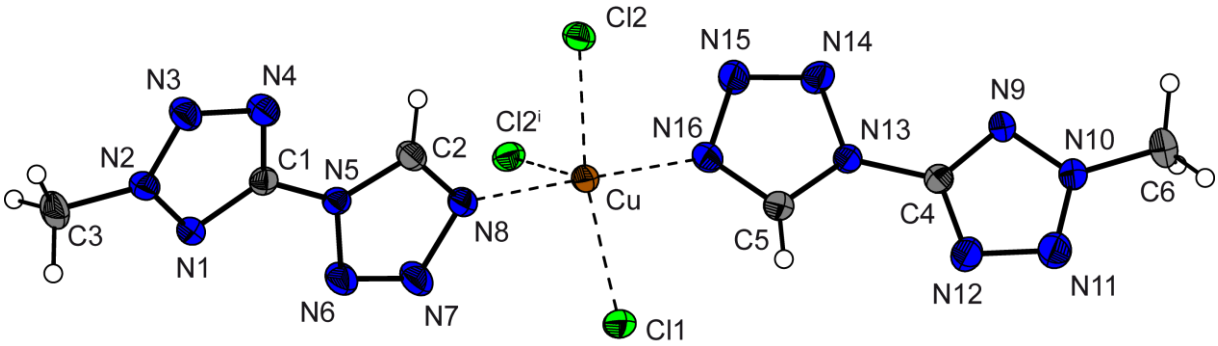

Figure 14.16 Molecular structure of complex **159**. Thermal ellipsoids represent the 50 % probability level. Selected coordination geometries: distances (Å): Cu–N8 = 2.015(3), Cu–N16 = 2.023(3), Cu–Cl1 = 2.2557(7), Cu–Cl2 = 2.2966(7), Cu–Cl2^{i} = 2.6664(7); angles (°): N8–Cu–N16 = 178.44(9), N8–Cu–Cl1 = 89.98(8), N16–Cu–Cl1 = 89.33(7), N8–Cu–Cl2 = 89.53(7), N16–Cu–Cl2 = 91.77(7), Cl1–Cu–Cl2 = 149.78(3), N8–Cu–Cl2^{i} = 87.02(7), N16–Cu–Cl2^{i} = 91.88(7), Cl1–Cu–Cl2^{i} = 108.84(2), Cl2–Cu–Cl2^{i} = 101.31(2), ; (i) 0.5+x, –0.5–y, z.

Also the 2-MeBT molecules do not coordinate as a chelating ligand. The copper atoms are pentacoordinated by two 2-methyl-1,5-bistetrazole molecules d(Cu–N8) = 2.02(3) Å and d(Cu–N16) = 2.02(3) Å and three chloride anions with d(Cu–Cl1) = 2.26(2), d(Cu–Cl2) = 2.30(1) and d(Cu–Cl2^{i}) = 2.67(1) Å [(i) 0.5+x, –0.5–y, z]. The coordination of the copper atom can be described as distorted trigonal bipyramide because of the almost planar fragment found in the crystal structure (torsion angle Cl1–Cl2–Cu–Cl2 = 177.9(3)°). In complex **159** the 2-methyl-1,5-bistetrazole molecules show a different geometry compared to the neutral compound **153**. The tetrazole rings of the ligand are only slightly twisted against each other (torsion angle N4–C1–N5–C3 = –4.8(5)°). In the structure of **153** this torsion angle is about 30°. This fact shows the influence on the neutral ligand by the coordinative bonding to the copper atom.

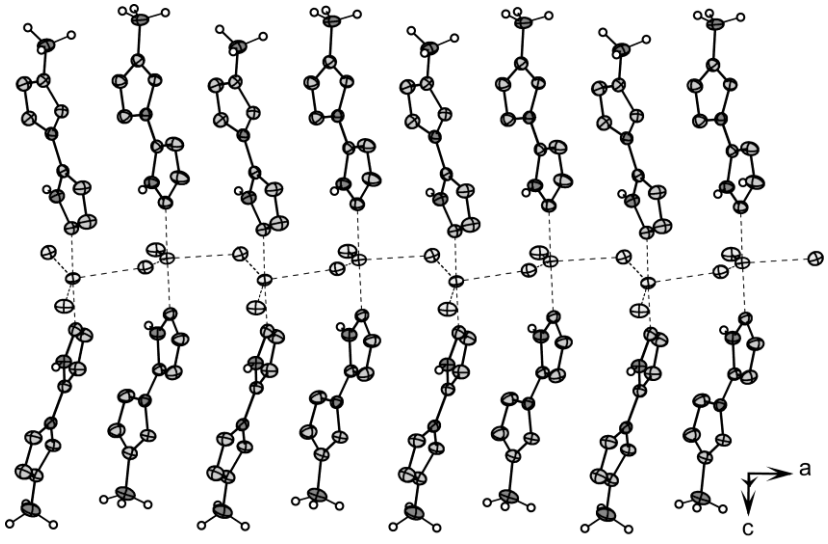

Figure 14.17 View on the chains formed by the bridging chlorido ligand Cl2.

The packing of the molecular moieties in the crystal structure is strongly influenced by the coordination of the copper atoms. The trigonal bipyramides are connected to each other over one shared chlorido ligand, resulting in linear fragments within the structure. This spatial arrangement in chains is represented by **Figure 14.17**. The pentacoordination of the copper atoms threw up some questions concerning the resulting spin momentum for the metal complex. Because of the crystal field dispartment for the coordination found in the structure there should be one unpaired electron in the dz^2 orbital for the Cu^{2+} ion (d^9 system). Therefore the metal complex should show paramagnetic characteristics in corresponding investigations. The existence of a spin super exchange path along the p_π orbitals of the chloride ligands can

be assumed. If this assumption is correct the complex should show diamagnetic characteristics. SQUID measurements of **159** are still under investigation.

Table 14.1 Bond lengths [Å] of **152**, **152**·H_2O, **153** and **154**.

Atoms	**152**·H_2O	**152**(1)	**152**(2)	**153**(1)	**153**(2)	**154**
N1–C1	1.314(2)	1.319(7)	1.316(6)	1.316(2)	1.319(2)	1.318(2)
N1–N2	1.326(2)	1.346(6)	1.333(6)	1.329(2)	1.337(2)	1.352(2)
N2–N3	1.312(2)	1.301(7)	1.310(6)	1.312(2)	1.316(2)	1.314(2)
N3–N4	1.332(2)	1.323(6)	1.324(6)	1.326(2)	1.327(2)	1.346(2)
N4–C1	1.330(2)	1.327(7)	1.334(6)	1.334(2)	1.330(2)	1.328(2)
C1–N5	1.404(2)	1.395(6)	1.399(3)	1.399(2)	1.405(2)	1.405(2)
N5–N6	1.359(2)	1.363(7)	1.371(5)	1.356(2)	1.356(2)	1.358(2)
N5–C2	1.336(2)	1.337(7)	1.333(6)	1.332(2)	1.347(2)	1.335(2)
N8–C2	1.307(2)	1.290(8)	1.302(8)	1.305(2)	1.306(2)	1.309(3)
N6–N7	1.292(2)	1.299(6)	1.297(6)	1.286(2)	1.292(2)	1.296(2)
N7–N8	1.366(3)	1.374(7)	1.370(6)	1.366(2)	1.370(2)	1.369(2)
N2–C3				1.454(3)	1.460(2)	

Table 14.2 Bond lengths [Å] of **155**, **156**, **157**, **158** and **159**.

Atoms	**155**	**156**	**157**	**158**	**159**(1)	**159**(2)
N1–C1	1.305(2)	1.319(2)	1.315(3)	1.318(3)	1.329(5)	1.320(5)
N1–N2	1.332(2)	1.350(2)	1.343(3)	1.344(3)	1.329(4)	1.325(4)
N2–N3	1.295(2)	1.311(2)	1.315(3)	1.313(3)	1.328(3)	1.323(4)
N3–N4	1.332(2)	1.348(2)	1.333(3)	1.346(3)	1.318(4)	1.327(4)
N4–C1	1.305(2)	1.323(2)	1.321(3)	1.314(3)	1.333(4)	1.337(4)
C1–N5	1.453(3)	1.407(2)	1.418(3)	1.415(3)	1.398(5)	1.405(5)
N5–N6	1.357(4)	1.357(2)	1.352(3)	1.355(3)	1.356(3)	1.358(3)
N6–N7	1.286(3)	1.290(2)	1.293(3)	1.293(3)	1.279(4)	1.275(4)
N7–N8	1.345(6)	1.364(2)	1.367(3)	1.358(3)	1.373(3)	1.373(3)
N5–C2	1.337(4)	1.341(2)	1.336(3)	1.334(3)	1.329(4)	1.332(4)
N8–C2	1.305(1)	1.319(2)	1.301(3)	1.308(3)	1.306(4)	1.300(4)
N2–C3					1.454(4)	1.456(5)

Table 14.3 Bond angles [°] of **152**, **152**·H_2O, **153** and **154**.

Atoms	**152**·H_2O	**152**(1)	**152**(2)	**153**(1)	**153**(2)	**154**
N2–N1–C1	100.5(1)	100.0(4)	99.3(3)	99.7(2)	99.9(1)	102.7(1)
C1–N4–N3	104.1(1)	105.1(4)	103.8(4)	104.4(1)	104.7(1)	102.8(1)
N1–N2–N3	114.0(1)	113.8(4)	114.5(4)	114.7(2)	114.1(1)	110.0(1)
N2–N3–N4	106.5(1)	106.7(5)	106.6(5	106.1(1)	106.2(1)	109.7(1)
N4–C1–N1	115.0(2)	114.4(4)	115.7(4)	115.1(2)	115.0(2)	114.9(2)
N1–C1–N5	123.0(2)	123.7(3)	122.6(3)	123.4(2)	123.0(1)	122.8(2)
N4–C1–N5	122.0(1)	122.0(3)	121.6(3)	121.5(2)	122.0(1)	122.3(2)
C1–N5–C2	130.0(2)	129.4(3)	129.9(3)	129.4(2)	129.7(2)	129.7(2)
C1–N5–N6	121.3(1)	121.6(3)	121.9(3)	122.6(2)	122.1(1)	121.8(1)
N5–C2–N8	108.7(2)	108.7(5)	109.0(4)	108.7(2)	109.1(2)	109.3(2)
N6–N5–C2	108.6(1)	109.0(4)	108.2(4)	107.9(2)	108.2(1)	108.4(2)
C2–N8–N7	106.0(1)	106.8(4)	106.7(4)	104.7(2)	105.5(1)	105.5(2)
N5–N6–N7	105.8(2)	105.2(4)	105.9(4)	105.8(2)	105.9(1)	105.7(2)
N6–N7–N8	110.9(1)	110.3(5)	110.2(4)	111.7(2)	111.3(1)	111.1(1)
N1–N2–C3				122.7(2)	123.5(2)	
N3–N2–C3				122.6(2)	122.3(2)	

Table 14.4 **Bond** angles [°] of **155**, **156**, **157**, **158** and **159**.

Atoms	**155**	**156**	**157**	**158**	**159**(1)	**159**(2)
N2–N1–C1	103.0(1)	102.7(1)	101.2(2)	101.7(2)	99.7(2)	100.0(3)
C1–N4–N3	103.0(1)	102.7(1)	103.6(2)	103.4(2)	104.3(3)	104.1(3)
N1–N2–N3	109.7(1)	109.8(1)	111.7(2)	111.2(2)	114.0(3)	114.3(3)
N2–N3–N4	109.8(1)	109.9(1)	108.2(2)	108.4(2)	106.7(2)	106.4(3)
N1–C1–N4	114.5(1)	114.9(1)	115.3(2)	115.4(2)	115.3(3)	115.2(4)
N1–C1–N5	106.7(2)	123.3(1)	122.5(2)	120.6(2)	123.0(3)	124.2(3)
N4–C1–N5	138.8(2)	122.1(1)	122.2(2)	124.1(2)	121.7(3)	120.6(3)
C1–N5–C2	123.8(3)	130.1(1)	130.5(2)	130.1(2)	130.0(3)	129.1(3)
C1–N5–N6	128.3(2)	121.6(1)	120.5(2)	121.2(2)	121.4(3)	122.0(3)
N5–C2–N8	108.6(4)	109.0(2)	108.7(2)	109.0(2)	108.7(3)	108.4(3)
N6–N5–C2	107.9(3)	108.3(1)	109.0(2)	108.7(2)	108.5(3)	108.5(3)
C2–N8–N7	106.4(6)	105.6(1)	105.9(2)	105.5(2)	106.0(3)	106.5(3)

N5–N6–N7	105.9(2)	105.8(1)	105.4(2)	105.2(2)	106.4(2)	106.5(2)
N6–N7–N8	111.2(4)	111.4(1)	111.0(2)	111.6(2)	110.4(2)	110.2(2)
N1–N2–C3					123.1(3)	123.5(3)
N3–N2–C3					122.9(3)	122.2(3)

14.4 NMR Spectroscopy

Multinuclear, particularly ^{1}H, ^{13}C and ^{15}N NMR spectroscopy is a valuable method to identify and characterize tetrazole derivatives. **152**·H_2O, **153** and **154** were determined by ^{1}H, ^{13}C and ^{15}N NMR spectroscopy. All NMR spectra were recorded in *d*$_6$-DMSO and chemical shifts are given with respect to TMS (^{1}H, ^{13}C) and CH_3NO_2 (^{15}N) as external standards. In the ^{1}H NMR spectra, the C–H proton resonance is observed as sharp signal at 10.20 (**152**), 10.26 (**153**) and 9.92 ppm (**154**). The nitrogen bonded proton in **152** is found at 7.77 ppm as broad resonance. In addition, crystal water is observed at 3.30 ppm. In **153** the methyl proton shifts are found at 4.51 ppm. The ammonia cation proton resonances in **154** are located 6.50 ppm. In all ^{13}C NMR spectra two signals of the tetrazole carbon atoms are observed. Both, the carbon atom (C1) resonances at 155.6 (**152**), 156.6 (**153**), 155.4 (**154**) ppm as well as the C2 resonances are in the same range. fields (144.2 (**152**), 143.8 (**153**), 144.2 (**154**) ppm). This is in contrast to e.g. 5-amino-1*H*-tetrazole (156.6 ppm) vs. 5-aminotetrazolate (164.8 ppm), in which a deprotonation yields to a highfield shifted carbon resonance for the case of the deprotonated species. The methyl group in **153** is found at 41.4 ppm. In **Figure 14.18** the ^{15}N spectra of **152**·H_2O, **153** and **154** are shown. In the case of **152**·H_2O also the proton de-coupled ^{15}N{^{1}H} spectrum was measured. According to the symmetry and fast proton exchange in DMSO, there are only six 1,5-bistetrazole nitrogen signals observed in the ^{15}N spectra of **152** and **154**. The assignments were done by evaluating the ^{15}N–^{1}H coupling constants and by comparison with ^{15}N spectra of known tetrazole derivatives. In the case of **152**·H_2O, signals at –153.8 (N3, d, $^{2}J_{N-H}$ = 9.5 Hz), –85.2 (N1, s), –51.3 (N6, d, $^{2}J_{N-H}$ = 12.3 Hz), –35.2 N2, s), –19.0 (N4, s) and 13.4 (N5, d, $^{3}J_{N-H}$ = 3.3 Hz) ppm can be observed. In contrast to nitrogen atom N5, there is no $^{3}J_{N-H}$ observed for atom N4. The N–H proton is located at the nitrogen atom N2 also in solution, which can be seen on the large downfield shift (Δ(N2) = 46.7 ppm) of resonance N2 in the spectrum of deprotonated **154** (11.5 ppm). In addition, **154** shows further signals shifted to lower shifts, e.g. at –148.3 (N3, d, $^{2}J_{N-H}$ = 9.4 Hz), –76.0 (N1, s) and –17.8 (N4, s) ppm, whereas

the resonances at –52.5 (N6, d, $^{2}J_{N-H}$ = 12.3 Hz) and N5 (11.0 ppm, d, $^{3}J_{N-H}$ = 3.3 Hz) show chemical shifts in the same range. The ammonium nitrogen core is found at –358.2 ppm. In the spectrum **153** eight nitrogen resonances are found at –154.3 (N5, d, $^{2}J_{N-H}$ = 9.7 Hz), –100.9 (N2, q, $^{2}J_{N-H}$ = 2.2 Hz), –89.7 (N1, q, $^{3}J_{N-H}$ = 1.7 Hz), –66.6 (N4, s), –50.8 (N8, d, $^{2}J_{N-H}$ = 12.3 Hz), –19.3 (N6, s), 1.9 (N3, q, $^{3}J_{N-H}$ = 1.5 Hz), 13.9 (N7, d, $^{3}J_{N-H}$ = 3.3 Hz) ppm.

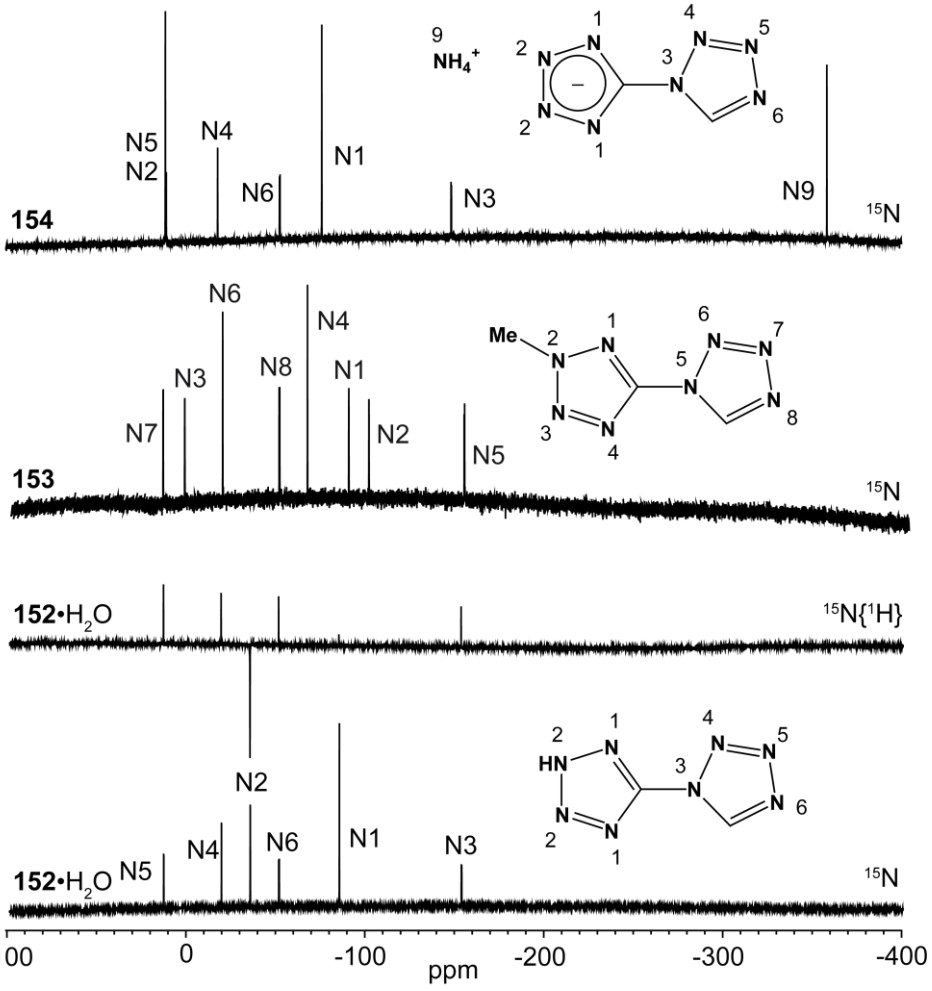

Figure 14.18 ^{15}N spectra of **152**·H_2O, **153** and **154**.

14.5 Energetic Properties

The energetic properties of the discussed compounds can be ranked in all classes of energetic materials: explosives, propellants and pyrotechnics. **152** are **152**·H_2O typical high explosives. Their performance, summarized in **Table 14.6**, belongs to the class of secondary explosives while the sensitivities belong to the class of primary explosives. **153** and **154** are promising combustible materials, which can be used as nitrogen-rich

fuel in modern smokeless propellant compositions. However, with regard to the development of new thermal stable explosives, the ammonium salt of 1,5-bistetrazole (**152**, NH_4_1,5-BT) shows promising characteristics ($T_{Dec.}$: 240 °C) and was even successfully upscaled (50 g) and tested by a "Koenen Test" (critical diameter > 10 mm). The metal salts and copper complexes, respectively, are new outstanding colorants in smokeless and low-polluting pyrotechnic compositions. **157** and **158** feature brilliant green flames, when combusted in *bunsen burner* flame, while **159** exhibits an intensive blue flame color. In the following important criteria of energetic material research are discussed, particularly thermal stability, heats of formation, sensitivities and performances.

14.5.1 Differential Scanning Calorimetry

DSC measurements were undertaken in order to determine the thermal behavior of **152**·H_2O, **153**, **154**, aminoguanidinium 1,5-bistetrazolate (AG-1,5-BT), **157** and **159**. AG-1,5-BT was synthesized (reaction of aminoguanidinium bicarbonate with **152** in water) to investigate the thermal behavior of a further nitrogen-rich derivative of 1,5-BT in comparison to promising **154**. The measurements were performed in covered Al-containers with a nitrogen flow of 20 mL min^{-1} on a Linseis PT10 DSC at a heating rate of 5 °C min^{-1}. In each measurement, the thermal behavior of approximately 1.5 mg of each compound was investigated in the range from 50–350 °C. The neutral compound **152**·H_2O decomposes already at 145°C without previous crystal water release whereas the ammonium salt **154** is much more stable. It melts at 115 °C and has a comparatively high decomposition temperature of 223°C despite less aromatic stabilization (**Figure 14.19**). The methyl substituted compound **153** melts at 97 °C and also decompose at lower temperatures above 137 °C. The sodium salt **155** shows a similar thermal behavior in comparison to **154**. In addition next to the melting point, loss of its crystal water is obtained in the range 100–110 °C. The copper complex **157** decompose at temperatures above 145 °C which is subsequent to the dehydration. **159** decompose at higher temperatures starting at 172 °C:

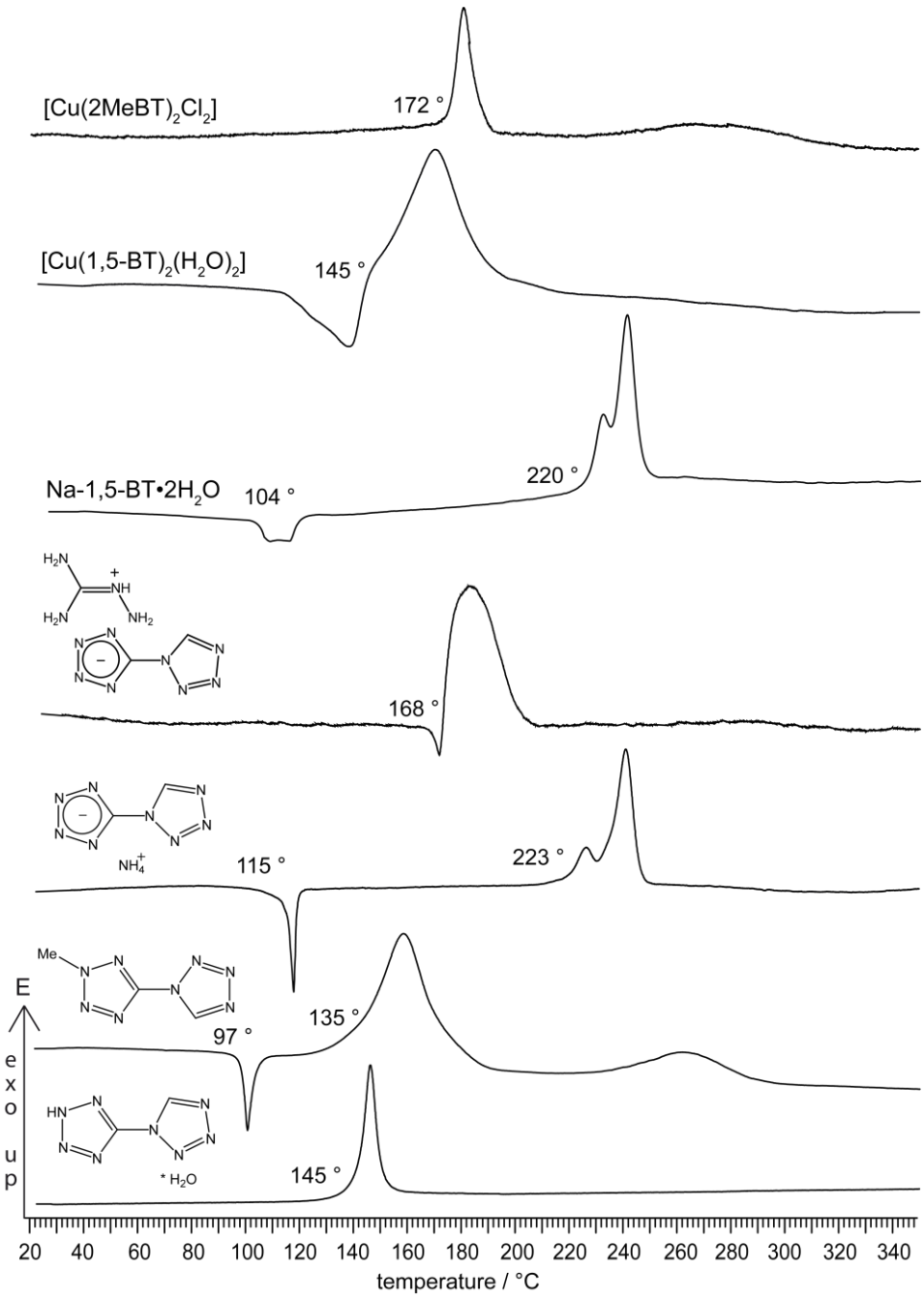

Figure 14.19 DSC plot (exo up) of compounds **152**·H_2O, **153**, **154**, aminoguanidinium 1,5-bistetrazolate, **157** and **159** (5° min^{-1}). T_{onset} (dec.): **152**·H_2O = 145 °C, **153** = 135 °C, **154** = 223 °C, AG-1,5-BT = 168 °C, **155** = 220 °C, **157** = 145 °C, **159** = 172 °C.

14.5.2 Heats of Formation

The heats of formation of **152**, **152**·H_2O, **153** and **154** have been computed (CBS-4M) using the atomization energy method. To check the calculation result of the

monohydrate **152**·H_2O a C_1 optimization and frequency analysis was performed on B3LYP/cc-pVDZ, whereby a stable minimum with NIMAG = 0 was obtained. From the gas-phase enthalpies of formation $\Delta_f H°$(g) (**152**: +168.5 kcal mol^{-1}, **152**·H_2O: +103.0 kcal mol^{-1}, **153**: +159.3 kcal mol^{-1} and **154**: (NH_4^+ = +151.9 kcal mol^{-1}, 1,5-BT$^-$ = +111.9 kcal mol^{-1}), the enthalpies of the solid state of neutral compounds can be calculated using the enthalpies of sublimation by the equation:

$$\Delta_f H°(s) = \Delta_f H°(g) - (\Delta_{sub} H)$$

For a solid compound the enthalpy of sublimation ($\Delta_{sub}H$) can be approximated on the basis of TROUTON's rule if the melting temperature or decomposition temperature (T_m in K) is known:

$$\Delta_{sub}H. \text{ [J mol}^{-1}\text{]} = 188\ T_m \text{ [K]}$$ ($\Delta_{sub}H$: **152**, **152**·H_2O = 18.8 kcal mol^{-1}, **153** = 16.4 kcal mol^{-1}).

The enthalpy of the salt **154** was computed with the *Jenkin*s equation by using the molecular volume (V_M(**154**) = 164Å^3) and the lattice enthalpies (ΔH_L(**154**) = 128.4 kcal mol^{-1}).

With the known enthalpies of formation of carbon dioxide ($\Delta_f H°_{298}(CO_{2(g)})$ = −394 kJ mol^{-1}) and water ($\Delta_f H°_{298}(H_2O_{(g)})$ = −242 kJ mol^{-1}) the enthalpies of formation of have been calculated and are listed in **Table 14.5**. **151**–**154** are strongly endothermic compounds.

Table 14.5 Solid state enthalpies ($\Delta_f H°$) and energies of formation ($\Delta_f U°$)

	$\Delta_f H°$(s) / kcal mol^{-1}	$\Delta_f H°$(s) / kJ mol^{-1}	Δn	$\Delta_f U°$(s) / kcal mol^{-1}	M / g mol^{-1}	$\Delta_f U°$(s) / kJ kg^{-1}
152·H_2O	+84.2	353	–6.5	88.0	156.1	+2358.7
152	+149.7	628	–5	152.7	138.1	+4626.3
153	+142.9	598	–6	146.5	152.1	+4030.0
154	+135.4	567	–7	139.5	155.1	+3763.2

14.5.3 Sensitivities

For initial safety testing, the impact and friction sensitivities as well as the electrostatic sensitivity of **152**–**159** were determined. The detailed values are summarized in **Table 14.6**. Water-free **152** is extremely sensitive towards impact (< 0.5 J) and can already be ignited by low finger pressure. It is also extremely sensitive towards friction (< 5 N) and

should therefore only be handled with utmost care. The impact sensitivity of **152**·H_2O (1 J), **153** (9 J) and **154** (10 J) is significantly lower. However, **152**·H_2O is also classified according to the "UN Recommendations on the Transport of Dangerous Goods" as *very sensitive* and should be considered to the class of primary explosives. **153** and **154** are classified as *sensitive* and are less sensitive than commonly used secondary explosives like RDX (8 J) and HMX (7 J). The same trends are observed regarding the friction sensitivity. While **152**·H_2O is *very sensitive* towards friction (120 N), **153** (240 J) and **154** (300 J) are significantly lower sensitive towards friction. Compounds **155**·$2H_2O$, **156**·$2H_2O$, **157**, and **158** are neither sensitive towards impact (> 50 J) nor friction (> 360 N). Complex **159** is weak sensitive towards impact (40 J), but not sensitive towards friction.

Electrostatic sensitivity tests of **152**·H_2O, **153** and **154** were carried out using an electric spark tester ESD 2010EN (OZM Research). The values of **152**·H_2O (0.12 J), **153** (0.30 J), **154** (0.60 J) are in agreement to those observed for commonly used secondary explosives like RDX (0.2 J) and also found in other nitramine compounds. Primary explosives like $Pb(N_3)_2$ (0.005 J) have much lower values. It should be mentioned that the test towards electrical discharge strongly depends on the particle size and shape. Although we tried to use fine crystalline materials (75–125 µm) a guarantee for the determined values cannot be given.

14.5.4 Performances and Koenen Test

The detonation parameters calculated with the EXPLO5 program using the experimentally determined densities and previously discussed heats of formation are summarized in **Table 14.6**. The most important criteria of high explosives are the detonation velocity, the detonation pressure ($p_{C\text{-}J}$ = RDX 299 kbar) and the energy of explosion ($\Delta_E U_m°$ = RDX –5902 kJ kg^{-1}). **152**–**154** have calculated detonation parameters which are lower than those of RDX but higher in comparison with TNT ($V_{Det.}$ = TNT: 7000, RDX: 8796, HMX: 9100 m s^{-1}) For applications as new powerful secondary explosives none of these compounds is suitable, although the detonation performance of **154** has been successfully proofed in a Koenen Steel Sleeve test using a critical diameter of 10 mm. Due to its high nitrogen content and its thermal stability **154** is a appropriate compound as nitrogen-fuel in solid propellant charges.

Table 14.6 Physico-chemical properties of **152–154**.

	152	**152·H_2O**	**153**	**154**
Formula	$C_2H_2N_8$	$C_2H_4N_8O$	$C_3H_4N_8$	$C_2H_5N_9$
Molecular Mass	156.13	156.13	152.12	155.15
Impact sensitivity (J) [a]	< 0.5	1	9	10
Friction sensitivity (N)[b]	< 5	120	240	300
Electrical discharge (J) [c]	n.d.	0.12	0.30	0.60
N (%) [d]	81.14	71.78	73.66	81.27
Ω (%) [e]	–51.14	–51.14	–84.1	–67.04
Combustion [f]	fulmination	very good	good	good
T_{dec} (°C) [g]	140	145	135	240
Density (g cm^{-3}) [h]	1.728	1.567	1.568	1.670
$\Delta_f H_m$ (kJ mol^{-1}) [j]	628	353	598	567
$\Delta_f U$ (kJ kg^{-1}) [k]	4626	2359	4030	3763
calculated values using EXPLO5:				
$-\Delta_E U_m°$ (J g^{-1}) [l]	4852	4084	4454	4289
T_E (K) [n]	3843	3220	3283	3181
p (kbar) [o]	290	242	222	248
D (m s^{-1}) [p]	8567	8010	7891	8413
Gas vol. (L kg^{-1}) [q]	723	780	726	815

[a] BAM drophammer; [b] BAM friction tester; [c] OZM small scale electrical discharge tester; [d] Nitrogen content; [e] Oxygen balance; [f] Flame test; [g] Temperature of decomposition by DSC (δ = 5 °C); [h] estimated from a structure determination; [i] Experimental (constant volume) combustion energy; [j] Molar enthalpy of formation; [k] Energy of formation; [l] Energy of Explosion, EXPLO5 V5.02; [l] explosion temperature; [m] detonation pressure; [n] detonation velocity; [o] Assuming only gaseous products.

Figure 14.20 shows the result of the Koenen steel sleeve test using a closing plate with a hole diameter of 10 mm. Unfortunately the high speed camera did not work and no detonation pictures are available. Since RDX destroys the sleeve only up to 8 mm it can be concluded that the detonation performance of **154** under confinement initiated by heat is greater than that of RDX.

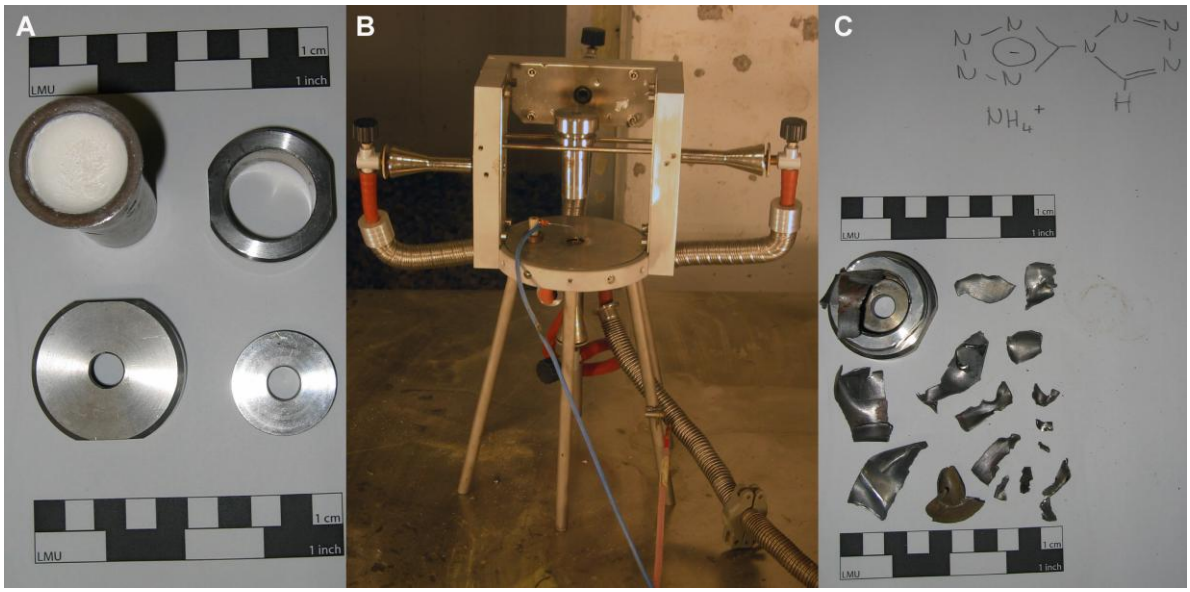

Figure 14.20 Koenen Steel Sleeve Test of 26 g **154**. A) Steel sleeve loaded with **154** and closing parts (hole: 10 mm); B) Koenen test setup; C) Collected fragments.

14.6 Experimental Part

CAUTION! 1,5-Bistetrazoles are energetic compounds with increased sensitivities against heat, impact and friction. Although we had no problems in synthesis, proper protective measures (safety glasses, face shield, leather coat, earthened equipment and shoes, Kevlar® gloves and ear plugs) should be used during work on ***152–159****. in larger scale. Highest safety precautions are needed when handling water-free* ***152****.*

*1,5-Bistetrazole monohydrate (**152**·H_2O):* To a suspension of 5-aminotetrazole (8.50 g, 0.10 mol) and sodium azide (7.80 g, 0.12 mol) in triethyl orthoformate (22.2 g, 0.15 mol) acetic acid (42.0 g, 0.70 mol) was added dropwise while intensive stirring. After three hours of refluxing at 90 °C the solvent was evaporated under vacuum and the product was extracted three times with 50 mL of cold ethyl acetate each. The solvent was evaporated and the product was washed with diethyl ether yielding 6.21 g (yield 45 %) of 1,5-bistetrazole monohydrate as colorless solid. Single crystals were grown from water. Highly explosive water-free **152** can be obtained by recrystallization from 20 % hydrochloric acid. **DSC** (T_{onset}, 5 °C min^{-1}): 145 °C (dec.); **IR** (ATR, cm^{-1}): $\tilde{\nu}$ = 3163 (m), 3130 (m), 3034 (m), 2971 (m), 2865 (m), 2766 (m), 2702 (m), 2649 (m), 1697 (w), 15+82 (vs), 1455 (m), 1385 (m), 1372 (m), 1272 (s), 1208 (m), 1178 (m), 1148 (m), 1114 (m), 1086 (s), 1021 (s), 993 (m), 957 (m), 913 (m), 891 (m), 871 (m), 742 (m), 649

(m); **Raman** (1064 nm, 400 mW, 25 °C, cm^{-1}): $\tilde{\nu}$ = 3117 (9), 1582 (100), 1543 (7), 1466 (6), 1398 (4), 1275 (17), 1182 (10), 1162 (19), 1124 (14), 1094 (5), 1025 (32), 994 (3), 959 (4), 741 (3), 426 (14), 378 (13); **^{1}H NMR** (*d*$_6$-DMSO, 25 °C, ppm): δ = 7.77 (s, -NH), 10.20 (s, -CH); **^{13}C NMR** (*d*$_6$-DMSO, 25 °C, ppm): δ = 144.2 (CN_4), 155.4 (N_4C-N); **^{15}N NMR** (*d*$_6$-DMSO, 25 °C, ppm): δ = –153.9 (N3), –85.2 (N1), –51.3 (N6), –35.2 (N4), –18.9 (N2), 13.5 (N5); **EA** ($C_2H_4N_8O$, 156.11) calcd.: C 15.39, H 2.58, N 71.78 %; found: C 15.33, H 2.67, N 70.99 %; **Δ*U*$_c$**: –2838 cal g^{-1}; **impact sensitivity**: 1 J; **friction sensitivity**: 120 N; **ESD**: 0.12 J.

*2-Methyl-1,5-bistetrazole (**153**):* A solution of 2-methyl-5-aminotetrazole (**11**) (1.98 g, 0.02 mol) and sodium azide (1.56 g, 0.024 mol) in triethyl orthoformate (4.44 g, 0.030 mol) was prepared. Glacial acetic acid (8.40 g, 0.14 mol) was added drop wise and the reaction mixture was refluxed at 100 °C for 3 hours. After the crude product precipitated as colorless powder, 20 mL of 1N hydrochloric acid (0.02 mol) was added. The solvent was removed and the residue was dissolved in boiling benzene and filtered off. Product **153** was achieved via crystallization from the filtered solution as colorless needles with a reaction yield of 36 % (1.10 g). **DSC** (T_{onset}, 5 °C min^{-1}): 92 °C, 135 °C (dec.); **IR** (KBr, cm^{-1}): $\tilde{\nu}$ = 3427 (w), 3142 (s), 3051 (w), 3967 (w), 2930 (w), 2886 (w), 2777 (w), 2710 (w), 2385 (w), 2342 (w), 2254 (w), 2129 (w), 1978 (w), 1781 (w), 1752 (w), 1588 (vs), 1534 (m), 1476 (m), 1467 (s), 1433 (m), 1414 (s), 1363 (w), 1351 (m), 1291 (m), 1266 (s), 1260 (s), 1198 (m), 1178 (m), 1134 (m), 1088 (vs), 1056 (s), 1038 (w), 1018 (w), 1001 (s), 944 (m), 893 (m), 880 (m), 808 (w), 743 (m), 721 (s), 713 (s), 684 (w), 652 (s), 501 (w); **Raman** (1064 nm, 400 mW, 25 °C, cm^{-1}): $\tilde{\nu}$ = 3123 (12), 2986 (23), 2968 (36), 1582 (100), 1478 (6), 1431 (13), 1414 (9), 1364 (10), 1261 (20), 1198 (7), 1136 (12), 1087 (7), 1058 (11), 1019 (39), 990 (5), 948 (4), 739 (4), 713 (14), 507 (4), 406 (28), 384 (14), 345 (9); **^{1}H NMR** (*d*$_6$-DMSO, 25 °C, ppm): δ = 10.26 (s, 1H, N*H*), 4.51 (s, 3H, C*H*$_3$); **^{13}C NMR** (*d*$_6$-DMSO, 25 °C, ppm): δ = 156.58 (CN_2H), 144.15 (CN_4), 41.38 (CH_3); **^{15}N NMR** (*d*$_6$-DMSO, 25 °C, ppm): δ = 13.9 (N7, d, $^3J_{NH}$ = 3.3 Hz), 1.9 (N3, d, $^2J_{NH}$ = 1.49 Hz), –19.3 (N6), –50.8 (N8, d, $^2J_{NH}$ = 12.3 Hz), –66.6 (N4), –89.7 (N1, d, $^2J_{NH}$ = 1.7 Hz), –100.9 (N2, t, $^3J_{NH}$ = 2.2 Hz), –154.3 (N5, d, $^2J_{NH}$ = 9.7 Hz); ***m/z*** (DEI$^+$): 153 (M^+); **EA** ($C_3H_4N_8$, 152.12) calcd.: C 23.69, H 2.65, N 73.66 %; found: C 23.64, H 2.67, N 73.56 %; **Δ*U*$_c$**.: 2708 cal g^{-1}; **impact sensitivity**: 9 J; **friction sensitivity**: 240 N; **ESD**: 0.30 J.

*Ammonium 1,5-bistetrazolate (**154**):* To a solution of 5.52 g (40.0 mmol) of 1,5-bis-tetrazole in 20 mL of water an excess of half concentrated ammonia was added. After

refluxing for five minutes the water was evaporated and the product was recrystallized from ethanol furnishing 5.46 g (35.2 mmol, yield 88 %) of ammonium 1,5-bistetrazolate as colorless single crystals. **DSC** (T_{onset}, 5 °C min^{-1}): 115 °C, 220 °C (dec.); **IR** (ATR, cm^{-1}): $\tilde{\nu}$ = 3377 (s), 3326 (vs), 3118 (s), 2290 (w), 2237 (w), 1795 (w), 1692 (w), 1655 (m), 1571 (w), 1552 (m), 1479 (m), 1437 (w), 1339 (w), 1279 (m), 1205 (w), 1176 (m), 1139 (m), 1084 (m), 1026 (w), 988 (m), 950 (w), 902 (w), 736 (m), 720 (w), 652 (m), 626 (m); **Raman** (1064 nm, 400 mW, 25 °C, cm^{-1}): $\tilde{\nu}$ = 3303 (3), 3120 (10), 1572 (20), 1552 (100), 1439 (15), 1280 (14), 1204 (3), 1142 (27), 1099 (5), 1087 (10), 1032 (27), 1002 (7), 951 (4), 741 (2), 482 (7), 428 (15), 383 (23); **^{1}H NMR** (d_6-DMSO, 25 °C, ppm): δ = 6.50 (s, NH_4^+), 9.92 (s, -CH); **^{13}C NMR** (d_6-DMSO, 25 °C, ppm): δ = 143.8 (CN_4), 155.6 (N_4C-N); **^{15}N NMR** (d_6-DMSO, 25 °C, ppm): δ = –358.2 (NH_4^+), –148.3 (N3, ^2J = 9.28 Hz), –76.0 (N1), –52.5 (N6, ^2J = 12.25 Hz), –17.8 (N4), –11.0 (N5, ^3J = 3.34 Hz), –11.5 (N2); ***m/z*** (FAB^-): 137.1 (1,5-bistetrazolate); **EA** ($C_2H_5N_9$, 155.12) calcd.: C 15.49, H 3.25, N 81.27 %; found: C 15.62, H 3.20, N 81.02 %; **ΔU_c**: –3186 cal g^{-1}; **impact sensitivity**: 10 J; **friction sensitivity**: 300 N; **ESD**: 0.6 J.

*Sodium 1,5-bistetrazolate dihydrate (**155**):* Sodium hydroxide (0.22 g, 5.4 mmol) was added to a solution of 1,5-*bis*tetrazole monohydrate (0.85 g, 5.4 mmol) in 10 mL H_2O. The reaction mixture was refluxed at 80 °C for 15 min and the solvent was removed under high vacuum. Recrystallization from EtOH/H_2O yielded colorless needles (847 mg, 80 % yield). **DSC** (T_{onset}, 5 °C min^{-1}): 80–81 °C, 222 °C (dec.); **Raman** (1064 nm, 300 mW, 25 °C, cm^{-1}): $\tilde{\nu}$ = 3310 (4), 2121 (11), 1572 (22), 1552 (102), 1439 (16), 1282 (15), 1203 (4), 1143 (29), 1103 (4), 1087 (11), 1032 (30), 1003 (9), 951 (5), 812 (4), 745 (4), 482 (9), 429 (17), 384 (26), 268 (4), 194 (4), 91 (4). **^{1}H NMR** (D_2O, 25 °C, ppm): δ = 10.70 (s, 1H, CH). **^{13}C NMR** (D_2O, 25 °C, ppm): δ = 155.5 (C), 143.3 (C); **EA** ($C_2H_5N_8O_2Na$, 196.10) calcd.: C 12.25; H 2.57; N 57.14 %; found: C 12.02; H 2.32; N 56.44 %; **impact sensitivity**: > 50 J; **friction sensitivity**: > 360 N.

*Potassium 1,5-bistetrazolate dihydrate (**156**):* **156** was prepared analogously to **155** by the reaction of potassium hydroxide (0.56 g, 10 mmol) was added to a solution of 1,5-bistetrazole monohydrate (1.56 g, 5.4 mmol) in 10 mL H_2O. The obtained solution was stirred for 10 min at 80 °C. Afterwards, the solvent was evaporated and the crude product recrystallized from water/ethanol.

*[Cu(1,5-BT)$_2$(H$_2$O)$_4$] (**157**):* Copper(II) nitrate trihydrate (242 mg, 1.0 mmol) was dissolved in 2 mL hot water and combined with a hot solution of 1,5-bistetrazole monohydrate (**152**·H$_2$O) (312 mg, 2 mmol) in 10 mL water. After stirring at 80 °C for 15 min, the solution was left for crystallization. Blue crystals suitable for X-ray analysis were obtained after one day of crystallization time at room temperature (331 mg, yield 81 %). **DSC** (T_{onset}, 5 deg min^{-1}): 145 °C (dec.); **EA** ($C_4H_{10}CuN_{16}O_4$, 409.77) calcd.: C 11.72, H 2.46, N 54.69 %; found: C 11.92, H 2.39, N 54.60 %; **impact sensitivity**: > 50 J; **friction sensitivity**: > 360 N.

*[Cu(1,5-BT)$_2$(H$_2$O)$_2$(NH$_3$)$_2$] (**158**):* Copper(II) nitrate trihydrate (242 mg, 1.0 mmol) was dissolved in 2 mL hot water and combined with a hot solution of 1,5-bistetrazole monohydrate (**152**·H$_2$O) (312 mg, 2 mmol) in 10 mL of 15 % ammonia solution. After stirring at 80 °C for 15 min, the solution was left for crystallization. Dark blue crystals suitable for X-ray analysis were obtained after one day of crystallization time at room temperature (253 mg, 62 % yield). **DSC** (T_{onset}, 5 °C min^{-1}): 155 °C (dec.); **EA** ($C_2H_{10}CuN_{16}O_4$, 407.80) calcd.: C 11.78, H 2.97, N 61.82 %; found: C 11.55, H 2.80, N 51.61 %; **impact sensitivity**: > 50 J; **friction sensitivity**: > 360 N.

*[Cu(2-Me-1,5-BT)$_2$Cl$_2$] (II) (**159**):* A solution of copper (II) chloride dihydrate (1.00 g, 0.006 mol) in 20 mL of water was prepared and heated up to 60 °C. Compound **153** (1.83 g, 0.012 mol) was dissolved in boiling water and added to the copper (II) solution. After the addition of 10 mL of 1N hydrochloric acid, the reaction mixture was heated up to 90 °C for 30 min. Compound **159** started to precipitate as green rods after two days. The green crystals, which where suitable for single X-ray diffraction measurements, were filtered off and washed with small amounts of ethanol and diethyl ether (371 mg, yield 14 %). **DSC** (T_{onset}, 5 °C min^{-1}): 172 °C (dec.); **IR** (KBr, cm^{-1}): $\tilde{\nu}$ = 3424 (w), 3160 (m), 3150 (m), 3039 (w), 2958 (w), 2322 (vw), 1779 (vw), 1750 (vw), 1647 (w), 1596 (vs), 1588 (vs), 1482 (m), 1462 (m), 1434 (m), 1414 (m), 1379 (w), 1301 (m), 1288 (m), 1200 (m), 1162 (s), 1143 (w), 1080 (vs), 1055 (m), 1005 (vs), 972 (m), 892 (w), 876 (w), 735 (m), 718 (s), 682 (w), 647 (m); **EA** ($C_4H_{10}CuN_{16}O_4$, 438.69) calcd.: C 16.43, H 1.84, N 51.09 %; found: C 16.52, H 2.10, N 50.69 %; **impact sensitivity**: 40 J; **friction sensitivity**: > 360 N.

14.7 Conclusion

From this experimental study the following conclusions can be drawn:

- 1,5-Bistetrazoles can be synthesized by the reactions of 5-aminotetrazoles, triethyl orthoformate and sodium azide in glacial acetic acid.

- By using 5-amino-1*H*-tetrazole as starting material 1,5-bistetrazole monohydrate (**152**·H_2O) is obtained. Recrystallization from half-conc. hydrochloric acid leads to highly explosive and sensitive water-free 1,5-bistetrazole (**152**). 2-Methyl-5-aminotetrazole leads to 2-methyl-1,5-bistetrazole. The reaction fails by using 1-methyl-5-aminotetrazole due to the sterical hindrance of the methyl-group.

- 1,5-Bistetrazole monohydrate (**152**·H_2O) can be easily deprotonated, which was proofed by the reaction with ammonia solution as well as sodium and potassium hydroxide yielding ammonium 1,5-bistetrazolate (**154**), sodium 1,5-bis-tetrazolate dihydrate (**155**) and potassium 1,5-bistetrazolate dihydrate (**156**).

- To investigate the ligand properties of **152** and **154**, three different copper complexes have been synthesized: $[Cu(1,5\text{-}BT)_2(H_2O)_4]$ (**157**), $[Cu(1,5\text{-}BT)_2(H_2O)_2(NH_3)_2]$ (**158**) and $[Cu(2Me\text{-}1,5\text{-}BT)Cl_2]$ (**159**). **152** as well as **154** do not act as a bidentate ligand.

- Single crystals of **152**, **152**·H_2O and **153**–**159** were determined by low temperature X-ray diffraction.

- **152**, **154** as well as deprotonated **152** do not act as bidentate ligands in copper(II) complexes.

- The energetic properties of **152**–**159** have been discovered. **152** is extremely sensitive towards impact and friction. The sensitivities are even higher than that observed for 5-azido-1*H*-tetrazole. Therefore it can be concluded, that 5-azidotetrazoles cannot be stabilized by the addition of HCN. Also **152**·H_2O, **153** and **154** are energetic materials with moderate sensitivities towards outer stimuli. The heats of formation of **152**, **152**·H_2O, **153** and **154** were calculated by the atomization energy method resulting in highly positive values.

- The calculated (EXPLO5) detonation parameters of **152**, **152**·H_2O, **153** and **154** are higher than those of TNT but lower than those of RDX.

- **154** was investigated by an *Koenen steel sleeve test* using an orifice of 10 mm. The steal sleeve has been fragmentated into more than 10 pieces.

- According to its (**154**) high nitrogen content of 81.27 %, its great combustion energy and also suitable good handling properties, ammonium 1,5-bistetrazolate may be a promising compound in solid propellant charges.

- Metal salts of 1,5-bistetrazole, including the copper complexes, are promising smokeless colorants for pyrotechnical compositions.

Chapter 15.

Bis(tetrazolyl)amines

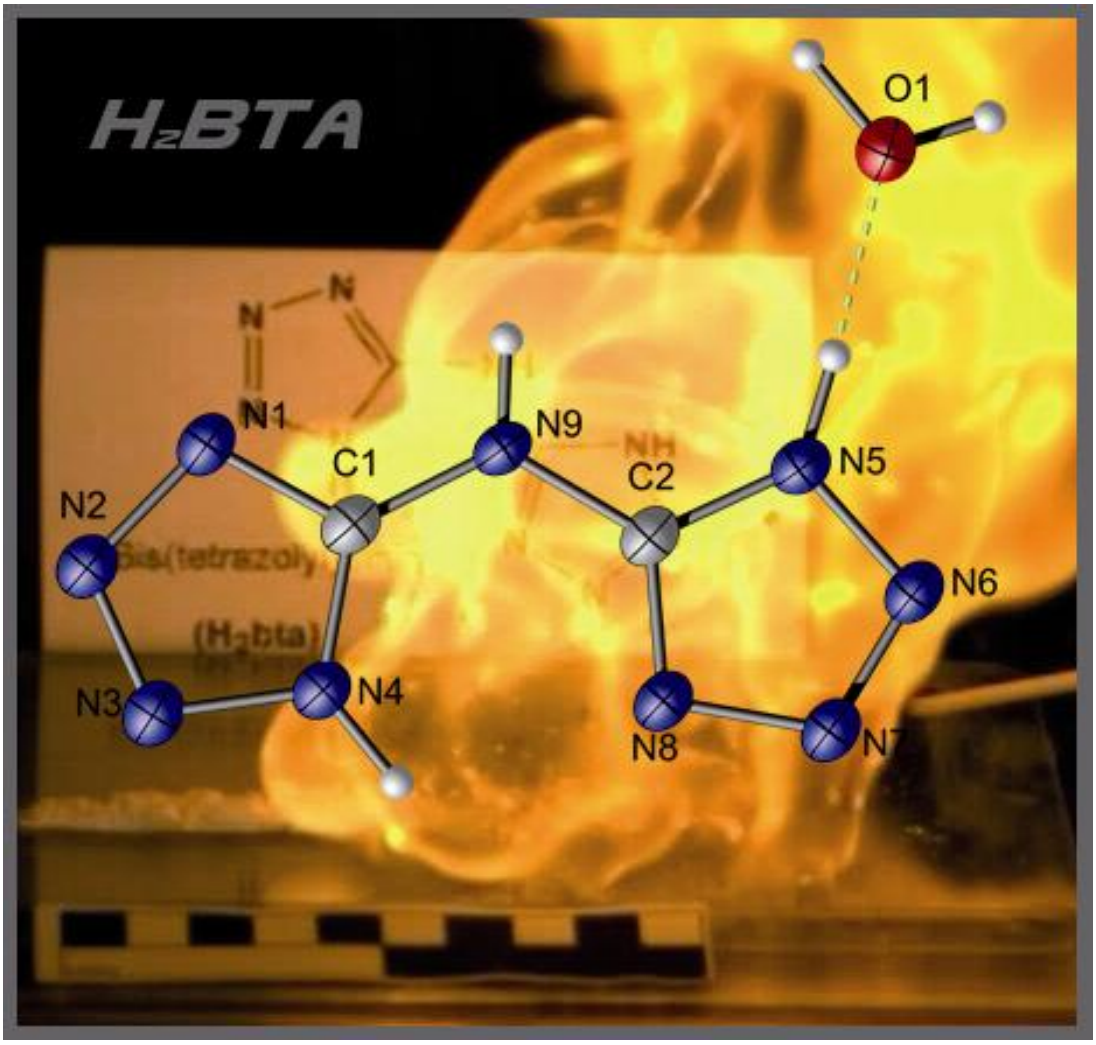

15.1 Introduction

In the continuous search for novel, green, energetic materials with high nitrogen but low carbon content, several groups around the world are currently investigating HEDMs (**H**igh **E**nergy **D**ense **M**aterials), based on tetrazoles. These energetic materials are applicable in low-smoke producing pyrotechnic compositions,[329] gas generators,[424] propellants,[425] high explosives,[279] and primers in primer charges (PC).[279] In particular, derivatives of tetrazole-5-yl-amines (**Figure 15.1**) are very promise and display low sensitivities and high thermal stabilities.

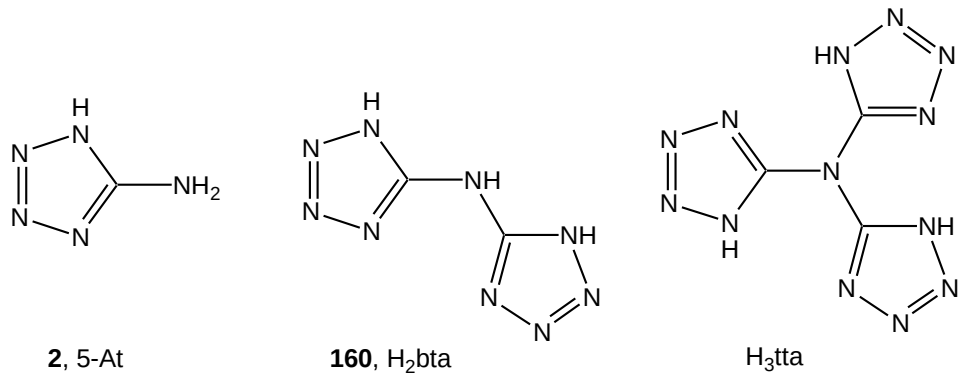

2, 5-At **160**, H_2bta H_3tta

Figure 15.1 Feasible tetrazol-5-yl-amines: 5-amino-1*H*-tetrazole (**2**), 5,5’-bis(1*H*-tetrazolyl)amine (**160**), 5,5’,5’’-tris(1*H*-tetrazolyl)amine

The *mono*-tetrazolyl-substituted 5-aminotetrazole (**2**, 5-At) represents a valuable building-block for the preparation of tetrazole-based high energetic materials, which can be seen in al chapters of this thesis. Metal salts of 5,5’-bis(1*H*-tetrazolyl)amines (**160**, H_2bta) were described as useful colorants in pyrotechnic compositions by Highsmith *et al.* [426] and Hiskey *et al.*.[427] In addition, several nitrogen-rich salts such as ammonium, hydrazinium, and guanidinium derivatives have been synthesized in our research group but were recently published as energetic materials by Shreeve *et al.*.[3c] The parent compound has only been sparingly described in the literature.[387b] To date, there are no reports on tris(tetrazolyl)amine (H_3tta). This may be due to the influence of electronic and/or steric factors which prohibit a viable synthesis.

A suitable precursor for the synthesis of **160** is the non-linear pseudohalide dicyanamide anion ($N(CN)_2^-$). The first synthesis of **160**, obtained as a monohydrate, was described by Norris *et al.* by refluxing sodium dicyanamide, sodium azide, and trimethylammonium chloride in water.[428] Currently, there are three synthetic

procedures for **160**, which are shown in **Scheme 15.1**: (1) The *in situ* reaction of hydrazoic acid (prepared form sodium azide and a weak acid like trimethylammonium chloride, boric acid, ammonium chloride) with sodium dicyanamide,[429] (2) the reaction of sodium dicyanamide with sodium azide in the presence of a catalyst like zinc chloride, bromide or perchlorate, followed by an acidic work-up,[430] and (3) the reaction of **2** with cyanogen bromide under base-catalyzed conditions forming the 5-cyaniminotetrazolinediide anion (CIT^{2-}),[387] followed by a subsequent cycloaddition of hydrazoic acid under acidic conditions.

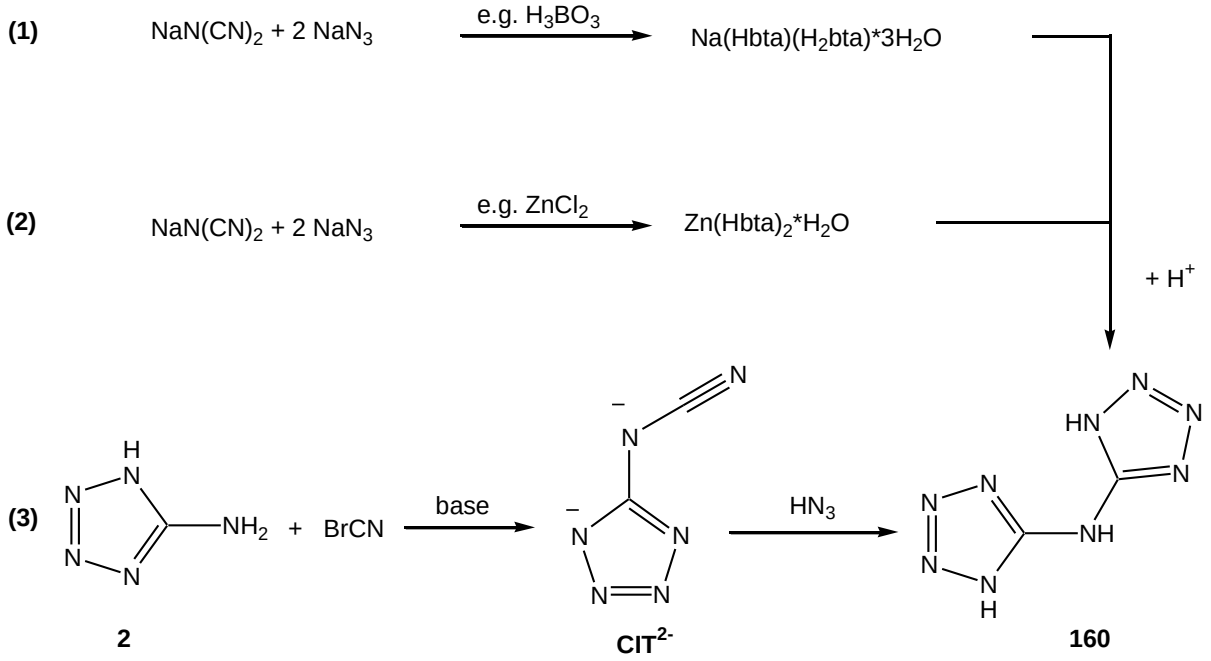

Scheme 15.1 Protocols for the synthesis of **160**.

Surprisingly, **160** has only been poorly characterized and the chemistry of methyl-derivatives of **160** has not been investigated. Therefore, a modified synthesis and full characterization of 5,5’-bistetrazolylamine **160** and its monohydrate **160**·H_2O is given in this chapter. Furthermore, the recrystallization of **160**·H_2O in DMSO resulted in the formation of **160**·H_2O·DMSO. In addition the results of the methylation reaction of **160** with MeI under basic conditions yielding the 5,5’-bis(2-methyl-tetrazolyl)amine (**161**, Me_2bta) as the main product are described.[347] The subsequent reaction of **161** with Me_2SO_4 under basic conditions afforded the 5,5’-bis(2-methyl-tetrazolyl)methylamine (**162**, Me_3bta) in good yields. Lastly, the two 1-substituted compounds 5-(2-methyltetrazolyl)-5’-(1*H*-tetrazolyl)amine (**163**) and 5-(2-ethyltetrazolyl)-5’-(1*H*-tetrazolyl)amine (**164**) have been obtained as byproducts during the work on this

thesis. All compounds were obtained in high purities as colorless, crystalline materials. The molecular structures of all compounds were confirmed by means of X-ray investigations at low temperature. Initial safety testing and energetic properties are reported. The cheap and facile synthetic route, high thermal stability, and low sensitivities of **160** and its derivatives bode well for the application of these compounds for use in novel propellant systems, pyrotechnic formulations [431] and/or in high-energy-capacity transition metal complexes.[157,158]

15.2 Synthesis

In contrast to the previously reported synthesis of **160**·H_2O by Norris *et al.*,[387b] **160**·H_2O is obtained in high yields and high purity by the reaction of sodium dicyanamide with two eq. of sodium azide and hydrochloric acid (**Scheme 15.2**). The reaction was performed in an aqueous ethanolic solution by slow addition of diluted hydrochloric acid at 80 °C in the course of 4 h and subsequently refluxing of the reaction mixture for further 48h.[354] Compound **160**·H_2O is insoluble in common organic solvents such as CH_2Cl_2, diethyl ether or THF and dissolves only poorly in MeOH or EtOH when heated. **160**·H_2O is soluble in water or mineral acids (e.g. HCl or $HClO_4$) when warmed. Single crystals of **160**·H_2O were obtained by recrystallization from 20 % perchloric acid. Recrystallization from DMSO yielded the adduct **160**·H_2O·DMSO. Anhydrous **160** is obtained when **160**·H_2O is dehydrated under vacuum (24 h, 10^{-2} mbar) at elevated temperature (120 °C).

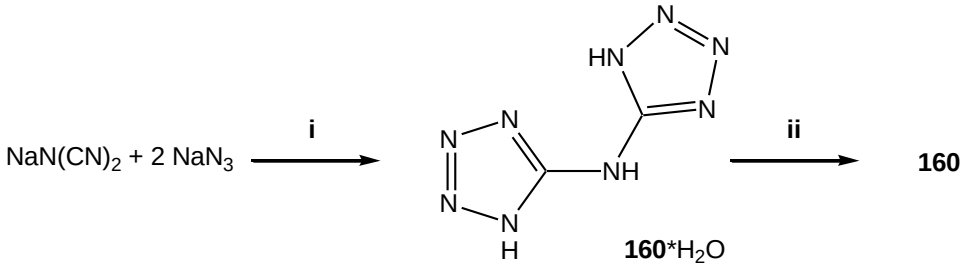

Scheme 15.2 Preparative route to **160**; i) EtOH/H_2O, 2M HCl. 80°C; ii) 120°C, 10^{-2} mbar.

Our two-step synthesis of **162** starts from **160**·H_2O (**Scheme 15.3**). In the first step, neutralization of an aqueous solution of **160** with two eq. sodium hydroxide at 60°C and addition of two eq. MeI in acetone, yields the dimethylated product **161** after 12 h of refluxing and further cooling to 4°C. The obtained precipitate was recrystallized from dilute HCl affording pure **161**. Interestingly, when the methylation was performed with

dimethyl sulfate *in lieu* of MeI, a mixture of 1- and 2-methylated isomers was obtained. However, the 1,1-, 1,2-, and 2,2-isomers were detected in the ^{13}C NMR spectrum of the reaction mixture. In the second step, **162** was obtained in 62% yield through methylation of **161** with an excess of dimethyl sulfate in refluxing aqueous sodium hydroxide solution. **162** is soluble in common solvents, e.g., ethanol, acetone, and acetonitrile, and was recrystallized from hot water yielding colorless needles.

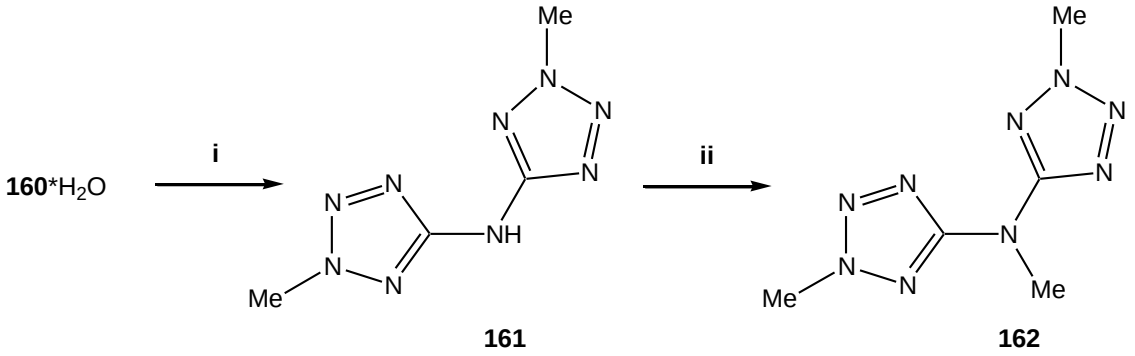

Scheme 15.3 Preparative route to **161** and **162**; i) NaOH, H_2O, MeI/acetone. 60°C; ii) NaOH, H_2O, Me_2SO_4, reflux.

The following products 5-(2-methyltetrazolyl)-5’-(1*H*-tetrazolyl)amine (**163**) and 5-(2-ethyltetrazolyl)-5’-(1*H*-tetrazolyl)amine (**164**) have been obtained accidentally as byproducts in the synthesis of the **152**·H_2O and **154** (**Scheme 15.4**), described in Chapter 14. However, both compounds should also be synthesized by the reaction of monodeprotonated **160** with MeI or EtI, respectively.

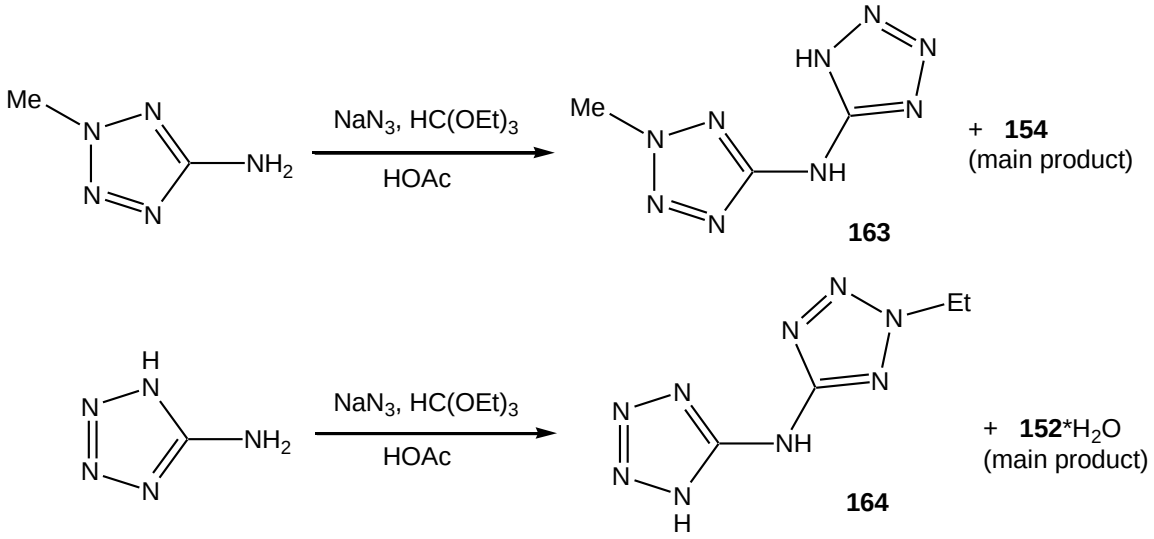

Scheme 15.4 Syntheses, in which **163** and **164** appear as by-products.

Although the mechanism could still not be clarified, a possible mechanism for the formation of **164** is given in **Scheme 15.5**. Firstly, a CN-moiety must be connected at the amino group of 5-aminotetrazole forming the acidic form of the CIT^{2-} anion (1*H*-tetrazol-5-yl-cyanamid). This cyano group may be react in a (2+3)-cycloaddition with an ethylazide moiety, which is formed by the reaction of ionic azide with triethyl orthoformate. The formation of **163** should proceed analogously. Finally, in the cycloaddition a ionic azide anion must react as the enophile.

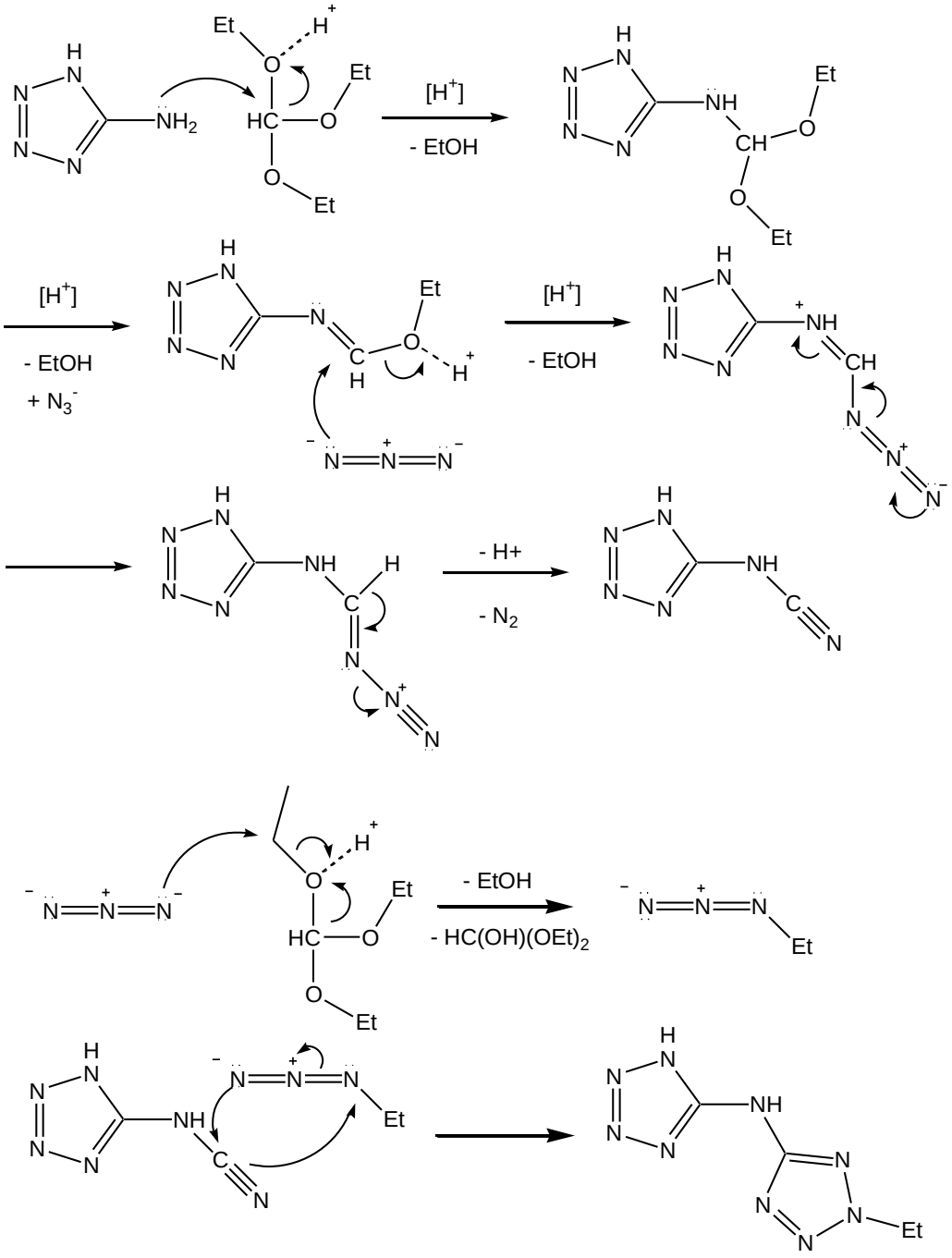

Scheme 15.5 Possible mechanism for the formation of 5-(2-ethyl-tetrazolyl)-5’-(1*H*-tetrazolyl)amine.

15.3 Crystal Structures

160, **160**·H_2O, **160**·H_2O·DMSO, **161**, **162**, **163** and **164** were determined by low temperature X-ray diffraction. Suitable crystals for the X-ray investigations were produced by recrystallization of **160**·H_2O and **161** from warm aqueous $HClO_4$ solutions (20 %). X-ray quality crystals of **160**·H_2O·DMSO were ascertained from warm DMSO solution and from water for **162**, **163** and **164**. Single crystals of water-free **160** were obtained from an organic tetranitromethane solution through a failed attempt to nitrate the secondary amine of **160**.

15.3.1 5,5’-Bis(1*H*-tetrazolyl)amine monohydrate (**160**·H_2O)

160·H_2O crystallizes in the monoclinic space group $P2_1/c$ with four molecules in the unit cell. Interestingly, the bistetrazolylamine molecules are planar (torsion angle C1–N1–C2–N9 = –179.6(1)°. The C–N bond distances to the amine nitrogen show lengths of N1–C1 = 1.370(2) Å and N1–C2 = 1.356(2) Å and are significantly shorter than C–N single bonds (1.47 Å) suggesting that, in addition to the planar geometry, there is a delocalization of the amine lone pair. The bond distances in the tetrazole rings are in the typical range of 1.29–1.36 Å between N–N single bonds (1.45 Å) and N=N double bonds (1.25 Å) and are given in **Table 15.1**.

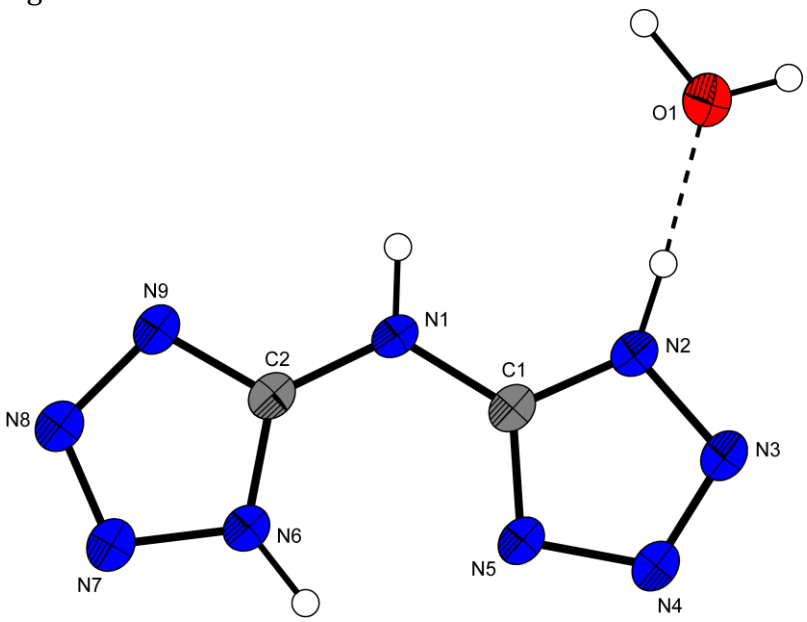

Figure 15.2 Molecular Structure of **160**·H_2O**.** Hydrogen atoms are shown as spheres of arbitrary radii and thermal displacements are set at 50 % probability.

160·H_2O forms a layer structure involving several hydrogen bonds (**Figure 15.3**). The strongest hydrogen bond is found between the water oxygen atom and the ring nitrogen (N2–H1···O1, D–H = 0.94(2), H···A = 1.69(2) Å, D···A = 2.623(2) Å, D–H···A = 177(2)°). Both water hydrogen atoms are directed to further bistetrazolylamine molecules with “D–A hydrogen bond distances” of about 2.8 Å. The distance between the layers is ~3.35 Å.

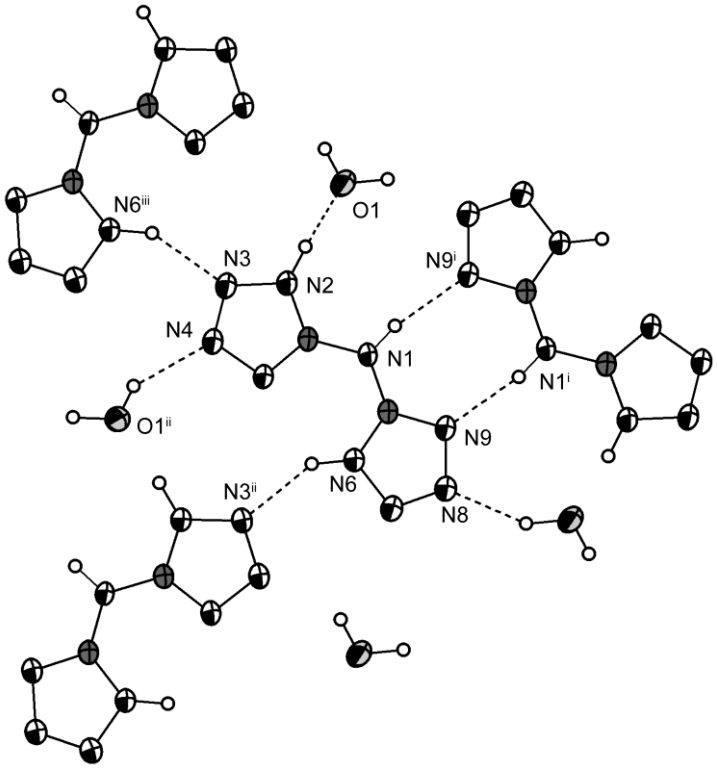

Figure 15.3 Hydrogen bonding of one **H_2bta** molecule within the layers; (i): 2–x, –y, –z; (ii) 1–x, 0.5+y, 0.5–z;(iii) 1–x, –0.5+y, 0.5–z).

15.3.2 5,5’-Bis(1*H*-tetrazolyl)amine (**160**)

Water-free **160** crystallizes in the orthorhombic space group *Pbca* with 16 molecules in the unit cell. The density of 1.861 g cm^{-3} is the highest of the investigated compounds in this chapter and is also higher in comparison to densities of other tetrazoles. The molecular structure shows a significant difference to that observed in **160**·H_2O and can be seen in **Figure 15.4**. In the structure of **160**, all hydrogen atoms are directed to one side of the molecule. This structure is anomalous and could not be achieved as a minimum in theoretical structure optimization. Once again, all hydrogen atoms participate in hydrogen bonds (**Figure 15.5**) and the molecule is nearly planar (torsion

angle C1–N1–C2–N9 = -4.4(3)°. The bonds to the tetrazole carbon atoms have lengths of C1–N1 = 1.365(2) Å and N1–C2 = 1.366(2) Å.

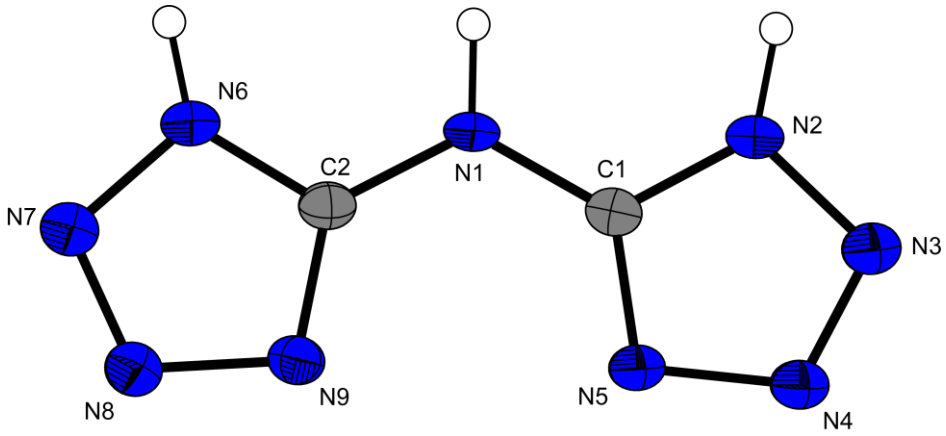

Figure 15.4 Molecular Structure of **160**. For clarity, only one molecule of the asymmetric unit is depicted. Thermal ellipsoids are drawn at the 50 % probability level and hydrogen atoms are shown as spheres of arbitrary radii.

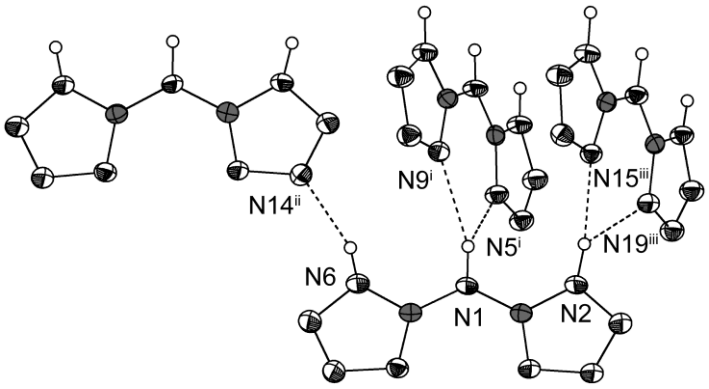

Figure 15.5 Selected Hydrogen bonds in **160**: (N1–H1···N9^{i}, 0.90(2), 2.18(2), 2.977(2) Å, 147(2)°; N1–H1···N5^{i}, 0.90(2), 2.39(2), 3.090(2) Å, 135(2)°; N6–H6···N14^{ii}, 0.87(2), 2.09(2), 2.914 (2) Å, 159(2)°; N2–H2···N15^{iii}, 0.92(2), 2.02(2), 2.871(2) Å, 152(2)°; N2–H2···N19^{iii}, 0.92(2), 2.48(2), 3.141(2) Å, 128(2)°; (i) 1.5–x, 0.5+y, z; (ii) 1.5–x, 0.5+y, z; (iii) 2–x, 0.5+y, 0.5–z.).

15.3.3 5,5’-Bis(1*H*-tetrazolyl)amine monohydrate DMSO adduct (**160**·H_2O·DMSO)

Recrystallization of **160**·H_2O from dimethyl sulfoxide yields colorless crystals containing, besides the bta molecule, one crystal water and one DMSO molecule,

abbreviated by **160**·H_2O·DMSO. This compound crystallizes in the monoclinic space group $C2/c$ with eight molecules in the unit cell and can be seen in **Figure 15.6**. The DMSO solvent molecule participates in a strong hydrogen bridge to the N2 atom through its oxygen atom (N2–H2···O2, 0.85(3), 1.89(3), 2.645(2) Å, 148(2)°). The distances and angles within the bistetrazolylamine are comparable to those found in the previously described H_2bta structures and are given also in **Table 15.1** and **Table 15.2**.

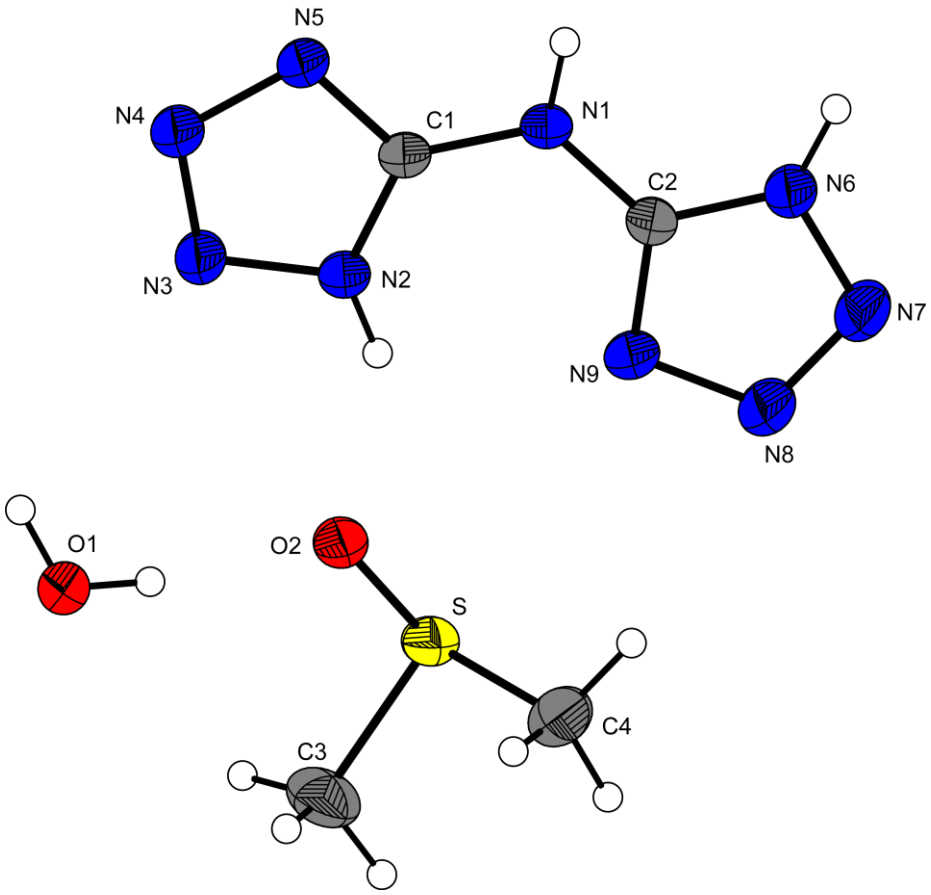

Figure 15.6 Molecular Structure of **160**·H_2O·DMSO. Thermal ellipsoids are drawn at the 50 % probability level and hydrogen atoms are shown as spheres of arbitrary radii.

15.3.4 5,5’-Bis(2-methyltetrazolyl)amine (**161**)

161 crystallizes in the monoclinic space group $P2_1/c$ with four molecules in the unit cell and a lower density of 1.530 g cm^{-3} in comparison to the structures of **160**. The molecular unit is shown in **Figure 15.7**.

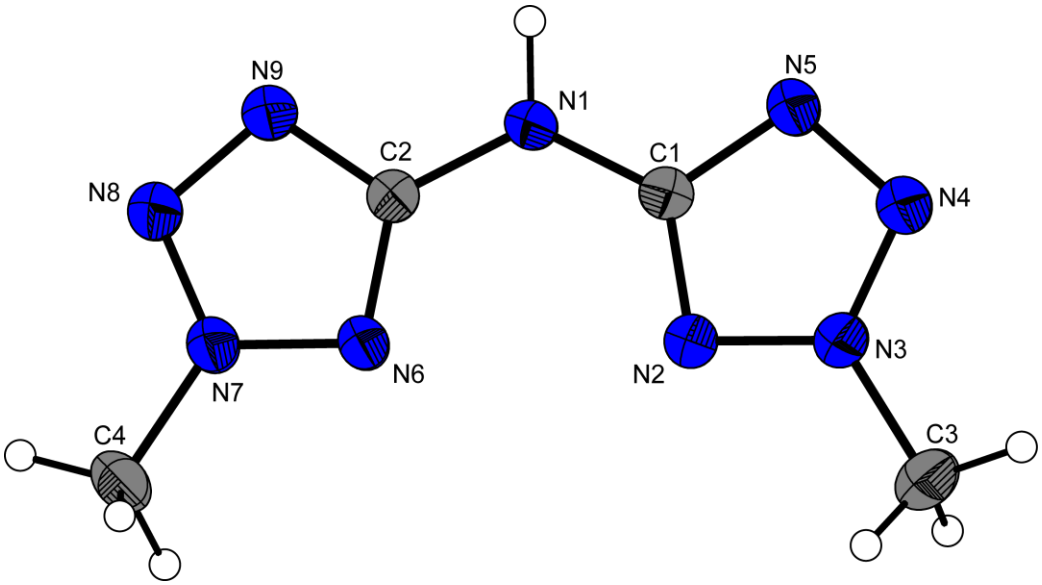

Figure 15.7 Molecular Structure of **161**. Thermal ellipsoids are drawn at the 50 % probability level and hydrogen atoms shown as spheres of arbitrary radii.

Both methyl groups are directed in the same direction. On the other side, a hydrogen bond between the nitrogen atoms N1 and N5 (N9–H7···N4^{i}: 0.92(2), 2.03(2), 2.946(2) Å, 174(2)°; (i) –x, 2–y, 2–z.) resulting in **R2,2(8)** graph sets. (**Figure 15.8**). Once again, the molecules are packed in layers with a larger distance of approximately 3.65 Å in comparison to those of **160**·H_2O.

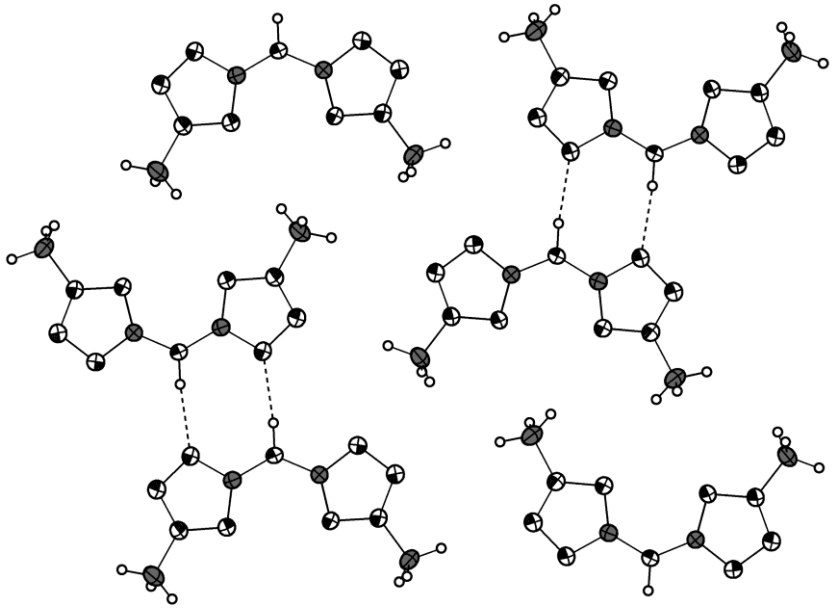

Figure 15.8 Formation of dimers in the layer structure of **161**.

15.3.5 5,5’-Bis(2-methyltetrazolyl)methylamine (**162**)

Me_3bta (**162**) crystallizes in the monoclinic space group $P2_1/m$ with 2 molecules in the unit cell. The atoms N1 and C5 on x, ¾, z are divided by the mirror plane generating the molecular unit shown in **Figure 15.9**.

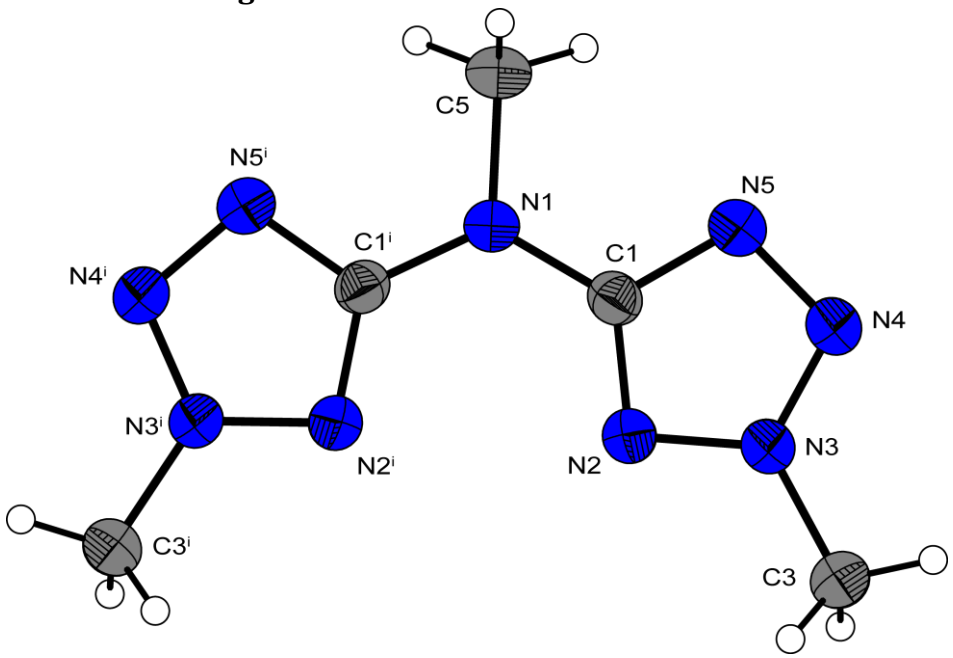

Figure 15.9 Molecular Structure of **162**. Thermal ellipsoids are drawn at the 50 % probability level and hydrogen atoms shown as spheres of arbitrary radii; (i) x, 1.5–y, z.

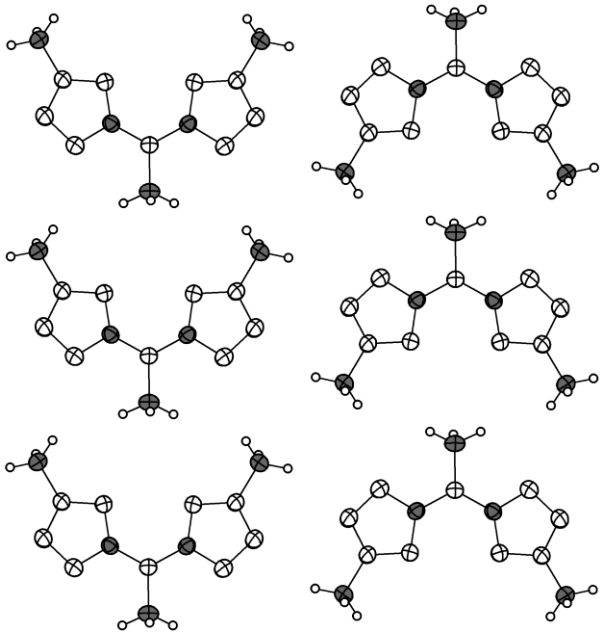

Figure 15.10 View along the *a*-axis on the Me_3bta molecules in the *b*-*c* layers.

The bond lengths and angles are in the same range as the previously discussed molecules, whereby the molecule is not observed to be planar (torsion angle N2–C1–N1–C1’ = 14.6(4)°). Me_3bta crystallizes in a layer structure (**Figure 15.10**), with only weak interactions between and within the layers. There are no hydrogen bonds since there are no N–H or O–H groups in these molecules, resulting in the lowest density of 1.51 g cm^{-3}, observed in this chapter.

15.3.6 5-(2-Methyltetrazolyl)-5’-(1*H*-tetrazolyl)amine (**163**)

Figure 15.11 shows the molecular structure of **163**, which crystallizes in the triclinic space group *P*–1 with two molecular moieties in the unit cell. The density of 1.665 g cm^{-3} was calculated between those observed for $H_2bta{\cdot}H_2O$ (1.693 g cm^{-3}) and Me_2bta (1.530 g cm^{-3}). The whole bistetrazolyl moiety is again found to be planar. The bond lengths and angles are in the expected range. The methyl group affects the structure only insignificantly. Also the bonds N5–C3 (1.363(2) Å) and N5–C1 (1.377(2) Å) are regulated and in agreement with other bis(tetrazolyl)amines.

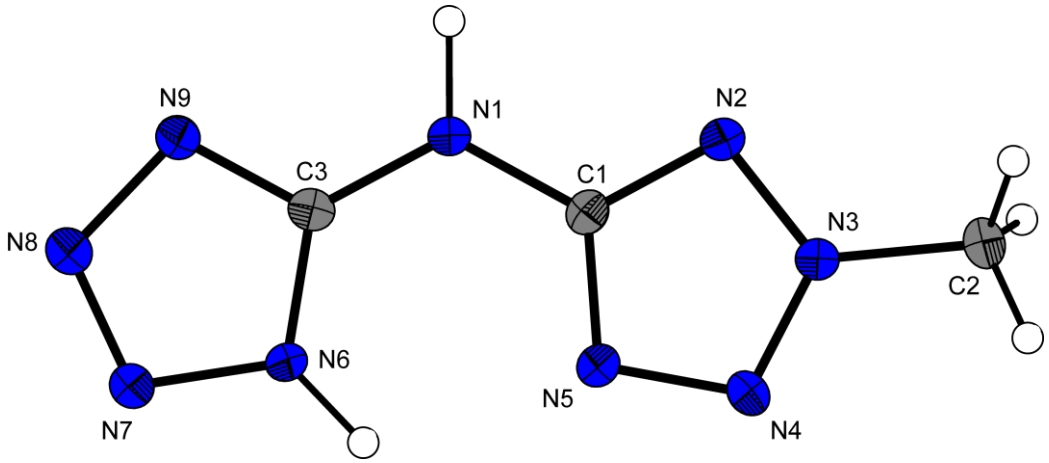

Figure 15.11 Molecular structure of 5-(2-methyltetrazolyl)-5’-(1*H*-tetrazolyl)amine. Thermal ellipsoids represent 50 % probability.

The packing of **163** is dominated by the formation of a layer structure. Inside the layers the two strong hydrogen bonds (**Figure 15.12**) N6–H6···$N3^{i}$ = 0.97(2), 2.15(2), 3.037(2) Å, 152(2)° and N5–N5···$N9^{ii}$ = 0.99(2), 1.84(2), 2.830 Å, 170°; (i) –1–x, 1–y, 1–z (ii) 1–x, 2–y, 1–z) form chains with a **C2,2(9)** graph set. In addition a important intramolecular hydrogen bond (N6–H6···N4 = 0.97(2), 2.17(2), 2.732(2) Å, 116(2)°)

with the graph set (**S1,1(6)**) can be found, which may also be a reason of the planar bistetrazolylamine moiety.

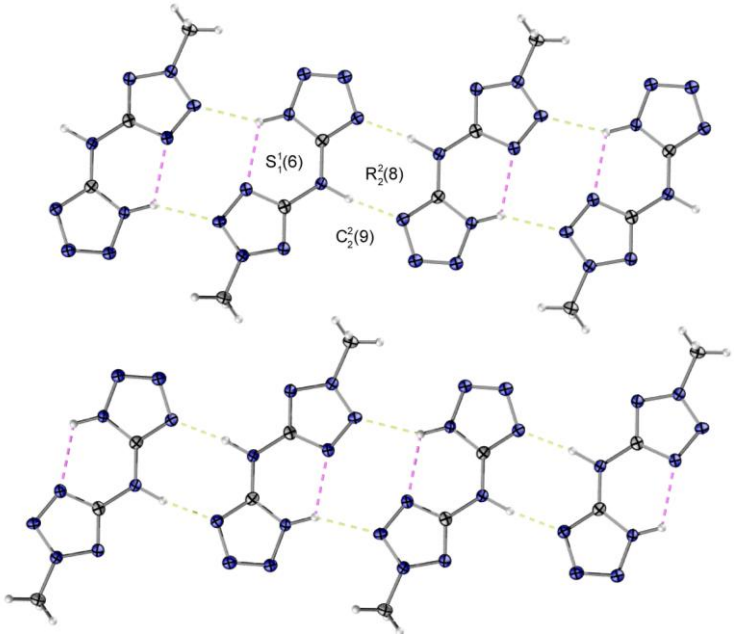

Figure 15.12 Hydrogen bonds in the layer structure of **163**. Important graph sets are drawn.

15.3.7 5-(2-Ethyltetrazolyl)-5’-(1*H*-tetrazolyl)amine (**164**)

164 crystallizes analogue to the former discussed structure of **163**. One molecule is shown in **Figure 15.13**. **164** also crystallizes in the triclinic space group *P*–1, with a slightly elongated metric. The density of 1.569 g cm^{-3} is lower than that of **163.** The molecular structure (bond distances and angles) as well as the packing is similar to that of **163**.

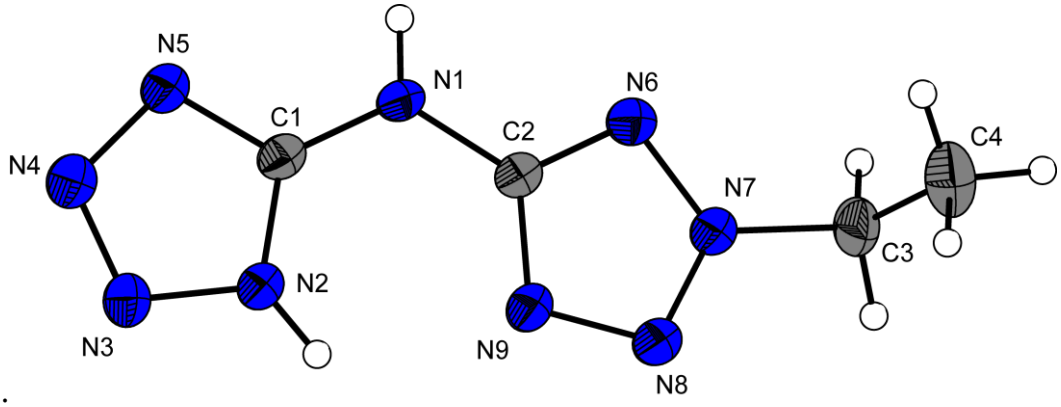

Figure 15.13 Molecular structure of 5-(2-ethyltetrazolyl)-5’-(1*H*-tetrazolyl)amine (**164**). Thermal ellipsoids represent 50 % probability.

Again the two hydrogen bonds N1–H1···N7^{i} = 0.87(2), 2.22(2), 3.034(2), 157(2)° and N5–H5···N4^{ii} = 0.83(2), 2.06(2), 2.882(2), 170(2)° (symmetry codes (i) –x, –y, –z (ii) 2–x, 1–y, –z) build chains (graph set: **C2,2(9)**) within the layers. (**Figure 15.14**) Again the intramolecular H-bond (N1–H1···N6 = 0.87(2), 2.25(2), 2.717(2), 114(2)°) yields to a planar condensed ring system.

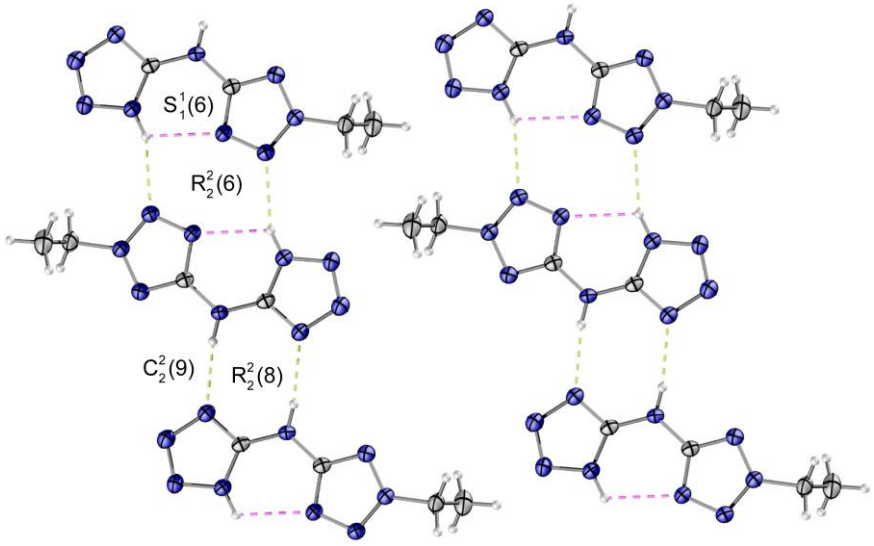

Figure 15.14 Hydrogen bonds in the layer structure of **164**. Important graph sets are drawn.

Table 15.1 Bond lengths [Å] of **160**, **160**·H_2O**, 160**·H_2O·DMSO**, 161**, **162**, **163** and **164**.

	160	**160**·H_2O	**160**·H_2O·DMSO	**161**	**162**	**163**	**164**
N1–C1	1.365(2)	1.370(2)	1.351(2)	1.366(2)	1.381(2)	1.377(2)	1.357(2)
N1–C2	1.366(2)	1.360(2)	1.358(2)	1.371(2)	1.381(2)	1.363(2)	1.374(2)
C1–N2	1.339(2)	1.330(2)	1.326(2)	1.329(2)	1.326(3)	1.337(2)	1.335(2)
C1–N5	1.317(2)	1.320(2)	1.316(2)	1.354(2)	1.354(3)	1.341(2)	1.325(2)
N2–N3	1.350(2)	1.353(2)	1.346(2)	1.347(2)	1.342(3)	1.338(2)	1.360(2)
N3–N4	1.287(2)	1.290(2)	1.278(2)	1.307(2)	1.307(3)	1.312(2)	1.291(2)
N4–N5	1.368(2)	1.360(2)	1.360(2)	1.329(2)	1.328(3)	1.332(2)	1.366(2)
C2–N6	1.339(2)	1.338(2)	1.322(3)	1.327(2)	1.326(3)	1.345(2)	1.330(2)
C2–N9	1.319(2)	1.323(2)	1.312(2)	1.349(2)	1.354(3)	1.326(2)	1.339(2)
N6–N7	1.352(2)	1.358(2)	1.348(2)	1.344(2)	1.342(3)	1.368(2)	1.337(2)
N7–N8	1.287(2)	1.286(2)	1.284(2)	1.312(2)	1.307(3)	1.296(2)	1.309(2)
N8–N9	1.371(2)	1.364(2)	1.361(2)	1.327(2)	1.328(3)	1.372(2)	1.336(2)
N3–C3				1.457(2)	1.454(3)	1.463(2)	

N7–C4		1.451(2)	1.454(3)		1.473(2)
N1–C5			1.468(4)		

Table 15.2 Bond angles [°] of **160**, **160**·H_2O**, 160**·H_2O·DMSO**, 161**, **162**, **163** and **164**.

	160	**160**·H_2O	**160**·H_2O·DMSO	**161**	**162**	**163**	**164**
C1–N1–C2	123.3(2)	122.5(1)	123.6(2)	126.4(1)	122.5(3)	123.3(2)	123.3(1)
N2–C1–N1	122.5(2)	124.4(1)	127.7(2)	127.0(1)	126.6(2)	122.9(2)	127.2(1)
N2–C1–N5	109.5(2)	110.2(1)	108.9(2)	113.1(1)	113.1(2)	114.0(2)	108.6(1)
N1–C2–N6	122.1(2)	126.8(1)	124.2(2)	127.0(1)	126.6(2)	127.2(2)	122.9(1)
N6–C2–N9	109.3(2)	109.1(1)	110.1(2)	113.7(1)	113.1(2)	109.0(2)	114.2(1)

15.4 Spectroscopy

The 5,5’-bistetrazolylamines **160**, **161**, and **162** were characterized and identified by IR, Raman and **NMR spectroscopy** as well as mass spectrometry and elemental analysis. The ^{1}H and ^{13}C NMR experiments were measured in d_6-DMSO at 25 °C. The ^{1}H NMR spectrum for **160** depicts a broad resonance (due to fast proton exchange) appearing at 11.92 ppm, a typical value for tetrazole protons.[432] The proton of the secondary amine is deshielded due to electronic effects of the tetrazole substituent and appears at 9.53 ppm. After methylation of **160**, the proton of the secondary amine in **161** is further deshielded and appears at 10.91 ppm. The range of resonances for methyl substituents is consistent with literature data [165]) and these protons are more deshielded for the methyl-azoles (4.27 (**161**) and 4.29 (**162**) ppm) than for the tertiary amine in **162** (3.60 ppm). The ^{13}C chemical shift can be used to distinguish between 1,5- and 2,5-disubstituted tetrazoles. The chemical shift for the tetrazole carbon atom in the 2,5-isomers is found at a higher frequency, typically with values greater than 160 ppm (162.7 (**161**) and 164.6 (**162**) ppm) for methyl-derivatives. The resonances of C-5 for the corresponding 1,5-isomers are expected to range from 145–160 ppm. Similar results are observed for the methyl group shifts. Once again, the 2,5-isomers display higher resonances (40.1 (**161**) and 40.3 (**162**) ppm) compared to those expected for the more shielded 1,5-isomers.[433]

The ^{15}N NMR shifts and the absolute values of the ^{15}N–^{1}H NMR coupling constants are presented in **Table 15.3**. The spectra of compounds **160**, **161**, and **162** are depicted in

Figure 15.15. Our assignments were mainly based on the analysis of the $^{15}N–^{1}H$ NMR coupling patterns and on previous investigations. In agreement with the correlations between ^{15}N NMR chemical shifts and electron densities at the nitrogen atoms, the ^{15}N NMR chemical shifts become increasingly more negative for 2,5-disubstituted tetrazoles: N3< N4< N1< N2. In the proton-coupled spectrum of **161** and **162**, the N1, N2, and N3 signals appear as quartets with $^{15}N–^{1}H$ coupling constants that are similar in magnitude, resulting from coupling to protons of the *N*-Me group. For **162**, the N5 signal also appears as a quartet due to coupling to protons of the *C*-Me group.

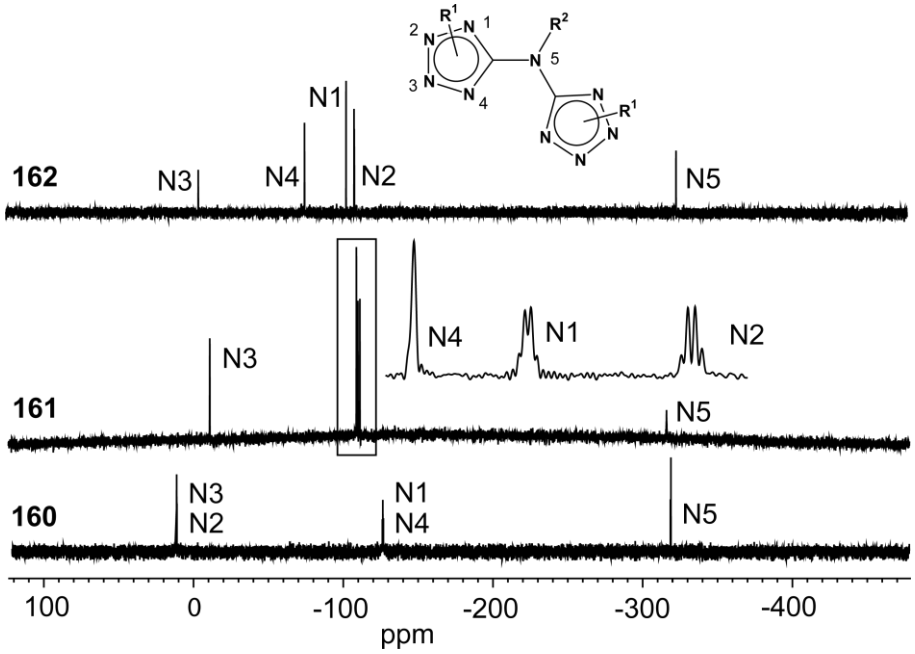

Figure 15.15 ^{15}N NMR spectra of compounds **160**, **161** and **162**.

Table 15.3 ^{15}N NMR chemical shifts (δ, ppm) and $^{15}N–^{1}H$ NMR coupling constants (Hz) for compounds **160**, **161** and **162**.

	N1	N2	N3	N4	N5
160[a]	–123.8	–17.9	---	---	–315.7
161[b]	–110.2	–111.5	–11.3	–109.2	–316.4
	q, ^{3}J = 1.9	q, ^{2}J = 2.1	q, ^{3}J = 1.9		
162[a]	–104.0	–110.5	–5.2	–76.2	–324.5
	q, ^{3}J = 1.9	q, ^{2}J = 2.2	q, ^{3}J = 1.9		q, ^{2}J = 2.2

[a] in d_6-DMSO; [b] in CF_3COOH.

Vibrational spectroscopy is another suitable method for identifying bis(tetrazolyl)-amines. The IR and Raman spectra (**Figure 15.16**) of the investigated compounds are characteristic for 5-aminotetrazoles.[434] Assignments were performed with the help of a frequency analysis after calculating (B3LYP/cc-pVDZ) the optimal structure with the GAUSSIAN03 software. Compared to the characteristic bands located at 1656 and 1556 cm^{-1}, assigned to the $\nu_{asym}(C_{tet}–N–C_{tet})$ and $\nu_{sym}(C_{tet}–N–C_{tet})$ stretching vibrations in **160**·H_2O, the corresponding bands are shifted to lower frequencies in the methylated compounds by approximately 8 to 12 cm^{-1}. Further bands can be attributed to the stretching vibrations of the N=N (1454 cm^{-1}), C=N (1352, 1337 cm^{-1}), and N–N (1282, 1268 cm^{-1}) bonds in the vibrational spectra of **160**·H_2O.[435] The IR and Raman spectra of the investigated compounds have in common the bands for the stretching and bending modes of the C–H (2950–3150 cm^{-1}) and N–H (3300–3450 cm^{-1}) groups from the protons of the tetrazole ring and of the secondary amino group.

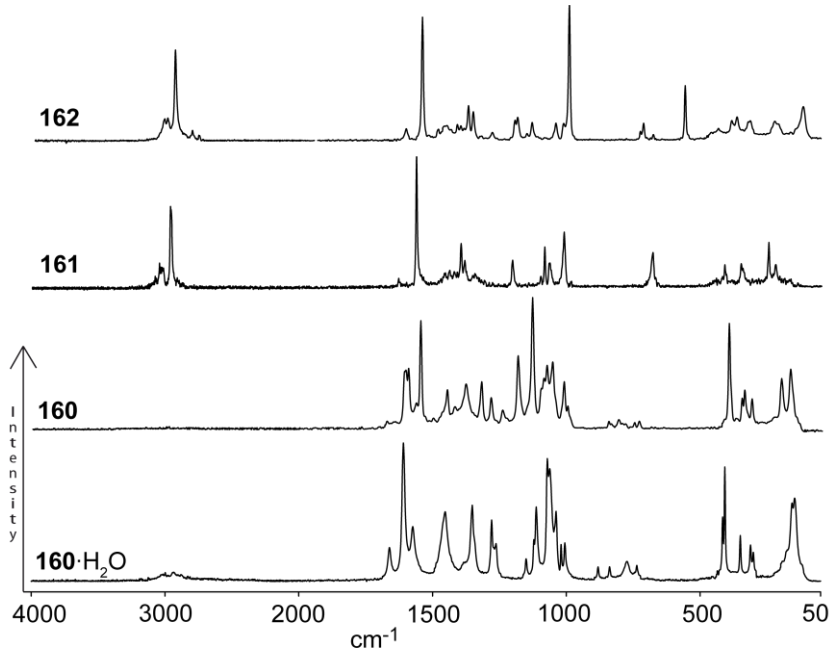

Figure 15.16 Raman spectra of compounds **160**·H_2O, **160**, **161** and **162**.

15.5 Physico-Chemical Properties

15.5.1 Differential Scanning Calorimetry (DSC)

DSC measurements to determine the melt- and decomposition temperatures of **160**·H_2O, **160**, **161**, **162**, **163** and **164** were performed in covered Al-containers with a nitrogen

flow of 20 mL min^{-1} on a Perkin-Elmer Pyris 6 DSC, at a heating rate of 5 °C min^{-1}. The DSC plots in **Figure 15.17** show the thermal behavior of 1.0 mg of **160**·H_2O, **160**, **161**, **162**, **163** and **164** in the 50–400°C temperature range. Temperatures are given as onset temperatures. The loss of water in **160**·H_2O starts at around 145 °C. However, **160** and **160**·H_2O show the same decomposition temperatures of about 250 °C. **161** is temperature-stable up to 263 °C, whereby it melts under decomposition. **162** melts at 138 °C and starts to decompose at 236 °C. Also the monosubstituted derivatives **163** and **164** show high decomposition temperatures of 273 °C (**163**) and 256 °C (**164**). *The decomposition temperature of **163** is the highest one, observed for all neutral tetrazole derivatives in this thesis.*

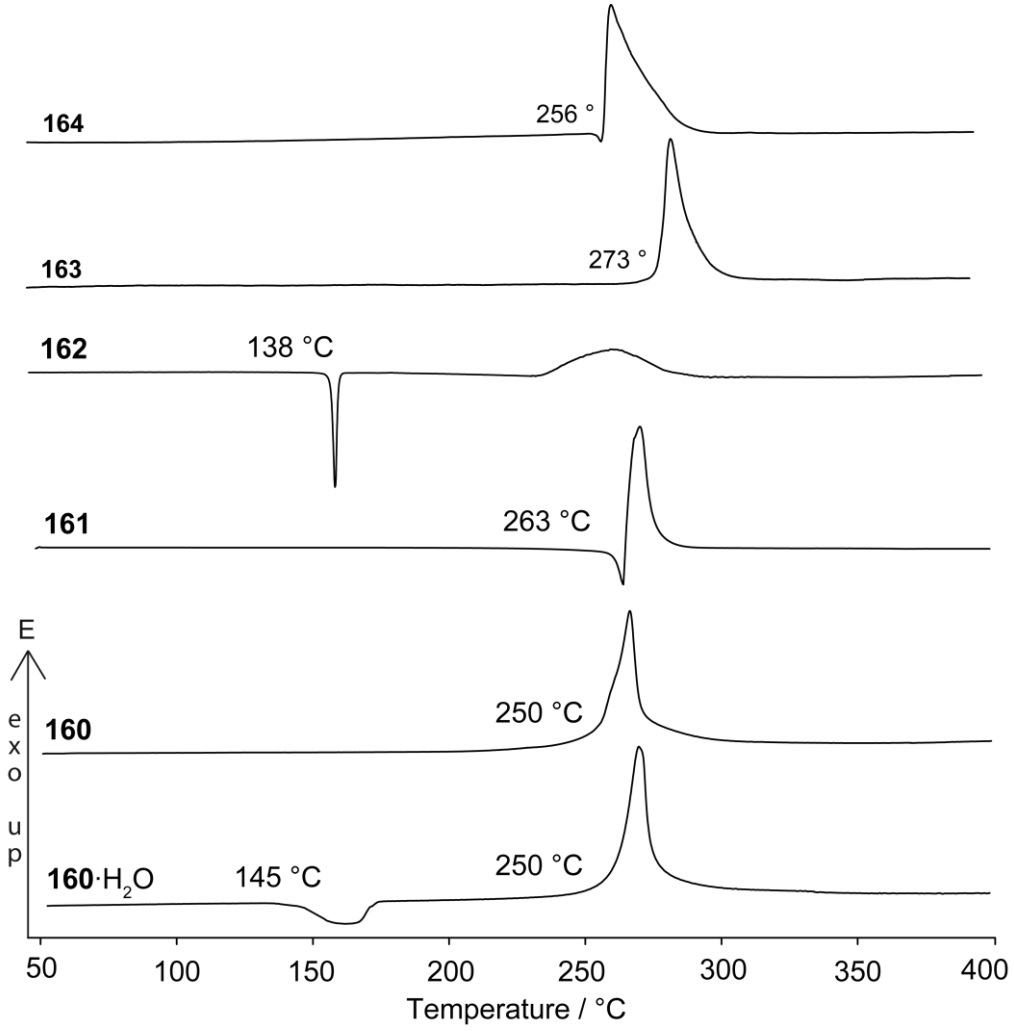

Figure 15.17 DSC thermograms (exo up) of compounds **160**·H_2O, **160**, **161**, **162**, **163** and **164** (heating rate of 5 ° min^{-1}).

15.5.2 Bomb Calorimetry

The heats of combustion of compounds **160**·H_2O, **160**, **161** and **162** were determined experimentally using a Parr 1356 bomb calorimeter. To achieve better combustion, the samples (~200 mg) were pressed with a defined amount of benzoic acid (~800 mg) forming a tablet. The standard molar enthalpy of combustion ($\Delta_c H°$) was derived from $\Delta_c H° = \Delta_c U + \Delta nRT$ ($\Delta n = \Delta n_i$ (products, g) – Δn_i(reactants, g); Δn_i is the total molar amount of gases in the products or reactants). The enthalpy of formation, $\Delta_f H°$, for each of the compounds was calculated at 298.15 K using Hess' law and the following combustion reactions. All investigated tetrazoles are strongly endothermic, which was expected by comparison with the literature ($\Delta_f H°$ **160**·H_2O: +203, **160**: + 633, **161**: + 350, **162**: + 586 kJ mol^{-1}). The influence of crystal water can be seen at the lower $\Delta_f H°$ of **160**·H_2O, in comparison to **160**.

The enthalpies of energetic materials are governed by the molecular structure of the compounds and, therefore, heterocycles with a higher nitrogen content, show higher heats of formation. From the experimentally determined heats of formation and densities obtained from single crystal structure X-ray diffraction, various thermochemical properties have been calculated using the EXPLO5 software (see below) and are summarized in **Table 15.4**.

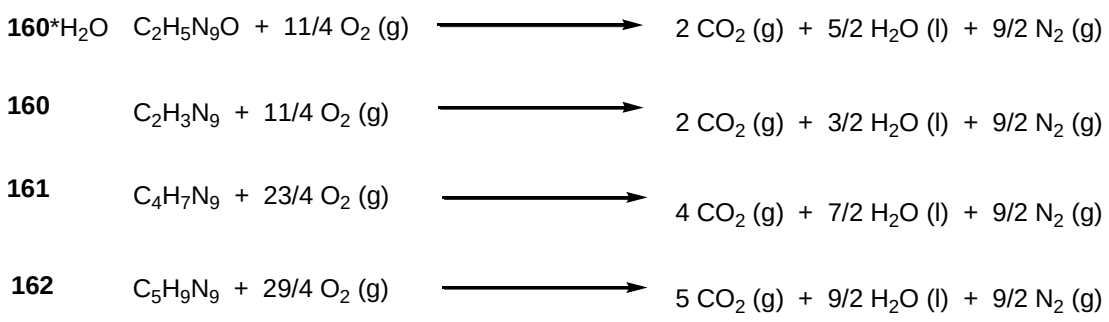

Scheme 15.6 Combustion reactions.

The heat of formation of water-free **160** was also calculated by the atomization energy method yielding a strongly positive value of 746 kJ mol^{-1}. By comparison with the experimentally determined one of 633 kJ mol^{-1}, the problem of meaningful heats of formation of nitrogen-rich materials can be seen. However, due to our experience we rather trust the calculated data.

15.5.3 Sensitivities

Since the investigated tetrazoles are energetic compounds with high nitrogen contents, the sensitivities toward friction and impact were tested. Powdered **160**·H_2O, **161, 163** and **164** are neither sensitive towards impact (< 100 J) nor friction (< 360 N), while **160** shows a low impact (> 30 J) and friction sensitivity (360 N). **162** is also only weak impact (30 J) but not friction sensitive. According to the “UN Recommendations on the Transport of Dangerous Goods”, compounds **160**·H_2O, **161**, and **162** are classified as “insensitive”, while water-free **160** is described as “less sensitive” but for all that should be handled with care and appropriate precautions. The electrostatic sensitivity tests were carried out using an electric spark tester ESD 2010EN (OZM Research).. The electrical spark sensitivities were determined to be 7.5 J (**160**), 12 J (**160**·H_2O), 10 J (**161**), and 20 J (**162**). These values are extremely low in comparison to commonly used secondary explosives like RDX (0.2 J).

15.5.4 Detonation Parameters

Some detonation parameters such as pressure, temperature, velocity, the heat of explosion, and the amount of gaseous decomposition products were calculated with the EXPLO5 V5.02 software. The results are given in **Table 15.4**. The most useful values for classifying new explosives are the detonation pressure and detonation velocity. In comparison with common explosives such as TNT (trinitrotoluol, $p_{C\text{-}J}$ = 202 kbar, $V_{Det.}$ = 7150 m s^{-1}), compounds **160**·H_2O, **160**, and **162** show higher detonation pressures (**160**·H_2O: 220, **160**: 343, **162**: 205 kbar) while compound **161** is lower (172 kbar). Due to the correlation of the detonation pressure and velocity, the same trend is observed regarding the detonation velocities. (**160**·H_2O: 7792, **160**: 9120, **161**: 7291, **162**: 7851 m s^{-1}). The calculated values of **160** are even higher than those of RDX (royal demolition explosive, $p_{C\text{-}J}$ = 340 kbar, $V_{Det.}$ = 8882 m s^{-1}). By using the calculated heat of formation of **160**, even higher values regarding the explosion performance were calculated. In this case a V_{Det} of 9275 m s^{-1} has been computed. To verify these data, the explosion performance of **160** was tested experimentally using a “Koenen” steel sleeve test.

15.5.5 Koenen Test

The explosion performance, under confinement of compound **160** ignited thermally, was investigated using a “Koenen test” steel sleeve apparatus. Data obtained from the Koenen test can be related to the performance of the compound and can be used to determine the shipping classification of a substance. TNT destroys the steel tube to a hole width 6 mm and RDX achieves this with a hole width of 8 mm. The result of the Koenen test can be seen in **Figure 15.18**. The test was performed with 24.0 g **160**, which was dried in a 160 °C oven for 24 h. Compound **160** destroyed the steel tube into more than 10 fragments using a hole of width 8 mm and also with a hole of 10 mm and it can, therefore, be assumed that compound **160** offers a greater explosion performance than RDX, which is in accordance with the calculated detonation values.

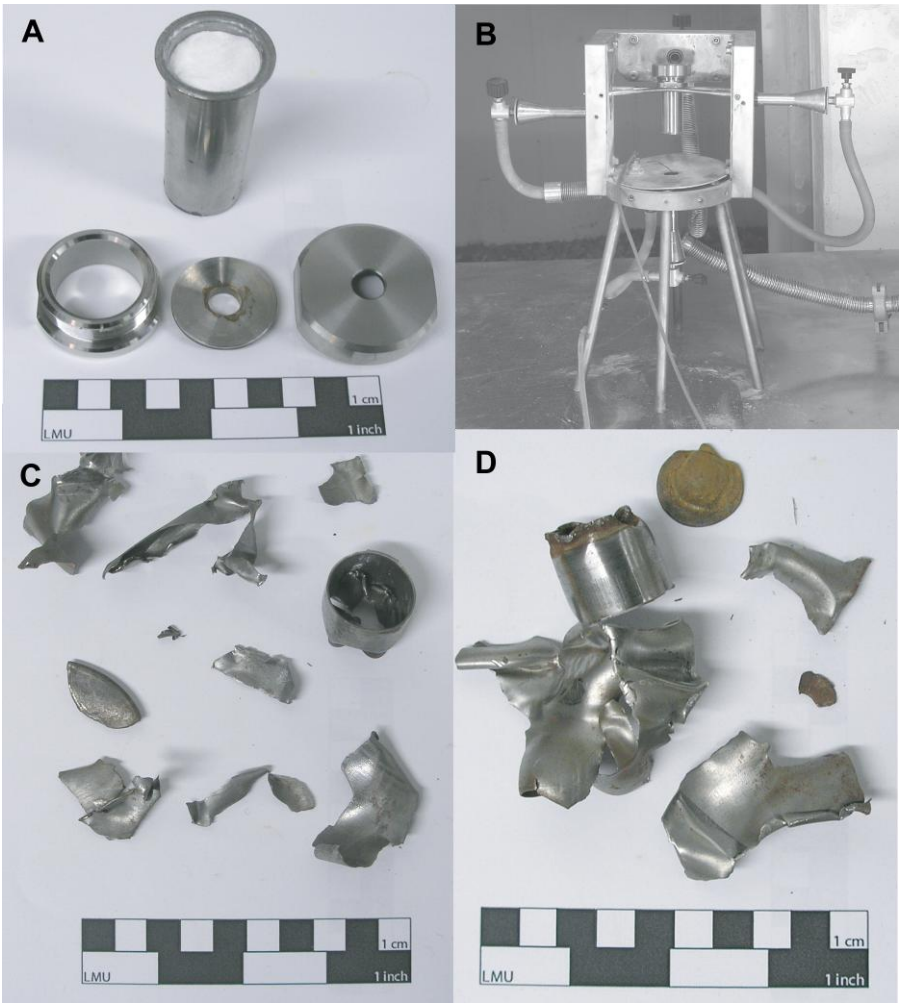

Figure 15.18 “Koenen test” of compound **160**. (A: filled steel sleeve; B: Koenen Test setup; C: collected fragments using a hole width of 8 mm; D: collected fragments using a hole width of 10 mm).

Table 15.4 Physico-chemical properties of **160**·H_2O, **160**, **161** and **162**.

	160·H_2O	**160**	**161**	**162**
Formula	$C_2H_5N_9O$	$C_2H_3N_9$	$C_4H_7N_9$	$C_5H_9N_9$
Molecular Mass (g mol^{-1})	171.15	153.13	181.19	195.21
Impact sensitivity (J)[a]	> 100	> 30	> 45	> 70
Friction sensitivity (N)[b]	> 360	> 360	> 360	> 360
ESD (J)[c]	12	7.5	10	20
Ω (%)[d]	73.67	82.34	69.6	64.59
N (%)[e]	–51.42	–57.47	–101.57	–118.85
Combustion	poor	very good	good	poor
$T_{dec.}$ (°C)[f]	263	263	263	232
Density (g cm^{-3})[g]	1.693	1.861	1.530	1.512
$-\Delta_{comb.}U$ (cal g^{-1})[h]	2392	2898	3865	4702
$-\Delta_{comb.}H$ (kJ mol^{-1})[i]	1714	1858	2932	3843
$\Delta_fH_m°$ (kJ mol^{-1})[j]	203	633(746)*	350	583
calculated values by EXPLO5:				
$-\Delta_EU°$ (J g^{-1})[k]	2985	4537 (4632)*	2684	3853
T_E (K)[l]	2555	3449 (3530)*	2184	2602
$p_{C\text{-}J}$ (kbar)[m]	220	343 (356)*	172	205
$V_{Det.}$ (m s^{-1})[n]	7792	9120 (9275)*	7291	7851
Gas vol. (L kg^{-1})[o]	808	753 (752)*	754	752

[a] BAM drophammer (grain size: 80–160 µm); [b] BAM friction tester (grain size: 80–160 µm); [c] OZM electric spark tester (grain size: 80–160 µm); [d] nitrogen content; [e] oxygen balance; [f] decomposition temperature from DSC (5 °C min^{-1}); [g] estimated from X-ray diffraction; [h] experimental (constant volume) combustion energy; [i] experimental molar enthalpy of combustion; [j] molar enthalpy of formation; [k] energy of explosion, EXPLO5 V5.02; [l] explosion temperature; [m] detonation pressure; [n] detonation velocity; [o] assuming only gaseous products; * values obtained by using the calculated heat of formation.

15.6 Experimental Part

CAUTION! *Tetrazole derivatives are considered energetic materials and tend to explode under certain conditions. Although we have not experienced any problems during the synthesis of the reported compounds, appropriate safety precautions should be taken at all*

*times, especially when manipulating **160**. Laboratories and personnel should be properly grounded and safety equipment such as Kevlar© gloves, leather coats, face shields, and ear plugs are necessary.*

*5,5’-Bis(1H-tetrazolyl)amine monohydrate (**160**·H_2O):* To a 2000 mL three-neck reaction flask containing a refluxing suspension of sodium dicyanamide (44.5 g, 0.5 mol), sodium azide (65.0 g, 1.0 mol), ethanol (400 mL), and water (250 mL) was added 2M HCl (750 mL) in the course of five hours. The reaction mixture was refluxed for a further 48 hours. After cooling to 0 °C in an ice bath and addition of conc. HCl (80 mL) **160**·H_2O was obtained as a fine colorless precipitate. The precipitate was filtered off and washed with small amounts of ethanol and diethyl ether and dried in vacuum. Yield: 75 g (0.43 mol, 88 %). The product can be recrystallized from dilute acids such as HCl or $HClO_4$. **DSC** (T_{onset}, 5 °C min^{-1}): 250 °C (dec.); **IR** (KBr, cm^{-1}): $\tilde{\nu}$ = 3456 (s), 3028 (s), 2932 (s), 2858 (s), 2671 (m), 2438 (m), 1796 (w), 1656 (vs), 1611 (s), 1556 (s), 1454 (m), 1352 (m), 1337 (m), 1282 (m), 1263 (m), 1154 (w), 1110 (m), 1072 (s), 1501 (s), 1036 (m), 1003 (m), 899 (m), 819 (m), 790 (m), 738 (m), 690 (m), 503 (m), 406 (w); **Raman** (1064 nm, 200 mW, 25 °C, cm^{-1}): $\tilde{\nu}$ = 3328 (11), 3120 (8, br), 1649 (9), 1618 (34), 1552 (54), 1480 (22), 1455 (17), 1370 (17), 1346 (15), 1267 (25), 1226 (26), 1151 (15), 1128 (15), 1073 (100), 1039 (42), 838 (7), 794 (17), 736 (9), 670 (7), 421 (22), 409 (48), 381 (9), 348 (20), 321 (48), 172 (100), 147 (46); **^{1}H NMR** (d_6-DMSO, 25 °C, ppm): δ = 11.92 (s, br), 9.53 (s, br); **^{13}C NMR** (d_6-DMSO, 25 °C, ppm): δ = 154.7 (C); **^{15}N{^{1}H} NMR** (d_6-DMSO, 25 °C, ppm): δ = –17.9 (N2), –123.8 (N1), –315.7 (NH); ***m/z*** (DEI^+): 153 (M^+–H_2O, 66), 128 (18), 127 (9), 97 (16), 96 (20), 70 (35), 69 (34), 68 (36), 57 (33), 53 (23), 43 (33), 42 (81), 41 (39), 29 (39), 28 (100); **EA** ($C_2H_5N_9O$, 171.15) calcd.: C 14.04, H 2.95, N 73.67 %; found: C 14.10, H 2.61, N 73.19 %; **impact sensitivity:** > 100 J; **friction sensitivity:** > 360 N; $\Delta_c U$: 2898 cal g^{-1}.

*5,5’-Bis(1H-tetrazolyl)amine (**160**):* Compound **160**·H_2O was dehydrated under vacuum (24 h, 10^{-2} mbar) at elevated temperature (120°C). **DSC** (T_{onset}, 5 °C min^{-1}): 250 °C (dec.); **IR** (KBr, cm^{-1}): $\tilde{\nu}$ = 3267 (m), 3136 (m), 3080 (m), 2934 (m), 1654 (vs), 1618 (s), 1607 (s), 1570 (s), 1547 (m), 1481 (m), 1445 (w), 1384 (w), 1321 (w), 1288 (w), 1228 (w), 1174 (w), 1133 (m), 1078 (w), 1057 (m), 1042 (m), 1014 (w), 835 (w), 806 (w), 749 (w), 719 (w), 600 (w); **Raman** (1064 nm, 200 mW, 25 °C, cm^{-1}): $\tilde{\nu}$ = 2986 (58), 1606 (47), 1595 (48), 1568 (22), 1550 (83), 1450 (32), 1422 (20), 1381 (37), 1322 (38), 1287 (27), 1243 (17), 1186 (57), 1132 (100), 1078 (50), 1057 (53), 1014 (38), 810 (13), 397

(81), 339 (32), 312 (26), 201 (41), 167 (47); **EA** ($C_2H_3N_9$, 153.11) calcd.: C 15.69, H 1.97, N 82.34 %; found: C 15.61, H 2.07, N 81.62 %; **impact sensitivity:** > 30 J; **friction sensitivity:** > 300 N; $\Delta_c U$: –4537 cal g^{-1}.

*5,5´-Bis(2-methyltetrazolyl)amine (**161**):* In a 500 mL three neck round bottom flask, **160**·H_2O (17.1 g, 0.1 mol) was neutralized with an aqueous NaOH solution (8.0 g, 0.2 mol in 100 mL water) and warmed to 60 °C until a clear dark-red solution was obtained. Methyl iodide (12.5 mL, 0.21 mol) in acetone (50 mL) was then added drop-wise to the reaction mixture. Afterwards the solution was heated under reflux for 12 hours. After cooling the reaction mixture (4 °C) compound **161** was obtained as colorless precipitate. The precipitate was filtered off and washed with acetone (2 x 30 mL) and dried in vacuum. Yield: 9.1 g (55 mmol, 55 %). The product can be recrystallized from dilute mineral acids such as HCl or $HClO_4$. **DSC** (T_{onset}, 5 °C min^{-1}): 263°C (dec.); **IR** (KBr, cm^{-1}): $\tilde{\nu}$ = 3417 (w), 3278 (m), 3194 (m), 3097 (m), 3049 (m), 2949 (w), 2890 (w), 2862 (w), 1644 (vs), 1565 (s), 1540 (s), 1465 (w), 1434 (w), 1417 (w), 1329 (w), 1202 (m), 1097 (w), 1055 (w), 1010 (w), 885 (w), 837 (w), 744 (m), 702 (w), 679 (w); **Raman** (1064 nm, 200 mW, 25 °C, cm^{-1}): $\tilde{\nu}$ = 3269 (4), 3197 (4), 3047(22), 3031(21), 2963 (81), 2821 (4), 1631 (7), 1563 (100), 1395 (8), 1455 (14), 1438 (14), 1419 (14), 1396 (33), 1381 (23), 1346 (11), 1204 (22), 1098 (14), 1084 (30), 1065 (24), 1011 (55), 748 (5), 680 (38), 446 (8), 386 (8), 348 (20), 247 (30), 222 (20); **^{1}H NMR** (d_6-DMSO, 25 °C, ppm): δ = 10.91 (s, NH), 4.27 (s, CH_3); **^{13}C NMR** (d_6-DMSO, 25 °C, ppm): δ = 162.7 (CN_4), 40.1 (CH_3); **^{15}N NMR** (CF_3–COOH, 25 °C, ppm): δ = –11.3 (N3, q, $^3J_{NH}$ = 1.86 Hz), –109.2 (N4, s), –110.2 (N1, q, $^3J_{NH}$ = 1.9 Hz), –111.5 (N2, q, $^2J_{NH}$ = 2.1 Hz), –316.4 (N5, s); ***m/z*** (DEI$^+$): 181 (M^+, 11), 153 (11), 96 (2), 82 (3), 67 (5), 56 (4), 53 (10), 43 (100), 42 (63), 39 (4), 28 (42), 27 (12), 15 (54); **EA** ($C_4H_7N_9$, 181.17) calcd.: C 26.52, H 3.89, N 69.59 %; found: C 26.50, H 3.93, N 69.27 %; **impact sensitivity**: > 45 J; **friction sensitivity**: > 360 N; $\Delta_c U$: –3865 cal g^{-1}.

*5,5´-Bis(2-methyltetrazolyl)methylamine (**162**):* Dimethyl sulfate (0.95 mL, 10 mmol) was slowly added to a stirred, warm (65 °C) solution of **161** (1.81 g, 10 mmol) and NaOH (0.40 g, 10 mmol) in H_2O (15 mL). The colorless mixture was heated for 2 h from which after cooling to RT the product **162** separated as a colorless precipitate. After filtration, **162** was washed with cold water and recrystallized. Yield: 1.41 g (7.2 mmol, 72 %). **DSC** (T_{onset}, 5 °C min^{-1}): 137 –139 °C, 236 °C (dec.); **IR** (KBr, cm^{-1}): $\tilde{\nu}$ = 3109 (w), 3038 (w), 2957 (w), 2576 (w), 2421 (w), 1968 (w), 1585 (s), 1553 (vs), 1471 (m), 1421 (m), 1385

(w), 1364 (w), 1293 (w), 1210 (m), 1167(m), 1147 (m), 1061 (w), 1009 (m), 745 (m), 735 (s), 697 (w), 666 (w), 580 (w); **Raman** (1064 nm, 200 mW, 25 °C, cm^{-1}): $\tilde{\nu}$ = 3038 (17), 3018 (18), 2961 (67), 1614 (11), 1553 (91), 1463 (13), 1425 (14), 1383 (27), 1366 (23), 1295 (8), 1202 (19), 1148 (15), 1060 (15), 1010 (100), 736 (15), 582 (42), 390 (19), 341 (16), 250 (16), 145 (27); **^{1}H NMR** (*d*$_6$-DMSO, 25 °C, ppm): δ = 4.29 (CH_3, s), 3.60 (N_sCH_3, s); **^{13}C NMR** (*d*$_6$-DMSO, 25 °C, ppm): δ = 164.6 (C2), 40.3 (C3), 36.8 (C1); **^{15}N NMR** (*d*$_6$-DMSO, 25 °C, ppm): δ = –5.2 (N3, q, $^{3}J_{N-H}$ = 1.9 Hz), –76.2 (N4, s), –104.0 (N1, q, $^{3}J_{N-H}$ = 1.9 Hz), –110.5 (N2, q, $^{2}J_{N-H}$ = 2.3 Hz), –324.5 (N5, q, $^{2}J_{N-H}$ = 2.3 Hz; **EA** ($C_5H_9N_9$, 195.22) calcd.: C 30.77, H 4.65, N 64.59 %; found: C 30.62, H 4.50, N 64.51 %; ***m/z*** (DEI): 195 [(M^+) (22)], 167 (9), 68 (8), 96 (48), 56 (21), 53 (12), 43 (100), 42 (37), 28 (34), 27 (8); **impact sensitivity**: > 70 J; **friction sensitivity**: > 360 N; $\Delta_c U$: –3853 cal g^{-1}.

*5-(2-Methyltetrazolyl)-5’-(1H-tetrazolyl)amine (**163**):* A solution of 2-methyl-5-amino-tetrazole (1.98 g, 0.02 mol) and sodium azide (1.56 g, 0.024 mol) in triethyl orthoformate (4.44 g, 0.030 mol) was prepared. Glacial acetic acid (8.40 g, 0.14 mol) was added drop wise and the reaction mixture was refluxed at 100 °C for 3 hours. After a crude product precipitated as colorless powder, 20 mL of 1N hydrochloric acid (0.02 mol) was added. The solvent was removed and the residue was dissolved in boiling benzene and filtered off. The 1,5-bistetrazole **153** was achieved via crystallization from the filtered solution as colorless needles with a reaction yield of 36 % (1.10 g). Before this, and after the addition of 1N hydrochloric acid, the solvent was removed from the reaction mixture. The residuum was dissolved in boiling water and filtered off, whereby **163** started to crystallize as colorless needles with a reaction yield of 24 % (0.80 g). **DSC** (T_{onset}, 5 °C min^{-1}): 273 °C (dec.); **IR** (KBr, cm^{-1}): $\tilde{\nu}$ = 3181 (vs), 3028 (s), 2889 (s), 2764 (s), 1663 (vs), 1570 (s), 1513 (s), 1436 (s), 1336 (m), 1292 (m), 1247 (m), 1199 (m), 1131 (w), 1084 (m), 1064 (m), 1027 (s), 1000 (m), 852 (w), 794 (m), 761 (m), 742 (m), 726 (s), 697 (s), 674 (s); **Raman** (1064 nm, 400 mW, 25 °C, cm^{-1}): $\tilde{\nu}$ = 3029 (6), 2986 (100), 2965 (30), 1648 (4), 1582 (18), 1521 (13), 1448 (6), 1316 (14), 1335 (14), 1297 (4), 1250 (4), 1204 (11), 1086 (6), 1060 (47), 1032 (14), 1005 (5), 858 (3), 786 (4), 698 (7), 455 (13), 366 (14), 318 (8), 282 (10), 144 (7); **^{1}H NMR** (*d*$_6$-DMSO, 25 °C, ppm): δ = 11.65 (s, 1H, C_2NH), 4.30 (s, 3H, CH_3); **^{13}C NMR** (*d*$_6$-DMSO, 25 °C, ppm): δ = 161.9 (C2, N_2C–N–H), 152.7 (C1, N_2C–N–Me), 41.4 (CH_3); ***m/z*** (DEI$^+$): 167.1 (M^+); **EA** ($C_3H_5N_9$, 167.13) calcd.: C 21.56, H 3.02, N 75.43 %; found: 21.52, H 3.17, N 75.43 %.

*5-(2-Ethyltetrazolyl)-5’-(1H-tetrazolyl)amine (**164**):* A 2000 mL three necked round bottom flask, equipped with a thermometer and a dropping funnel was charged with 5-aminotetrazole (21.3 g, 0.25 mol) and NaN_3 (78.0 g, 1.2 mol), which were suspended in triethyl orthoformate (196.4 g, 1.5 mol) and heated to 55 °C. Glacial acetic acid (500 mL, 8.74 mol) is slowly added under vigorous stirring, as a thick, white precipitate forms. After addition of the glacial acetic acid, the mixture is heated to 105 °C and the precipitate dissolves. It is now kept at 105 °C for 2 days under reflux conditions. The solution is allowed to cool down to room temperature and concentrated hydrochloric acid (118.3 g, 1.2 mol) is added dropwise. The mixture is filtered off and the solvent is removed from the filtrate in a rotary evaporator to give a viscous liquid, in which the product starts to precipitate. The precipitate was filtered off, stirred with water and filtered off again and recrystallized from ethanol to give 4.50 g (24.8 mmol, 10 % yield) 2-ethyl-bistetrazolylamine. **DSC** (T_{onset}, 5 °C min^{-1}): 256 °C (dec.); **IR** (KBr, cm^{-1}): $\tilde{\nu}$ = 3178 (vs), 3038 (s), 2861 (s), 1667 (vs), 1569 (vs), 1513 (vs), 1554 (s), 1355 (m), 1340 (m), 1318 (m), 1247 (m), 1223 (w), 1197 (m), 1129 (w), 1083 (s), 1057 (s), 1032 (s), 999 (m), 973 (m), 848 (w), 785 (s), 763 (s), 729 (s), 699 (m), 677 (s), 667 (s); **Raman** (1064 nm, 300 mW, 25 °C, cm^{-1}): $\tilde{\nu}$ = 3000 (25), 2954 (38), 1643 (9), 1579 (32), 1514 (22), 1447 (29), 1356 (17), 1338 (33), 1248 (6), 1225 (11), 1200 (26), 1098 (19), 1084 (21), 1058 (100), 1037 (50), 1002 (9), 978 (12), 852 (7), 774 (10), 667 (8), 436 (11), 371 (12), 299 (16), 281 (12); **^{1}H NMR** (d_6-DMSO, 25 °C, ppm): δ = 11.66 (s, NH), 4.59 (q, *J* = 7.4 Hz, CH_2), 1.50 (t, J = 7.4 Hz, CH_3); **^{13}C NMR** (d_6-DMSO, 25 °C, ppm): δ = 161.7(CN_4), 152.2 (CN_4), 48.9 (CH_2), 14.5 (CH_3); ***m/z*** (FAB$^+$): 182.2 $[M+H]^+$, 154.1 $[M–Et+H]^+$; **EA** ($C_4H_7N_9$, 181.16) calcd.: C 26.52, H 3.89, N 69.59 %; found: C 26.28, H 3.79, N 69.57 %; **impact sensitivity**: > 100 J; **friction sensitivity**: > 360 N ; **ESD**: > 2.5 J.

15.7 Conclusions

From this experimental study the following conclusions can be drawn:

- 5,5’-Bis-(1*H*-tetrazolyl)amine monohydrate (**160**·H_2O) can be synthesized in high yield and pure quality by the reaction of sodium dicyanamide and 2 eq. sodium azide in aqueous/ethanolic solution by adding diluted hydrochloric acid. 5,5’-Bis(2-methyl-tetrazolyl)amine (Me_2bta, **161**) and 5,5’-bis(2-methyltetrazol-

yl)methylamine (Me_3bta, **162**) can be obtained by methylation of deprotonated H_2bta and Me_2bta, respectively.

- H_2bta·H_2O can be dehydrated at 120 °C under reduced pressure ($1 \cdot 10^{-2}$ mbar) yielding water-free H_2bta (**160**).

- The mono-substituted bis(tetrazolyl)amines 5-(2-methyltetrazolyl)-5’-(1*H*-tetrazolyl)amine (**163**) and 5-(2-ethyltetrazolyl)-5’-(1*H*-tetrazolyl)amine (**164**) have been discovered as byproducts in the synthesis of 1,5-bistetrazole and 2-methyl-1,5-bistetrazole. A potential mechanism for the formation of **163** and **164** is presented.

- The structures of **160**, **160**·H_2O, **160**·H_2O·DMSO, **161**, **162**, **163** and **164** in the crystalline state were determined using X-ray diffraction, showing monoclinic (**160**·H_2O, **161**, **162** and triclinic (**163**, **164**) crystal systems, which are packed in layer structures (**160**·H_2O, **161**, **162**, **163** and **164**) as well as an orthorhombic structure (**160**) with a high density.

- The investigated compounds were fully characterized and a detailed discussion of the vibration spectroscopy as well as the heterocore NMR spectra is given in this work.

- Bis(tetrazolyl)amines are suitable energetic materials with low sensitivities and high thermal stabilities (> 250 °C) and can be used in smokeless high-nitrogen composite propellants.

- Water-free **160** can also be used as a secondary explosive since it is a highly endothermic compound and show great calculated detonation parameters such as the detonation pressure and explosion velocity (~9200 m s^{-1}). The explosion performance of **160** was verified using a steel sleeve test. **160** destroyed the steal sleeve using a critical diameter of 8 mm as well as 10 mm.

- Further advantages of **160** are its low sensitivity and a facile synthetic route, which can also be performed in larger scales.

- Bis(tetrazolyl)amines can be used as chelating ligands in novel transition metal complexes (Chapter 16).

Chapter 16.

Complexes of Bis(tetrazolyl)amines

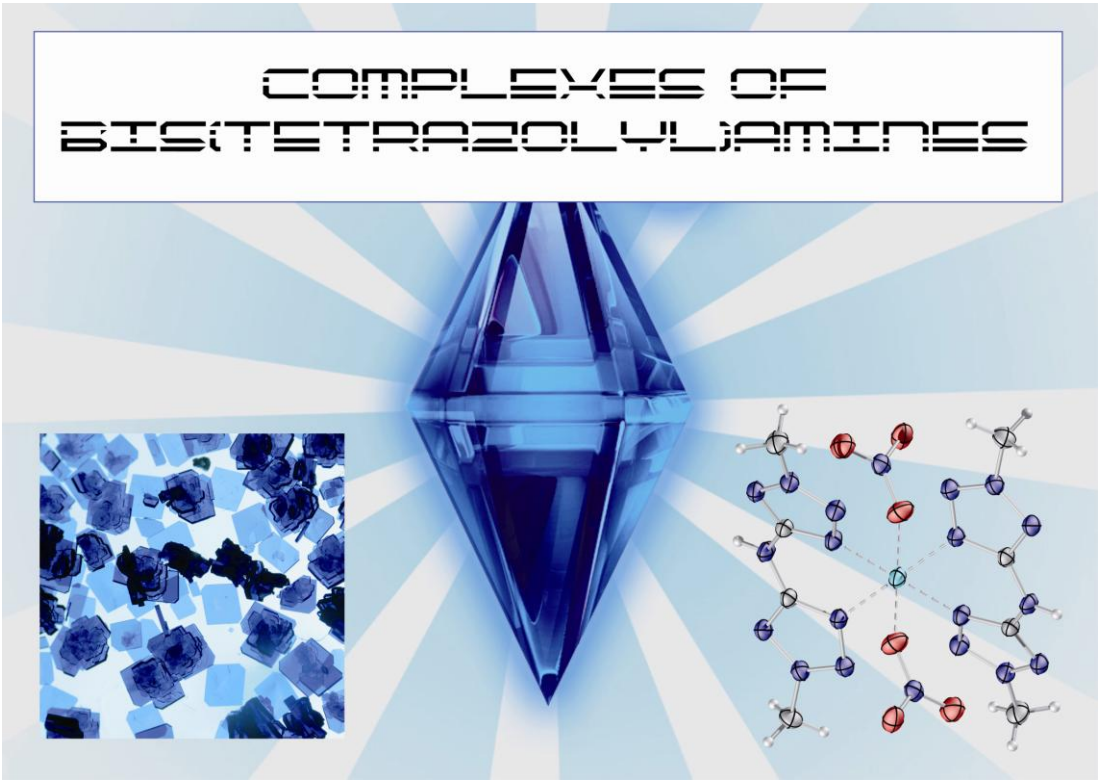

16.1 Introduction

High-nitrogen complexes of bis(tetrazolyl)amines are very profitable due to their various properties and applications as smokeless colorants, primary explosives and laser inducible igniters. Since several transition metal complexes of **160** are described in the dissertation of Jan J. Weigand [57] and in the diploma thesis of Jörg Stierstorfer,[436] only new as well as a summary of the most important compounds are given in this thesis.

Neutral as well as ionic azides can undergo cycloaddition with cyano groups yielding a huge variety of different tetrazole derivatives. An interesting precursor for cycloaddition reactions with azide is the non-linear pseudohalide dicyanamide anion ($N(CN)_2^-$), which exhibits a rich variety of bonding modes for coordination in for example *3d*-complexes. Dicyanamide complexes have attracted much interest in recent years in the construction of supramolecular aggregates due to their intriguing network topologies and potential functions as a new class of materials.[437]

The reaction of sodium dicyanamide with sodium azide under acid catalyzed condition yield the corresponding 5,5’-bis(1*H*-tetrazolyl)amine as monohydrate (abbreviated as H_2bta, **160**) (Chapter 15). In the continuous search of novel energetic materials with high nitrogen content for application, for example as low-smoke producing *pyrotechnic compositions*, *gas generators*, *propellants* and *primers* in primer charges (PC), high-energy-capacity transition metal complexes are of special interest and **160** might play an important role in future investigations as well as in applications. Still modern primary explosives may be represented by lead azide as the main filling detonator,[308] and by lead styphnate as the main filling for primers, which is usually associated with tetrazene as a sensitizer. Recently, coordination compounds containing near stoichiometric fuel and oxidizer fractions have evinced great interest.[438] The extensive study on the relationship between structure of coordination compound and explosive properties has been reported by various research groups.[439,57] Nickel, copper and cobalt complexes appear suitable for detonator applications.[440] For example, nickel hydrazinium nitrate (NHN) [441] may find wide ranging applications in conventional detonators, whereas bis(5-nitrotetrazolato-*N*2)-tetraamine cobalt perchlorate

(BNCP) [442] has emerged as an energy producing component for semi-conducting bridge (SCB) initiator applications.

Low-smoke high energy materials are thought as suitable fuel components in new coordination compounds used in novel priming charges (PCs). Derivatives of tetrazoles seem to be the most promising substance class since they are characterized by extreme properties among heterocycles e.g. by the highest N–H-acidity, lowest basicity and the presences of several “pyridine-like” nitrogen atoms important in new ligand systems as appropriate metal binding sites. Tetrazole containing substituents with potential coordination centers are of interest because of their added chelating properties and it is known that tetrazoles are well known ligands for ions of many metals.[443] With respect to new PCs, 5,5’-bis(1*H*-tetrazolyl)amine (**160**), 5,5’-bis(2-methyltetrazolyl)amine (**161**) and 5,5’-bis(2-methyltetrazolyl)methylamine (**162**) were investigated to see if they could serve as new high-nitrogen content ligand systems for new copper- and zinc-based primary explosives. Latter ones are a novel attempt in the development of new “green” high explosives, since the coordination of tetrazole derivatives to nontoxic metal centers, such as zinc(II) leads to environmentally benign compounds. Several zinc tetrazolate complexes are described in the literature,[444,445] however, the energetic properties are rarely described.

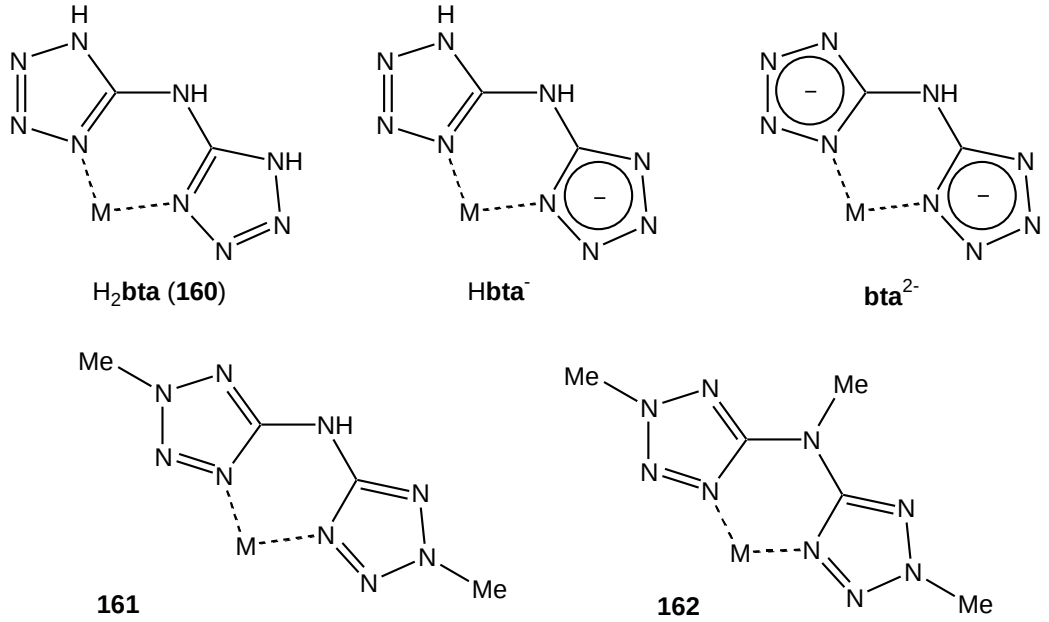

Figure 16.1 Possible chelating coordination modes of **160** and its deprotonated forms as well as **161** and **162**.

Compounds **160**, **161** and **162** are well bidentate chelating ligands. In contrast to the methyl analogues, **160** is a ligand with multiproton donor sites, it is able to coordinate to a metal with three reversible types of protonated and deprotonated modes: neutral (H_2**bta**), mono-deprotonated (H**bta**$^-$), and di-deprotonated (**bta**$^{2-}$) types (**Figure 16.1**). Moreover, H_2**bta** can be utilized as a new bridging ligand for controlling the molecular architectures which, in combination with appropriate outer- and inner-sphere ligands, allows the variation of physicochemical and explosive properties within a wide range.

The occurrence of energetic oxygen rich cations is comparable few but required to assure an appropriate oxygen balance. Therefore, counterions such as nitrate (NO_3^-) or perchlorate (ClO_4^-) anion are required in combination with the **bta** ligand system. In such systems, of course, the **bta** needs to coordinate in its protonated form. The reaction of metal salts (e.g. Cl^-, NO_3^-, ClO_4^-) in the corresponding acid with **160**, **161** and **162**, respectively, strongly depends on the reaction conditions like temperature, reaction time and concentration of the acid. By variation of those parameters a series of highly energetic **bta** complexes were obtained. The complexes are crystalline compounds and dissolves in water mostly under decomposition. They were characterized by means of IR spectroscopy, elemental analysis and X-ray structure determination.

16.2 Synthesis

The zinc complexes **165** and **166** were synthesized using zinc(II) nitrate and perchlorate, respectively as well as two equivalents of 5,5’-bis(1*H*-tetrazolyl)amine in the corresponding acids according to **Scheme 16.1**.

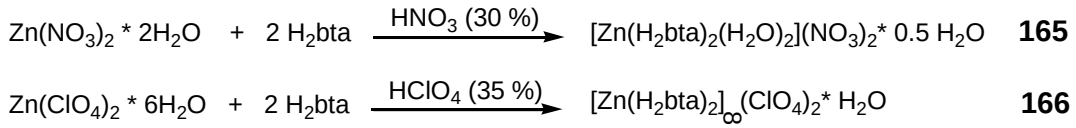

Scheme 16.1 Synthesis of compounds **165** and **166**.

The copper complexes $[Cu(H_2bta)_2](NO_3)_2{\cdot}0.5H_2O]$ (**167**), $[Cu(H_2bta)_2](ClO_4)_2$ (**168**), $[Cu(Me_2bta)_2(NO_3)_2]$ (**169**), $[Cu(Me_2bta)_2(ClO_4)_2]$ (**170**), $[Cu(Me_3bta)_3(ClO_4)_2]$ (**171**) and $[Cu(Me_3bta)Cl_2]$(**172**) have been synthesized according to **Scheme 16.2**.

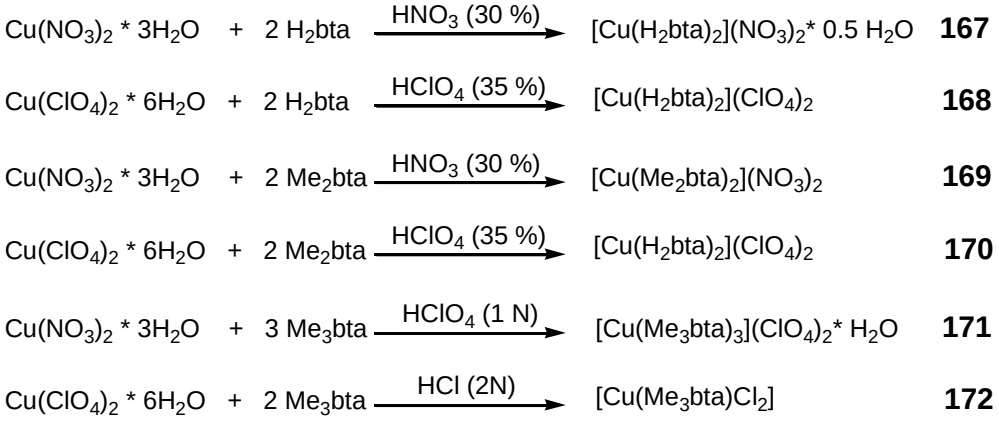

Scheme 16.2 Synthesis of copper complexes **167**–**172**.

The synthesis of the Cu(II) complexes strongly depends on the volume of the solvents, concentration of the acids, temperature, and the growing time of the crystals. Interestingly, it is possible to obtained different complexes by changing certain reaction conditions. Crystals of **167** were obtained by the addition of a warm copper nitrate solution to a warm H_2bta solution in conc. HNO_3. **167** crystallizes as beautiful blue plates suitable for X-ray determination within one day. The reaction of $Cu(ClO_4)_2 \cdot 6H_2O$ in conc. $HClO_4$ with two equivalents of the ligand **160** under harsh condition (70 °C) yielded in the formation of the very explosive, sensitive and hygroscopic water free complex **168**. It is important to mention that the preparation of **168** is aligned with a high risk of explosion. Never heat reaction mixtures where the crystallization is already in progress. In the case of **168**, the solution with separated crystals shows an increased shock sensitivity and tend to explode without any obvious external impact. Special precautions have to be applied to synthesize and separate those crystals from the reaction mixture.

Analog this reactions the copper Me_2**bta** and Me_3**bta** complexes, which are all green colored, were synthesized. The highly energetic complex **169** was obtained by the reaction of copper perchlorate and 2 equivalents of **161** in half concentrated perchloric acid after a few days. **170** crystallizes from half.-conc. HNO_3 after one day forming air stable, green-blue dichroitic crystals. The copper-Me_3**bta** complexes **171** and **172** were obtained from diluted perchloric and hydrochloric acid, respectively, by crystallization within a few hours. The corresponding reaction of **162** with copper(II) nitrate does not form suitable crystals and was refused.

16.3 Crystal Structures

Complexes **165**–**172** were determined by low temperature X-ray diffraction. A detailed description of the molecular structures follows.

16.3.1 $[Zn(H_2bta)_2(H_2O)_2](NO_3)_2 \cdot 0.5H_2O$ (**165**)

Bis(aqua-5,5’-bis(1*H*-tetrazolyl)amino-κ²N,N’)zinc(II) nitrate sesquihydrate (**165**) crystallizes in the monoclinic space group $P2_1/c$ with two molecules in the unit cell and a density of 2.09 g cm^{-3}. The zinc(II) cations are coordinated octahedrally by two H_2bta ligands and two crystal waters. (**Figure 16.2**) The equatorial positions are occupied by two chelating nitrogen atoms of **160** in distances of Zn–N2 = 2.137(3) Å, Zn–N6 = 2.132(3) Å, Zn–N12 = 2.157(3) Å and Zn–N16 = 2.146(3) Å, which is typical and could also be found in zinc nitrogen complexes in the literature.[444] The axial positions are filled by two coordination crystal water molecules with distances of Zn–O1 = 2.049(3) Å and 2.057(3) Å for Zn–O2.

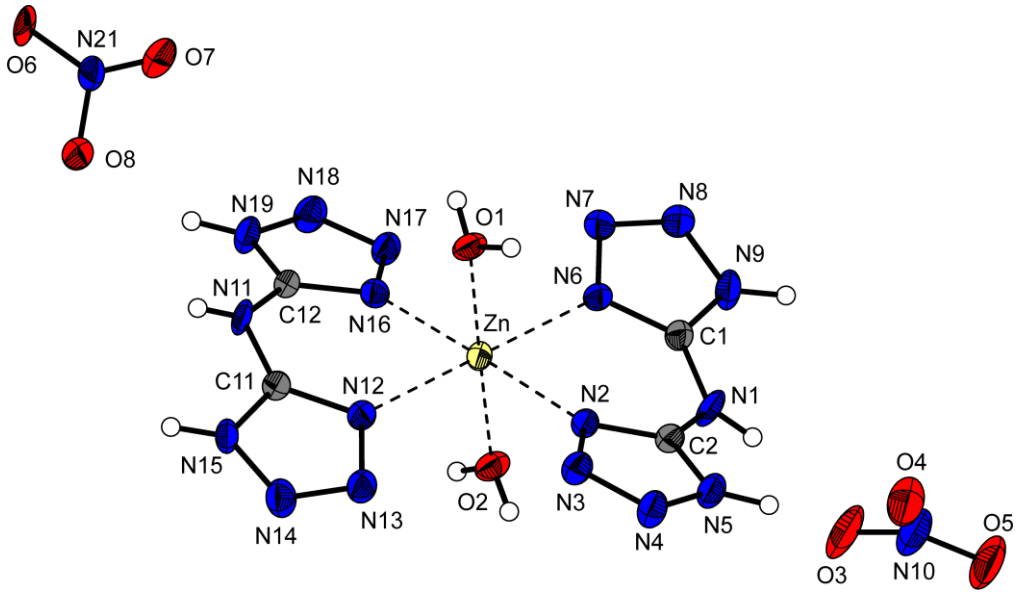

Figure 16.2 Molecular structure of **165**, without the non-coordinating crystal water. ORTEP plot drawn at the 50 % probability level, and hydrogen atoms are shown as spheres of arbitrary radii. Selected coordination geometries of **165**: Zn–O1 = 2.049(3) Å, Zn–O2 = 2.057(3) Å, Zn–N2 = 2.137(3) Å, Zn–N6 = 2.132(3) Å, Zn–N12 = 2.157(3) Å, Zn–N16 = 2.146(3) Å, O1–Zn–O2 = 178.7(1)°, N2–Zn–N6 = 81.5(1)°, N2–Zn–N16 = 98.6(1)°, N12–Zn–N16 = 81.8(1)°, N6–Zn–N12 = 98.2(1)°.

The bistetrazolylamine zinc(II) cations build stags, in between the nitrate anions and the half crystal water are placed, whereby the nitrate anions as well as the crystal water is strongly disordered, due to available space between the stags (**Figure 16.3**).

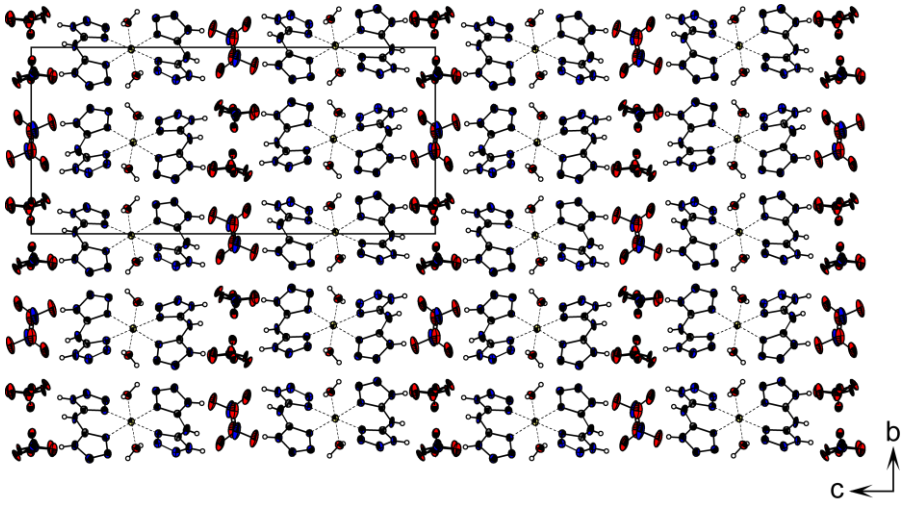

Figure 16.3 A projection of the structure of **165** along the *a* axis, showing the packing of the unit cell.

16.3.2 $[Zn(H_2bta)_2](ClO_4)_2{\cdot}H_2O$ (**166**)

Bis(5,5’-bis(1*H*-tetrazolyl)amino-κ²N,N’)zinc(II) perchlorate monohydrate (**166**) crystallizes in the triclinic space group *P*–1 forming a density of 2.178 g cm^{-3}. The zinc centers are surrounded by six nitrogen atoms (N2, N6, N12, N16, N7^{i} and N13^{ii}) forming a octahedral coordination sphere (**Figure 16.5**). Due to the coordination of N7^{i} and N13^{ii} chains along the *a* axis are formed. (**Figure 16.4**)

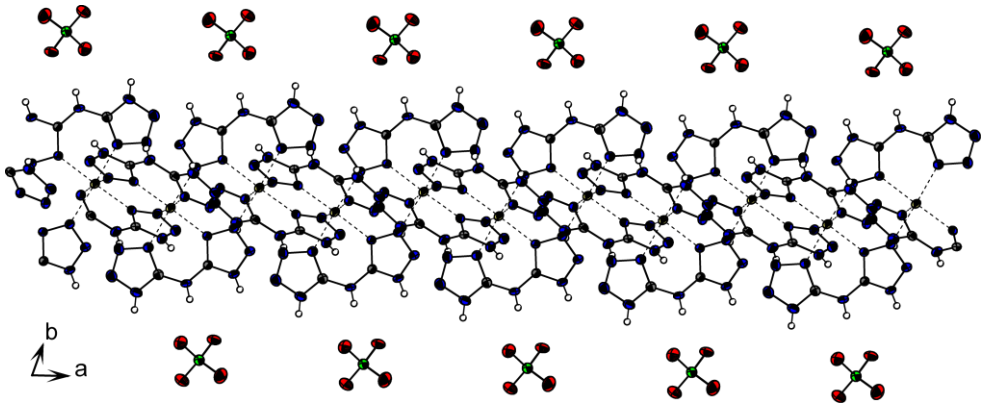

Figure 16.4 A projection of the structural motive of **166** along the *c* axis, showing the chains along the *a* axis.

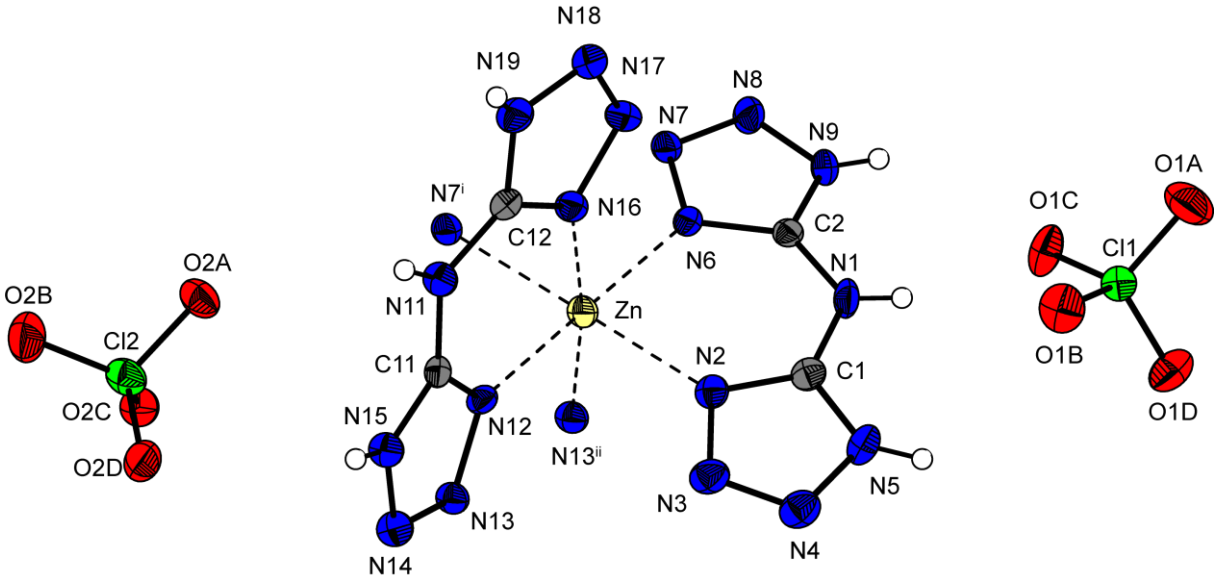

Figure 16.5 Asymmetric unit of **166** without crystal water. Thermal ellipsoids are drawn at the 50 % probability level, and hydrogen atoms are shown as spheres of arbitrary radii. Selected bond geometries of **166**: Zn–N2 = 2.11(2) Å, Zn–N6 = 2.12(2) Å, Zn–N12 = 2.12(2) Å, Zn–N16 = 2.111(7) Å, Zn–N7^{i} = 2.30(2) Å, Zn–N13^{ii} = 2.287(6) Å, N2–Zn–N6 = 84.41(9)°, N2–Zn–N16 = 99.09(9)°, N12–Zn–N16 = 84.03(9)°, N6–Zn–N12 = 176.25(10)°; N13^{ii}–Zn–N7^{i} = 84.98(8)°, N2–Zn–N7^{i} = 173.19(9)°; (i) 1–x, –y, 1–z; (ii) 2–x, –y, 1–z.

16.3.3 $[Cu(H_2bta)_2](NO_3)_2 \cdot ½H_2O$ (**167**)

167 crystallizes in the orthorhombic space group *Pbcm* in beautiful blue plates (illustrated on the right side) with four molecular moieties in the unit cell. The structure is more complex than illustrated in **Figure 16.6**. The copper centers are coordinated by four nitrogen atoms forming a distorted tetrahedral coordination sphere. Selected coordination geometries are given in **Figure 16.6**.

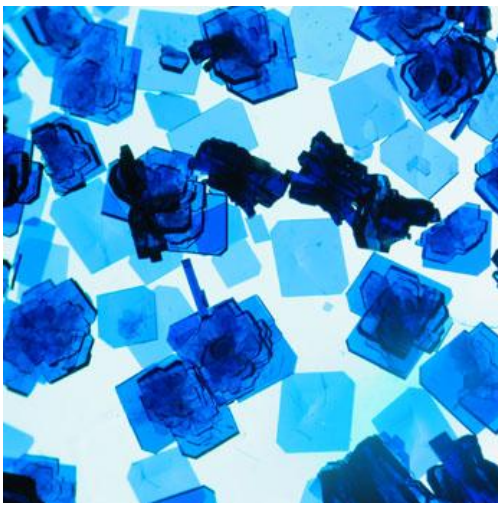

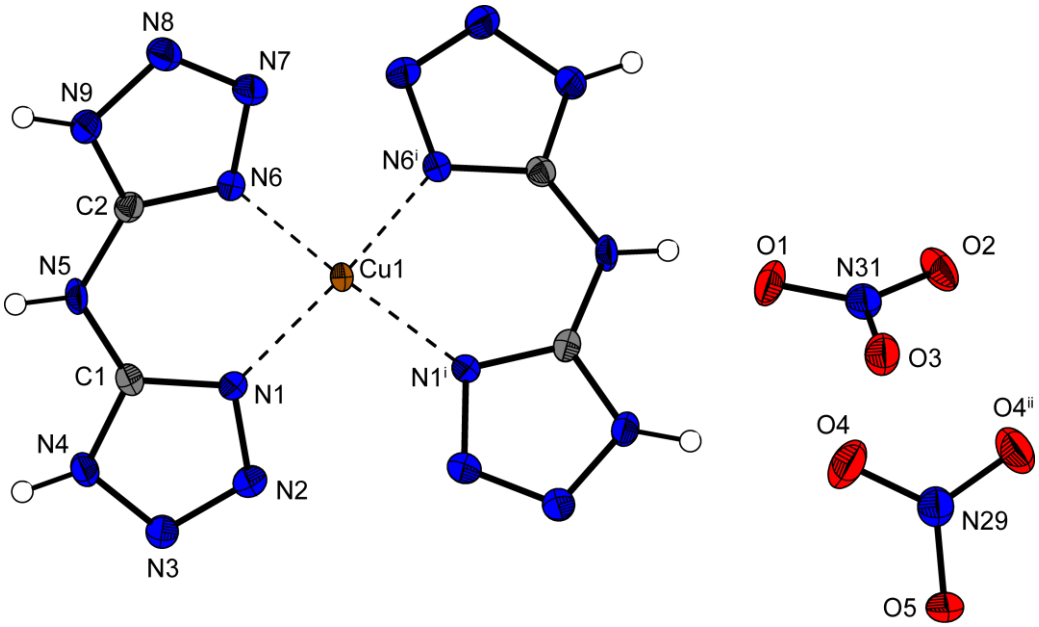

Figure 16.6 Molecular moiety of **167** without crystal water. Thermal ellipsoids are drawn at the 50 % probability level and hydrogen atoms are shown as spheres of arbitrary radii. Selected coordination geometries of **167**: Cu1–N1 = 1.958(2) Å, Cu1–N6 = 1.953(2) Å, N1–Cu1–N6 = 87.81(7)°, N1–Cu1–N1^{i} = 99.42(7), N1–Cu1–N6^{i} = 151.87(7)°, (i) x, 0.5–y, –z; (ii) x, y, 0.5–z

16.3.4 $[Cu(H_2bta)_2](ClO_4)_2$ (**168**)

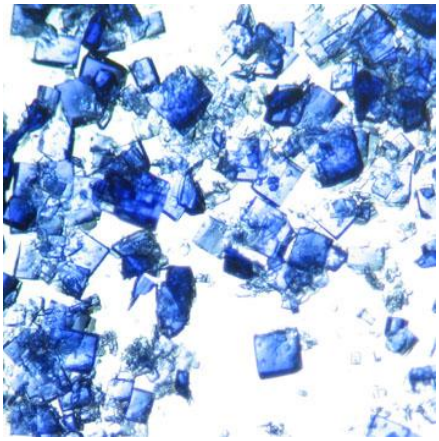

The molecular structure of bis(5,5’-bis(1*H*-tetrazol-yl)amino-κ^{2}N,N’)copper(II) perchlorate (**168**) with the labeling scheme of its atoms is shown in **Figure 16.7**. **168** crystallizes in the monoclinic space group $P2_1/c$ with two formula units in the unit cell. The Cu atom displays a distorted octahedral geometry and is positioned at (0,0,0). It lies on an inversion centre, bonded to four nitrogen atoms of the two ligands in the equatorial plane (Cu–N1 = 1.996(3) Å; Cu–N6 = 1.974(3) Å). It is bonded more weekly to two nitrogen atoms of the tetrazole ring of adjacent molecules (Cu–N3^{ii} and Cu–N3^{iii} = 2.943(5) Å; (ii) –x, –0.5+y, 0.5–z; (iii) x, 0.5–y, –0.5+z) in the axial position. The weak Cu–N3 interactions link the molecules into layers parallel to [011], whereas parallel stacking of these layers in the x

direction is achieved via hydrogen bonds between the NH groups and the oxygen atoms of the perchlorate anion (N5–H5···O3^{i}: d(D–A) = 2.854(4) Å, N9–H9···O1^{iv}: d(D–A) = 2.848(4) Å, N9–H9···O3^{iv}: d(D–A) = 2.964(4) Å, N4–H4···O2^{vi}: d(D–A) = 2.958(3) Å, N4–H4···O1^{iv}: d(D–A) = 3.004(4) Å; (iv) 1–x, –y, –z; (v) –x, –0.5–y, 0.5+z; (vi) x, y, 1+z; (vii) x, 0.5–y, 0.5+z). The oxygen atom O4 of the perchlorate anion is not involved in any hydrogen bonding.

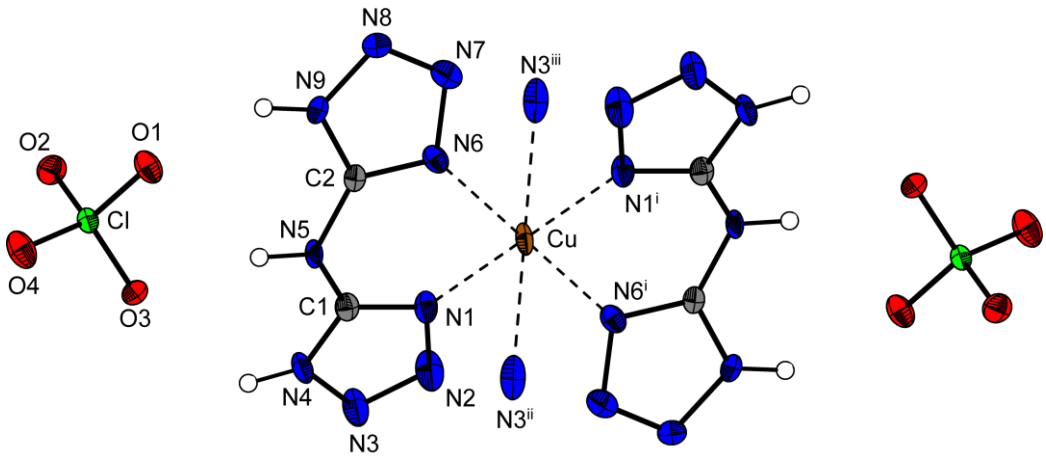

Figure 16.7 The coordination environment of the Cu^{2+} cation in **168**, showing the atom-labeling scheme. Displacement ellipsoids are drawn at the 50 % probability level and hydrogen atoms are shown as spheres of arbitrary radii. Selected bond length [Å]: Cu–N1 = 1.996(3), Cu–N6 = 1.974(3), Cu–N3^{i} = 2.943(5), Selected bond angle [°]: N1–Cu–N6 = 85.6(3), N1–Cu–N6^{i} = 94.4(4), N1–Cu–N3^{ii} = 100.3(1), N6–Cu–N3^{ii} = 79.8(2). Symmetry code: (i) –x, –y, –z; (ii) –x, –0.5+y, 0.5–z; (iii) x, 0.5–y, –0.5+z.

16.3.5 [Cu(Me$_2$bta)$_2$](NO$_3$)$_2$ (**169**)

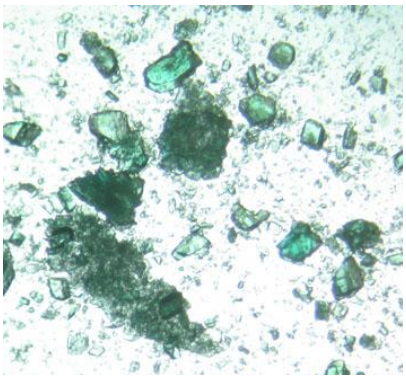

Bis(nitrato-bis-5,5’(2-methyl-tetrazolyl)amino-κ^{2}N,N’)-copper(II) (**169**) crystallizes in the triclinic space group *P*–1 with one formula unit in the unit cell. Again, the coordination sphere of the copper is a distorted octahedron, in which the copper atom lies on the inversion centre (1,1/2.1) and is bonded to four nitrogen atoms belonging to the two Me$_2$**bta** ligands in the equatorial plane (Cu–N1 = 1.998(2) Å, Cu–N6 = 2.018(2) Å). It is weakly bonded to two oxygen atoms O1 and O1^{i} (Cu–O1 = 2.367(2) Å;

(i) 2–x, 1–y, 2–z) of the two nitrate anions in the axial position. The molecular moiety is depicted in **Figure 16.8**.

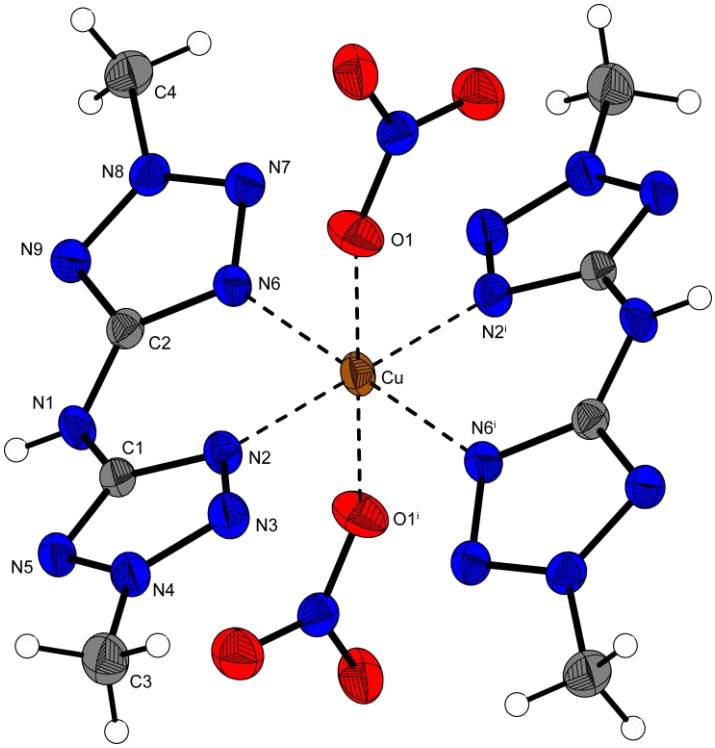

Figure 16.8 The coordination environment of the Cu^{II} ion in **169**, showing the atom-labeling scheme. Displacement ellipsoids are drawn at the 50 % probability level and H atoms are shown as spheres of arbitrary radii. Selected bond length [Å]: Cu–N1 = 1.998(2), Cu–N6 2.018(2), Cu–O1 = 2.367(2), Selected bond angle [°]: N1–Cu–N6 = 84.37(7), N1–Cu–N6^{i} = 95.63(7), N1^{i}–Cu–O1 = 92.39(6), N6–Cu–O1 = 88.45(6), (i) 2–x, 1–y, 2–z.

16.3.6 $[Cu(Me_2bta)_2](ClO_4)_2$ (**170**)

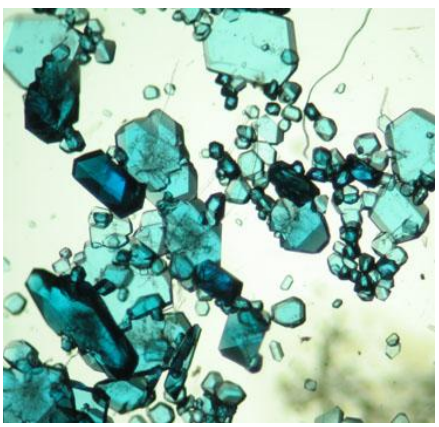

In contrast to the structure of **169**, diperchlorato-bis(5,5’-bis(2-methyl-tetrazol)amino-κ²N,N’)copper crystallizes in the monoclinic space group $P2_1/c$ with two formula unit in the unit cell. The density of 1.902 g cm^{-3} is higher than that of **169** (1.807 g cm^{-3}). However, the coordination of the copper centers (**Figure 16.9**) follows exactly that observed for **169**. The Cu–O distance of 2.383(2) Å to the perchlorate anions is slightly longer than the corresponding distance in the structure of **169** (2.367(2) Å).

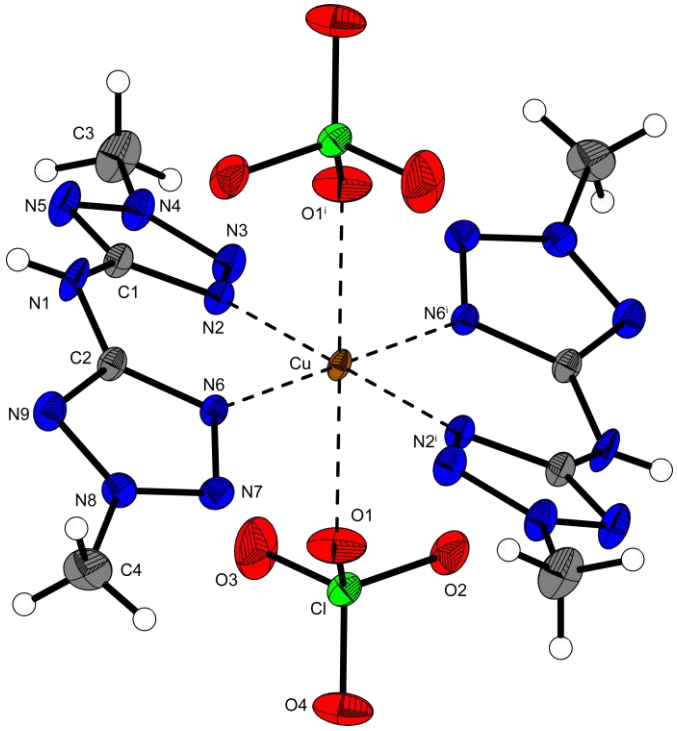

Figure 16.9 Molecular moiety of **170**. Thermal ellipsoids are drawn at the 50 % probability level, and H atoms are shown as spheres of arbitrary radii. Selected coordination geometries of **170**: Cu–N2 = 2.019(6) Å, Cu–N6 = 1.990(6) Å, Cu–O1 = 2.383(2) Å, N2–Cu–N6 = 85.06(5)°, N2–Cu–O1 = 96.52(5)°, N6–Cu–O1 = 89.42(5)°, N2–Cu–N6^{i} = 94.94(5)°, (i) 1–x, –y, –z.

16.3.7 $[Cu(Me_3bta)_3](ClO_4)_2$ (**171**)

Tris(5,5’-bis(2-methyltetrazolyl)methylamino-κ^{2}N,N’)copper(II) perchlorate (**171**) crystallizes in the monoclinic space group $C2/c$ with four molecular moieties in the unit cell and a lower density of 1.647 g cm^{-3}. The perchlorate anions are strongly disordered and has been splitted in the solution. Also the outer carbon atoms of the methyl groups show large thermal ellipsoids. **171** is the only structure observed in which three bis(tetrazolyl)amino ligands could be coordinated to the copper centers forming a distorted elongated octahedral coordination (**Figure 16.10**). Also by using an excess of copper perchlorate in the synthesis of **171** this coordination mode is the only one formed. This coordination mode leads to a decrease of the bite angle of two bis(tetrazolyl)amine ligands to 80.1(1)°, which is significantly lower than that observed for structures **165**–**170**.

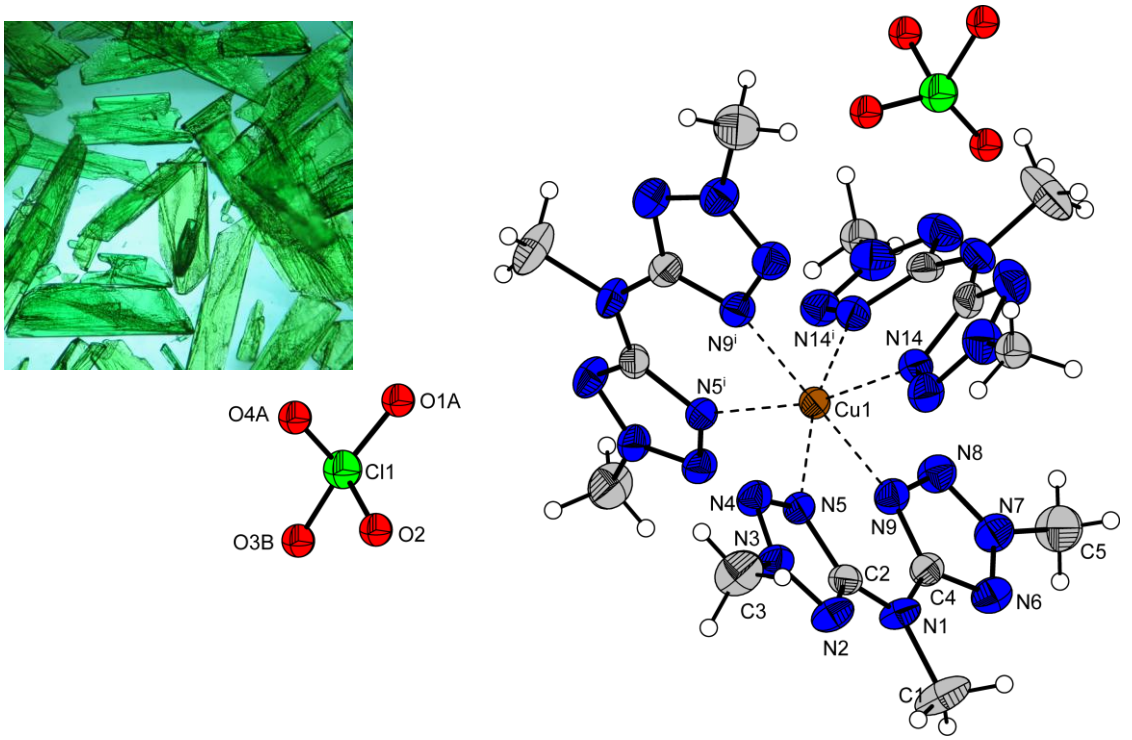

Figure 16.10 Molecular moiety of **171** without crystal water. Thermal ellipsoids are drawn at the 50 % probability level, and H atoms are shown as spheres of arbitrary radii. Oxygen atoms are represented in the ball-and-stick model. Selected coordination geometries of **171**: Cu–N5 = 2.040(9) Å, Cu–N9 = 2.237(5) Å, Cu–N14 = 2.02(1) Å, N5–Cu–N9 = 80.1(1)°, N5–Cu–N14 = 90.8(1)°, N9–Cu–N14 = 87.6(1)°, N14–Cu–N14^{i} = 85.3(1)°, N5–Cu–N14^{i} = 167.0(1)°, (i) 1–x, y, 0.5–z.

16.3.8 $[Cu(Me_3bta)Cl_2]_2$ (**172**)

Dichlorido-(5,5’-bis(2-methyltetrazolyl)amino-κ^{2}N,N’)copper(II) crystallizes in the monoclinic space group $P2_1/c$ with two formula unit in the unit cell and a density of 1.897 g cm^{-3}. Also by using an excess of ligand, **172** is the only complex formed in this synthesis. **172** is best described as a binuclear complex (**Figure 16.11**). Of particular interest is the coordination sphere of the copper cations, which is distorted tetragonal pyramid. The next atoms (N) below the copper centers at its unoccupied side are not before 3.64 Å. The Cu–N distances are in an usual range of ~2.04 Å. The Cu–Cl coordination bonds are found to have distances between 2.22 and 2.76 Å.

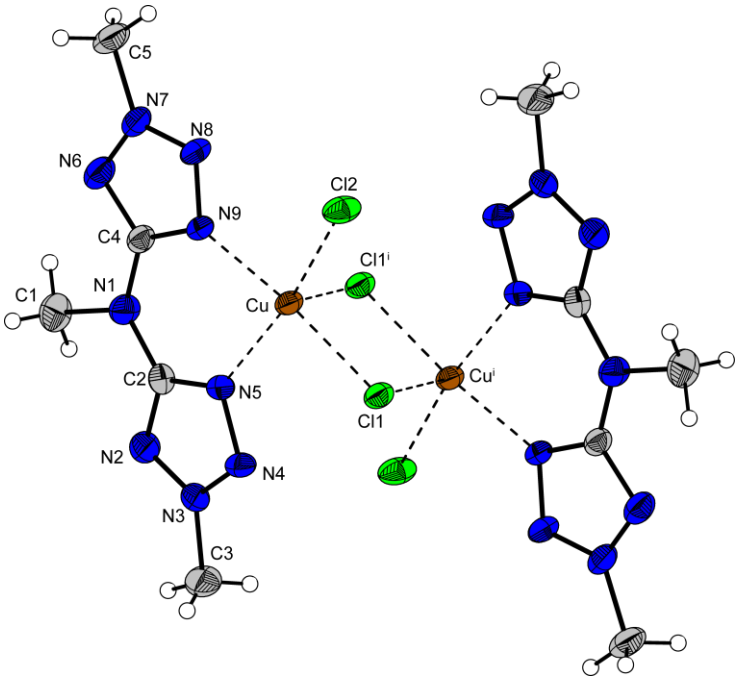

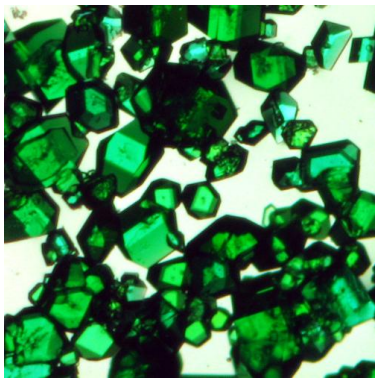

Figure 16.11 Molecular structure of the binuclear complex **172**, showing the atom-labeling scheme. Displacement ellipsoids are drawn at the 50 % probability level and hydrogen atoms are shown as spheres of arbitrary radii. Selected bond length [Å]: Cu–N5 = 2.037(3), Cu–N9 = 2.039(9), Cu–Cl1 = 2.272(11), Cu–Cl2 = 2.229(2), Cu–Cl1^{i} = 2.755(7); Selected bond angle [°]: Cl1–Cu–Cl2 = 92.11(3), Cl1^{i}–Cu–Cl2 = 106.64(3), Cl1^{i}–Cu–Cl1 = 93.29(3), N5–Cu–N9 = 83.4(1), N5–Cu–Cl1 = 91.76(7), N5–Cu–Cl2 = 167.19(8), N5–Cu–Cl1^{i} = 85.32(7), N9–Cu–Cl2 = 92.04(8), N9–Cu–Cl1 = 174.50(8), Cu–Cl1–Cu^{i} = 86.71(3); (i) 1–x, –y, 1–z.

16.4 Vibrational Spectroscopy

Except for the zinc complexes **165** and **166** as well as **172** all investigated copper complexes show photosensitive behavior and explode by laser irradiation in Raman experiments. (Laser: Nd/YAG 1064 nm). However, **172** could also not be determined by Raman spectroscopy due to strong fluorescence.

The IR spectra of the bis(tetrazolyl)amino ligands (**160**–**162**) are characteristic for aminotetrazoles (see chapter 15). The changes in the bands that are composed from combinations of the vibrations of the tetrazole ring components indicates the formation of a coordination bond trough the nitrogen atoms of the two tetrazole rings of **160**–**162** involved. Although those absorptions bands showing medium or weak intensities, the

shift and change in intensity can be used for the demonstration of the direct participation of the tetrazole cycle in the complexation. The characteristic bands located at 1656 and 1556 cm^{-1} and assigned to the $\nu_{asym}(C_{tet}–N–C_{tet})$ and $\nu_{sym}(C_{tet}–N–C_{tet})$ stretching vibrations in **160** are shifted to lower frequencies by approximately 8 to 10 cm^{-1}. The bands attributed to the stretching vibrations of the N=N (1454 cm^{-1}), C=N (1352, 1337 cm^{-1}) and N–N (1282, 1268 cm^{-1}) bonds in the IR spectrum of the free H_2bta ligand are shifted to higher wavenumbers after complexation associated with a decrease of intensity.[446] The IR spectra of the compounds have in common the bands for the stretching and bending modes of the N–H groups from the protons at the tetrazole ring and the secondary amino group. As it was found for other copper-tetrazole complexes the bands between 3500–3000 cm^{-1} assigned to stretching vibrations of the N–H groups of **160** and **161** are shifted to higher frequencies with respect to those of the free ligand. Furthermore it is observed that those bands in the complexes are less well resolved compared to the free ligands **160** and **161**. This can be best explained due to the formation of intermolecular hydrogen bonds in the crystalline network. A red shift of the stretching modes establish that the heteromolecular hydrogen-bond interaction between the N–H (donor) groups of the ligand **160** and corresponding acceptors (e.g. counter anion and water) are strong. In all spectra the bands of the respective energetic anions (ClO_4^- (**166**, **168**, **170** and **171**) and NO_3^- (**165**, **167**, **169**)) were obvious and as these bands usually have characteristic fingerprints in IR spectra, they could be identified easily. The presence of nonsplit, strong absorption bands at 1384 cm^{-1} (NO_3^-) [447] in **169**, 1090 and 626 cm^{-1} (ClO_4^-) [448] in **170** points to a lack of strong deviation of the trigonal planar and tetrahedral symmetry in the nitrate and perchlorate anion, respectively.[449]

16.5 Energetic Properties

The thermal stabilities of **165–172** have been discovered by DSC measurements with heating rates of 2 as well as 5 °C min^{-1}. All compounds have decomposition temperatures above 145 °C (**165** = 180 °C, **166** =150 °C, **167** = 147 °C, **168** = 162 °C, **169** = 193 °C, **170** = 265 °C, **171** = 267 °C and **172** = 192 °C). In general the methylated analogues have higher thermal stabilities than the H_2bta complexes. Interestingly, in the case of the copper complexes, the perchlorates have higher temperatures of decomposition than the corresponding nitrates.

For initial safety testing, the impact and friction sensitivity was tested according to BAM methods with a “BAM drophammer” and a “BAM friction tester”. Due to the extreme hygroscopicity and sensitivity of compound **168** suitable values for the friction and impact sensitivity cannot be given but we experienced that compound **168** is extremely sensitive toward friction and impact and two explosions during preparation occurred even without obvious external impact. The zinc H_2bta complexes are sensitive towards impact (**165**: 6 J, **166**: 4 J) and friction (**165**: 350 N, **166**: 35 N). The shock sensitivity values are comparable to those of $Pb(N_3)_2$ (2.5 J; 10 N) and indicate that this salt belongs to the group of primary explosives. Also copper nitrate **167** (4 J; 196 N) is sensitive in both categories.
The Me_2bta and Me_3bta analogs represent a safer class of compounds because of the higher carbon content. However, **169** and **170** are both sensitive towards impact (**169**: 7 J, **170**: 3 J) and friction (**169**: 305 N, **170**: 100 N). Perchlorate **171** has moderate impact (10 J) and also a moderate friction sensitivity (150 N). **172** is neither friction nor impact sensitive.

Due to their specific energetic behavior the compounds can be used for example as (i) “green” primary explosives (**165**, **166**, **167**, **170**, **171**) (ii) colorants in smokeless pyrotechnical compositions (**169**, **172**) and (iii) laser inducible primary explosives (**167**, **169**, **170**).

16.6 Experimental Part

*CAUTION! Complexes of bis(tetrazolyl)amines in combination with oxygen-rich counter-anions are highly energetic compounds with increased sensitivities against heat, impact and friction. Proper protective measures (safety glasses, face shield, leather coat, earthened equipment and shoes, Kevlar® gloves and ear plugs) should be used during work, especially on compounds **165–179**. Highest safety precautions are needed when handling water-free complex **168**.*

*$[Zn(H_2bta)_2(H_2O)_2](NO_3)_2 \cdot 0.5\ H_2O$ (**165**):* **160**·H_2O (1.37 g, 8 mmol) was dissolved in 40 mL nitric acid (65 %) and warmed to 80 °C. A solution of $Zn(NO_3)_2 \cdot 6H_2O$ in (1.19 g, 4 mmol) in 10 mL of hot water was added and stirred for 30 min at this temperature. The reaction mixture was cooled to RT and left for crystallization. After one day **165**

started to precipitate in colorless crystals suitable for X-ray determination. The product was isolated by filtration and washed with diethyl ether (1.41 g, yield 65 %). **DSC** (T_{onset}, 5 °C min^{-1}): 180 °C (dec.); **IR** (KBr, cm^{-1}): $\tilde{\nu}$ = 3371 (m), 3235 (m), 3065 (m), 2929 (m), 2851 (m), 2676 (w), 1655 (vs), 1616 (s), 1572 (m), 1495 (w), 1462 (m), 1384 (s), 1351 (m), 1311 (m),, 1292 (m), 1275 (m), 1154 (w), 1136 (w), 1042 (w), 1028 (w), 1018 (w), 845 (w), 820 (w), 735 (w), 724 (w), 686 (w), 668 (w), 609 (w), 457 (w); **Raman** (200 mW, 25 °C, cm^{-1}): $\tilde{\nu}$ = 3351 (9), 3227 (9), 3087 (8), 2892 (8), 2853 (10), 2581 (7), 2528 (7), 2442 (7), 2380 (8), 1931 (8), 1702 (8), 1623 (91), 899 (11), 846 (12), 724 (16), 474 (14), 416 (36), 378 (29), 365 (27), 303 (19), 169 (40); **^{1}H NMR** (*d*$_6$-DMSO, 25 °C, ppm): δ = 8.65 (s, br); **^{13}C NMR** (*d*$_6$-DMSO, 25 °C, ppm): δ = 153.83 (s, CN_4); **^{14}N NMR** (*d*$_6$-DMSO, 25 °C, ppm): δ = –7.72 (s, NO_3^-); **EA** ($ZnC_4H_{11}N_{20}O_{8.5}$, 540.65) calcd.: C 8.89, H 2.05, N 51.81 %; found: C 8.97, H 2.16, N 51.87 %; **impact sensitivity**: > 6 J; **friction sensitivity**: 350 N; **Δ*U*$_c$**: 1485 cal g^{-1}.

*[Zn(H$_2$bta)$_2$](ClO$_4$)$_2$·H$_2$O (**166**):* To a 90 °C hot solution of **160**·H_2O (1027 mg, 6 mmol) in 25 mL perchloric acid (35 %) a solution of $Zn(ClO_4)_2$·$6H_2O$ (1117 mg, 3 mmol) in 10 ml of hot water was added and stirred for 30 min at this temperature. The reaction mixture was cooled to RT and left for crystallization. After 2 hours compound **166** started to precipitate in colorless crystals suitable for X-ray determination. **166** was isolated by filtration and washed with diethyl ether (881 mg, yield 50 %). **DSC** (T_{onset}, 5 °C min^{-1}): 150 °C (dec.); **IR** (KBr, cm^{-1}): $\tilde{\nu}$ = 3931 (w), 3592 (m), 3527 (m), 3458 (m), 3303 (m), 3236 (m), 3152 (s), 3085 (s), 2963 (m), 2863 (m), 2670 (m), 2456 (w), 2056 (w), 1652 (vs), 1616 (vs), 1551 (s), 1483 (w), 1456 (w), 1384 (w), 1336 (w), 1305 (w), 1282 (w), 1263 (w), 1121 (s), 1086 (s), 1032 (s), 1012 (s), 940 (w), 916 (w), 842 (w), 801 (w), 723 (m), 690 (w), 636 (m), 625 (m), 526 (w), 468 (w); **EA** ($ZnC_4H_8N_{18}O_9Cl_2$, 588.52) calcd.: C 8.16, H 1.37, N 42.84, Cl 12.05 %; found: C 8.38, H 1.51, N 42.78 %; **impact sensitivity**: > 4 J; **friction sensitivity**: > 35 N; **Δ*U*$_c$**: 1331 cal g^{-1}.

*[Cu(H$_2$bta)$_2$](NO$_3$)$_2$·0.5H$_2$O (**167**):* Single crystals suitable for X-ray analysis were obtained as follows: To a warm (60 °C) solution of H_2bta·H_2O (0.684 g, 4.0 mmol) in 5 mL HNO_3 (65 %), a solution of $Cu(NO_3)_2$·$3H_2O$ (0.482 g, 2 mmol) in 4 mL 2N HNO_3 was added, producing a dark-blue solution. This solution was stirred for 10 minutes at 60 °C and left to crystallize. After one day, **167** was obtained as blue crystals suitable for X-ray diffraction determination (651 mg, 65 % yield). **DSC** (T_{onset}, 2 °C min^{-1}): 147 °C (dec.); **IR** (KBr, cm^{-1}): $\tilde{\nu}$ = 3455 (m), 3252 (m), 3031 (m), 2923 (m), 2846 (m), 2675 (m), 1651

(s), 1559 (m), 1511 (w), 1467 (m), 1384 (vs), 1265 (m), 1160 (w), 1131 (w), 1054 (m), 1017 (w), 824 (w), 815 (w), 726 (m), 664 (w), 625 (w); **Raman** (1064 nm, 150 mW, 25 °C, cm^{-1}): decomposition; **EA** ($C_4H_7N_{20}CuO_{13/2}$, 502.78) calcd.: C 9.6, H 1.4, N 55.7 %; found: C 9.6, H 1.4, N 55.9 %; **impact sensitivity**: 4 J; **friction sensitivity**: 196 N.

*[Cu(H₂bta)₂](ClO₄)₂ (**168**):* Single crystals suitable for X-ray analysis were obtained as follows: To a warm (70 °C) solution of $H_2bta{\cdot}H_2O$ (0.342 g, 2.0 mmol) in 10 mL $HClO_4$ (72 %), a warm (70 °C) solution of $Cu(ClO_4)_2{\cdot}6H_2O$ (0.371 g, 1.0 mmol) in 4 mL $HClO_4$ (72 %) was added, producing a dark blue solution. This solution was stirred for further two minutes at this temperature and left to crystallize. After one hour, the highly explosive and hygroscopic product **168** was obtained as dark-blue crystals suitable for XRD (~70% yield). **DSC** (T_{onset}, 5 °C min^{-1}): 162 °C (dec.); **IR** (KBr, cm^{-1}): $\tilde{\nu}$ = 3430 (s), 2956 (m), 2925 (s), 2851 (m), 1652 (s), 1569 (m), 1454 w), 1384 (w), 1259 (w), 1141 (m), 1105 (s), 1090 (s), 1009 (w), 938 (w), 798 (w), 726 (w), 626 (m), 540 (w); **EA** ($C_4H_6Cl_2CuN_{18}O_8$, 568.66): calcd.: C 8.45, H 1.06, N 44.34 %; found: not determinable; **impact sensitivity**: < 1 J; **friction sensitivity**: < 5 N.

*[Cu(Me₂bta)₂(NO₃)₂] (**169**):* Single crystals suitable for X-ray analysis were obtained as follows: To a warm (80 °C) solution of 2,2’-Me_2bta (0.362 g, 2.0 mmol) in 4 mL HNO_3 (40 %), a solution of $Cu(NO_3)_2{\cdot}3H_2O$ (0.241 g, 1.0 mmol) in 3 mL H_2O was added, producing a dark-green solution. This solution was stirred for ten minutes at 80 °C, followed by removal of 90 % of the solvent under high vacuum. The residue was dissolved in 40 mL methanol and left to crystallize. After a few hours, **169** was obtained as green crystals suitable for X-ray structure determination (352 mg, 64 % yield). **DSC** (T_{onset}, 2 °C min^{-1}): 193 °C (dec.); **IR** (KBr, cm^{-1}): $\tilde{\nu}$ = 3441 (w), 3277 (w), 3137 (w), 3041 (m), 2896 (m), 2767 (m), 1639 (vs), 1572 (m), 1492 (m), 1444 (m), 1422 (m), 1384 (s), 1318 (s), 1197 (w), 1117 (w), 1082 (w), 1043 (w), 1026 (w), 880 (w), 813 (w), 797 (w), 751 (m), 742 (w), 722 (w), 679 (m), 467 (w); **Raman** (1064 nm, 200 mW, 25 °C, cm^{-1}): decomposition; **EA** ($C_8H_{14}CuN_{20}O_6$, 549.88): calcd.: C 17.5, H 2.6, N 51.0 %; found: C 17.5, H 2.5, N 50.9 %; **impact sensitivity**: 7 J; **friction sensitivity**: 305 N.

*[Cu(Me₂bta)₂(ClO₄)₂] (**170**):* Single crystals suitable for X-ray analysis were obtained as follows: To a hot (90 °C) solution of 2,2´-Me_2bta (0.362 g, 2.0 mmol) in 30 mL H_2O and 2 mL $HClO_4$ (72 %), a solution of $Cu(ClO_4)_2{\cdot}6H_2O$ (0.371 g, 1.0 mmol) in 5 mL $HClO_4$ (72 %) was added, producing a green solution. From this solution, **170** was obtained as

green-blue crystals after two weeks (437 mg, 70 % yield). **DSC** (T_{onset}, 2 °C min^{-1}): 265 °C (dec.); **IR** (KBr, cm^{-1}): $\tilde{\nu}$ = 3412 (w), 3283 (m), 3154 (m), 3065 (s), 3055 (s), 2961 (m), 2939 (m), 2829 (s), 2445 (vw), 1639 (vs), 1571 (s), 1490 (s), 1451 (s), 1418 (w), 1382 (w), 1345 (w), 1325 (w), 1199 (m), 1146 (s), 1118 (vs), 1054 s), 935 (m), 878 (m), 826 (m), 754 (s), 740 (w), 733 (w), 680 (s), 629 (s), 618 (s), 467 (w); **Raman** (1064 nm, 100 mW, 25 °C, cm^{-1}): explosion; **EA** ($C_8H_{14}Cl_2CuN_{18}O_8$, 624.76): calcd.: C 15.4, H 2.3, N 40.4 %; found: C 15.5, H 2.3, N 40.2 %; **impact sensitivity**: 3 J; **friction sensitivity**: 100 N.

*[Cu(Me$_3$bta)$_3$](ClO$_4$)$_2$ (**171**):* Copper(II) perchlorate hexahydrate (370 mg, 1 mmol) and 5,5’-bis-(2-methyltetrazolyl)-methylamine (**162**) (586 mg, 3 mmol) were dissolved in 15 mL water and heated for 20 minutes at 90 °C. The green solution was cooled to RT and left for crystallization. After 6 hours green crystals suitable for X-ray diffraction were obtained (636 mg, yield 75 %). **DSC** (T_{onset}, 2 °C min^{-1}): 267 °C (dec.); **IR** (KBr, cm^{-1}): $\tilde{\nu}$ = 3429 (w), 3042 (w), 2963 (w), 2020 (w), 1584 (s), 1576 (s), 1448 (m), 1412 (w), 1387 (w), 1231 (w), 1209 (w), 1095 (vs), 893 (vw), 885 (vw), 743 (w), 738 (w), 686 (m), 673 (w), 623 (m), 601 (w); **EA** ($C_{15}H_{27}Cl_2CuN_{27}O_8$, 848.0): calcd.: C 21.25, H 3.21, N 44.60 %; found: C 21.17, H 3.22, N 44.66 %; **impact sensitivity**: 10 J; **friction sensitivity**: 150 N.

*[Cu(Me$_3$bta)Cl$_2$] (**172**):* 5,5’-Bis(2-methyltetrazolyl)methylamine (390 mg, 2 mmol) and $CuCl_2 \cdot 2\ H_2O$ (170.5, 1 mmol) were combined and dissolved in 10 mL hot water. The intensive green solution was concentrated using vacuum and left for 24 hour till the light green product started to precipitate (273 mg, yield 83 %), **DSC** (T_{onset}, 5 °C min^{-1}): 292 °C (dec.); **IR** (KBr, cm^{-1}): $\tilde{\nu}$ = 3390 (w), 3024 (w), 2925 (w), 2854 (w), 1625 (m), 1596 (s), 1567 (m), 1444 (w), 1405 (w), 1384 (w), 1322 (w), 1262 (w), 1234 (w), 1192 (w), 1107 (w), 1070 (w), 889 (w), 802 (w), 741 (w), 682 (m), 672 (w), 615 (w), 450 (w); **Raman** (1064 nm, 200 mW, 25 °C, cm^{-1}): $\tilde{\nu}$ = fluorescence effects; **EA** ($C_5H_9Cl_2CuN_9$, 329.64) calcd.: C 18.22, H 2.75, N 38.24 %; found: C 18.15, H 2.81, N 38.15 %; **impact sensitivity**: > 100 J; **friction sensitivity**: > 360 N.

16.7 Conclusions

In this chapter selected results on a series of zinc and copper bta salts (**165–172**) are presented. They might play an important role in the development of safe non-toxic PC formulations, as possibly photosensitive compounds utilized in laser detonators as well as colorants in pyrotechnic formulations. The following conclusions can be drawn:

- H_2bta (**160**), Me_2bta (**161**) and Me_3bta (**162**) can be used as a suitable neutral ligands in transition metal complexes. The nitrogen rich zinc(II) complexes $[Zn(H_2bta)_2(H_2O)_2](NO_3)_2{\cdot}0.5H_2O$ (**165**) and $[Zn(H_2bta)_2(ClO_4)_2]{\cdot}H_2O$ (**166**) as well as the copper complexes $[Cu(H_2bta)_2](NO_3)_2{\cdot}0.5H_2O$ (**167**), $[Cu(H_2bta)_2](ClO_4)_2$ (**168**), $[Cu(Me_2bta)_2(NO_3)_2]$ (**169**), $[Cu(Me_2bta)_2(ClO_4)_2]$ (**170**), $[Cu(Me_3bta)_3](ClO_4)_2$ (**171**), $[Cu(Me_3bta)Cl_2]$ (**172**) have been synthesized. The reactions strongly depends on the concentrations of the corresponding acids. The syntheses are performed with cheap starting materials and pass mostly with good yields.

- Suitable single crystals of **165**–**172** were investigated by low temperature X-ray diffraction. The bis(tetrazolyl)amines act as bidentate ligands with different coordination modes. In the case of **172** one ligand, in the cases of **165**–**170** two ligands and in **172** three ligands coordinate to the copper(II) centers. Except for **167** and **172** the coordination geometries are dominated by the Jahn Teller effect forming elongated octahedral.

- The energetic properties of **165**–**172** were discovered. All compounds have appropriate decomposition temperatures above 145 °C Except for **172** all compounds are sensitive towards friction and impact. In the case of **168** also the concentrated reaction solution is extremely sensitive towards shock!

- **167**–**170** can be ignited by laser irradiation (1064 nm, 50–300 mW), which makes them promising for novel light inducible primary explosives.

Chapter 17.

Exciting Reactions, Ongoing Projects and Selected Structures

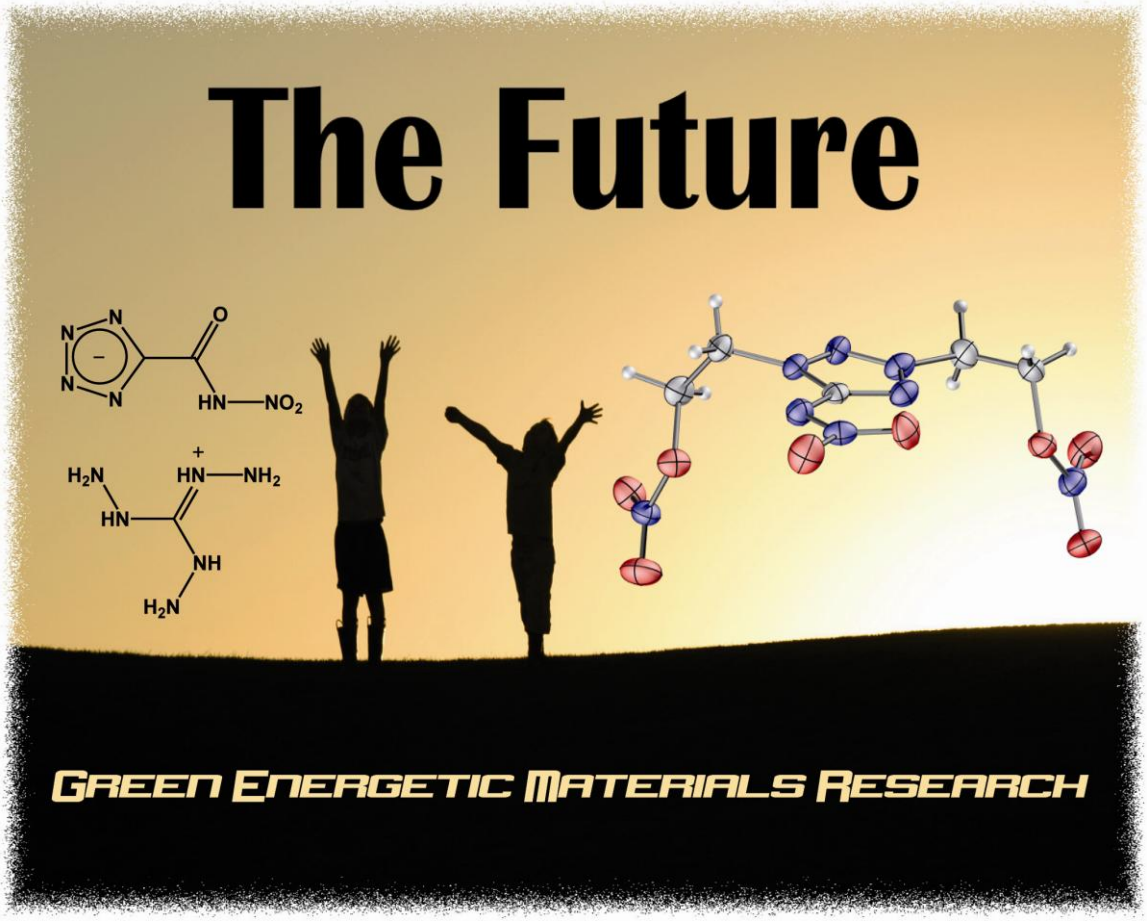

17.1 Nitration of 5-Aminotetrazole with NO_2BF_4

Due to the great risk of explosion in the former synthetic procedure of H_2AtNO_2 (**43**) a new synthesis should be discovered. The nitration of 5-aminotetrazole (**2**) with nitronium tetrafluoroborate was performed in the ratio 1:1 in dry MeCN (**Scheme 17.1**). At this, **2** (840 mg, 10 mmol) was suspended in 10 mL dry MeCN and cooled to 0 °C. NO_2BF_4 (1.33 g, 10 mmol) was added and the solution was stirred for 12 h at ambient temperature. The solution was evaporated and ethanol (15 mL) was added. From this solution, colorless single crystals were obtained, which have been proofed to be 5-aminotetrazolium tetrafluoroborate (**173**).

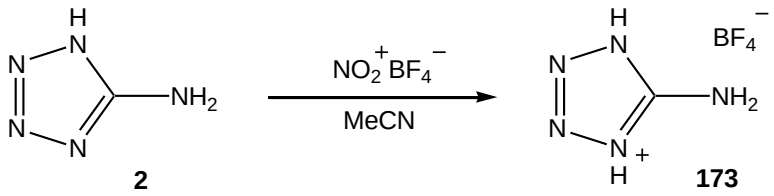

Scheme 17.1 Reaction of 5-aminotetrazole with NO_2BF_4 yields 5-aminotetrazolium tetrafluoroborate (**173**).

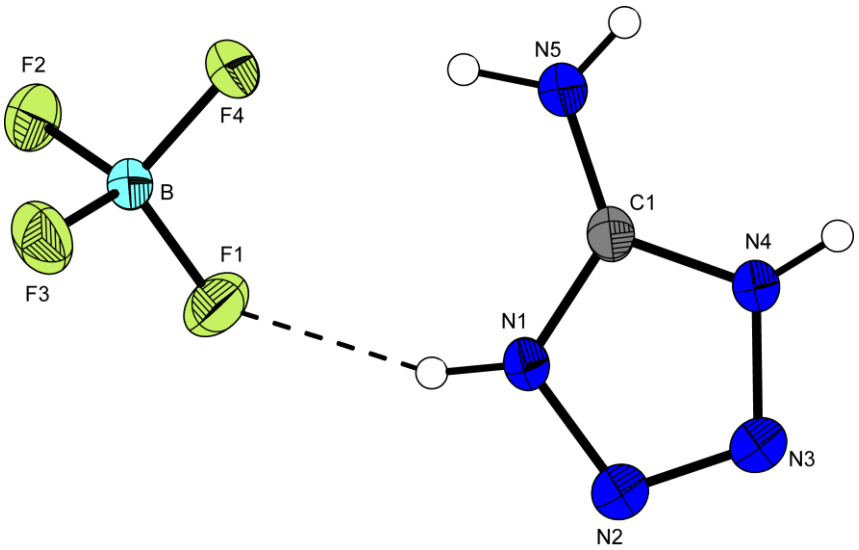

Figure 17.1 Molecular structure of 5-aminotetrazolium tetrafluoroborate (**173**). Thermal ellipsoids are drawn at the 50 % probability level, and H atoms are shown as spheres of arbitrary radii. Bond lengths (Å): N1–N2 = 1.363(2), N2–N3 = 1.264(2), N3–N4 = 1.363(2), N4–C1 = 1.336(2), N5–C1 = 1.307(2), N1–C1 = 1.332(2), F1–B1 = 1.381(2), F4–B1 = 1.400(2), F2–B1 = 1.390(2), F3–B1 = 1.387(2).

173 crystallizes in the triclinic crystal system (space group *P*–1) with two formula units in the unit cell. The density of 1.874 g cm^{-3} is comparable to this observed for 5-aminotetrazolium dinitramide (**31**) (Chapter 3). The molecular moiety is depicted in **Figure 17.1**. The bond lengths in the cation are also similar to these observed in **31**. The B–F distances have values of 1.38 to 1.40 Å. The packing of **173** is strongly dominated by the formation of H···F hydrogen bonds, which are listed in **Table 17.1**. The coordination mode of one tetrafluoroborate anion is depicted in **Figure 17.2**.

Table 17.1 Hydrogen bonds in the structure of **173**.

D–H···A	d(D–H)	d(H···A)	d(D···A)	∢(D–H···A)
N1–H1···F1	0.84(2)	2.07(2)	2.854(1)	156(2)
N1–H1···N2^{i}	0.84(2)	2.53(2)	3.013(2)	118 (1)
N4–H4···F2^{ii}	0.83(2)	2.04 (2)	2.792(1)	151(2)
N4–H4···F3^{iii}	0.83(2)	2.47(2)	3.001(1)	123(1)
N5–H5A···F4	0.87 (2)	1.98(2)	2.839(2)	167(2)
N5–H5A···F4^{iv}	0.87(2)	2.44(2)	2.890(1)	113(1)
N5–H5B···F3^{iii}	0.79(2)	2.23 (2)	2.886(2)	141(2)
N5–H5B···F2^{iv}	0.79(2)	2.54(2)	3.126(2)	133(1)

(i) 2–x, –y, 1–z; (ii) 1+x, 1+y, z; (iii) x, 1+y, z; (iv) –x, –y, 2–z.

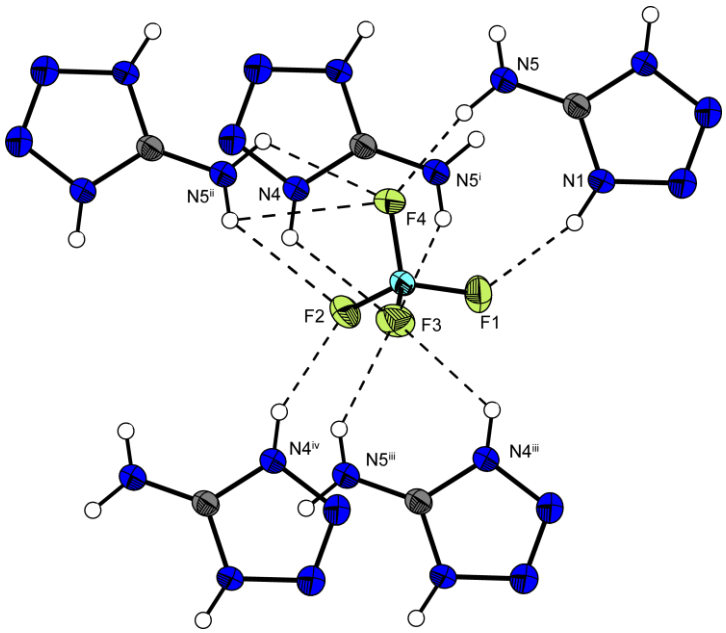

Figure 17.2 Hydrogen bonding of one tetrafluoroborate anion; (i) 1–x, –y, 2–z; (ii) –x, –y, 2–z; (iii) x, –1+y, z; (iv) –1+x, –1+y, z.

17.2 Reaction of 5-Aminotetrazole with Tosyl Chloride under Basic Conditions

The reaction of 5-aminotetrazole with triethyl amine and tosyl chloride leads under ring opening to the formation of tosyl-azidoformamidine (**174**). This compound may be a valuable transfer agent of 5-aminotetrazole to form substituted 5-aminotetrazole derivatives (**Scheme 17.2**). The reaction of **174** with hydroxyl amine followed by an basic work up should be a new way to 1,5-diaminotetrazole or 5-hydrazino-1*H*-tetrazole.

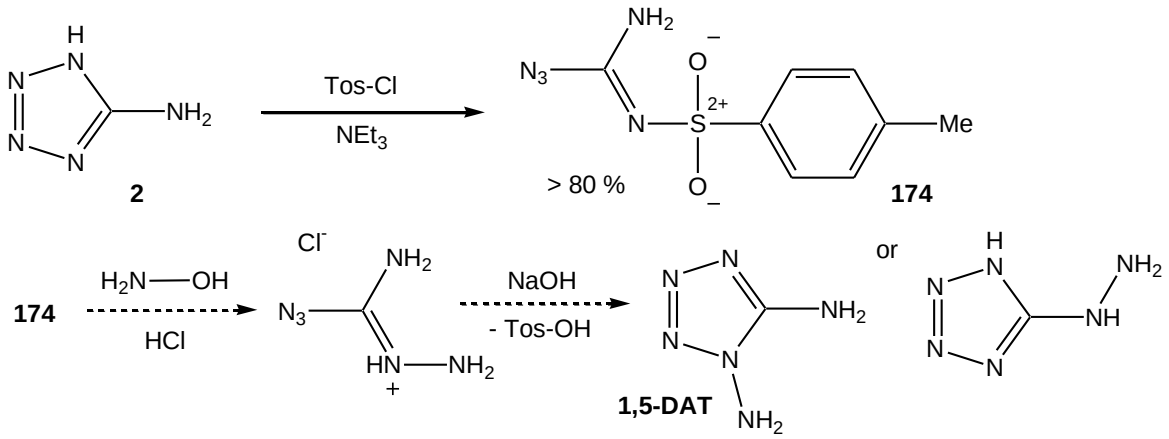

Scheme 17.2 Reaction of 5-aminotetrazole with triethyl amine and tosyl chloride.

Tosyl-azidoformamidine (**174**) crystallizes in the triclinic space group *P*–1 with two molecules in the unit cell and a density of 1.516 g cm^{-3}. The molecular structure is depicted in **Figure 17.3**.

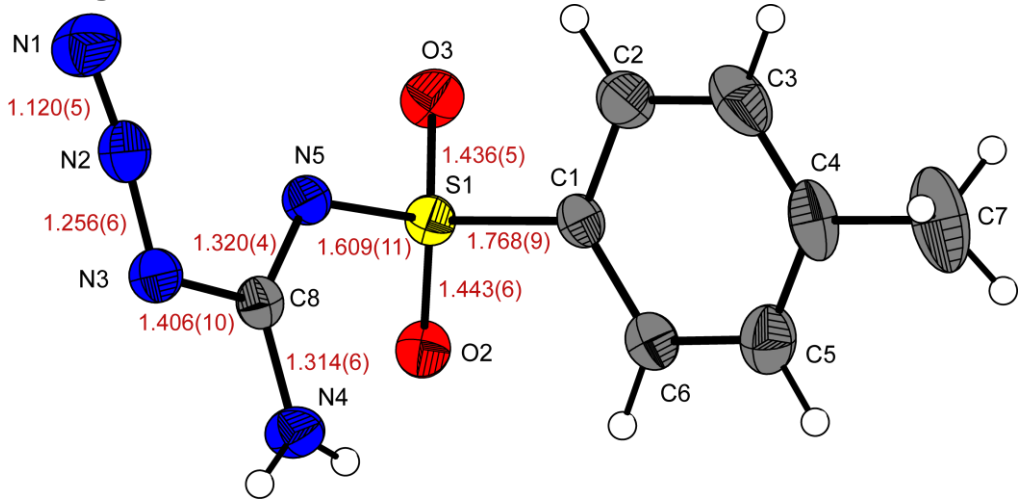

Figure 17.3 Molecular structure of tosyl-azidoformamidine (**174**). Selected bond lengths (Å) are depicted. Thermal ellipsoids are drawn at the 50 % probability level.

17.3 Nitration of 2-(2-Hydroxyethyl)-5-aminotetrazole with 100 % Nitric Acid

The nitration of 2-(2-hydroxyethyl)-5-aminotetrazole (**47**) using 100 % nitric acid leads to the formation of **OCX** (**175**, **oc**topus e**x**plosive) and a byproduct (detected by NMR spectroscopy) which could not be identified yet (**Scheme 17.3**).

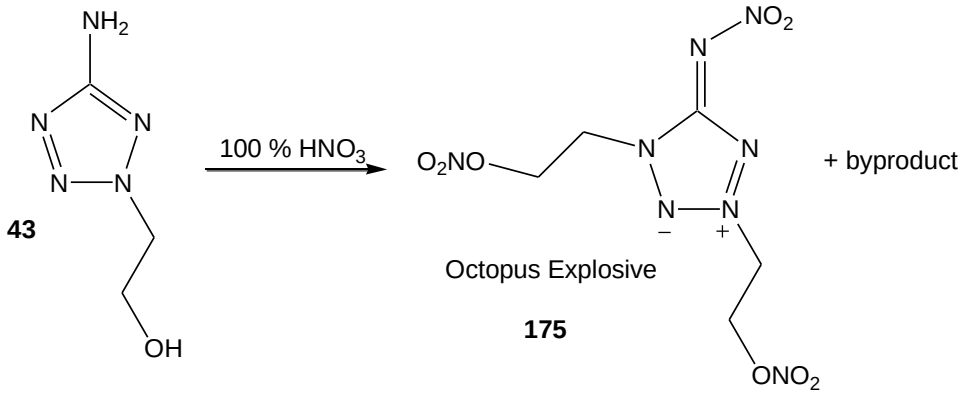

Scheme 17.3 Synthesis of **OCX** (**175**) by nitration of 2-(2-hydroxyethyl)-5-aminotetrazole.

The extraction of the nitration mixture followed by recrystallization from MeOH afforded the first tetrazolyl-oxatriazolio-oxid: 3-[2-(2-Nitrato-ethyl)-2*H*-tetrazol-5-yl]-[1,2,3,4]oxatriazol-5-one (**176**). **175** as well as **176** are zwitter ionic compounds, which can be seen on their lewis structure in **Scheme 17.4**.

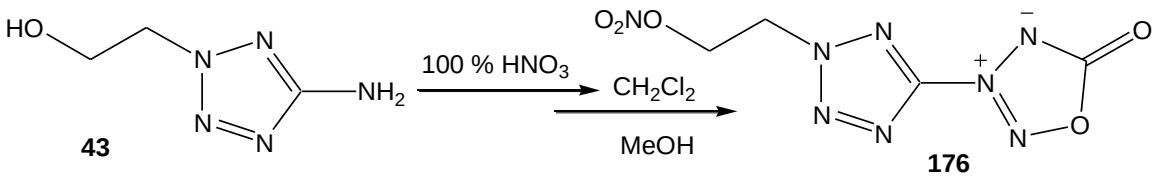

Scheme 17.4 Synthesis of the first tetrazolyl-oxatriazolio-oxid (**176**).

OCX crystallizes in the monoclinic space group $P2_1$ with two molecules in the unit cell. The *Friedel pairs* have been merged. The density of 1.791 g cm^{-3} is promising high with regard to develop new high explosives. The molecular unit is shown in **Figure 17.4**. Although a zwitter ionic tetrazole is formed the structure of the ring system is not affected and is in agreement with most of the other neutral tetrazoles in this work.

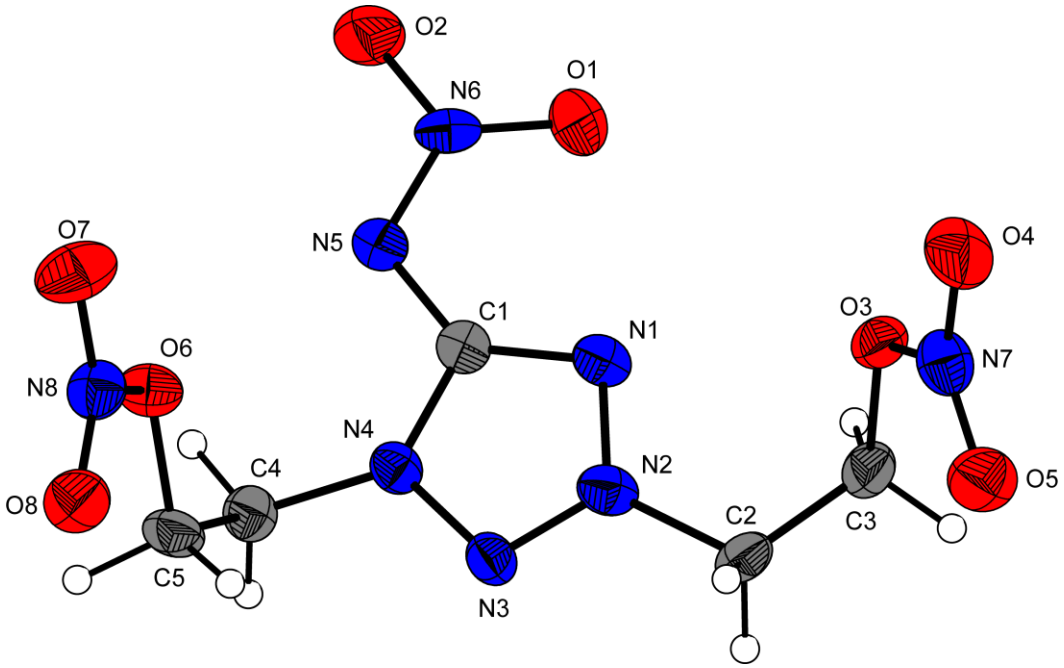

Figure 17.4 Molecular structure of **175**. Thermal ellipsoids are drawn at the 50 % probability level. Bond distances (Å): O3–N7 = 1.394(3), O3–C3 = 1.457(4), O6–N8 = 1.387(3), O6–C5 = 1.466(4), O8–N8 = 1.201(3), O5–N7 = 1.198(3), O2–N6 = 1.238(3), N8–O7 = 1.204(3), O4–N7 = 1.203(4), N1–C1 = 1.336(3), N1–N2 = 1.341(3), O1–N6 = 1.234(3), N4–N3 = 1.342(3), N4–C1 = 1.371(4), N4–C4 = 1.456(4), N5–N6 = 1.341(3), N5–C1 = 1.358(3), N2–N3 = 1.283(3), N2–C2 = 1.493(4), C5–C4 = 1.488(5), C2–C3 = 1.479(5).

Since **OCX** shows an decomposition temperature not until 164 °C, the energetic properties have been discovered and the heat of formation as well as the detonation parameters were calculated. The heat of formation $\Delta_f H°$(s, **OCX**) was calculated by the atomization energy method yielding a value of +30.8 kcal mol^{-1} (129 kJ mol^{-1}). With that value and the X-ray density of 1.791 g cm^{-3} several detonation parameters, such as the detonation velocity and pressure have been computed with the EXPLO5.V2 program. OCX shows a detonation velocity of ~8700 m s^{-1}, which is close to these of RDX. The exact values are summarized in **Table 17.2**. Unfortunately, **OCX** is sensitive towards impact (2.5 J) and friction (145 N).

Table 17.2 Energetic properties **of OCX**

	OCX (**175**)	EXPLO5 values:	
impact sensitivity / J	2.5	Q_v / kJ kg^{-1}	–5874
friction sensitivity / N	145	T_{ex} / K	4268
$T_{Dec.}$ / °C	164	p/ kbar	325
ρ / g cm^{-3}	1.792	$V_{Det.}$ / m s^{-1}	8701
Ω / %	–31.2	V_0 / L kg^{-1}	768

For **OCX** a preliminary experimental procedure follows: HNO_3 (100 %, 15 mL) was cooled to 0 °C and gelantinous 2-(2-hydroxyethyl)-1*H*-tetrazol-5-ylamine (4.00 g, 27.2 mmol) was added dropwise. The obtained solution was stirred at ambient temperature for 48 hours. The reaction mixture was poured on ice and extracted with CH_2Cl_2. To the DCM phase 20 mL MeOH was added and the raw product emerged which was filtrated and washed with small amounts of EtOH and diethyl ether. The recrystallization from acetone resulted in colorless plates (yield ~40 %). **DSC** (T_{onset}, 5 °C min^{-1}): 164–165 °C (dec.); **IR** (KBr, cm^{-1}): $\tilde{\nu}$ **=** 3233 (w, br), 3037 (w), 2984 (w), 2965 (w), 2905 (w), 1668 m), 1633 (s), 1533 (s), 1474 (m), 1424 (m), 1371 (m), 1278 (s br), 1242 (s), 1207 (m), 1186 (m),1007 (m), 977 (m), 893 (s), 850 (s), 757 (m), 707 (m), 667 (m); **Raman** (1064 nm, 300 mW, 25 °C, cm^{-1}): $\tilde{\nu}$ = 2965 (17), 1632 (17), 1524 (50), 1469 (24), 1435 (31), 1320 (25), 1284 (41), 1208 (24), 1198 (26), 1047 (29), 987 (25), 899 (19), 848 (25), 757 (40), 709 (22), 566 (36), 460 (36), 460 (34), 443 (34), 399 (34), 311 (38), 273 (37); **^{1}H NMR** (d_6-DMSO, 25 °C, ppm): δ = 5.17 (t, ^3J=5 Hz, 2H, CH_2), 5.01 (t, ^3J=5 Hz, 2H, CH_2), 4.87 (t, ^3J=5 Hz, 2H, CH_2), 4.68 (t, ^3J=5 Hz, 2H, CH_2); **^{13}C NMR** (d_6-DMSO, 25 °C, ppm): δ = 159.8 (C), 69.6 (2 CH_2), 54.1 (CH_2), 45.7(CH_2); **^{14}N NMR** (d_6-DMSO, 25 °C, ppm): δ = –17.6 (NO_2), –45.6 (NO_2). ***m/z*** (DEI): 308 [$(M)^+$], 125 (23), 60 (50), 55 (60), 46 (78), 45 (57), 44 (25), 43 (100), 30 (71), 29 (25), 28 (26), 27 (64); **impact sensitivity**: 2.5 J; **friction sensitivity**: 145 N.

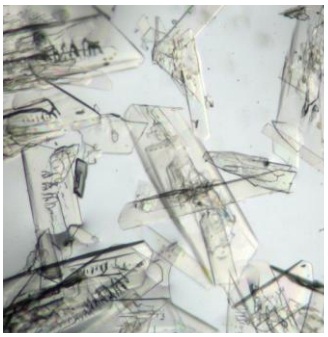

Except for the crystal structure there exists no further characterization of the tetrazolyl-oxatriazolio-oxid **176**. Compound **176** crystallizes in the monoclinic space group $P2_1/c$ with four molecules in the unit cell and a density of 1.827 g cm^{-3}. The molecular structure can be seen in **Figure 17.5**. Due to the long distance C1–N5 of 1.42 Å there should

be no delocalized electron system between the heterocycles. In addition the two planar rings are not coplanar (torsion angle N4–C1–N5–N7 = –2.1(3)°).

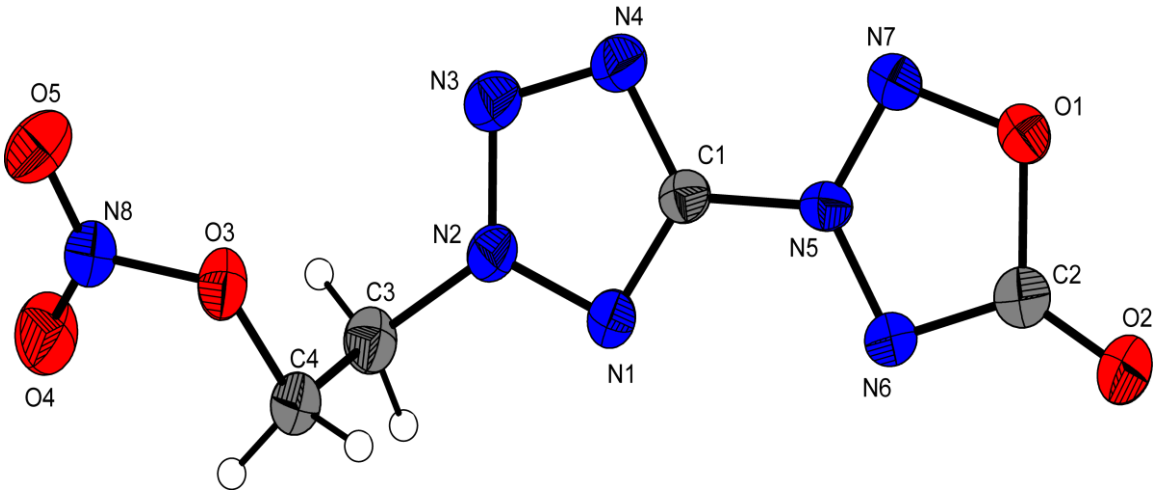

Figure 17.5 Molecular structure of **176**. Thermal ellipsoids are drawn at the 50 % probability level. Bond distances (Å): O5–N8 = 1.201(2), O3–N8 = 1.408(2), O3–C4 = 1.451(3), N4–C1 = 1.334(3), O4–N8 = 1.195(2), N1–C1 = 1.316(3), N1–N2 = 1.329(2), N2–N3 = 1.331(3), N4–N3 = 1.323(2), N2–C3 = 1.466(3), N5–N7 = 1.290(2), N5–N6 = 1.326(2), N5–C1 = 1.419(3), C4–C3 = 1.508(3), O1–N7 = 1.358(2), O1–C2 = 1.431(3), N6–C2 = 1.361(3), C2–O2 = 1.198(3).

Note from the author: It would be of great interest to continue this work on nitrated 2-substituted 5-aminotetrazoles to (i) understand the mechanism of formation (ii) discover and characterize all by-products and (iii) obtained highly dense new energetic materials.

17.4 The Energetic Compound 5-Nitratoethyl-5-nitramino-1*H*-tetrazole

In accordance to the past discussed reactions a further energetic compound based on nitration of 2-substituted 5-aminotetrazols was obtained. The nitration of 2-methyl-5-aminotetrazole with fuming nitric acid was discussed in Chapter 4. After pouring the reaction on ice, 2-methyl-5-nitraminotetrazole (**45**) precipitated. The wet (HNO_3/water) raw product was recrystallized from a small amount of EtOH, whereby the following product ($C_3H_5O_5N_7$, M = 219.12 g mol^{-1}) was obtained (**Scheme 17.5**).

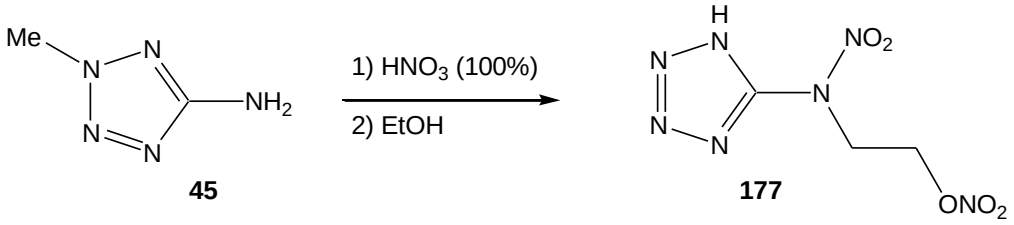

Scheme 17.5 Formation of 5-nitratoethyl-5-nitramino-1*H*-tetrazole (**177**).

5-Nitratoethyl-5-nitramino-1*H*-tetrazole (**177**) is an interesting energetic material since it shows (i) a high density (1.829 g cm^{-3}) (ii) an appropriate oxygen balance (Ω = –25.6 %) (iii) an acid ring proton, which can be deprotonated to form thermally stable salts, e.g. triaminoguanidinium 5-nitratoethyl-5-nitramino-1*H*-tetrazolate. Except for the crystal structure of **177**, no further characterization has been done. **177** crystallizes in the monoclinic space group $P2_1/c$ with four molecules in the unit cell. Due to the ring proton chains (graph set **C1,1(6)**) are formed by the hydrogen bond N1–H1···N2^{i} (0.90(3), 2.08(3), 2.912(7) Å, 153(3)°;(i) 1–x, –0.5+y, 2.5–z).

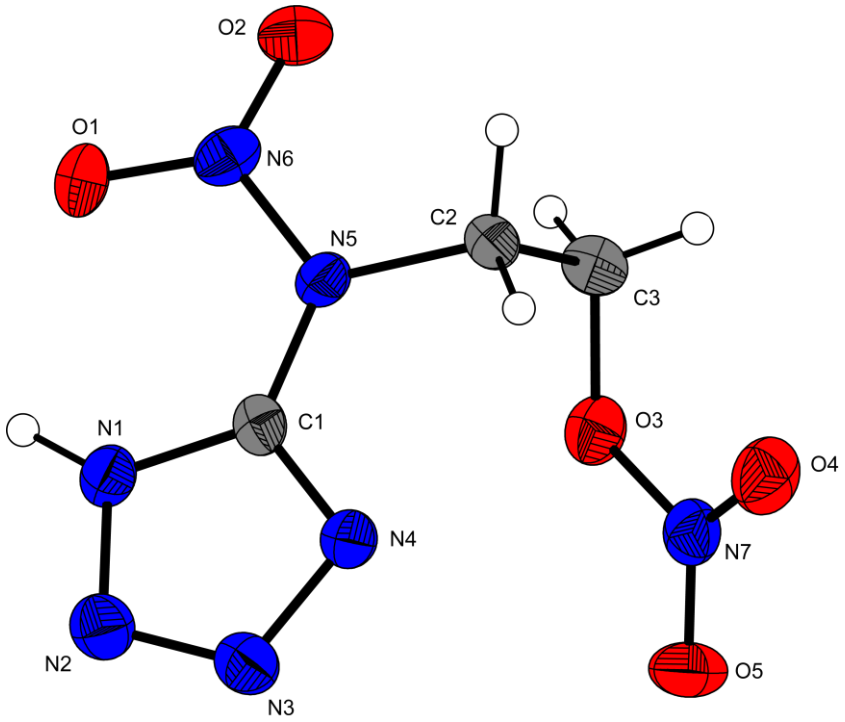

Figure 17.6 Molecular structure of **177**. Thermal ellipsoids are drawn at the 50 % probability level. Bond distances (Å): O2–N6 = 1.210(3), N1–C1 = 1.341(4), N1–N2 = 1.347(4), O1–N6 = 1.232(3), O3–N7 = 1.399(3), O3–C3 = 1.450(4), N6–N5 = 1.387(4), N4–C1 = 1.321(4), N4–N3 = 1.366(3), O5–N7 = 1.210(3), C1–N5 1.381(4), N3–N2 = 1.302(4), N7–O4 = 1.209(3), N5–C2 = 1.473(4), C2–C3 = 1.503(5).

17.5 1,4-Di(2-chloroethyl)-5-aminotetrazolium chloride

In the synthesis of 1-(2-chloroethyl)-5-aminotetrazole (**51**) the interesting byproduct 1,4-di(2-chloroethyl)5-aminotetrazolium chloride (**178**) could be discovered, which may be precursor for the formation of a new nitrogen-rich azide salt (**Scheme 17.6**). Up to now only the crystal structure of **178** has been investigated.

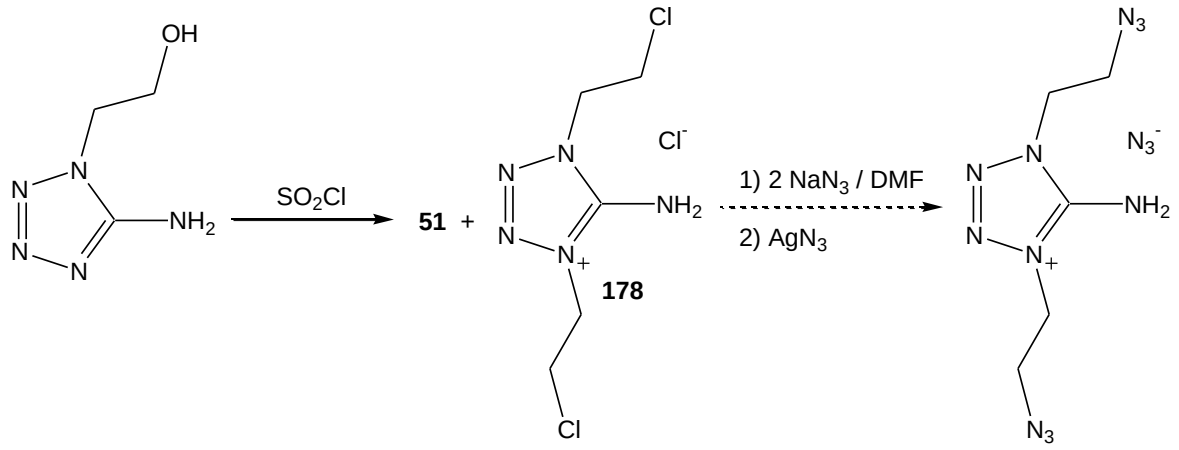

Scheme 17.6 Formation of **178** and potential synthesis of a new disubstituted tetrazolium based azide.

1,4-Di(2-chloroethyl)-5-aminotetrazolium chloride (**178**) crystallizes in the monoclinic space group $P2_1/c$ with four molecules in the unit cell and a density of 1.516 g cm^{-3}. The molecular structure is shown in **Figure 17.7**.

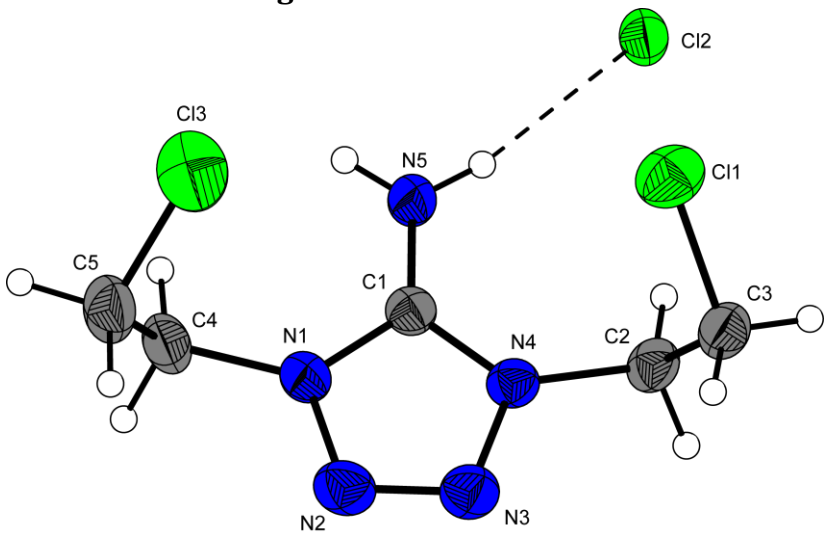

Figure 17.7 Molecular structure of 1,4-di(2-chloroethyl)5-aminotetrazolium chloride (**178**). Thermal ellipsoids are drawn at 50 % probability, and hydrogen

atoms are shown as spheres of arbitrary radii. Bond distances (Å): Cl1–C3 = 1.788(2), Cl3–C5 = 1.796(3), N4–C1 = 1.343(3), N4–N3 = 1.364(3), N4–C2 = 1.464(3), N2–N3 = 1.279(3), N2–N1 = 1.368(3), N1–C1 = 1.345(3), N1–C4 = 1.461(3), C1–N5 = 1.307(3), C3–C2 = 1.505(3), C5–C4 = 1.499(4).

17.6 Energetic Materials based on 5-Cyanotetrazole

5-Cyano-2*H*-tetrazole (**179**) is a valuable tetrazole derivative which is easily available by the reaction of dicyan with one equivalent of sodium azide, followed by protonation using diluted mineralic acids. However, **179** is only rarely described in the literature.[450] The hydrolysis of **179** yields to just as little described *1H*-tetrazole-5-carboxylic acid amide (**180**). Both compounds can be utilized to form thermally stable nitrogen-rich as well as metal salts. These compounds may be used as nitrogen-rich fuels or as smokeless colorants for pyrotechnical compositions. The energetic character of **180** should be further increased by the nitration of the primary amine forming *1H*-tetrazole-5-carboxylic acid nitramine (**181**) (**Scheme 17.7**). This compound should be highly stabilized and act as a promising starting material for several new tetrazolate-based energetic materials. In this contribution, the crystal structures of 5-cyano-2*H*-tetrazole (**179**), *1H*-tetrazole-5-carboxylic acid amide (**180**) and a mixed ammonia/sodium salt (**181**) of **179** are presented as preliminary results.

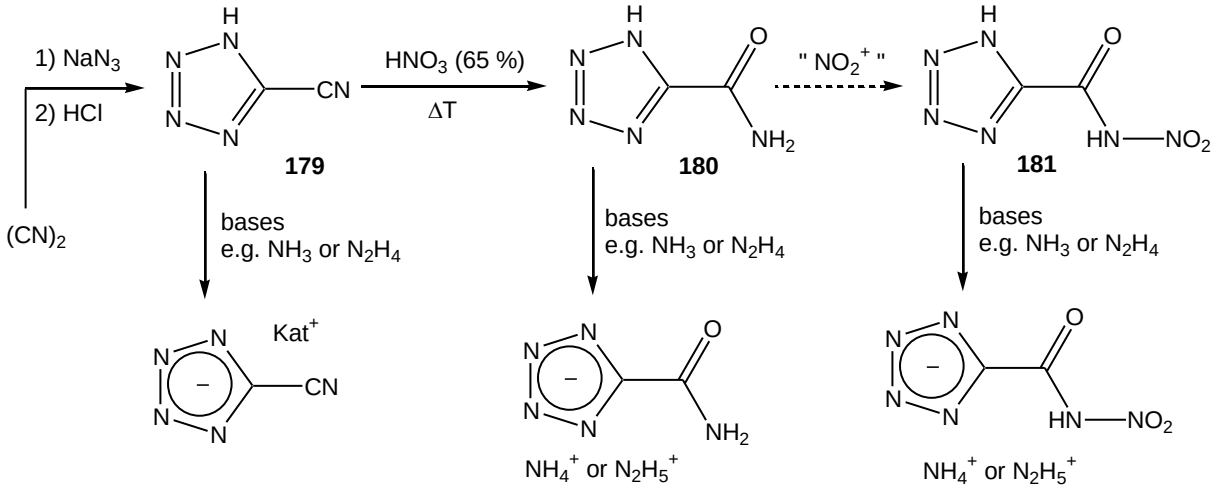

Scheme 17.7 Reaction pathways of the ongoing project "Energetic materials based on 5-cyano-2*H*-tetrazole".

5-Cyano-2*H*-tetrazole (**179**) crystallizes in the monoclinic crystal system ($P2_1/m$) with two molecules in the unit cell and a density of 1.635 g cm^{-3}. The molecular structure is depicted in **Figure 17.8**. To the best of our knowledge, next to 5-nitro-2*H*-tetrazole (**147**) and 1,5-bistetrazole (**152**), compound **179** is the third structural characterized compound, in which the ring proton is located at the ring nitrogen N2. The structure of the tetrazole ring is similar to that of 5-nitro-2*H*-tetrazole. The external cyano group follows the ring plane and is characterized by a C–N bond length of 1.137(2) Å.

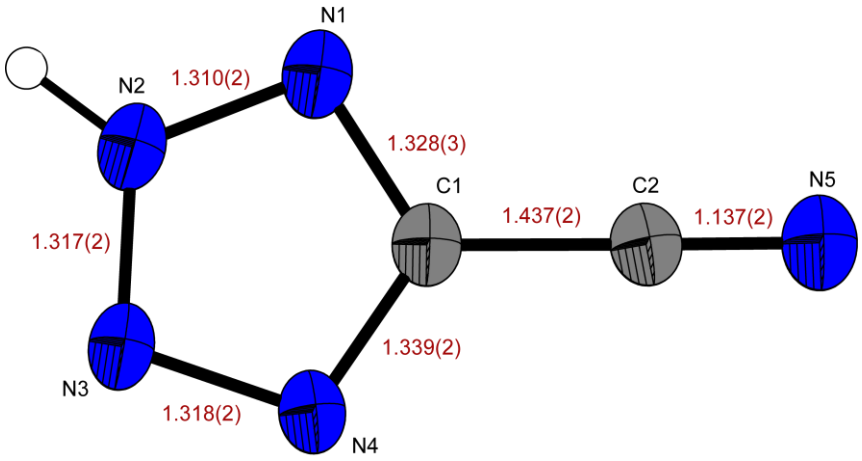

Figure 17.8 Molecular structure of 5-cyano-2*H*-tetrazole (**179**). Bond lengths (Å) are drawn. Thermal ellipsoids are drawn at 50 % probability, and hydrogen atoms are shown as spheres of arbitrary radii.

179 crystallizes in layers within the *a*-*c* plane, which are connected by the hydrogen bonds N2–H2···N4^{i} (0.86(2), 2.28(2), 3.003(5) Å, 141(1)°) and N2–H2···N5^{ii} (0.86(2), 2.31(2), 2.949(3) Å, 131(1)°), shown in **Figure 17.9**.

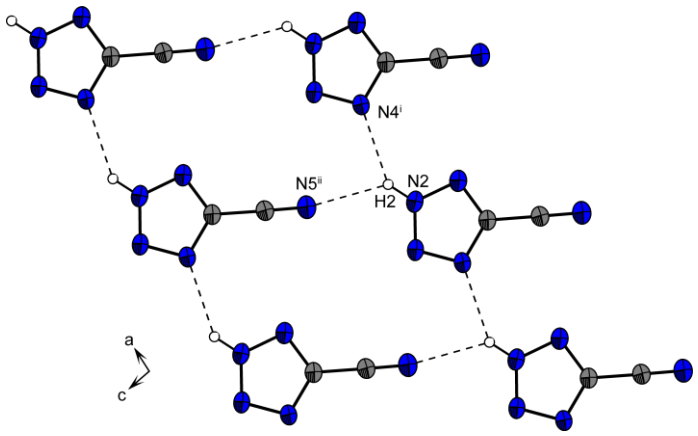

Figure 17.9 View along the *b* axis on the layers in the packing of **179**. Bifurcated hydrogen bonds are marked; (i) –1+x, y, z; (ii) –1+x, y, –1+z.

The mixed sodium/ammonium salt of 5-cyanotetrazolate (**182**) was obtained by deprotonation of impure **179** (residue of sodium 5-cyanotetrazolate) by using diluted ammonia solution. **182** crystallizes as a dihydrate in the monoclinic space group $C2/m$ with four molecular moieties in the unit cell. Interestingly its density of 1.448 g cm^{-3} is lower than this of neutral **179**. The coordination of the sodium cations is depicted in **Figure 17.10**. Due to this coordination chains along the *b* axis are formed, which are illustrated in **Figure 17.11**.

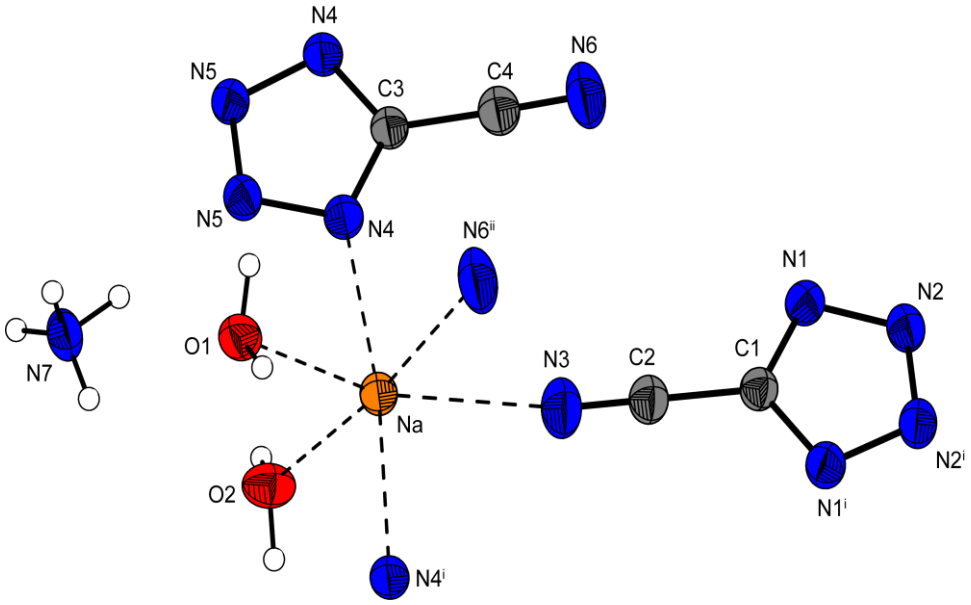

Figure 17.10 Molecular structure and coordination geometry of the sodium atoms in the structure of **182**. Thermal ellipsoids are drawn at the 50 % probability level and hydrogen atoms are shown as spheres of arbitrary radii. Selected coordination distances (Å): Na–O1 = 2.45(1), Na–O2 = 2.310(7), Na–N3 = 2.519(7), Na–N4 = 2.476(1), Na–N4^{i} = 2.476(1), Na–N6^{ii} = 2.671(7); (i) x, 1–y, z (ii) 0.5–x, 0.5+y, –z.

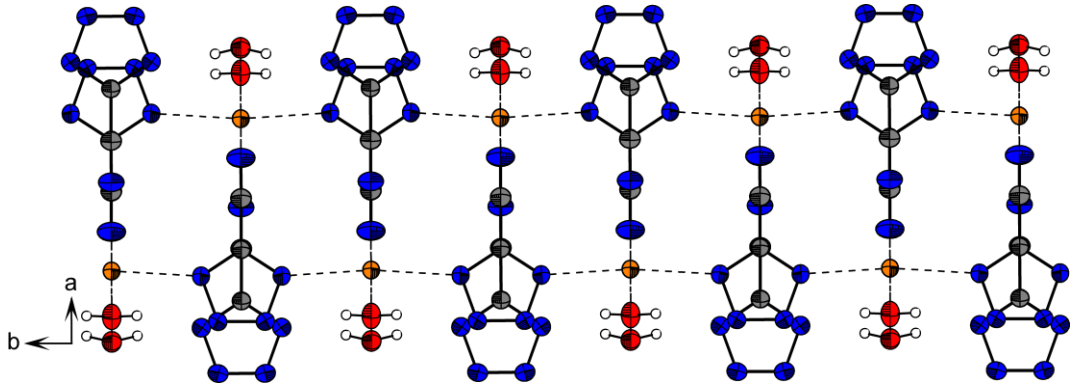

Figure 17.11 Formation of chains along the *b* axis in the structure of **182**. View along the *c* axis.

1H-Tetrazole-5-carboxylic acid amide (**180**) crystallizes in the monoclinic crystal system (space group $P2_1/m$) with two molecules in the unit cell and a density of 1.730 g cm^{-3}. The molecular moiety is shown in **Figure 17.12**. The C–C bond length of 1.488(2) Å is significantly longer than that in 5-cyano-2*H*-tetrazole.

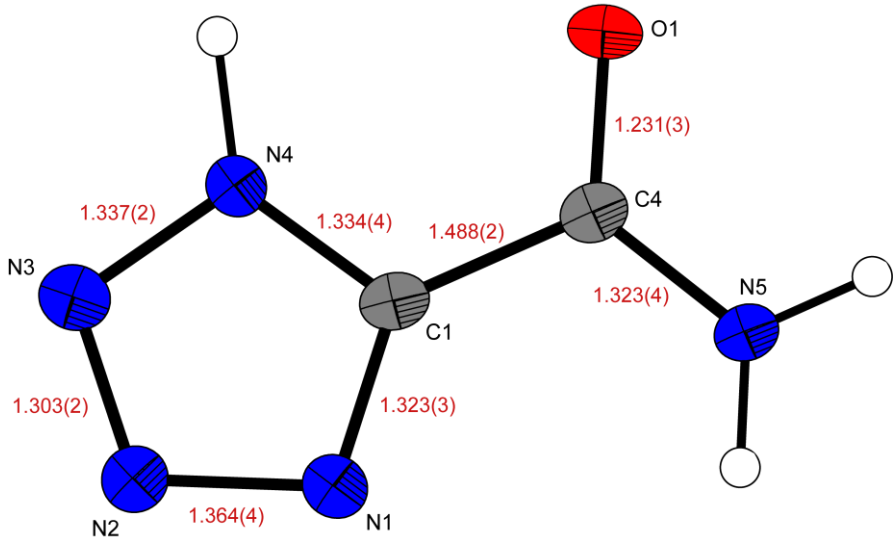

Figure 17.12 Molecular structure of 1*H*-tetrazole-5-carboxylic acid amide (**180**). Bond lengths (Å) are drawn. Thermal ellipsoids are drawn at the 50 % probability level and hydrogen atoms are shown as spheres of arbitrary radii.

In agreement to **179**, compound **180** also crystallizes in a layer structure. The layers along the *a*-*c* plane are build by four strong hydrogen bonds (**Table 17.3**) forming the several graph sets, e.g. **C1,1(4)**, **C1,1(6)**, **C2,2(8)**, **R2,2(10)** and **R4,4(13)** (**Figure 17.13**).

Table 17.3 H-bonding in the structure of *1H*-tetrazole-5-carboxylic acid amide (**180**).

D–H···A	d(D–H)	d(H···A)	d(D···A)	∢(D–H···A)
N5–H62···N2^{i}	0.94(2)	2.23(2)	3.121(2)	158(2)
N4–H4···N1^{ii}	1.02(3)	1.82(3)	2.845(2)	175(3)
N4–H4···N2^{ii}	1.02(3)	2.54(3)	3.415(2)	144(3)
N5–H61···O1^{iii}	0.92(3)	1.90(3)	2.803(2)	169(2)

(i) x, y, 1+z; (ii) –1+x, y, z; (iii) 1+x, y, z.

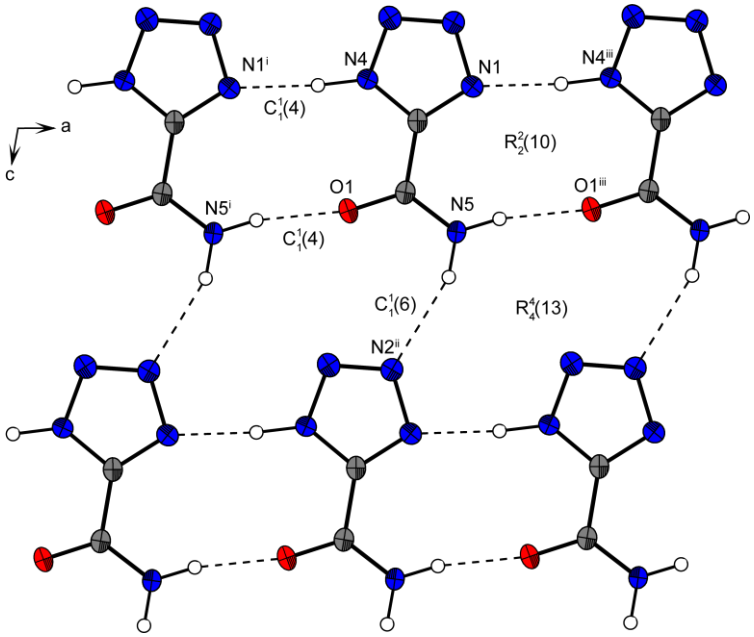

Figure 17.13 View on the layers in **180** along the *b* axis. Hydrogen bond graph sets are drawn; (i) –1+x, y, z (ii) x, y, 1+z (iii) 1+x, y, z.

17.7 A new Modification of 3,6-Diamino-1,2,4,5-tetrazine (183)

3,6-Diamino-1,2,4,5-tetrazine ($C_2H_4N_6$) belongs to the exiting class of nitrogen-rich tetrazine heterocycles. Promising 1,4-diaminotetrazine based energetic materials are described in literature.[451] During attempts to synthesize new tetrazine derivative, single crystals of **183** have been grown from DMF. The structure presented here represents a new polymorph of **183**, crystallizing in the monoclinic space group *C*2/*m* (Z = 2) with a density of 1.624 g cm^{-3}. The previously described structure of 1,4-diaminotetrazine by Krieger *et al.* crystallizes in the orthorhombic space group *Amam* with a slightly lower density of 1.611 g cm^{-3}.[452] The molecular structure of **183** is shown in **Figure 17.14**. The bond lengths of the symmetric 1,4-diaminotetrazine molecule are 1.337(3) Å (N1–C1), 1.351(2) Å (N2–C1) and 1.326(2) Å (N2–N2^{i}).

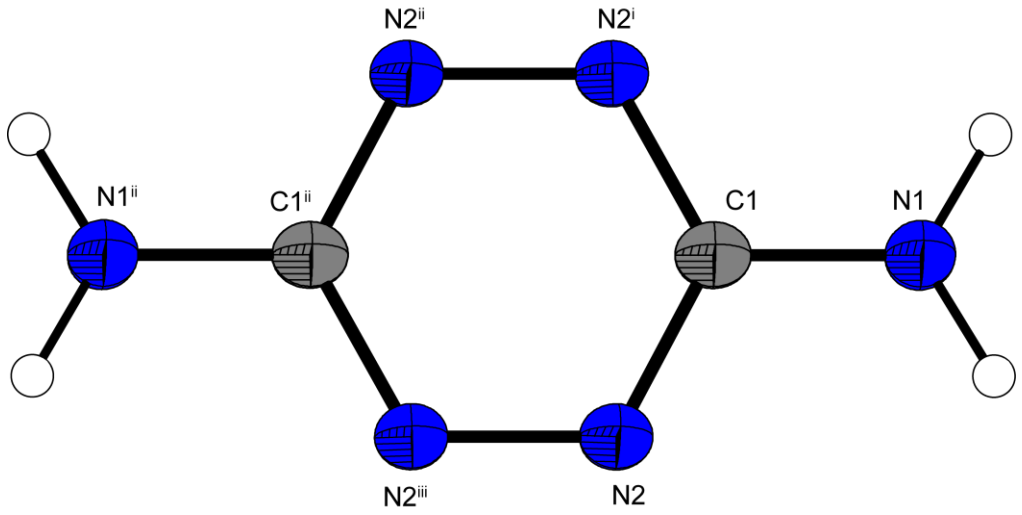

Figure 17.14 Molecular structure of 1,4-diaminotetrazine (**183**). Thermal ellipsoids are drawn at the 50 % probability level, and H atoms are shown as spheres of arbitrary radii. (i) –x, y, 1–z (ii) –x, –y, 1–z (iii) x, –y, z.

The 1,4-diaminotetrazine molecules form a layer structure (**Figure 17.15**), which is stabilized by the hydrogen bond N1–H1···N2^{i} (0.92(2), 2.16(2), 3.080(3) Å, 176(2)°; (i) 0.5–x, 0.5–y, 2–z).

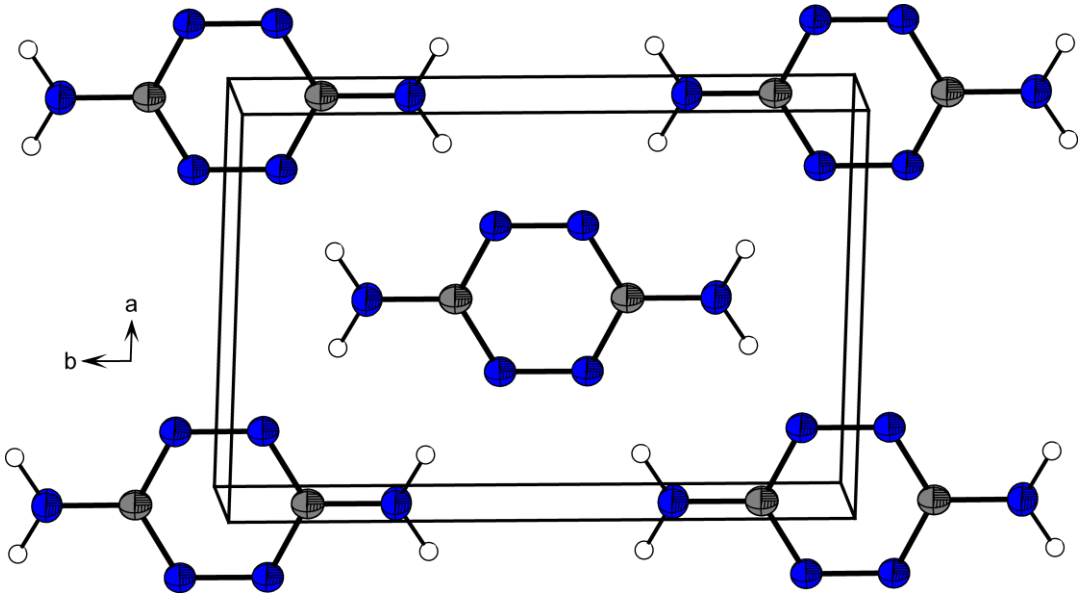

Figure 17.15 Unit cell of **183**. View along the *c* axis.

17.8 Pyrotechnic Colorants Based on 5-Chlorotetrazole

5-Chlorotetrazoles can be synthesized from 5-aminotetrazole by diazotation with sodium nitrite during the presence of Cu(I)Cl and sodium chloride (**Scheme 17.8**). Metal salts of 5-chlorotetrazole represent an exciting class of new materials, which can be used as future colorants in modern smokeless pyrotechnical composition. Within this thesis the crystal structure of the sodium salt (**184**) of 5-chlorotetrazole is presented, which is the first example of a structural characterized unsubstituted 5-chlorotetrazole. **184** crystallizes as a dihydrate in the orthorhombic space group Pnma with four molecular formula in the unit cell and a density of 1.830 g cm^{-3}. The coordination of the sodium cations is distorted octahedral, which is shown in **Figure 17.16**. Due to this coordination mode, chains, depicted in **Figure 17.17**, are formed along the *a* axis.

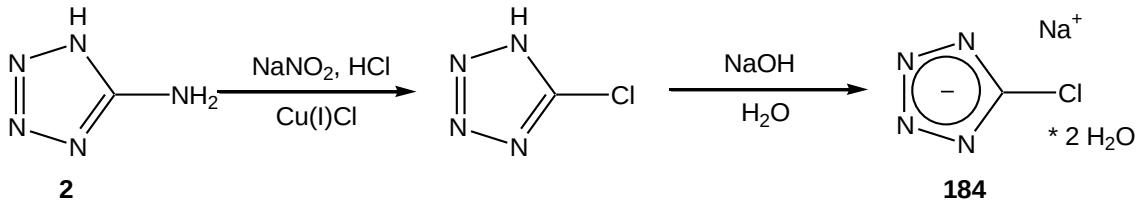

Scheme 17.8 Synthesis of sodium 5-chlorotetrazolate dihydrate (**184**).

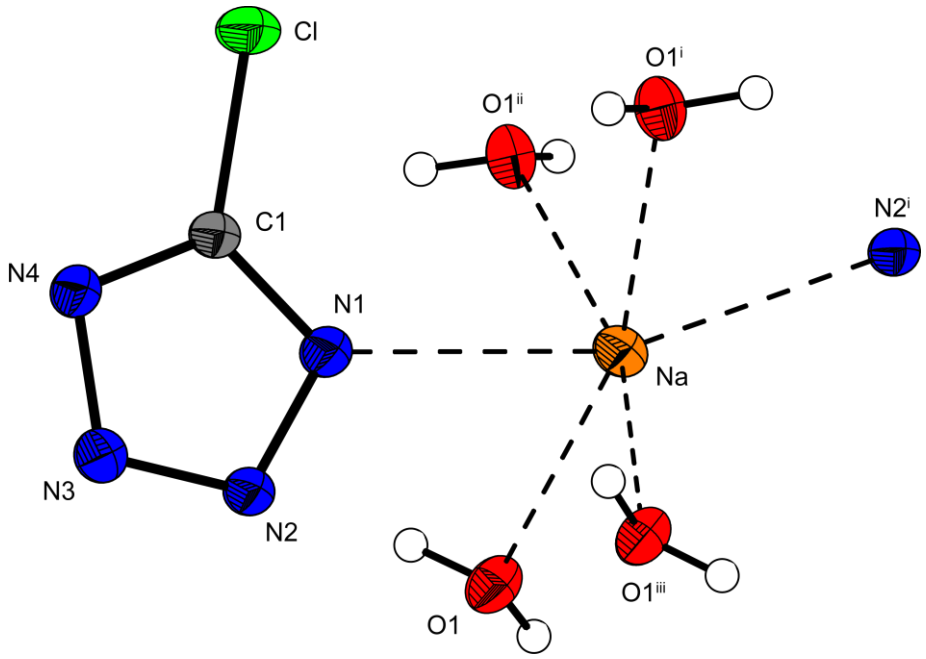

Figure 17.16 Molecular structure and coordination geometry of the sodium atoms in the structure of **184**. Thermal ellipsoids are drawn at the 50 % probability level, and H atoms are shown as spheres of arbitrary radii. Selected distances(Å): Cl–C1 = 1.706(2), Na–O1 = 2.419(1), Na–O1^{iii} = 2.419(1), Na–O1^{i} = 2.428(1), Na–O1^{ii} = 2.428(1), Na–N1 = 2.574(2), N2–N3 = 1.314(3), N2–N1 = 1.350(3), N3–N4 = 1.349(3), N1–C1 = 1.331(3), N4–C1 = 1.319(3); (i) 0.5+x, 0.5–y, 1.5–z; (ii) 0.5+x, y, 1.5–z; (iii) x, 0.5–y, z.

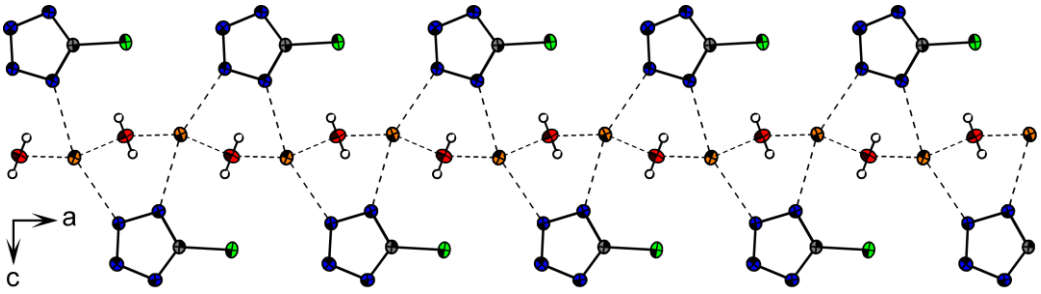

Figure 17.17 Formation of chains along the *a* axis in the structure of **184**. View along the *b* axis.

Summary

The main goals of the present thesis are:

(i) Replacement of RDX.
(ii) New red and green colorants for pyrotechnical compositions.
(iii) Nitrogen-rich derivatives for smokeless propellant charges.
(iv) Green replacement of lead(II) azide in priming charges.

In all of these topics promising technical advances have been made and are described in this thesis.

(i) Replacement of RDX

The substitution of RDX in secondary detonation charges is very challenging, due to the great performance of RDX, its low sensitivities as well as its good thermal behavior. Based on the results of this thesis, three compounds (**Figure 18.1**) are under current investigation as new replacements:

(a) Triaminoguanidinium dinitramide (TAGDN, **37**)
(b) Triaminoguanidinium 1-methyl-5-nitriminotetrazolate (TAG-1MeAtNO$_2$, **88**)
(c) Bis(1*H*-tetrazolyl)amine (H_2bta, **160**)

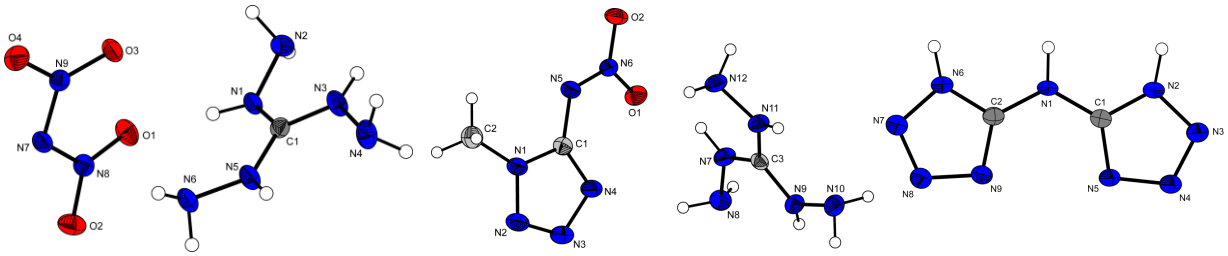

Figure 18.1 Molecular structures of TAGDN (left), TAG-1MeAtNO2 (middle) and H_2bta (right)

A comparison of their energetic properties with those of RDX is given in **Table 18.1**.

Table 18.1 Comparison of investigated explosives with hexogen.

	RDX	TAGDN	TAG-1MeAtNO$_2$	H$_2$bta
Impact / J	7	3	6	> 30
Friction / N	120	24	240	> 360
ESD / J	0.15–0.2	0.79	0.2	7.5
Steel shell / mm	8	≥ 10	≥ 10	≥ 10
N / %	37.8	59.7	67.7	82.3
Ω / %	-21.6	-18.9	-64.5	-57.5
$T_{dec.}$ / °C	213	180	210	250
ρ / g cm^{-3}	1.82	1.628	1.57	1.861
ΔU_{ex} / kJ kg^{-1}	-6043	-5902	-4888	-4537
V_{Det} / m s^{-1}	8750	8796	8770	9120
$p_{C\text{-}J}$ / kbar	346	299	273	343
T_{ex} / °C	4321	3986	3210	3449

Within the framework of the study of new high explosives, several manuscripts have been published, e.g. in Chemistry of Materials,[145] Dalton Transactions,[133] European Journal of Inorganic Chemistry,[134] Physical Chemistry Chemical Physics[135] and Journal of Materials Chemistry.[156] Two of them were selected as front covers on the corresponding journals.

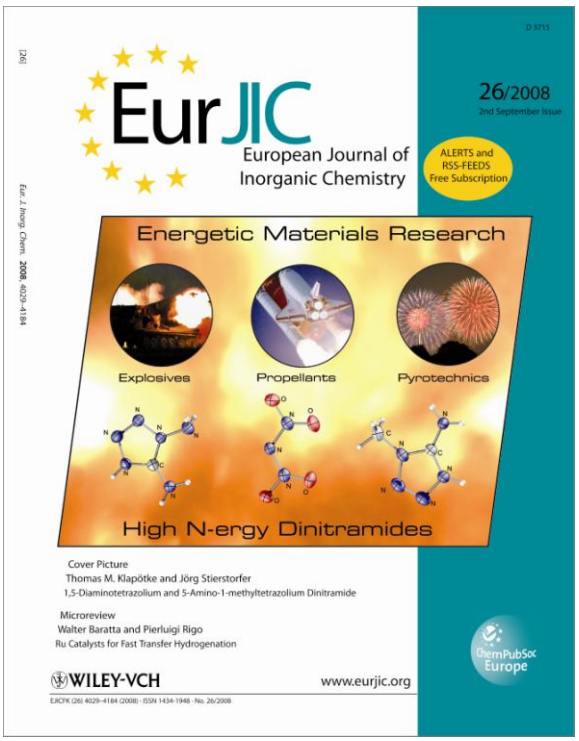

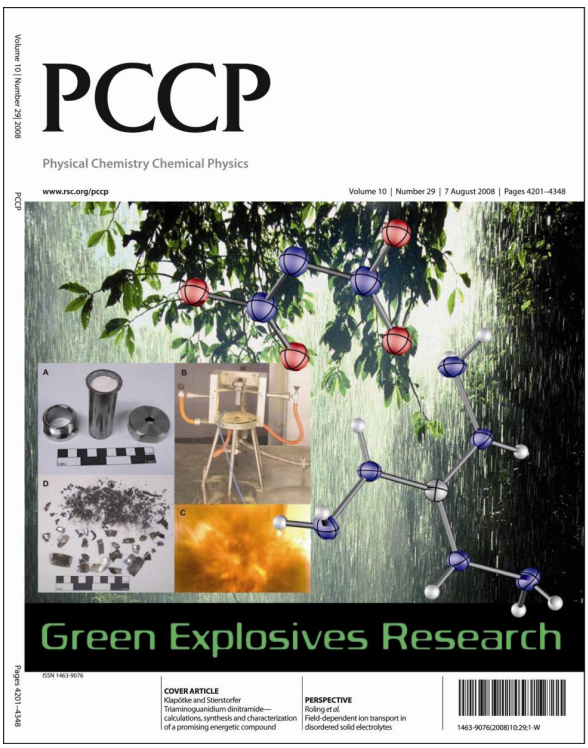

(ii) New red and green colorants for pyrotechnical compositions

Red and green colorants in pyrotechnical compositions still contain polluting salts, e.g. barium(II) and perchlorates. Several strontium and copper based tetrazole salts and complexes have been synthesized and characterized. Within this thesis, two very appropriate red colorants have been discovered, which show brilliant red flame colors. These compounds are already under current investigation at our co-operation partners at ARDEC (Armament Research, Development and Engineering Center):

(a) Strontium tetrazolate pentahydrate ($Sr(Tz)_2 \cdot 5H_2O$, **134**)
(b) Strontium 1-methyl-5-nitriminotetrazolate hydrate ($Sr(1MeAtNO_2)_2) \cdot H_2O$, **82**)

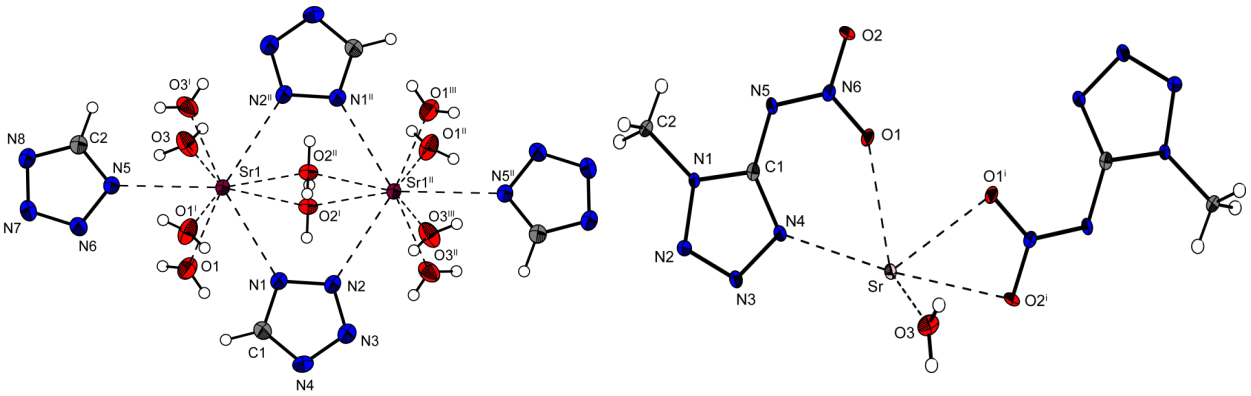

Figure 18.2 Molecular structures of ($Sr(Tz)_2 \cdot 5H_2O$) (left) and ($Sr(1MeAtNO_2)_2) \cdot H_2O$) (right).

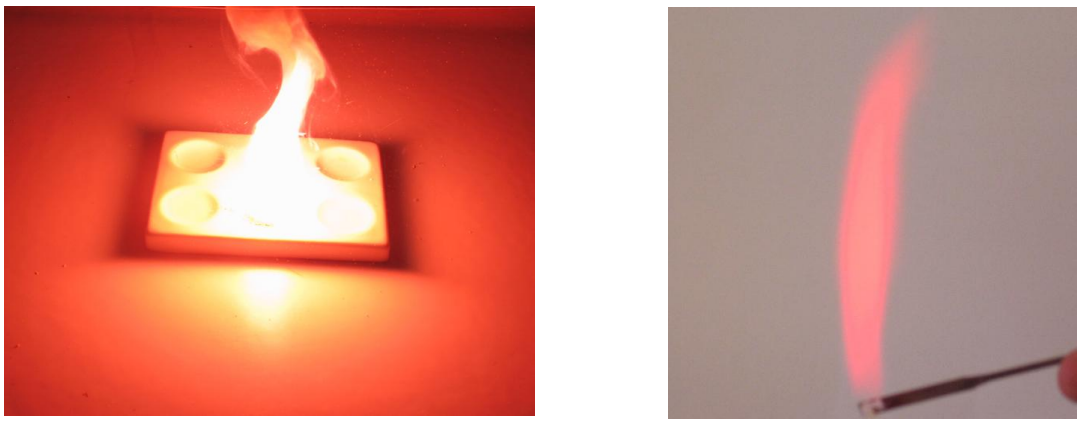

Figure 18.3 Combustion of ($Sr(Tz)_2 \cdot 5H_2O$) with magnesium (left) and ($Sr(1MeAtNO_2)_2) \cdot H_2O$) (right).

Also several copper complexes were synthesized and characterized. Although most of them exhibit brilliant green flame colors when combusted in the flame tests, they nevertheless show problems reaching this green colors when mixed with magnesium and binders. Two of the most promising copper complexes based on 5-nitriminotetrazoles are:

(a) $[Cu(AtNO_2)(NH_3)_3]_2$
(b) $[Cu(1MeAtNO_2)(NH_3)_2]$

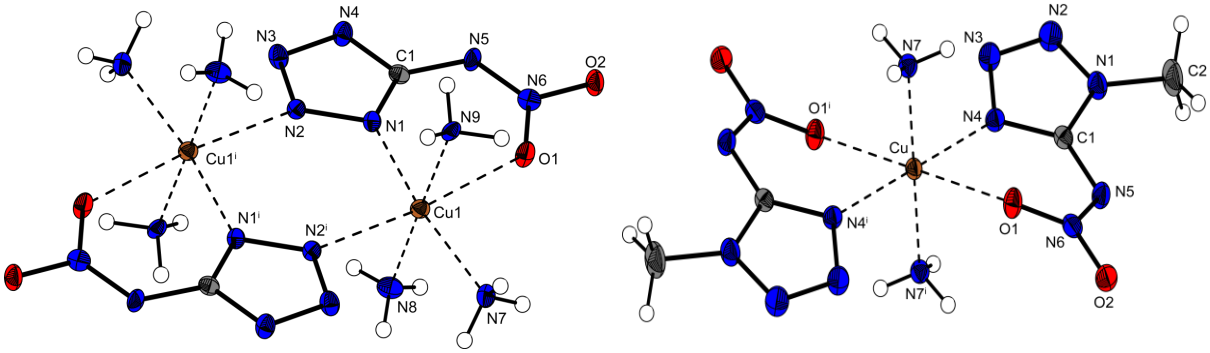

Figure 18.4 Molecular structures of $[Cu(AtNO_2)(NH_3)_3]_2$ (left) and $[Cu(1MeAtNO_2)(NH_3)_2]$ (right).

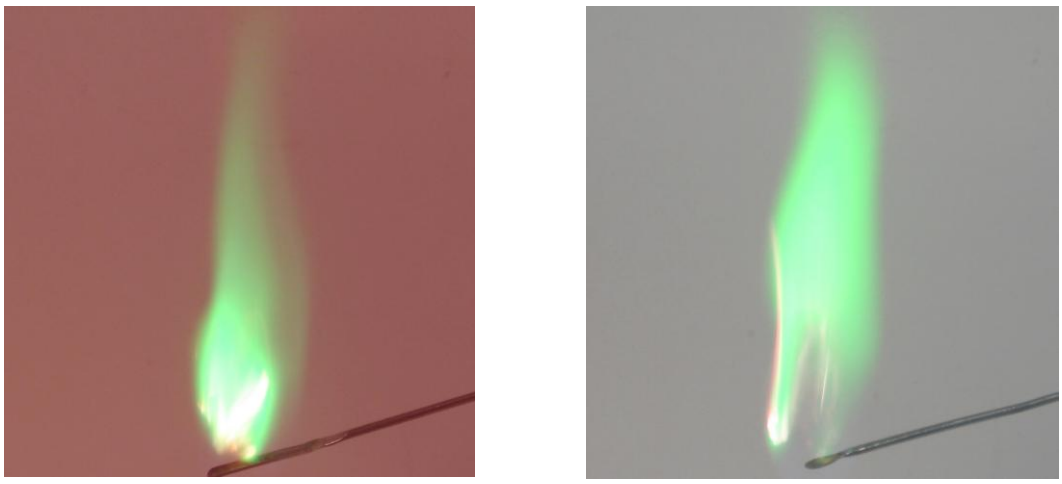

Figure 18.5 Combustion of the complexes $[Cu(AtNO_2)(NH_3)_3]_2$ (left) and $[Cu(1MeAtNO_2)(NH_3)_2]$ (right).

(iii) Nitrogen-rich derivatives for smokeless propellant charges.

Nitrogen-rich salts of 5,5'-azotetrazolate are promise as additives in solid propellant charges. However, these compounds are not compatible towards acidic conditions. Many new nitrogen-rich compounds of tetrazole derivatives are presented in this thesis. Also compounds with high nitrogen contents are very challenging, since a high thermal stability and low sensitivity are needed. Next to H_2bta (**160**), which may also be an outstanding additive in solid propellants, the three best compounds, with regard to technical applications are:

(a) Ammonium 1,5-bistetrazolate (NH_4-1,5BT, **154**)
(b) Ammonium bis(1-methyltetrazolyl)triazenate (NH_4-1MeBTT, **120**)
(c) Hydrazinium 5-aminotetrazolate (N_2H_5At, **30**)

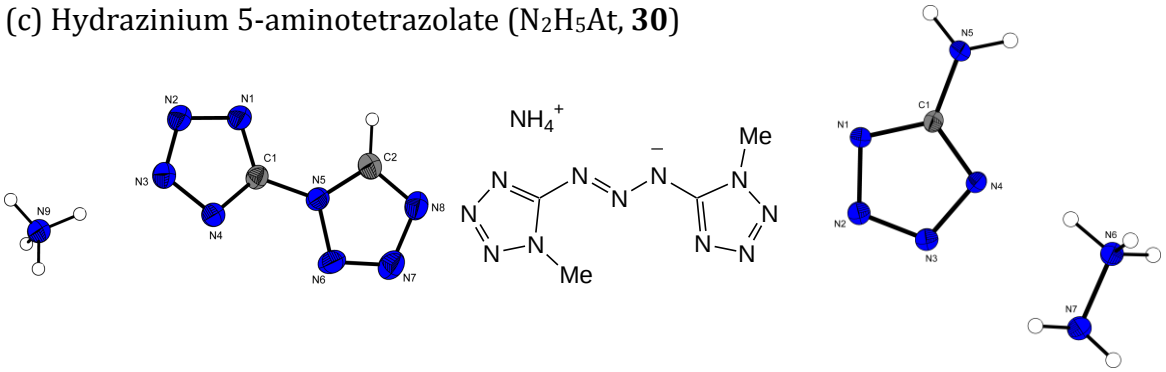

Figure 18.6 Molecular structures of NH_4-1,5BT (left) and N_2H_5At (right) as well as lewis structure of NH_4-1MeBTT (middle).

Table 18.2 Physico-chemical properties of selected nitrogen-rich derivatives.

	NH_4-1,5BT	NH_4-1MeBTT	N_2H_5At
Impact / J	10	7.5	> 100 J
Friction / N	300	360	> 360 N
ESD / J	0.60	1.2	3.0
Steel shell / mm	10		
N / %	81.27	74.31	83.72
Ω / %	–67.04	–91.95	–75.14
$T_{dec.}$ / °C	240	236	186
ρ / g cm^{-3}	1.670	1.60	1.547
ΔU_{ex} / kJ kg^{-1}	–4289	–3714	–4295
V_{Det} / m s^{-1}	8413	8484	9516
$p_{C\text{-}J}$ / kbar	248	248	296
T_{ex} / °C	3181	2626	2759

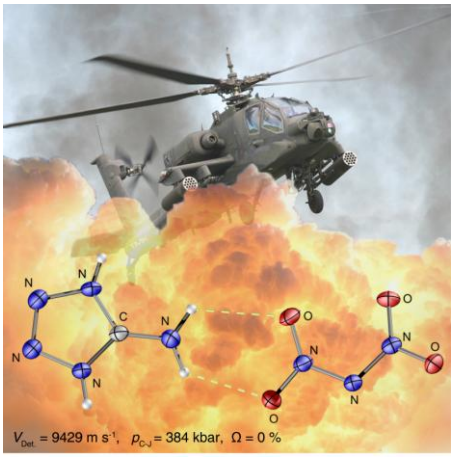

Hydrazinium 5-aminotetrazolate shows the **highest calc. $V_{Det.}$** (9516 m s^{-1}) of all compounds investigated in this thesis. The compounds with the second (9450 m s^{-1}) and third (9428 m s^{-1}) highest $V_{Det.}$ are 5-nitriminotetrazole (**43**) and 5-aminotetrazolium dinitramide (**31**, right picture). However, the first mentioned cannot be used as a secondary explosive, since even PETN based initiators were not able to initiate hydrazinium 5-aminotetrazolate. The full contribution has been published in "Central European Journal of Energetic Materials".[130] The work concerning bis(methyltetrazolyl)triazenes has been published in "Polyhedron".[151]

Many other compounds with partly very high nitrogen contents have been introduced. Since most of these compounds are characterized by extremely high sensitivities, they are more of academic interest. A full reinvestigation of 5-azidotetrazole (**135**) was performed which was also presented on the front cover of the "Zeitschrift für Anorganische und Allgemeine Chemie" in June 2008.[153] Deprotonation of 5-azido-1*H*-tetrazole yields highly energetic salts, which contain the rarely described CN_7^- anion. Next to the new hydrazinium 5-azidotetrazolate (**136**), which represents the tetrazole salt with the highest nitrogen content (88.1 %), eight different salts have been introduced and published in the "Journal of the American Chemical Society".[154]

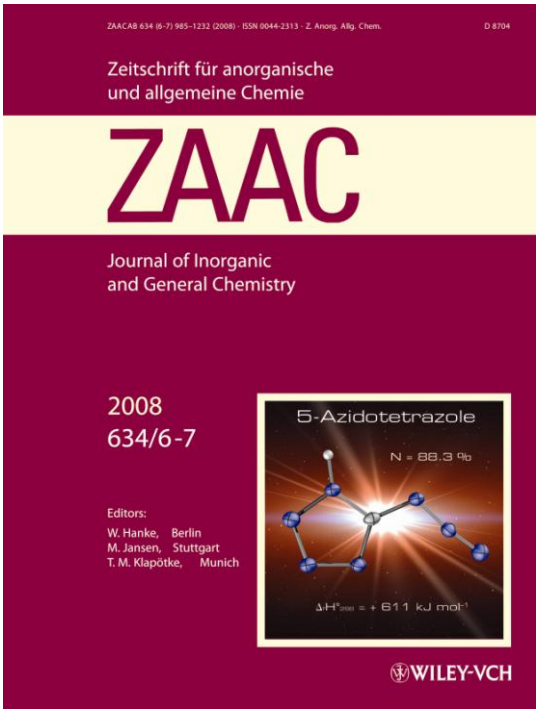

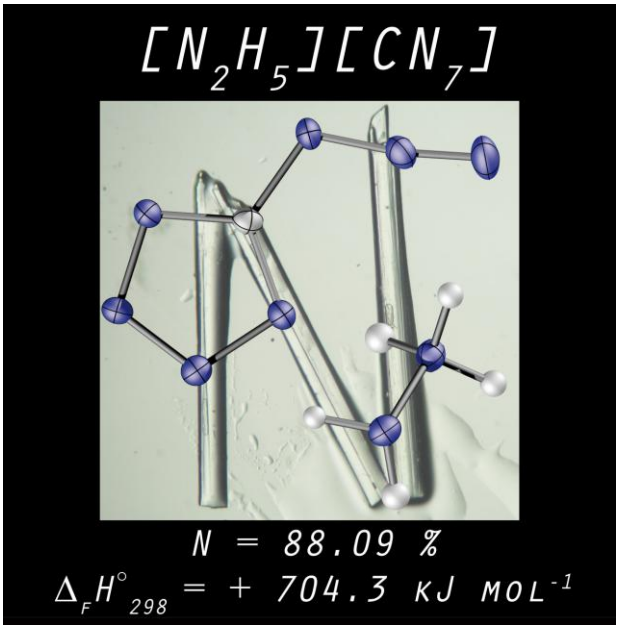

(iv) Green replacement of lead(II) azide in priming charges.

Thousands of tons of extremely toxic lead(II) azide each year are still used in priming charges and detonators. The searching for new substituents of $Pb(N_3)_2$, in this thesis, afforded two new nitriminotetrazole derivatives, which show very promising characteristics (**Figure 18.7**). For use in detonators calcium 5-nitriminotetrazolate (**90**) may be used. This compound is very stable towards temperature and is also lower in sensitivity and toxicity than lead azide. For shock initiated priming applications copper 1-methyl-5-nitriminotetrazolate (**109**) could be used. It shows next to a great thermal stability a higher impact but much less friction sensitivity than lead azide. Both new compounds can be prepared in safe large scale syntheses with low costs.

a) Calcium 5-nitriminotetrazolate
b) Copper 1-methyl-5-nitriminotetrazolate

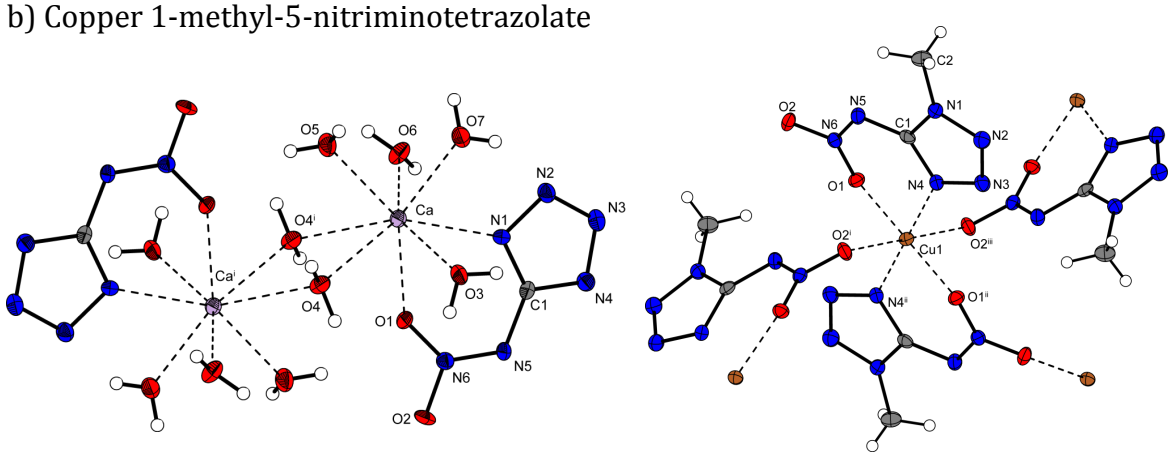

Figure 18.7 Details of the crystal structures of $CaCN_6O_2{\cdot}5H_2O$ (left) and $[Cu(1MeAtNO_2)_2]$ (right).

Table 17.4 Comparison of **90** and **109** with lead azide.

	90	**109**	$Pb(N_3)_2$
$\Delta_{Ex}H°$ / kJ kg^{-1}	–4632		–1638
Impact sensitivity / J	50	< 1	2–4
Friction Sensitivity / N	112	40 N	0.1–1 N
ESD / J	0.15	0.10	0.005
Hot plate test	fulmination	fulmination	fulmination
$T_{dec.}$ / °C	360	252	320

Crystallographic Summary

In this thesis, 156 crystal structures are presented. The following table and diagrams summarize the frequency of the corresponding space groups. Nearly half of the compounds (in this thesis) investigated by XRD crystallize in the space group 14 ($P2_1/n$ and $P2_1/c$).

Space group	Amount	Space group	Amount	Space group	Amount
$P2_1/c$	56	$Pnma$	4	$C222_1$	1
$P2_1/n$	19	$C2/m$	2	$Pmma$	1
P-1	27	Pc	1	$Pnnm$	1
$C2/c$	8	$Pbcn$	1	Pn	1
$Pbca$	8	$Fdd2$	1	$Pna2_1$	1
$P2_1/m$	7	$I2/a$	1	$Pbcm$	1
$P2_1$	6	$Pca2_1$	1	P-6	1
$P2_12_12_1$	5	$Ccca$	1	$P63/m$	1

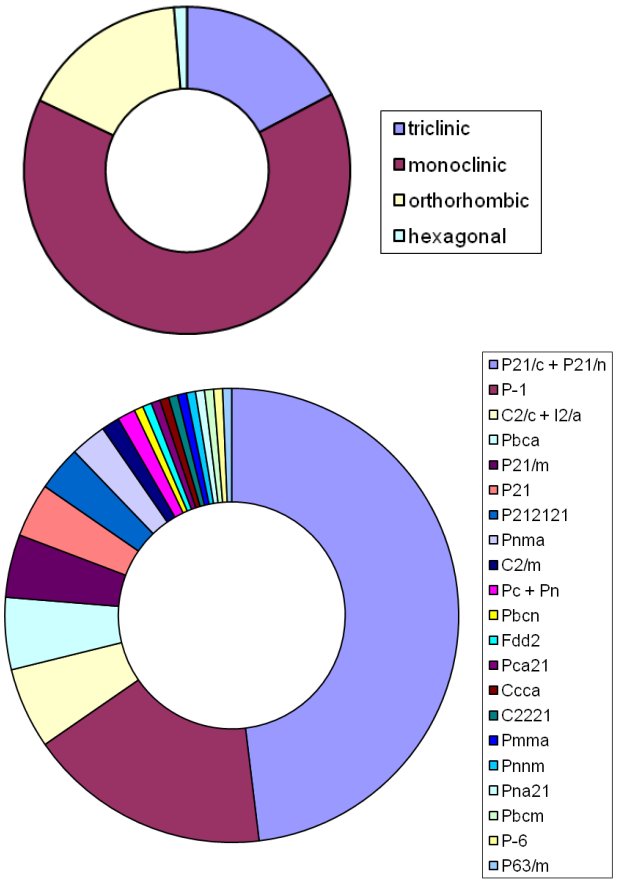

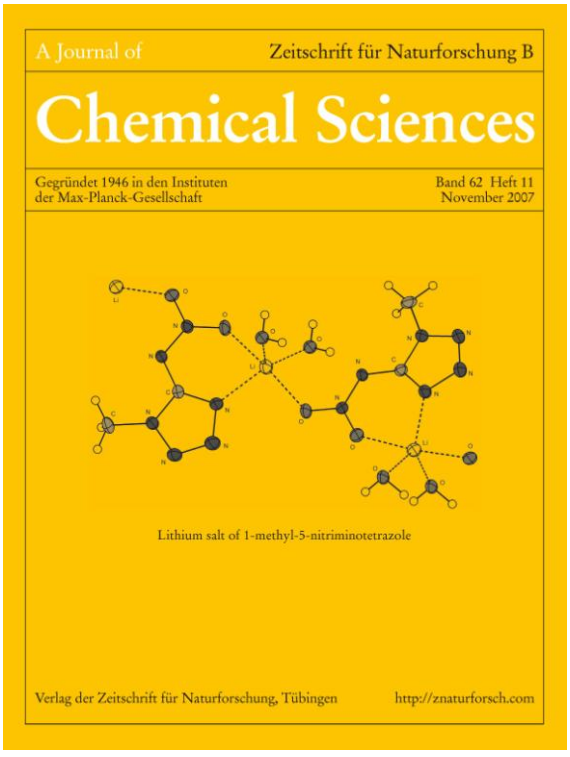

Front cover of *Z. Naturforschung* **2007**, *62b*, 1343–1352, illustrating a view on the structure of lithium 1-methyl-5-nitriminotetrazolate (**77**).

References

[1]J. Giles, *Nature*, **2004**, *427*, 580–581.

[2](a) K. O. Christe, W. W. Wilson, J. A. Sheehy, J. A. Boatz, *Angew. Chem.* **1999**, *111*, 2112–2118; *Angew. Chem. Int. Ed.* **1999**, *38*, 2004–2009; (b) R. Haiges, S. Schneider, T. Schroer, K. O. Christe, *Angew. Chem.* **2004**, *116*, 5027–5032, *Angew. Chem. Int. Ed.* **2004**, *43*, 4919–4924; (c) M. A. Petrie, J. A. Sheehy, J. A. Boatz, G. Rasul, G. K. Surya Prakash, G. A. Olah, K. O. Christe, *J. Am. Chem. Soc.* **1997**, *229*, 8802–8808.

[3](a) Y.–H. Joo, B. Twamley, S. Garg, J. M. Shreeve, *Angew. Chem.* **2008**, *120*, 6332–6335; *Angew. Chem*. *Int. Ed.* **2008**, *47,* 6236–6239. (b) H. Xue, H. Gao, B. Twamley, J. M. Shreeve, *Chem. Mater.* **2007**, *19,* 1731–1739; (c) Y. Guo, H. Gao, B. Twamley, J. M. Shreeve, *Adv. Mater.* **2007***, 19,* 2884–2888; (d) H. Gao, C. Ye, O. D. Gupta, J.–C. Xiao, M. A. Hiskey, B. Twamley, J. M. Shreeve, *Chem. – Europ. J.* **2007**, *13*, 3853–3860.

[4](a) D. E. Chavez, M. A. Hiskey, D. L. Naud, D. Parrish, *Angew. Chem.* **2008**, *120*, 8431–8433; *Angew. Chem., Int. Ed.* **2008**, *47*, 8307–8309; (b) M. H. V. Huynh, M. A. Hiskey, T. J. Meyer, M. Wetzler, *Proceedings of the National Academy of Sciences of the United States of America,* **2006**, *103*, 5409–5412; (c) M. H. V. Huynh, M. A. Hiskey, D. E. Chavez, D. L. Naud, R. D. Gilardi, *J. Am. Chem. Soc.* **2005**, *127*, 12537–12543.

[5](a) all authors, in "*High Energy Density Materials"*, T. M. Klapötke (Hrsg.), Springer, Berlin, Heidelberg, **2007**, 1; (b) C. Darwich, T. M. Klapötke, C. Miró Sabaté, *Chemistry – Europ. J.* **2008**, *14*, 5756–5771; (c) T. M. Klapötke, C. Miró Sabaté, *Chem. Mater*. **2008**, *20(5)*, 1750–1763.

[6](a) J. Vavra, P. Vavra, P. *New Trends in Research of Energetic Materials, Proceedings of the Seminar,* 7th, Pardubice, Czech Republic, Apr. 20–22, **2004**, *2*, 700–706; (b) L. Nock, D. Porada, G. King, *CPIA Publication*, **2002**, 708, JANNAF 30th Propellant Development & Characterization Subcommittee Meeting, , 1–11.

[7]J. Akhaven, in „The chemistry of explosives", RSC Paperbacks, Cambridge, **1998**, pp. 18–24.

[8]R. Meyer, J. Köhler, A. Homburg, in „Explosives", 6th edn., Wiley-VCH, Weinheim, **2007**, 128–129.

[9]G.-C. Guo, Q.-M. Wang, T. C. W. Mak, *J. Chem. Crystallogr.* **1999**, *29*, 56.

[10]W. Beck, J. Evers, M. Göbel, T. M. Klapötke, G. Oehlinger, *Z. Anorg. Allg. Chem*. **2007***, 633*, 1417–1422.

[11]D. Adam, K. Karaghiosoff, T. M. Klapötke, G. Holl, M. Kaiser, *Propellants, Explos. Pyrotech.* **2002**, *27*, 7.

[12]W. E. Deal, *J. Chem. Phys.* **1957**, *27(1)*, 796.

[13]C. L. Mader, Report LA-2900, *Los Alomos Scientific Laboratory, Fortran BKW Code for computing the detonation properties of explosives*, Los Alamos, NM, July **1963**.

[14]J. Köhler, R, Meyer, in „Explosivstoffe", Wiley-VCH, D-Weinheim, D, 9th edn., **1998**.

[15]P. F. Pagoria, G. S. Lee, A. R. Michell, R. D. Schmidt, *Thermochim. Acta* **2002**, *384*, 187.

[16](a) E. Anderson, *Prog. Astronout. Aeronout.* **1993**, *155*, 81; (b) P. A. Kempa, J. Kerth, *32th Int. Annual Conf. of ICT*, Karlsruhe, Germany, **2001**, 147; (c) Y. Akutsu, R. Che. M. Tamura, *J. Energ. Mater.* **1993**, *11*, 173; (d) M. J. Kamlet, H. J. Hurwitz, *J. Chem. Phys.* **1968**, *23*, 3685; (e) L. R. Rothstein, R. Peterson, *Propellants, Expl. Pyrotech.* **1979**, *4*, 56; (f) R. J. Spear, I. J. Dagley, *in Organic Energetic Compounds* (Marinkas P. L. (ed.)), Nova, Commack, NY, **1996**, chapt. 2.

[17]T. G. Archibald, R. Gilardi, K. Baum, C. George, *J. Org. Chem*. **1990**, 55, 143.

[18](a) J. Evers, T. M. Klapötke, P. Mayer, G. Oehlinger, J. Welch, *Inorg. Chem.* **2006**, *45*, 4996–5007; (b) M.-J. Crawford, J. Evers, M. Göbel, T. M. Klapötke, P. Mayer, G. Oehlinger, J. Welch, *Propellants, Explos. Pyrotech.* **2007**, *32*, 478–495.

[19]U. Bemm, H. Östmark, *Acta Cryst.**1998**, C54*, 1997–1999.

[20]K. Karaghiosoff, T. M. Klapötke, A. Michailowski, G. Holl, *Acta Crystallogr.* **2002**, *C58*, o580.

[21]M.-X. Zhang, P. E. Eaton, R. Gilardi, *Angew. Chem.* **2000**, *112*, 422–426

[22]T. Urbanski, "Chemistry and technology of explosives", Pergamon Press, England, **1985**.

[23]M. Suceska, *Materials Science Forum*, **2004**, *465–466*, 325–330.

[24](a) R. Huisgen, I. Ugi, *Angew. Chem. Int. Ed.* **1956**, *68*, 736; (b) J. D. Wallis, J. D. Dunitz, *J. Chem. Soc., Chem. Commun.* **1983**, 910. (c) M. S. Workentin, B. D. Wagner, F. Negri, M. Z. Zgierski, J. Lusztky, W. Silberand, D. D. M. Wyner, *J. Phys. Chem.* **1995**, *99(1)*, 94. (d) M. S. Workentin, B. D. Wagner, J. Lusztyk, D. D. M. Wayner, *J. Am. Chem. Soc.* **1995,** *117*, 119.

[25](a) R. J. Buenker, S. D. Peyerimhoff, *J. Chem. Phys.* **1968**, *48*, 354; (b) J. S. Murray, J. M. Seminario, P. Lane, P. Politzer, *J. Mol. Struct.* **1990**, *66(3–4)*, 193; (c) R. Engelke, *J. Chem. Phys.* **1992**, *96*, 10789; (d) R. Engelke, *J. Am. Chem. Soc.* **1993**, *115*, 2961; (e) T. M. Klapötke, *J. Mol. Struct.* **2000**, *499*, 99; (f) H. H. Michels, J. A. Montgomery, K. O. Christe, D. A. Dixon, *J. Phys. Chem.* **1995**, *99*, 187;(g) T. M. Klapötke, R. D. Harcourt, *J.*

Mol. Struct. **2001**, *541*, 237; (h) L. Gagliardi, G. Orlandi, *J. Chem. Phys.* **2001**, *114*, 10733; (i) D. L. Strout, *J. Phys. Chem. A* **2002**, *106*, 816; (j) S. Fau, K. J. Wilson, R. J. Bartlett, *J. Phys. Chem. A* **2002**, *106*, 4639; (k) A. Hammerl, T. M. Klapötke, P. Schwerdtfeger, *Chem. – Eur. J.* **2003**, *9*, 5511.

[26](a) K. O. Christe, W. W. Wilson, J. A. Sheehy, J. A. Boatz, *Angew. Chem. Int. Ed.* **1999**, *38*, 2004; (b) A. Vij, W. W. Wilson, V. Vij, F. S. Tham, V. Jeffrey, K. O. Christe, *J. Am. Chem. Soc.* **2001**, *123(26)*, 6308; (c) D. A. Dixon, D. Feller, K. O. Christe, W. W. Wilson, A. Vij, V. Vij, H. D. B. Brooke, R. M. Olson, M. S. Gordon, *J. Am. Chem. Soc.* **2004**, *126(3)*, 834.

[27]M. I. Eremets, A. G. Gavriliuk, I. A. Trojan, D. A. Dzivenko, R. Boehler, R. *Nature Mater.* **2004**, *3*, 558–563.

[28](a) M. I. Eremets, M. Yu. Popov, I. A. Trojan, V. N. Denisov, R. Boehler, R. J. Hemley, *J. Chem. Phys*. **2004**, *120*, 10618–10623. (b) M. I. Eremets, A.G. Gavriliuk, N. R. Serebrianaya, I. A. Trojan, D. A. Dzivenko, R. Boehler, H. K. Mao, R. J. Hemley, *J. Chem. Phys.* **2004**, *121*, 11296–11300.

[29]Jennifer A. Ciezak, *Proc. Army Science Conference,* **2008**.

[30](a) T. M. Klapötke, in *Moderne Anorganische Chemie*, E. Riedel (Hrsg.), 3rd edn, Walter de Gruyter, Berlin, New York, **2007**, 99–104. (b) R. P. Singh, R. D. Verma, D. T. Meshri, J. M. Shreeve, *Ang. Chem. Int. Ed.* **2006**, *45*, 3584. (c) T. M. Klapötke, in *High Energy Density Materials*, T. M. Klapötke (Hrsg.), Springer, Berlin, Heidelberg, **2007**, 85–122. (d) R. D. Chapman, in *High Energy Density Materials*, T. M. Klapötke (Hrsg.), Springer, Berlin, Heidelberg, **2007**, 123–152.

[31]R. C. West, S. M. Selby, *Handbook of Chemistry and Physics*, 48th ed.; The Chemical Rubber Co.; Cleveland, OH, 1967–1968; pp D22–D51.

[32]V. A. Ostrovskii, M. S. Pevzner, T. P. Kofman, I. V. Tselinskii, *Targets Heterocycl. Syst.* **1999**, *3*, 467.

[33]M. A. Hiskey,D . E. Chavez, D. L. Naud, S. F. Son, H. L. Berghout, C. A. Bolme, *Proc. Int. Pyrotech. Semin.* **2000**, 27, 3–14.

[34]E. Fischer, *Liebigs Ann.* **1878**, *190*, 138.

[35](a) J. A. Bladin, *Ber. Dtsch. Chem. Ges.* **1885**, *18*, 1544. (b) J. A. Bladin, *Ber. Dtsch. Chem. Ges.* **1885**, *18*, 2907. (c) J. A. Bladin, *Ber. Dtsch. Chem. Ges.* **1886**, *25*, 2589.

[36]F. R. Benson, in "Heterocyclic Compounds", Vol. 8, R. C. Elderfield (ed.), Wiley, New York, **1967**, p. 1.

[37](a) C. V. Reddy Sastry, *Ind. J. Chem*., **1990**, *29B*, 396. (b) E. Makino, N. Iwasaki, N. Yagi, H. Kato, Y. Ito, H. Azuma, *Chem. Pharm. Bull*., **1990**, *38,* 201.

[38]P. Desos. G. Schlewer, C. G. Wermuth, *Heterocycles*, **1989**, 28, 1085.

[39]M. Uchida, M. Komatsu, S. Morita, T. Kanbe, K. Nagakawa, *Chem. Parm. Bull.,* **1989**, *37*, 322

[40]R. N. Butler, A. R. Katritzky, C. W. Rees, *Comprehensive Hetreocyclic Chemistry*, Vol. 21, Academic press, New York, **1977,** p. 323.

[41]SCIFINDER SCHOLAR, Version **2006**, *Am. Chem. Soc*.

[42]V. Grakauskas, A. H. Albert, *J. Heterocycl. Chem*., **1981**, *18*, 1477

[43]K. A. Jensen, A. Friedinger, *Kgl. Danske Videnskab. Selskab. Mat.-Fys. Medd.* **1943**, *20*, 1.

[44]M. Roche, L. Pujal, *Bull. Soc. Chim. France* **1969**, 1097.

[45]M. J. S. Dewar, G. J. Gleicher, *J. Chem. Phys.* **1966**, *44*, 759.

[46]R. N. Butler, *Advances in heterocyclic chemistry*, No 21, p. 323, Academic Press, New York **1977**.

[47]R. N. Butler, *Comprehensive heterocyclic chemistry*, No 5, p. 791, Pergamon Press, Oxford, **1984**.

[48]M. Sainsbury, *Rodd´s Chemistry of Carbon Compounds*, No IV, part D, p. 211, Elsevier, Amsterdam, **1986**.

[49]A. J. Owen, *Tetrahedron* **1961**, *14*, 237.

[50]M. Tišler, *Synthesis* **1973**, *80*, 123.

[51]R. N. Butler, *Chem. Ind. (London)* **1973**, 371.

[52]M. M. Sokolova, V. A. Ostrovskii, G. I. Goldobstii, V. V. Melnikov, B. V. Gidaspov, *Zh. Org. Khim*. **1974,** *10*, 1085.

[53]G. B. Barlin, *T. J. Batterham, J. Chem. Soc. (B)* **1967**, 516.

[54]R. Huisgen, C. Axen, H. Seidl, *Chem. Ber*. **1965**, *98*, 2966.

[55]R. Huisgen, J. Sauer, M. Seidl, *Chem. Ber*. **1961**, *94*, 2503.

[56]J. Thiele, J. T. Marais, *Liebigs Ann.* **1893**, *273*, 144–160.

[57]J. J. Weigand, High Energy Density Materials Based on Tetrazole and Nitramine Compounds – Synthesis, Scale-up and Testing, *dissertation*, Ludwig-Maximilian University, **2005.**

[58]J. Thiele, *Liebigs Ann.* **1892**, *270*, 1.

[59]R. Stollé, *Ber. Dtsch. Chem. Ges.* **1929**, *62*, 1118.

[60]D. D. Bray, J. G. White, *Acta Cryst.* **1979**, B*35*, 3039.

[61](a) M. Denffer, T. M. Klapötke, G. Kramer, G. Spiess, J. M. Welch, G. Heeb, *Propellants, Explos., Pyrotech.* **2005**, *30(3)*, 191–195; (b) G. Ma, Z. Zhang, J. Zhang, K. Yu, *Thermochimica Acta* **2004**, *423(1–2)*, 137–141.

[62]C.-M. Jin, C. Ye, C. Piekarski, B. Twamley, J. M. Shreeve, *Eur. J. of Inorg. Chem.* **2005**, *18*, 3760–3767.

[63]M. von Denffer, T. M. Klapötke, C. M. Sabaté, *Z. Anorg. Allg. Chem.* **2008**, *634*, 2575–2582.

[64](a) V. P. Sinditskii, A. I. Levshenkov,V. Y. Egorshev, V. V. Serushkin, *New Trends in Research of Energetic Materials, Proceedings of the Seminar*, 7th, Pardubice, Czech Republic, **2004**, *2*, 649–658; (b) H. R. Blomquist, *U.S. patent* **1999**, US 6004410, A 19991221; (c) C. J. Hinshaw, R. B. Wardle, T. K. Highsmith, *U.S. patent* **1998**, US 5741998, A 19980421.

[65]R. A. Henry, W. G. Finnegan, *J. Am. Chem. Soc.* **1954**, *76,* 923.

[66]R. M. Herbst, C. W. Roberts, E. J. Harvill, *J. Org. Chem.* **1951**, *16*, 139.

[67]V. Ernst, T. M. Klapötke, J. Stierstorfer, *Z. Anorg. Allg. Chem.* **2007**, *633*, 879.

[68]K. Karaghiosoff, T. M. Klapötke, P. Mayer, C. M. Sabate, A. Penger, J. M. Welch, *Inorg. Chem.* **2008**, *47(3)*, 1007–1019.

[69]T. M. Klapötke, K. Karaghiosoff, P. Mayer, A. Penger, J. M. Welch, *Propellants, Explos. Pyrotech.* **2006**, *31*, 188–195.

[70]J. Thiele, *Justus Liebigs Ann. Chem.* **1898**, *303*, 57–75.

[71](a) M. A. Hiskey, D. E. Chavez, D. L. Naud, S. F. Son, H. L. Berghout, C. A. Bolme,. *Proc. Int. Pyrotech. Semin.* **2000**, *27*, 3–14; (b) M. A. Hiskey, N. Goldman, J. R. Stine, *J. Energ. Mater.* **1998**, *16*(2, 3), 119–127; (c) A. Hammerl, T. M. Klapötke, H. Nöth, M. Warchhold, G. Holl, M. Kaiser U. Ticmanis, *Inorg. Chem.* **2001**, *40*, 3570–3575; (d) A. Hammerl, G. Holl, T. M. Klapötke, P. Mayer, H. Nöth, H. Piotrowski, M. Warchhold, *Eur. J. Inorg. Chem.* **2002**, *4*, 834–845; (e) H. Ang, W. Frank, K. Karaghiosoff, T. M. Klapötke, H. Nöth, J. Sprott, M. Suter, M. Vogt, M. Z. Warchhold, *Anorg. Allg. Chem.* **2002**, *628*, 2901–2906; (f) Y. Peng, C. Wong, *U.S. Patent* **1999**, US 5877300; *Chem. Abstr.* **1999**, *130*, 196656; (g) M. Tremblay, *Can. J. Chem.* **1964**, *42*, 4–1157. (h) A. Hammerl, G. Holl, M. Kaiser, T. M. Klapötke, P. Mayer, H. Piotrowski, M. Vogt, *Z. Naturforsch.* **2001**, *56* (9), 847–856; (i) A. Hammerl, G. Holl, M. Kaiser, T. M. Klapötke, P. Mayer, H. Nöth, H. Piotrowski, M. Suter, *Z. Naturforsch.* **2001**, *56* (9), 857–870.

[72]A. Hammerl, M. A. Hiskey, G. Holl, T. M. Klapötke, K. Polborn, J. Stierstorfer, J. J. Weigand, *Chem. Mater.* **2005**, *17*, 3784–3793.

[73]J. Thiele, *Just. Lieb. Ann. Chem.* **1898**, *303*, 57–75.

[74]T. M. Klapötke, Carles Miró Sabaté. *Chem. Mater*. **2008**, *20*, 3629–3637.

[75]J. M. Welch, *dissertation*, Ludwigs-Maximilian University Munich, **2008**.

[76]T. M. Klapötke, P. Mayer, K. Polborn, J. M. Welch, *New Trends in Research of Energetic Materials, Proceedings of the Seminar*, 9th, Pardubice, Czech Republic, Apr. 19–21, **2006**, 631–640.

[77]C. Darwich, T. M. Klapötke, J. M. Welch, M. Suceska, *Propellants Explosiv. Pyrotech.* **2007,** *32(3)*, 235 – 243.

[78]T. M. Klapötke, P. Mayer, C. Miró Sabaté, J. M. Welch, N. Wiegand, *Inorg. Chem*. **2008**, submitted.

[79](a) H. Xue, S. W. Arritt, B. Twamley, J. M. Shreeve, *Inorg. Chem.* **2004**, *43* (25), 7972. (b) R. L. Willer, R. A. Henry, *J. Org. Chem.* **1988**, *53*, 5371. (c) V. P. Sinditskii, A. E. Fogelzang, *Russ. Khim. Zh.* **1997**, *4*, 74.

[80](a) P. N. Gaponik, V. P. Karavai, *Khim. Geterotsikl. Soedin.* **1984**, 1388. (b) R. L. Willer, R. A. Henry, *J. Org. Chem.* **1988**, *53*, 5371.

[81]R. Stolle, H. Netz, O. Kramer, S. Rothschild, E. Erbe, O. Schick, *J. Prakt. Chem.* **1933**, *138*, 1.

[82]CrysAlis CCD, Oxford Diffraction Ltd., Version 1.171.27p5 beta (release 01-04-2005 CrysAlis171 .NET).

[83]CrysAlis RED, Oxford Diffraction Ltd., Version 1.171.27p5 beta (release 01-04-2005 CrysAlis171 .NET).

[84]A. Altomare, G. Cascarano, C. Giacovazzo, A. Guagliardi, *J. Appl. Cryst.* **1993**, *26*, 343.

[85]A. Altomare, M. C. Burla, M. Camalli, G. L. Cascarano, C. Giacovazzo, A. Guagliardi, A. G. G. Moliterni, G. Polidori, R. Spagna, *J. Appl. Cryst.* **1999** *32*, 115–119.

[86]G. M. Sheldrick SHELXS-97, Program for Crystal Structure Solution, Universität Göttingen, **1997**.

[87]G. M. Sheldrick, Shelxl-97, Program for the Refinement of Crystal Structures. University of Göttingen, Germany, **1994**.

[88]L. J. Farrugia, *J. Appl. Cryst.* **1999**, *32*, 837–838.

[89]A. L. Spek, Platon, A Multipurpose Crystallographic Tool, Utrecht University, Utrecht, The Netherlands, **1999**.

[90]S. R. Hall, F. H. Allen, I. D. Brown, *Acta Crystallogr.* **1991**, *A47*, 655–685.

[91]http://journals.iucr.org/services/cif/checkcif.html

[92]K. Brandenburg, *Diamond 2.1.c*, **1996–1999**, Crystal Impact GbR.

[93]Z. Otwinowski and W. Minor "Processing of X-ray Diffraction Data Collected in Oscillation Mode", Methods in Enzymology, Volume 276: Macromolecular Crystallography, part A, p. 307–326, **1997**, C.W. Carter, Jr. and R.M. Sweet, Eds., Academic Press (New York)

[94]http://www.linseis.de

[95]http://www.perkin-elmer.de

[96]http://www.parrinst.de

[97]http://www.systag.ch

[98]http://www.setaram.com

[99]*NATO standardization agreement (STANAG) on explosives, impact sensitivity tests, no. 4489*, Ed. 1, Sept. 17, **1999**.

[100]*WIWEB-Standardarbeitsanweisung 4-5.1.02, Ermittlung der Explosionsgefährlichkeit, hier der Schlagempfindlichkeit mit dem Fallhammer*, Nov. 8, **2002**.

[101]http://www.bam.de

[102]http://www.reichel-partner.de/

[103]*NATO standardization agreement (STANAG) on explosive, friction sensitivity tests, no. 4487*, Ed. 1, Aug. 22, **2002**.

[104]*WIWEB-Standardarbeitsanweisung 4-5.1.03, Ermittlung der Explosionsgefährlichkeit oder der Reibeempfindlichkeit mit dem Reibeapparat*, Nov. 8, **2002**.

[105]http://www.bam.de

[106]http://www.reichel-partner.de/

[107]Impact: Insensitive > 40 J, less sensitive ≥ 35 J, sensitive ≥ 4, very sensitive ≤ 3 J; friction: Insensitive > 360 N, less sensitive = 360 N, sensitive < 360 N a. > 80 N, very sensitive ≤ 80 N, extreme sensitive ≤ 10 N; According to the UN Recommendations on the Transport of Dangerous Goods (+) indicates: not safe for transport.

[108](a) S. Zeman, V. Pelikán, J. Majzlík, *Centr. Eur. J. Energy. Mater*. **2006**, *3*, 45–51; (b) D. Skinner, D. Olson, A. Block-Bolten, *Propellants, Explos., Pyrotechn.* **1997**, *23*, 34–42; (c) OZM research, Czech Republic, http://www.ozm.cz/testing-instruments/pdf/TI-SmallSpark.pdf.

[109]R. Meyer, J. Köhler, A. Homburg, in ‚Explosives', 6th edn., Wiley-VCH, Weinheim, **2007**, 45–46.

[110](a) J. Köhler, R. Meyer, A. Homburg, in "Explosives", 6th edn., Wiley-VCH, Weinheim, **2007**, p. 162 (b) Prüfung der thermischen Empfindlichkeit (Stahlhülsenverfahren), WIWEB Standardarbeitsanweisung 410/001, Neufassung, 1st edn., 01.06.1997 (c) http://www.sms-ink.com/ products_koenen.html

[111]V. A. Ostrovskii, M. S. Pevzner, T. P. Kofman, I. V. Tselinskii, *Targets Heterocycl. Syst.* **1999**, *3*, 467.

[112]J. Köhler, R. Meyer, Explosivstoffe, 9th edn., Wiley-VCH, Weinheim, **1998**, pp 166–168.

[113]A. Leo, C. Hantsch, D. Elkins, *Chemical Reviews* **1971***, 71(6)*, 525–616.

[114]W. B. Neely, D. R. Branson, G. E. Blau, *Environmental Science and Technology* **1974***, 8(13)*, 1113–1115.

[115]Gaussian 03, Revision A.1, M. J. Frisch, G. W. Trucks, H. B. Schlegel, G. E. Scuseria, M. A. Robb, J. R. Cheeseman, J. A. Montgomery, Jr., T. Vreven, K. N. Kudin, J. C. Burant, J. M. Millam, S. S. Iyengar, J. Tomasi, V. Barone, B. Mennucci, M. Cossi, G. Scalmani, N. Rega, G. A. Petersson, H. Nakatsuji, M. Hada, M. Ehara, K. Toyota, R. Fukuda, J. Hasegawa, M. Ishida, T. Nakajima, Y. Honda, O. Kitao, H. Nakai, M. Klene, X. Li, J. E. Knox, H. P. Hratchian, J. B. Cross, C. Adamo, J. Jaramillo, R. Gomperts, R. E. Stratmann, O. Yazyev, A. J. Austin, R. Cammi, C. Pomelli, J. W. Ochterski, P. Y. Ayala, K. Morokuma, G. A. Voth, P. Salvador, J. J. Dannenberg, V. G. Zakrzewski, S. Dapprich, A. D. Daniels, M. C. Strain, O. Farkas, D. K. Malick, A. D. Rabuck, K. Raghavachari, J. B. Foresman, J. V. Ortiz, Q. Cui, A. G. Baboul, S. Clifford, J. Cioslowski, B. B. Stefanov, G. Liu, A. Liashenko, P. Piskorz, I. Komaromi, R. L. Martin, D. J. Fox, T. Keith, M. A. Al-Laham, C. Y. Peng, A. Nanayakkara, M. Challacombe, P. M. W. Gill, B. Johnson, W. Chen, M. W. Wong, C. Gonzalez, and J. A. Pople, Gaussian, Inc., Pittsburgh PA, **2003**.

[116](a) C. Møller, M. S. Plesset, *Phys. Rev.* **1934**, *46*, 618; (b) M. J. Frisch, M. Head-Gordon, J. A. Pople, *J. Chem. Phys.* **1990**, *141*, 189; (c) M. Head-Gordon, J. A. Pople, M. J. Frisch, *Chem. Phys. Lett.* **1988**, *153*, 503; (d) M. J. Frisch, M. Head-Gordon, J. A. Pople, Chem. Phys. Lett. **1990**, 166, 275. (e) M. J. Frisch, M. Head-Gordon, J. A. Pople, *Chem. Phys. Lett.* **1990**, *166*, 281.

[117](a) D. E. Woon and T. H. Dunning Jr., *J. Chem. Phys.* **1993***, 98*, 1358; (b) R. A. Kendall, T. H. Dunning Jr., and R. J. Harrison, *J. Chem. Phys.* **1992**, *96*, 6796; (c) T. H. Dunning Jr., *J. Chem. Phys.* **1989**, 90, 1007; (d) K. A. Peterson, D. E. Woon, and T. H. Dunning

Jr., *J. Chem. Phys.* **1994**, *100*, 7410. (e) A. Wilson, T. van Mourik, and T. H. Dunning Jr., *J. Mol. Struct.* **1997**, *388*, 339.

[118] (a) H. D. B. Jenkins, H. K. Roobottom, J. Passmore, L. Glasser, *Inorg. Chem.* **1999**, *38*, 3609–3620. (b) H. D. B. Jenkins, D. Tudela, L. Glasser, *Inorg. Chem.* **2002**, *41*, 2364–2367.

[119] A. J. Bracuti, *Large Caliber Weapon Syst. Lab., Army Armament Res. Dev. Command*, Dover, NJ, USA. *Avail. NTIS. Report* , **1979**, (ARLCD-TR-78050, AD-E400296; Order No. AD-A067293), 22 pp. From: Gov. Rep. Announce. Index (U. S.) **1979**, *79(17)*, 224.

[120] J. P. Ritchie, E. A. Zhurova, A. Martin, A. A. Pinkerton, *J. Phys. Chem. B* **2003**, *107*, 14576–14589.

[121] T. M. Klapötke, A. Schulz, in "Quantum Chemical Methods in Main-Group Chemistry", Wiley, Chichester, **1996**, 89–95.

[122] P. J. Linstrom, W. G. Mallard, NIST Chemistry WebBook, NIST Standard Reference Database Number 69, June **2005**, National Institute of Standards and Technology, Gaithersburg MD, 20899, http://webbook.nist.gov.

[123] J. W. Ochterski, G. A. Petersson, J. A. Montgomery Jr., *J. Chem. Phys.* **1996,** *104*, 2598.

[124] J. A. Montgomery Jr., M. J. Frisch, J. W. Ochterski, G. A. Petersson, *J. Chem. Phys.* **2000**, *112*, 6532.

[125] L. A. Curtiss, K. Raghavachari, P. C. Redfern, J. A. Pople, *J. Chem. Phys.* **1997**, *106(3)*, 1063.

[126] (a) E. F. Byrd, B. M. Rice, *J. Phys. Chem.* **2006**, *110(3)*, 1005–1013; (b) B. M. Rice, S. V. Pai, J. Hare, *Combust. Flame* **1999**, *118(3)*, 445–458.

[127] (a) M. Sućeska, *Propellants, Explos., Pyrotech.* **1991**, *16*, 197–202 ; (b) M. Sućeska, *Propellants Explos. Pyrotech.* **1999**, *24*, 280–285.

[128] (a) EXPLO5.V2, M. Sućeska, *Proc. of 32nd Int. Annual Conference of ICT*, July 3-6, Karlsruhe, Germany, **2001**, pp. 110/1 a software for determining detonation parameter; (b) M. Suceska, *Proc. of 30th Int. Annual Conference of ICT*, June 29–July 2, Karlsruhe, Germany, **1999**, 50/1

[129] M. L. Hobbs, M. R. Baer. Calibration of the BKW-EOS with a Large Product Species Data Base and Measured C-J Properties, *Proc. of the 10th Symp. on Detonation*, ONR 33395–12, Boston, MA, July 12–16, **1993**, p. 409.

[130] N. Fischer, T. M. Klapötke, S. Scheutzow, J. Stierstorfer, *Centr. Europ. J. Energ. Mater.* **2008**, *5*(3–4), 3–18.

[131]T. M. Klapötke, J. Stierstorfer, *Centr. Europ. J. Energ. Mat.* **2008**, *5*, 13–30.

[132]T. M. Klapötke, C. M. Sabaté, J. Stierstorfer, *Z. Anorg. Allg. Chem.* **2008**, *634*, 1867–1874.

[133]T. M. Klapötke, J. Stierstorfer, *Dalton Transactions*, **2008**, *4*, 643–653.

[134]T. M. Klapötke, J. Stierstorfer, *Eur. J. Inorg. Chem.* **2008**, *26*, 4055–4062.

[135]T. M. Klapötke, J. Stierstorfer, *Phys. Chem. Chem. Phys.* **2008**, *10*, 4340–4346.

[136]T. M. Klapötke, J. Stierstorfer, *New Trends in Research of Energetic Materials, Proceedings of the Seminar*, 11th, Pardubice, Czech Republic, **2008**, *2*, 810–831.

[137]T. M. Klapötke, J. Stierstorfer, *New Trends in Research of Energetic Materials, Proceedings of the Seminar*, 10th, Pardubice, Czech Republic, **2007**, *2*, 674.

[138]T. M. Klapötke, J. Stierstorfer, *Helv. Chim. Acta* **2007**, *90*, 2132–2150.

[139]N. Fischer, T. M. Klapötke, J. Stierstorfer, *Z. Anorg. Allg. Chem.* **2008**, *accepted*.

[140]J. Stierstorfer, K. Tarantik, T. M. Klapötke, *Chem. – Europ. J.* **2008**, *accepted*.

[141]N. Fischer, K. Karaghiosoff, T. M. Klapötke, J. Stierstorfer, *Helv. Chim Acta*, **2008**, *submitted*.

[142]T. M. Klapötke, H. A. Laub, J. Stierstorfer, *Propellants Explos. Pyrotech.* **2008**, *33*, 421–430.

[143]T. M. Klapötke, H. Radies, J. Stierstorfer, *Z. Naturforschung,* **2007**, *62b*, 1343–1352.

[144]T. M. Klapötke, J. Stierstorfer, A. Wallek, *New Trends in Research of Energetic Materials, Proceedings of the Seminar*, 11th, Pardubice, Czech Republic, **2008**, *2*, 832–854.

[145]T. M. Klapötke, J. Stierstorfer, A. U. Wallek, *Chem. Mater.* **2008**, *20*, 4519–4530.

[146]T. M. Klapötke, J. Stierstorfer, K. R. Tarantik, I. Thoma, *Z. Anorg. Allg. Chem.* **2008**, *634*, 2777–2784.

[147]T. M. Klapötke, J. Stierstorfer, *Chem. Mater.* **2008**, *submitted*.

[148]V. Ernst, T. M. Klapötke, J. Stierstorfer, *New Trends in Research of Energetic Materials, Proceedings of the Seminar*, 10th, Pardubice, Czech Republic, **2007**, *2*, 575.

[149]G. Geisberger, T. M. Klapötke, J. Stierstorfer, *Eur. J. Inorg. Chem.* **2007**, *30*, 4743–4750.

[150]T. M. Klapötke, J. Stierstorfer, B. Weber, *Inorg. Chim. Acta*. **2008**, 10.1016/ j.ica.2008.10.014.

[151]T. M. Klapötke, N. Minar, J. Stierstorfer, *Polyhedron*, **2009**, *28*, 13–26.

[152]T. M. Klapötke, M. Stein, J. Stierstorfer, *Z. Anorg. Allg. Chem.* **2008**, *634*, 1711–1723.

[153]J. Stierstorfer, T. M. Klapötke, A. Hammerl, R. D. Chapman, *Z. Anorg. Allg. Chem.* **2008**, *634*, 1051–1057.

[154]T. M. Klapötke, J. Stierstorfer, *J. Am. Chem. Soc.* **2009**, *131,* 1122–1134.

[155]T. M. Klapötke, C. M. Sabaté, J. Stierstorfer, *New J. Chem.* **2009**, *33*, 136–147.

[156]T. M. Klapötke, P. Mayer, J. Stierstorfer, J. J. Weigand, *J. Mater. Chem.* **2008**, *18*, 5248–5258.

[157]T. M. Klapötke, P. Mayer, K. Polborn, J. Stierstorfer, J. J. Weigand, *New Trends in Research of Energetic Materials, Proceedings of the Seminar* **2006**, *2*, 641–651.

[158]T. M. Klapötke, P. Mayer, K. Polborn, J. Stierstorfer, J. J. Weigand, *37th International Annual Conference of ICT*, Karlsruhe, Federal Republic of Germany, **2006**, 134/1–134/14.

[159]P. N. Gaponik, S. V. Voitekhovich, O. A. Ivashkevich, *Russ. Chem. Rev.* **2006**, *75* (6), 507.

[160]H. Nöth, W. Beck, K. Burger, *Eur. J. Inorg. Chem.* **1998**, 93–99.

[161](a) E. Lieber, S. H. Patinkin, H. H. Tao, *J. Am. Chem. Soc.* **1951**, *73*, 1792; (b) A. Hammerl, T. M. Klapötke, P. Mayer, J. J. Weigand, *Propellants, Explos. Pyrotech.* **2004**, *29(6)*, 325 and references therein.

[162]G. B. Barlin, T. J. Batterham, *J. Chem. Soc. (B)* **1967**, *516*, 38.

[163]M. Sainsburry, M. *odd's Chemistry of Carbon Compounds*, Vol IV, Part D, 211, Elsevier, Amsterdam, **1986**.

[164](a) R. Huisgen, J. Sauer, M. Seidel, *Chem. Ber.* **1960**, *93*, 2885; (b) D. Martin, A. Weise, C*hem. Ber.* **1966**, *99*, 317.

[165]J. H. Markgraf, W. T. Bachmann, D. P. Hollis, *J. Org. Chem.* **1965**, *30*, 3472.

[166]N. Wiberg, in: *Lehrbuch der Anorganischen Chemie / Holleman-Wiberg*, 101st edn., de Gruyter, Berlin, **1995**, p. 1842.

[167]N–N values and N=N values from: Internationl tables for X-ray crystallography; Kluwer Academic Publisher: Dordrecht, The Netherlands, **1992**, Vol. C.

[168]A. F. Holleman, E. Wiberg, *Lehrbuch der anorganischen Chemie*, 101st edn., de Gruyter, Berlin, **1995**, p. 1176

[169]J. H. Bryden, *Acta Cryst.* **1958**, *11*, 31–37.

[170] A. J. Bracuti, J. M. Troup, M. W. Extine, *Acta Crystallogr.* **1986**, *C42*, 505–506.

[171] A. Hammerl, G. Holl, M. Kaiser, T. M. Klapötke, H. Piotrowski, *Z. Anorg. Allg. Chem.* **2003**, *629*, 2117–2121.

[172] A. Hammerl, G. Holl, M. Kaiser, T. M. Klapötke, H. Nöth, U. Ticmanis, M. Warchhold, *Inorg. Chem.* **2001**, *40*, 3570–3575.

[173] R. M. Doherty, Novel Energetic Materials for Emerging Needs, 9th-IWCP on Novel Energetic Materials and Applications, Lerici (Pisa), Italy, September 14–18 (**2003**).

[174] T. Brinck, J. S. Murray, P. Politzer, *J. Org. Chem.* **1991**, *56*, 5012–5015.

[175] (a) K. O. Christe, W. W. Wilson, M. A. Petrie, H. H. Michels, J. C. Bottaro, R. Gilardi, *Inorg. Chem.* **1996**, *35*, 5068–5071; (b) V. A. Shlyapochnikov, M. A. Tafipolsky, I. V. Tokmakov, E. S. Baskir, O. V. Anikin, Yu.A. Strelenko, O. A. Luk'yanov, V. A. Tartakovsky, *J. Molec. Struct.* **2001**, *559*, 147–166; (c) J. C. Bottaro, P. E. Penwell, R. J. Schmitt, *Synth. Commun.* **1991**, *21*, 945; (d) O. A. Luk'yanov, V. P. Gorelik, V. A. Tartakovskii, *Russ. Chem. Bull.* **1994**, *43*, 89.

[176] Y. N. Matyushin, T. S. Kon'kova, A. B. Vorob'ev, Y. A. Lebedev, *International Annual Conference of ICT,* **2005**, 36th, 92/1–92/9.

[177] N. Wingborg, N. V. Latypov, *Propellants, Explos., Pyrotech.* **2003**, *28(6)*, 314–318.

[178] H. R. Blomquist, *U.S. patent* **1999**, 9 pp. US 6004410 A 19991221.

[179] (a) C. E. Gregory, Explosives for North American Engineers, Vol. 5, Trans Tech Publications, Clausthal-Zellerfeld, **1984**. (b) T. L. Davis, The Chemistry of Powder and Explosives, Vol. 2, Wiley,New York, **1943**.

[180] (a) A. Hammerl, T. M. Klapötke, H. Nöth and M. Warchhold, G. Holl, M. Kaiser, *Inorg. Chem*. **2001**, *40*, 3570–3575. (b) A. Hammerl, G. Holl, M. Kaiser, T. M. Klapötke, P. Mayer, H. Piotrowsky, M. Vogt, *Z. Naturforsch.* **2001**, *56b*, 857–870.

[181] T. M. Klapötke, J. Stierstorfer, *New Trends in Research of Energetic Materials, Proceedings of the Seminar*, 11th, Pardubice, Czech Republic, **2008**, *2*, 810–831.

[182] H. Xue, J . M. Shreeve, *Adv. Mater.* **2005**, *17*, 2142–2146.

[183] R. Gilardi, R. J. Butcher, *J. Chem. Cryst.* **2002**, *32(11)*, 477–484.

[184] M. E. Sitzmann, R. Gilardi, R. J. Butcher, W. M. Koppes, A. G. Stern, J. S. Trasher, N. J. Trivedi, Z.-Y. Yang, *Inorg. Chem.* **2000**, *39*, 843–850.

[185] N. B. Bolotina, M. J. Hardie, A. A. Pinkerton, *J. Appl. Crystallogr.* **2003**, *36(6)*, 1334–1341.

[186] (a) T. M. Klapötke, P. Mayer, A. Schulz, J. J. Weigand, *J. Am. Chem. Soc.* **2005**, *127(7)*, 2032–2033; (b) G. Fischer, G. Holl, T. M. Klapötke, P. Mayer, J. J. Weigand, *New*

Trends in Research of Energetic Materials, Proceedings of the Seminar, 8th, Pardubice, Czech Republic, **2005**, *1*, 190–199.

[187] C. J. Hinshaw, R. B. Wardle, T. K. Highsmith, *U.S. patent* 1998, US 5741998, A 19980421.

[188] J. Thiele, *Liebigs Ann.* **1892**, *270*, 1.

[189] R. Stollé, *Ber. Dtsch. Chem. Ges.* **1929**, *62*, 1118.

[190] K. E. Gutowski, R. D. Rogers, D. A. Dixon, *J. Phys. Chem. B*, **2007**, *111(18)*, 4788–4800.

[191] Y. Ohnishi, S. Tanimoto, *Tetrahedron Letters*, **1977**, *18(22)*, 1909–1912.

[192] J. Köhler, R. Meyer, Explosivstoffe, 9th edn., Wiley-VCH, Weinheim, **1998**, pp. 251–252.

[193] (a) H. Oehme, **1922**, *US patent* 1426313 19220815. (b) E. Vernazza, *Industria Chimica*, **1929**, *4*, 990–999; (c) J. Köhler, R. Meyer, Explosivstoffe, 9th edn., Wiley-VCH, Weinheim, **1998**, pp. 222–223.

[194] (a) A. Stettbacher, *Nitrocellulose*, **1934**, *5*, 159–162, 181–184, 203–206; (b) W. C. Crater, **1938**, *US patent* 2112749 19380329.

[195] M. D. Lind, *Acta Crystallogr. B* **1970**, *B26*, 590.

[196] (a) E. T. Urbansky, *Environmental Science and Polluting Research International*, **2002**, *9(3)*, 187–192; (b) J. M. Hershman, *Thyroid*, **2005**, *15(5)*, 427–431; (c) C. J. Siglin, D. R. Mattie, D. E. Dodd, P. K. Hildebrandt, W. H. Baker, *Toxicological Sciences*, **2000**, *57(1)*, 61–74.

[197] J. Köhler, R. Mayer, *Explosivstoffe*, VCH Verlagsgesellschaft, Weinheim, 9th edn., **1998**. pp. 66–67.

[198] N. Wiberg, in: *Lehrbuch der Anorganischen Chemie / Holleman-Wiberg*, 101st edn., de Gruyter, Berlin, **1995**, pp. 481.

[199] (a) C. S. Choi, H. J. Prask, E. Prince, *J. Phys. Chem.* **1974**, *61(9)*, 3523–3529; (b) G. Peyronel, A. Pignedoli, *Acta Cryst.* **1975**, *B32*, 2052–2056; (c) C. S. Choi, H. J. Prask, *Acta Cryst.* **1976**, *B32*, 2919–2920.

[200] (a) G. M. Gore, F. R. Tipare, C. N. Divekar, R. G. Bhatewara, S. N. Asthana, *J. Energ. Mater.* **2002**, *20(3)*, 255–278; (b) M. Celina, L. Minier, R. Assink, *Thermochimica Acta*, **2002**, *384(1–2)*, 343–349.

[201] N. Wiberg, in: *Lehrbuch der Anorganischen Chemie / Holleman-Wiberg*, 101st edn., de Gruyter, Berlin, **1995**, p. 238.

[202]J. C. Galvez-Ruiz, G. Holl, K. Karaghiosoff, T. M. Klapötke, K. Löhnwitz, P. Mayer, H. Nöth, K. Polborn, C. J. Rohbogner, M. Suter, J. J. Weigand, *Inorg. Chem.*, **2005**, *44*, 4237–4253.

[203]R. N. Butler, J. P. Duffy, E. P. N. Bhradaigh, P. D. McArdle, D. Cunningham, *J. Chem. Res.* **1994**, *6*, 216–217.

[204](a) Z. Pajak, M. Grottel, A. E. Koziol, *J. Chem. Soc., Faraday Trans.*, *2*, **1982**, *78*, 1529–1538; (b) A. E. Koziol, *Z. Kristallogr*. **1984**, *168(1–4)*, 313–315.

[205]M. J. Begley, P. Hubberstey, C. H. M. Moore, *J. Chem. Res., Synopses*, **1985**, *12*, 380–381.

[206]A. Martin, A. A. Pinkerton, *Acta Cryst.*, **1996**, *C52*, 1048–1052.

[207]**AGClO4:** W. Sauermilch, *Explosivstoffe*, **1964**, *12(9)*, 197–199; **TAGClO4:** (a) Y. N. Matyushin, T. S. Konkova, K. V. Titova, V. Y. Rosolovskii, Y. A. Lebedev, *Seriya Khimicheskaya*, **1982**, *3*, 498–501;(b) S. F. Bedell, U.S. patent, **1966**, US 3293853.

[208]J. Bernstein, R. E. Davis, L. Shimoni, N. Chang, *Angew. Chem. Int. Ed.* **1995**, *34(15)*, 1555–1573.

[209]http://www.ccdc.cam.ac.uk/support/documentation/rpluto/TOC.html.

[210]J. H.Bryden, *Acta Cryst*, **1957**, *10*, 677–680.

[211]A. Akella, D. A. Keszler, *Acta Cryst.* **1994**, *C50*, 1974–1976.

[212](a) Y. Okaya, R. Pepinsky, *Acta Cryst.* **1957**, *10*, 681–684; (b) A. J. Bracuti, *Acta Cryst.* **1983**, *C39*, 1465–1467.

[213]A. J. Bracuti, *Acta Cryst.* **1979**, *B35*, 760–761.

[214]T. M. Klapötke, in: *Moderne Anorganische Chemie*, E. Riedel (Hrsg.), 2nd edn., Walter de Gruyter, Berlin, New York, **2003**, pp. 84–86.

[215]U. Müller, H. Bärnighausen, *Acta Cryst.*, **1970**, *26(B)*, 1671–1679.

[216]M. J. Begley, P. Hubberstey, C. H. M. Moore, *J. Chem. Res., Synopses* **1985**, *12*, 380–381.

[217]A. Martin, A. A.Pinkerton, *Acta Crystallogr.* **1996**, *C52*, 1048–1052.

[218]M. v. Denffer, T. M. Klapötke, G. Kramer, G. Spieß, J. M. Welch, G. Heeb, *Propellants Explos. Pyrotech.* **2005**, *30*, 1191–1195.

[219]C.-M. Jin, C. Ye, C. Piekarski, B. Twamley, J. M. Shreeve, *Eur. J. Inorg. Chem.* **2005**, *18*, 3760–3767.

[220] T. M. Klapötke, C. M. Sabate, *Z. Anorg. Allg. Chem.* **2008**, *634(6–7)*, 1017–1024.

[221](a) N. van der Putten, D. Heijdenrijk, H. Schenk, *Cryst. Struct. Commun.* **1974**, *3*, 321; (b) R. Goddard, O. Heinemann, C. Krüger, *Acta Crystallogr.* **1997**, *C53*, 590–592.

[222]Y. Ohno, Y. Akutsu, M. Arai, M. Tamura, T. Matsunaga, *Acta Crystallogr.* **1999**, *C55*, 1014.

[223]C. A. K. Diop, M. F. Mahon, K.C. Molloy, L. Ooi, P. R. Raithby, M. M. Venter, S. J. Teat, *Cryst. Eng. Comm.* **2002**, *4*, 462.

[224]P. J. Steel, *J. Chem. Cryst.* **1996**, *26*, 399.

[225]A. F. Hollemann, E. Wiberg, Lehrbuch der anorganischen Chemie, 101st edn., Walter de Gruyter, Berlin, **1995**, p. 661.

[226]A. Hammerl, G. Holl, T. M. Klapötke, H. Nöth, M. Warchhold, *Propellants. Explos. Pyrotech.* **2003**, *28 (4)*, 165–173.

[227](a) W. Fraenk, T. Habereder, A. Hammerl, T. M. Klapötke, B. Krumm, P. Mayer, H. Nöth, M. Warchhold, *Inorg. Chem.* **2001**, *40*, 1334–1340; (b) A. Hammerl, T. M. Klapötke, *Inorg. Chem.* **2002**, *41*, 906–912.

[228]T. M. Klapötke, C. Miró Sabaté, *Z. Anorg. Allg. Chem.,* **2008**, *634*, 1017–1024.

[229](a) P. Geißler, T. M. Klapötke, H. J. Kroth, *Spectroch. Acta.*, **1995**, Part A, *51A(6)*, 1075–1078; (b) M. Göbel, K. Karaghiosoff, T. M. Klapötke, *Angew. Chem*. **2006**, *118(3)*, 6183–6186; *Angew, Chem. Int. Ed.* **2006**, *45*, 6037–6040.

[230](a) H. Cohn, *J. Chem. Soc.* **1952**, 4282–4284; (b) O. Redlich, E. K. Holt, J. Biegeleisen, *J. Am. Chem. Soc.* **1944**, *55*, 13–16.

[231](a) G. Drake, T. Hawkins, A. Brand, L. Hall, M. Mckay, A. Vij, I., *Propellants, Explos., Pyrotech.* **2003**, *28*, 174; (b) H. Cohn, *J. Chem. Soc*., **1952**, 4282; (c) P. Redlich, J. Holt, T. Biegeleisen, *J. Am. Chem. Soc*. **1944**, *66*, 13.

[232]N. B. Colthup, L. H. Daly, S. E. Wiberley, *Introduction to Infrared and Raman Spectroscopy*, Academic Press: Boston, **1990**.

[233]K. Karaghiosoff, T. M. Klapötke, A. Michailovski, H. Nöth, M.Suter, *Propellants, Explos., Pyrotech*., **2003**, *28(1)*, 1.

[234]T. M. Klapötke, P. Mayer, V. Verma, *Propellants, Explos., Pyrotech.* **2006**, *31*(4), 263

[235]W. E. Deal, *J. Chem. Phys.* **1957**, *27(1)*, 796.

[236]C. L. Mader, Report LA-2900, *Los Alomos Scientific Laboratory, Fortran BKW Code for computing the detonation properties of explosives*, Los Alamos, NM, July **1963**.

[237]T. Urbanski, in "Chemistry and technology of explosives", Pergamon Press, England, **1985**.

[238]A. M. Astakhov, A. D. Vasilev, M. S. Molokeev, V. A. Revenko, R. S. Stepanov, *Russ. J. Org. Chem.* **2005**, *41(6)*, 910.

[239]J. H. Bryden, *Acta Cryst.* **1953**, *6*, 669.

[240]K. Karahiosoff, T. M. Klapötke, P. Mayer, H. Piotrowski, K. Polborn, R. L. Willer, J. J. Weigand, *J. Org. Chem.* **2005**, *71*, 1295.

[241]B. C. Tappan, R. W. Beal, T. B. Brill, *Thermochimica Acta* **2002**, *288(1–2)*, 227.

[242]B. C. Tappan, C. D. Incarnito, A. L. Rheingold, T. B. Brill, *Thermochimica Acta* **2002**, *384(1–2)*, 113.

[243]T. B. Brill, B. C. Tappan, R. W. Beal, *New Trends in Research of Energetic Materials*, Proc. Of the Sem. *4th*, Pardubice, Czech Rep. **2001**, 17.

[244]J. Thiele, *Ann.* **1892**, 270, 1.

[245]R. M. Herbst, J. A. Garrison*, J. Org. Chem.* **1953**, *18,* 941.

[246]A. M. Astakhov, A. A. Nefedo, A. D. Vasiliev, L. A. Kruglyakova, K. P. Dyugaev, R. S. Stepanov, *Internatual Conference of ICT*, 36th, Germany, **2005**, 113/1.

[247]E. Lieber, E. Sherman, R. A. Henry, J. Cohen, *J. Am. Chem. Soc*. **1951**, *73*, 2327.

[248]E. Lieber, Patinkin, Tao, *J. Am. Chem. Soc.* **1951**, *73*, 1792.

[249]E. Riedel, *Anorganische Chemie*, 4th edn., de Gruyter, Berlin, **1999**, p. 134

[250]N. Wiberg, in *Lehrbuch der Anorganischen Chemie / Holleman-Wiberg*, 101st edn., de Gruyter, Berlin, **1995**, p. 1842.

[251]E. Lieber, D. R. Levering, L. J. Patterson, *Anal. Chem.* **1951**, *23*, 1594.

[252]Z. Daszkiewicz, E. M. Nowakowska, W. W. Preźdo, J. B. Kyzioł, *Pol. J. Chem.* **1995**, *69*, 1437.

[253]M. S. Westwell, M. S. Searle, D. J. Wales, D. H. Williams, *J. Am. Chem. Soc*. **1995**, *117*, 5013.

[254]K. Nakamoto, *Infrared and Raman Spectra of Inorganic and Coodination Compounds*, 4th ed.; Wiley & Sons: New York, Chichester, Brisbane, Toronto, Singapore, **1986**.

[255]HyperChem 7.52, Molecular *Visualization and Simulation Program Package,* Hypercube, Gainsville, FL, **2002**.

[256]B. M. Rice, J. J. Hare, *J. Phys. Chem.* **2002**, *106A*, 1770.

[257](a) P. Politzer, J.S. Murray, J. M. Seminario, P. Lane, M. E. Grice, M. C. Concha, *J. Mol. Struct.* **2001**, *573*, 1; (b) J.S. Murray, P. Lane, P. Politzer, *Mol. Phys.* **1995**, *85*, 1.

[258]T. M. Klapötke, C. M. Sabatè, *Dalton Trans.* **2008**, accepted.

[259]G. Holl, T. M. Klapötke, K. Polborn, C. Rienäcker, *Propellants, Explos., Pyrotech.* **2003**, *28*, 153–156.

[260](a) J. Geith, G. Holl, T. M. Klapötke, J. J. Weigand, *Combust. Flame* **2004**, *139*, 358–366; (b) J. Geith, T. M. Klapötke, J. J. Weigand, G. Holl, *Propellants, Explos., Pyrotech.* **2004**, *29*, 3–8.

[261]E. Lieber, E. Sherman, R. A. Henry, J. Cohen, *J. Am. Chem. Soc.* **1951**, *73*, 2327–2329.

[262]J. A. Garrison, R. M. Herbst, *J. Org. Chem.* **1957**, *22*, 278–283.

[263]W. G. Finnegan, R. A. Henry, *J. Org. Chem.* **1959**, *24*, 1565–1567.

[264]A. S. Lyakhov, A. N. Vorobiov, P. N. Gaponik, L. S. Ivashkevich, V. E. Matulis, O. A. Ivashkevich, *Acta Crystallogr.* **2003**, *C59*, o690–o693.

[265]A. S. Lyakhov, Yu.V. Grigoriev, L. S. Ivashkevich, P. N. Gaponik, *Acta Crystallogr.*, **2007**, *63*, 2579.

[266]C. M. Grunert, P. Weinberger, J. Schweifer, C. Hampel, A. F. Stassen, K. Mereiter, W. Linert, *J. Molec. Struct.* **2005**, *733*, 41–52.

[267]Y. Shvedenkov, M. Bushuev, G. Romanenko, L. Lavrenova, V. Ikorskii, P. Gaponik, S. Larionov, *Eur. J. Inorg.* Chem. **2005**, *9*,1678–1682.

[268]D. O. Ivashkevich, A. S. Lyakhov, P. N. Gaponik, A. N. Bogatikov, A. A. Govorova, *Acta Crystallogr.* **2001**, *E57*, m335–m337.

[269](a) J. S. Murray, P. Lane, T. Clark, P. Politzer, *J. Mol. Model.* **2007**, *13(10)*, 1033–1038; (b) P. Politzer, J. S. Murray, P. Lane, *Int. J. Quantum Chem.* **2007**, *107(15)*, 3046–3052; (c) P. Politzer, J. Murray, M. C. Concha *J. Mol. Model.* **2008**, *14(8)*, 659–65; (d) P. Metrangolo, F. Meyer, T. Pilati, G. Resnati, G. Terraneo, *Ang*e*w. Chem. Int. Ed.* **2008**, *47*, 6114–6127.

[270]A. D. Vasiliev, A. M. Astakhov, A. A. Nefedov, R. S. Stepanov, *J. Struct. Chem.* **2003**, *44(2)*, 322–325.

[271]A. F. Stassen, W. L. Driessen, J. G. Haasnoot, J. Reedijk, *Inorg. Chim. Acta.* **2003**, *350*, 57–61.

[272]A. F. Stassen, H. Kooijman, A. L.Spek, L. J. de Jongh, J. G. Haasnoot, J. Reedijk, *Inorg.Chem.* **2002**, *41*, 6468–6473.

[273]A. F. Stassen, H. Kooijman, A. L. Spek, J. G. Haasnoot, J. Reedijk, *J. Chem. Cryst.* **2001**, *31*, 307–314.

[274](a) E. Dova, R. Peschar, M. Sakata, K. Kato, H. Schenk, *Chem. – Eur. J*. **2006**, *12*, 5043–5052; (b) E. Dova, R. Peschar, M. Takata, E. Nishibori, H. Schenk, A. F. Stassen, J. G. Haasnoot, *Chem. – Eur. J.* **2005**, *11*, 5855–5865.

[275] R. N. Butler, T. M. McEvoy, *Proc. R. Irish Acad.* **1977**, *77B*, 359.

[276] H. R. Meier, H. Heimgartner, in *Methoden der organischen Chemie* (Houben-Weyl), 4th edn., vol. E8d, E. Schaumann, E., Thieme: Stuttgart, **1994**, 664.

[277] M. Tremblay, *Canad. J. Chem.* **1965**, *43*, 1154–1157.

[278] J. Svetlik, A. Martvon, J. Lesko, *Chem. Papers*, **1979**, *33*, 521.

[279] *primary explosives:* (a) G. Geisberger, T. M. Klapötke, J. Stierstorfer, *Eur. J. Inorg. Chem.* **2007**, *30*, 4743–4750; (b) T. M. Klapötke, J. Stierstorfer, *Centr. Europ. J. Energ. Mat.* **2008**, *5(1)*, 13–30; *secondary explosives:* J. Akhavan, The Chemistry of Explosives, 2nd edn. London, RSC press, **2004**; *propellants:* (a) Ref. 174; (b) T. M. Klapötke, P. Mayer, J. Stierstorfer, J. J. Weigand, *J. Mat. Chem.* **2008**, *18*, 5248–5258. *pyrotechnics:* (a) G. Steinhauser, T. M. Klapötke, *Angew. Chem. Int. Ed.* **2008**, *47*, 3330. (b) T. M. Klapötke, J. Stierstorfer, K. R. Tarantik, I. Thoma, *Z. Anorg. Allg. Chem.* **2008**, *634*, 2777–2784.

[280] R. Boese, T. M. Klapötke, P. Mayer, V. Verma, *Propellants, Explos., Pyrotech.* **2006**, *31*, 263–268

[281] G. A. Gareev, L. P. Kirillova, V. M. Shul´gina, S. R. Buzilova, L. P. Vologdina, L. I.Vereshchagin, *J. Org. Chem. USSR* (Engl. Transl.) **1988**, *24*, 2003–2007.

[282] J. Denkstein, V. Kaderabek, *Coll. Czech. Commun*. **1960**, *25*, 2334–2340.

[283] J. H. Bryden, *Acta Cryst.* **1956**, *9*, 874.

[284] J. M. Welch, *Dissertation*, Ludwig Maximilian University Munich, **2008**.

[285] M. Tremblay, *Canad. J. Chem*. **1965**, *43*, 1154.

[286] J. Svetlik, A. Martvon, J. Lesko, *Chem. Papers* **1979**, *33*, 521.

[287] M. Hesse, H. Meier, B. Zeeh, *Spektroskopische Methoden in der organischen Chemie*, 7th edn., Thieme, Stuttgart, New York, **2005**.

[288] N. Wiberg, in *Lehrbuch der Anorganischen Chemie / Holleman-Wiberg*, 101st edn., de Gruyter, Berlin, **1995**, p. 51.

[289] N. Wiberg, in *Lehrbuch der Anorganischen Chemie / Holleman-Wiberg*, 101. edn., de Gruyter, Berlin, **1995**, p. 141.

[290] Proceedings of Partners in Environmental Technology Symposium, Strategic Environmental Research and Development Program (SERDEP) and Environmental Security Technology Certification Program (ESTCP), Nov 30-Dec 2, **2004**, Washignton DC, USA.

[291] A. Hammerl, T. M. Klapötke, H. Nöth, M. Warchhold, *Inorg. Chem*. **2001**, *40*, 3570–3575.

[292](a) J. Thiele, J. T. Marais, *J. Liebigs Ann..* **1893**, *273*, 144–160; (b) J. Thiele, *Liebigs Ann.* **1898**, *303*, 57–75.

[293]T. M. Klapötke, P. Meyer, A. Schulz, J. J. Weigand, *Propellants, Explos., Pyrotech.* **2004**, *29*, 325–332.

[294]C. Ye, J.-C. Xiao, B. Twamley, J. M. Shreeve, *Chem. Comm.* **2005**, *21*, 2750–2752.

[295]H. Xue, B. Twamley, J. M. Shreeve, *Inorg. Chem.* **2004**, *43*, 7972–7977.

[296]J. A. Garrison, R. M. Herbst, *J. Org. Chem.* **1957**, *22*, 278–283.

[297](a) S. Fukumoto, E. Imamiya, K. Kusumoto, S. Fujiwara, T. Watenabe, M. J. Shiraishi, *Med. Chem.* **2002**, *45(14)*, 3009–3021; (b) I. Jedidi, P. Therond, S. Zarev, C. Cosson, M. Couturier, C. Massot, D. Jore, M. Gardes-Albert, A. Legrand, D. Bonnefondt-Rousselot, *Biochemistry* **2003**, *42(38)*, 11356–11365; (c) K. A. Schug, W. Lindner, *Chem. ReV.* **2005**, *105(1)*, 67–114; (d) A. W. Nineham, *Chem. Rev.* **1955**, *55*, 355–483; (e) T. K. Brothrton, J. W. Lynn, *Chem. Rev.* **1959**, *59(5)*, 841–883; (f) J. Neutz, O. Grosshardt, S. Schäufele, H. Schnuppler, W. Schweikert, *Propellants, Explos., Pyrotech.***2003**, *28(4)*, 181–188; (g) N. Wingborg, N. Latypov, *Propellants, Explos., Pyrotech.* **2003**, *28(6)*, 314–318.

[298]J. Köhler, R. Meyer, *Explosivstoffe*, Wiley-VCH, D-Weinheim, 9th edn., **1998**, 138.

[299](a) D. E. Chavez, M. A. Hiskey, M. H. Huynh, D. L. Naud, S. F. Son, B. C. Tappan, *J. Pyrotech.* **2006**, *23*, 70–80; (b) D. E. Chavez, M. A. Hiskey, D. L. Naud, *J. Pyrotech.* **1999**, *10*, 17–36; (c) M. A. Hiskey, D. E. Chavez, D. L. Naud, *U.S. patent* **2001**, US 6214139.

[300]A. Akella, D. A. Keszler, *Acta Cryst.* **1994**, *C50*, 1974–1976.

[301]J. H. Bryden, *Acta Cryst.* **1957**, *10*, 677–680.

[302]D. T. Cromer, J. H. Hall, K.-Y. Le, R. R. Ryan, *Acta Cryst.* **1988,** *C44***,** 2206–2208.

[303]T. M. Klapötke, in *Moderne Anorganische Chemie*, E. Riedel (Hrsg.), 3rd edn., Walter de Gruyter, Berlin, New York, **2007**, 84–86.

[304](a) http://secure2.pnl.gov/nsd/nsd.nsf/Welcome; (b) R. Mecke, F. Langenbucher, *Infrared Spectra*, Heyden & Son, **1965**, London, Serial No. 6.

[305]T. Shimanouchi*, Tables of Molecular Vibrational Frequencies Consolidated* Volume II*,* J*. Phys. Chem. Ref. Data* **1972**, *6(3)*, 993.

[306]T. Shimanouchi, *Tables of Molecular Vibrational Frequencies Consolidated* Volume I, National Bureau of Standards *1*, **1972**.

[307]R. P. Singh, H. Gao, D. T. Meshri, J. M. Shreeve, in *High Energy Density Materials*, T. M. Klapötke (Hrsg.), Springer, Berlin, Heidelberg, **2007**, 36–80.

[308]R. Meyer, J. Köhler, A. Homburg, in *Explosives*, 6th edn., Wiley-VCH, Weinheim, **2007**, pp 194–195.

[309]G. O. Reddy, *Propellants, Explos., Pyrotech.* **1992**, *17*, 241–248.

[310] M. H. V. Huynh, M. A. Hiskey, T. J. Meyer, M. Wetzler, *PNAS*, **2006**, *103*, 5409–5412.

[311]A. Yu. Zhilin, M. A. Ilyushin, I. V. Tselinskii, A. S. Brykov, *Zh. Prikl. Khim*., **2001**, *74*, 96–99.

[312]A. Yu. Zhilin, M. A. Ilyushin, I. V. Tselinskii, A. S. Kozlov, N. E. Kuzmina, *Russ. J. Appl. Chem.* **2002***, 75,* 1849–1851.

[313]P. N. Gaponik, S. V. Voitekhovich, O. A. Ivashkevich, *Russian Chem. Rev.* **2006**, *75*, 508.

[314](a) A. M. Astakhov, A. D. Vasilev, M. S. Molokeev, A. M. Sirotinin, L. A. Kruglyakova, R. S. Stepanov, *Zh. Strukt. Khim. (Russ.)* **2004**, *45*, 175–180; (b) A. D. Vasilev, A. M. Astakhov, A. A. Nefedov, R. S. Stepanov, *J. Struct. Chem (Russ.)* **2003**, *44(2)*, 359–361.

[315]A. D. Vasilev, A. M. Astakhov, A. A. Nefedov, R. S. Stepanov, *Zh. Strukt. Khim.* **2003**, *44*, 359.

[316](a) S. Natarajan, K. V. Vijitha, S. A. Martin Britto Dhas, J. Sureshb, P. L. Nilantha Lakshman, *Acta Crystallogr.***2008**, *E64*, 581; (b) Shan Gao, Zhu-Yan Zhang, Li-Hua Huo, Hui Zhao, Jing-Gui Zhao, *Acta Crystallogr.***2004**, *E60*, 444.

[317] M. V. Kirillova, A. M. Kirillov, M. F. C. G. da Silva, M. N. Kopylovich, J. J. R. F. da Silva, A. J. L. Pombeiro, *Inorg. Chim. Acta* **2008***, 361,* 1728–1737.

[318] V. A. Ostrovskii, G. I. Koldobskii, R. E. Trifonov, in "*Comprehensive Heterocyclic Chemistry III*", Volume 6, V. V. Zhdankin, A. R. Katritzky (Ed.), Elsevier, **2008**, p. 301.

[319]N. Wiberg, in „Lehrbuch der anorganischen Chemie", A. F. Holleman, E. Wiberg, 101st edn., de Gruyter, Berlin, New York, **1995**, 1262–1264.

[320]J. Köhler, R. Meyer, *Explosivstoffe*, Wiley-VCH, D-Weinheim, 9th edn., **1998**, 174.

[321]K. Karaghiosoff, T. M. Klapötke, A. N. Michailovski, H. Nöth, M. Suter, G. Holl, *Propellants, Explos., Pyrotech.* **2003**, *28(1)*, 1.

[322](a) G. Pfefferkorn, *Z. Naturforsch.* **1948**, *3a*, 364; (b) B. Reitzner, R. P. Manno, *Nature* **1963**, *198*, 4884; (c) C. M. Ho, S. T. Lee, , P. C. Chen, G. H. Wei, J. S. Shiau, P. H. Chen, H. C. Fan, J. Y. Huan, *Huoyao Jishu* **1992**, *8*, 31; (d) G. L. Glen, *J. Am. Chem. Soc.* **1963**, *85*(23), 3892.

[323](a) M. Stammler, J. E. Abel, R. C. Ling, *Nature* **1961**, *192*, 626; (b) M. Stammler, J. E. Abel, J. V. R. Kaufman, *Nature* **1960**, *185*, 4560; (c) J. Roth, *J. Chem. Phys.* **1964**, *41(7)*, 1929; (d) G. Todd, E. Parry, *Nature* **1962**, *196*, 250.

[324]J. Köhler, R. Meyer, *Explosivstoffe*, Wiley-VCH, Weilheim, 9th edn., **1998**, 54.

[325](a) A. Stettbacher, *Nitrocellulose* **1937**, *8*, 3–6, 21–27; (b) J. R. Payne, *Thermochim. Acta* **1994**, *242(1–2)*, 13; (c) H. C. J. Saint, J. Hewson, *Analyst* **1959**, *84*, 183; (d) F. C. Tompkins, D. A. Young, *J. Chem. Soc.* **1956**, 3331; (e) W. C. McCrone, O. W. Adams, *Anal. Chem.* **1955**, *27*, 2014.

[326](a) W. Beck, J. Evers, M. Göbel, G. Oehlinger, T. M. Klapötke, *Z. Anorg. Allg. Chem.* **2007**, *633*, 1417–1422; (b) S. Singh, *J. Phys. Soc. Japan* **1959**, *14*, 540; (c) L. Wohler, A. Berthmann, *Angew. Chem.* **1930**, *43*, 59; (d) A. Langhans, *J. Soc. Chem. Ind.* **1918**, *38*, 389A. (e) M. E. Brown, G. M. Swallowe, *Thermochim. Acta* **1981**, *49*(2–3), 333.

[327](a) S. H. Patinkin, J. P. Horwitz, E. Lieber, *J. Am. Chem. Soc.* **1955**, *77*, 562; (b) J. R. C. Duke, J. *Chem. Soc. Sect. D* **1971**, *1*, 2; (c) G. C. Mei, J. W. Pickett, *Propellants, Explos., Pyrotech.* **1998**, *23(4)*, 172.

[328]M. H. V. Huynh, M. A. Hiskey, T. J. Meyer, M. Wetzler, *Proc. Natl. Acad. Sci. U.S.A.* **2006**, *103(14)*, 5409.

[329]G. Steinhauser, T. M. Klapötke, *Angew. Chem. Int. Ed.* **2008**, *47*, 2–20.

[330]J. Köhler, R. Meyer, *Explosivstoffe*, Wiley-VCH, D-Weinheim, 9th edn., **1998**, 138.

[331](a) D. E. Chavez, M. A. Hiskey, M. H. Huynh, D. L. Naud, S. F. Son, B. C. Tappan, *J. Pyrotech.* **2006**, *23*, 70; (b) D. E. Chavez, M. A. Hiskey, D. L. Naud, *J. Pyrotech.* **1999**, *10*, 17; (c) M. A. Hiskey, D. E. Chavez, D. L. Naud, *U.S. patent* **2001**, US 6214139.

[332](a) D. E. Chavez, M. A. Hiskey, D. L. Naud, *J. Pyrotech.* **1999**, *10*, 17; (b) G. Steinhauser, K. Tarantik, T. M. Klapötke, *J. Pyrotech.* **2008**, *27*, 3; (c) G. Steinhauser, K. Karaghiosoff, T. M. Klapötke, *Z. Anorg. Allg. Chem*. **2008**, *634*, 892; (d) D. E. Chavez, M. A. Hiskey, M. H. Huynh, D. L. Naud, S. F. Son, B. C. Tappan, *J. Pyrotech.* **2006**, *23*, 70; (e) B. C. Tappan, M. H. Huynh, M. A. Hiskey, D. E. Chavez, E. P. Luther, J. T. Mang, S. F. Son, *J. Am. Chem. Soc.* **2006**, *128*, 6589.

[333]B. Morosin, *Acta Cryst.* **1976**, *B32*, 1237.

[334]E. Riedel, *Anorganische Chemie*, 4th edn., de Gryter, Berlin, **1999**, 677 and 722.

[335](a) R. Prins, M. Biagini-Cingi, R. A. G. De Graff, J. Haasnoot, A.-M. Manotti-Lanfredi, P. Rabu, P. Reedijk, E. Ugozzli, *Inorg. Chim. Acta* **1996**, *248*, 35; (b) R. Bronisz, *Inorg. Chim. Acta* **2004**, *357*, 396; (c) P. Børsting, J. J. Steel, *Eur. J. Inorg. Chem.* **2004**, 376; (d) P. E. M. Wijnands, J. S. Wood, J. Reedijk, W. J. A. Maaskant, *Inorg. Chem.* **1996**, *35*, 1214.

[336]S. F. Palopoli, S. J. Geib, A. L. Rheingold, T. B. Brill, *Inorg. Chem.* **1988**, 27, 2963.

[337]A. M.Astakhov, A. D.Vasil'ev, M. S. Molokeev, A. M. Sirotinin, L. A. Kruglyakova, R. S. Stepanov, *J.Struct.Chem.* **2004**, 45, 181.

[338](a) H. Nakai and Y. Deguchi, *Bull. Chem. Soc. Jap.* **1975**, *48*, 2557; (b) H. E. Heldal , J. Sletten, *Acta Chem. Scand.* **1997**, *51*, 122.

[339]F. Mazzi, *Acta Cryst.* **1955**, *8*, 137.

[340]N. Wiberg, in Lehrbuch der anorganischen Chemie, A. F. Holleman, E. Wiberg, 101st edn., de Gruyter, Berlin, New York, **1995**, 1838–1839.

[341](a) O. Kahn, "Molecular Magnetism" *VHC* **1993**; (b) J. C. Bonner, M. E. Fisher, *Phys. Rev.* **1964**, 135, 640.

[342]M. H. V. Huynh, M. A. Hiskey, T. J. Meyer, M. Wetzler, *Proc. Natl. Acad. Sci. U.S.A.* **2006**, *103*, 5409.

[343](a) R. Escales, in 'Schwarzpulver und Sprengsalpeter', 1st edn., Survival press, **2003,** 1–488; (b) M. Baetz, in 'Schwarzpulver für Survival, 1st edn., Books on Demand, **2004**; (c) J. P. Agrawal, R. Hodgson, in 'Organic Chemistry of Explosives', 1st edn., Wiley, **2007**, 1–414; (d) J. Akhavan, in 'The chemistry of Explosives', 2nd edn., RSC, **2004**, 1–180

[344]P. Folly, P. Mäder, *Chimia*, **2004**, *58*, 374–382.

[345]N. Kubota, *Propellants and Explosives*, *2nd edn.*; Wiley-VCH, Weinheim,

2007, 360–363.

[346](a) J. Reilly, J. Teegan, M. Carey, *Nature* **1947**, *159*, 643; b) V. P. Shchipanov, A. I. Zabolotskaya, R. A. Badryzlova, *Chem. Heterocycl. Compd.* **1975**, 6, 850–854.

[347]K. Hattori, E. Lieber, J. P. Horwitz, *J. Am. Chem. Soc.* **1956**, *78*, 411–415.

[348]R. N. Butler, F. L. Scott, *J. Org. Chem.* **1967**, *32*, 1224–1226.

[349]R. N. Butler, V. C. Garvin, Victor C. *J. Chemi. Res. Synopses* **1982**, *7*, 183.

[350]A. S. Lyakhov, P. N. Gaponik, D. S. Pytleva, S. V. Voitekhovich, L. S. Ivashkevich, *Acta Cryst.* **2004**, *C60*, 421–422.

[351]J. Thiele, J. T. Marais, *Liebigs Ann.* **1893**, *273*, 144–160.

[352]V. P. Shchipanov, A. I. Zabolotskaya, R. A. Badryzlova, *Khimiya Geterotsiklicheskikh Soedinenii* **1975**, *6*, 850–854.

[353](a) E. Makino, N. Iwasaki, N. Yagi, H. Kato, Y. Ito, H. Azuma, *Chem. Pharm. Bull*. **1990**, *38*, 201; (b) C. V. Reddy Sastry, *Ind. J. Chem*. **1990**, *29B*, 396; (c) C. T.

Alabaster, *J. Med. Chem*. **1989**, *32*, 575; (d) M. Uchida, M. Komatsu, S. Morita, T. Kanbe, K. Nagakawa, *Chem. Parm. Bull.* **1989**, *37*, 322.

[354] M. Friedrich, J. C. Gálvez-Ruiz, T. M. Klapötke, P. Mayer, B. Weber, J. J. Weigand, *Inorg. Chem*, **2005**, *44(22)*, 8044.

[355] (a) R. Bronisz, *Inorg. Chim. Acta **2002**, 340,* 215–220; b) F. Jiang, *Peop. Rep. China. Faming Zhuanli Shenqing Gongkai Shuomingshu,* **1993**, CN 92-108636, 19921117.

[356] J. S. Mihina, R. M. Herbst, *J. Org. Chem.* **1950**, *15*, 1082.

[357] A. Catino, *Ann. Chim.* **1966**, *56(11),* 1332.

[358] W. S. McEwan, M. W. Rigg, *J. Am. Chem. Soc.* **1951**, *76*, 4725–4727.

[359] A. M. Astakhov, A. D. Vasiliev, M. S. Molokeey, A. M. Sirotinin, L. A. Kruglyakova, R. S. Stepanov, *J. Struct. Chem.* **2004**, *45(1)*, 175–180.

[360] E. A. Goiko, N. V. Grigoreva, N. V. Margolis, A. A. Mel'nikov, T. K. Strochkina, I. V. Tselinskii, *J. Struct. Chem.* **1980**, *21(5)*, 177–180.

[361] M. Alcami, O. Mo, M. Yanez, *J. Phys. Chem.* **1989**, *93*, 3929–3936.

[362] G. J. Palenik, *Acta Cryst.* **1963**, *16*, 596–600.

[363] H. P. H. Arp, A. Decken, J. Passmore, D. J. Wood, *Inorg. Chem.* **2000**, *39(9)*, 1840–1848.

[364] B. C. Tappan, C. D. Incarvito, A. L. Rheingold, T. B. Brill, *Thermochim. Acta* **2002**, *384(1–2)*, 113–120.

[365] O. A. Ivanshkevich, P. N. Gaponik, N. I. Sushko, V. A. Krasitskii, *Zhurnal Prikladnoi Spektroskopii* **1994**, *61(1–2)*, 45–49.

[366] R. Goddard, O. Heinemann, C. Kruger, *Acta Cryst.* **1997**, *C53(5)*, 590.

[367] M. I. Eremets, A. G. Gavriliuk, I. A. Trojan, *Appl. Phys. Lett.* **2007**, *90(17)*, 171904/1-171904/3.

[368] (a) M. Tobita, R. J. Bartlett, *J. Phys. Che*m. A **2001**, *105(16)*, 4107–4113; b) S. A. Perera, R. J. Bartlett, *Chem. Phys. Let.* **1999**, *314(3,4)*, 381–387; (c) W. J. Lauderdale, J. F. Stanton, R. J. Bartlett, *J. Phys. Chem*. **1992**, *96(3),* 1173–1178; (b) T. M. Klapötke, *J. Mol. Struct.* **2000**, *499*, 99–104; (c) T. M. Klapötke, R. D. Harcourt, *J. Mol. Struct.* **2001**, *541*, 237–242.

[369] (a) P. Gray, Chemistry of the Inorganic Azides, *Quart. Rev.* **1963**, *17*, 441–473; (b) Ullmann, 5th edn., **1989**, *A13*, 193–197; (c) I. C. Tornieporth-Oetting, T. M. Klapötke, Covalent inorganic nonmetal azides, *Combustion Efficiency and Air Quality,* **1995**, 51–62.

[370]R. Haiges, S. Schneider, T. Schroer, K. O. Christe, *Angew. Chem. Int. Ed.* **2004**, *43(37)*, 4919–4924.

[371](a) K. Banert, Y.-H. Joo, T. Rueffer, B. Wlafort, H. Lang, *Angew. Chem. Int. Ed.* **2007**, *46(7)*, 1168–1171; (b) Q. S. Li, H. X. Duan, *J. Phys. Chem. A* **2005**, *109(40)*, 9089–9094.

[372](a) T. Curtius, *Ber. Dtsch. Chem. Ges.* **1891**, *24*, 3341; (b) E. P. Kirpichev, A. P. Alekseev, Yu. I. Rubtsov, G. B. Manelis, *Russ. J. Phys. Chem.* **1973**, *47*, 1654.

[373]N. Wiberg, in „Lehrbuch der Anorganischen Chemie“ *Holleman-Wiberg*, 102nd edn., de Gruyter, Berlin, **2007**, p. 659 (ammonium azide), p. 692–693 (tetrazene).

[374](a) S. Hünig, H. R. Müller, W. Thier, *Angew. Chem.* **1965**, *77*, 368–377; *Ang. Chem. Int. Ed.* **1965**, *4*, 271; (b) C. E. Miller, *J. Chem. educ.* **1965**, *42*, 254–259.

[375]A. Hammerl, T. M. Klapötke, H. Piotrowski, *Propellants, Explosiv., Pyrotech.* **2001**, *26*, 161–164.

[376]Ullmann, 5th Ed. **1989**, *A13*, 177–191.

[377]W. Friedrich, K. Flick, **1942**, DE 719135. b) W. Friederich, **1940**, GB 519069 19400315. c) W. Friedrich, K. Flick, **1939**, US 2179783 19391114.

[378](a) A. Hammerl, T. M. Klapötke, P. Mayer, J. J. Weigand, *Propellants, Explos., Pyrotech.* **2005**, *30(1)*, 17–26; (b) A. Hammerl, T. M. Klapötke, H. Nöth, M. Warchhold, G. Holl, *Propellants, Explos., Pyrotech.* **2003**, *28(4)*, 165–173.

[379]F. D. Marsh, *J. Org. Chem.* **1972**, *37(19)*, 2966–2969.

[380]A. J. Barratt, L. R. Bates, J. M. Jenkins, J. R. White, *U. S. Nat. Tech. Inform. Serv.* **1971**, *No. 752370*, 25 pp.

[381](a) N. Wiberg, in: *Lehrbuch der Anorganischen Chemie / Holleman-Wiberg*, 101st edn., de Gruyter, Berlin, **1995**, pp. 873–876; (b) Ullmann, 5th edn., **1989** pp. 139–200.

[382]B. Jürgens, E. Irran, E. W. Schnick, *J. Solid State Chem.* **2001**, *157*, 241–249.

[383]general: (a) M. Becker, M. Jansen, A. Lieb, W. Milius, W. Schnick, *Z. Anorg. Allg. Chem.* **1998**, *624 (1)*, 113–118; (b) R. Riedel, E. Kroke, A. Greiner, A. O. Gabriel, L. Ruwisch, J. Nicolich, *Chem. Mater.* **1998**, *10*, 2964–2970. structure: (a) M. A. Bredig, *J. Am. Chem. Soc.* **1942**, *64*, 1730–1731; (b) N. G. Vannerberg, *Acta Chem. Scand.* **1962**, *16*, 2263–2266; (c) M. J. Cooper, Acta Cryst. **1964**, *17(11)*, 1452–1456; (d) M. G. Down, M. J. Haley, P. Hubberstey, R. J. Pulham, A. E. Thunder, *J. Chem. Soc. (Chem. Comm.)* **1978**, *2*, 52–53.

[384] (a) W. Madelung, E. Kern, *Liebigs Ann. Chem*. **1922**, *427*, 26; (b) B. Jürgens, E. Irran, J. Schneider, W. Schnick, *Inorg. Chem.* **2000**, *39,* 665–670; (c) E. Irran, B. Jürgens, W. Schnick, *Solid State Sci.* **2002**, *4*, 1305–1311; (d) E. Irran, B. Jürgens, W. Schnick *Chem. Eur. J.* **2001**, *7*, 5372–5381.

[385] (a) J. R. Witt, D. Britton, *Acta Crystallogr.* **1971**, *B27*, 1835–1836; (b) L. Jäger, M. Kretschmann, H. Köhler, *Z. Anorg. Allg. Chem.* **1992**, *611*, 68–72; (c) H. Köhler, M. Jeschke, V. I. Nefedov, *Z. Anorg. Allg. Chem.* **1987**, *552*, 210–214; (d) P. Andersen, B. Klewe, E. Thom, *Acta Chem. Scand.* **1967**, *21* (6), 1530–1542.

[386] (a) H. P. H. Arp, A. Decken, J. Passmore, D. J. Wood, *Inorg. Chem.* **2000**, *39*, 1840–1848; (b) E. J. Graeber, B. Morosin, *Acta Crystallogr.* **1983**, *C39*, 567–570.

[387] (a) T. M. Klapötke. C. Kuffer, P. Mayer, K. Polborn, A. Schulz, J. J. Weigand, *Inorg. Chem.* **2005**, *44(16),* 5949–5958; (b) W. P. Norris, R. A. Henry, *J. Am. Chem. Soc.* **1963**, *29*, 650–660.

[388] (a) R. Reed, V. L. Brady, J. M. Hirtner, *Proceedings of the 18th International Pyrotechnics Seminar*; July 13–17, **1992**, 939–972; (b) Y. Akutsu, M. J. Tamura, *Energ. Mater.* **1993**, *16*, 205–218.

[389] (a) J. Lifschitz, *Chem. Ber.* **1915**, *48*, 410–420; (b) T. Curtius, A. Darapsky, E. Müller, *Chem. Ber.* **1915**, *48*, 1614–1634; (c) J. Lifschitz, *Chem. Ber.* **1916**, *49*, 489–493; (d) J. Lifschitz, W. F. Donath, *Recl. Trav. Chim. Pays-Bas* **1918**, *37*, 270–284.

[390] E. Lieber, D. R. Levering, *J. Am. Chem. Soc.* **1951**, *73*, 1313–1317.

[391] M. A. Hiskey, *Chemical & Engineering News*, **2005**, *83(30)*, 5.

[392] S. H. Patinkin, J. P. Horwitz, E. Lieber, *J. Am. Chem. Soc.* **1955**, *77*, 562–567.

[393] K. Sakurai, Y. Tomiie, *Acta Cryst.* **1952**, *5*, 293–294.

[394] A. Akella, D. A. Keszler, *Acta Cryst.* **1994**, *C50*, 1974–1976.

[395] A. Bondi, *J. Phys. Chem.* **1964**, *68*, 441.

[396] D. J. Haas, D. R. Harris, H. H. Mills, *Acta Cryst*. **1995**, *19*, 676–679.

[397] Z. Pajak, M. Grottel, A. E. Koziol, *J. Chem.Soc., Faraday Trans.* **1982**, *78*, 1529.

[398] D. A. Baldwin, L. Denner, T. J. Egan, A. J. Markwell, *Acta Crystallogr.* **1986**, *C42*, 1197.

[399] B. C. Tappan, C. D. Incarvito, A. L. Rheingold, T. B. Brill, *Thermochim. Acta* **2002**, *384(1–2)*, 113–120.

[400] A. R. Kennedy, J. B. A. Kirkhouse, K. M. McCarney, O. Puissegur, W. E. Smith, E. Staunton, S. J. Teat, J. C. Cherryman, R. James, *Chem. – Eur. J.* **2004**, *10*, 4606.

[401] M. Bichay, J. W. Fronabarger, R. Gilardi, R. J. Butcher, W. B. Sanborn, M. E. Sitzmann, M. D. Williams, *Tetrahedron Lett.* **2006**, *47*, 6663–6666

[402] L. Stefaniak, J. D. Roberts, M. Witanowski, G. A. Webb, *Org. Magn. Reson.* **1984**, *22*, 209.

[403] (a) G. L'Abbe, P. Van Stappen, S. Toppet, *Tetrahedron*, **1985**, *41*, 4621–4631; (b) P. Geißler, T. M. Klapötke, H. J. Kroth, *Spectrochim. Acta Part A*, **1995**, 51,1075.

[404] (a) M. Roche, L. Pujol, *Bull. Soc. Chim.,* **1969**, 1097–1102; (b) M. J. S. Dewar, G. J. Gleicher, *J. Chem. Phys*., **1966**, *44(2)*, 759–773.

[405] M. S. Westwell, M. S. Searle, D. J. Wales, D. H. Williams, *J. Am. Chem. Soc.*, **1995**, *117*, 5013–5015.

[406] J. Wilbrand, *Liebigs Ann.* **1863**, *128*, 178–179.

[407] G. I. Koldobskii, D. S. Soldatenko, E. S. Gerasimova, N. R. Khokhryakova, M. B. Shcherbinin, V. P. Lebedev, V. A. Ostrovskii, *Russ. J. Org. Chem.* **1997***, 33*, 1771–1783.

[408] E. Oliveri-Mandala and T. Passalaqua, *Gazzetta Chim. Ital.* **1912**, *41(II),* 430–435.

[409] (a) G. F. Holland and J. N. Pereira, *J. Med. Chem.* **1967**, *10(2),* 149–154; (b) S. V. Voitekhovich, P. N. Gaponik, A. O. Koren, *Mendeleev Commun.* **1997**, *1*, 41–42; (c) P. N. Gaponik, S. V. Voitekhovich, B. G. Klyaus, *Russ. J. Org. Chem.* **2004**, *40(4)*, 598–600; (d) M. D. Cullen, B. L. Deng, T. L. Hartman, K. M. Watson, R. W. Jr. Buckheit, C. Pannecouque, E. De Clercq, M. Cushman, *J. Med. Chem.* **2007**, *50(20)*, 4854–4867.

[410] (a) C. Stadler, J. Daub, J. Köhler, R. W. Saalfrank, V. Coropceanu, V. Schuenemann, C. Ober, A. X. Trautwein, S. F. Parker, M. Poyraz, T. Inomata, R. D. Cannon, *J. Chem. Soc. Dalton Trans.* **2001**, *22*, 3373–3383; (b) S. Achamlale, A. Elachqar, A. El Hallaoui, A. Alami, S. Elhajji, M. L. Roumestant, P. Viallefont, *Phosphorus, Sulfur Silicon Relat. Elem.* **1998**, *140*, 103–111; (c) A. O. Koren, P. N. Gaponik, O. A. Ivashkevich, T. B. Kovalyova, *Mendeleev Commun.* **1995**, *1*, 10–11.

[411] A. M. Churakov, S. E. Semenov, S. L. loffe, Y. A. Strelenko and V. A. Tartakovskii, *Mendeleev Commun.* **1995**, *5*, 102–103.

[412] M. M. Sokolova, V. V. Melnikov, A. A. Melnikov, B. V. Gidaspov, *Chem. Heterocyclic Comp*. **1977**, *6*, 689–692.

[413] (a) T. M. Klapötke, P. Mayer, K. Polborn, J. M. Welch, *New Trends in Research of Energetic Materials, Proceedings of the Seminar,* 9th, Pardubice, Czech Republic, Apr. 19-21, **2006**, 631-640; (b) T. M. Klapötke, P. Mayer, C. Miró Sabaté, J. M. Welch, N. Wiegand, *Inorg. Chem*. **2009**, accepted.

[414]T. M. Klapötke, C. Miró Sabaté, J. M. Welch, *Dalton Trans.* **2008**, 6372–6380**,** DOI: 10.1039/b811410b

[415]W. G. Finnegan, R. A. Henry, R. Lofquist, *J. Am. Chem. Soc*. **1958**, *80*, 3908.

[416](a) E. Oliveri-Mandala, *Gazz. Chim. Ital.* **1914**, *43*, 465–475; (b) E. Oliveri-Mandala, *Gazz. Chim. Ital.* **1920**, *50*, 256–261; (c) W. Friedrich, D. B. P. 952 811, **1956**; (d) G. I. Koldobskii, V. A. Ostrovskii, B. V. Gidaspov, *Khim. Geterotsikl. Soedin.* **1980**, *7*, 867–879; (e) V. Yu. Zubarev, V. A. Ostrowskii, *Chem. Heterocycl. Compd.* **2000**, *36*, 759–774; (f) P. J. Steel, J. *Chem. Crystallogr.* **1996**, *26*, 399–402; (g) J. H. Nelson, N. E. Takach, R. A. Henry, D. W. Moore, W. M. Tolles, G. A. Gray, *Magn. Reson. Chem.* **1986**, *24*, 984–994.

[417]A. Onishi, H. Tanaka, K. Shimamoto, *Jpn. Kokai Tokkyo Koho* **1998**, 29 pp. JP 10298168 A 19981110.

[418]H. Tanaka, K. Shimamoto, A. Onishi, *U.S. patent*, **2001**, 10 pp. 6300498 B1 20011009.

[419](a) H. P. H. Arp, A. Decken, J. Passmore, D. J. Wood, *Inorg. Chem.* **2000**, *39*, 1840 – 1848; (b)W. Selig, *Microchim. Acta* **1979**, 53–59; (c) M. A. Pierce-Butler, *Acta Crystallogr*. **1982**, *B38*, 2681–2683.

[420](a) P, N. Gaponik, V. P. Karavai, N. X. Chernavina, *Vestn. Beloruss. Gos. Univ.* **1983**, *2*, 23; (b) P. N. Gaponik, V. P. Karavai, *Khim. Geterotskikl. Soediu.* **1985**, *10*, 1422.

[421]P. N. Gaponik, V. P. Karavai, Y. V. Grigor'ev, *Khimiya Geterotsiklicheskikh Soedinenii*, **1985**, *11*, 1521–1524.

[422]Y. Gao, C. Ye, B. Twamley, J. M. Shreeve, *Chem. – Eur. J.* **2006**, *12*, 9010–9018.

[423]P. J. Steel, *J. Chem. Cryst*. **1996**, *26*, 399–402.

[424]S. Oga, *Jpn. Kokai Tokkyo Koho* **2006**, JP 2006249061, A 20060921.

[425]T. M. Klapötke, G. Holl. J. Geith, A. Hammerl, J. J. Weigand, *New Trends in Research of Energetic Materials*, *Proceedings of the Seminar,* 7th, Pardubice, Czech Republic, **2004**.

[426]T. K. Highsmith, R. J. Blau, G. K. Lund, US patent *5682014*, **1995**.

[427](a) M. A. Hiskey, D. E. Chavez, D. L. Naud, *US patent* 6214139, **2001**; (b) M. A. Hiskey, D. E. Chavez, D. L. Naud, D. L. *US patent* 6458227, **2003**; (c) M. A. Hiskey *et. al*, *US patent* 5917146, **2000**.

[428]W. P. Norris, R. A. Henry, *J. Org. Chem.* **1964**, *29(3)*, 650.

[429]T. K. Highsmith, R. M. Hajik, R. B. Wardle, G. K. Lund, R. J. Blau, *US patent* 5468866, **1995**.

[430]P. Mareček, K. Dudek, F. Liška, *New Trends in Research of Energetic Materials, Proceedings of the Seminar*, 7th, Pardubice, Czech Republic, April 20–22, **2004**, *2*, 566.

[431]D. E. Chavez, M. A. Hiskey, *J. Pyrotech.* **1998**, *7*, 11.

[432](a) R. N. Butler, *J. Chem. Soc. B*, **1969**, *6*, 980–981; (b) L. A. Lee, J. W. Wheeler, *J. Org. Chem.* **1972**, *37(3),* 348–351.

[433]N. N. Sveshnikov, J. H. Nelson, *Magn. Reson. Chem.* **1997**, *35*, 209.

[434]M. M. Degtyarik, P. N. Gaponik, V. N. Naumenko, A. I. Lesnikovich, M. V. Nikanovich, *Spectrochim. Acta.* **1987***, 43A*, 349.

[435]P. N. Gaponik, V. P. Karavai, Y. V. Grigorev, *Him. Geterotsikl. Soed.* **1985**, 1521.

[436]J. Stierstorfer, Chemistry of Bistetrazolylamines, *diploma thesis*, Ludwig-Maximilian University Munich, **2005**.

[437](a) M. Eddaoudi, J. Kim, N. Rosi, D. Vodak, J. Wachter, M. O'Keeffe, O. M. Yaghi, *Science* **2002**, *295*, 469; (b) H. Li, M. Eddaoudi, M. O'Keeffe, O. M. Yaghi, *Nature* **1999**, *402*, 276; (c) S. R. Batten, P. Jensen, B. Moubaraki, K. S. Murray, R. Robson, *Chem. Commun.* **1998**, 439.

[438](a) V. G. Leontjev, E K. Shesttakov, *Proceedings of International Pyrotechnoology Seminar*, 520, **1995**; (b) K. C. Patil, V. R. Vernekar Pai, *Synth. React. Inorg. Met. Org. Chem.* **1982**, *12*, 383; (c) A. Yu Zhilin, M. A. Ilyshin, I. V. Tselinskii, A. S. Kozlov, N. E. Kuz'mina, *Russ. J. Appl. Chem.* **2002**, *75(11)*, 1849; (d) A. V. Smirnov, M. A. Ilyushin, I. V. Tselinskii, *Russ. J. Appl. Chem.* **2004**, *77(5)*, 794.

[439](a) W. R. Tomlinson, K. G. Ottoson, L. F. Audriete, *J. Am. Chem. Soc.* **1949**, *71*, 375; (b) T. B. Joyner, *Can. J. Chem.* **1969**, *74*, 2729; (c) S. V. Sinditskii, V. V. Serushkin, *Def. Sci. J.* **1996**, *46*, 371.

[440](a) S. Zhu, Y. Wu, W. Zhang and J. Mu, *Propellants, Explos., Pyrotech.* **1996**, *22(6)*, 317; (b) M. L. Liebarger, *Ind. Eng. Chem. Prod. Res. Dev.* **1985**, *24*, 438.

[441]S. Zh, Y. Wu, W. Zhang, J. Mu, J. *Propellants, Explos. Pyrotech.* **1996**, *22(6)*, 317.

[442]M. Parry, P. M. Dickson and J. E. Field, *19th International Annual Conference ICT*, Karlsruhe, 44/1, **1988**.

[443](a) R. Bronisz, *Eur. J. Inorg. Chem.* **2004**, 3688; (b) P. J. van Koningsbruggen, Y. Garcia, L. Fourne`s, H. Kooijman, A. L. Spek, J. G. Haasnoot, J. Moscovici, K. Provost, A. Michalowicz, F. Renz, P. Gütlich, *Inorg. Chem.* **2000**, *39*, 1891; (c) A. F. Stasse, W. L. Driesse, J. G. Haasnoot, J. Reedijk, *Inorg. Chim. Acta* **2003**, *350*, 57; (d) P. N. Gaponik, S. V. Votekhovich, A. S. Lyakhov, V. E. Matulis, O. A. Ivashkevich, M. Quesada, J. Reedijk, *Inorg. Chim. Acta* **2005**, *358*, 2549; (e) P. N. Gaponik, M. M.

Degtyarik, A. S. Lyakhov, V. E. Matulis, O. A. Ivashkevich, M. Quesada, J. Reedijk, *Inorg. Chim. Acta* **2005**, *358*, 3949.

[444] N. C. Baenziger, R.J. Schultz, *Inorg. Chem.* **1971**, *10*, 661–667.

[445] P. E. M. Wijnands, J. S. Wood, J. Reedijk, W. J. A. Maaskant, *Inorg. Chem.* **1996**, *35(5)*, 1214–1222.

[446] P. N. Gaponik, V. P. Karavai, Y. V. Grigorev, *Him. Geterotsikl. Soed.* **1985**, 1521

[447] (a) K. Williamson, P. Li, J. P. Devlin, *J. Chem. Phys.* **1968**, *48*, 3891; (b) J. R. Fernandes, S. Ganguly, C. N. R. Rao, *Spectrochim. Acta* **1979**, *35A*, 1013.

[448] (a) H. J. Cohn, *Chem. Soc.* **1952**, 4282; (b) P. Redlich, J. Holt, T. Biegeleisen, *J. Am. Chem. Soc.* **1944**, *66*, 13; (c) H. Grothe, H. Willner, *Angew. Chem.* **1996**, *108*, 816.

[449] K. Nakamoto, *Infrared and Raman spectra of Inorganic and Coordination Compounds*, 4th edn., Wiley, New York, **1986**.

[450] P. L. Franke, W. L. Groeneveld, *Transition Met. Chem.* **1980**, *5*, 240–244.

[451] M. Göbel, T. M. Klapötke, *Adv. Funct. Mat.* **2009**, DOI: 10.1002/adfm200801389.

[452] C. Krieger, H. Fischer, F. A. Neugebauer, *Acta Cryst.* **1987**, *C43*, 1320–1322.

X-ray data and parameters

	2·H_2O	**21**	**22**
Formula	$CH_3N_5 \cdot H_2O$	$LiCH_2N_5$	$NaCH_8N_5O_3$
Form. weight [g mol^{-1}]	103.10	91.02	161.11
Crystal system	monoclinic	monoclinic	triclinic
Space Group	$P2_1/c$ (14)	$P2_1/c$ (14)	P–1 (2)
Color / Habit	colorless rods	colorless prism	colorless needle
Size [mm]	0.07 x 0.08 x 0.09	0.20 x 0.23 x 0.25	0.42 x 0.21 x 0.20
a [Å]	6.389(4)	4.7900(5)	5.8689(7)
b [Å]	7.198(5)	10.614(1)	10.0258(9)
c [Å]	9.819(6)	7.0369(8)	12.171(1)
α [°]	90	90	87.34(1)
β [°]	90.198(5)	103.260(9)	77.546(9)
γ [°]	90	90	80.059(9)
V [Å^3]	451.6(5)	348.22(7)	688.76(13)
Z	4	4	4
$\rho_{calc.}$ [g cm^{-3}]	1.516	1.736	1.554
μ [mm^{-1}]	0.129	0.130	0.190
$F(000)$	216	184	336
$\lambda_{MoK\alpha}$[Å]	0.71073	0.71073	0.71073
T [K]	200	120	200
Theta Min-Max [°]	4.3, 26.0	4.4, 26.7	4.3, 26.0
Dataset [h; k; l]	–5:7; –8:7; –11:12	–6:6; –13:13; –8:8	–7:7; –12:12; –14:14
Reflection collected	2239	3658	7001
Independent reflection	874	736	2687
R_{int}	0.042	0.028	0.019
Observed reflection	748	714	2437
No. parameters	84	72	245
R_1 (obs)	0.0540	0.0425	0.0339
wR_2 (all data)	0.1254	0.0939	0.0837
S	1.17	1.20	1.11
Min./Max. Resd. [e Å^{-3}]	–0.15, 0.23	–0.20, 0.17	–0.20, 0.17
Device type	Oxford Xcalibur3 CCD	Oxford Xcalibur3 CCD	Oxford Xcalibur3 CCD
Solution	SHELXS-97	SHELXS-97	SIR-97
Refinement	SHELXL-97	SHELXL-97	SHELXL-97
Absorption correction	multi-scan	multi-scan	multi-scan
CCDC No.	---	631339	631337

	23	**24**	**25**
Formula	KCH_2N_5	$RbCH_2N_5$	$CsCH_2N_5$
Form. weight [g mol^{-1}]	123.18	169.55	216.99
Crystal system	monoclinic	orthorhombic	orthorhombic
Space Group	$P2_1/c$ (14)	*Pnma* (62)	*Pnma* (62)
Color / Habit	colorless rods	colorless prism	colorless prism
Size [mm]	0.14 x 0.18 x 0.25	0.04 x 0.09 x 0.13	0.15 x 0.08 x 0.07
a [Å]	6.8702(8)	7.4221(9)	8.0538(7)
b [Å]	9.8516(9)	6.8053(8)	6.9305(6)
c [Å]	6.8372(7)	9.0133(9)	9.1021(8)
α [°]	90	90	90
β [°]	115.61(1)	90	90
γ [°]	90	90	90
V [Å^3]	417.29(8)	455.26(9)	508.05(8)
Z	4	4	4
$\rho_{calc.}$ [g cm^{-3}]	1.961	2.474	2.837
μ [mm^{-1}]	1.113	10.729	7.157
$F(000)$	248	320	392
$\lambda_{MoK\alpha}$ [Å]	0.71073	0.71073	0.71073
T [K]	120	125	200
Theta Min-Max [°]	4.1, 26.5	4.5, 27.5	4.5, 26.5
Dataset [h; k; l]	–8:8; –12:12; –8:8	–9:9; –8:8; –11:11	–10:10; –8:8; –11:11
Reflection collected	4269	4841	4973
Independent reflection	863	569	570
R_{int}	0.028	0.055	0.028
Observed reflection	829	544	568
No. parameters	72	41	42
R_1 (obs)	0.0269	0.0295	0.0180
wR_2 (all data)	0.0673	0.0443	0.0369
S	1.11	1.18	1.15
Min./Max. Resd. [e Å^{-3}]	–0.28, 0.29	–0.51, 0.78	–0.47, 0.98
Device type	Oxford Xcalibur3 CCD	Oxford Xcalibur3 CCD	Oxford Xcalibur3 CCD
Solution	SIR-92	SHELXS-97	SIR-92
Refinement	SHELXL-97	SHELXL-97	SHELXL-97
Absorption correction	multi-scan	multi-scan	multi-scan
CCDC No.	631335	631336	631338

	26	**29**	**30**
Formula	$C_2H_{12}MgN_{10}O_4$	$Ba_2C_4H_{23}N_{20}O_9$	CH_7N_7
Form. weight [g mol^{-1}]	264.50	763.12	117.14
Crystal system	triclinic	monoclinic	orthorhombic
Space Group	$P\bar{1}$ (2)	$P2_1/n$ (14)	$P2_12_12_1$ (18)
Color / Habit	colorless rods	colorless needles	colorless needles
Size [mm]	0.08 x 0.10 x 0.10	0.03 x 0.03 x 0.13	0.04 x 0.09 x 0.09
a [Å]	5.950(1)	7.2980(5)	9.7179(6)
b [Å]	7.345(2)	23.759(2)	13.5958(8)
c [Å]	7.397(2)	13.929(1)	3.8056(3)
α [°]	106.11(3)	90	90
β [°]	106.54(2)	92.206(6)	90
γ [°]	111.90(2)	90	90
V [Å^3]	259.38(15)	2413.5(3)	502.81(6)
Z	1	4	4
$\rho_{calc.}$ [g cm^{-3}]	1.693	2.128	1.547
μ [mm^{-1}]	0.201	3.322	0.122
$F(000)$	138	1496	248
$\lambda_{MoK\alpha}$[Å]	0.71073	0.71073	0.71073
T [K]	100	200	200
Theta Min-Max [°]	4.7, 27.5	4.0, 27.5	3.7, 31.5
Dataset [h; k; l]	–7:7; –9:9; –9:9	–9:9; –30:30; –18:18	–9:14; –19:19; –5:5
Reflection collected	2978	27278	3815
Independent reflection	1190	5531	1013
R_{int}	0.016	0.037	0.065
Observed reflection	1145	5245	522
No. parameters	103	420	101
R_1 (obs)	0.0274	0.0525	0.0398
wR_2 (all data)	0.0613	0.1095	0.0778
S	1.10	1.42	0.85
Min./Max. Resd. [e Å^{-3}]	–0.24, 0.19	–1.07, 2.89	–0.26, 0.20
Device type	Oxford Xcalibur3 CCD	Oxford Xcalibur CCD	Oxford Xcalibur CCD
Solution	SIR-92	SIR-92	SIR-92
Refinement	SHELXL-97	SHELXL-97	SHELXL-97
Absorption correction	multi-scan	multi-scan	multi-scan
CCDC No.	---	---	697710

	31	**32**	**33**
Formula	$CH_4N_8O_4$	$CH_6N_8N_3O_5$	$CH_5N_9O_4$
Form. weight [g mol^{-1}]	192.12	210.14	207.14
Crystal system	monoclinic	monoclinic	monoclinic
Space Group	Pc (7)	$P2_1/m$ (11)	$P2_1/c$ (14)
Color / Habit	colorless rods	colorless plates	colorless blocks
Size [mm]	0.04 x 0.06 x 0.07	0.07 x 0.09 x 0.09	0.07 x 0.10 x 0.12
a [Å]	4.6283(3)	7.2806(8)	15.7942(8)
b [Å]	9.4580(6)	5.9376(7)	10.1115(4)
c [Å]	9.0071(5)	9.8324(5)	10.2757(5)
α [°]	90	90	90
β [°]	119.343(4)	110.609(7)	108.817(6)
γ [°]	90	90	90
V [Å^3]	343.70(4)	397.85(7)	1553.35(14)
Z	2	2	8
$\rho_{calc.}$ [g cm^{-3}]	1.856	1.754	1.771
μ [mm^{-1}]	0.175	0.168	0.165
$F(000)$	196	216	848
$\lambda_{MoK\alpha}$[Å]	0.71073	0.71073	0.71073
T [K]	200	200	200
Theta Min-Max [°]	4.3, 33.4	4.1, 28.0	4.0, 26.0
Dataset [h; k; l]	–4:7; –13:14; –13:9	–9:9; –7:7; –12:12	–19:19; –11:12; –12: 12
Reflection collected	2691	4540	9875
Independent reflection	1236	1051	3048
R_{int}	0.025	0.041	0.033
Observed reflection	848	703	1628
No. parameters	134	103	293
R_1 (obs)	0.0307	0.0372	0.0328
wR_2 (all data)	0.0638	0.0911	0.0702
S	0.86	0.92	0.84
Min./Max. Resd. [e Å^{-3}]	–0.26, 0.15	–0.29, 0.31	–0.23, 0.17
Device type	Oxford Xcalibur3 CCD	Oxford Xcalibur3 CCD	Oxford Xcalibur3 CCD
Solution	SIR-92	SIR-92	SIR-92
Refinement	SHELXL-97	SHELXL-97	SHELXL-97
Absorption correction	multi-scan	multi-scan	multi-scan
CCDC No.	680293	674701	680292

	34	**35**	**36**
Formula	$C_2H_6N_8O_4$	$C_2H_6N_8O_4$	$CH_3N_7O_4$
Form. weight [g mol^{-1}]	206.15	206.15	177.10
Crystal system	monoclinic	triclinic	monoclinic
Space Group	$P2_1/m$ (11)	$P\text{–}1$ (2)	$C2/c$ (15)
Color / Habit	colorless rods	colorless rods	colorless plates
Size [mm]	0.06 x 0.08 x 0.09	0.05 x 0.10 x 0.10	0.02 x 0.09 x 0.13
a [Å]	7.2601(7)	6.6567(8)	6.904(2)
b [Å]	5.9178(5)	7.265(1)	7.668(2)
c [Å]	9.8713(7)	9.818(1)	12.200(4)
α [°]	90	110.75(1)	90
β [°]	101.185(8)	97.59(1)	93.01(3)
γ [°]	90	105.95(1)	90
V [Å^3]	416.05(6)	412.77(11)	645.0(3)
Z	2	2	4
$\rho_{calc.}$ [g cm^{-3}]	1.646	1.659	1.824
μ [mm^{-1}]	0.151	0.152	0.174
$F(000)$	212	212	360
$\lambda_{MoK\alpha}$[Å]	0.71073	0.71073	0.71073
T [K]	200	150	200
Theta Min-Max [°]	3.9, 27.5	4.1, 25.5	4.0, 29.2
Dataset [h; k; l]	–7:9; –7:7; –12:12	–8:6; –8:8; –8:11	–6:9; –10:10; –16:16
Reflection collected	2315	2047	2058
Independent reflection	1024	1513	871
R_{int}	0.038	0.027	0.047
Observed reflection	508	778	341
No. parameters	101	151	85
R_1 (obs)	0.0371	0.0363	0.0322
wR_2 (all data)	0.1016	0.0865	0.0613
S	0.91	0.86	0.75
Min./Max. Resd. [e Å^{-3}]	–0.25, 0.18	–0.26, 0.19	–0.13, 0.16
Device type	Oxford Xcalibur3 CCD	Oxford Xcalibur3 CCD	Oxford Xcalibur3 CCD
Solution	SIR-92	SIR-92	SHELXS-97
Refinement	SHELXL-97	SHELXL-97	SHELXL-97
Absorption correction	multi-scan	multi-scan	multi-scan
CCDC No.	680291	693659	693661

	37	**38**	**38**·5-At
Formula	CH_9N_6, N_3O_4	$C_2H_4N_5O_4Cl$	$C_2H_7N_{10}O_4Cl$
Form. weight [g mol^{-1}]	211.17	197.54	270.63
Crystal system	orthorhombic	monoclinic	monoclinic
Space Group	*Pbca* (61)	$P2_1/n$ (14)	$P2_1/n$ (14)
Color / Habit	colorless rods	colorless rods	colorless rods
Size [mm]	0.07 x 0.08 x 0.09	0.19 x 0.12 x 0.09	0.25 x 0.15 x 0.12
a [Å]	12.5217(3)	5.3691(6)	5.2325(2)
b [Å]	8.1036(2)	7.8470(6)	8.4958(3)
c [Å]	16.9859(4)	15.277(1)	21.4225(7)
α [°]	90	90	90
β [°]	90	91.381(8)	96.683(3)
γ [°]	90	90	90
V [Å^3]	1723.57(7)	643.45(10)	945.85(6)
Z	8	4	4
$\rho_{calc.}$ [g cm^{-3}]	1.628	1.915	1.901
μ [mm^{-1}]	0.150	0.572	0.436
$F(000)$	880	572	552
$\lambda_{MoK\alpha}$[Å]	0.71073	0.71073	0.71073
T [K]	100	200	200
Theta Min-Max [°]	3.8, 27.5	3.7, 26.0	3.7, 26.5
Dataset [h; k; l]	–16:16; –10:10; –22:22	–6:6; –9:9; –18:12	–6:6; –10:10; –26:26
Reflection collected	18469	3184	7716
Independent reflection	1986	1266	1962
R_{int}	0.034	0.047	0.020
Observed reflection	1419	748	1796
No. parameters	163	116	182
R_1 (obs)	0.0306	0.0403	0.0251
wR_2 (all data)	0.0891	0.0977	0.0687
S	1.02	0.94	1.05
Min./Max. Resd. [e Å^{-3}]	–0.22, 0.25	–0.37, 0.40	–0.47, 0.31
Device type	Oxford Xcalibur3 CCD	Oxford Xcalibur CCD	Oxford Xcalibur CCD
Solution	SIR-92	SIR-92	SIR-92
Refinement	SHELXL-97	SHELXL-97	SHELXL-97
Absorption correction	multi-scan	multi-scan	multi-scan
CCDC No.	674702	689306	689307

	39	**40**	**41**
Formula	$CH_7N_4ClO_4$	$CH_9N_6ClO_4$	$CH_4N_5ClO_4$
Form. weight [g mol^{-1}]	174.56	204.59	185.54
Crystal system	monoclinic	monoclinic	orthorhombic
Space Group	$P2_1/c$ (14)	$P2_1/c$ (14)	$Pbca$ (61)
Color / Habit	colorless needles	colorless rods	colorless rods
Size [mm]	0.04 x 0.06 x 0.09	0.02 x 0.07 x 0.09	0.02 x 0.07 x 0.11
a [Å]	7.988(1)	10.2506(3)	8.5992(3)
b [Å]	8.498(1)	15.0671(4)	11.0586(4)
c [Å]	9.958(2)	10.3572(3)	14.1919(4)
α [°]	90	90	90
β [°]	103.50(1)	102.443(3)	90
γ [°]	90	90	90
V [Å^3]	657.3(2)	1562.06(8)	1349.58(8)
Z	4	8	8
$\rho_{calc.}$ [g cm^{-3}]	1.764	1.740	1.826
μ [mm^{-1}]	0.549	0.483	0.545
$F(000)$	360	848	752
$\lambda_{MoK\alpha}$[Å]	0.71073	0.71073	0.71073
T [K]	200	100	200
Theta Min-Max [°]	4.4, 26.0	3.7, 26.0	4.0, 26.0
Dataset [h; k; l]	–9:9; –10:10; –12:12	–12:12; –18:18; –12:12	–9:10; –9:13; –17:16
Reflection collected	6373	15530	6468
Independent reflection	1291	3068	1325
R_{int}	0.030	0.063	0.034
Observed reflection	1214	1930	974
No. parameters	119	289	116
R_1 (obs)	0.0343	0.0343	0.0297
wR_2 (all data)	0.0864	0.0844	0.0802
S	1.07	0.94	1.02
Min./Max. Resd. [e Å^{-3}]	–0.35, 0.32	–0.36, 0.29	–0.47, 0.19
Device type	Oxford Xcalibur3 CCD	Oxford Xcalibur3 CCD	Oxford Xcalibur3 CCD
Solution	SIR-92	SIR-92	SIR-92
Refinement	SHELXL-97	SHELXL-97	SHELXL-97
Absorption correction	multi-scan	multi-scan	multi-scan
CCDC No.	664916	664917	664918

	42	**43**	**44**
Formula	$CH_3ClN_4O_4$	$CH_2N_6O_2$	$C_2H_4N_6O_2$
Form. weight [g mol^{-1}]	170.52	130.09	144.11
Crystal system	monoclinic	monoclinic	orthorhombic
Space Group	$P2_1/n$ (14)	$P2_1/c$ (14)	$P2_12_12_1$ (19)
Color / Habit	colorless plates	colorless cuboids	colorless rods
Size [mm]	0.07 x 0.18 x 0.18	0.18 x 0.13 x 0.08	0.19 x 0.16 x 0.08
a [Å]	4.9338(4)	9.4010(3)	6.6140(1)
b [Å]	7.4893(5)	5.4918(1)	8.5672(2)
c [Å]	15.1744(10)	9.3150(3)	19.2473(4)
α [°]	90	90	90
β [°]	92.073(6)	105.762(3)	90
γ [°]	90	90	90
V [Å^3]	560.34(7)	462.84(2)	1090.62(4)
Z	4	4	8
$\rho_{calc.}$ [g cm^{-3}]	2.021	1.867	1.755
μ [mm^{-1}]	0.642	0.169	0.153
$F(000)$	344	264	592
$\lambda_{MoK\alpha}$[Å]	0.71073	0.71073	0.71073
T [K]	200	100	100
Theta Min-Max [°]	3.8, 27.0	4.3, 32.1	3.7, 32.1
Dataset [h; k; l]	–6:6; –9:9; –19:19	–13:13; –8:8; –13:13	–9:9; –12:12; –28:27
Reflection collected	5406	6375	15881
Independent reflection	1231	1537	2104
R_{int}	0.017	0.037	0.034
Observed reflection	1071	1050	1616
No. parameters	104	90	213
R_1 (obs)	0.0237	0.0343	0.0297
wR_2 (all data)	0.0714	0.0960	0.0696
S	1.12	1.00	0.99
Min./Max. Resd. [e Å^{-3}]	–0.45, 0.22	–0.23, 0.31	–0.32, 0.21
Device type	Oxford Xcalibur3 CCD	Oxford Xcalibur3 CCD	Oxford Xcalibur3 CCD
Solution	SIR-92	SIR-92	SIR-92
Refinement	SHELXL-97	SHELXL-97	SHELXL-97
Absorption correction	multi-scan	none	multi-scan
CCDC No.	693660	635164	635163

	45	**43**·H_2O	**44**·H_2O
Formula	$C_2H_4N_6O_2$	$CH_4N_6O_3$	$C_2H_6N_6O_3$
Form. weight [g mol^{-1}]	144.11	148.10	162.13
Crystal system	monoclinic	monoclinic	monoclinic
Space Group	$P2_1/c$ (14)	$P2_1/c$ (14)	$P2_1/n$ (14)
Color / Habit	colorless blocks	colorless rods	colorless rods
Size [mm]	0.24 x 0.18 x 0.15	0.11 x 0.16 x 0.18	0.08 x 0.13 x 0.17
a [Å]	9.5278(9)	8.4443(5)	9.8838(6)
b [Å]	7.7308(7)	8.7433(5)	5.4265(3)
c [Å]	8.4598(9)	7.4478(4)	12.3380(7)
α [°]	90	90	90
β [°]	112.875(9)	98.395(5)	97.888(6)
γ [°]	90	90	90
V [Å^3]	574.1(1)	543.99(5)	655.48(7)
Z	4	4	4
$\rho_{calc.}$ [g cm^{-3}]	1.667	1.808	1.643
μ [mm^{-1}]	0.145	0.168	0.148
$F(000)$	296	304	336
$\lambda_{MoK\alpha}$[Å]	0.71073	0.71073	0.71073
T [K]	200	100	200
Theta Min-Max [°]	4.6, 26.0	4.1, 26.3	4.1, 25.8
Dataset [h; k; l]	–11:11; –9:9; –10:10	–10:7; –8:10; –7:9	–12:11; –4:6; –15:14
Reflection collected	5625	2833	3141
Independent reflection	1128	1096	1249
R_{int}	0.034	0.025	0.039
Observed reflection	1087	672	691
No. parameters	107	107	124
R_1 (obs)	0.0440	0.0326	0.0356
wR_2 (all data)	0.0950	0.0746	0.0740
S	1.21	0.88	0.81
Min./Max. Resd. [e Å^{-3}]	–0.22, 0.17	–0.29, 0.17	–0.24, 0.19
Device type	Oxford Xcalibur3 CCD	Oxford Xcalibur3 CCD	Oxford Xcalibur3 CCD
Solution	SIR-92	SIR-92	SHELXS-97
Refinement	SHELXL-97	SHELXL-97	SHELXL-97
Absorption correction	multi-scan	multi-scan	multi-scan
CCDC No.	635160	652904	652905

	46	**47**	**48**
Formula	$C_3H_7N_5O$	$C_3H_7N_5O$	$C_3H_6ClN_5$
Form. weight [g mol^{-1}]	129.14	129.14	147.58
Crystal system	monoclinic	monoclinic	triclinic
Space Group	$P2_1/c$ (14)	$P2_1/c$ (14)	$P\bar{1}$ (2)
Color / Habit	colorless rods	colorless rods	colorless rods
Size [mm]	0.15 x 0.20 x 0.25	0.04 x 0.09 x 0.12	0.15 x 0.21 x 0.25
a [Å]	7.006(5)	4.624(2)	4.6620(6)
b [Å]	6.0570(7)	12.519(2)	5.3220(7)
c [Å]	13.864(2)	10.401(3)	13.42(2)
α [°]	90	90	96.15(1)
β [°]	103.17(2)	99.237(2)	90.75(1)
γ [°]	90	90	106.66(1)
V [Å^3]	572.86(14)	594.3(3)	316.81(7)
Z	4	4	2
$\rho_{calc.}$ [g cm^{-3}]	1.497	1.443	1.547
μ [mm^{-1}]	0.118	0.114	0.514
$F(000)$	272	272	152
$\lambda_{MoK\alpha}$[Å]	0.71069	0.71069	0.71073
T [K]	200	200	200
Theta Min-Max [°]	4.5, 26.0	3.8, 26.0	4.1, 26.0
Dataset [h; k; l]	–8:8; –7:7; –17:17	–5:5; –15:15; –12:12	–5:5; –6:6; –16:16
Reflection collected	5524	5900	3237
Independent reflection	1127	1167	1249
R_{int}	0.033	0.019	0.024
Observed reflection	1070	921	1191
No. parameters	110	110	106
R_1 (obs)	0.0582	0.0273	0.0305
wR_2 (all data)	0.1266	0.0780	0.0776
S	1.22	1.12	1.05
Min./Max. Resd. [e Å^{-3}]	–0.17, 0.29	–0.18, 0.13	–0.25, 0.23
Device type	Oxford Xcalibur3 CCD	Oxford Xcalibur3 CCD	Oxford Xcalibur3 CCD
Solution	SIR-92	SIR-97	SIR-92
Refinement	SHELXL-97	SHELXL-97	SHELXL-97
Absorption correction	multi-scan	multi-scan	multi-scan
CCDC No.	704303	---	704306

	49a	**49b**	**50**
Formula	$C_3H_6N_8$	$C_3H_6N_8$	$C_3H_6N_6O_3$
Form. weight [g mol^{-1}]	154.16	154.16	174.14
Crystal system	monoclinic	triclinic	triclinic
Space Group	$P2_1/c$ (14)	$P\bar{1}$ (2)	$P\bar{1}$ (2)
Color / Habit	colorless needles	colorless rods	colorless blocks
Size [mm]	0.10 x 0.10 x 0.12	0.10 x 0.10 x 0.16	0.30 x 0.22 x 0.12
a [Å]	6.0263(6)	4.8512(3)	7.129(1)
b [Å]	7.8546(6)	5.9583(4)	7.130(1)
c [Å]	14.559(1)	12.3508(9)	7.922(1)
α [°]	90	92.037(5)	66.21(2)
β [°]	98.303(7)	94.938(6)	89.24(1)
γ [°]	90	105.130(6)	66.86(2)
V [Å^3]	681.9(1)	342.72(4)	333.7(1)
Z	4	2	2
$\rho_{calc.}$ [g cm^{-3}]	1.502	1.494	1.733
μ [mm^{-1}]	0.114	0.114	0.152
$F(000)$	320	160	180
$\lambda_{MoK\alpha}$[Å]	0.71073	0.71073	0.71073
T [K]	200	200	200
Theta Min-Max [°]	4.3, 26.0	3.8, 26.0	4.6, 26.5
Dataset [h; k; l]	–7:7; –9:9; –17:17	–5:5; –7:7; –15:15	–8:8; –8:8; –9:9
Reflection collected	6660	3331	3516
Independent reflection	1343	1329	1367
R_{int}	0.030	0.022	0.023
Observed reflection	1343	909	1210
No. parameters	124	124	133
R_1 (obs)	0.0305	0.0349	0.0359
wR_2 (all data)	0.0776	0.1048	0.0921
S	1.14	1.02	1.05
Min./Max. Resd. [e Å^{-3}]	–0.19, 0.14	–0.18, 0.30	–0.28, 0.19
Device type	Oxford Xcalibur3 CCD	Oxford Xcalibur3 CCD	Oxford Xcalibur3 CCD
Solution	SIR-92	SIR-92	SIR-92
Refinement	SHELXL-97	SHELXL-97	SHELXL-97
Absorption correction	multi-scan	multi-scan	multi-scan
CCDC No.	704301	705303	704309

	51	**52**	**53**
Formula	$C_3H_5ClN_6O_2$	$C_3H_7N_7O_6$	$C_3H_5N_9O_2$
Form. weight [g mol^{-1}]	192.58	237.16	199.16
Crystal system	orthorhombic	triclinic	monoclinic
Space Group	$P2_12_12_1$ (19)	$P\bar{1}$ (2)	$P2_1/n$ (14)
Color / Habit	colorless rods	colorless plate	colorless rods
Size [mm]	0.10 x 0.13 x 0.20	0.03 x 0.10 x 0.10	0.05 x 0.11 x 0.12
a [Å]	5.207(5)	6.324(1)	6.2652(7)
b [Å]	7.197(5)	7.198(1)	7.9142(9)
c [Å]	19.804(5)	10.711(2)	16.026(2)
α [°]	90	82.99(2)	90
β [°]	90	82.73(2)	90.204(9)
γ [°]	90	66.52(2)	90
V [Å^3]	742.2(9)	442.22(15)	794.63(16)
Z	4	2	4
$\rho_{calc.}$ [g cm^{-3}]	1.724	1.781	1.665
μ [mm^{-1}]	0.484	0.168	0.140
$F(000)$	392	244	408
$\lambda_{MoK\alpha}$[Å]	0.71073	0.71073	0.71073
T [K]	200	200	200
Theta Min-Max [°]	4.1, 25.5	4.4, 26.0	4.2, 25.5
Dataset [h; k; l]	–6:6; –8:8 ; –23: 14	–7:7; –8:8; –13:13	–7:7; –6:9; –18:19
Reflection collected	3737	4503	3849
Independent reflection	1382	1723	1487
R_{int}	0.071	0.040	0.036
Observed reflection	949	1293	824
No. parameters	129	173	247
R_1 (obs)	0.0529	0.0658	0.0332
wR_2 (all data)	0.0692	0.1971	0.0755
S	0.93	1.14	0.88
Min./Max. Resd. [e Å^{-3}]	–0.20, 0.26	–0.61, 1.13	–0.20, 0.15
Device type	Oxford Xcalibur3 CCD	Oxford Xcalibur3 CCD	Oxford Xcalibur3 CCD
Solution	SIR-92	SIR-92	SIR-92
Refinement	SHELXL-97	SHELXL-97	SHELXL-97
Absorption correction	multi-scan	multi-scan	multi-scan
CCDC No.	704302	704310	704312

	54	**55**	**56**
Formula	$C_3H_4KN_9O_2$	$C_3H_4ClN_6NaO_2$	$C_3H_8ClN_7O_2$
Form. weight [g mol^{-1}]	237.25	214.56	209.61
Crystal system	triclinic	monoclinic	monoclinic
Space Group	$P\bar{1}$ (2)	$P2_1/c$ (14)	$P2_1/c$ (14)
Color / Habit	colorless plates	colorless rods	colorless blocks
Size [mm]	0.02 x 0.10 x 0.15	0.13 x 0.18 x 0.19	0.15 x 0.16 x 0.23
a [Å]	6.8683(4)	10.239(1)	10.1928(9)
b [Å]	10.8930(7)	9.4797(9)	9.9612(9)
c [Å]	18.178(1)	8.3739(9)	8.7198(8)
α [°]	96.491(5)	90	90
β [°]	97.054(5)	109.65(1)	106.092(8)
γ [°]	96.038(5)	90	90
V [Å^3]	1331.22(14)	765.4(2)	850.7(1)
Z	6	4	4
$\rho_{calc.}$ [g cm^{-3}]	1.776	1.862	1.637
μ [mm^{-1}]	0.599	0.530	0.530
$F(000)$	720	432	432
$\lambda_{MoK\alpha}$[Å]	0.71073	0.71073	0.71073
T [K]	200	200	200
Theta Min-Max [°]	3.8, 26.5	4.2, 26.0	4.2, 26.0
Dataset [h; k; l]	–8:8; –13:13; –22:22	–12:12; –11:11 ; –10:10	–12:12; –12:12; –10:10
Reflection collected	14218	7497	8074
Independent reflection	5503	1507	1576
R_{int}	0.036	0.026	0.032
Observed reflection	2921	1418	1463
No. parameters	406	134	150
R_1 (obs)	0.0418	0.0348	0.0444
wR_2 (all data)	0.1065	0.0892	0.0999
S	0.90	1.09	1.16
Min./Max. Resd. [e Å^{-3}]	–0.70, 0.94	–0.31, 0.28	–0.23, 0.22
Device type	Oxford Xcalibur3 CCD	Oxford Xcalibur3 CCD	Oxford Xcalibur3 CCD
Solution	SIR-92	SIR-92	SIR-92
Refinement	SHELXL-97	SHELXL-97	SHELXL-97
Absorption correction	multi-scan	multi-scan	multi-scan
CCDC No.	705304	704307	704308

	57	**58**	**59**
Formula	$C_3H_8N_6O_4$	$C_3H_7N_9O_3$	$C_3H_9ClN_8O_5$
Form. weight [g mol^{-1}]	192.15	217.18	272.63
Crystal system	monoclinic	monoclinic	monoclinic
Space Group	$P2_1/c$ (14)	$P2_1/c$ (14)	$P2_1/c$ (14)
Color / Habit	colorless rods	colorless rods	colorless rods
Size [mm]	0.01 x 0.09 x 0.10	0.03 x 0.13 x 0.29	0.05 x 0.09 x 0.12
a [Å]	10.599(1)	11.639(2)	7.748(2)
b [Å]	5.3468(5)	5.2940(11)	25.801(3)
c [Å]	14.945(1)	14.827(3)	5.900(2)
α [°]	90	90	90
β [°]	109.86(1)	108.33(3)	111.899(5)
γ [°]	90	90	90
V [Å^3]	796.56(14)	867.2(3)	1094.3(5)
Z	4	4	4
$\rho_{calc.}$ [g cm^{-3}]	1.602	1.663	1.655
μ [mm^{-1}]	0.144	0.144	0.379
$F(000)$	400	448	560
$\lambda_{MoK\alpha}$[Å]	0.71073	0.71073	0.71073
T [K]	150	200	200
Theta Min-Max [°]	4.1, 25.7	3.7, 26.0	3.7, 26.0
Dataset [h; k; l]	–11:12; –4:6; –18:17	–14:14; –6:6; –18:18	–9:8; –31:30; –7: 6
Reflection collected	3733	3151	5666,
Independent reflection	1519	1715	2149
R_{int}	0.100	0.014	0.032
Observed reflection	499	1426	1324
No. parameters	150	165	190
R_1 (obs)	0.0560	0.0612	0.0361
wR_2 (all data)	0.1486	0.2018	0.0920
S	0.81	1.12	0.92
Min./Max. Resd. [e Å^{-3}]	–0.24, 0.52	–0.52, 0.45	–0.39, 0.32
Device type	Oxford Xcalibur3 CCD	Oxford Xcalibur3 CCD	Oxford Xcalibur3 CCD
Solution	SHELXS-97	SIR-92	SIR-92
Refinement	SHELXL-97	SHELXL-97	SHELXL-97
Absorption correction	multi-scan	multi-scan	none
CCDC No.	704315	704314	704311

	60	**61**	**62**
Formula	$C_6H_{14}CuN_{12}O_8$	$C_6H_{16}Cl_2CuN_{12}O_8$	$C_6H_{12}CuN_{18}O_6$
Form. weight [g mol^{-1}]	445.84	518.75	495.83
Crystal system	monoclinic	monoclinic	monoclinic
Space Group	$P2_1/c$ (14)	$P2_1/c$ (14)	$P2_1/n$ (14)
Color / Habit	blue rods	light blue rods	blue rods
Size [mm]	0.08 x 0.12 x 0.14	0.10 x 0.13 x 0.17	0.01 x 0.10 x 0.10
a [Å]	7.5380(4)	6.0251(3)	12.5699(6)
b [Å]	8.4400(4)	21.7937(9)	6.5342(3)
c [Å]	12.7970(6)	7.0960(4)	22.792(1)
α [°]	90	90	90
β [°]	92.974(4)	98.856(4)	94.291(4)
γ [°]	90	90	90
V [Å^3]	813.06(7)	920.66(8)	1866.75(15)
Z	2	2	4
$\rho_{calc.}$ [g cm^{-3}]	1.821	1.871	1.764
μ [mm^{-1}]	1.415	1.545	1.244
$F(000)$	454	526	1004
$\lambda_{MoK\alpha}$[Å]	0.71073	0.71073	0.71073
T [K]	200	200	200
Theta Min-Max [°]	4.0, 26.0	4.2, 26.5	3.8, 26.0
Dataset [h; k; l]	–9:9; –10:10; –15:15	–7:7; –27:27; –8: 8	–15:14; –8:8; –20:28
Reflection collected	7897	9620	8800
Independent reflection	1584	1908	3624
R_{int}	0.020	0.022	0.084
Observed reflection	1563	1885	1687
No. parameters	152	165	328
R_1 (obs)	0.0275	0.0268	0.0585
wR_2 (all data)	0.0754	0.0627	0.1653
S	1.09	1.07	0.94
Min./Max. Resd. [e Å^{-3}]	–0.39, 0.33	–0.35, 0.45	0.54, 0.99
Device type	Oxford Xcalibur3 CCD	Oxford Xcalibur3 CCD	Oxford Xcalibur3 CCD
Solution	SIR-92	SIR-92	SIR-92
Refinement	SHELXL-97	SHELXL-97	SHELXL-97
Absorption correction	multi-scan	multi-scan	multi-scan
CCDC No.	704304	704305	704313

	66	**67**	**68**·H_2O
Formula	$C_3H_7N_7O_2$	$C_3H_6N_6O_2$	$C_3H_8N_8O_5$
Form. weight [g mol^{-1}]	173.16	158.14	236.17
Crystal system	monoclinic	monoclinic	monoclinic
Space Group	$P2_1/c$ (14)	$P2_1$ (4)	$P2_1/c$ (14)
Color / Habit	colorless rods	colorless plates	colorless rods
Size [mm]	0.04 x 0.12 x 0.14	0.06 x 0.10 x 0.15	0.16 x 0.18 x 0.25
a [Å]	8.6244(4)	6.0193(3)	6.3626(3)
b [Å]	6.8715(4)	6.4786(3)	22.1364(8)
c [Å]	12.0481(6)	8.4598(4)	6.9804(3)
α [°]	90	90	90
β [°]	98.263(4)	98.952(5)	113.982(6)
γ [°]	90	90	90
V [Å^3]	706.59(6)	325.89(3)	898.28(8)
Z	4	2	4
$\rho_{calc.}$ [g cm^{-3}]	1.628	1.612	1.746
μ [mm^{-1}]	0.136	0.136	0.160
$F(000)$	360	164	488
$\lambda_{MoK\alpha}$[Å]	0.71073	0.71073	0.71073
T [K]	200	200	200
Theta Min-Max [°]	3.9, 26.0	3.9, 32.4	4.0, 26.2
Dataset [h; k; l]	–10:10; –8:7; –11:14	–8:9; –9:9; –12:12	–7:7; –26:27; –8:3
Reflection collected	3508	4877	4690
Independent reflection	1379	1206	1792
R_{int}	0.049	0.021	0.018
Observed reflection	743	1042	1343
No. parameters	137	124	177
R_1 (obs)	0.0323	0.0251	0.0371
wR_2 (all data)	0.0742	0.0656	0.1057
S	0.82	1.08	1.09
Min./Max. Resd. [e Å^{-3}]	–0.16, 0.18	–0.19, 0.24	–0.43, 0.41
Device type	Oxford Xcalibur3 CCD	Oxford Xcalibur3 CCD	Oxford Xcalibur3 CCD
Solution	SIR-92	SIR-92	SIR-92
Refinement	SHELXL-97	SHELXL-97	SHELXL-97
Absorption correction	multi-scan	multi-scan	multi-scan
CCDC No.	652906	703983	703979

	68·EtOH	**69**	**70**
Formula	$C_5H_{12}N_8O_5$	$C_5H_{10}N_{10}O_6$	$C_4H_8N_8O_4$
Form. weight [g mol^{-1}]	264.20	306.23	232.18
Crystal system	monoclinic	monoclinic	monoclinic
Space Group	$P2_1/c$ (14)	$P2_1$ (4)	$P2_1/c$ (14)
Color / Habit	colorless rods	colorless needles	colorless rods
Size [mm]	0.09 x 0.13 x 0.14	0.05 x 0.06 x 0.14	0.06 x 0.15 x 0.20
a [Å]	5.6304(4)	9.175(1)	11.1953(6)
b [Å]	24.810(2)	6.177(1)	9.3248(4)
c [Å]	8.5116(6)	11.171(2)	9.9411(4)
α [°]	90	90	90
β [°]	109.103(6)	90.38(1)	111.217(5)
γ [°]	90	90	90
V [Å^3]	1123.52(14)	633.09(17)	967.45(8)
Z	4	2	4
$\rho_{calc.}$ [g cm^{-3}]	1.562	1.606	1.594
μ [mm^{-1}]	0.137	0.144	0.140
$F(000)$	552	316	480
$\lambda_{MoK\alpha}$[Å]	0.71073	0.71073	0.71073
T [K]	200	200	200
Theta Min-Max [°]	3.8, 25.3	3.8, 30.1	3.9, 26.0
Dataset [h; k; l]	–6:6; –29:29; –10:10	–12:12; –8:8; –15:15	–8:13; –7:11; –12:12
Reflection collected	10537	8408	4064
Independent reflection	2032	2007	1890
R_{int}	0.036	0.050	0.026
Observed reflection	1398	1034	1125
No. parameters	193	208	177
R_1 (obs)	0.0487	0.0318	0.0342
wR_2 (all data)	0.1557	0.0698	0.0757
S	1.07	0.91	0.89
Min./Max. Resd. [e Å^{-3}]	–0.39, 0.91	–0.17, 0.18	–0.24, 0.20
Device type	Oxford Xcalibur3 CCD	Oxford Xcalibur3 CCD	Oxford Xcalibur3 CCD
Solution	SIR-92	SIR-92	SIR-92
Refinement	SHELXL-97	SHELXL-97	SHELXL-97
Absorption correction	multi-scan	multi-scan	multi-scan
CCDC No.	703978	703984	652908

	71	**72**	**73**
Formula	$C_4H_8N_8O_4$	$C_4H_9N_7O_2$	$C_4H_8N_8O_4$
Form. weight [g mol^{-1}]	232.18	187.18	232.18
Crystal system	orthorhombic	monoclinic	monoclinic
Space Group	*Pbca* (61)	$P2_1/c$ (14)	$P2_1/c$ (14)
Color / Habit	colorless blocks	colorless rods	colorless rods
Size [mm]	0.05 x 0.05 x 0.07	0.09 x 0.13 x 0.16	0.08 x 0.11 x 0.12
a [Å]	9.413(2)	5.8461(3)	9.2526(5)
b [Å]	9.225(2)	18.4860(7)	11.3617(6)
c [Å]	21.355(4)	8.0667(4)	9.5915(6)
α [°]	90	90	90
β [°]	90	110.769(5)	106.156(6)
γ [°]	90	90	90
V [Å^3]	1854.5(6)	815.13(7)	968.49(10)
Z	8	4	4
$\rho_{calc.}$ [g cm^{-3}]	1.663	1.525	1.592
μ [mm^{-1}]	0.146	0.125	0.140
$F(000)$	960	392	480
$\lambda_{MoK\alpha}$[Å]	0.71073	0.71073	0.71073
T [K]	200	200	200
Theta Min-Max [°]	3.6, 26.0	3.9, 26.0	4.0, 26.0
Dataset [h; k; l]	–11:8; –10:11; –26:18	–7:6; –21:22; –8:9	–10:11; –14:10; –11:10
Reflection collected	8975	4004	4883
Independent reflection	1814	1580	1890
R_{int}	0.147	0.041	0.027
Observed reflection	643	1085	1146
No. parameters	177	154	177
R_1 (obs)	0.0415	0.043	0.0349
wR_2 (all data)	0.0917	0.0884	0.0904
S	0.78	1.01	0.94
Min./Max. Resd. [e Å^{-3}]	–0.29, 0.24	–0.20, 0.21	–0.24, 0.20
Device type	Oxford Xcalibur3 CCD	Oxford Xcalibur3 CCD	Oxford Xcalibur3 CCD
Solution	SHELXS-97	SIR-92	SIR-92
Refinement	SHELXL-97	SHELXL-97	SHELXL-97
Absorption correction	multi-scan	multi-scan	multi-scan
CCDC No.	652907	703982	703980

	74	**75**	**76**
Formula	$C_3H_6N_6O_2$	$C_2H_7N_7O_2$	$C_2H_7N_7O_2$
Form. weight [g mol^{-1}]	158.12	161.15	161.15
Crystal system	orthorhombic	monoclinic	monoclinic
Space Group	*Pbca* (61)	$P2_1/c$ (14)	$P2_1$ (4)
Color / Habit	colorless blocks	colorless rods	Colorless needles
Size [mm]	0.03 x 0.14 x 0.15	0.17 x 0.13 x 0.07	0.16 x 0.11 0.04
a [Å]	14.2278(5)	3.7006(2)	3.6539(2)
b [Å]	6.1607(2)	20.7906(9)	7.8882(5)
c [Å]	31.200(1)	8.5969(5)	11.2495(7)
α [°]	90	90	90
β [°]	90	99.120(5)	91.818(6)
γ [°]	90	90	90
V [Å^3]	2734.81(16)	653.06(6)	324.08(3)
Z	16	4	2
$\rho_{calc.}$ [g cm^{-3}]	1.536	1.639	1.651
μ [mm^{-1}]	0.129	0.141	0.142
$F(000)$	1312	336	168
$\lambda_{MoK\alpha}$[Å]	0.71073	0.71073	0.71073
T [K]	100	200	100
Theta Min-Max [°]	3.8, 26.0	3.8, 26.0	4.4, 32.3
Dataset [h; k; l]	–17:17; –7:7; –38:38	–4:4; –25:25; –10:10	–5:5; –11:11; –16:16
Reflection collected	25785	5207	4708
Independent reflection	2676	1284	1148
R_{int}	0.080	0.042	0.036
Observed reflection	1386	746	792
No. parameters	247	128	128
R_1 (obs)	0.0369	0.0343	0.0318
wR_2 (all data)	0.0893	0.0782	0.0638
S	0.98	0.91	0.94
Min./Max. Resd. [e Å^{-3}]	–0.25, 0.17	–0.24, 0.16	–0.20, 0.21
Device type	Oxford Xcalibur3 CCD	Oxford Xcalibur3 CCD	Oxford Xcalibur3 CCD
Solution	SHELXS-97	SIR-92	SIR-92
Refinement	SHELXL-97	SHELXL-97	SHELXL-97
Absorption correction	multi-scan	multi-scan	multi-scan
CCDC No.	703981	635161	635162

	77	**78**	**79**
Formula	$C_2H_5LiN_6O_3$	$C_2H_3N_6NaO_2$	$C_2H_3KN_6O_2$
Form. weight [g mol^{-1}]	168.06	166.09	182.19
Crystal system	monoclinic	monoclinic	monoclinic
Space Group	$P2_1$ (4)	$P2_1/n$ (14)	$P2_1/c$ (14)
Color / Habit	colorless rods	colorless needles	colorless needles
Size [mm]	0.05 x 0.12 x 0.16	0.04 x 0.13 x 0.15	0.08 x 0.08 x 0.21
a [Å]	3.5152(3)	3.6071(2)	3.6310(1)
b [Å]	12.3308(9)	8.3254(5)	8.6487(2)
c [Å]	7.3381(5)	18.955(1)	19.8598(5)
α [°]	90	90	90
β [°]	92.068(7)	91.365(6)	94.945(2)
γ [°]	90	90	90
V [Å^3]	317.86(4)	569.07(6)	621.34(3)
Z	2	4	4
$\rho_{calc.}$ [g cm^{-3}]	1.756	1.939	1.948
μ [mm^{-1}]	0.153	0.227	0.810
$F(000)$	172	336	368
$\lambda_{MoK\alpha}$[Å]	0.71073	0.71073	0.71073
T [K]	200	200	100
Theta Min-Max [°]	4.3, 30.0	4.1, 26.0	3.9, 26.5
Dataset [h; k; l]	–3:4; –17:17; –10:6	–4:2; –10:9; –23:21	–4:3; –10:10; –23:24
Reflection collected	2174	2894	3667
Independent reflection	947	1125	1287
R_{int}	0.041	0.049	0.023
Observed reflection	649	558	1130
No. parameters	114	112	112
R_1 (obs)	0.0402	0.0317	0.0213
wR_2 (all data)	0.0942	0.0614	0.0568
S	0.89	0.81	1.05
Min./Max. Resd. [e Å^{-3}]	–0.27, 0.37	–0.31, 0.24	–0.32, 0.25
Device type	Oxford Xcalibur3 CCD	Oxford Xcalibur3 CCD	Oxford Xcalibur3 CCD
Solution	SIR-92	SIR-92	SIR-92
Refinement	SHELXL-97	SHELXL-97	SHELXL-97
Absorption correction	multi-scan	multi-scan	multi-scan
CCDC No.	643232	643231	643233

	80	**81**	**82**
Formula	$C_4H_6N_{12}O_4Rb_2$	$C_2H_3CsN_6O_2$	$C_4H_8N_{12}O_5Sr$
Form. weight [g mol^{-1}]	457.15	276.01	391.84
Crystal system	monoclinic	monoclinic	monoclinic
Space Group	$P2_1/n$ (14)	$P2_1/n$ (14)	$C2/c$ (15)
Color / Habit	colorless rods	colorless rods	colorless needles
Size [mm]	0.07 x 0.08 x 0.16	0.02 x 0.05 x 0.05	0.07 x 0.08 x 0.19
a [Å]	8.7948(2)	6.3539(1)	20.5634(7)
b [Å]	10.1640(2)	13.4762(3)	6.9792(2)
c [Å]	15.0571(3)	8.2876(2)	8.3283(3)
α [°]	90	90	90
β [°]	92.470(2)	99.245(2)	95.949(3)
γ [°]	90	90	90
V [Å^3]	1344.71(5)	700.42(3)	1188.81(7)
Z	4	4	4
$\rho_{calc.}$ [g cm^{-3}]	2.258	2.618	2.189
μ [mm^{-1}]	7.322	5.247	4.592
$F(000)$	880	512	776
$\lambda_{MoK\alpha}$[Å]	0.71073	0.71073	0.71073
T [K]	100	100	100
Theta Min-Max [°]	4.0, 26.0	3.8, 26.0	3.9, 26.0
Dataset [h; k; l]	–10:10; –12:12; –18:18	–7:7; –16:11; –10:10	–20:25; –8:8; –8:10
Reflection collected	14582	3552	2951
Independent reflection	2642	1373	1175
R_{int}	0.042	0.026	0.027
Observed reflection	2012	1105	1045
No. parameters	201	112	117
R_1 (obs)	0.0243	0.0229	0.0222
wR_2 (all data)	0.0599	0.0517	0.0468
S	1.01	0.93	1.01
Min./Max. Resd. [e Å^{-3}]	–0.50, 0.77	–0.75, 1.19	–0.35, 0.68
Device type	Oxford Xcalibur3 CCD	Oxford Xcalibur3 CCD	Oxford Xcalibur3 CCD
Solution	SIR-92	SIR-92	SIR-92
Refinement	SHELXL-97	SHELXL-97	SHELXL-97
Absorption correction	multi-scan	multi-scan	multi-scan
CCDC No.	643234	643235	686401

	83	**84**	**85**
Formula	$C_4H_{14}N_{12}O_8Sr$	$C_2H_3AgN_6O_2$	$C_3H_9N_9O_2$
Form. weight [g mol^{-1}]	445.89	250.97	203.19
Crystal system	monoclinic	monoclinic	monoclinic
Space Group	$C2/c$ (15)	$P2_1/c$ (14)	$C2/c$ (15)
Color / Habit	colorless rods	colorless blocks	colorless needles
Size [mm]	0.05 x 0.08 x 0.15	0.03 x 0.08 x 0.09	0.05 x 0.17 x 0.22
a [Å]	11.7428(5)	10.7740(3)	21.2356(8)
b [Å]	8.9262(3)	8.4315(2)	6.8969(2)
c [Å]	16.2326(3)	6.4111(2)	12.1761(4)
α [°]	90	90	90
β [°]	108.401(4)	103.816(3)	102.457(2)
γ [°]	90	90	90
V [Å^3]	1614.48(10)	565.54(3)	574.1(1)
Z	4	4	8
$\rho_{calc.}$ [g cm^{-3}]	1.834	2.948	1.550
μ [mm^{-1}]	3.407	3.513	0.129
$F(000)$	896	480	848
$\lambda_{MoK\alpha}$[Å]	0.71073	0.71073	0.71073
T [K]	200	100	200
Theta Min-Max [°]	3.8, 26.0	3.9, 26.2	3.5, 25.3
Dataset [h; k; l]	–14:7; –11:10; –19:20	–13:13; –10:10; –7:7	–25:25; –7:8; –14:14
Reflection collected	3896	5491	5055
Independent reflection	1569	1130	1574
R_{int}	0.032	0.025	0.034
Observed reflection	1370	970	1330
No. parameters	142	112	164
R_1 (obs)	0.0293	0.0190	0.0487
wR_2 (all data)	0.0798	0.0494	0.1359
S	1.05	1.08	1.15
Min./Max. Resd. [e Å^{-3}]	–0.33, 0.77	–0.58, 1.48	–0.26, 0.26
Device type	Oxford Xcalibur3 CCD	Oxford Xcalibur3 CCD	Kappa CCD
Solution	SIR-92	SIR-92	SIR-92
Refinement	SHELXL-97	SHELXL-97	SHELXL-97
Absorption correction	multi-scan	multi-scan	none
CCDC No.	686403	670917	670921

	87	**88**	**89**
Formula	$C_3H_{13}N_{11}O_3$	$C_3H_{12}N_{12}O_2$	$C_3H_7N_{11}O_2$
Form. weight [g mol^{-1}]	251.24	248.25	229.20
Crystal system	triclinic	triclinic	monoclinic
Space Group	P–1 (2)	P–1 (2)	$P2_1/c$ (14)
Color / Habit	colorless needles	colorless needles	colorless needles
Size [mm]	0.04 x 0.13 x 0.19	0.09 x 0.13 x 0.14	0.09 x 0.12 x 0.14
a [Å]	7.081(2)	6.8650(2)	7.9410(2)
b [Å]	7.361(2)	7.9800(2)	6.7131(1)
c [Å]	10.515(3)	10.5180(3)	17.7867(3)
α [°]	80.68(2)	101.311(2)	90
β [°]	88.59(2)	103.776(2)	95.269(2)
γ [°]	74.05(2)	103.123(2)	90
V [Å^3]	519.9(3)	525.60(3)	944.18(3)
Z	2	2	4
$\rho_{calc.}$ [g cm^{-3}]	1.605	1.569	1.612
μ [mm^{-1}]	0.137	0.130	0.135
$F(000)$	264	260	472
$\lambda_{MoK\alpha}$[Å]	0.71073	0.71073	0.71073
T [K]	100	200	100
Theta Min-Max [°]	3.8, 26.3	3.2, 26.0	3.8, 26.0
Dataset [h; k; l]	–8:8; –9:9; –13:13	–8:8; –9:9; –12:12	–9:9; –8:8; –21:21
Reflection collected	5496	3943	9050
Independent reflection	2086	2056	1855
R_{int}	0.021	0.011	0.026
Observed reflection	1669	1886	1580
No. parameters	206	202	173
R_1 (obs)	0.0315	0.0354	0.0298
wR_2 (all data)	0.0889	0.1131	0.0735
S	1.11	1.19	1.08
Min./Max. Resd. [e Å^{-3}]	–0.26, 0.20	–0.43, 0.30	–0.24, 0.19
Device type	Oxford Xcalibur3 CCD	Kappa CCD	Oxford Xcalibur3 CCD
Solution	SIR-92	SIR-92	SIR-92
Refinement	SHELXL-97	SHELXL-97	SHELXL-97
Absorption correction	multi-scan	none	multi-scan
CCDC No.	670918	670920	670919

	90·5H_2O	**93**	**94**
Formula	$C_2H_{20}Ca_2N_{12}O_{14}$	$C_2H_{12}CaN_{12}O_9$	$C_2H_{10}N_{12}O_8Sr$
Form. weight [g mol^{-1}]	516.46	388.32	417.84
Crystal system	triclinic	monoclinic	orthorhombic
Space Group	*P*–1 (2)	$P2_1/n$ (14)	*Pbcn* (60)
Color / Habit	colorless needles	colorless rods	colorless rods
Size [mm]	0.04 x 0.05 x 0.18	0.03 x 0.08 x 0.16	0.03 x 0.04 x 0.07
a [Å]	6.5227(2)	6.4500(3)	20.8342(6)
b [Å]	7.4533(1)	21.712(1)	9.6153(3)
c [Å]	10.380(2)	9.9493(4)	6.2901(2)
α [°]	74.371(2)	90	90
β [°]	72.29(2)	91.822(4)	90
γ [°]	74.660(2)	90	90
V [Å^3]	453.68(16)	1392.64(11)	1260.08(7)
Z	1	4	4
$\rho_{calc.}$ [g cm^{-3}]	1.890	1.852	2.203
μ [mm^{-1}]	0.729	0.531	4.357
F(000)	268	800	832
$\lambda_{MoK\alpha}$[Å]	0.71073	0.71073	0.71073
T [K]	200	200	200
Theta Min-Max [°]	3.8, 26.0	3.7, 26.0	4.0, 26.5
Dataset [h; k; l]	–5:8; –7:9; –9:12	–7:7; –26:26; –12:12	–23:26; –10:12; –7:7
Reflection collected	2373	13801	6055
Independent reflection	1765	2731	1300
R_{int}	0.019	0.058	0.049
Observed reflection	1254	1759	877
No. parameters	176	265	125
R_1 (obs)	0.0305	0.0297	0.0312
wR_2 (all data)	0.0665	0.0665	0.0844
S	0.91	0.99	1.00
Min./Max. Resd. [e Å^{-3}]	–0.35, 0.45	–0.30, 0.31	–0.35, 1.36
Device type	Oxford Xcalibur3 CCD	Oxford Xcalibur3 CCD	Oxford Xcalibur3 CCD
Solution	SIR-92	SIR-92	SHELXS-97
Refinement	SHELXL-97	SHELXL-97	SHELXL-97
Absorption correction	multi-scan	multi-scan	multi-scan
CCDC No.	708342	---	686402

	95	**96**	**98**
Formula	$CH_4N_6O_4Sr$	$CH_4BaN_6O_4$	$C_2H_{14}N_{12}O_{10}Zn$
Form. weight [g mol^{-1}]	251.72	301.43	431.59
Crystal system	orthorhombic	triclinic	monoclinic
Space Group	*Fdd*2 (43)	*P*–1 (2)	$P2_1/c$ (14)
Color / Habit	colorless blocks	colorless needles	colorless rods
Size [mm]	0.09 x 0.15 x 0.18	0.05 x 0.06 x 0.12	0.10 x 0.12 x 0.15
a [Å]	16.3396(4)	6.787(1)	6.6818(3)
b [Å]	25.9703(6)	7.1494(9)	22.195(1)
c [Å]	6.5045(2)	8.201(1)	11.1950(5)
α [°]	90	102.89(1)	90
β [°]	90	97.15(1)	119.098(3)
γ [°]	90	114.00(1)	90
V [Å^3]	2760.2(1)	343.87(11)	1450.70(12)
Z	16	2	4
$\rho_{calc.}$ [g cm^{-3}]	2.423	2.911	1.967
μ [mm^{-1}]	7.803	5.765	1.779
$F(000)$	1952	280	872
$\lambda_{MoK\alpha}$[Å]	0.71073	0.71073	0.71073
T [K]	200	200	120
Theta Min-Max [°]	4.0, 26.5	3.8, 26.0	4.1, 27.0
Dataset [h; k; l]	−20:20; −32:32; −8:8	−8:8; −8:8; −10:10	−8:8; −28:28; −14: 14
Reflection collected	6971	3507	15807
Independent reflection	1415	1347	3155
R_{int}	0.035	0.035	0.032
Observed reflection	1314	1266	2864
No. parameters	125	125	274
R_1 (obs)	0.0171	0.0161	0.0353
wR_2 (all data)	0.0376	0.0379	0.0845
S	1.06	1.06	1.12
Min./Max. Resd. [e Å^{-3}]	−0.39, 0.31	−0.69, 0.90	−0.29, 1.02
Device type	Oxford Xcalibur3 CCD	Oxford Xcalibur3 CCD	Oxford Xcalibur3 CCD
Solution	SIR-92	SIR-92	SIR-92
Refinement	SHELXL-97	SHELXL-97	SHELXL-97
Absorption correction	multi-scan	multi-scan	multi-scan
CCDC No.	686400	---	---

	99	**101**	**102**
Formula	$C_4H_{18}N_{12}O_{10}Zn$,	$CH_{12}N_{10}O_3$,	$C_3H_9N_{11}O_3$
Form. weight [g mol^{-1}]	459.67	212.21	247.21
Crystal system	orthorhombic	Orthorhombic	monoclinic
Space Group	*Pbca* (61)	$P2_12_12_1$ (19)	$P2_1/c$ (14)
Color / Habit	colorless plates	colorless plates	colorless rods
Size [mm]	0.04 x 0.09 x 0.09	0.12 x 0.12 x 0.18	0.06 x 0.14 x 0.17
a [Å]	12.0051(4)	3.633(5)	7.1470(6)
b [Å]	10.2285(3)	12.888(5)	7.3979(6)
c [Å]	13.0886(4)	18.415(5)	19.8509(2)
α [°]	90	90	90
β [°]	90	90	100.291(7)
γ [°]	90	90	90
V [Å^3]	1607.20(9)	862.2(13)	1032.69(15)
Z	4	4	4
$\rho_{calc.}$ [g cm^{-3}]	1.900	1.635	1.590
μ [mm^{-1}]	1.612	0.145	0.137
$F(000)$	944	448	512
$\lambda_{MoK\alpha}$[Å]	0.71073	0.71073	0.71073
T [K]	200	200	200
Theta Min-Max [°]	3.9, 26.0	4.4, 27.6	4.3, 25.5
Dataset [h; k; l]	–14:12; –10:12; –15:16	–3:4; –16:16; –22:23	–8:8; –8:8; –24:23
Reflection collected	7453	4610	9653
Independent reflection	1577	1209	1912
R_{int}	0.055	0.056	0.029
Observed reflection	972	1056	1777
No. parameters	149	127	190
R_1 (obs)	0.0331	0.0467	0.0432
wR_2 (all data)	0.1043	0.0892	0.1180
S	1.09	1.04	1.14
Min./Max. Resd. [e Å^{-3}]	–0.42, 0.51	–0.19, 0.17	–0.22, 0.23
Device type	Oxford Xcalibur3 CCD	Oxford Xcalibur3 CCD	Oxford Xcalibur3 CCD
Solution	SHELXS-97	SHELXS-97	SIR-92
Refinement	SHELXL-97	SHELXL-97	SHELXL-97
Absorption correction	multi-scan	multi-scan	multi-scan
CCDC No.	---	---	705789

	103	**104**	**105**
Formula	$C_3H_7N_{11}O_2$	$C_2H_{10}CuN_{12}O_8$	$C_2H_{18}Cu_2N_{18}O_4$
Form. weight [g mol^{-1}]	229.20	393.76	485.42
Crystal system	monoclinic	triclinic	monoclinic
Space Group	$P2_1/c$ (14)	$P\bar{1}$ (2)	$P2_1/n$ (14)
Color / Habit	colorless rods	blue blocks	dark-blue rods
Size [mm]	0.05 x 0.10 x 0.10	0.08 x 0.12 x 0.15	0.03 x 0.11 x 0.12
a [Å]	14.7640(6)	6.5850(8)	7.1064(3)
b [Å]	9.1430(6)	7.549(1)	16.5738(5)
c [Å]	6.810(1)	7.793(1)	7.4191(3)
α [°]	90	104.23(1)	90
β [°]	92.161(7)	104.70(1)	113.382(5)
γ [°]	90	113.240(1)	90
V [Å^3]	918.61(18)	317.17(9)	802.06(6)
Z	4	1	2
$\rho_{calc.}$ [g cm^{-3}]	1.657	2.062	2.010
μ [mm^{-1}]	0.139	1.799	2.712
$F(000)$	472	199	492
$\lambda_{MoK\alpha}$[Å]	0.71073	0.71073	0.71073
T [K]	200	200	100
Theta Min-Max [°]	3.7, 26.0	4.4, 26.5	3.9, 26.0
Dataset [h; k; l]	–18:18; –11:11; –8:5	–8:8; –9:9; –9:9	–8:7; –19:20; –9:8
Reflection collected	4640	3371	4117
Independent reflection	1804	1313	1571
R_{int}	0.041	0.025	0.034
Observed reflection	1003	1270	1159
No. parameters	173	122	154
R_1 (obs)	0.0321	0.0276	0.0303
wR_2 (all data)	0.0716	0.0624	0.0681
S	0.85	1.09	0.94
Min./Max. Resd. [e Å^{-3}]	–0.19, 0.15	–0.37, 0.34	–0.47, 0.74
Device type	Oxford Xcalibur3 CCD	Oxford Xcalibur CCD	Oxford Xcalibur CCD
Solution	SIR-92	SIR-92	SHELXS-97
Refinement	SHELXL-97	SHELXL-97	SHELXL-97
Absorption correction	multi-scan	multi-scan	multi-scan
CCDC No.	705790	695924	695927

	106	**107**	**108**
Formula	$C_2H_{12}CuN_{14}O_6$	$CuC_4H_{14}N_{12}O_8$	$CuC_4H_{10}N_{12}O_6$
Form. weight [g mol^{-1}]	391.80	421.81	385.78
Crystal system	monoclinic	monoclinic	monoclinic
Space Group	$P2_1/c$ (14)	$P2_1/c$ (14)	$P2_1/n$ (14)
Color / Habit	blue needles	blue rods	green plates
Size [mm]	0.04 x 0.10 x 0.16	0.08 x 0.17 x 0.18	0.08 x 0.12 x 0.16
a [Å]	7.5964(2)	5.9934(4)	5.7451(6)
b [Å]	12.7389(2)	14.3068(8)	9.482(1)
c [Å]	6.6865(1)	8.9967(6)	11.574(1)
α [°]	90	90	90
β [°]	90.309(2)	103.753(6)	92.935(9)
γ [°]	90	90	90
V [Å^3]	647.04(2)	749.32(8)	629.7(1)
Z	2	2	2
$\rho_{calc.}$ [g cm^{-3}]	2.011	1.870	2.035
μ [mm^{-1}]	1.756	1.529	1.799
$F(000)$	398	430	390
$\lambda_{MoK\alpha}$[Å]	0.71073	0.71073	0.71073
T [K]	200	120	200
Theta Min-Max [°]	4.2, 27.5	4.5, 26.5	4.1, 26.5
Dataset [h; k; l]	–5:9; –16:16; –8:7	–7:7; –17:17; –11:11	–7:7; –11:11; –14:14
Reflection collected	3698	7776	6422
Independent reflection	1482	1551	1295
R_{int}	0.019	0.025	0.038
Observed reflection	1277	1473	1170
No. parameters	130	143	126
R_1 (obs)	0.0234	0.0254	0.0352
wR_2 (all data)	0.0674	0.0616	0.0782
S	1.10	1.12	1.16
Min./Max. Resd. [e Å^{-3}]	–0.50, 0.35	–0.24, 0.34	–0.31, 0.39
Device type	Oxford Xcalibur CCD	Oxford Xcalibur3 CCD	Oxford Xcalibur3 CCD
Solution	SIR-92	SIR-92	SIR-92
Refinement	SHELXL-97	SHELXL-97	SHELXL-97
Absorption correction	multi-scan	multi-scan	multi-scan
CCDC No.	695928	641972	641973

	109	**110**	**111**
Formula	$CuC_4H_6N_{12}O$	$C_6H_{18}CuN_{12}O_8$	$C_4H_{12}CuN_{14}O_4$
Form. weight [g mol^{-1}]	349.75	449.87	383.82
Crystal system	monoclinic	monoclinic	monoclinic
Space Group	$P2_1/c$ (14)	$P2_1/n$ (14)	$P2_1/c$ (14)
Color / Habit	green rods	light-blue needles	blue rods
Size [mm]	0.03 x 0.04 x 0.10	0.03 x 0.05 x 0.12	0.04 x 0.08 x 0.11
a [Å]	9.1982(5)	6.9382(3)	11.4080(3)
b [Å]	6.7004(3)	12.1607(7)	8.5520(3)
c [Å]	9.3453(4)	10.1950(5)	7.2660(4)
α [°]	90	90	90
β [°]	102.653(5)	93.188(5)	103.643(3)
γ [°]	90	90	90
V [Å^3]	561.98(5)	858.86(7)	688.88(5)
Z	2	2	2
$\rho_{calc.}$ [g cm^{-3}]	2.067	1.740	1.850
μ [mm^{-1}]	1.991	1.340	1.637
$F(000)$	350	462	390
$\lambda_{MoK\alpha}$[Å]	0.71073	0.71073	0.71073
T [K]	100	100	200
Theta Min-Max [°]	3.8, 26.0	3.7, 26.0	3.7, 26.0
Dataset [h; k; l]	–11:11 ; –8:8; –11:11	–8:8; –13:15; –12:12	–14:10; –9:10; –8:8
Reflection collected	5473	4363	3459
Independent reflection	1102	1689	1351
R_{int}	0.044	0.041	0.038
Observed reflection	837	1060	998
No. parameters	109	160	130
R_1 (obs)	0.0267	0.0291	0.0274
wR_2 (all data)	0.0669	0.0612	0.0656
S	0.96	0.88	0.94
Min./Max. Resd. [e Å^{-3}]	–0.32, 0.42	–0.33, 0.41	–0.31, 0.38
Device type	Oxford Xcalibur3 CCD	Oxford Xcalibur3 CCD	Oxford Xcalibur CCD
Solution	SIR-92	SIR-92	SIR-92
Refinement	SHELXL-97	SHELXL-97	SHELXL-97
Absorption correction	multi-scan	multi-scan	multi-scan
CCDC No.	642162	642161	695925

	112	**113**	**114**
Formula	$C_8H_{14}CuN_{24}O_8$	$C_4H_6CuN_{12}O_4$	$C_4H_{12}CuN_{14}O_4$
Form. weight [g mol^{-1}]	637.98	349.75	383.82
Crystal system	triclinic	monoclinic	monoclinic
Space Group	$P\bar{1}$ (2)	$P2_1/c$ (14)	$C2/c$ (15)
Color / Habit	green plates	green rods	blue rods
Size [mm]	0.08 x 0.12 x 0.13	0.06 x 0.08 x 0.16	0.05 x 0.12 x 0.14
a [Å]	7.5580(8)	8.6890(4)	12.5744(5)
b [Å]	8.3910(9)	8.9998(3)	12.2013(4)
c [Å]	9.199(1)	7.6978(3)	9.4163(4)
α [°]	83.965(9)	90	90
β [°]	79.786(9)	111.448(5)	108.775(4)
γ [°]	85.377(8)	90	90
V [Å^3]	569.8(1)	560.28(4)	1367.8(1)
Z	1	2	4
$\rho_{calc.}$ [g cm^{-3}]	1.859	2.073	1.864
μ [mm^{-1}]	1.055	1.997	1.649
$F(000)$	323	350	780
$\lambda_{MoK\alpha}$[Å]	0.71073	0.71073	0.71073
T [K]	200	100	200
Theta Min-Max [°]	3.8, 26.0	3.8, 26.0	4.1, 26.3
Dataset [h; k; l]	–9:9; –10:10; –11:11	–10:10; –11:11; –9:9	–15:13; –12:15; –7:11
Reflection collected	5758	5488	3541
Independent reflection	2232	1094	1369
R_{int}	0.024	0.027	0.031
Observed reflection	1838	900	991
No. parameters	215	109	134
R_1 (obs)	0.0253	0.0251	0.0243
wR_2 (all data)	0.0686	0.0713	0.0649
S	1.07	1.10	1.00
Min./Max. Resd. [e Å^{-3}]	–0.38, 0.28	–0.20, 0.42	–0.34, 0.41
Device type	Oxford Xcalibur CCD	Oxford Xcalibur CCD	Oxford Xcalibur CCD
Solution	SIR-92	SIR-92	SIR-92
Refinement	SHELXL-97	SHELXS-97	SHELXL-97
Absorption correction	multi-scan	multi-scan	multi-scan
CCDC No.	695929	695930	695926

	115	**117**	**118**
Formula	$C_4H_{20}CuN_{16}O_5$	$C_8H_8N_6$	$C_4H_9N_{11}O$
Form. weight [g mol^{-1}]	435.91	188.20	227.19
Crystal system	triclinic	triclinic	orthorhombic
Space Group	*P*–1 (2)	*P*–1 (2)	*Pnma* (62)
Color / Habit	lavender plates	colorless rods	colorless needles
Size [mm]	0.02 x 0.10 x 0.13	0.06 x 0.10 x 0.15	0.03 x 0.10 x 0.11
a [Å]	6.7814(5)	7.8476(5)	23.548(5)
b [Å]	9.366(2)	8.9957(5)	6.309(1)
c [Å]	13.386(2)	12.6307(8)	6.649(1)
α [°]	82.977(1)	89.759(5)	90
β [°]	86.859(2)	88.260(5)	90
γ [°]	89.968(1)	88.936(5)	90
V [Å^3]	842.51(19)	891.09(9)	987.90(4)
Z	2	4	4
$\rho_{calc.}$ [g cm^{-3}]	1.718	1.403	1.528
μ [mm^{-1}]	1.357	0.096	0.121
$F(000)$	450	392	472
$\lambda_{MoK\alpha}$[Å]	0.71073	0.71073	0.71073
T [K]	200	200	173
Theta Min-Max [°]	3.7, 26.0	3.8, 26.0	3.2, 26.5
Dataset [h; k; l]	–8:8; –11:11; –16:16	–9:9; –11:11; –15:15	–30:30; –8:8; –8:8
Reflection collected	7828	9098	1938
Independent reflection	2210	3490	1118
R_{int}	0.119	0.027	0.026
Observed reflection	2210	2184	894
No. parameters	249	277	108
R_1 (obs)	0.0553	0.0337	0.0405
wR_2 (all data)	0.1786	0.0865	0.1056
S	1.22	0.99	1.15
Min./Max. Resd. [e Å^{-3}]	–0.75, 0.68	–0.20, 0.14	–0.21, 0.32
Device type	Nonius Kappa CCD	Oxford Xcalibur3 CCD	Nonius Kappa CCD
Solution	SIR-97	SIR-92	SIR-92
Refinement	SHELXL-97	SHELXL-97	SHELXL-97
Absorption correction	none	multi-scan	multi-scan
CCDC No.	695923	---	699132

	119	**122**·MeOH	**124**
Formula	$C_4H_7N_{11}$	$C_5H_{10}N_{11}NaO$	$C_5H_9N_{11}$
Form. weight [g mol^{-1}]	209.21	263.23	223.20
Crystal system	monoclinic	monoclinic	orthorhombic
Space Group	$I2/a$ (15)	$P2_1/c$ (14)	$Pca2_1$ (29)
Color / Habit	colorless needles	yellow rods	colorless needles
Size [mm]	0.04 x 0.13 x 0.17	0.07 x 0.08 x 0.15	0.11 x 0.14 x 0.23
a [Å]	13.9626(5)	6.905(1)	10.395(2)
b [Å]	6.7239(3)	9.177(2)	12.313(3)
c [Å]	19.3318(7)	20.919(4)	14.865(3)
α [°]	90	90	90
β [°]	91.750(3)	96.32(3)	90
γ [°]	90	90	90
V [Å^3]	1814.1(1)	1317.5(5)	1902.6(7)
Z	8	4	8
$\rho_{calc.}$ [g cm^{-3}]	1.532	1.327	1.559
μ [mm^{-1}]	0.117	0.130	0.117
$F(000)$	864	544	928
$\lambda_{MoK\alpha}$[Å]	0.71073	0.71073	0.71073
T [K]	200	200	200
Theta Min-Max [°]	3.7, 26.0	3.0, 26.0	3.2, 26.4
Dataset [h; k; l]	–17:17; –8:8; –23:23	–8:8; –10:10; –25:25	–12:12; –15:15; –18:17
Reflection collected	8764	4817	11948
Independent reflection	1778	2512	2015
R_{int}	0.047	0.024	0.044
Observed reflection	1130	1902	1748
No. parameters	164	170	361
R_1 (obs)	0.0376	0.0424	0.0505
wR_2 (all data)	0.1028	0.1196	0.1391
S	0.99	1.05	1.06
Min./Max. Resd. [e Å^{-3}]	–0.21, 0.23	–0.29, 0.21	–0.31, 0.48
Device type	Oxford Xcalibur3 CCD	Nonius Kappa CCD	Nonius Kappa CCD
Solution	SIR-92	SHELXS-97	SIR-92
Refinement	SHELXL-97	SHELXL-97	SHELXL-97
Absorption correction	multi-scan	multi-scan	multi-scan
CCDC No.	699130	699133	699131

	126	**127**	**128**
Formula	$C_8H_{36}N_{22}MgO_{12}$	CH_7N_5O	CH_6N_6
Form. weight [g mol^{-1}]	656.90	105.12	102.12
Crystal system	triclinic	monoclinic	orthorhombic
Space Group	*P*–1 (2)	$P2_1/n$ (14)	*Ccca* (68)
Color / Habit	colorless rods	colorless platelets	colorless rods
Size [mm]	0.10 x 0.14 x 0.17	0.06 x 0.18 x 0.25	0.05 x 0.05 x 0.18
a [Å]	8.2922(5)	7.211(1)	6.763(1)
b [Å]	9.1757(6)	4.0108(8)	17.7510(4)
c [Å]	10.0013(6)	17.991(4)	16.3160(8)
α [°]	87.597(5)	90	90
β [°]	89.622(5)	91.97(3)	90
γ [°]	78.714(5)	90	90
V [Å^3]	745.59(8)	520.0(2)	1958.7(3)
Z	1	4	16
$\rho_{calc.}$ [g cm^{-3}]	1.463	1.343	1.385
μ [mm^{-1}]	0.148	0.113	0.108
F(000)	346	224	864
$\lambda_{MoK\alpha}$[Å]	0.71073	0.71073	0.71073
T [K]	200	200	200
Theta Min-Max [°]	3.7, 26.0	4.3, 26.0	3.4, 27.5
Dataset [h; k; l]	–10:10; –11:11; –12:12	–8:8; –4:4; –22:22	–8:8; –22:22; –21:21
Reflection collected	7614	1869	7045
Independent reflection	2929	1012	1127
R_{int}	0.028	0.021	0.117
Observed reflection	1794	874	1127
No. parameters	268	93	92
R_1 (obs)	0.0309	0.0323	0.0985
wR_2 (all data)	0.0728	0.0957	0.2031
S	0.90	1.11	1.28
Min./Max. Resd. [e Å^{-3}]	–0.19, 0.19	–0.12, 0.16	–0.32, 0.58
Device type	Oxford Xcalibur3 CCD	KappaCCD	KappaCCD
Solution	SHELXS-97	SIR-92	SIR-97
Refinement	SHELXL-97	SHELXL-97	SHELXL-97
Absorption correction	multi-scan	none	none
CCDC No.	699134	678881	678884

	129	**130**	**131**
Formula	$CHLiN_4$	CH_3N_4NaO	$CHKN_4$
Form. weight [g mol^{-1}]	75.99	110.05	108.14
Crystal system	orthorhombic	orthorhombic	hexagonal
Space Group	$C222_1$ (20)	*Pmma* (51)	*P*–6 (174)
Color / Habit	colorless blocks	colorless rods	colorless blocks
Size [mm]	0.09 x 0.13 x 0.15	0.04 x 0.09 x 0.15	0.15 x 0.24 x 0.25
a [Å]	13.499(2)	6.400(2)	14.0037(2)
b [Å]	14.389(3)	5.837(1)	14.0037(2)
c [Å]	14.125(3)	5.608(2)	10.7285(2)
α [°]	90	90	90
β [°]	90	90	90
γ [°]	90	90	120
V [Å^3]	2743.6(9)	209.51(9)	1822.03(5)
Z	8	2	6
$\rho_{calc.}$ [g cm^{-3}]	1.472	1.745	1.774
μ [mm^{-1}]	0.108	0.229	1.127
$F(000)$	1216	112	972
$\lambda_{MoK\alpha}$[Å]	0.71073	0.71073	0.71073
T [K]	200	200	200
Theta Min-Max [°]	3.2, 27.5	5.0, 27.5	3.4, 27.5
Dataset [h; k; l]	–17:17; –18:18; –18:18	–8:7; –7:3; –7:7	–17:18; –18:18; –12:13
Reflection collected	3153	1051	13968
Independent reflection	1766	281	2922
R_{int}	0.017	0.024	0.050
Observed reflection	1515	279	2587
No. parameters	235	30	173
R_1 (obs)	0.0382	0.0223	0.0425
wR_2 (all data)	0.1027	0.0627	0.1094
S	1.12	1.14	1.08
Min./Max. Resd. [e Å^{-3}]	–0.27, 0.21	–0.16, 0.22	–0.46, 0.62
Device type	KappaCCD	Oxford Xcalibur3 CCD	KappaCCD
Solution	SIR-92	SIR-92	SIR-92
Refinement	SHELXL-97	SHELXL-97	SHELXL-97
Absorption correction	none	multi-scan	none
CCDC No.	678888	678885	678882

	132	**133**	**134**
Formula	CHN_4Rb	$CHCsN_4$	$C_2H_{12}N_8O_5Sr$
Form. weight [g mol^{-1}]	154.51	201.95	315.79
Crystal system	hexagonal	orthorhombic	orthorhombic
Space Group	$P6_3/m$ (176)	$Pbca$ (61)	$Pnnm$ (58)
Color / Habit	colorless prisms	colorless rods	colorless platelets
Size [mm]	0.05 x 0.08 x 0.12	0.05 x 0.07 x 0.13	0.04 x 0.09 x 0.18
a [Å]	8.260(2)	7.3406(8)	11.314(2)
b [Å]	8.260(2)	9.610(1)	13.876(3)
c [Å]	11.009(3)	12.199(1)	7.121(1)
α [°]	90	90	90
β [°]	90	90	90
γ [°]	120	90	90
V [Å^3]	650.5(3)	860.5(2)	1117.9(4)
Z	6	8	2
$\rho_{calc.}$ [g cm^{-3}]	2.367	3.118	1.877
μ [mm^{-1}]	11.244	8.433	4.848
$F(000)$	432	720	632
$\lambda_{MoK\alpha}$[Å]	0.71073	0.71073	0.71073
T [K]	200	200	200
Theta Min-Max [°]	4.7, 26.0	3.9, 25.0	3.2, 27.5
Dataset [h; k; l]	–8:10; –10:5; –13:12	–8:8; –11:11; –14:14	–14:14; –17:18; –8:9
Reflection collected	3302	73475	15656
Independent reflection	450	760	1387
R_{int}	0.073	0.039	0.055
Observed reflection	395	755	1215
No. parameters	34	60	117
R_1 (obs)	0.0344	0.0307	0.0233
wR_2 (all data)	0.0787	0.0521	0.0494
S	1.19	1.37	1.02
Min./Max. Resd. [e Å^{-3}]	–0.54, 0.73	–0.64, 0.74	–0.31, 0.78
Device type	Oxford Xcalibur3 CCD	Oxford Xcalibur3 CCD	KappaCCD
Solution	SHELXS-97	SHELXS-97	SIR-92
Refinement	SHELXL-97	SHELXL-97	SHELXL-97
Absorption correction	multi-scan	multi-scan	sphere
CCDC No.	678886	578887	678883

	135	**136**	**137**
Formula	CHN_7	CH_5N_9	CH_4N_8
Form. weight [g mol^{-1}]	111.09	143.14	128.12
Crystal system	monoclinic	monoclinic	monoclinic
Space Group	$P2_1/c$ (14)	$P2_1/c$ (14)	$P2_1$ (4)
Color / Habit	colorless needles	colorless needles	colorless needles
Size [mm]	0.03 x 0.04 x 0.10	0.07 x 0.07 x 0.21	0.01 x 0.05 x 0.08
a [Å]	13.265(2)	10.8114(5)	3.9103(3)
b [Å]	4.9693(6)	7.4641(4)	6.9140(4)
c [Å]	16.304(3)	7.6676(4)	9.9127(6)
α [°]	90	90	90
β [°]	127.04(1)	101.437(5)	99.177(6)
γ [°]	90	90	90
V [Å^3]	857.9(3)	606.47(5)	264.57(3)
Z	8	4	2
$\rho_{calc.}$ [g cm^{-3}]	1.720	1.568	1.608
μ [mm^{-1}]	0.139	0.126	0.129
$F(000)$	448	296	132
$\lambda_{MoK\alpha}$[Å]	0.71073	0.71073	0.71073
T [K]	100	100	200
Theta Min-Max [°]	3.8, 26.0	3.8, 26.0	4.2, 27.1
Dataset [h; k; l]	–16:16; –6:6; –20:20	–12:13; –9:8; –9:8	–4:5; –8:8 ; –12:12
Reflection collected	8224	3021	2806
Independent reflection	1696	1192	623
R_{int}	0.063	0.025	0.059
Observed reflection	1154	824	383
No. parameters	153	111	98
R_1 (obs)	0.0306	0.0305	0.0307
wR_2 (all data)	0.0806	0.0767	0.0637
S	1.00	0.93	0.91
Min./Max. Resd. [e Å^{-3}]	–0.21, 0.19	–0.24, 0.19	–0.16, 0.22
Device type	Oxford Xcalibur3 CCD	Oxford Xcalibur3 CCD	Oxford Xcalibur3 CCD
Solution	SIR-92	SIR-92	SIR-92
Refinement	SHELXL-97	SHELXL-97	SHELXL-97
Absorption correction	none	multi-scan	multi-scan
CCDC No.	673182	677382	675485

	138	**139**	**140**
Formula	$C_2H_7N_{11}$	$C_4H_{14}N_{20}O$	CH_2N_7OLi
Form. weight [g mol^{-1}]	185.19	358.35	135.03
Crystal system	triclinic	monoclinic	monoclinic
Space Group	$P\bar{1}$ (2)	$P2_1/c$ (14)	$P2_1/c$ (14)
Color / Habit	colorless blocks	colorless rods	colorless needles
Size [mm]	0.03 x 0.07 x 0.18	0.03 x 0.05 x 0.06	0.05 x 0.06 x 0.17
a [Å]	9.7652(8)	9.5374(8)	8.9207(5)
b [Å]	9.7803(9)	15.3120(9)	4.6663(2)
c [Å]	10.0434(9)	10.5731(6)	12.8648(6)
α [°]	71.327(8)	90	90
β [°]	74.399(7)	94.361(7)	95.608(5)
γ [°]	63.962(9)	90	90
V [Å^3]	807.2(1)	1539.6(2)	532.96(5)
Z	4	4	4
$\rho_{calc.}$ [g cm^{-3}]	1.524	1.546	1.683
μ [mm^{-1}]	0.120	0.125	0.139
$F(000)$	384	744	272
$\lambda_{MoK\alpha}$[Å]	0.71073	0.71073	0.71073
T [K]	200	100	200
Theta Min-Max [°]	3.9, 26.0	3.8, 25.5	4.1, 26.5
Dataset [h; k; l]	–11:12; –12:11; –12:12	–11:11; –18:16; –12:6	–10:11; –5:5 ; –14:16
Reflection collected	4173	7183	2650
Independent reflection	3118	2835	1096
R_{int}	0.027	0.082	0.029
Observed reflection	1552	1128	785
No. parameters	291	282	99
R_1 (obs)	0.0450	0.0490	0.0313
wR_2 (all data)	0.1154	0.1288	0.0869
S	0.93	0.88	1.05
Min./Max. Resd. [e Å^{-3}]	–0.22, 0.21	–0.23, 0.27	–0.19, 0.19
Device type	Oxford Xcalibur3 CCD	Oxford Xcalibur3 CCD	Oxford Xcalibur3 CCD
Solution	SIR-92	SIR-92	SIR-92
Refinement	SHELXL-97	SHELXL-97	SHELXL-97
Absorption correction	multi-scan	multi-scan	multi-scan
CCDC No.	699844	699848	699845

	141	**142**	**143**
Formula	CN_7Na*H_2O	CN_7K	CN_7Cs
Form. weight [g mol^{-1}]	151.09	149.18	242.99
Crystal system	monoclinic	monoclinic	orthorhombic
Space Group	$P2_1/c$ (60)	$P2_1/c$ (60)	$P2_12_12_1$ (19)
Color / Habit	colorless needles	colorless rods	colorless plates
Size [mm]	0.04 x 0.05 x 0.09	0.03 x 0.07 x 0.14	0.05 x 0.06 x 0.07
a [Å]	11.203(2)	9.7759(9)	4.3082(1)
b [Å]	7.138(2)	6.2990(6)	7.1345(2)
c [Å]	14.409(2)	8.4533(6)	18.6869(9)
α [°]	90	90	90
β [°]	91.630(1)	96.720(8)	90
γ [°]	90	90	90
V [Å^3]	1151.8(4)	516.96(8)	574.38(3)
Z	8	4	4
$\rho_{calc.}$ [g cm^{-3}]	1.743	1.917	2.810
μ [mm^{-1}]	0.207	0.927	6.357
$F(000)$	608	296	440
$\lambda_{MoK\alpha}$[Å]	0.71073	0.71073	0.71073
T [K]	200	100	100
Theta Min-Max [°]	4.0, 26.0	4.0, 25.5	4.3, 26.8
Dataset [h; k; l]	–13:13; –8:8; –17:14	–11:9; –7:7; –10:10	–5:5; –8:9 ; –13:23
Reflection collected	5726	2090	3179
Independent reflection	2254	956	1227
R_{int}	0.041	0.028	0.027
Observed reflection	830	678	1074
No. parameters	197	82	82
R_1 (obs)	0.0313	0.0315	0.0227
wR_2 (all data)	0.0798	0.0763	0.0398
S	0.71	0.99	0.92
Min./Max. Resd. [e Å^{-3}]	–0.22, 0.39	–0.35, 0.60	-0.42, 0.85
Device type	Oxford Xcalibur3 CCD	Oxford Xcalibur3 CCD	Oxford Xcalibur3 CCD
Solution	SIR-92	SIR-92	SIR-92
Refinement	SHELXL-97	SHELXL-97	SHELXL-97
Absorption correction	multi-scan	multi-scan	multi-scan
CCDC No.	675486	699847	699846

	144	**145**	**146**
Formula	$C_6H_{32}Ca_3N_{42}O_{16}$	$C_2H_3N_7$	$C_2H_3N_7$
Form. weight [g mol^{-1}]	1068.98	125.11	125.11
Crystal system	monoclinic	monoclinic	monoclinic
Space Group	$C2/c$ (15)	$P2_1/m$ (11)	$P2_1/c$ (14)
Color / Habit	colorless needles	colorless needles	colorless rods
Size [mm]	0.05 x 0.06 x 0.09	0.06 x 0.10 x 0.26	0.10 x 0.12 x 0.13
a [Å]	24.448(5)	8.7382(4)	6.6219(5)
b [Å]	6.616(5)	6.2408(4)	8.7588(7)
c [Å]	28.057(5)	10.2986(6)	9.6392(8)
α [°]	90	90	90
β [°]	109.246(5)	90.722(4)	108.858(7)
γ [°]	90	90	90
V [Å^3]	4285(3)	561.57(6)	529.06(8)
Z	4	4	4
$\rho_{calc.}$ [g cm^{-3}]	1.657	1.480	1.571
μ [mm^{-1}]	0.495	0.115	0.123
$F(000)$	2200	256	256
$\lambda_{MoK\alpha}$[Å]	0.71073	0.71073	0.71069
T [K]	100	200	200
Theta Min-Max [°]	3.7, 25.5	3.8, 26.0	4.0, 26.0
Dataset [h; k; l]	–23:29; –8:7; –3:28	–10:8; –7:7; –12:8	–5:8; –10:8; –10:11
Reflection collected	9922	2919	2662
Independent reflection	3947	1206	1037
R_{int}	0.064	0.037	0.036
Observed reflection	2220	729	674
No. parameters	369	112	94
R_1 (obs)	0.0423	0.0320	0.0331
wR_2 (all data)	0.0992	0.0926	0.0854
S	0.96	0.97	0.90
Min./Max. Resd. [e Å^{-3}]	–0.52, 0.46	–0.18, 0.16	–0.16, 0.18
Device type	Oxford Xcalibur3 CCD	Oxford Xcalibur3 CCD	Oxford Xcalibur3 CCD
Solution	SIR-92	SIR-92	SIR-92
Refinement	SHELXL-97	SHELXL-97	SHELXL-97
Absorption correction	multi-scan	multi-scan	multi-scan
CCDC No.	699849	707542	707543

	148	**149**	**150**
Formula	$C_2H_3N_5O_2$	$C_2H_3N_5O_2$	$C_2H_3ClN_4$
Form. weight [g mol^{-1}]	129.09	129.09	118.53
Crystal system	monoclinic	monoclinic	orthorhombic
Space Group	$P2_1/n$ (14)	$P2_1/c$ (14)	$Pbca$ (61)
Color / Habit	colorless rods	colorless rods	colorless blocks
Size [mm]	0.04 x 0.08 x 0.10	0.03 x 0.18 x 0.27	0.10 x 0.16 x 0.17
a [Å]	10.0578(4)	6.331(1)	10.8096(5)
b [Å]	9.7055(4)	4.993(1)	7.3646(3)
c [Å]	16.5331(6)	16.388(3)	12.1244(6)
α [°]	90	90	90
β [°]	101.701(4)	97.13(3)	90
γ [°]	90	90	90
V [Å^3]	1580.36(11)	514.0(2)	965.20(8)
Z	12	4	8
$\rho_{calc.}$ [g cm^{-3}]	1.628	1.668	1.631
μ [mm^{-1}]	0.143	0.146	0.648
$F(000)$	792	264	480
$\lambda_{MoK\alpha}$[Å]	0.71073	0.71073	0.71073
T [K]	200	200	150
Theta Min-Max [°]	3.9, 25.0	3.2, 26.0	3.8, 27.5
Dataset [h; k; l]	–11:10; –11:11; –19:15	–7:7; –6:6; –20:19	–14:13; –9:9; –7:15
Reflection collected	7250	3454	5086
Independent reflection	2766	1003	1100
R_{int}	0.064	0.037	0.026
Observed reflection	1139	862	833
No. parameters	258	94	76
R_1 (obs)	0.0664	0.0364	0.0323
wR_2 (all data)	0.2102	0.0946	0.0999
S	0.91	1.08	1.10
Min./Max. Resd. [e Å^{-3}]	–0.27, 0.85	–0.22, 0.14	–0.24, 0.27
Device type	Oxford Xcalibur3 CCD	Oxford Xcalibur3 CCD	Oxford Xcalibur3 CCD
Solution	SIR-92	SIR-92	SIR-97
Refinement	SHELXL-97	SHELXL-97	SHELXL-97
Absorption correction	multi-scan	none	multi-scan
CCDC No.	689201	689203	---

	151	**152**	**152**·H_2O
Formula	$C_4H_6N_{10}O$	$C_2H_2N_8$	$C_2H_4N_8O$
Form. weight [g mol^{-1}]	210.19	138.12	156.13
Crystal system	monoclinic	monoclinic	monoclinic
Space Group	$P2_1/m$ (11)	Pn (7)	$P2_1/c$ (14)
Color / Habit	colorless rods	colorless rods	colorless plates
Size [mm]	0.03 x 0.08 x 0.12	0.08 x 0.12 x 0.15	0.02 x 0.11 x 0.13
a [Å]	6.6970(4)	6.8512(6)	5.4394(3)
b [Å]	6.0510(3)	7.9270(7)	17.8798(8)
c [Å]	10.9310(6)	9.7809(8)	6.8156(5)
α [°]	90	90	90
β [°]	106.596(6)	91.655(7)	110.470(6)
γ [°]	90	90	90
V [Å^3]	424.51(4)	530.97(8)	621.00(7)
Z	2	4	4
$\rho_{calc.}$ [g cm^{-3}]	1.644	1.728	1.670
μ [mm^{-1}]	0.131	0.136	0.138
$F(000)$	216	280	320
$\lambda_{MoK\alpha}$[Å]	0.71073	0.71073	0.71073
T [K]	150	150	200
Theta Min-Max [°]	3.9, 27.5	3.9, 33.6	3.9, 26.0
Dataset [h; k; l]	–8:8; –5:7; –11:14	–6:10; –11:7; –14:11	–6:5; –22:13; –8:7
Reflection collected	2470	4154	3073
Independent reflection	1063	1909	1218
R_{int}	0.035	0.048	0.031
Observed reflection	744	923	799
No. parameters	105	197	116
R_1 (obs)	0.0384	0.0337	0.0363
wR_2 (all data)	0.1086	0.0686	0.0883
S	0.94	0.86	0.98
Min./Max. Resd. [e Å^{-3}]	–0.31, 0.40	–1.26, 0.26	–0.16, 0.18
Device type	Oxford Xcalibur3 CCD	Oxford Xcalibur3 CCD	Oxford Xcalibur3 CCD
Solution	SIR-92	SIR-92	SIR-92
Refinement	SHELXL-97	SHELXL-97	SHELXL-97
Absorption correction	multi-scan	multi-scan	multi-scan
CCDC No.	---	709126	709127

	153	**154**	**155**
Formula	$C_3H_4N_8$	$C_2H_5N_9$	$C_2H_5N_8NaO_2$
Form. weight [g mol^{-1}]	152.12	155.15	196.13
Crystal system	monoclinic	monoclinic	triclinic
Space Group	$P2_1/n$ (14)	$P2_1/c$ (14)	P–1 (2)
Color / Habit	colorless needles	colorless rods	colorless rods
Size [mm]	0.10 x 0.12 x 0.16	0.06 x 0.09 x 0.24	0.07 x 0.12 x 0.16
a [Å]	10.987(2)	8.447(2)	6.4458(4)
b [Å]	8.1663(2)	7.366(2)	8.453(5)
c [Å]	14.547(3)	10.675(2)	8.456(6)
α [°]	90	90	83.733(4)
β [°]	98.98(3)	98.14(3)	67.666(5)
γ [°]	90	90	67.670(6)
V [Å^3]	1289.2(4)	657.5(2)	393.9(4)
Z	8	4	2
$\rho_{calc.}$ [g cm^{-3}]	1.568	1.567	1.645
μ [mm^{-1}]	0.120	0.123	0.185
$F(000)$	624	320	200
$\lambda_{MoK\alpha}$[Å]	0.71073	0.71073	0.71073
T [K]	200	200	200
Theta Min-Max [°]	3.3, 25.5	3.4, 26.0	3.7, 27.6
Dataset [h; k; l]	–13:13; –9:9; –17:17	–10:10; –9:9; –13:13	–8:8; –11:11; –11:10
Reflection collected	4604	4698	4540
Independent reflection	2401	1282	1813
R_{int}	0.027	0.042	0.025
Observed reflection	1801	968	1813
No. parameters	232	120	183
R_1 (obs)	0.0388	0.0396	0.0294
wR_2 (all data)	0.1105	0.1080	0.0743
S	1.04	1.08	0.94
Min./Max. Resd. [e Å^{-3}]	–0.18, 0.21	–0.22, 0.19	–0.22, 0.14
Device type	Nonius Kappa CCD	Nonius Kappa CCD	Oxford Xcalibur3 CCD
Solution	SIR-92	SIR-92	SHELXS-97
Refinement	SHELXL-97	SHELXL-97	SHELXL-97
Absorption correction	none	none	multi-scan
CCDC No.	709125	709124	709132

	156	**157**	**158**
Formula	$C_2H_5KN_8O_2$	$C_4H_{10}CuN_{16}O_4$	$C_4H_{12}CuN_{18}O_2$
Form. weight [g mol^{-1}]	212.24	409.82	407.86
Crystal system	triclinic	monoclinic	triclinic
Space Group	*P*–1 (2)	$P2_1/n$ (14)	*P*–1 (2)
Color / Habit	colorless rods	light blue rods	dark blue rods
Size [mm]	0.09 x 0.10 x 0.12	0.09 x 0.11 x 0.15	0.02 x 0.08 x 0.12
a [Å]	7.2121(6)	5.4888(1)	5.7360(4)
b [Å]	7.6842(6)	6.3797(2)	6.7215(5)
c [Å]	7.8868(6)	19.5884(5)	10.2341(9)
α [°]	85.874(7)	90	106.896(7)
β [°]	84.457(7)	95.165(2)	100.421(7)
γ [°]	86.231(7)	90	90.932(6)
V [Å^3]	433.15(6)	683.14(3)	370.32(5)
Z	2	2	1
$\rho_{calc.}$ [g cm^{-3}]	1.627	1.992	1.829
μ [mm^{-1}]	0.599	1.662	1.526
F(000)	216	414	207
$\lambda_{MoK\alpha}$[Å]	0.71073	0.71073	0.71073
T [K]	200	200	200
Theta Min-Max [°]	3.8, 26.0	3.8, 26.2	3.8, 26.0
Dataset [h; k; l]	–8:8; –9:9; –9:7	–6:6; –7:7; –24:24	–6:7; –8:8; –12:11
Reflection collected	2278	4055	1940
Independent reflection	1689	1366	1442
R_{int}	0.012	0.018	0.017
Observed reflection	1398	1002	1164
No. parameters	138	135	139
R_1 (obs)	0.0252	0.0337	0.0301
wR_2 (all data)	0.0689	0.0978	0.0683
S	1.07	1.02	1.01
Min./Max. Resd. [e Å^{-3}]	–0.25, 0.23	–0.30, 1.34	–0.32, 0.40
Device type	Oxford Xcalibur3 CCD	Oxford Xcalibur3 CCD	Oxford Xcalibur3 CCD
Solution	SHELXS-97	SHELXS-97	SHELXS-97
Refinement	SHELXL-97	SHELXL-97	SHELXL-97
Absorption correction	multi-scan	multi-scan	multi-scan
CCDC No.	709131	709128	709129

	159	**160**·H_2O	**160**
Formula	$C_6H_8Cl_2CuN_{16}$	$C_2H_5N_9O$	$C_2H_3N_9$
Form. weight [g mol^{-1}]	438.69	171.15	153.13
Crystal system	orthorhombic	monoclinic	orthorhombic
Space Group	$Pna2_1$ (33)	$P2_1/c$ (14)	$Pbca$ (61)
Color / Habit	green rods	colorless plates	colorless needles
Size [mm]	0.03 x 0.09 x 0.09	0.04 x 0.10 x 0.15	0.05 x 0.06 x 0.19
a [Å]	6.8906(1)	9.367(2)	11.109(2)
b [Å]	10.5373(2)	10.531(2)	9.227(2)
c [Å]	21.1159(4)	6.808(1)	21.327(4)
α [°]	90	90	90
β [°]	90	90.42(3)	90
γ [°]	90	90	90
V [Å^3]	1533.19(5)	671.6(2)	2186.1(7)
Z	4	4	16
$\rho_{calc.}$ [g cm^{-3}]	1.901	1.693	1.861
μ [mm^{-1}]	1.806	0.140	0.147
$F(000)$	876	352	1248
$\lambda_{MoK\alpha}$[Å]	0.71073	0.71073	0.71073
T [K]	200	200	200
Theta Min-Max [°]	3.7, 27.5	3.6, 27.4	3.5, 26.5
Dataset [h; k; l]	–8:8; –13:13; –27:16	12:12; –13:13; –8: 8	–13:13; –11:11; –26:26
Reflection collected	8320	2966	4201
Independent reflection	2706	1529	2257
R_{int}	0.030	0.019	0.026
Observed reflection	2383	1257	1618
No. parameters	236	129	223
R_1 (obs)	0.0241	0.0367	0.0396
wR_2 (all data)	0.0522	0.0998	0.1022
S	1.01	1.08	1.06
Min./Max. Resd. [e Å^{-3}]	–0.50, 0.25	–0.28, 0.19	–0.28, 0.25
Device type	Oxford Xcalibur3 CCD	Nonius Kappa CCD	Nonius Kappa CCD
Solution	SIR-92	SIR-92	SHELXS-97
Refinement	SHELXL-97	SHELXL-97	SHELXL-97
Absorption correction	multi-scan	none	none
CCDC No.	709130	687771	299051

	160·H_2O·DMSO	**161**	**162**
Formula	$C_4H_{11}N_9OS$	$C_4H_7N_9$	$C_5H_9N_9$
Form. weight [g mol^{-1}]	249.54	181.19	195.21
Crystal system	monoclinic	monoclinic	monoclinic
Space Group	$C2/c$ (15)	$P2_1/c$ (14)	$P2_1/m$ (11)
Color / Habit	colorless rods	colorless needles	colorless rods
Size [mm]	0.04 x 0.11 x 0.11	0.08 x 0.16 x 0.23	0.12 x 0.15 x 0.26
a [Å]	15.933(1)	10.279(2)	3.852(1)
b [Å]	6.8863(6)	11.338(2)	19.395(5)
c [Å]	19.920(2)	6.772(1)	5.769 (2)
α [°]	90	90	90
β [°]	104.227(7)	94.74(3)	95.60(3)
γ [°]	90	90	90
V [Å^3]	2118.6(3)	786.5(3)	428.9(2)
Z	8	4	2
$\rho_{calc.}$ [g cm^{-3}]	1.563	1.530	1.512
μ [mm^{-1}]	0.312	0.115	0.112
$F(000)$	1040	376	204
$\lambda_{MoK\alpha}$[Å]	0.71073	0.71073	0.71073
T [K]	200	200	200
Theta Min-Max [°]	4.3, 25.5	3.5, 27.5	4.1, 26.0
Dataset [h; k; l]	–19:19; –8:8; –24:24	–13:13; –14:14; –8:8	–4:4; –17:23; –6:7
Reflection collected	9776	3457	2226
Independent reflection	1965	1803	862
R_{int}	0.029	0.023	0.033
Observed reflection	1846	1383	724
No. parameters	165	146	86
R_1 (obs)	0.0406	0.0407	0.0570
wR_2 (all data)	0.1067	0.1171	0.1353
S	1.11	1.14	1.18
Min./Max. Resd. [e Å^{-3}]	–0.34, 0.34	–0.26, 0.19	–0.23, 0.22
Device type	Oxford Xcalibur3 CCD	Nonius Kappa CCD	Oxford Xcalibur3 CCD
Solution	SIR-92	SHELXS-97	SIR-92
Refinement	SHELXL-97	SHELXL-97	SHELXL-97
Absorption correction	multi-scan	none	multi-scan
CCDC No.	687768	687770	687769

	163	**164**	**165**
Formula	$C_3H_5N_9$	$C_4H_7N_9$	$C_4H_{11}N_{20}ZnO_{17/2}$
Form. weight [g mol^{-1}]	167.16	181.19	540.65
Crystal system	triclinic	triclinic	monoclinic
Space Group	*P*–1 (2)	*P*–1 (2)	$P2_1/c$ (14)
Color / Habit	colorless rods	colorless rods	colorless needles
Size [mm]	0.03 x 0.09 x 0.09	0.02 x 0.11 x 0.14	0.19 x 0.11 x 0.08
a [Å]	5.0808(8)	5.1505(4)	6.0448(8)
b [Å]	7.009(1)	7.3074(6)	11.429(1)
c [Å]	9.873(2)	10.7388(8)	25.236(3)
α [°]	102.94(2)	98.189(6)	90
β [°]	91.46(1)	96.183(6)	100.41(1)
γ [°]	102.51(1)	104.214(7)	90
V [Å^3]	333.51(1)	383.49(5)	1714.7(4)
Z	2	2	2
$\rho_{calc.}$ [g cm^{-3}]	1.665	1.569	2.091
μ [mm^{-1}]	0.128	0.118	1.535
F(000)	172	188	367
$\lambda_{MoK\alpha}$[Å]	0.71073	0.71073	0.71073
T [K]	100	100	200
Theta Min-Max [°]	4.1, 26.0	3.8, 26.5	3.7, 26.0
Dataset [h; k; l]	–6:6; –8:8; –12:12	–6:6; –9:9; –13:13	–7:7; –14:15; –31:31
Reflection collected	3443	4034	17112
Independent reflection	1319	1584	3352
R_{int}	0.043	0.042	0.058
Observed reflection	1319	1584	2795
No. parameters	129	146	383
R_1 (obs)	0.0359	0.0342	0.0529
wR_2 (all data)	0.0900	0.0978	0.1085
S	1.13	1.14	1.15
Min./Max. Resd. [e Å^{-3}]	–0.23, 0.18	–0.28, 0.17	–0.34, 0.58
Device type	Oxford Xcalibur3 CCD	Oxford Xcalibur3 CCD	Oxford Xcalibur3 CCD
Solution	SIR-92	SIR-92	SIR-92
Refinement	SHELXL-97	SHELXL-97	SHELXL-97
Absorption correction	multi-scan	multi-scan	multi-scan
CCDC No.	---	---	---

	166	**167**	**168**
Formula	$C_4H_8N_{18}ZnCl_2O_9$	$C_8H_{14}N_{40}Cu_2O_{13}$	$C_4H_6N_{18}Cl_2CuO_4$
Form. weight [g mol^{-1}]	588.57	1499.53	568.66
Crystal system	triclinic	orthorhombic	monoclinic
Space Group	*P*–1 (2)	*Pbcm* (57)	$P2_1/c$ (14)
Color / Habit	colorless plates	blue plates	blue plates
Size [mm]	0.22 x 0.18 x 0.16	0.22 x 0.31 x 0.19	0.12 x 0.26 x 0.38
a [Å]	7.513(1)	7.4675(1)	10.7325(9)
b [Å]	11.700(1)	25.5259(3)	8.7712(5)
c [Å]	12.203(1)	24.4201(3)	8.9550(6)
α [°]	62.47(1)	90	90
β [°]	83.65(1)	90	91.988(9)
γ [°]	70.87(1)	90	90
V [Å^3]	897.6(2)	4654.8(1)	842.5(1)
Z	2	4	2
$\rho_{calc.}$ [g cm^{-3}]	2.178	2.140	2.242
μ [mm^{-1}]	1.763	1.502	1.709
$F(000)$	588	486	160
$\lambda_{MoK\alpha}$[Å]	0.71073	0.71073	0.71073
T [K]	200	200	200
Theta Min-Max [°]	4.1, 26.0	3.2, 27.5	3.3, 24.0
Dataset [h; k; l]	–9:9; –12:14; –15:14	–9:9; –33:32; –31:31	–11:11; –9:9; –9:10
Reflection collected	4690	10017	3328
Independent reflection	3501	5456	974
R_{int}	0.018	0.023	0.088
Observed reflection	2848	3753	892
No. parameters	339	3004	566
R_1 (obs)	0.0337	0.0378	0.0278
wR_2 (all data)	0.0841	0.1162	0.0839
S	1.04	1.04	1.12
Min./Max. Resd. [e Å^{-3}]	–0.57, 0.46	–0.54, 0.93	–0.43, 0.26
Device type	Oxford Xcalibur3 CCD	STOE IPDS	NONIUS Kappa CCD
Solution	SIR–97	SIR-97	SIR-97
Refinement	SHELXL-97	SHELXL-97	SHELXL-97
Absorption correction	multiscan	none	none
CCDC No.	---	---	---

	169	**170**	**171**
Formula	$C_8H_{14}N_{20}CuO_6$	$C_8H_{14}N_{18}Cl_2CuO_8$	$C_{15}H_{27}CuN_{27}Cl_2O_4$
Form. weight [g mol^{-1}]	549.94	624.77	848.09
Crystal system	triclinic	monoclinic	monoclinic
Space Group	$P\bar{1}$ (2)	$P2_1/n$ (14)	$C2/c$ (15)
Color / Habit	green plates	green plates	green prismn
Size [mm]	0.28 x 0.30 x 0.18	0.12 x 0.25 x 0.37	0.06 x 0.11 x 0.14
a [Å]	8.4540(9)	9.7673(8)	26.304(3)
b [Å]	8.5751(8)	7.6168(8)	9.6080(7)
c [Å]	9.0260(7)	14.664(1)	17.188(2)
α [°]	102.007(8)	90	90
β [°]	111.213(9)	90.48(1)	128.00(1)
γ [°]	114.16(1)	90	90
V [Å^3]	505.4(1)	1090.9(2)	3423.2(8)
Z	1	2	4
$\rho_{calc.}$ [g cm^{-3}]	1.807	1.902	1.646
μ [mm^{-1}]	1.161	1.329	0.878
$F(000)$	188	630	1732
$\lambda_{MoK\alpha}$[Å]	0.71073	0.71073	0.71073
T [K]	200	200	200
Theta Min-Max [°]	4.1, 26.6	2.5, 28.0	4.1, 26.0
Dataset [h; k; l]	–10:10; –10:10; –11:11	–12:12; –10:10; –19:19	–32:32; –11:11; –21:21
Reflection collected	12885	9031	16978
Independent reflection	2026	2614	3348
R_{int}	0.044	0.044	0.050
Observed reflection	1941	2237	3017
No. parameters	188	197	319
R_1 (obs)	0.0331	0.0270	0.0649
wR_2 (all data)	0.0793	0.0700	0.1420
S	1.09	1.02	1.17
Min./Max. Resd. [e Å^{-3}]	–0.32, 0.41	–0.58, 0.35	–0.38, 0.55
Device type	Oxford Xcalibur3 CCD	STOE IPDS	Oxford Xcalibur3 CCD
Solution	SIR-92	SIR-97	SIR-92
Refinement	SHELXL-97	SHELXL-97	SHELXL-97
Absorption correction	multi-scan	none	multi-scan
CCDC No.	---	---	---

	172	**173**	**174**
Formula	$C_5H_9Cl_2CuN_9$	$CH_4N_5BF_4$	$C_8H_9N_5O_2S$
Form. weight [g mol^{-1}]	329.65	172.88	239.26
Crystal system	monoclinic	triclinic	triclinic
Space Group	$P2_1/c$ (14)	$P\bar{1}$ (2)	$P\bar{1}$ (2)
Color / Habit	green rods	colorless plates	colorless plates
Size [mm]	0.11 x 0.12 x 0.15	0.05 x 0.07 x 0.10	0.02 x 0.06 x 0.12
a [Å]	8.3620(9)	5.0408(4)	6.8569(8)
b [Å]	16.8770(2)	7.5664(5)	7.2247(8)
c [Å]	8.4180(9)	8.4364(6)	11.358(1)
α [°]	90	82.400(6)	92.074(9)
β [°]	103.669(9)	73.911(7)	93.570(9)
γ [°]	90	88.757(5)	110.71(1)
V [Å^3]	1154.4(2)	306.41(4)	524.3(1)
Z	4	2	2
$\rho_{calc.}$ [g cm^{-3}]	1.897	1.874	1.516
μ [mm^{-1}]	2.348	0.212	0.302
$F(000)$	660	172	248
$\lambda_{MoK\alpha}$[Å]	0.71073	0.71073	0.71073
T [K]	200	150	200
Theta Min-Max [°]	4.1, 26.0	4.0, 26.0	4.6, 26.0
Dataset [h; k; l]	–10:8; –20:20; –8:10	–6:6; –9:9; –10:10	–8:8; –8:8; –13:13
Reflection collected	5946	3051	5343
Independent reflection	2270	1196	2042
R_{int}	0.030	0.015	0.030
Observed reflection	1872	956	1700
No. parameters	190	116	181
R_1 (obs)	0.0351	0.0245	0.0400
wR_2 (all data)	0.0857	0.0653	0.1069
S	1.03	1.10	1.07
Min./Max. Resd. [e Å^{-3}]	–0.31, 0.67	–0.19, 0.17	–0.25, 0.27
Device type	Oxford Xcalibur3 CCD	Oxford Xcalibur3 CCD	Oxford Xcalibur3 CCD
Solution	SIR-92	SIR-97	SIR-92
Refinement	SHELXL-97	SHELXL-97	SHELXL-97
Absorption correction	multi-scan	multi-scan	multi-scan
CCDC No.	---	---	---

	175	**176**	**177**
Formula	$C_5H_8N_8O_8$	$C_4H_4N_8O_5$	$C_3H_5N_7O_5$
Form. weight [g mol^{-1}]	308.19	244.15	219.14
Crystal system	monoclinic	monoclinic	monoclinic
Space Group	$P2_1$ (4)	$P2_1/c$ (14)	$P2_1/c$ (14)
Color / Habit	colorless plates	colorless rods	colorless needles
Size [mm]	0.02 x 0.06 x 0.08	0.02 x 0.09 x 0.10	0.04 x 0.05 x 0.13
a [Å]	5.3958(3)	6.8250(8)	14.990(3)
b [Å]	9.8988(5)	5.082(2)	5.2214(9)
c [Å]	10.9859(6)	25.623(9)	10.166(2)
α [°]	90	90	90
β [°]	103.192(6)	92.802(9)	90.11(1)
γ [°]	90	90	90
V [Å^3]	571.29(5)	887.7(5)	795.7(2)
Z	2	4	4
$\rho_{calc.}$ [g cm^{-3}]	1.792	1.827	1.829
μ [mm^{-1}]	0.168	0.166	0.170
$F(000)$	316	496	448
$\lambda_{MoK\alpha}$[Å]	0.71073	0.71073	0.71073
T [K]	200	200	200
Theta Min-Max [°]	3.8, 33.4	4.1, 26.0	4.2, 26.0
Dataset [h; k; l]	–8:4; –14:14; –16:16	–8:8; –6:6; –31:31	–18:14; –6:4; –12:12
Reflection collected	4396	8549	3978
Independent reflection	2097	1749	1568
R_{int}	0.061	0.043	0.057
Observed reflection	874	1496	978
No. parameters	222	170	156
R_1 (obs)	0.0376	0.0494	0.0578
wR_2 (all data)	0.0685	0.1050	0.1081
S	0.78	1.17	1.08
Min./Max. Resd. [e Å^{-3}]	–0.20, 0.25	–0.25, 0.17	–0.22, 0.22
Device type	Oxford Xcalibur3 CCD	Oxford Xcalibur3 CCD	Oxford Xcalibur3 CCD
Solution	SHELXS-97	SIR-92	SHELXS-97
Refinement	SHELXL-97	SHELXL-97	SHELXL-97
Absorption correction	multi-scan	multi-scan	multi-scan
CCDC No.	---	---	---

	178	**179**	**180**
Formula	$C_5H_{10}Cl_3N_5$	C_2HN_5	$C_2H_3N_5O$
Form. weight [g mol^{-1}]	246.53	95.08	113.09
Crystal system	monoclinic	monoclinic	monoclinic
Space Group	$P2_1/c$ (14)	$P2_1/m$ (11)	$P2_1/m$ (11)
Color / Habit	colorless rods	colorless plates	colorless plates
Size [mm]	0.05 x 0.09 x 0.18	0.03 x 0.13 x 0.14	0.04 x 0.18 x 0.24
a [Å]	11.5872(9)	5.085(3)	4.9867(3)
b [Å]	9.1972(7)	6.103(2)	6.1274(4)
c [Å]	10.6148(9)	6.294(2)	7.2221(4)
α [°]	90	90	90
β [°]	107.265(7)	98.54(4)	100.421(5)
γ [°]	90	90	90
V [Å^3]	1080.3(2)	193.17(15)	217.04(2)
Z	4	2	2
$\rho_{calc.}$ [g cm^{-3}]	1.516	1.635	1.730
μ [mm^{-1}]	0.813	0.126	0.143
$F(000)$	504	96	116
$\lambda_{MoK\alpha}$[Å]	0.71073	0.71073	0.71073
T [K]	200	200	200
Theta Min-Max [°]	4.3, 25.0	4.7, 27.0	4.2, 28.2
Dataset [h; k; l]	–13:13; –10:10; –12:12	–6:6; –7:5; –7:8	–6:6; –7:8; –9:7
Reflection collected	9705	1067	1328
Independent reflection	1890	458	582
R_{int}	0.024	0.058	0.033
Observed reflection	1768	362	417
No. parameters	158	47	58
R_1 (obs)	0.0376	0.0531	0.0343
wR_2 (all data)	0.0989	0.1498	0.0914
S	1.12	1.13	0.94
Min./Max. Resd. [e Å^{-3}]	–0.36, 0.50	–0.26, 0.35	–0.18, 0.29
Device type	Oxford Xcalibur3 CCD	Oxford Xcalibur3 CCD	Oxford Xcalibur3 CCD
Solution	SIR-92	SHELXS-97	SIR-92
Refinement	SHELXL-97	SHELXL-97	SHELXL-97
Absorption correction	multi-scan	multi-scan	multi-scan
CCDC No.	---	---	---

	182	**183**	**184**
Formula	$C_4H_{12}N_{12}NaO_2$	$C_2H_4N_6$	$CH_4ClN_4NaO_2$
Form. weight [g mol^{-1}]	283.25	112.11	162.52
Crystal system	monoclinic	monoclinic	orthorhombic
Space Group	$C2/m$ (12)	$C2/m$ (12)	$Pnma$ (62)
Color / Habit	colorless plates	colorless blocks	colorless blocks
Size [mm]	0.08 x 0.10 x 0.18	0.13 x 0.21 x 0.24	0.08 x 0.09 x 0.13
a [Å]	26.329(2)	7.404(4)	6.882(1)
b [Å]	7.1694(6)	9.465(6)	6.964(1)
c [Å]	6.9333(6)	3.620(3)	12.306(2)
α [°]	90	90	90
β [°]	96.812(7)	115.32(4)	90
γ [°]	90	90	90
V [Å^3]	1299.5(2)	229.3(3)	589.8(2)
Z	4	2	4
$\rho_{calc.}$ [g cm^{-3}]	1.448	1.624	1.830
μ [mm^{-1}]	0.145	0.125	0.645
$F(000)$	588	116	328
$\lambda_{MoK\alpha}$[Å]	0.71073	0.71073	0.71073
T [K]	200	200	200
Theta Min-Max [°]	4.2, 26.0	4.3, 26.2	4.4, 26.0
Dataset [h; k; l]	–32:32; –8:8; –8:8	–9:9; –11:11; –4:4	–6:8; –8:8; –15:15
Reflection collected	6613	1206	2877
Independent reflection	1381	250	631
R_{int}	0.022	0.019	0.033
Observed reflection	1277	229	586
No. parameters	124	24	61
R_1 (obs)	0.0365	0.0365	0.0295
wR_2 (all data)	0.1025	0.0930	0.0781
S	1.10	1.18	1.14
Min./Max. Resd. [e Å^{-3}]	–0.21, 0.24	–0.20, 0.17	–0.27, 0.27
Device type	Oxford Xcalibur3 CCD	Oxford Xcalibur3 CCD	Oxford Xcalibur3 CCD
Solution	SHELXS-97	SIR-92	SIR-97
Refinement	SHELXL-97	SHELXL-97	SHELXL-97
Absorption correction	multi-scan	multi-scan	multi-scan
CCDC No.	---	---	---

List of Abbreviations

1,5-BT	1,5-bistetrazolate anion
1,5-HBT	1,5-bistetrazole
1MeAt	1-methyl-5-aminotetrazole
1MeAtNO_2	1-methyl-5-nitriminotetrazolate anion
1MeHAtNO_2	1-methyl-5-nitriminotetrazole
5-At	5-amino-1*H*-tetrazole
2MeAtNO_2	2-methyl-5-nitriminotetrazolate anion
2MeHAtNO_2	2-methyl-5-nitraminotetrazole
Å	angstrom (10^{-10} m)
AF	azidoformamidinium
AG	aminoguanidinium
ADN	ammonium dinitramide
AP	ammonium perchlorate
ARL	army research laboratory
AtNO_2	5-nitriminotetrazolate dianion
a.u.	atomic units (Hartree)
BAM	Bundesanstalt für Materialforschung und -prüfung
bp.	boiling point
br	bright
bta	bis(tetrazolyl)amine
BTH	bis(1*H*-tetrazolyl)hydrazine
BTT	bis(tetrazolyl)triazene
calcd.	calculated
C-J	Chapman-Jouguet
CL-20	hexanitro-hexaaza-isowurtzitane
d	dublett
δ	chemical shift
DAG	diaminoguanidinium
dec.	decomposition
DEI	desorption electron ionization
DMSO	dimethyl sulfoxide
DMF	dimethyl formamide
DN	dinitramide
DSC	differential scanning calorimetry
DTA	differential thermoanalysis
EA	elemental analysis

EI	electrical ionization
ESD	electrostatic discharge device
Et	ethyl
EtOH	ethanol
F	fuel
FID	free induction decay
FT	fourier transformation
FW	formula weight
g	gaseous
G	guanidinium
h	hour
H	hartree
H_2AtNO_2	5-nitrimino-1,4*H*-tetrazole
H_2bta	5,5'-bis(tetrazolyl)amine
HE	high explosives
HEDM	high energetic dense materials
HMX	high melting explosive, octogen
IR	infrared spectrum
J	coupling constant
l	liquid
m	medium (IR), multiplett (NMR)
Me	methyl
MeOH	methanol
mp.	melting point
min	minute
$MeNO_2$	nitromethane
MS	mass spectrometry
NAP	2-nitro-2-aza-propyl
NC	nitrocellulose
NG	nitroglycerine
NQ	nitroguanidine
NMR	nuclear magnetic resonance
NOE	nuclear overhauser effect
O	oxidizer
Ω	oxygen balance
OCX	octopus explosive
ONC	octanitrocubane
ρ	density
Ω	oxygen balance

OCX	octopus explosive
ONC	octanitrocubane
ρ	density
PC	priming charges
$p_{C\text{-}J}$	detonation pressure
PE	primary explosive
PETN	pentaerythritol tetranitrate
Ph	phenyl
ppm	parts per million
q	quartett
RDX	royal demolition explosive, research department explosive, hexogen, 1,3,5-trinitro-1,3,5-triazine
rt	room temperature
s	strong (IR), singulett (NMR), solid
sens.	sensitivity
STANAG	standardization agreement
t	triplett
T	temperature
T_E	temperature of explosion
TAG	triaminoguanidinium
THF	tetrahydrofuran
TMS	tetramethyl silane
Tz	tetrazole
$V_{Det.}$	velocity of detonation
vs	very strong
vw	very weak
w	weak

Jörg Stierstorfer
Kolpingstr. 16
82234 Wessling

CURRICULUM VITAE

PERSONAL DATA

Date of birth	29.11.1979
Place of birth	Munich
Nationality	German
Family status	single

Tel: + 49 (0)8153 / 953074
Mobil: + 49 (0)170 / 4708191
E-Mail: joerg.stierstorfer@gmx.de

EDUCATION

09/1986 – 09/1988	Primary school: Hallbergmoos, Germany
09/1988 – 09/1990	Primary school: Wessling, Germany
09/1990 – 06/1999	Secondary school: Gilching, Germany *Degree:* Abitur
09/1999 – 08/2000	Civilian service at Nachbarschaftshilfe Wessling
10/2000 – 09/2002	Undergraduate studies at the Ludwig-Maximilian University of Munich
10/2002 – 12/2005	Graduate studies at the Ludwig-Maximilian University of Munich *Degree:* Diplom Chemiker
01/2006 – 02/2009	Ph. D. student and scientific co-worker at the Ludwig-Maximilian University of Munich in the research group of Prof. Dr. T. M. Klapötke

WORK EXPERIENCE

08/2000 – 10/2000	Practical at 3M Espe AG, chemical analytics
08/2002 – 09/2002	Temporary job at 3M Espe AG, chemical research
05/2004 – 05/2005	Temporary job as private tutor for math, physics and chemistry at Schülerhilfe Gilching
01/2006 – 02/2009	Scientific co-worker at the LMU Munich in the research group of Prof. T. M. Klapötke

SUPPLEMENTARY

Computer literacy	MS Office, chemical software, Adobe CS3 Suite, html, unix systems
Language skills	German and English
Miscellaneous	Ambulance education

Wessling, 29.02.2009

BIBLIOGRAPHY

PUBLICATIONS

1. M. Hiskey, A. Hammerl, G. Holl, T. M. Klapötke, K. Polborn, J. Stierstorfer, J. J. Weigand, Azidoformamidinium and Guanidinium 5,5'-Azotetrazolate Salts, *Chem. Mater.* **2005**, *17*, 3784–3793.

2. T. M. Klapötke, P. Meyer, K. Polborn, J. Stierstorfer, J. J. Weigand, 5,5'-bis(1*H*-tetrazolyl)amine (H_2BTA): a promising ligand in novel copper based priming charges (PC), *New Trends in Research of Energetic Materials, Proceedings of the Seminar,* 9th, Pardubice, Czech Republic, **2006**, *2*, 641–651.

3. T. M. Klapötke, P. Mayer, K. Polborn, J. Stierstorfer, J. J. Weigand, 5,5'-bis-(1*H*-tetrazolyl)amine (H_2BTA) and 5,5'-bis-(2-methyl-tetrazolyl)amine (Me_2BTA), promising ligands in new copper based priming charges, *37th International Annual Conference of ICT*, Karlsruhe, Federal Republic of Germany, **2006**, 134/1–134/14.

4. V. Ernst, T. M. Klapötke, J. Stierstorfer, Alkali Salts of 5-Aminotetrazole – Structures and Properties, *Z. Anorg. Allg. Chem.* **2007**, *633*, 879–887.

5. T. M. Klapötke, J. Stierstorfer, Investigations of Nitrated Aminotetrazoles as Promising Energetic Materials – Synthesis, Structures and Properties, *New Trends in Research of Energetic Materials, Proceedings of the Seminar*, 10th, Pardubice, Czech Republic, **2007**, *2*, 674.

6. V. Ernst, T. M. Klapötke, J. Stierstorfer, Nitriminotetrazolates as Energetic Ingredients in Innovative Pyrotechnical Compositions – A Comprehensive Characterization, *New Trends in Research of Energetic Materials, Proceedings of the Seminar*, 10th, Pardubice, Czech Republic, **2007**, *2*, 575.

7. G. Geisberger, T. M. Klapötke, J. Stierstorfer, Copper Bis(1-methyl-5-nitrimino-tetrazolate): A Promising New Primary Explosive, *Eur. J. Inorg. Chem.* **2007**, *30*, 4743–4750.

8. T. M. Klapötke, J. Stierstorfer, Nitration Products of 5-Amino-1*H*-tetrazole and Methyl-5-amino-1*H*-tetrazoles – Structures and Properties of Promising Energetic Materials, *Helv. Chim. Acta* **2007**, *90*, 2132–2150.

9. T. M. Klapötke, H. Radies, J. Stierstorfer, Alkali Salts of 1-Methyl-5-nitriminotetrazole – Structures and Properties, *Z. Naturforschung,* **2007**, *62b*, 1343–1352.

10. T. M. Klapötke, H. A. Laub, J. Stierstorfer, Synthesis and Characterization of a New Class of Energetic Compounds – Ammonium Nitriminotetrazolates, *Propellants Explos. Pyrotech.* **2009**, *33*, 421–430.

11. T. M. Klapötke, J. Stierstorfer, Synthesis and Characterization of the Energetic Compounds Aminoguanidinium-, Triaminoguanidinium- and Azidoformamidinium Perchlorate, *Centr. Europ. J. Energ. Mat.* **2008**, *5*, 13–30.

12. J. Stierstorfer, T. M. Klapötke, A. Hammerl, R. D. Chapman, 5-Azido-1*H*-tetrazole – Improved Synthesis, Crystal Structure and Sensitivity Data, *Z. Anorg. Allg. Chem.* **2008**, *634*, 1051–1057.

13. T. M. Klapötke, J. Stierstorfer, Triaminoguanidinium dinitramide – calculations, synthesis and characterization of a promising energetic compound, *Phys. Chem. Chem. Phys.* **2008**, *10*, 4340–4346.

14. T. M. Klapötke, J. Stierstorfer, A. Wallek, Nitrogen-rich salts of 1-methyl-5-nitriminotetrazole, *New Trends in Research of Energetic Materials, Proceedings of the Seminar*, 11th, Pardubice, Czech Republic, **2008**, *2*, 832–854.

15. T. M. Klapötke, J. Stierstorfer, Recent Developments on Energetic Materials based on 5-aminotetrazole, *New Trends in Research of Energetic Materials, Proceedings of the Seminar*, 11th, Pardubice, Czech Republic, **2008**, *1*, 278–298.

16. T. M. Klapötke, J. Stierstorfer, Nitrogen-rich dinitramides – a class of energetic compounds with a well balanced oxygen content, *New Trends in Research of Energetic Materials, Proceedings of the Seminar*, 11th, Pardubice, Czech Republic, **2008**, *2*, 810–831.

17. T. M. Klapötke, J. Stierstorfer, The New Energetic Compounds 1,5-Diaminotetrazolium and 5-Amino-1-methyltetrazolium Dinitramide – Synthesis, Characterization and Testing, *Eur. J. Inorg. Chem.* **2008**, *26*, 4055–4062.

18. T. M. Klapötke, J. Stierstorfer, A. U. Wallek, Nitrogen-Rich Salts of 1-Methyl-5-nitriminotetrazolate: An Auspicious Class of Thermally Stable Energetic Materials, *Chem. Mater.* **2008**, *20*, 4519–4530.

19. T. M. Klapötke, M. Stein, J. Stierstorfer, Salts of 1*H*-Tetrazole – Synthesis, Characterization and Properties, **2008***, 634*, 1711–1723.

20. T. M. Klapötke, P. Mayer, J. Stierstorfer, J. J. Weigand, Bistetrazolylamines – synthesis and characterization *J. Mat. Chem.* **2008**, *18*, 5248–5258.

21. T. M. Klapötke, J. Stierstorfer, Azidoformamidinium and 5-Aminotetrazolium Dinitramide – Two Highly Energetic Isomers with a Balanced Oxygen Content *Dalton Transactions*, **2008**, *4*, 643–653..

22. T. M. Klapötke, C. M. Sabaté, J. Stierstorfer, Hydrogen-bonding Stabilization in Energetic Perchlorate Salts: 5-Amino-1*H*-tetrazolium Perchlorate and its Adduct with 5-Amino-1*H*-tetrazole, *Z. Anorg. Allg. Chem.* **2008**, *634*, 1867–1874.

23. T. M. Klapötke, J. Stierstorfer, K. R. Tarantik, I. Thoma, Strontium Nitriminotetrazolates – Suitable Colorants in Smokeless Pyrotechnic Compositions, *Z. Anorg. Allg. Chem.* **2008**, *634*, 2777–2784.

24. N. Fischer, T. M. Klapötke, S. Scheutzow, J. Stierstorfer, Hydrazinium 5-aminotetrazolate: An insensitive energetic material containing 83.72 % nitrogen*, Centr. Europ. J. Energ. Mater.* **2008**, *5*, 3–18.

25. T. M. Klapötke, C. M. Sabaté, J. Stierstorfer, Neutral 5-nitrotetrazoles: easy initiation with low pollution, *New J. Chem.* **2009***, 33*, 136–147.

26. T. M. Klapötke, N. Minar, J. Stierstorfer, Investigations of *bis*(Methyl-tetrazolyl)triazenes as Nitrogen-Rich Ingredients in Solid Propellant Charges: Synthesis, Characterization and Properties, *Polyhedron*, **2008**, *28, 13–26*.

27. T. M. Klapötke, J. Stierstorfer, B. Weber, New energetic materials: Synthesis and characterization of copper 5-nitriminotetrazolates, *Inorg. Chim. Acta* **2008**, 10.1016/j.ica.2008.10.014.

28. T. M. Klapötke, P. Mayer, J. Stierstorfer, Crystal Structures of Mono-, Di- and Triaminoguanidinium Sulfate as well as Azidoformamidinium Sulfate: Important Precursors for Syntheses of Nitrogen Rich Ionic Compounds. *Phosphorus, Sulfur Silicon Relat. Elem.* **2008**, *in press*.

29. N. Fischer, K. Karaghiosoff, T. M. Klapötke, J. Stierstorfer, New Energetic Materials feat. Tetrazoles and Nitramines – Synthesis, Characterization and Properties, *Helv. Chim. Acta* **2008**, *accepted.*

30. T. M. Klapötke, J. Stierstorfer, The CN_7^-Anion, *J. Am. Chem. Soc.* **2009**, *131,* 1122–1134.

31. J. Stierstorfer, K. Tarantik, T. M. Klapötke, New Energetic Materials: Functionalized 1-Ethyl-5-aminotetrazoles and 1-Ethyl-5-nitriminotetrazoles, *Chem. – Europ. J.* **2009**, *in press*.

32. N. Fischer, T. M. Klapötke, J. Stierstorfer, New Nitriminotetrazoles – Synthesis, Structures and Characterization, *Z. Anorg. Allg. Chem.* **2009**, *635,* 271–281.

33. T. M. Klapötke, S. Sproll, J. Stierstorfer, J. J. Weigand, Synthesis and Characterization of Methyl-5-azidotetrazoles, *Chem. Comm.* **2009**, *submitted*.

34. T. M. Klapötke, J. Stierstorfer, Calcium 5-Nitriminotetrazolate – A new green replacement for lead azide in priming charges, *Chem. Mater.* **2008**, *submitted*.

PRESENTATIONS

1. J. Stierstorfer, Energetic Materials based on 5-Aminotetrazole, 11th NTREM conference in Pardubice, **2008**, Czech Republic.
2. J. Stierstorfer, High Nitrogen Compounds for use in Low-erosivity Gun Propellants, Army Science Conference, **2008**, Orlando, Florida, USA.

POSTER PRESENTATIONS

1. 5,5'-Bis(1*H*-tetrazolyl)amine (H_2BTA): A Promising Ligand in Novel Copper Based Priming Charges (PC), T. M. Klapötke, P. Meyer, K. Polborn, J. Stierstorfer, J. J. Weigand, *New Trends in Research of Energetic Materials, Proceedings of the Seminar*, 9th, Pardubice, Czech Republic, **2006**.
2. New methods of synthesis of 1,5-Diamino-(1*H*)-tetrazole, C. Darwich, J. Stierstorfer, *New Trends in Research of Energetic Materials, Proceedings of the Seminar*, 9th, Pardubice, Czech Republic, **2006**.
3. 5,5´-Bis(1*H*-tetrazolyl)amine (H_2bta) and 5,5´-Bis-(2-Methyltetrazolyl)amine (Me_2bta): Promising Ligands in New Copper Based Priming Charges (PC), T. M. Klapötke, P. Mayer, J. Stierstorfer, B. Weber and J. J. Weigand, Karlsruhe, Federal Republic of Germany, **2006**.
4. T. M. Klapötke, J. Stierstorfer, Investigations of Nitrated Aminotetrazoles as Promising Energetic Materials – Synthesis, Structures and Properties, *New Trends in Research of Energetic Materials,* 10th, Pardubice, Czech Republic, **2007**.
5. V. Ernst, T. M. Klapötke, J. Stierstorfer, Nitriminotetrazolates as Energetic Ingredients in Innovative Pyrotechnical Compositions – A Comprehensive Characterization – *New Trends in Research of Energetic Materials,* 10th, Pardubice, Czech Republic, **2007**.
6. T. M. Klapötke, J. Stierstorfer, A. Wallek, Nitrogen-rich salts of 1-methyl-5-nitriminotetrazole – an auspicious class of thermally stable high explosives, *New Trends in Research of Energetic Materials, Proceedings of the Seminar*, 11th, Pardubice, Czech Republic, **2008**.
7. T. M. Klapötke, J. Stierstorfer, Nitrogen-rich dinitramides – a class of energetic compounds with a well balanced oxygen content, *New Trends in Research of Energetic Materials, Proceedings of the Seminar*, 11th, Pardubice, Czech Republic, **2008**.

8. T. M. Klapötke, J. Stierstorfer, Energetic Dinitramides, Gordon Research Conference, **2008**, Tilton, NH, USA.
9. T. M. Klapötke, J. Stierstorfer, The CN_7^- Anion, Gordon Research Conference, **2008**, Tilton, NH, USA.
10. T. M. Klapötke, J. Stierstorfer, Nitrogen-rich salts of 1-methyl-5-nitriminotetrazole – an auspicious class of thermally stable high explosives, Gordon Research Conference, **2008**, Tilton, NH, USA.
11. T. M. Klapötke, N. Mayr, J. Stierstorfer, New Enregetic Materials containing the Dinitramide and Triaminoguanidinium moieties, **2008**, Orlando, Florida, USA.

AWARDS

1. Award for best poster presentation, 9th Conference in Pardubice, Czech Republic, *New Trends in Research of Energetic Materials,* **2006**.
2. Award for excellent poster presentation, 10th Conference in Pardubice, Czech Republic, *New Trends in Research of Energetic Materials,* **2007**.
3. Römer price of the "Dr. Klaus Römer foundation" at the Ludwig-Maximilian University Munich for excellent scientific results in chemistry and biochemistry, **2007**.
4. Award for best oral presentation, 11th Conference in Pardubice, Czech Republic, *New Trends in Research of Energetic Materials,* **2008**.